Mid-Atlantic U.S. Offshore Carbon Storage Resource Assessment Project

Final Technical Report

MID-ATLANTIC U.S. OFFSHORE
CARBON STORAGE RESOURCE
ASSESSMENT PROJECT

U.S. Department of Energy (DOE) Project – DE-FE0026087
Battelle Project Number – 100068380

Prepared by:

Battelle
505 King Avenue
Columbus, Ohio 43201
Principal Investigator: Dr. Neeraj Gupta
Project Manager: Ms. Lydia Cumming

Submitted to:

U.S. DOE
National Energy Technology Laboratory (NETL)
Project Manager: Mr. William O'Dowd
William.ODowd@NETL.DOE.GOV

September 25, 2019

Disclaimer

Acknowledgements

This material is based upon work supported by the Department of Energy under Award Number DE-FE0026087. The Project Team is led by Battelle and includes the state geological surveys of Delaware, Maryland, and Pennsylvania; United States Geological Survey (USGS); Lamont-Doherty Earth Observatory at Columbia University (LDEO); and Rutgers University. Harvard University, Texas Bureau of Economic Geology, and Virginia Department of Mines, Minerals & Energy serve as technical advisors.

Battelle was responsible for the overall project execution, including project management and technical analysis, with **Dr. Neeraj Gupta as Principal Investigator and Ms. Lydia Cumming providing project management** and technical coordination between team members. Project management support was also provided by Ms. Christa Duffy and Ms. Kathryn Johnson.

Authors/Principal Technical Contributors: Task 2 correlation of seismic data with well-log data and sequence stratigraphic characterization of geologic storage zones were performed by Rutgers University, including: Dr. Ken Miller, Dr. Gregory Mountain, Dr. Christopher Lombardi, Ms. Alex Adams, Ms. Kimberly Baldwin, Mr. Stephen Graham, Ms. Leslie Jordan, Mr. Paul Romero, and Mr. William Schmelz; and USGS team members Dr. Uri ten Brink and Mr. Guy Lang (Haifa University). **Task 3** seismic processing, interpretation, and inversion to support structural and stratigraphic framework development was overseen by Dr. Will Fortin, Dr. Dave Goldberg, and Dr. Angela Slagle at LDEO. **Task 4** hydrological data compilation and characterization efforts were undertaken by Dr. Mojisola KunleDare and Dr. Peter McLaughlin at the Delaware Geological Survey. **Task 5** storage resource calculations were overseen by Ms. Isis Fukai from Battelle. **Task 6** risk factor analysis was led by Mr. Joel Sminchak at Battelle. Ms. Kristin Carter from the Pennsylvania Geological Survey (PaGS) led the **Task 7** stakeholder engagement effort.

Additional Technical Contributors: Other Battelle Project Team members contributing to this project include (in alphabetical order) Dr. Jit Bhattacharya, Ms. Carol Brantley, Mr. Andrew Burchwell, Ms. Priya Ravi Ganesh, Mr. Martin Jimenez, Ms. Laura Keister, Mr. Sanjay Mawalkar, Dr. Heather McCarren, and Ms. Desiree Padgett. Well-log digitization efforts and guidance on petrophysical calculation methods and mineralogical/geochemical data used in Task 2, 4, and 5 for characterization of storage zones and caprocks was provided by Ms. Kristin Carter, Mr. Brian Dunst, and Dr. Steve Shank at the PaGS. Management of the ArcGIS online database and correlation of onshore-offshore coastal plain stratigraphy was conducted by Mr. David Andreasen, Mr. Richard Ortt, Ms. Heather Quinn, and Mr. Andrew Stanley at the Maryland Geological Survey. This project also benefited from research performed by the Bureau of Ocean Energy Management and offshore drilling programs along the Mid-Atlantic from the 1970s to 1980s.

Table of Contents

Page

Attachments

List of Tables

Page

List of Figures

Page

List of Acronyms and Abbreviations

2D	Two-dimensional
3D	Three-dimensional
AGOL	ArcGIS Online
AI	Absolute Imaging, Inc.
API	American Petroleum Institute
BCT	Baltimore Canyon Trough
BEG	Bureau of Economic Geology
BOEM	Bureau of Ocean Energy Management
BSE	backscatter electron
ca.	circa
CAMP	Central Atlantic Magmatic Province
CCS	Carbon Capture and Storage
CCUS	Carbon Capture Utilization and Storage
CMP	Common mid-point
CO_2	Carbon Dioxide
CO_2-SCREEN	CO_2 Storage prospeCtive Resource Estimation Excel aNalysis
COST	Continental Offshore Stratigraphic Test
CSLF	Carbon Sequestration Leadership Forum
DC	Dawson Canyon
DGS	Delaware Geological Survey
DMME	Department of Mines, Minerals & Energy
DOE	U.S. Department of Energy
EDS	energy dispersive spectroscopy
EDX	NETL Energy Data eXchange
EEZ	Exclusive Economic Zone
EIA	U.S. Energy Information Administration
EPA	U.S. Environmental Protection Agency
FAD	First Appearance Datum
FG	Fills a data gap
FOA	Funding Opportunity Announcement
ft	Foot
g	gram
gal	gallon
gAPI	American Petroleum Institute Gamma Ray Unit
GBB	Georges Bank Basin
GCSSEPM	Gulf Coast Section SEPM
GHGT	Greenhouse Gas Control Technologies
GR	Gamma Ray
GSD	Great Stone Dome
Gt	Gigatonne (1 billion metric tons or 1,000,000,000,000 kg)
HST	highstand systems tract
IEAGHG	International Energy Agency Greenhouse Gas
IODP	International Ocean Discovery Program
kg	kilogram

km	Kilometer
L	Liter
LAS	Log ASCII Standard
lb	pound
LC	Logan Canyon
LDEO	Lamont-Doherty Earth Observatory
LIP	Long Island Platform
LK#	Lower Cretaceous Sequence Number
LOC	line of correlation
LST	lowstand systems tract
m	Meter
Ma	million years ago
MAOCSRAP	Mid-Atlantic U.S. Offshore Carbon Storage Resource Assessment Project
mbsf	meters below sea floor
MCS	multichannel seismic
mD	Millidarcy
MFS	maximum flooding surface
Mg	milligram
MGS	Maryland Geological Survey
mi	mile
MIT	Massachusetts Institute of Technology
MK#	Middle Cretaceous Sequence Number
ml	milliliter
mm	millimeter
MMS	Minerals Management Service
MRCSP	Midwest Regional Carbon Sequestration Partnership
ms	Millisecond
msl	mean sea level
Mt	Megatonne (1 million metric tons or 1,000,000,000 kg)
NAMSS	National Archive of Marine Seismic Surveys
NE	Northeast
NETL	National Energy Technology Laboratory
NGO	non-government organization
NRAP	National Risk Assessment Partnership
NW	Northwest
OCS	Outer Continental Shelf
P10	low probability
P50	median probability
P90	high probability
Pa	Pascal
PaGS	Pennsylvania Geological Survey
ppt	parts per thousand
psi	Pounds per Square Inch
QA/QC	Quality Assurance/Quality Control
R&D	research and development
R/V	Research Vessel

s	second
SB	Sequence Boundary
SBCT	Southern Baltimore Canyon Trough
SE	Southeast
SEM	scanning electron microscopy
SLA	Submerged Lands Act
SP	spontaneous potential
SPE	Society of Petroleum Engineers
SRMS	Storage Resources Management System
SW	southwest
TS	transgressive surface
TST	transgressive systems tract
TWT	two way time
TWTT	two way travel time
UJ#	Upper Jurassic Sequence Number
UK#	Upper Cretaceous Sequence Number
UMASS	University of Massachusetts
USGS	United States Geological Survey
VE	Helps to verify empirically derived permeability values
Vp	Primary-wave velocity
Vs	Secondary-wave velocity
WRI	World Resources Institute
XRD	X-ray Diffraction
XRF	X-ray Fluorescence

Executive Summary

The greatest potential for carbon storage in the northeastern United States lies in the offshore geologic formations comprising the continental shelf (Monteverde et al., 2011). Offshore storage can be linked to large point-sources of carbon dioxide (CO_2) while avoiding many of the logistical difficulties and potential risks encountered when siting onshore projects, especially in densely populated areas of the East Coast. Recent assessments of domestic offshore CO_2 storage suggest a majority of the storage potential is in sandstone and carbonate saline reservoirs, with less potential in depleted oil fields and enhanced oil recovery projects (e.g., Gulf of Mexico). Other potential storage formations such as basalts have not been comprehensively assessed, although they may become significant reservoir candidates in the Atlantic and Pacific. Internationally, offshore CO_2 storage has been underway in Norway for the past 20 years, and considerable research has been completed in countries including Japan, Australia, Brazil, and South Africa. Offshore CO_2 storage assessment and research in the United States is underway to address uncertainty in potential storage resources, particularly in the mid- and north-Atlantic offshore area (Figure ES-1).

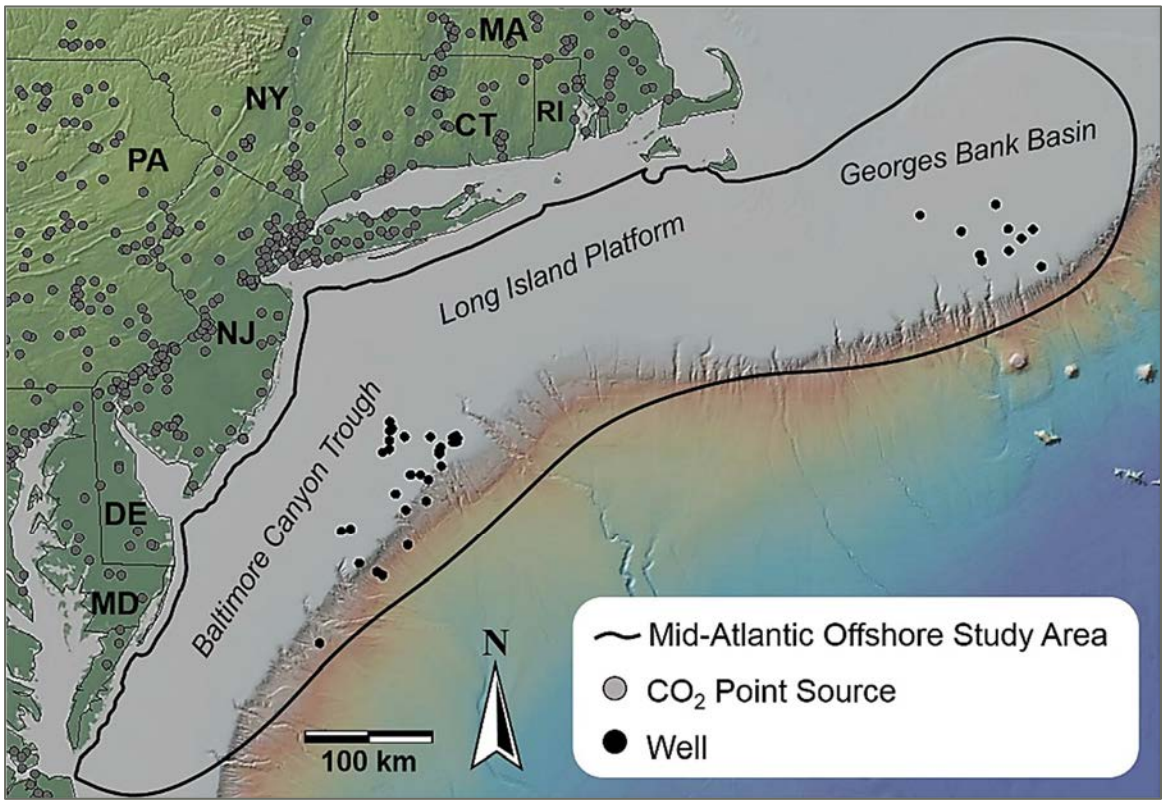

Figure ES-1. Map of the eastern United States coastal region showing location of the mid-Atlantic U.S. offshore study area, as well as locations of stationary CO_2 sources.

Given the current knowledge base and access to publicly available data, the objectives of the Mid-Atlantic U.S. Offshore Carbon Storage Resource Assessment Project (MAOCSRAP) are fourfold: (1) complete a systematic carbon storage resource assessment of the mid-Atlantic offshore coastal region from the Georges Bank Basin (GBB) through the Long Island Platform (LIP) to the southern Baltimore Canyon Trough (BCT); (2) define key input parameters to reduce uncertainty for offshore storage resource and efficiency estimates; (3) perform a preliminary assessment of risk factors, uncertainties, and data gaps; and (4) engage industry

and regulatory stakeholders through development of a Road Map to assist future project planning and implementation.

Over the past 3 years, the Project Team has compiled, inventoried, and assimilated various publicly available data sets to provide a strong technical basis on which future carbon storage studies and applications can be built. The knowledge infrastructure necessary to support the development of full-scale offshore carbon storage include:

- Defining the geologic characteristics of candidate storage sites (Chapter 2)
- Using existing seismic data to better define the continuity of the storage zones and seals (Chapter 3)
- Cataloguing the hydrogeologic properties of mid-Atlantic offshore storage sites (Chapter 4)
- Calculating prospective CO_2 storage resources using net effective pore volumes and fluid displacement properties specific to offshore lithologies (Chapter 5)
- Examining risk factors related to offshore storage (Chapter 6)
- Communicating with industry and other stakeholders about the future prospects for offshore storage (Chapter 7)
- Ensuring technology transfer to industry and other stakeholders (Chapter 8).

Led by Battelle, this project was conducted by public and private entities with expertise in offshore geology and resources for the study region, including state geological surveys of Delaware, Maryland, and Pennsylvania; United States Geological Survey-Woods Hole Coastal and Marine Science Center and Haifa University; Rutgers University; Harvard University; and Lamont-Doherty Earth Observatory (LDEO) at Columbia University. The storage resource assessment was completed for a broad region offshore of the U.S. East Coast, from Massachusetts to Virginia. The team built on the success of the Midwest Regional Carbon Sequestration Partnership (MRCSP) program (www.mrcsp.org), using a regional approach for screening and identifying candidate storage sites with the potential to deliver the most value for the East Coast. The results include high-level storage resource estimates for areas not previously characterized and improved storage resource estimates for geographically expansive portions of offshore geologic units.

Key Findings

Results of the project provide a foundation for developing CO_2 storage along offshore areas of the mid-Atlantic United States. A combination of information was used to provide confidence in project results. Key findings of the major project tasks are summarized as follows.

Subsurface Data Analysis:

- Legacy seismic, well-log, core, and biostratigraphic data were digitized, reprocessed, and analyzed using modern techniques, augmenting previous characterization efforts.
- The sequence stratigraphic framework for the Cretaceous and Jurassic strata was developed by correlating well-log depositional sequences to seismic reflectors identified in the BCT, LIP, and GBB.
- The integration of well-log stratigraphy with seismic stratigraphy and petrophysical analysis helped to identify and map potential storage zones within sequences of the Logan Canyon (LC), Missisauga, and Mohawk formations, as well as the regionally extensive caprock comprised of the Dawson Canyon shale.
- Approximately 4,000 kilometers (km) of seismic data was reprocessed to create a structural framework that was used to tie together all available well data, constrain sequence

stratigraphic interpretations, and make regional assessments of offshore carbon storage resources.

- Prospective storage resource estimates were 150 to 1136 megatons (Mt) for the combined storage zones. This suggests mid-Atlantic U.S. offshore formations can store decades of CO_2 from industrial sources in the region.
- Preliminary local reservoir simulations suggest that injection rates of 1 Mt CO_2/year may be sustained for 30 years in single injection wells in the BCT. Advanced geologic modeling and new data acquisition are needed to address data gaps and advance carbon capture and storage (CCS) in key offshore areas selected for further investigation.

Offshore Risk Factors:

- Offshore geologic risk factors include soft sediment deformation, unit continuity, sedimentological and structural features, seismicity and hydrates.
- CO_2 storage risks include inadequate seals, migration/leakage, and chemical interactions leading to decreased storage.
- Sensitive habitats, environmental impacts, disturbance to seafloor, and other risks need to be identified in advance of project activities and integrated into detailed mitigation plans for all project phases.

Stakeholder Engagement:

- Input and participation from government, industry, and environmental groups provided input into the Road Map and address next steps needed for project deployment (Figure ES-2).
- Early engagement and ongoing communication, as well as policy framework development, is key to large-scale deployment of CCS.

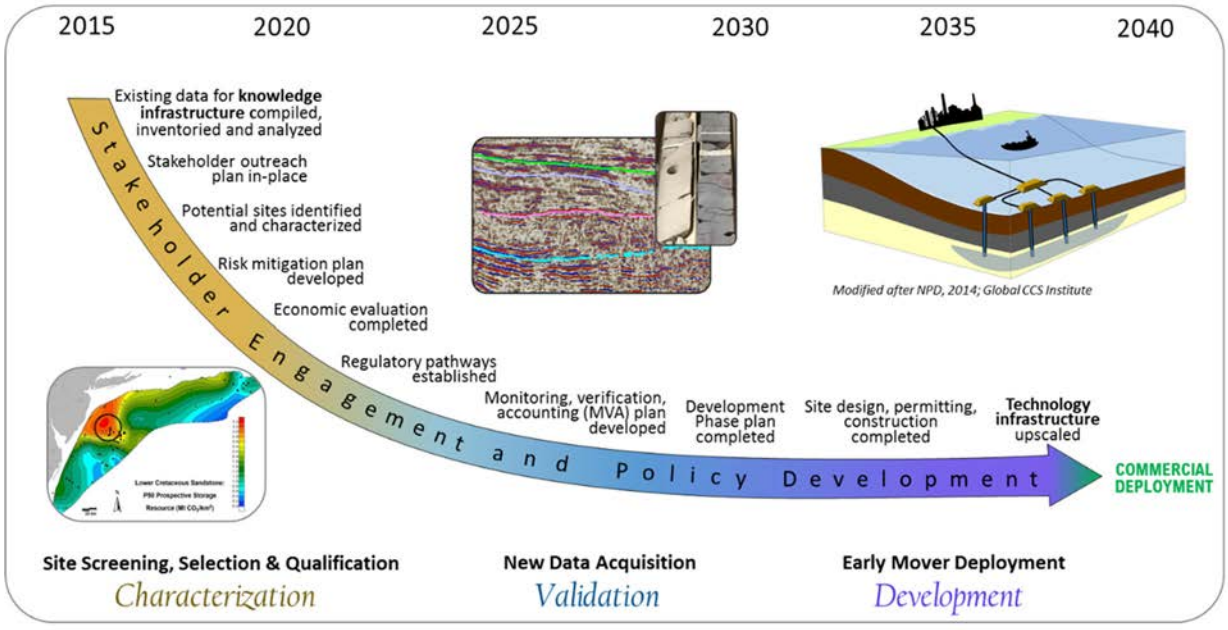

Figure ES-2. Preliminary Mid-Atlantic Offshore CCS Deployment Road Map.

Next Steps

This project represents an important first step by completing a high-level CO_2 storage resource assessment and building the knowledge infrastructure necessary to improve quantitative storage resource estimates. The data sets that have been curated under this project provide an opportunity to conduct research and development (R&D) needed to address data gaps and reduce risk and uncertainty. Offshore characterization and validation strategies that are systematically designed to provide data and infrastructure that can be upscaled to meet commercial requirements should be developed. Recommended actions for future CCS project planning and implementation offshore of the mid-Atlantic United States are listed below.

Near-Term Actions (Characterization Stage):

- As a practical next step, the Project Team could use existing data sets to develop advanced static and dynamic geologic models to determine the geospatial variability of key storage parameters, complete the site screening process, and provide a better understanding of offshore subsurface storage opportunities and risks.
- Complete advanced reprocessing using existing seismic data and interpretation of modern seismic data from recent cruises to evaluate rift basin properties and reservoir capacity.
- Implement a stakeholder outreach strategy to create champions for CCS R&D in the offshore region and streamline public acceptance of data collection in the marine environment as early as possible.
- Identify common industry and research goals for collaboration with international projects to build partnerships that lower research costs. Pursuit of onshore or analog data collection opportunities (e.g., drilling, core collection) could also help lower the cost of data collection.
- Develop regulatory certainty facilitated through U.S. regulator meetings with countries (e.g., Norway) where there is experience with offshore CCS operations.

Mid-Term Actions (Validation Stage):

- New data collection efforts should initially focus on addressing subsurface data gaps and requirements for qualifying potential sites, mitigating risk, and addressing potential regulatory/permit requirements.
- New data will be needed to validate caprock petrophysical properties, fracture pressure gradients, leakage risks, reservoir injectivity, and baseline geomechanical, geochemical, and hydrologic properties of storage zones and caprocks.
- Due to the higher costs and challenges associated with offshore characterization wells, a cost-benefit analysis will be needed to ensure the value of new data acquired meets the specific technical and economic requirements defined for the project.
- Appropriate monitoring methods will need to be investigated and validated prior to full-scale deployment and incorporated into the development phase plan.

Long-Term Actions (Development Stage):

- The development stage will establish and implement a detailed plan for large-scale CCS operations based on the findings of the preceding phases and the development of sufficient regulatory and pricing mechanisms to enable financially viable deployment. The progression to development also will depend on the strength of the stakeholder buy-in into the offshore CCS deployment in the mid-Atlantic area.
- The development stage activities typically include the assessment of CO_2 sources and transport, final site selection, detailed design, permitting, construction, operations, and

monitoring. Advances in offshore technologies such as advanced characterization, robotics, sub-sea structures, safety mechanisms, and remote operations over the next decade may facilitate cost-effective deployment with enhanced stakeholder confidence.

- Early mover projects in the United States and globally may help accelerate deployment of CCS through upscaling of technologies that reduce economic and policy barriers to commercial-scale CCS.

1. Introduction

The *Mid-Atlantic U.S. Offshore Carbon Storage Resource Assessment Project* (MAOCSRAP was part of the U.S. Department of Energy (DOE) National Energy Technology Laboratory's (NETL's) Carbon Storage program to improve the effectiveness and reduce the costs of carbon storage implementation (FE0026087). MAOCSRAP was selected for award under Funding Opportunity Announcement (FOA) DE-FOA-001246 Offshore Storage Resource Assessment. This project goal was to develop an informative picture of offshore storage potential and viable geologic storage options for the mid-Atlantic United States (i.e., New York, New Jersey, Pennsylvania, Delaware, and Maryland) (Figure 1-1). Over the past 3 years, the Project has compiled, inventoried, and assimilated various publicly available data sets to begin developing the knowledge infrastructure necessary to support the development of full-scale offshore carbon storage and to prudently transfer onshore technology knowledge to offshore applications.

This study gathered and integrated data from a wide variety of sources: geologic samples from research borehole cores, Continental Offshore Stratigraphic Test (COST) wells, and petroleum exploration wells drilled in the Atlantic Outer Continental Shelf (OCS); analog data from onshore coastal plain studies; and publicly available seismic data. This data was used to understand the regional geologic framework and continuity of potential carbon storage reservoirs and seals, as well as hydrologic properties and other characteristics of the deep sedimentary layers and rift basins. In turn, this information was used by the Project Team to develop site selection criteria, geologic storage efficiency factors, and risk factors specific to the mid-Atlantic U.S. offshore environment.

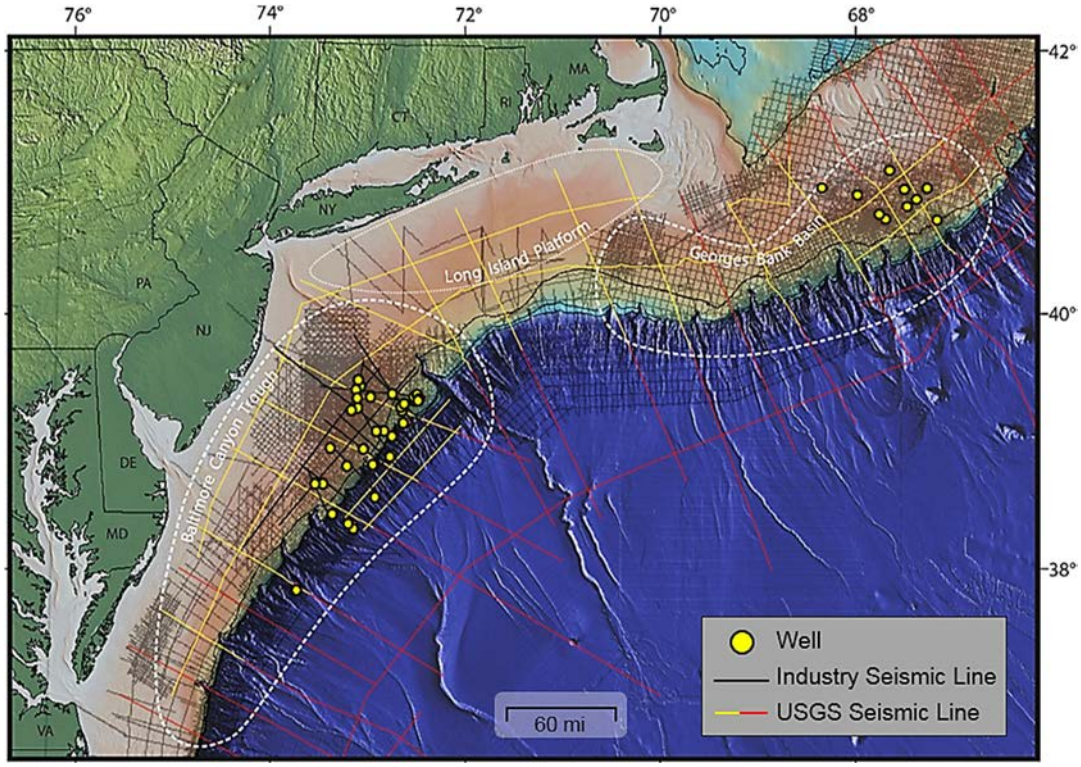

Figure 1-1. Map of the MAOCSRAP study area showing outlines of the three main subregions with the locations of wells and seismic lines.

Note: Dashed lines approximate the subregion outlines based on minimum of 5-km sediment thickness.

1.1 Project Objectives

The project objectives were aligned with DOE's goals to support industry's ability to predict CO_2 storage capacity in geologic formations to within ± 30 percent and to develop Best Practices Manuals for monitoring, verification, accounting, site screening, site selection, initial characterization, public outreach, well management, risk analysis, and simulation.

The objectives of this project were to (1) complete a systematic carbon storage resource assessment of the offshore study area; (2) define key input parameters to reduce uncertainty for offshore resource assessment and efficiency estimates; (3) examine risk factors that may impact storage resource estimates; and (4) engage industry and regulatory stakeholders through development of a Road Map to assist future project planning and implementation.

1.2 Project Organization

The Project Team included Battelle, the state geological surveys of Maryland, Delaware, and Pennsylvania; the United States Geological Survey (USGS in conjunction with Haifa University; Rutgers University; Harvard University; and Lamont-Doherty Earth Observatory (LDEO) at Columbia University. The Texas Bureau of Economic Geology (BEG) and Virginia Department of Mines, Minerals & Energy (DMME) served as technical advisors to the Project Team.

The project consisted of eight tasks, including Project Management and Planning (Task 1), Offshore Geological Characterization (Task 2), Seismic Evaluation (Task 3), Hydrologic Properties Characterization (Task 4), Carbon Storage Resource Calculations (Task 5), Risk Factors Assessment (Task 6), Stakeholder Education and Engagement (Task 7), and Reporting and Technology Transfer (Task 8). Figure 1-2 shows the project's high-level organization, the tasks, and the task leaders. Each task leader was responsible for completing the project objectives and subtask work. More detail on specific task approach and accomplishments are provided in the following sections.

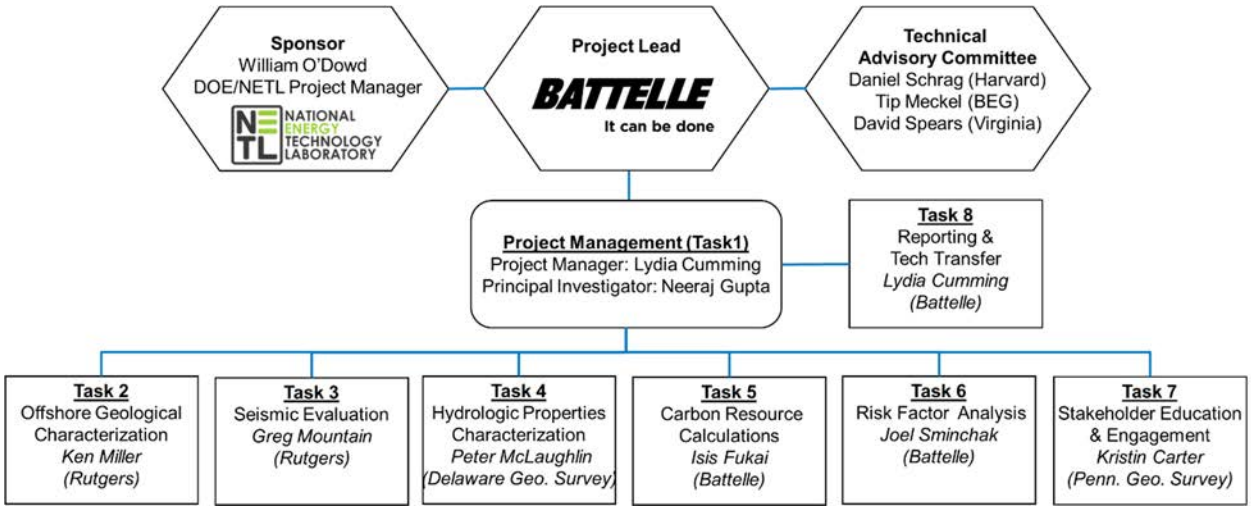

Figure 1-2. Project Organization Chart

2. Offshore Geologic Characterization

The mid-Atlantic offshore study area encompasses nearly 171,000 square kilometers (km^2) along the mid-Atlantic states of Virginia, Maryland, Delaware, New York, New Jersey, and Pennsylvania (Figure 1-1). The study area comprises three major subregions: Georges Bank Basin (GBB), Long Island Platform (LIP), and Baltimore Canyon Trough (BCT). The project study area extends from within 10 kilometers (km) to 300 km offshore, encompassing the inner continental shelf to portions of the continental slope. Water depths in the mid-Atlantic continental shelf grade gently from zero depth along the shoreline to the depths of 100 meters (m) to 200 m at the continental slope. Along the continental slope, water depths plummet more than 2,000 m into the North Atlantic Basin.

Task 2 geologic characterization focused on defining a detailed regional geologic framework encompassing the BCT, LIP, and the GBB through biostratigraphic correlations and seismic stratigraphy integrated with well-log analysis and core data. The sequence stratigraphic framework developed for the study area provides enhanced predictability of storage zone geometry and reservoir properties across the region (Miller et al., 2013). An extensive data compilation and database development effort was first undertaken to support geocharacterization activities, and the three major subregions of interest were then selected for more detailed evaluation based on data availability and storage reservoir quality.

Data collection and database development conducted as part of the data management effort for this project are described in the Task 2 Final Data Collection Report provided in Attachment A.

2.1 Geologic Background

The mid-Atlantic U.S. passive continental margin contains thick (2- to 16-km) post-rift (upper Lower Jurassic and younger) sediments in the offshore basins, and thinner (0- to 2.4-km) uppermost Jurassic to Holocene sediment in the onshore coastal plain in the Salisbury Embayment (Grow and Sheridan, 1988). Rifting occurred during the Late Triassic to earliest Jurassic (i.e., 230 to 198 million years ago [Ma]) followed by extrusion of Early Jurassic seaward-dipping basalts. Seafloor spreading began prior to the Callovian (~165 Ma; Middle Jurassic) (Grow and Sheridan, 1988), with the likely opening beginning off Georgia circa [ca.] 200 Ma and progressing northward off the mid-Atlantic margin by ca. 180 Ma (Withjack et al., 1998). This south-to-north “zipper” onset of seafloor spreading is associated with a diachronous post-rift unconformity that separates active “rift-stage” deposits from more passive margin “drift-stage” deposits that accumulated in an ever-widening and deepening basin open to the ocean. Post-rift history was generally dominated by passive simple thermoflexural subsidence and loading (Steckler and Watts, 1982; Grow and Sheridan, 1988; Kominz et al., 1998; Kominz et al., 2002). Subsidence began offshore in the Early Jurassic and progressively moved onshore from the Late Jurassic to Early Cretaceous (ca. 150 to 125 Ma) as a thermoflexural response to increasing crustal rigidity (Watts, 1981; Grow and Sheridan, 1988; Olsson et al., 1988). The region has provided an excellent record of relative sea-level changes (Olsson et al., 1988; Miller et al., 2005), though glacial isostatic adjustments complicate the Pliocene and younger record (Peltier, 1998; Raymo et al., 2011), and deposition has been impacted by mantle-based dynamic topography changes (Moucha et al., 2008; Rowley et al., 2011).

The offshore basins contain a thick succession of Paleogene-to-Jurassic sedimentary rocks above crystalline basement that lies at depths of 5 to 15 km. The sedimentary rocks consist of layers of mudstone, shales, sandstone, carbonates, and evaporites that dip to the east-

southeast toward the continental slope (Libby-French, 1984). The sedimentary rocks overlie deeper rift basin strata, Early Jurassic flows and sills associated with the Central Atlantic Magmatic Province (CAMP), continental crust, and oceanic crust. Younger quaternary clay, siltstone, and sand overlie the Paleogene-Triassic sedimentary rocks, with ocean sediments present at the ocean floor. Local structures such as igneous intrusions, salt diapirs, growth faults, and escarpments are present in portions of the mid-Atlantic offshore study area.

Previous work indicates that Cretaceous and Jurassic-age sandstone formations in this region have porosities of 25% and permeabilities greater than 100 millidarcys (mD) (Amato and Bebout, 1980; Slater, et al. 2010). Case studies from the northern Newark basin (i.e., onshore New York Metropolitan area) suggest that storage mechanisms at this candidate CO_2 storage site may translate to analog Mesozoic rift basins offshore in the LIP (Post and Coleman, 2015). This suggests an extremely large capacity for potential storage of CO_2 in the mid-Atlantic offshore study area. Preliminary investigation of storage resource near a geologic structure known as the Great Stone Dome (GSD) in the northern BCT suggests that as much as 5.9 gigatons (Gt) of CO_2 could be stored and structurally trapped at this location. Further work was required to define the structural and stratigraphic framework of Cretaceous and Jurassic-age formations in the GBB, LIP, and BCT, and determine the regional extent of the potential storage zones and caprocks.

2.2 Data Compilation and Database Construction

The Project Team identified data sources and collected legacy well data, seismic survey data, geophysical well logs, core test data, biostratigraphic data, and previous literature/research papers on mid-Atlantic offshore geology. Much of the geologic information gathered for the Project was derived from the 44 deep exploratory wells and seismic surveys completed during the 1970s and 1980s. Lack of hydrocarbon resources and restrictions on offshore exploration have since limited acquisition of additional, newer subsurface data.

The Project Team worked collaboratively to build and maintain six main databases to store, manage, analyze, and share/distribute information compiled and generated as part of the Project: (1) Box, (2) ArcGIS online (AGOL), (3) Petra®, (4) IHS Kingdom®, (5) Petrel®, and (6) Microsoft Access. A significant effort was made to create electronic versions of paper logs, well reports, and core laboratory reports, as the data quality and format varied widely. Well logs, for example, were available as paper logs, raster images, and/or Log ASCII Standard (LAS) files, and it was necessary to convert all well-log data into the LAS format. In addition, the physical samples located at the Delaware Geological Survey (DGS) required inventorying as well as sample preservation conducted as part of Task 4 (Section 4). Well reports were compiled to provide information acquired on geologic formations, geotechnical rock properties, geologic structures, and petrophysical properties for Task 2 (Sections 2.3 – 2.6), Task 5 (Section 5), and Task 6 (Section 6). A subset of the seismic data was selected for reprocessing as part of Task 3 to enhance resolution in target areas and to assist the correlation of rock layers in areas with no deep wells (Section 3).

2.3 Georges Bank Basin

The geologic characterization of the GBB was conducted primarily by two Rutgers University students, Stephen Graham and Alex Adams. Their work has resulted in two end products in the form of Master's theses: *Georges Bank Basin stratigraphy: Cretaceous gamma log sequences correlated with seismic data* (Graham, 2018), and *Seismic stratigraphy of the Georges Bank*

Basin: implications for carbon sequestration (Adams, 2019). A summary of their work is presented in the following subsections.

2.3.1 Background

The elongate, asymmetric GBB, located approximately 150 km southeast (SE) of Cape Cod, MA, encompasses an area of approximately 70,000 km^2. The basin contains 6-10 km of accumulated post-rift sediments, and has an average water depth of 80 m. The GBB is a collection of smaller Triassic rift basins formed during the breakup of Pangea. The basement is made up of Paleozoic and older block-faulted crystalline rocks, which are overlain by various terrestrial sandstones and marine shelf dolomites. The Jurassic Western Bank Group (i.e., Abenaki, Mohawk, and Mic-Mac Formations) contributed to the prograding Middle Jurassic carbonate platform, interfingered with and overlain by siliciclastics above. The largely siliciclastic Lower Cretaceous to lower Upper Cretaceous Nova Scotia Group is made up of the Missisauga, the Naskapi Shale, the Logan Canyon (LC), and the Dawson Canyon formations. The Mohawk, Missisauga, and LC formations were evaluated as potential storage zones, with the Dawson Canyon and Naskapi shale evaluated as potential caprocks.

2.3.2 Methods

Two-dimensional (2D) multichannel seismic (MCS) profiles and industry drilling data provide a baseline for evaluation of the GBB. In the 1970s, the USGS collected 6,400 km of MCS reflection data over 32 tracklines across the offshore Massachusetts to offshore Maryland region. USGS reconnaissance seismic data were reprocessed in 2016 by Canada-based Absolute Imaging (AI) Inc.. Imaging was greatly improved by velocity modeling, data migration, and noise and spike suppression, among other modern reprocessing steps. In addition, seismic data originally collected for exploratory purposes was recently released by the Bureau of Ocean Energy Management (BOEM)/USGS as a part of the National Archive of Marine Seismic Surveys (NAMSS) (Triezenberg et al., 2016). MCS reflection profiles from six seismic surveys in the NAMSS database were used in this study. The six surveys recorded a total of 45,000 km of data over 759 tracklines along the entire United States margin. Ten exploratory wells drilled in the eastern subregion of the GBB between 1976 and 1982 provide wireline log data to investigate the storage potential of two Middle Cretaceous sand units: the LC and the Missisauga Formation.

By means of Petrel ver. 2017 (i.e., an advanced MCS and well-log analysis software package produced by Schlumberger), Graham (2018) utilized gamma ray (GR) logs reinforced with neutron porosity logs, density porosity logs, and previously published permeability and porosity data to correlate stratigraphic signatures across 10 exploratory wells drilled in the eastern GBB. To determine general lithologies, trends in GR logs were examined for high or low readings, inferred to represent mud/shale-rich or sand-prone units, respectively. Using “back to basics” technique of sequence stratigraphy (Miller et al., 2018; identifying coarsening- and fining-upward packages and stratal stacking patterns), well-log sequence boundaries were delineated and depositional sequences within the LC Formation and Missisauga Formation were identified. Eastern GBB well-log sequences were correlated to major seismic reflectors, originally identified in the BCT.

Interpretations of MCS profiles within the western GBB were guided by the interpreted eastern well-log seismic stratigraphy. Significant seismic reflectors identified in the eastern GBB were traced into the western GBB with the guidance of intersecting seismic profiles. Due to the lack of wells in the western GBB, the interpretation of the seismic reflectors on the profiles were based

strictly on internal reflection geometry and subsequent reflection terminations. The ages assigned to the reflectors are based generally on the well-log-seismic stratigraphic results in the eastern GBB.

2.3.3 Results

In all, seven depositional sequences (i.e., oldest to youngest: MS3, MS2, MS1, LC3, LC2, LC1, DCx,) were identified in the eastern GBB well logs (Figure 2-1, Table 2-1). The sequences can be mostly correlated with seven distinct seismic reflectors (i.e., UJ1, LK2, LK1, MK3, MK2, MK1, UK2GB [upper bounding surface]) that are identified across the entirety of the GBB (Figure 2-2). The LC Formation is comprised of three depositional sequences: the LC3, LC2, LC1, (correlating with basal seismic reflectors: LK1, MK3, MK2, respectively) from oldest to youngest. The Missisauga Formation is comprised of three depositional sequences: the MS3, MS2, M1, oldest to youngest, that are bound by the basal seismic reflector LK2 and reflector LK1 at the top of the sequence. Using the techniques of sequence stratigraphy, the top of the LC Sandstone (LC1 sequence bound by basal reflector MK2 and upper reflector MK1) is mapped shallower in the eastern GBB than in previous interpretations; approximately 55% of the LC1/MK2 sequence is deeper than the minimum depth required to maintain the supercritical form of CO_2 (>800 m). The top of the Missisauga Formation (MS1 [upper reflector LK1]) in the EGBB is mapped at depths (>1,000 meters below sea floor [mbsf]). The LC and Missisauga Formations are loosely mapped at depths below 800 mbsf everywhere in the WGBB. The observation of prograding clinoforms within the thick, deep, sandy LC2 and LC1 depositional sequences along the southeastern margin of the WGBB (Figure 2-3) indicate a potential target for storage.

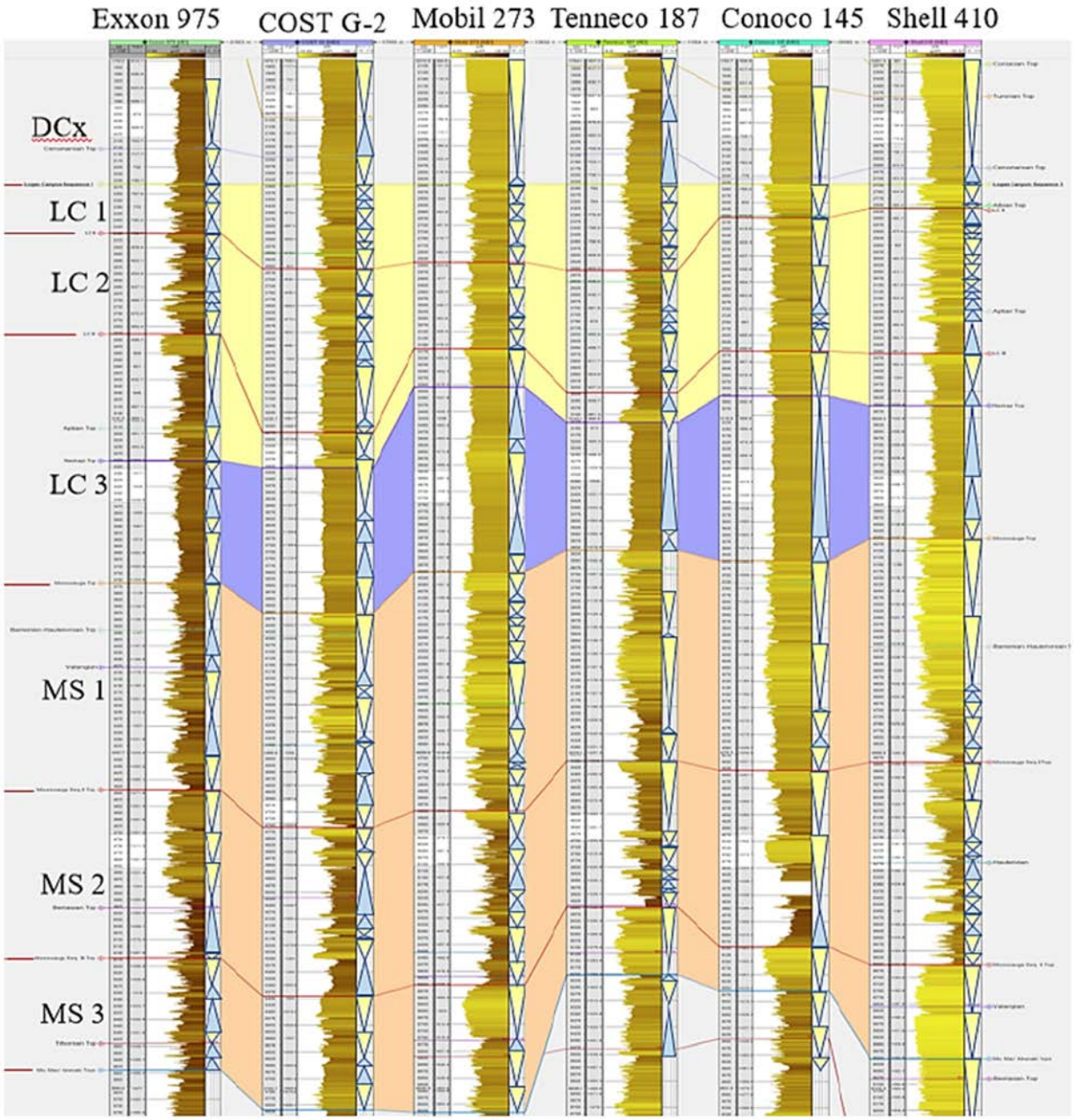

Figure 2-1. Gamma Log cross section from northeast to southwest (left to right) showing seven depositional sequences identified in the eastern GBB.

Note: Cross section from Graham (2018). Both measured depth in feet and two-way time (TWT) in milliseconds (ms), are shown for each log. Well logs are hung from the youngest LC sequence (i.e., LC1). Sequences boundaries are denoted in red, yellow-shaded hues (i.e., low gamma values) correlate to sand lithology, brown-shaded hues (i.e., high values) correlate with muds or shales. Exxon 133 and Exxon 975 wells were integrated with seismic line USGS 12 to create well-seismic ties and allow loop correlation closure between the EGBB and WGBB seismic grids. (From Adams, 2019).

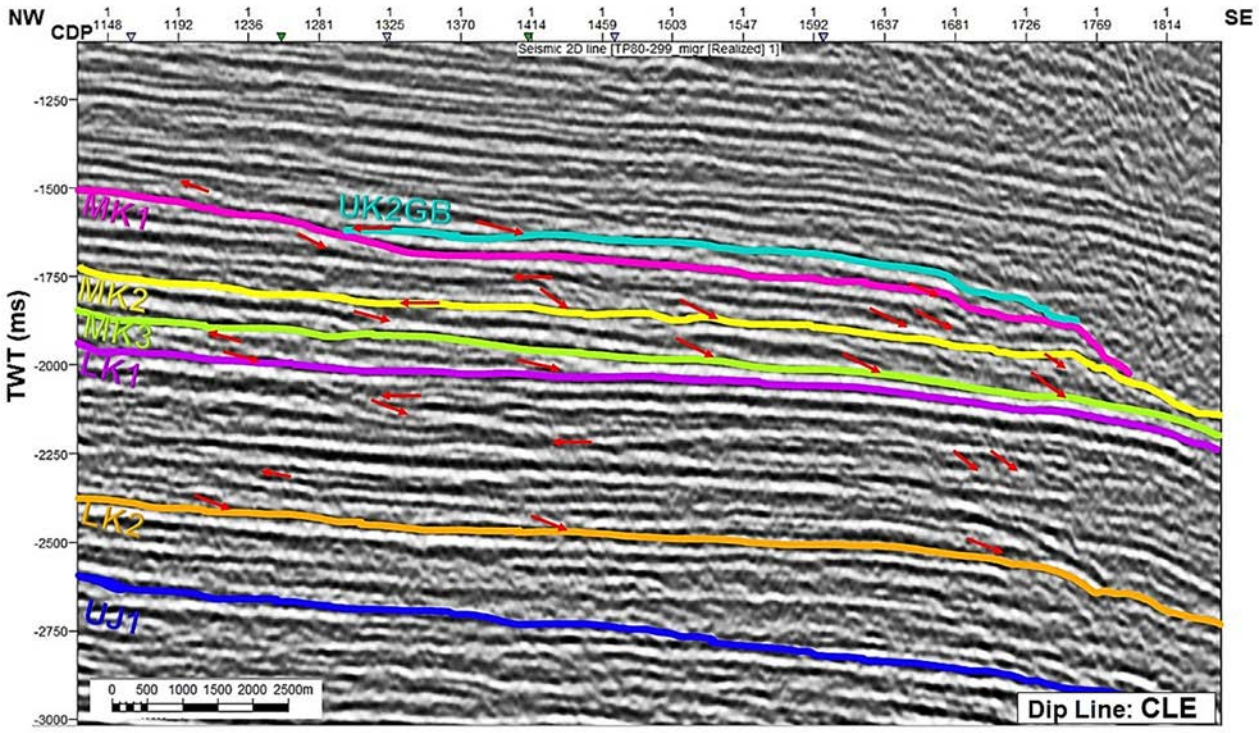

Figure 2-2. 2D along-dip MCS profile CLE (TP80-299) from survey B-04-80 interpreted for reflection terminations.

Note: Interpretations include onlap surfaces, downlap surfaces, toplaps, and truncations (indicated by red arrows), and seismic reflectors. Seismic reflectors mapped (oldest to youngest) include: UJ1 (in blue) seismic horizon represents the basal surface of the JU1 depositional sequence (Mic-Mac); LK2 (orange) seismic horizon represents basal surface of Missisauga depositional sequence (MS1); LK1 (purple) seismic horizon represents basal surface of LC3 depositional sequence/top Miss; MK3 (green) seismic horizon represents basal surface of LC2 depositional sequence/top LC3; MK2 (yellow) seismic horizon represents basal surface of LC1 depositional sequence/top LC2; MK1 (pink) seismic horizon represents basal surface of DCx depositional sequence/top LC1. Capping surface UK2GB is in teal. Cross section is in northwest (NW) to southeast (SE) direction. XY scale is 1:62500, and vertical exaggeration is 5. Common depth point numbers are above seismic line on the X-axis, vertical axis is in TWT (1,250-3,000 ms). This is a primary dip line in recognizing higher order sequences in the southeastern subarea of the western GBB.

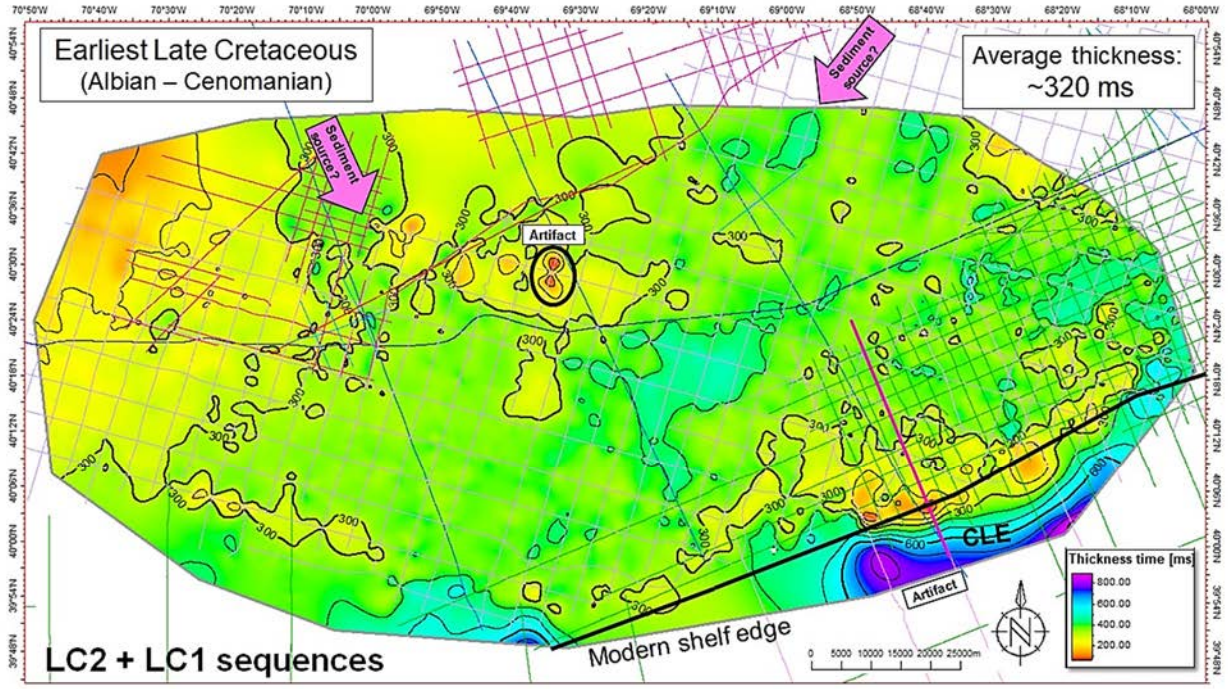

Figure 2-3. Isopleth (~isopach) map of the LK1 package. Scale is 1:705044 m.

Note: Thickness was calculated in Petrel by using the LK1 as the basal surface of the package and seismic surface MK3 as the upper boundary. Contour interval is 100 ms. Minimum thicknesses are represented by red, increasing from yellow to green to blue, with purple as maximum thicknesses. Thicknesses range from 25 to 620 ms, averaging ~150 ms. The black line indicates the modern shelf-slope break; all data southeast of the line was potentially inaccurately interpolated by Petrel (details in the contour lines are likely artifacts) and not considered for carbon storage. Pink arrows represent the possible direction of sediment supply sources.

2.4 Long Island Platform

The two basins evaluated in this project, the BCT and GBB, are separated by a structural high, the LIP. It contains a much thinner post-rift sedimentary record (2-5 km thick) than the thick post-rift sections of the BCT (>15 km) and GBB (>7 km) (Klitgord et al., 1988). Because the mid-Cretaceous reservoir sands found in the eastern GBB occur at above supercritical depths (>800 m), studies of the LIP focused on two aspects: (1) identification and evaluation of rift basins buried beneath the LIP (Fortin, 2018); and (2) interregional correlations between the GBB and BCT across the LIP conducted in collaboration with G. Lang (Ph.D. studies at Haifa University) and U. ten Brink (at USGS).

Lack of deep boreholes at the LIP does not allow in situ stratigraphic investigation of the sedimentary section. Instead, the stratigraphy presented here relies on seismic correlations between the two adjacent basins: GBB and BCT, where borehole control is available (Figure 2-4 [USGS line 12]). The thin (i.e., 2-5 km) sediment cover at the LIP is composed of numerous unconformities. Some seismic horizons onlap on deeper or are truncated by shallower horizons. This makes their distribution along the LIP, limited or absent. For example, the LK1 horizon onlaps on the LK2 at the western and eastern edges of the platform and could only be traced at the southeasternmost part of the platform (Figure 2-4 [USGS line 12]). Thus, only three seismic boundaries were correlated successfully across the LIP: LK2, MK1 and UK1. In addition, the sediment cover thins landward (that is toward the north northwest), making the correlation more

difficult at these areas. The reprocessed USGS line 12 had a significant role in the across-platform correlation as it connects the GBB and BCT along the LIP OCS.

As the mapped horizons mark unconformities, analysis of seismic facies and reflector terminations provides constrains for their seismic interpretation. The LK2 delineates a low continuity, low amplitude Jurassic strata below from higher continuity Cretaceous reflectors above (Figure 2-4 [USGS line 12], Figure 2-5 [USGS line 23]). While deeper reflectors toplap the LK2 toward the platform, shallower reflectors onlap it. The lower to middle Cretaceous unit (LK2 to MK1) has a high continuity, high-amplitude seismic facies under the LIP shelf. The LK1 and LK2 comprise its base at the outer shelf while under the inner shelf onlaps syn-rift and basement rocks (i.e., bounded by the post-rift unconformity, Klitgord et al., 1988). It is unconformably topped by the MK1, which truncates some of its higher reflectors. The Upper Cretaceous is the thickest interval mapped along the LIP (Figure 2-5 [USGS line 23]). It reaches up to ~900 ms at the upper continental slope and thins gradually landward where it is truncated by younger tertiary unconformities. Its lower part has relatively high amplitudes and low continuity seismic facies, while its upper part is more continuous and has moderate seismic amplitudes. The UK1 seismic boundary constitutes the top of this interval. It is a noticeable unconformity that truncates Cretaceous reflectors and is both onlapped and toplapped by tertiary strata. Following the seismic facies and stratigraphic relationships describe above, the LK2, MK1, and UK1 seismic horizons were mapped across the LIP and interpolated to form TWT structural maps (Figure 2-6; Figure 2-7; Figure 2-8, respectively).

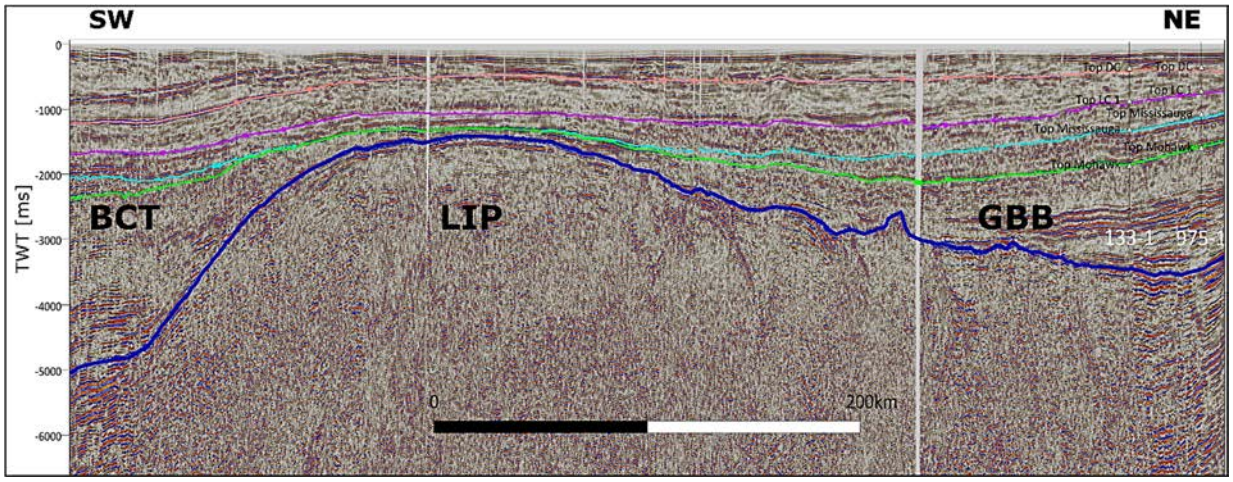

Figure 2-4. Interpreted 2D along-strike reprocessed MCS profile USGS 12.

Note: Seismic reflectors mapped (oldest to youngest) include: PRU (dark blue), LK2 (green), LK1 (light blue), MK1 (pink), and UK1 (orange). Two wells (133-1 and 975-1) located at the GBB and their stratigraphic information are projected on to the section. Cross section is in NE to SW direction. Vertical axis is in TWT (0-6,500 ms). This is a primary strike line in correlating seismic horizons across the LIP.

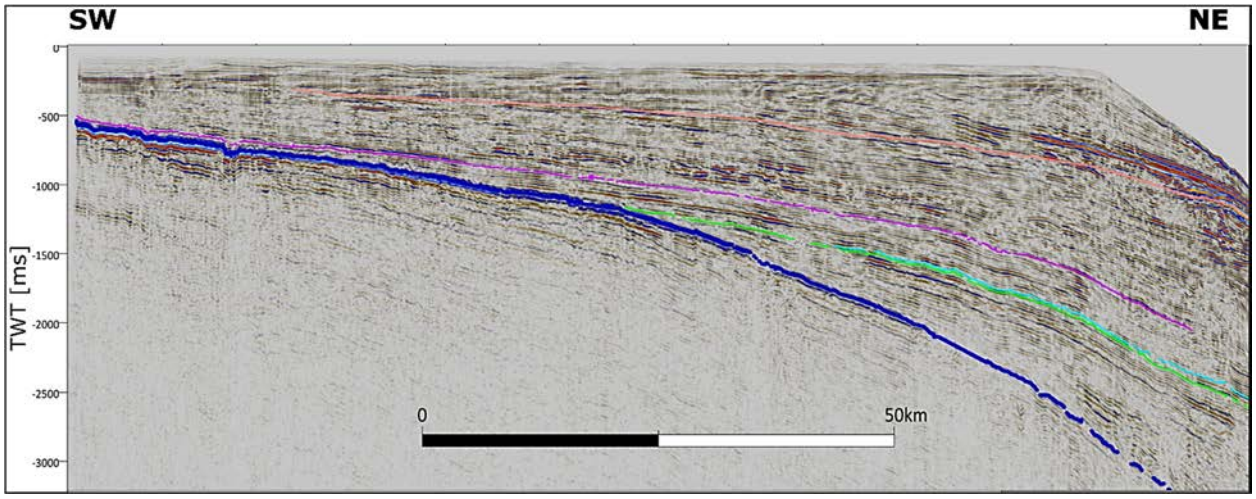

Figure 2-5. Interpreted 2D along-dip reprocessed MCS profile USGS 23.

Note: Seismic reflectors mapped (oldest to youngest) include PRU (dark blue), LK2 (green), LK1 (light blue), MK1 (pink) and UK1 (orange). Cross section is in NW to SE direction. Vertical axis is in TWT (0-3,200 ms).

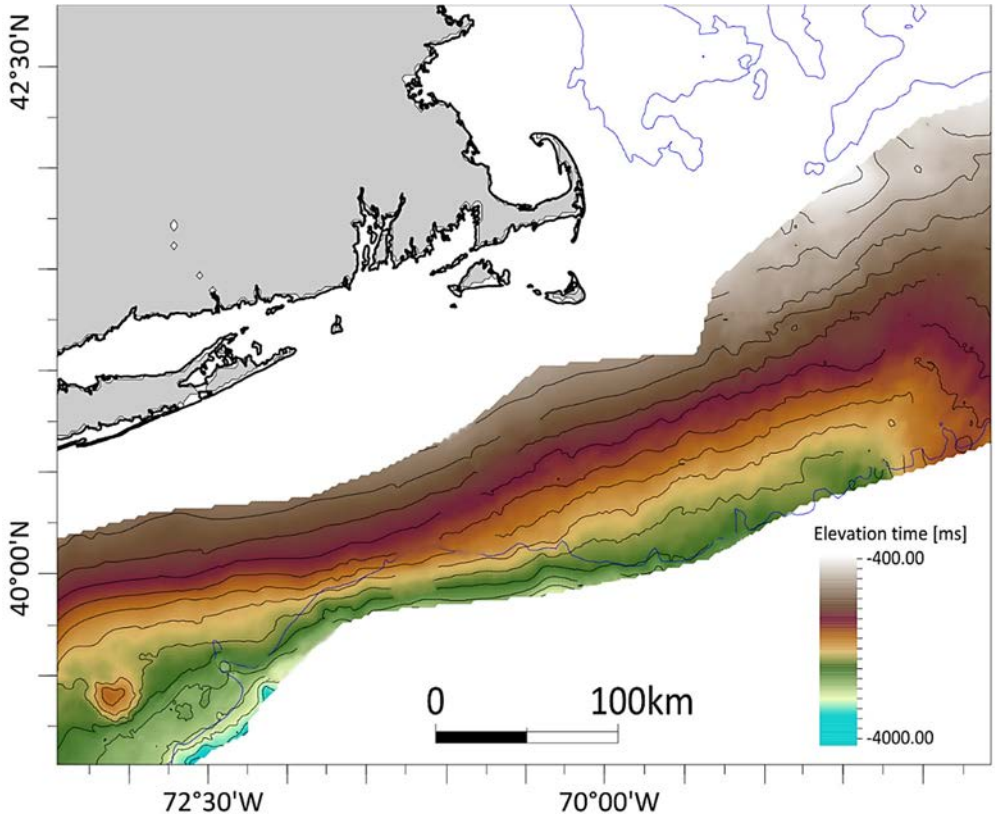

Figure 2-6. TWT structural map of the LK2 seismic horizon across the western GBB, LIP and northern BCT.

Note: Minimum TWT values are in white increasing from brown to green, with blue as maximum TWT. TWT values ranges from -400 at the northeastern GBB to -4000 at the seaward edge of the BCT. The black line indicates the modern coastline..

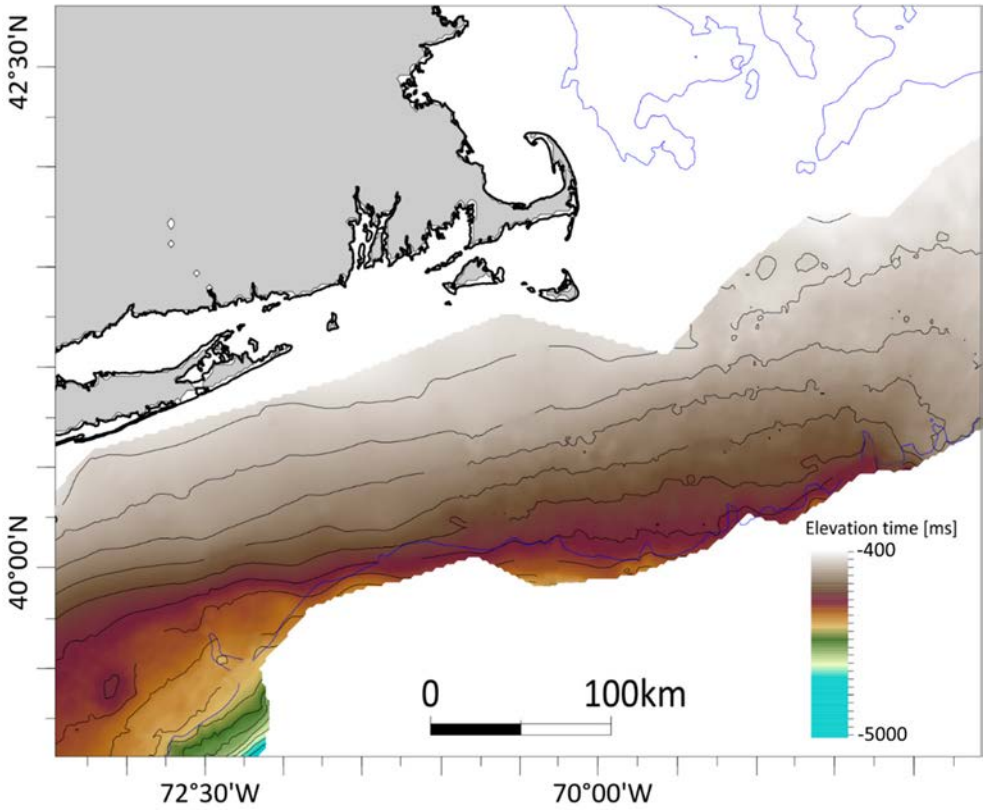

Figure 2-7. TWT structural map of the MK1 seismic horizon across the western GBB, LIP and northern BCT.

Note: Minimum TWT values are in white increasing from brown to green, with blue as maximum TWT. TWT values ranges from -500 at the northeastern GBB to -5000 at the seaward edge of the BCT. The black line indicates the modern coastline.

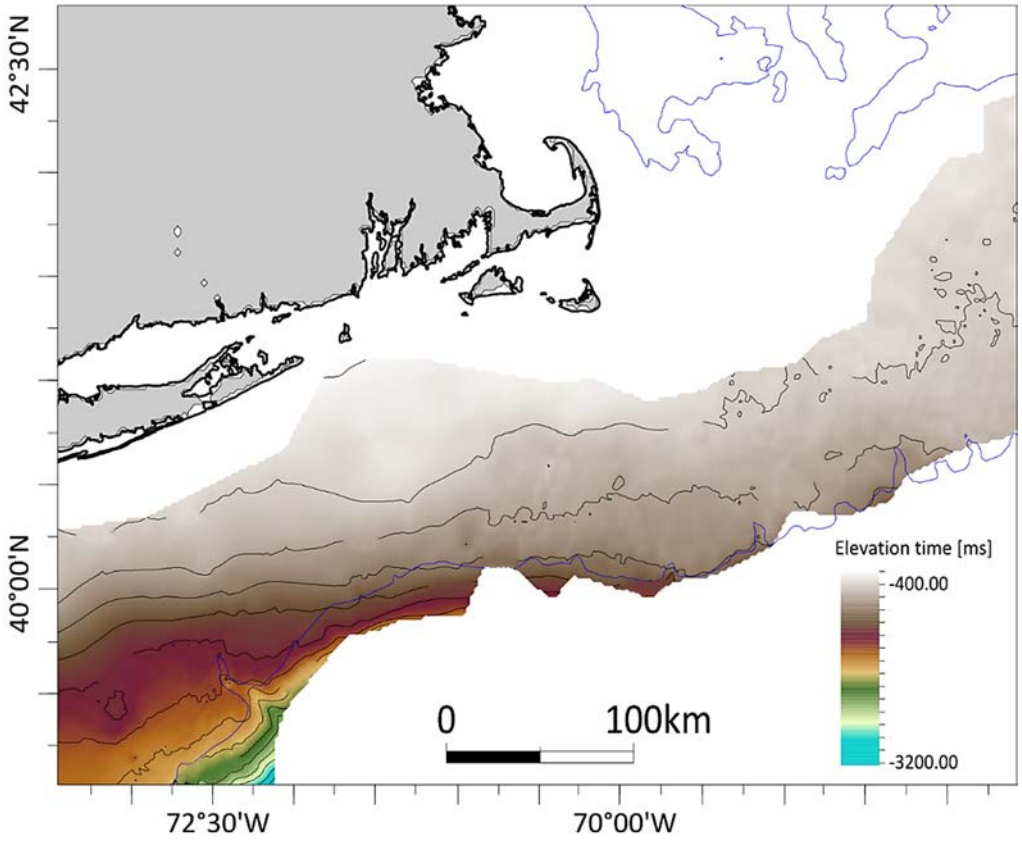

Figure 2-8. TWT structural map of the UK1 seismic horizon across the western GBB, LIP and northern BCT.

Note: Minimum TWT values are in white increasing from brown to green, with blue as maximum TWT. TWT values ranges from -200 at the northeastern GBB to -3200 at the seaward edge of the BCT. The black line indicates the modern coastline.

2.5 Baltimore Canyon Trough

Geological characterization of the BCT was initially conducted by Lombardi (2017) and resulted in the publication *Back to basics of sequence stratigraphy: early Miocene and mid-Cretaceous examples from the New Jersey paleoshelf* (Miller et al., 2018). Additional detailed studies of the southern and northern BCT expanded previous results to assess carbon storage potential across the entire offshore mid-Atlantic, resulting in one accepted and one in review publication: *Onshore-offshore correlations of Cretaceous fluvial-deltaic sequences, southern Baltimore Canyon Trough* (Schmelz et al., 2019) and *Cretaceous sequence stratigraphy of the northern Baltimore Canyon Trough: Implications for tectonic, paleogeographic, and sea-level evolution* (Baldwin et al., in review). In addition, funding from MAOCSRAP supported the completion of Leslie Jordan's Master's thesis (2019): *Quantitative biostratigraphic analysis of middle Cretaceous sequences in the Baltimore Canyon Trough, offshore mid-Atlantic U.S. Margin*. All completed work is summarized below.

2.5.1 Background

The uppermost Jurassic and Cretaceous sedimentation within the BCT began approximately 50 Ma after the CAMP. The presence of post-rift Lower Jurassic strata is uncertain (cf., Klitgord

et al., 1988; Manspeizer and Cousminer, 1988), and due to the location of deep-penetration wells, there are few samples of Middle to lower Upper Jurassic strata. An initial post-rift period of evaporite precipitation in the embryo of the present-day Atlantic Ocean was followed by a carbonate shelf regime with a fringing progradational reef that was subsequently buried in the mid-Cretaceous by siliciclastic deposition (Jansa, 1981). For the majority of the BCT, the reef was buried in the Barremian when sediments overtopped the reef structure and were deposited on top of the Neocomian (i.e., Hauterivian, Valanginian, and Berriasian) deep sea reflector β identified beneath the modern continental rise (Mountain and Tucholke, 1985). The carbonate platform was generally progradational (Poag and Valentine, 1988), with continentally sourced siliciclastics locally interfingering with the Upper Jurassic and Lower Cretaceous carbonates (Poag, 1985). Proximally, the subsurface Neocomian sediments of the New Jersey Coastal Plain record the fluvial deposition of the Waste Gate Formation in Maryland and southern New Jersey (Doyle, 1982; Hansen, 1982; Miller et al., 2017). Under the modern shelf, the heterolithic Valanginian to Barremian interval contains facies equivalent to the Missisauga Formation of the Scotian shelf (Libby-French, 1984; Table 2-1). The siliciclastic sediments that eventually buried the carbonate platform are coarser than the finer mid- to Upper Cretaceous sediments they were buried by (Poag and Valentine, 1988), the upward fining succession reflects an increase in base-level that began in the mid-Cretaceous.

The mid-Cretaceous sandstones of the BCT, described as the lithological equivalent to the LC Formation of the Scotian shelf (Libby-French, 1984; Poag, 1985), were deposited following the mixed siliciclastic-carbonates of the Barremian to Neocomian Missisauga Formation equivalent (Libby-French, 1984; Poag, 1985; Table 2-1). The sandstones were originally partitioned into an upper and lower LC Sandstone by Libby-French (1984). These two sands were thought to be separated by a fine-grained unit called the Sable Shale. Closer examination of the lithological transitions and biostratigraphy in the northern BCT led Miller et al. (2018) to conclude that the LC was actually comprised of three distinct depositional sequences. The LC3 (oldest), LC2, and LC1 (youngest) sequences, each possess: (1) lower regressive, lowstand systems tract (LST) interbedded silts and sands; (2) transgressive systems tract (TST) silts; and (3) upper regressive, highstand systems tract (HST) sands. The revised stratigraphic packaging presents a more detailed portrayal of the sand-prone units in the regressive LST and HSTs and offers a predictive framework for reservoir sand and confining shale prone capstone units associated with the major flooding surfaces. These three depositional sequences are best observed in the northern BCT on a well-log transect between the GSD and the OCS (Miller et al., 2018). In this location, they were apparently deposited within estuarine, delta front, and prodelta paleoenvironments (Miller et al., 2018) that follow a first-order deepening upsection. These offshore sands are coeval with the predominantly terrestrial/nonmarine Potomac Formation sequences of the mid-Atlantic Coastal Plain (Table 2-1; Miller et al., 2004; Browning et al., 2008; Miller et al., 2017; Miller et al., 2018).

The Upper Cretaceous of the BCT is characterized by a number of transgressive-regressive cycles that have been subdivided into depositional sequences on the mid-Atlantic Coastal Plain, where sedimentation was predominantly deltaic, with some terrestrial and non-deltaic marine sedimentation during major sea-level lowstands and highstands, respectively (Miller et al., 2004; Browning et al., 2008). Offshore, the section is largely comprised of the shaly Dawson Canyon equivalent (Table 2-1; Libby-French, 1984). A single regionally persistent sandstone unit, the Middle Sandstone, was identified by Libby-French (1984) that ranges from Coniacian to Campanian in age, according to biostratigraphic reports associated with wells drilled on the OCS (Seker, 2012). It may be coeval with any of several onshore sand units, from the Coniacian Magothy to the Campanian Mount Laurel Formation of the New Jersey Coastal Plain. The highest Late Cretaceous global sea levels occur close to the Cenomanian/Turonian

boundary (Miller et al., 2005; Haq, 2014), producing the prodelta and shelfal sediments of the onshore Raritan and Bass River Formations (Browning et al., 2008) that caps the underlying, sand-prone fluvial sediments of the Potomac Formation. This onshore interval of Raritan and Bass River Formation shales corresponds to the Dawson Canyon Formation offshore, similarly, capping the deltaic sands of the LC sequences identified by Miller et al. (2018). Additionally, Maastrichtian strata are deposited during a second long-term rise in sea level that ultimately culminates with a regional sea-level peak in the Eocene (Miller et al., 2005). The strata deposited during this base-level increase also comprise a major confining unit both onshore (the Composite Confining Unit of Zapecza, 1989) and offshore (Table 2-1).

Table 2-1. Correlation of the variety of names used to identify the Cretaceous strata of the BCT and GBB.

Seismic boundary	Well log sequence	Lithologic Units (Libby-French, 1984)	Onshore equivalent	Age/stage	Reservoir characteristics
UK1	?	Dawson Canyon Shale	Navesink	Maastrichtian	Equivalent of onshore Composite Confining Unit (CCU)
UK2	?	Middle Sandstone?	Magothy?	upper Turonian?	?
MK1	DCx	Dawson Canyon Shale & Middle Sandstone	Marshal. to Bass R.*	Cenomanian-Campanian	Middle Sandstone too shallow (for CO^2) and thin in SBCT?
MK2	LC1	Upper Logan Canyon Sandstone & Sable Shale	Potomac III	lower Cenomanian	HST sandstone reservoir shales into basin
MK2.1	LC2	Upper Logan Canyon Sandstone & Sable & Naskapi Shales	Potomac II	Albian	High porosity & permeability(?) in HST sandstone reservoir
MK3	LC3	Lower Logan Canyon Sandstone & Naskapi Shale	Potomac I	Aptian	High porosity & permeability(?) in HST sandstone reservoir
LK1	Miss.	Naskapi Shale & Missisauga Sandstone	Wastegate	Berriasian-Barremian	Heterolithic reservoirs
LK2	?	Mic Mac, Mohawk, and older units	unnamed	Upper Jurassic	?

Note: Abbreviations: Bass R. = Bass River; DC = Dawson Canyon; HST = highstand systems tract; LC = Logan Canyon; LK = Lower Cretaceous; Marshal. = Marshaltown; Miss. = Missisauga; MK = mid-Cretaceous; SBCT = southern Baltimore Canyon Trough; UK = Upper Cretaceous. From Schemlz et al., 2019.

2.5.2 Methods

2.5.2.1 Offshore Biostratigraphy

By creating a composite standard biostratigraphic section of the BCT, the position of sequence boundaries was constrained, and ages were assigned to sequences and unconformities originally proposed in Miller et al. (2018). Biostratigraphic packages that correspond to each of the major sequences were defined by chronostratigraphically significant taxa identified through the use of this quantitative method.

The Dawson Canyon sequence has been assigned an age of late Cenomanian due to the consistent occurrence of Rotalipora cushmani and R. greenhornensis (Figure 2-9). These planktonic foraminifera also helped constrain the depth at which OAE2 black shales were deposited in an interval that is composed of relatively homogenous shales. The LC1 sequence is defined by its lack of identifying taxa, with wells such as COST B2 subject to reworking in this interval. The LC2 and LC3 sequences both have facies shifts that can be identified by changes in the biostratigraphy. HST in LC2 are characterized by nannofossils and foraminifera, particularly Podorhabdus albianus, Braarudosphaera africana, Planomalina buxtorfi, and Biticinella breggiensis (Figure 2-9). The shift from palynomorphs Spinidinium vestitum, Concavissimisporites punctatus, and Rugubivesiculites rugosus is evidence for a TST. The LC2 sequence has been assigned an age of middle to late Albian based on these taxa. A similar shift in facies is seen in the LC3 sequence, where the nannofossils Nannoconus globulus and Cyclagelosphaera margereli are present in the HST facies, and the absence of biostratigraphic markers in the lower part of the sequence indicate a TST (Figure 2-9). This sequence is early Aptian. Lastly, dinoflagellates Muderongia simplex, Aptea anaphrissa, and Pseudoceratium pelliferum define the nonmarine facies in the Missisauga sequence and has been assigned an age of early Aptian to Barremian (Figure 2-9).

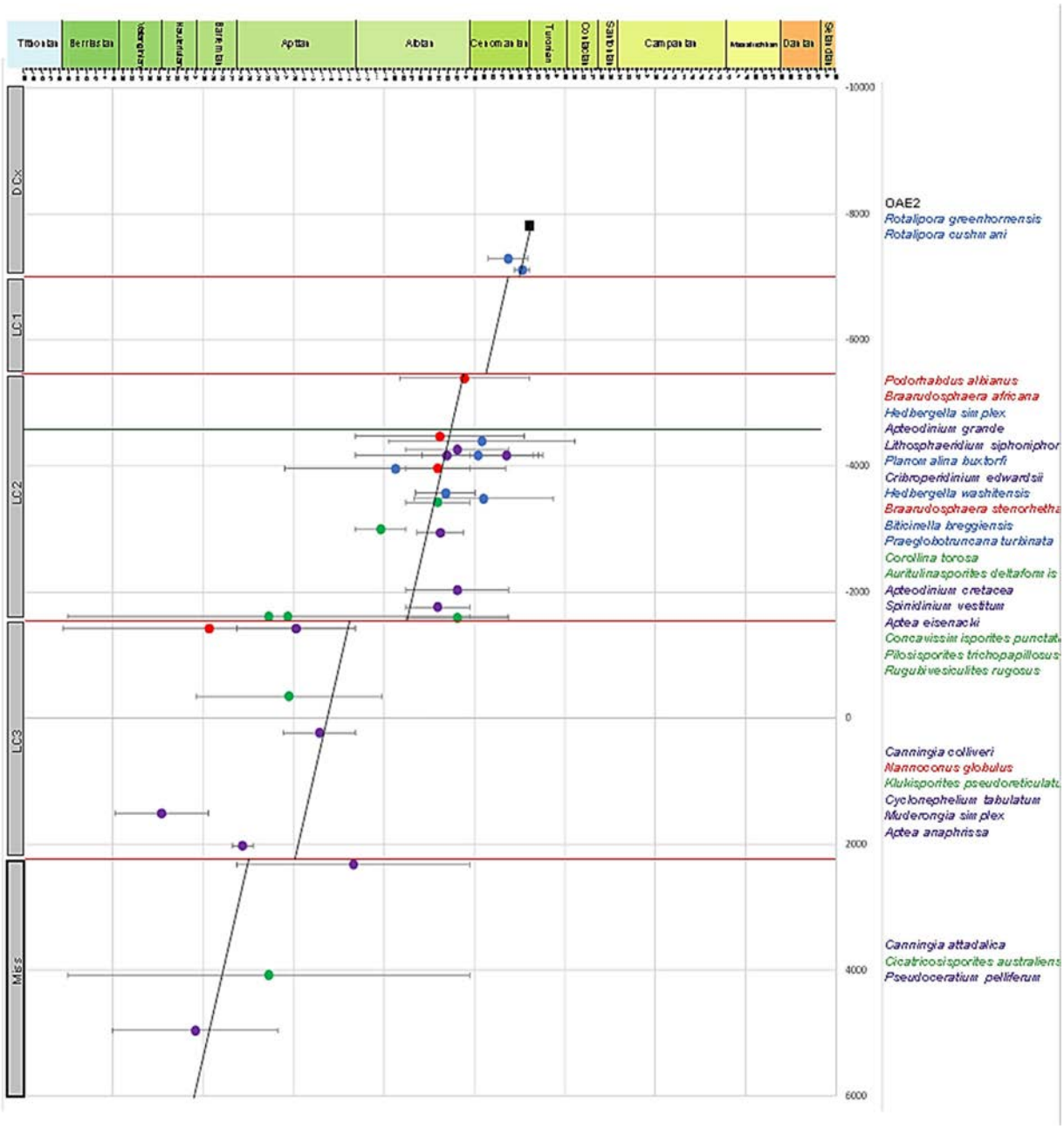

Figure 2-9. Age depth plot using the First Appearance Datum (FAD) determined by the graphic correlation analysis.

Note: Higher resolution version is provided as an attachment in Attachment B. Depths are in composite standard units (feet below kelly bushing). Biostratigraphic events were selected if they were on or near the line of correlation (LOC). Sequence boundaries are plotted in red, with the LOC shown in black. (From Jordan, 2019)

2.5.2.2 Well-Log and Core Analysis

Stratigraphic sequences were interpreted from GR log stacking patterns and guided by biostratigraphy for 29 out of 34 exploration wells drilled in the BCT from 1978 to 1984 (Figure 2-10), in addition to 3 wells (i.e., Maryland Esso 1, Mobil Bethards, and Ohio Oil Hammond) drilled onshore on the Maryland Coastal Plain. Sequences in five of the offshore wells were not assigned for several reasons, including: (1) lack of GR or spontaneous potential (SP) logs; (2)

lack of GR or SP logs associated with the target sequence depths; or (3) the well is located on the modern slope in an environment where carbonate deposition and down-slope processes have been dominant, thus, complicating the correlation of well, log, and seismic information.

The procedure for identification of systems tracts and surfaces in wells was modeled after the sequence stratigraphic analysis of the COST B-2 “Rosetta Stone” used by Miller et al. (2018). COST B-2 is referred to as the “Rosetta Stone” because it is well studied and contains geophysical log and core data that overlap within the middle Cretaceous sequences of this study, thus making it possible to ground-truth sequence stratigraphic interpretations with lithology and sedimentary structures observed in the core. All surfaces and systems tracts were derived objectively in each well by coarsening and fining upward patterns in geophysical well logs (Miller et al., 2018). Sequences generally follow a repetitive transgressive-regressive pattern that define three packages: the LST, the TST, and the HST (Figure 2-11a, b).

Sequence boundaries were placed at the top of the HST, following Miller et al. (2018). In most wells, this was located at the top of a blocky sand that capped a series of genetically related coarsening upward parasequences (Figure 2-11a,b). The contact between the HST below and LST above, at which the sequence boundary was placed, was generally sharp and regionally traceable on wells. In addition, biostratigraphy guided sequence stratigraphic interpretations, and was used to maintain a consistent age within each sequence and across wells. A lack of clear coarsening and fining upward parasequences within the LC1 sequence of some wells (i.e., Figure 2-11b) made placing the DCx sequence boundary difficult. In wells where this was the case, biostratigraphy and seismic stratigraphy was heavily relied upon.

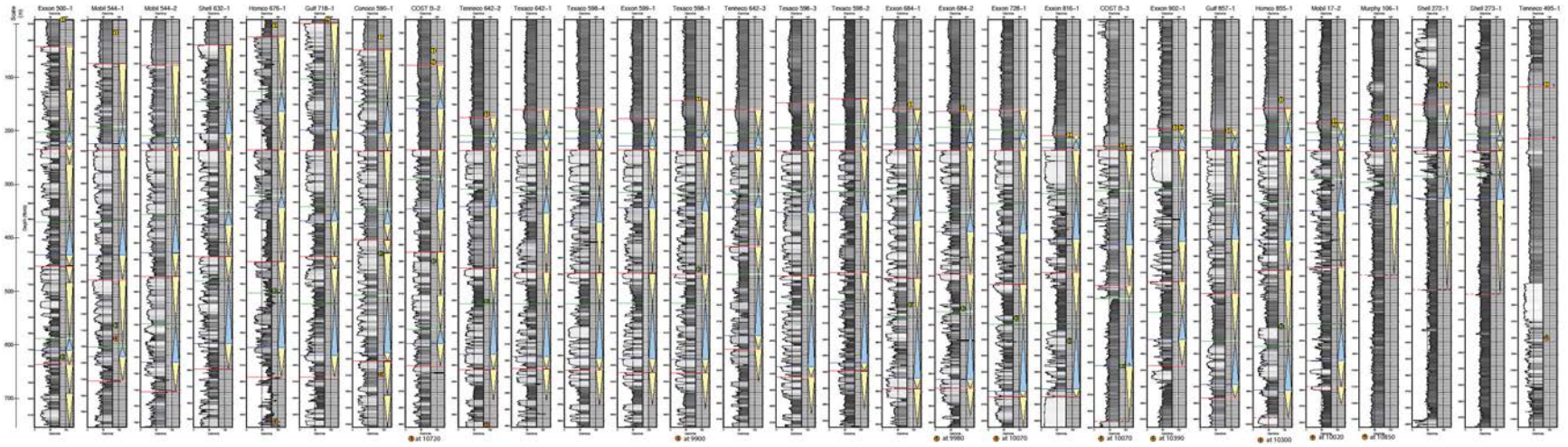

Figure 2-10. Well-log interpretation compilation for 29 of the 34 deep-penetrating wells in the BCT.

Note: Higher resolution version is provided as an attachment in Attachment C. GR log data is shaded so that the lowest values are white (assuming low GR=quartz sand) and the highest values are black (assuming high GR=mud/shale), to indicate the assumed lithology and aid in the visualization of stacking patterns (Miller et al., 2018). Circles indicating biostratigraphic analyses are color coded by approximate age (yellow=Cenomanian; green=Aptian, orange=Barremian) and numbered by species (1 = Rotalipora cushmani; 2 = R. greenhornensis; 3 = Cyclonephelium tabulatum; 4 = Muderongia simplex). Sequence boundaries derived from well-log stacking patterns are represented by red lines. Dashed red lines represent well-log sequence boundaries that are uncertain. Triangles next to the GR log show coarsening (yellow) and fining (blue) upward patterns. Blue lines indicate a transgressive surface; green lines indicate a maximum flooding surface. Units are logging units (feet below kelly bushing), but a scale is given in m. From Baldwin et al., (in review).

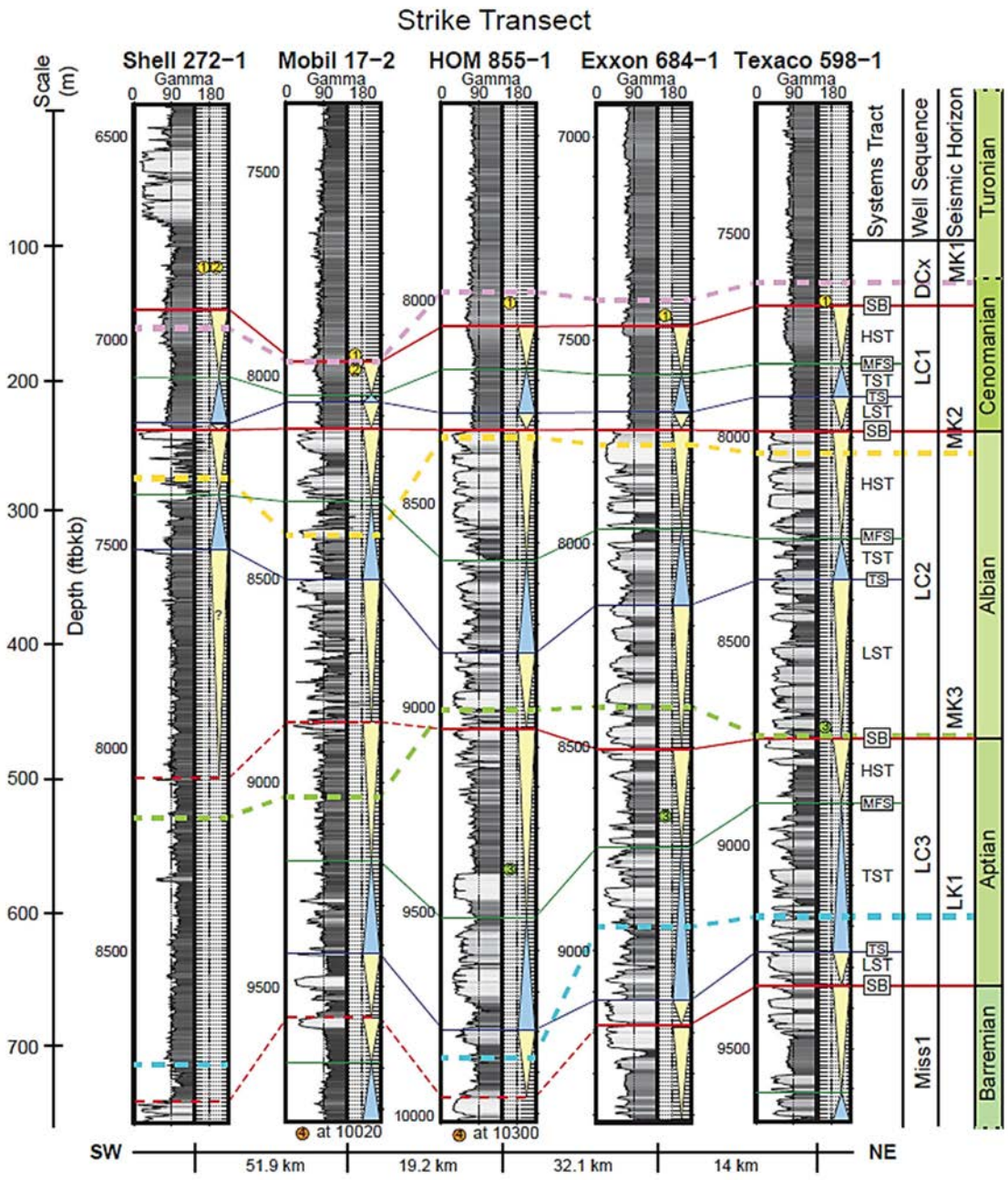

Figure 2-11a. Well-log transect across the Northern BCT OCS in the SW-NE strike direction (location map: inset of Figure 2-1).

Note: GR log data is shaded so that the lowest values are white (assuming low GR=quartz sand) and the highest values are black (assuming high GR=mud/shale), to indicate the assumed lithology and aid in the visualization of stacking patterns (Miller et al., 2018). Circles indicating biostratigraphic analyses are color coded by approximate age (yellow=Cenomanian; green=Aptian, orange=Barremian) and numbered by species (1 = Rotalipora cushmani; 2 = R. greenhornensis; 3 = Cyclonephelium tabulatum; 4 = Muderongia simplex). Sequence boundaries derived from well-log stacking patterns are represented by red lines. Dashed red lines represent well-log sequence boundaries that are uncertain. Seismic horizons, representing seismic sequence boundaries, are tied to wells using checkshot surveys and synthetic seismograms and are shown with thick, dashed, colored lines. Units are logging units (feet below kelly bushing), but a scale is given in m. Abbreviations: SB=sequence boundary; HST= highstand systems tract; MFS= maximum flooding surface; TST=transgressive systems tract; TS= transgressive surface; LST=lowstand systems tract; Barr. = Barremian. From Baldwin et al., (in review).

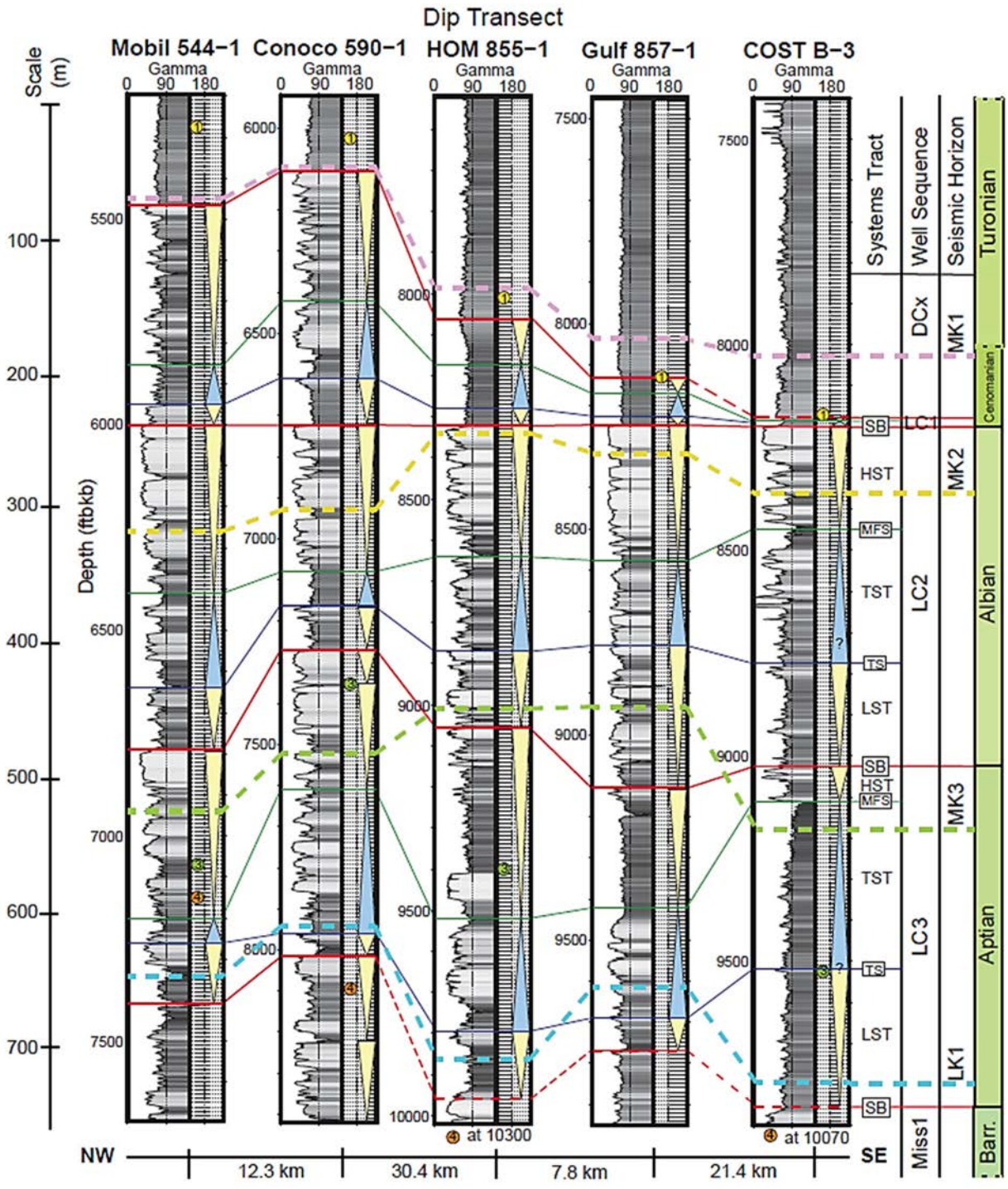

Figure 2-11b. Well-log transect across the GSD in the NW-SE dip direction. See Figure 2-11a for extended figure caption. From Baldwin et al., (in review).

2.5.2.3 Seismic Evaluation

Sequences in seismic data were determined independently from well data using reflection terminations (Figure 2-12, Figure 2-13). Reflection terminations, including erosional truncation, toplap, onlap, and downlap, highlight major regional unconformities that form as a result of erosion or non-deposition and bound a depositional sequence (Mitchum et al., 1977). The majority of interpreted seismic data include >10,000 km of MCS reflection profiles collected by industry for exploration purposes in the 1970s and 80s, covering ~30,000 km^2 of the OCS and slope with ~2 km line spacing. These data were recently released by the NAMSS (Triezenberg et al., 2016). Within the interval of interest for this study (~1-3 seconds [s] Two-Way Travel Time [TWTT]), the vertical seismic resolution decreases with depth and ranges from approximately 25 m to 75 m respectively.

The dataset was supplemented by two slightly higher resolution seismic surveys. The first includes ~500 km of USGS seismic lines collected between 1973 and 1978, and recently reprocessed in 2016-2017 by AI Inc. for this project. The second is a 2D MCS academic survey collected on the Research Vessel (R/V) Ewing in 1990, covering area on both the inner and OCS offshore NJ. The Ewing sound source achieved slightly better seismic resolution (~10 m) than the aforementioned datasets, yet the useful acoustic penetration was limited to roughly 1 s TWTT (~1 km). Although low penetration caused difficulty tracing seismic reflections within this dataset, the Ewing seismic profiles were useful in correlating seismic horizons landward of the GSD.

Key seismic horizons were identified using seismic sequence principles originally laid out by Mitchum et al. (1977) and Mitchum and Vail (1977). The identification of reflection terminations (e.g., red arrows in Figure 2-3), including those that constituted onlap, toplap, downlap, and erosional truncation, helped us identify surfaces of discontinuity that bound a depositional sequence and guided the placement of sequence boundaries. These surfaces could be loop correlated across >10,000 km of seismic lines, encompassing the entirety of the northern and southern BCT (SBCT) within the restrictions of seismic resolution. Seismic facies derived from internal reflections were used to infer depositional environments and lithology within each sequence following Mitchum et al. (1977).

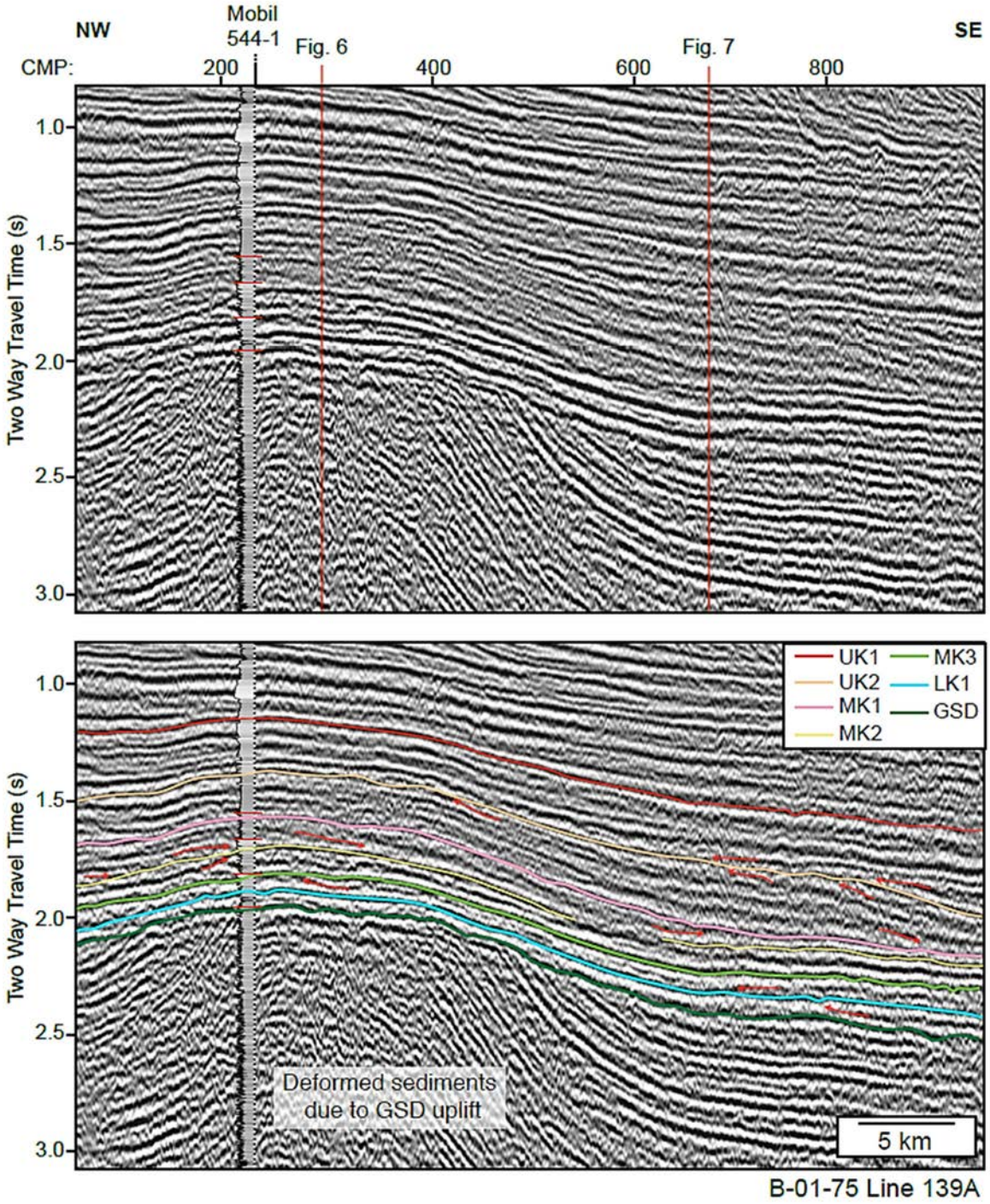

Figure 2-12. Seismic reflection dip profile across the GSD.

Note: Seismic horizons representing sequence boundaries are colored. Well-log sequences are represented by horizontal red lines at the well location. Vertical red lines indicate locations of intersecting seismic lines in subsequent figures. From Baldwin et al., (in review).

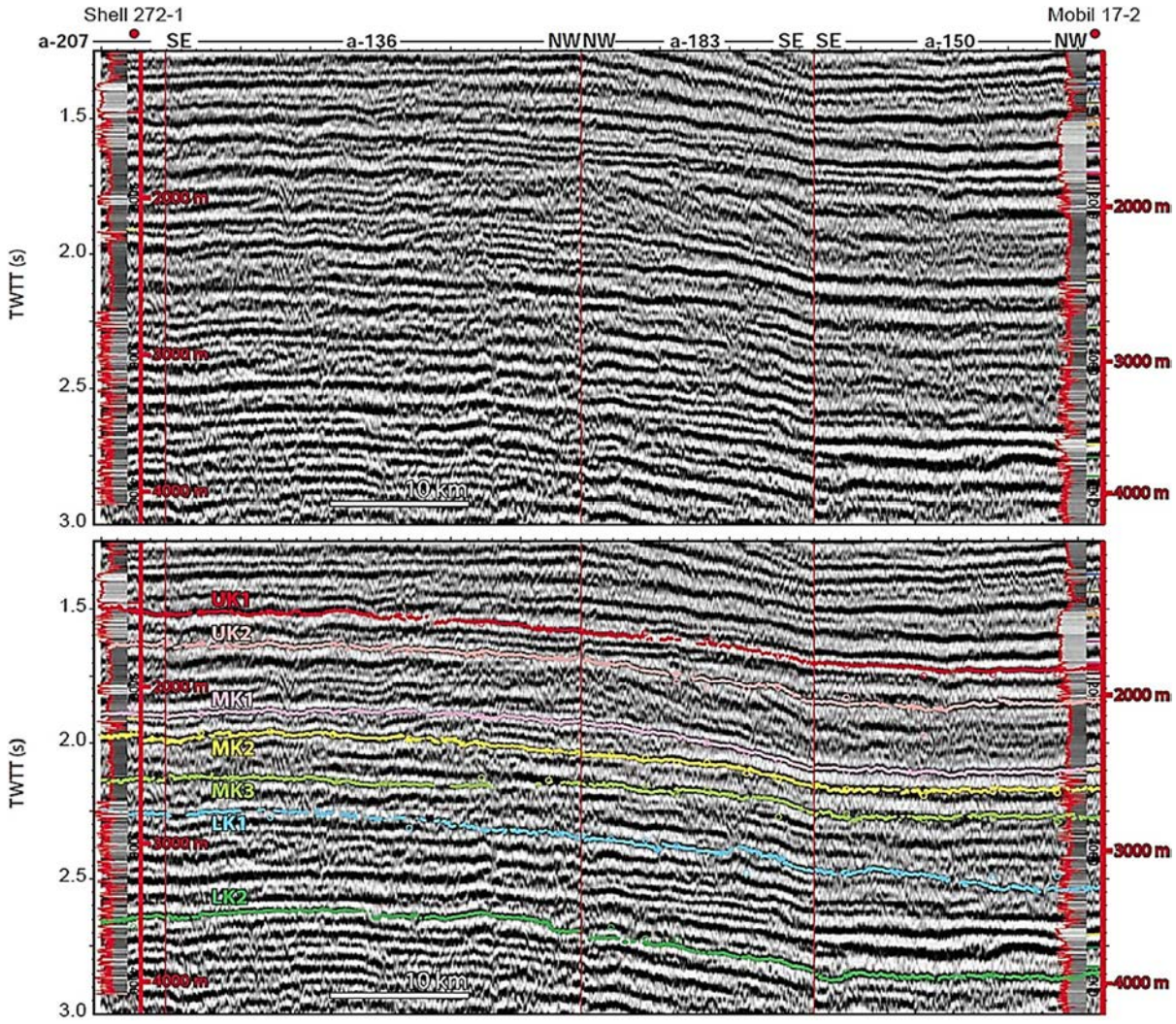

Figure 2-13. Seismic correlation between the Shell 272-1 and Mobil 17-2 wells.

Note: Wells are located on the OCS offshore southern New Jersey and correlations used the a-207, a-136, a-183, and a-150 seismic profile lines from the B-01-75-AT seismic survey. The biostratigraphic picks within the wells are used to assign preliminary ages to the mapped seismic packages. From Schmelz et al., (2019).

2.5.2.4 Regional Time-Depth Conversion

The conversion of TWTT to depth is required to generate structural contours and isopach maps in meters. Velocity-depth grids generated by Klitgord et al. (1988) were initially considered, and supplemented by incorporating a more detailed time-depth profile for the upper second (i.e., TWTT) of sediments generated by Mountain and Monteverde (2012) based on seismic data acquired from the R/V Oceanus expedition OC270 and well data from International Ocean Discovery Program (IODP) Exp. 313. The accuracy of the conversion of the seismic data (i.e., TWTT) to depth was checked against values obtained from OCS well velocity surveys at the well locations (i.e., checkshot surveys and velocity logs).

2.5.3 Results

An updated sequence stratigraphic framework was developed for the Cretaceous fluvial-deltaic sedimentary sequences of the BCT and identify five well-log sequences in Lower to Upper

Cretaceous strata (i.e., Miss, LC3, LC2, LC1, DCx) (Table 2-1; Figure 2-10, Figure 2-11a, Figure 2-11b) that correlate (within 50 m) to six seismic sequences (i.e., LK2, LK1, MK3, MK2, MK1/UK2) (Figure 2-12, Figure 2-13). In the northern BCT, the Aptian LC3/LK1 sequence contains thick, blocky sands updip on the GSD; it shales out down dip and to the SW part of our study area (Figure 2-11a). This sequence is thickest south of the GSD, near the structural high of the dome (Figure 2-14). The Albian LC2/MK3 sequence is thinner than the Aptian sequence and contains thick, blocky sands in the northern part of the study area that shale out to the SW (Figure 2-11a, Figure 2-11b). The lower Cenomanian LC1/MK2 sequence is the thickest of the three sequences, is located on the inner continental shelf, and thins and loses sand content down dip.

A total of seven seismic stratigraphic surfaces were identified that can be traced from the SBCT offshore New Jersey, south to the continental shelf off the coast of Maryland, constrained in age by biostratigraphic data from five wells offshore southern New Jersey and a cross section of three wells on the Maryland Coastal Plain (Figure 2-15). A regional velocity-depth model is developed to convert the legacy seismic data to depth, and an onshore-offshore correlation is made between the depth converted seismic surfaces of the Maryland Shelf and the onshore well-log stratigraphy (Miller et al., 2017) within the three deep stratigraphic test wells in Maryland (Figure 2-15). The onshore-offshore correlation provides additional, albeit coarse, constraints on absolute age.

The onshore stratigraphy was integrated for the mid-Atlantic Coastal Plain (Miller et al., 2004; Miller et al., 2017) with the depth converted seismic stratigraphy ultimately producing regional structural contour maps and isopachs for the entire SBCT (Figure 2-16). These maps were combined with Wheeler diagrams to generate for dip lines of the Maryland Shelf and establish a better understanding of spatiotemporal variations of Cretaceous sedimentation in the SBCT. The 3-dimensional (3D) movement (i.e., planimetric space and time) of the sedimentary depocenter was delineated from a distal and southerly Lower Cretaceous position to a more proximal but still southerly location in the mid-Cretaceous, followed by predominantly northerly and distal Upper Cretaceous sedimentation. These spatial variations in sedimentary thickness correspond with a deepening of depositional environment from the Early Cretaceous to a maximum paleodepth at the Cenomanian/Turonian boundary, followed by a Late Cretaceous shoaling.

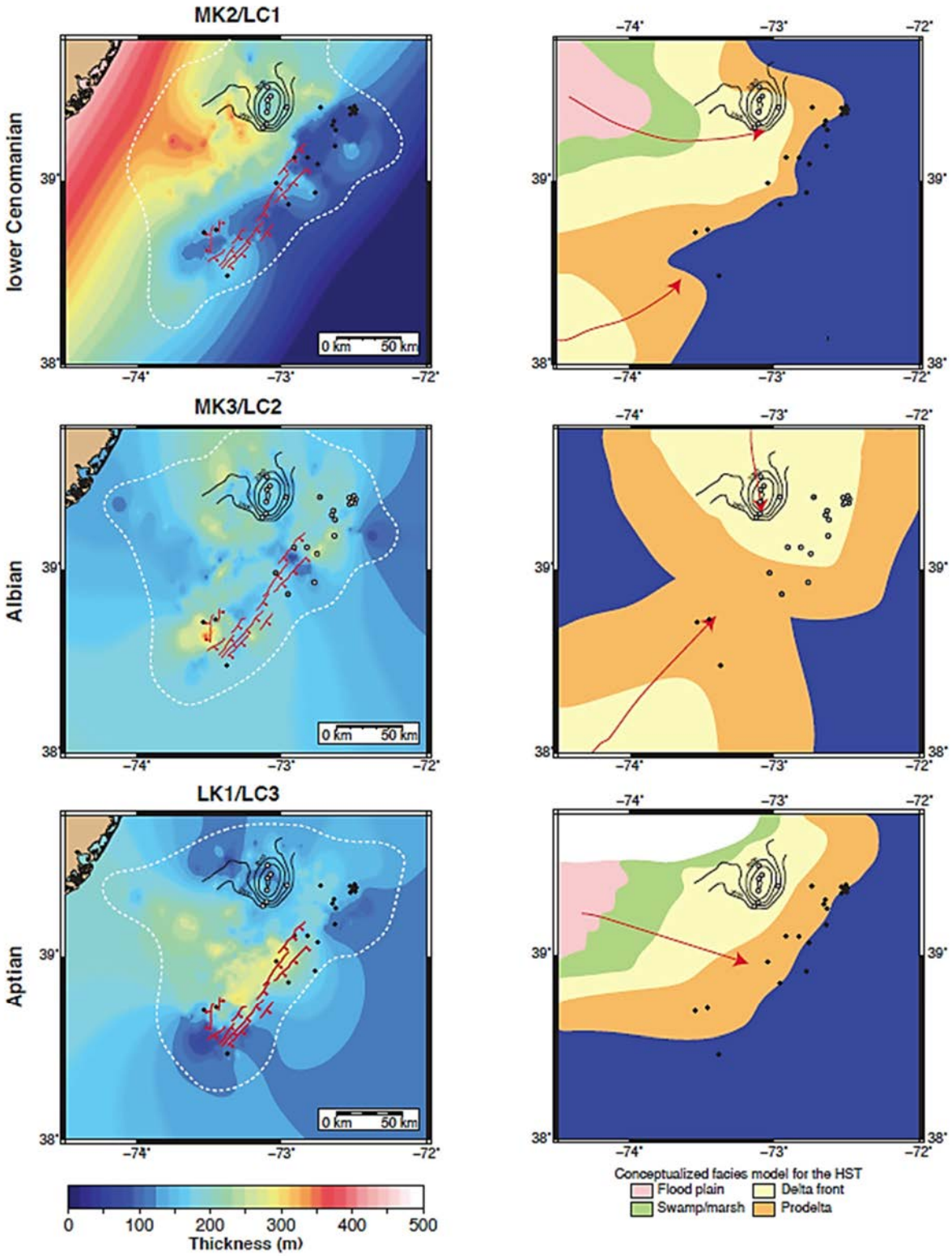

Figure 2-14. Isopach maps (left) and facies interpretations (right) of sequences LC3, LC2 and LC1.

Note: Dots represent well locations, color coded to indicate generalized % sand content of each sequence (<25 black, >25 gray <75, white >75.). Facies models for the HST of each sequence are based on sequence thickness, calculated sedimentation rate, and inferred lithologic composition. From Baldwin et al., (in review).

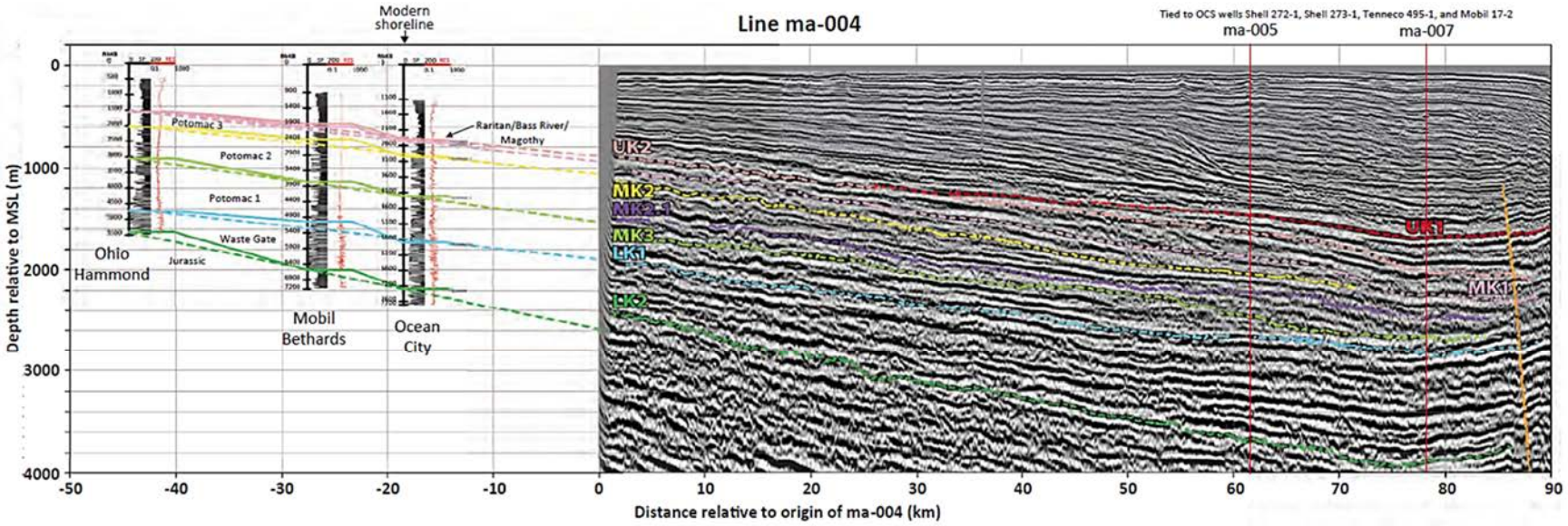

Figure 2-15. Correlation of the Potomac Formation/Group and Waste Gate sequences from a well-log cross section comprised of the three deep stratgraphic test wells on the Maryland Coastal Plain.

Note: Interpreted by Miller et al. (2017), with the Ma-004 seismic section converted from TWTT to depth using a splice of the GDUSNAM (Klitgord et al., 1988) and the TD function of Mountain & Monteverde (2012) (in the upper 1s of sediments). The onshore Potomac and Waste Gate sequences (Miller et al., 2017) are projected onto the seismic line through extrapolation of a spatial linear regression through the sequence picks in each of the wells across the transect. The resulting correlation matches the Potomac and Waste Gate sequence boundary surfaces with the Cretaceous seismic sequences interpreted herein. From Schmelz et al., (2019).

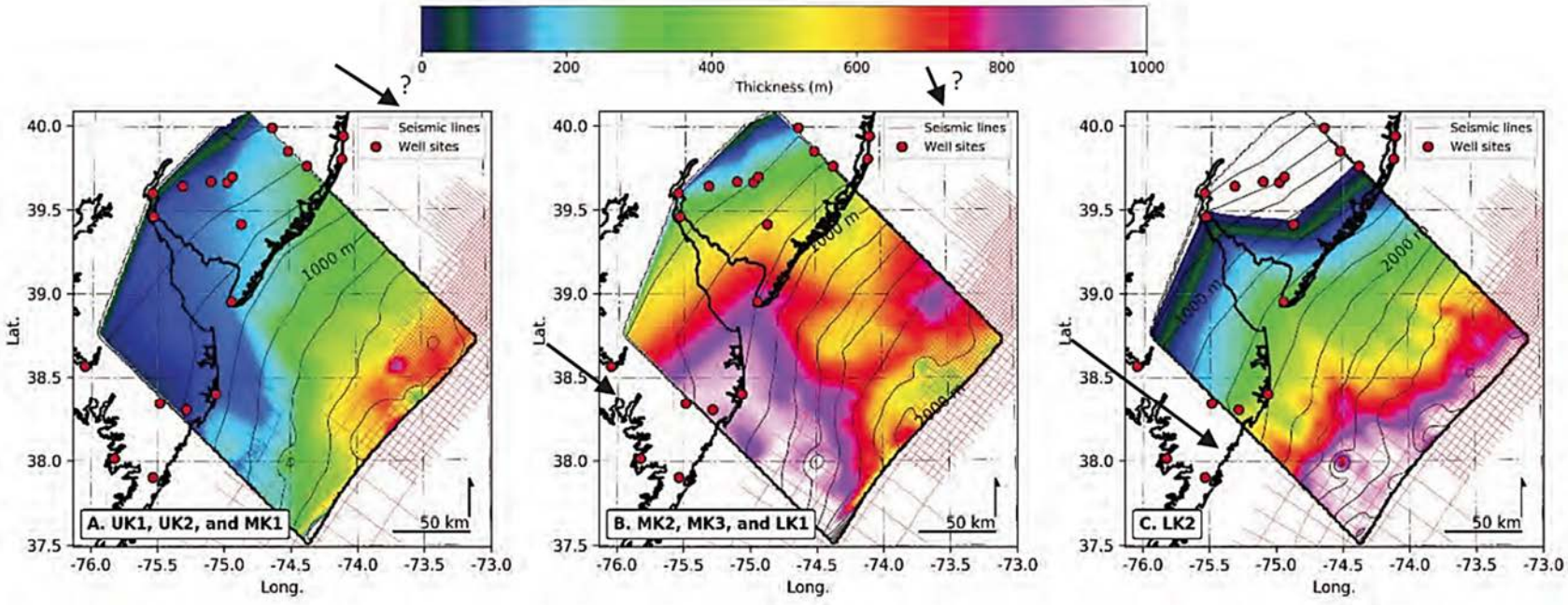

Figure 2-16. Uninterpreted and interpreted seismic profiles and Wheeler diagram for mid-Cretaceous depositional sequences identified on line ma-006.

Note: Line ma-006 is 10 km (6 miles) south of ma-004. Sediments bound by the reflections marked with blue lines are assigned to the LST, with green lines to the TST, and with yellow lines to the HST. The red lines are sequence boundaries. From Schmelz et al., (2019).

2.6 Onshore Coastal Plain Studies: Implications for Offshore Storage

Studies conducted onshore in Maryland by the Maryland Geological Survey (MGS) and Miller et al. (2017) and in New Jersey and Delaware by Thornburg et al. (2016) and Thornburg et al. (2019) are updip of the MAOSCRAP study area. These updip studies provide information about (1) excellent onshore and nearshore Waste Gate-Potomac I reservoirs (Miller et al., 2017); (2) facies distribution of the updip reservoirs and their confining units that can be directly exported to offshore reservoirs and confining units; and (3) continuity of confining beds updip of proposed carbon storage sites nearshore in the Waste Gate-Potomac I sequence off Maryland and offshore on the GSD off New Jersey.

In the MGS study, data from three updip coreholes in Cecil County, Maryland, were used to fill some data gaps and test previous correlations. Results indicate some previous correlations in the study area that were derived largely from geophysical log interpretations, need to be revised. This study underscored the difficulty of interpreting the original genetic relationships of Potomac Group strata across distances without corroborating data (e.g., biostratigraphy) to tie ages to sediments. Where interpretative stratigraphic techniques are used to correlate strata across data-limited areas and predict the extent and/or continuity of storage or capping units in the Potomac Group, the provisional nature of such correlations needs to be clearly conveyed. ***The draft report summarizing the geologic characterization of core data from the Potomac Group on the coastal plain of Maryland is provided in Attachment D***.

Similarly, Thornburg et al. (2016) and Thornburg et al. (2019) evaluated the paleoenvironments of the onshore New Jersey and Delaware Potomac Formation with coreholes at Medford, NJ, Fort Mott, NJ, and Summit Marina, DE. These studies allow placement of the Potomac Formation into a regional context, emphasize the importance of biostratigraphy and sequence stratigraphy in interpreting genetic relationships, and provide for the addition of Delaware to our stratigraphic correlations chart. Though these three coreholes are updip, they inform us of facies and paleoenvironmental changes to the potential targets for onshore sequestration.

Miller et al. (2017) show that the Waste Gate-Potomac I reservoirs are excellent in both New Jersey and Maryland. Confinement in New Jersey appears to be widespread and continuous; the updip confinement of this reservoir in Maryland is less certain. Volume storage estimates for the Potomac I-Waste Gate in the mid-Atlantic Coastal Plain are 8.4–33.5 Gt CO_2, adequate to store CO_2 captured from 24–95 GW of natural gas generation for a century.

2.7 Key Findings

2.7.1 Georges Bank Basin

The sequence stratigraphic framework for the Cretaceous strata of the GBB allowed us to correlate six well-log depositional sequences to seven seismic reflectors identified in the eastern and western subregion. The integration of eastern well-log stratigraphy with western seismic stratigraphy resulted in surface contour maps and isopach maps (e.g., Figure 2-3), where Cretaceous sedimentation patterns are similar between both regions, and sediment sources likely lie toward the north, outside the boundaries of the GBB. The LC sands in the eastern GBB are too shallow and therefore unsuitable, in the eastern GBB for carbon storage. However, the deeper Missisauga sands are still a viable target in the eastern subregion. The LC sands along the southeast margin in the western GBB have potential to be a suitable target for carbon storage because they are likely to be comparable to the LC sands that are thick, porous and

permeable in the eastern GBB. In the western GBB, these sands are below the burial depth needed for supercritical storage (>800 m), and are capped by thick shales. Yet, without well data and cores in the western GBB, it is difficult to know the lithologic composition, porosity, and permeability of the target sands; drilling must be done before considering the western GBB a potential target for carbon storage.

2.7.2 Baltimore Canyon Trough

In general, sands are thickest on the GSD offshore NJ, within the LC3, LC2, and LC1 sequences. Porosity and permeability measurements suggest good storage capability and the DCx sequence provides a good cap rock and seal for the reservoirs below. In addition, differential compaction, forming an anticline around the GSD, has created a structural trap suggesting excellent closure for storage. The HST and LST sands within the mid-Cretaceous sequences in the vicinity of the GSD appear to be the optimum storage location for supercritical CO_2 in the northern BCT, and a world-class target for carbon sequestration.

Based on the seismic facies the correlation was observed to coeval fluvial depositional facies in well data from the MD and NJ Coastal Plains (Browning et al., 2008; Miller et al., 2017), suggesting there are likely mid-Cretaceous, sand-prone deltaic facies offshore Maryland. This interval is largely shale offshore southern New Jersey but thickens to the south, indicating a location more proximal to a deltaic sediment source. This package is thick and is likely to contain sedimentary facies that comprise a viable reservoir for storage of supercritical CO_2 or oil and/or natural gas. It is also capped by muds and shales onshore and offshore. However, since a viable source rock for hydrocarbon accumulation in these potential reservoir sands has yet to be identified, they have potential to be CO_2 storage reservoirs. Beneath this mid-Cretaceous interval, there is also a thick package of Lower Cretaceous sediments that likely contain sand-prone siliciclastics deposited behind a fringing carbonate platform. These sands might also present attractive targets for CO_2 storage (or hydrocarbon exploration) if the sand bodies are locally amalgamated and hydrologically connective.

3. Seismic Data Evaluation

This section summarizes the seismic evaluation completed by the research team, primarily through the LDEO and Rutgers University. This work included seismic reprocessing and interpretation associated with the project, focusing on the re-evaluation of 1970s vintage legacy data using modern techniques. These methods achieved marked improvements in seismic imaging that enabled the Project Team to better estimate storage potential and make new geological interpretations along the U.S. mid-Atlantic margin. Seismic data was especially valuable in areas where these is no well control. Results from these activities are summarized in the following section.

3.1 Seismic Processing: Recovering and Reprocessing Legacy Seismic Data

One of the major objectives of this project was the recovery and reprocessing of legacy seismic data collected by the USGS in the 1970s and 1980s. These data are foundational to the offshore work done as part of this project, as they provide the framework for building our regional geologic models and provide surfaces to interpolate data recovered from drilled boreholes (Figure 3-1). Data from these USGS transects was chosen for this project for three major reasons: (1) they are the most comprehensive data available in the region despite their age; (2) exploration wells are located along or close to these seismic lines; and (3) this type of multi-channel marine data can be heavily improved with modern methods, including attribute analyses from full waveform inversion. The vintage data presented a variety of challenges and required specialized approaches outlined here.

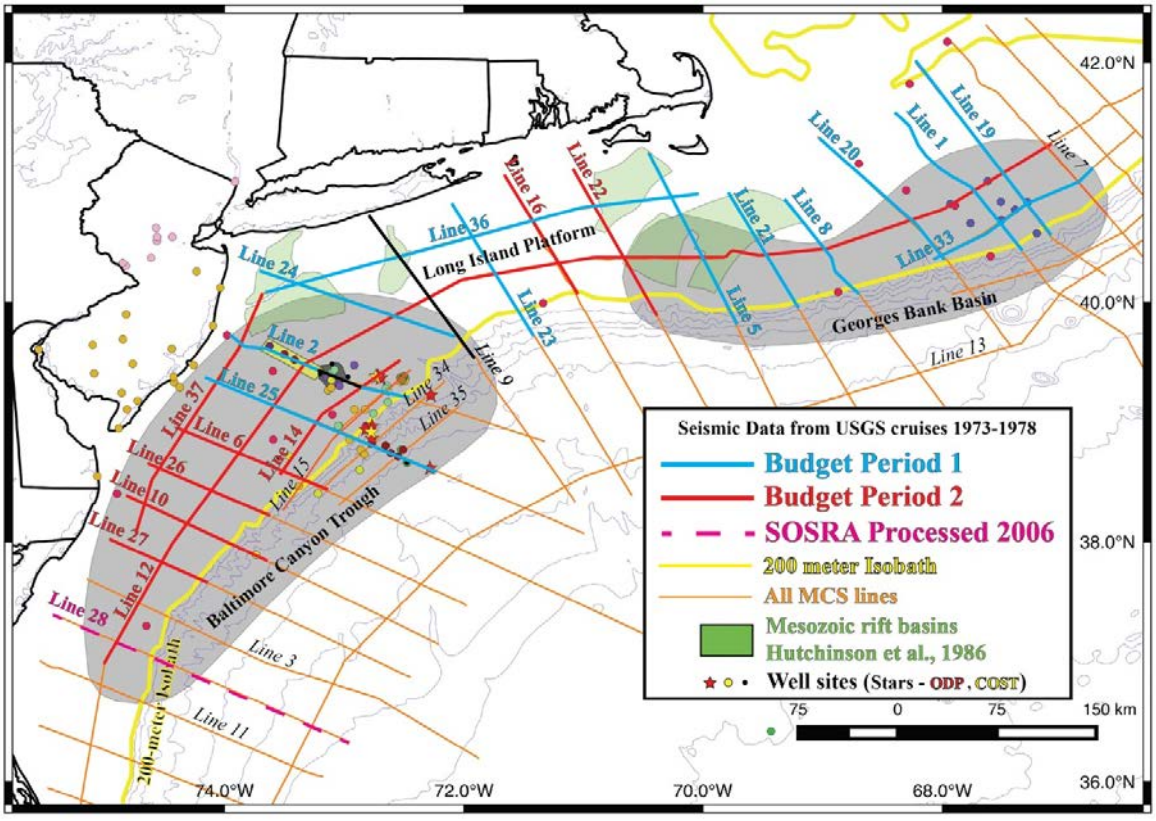

Figure 3-1. Seismic Data from USGS cruises 1973-1978 used for the framework for building geological models and providing surfaces for data interpolation from drilled boreholes

The selection and recovery of the seismic data was an iterative process, as LDEO worked to meet the project goals with the availability and quality of the data. LDEO first mapped the original transects along with wells and major interpreted geologic boundaries (e.g., GSD, rift basins). From this map, LDEO selected our primary targets and searched the available data on the USGS database. LDEO found significant portions of the data missing online but were able to recover some from the USGS data storage facility in Woods Hole, MA, via archived compact discs. Not all of the data could be recovered, most notably: the entirety of line 9 (except a paper copy of a stack) and the region around the GSD on line 2. With these limitations, the targets were re-ranked and split the data into two processing batches totaling ~2,000 km of seismic line length each, one for each project budget period. Despite the extensive data recovery, there still remained gaps in data, navigational information, and acquisition geometries since the data was collected on multiple research vessels with significant variations in acquisition geometry. As such, commercial processing experts were consulted to achieve the highest quality results possible.

Seismic data reprocessing was completed under contract with AI Inc. of Calgary, Canada. Legacy processing (i.e., ~1980s) was heavily limited by the computational capabilities available at the time of data collection; reprocessing using a full suite of state-of-the-art techniques greatly improved seismic image quality and geologic interpretation potential. In particular, detailed velocity modeling and data migration accounted for many of the imaging improvements. Seismic data migration relies on accurate, detailed velocity models to properly locate reflected seismic energy from dipping stratigraphic layers, a standard and necessary procedure in all modern processing. Other significant improvements included spike suppression, predictive deconvolution, and noise suppression. Removing noise and de-convolving the pre-stack seismic data with the predicted source wavelet produced sharper images, and ultimately, more reliably interpreted geology.

The full seismic reprocessing report from Absolute Imaging Inc. and Columbia University is provided as Attachment E of this report. This report describes seismic products including: pre-stack time migrated seismic gathers and sections (SEGY and TIFF), time domain velocity models (SEGY: interval and RMS), navigation information (ASCII). The final seismic processing dataset was uploaded to DOE's EDX website (https://edx.netl.doe.gov/) at the conclusion of this project. The underlying raw dataset used for this seismic processing are described in our Task 2 report titled "Final Regional Stratigraphic Framework Topical Report" issued on July 31, 2017 and can be obtained from USGS website at https://walrus.wr.usgs.gov/namss/search/ or at https://cotuit.er.usgs.gov/data/.

3.2 Extent Integration of Seismic Data to Provide Sequence Stratigraphic Framework

Seismic profiles can extend interpretations made on sparse well and core data to an entire basin; however, seismic data is typically recorded in TWTT as opposed to well logs, which are recorded in depth. Thus, well logs must be converted to TWTT and projected onto seismic profiles in order to integrate well-log and core interpretations with seismic sequence interpretations. Checkshot surveys provided the primary means of converting from depth to TWTT; they were collected by industry during the time of seismic acquisition and measure the travel time from a source to a known depth at a specific location. A time-depth chart was made from averaged checkshot data. Synthetic seismograms were than created to better evaluate well-seismic ties. Synthetic seismic data were created using density and velocity logs with an estimated time-depth chart to calculate impedance and convolving the result with a hypothetical wavelet. Synthetic seismograms provided a way to match acquired seismic data with modeled

seismic data. IHS Kingdom Suite allowed manipulation of time-depth relationships after synthetic generation to better match modeled synthetic to seismic data. After comparison between our modeled and real seismic trace, the original time-depth chart was shifted (+/- 10 ms) using IHS Kingdom to best fit the correlation between the synthetic and seismic traces. Error for the seismic-well tie increased for wells that were drilled on the GSD that encountered significant topography in Cretaceous strata (e.g., Conoco 590-1), as well as for wells that were drilled at a significant distance from a seismic line (e.g., Exxon 684-1). Once a time-depth conversion is established, well-log information can be integrated with seismic interpretations. This allows integration of facies, systems tracts, sequence boundaries, and biostratigraphy observed in wells with sequences determined by seismic sequence analysis.

3.3 Refined Offshore Rift Basins Extent

The discovery of offshore rift basins along the LIP was among the chief results of the original data collection. Offshore rift basins were a specific target for the re-evaluation of these data for this project (Hutchinson et al., 1986). These buried basins fit within the scope of this project as analogous onshore basins containing basaltic facies. Recently, work in other onshore locations has proven the viability of CO_2 storage in basaltic reservoirs in a solid state through mineralization processes (Matter et al., 2016). Injected dissolved or liquid CO_2 can mineralize on basaltic surfaces, thereby sequestering CO_2 permanently and without risk of later reservoir leakage. Though potential basalt storage reservoirs are not the primary focus for the project, these basins are prime for cutting-edge research and could be ideal storage reservoirs due to their vast size, location offshore, and ability to store CO_2 in a solid state via mineral trapping.

Research goals in this project related to the rift basins were two-fold. First, the reprocessing of the seismic data enabled LDEO to better map the areal extent of the basins. The improved velocity models and imaging helped outline the shape and presence of any structures within the basins. Second, LDEO used advanced computational methods to examine the character of the basin fill. In particular, LDEO applied prestack waveform inversion on selected spots within the dataset to estimate the porosity and rock composition. This work is currently being prepared for future publication (Fortin et al., 2018*)*. These results also aided in the regional estimation of CO_2 storage resource by providing seismic “pseudo-wells” where borehole geophysical data was lacking.

LDEO’s efforts to update and refine the areal extent of the rift basins with reprocessed seismic data were successful (Fortin et al., 2018). Not only has the imaging of known basin extents improved, LDEO discovered a previously un-imaged basin (Fortin et al., 2018.). The original mapping of the basins was performed using these same seismic data, and their shape between transects was largely inferred from magnetic data resulting from the prevalence of straight edges and corners defining many boundaries. More recent investigations of the region have been using small or single-channel seismic systems incapable of penetrating the subsurface far enough to image the deeply buried basins. North of this study area, similar rift basins have been mapped using seismic, gravity, and magnetic data showing elongated basins running SW to NE. In the GBB, LDEO imaged complex boundary edges for the rift basins and drew our interpreted basins to match those found to the north. Along the LIP, the basins largely retained their previously mapped shape.

The interior of the rift basins also shows much greater detail in the reprocessed data. This result is unsurprising, as the basin fill should contain layers, some of which are thought to be basaltic and have significantly different seismic responses. Figure 3-2 illustrates the improvements in imaging within the rift basin, particularly from ~55-65 km and 1.5-2.5 s. Seismic waveform

inversion results are detailed enough to show significant velocity anomalies suggesting some layers to be basaltic. These layers are ~10 m thick and have porosities high enough (i.e., in some cases >20%) to merit consideration for carbon storage (Figure 3-3). These results, conducted at basins imaged in lines 16, 27, and 36, encourage further data collection and analyses (Fortin et al., 2018.).

Porosity was calculated from inverted seismic velocities following the empirical, global relationship outlined in Erickson and Jarrard (1998) with a normal consolidation history. The velocity-porosity relationship assumes the velocity of water to be 1.51 km/s, the velocity of a pure sandstone matrix to be 5.49 km/s, and the velocity of a pure shale matrix to be 4.3 km/s. The relationship ignores the effects of temperature, microcracks, exhumation, rebound, overpressure, anisotropy, pore fluids other than water, or biogenic sediment components. LDEO also produced a few seismic pseudo-wells used to inform regional porosity maps and subsequent estimates of carbon storage. These results are included and discussed in Section 5 for the Task 5 CO_2 Storage Resource Calculations.

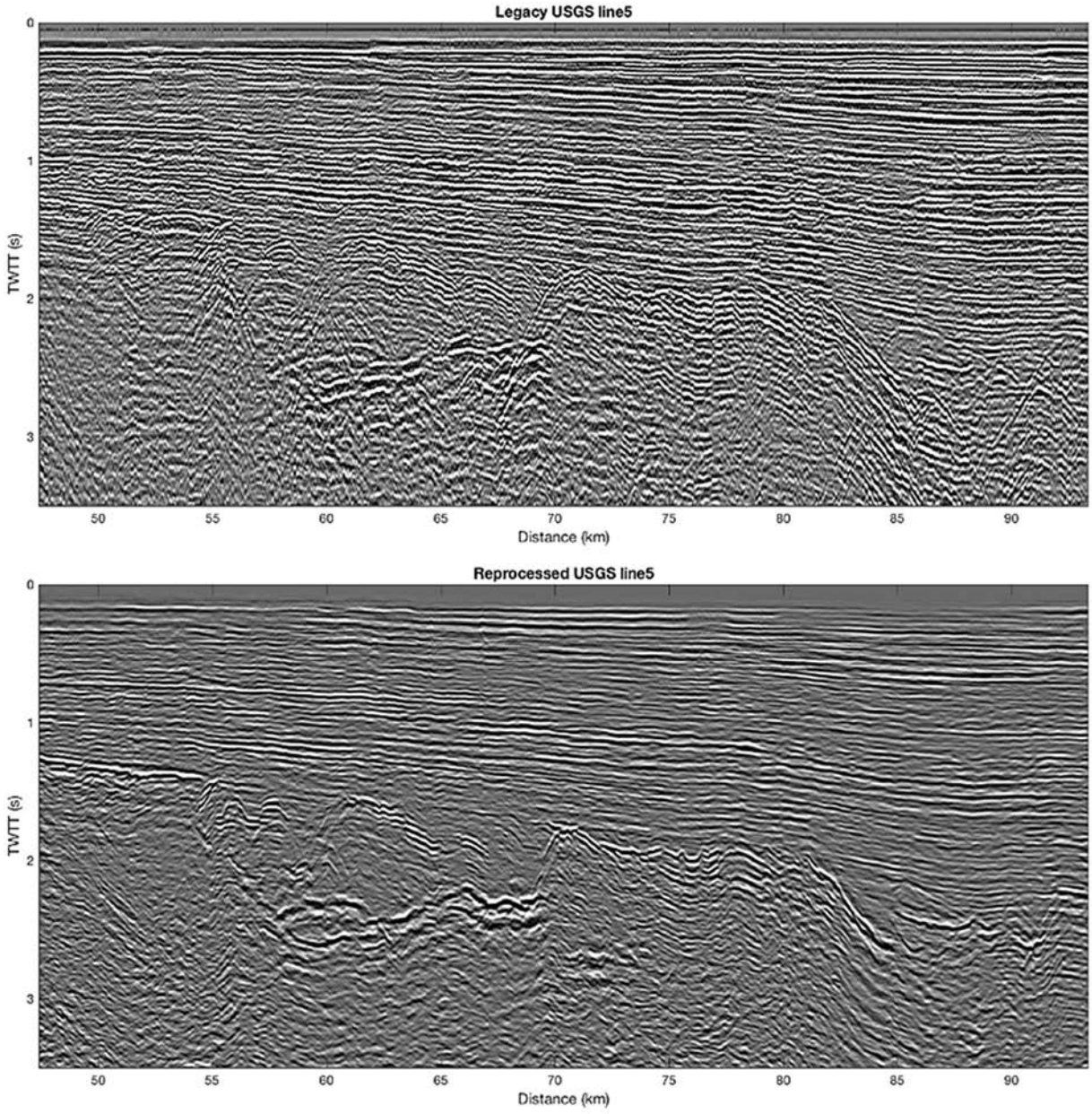

Figure 3-2. Legacy processing of line 5 showing a rift basin (above) and the reprocessed result (below). Note the much clearer definition of the bottom boundary as well as the interior structures.

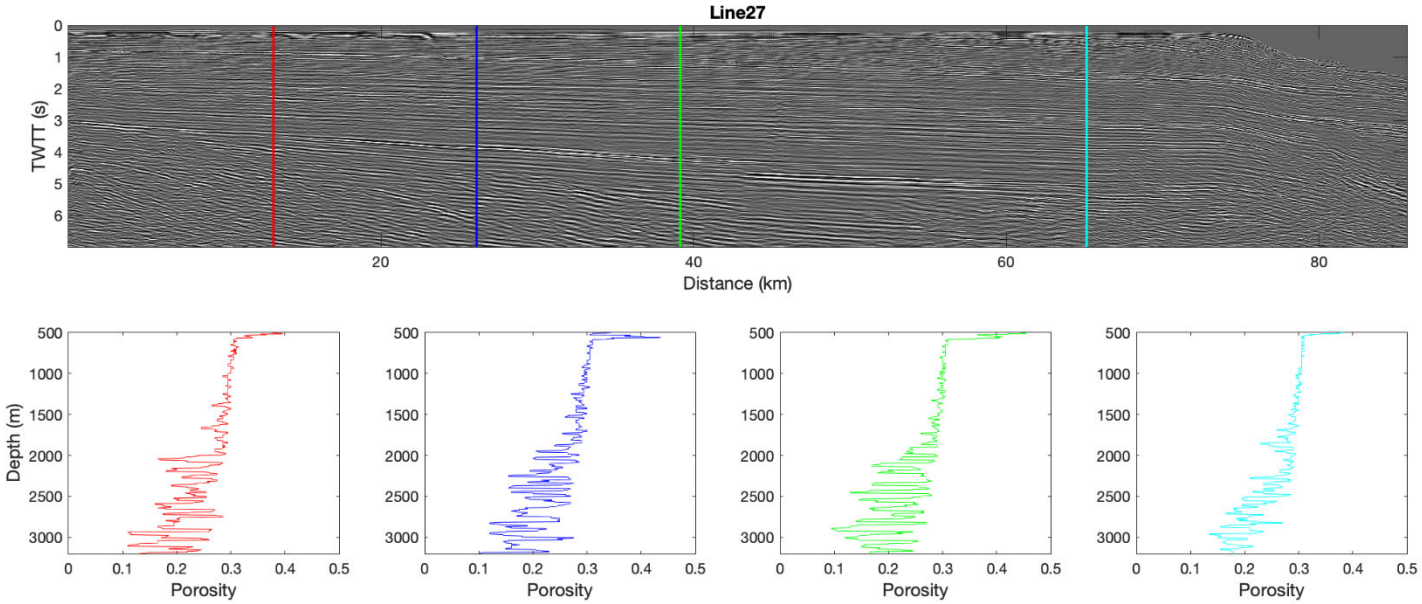

Figure 3-3. Porosity calculated from prestack waveform inversion on line 27 at four locations. Results were incorporated in regional storage capacity estimates discussed in section 5

3.4 Key Findings

In total, the team reprocessed approximately 4,000 km of seismic data to create a structural framework that was used to tie together all available well data, constrain sequence stratigraphic interpretations, and make regional assessments of carbon storage potential offshore of the eastern United States. Despite the 1970s vintage, these data are the best available for this study area. The age of these data sets introduced challenges in both data collection and data processing. LDEO found that some data in the region was missing, and some was unable to be reprocessed to modern standards. Despite these challenges, the research team produced 21 seismic transects ranging in length of 104 km to 940 km as summarized in Table 3-1 and shown in Figure 3-2.

Reprocessing of these data was needed to meet the goals of this project, and most likely, those of any future research in the region. The data had been recorded in an outdated format, and the processing was completed to what is now inadequate standards. In particular, all profiles were migrated to shift seismic reflections to their proper spatial location. Without this step, interpreting subsurface boundaries would ignore the real geometries and relative positions of subsurface sediment packages. The result is seismic data that has been updated and preserved to be useful both for this project and for other future research activities. The higher frequencies preserved in the reprocessed data and improvements in seismic amplitude handling improved the accuracy and reliability of geologic interpretations. This applied to both the shallower sedimentary, semi-consolidated, and consolidated facies that have been drilled as well as sediments and possible sills in the deeper rift basins. Stratigraphic interpretation among wells was improved, as interpretation could be conducted accurately along more clearly defined (i.e., higher frequency) horizons, and lateral changes were better represented. Rift basin mapping was improved by better locations of basin boundaries and greatly improved imaging of basin infill. These improvements led to a better overall estimation of carbon storage potential for the region.

Results from these reprocessed data provided higher resolution images and, as such, more accurate models of subsurface characteristics. Advanced computational methods were applied to inform rift basin content and provide insight into regional storage capacities in regions lacking well data. The original data were compiled, reprocessed into current data formats, and updated to modern standards to allow effective preservation for other research activities in the future. Results were also presented and published at various conferences, including the American Geophysical Union fall meeting in 2017 and 2018, LDEO MG&G seminars in 2017 and 2018, and the Greenhouse Gas Control Technology conference in 2018 [Fortin et al., 2018]. Two further publications will be submitted in 2019 to *Geophysics Research Letters* and an undecided publication covering the updated basin extent and composition derived from prestack waveform inversion.

Table 3-1. Line number, length, and number of gathers for the 21 reprocessed seismic transects.

Region – Line Number	Length (*km*)	Gathers (#)
Baltimore Canyon Trough – Line 27	152	3425
Baltimore Canyon Trough – Line 10	152	4700
Baltimore Canyon Trough – Line 26	104	4400
Baltimore Canyon Trough – Line 6	107	4850
Baltimore Canyon Trough – Line 25	187	11423
Baltimore Canyon Trough – Line 2	178	3515
Baltimore Canyon Trough – Line 37	240	9652
Baltimore Canyon Trough – Line 14	140	5547
Long Island Platform – Line 24	154	6221
Long Island Platform – Line 23	157	6334
Long Island Platform – Line 16	123	4950
Long Island Platform – Line 22	107	6150
Long Island Platform – Line 36	320	6408
Georges Bank Basin – Line 5	157	6386
Georges Bank Basin – Line 21	114	4614
Georges Bank Basin – Line 8	116	4717
Georges Bank Basin – Line 20	155	6223
Georges Bank Basin – Line 1	171	3388
Georges Bank Basin – Line 19	192	8546
Georges Bank Basin – Line 33	107	4295
BCT, LIP & GBB – Line 12	940	37736

4. Hydrologic Properties Characterization

The objective of the hydrologic property analysis conducted for this project was to assemble a comprehensive dataset from mid-Atlantic OCS wells that will support two of the project's main goals: to assess pore space available for CO_2 storage and to characterize potential storage zones and confining caprocks. This task involved compiling information on all available existing rock samples and testing data, as well as generating new data from new laboratory analyses.

Analysis of hydrologic properties requires data on lithology, mineralogy, porosity, and permeability derived from sample analyses and geophysical logs. The Project Team first identified all available, relevant existing well samples and data, most of which are housed at the DGS OCS Sample Repository. Following this review, a comprehensive inventory was made of the sample materials at the DGS. Next, an inventory was made of relevant reports and publications that contain reservoir quality data for the mid-Atlantic OCS wells drilled in the 1970s and 1980s. Those legacy reservoir data were compiled in a database to facilitate hydrologic characterization and resource assessment of OCS formations of interest. With the data compiled, gaps in existing data coverage were identified in intervals of interest; additionally, legacy data points with notable hydrologic properties (i.e., very high permeability) were identified as candidates for validation. Finally, sample materials were selected from the data gaps and validation candidates and sent to vendor and partner laboratories for analysis of hydrologic properties and composition.

The large volume of hydrologic property data assembled for the project were used primarily to characterize potential storage resources as well as potential caprock units. However, the interdisciplinary nature of the research effort requires the integration of data generated from the different tasks. These data were applied to other tasks as needed, such as stratigraphic analysis, well-log calibration and characterization, seismic inversion, and risk assessment.

The topical report associated with this task is provided as Attachment F. Original source image files are available, in addition to the workbooks, on the NETL's Energy Data Exchange (EDX) website (https://edx.netl.doe.gov/).

4.1 Hydrologic Properties Data Collection and Testing

The collection of existing hydrologic property data was focused on samples and reports housed at the DGS OCS Sample Repository. This task involved compiling information on all available existing samples and data in order to generate new data from new laboratory analyses. The collection inventory work included compilation of the type, number, stratigraphic and spatial distribution of cores, cuttings, and prepared sample materials. The collection of legacy hydrologic property data included mining of proprietary and published reports in DGS files as well as public records and the literature.

A detailed inventory of the DGS Atlantic OCS Sample Repository collection was carried out to identify specific materials available for this study. The DGS Atlantic OCS sample collection represents an agglomeration of numerous samples from wells drilled on the U.S. Atlantic OCS between 1975 and 1984; these samples exist in a variety of states of organization and preservation. The collection includes raw samples such as cores, washed cuttings, and unwashed cuttings, as well as prepared sample materials such as thin sections and micropaleontologic slides. The inventory work also allowed for an assessment of the condition of the samples. Materials in deteriorating packaging that were most immediately at risk were repackaged to ensure sample integrity for analytical work.

The sample inventory was tabulated in a master spreadsheet file composed of numerous worksheets that contain summary data and detailed inventories for each class of sample material. The extensive inventory effort resulted in a highly detailed, comprehensive listing of every item for each sample type in the collection. Approximately 100,000 items were inventoried that were potentially applicable to this project. Of most importance were the core samples, which allowed precisely located analyses of hydrologic properties and composition in potential storage and sealing units. Core sample types in the collection included large core slabs as well as smaller slices and chips taken from the cores. The number of core chips in the collection totaled more than 1,700.

Cuttings were the most numerous sample type in the collection; the cuttings were mostly washed but many were unwashed as well. More than 76,000 individual washed cutting sample envelopes and bags were inventoried. The coverage of washed cuttings from the OCS wells was extensive, but these materials have the disadvantage of being composed of smaller pieces and commonly suffering from some degree of mixing of materials from outside designated depth range of a sample. They were expected to be less useful for analysis of hydrologic properties than the cores.

A significant data mining effort was undertaken to obtain existing relevant geologic data from public records, published reports, and the literature. These data were generated during and shortly after the exploratory drilling in the Atlantic OCS in the 1970s and 1980s to evaluate the petroleum geology associated with the exploration targets. These data were compiled for this project to characterize important physical properties of the CO_2 storage reservoirs and caprock formations. A complete inventory was essential to assess available hydrologic property data for the Atlantic OCS wells and to identify data gaps where additional analyses may be warranted.

Mining of the legacy data was led by DGS staff and conducted in collaboration with staff from Battelle, the MGS, and the Pennsylvania Geological Survey (PaGS). The Project Team searched files and literature for relevant reservoir-related data on the petroleum geology of the Atlantic OCS wells. Numerous reports and publications were identified and collected from a number of sources, including hard copies of proprietary reports in DGS files, microfilm copies of reports available at the DGS, digital copies (e.g., PDF) of reports available from the Minerals Management Service (MMS), government publications (e.g., USGS, MMS), and open literature. Sample descriptions and porosity, permeability, mineralogical, and stratigraphic data were compiled into a master spreadsheet of hydrologic properties and subjected to quality control checks by the team.

The data mining effort resulted in the compilation of a master spreadsheet of hydrologic properties records from more than 9,000 individual sample/observation depths in 42 wells. The hydrologic property database includes more than 4,800 porosity measurements and more than 4,200 permeability measurements within the defined interval of interest for this study for hydrologic properties, between the top of the Dawson Canyon unit and the bottom of the Mohawk unit.

A close review of the data reveals a number of values that are somewhat anomalous compared to other values in the same intervals. Cases where permeability values are unusually high are of special interest. These data points were highlighted for possible verification to determine whether the data are reproducible. Damaged sample materials, poor analytical work, and/or outdated techniques were other possible sources of data quality problems to be considered. In addition, evaluation of the distribution of the data revealed data gaps in intervals of potential interest for carbon storage where additional analyses were warranted.

4.1.1 Sample Selection Methodology

The available rock properties and hydrologic characteristics data were analyzed in detail to find data gaps and to identify existing data where verification or calibration would be beneficial. These intervals of interest were identified as potential targets for new sample analyses. The availability of sample materials in these data gaps was assessed using a series of data queries in Microsoft Access and Microsoft Excel as well as graphically by viewing plots of data versus well logs in Petra.

Due to the large number of data line entries, repeatable automated approaches were used to identify data gaps. The DGS investigated and defined processes for applying Microsoft Access querying capabilities and Microsoft Excel sorting functions for the data gap analysis. The data gap analysis involved three primary datasets: (1) hydrologic property data compiled from mining of well reports and publications; (2) stratigraphic picks for the wells that are used to frame the interval of interest; and (3) a detailed item-by-item inventory of sample holdings in the DGS OCS Sample Repository.

The data gap analysis provided a basis for sample selection. The criteria for sample selection included the following requirements and decision factors:

- **Criterion 1**. **Fills a data gap (FG).** Where possible, samples were selected to fill gaps in existing porosity, permeability, and grain density data.
- **Criterion 2**. **Helps to verify empirically derived permeability values (VE).** Existing permeability data for sidewall cores may be verified by obtaining new measured values on corresponding conventional core samples and/or remaining sidewall core materials, where available.
- **Criterion 3**. **Helps to calibrate existing legacy data (LC).** Samples were also selected to examine changes in permeability in the sample material over time and help calibrate porosity log data.

The DGS hosted three workshops to select samples for hydrologic property analyses based on these criteria. At these workshops, sampling strategies were discussed, sample priorities were determined, and cores were examined to make final sample selections. The first workshop, which focused on planning of sampling and analysis, was held on May 10, 2017. The sampling analysis plan was designed to evaluate hydrologic properties using several analytical methods on samples from the same depth. This allowed direct comparison of data obtained from different types of laboratory measurements and thin-section analysis.

During sampling workshops held on July 13 and July 31, 2017, the Project Team evaluated sample materials available in intervals targeted for new analyses. Conventional core slabs, chips, and slices and sidewall core samples were examined to determine whether a sufficient quantity of the sample was available. A flow chart summarizing the selection criteria is shown in Figure 4-1. In total, 75 sample points from 17 wells were selected.

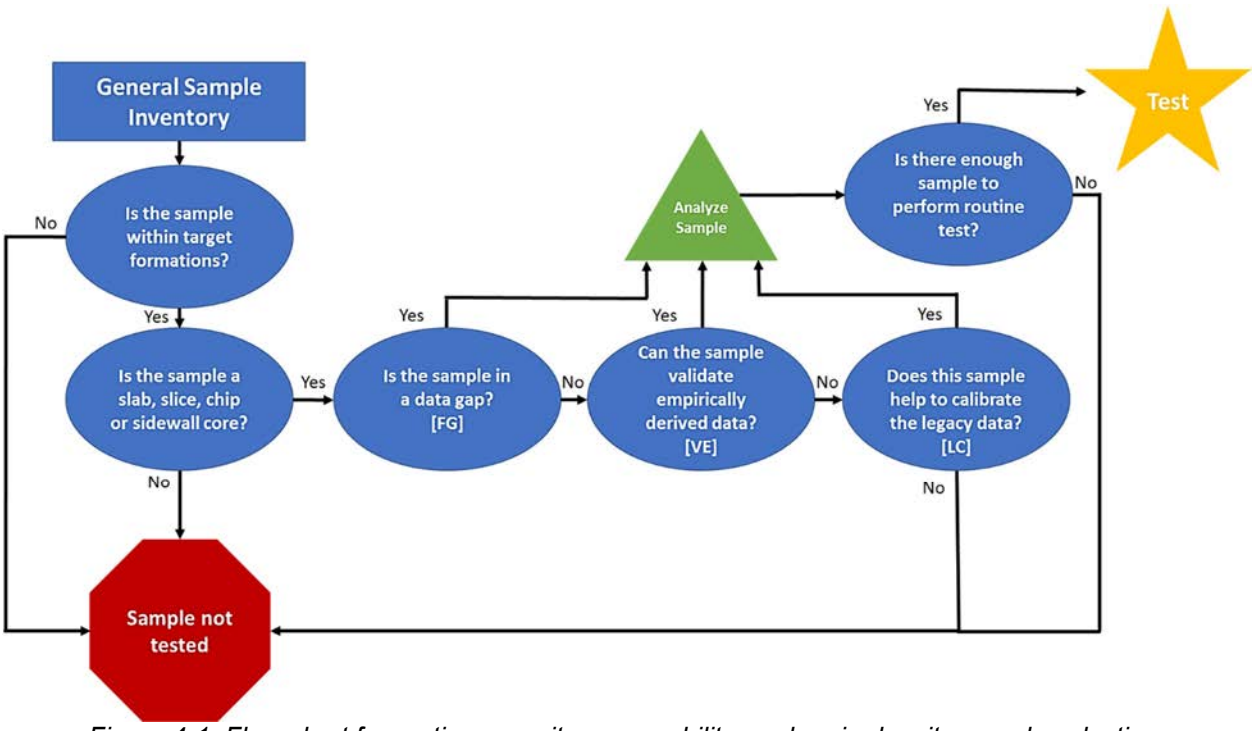

Figure 4-1. Flow chart for routine porosity, permeability, and grain density sample selection.

4.1.2 Laboratory Methods of Analysis

This section describes the laboratory analyses conducted on sample materials from 17 wells in the mid-Atlantic OCS. Hydrologic properties of the selected sample materials were assessed by measuring porosity, permeability, and grain density. Thin sections were used to evaluate porosity and to identify the mineral composition of the selected samples. Three types of instrumental analyses were performed to identify and characterize the framework grains, matrix, cements and porosity properties: X-ray fluorescence (XRF), X-ray diffraction (XRD), and scanning electron microscopy (SEM). Additionally, SEM analysis provides information on the crystalline nature of minerals, pore space geometry, and cement conditions of the samples. Table 4-1 summarizes the analyses carried out for each well.

Table 4-1. Summary of new analyses by well.

Well name	Permeability		Porosity (plug)	Grain density (plug)	Thin section	XRF	XRD	SEM
	(probe)	(plug)						
Conoco 145-1	--	--	--	--	1	1	1	--
COST B-2	17	15	15	15	18	15	17	5
COST B-3	12	6	6	6	13	13	13	4
COST G-1	8	4	4	4	7	5	6	2
COST G-2	3	2	2	2	2	2	2	--
Exxon 599-1	2	1	1	1	3	4	3	--
Exxon 684-1	10	4	4	4	10	10	8	4
Exxon 684-2	1	1	1	1	1	1	--	--
Mobil 544-1	12	1	1	1	12	11	12	1
Shell 273-1	2	--	--	--	2	2	1	--

Well name	Permeability		Porosity (plug)	Grain density (plug)	Thin section	XRF	XRD	SEM
	(probe)	(plug)						
Shell 372-1	2	--	--	--	2	1	1	--
Shell 586-1	2	1	1	1	1	1	1	1
Shell 587-1	1	--	--	--	1	1	1	--
Shell 632-1	3	1	1	1	3	3	3	--
Shell 93-1	1	--	--	--	1	1	1	--
Texaco 598-1	3	3	3	3	3	3	3	1
Texaco 642-1	2	1	1	1	2	2	2	--
Totals	**81**	**40**	**40**	**40**	**82**	**76**	**75**	**18**

XRF = X-ray fluorescence; XRD = X-ray diffraction; SEM = scanning electron microscopy.

Hydrologic Property Measurements

Seventy-four depth points were identified for analysis where core materials were available, including conventional core slabs, chips, slices, and sidewall cores. One-inch core plugs were cut for 40 samples of those materials and analyzed for porosity, permeability, and grain density by Core Laboratories. A total of 81 Pressure-Decay Profile Permeameter measurements were made at 75 depth points, 6 of which had duplicate measurements made on the same sample. Where possible, probe permeameter measurements were taken at the same depth point, or otherwise at the closest point, as the core plugs measured with the core measurement system instrument to allow for comparison of results from these methods.

Thin-Section Preparation and Analysis

Upon completion of the hydrologic property analyses by Core Laboratories, remaining sample materials were returned to the DGS. These materials were then shipped to Wagner Petrographic for thin-section preparation. The samples were impregnated with blue epoxy, and thin-section slides were prepared. One-half of each prepared slide was stained for potassium feldspar, plagioclase feldspar, and calcite, and the thin section was covered with a coverslip. Eighty new thin sections, plus two previously prepared thin sections from the DGS repository, were sent to the PaGS for petrographic analysis of mineralogy and porosity. Petrographic analysis of these thin sections included the preparation of standard point counts, visual descriptions of porosity, and photomicrographs. In general, point-count analyses followed the Gazzi-Dickinson method for the measurement of framework grains and matrix spaces. Because the purpose of this work was also to describe the nature and extent of porosity in these samples, 10 specific pore types were also included as matrix space categories in the point counts. Each count targeted a minimum of 400 points to ensure 95% confidence. Those thin sections with counts of fewer than 400 either did not have a large enough area to perform a full count or were made up of very fine-grained material with indeterminable mineral content. Photomicrograph images were collected to document mineralogical composition, cementing materials, and porosity conditions.

X-ray Fluorescence

XRF analysis was carried out at the DGS by PaGS staff to determine quantitative bulk-rock geochemistry. Measurements were made using a handheld portable Thermo Scientific Niton XL3t GOLDD+ handheld analyzer. The XRF analysis allows for bulk compositional analysis to quantify the bulk concentrations of major, minor, and trace elements. The first two batches were analyzed on July 13 and July 20, 2017, prior to sample shipment to Core Laboratories. The last

batch was analyzed on December 5, 2017, after samples were returned from Core Laboratories and before shipment to Wagner Petrographic. The Thermo Scientific handheld analyzer was used to analyze 76 rock core samples. Analyses were conducted using the built-in TestAllGeo calibration. These XRF results add to the data available to make detailed comparisons between results from different analytical methods on samples from the same or close depths and in validating and interpreting both legacy and new data.

X-ray Diffraction Analysis

Semi-quantitative estimates of the bulk mineralogy of 75 rock core samples were determined using X-ray powder diffraction. The analyses were run using a PANalytical Empyrean X-ray diffractometer. The samples were loaded in 16-millimeter (mm)-diameter back-packed sample holders that were mounted in a sample spinner.

Analyses were performed with PANalytical HighScore Plus software and the ICDD PDF-4 database. Replicate analyses of nine samples were run as a test of precision. Semi-quantitative results were interpreted using the Rietveld method, which utilizes the whole X-ray pattern to find agreement between observed patterns and the published crystal structure data of the minerals through least-squares analyses. Quantities are then calculated based on these analyses. This method can account for such factors as preferred orientation and peak shape that can present problems in dealing with layered silicate minerals. The HighScore Plus software enabled the programming of an automated Rietveld procedure that took these factors into account and was therefore able to provide a level of precision sufficient for classifying the lithologies that were encountered.

Scanning Electron Microscope

Bulk mineralogy and porosity characteristics underwent further evaluation at the PaGS. Remaining billets from thin-section preparation were analyzed using a Hitachi S-2600N SEM with backscatter electron (BSE) and energy dispersive spectroscopy (EDS) detectors. The EDS system was manufactured by Gresham Scientific Instruments (now Teledyne e2v), and Quartz Imaging software was used for data acquisition and display. The SEM analysis produced individual and composite geochemical maps displaying distribution of aluminum (Al), calcium (Ca), iron (Fe), potassium (K), magnesium (Mg), sodium (Na), oxygen (O), sulfur (S), and silicon (Si). Operating conditions are reported with the images. Two maps each were created per sample. Images showing high-resolution crystalline texture and pore space geometry were also taken. Most samples were polished to improve image quality. Figure 4-2 shows sample images of BSE analysis results and composite element maps from EDS analysis for the COST B-2 and COST B-3 wells, highlighting properties such as composition, porosity, and cementation. The results identify the different lithologies of the samples and the composition of matrix and cement. This is invaluable in facilitating detailed comparisons between results from different analytical methods and to understanding the relationship of composition to measured porosity and permeability values.

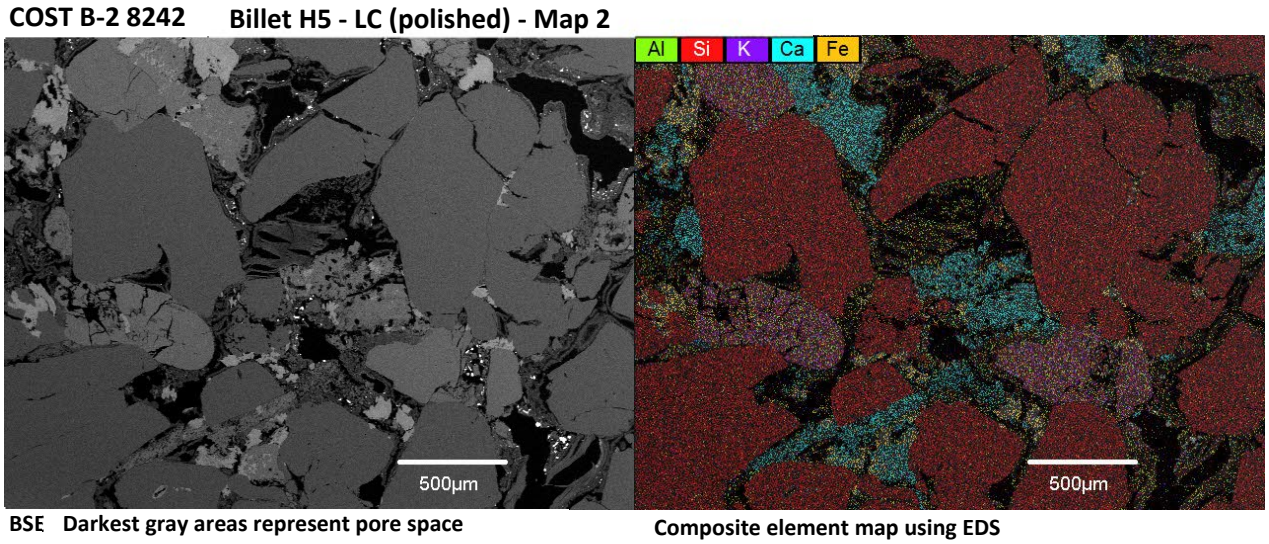

Figure 4-2. Sample SEM results from potential sandstone storage target in COST B-2 well.

Petrographic Analysis

Petrographic analysis of porosity and mineralogy was conducted on 82 standard thin sections from 17 different wells by the PaGS. Thin-section locations targeted various depths and lithologies in these wells to assess various potential reservoir and caprock characteristics. Porosity point counts (i.e., a proxy for volumetric porosity as a percentage) were prepared for each thin section as part of the petrographic analysis, including total porosity estimates and percentages of 10 different porosity types. For most of the relatively porous (>10%) samples, the largest component of the porosity volumes was intergranular porosity, commonly followed by grain/cement dissolution porosity. Comparisons of the new, laboratory-measured porosity data to the thin-section-based porosity measurements show that the laboratory measurements are much higher than the thin-section-based porosity estimates. The thin-section porosity and laboratory porosity measurements yield comparable numbers in some intervals, with the laboratory measurements overall slightly higher, most commonly in those samples with high percentage of visible porosity (i.e., macroporosity) such as intergranular and dissolution porosity. Thin-section analytical results were used to determine which samples warranted further scrutiny using SEM techniques. Figure 4-3 is an example of the observations made on framework grains, matrix, cementation, and porosity, which allow for a more robust assessment and characterization of potential storage targets and caprocks.

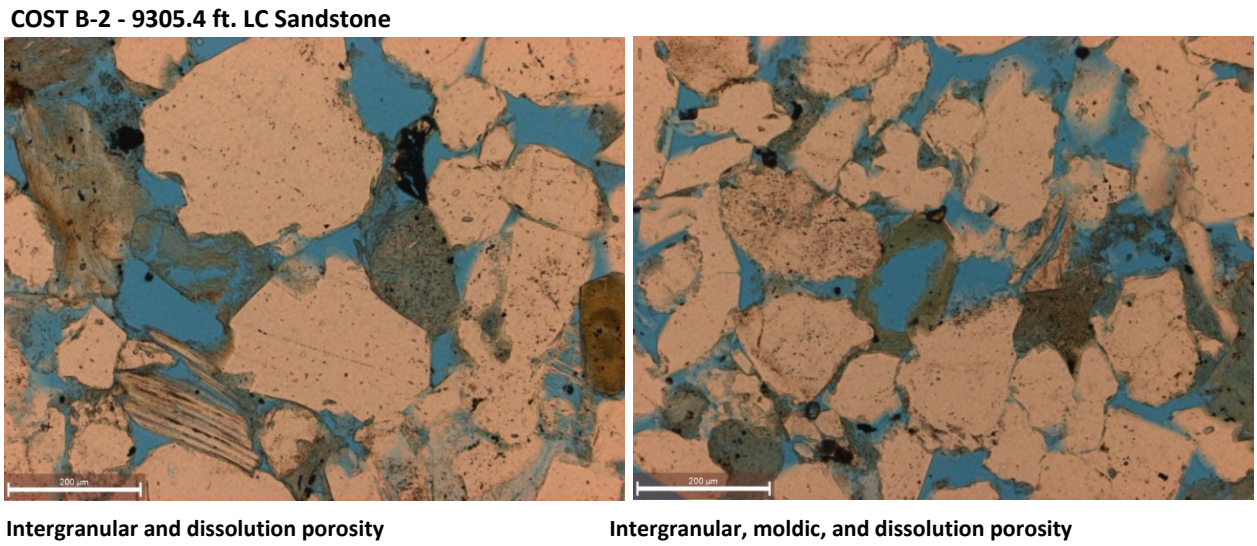

Figure 4-3. Photomicrographs from potential sandstone storage target in COST B-2 well showing different porosity types.

4.1.3 Hydrologic Properties Integration

The new analytical results were integrated with the mined legacy data spreadsheets and imported into the Microsoft Access database. This integration process involved assessing and validating each value through cross-comparison of mined legacy data with new data from all the studies performed. This work involved scrutinizing data values from core plug analysis (i.e., 40 analysis points each for permeability, porosity, and grain density), probe permeability (i.e., 81 analysis points), petrographic analysis (i.e., 82 analysis points), and mineralogical and geochemical analyses (i.e., 76 XRF analysis points, 75 XRD analysis points, and 18 SEM analysis points). These data were combined with the stratigraphic and petrophysical analyses. This large volume of data available, both from mined legacy data and new data generated specifically for this project, is applied and cross-correlated to allow for a robust interpretation and application of the data to storage resource assessments.

Initial results verify the observed variability; however, the more robust core plug measurements did not reproduce the highest permeability values (>1000 mD) at corresponding or close sample points, suggesting that these values needed to be scrutinized further when integrating all the available data. These steps—analysis, cross-validation, and integration of analyses results—proved to be crucial in the utilization of all the data for the project.

Some observations were made that informed how these data were applied for resource calculations as well as other project tasks. Generally, thin-section porosity estimates are lower than measured porosity, which may be due to the fact that point counting only accounts for visible porosity. This result suggests that microporosity may have a significant effect on the hydrologic properties of the units. Several samples where macroporosity dominates show closer correlation between measured and thin-section porosity values. This correlation is not observed where microporosity may be an important factor. Overall, these data were applied to other tasks as needed, such as stratigraphic analysis, well-log calibration and characterization, seismic inversion, and risk assessment; the results were integrated to validate and /or update previous and ongoing interpretation.

It is important to note that the analytical results provided in the Task 4 Topical Report (Attachment F) have provisional formation names assigned based on the stratigraphic picks that were available at the time of sampling using a lithostratigraphic approach that was developed to guide the selection of formation tops and bases from well-log signatures. After this effort was complete, sequence stratigraphy was used to correlate rock units across the study area, using seismic data where well data are not available. The provisional picks were subsequently revised as the seismic data evaluation and storage resource calculation tasks progressed. As a result, there will be differences in the formations assigned to some samples in the database as compared to the final reporting.

4.2 Key Accomplishments and Findings

The objective of the hydrologic property analyses conducted for this project was to assemble a comprehensive dataset from mid-Atlantic OCS wells that will support two of the project's main goals: to assess pore space available for CO_2 storage and to characterize the physical properties of potential storage zones and confining caprocks. Data were compiled on the porosity, permeability, and composition of sample materials. Work involved a comprehensive compilation of existing data from well reports and other publications as well as generation of new data from new laboratory analyses. The use of multiple methodologies for analysis of porosity, permeability, and sample composition allows for the understanding of rock properties at different scales and from different physical measures. Porosity was measured by laboratory tests of core plugs and examination of thin sections. Permeability was measured by laboratory measurements of core plugs and probe permeameter measurements on sample surfaces. Composition was measured using XRD of powdered samples, XRF measurements on sample surfaces, SEM of small sample surfaces, and examination of thin sections.

A large volume (>9,000 individual entries) of legacy hydrologic property data was assembled by mining well reports, documents, and published material. Gaps in the compiled data within the stratigraphic intervals of interest (i.e., Dawson Canyon to Mohawk) were assessed using an automated method built into a Microsoft Access database. This process was also used to assess the availability of samples at the DGS OCS repository to enable new analyses to be carried out to fill gaps in data coverage and validate existing data where applicable.

A series of workshops were held to plan sample analyses and to select samples. Seventy-five sample points from 17 wells were selected for analysis. Porosity, permeability, and grain density measurements carried out by a commercial laboratory yielded important new data that filled gaps in legacy data coverage and provided new analyses to verify legacy data of special interest. Petrographic, mineralogical, and geochemical analyses conducted at the PaGS generated additional porosity and compositional data that were used to understand the relationship of hydrologic properties and mineralogy of samples. In total, the new analyses provided 40 new data points for permeability, porosity, and grain density from core plug samples, 81 points of permeability measurement from probe permeameter analyses, 82 points with new porosity and mineralogy data measured in thin sections, and a large dataset of new instrumental measurements of sample mineralogy and geochemistry (i.e., 76 XRF analysis points, 75 XRD analysis points, and 18 SEM analysis points). The new hydrologic property data have been integrated with existing legacy data in a Microsoft Access database.

Overall, the results confirm that the most promising storage resources are in the LC and Missisauga Formations and that the Naskapi and Mic-Mac Formations are locally important as seals. The results also show that the units are heterogeneous, with stratigraphic and areal (i.e.,

geographic) variations in lithologies and hydrologic properties observed. These variations must be taken into consideration in the assessment of each unit.

The results of these analyses provide a basis for improved understanding of the potential storage resource and caprock units. Where legacy data were reproduced, the existing data were validated, which allows for confident application to other tasks such as well-log calibration and risk assessment. Where there are discrepancies, results from multiple analyses allow for scrutiny and validation of property values. Calibration of sample-based hydrologic property measurements to geophysical log data can be extended spatially in future work through the relationship of geophysical log data to seismic character. The large volume of both mined legacy data and new analytical data compiled for this project task, combined with stratigraphic and petrophysical analyses conducted for other project tasks, allows for a robust interpretation of hydrologic properties of the subsurface formations of the Atlantic OCS, resulting in insights that can ultimately be applied to the assessment of carbon storage resource volumes present in the study area.

5. Storage Resource Assessment

Storage resource assessment is a critical component of the site screening and characterization process necessary to advance development of deep geologic resources for CO_2 storage in a region. Regional static volumetric CO_2 storage estimates and simplified dynamic models are useful for delineating prospective storage targets at the basin or sub-basin scale, and therefore play a key role in the initial stages of site screening and selection for a geologic CO_2 storage project (DOE-NETL, 2017; Gorecki et al., 2015). CO_2 storage resource estimates were calculated at the regional and local scales using static volumetric and dynamic methods to establish screening-level constraints on deep saline CO_2 storage potential in the mid-Atlantic offshore study region.

Risk factors identified in Task 6, such as basin age and maturity, sediment lithification, and hydrostatic pressures, were integrated with recommended best practices for onshore geologic CO_2 storage (DOE-NETL, 2013) to develop the following screening criteria for offshore storage resource assessment:

- Formation depth must be adequate (i.e., approximately 1,000 m) to ensure (1) temperature and pressure conditions are sufficient to store CO_2 in a supercritical phase; and (2) the risk of soft sediment deformation is minimized.
- A suitable seal/caprock overlies the targeted storage zone to inhibit the vertical migration of CO_2 to the surface.
- Hydrogeologic conditions such as structural, stratigraphic, and hydrodynamic traps are present to retain the injected CO_2 within the targeted storage zone(s).

These screening criteria were used along with structural, stratigraphic, and petrophysical analysis to calculate offshore-specific storage efficiencies and CO_2 storage resources for three deep saline formations of interest.

The general workflow used for Task 5 storage resource calculations is shown in Figure 5-1. Geophysical logs from 44 existing offshore test well locations were scanned and digitized to inform interpretations of storage zone sequence stratigraphy, lithofacies, and petrophysical properties. Seismic and well-log sequence stratigraphy was used to define the structural and stratigraphic framework of the caprocks and storage zones. Biostratigraphic data provided age control to help align and correlate storage zone lithofacies with sequence boundaries. Log data was integrated with laboratory-derived core analyses to better characterize effective reservoir lithology, porosity, and permeability. The newly reprocessed seismic data provided by this project were also used to derive estimates of porosity in areas without well data.

The integrated dataset was used to develop regional depth, thickness, and porosity maps for each storage zone. Map grids served as input for regional-scale CO_2 storage resource calculations using the static volumetric methodology and CO_2-SCREEN tool (Sanguinito et al., 2016) developed by DOE-NETL (Goodman et al., 2011; 2016) for onshore deep saline formations. Offshore formation-specific storage efficiency values were determined using regional geospatial and statistical distributions of net-to-gross reservoir pore volume and permeability for the three storage zones of interest. Regional results were mapped, and locations exhibiting high CO_2 storage resource (≥ 2.5 Mt CO_2/km^2) constrained by data from three or more nearby wells were selected for dynamic simulation. Offshore geologic storage resources were classified and categorized following industry-standard guidelines established by

the Society of Petroleum Engineers (SPE) Storage Resources Management System (SPE, 2017) .

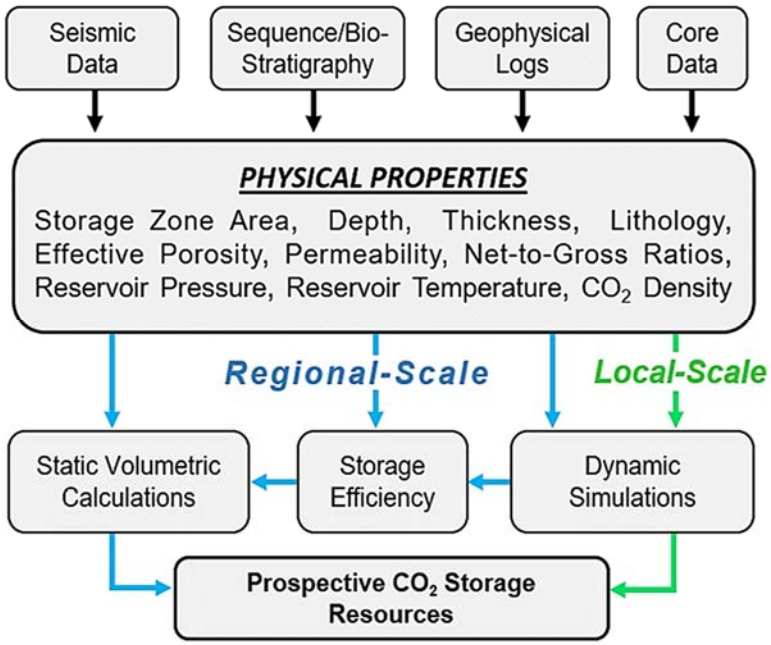

Figure 5-1. Schematic showing data input and workflow used for estimating offshore CO_2 storage resources in Task 5.

The topical report associated with this task, which describes the methodologies for data integration and mapping, petrophysical analysis, and storage resource calculations, is provided in Attachment G.

5.1 Storage Zone Reservoir Properties

Regional interpretation and correlation of seismic data was used to define the structural and stratigraphic framework of offshore Cretaceous and Jurassic sequences, with three storage zones and two caprocks identified in the BCT (Figure 5-2), and three storage zones and three caprocks identified in the GBB. Interpreted seismic horizons from Task 2 and 3 were depth converted, tied to nearby wells, and integrated into a continuous, interpolated 2D grid surface to derive regional structure and thickness maps for each zone of interest. A quality assurance/quality control (QA/QC) procedure was performed to ensure seismic horizons, biostratigraphic markers, well-log sequence stratigraphic picks, and well-log lithostratigraphic picks were consistent to within ± 100 m.

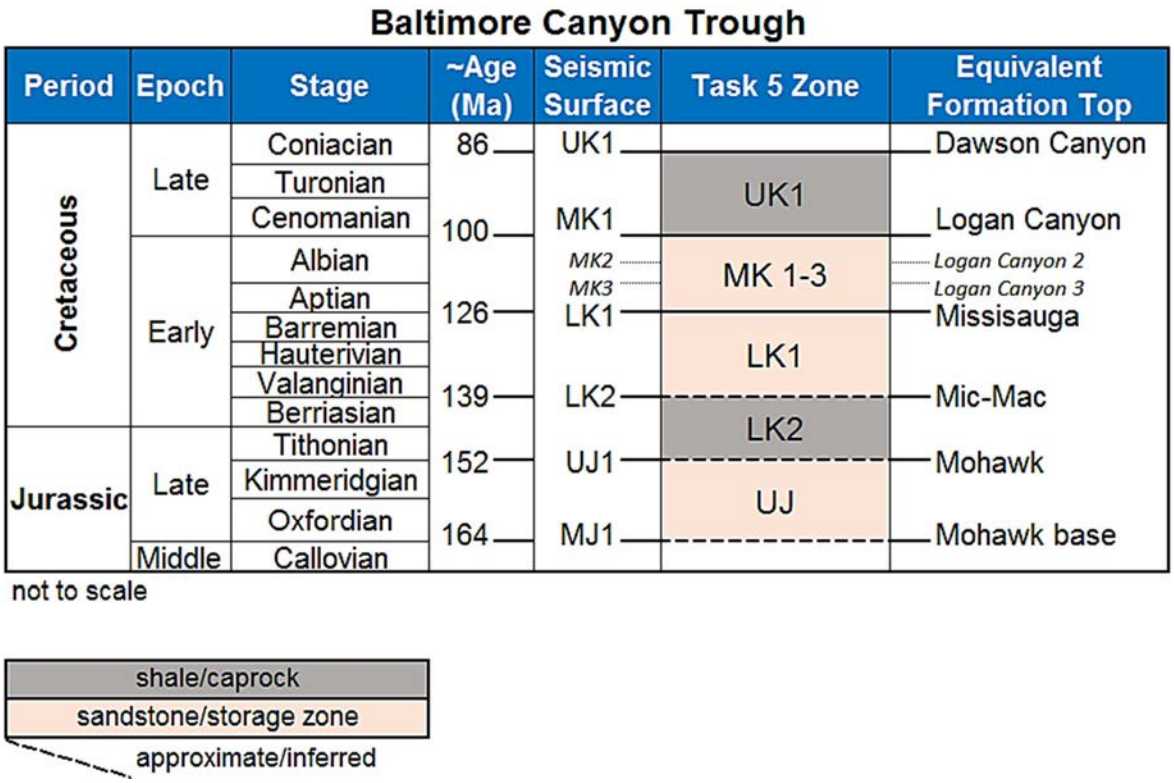

Figure 5-2. Correlation of chrono-, sequence-, and seismic stratigraphy and formation tops used to define Task 5 storage zone tops and bases for the BCT.

Core porosity, permeability, and grain density data from the Hydrologic Properties Database were used to correct/calibrate log data and quantify lithologic and petrophysical properties of the three storage zones. Cross-plots of porosity and permeability were then generated from 914 unique laboratory-derived core measurements to derive permeability transforms for the three storage zones of interest (Figure 5-3).

Total and net reservoir intervals were quantified and mapped using lithofacies logs to delineate clean sandstone reservoir intervals and using permeability as a proxy for connected pore volumes. Lithofacies logs generated via integration of core mineralogy and GR log data were also used to calculate effective porosity curves. The effective porosity logs were then calibrated to core porosity data and used to generate permeability curves using the transform relationship shown in Figure 5-3 for each storage zone. Twenty pseudo-wells were created to better constrain porosity map grids in areas with well data gaps. Average effective porosities from the three nearest wells were assigned to storage zones in 15 pseudo-wells. Porosities derived from seismic inversion methods were used to characterize storage zones in five pseudo-wells.

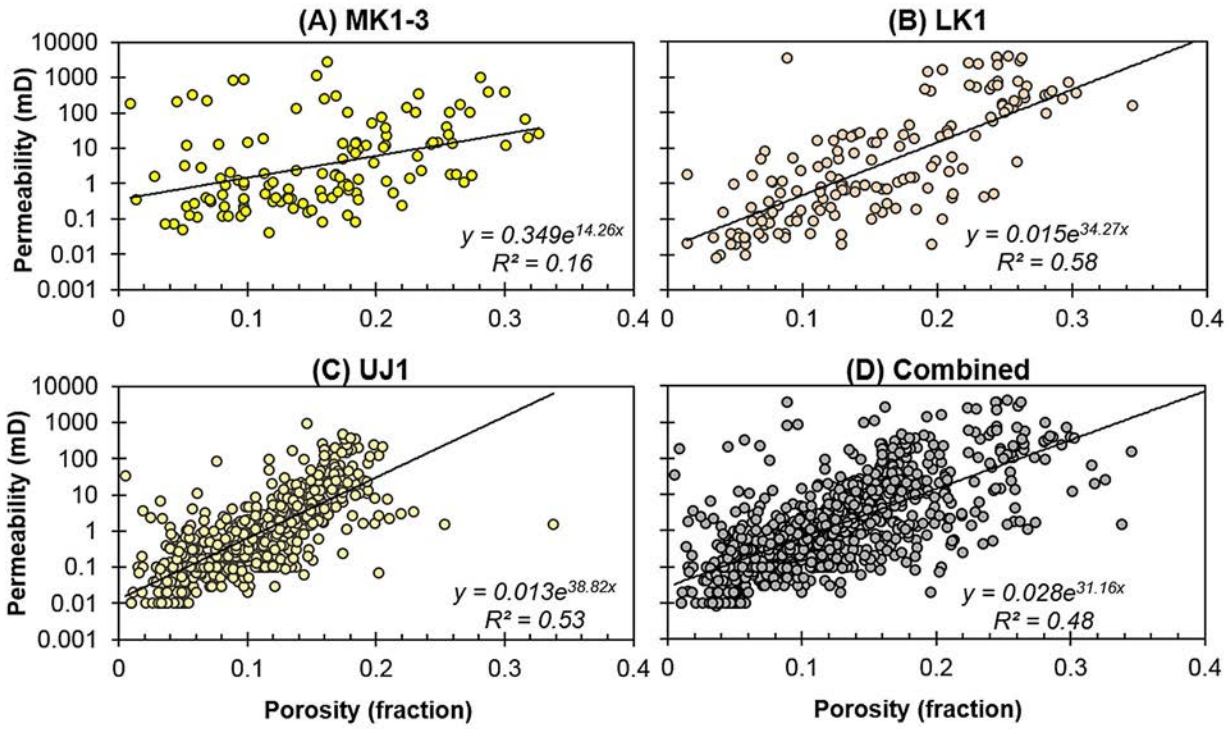

Figure 5-3. Porosity-permeability transforms derived from core data for (A) the MK1-3; (B) the LK1; (C) the UJ1; and (D) all three storage zones combined.

Using a permeability cut-off of 10 mD or greater and a lithologic cut-off for clean sandstone, petrophysical properties were calculated and mapped to generate regional 2D grids representing the total reservoir pore volume in each storage zone. The associated means and standard deviations (σ)[1] of the total reservoir pore volume grids for in each storage zone are shown in Table 5-1. The MK1-3 exhibits an average thickness of 181 m and an average effective porosity of 23%, covering a total area of 92,928 km^2. The resulting total reservoir pore volume for the MK1-3 grid is 3,668 km^3. The LK1 zone has a total area of 117,493 km^2, with an average thickness of 154 m and an average effective porosity of 26%, resulting in a total reservoir pore volume of 4,635 km^3. The UJ1 zone exhibits the largest area and thickness of the three zones evaluated, resulting in a total reservoir pore volume of 6,511 km^3. Mean permeabilities of the total reservoir intervals range from 45 mD in the UJ1 to 71 mD in the MK1-3 zone.

Table 5-1. Total reservoir pore volume (sum) and mean petrophysical properties calculated from the regional grid data (n=300 cells) for each storage zone[2].

[1] Geometric means and standard deviations are reported for permeability to better represent the lognormal distribution expected for effective permeability in heterogenous formations (Jensen et al., 2000; Mishra and Datta-Gupta, 2018). Arithmetic means and standard deviations are reported for grain density and porosity.

[2] The total pore volumes reported are calculated directly as the *sum* of the 300 grid cells. Total pore volumes calculated using the *mean* grid values will be slightly different and less accurate.

Storage Zone	Area (km²)	Thickness (m)		Effective Porosity (%)		Permeability (mD)*		Total Pore Volume (km³)
		Mean	σ	Mean	σ	Mean	σ	
MK1-3	92,928	181	112	23	2	71	4	3,668
LK1	117,493	154	82	26	3	65	4	4,635
UJ1	134,578	211	292	21	2	45	3	6,511

*geometric mean and standard deviation

A second permeability cut-off of 100 mD or greater was then applied to estimate the net effective (i.e., connected) reservoir pore volume to be occupied by CO_2 and derive formation-specific storage efficiency values. The 100 mD or greater cut-off is intended to account for uncertainty in the estimated net pore volume available for CO_2 storage, and represents an order of magnitude of potential error in the permeability curves calculated from porosity-permeability transforms. The effective pore volume and petrophysical properties associated with the net reservoir interval in each storage zone are summarized in Table 5-2. Relative to the LK1 and UJ1 storage zones, the net reservoir interval in the MK1-3 zone exhibits the highest average net thickness of 55 m and the smallest net area of 79,918 km^2, with an average net effective porosity of 27% and a net reservoir pore volume of 1,371 km^3. The LK1 exhibits the largest net area (117,102 km^2), highest average net effective porosity (29%), and largest net reservoir pore volume (1,430 km^3) of the three storage zones evaluated. In contrast to the ≥10 mD cut-off used for total pore volume calculations, the ≥100 mD cut-off in the UJ1 zone results in the lowest net thickness (32 m) and smallest net reservoir pore volume (1,049 km^3) of the three storage zones. Mean permeabilities of 264 mD, 314 mD, and 339 mD are estimated for the net reservoir intervals in the UJ1, MK1-3, and LK1, respectively.

Table 5-2. Net reservoir pore volume (sum) and mean net petrophysical properties calculated from the regional grid data (n=300 cells) for each storage zone.

Storage Zone	Net Area (km²)	Net Thickness (m)		Net Effective Porosity (%)		Net Permeability (mD)*		Net Pore Volume (km³)
		Mean	σ	Mean	σ	Mean	σ	
MK1-3	79,918	55	64	27	3	314	2	1,371
LK1	117,102	40	45	29	5	339	3	1,430
UJ1	88,372	32	41	25	8	264	3	1,049

*geometric mean and standard deviation

5.2 Regional Static Storage Resource Calculations

Static CO_2 storage calculations use subsurface pore volume estimates and storage efficiency coefficients to derive an equivalent quantity of CO_2 that could be stored in a formation. Regional static storage resource estimates were calculated stochastically using a volumetric approach and offshore-specific storage efficiency values, with uncertainty reported statistically as P10, P50, and P90 results. Storage efficiency was evaluated in terms of geologic and displacement efficiency using statistical distributions from regional net-to-total pore volume grid data and outcomes from 90 numerical injection simulations representing a range of deep saline formation (MK1-3) properties/conditions observed in the offshore study region.

The low (P10), median (P50), and high probability (P90) values derived for geologic and displacement efficiency components are shown in Table 5-3. The geologic efficiency values from the combined net-to-total pore volume dataset from the three storage zones range from 0.10 (P10) to 0.58 (P90), with a median value of 0.31. The geologic efficiencies for the MK1-3 zone exhibit the largest probability range. A P50 value of 0.36 is observed in both the MK1-3 and LK1 zones. UJ1 exhibits the smallest geologic efficiency values and probability ranges of the three storage zones. Offshore-specific displacement efficiencies range from 0.09 to 0.26,

with a P50 value of 0.18. Using the combined dataset of geologic and displacement efficiency values from the three storage zones, the resulting total storage efficiency (E_{saline}) estimates exhibit a range of 0.01 to 0.11 and a P50 value of 0.04 (Table 5-3).

Table 5-3. Storage efficiencies of offshore storage zones and comparison with onshore values.

Storage Zone	Geologic Efficiency			Displacement Efficiency			Total Storage Efficiency (E_{saline})		
	P10	P50	P90	P10	P50	P90	P10	P50	P90
MK1-3	0.09	0.36	0.70	0.09	0.18	0.26	0.01	0.05	0.13
LK1	0.12	0.36	0.59	not analyzed	not analyzed	not analyzed	0.02	0.05	0.11
UJ1	0.08	0.19	0.38	not analyzed	not analyzed	not analyzed	0.01	0.03	0.07
Offshore Combined	0.10	0.31	0.58	0.09	0.18	0.26	0.01	0.04	0.11
DOE-NETL Clastics*	0.05	0.15	0.33	0.07	0.14	0.24	0.01	0.02	0.05

*Goodman et al., (2011; 2016).

Table 5-3 and Figure 5-4 show storage efficiency P-values determined in this study compared to those reported by the DOE-NETL for onshore clastic deep saline formations. Higher P50 values and larger probability ranges are observed in offshore geologic and total storage efficiency results relative to those reported for onshore clastic formations. This result may reflect greater variation in sediment compaction and lithification in offshore environments, which could contribute to higher porosity and permeability relative to onshore basins. Offshore displacement efficiencies exhibit slightly higher P50 values and the same range as onshore formations.

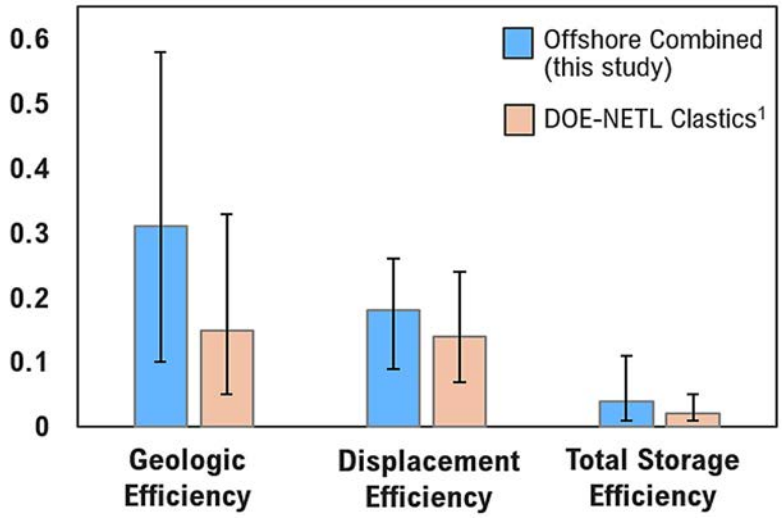

Figure 5-4. P50 storage efficiency values determined in this study compared to those reported by the DOE-NETL. Error bars represent the P10 and P90 values.

Regional grid data representing total reservoir pore volumes were used as input along with the formation-specific storage efficiency p-values to estimate and map the CO_2 storage resources of each offshore storage zone. The regional-scale storage resources estimated for MK1-3 range from 37 Gt (P10) to 378 Gt (P90), with a P50 value of 148 Gt (Figure 5-5A). The highest storage resources were calculated for the LK1 zone, with estimates exhibiting a range of 59 to 403 Gt (Figure 5-5B). Low and high values of 54 Gt and 355 Gt were calculated, respectively, for the UJ1 zone, representing the smallest probability range of the three offshore storage zones evaluated (Figure 5-5C). For comparison, annual CO_2 emissions from power generation and industrial sources in the eastern United States were approximately 0.15 Gt in 2016 (Battelle, 2018). Even with CO_2 emission expected to increase by an average of 6% annually (EIA, 2018),

P10 values of 37 to 59 Gt suggest a high probability that the offshore storage resources evaluated could accommodate commercial quantities of CO_2 emitted from nearby point-sources in the mid-Atlantic region for decades.

The regional spatial distribution of P50 storage resources estimated for the MK1-3 zone is shown in Figure 5-5A. The highest storage resource values (≥2.5 Mt CO_2/km^2) occur in the northern BCT near the GSD. P50 values ≤0.2 Mt CO_2/km^2 occur along the southeastern extent of the MK1-3 map boundary. LK1 storage resource values ≥2.5 Mt CO_2/km^2 (P50) are also observed in the northern BCT near the GSD (Figure 5-5B). The P50 storage resource map for the UJ1 zone exhibits values of 3.2 Mt CO_2/km^2 and higher in the northern BCT, with estimates decreasing to 0.2 Mt CO_2/km^2 along the southeastern margin of the study area (Figure 5-5C).

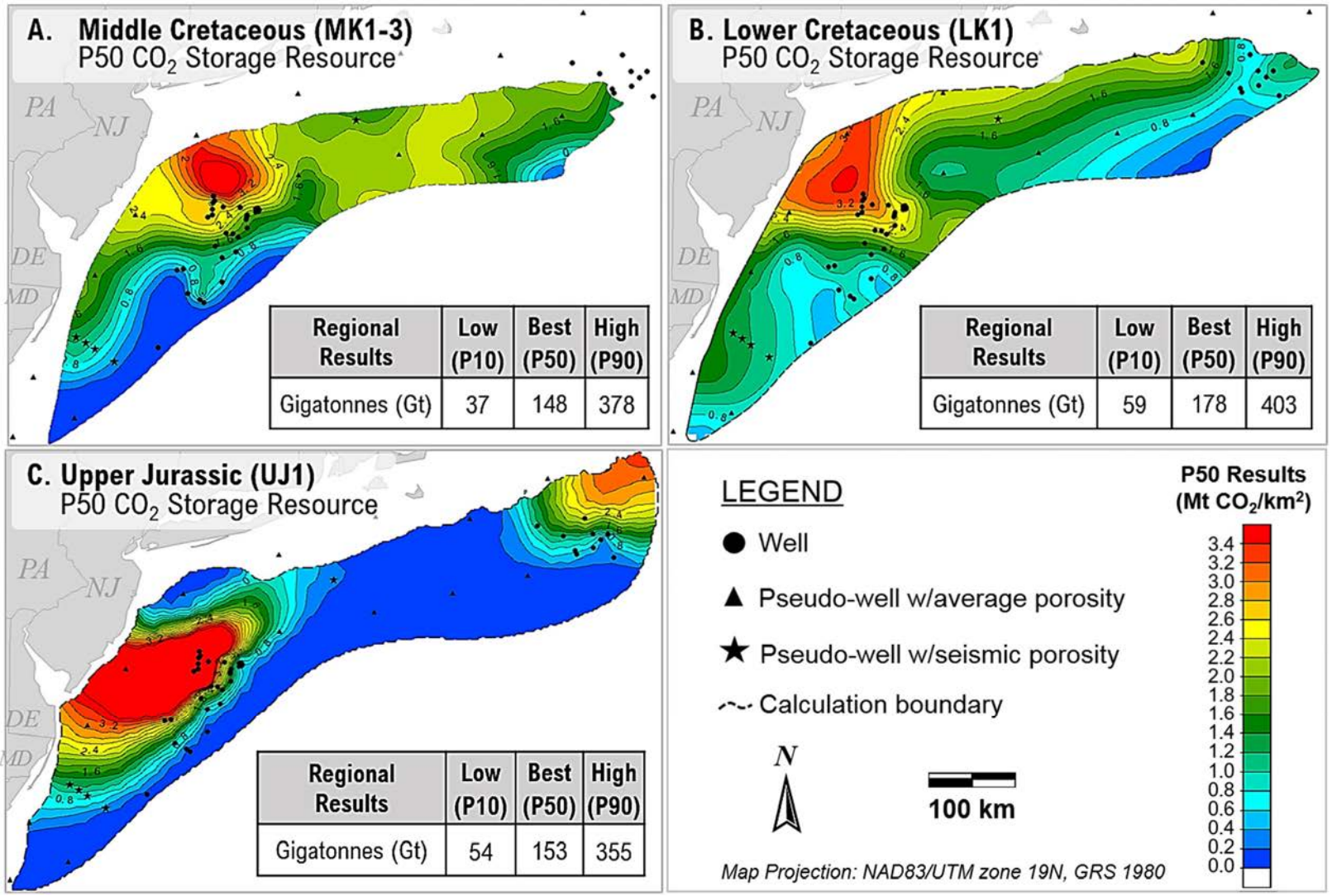

Figure 5-5. The regional P50 static storage resource maps for (A) the MK1-3 zone, (B) the LK1 zones, and (C) the UJ1 zone. The total calculated P10, P50, and P90 estimates are also shown for each storage zone.

5.3 Local Dynamic Storage Resource Simulations

The area near the GSD in the northern BCT was selected to simulate CO_2 injection and storage performance under specific pressure, time, and operational constraints via simplified dynamic modeling. A 3D site model covering an area of 596 km^2 was delineated by net thicknesses ≥100 m and effective porosities ≥20% for the Cretaceous-Jurassic interval extending from the MK1-3 to the base of the UJ1 (Figure 5-6). The model injection well was positioned in the area with the highest net thickness, between three existing wells on the eastern margin of the GSD. An interval at the top of the MK3 zone having an average net thickness of 51 m was identified as the most vertically and laterally continuous net pay interval (GR <75 gAPI, permeability ≥100 mD, continuous pay thickness ≥6.1 m) within the Cretaceous-Jurassic section of interest and was selected as the model injection zone (Figure 5-7).

Three scenarios were evaluated for the 30-year simulation timeframe: (1) a maximum injection scenario where injection rates are varied to maintain maximum injection pressures based on an assumed fracture pressure gradient of 14.7 kPa/m; (2) a reference case using an injection rate of 1.5 Mt CO_2/year; and (3) a variant case using a rate of 1.0 Mt CO_2/year.

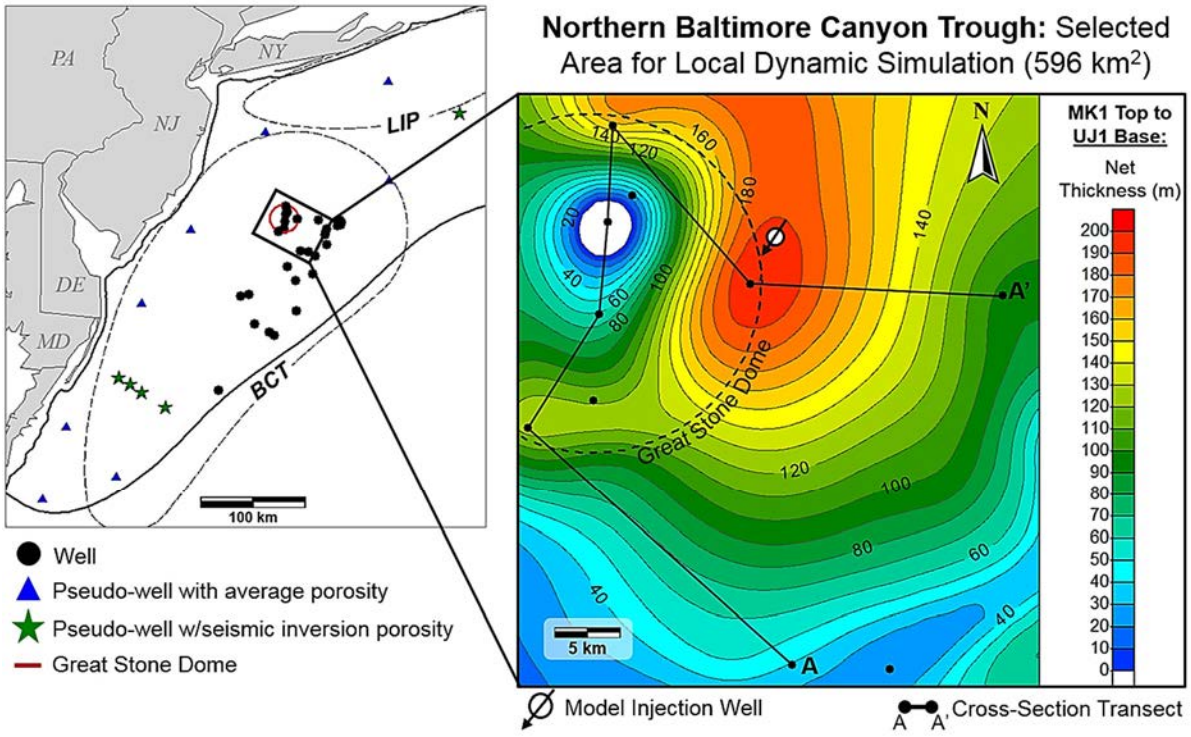

Figure 5-6. Local area in the northern BCT selected for dynamic CO_2 injection simulation.

The maximum amount of CO_2 that could be injected over a 30-year period was found to be 51 Mt for injection rates corresponding to the maximum allowable injection pressure of 31,000 kPa measured at bottom-hole conditions. In both the reference and variant case, 45 and 30 Mt of CO_2 were able to be injected and stored over 30 years, respectively, without reaching the maximum allowable bottom-hole pressure constraint (Figure 5-8). The resulting CO_2 plume had an area of 32 km^2 (6.4 km diameter) at the end of the 30-year the injection period.

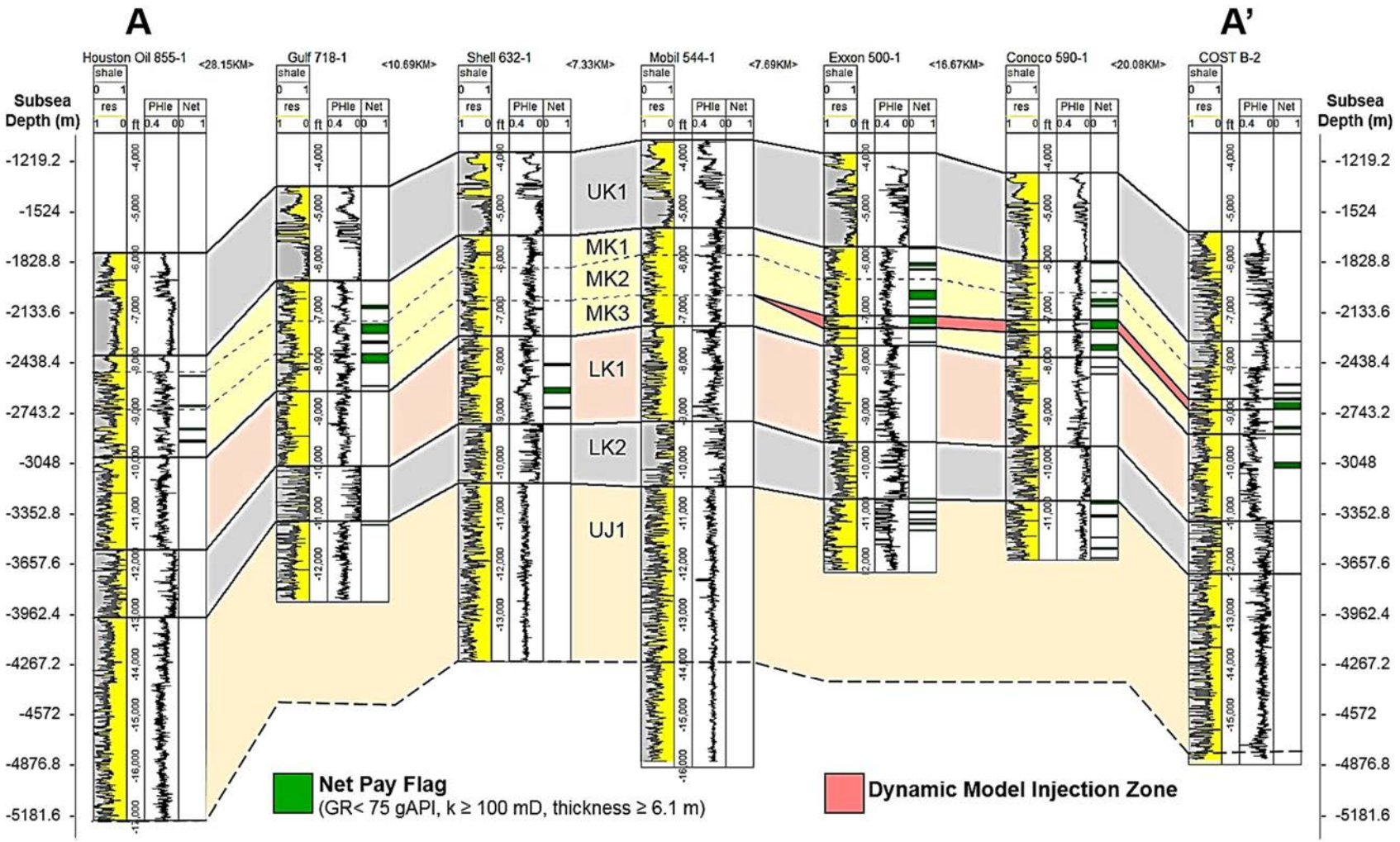

Figure 5-7. Structural cross section (see Figure 5-6 for areal transect) across the GSD showing net pay flags calculated over the three storage zones and the selected injection zone for the dynamic reservoir simulation at the top of the MK3.

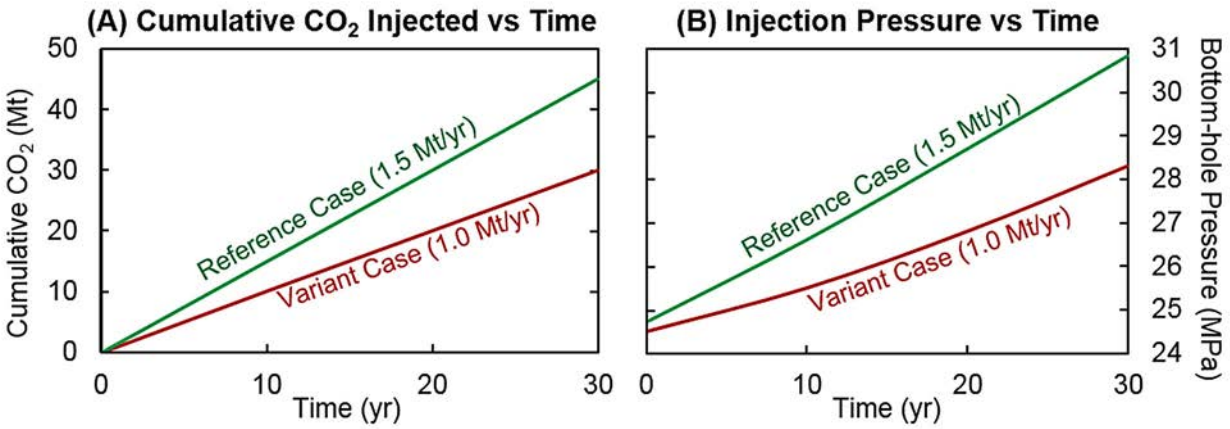

Figure 5-8. Results of the reference and variant injection scenarios showing (A) cumulative CO_2 injected and (B) bottom-hole injection pressure response for the 30-year simulation timeframe.

In 2016, there were 39 power plants and five petroleum processing facilities with emissions greater than 1 Mt per year in the eastern United States (see Section 6.3). The preliminary dynamic simulation results for the reference and variant injection scenarios suggest a 51-m-thick zone in the MK3 sandstone sequence could accommodate injection of annual and 30-year cumulative CO_2 emissions from an individual nearby power plant or industrial source. Net pay flags were also observed in the MK1, MK2, LK1, and UJ1 zones within the selected area near the GSD, with the MK2 net pay flag exhibiting lateral and vertical continuity comparable to that observed in the MK3 model injection zone (Figure 5-7). These findings suggest that stacked storage could potentially enhance commercial-scale CO_2 storage resources in the selected area. Results from the local-scale dynamic injection and storage simulation in this study are consistent with results of previous work that suggest large-scale CO_2 storage is feasible in the northern BCT (Slater et al., 2010; Brown et al., 2011; New Jersey Geological Survey, 2011).

5.4 Key Findings

The SPE's CO_2 Storage Resources Management System has been adopted to communicate project risk and commercial potential to investors using an industry-standard classification framework. The results derived from static and dynamic assessment methods employed in this study are categorized as prospective storage resources. Prospective storage resource estimates do not account for regulatory issues or system-wide techno-economics of a CCS project. Regional storage resources reported in this work can be classified at the "Play" level in terms of project maturity. Advancing to the "Lead" level would require identification of a prospective drilling target, which could be accomplished via development of a 3D static earth model to better characterize the geospatial variability of accessible pore volumes, reservoir injectivity, and trapping mechanisms in the selected area of the GSD.

As part of the Storage Resource Calculation task, a systematic workflow has been employed to quantify and categorize CO_2 storage resources for the mid-Atlantic U.S. offshore region extending from Maryland to Massachusetts. Results of this work suggest offshore storage resource estimates should be based on comprehensive data integration methods that incorporate analysis of risks and other factors unique to offshore environments, such as immature basin conditions, sediment lithification, and formation-specific storage efficiencies. Other key outcomes and findings from Task 5 are summarized as follows:

- Detailed characterization of key petrophysical properties (e.g., pore volume, permeability) for the three potential storage zones suggests targeted reservoir intervals contain average porosities ranging from 21% to 29%, and mean permeabilities ranging from 45 mD to 339 mD. These values are within the range of porosities and permeabilities reported for other offshore reservoirs currently being used or evaluated for commercial-scale CO_2 storage (Norwegian Petroleum Directorate, 2011; 2013; Trevino and Meckel, 2017).
- Offshore formation-specific probability ranges were determined for geologic and displacement efficiencies based on an integrated dataset of regional core, log, seismic, and biostratigraphic data. The total storage efficiency of the combined Cretaceous-Jurassic interval of interest ranged from 0.01 to 0.11, with a P50 of 0.04.
- Regional prospective storage resources were calculated and mapped, and results from the three storage zones range from 37 Gt to 403 Gt of CO_2. In all three storage zones, storage resources of 2.5 Mt CO_2/km^2 or greater are observed in the northern BCT near the GSD structure (e.g., Figure 5-9).
- Preliminary results of simplified dynamic reservoir simulation performed for one 51-m-thick net reservoir interval within the MK3 sequence near the GSD suggest approximately 30 Mt to 51 Mt of CO_2 could be stored over 30 years for the specific injection scenarios and pressure constraints evaluated.
- Both the regional static storage resource calculations and local-scale dynamic simulation suggest a high probability that the storage resources of the three storage zones evaluated could accommodate commercial quantities of CO_2 emitted from nearby power plants or industrial sources in the mid-Atlantic region for decades.

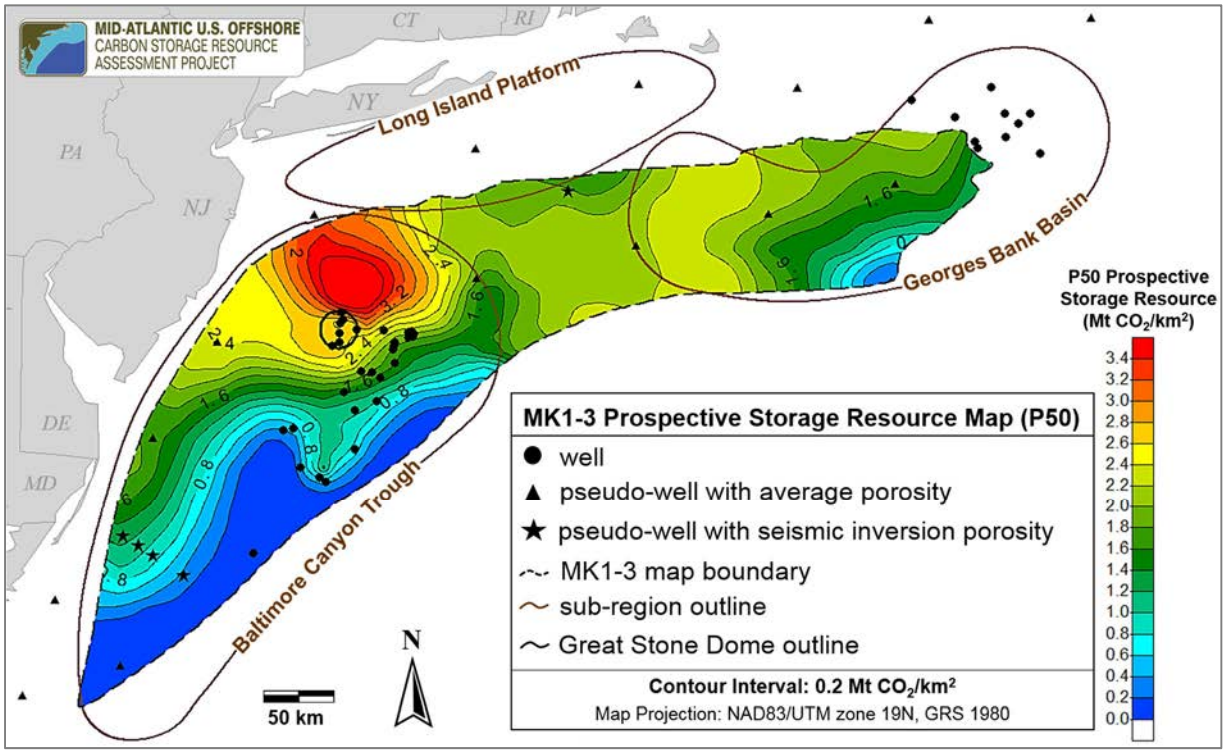

Figure 5-9. Map showing well locations, the three subregions, and the GSD outline alongside prospective storage resource estimates in Mt CO_2/ km^2 for MK1-3 zone.

Recommendations for Further Study

Preparation of this regional storage resource assessment is seen as the first step in analyzing and building the knowledge infrastructure necessary to drive offshore CCS forward. Given the findings reported herein, meaningful next steps should include the following:

- Acquire and analyze additional subsurface data to reduce uncertainty and close data gaps within each of the offshore subregions.
- Identify potential injection site(s) through careful consideration of geologic, environmental, cultural and economic conditions in prospective areas.
- Develop a 3D static earth model, which would help to better characterize the geospatial variability of accessible pore volumes, reservoir injectivity, caprock/confining mechanisms, and estimated storage resources in the selected area(s).
- Consider potential regulatory pathways, storage site requirements, and affected communities in the mid-Atlantic region even as the selected area(s) is (are) being assessed from a resource standpoint.

These activities will carry the current “Play” level assessment through the “Lead” level to the “Prospect” level. With the necessary knowledge and technology infrastructure in place, offshore carbon storage can be implemented.

6. Risk Factor Analysis

The Task 6 Risk Factor Analysis completed an initial assessment of technical risk factors present in mid-Atlantic offshore areas that may affect CO_2 storage resource estimates in terms of geologic storage processes, long-term potential for CO_2 migration, and environmental factors for deployment of an offshore carbon storage project. The risk analysis was based on results from previous tasks on hydrologic characterization, seismic interpretation, geologic mapping, and previous research on the offshore mid-Atlantic. Results were used to constrain CO_2 storage resource calculations and provide guidance for future exploration and development activities for CO_2 storage along the offshore mid-Atlantic. The risk analysis benefited from previous research on risk assessment for CO_2 storage (DOE-NETL, 2011; Savage et al., 2004; WRI, 2008; Pawar et al., 2014) and offshore carbon storage (Brown, 2017; Hannis et al., 2017; IEAGHG, 2016; Blackford et al., 2014; Leighton & White, 2012). At this early stage of CO_2 storage resource assessment, the analysis was centered on a qualitative review of risk factors rather than a more formal risk assessment or probability-consequence evaluation.

The topical report associated with this task is included as Attachment H.

6.1 Offshore Geological Risk Factors

Geological risk factors were analyzed for the study areas based on geotechnical data, geologic features, and hydrologic conditions. The information was used to constrain resource estimates in terms of depth and spatial extent.

Geological Setting- The GBB, LIP, and BCT geologic structures contain sequences of sedimentary rocks deposited over four geologic time periods: the Paleogene (23 to 66 Ma), the Cretaceous (66 to 145 Ma), the Jurassic (145 to 201 Ma), and the Triassic (252 to 201 Ma). More recent unconsolidated marine sediments and Neogene deposits are present at the shallow seabed. Total thickness of the sediments varies from less than 200 m (700 ft) near the coastline to more than 7,600 m (25,000 ft) in the trough areas. Rifting occurred during the late Triassic to earliest Jurassic (230 to 198 Ma) followed by extrusion of early Jurassic seaward-dipping basalts. Seafloor spreading began prior to the Callovian (~165 Ma; middle Jurassic), with the likely opening beginning off Georgia ca. 200 Ma and progressing northward off the mid-Atlantic margin by ca. 180 Ma (Withjack et al., 1998). Post-rift history was generally dominated by passive thermoflexural subsidence and loading. The U.S. mid-Atlantic offshore is a classic passive continental margin (i.e., there is sedimentation occurring above an inactive plate boundary). This tectonic setting poses inherently fewer operational and long-term storage risks than an active margin with crustal subduction or extrusion and the associated hazards such as earthquakes, faults, and volcanic activity.

Lithology- The offshore basins contain a thick succession of Paleogene-to-Jurassic sedimentary rocks above crystalline basement at depths of 5 to 15 km (3 to 9 mi). The sedimentary rocks consist of layers of mudstone, shales, sandstone, carbonates, and evaporites that dip to the east-southeast toward the continental slope (Libby-French, 1984). Sedimentary rocks overlie deeper rift basin strata, early Jurassic flows and sills, continental crust, and oceanic crust. Younger quaternary clay, siltstone, and sand overlie the Paleogene-Triassic sedimentary rocks, with ocean sediments present at the ocean floor. Local structures such as igneous intrusions, salt diapirs, growth faults, and escarpments are present in portions of the mid-Atlantic offshore region.

Structural Features- Reconnaissance of 2D seismic lines and review of existing literature were conducted to determine general trends in structural features and faulting within the study areas.

The present-day seafloor structure contains a broad and relatively flat shelf, an area with steeper gradient commonly referred to as the slope, and a rise which grades more gently seaward to the abyssal plain (Brothers et al., 2013). The outer shelf edge is a relic of the Eocene-Miocene carbonate ramp and is not related to the paleo shoreline (Steckler et al., 1982). The other main structural feature present in the study area is the GSD, a sedimentary dome structure related to a Cretaceous age igneous intrusion in basement rocks. Situated in the BCT, this four-way structural closure covers an area of 400 km^2 (200 mi^2) and has 270 m (890 ft) of relief, which made it a target for oil and gas exploration in the 1970s.

Faults have been identified on seismic data by the vertical offset of horizontal parallel reflections or the presence of a relatively isolated vertical trending zones. In general, extensional mode normal faulting is observed in the subsurface near the structural shelf break, at the terminus of the buried carbonate reefs, and along the continental rise. Figure 6-1 shows a seismic cross section from northern GBB, exhibiting normal faults with offset likely less than 300 m (1,000 ft), consistent with trends across the study area. The faults offset parallel and sub-parallel reflections below the Upper Cretaceous horizon through high-amplitude, chaotic seismic facies at depth interpreted as carbonate reef material. BCT faulting along the structural shelf break continued into the Miocene, evidenced by the offset of the expanded Miocene section. Normal faults sole out into high-amplitude reflections, likely representing carbonate reefs as seen in GBB. Faults in BCT appear to have more listric characteristics compared to those in GBB and exhibit sediment growth on the downthrown side (Figure 6-1).

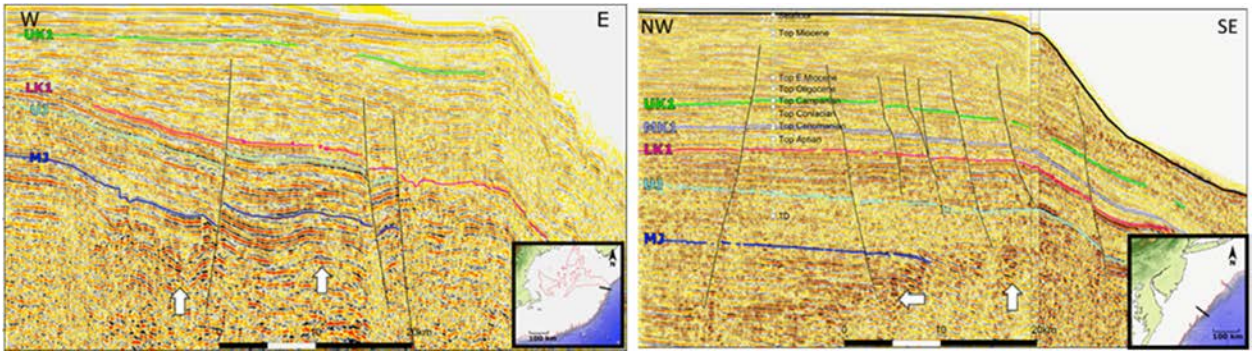

Figure 6-1. West- to east-trending seismic cross section along structural dip within GBB (left) and Northwest- to southeast-trending seismic cross section along structural dip within BCT (right).

Outer Continental Shelf Factors- A variety of features may be present along the OCS seafloor that are indicators of risk factors for exploration activities, subsurface storage, and project construction. Seawater along the shelf is 25 to 200 m (80 to 700 ft) deep, a relatively shallow depth, which reduces challenges associated with deepwater drilling and equipment. The seafloor features reflect a combination of many Quaternary glacial erosion, deposition, and subsidence events related to eustatic sea-level changes (Brothers et al., 2013). Portions of the shelf are dissected by channels and canyons. More substantial relief and mass flow features are present along the slope and continental rise.

As described by Kramer & Shedd (2017), high-resolution seabed image analysis may show the presence of features related to subsurface geologic features such as gas pockmarks, salt domes, faulting, folding, escarpments, slump blocks, slides, canyons, channels, and gas chimneys. These items may be indicators of deeper geologic structures, gas migration, and other geological risk factors for CO_2 storage applications. To examine continental shelf features on the seabed, high-resolution bathymetry data were mapped and inspected for geomorphic features that may be indicators of subsurface geological processes or structures (Figure 6-2).

The relief model was examined in more detail for indicators of more localized features, and there are few indications of extensive features like pockmarks, gas chimneys, faulting, salt domes, or sediment deformation. Along the slope, many more steeply incised canyons, mass flows, and escarpments were evident. More detailed seabed surveys would be necessary to determine site-specific features. Active methane venting has been investigated along the mid-Atlantic continental shelf edge (Newman et al., 2008), noting some active venting sites present as elongate pockmarks on kilometers in scale located near the shelf/slope margin and are elongated parallel to the shelf edge with steep landward walls (Hill et al., 2004).

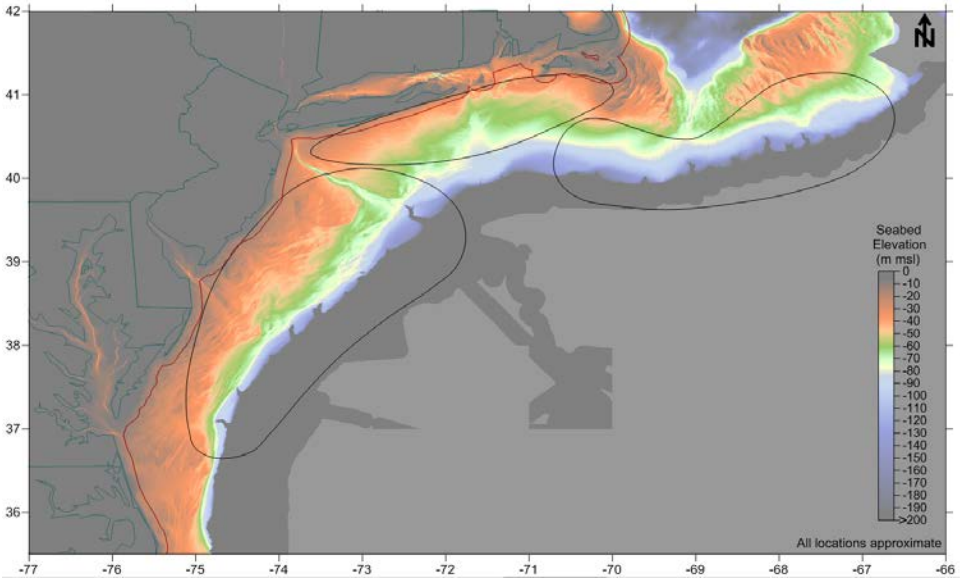

Figure 6-2. High-resolution coastal relief image for the mid-Atlantic OCS.

Storage Zone/Caprock Factors- Properties of the potential CO_2 storage zones and caprocks were characterized to assess upward migration, density effects, pressure changes, and trapping mechanisms in the study areas. Hannis et al. (2017) describe 'containment assurance' for offshore carbon storage in terms of deep- and shallow-focused elements. Deep containment is focused on CO_2 storage security in the reservoir zone, where containment often relies on structural traps, low-permeability caprocks, and capillary trapping. Shallow containment examines potential CO_2 leakage at the seabed into the ocean water, where gas migration along fractures, soft sediment deformation zones, and gas seeps may occur.

Figure 6-3 shows stratigraphic columns for wells in BCT and GBB, illustrating the relationship of deep storage zones, caprocks, shallow sediments, and seawater along the mid-Atlantic OCS. The offshore wells generally note soft to semi-consolidated Miocene- to Paleocene-age clay, mud, siltstone, limestone, shell, and sand sediments. These layers reflect various depositional and erosional periods during sea-level change and vary across the shelf. Logs and notes from exploration wells along the mid-Atlantic OCS describe unconsolidated sediments at depths of 500 to 1,500 m (2,000 to 4,900 ft), depending upon their location along the shelf. Sonic logs also show a notable increase in velocities at depths greater than approximately 1,200 m (3,900 ft), which may be an indicator of a transition from semi-consolidated sediments to more lithified rocks. Combined with the phase behavior of CO_2, processes like soft sediment deformation may present risk factors in intervals above a depth of 1,000 m (3,000 ft) below mean sea level.

Variability of reservoir zones and caprocks has the potential to affect storage security and injection well performance. Variability in the storage zones and caprock reflects series of depositional and erosional events that affected sediments over geologic time. Consequently,

many of the reservoir zones have interbedded layers of sandstone, siltstone, and clay as discussed in Chapters 2 through 4. The confining layers appear more consistent and continuous in both spatial and vertical extents.

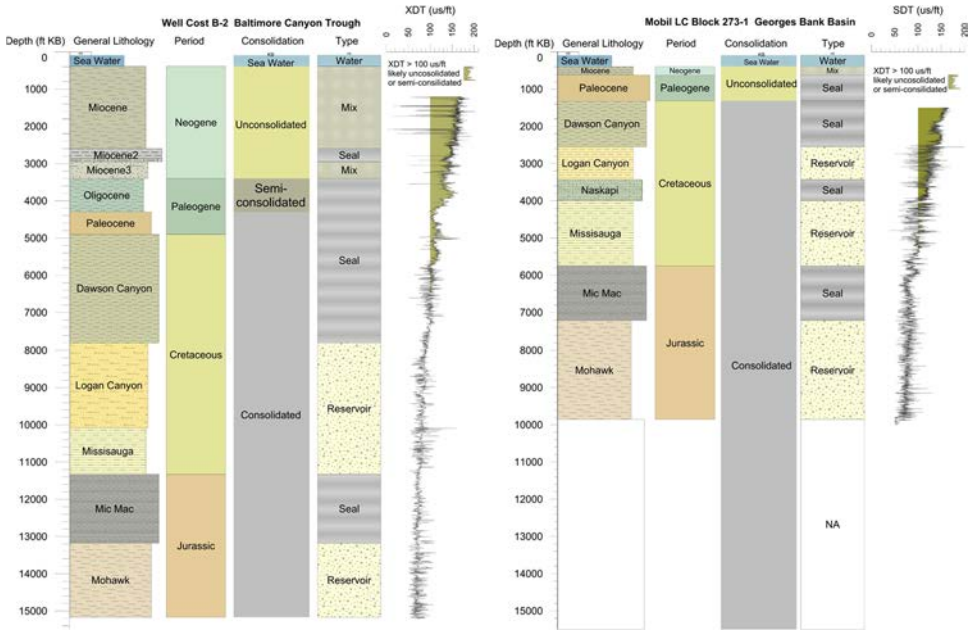

Figure 6-3. Geologic diagram illustrating sonic log (XDT) behavior in unconsolidated/semi-consolidated rocks in BCT COST B-2 and GBB Mobil 273-1 wells.

Hydrologic Conditions- Pressure conditions, pore water salinity, geothermal gradients, and gas hydrate occurrence were analyzed based on tests, logs, and sample analysis from exploratory wells in the mid-Atlantic offshore region. These conditions are important to ensure storage of CO_2 in supercritical fluid phase and assess potential upward/updip migration of CO_2.

To assess subsurface pore pressure conditions in the offshore mid-Atlantic, repeat formation tests and mud weights were analyzed for exploratory wells. Data from 181 repeat formation tests were compiled from 12 wells in the mid-Atlantic offshore region. Figure 6-4 shows a plot of measured pressures versus depth for the repeat formation tests. Data indicate very good correlation to a 0.45-psi/ft (10,000 Pa/m) pressure gradient, which likely reflects salinity of more than 35,000 milligrams per liter (mg/L).

Subsurface salinity is important to determine the amount of CO_2 that may dissolve in formation fluids. Dissolved CO_2 is considered a secure CO_2 storage mechanism and will be higher at lower salinity pore waters. Research on salinity trends along the mid-Atlantic OCS suggests that paleo-waters trapped in the deeper rock formations have fairly low salinity (0 to 25 parts per thousand [ppt]) near shore with salinity increasing to 25 ppt to more than 50 ppt further offshore (van Geldern et al., 2013; Mountain et al., 2010; Cohen et al., 2010; Pope & Gordon, 1999; Kohout et al., 1977). Fluid samples from the repeat formation tests, mud weights, and resistivity logs from the offshore wells suggest a trend of increasing salinity with depth but are difficult to interpret in terms of specific salinity values. Overall, the precise salinity of the formation fluids in the deeper rock formations along the mid-Atlantic OCS is challenging to define based on available information. Research and fluid sampling offshore wells (Mountain et al., 2010) suggest that salinity in the deeper formations would likely be >40,000 mg/L (>0.3 lb/gal), especially in areas farther offshore.

Subsurface temperature conditions are a factor for CO_2 storage in terms of phase behavior. Abnormal temperatures may result in CO_2 transition to gas phase, liquid phase, or hydrate

formation, which could affect injection operations and storage processes in the subsurface. Review of temperature logs and other research for mid-Atlantic OCS wells suggests a geothermal gradient range of 16 to 24 °C/km (0.9 to 1.5 °F/100 ft), with an average gradient of approximately 23 °C/km (1.35 °F/100 ft). Some wells (e.g., Shell 93-1, Exxon 684-1) in the thicker basin portions of the OCS appear to have lower geothermal gradients, which may be related to seawater depth and proximity to oceanic crust (Robbins, 1979; Fry, 1987).

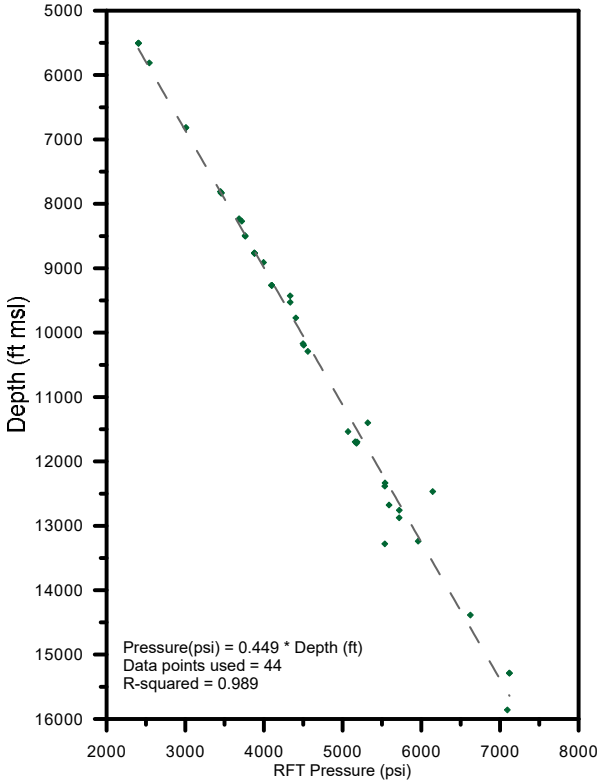

Figure 6-4. Pressure gradients from wireline repeat formation tests.

Methane gas hydrates have been observed along some areas of the Atlantic offshore continental slope. Gas hydrates may cause problems with drilling activities and CO_2 injection. Most gas hydrate formations have been observed south of BCT, generally outside of the project study area. The hydrates are also more common along the continental slope. Subsurface temperature and pressure conditions along the offshore mid-Atlantic would generally not result in hydrate formation, mostly because the geothermal gradient is high enough in the deep rock formations to prevent hydrate formation.

Seismic Activity along the Mid-Atlantic OCS- Earthquake activity along the offshore mid-Atlantic is low. The Atlantic OCS is a passive continental margin with very little seismic activity, tectonic movement, and/or volcanoes. No earthquakes have been observed in GBB and BCT. Three earthquakes have been observed along the south-central portion of the LIP with low magnitudes of 2.5 to 3.7. Hypocenters were 10 to 30 km (20 mi) deep. Seismic hazards along the East Coast are also rated as mostly low hazard, with a medium rating in the Pennsylvania-New Jersey-New York tristate area. Stress orientations along the offshore mid-Atlantic are related to tectonic forces and mid-Atlantic spreading of oceanic crust, which results in a principal stress direction in the northeast-southwest orientation. Strike-slip and thrust stress regimes are most likely in the region. More detailed geomechanical characterization would be necessary for

any site-specific CO_2 storage project. Escarpments and troughs near the continental slope would require careful consideration.

6.2 Long-term Storage Risk Factors

Long-term CO_2 storage risk factors were examined in terms of confining/trapping mechanisms, long-term migration patterns, and wellbore integrity. The objective of the analysis was to ensure that CO_2 would remain in the deep rock formations for geologic time periods.

Confining Layers Description- Table 6-1 summarizes the general properties of the confining layers in the mid-Atlantic OCS. The primary caprock for the LC/mid-Cretaceous sands interval is the Upper Cretaceous shales/Dawson Canyon Formation. Secondary containment may be provided by shallower Miocene-Paleocene layers. However, these layers may be unconsolidated to semi-consolidated, and there may be potential for soft sediment deformation in intervals less than 3,500 ft (1,100 m). The primary caprock for the lower Cretaceous sands/Missisauga Formation is the mid-Cretaceous Naskapi Formation, and the upper Jurassic Mic-Mac formation is the caprock for the Jurassic Mohawk sandstone. The individual confining layers are generally 200 to 2,500 ft (60 to 760 m) thick. In addition, the units are fairly continuous across the mid-Atlantic OCS, although the rock properties vary with location. The depth of the Upper Cretaceous shales/Dawson Canyon formation is much shallower in the GBB and LIP than in the BCT. Therefore, risk factors for containment would be present for CO_2 storage in the mid-Cretaceous sands/LC in these areas. Threshold entry pressure tests were completed on 17 samples from the BCT within the upper Jurassic Mic-Mac Formation that had porosity of 0.6 to 5.7% and vertical permeability of 0.000001 to 0.00168 mD. Threshold pressures were mostly listed as 800 to 1,000+ psi (6 to 7 MPa), which are very high considering that pressures of 300 to 700 psi (2 to 5 MPa) have been observed for other CO_2 storage caprocks (Espinoza and Santamaria, 2017; Zhou et al., 2017).

Table 6-1. General properties of confining layers in the mid-Atlantic OCS.

Property	Confining Layer			
	Miocene-Paleocene	UK Caprock/ Dawson Canyon	MK4/Naskapi	LK2/Mic-Mac Abenaki
Geologic Period	Tertiary	Upper Cretaceous	Middle Cretaceous	Lower Cretaceous - Upper Jurassic
Age (~Ma)	23-66	85	125	135 - 145
Lithology	Mixed clay, silt, sand	Mixed siliciclastic	Shale	Mixed siliciclastic
Thickness (ft)	>1,000	1,813	593	1,757
Porosity (fraction)	NA	0.23	0.24	0.20
Permeability (mD)	NA	407	NA	122

CO_2 Phase Behavior Analysis- To examine the potential for vertical migration of CO_2, the phase behavior of CO_2 with depth was completed for the mid-Atlantic OCS study areas. Supercritical CO_2 has a density of 0.6 to 0.9 g/ml (5 to 8 lb/gal) and will migrate upward along structural trends, caprock layers, and geologic flow pathways. Along the mid-Atlantic OCS, the rock formations being considered for CO_2 storage have a depth range of 2,000 to 15,000+ ft (600 to 5,000 m) below mean sea level with a wide range of temperature and pressure conditions. In the targeted storage zones, the conditions are firmly in the supercritical phase region. Based on pressures measured with downhole repeat formation tests and geothermal

gradients in the study areas, the density of supercritical CO_2 fluid is likely to range from 0.7 to 0.75 g/ml (6 lb/gal) at depths of 4,000 to 16,000 ft (1,000 to 5,000 m) mean sea level (msl) (Figure 6-5).

In general, the density would result in considerable buoyancy effects, because the CO_2 will be 25 to 30% lighter than existing fluid in the reservoir. The pressure-temperature trends at depth suggest that a minimum depth of approximately 1,000 m (3,280 ft) below msl may be required for supercritical fluid phase storage. At depths less than 1,000 m (3,280 ft), CO_2 could potentially transition to gas phase with density less than 0.3 g/ml (3 lb/gal). Soft sediment deformation may be possible in these zones. In the shallower storage zones, caprock and reservoir structures should be carefully characterized to ensure storage permanence.

These risk factors would affect the GBB and LIP, where rock formations are shallower. For example, the top of the LC in the entire GBB and LIP is less than 1,000 m (3,300 ft) msl deep. An updip flow vector analysis completed for the study areas indicated that CO_2 will tend to migrate updip due to buoyancy processes unless there is a geologic structure, sealing fault/feature, or stratigraphic trap. The dip of the rock layers along the shelf is fairly low, at 0.001 to 0.02 m/m (10 to 100 ft/mi), and migration will be slow. Analog studies of similar offshore geologic settings suggest that lateral depositional pinch-out traps and lateral facies changes provide additional trapping mechanisms for the study areas.

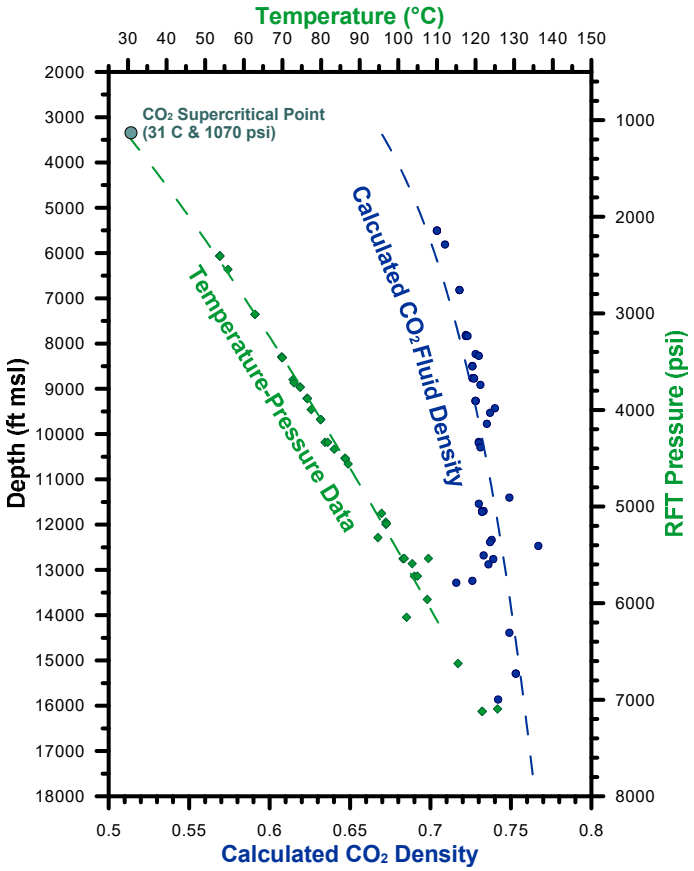

Figure 6-5. CO_2 density, pressure, and temperature trends for the offshore mid-Atlantic.

Long-term CO_2 Storage Processes- Long-term processes such as CO_2 dissolution, residual saturation, and mineralization were analyzed for the offshore geologic environments along the

mid-Atlantic OCS. These processes have been identified by Benson et al. (2009) as long-term, permanent mechanisms for CO_2 storage. The storage processes are important to understand the mobility of CO_2 in the subsurface in addition to stratigraphic and structural trapping.

CO_2 solubility at depth based on observed repeat formation test pressure, subsurface temperature, and salinity of 40,000 mg/L (0.3 lb/gal) was calculated with the methods described by Zhao et al. (2015). The analysis suggests that CO_2 solubility will be 1.0 to 1.4 mole/kg (0.5 to 0.6 mole/lb) in the subsurface along the OCS. This equates to approximately 44,000 to 60,000 mg/kg, or approximately 5% dissolved CO_2/kg water by weight. To estimate CO_2 residual trapping potential, the porosity distributions of mid-Atlantic offshore thin-section samples with 15 to 25% porosity were compared to brine-CO_2 relative permeability tests performed by Bachu (2013) for western Canada sandstone samples with similar 15 to 25% porosity. Both sets of samples have total porosity of 15 to 25% with 70 to 90% macro (or intergranular) porosity, 8 to 11% mesoporosity, and 15 to 17% microporosity. Potential for CO_2 mineralization was estimated based on the major-element bulk-rock geochemical compositions and mineral assemblages observed in the caprocks and storage zones of interest.

Hydrologic conditions, geotechnical rock properties, and mineralogy of the deep rock formations in the mid-Atlantic offshore suggest that structural and stratigraphic trapping of free-phase CO_2 and residual trapping would be the primary mechanisms for storage (Figure 6-6). CO_2 dissolution may account for 3 to 5%. Mineral trapping is expected to be low at less than 1%, but there are a moderate amount of reactive clays and feldspars that may be expected to react with CO_2. CO_2 contact with formation water, plume migration, mixing with water, and reservoir variability will affect these trapping processes over time.

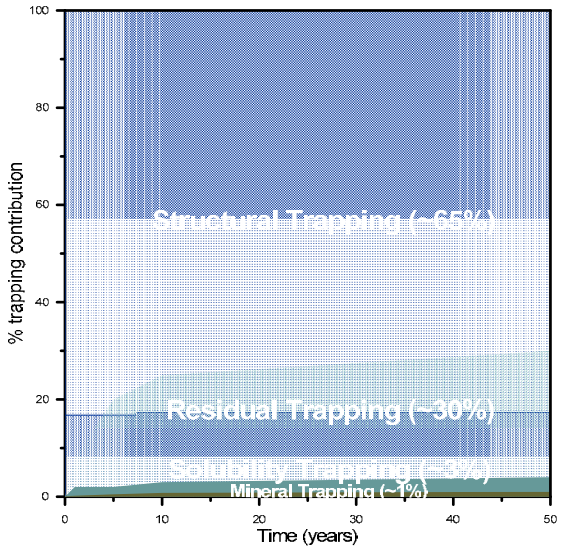

Figure 6-6. Conceptual diagram illustrating trapping processes for offshore mid-Atlantic.

Wellbore Integrity- Wellbore integrity may be a risk factor in areas with many legacy oil and gas wells, because the wells are a potential pathway for CO_2 migration. The mid-Atlantic offshore has only 44 deep exploration wells, all of which have been plugged and abandoned. In general, the offshore wells were completed with three to five casing strings cemented in place according to industry best practices and in compliance with regulatory requirements. Because the wells were considered exploratory, a “drill and plug” procedure was followed, and the wells were plugged after drilling was completed. Records suggest that typical offshore materials (i.e.,

Class H cement and carbon steel casing) were used for well construction. Most wells indicate that conductor casings were cut several hundred feet below the seafloor, and the drilling area was surveyed before final site demobilization. No additional monitoring or surveying of the well sites has occurred since they were drilled, and no well leakage incidents have been noted to the best of our knowledge.

6.3 Deployment Factors

This section provides a brief description of environmental risk factors, marine features, sources of CO_2, and stakeholder risk factors that could influence efforts to implement carbon storage projects in the mid-Atlantic region.

Environmental Risk Factors- Activities that may be associated with CO_2 storage projects such as conducting seismic surveys, drilling deep wells, installing pipelines, and placing bottom-founded equipment or structures could cause physical disturbances on the seafloor as outlined by a BOEM study (2014). Development of an offshore carbon storage project would likely require a variety of exploration activities very similar to oil and gas operations. Activities related to offshore drilling and exploration that may have an environmental impact were listed as “active acoustic sound sources; vessel and equipment noise; vessel traffic; aircraft traffic and noise; vessel exclusion zones; trash and debris; seafloor disturbance; drilling discharges; onshore support activities; and accidental fuel spills.”

Marine Features- Natural and man-made features were analyzed to determine their impact on exploration, drilling, and facility construction for a potential carbon storage on the mid-Atlantic OCS. Geologic hazards such as slumping, unconsolidated sediments, basins, troughs, escarpments, sand waves, and water currents may present additional technical challenges for offshore CO_2 storage projects. Many environmentally sensitive areas for marine species and habitats are present in the study areas. In terms of CO_2 storage applications, marine features and boundaries would mainly impact exploration and infrastructure development. Figure 6-7 illustrates the locations of these features in relation to the offshore continental shelf study areas. CO_2 pipelines, injection wells, offshore wind development areas, and seismic surveys may be limited in certain areas due to their potential to disturb the seabed or ocean surface activities. Most of the features are in nearshore areas, which may be more accessible by pipeline but less likely to be selected for a CO_2 storage site. The majority of the mid-Atlantic OCS would be accessible for CO_2 storage projects, and marine features have no direct impact on resource calculations since the storage zones are isolated rock layers deep beneath the seabed.

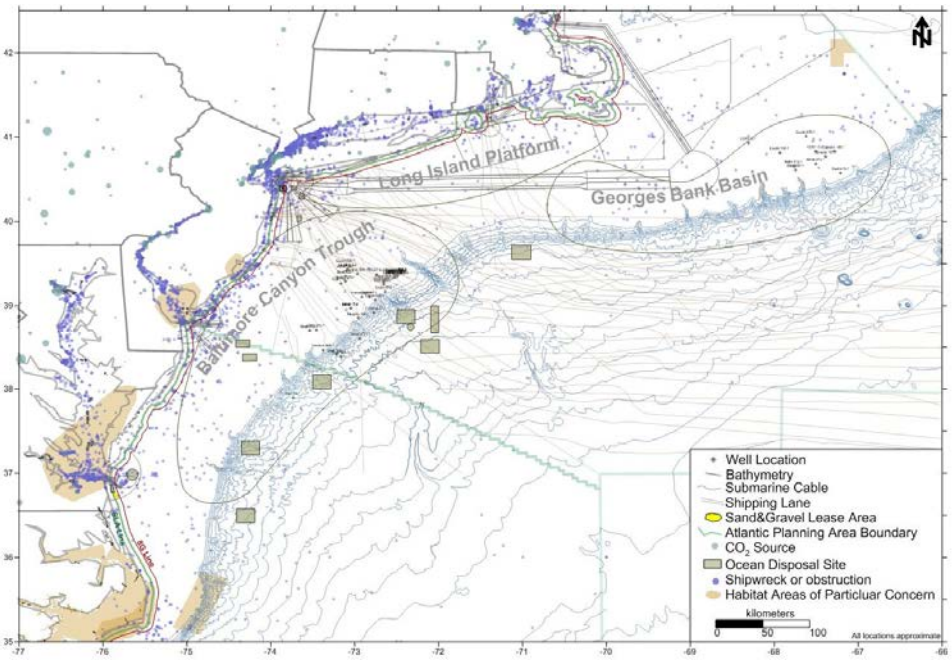

Figure 6-7. Map showing environmental and marine features in the mid-Atlantic OCS.

CO_2 Sources in the Mid-Atlantic Region- CO_2 sources in the mid-Atlantic region were examined to determine the feasibility of linking the sources to the offshore resource locations. Figure 6-8 shows a map of CO_2 industrial point-sources in the region based on the 2016 U.S. Environmental Protection Agency (EPA) Greenhouse Gas Reporting Program. There are approximately 489 sources in the region as defined by -77° W, 35° N to -66° W, 42.5° N domain. Total emissions were approximately 147 Mt in 2016 based on EPA Greenhouse Gas Reporting Program data. Many of the sources are clustered along industrial corridors, which have a higher CO_2 emissions intensity. The CO_2 sources in the region reflect a mix of power generation, chemical facilities, petroleum processing, mineral and metal plants, pulp and paper, waste facilities, and other industry. There were 39 power plants and 5 petroleum processing facilities with emissions >1 Mt/year. Many of the larger power plant sources are located inland from the coast. There are numerous small to moderate-sized sources in areas with significant combined CO_2 emissions. Connecting CO_2 sources to the mid-Atlantic OCS CO_2 storage resources would likely require a pipeline network connecting multiple sources. The BCT and LIP are most accessible to existing industrial corridors. The GBB is more distant from CO_2 sources.

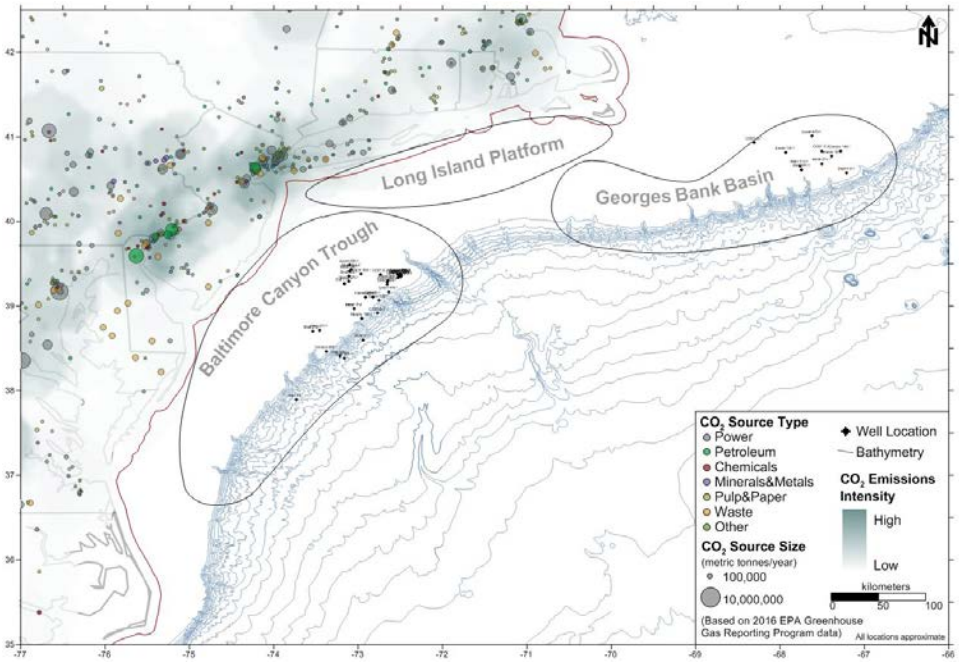

Figure 6-8. Locations of CO_2 sources in the mid-Atlantic region.

CO_2 Storage Stakeholder Risk Factors in the Mid-Atlantic Region- This project contributed to the stakeholder outreach effort by providing scientific-based data for future detailed risk assessments, which is important for building the public acceptance of offshore carbon storage. As part of the activities in this project, Battelle also co-hosted a stakeholder workshop on the MAOCSRAP effort at the Harvard University Center for the Environment in April 2018. The objective was to discuss the challenges and hurdles for offshore CCS and learn how to overcome them. Stakeholders included industry (e.g., Statoil, BP), non-governmental organizations (NGOs) (e.g., Natural Resources Defense Council, Clean Air Task Force), universities (e.g., Massachusetts Institute of Technology [MIT], University of Massachusetts [UMASS] Boston), and international regulators (e.g., Norwegian Petroleum Directorate). Workshop participants emphasized the need for early stakeholder outreach to identify and address *perceived* risks that are of most importance to offshore CCS stakeholders. Recommendations discussed included (1) establishing regulation and protocols specific to the offshore environment that leverage the experience of Norway, which has had an active offshore CCS industry for more than 20 years; (2) articulating risks using a quantitative analysis; (3) building a consensus that offshore CCS is for the greater good; and (4) conducting early briefings with regulators, NGOs, and the financial communities.

6.4 Key Findings

An initial assessment was completed on technical risk factors in mid-Atlantic offshore areas that may affect CO_2 storage resource estimates by constraining the prospective resource assessment boundaries. The risk factor analysis considered geologic storage processes, long-term potential for CO_2 migration, and environmental setting factors that could affect the feasibility of developing a carbon storage facility.

The results of the risk factor analysis provide guidance for geologic storage implementation by providing stakeholders (e.g., operators, project developers, regulators, the public) with preliminary information relevant to the long-term fate and associated risks of CO_2 injection into the subsurface, focusing on long-term CO_2 storage capacity, potential risks associated with CO_2

leakage, and other factors that have potential adverse impacts to logistics, economics, and infrastructure. The risk factor analysis was based on readily available reports, maps, and data for the area. Any site-specific project would require more detailed site selection, test well drilling, geophysical logging, injection testing, seismic surveys, and storage system design.

Overall, the mid-Atlantic offshore area benefits from the large spatial extent, thick sequences of Cretaceous- and Jurassic-age sands, lack of previous oil and gas wellbores, and distance from populated development. No highly critical risk factors were identified that would impede CO_2 storage along the study areas. Faults and geomechanical stability along the mid-Atlantic slope were identified as a moderate risk factor. Reservoir variability was also noted as a moderate risk factor, especially in Cretaceous sands that have interbedded silt and clay layers. Soft sediment deformation was identified as a risk factor for semi- or unconsolidated sediments <1,000 m deep, which are more prevalent in the GBB and LIP. CO_2 migration pathways and trapping mechanisms were not considered a significant risk factor for the deeper rock formations along the mid-Atlantic offshore.

Many environmental factors (e.g., habitat areas of particular concern, man-made features on the seabed, marine protected areas) are found along the mid-Atlantic seaboard. Most of these features are located closer to the shoreline. CO_2 sources are mainly clustered adjacent to the BCT. Dense population centers along the coastline may present challenges for stakeholder outreach and communication. In addition, there is little history of oil and gas development in the region, which would provide a level of familiarity with typical exploration activities.

7. Stakeholder Engagement

The objective of Task 7 was to provide stakeholders in the mid-Atlantic U.S. with educational and technical information on CO_2 storage resources for the offshore mid-Atlantic. There are large population centers along the mid-Atlantic coastline, so early communication of CO_2 storage technologies is important to establishing CO_2 storage in the region.

The results from this project were presented by the Project Team to technical advisors and to mid- and north-Atlantic CCS stakeholders for input and feedback. A short list of fact sheets was prepared to disseminate Project findings at the final stakeholder workshop.

The stakeholder engagement plan for this task is provided in Attachment I along with Attachment J, the memorandum detailing the Road Map for future CCS project planning and implementation in the offshore mid-Atlantic study region.

7.2 Stakeholder Workshops

Early and continuous stakeholder engagement has been identified as an important strategic element to any CCS project. Building relationships with government agencies, utilities, industry, NGOs and other interested parties is crucial. Communication is intended to facilitate a greater understanding of the benefits of CCS in an offshore setting and gain an understanding of how the associated activities may be successfully planned, implemented, and regulated.

To this end, two stakeholder workshops were held over the course of the Project: the first at the Harvard University Center for the Environment (Cambridge, MA) in April 2018 and the second at the Maryland State Capital (Annapolis, MD) in November 2018.

April 2018 Workshop

The first stakeholder workshop was intended to provide feedback regarding the Project Team's preliminary findings and solicit insight on the planning and application of CCS technologies in the mid-Atlantic U.S. offshore region. Stakeholders included industry (e.g., Statoil, BP), NGOs (e.g., Natural Resources Defense Council, Clean Air Task Force), universities (e.g., MIT, UMASS Boston), and regulators (e.g., Norwegian Petroleum Directorate). A roundtable discussion concentrated on three themes: (1) developing appropriate regulations; (2) the role of this Project and its work product to foster communication and public acceptance; and (3) identifying and addressing risk factors likely to be associated with an offshore CCS project.

- Regulatory framework – Norway has regulations in place from their CCS projects that have been in operation for more than 20 years. These regulations can be a starting point for the development of regulations in the United States. Regulatory and industry perspectives are crucial to build protocols and regulations.
- Science/public acceptance – It is important to initiate and maintain communication with entities that have the most at stake and/or stand to benefit the most (i.e., coastal communities, NGOs, and regulatory agencies). Public outreach should be initiated early on and outreach continued throughout project development; additional stakeholders may be identified through this process. Any project will need to demonstrate its scientific merit to regulators and potential environmental benefits versus anticipated and/or perceived risks as defined by stakeholders. Engaging a neutral party to solicit stakeholder input will support buy-in and understanding on the part of all interested stakeholders.

- Risk – A quantitative risk analysis that addresses stakeholder concerns is necessary. Understanding CCS technologies relative to risk factors is vital to reduce misinformation and manage perceived risk. Financial institutions require an understanding of risk and mitigation to provide appropriate funding and insurance.

November 2018 Workshop

The November 2018 workshop presented near-to-final Project results to a larger invited group of industry, government, and NGOs, and was held in conjunction with the annual MRCSP meeting. Having stakeholders for both projects at this workshop afforded attendees an opportunity to learn from each other, discuss similarities/differences in the prospects of onshore versus offshore CCS, and build synergy. Along with technical presentations on Project tasks, a facilitated discussion sought input on the draft CCS Road Map developed for the Project. Four components were brought to the floor for discussion and comment:

- **Goals** – Not enough information was available to reach a consensus on this topic. However, either a pilot-scale or commercial-scale project was envisioned to initiate CCS in an offshore setting, and that either could be used to demonstrate the viability of the technology. This project will help focus development of a regulatory framework.
- **Strategies** – Early stakeholder engagement is critical, particularly with coastal communities. Regulatory and policy unknowns can halt a project, so it is desirable to implement an early mover project to facilitate regulatory confidence and certainty.
- **Milestones** – Develop a stakeholder outreach plan that includes all appropriate organizations and is flexible enough to incorporate new stakeholders along the way. Establish a practicable permitting/regulatory pathway for CCS in the offshore environment.
- **Timelines** – Large-scale CCS deployment by 2040 was identified as necessary to meet established climate initiative goals.

7.3 Fact Sheet Preparation

Four fact sheets were developed in advance of the November 2018 workshop and are provided in Attachment J.

The *Project Overview* communicates the Project's technical approach to use publicly available data to meet four objectives: (1) complete a systematic assessment of the mid-Atlantic offshore coastal region (i.e., GBB through the LIP to the southern BCT); (2) define key parameters to reduce uncertainty for offshore storage resource and efficiency estimates; (3) perform a preliminary assessment of risk factors, uncertainties, and data gaps; and (4) develop a Road Map to engage stakeholders and guide future project planning and implementation.

The *Risk Factor Analysis* provides a summary of the Project's assessment of geologic risk factors, including the characteristics of shale and mudstone caprocks, shallow unconsolidated deposits, regional seismicity, and geomechanical stability. In particular, long-term CO_2 trapping mechanisms were determined to offer low risk, given the geologic characteristics of the region. Environmental factors to be considered in siting a storage location include marine life migration patterns and sensitive habitats; existing offshore infrastructure and industry activity (e.g., submarine cables, shipping lanes); and distance from population centers and CO_2 sources. No highly critical geologic, environmental, or long-term storage risks were identified that would preclude deployment of CCS in the mid-Atlantic U.S. offshore study region.

The *CO_2 Storage Resource Estimation* describes the step-wise approach used to estimate the storage resource associated with the mid-Atlantic U.S. offshore region. This approach started with data integration and mapping, then turned to a regional-scale storage resource estimate assessment and concluded with local-scale dynamic injection and storage simulation efforts. Reprocessed and newly available seismic data, stratigraphic reinterpretations, existing core, and geophysical logs mapped potential storage and confining units. New petrophysical analyses confirmed that potential storage reservoirs have the requisite porosity and permeability characteristics. Decades of CO_2 storage exist on a regional scale, based on the regional storage assessment. On a local scale, one potential site near one geologic feature could store gigatonnes of CO_2 within pressure constraints considered to be safe.

The *Road Map for U.S. Offshore CCS Deployment* was revised based on feedback from the facilitated discussion at the November 2018 workshop. The timeline moves from the early stages of offshore CO_2 storage assessment, in which knowledge infrastructure is developed, to continued stakeholder and public participation, which reduces risk and uncertainty, to eventual commercial deployment once the technology infrastructure has been established. A deliberate approach is proposed to move from characterization, to validation, to site development.

- **Characterization** – Advanced static and dynamic model development during the characterization phase can complete the site screening process. It will also provide a more thorough understanding of storage opportunities and risks. Reprocessing seismic data from recent surveys can evaluate rift basin properties and reservoir capacity. Onshore analogs and collaboration with industry and research organizations build partnerships and lower costs. Development of regulatory certainty and development of a stakeholder outreach strategy are other key components of this phase.
- **Validation** – Data gaps identified during this Project can be addressed through new data collection to address potential site locations, risk mitigation, and addressing regulatory/permitting requirements. New analyses will be needed to validate caprock petrophysical properties, fracture pressure gradients, leakage risks, reservoir injectivity, and supplement current knowledge of storage zones and caprocks. A cost-benefit analysis will be needed to ensure higher costs associated with offshore characterization are acceptable. Finally, monitoring methods should be investigated and designed in anticipation of the site development phase.
- **Development** – The progression to large-scale CCS development depends on the findings of previous stages and stakeholder support. This stage typically includes the assessment of CO_2 sources and transport, final site selection, detailed design, permitting, construction, operations, and monitoring. Technology advances, particularly with regard to characterization, robotics, sub-sea structures, safety mechanisms, and remote operations, may facilitate cost-effective deployment with enhanced stakeholder confidence. Regulatory requirements and pricing mechanisms must support economic viability. Early mover projects may help deployment of CCS through upscaling of technologies that reduce economic and policy barriers to commercial-scale ventures.

8. Reporting and Technology Transfer

Task 8 included reporting of project progress, technical reports, and technology transfer.

This task included preparation of monthly updates, quarterly progress reports, financial reports, and milestone tracking. In addition, topical reports were prepared as listed in Table 8-1 and have been included in this final technical report at the end of the Project.

Throughout the Project period, team members developed and presented technical papers at various professional meetings,. including the Annual Carbon Capture Utilization and Storage (CCUS) Conference, Greenhouse Gas Control Technologies (GHGT) Conference, American Geophysical Union, and other professional organization meetings. In addition, a significant component of technology transfer was through presentations (Table 8-1), posters (Table 8-2), peer-reviewed publications (Table 8-3), and theses prepared by graduate students (Table 8-4) working in team member institutions.

Table 8-1. List of presentations and lectures presented on the Mid-Atlantic Carbon Storage Resource Assessment Project.

Date	Title	Org.	Location	Author(s)
January, 2016	Palynological constraints on the stratigraphy of the Magothy Formation (Cretaceous), New Jersey and Delaware, and implications for interstate aquifer correlation	GSA	Denver, CO	McLaughlin, P.P. et al.
January, 2016	Sequence stratigraphic framework of the mid-Cretaceous nonmarine Potomac Formation in New Jersey and Delaware	GSA	Denver, CO	Thornburg, J.D. et al.
March, 2016	Mid-Atlantic U.S. Offshore Carbon Storage Resource Assessment	SECARB	Atlanta, GA	Cumming, L. et al.
May, 2016	Overview of the Mid-Atlantic U.S. Offshore Carbon Storage Resource Assessment	CCUS	Tysons, VA	Cumming, L. et al.
September, 2016	Sequence Stratigraphy in the Northern Baltimore Canyon Trough, Offshore Eastern U.S.	GSA	Denver, CO	Lombardi, C. J. et al.
March, 2017	Cretaceous Sedimentation Patterns in the Southern Baltimore Canyon Trough: Correlating the Maryland Coastal Plain to the Continental Rise	SE GSA	Richmond, VA	Schmelz, W.J. et al.
April, 2017	Carbon sequestration potential offshore the US east coast: teaching old data new tricks	REI	New Brunswick, NJ	Fortin, W.
May, 2017	Geology (and Policy) matters: The challenging case for carbon storage, U.S. Mid-Atlantic region	REI	New Brunswick, NJ	Miller, K.
June, 2017	Mid-Atlantic U.S. Offshore Carbon Storage Resource Assessment: Project Developments and Status Update	IEAGHG	Beaumont, TX	Gupta, N., and Cumming, L.
October, 2017	Delineating Mid-Cretaceous Seismic and Well-Log Sequences to Assess Carbon Storage Potential in the Northern Baltimore Canyon Trough	GSA	Seattle, WA	Baldwin, K. E. et al.

Date	Title	Org.	Location	Author(s)
October, 2017	Cross Sections from the Midwest Regional Carbon Sequestration Partnership: Visualizing Subsurface Carbon Storage Opportunities Across the Central and Eastern United States	GSA	Seattle, WA	Dinterman P. A., et al.
October, 2017	Sequence stratigraphic analysis of Cretaceous strata in the Southern Baltimore Canyon Trough: An integration of geological and geophysical data	GSA	Seattle, WA	Schmelz, W. et al.
October, 2017	Back to basics of sequence stratigraphy: Early Miocene and Mid-Cretaceous examples from the New Jersey paleoshelf	GSA	Seattle, WA	Miller, K. G. et al.
November, 2017	Mid-Atlantic U.S. Offshore Carbon Storage Resource Assessment	MRCSP	Washington D.C., MD	Cumming, L., and Gupta, N.
December, 2017	Carbon Sequestration Potential in Mesozoic Rift Basins Offshore the US East Coast: Teaching Old Seismic Data New Tricks	AGU	New Orleans, LA	Fortin, W., et al.
May, 2018	Leveraging a Legacy Sample and Data Collection for Carbon Storage Resource Assessment	AAPG ACE	Salt Lake City, UT	KunleDare, M. A., McLaughlin, P. P.
May, 2018	Mid-Atlantic U.S. Offshore Carbon Storage Resource Assessment	IEAGHG	Oslo Norway	Cumming et al.
August, 2018	Mid-Atlantic U.S. Offshore Carbon Storage Resource Assessment	DOE-NETL	Pittsburgh, PA	Cumming, L.
September, 2018	Mid-Atlantic U.S. Offshore seismic analysis, rift basin map update, preliminary petrophysical profiles	LDEO	Palisades, NY	Fortin, W.
September, 2018	Mid-Atlantic U.S. Offshore Carbon Storage Resource Assessment DE-FE0026087	DOE-NETL	Web-based	Gupta, N.
October, 2018	CCS Potential in Basaltic Rift Basins Offshore the East Coast: New Methods on Legacy Data	GHGT-14	Melbourne, Australia	Fortin, W. F et al.
November, 2018	Quantitative Biostratigraphic Analysis of Middle Cretaceous Sequences in Baltimore Canyon Trough, Offshore Mid Atlantic U.S Margin	GSA	Indianapolis, IN	Jordan, L. M. et al.
December, 2018	Carbon Capture and Storage Potential Offshore the US East Coast: New Methods and Insights from Legacy Data	GHGT-14	Melbourne, Australia	Fortin, W.
December, 2018	Crustal structure and rift architecture of the Georges Bank, U.S. Atlantic margin	AGU	Washington, D.C.	ten Brink, et al.

Table 8-2. List of posters presented on the Mid-Atlantic Carbon Storage Resource Assessment Project.

Date	Title	Org.	Location	Author(s)
May, 2016	Mid-Atlantic U.S. Offshore Carbon Storage Resource Assessment	CSLF	Austin, TX	Gupta, Fukai, Cumming
September, 2016	Carbon Storage Potential at the Great Stone Dome, Northern Baltimore Canyon Trough	GSA	Denver, CO	Lombardi, C. et al.
September, 2016	Potential for Carbon Capture and Sequestration (CCS) in the Eastern Georges Bank Basin, Offshore Massachusetts	GSA	Denver, CO	Graham, et al.
November, 2016	Mid-Atlantic U.S. Offshore Carbon Storage Resource Assessment	GHGT-13	Lausanne, SW	Cumming et al.
October, 2017	Using seismic stratigraphic principles to map carbon sequestration potential in the northern Baltimore Canyon Trough	GSA	Seattle, WA	Baldwin, K. E., et al.
October, 2017	Cross Sections from the Midwest Regional Carbon Sequestration Partnership: Visualizing Subsurface Carbon Storage Opportunities Across the Central and Eastern United States	GSA	Seattle, WA	Dinterman, P. A., et al.
October, 2017	Sequence stratigraphic analysis of Cretaceous strata in the Southern Baltimore Canyon Trough: An integration of geological and geophysical data	GSA	Seattle, WA	Schmelz, W., et al.
May, 2018	Revised Stratigraphic Synthesis of the Baltimore Canyon Trough: Implications for Reservoir Identification and Analysis	AAPG ACE	Salt Kale City, UT	Schmelz, W., et al.
October, 2018	Performing Carbon Storage Resource Assessments for Offshore Mid-Atlantic United States	GHGT-14	Melbourne, AU	Cumming, L. et al.
December, 2018	Potential for CO_2 sequestration in Rift Basins Offshore the US East Coast: Updated basin extent and composition from pre-stack seismic inversion	AGU	Washington, D.C.	Fortin, W. et al.

Table 8-3. List of peer-reviewed publications submitted as part of the Mid-Atlantic Carbon Storage Resource Assessment Project.

Date	Title	Journal	Author(s)
2017	Lower to Mid-Cretaceous sequence stratigraphy and characterization of CO_2 storage potential in the Mid-Atlantic U.S. Coastal Plain	Journal of Sedimentary Research	Miller, K. G. et al.
2018	Back to Basics of Sequence Stratigraphy: Early Miocene and Mid-Cretaceous Examples from the New Jersey Paleoshelf	Journal of Sedimentary Research	Miller, K. G. et al.
accepted	Onshore-offshore correlations of fluvial-deltaic sequences from the mid-Cretaceous of the southern Baltimore Canyon Trough	AAPG Bulletin	Schmelz, W.J. et al.
2019	Mid-Cretaceous Paleopedology and Landscape Reconstruction of the mid-Atlantic U.S. Coastal Plain	Journal of Sedimentary Research	Thornburg, J.D. et al.
submitted	Delineating Mid-Cretaceous seismic and well-log sequences to assess carbon storage potential in the northern Baltimore Canyon Trough	Geosphere	Baldwin, K.W. et al.
in prep.	Revised age constraints for Barremian to Cenomanian sequences, offshore U.S. mid-Atlantic margin	Geosphere	Jordan, L. et al.
2019	Summary of geologic data from three core holes drilled through the Potomac Group in the Coastal Plain of Cecil County, Maryland: Report of Investigations No. 87, DNR Publication No. 12-051419-149	Department of Natural Resources - MGS, Resource Assessment Service	Quinn, H.A.

Table 8-4. List of graduate student theses written as part of the Mid-Atlantic Carbon Storage Resource Assessment Project.

Date	Title	School	Student
2019	Seismic stratigraphy of the Georges Bank Basin: Implications for seismic stratigraphy and Carbon Capture and Storage	Rutgers University, master's thesis	Adams, A.
2017	Sequence stratigraphic interpretation of mid-Cretaceous strata from the Great Stone Dome to the continental slope, northern Baltimore Canyon Trough: Implications to sea level and Carbon Capture and Sequestration	Rutgers University, Ph.D. thesis	Lombardi, C.
2019	New Insights on the Mesozoic evolution of the Mid-Atlantic Continental Margin from Integrated Sequence Stratigraphy and Numerical Modeling	Rutgers University, master's thesis	Schmelz, W.
2019	Quantitative Biostratigraphic Analysis of Middle Cretaceous Sequences in Baltimore Canyon Trough, Mid Atlantic U.S. Margin	Rutgers University, master's thesis	Jordan, L.
2019	Georges Bank Basin Stratigraphy: Cretaceous Gamma Log Sequences Correlated with Seismic Data	Rutgers University, master's thesis	Graham, S.

9. Conclusions

The greatest potential for carbon storage in the northeastern United States lies in the offshore geologic formations comprising the continental shelf (Monteverde et al., 2011). Offshore storage can be linked to large point-sources of CO_2 while avoiding many of the logistical difficulties and potential risks encountered when siting onshore projects, especially in densely populated areas of the East Coast. The objectives of the MAOCSRAP are fourfold: (1) complete a systematic carbon storage resource assessment of the mid-Atlantic Offshore coastal region from the GBB through the LIP to the southern BCT; (2) define key input parameters to reduce uncertainty for offshore storage resource and efficiency estimates; (3) perform a preliminary assessment of risk factors, uncertainties and data gaps; and (4) engage industry and regulatory stakeholders through development of a Road Map to assist future project planning and implementation.

Over the past 3 years, the Project Team has compiled, inventoried, and assimilated various publicly available data sets to provide a strong technical basis on which future carbon storage studies and applications can be built. The knowledge infrastructure necessary to support the development of full-scale offshore carbon storage include:

- Defining the geologic characteristics of candidate storage sites (Section 2)
- Using existing seismic data to better define the continuity of the storage zones and seals (Section 3)
- Cataloguing the hydrogeologic properties of mid-Atlantic offshore storage sites (Section 4)
- Calculating prospective CO_2 storage resources using net effective pore volumes and fluid displacement properties specific to offshore lithologies (Section 5)
- Examining risk factors related to offshore storage (Section 6)
- Communicating with industry and other stakeholders about the future prospects for offshore storage (Section 7)
- Ensuring technology transfer to industry and other stakeholders (Section 8)

Led by Battelle, this project was conducted by public and private entities that have expertise in offshore geology and resources for the study region, including state geological surveys of Delaware, Maryland and Pennsylvania; USGS-Woods Hole Coastal and Marine Science Center and Haifa University; Rutgers University; Harvard University; and the LDEO at Columbia University. The storage resource assessment was completed for a broad region offshore of the U.S. East Coast, from Massachusetts to Virginia. The team built on the success of the MRCSP program (www.mrcsp.org), using a regional approach for screening and identifying candidate storage sites with the potential to deliver the most value for the East Coast. The results include high-level storage resource estimates for areas not previously characterized and improved storage resource estimates for geographically expansive portions of offshore geologic units.

Key Outcomes and Results

Legacy seismic, well-log, core, and biostratigraphic data were digitized, reprocessed, and analyzed using modern techniques, augmenting previous characterization efforts. The sequence stratigraphic framework for the Cretaceous and Jurassic strata was developed by correlating well-log depositional sequences to seismic reflectors identified in the BCT, LIP, and GBB. The integration of well-log stratigraphy with seismic stratigraphy and petrophysical analysis helped to identify and map potential storage zones within sequences of the LC, Missisauga, and Mohawk formations.

In total, the Project Team integrated approximately4,000 km of reprocessed seismic data; 2,294 well logs; 2,296 core samples; and 25,000 hydrogeologic property data from 6,640 individual samples. These data were in various conditions and dispersed across several different agencies. Oil and gas operators spent over $1 billion drilling and testing the 44 offshore wells in the study area in the 1970s and 1980s. Therefore, integration and preservation of the information into a database available on EDX is a valuable product for developing CO_2 storage along the offshore Northeast United States.

The data were analyzed to create a structural framework that was used to tie together all available well data, constrain sequence stratigraphic interpretations, and make regional assessments of offshore carbon storage resources. Prospective storage resource estimates suggest mid-Atlantic U.S. offshore formations have combined resources of 150 to 1,136 Mt, enough to store decades of CO_2 from industrial sources in the region.

Offshore geologic risk factors include soft sediment deformation, unit continuity, sedimentological and structural features, seismicity, and hydrates. CO_2 storage risks include inadequate seals, migration/leakage, and chemical interactions leading to decreased storage. Sensitive habitats, environmental impacts, disturbance to seafloor, and other risks need to be identified in advance of project activities and integrated into detailed mitigation plans for all project phases.

Meetings with key stakeholders in the Northeast United States were instrumental in defining the concerns and issues with establishing CCS in the offshore mid-Atlantic. Early engagement and ongoing communication, as well as policy framework development, is key to large-scale deployment of CCS. Input and participation from government, industry, and environmental groups provided input into the Road Map and address next steps needed for project deployment (Figure 9-1).

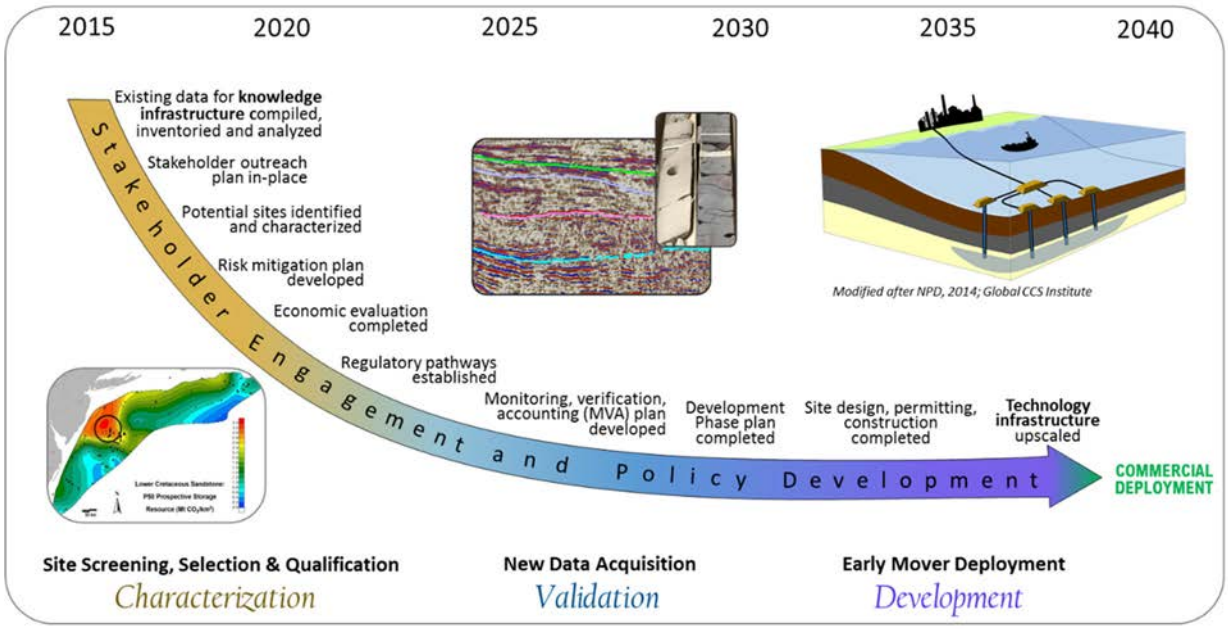

Figure 9-1.Mid-Atlantic Offshore CCS Deployment Road Map.

Next Steps

This project represents an important first step by completing a high-level CO_2 storage resource assessment and building the knowledge infrastructure necessary to improve quantitative storage resource estimates. The data sets that have been curated under this project provide an opportunity to conduct R&D needed to address data gaps and reduce risk and uncertainty. Offshore characterization and validation strategies that are systematically designed to provide data and infrastructure that can be upscaled to meet commercial requirements should be developed.

Near-term actions for further site selection and characterization include use of existing data sets to develop advanced static and dynamic geologic models in the selected area of the GSD to determine the geospatial variability of key storage parameters, site-specific risks, and offshore development potential. Advanced reprocessing using existing seismic data and interpretation of modern seismic data from recent cruises should be performed to evaluate rift basin properties and reservoir capacity. A stakeholder outreach strategy to create champions for CCS R&D in the offshore region and streamline public acceptance of data collection in the marine environment should be implemented as early as possible. Identifying common industry and research goals for collaboration with international projects can build partnerships that lower research costs. Pursuit of onshore or analog data collection opportunities (e.g., drilling, core collection) could also help lower the cost of data collection. Development of regulatory certainty could be facilitated through U.S. regulator meetings with countries (e.g., Norway) where CCS is currently implemented and experiences from offshore oil and gas activities.

Mid-term actions needed for storage feasibility validation include acquisition of new data to address subsurface data gaps for qualifying potential storage sites, mitigating risk, and addressing potential regulatory/permit requirements. New data will be needed to validate caprock petrophysical properties, fracture pressure gradients, leakage risks, reservoir injectivity, and baseline geomechanical, geochemical, and hydrologic properties of storage zones and caprocks. Due to the higher costs and challenges associated with offshore characterization wells, a cost-benefit analysis will be needed to ensure the value of new data acquired meets the specific technical and economic requirements defined for the project. Appropriate monitoring methods will need to be investigated and validated prior to full-scale deployment and incorporated into the development phase plan.

Long-term actions associated with the development stage will include establishing and implementing a detailed plan for large-scale CCS operations based on the findings of the preceding phases and the development of sufficient regulatory and pricing mechanisms to enable financially viable deployment. The progression to development also will depend on the strength of the stakeholder buy-in for offshore CCS deployment in the mid-Atlantic area. Development stage activities typically include the assessment of CO_2 sources and transport, final site selection, detailed design, permitting, construction, operations, and monitoring. Advances in offshore technologies such as advanced characterization, robotics, sub-sea structures, safety mechanisms, and remote operations over the next decade may facilitate cost-effective deployment with enhanced stakeholder confidence. Early mover projects in the United States and globally may help accelerate deployment of CCS through upscaling of technologies that reduce economic and policy barriers to commercial-scale CCS.

10. References

Adams, A. 2019. Seismic stratigraphy of the Georges Bank Basin: implications for carbon sequestration. Master's thesis. Rutgers University: New Brunswick, NJ.

Amato, R., and Bebout, J.W. 1980. Geological and operational summary, COST No. GE-1 well, Southeast Georgia Embayment area, South Atlantic OCS. USGS Open-File Report 78-668.

Baldwin, K.E., Miller, K.G., Schmelz, W.J., Mountain, G.S., Jordan, L.M., and Browning, J.V. 2019 (in review). Cretaceous sequence stratigraphy of the northern Baltimore Cnayone Trough: Implications for tectonic, paleogeographic, and sea-level evolution. Geosphere.

Bachu, S. 2013. Drainage and imbibition CO_2/brine relative permeability curves at in-situ conditions for sandstone formations in western Canada. *Energy Procedia, 37*, 4428-4436.

Battelle. 2018. Mid-Atlantic U.S. Offshore Carbon Storage Resource Assessment Project: Task 6 Risk Factor Analysis Report. Submitted June 30, 2018. DOE Award Number DE-FE0026087.

Benson, S., Esposito, A., Li, B., Krause, M., Krevor, S., Kuo, W., and Zou, L. 2009. Residual Trapping of Carbon Dioxide. Annual Report: Stanford Dept. of Energy Resources. 41 p.

Blackford, J. C., Stahl, H., Bull, J. M., Bergès, B. J. P., Cevatoglu, M., Lichtschlag, A., … Widdicombe, S. 2014. Detection and impacts of leakage from sub-seafloor deep geological carbon dioxide storage. *Nature Climate Change, 4*, 1011-1016.

BOEM (Bureau of Ocean Energy Management). 2014. *Atlantic OCS Proposed Geological and Geophysical Activities Mid-Atlantic and South Atlantic Planning Areas Final Programmatic Environmental Impact Statement*, Bureau of Ocean Energy Management. Prepared under Task Order No. M11PD00013. 788 p.

Brothers, D.S., ten Brink, U.S., Andrews, B.D., and Chaytor, J.D. 2013. Geomorphic characterization of the U.S. Atlantic continental margin. *Marine Geology*, *338*, 46-63.

Brown, A., Berlin, E., Butsch, R., Senel, O., Mills, J., Harichandran, A., and Wang, J. 2011. Carbon Capture and Sequestration: Ascertaining CO_2 Storage Potential, Offshore New Jersey, USA. Offshore Technology Conference, Houston Texas, May 2-5, 2011.OTC 21995.

Brown, G. 2017. Marine Monitoring for CCS…or Boaty McBoatFace's next adventure. IEAGHG Monitoring Meeting, Traverse City, MI. June 2017.

Browning, J.V., Miller, K.G., Sugarman, P.J., Kominz, M.A., McLaughlin, P.P., Kulpecz, A.A., and Feigenson, M.D.. 2008. 100 Myr record of sequences, sedimentary facies and sea level change from Ocean Drilling Program onshore coreholes, US mid-Atlantic coastal plain: Basin Research, v. 20, p. 227-248.

Cohen, D., Person, M., Wang, P., Gable, C., Hutchinson, D., Marksamer, A., … Lane, J. W. Jr. 2010. Origin and Extent of Fresh Paleowaters on the Atlantic Continental Shelf, USA. *Ground Water*, *48*(1), 143-158.

DOE-NETL. 2011. Best Practices for Risk Analysis and Simulation for Geologic Storage of CO_2, version 1.0. U.S. Department of Energy, National Energy Technology Laboratory, DOE/NETL-2011/1459.

DOE-NETL. 2013. Best Practices for Risk Analysis and Simulation for Geologic Storage of CO_2, version 2.0. U.S. Department of Energy, National Energy Technology Laboratory, DOE/NETL-2013/1459.

DOE-NETL. 2017. Best Practices for Site Screening, Selection, and Initial Characterization for Storage of CO_2 in Deep Geologic Formations. DOE/NETL-2017/1844.

Doyle, J. 1982. Palynology of continental Cretaceous sediments, Crisfield geothermal test well, eastern Maryland, pt. 2: in: Waste Gate Formation: Maryland Department of Natural Resources, Geological Survey Open-File Report, p. 82-02.

EIA (United States Energy Information Administration). 2018. Annual Energy Outlook 2018 with projections to 2050. U.S. Energy Information Administration Office of Energy Analysis, February 2018.

Erickson, S. N., and Jarrard, R. D. 1998. Velocity-porosity relationships for water-saturated siliciclastic sediments, *J. Geophy. Res.*, *103*(B12), 30385–30406, doi:10.1029/98jb02128.

Espinoza, D.N., and Santamaria, J.C. 2017. CO_2 breakthrough- Caprock sealing efficiency and integrity for carbon geological storage. International Journal of Greenhouse Gas Control, 66: 218-229.

Fortin, W., Goldberg, D., and Slagle, A. 2018. Carbon Capture and Storage Potential Offshore the U.S. East Coast: New Methods and Insights from Legacy Seismic Data. 14th Greenhouse Gas Control Technologies Conference Melbourne 21-26 October 2018 (GHGT-14). Available at SSRN: https://ssrn.com/abstract=3365637

Fry, C. 1987. Geothermal Gradient in Geologic and Operational Summary, COST No. B-3 Well, Baltimore Canyon Trough Area, Mid-Atlantic OCS, Open File Report 79-1159.

Goodman, A., Hakala, A., Bromhal, G., Deel, D., Rodosta, T., Frailey, S., Small, M., Allen, D., Romanov, V., Fazio, J., Huerta, N., McIntyre, D., Kutchko, B., and Guthrie, G. 2011. U.S. DOE methodology for the development of geologic storage potential for carbon dioxide at the national and regional-scale. Int. J. Greenh. Gas Con., vol. 5, pp. 952–965.

Goodman, A., Sanguinito, S., and Levine, J.. 2016. Prospective CO_2 resource estimation methodology: Refinement of existing US DOE-NETL methods based on data availability. Int. J. Greenh. Gas Con., vol. 54, pp. 242-249.

Gorecki, C., Ayash, S., Guoxiang, L.l Braunberger, J., Dotzenrod, N. 2015. A comparison of volumetric and dynamic CO_2 storage resource and efficiency in deep saline formations. Int. J. Greenh. Gas Con., 42, 213–225.

Graham, S. 2018. Georges Bank Basin stratigraphy: Cretaceous gamma log sequences correlated with seismic data: Master’s thesis. Rutgers University: New Brunswick, NJ.

Grow, J. A., and Sheridan, R. E. (Eds.). 1988. U.S. Atlantic continental margin: A typical Atlantic-type or passive continental margin. *The Atlantic Continental Margin* (Vol. 1-2, pp. 1-7). Geological Society of America.

Hannis, S., Chadwick, A., Connelly, D., Blackford, J., Leighton, T., Jones, D., … Dixon, T. 2017. Review of Offshore CO_2 Storage Monitoring: Operational and Research Experiences of Meeting Regulatory and Technical Requirements. *Energy Procedia*, *114*, 5967-5980.

Hansen, H. 1982. Hydrogeologic framework and potential utilization of the brine aquifers of the Waste Gate Formation, a new unit of the Potomac Group underlying the Delmarva Peninsula, pt. 1: Waste Gate Formation: Maryland Department of Natural Resources, Geological Survey Open-File Report, p. 82-02.

Haq, B. U. 2014. Cretaceous eustasy revisited: Global and Planetary Change, v. 113, p. 44-58.

Hill, J.C., Driscoll, N.W., Weissel, J.K., and Goff, J.A. 2004. Large-scale elongate gas blowouts along the U.S. Atlantic margin. J. Geophys. Res. 109, B09101.

Hutchinson, D.R., Klitgord, K.D., and Detrick, R.S. 1986. Rift basins of the Long Island platform. *Geologic Society of America Bulletin,* 97, 688-702.

IEAGHG (International Energy Agency Greenhouse Gas). 2016. International Workshop on Offshore Geologic CO_2 Storage. Report: 2016/TR2, May 2016.

Jansa, L. F. 1981. Mesozoic carbonate platforms and banks of the eastern North American margin: Marine Geology, v. 44, p. 97-117.

Jensen, J., Lake, L.W, Corbett, P., and Goggin, D. 2000. Statistics for Petroleum Engineers and Geoscientists. Elsevier, New York, NY.

Jordan, L. 2019. Quantitative biostratigraphic analysis of middle Cretaceous sequences in the Baltimore Canyon Trough, offshore mid-Atlantic U.S. Margin: Master's thesis. Rutgers University. New Brunswick, NJ.

Klitgord, K. D., D. R. Hutchinson, and H. Schouten. 1988. U.S. Atlantic continental margin; Structural and tectonic framework, in R. E. Sheridan, and J. A. Grow, eds., The Atlantic Continental Margin, U.S.: The Geology of North America, v. I-2: Boulder, CO, The Geological Society of America, p. 19-55.

Kohout, F. A., Hathaway, J., Folger, D., Bothner, M., Walker, E., Delaney, D., … Rhodehamel, E. 1977. Fresh groundwater stored in aquifers under the continental shelf, implications from a deep test, Nantucket Island, Massachusetts. J*ournal of the American Water Resources Association, 13*(2), 373-386.

Kominz, M.A., Miller, K.G., and Browning, J.V. 1998. Long-term and short-term global Cenozoic sea-level estimates: Geology, v. 26, p. 311-314.

Kominz, M.A., Van Sickel, W.A., Miller, K.G., and Browning, J.V.. 2002. Sea-level estimates for the latest 100 million years: one-dimensional backstripping of onshore New Jersey boreholes, in: Armentrout, J., and Rosen, N., eds., Sequence Stratigraphic Models for Exploration and Production: Evolving Methodology, Emerging Models and Application Case Histories: 22nd

Annual Gulf Coast Section, SEPM Foundation, Bob F. Perkins Research Conference, Proceedings, p. 303–315.

Kramer, K. V., and Shedd, W. W. 2017. A 1.4-billion-pixel map of the Gulf of Mexico seafloor, Eos, 98, https://doi.org/10.1029/2017EO073557. Published on 24 May 2017.

Libby-French, J. 1984. Stratigraphic Framework and Petroleum Potential of Northeastern Baltimore Canyon Trough, Mid-Atlantic Outer Continental Shelf. *AAPG Bulletin, 68*(1), 50-73.

Leighton, T. G., and White, P. R. 2012. Quantification of undersea gas leaks from carbon capture and storage facilities, from pipelines and from methane seeps, by their acoustic emissions. *Proceedings of the Royal Society 2012*, *468*, 485-510.

Lombardi, C. 2017. Sequence stratigraphic interpretation of mid-Cretaceous strata from the Great Stone Dome to the continental slope, northern Baltimore Canyon Trough: Implications to sea level and Carbon Capture and Sequestration. Rutgers University, Ph.D. thesis.

Manspeizer, W., and Cousminer, H. 1988. Late Triassic Early Jurassic synrift basins of the U.S. AtlanticMargin; in Sheridan, R.E. and Grow, J.A. (eds.), The Geology of North America, vol. 1 2, The Atlantic Continental Margin, U.S.: Geol. Soc. America, p. 197 216.

Matter, J.M., Stute, M., Snæbjçrnsdottir, S.Ó., Oelkers, E. H., Gislason, S.R., Aradottir, E. S., Sigfusson, B., Gunnarsson, I., Sigurdar-dottir, H., Gunnlaugsson, E., Axelsson, G., Alfredsson, H. A., Wolff-Boenisch, D., Mesfin, K., Fernandez de la Reguera Taya, D., Hall, J., Dideriksen, K., and Broecker, W. S. 2016. Rapid carbon mineralization for permanent disposal of anthropogenic carbon dioxide emissions, *Science*, 352 ,1312–1314, doi: 10.1126/science.aad8132.

Miller, K. G., Sugarman, P. J., Browning, J. V., Kominz, M. A., Olsson, R. K., Feigenson M. D., and Hernández, J. C.. 2004. Upper Cretaceous sequences and sea-level history, New Jersey coastal plain: Geological Society of America Bulletin, v. 116, p. 368-393.

Miller, K. G., Kominz, M. A., Browning, J. V., Wright, J. D., Mountain, G. S., Katz, M. E., Sugarman, P. J., Cramer, B. S., Christie-Blick, N., and Pekar, S. F.. 2005. The Phanerozoic record of global sea-level change: Science, v. 310, p. 1293-1298.

Miller, K.G., Browning, J.V., Mountain, G.S., Bassetti, M.A., Monteverde, D., Katz, M.E., Inwood, J., Lofi, J., and Proust, J.-N. 2013. Sequence boundaries are impedance contrasts: Core-seismic-log integration of Oligocene-Miocene sequences, New Jersey shallow shelf: Geosphere, v. 9, p. 1257-1285, doi:10.1130/GES00858.1

Miller, K.G., Browning, J.V., Sugarman, P.J., Monteverde, D.H., Andreasen, D.C., Lombardi, C., Thornburg, J., Fan, Y., and Kopp, R.E. 2017. Lower to mid-Cretaceous sequence stratigraphy and characterization of CO_2 storage potential in the Mid-Atlantic US Coastal Plain: Journal of Sedimentary Research, v. 87, no. 6, p. 609-629.

Miller, K.G., Lombardi, C.J., Browning, J.V., Schmelz, W.J., Gallegos, G., Mountain, G.S., and Baldwin, K.E. 2018. Back to basics of sequence stratigraphy: early Miocene and mid-Cretaceous examples from the New Jersey paleoshelf: Journal of Sedimentary Research, v. 88, no. 1, p. 148-176.

Mishra, S., and Datta Gupta, A. 2018. Applied Statistical Modeling and Data Analytics: A Practical Guide for the Petroleum Geosciences. Elsevier, Cambridge, MA.

Mitchum, R., and Vail, P. 1977. Seismic Stratigraphy and Global Changes of Sea Level: Part 7. Seismic Stratigraphic Interpretation Procedure: Section 2. Application of Seismic Reflection Configuration to Stratigraphic Interpretation, in C. E. Payton, ed., Seismic Stratigraphy--Applications to Hydrocarbon Exploration: Memoir, v. 26, American Association of Petroleum Geologists.

Mitchum, R., Vail, P., and Sangree, J. 1977. Seismic stratigraphy and global changes of sea level: Part 6. Stratigraphic interpretation of seismic reflection patterns in depositional sequences: Section 2. Application of seismic reflection configuration to stratigraphic interpretation, in C. E. Payton, ed., Seismic Stratigraphy--Applications to Hydrocarbon Exploration: Memoir, v. 26, American Association of Petroleum Geologists.

Monteverde, D.H., Sugarman, P.J., Miller, K.G., Brownign, J.V., Mountain, G.S., Reinfelder, Y., Romero, P., and Seker, Z. 2011. Characterization of the carbon dioxide storage potential beneath the continental shelf and slope offshore New Jersey, in New Jersey Geological Survey, Preliminary Characterization of CO_2 Sequestration Potential in New Jersey and the Offshore Coastal Region: Midwest Regional Carbon Sequestration Partnership, Final Report.

Moucha, R., Forte, A.M., Mitrovica, J.X., Rowley, D.B., Quere, S., Simmons, N.A., and Grand, S.P. 2008. Dynamic topography and long–term sea level variations: there is no such thing as a stable continental platform: Earth and Planetary Science Letters, v. 271, p. 101–108.

Mountain, G. S., and Tucholke, B. E. 1985. Mesozoic and Cenozoic geology of the US Atlantic continental slope and rise, in C. W. Poag, ed., Geologic Evolution of the United States Atlantic Margin, Van Nostrand Reinhold Co., p. 293-341.

Mountain, G., Proust, J.-N., McInroy, D., Cotterill, C., and the Expedition 313 Scientists. 2010. *Proceedings of the Integrated Ocean Drilling Program, 313*: Tokyo, Integrated Ocean Drilling Program Management International, Inc.

Mountain, G., and D. Monteverde. 2012. If You've Got the Time, We've Got the Depth: The Importance of Accurate Core-Seismic Correlation: AGU Fall Meeting Abstracts.

New Jersey Geological Survey. 2011. Preliminary Characterization of CO_2 Sequestration Potential in New Jersey and the Offshore Coastal Region: Midwest Regional Carbon Sequestration Partnership. Final Report, 98 pp;. http://www.mrcsp.org/phase-ii-geologic-reports

Newman, K.R., Cormier M.H., Weissel J.K., Driscoll N.W., Kastner M., Solomon E.A., Robertson G., Hill J.C., Singh H., Camilli R., and Eustice R. 2008. Active methane venting observed at giant pockmarks along the U.S. mid-Atlantic shelf break. Earth and Planetary Science Letters. 267:341-352.

Norwegian Petroleum Directorate. 2011. CO_2 Storage Atlas: Norwegian North Sea. Norwegian Petroleum Directorate, Stavanger. www.npd.no/Global/Norsk/3-Publikasjoner/Rapporter/PDF/CO_2-ATLAS-lav.pdf.

Norwegian Petroleum Directorate. 2013. CO_2 Storage Atlas: Barents Sea. Norwegian Petroleum Directorate, Stavanger. www.npd.no/Global/Norsk/3-Publikasjoner/Rapporter/PDF/CO_2-ATLAS-lav.pdf.

Olsen, P. E. 1997. Stratigraphic record of the early Mesozoic breakup of Pangea in the Laurasia–Gondwana rift system. *Annual Review of Earth and Planetary Sciences, 25*, 337-401.

Olsson, R.K., Gibson, T.G., Hansen, H.J., and Owens, J.P. 1988. Geology of the northern Atlantic coastal plain: Long Island to Virginia, *in* Sheridan, R.E., and J.A. Grow, eds., The Atlantic Continental Margin: Geological Society of America, Geology of North America, v. 1–2, p. 87–105.

Pawar, R., Chu, S., Stauffer, P., Bromhal, G., Dilmore, R., Guthrie, G., … Gastelum, J. 2014. Quantification of key long-term risks at CO_2 sequestration sites: Latest results from US DOE's National Risk Assessment Partnership (NRAP) Project. *Energy Procedia. 4*, 2014, Proceedings of the 12th International Conference on Greenhouse Gas Control Technologies, Austin, Texas, USA.

Peltier, W.R. 1998. Postglacial variations in the level of the sea: Implications for climate dynamics and solid-Earth geophysics: Reviews of Geophysics, v. 36, p. 603-689.

Poag, C. W. 1985. Depositional history and stratigraphic reference section for central Baltimore Canyon trough, in C. W. Poag, ed., Geologic Evolution of the United States Atlantic Margin: New York, Van Nostrand Reinhold, p. 217-263.

Poag, C. W., and Valentine, P. C. 1988. Mesozoic and Cenozoic stratigraphy of the United States Atlantic continental shelf and slope, in R. E. Sheridan, and J. A. Grow, eds., The Atlantic Continental Margin: US: The Geology of North America, v. I-2: Boulder, CO, The Geological Society of America, p. 67-86.

Pope, D. A., and Gordon, A. D. 1999. Simulation of groundwater flow and movement of the freshwater-saltwater interface in the New Jersey Coastal Plain. U.S. Geological Survey Water-Resources Investigations Report, 98–4216, 169 p.

Post, P., and Coleman, J. 2015. Mesozoic Rift Basins of the U.S. Central Atlantic Offshore: Comparisons with Onshore Basins, Analysis, and Potential Petroleum Prospectivity Petroleum Systems in “Rift” Basins. Gulf Coast Section SEPM (GCSSEPM), Houston, Texas, USA, 12-16 December 2015.

Raymo, M.E., Mitrovica, J.X., O’Leary, M.J., DeConto, R.M., and Hearty, P.J. 2011. Departures from eustasy in Pliocene sea-level records: Nature Geoscience, v. 4, p. 328-332.

Robbins, E. 1979. Geological Studies of the COST GE-1 Well, U.S. South Atlantic Outer Continental Shelf Area: Geothermal Gradients. U.S. Geological Survey Circular 800, 119 p.

Rowley, D.B., Forte, A.M., Moucha, R.R., Mitrovica, J.X., Simmons, N.A., and Grand, S.P. 2011. Dynamic Topography Change of the Eastern U.S. since 4 Ma: Implications for Sea Level and Stratigraphic Architecture of Passive Margins: Science, v. 340, p. 1563-1563.

Sanguinito, S., Goodman, A., and Levine, J.S. 2016. NETL CO_2 Storage prospeCtive Resource Estimation Excel aNalysis (CO_2-SCREEN) User’s Manual; NETL-TRS-X-2016; Technical Report

Series; U.S. Department of Energy, National Energy Technology Laboratory: Pittsburgh, Pennsylvania, 2016; p. 31.

Savage, D., Maul, P. R., Benbow, S., and Walke, R. C. 2004. A Generic FEP Database for the Assessment of Long-Term Performance and Safety of the Geological Storage of CO_2, Version 1.0. Quintessa Document # QRS-1060A-1.

Schmelz, W.J., Miller, K.G., Mountain, G.S., Browning, J.V., and Baldwin, K.E. 2019 (accepted). Onshore-offshore correlations of Cretaceous fluvial-deltaic sequences, southern Baltimore Canyon Trough: AAPG Bulletin.

Seker, Z. 2012. Cretaceous well-log and sequence stratigraphic correlation of the outer continental shelf and upper slope off of New Jersey: Master's thesis, Rutgers University, New Brunswick, NJ, 155 p.

Slater, B., Stolorow, A., and Smith, L. 2010. Potential for Supercritical Carbon Sequestration in the Offshore Bedrock Formations of the Baltimore Canyon Trough, in AAPG Eastern Section Meeting, Kalamazoo, Michigan.

SPE (Society of Petroleum Engineers). 2017. Storage Resources Management System (SRMS).

Steckler, M. S., and Watts, A. B. 1982. Subsidence history and tectonic evolution of Atlantic-type continental margins. *Dynamics of Passive Margins*, Scrutton, R. A., ed., AGU Geodynamic Ser: 6: 184-196.

Thornburg, J.D., Miller, K.G., Browning, J.V., McLaughlin, P.P., and Sugarman, P.J. 2016. Sequence stratigraphic framework of the mid-Cretaceous nonmarine Potomac Formation in New Jersey and Delaware. Geological Society of America, Denver, CO. January 2016.

Thornburg, J.D., Miller, K.G., Browning, J.V., and Wright, J.D. 2019. Mid-Cretaceous. Paleopedology and Landscape Reconstruction of the Mid-Atlantic U.S. Coastal Plain. Journal of Sedimentary Research, 89, 253–272. DOI: http://dx.doi.org/10.2110/jsr.2019.12

Trevino, R. and Meckel, T., (Eds). 2017. Geologic CO_2 Sequestration Atlas of Miocene Strata, Offshore Texas State Waters. Bureau of Economic Geology. The University of Texas at Austin. Report of Investigations No. 283.

Triezenberg, P., Hart, P., and Childs, J. 2016. National Archive of Marine Seismic Surveys: A USGS Data Website for the curation and dissemination of marine seismic reflection profile data within the US Exclusive Economic Zone (EEZ) and Extended Continental Shelf, United States Geological Survey.

van Geldern, R., Hayashi, T., Bottcher, M., Mottl, M., Barth, J., and Stadler, S. 2013. Stable isotope geochemistry of pore waters and marine sediments from the New Jersey shelf: Methane formation and fluid origin. *Geosphere, 9*(1), 96–112.

Watts, A.B. 1981. The U.S. Atlantic continental margin: subsidence history, crustal structure, and thermal evolution, *in* Bally, A.W., ed., Geology of Passive Continental Margins: History, Structure, and Sedimentologic Record: American Association of Petroleum Geologists, Education Course Note Series 19, p. 1–70.

Withjack, M. O., Schlische, R. W., and Olsen, P. E. 1998. Diachronous rifting, drifting, and inversion on the passive margin of central eastern North America: An analog for other passive margins. *American Association of Petroleum Geologists Bulletin, 82*, 817-835.

WRI (World Resources Institute). 2008. Guidelines for the capture, transportation and storage of carbon dioxide. Washington DC.

Zapecza, O. S. 1989. Hydrogeologic framework of the New Jersey coastal plain, Open-File Report, United States Geological Survey, p. 61

Zhao, H., Fedkin M. V., Dilmore, R. M., and Lvov, S. N. 2015. Carbon dioxide solubility in aqueous solutions of sodium chloride at geological conditions: Experimental results at 323.15, 373.15, and 423.15 K and 150 bar and modeling up to 573.15 K and 2000 bar. Geochimica et Cosmochimica Acta, 149, 165 189.

Zhou, Y., Dimitrios G., Hatzignatiou, Y. G., and Helland, J. O. 2017. On the estimation of CO_2 capillary entry pressure: Implications on geological CO_2 storage. *International Journal of Greenhouse Gas Control, 63*, 26-36.

Attachment A: Task 2 Final Report - Data Collection Report

Mid-Atlantic U.S. Offshore Carbon Storage Resource Assessment Project

Final Regional Stratigraphic Framework Topical Report

MID-ATLANTIC U.S. OFFSHORE CARBON STORAGE RESOURCE ASSESSMENT PROJECT

DOE Award Number DE-FE0026087

Prepared by:
Battelle
505 King Avenue
Columbus, OH 43201-2696
Principal Investigator: Dr. Neeraj Gupta
Project Manager: Ms. Lydia Cumming

Prepared for:
The U.S. Department of Energy
National Energy Technology Laboratory
Project Manager: Mr. William O'Dowd

July 31, 2017

Disclaimer

This report was prepared as an account of work sponsored by an agency of the United States Government. Neither the United States Government, nor any agency thereof, nor any of their employees, makes any warranty, express or implied, or assumes any liability or responsibility for the accuracy, completeness, or usefulness of any information, apparatus, product, or process disclosed, or represents that its use would not infringe privately owned rights. Reference herein to any specific commercial product, process, or service by trade name, trademark, manufacturer, or otherwise does not necessarily constitute or imply its endorsement, recommendations, or favoring by the United States Government or any agency thereof. The views and the opinions of authors expressed herein do not necessarily state or reflect those of the United States Government or any agency thereof.

This technical summary report contains preliminary findings related to project progress and should not be considered final.

Acknowledgements

This material is based upon work supported by the Department of Energy under Award Number DE-FE0026087. The Project Team is led by Battelle and includes the state geological surveys of Delaware, Maryland, and Pennsylvania; United States Geological Survey (USGS); Lamont-Doherty Earth Observatory at Columbia University (LDEO); and Rutgers University. Harvard University, Texas Bureau of Economic Geology, and Virginia Department of Mines, Minerals, & Energy serve as technical advisors.

Battelle was responsible for the overall project execution, including project management and technical analysis. Dr. Neeraj Gupta was the Battelle Principal Investigator for this work and Ms. Lydia Cumming provided project management and technical coordination between team members. Other Battelle team members contributing to this report included Ms. Isis Fukai, Mr. Andrew Burchwell, and Mr. Joel Sminchak. Correlation of seismic data with well log data and characterization of geologic storage zones were performed by Rutgers University (Dr. Ken Miller, Dr. Gregory Mountain, Dr. Christopher Lombardi, Mr. William Schmelz, Ms. Kimberly Baldwin, Mr. Stephen Graham, and Mr. Paul Romero) and USGS (Dr. Uri ten Brink and Mr. Guy Lang (Haifa University).

The authors are especially thankful for support relating to Task 2, including: the geological data compilation efforts undertaken by Dr. Mojisola KunleDare and Dr. Peter McLaughlin at the Delaware Geological Survey, well log digitization efforts led by Ms. Kristen Carter and Mr. Brian Dunst at the Pennsylvania Geological Survey, and management of the ArcGIS online database by Mr. Andrew Stanley and Mr. David Andreasen at the Maryland Geological Survey.

Table of Contents

List of Figures

List of Tables

List of Appendices

Acronyms

2D	Two-dimensional
3D	Three-dimensional
AGOL	ArcGIS Online
API	American Petroleum Institute
BCT	Baltimore Canyon Trough
BOEM	Bureau of Ocean Energy Management
CALI	Caliper
CDP	Common Depth Point
CO_2	Carbon Dioxide
COST	Continental Offshore Stratigraphic Test
CS	Checkshot
DT	Sonic Log
DGS	Delaware Geological Survey
EPA	Environmental Protection Agency
FSST	Falling Stage Systems Tract
ft	foot
GAPI	American Petroleum Institute Gamma Ray Unit
GBB	Georges Bank Basin
GIS	Geographic Information System
GR	Gamma Ray
GSD	Great Stone Dome
Gt	Gigaton
HO	Highest Occurrence
HST	Highstand Systems Tract
ISWT	Integrated Seismic Well Tie
KB	Kelly Bushing
km	kilometer
K/Pg	Cretaceous-Paleogene Boundary
LAS	Log ASCII Standard
LC1, etc.	Logan Canyon 1, etc. (sequence)

LDEO	Lamont-Doherty Earth Observatory
LST	Lowstand Systems Tract
Ma	Million Years Ago
mbsf	Meters Below Sea Floor
MCS	Multichannel Seismic
mD	Millidarcy
MFS	Maximum Flooding Surface
MICP	Mercury Injection Capillary Pressure
MK1, etc.	Middle Cretaceous 1, etc. (sequence)
MRCSP	Midwest Regional Carbon Sequestration Partnership
ms	millisecond
MS	Microsoft
NAMSS	National Archive of Marine Seismic Surveys
NETL	National Energy Technology Laboratory
NOAA	National Oceanic and Atmospheric Administration
NPHI	Neutron Porosity
NSF	National Science Foundation
OCS	Outer Continental Shelf
OPD	Official Protraction Diagram
PGS	Pennsylvania Geological Survey
PRS	Formation Pressure
PSTM	Pre-Stack Time-Migration
QA/QC	Quality Assurance/Quality Control
RHOB	Bulk Density
RT	Resistivity
s	Second
SEG Y	Society of Exploration Geophysicists “Y” format
Son Cal	Sonic Calibration
SP	Spontaneous Potential
SWC	Sidewall Core
TD	Total Depth (measured)

TEMP	Formation Temperature
TS	Transgressive Surface
TST	Transgressive Systems Tract
TVD	Total Vertical Depth
TWTT	Two-Way Travel Time
UK1	Upper Cretaceous 1 (sequence)
U.S. DOE	U.S. Department of Energy
USGS	United States Geological Survey
V-D	Velocity-Depth
XRF	X-ray fluorescence

Executive Summary

The Mid-Atlantic U.S. Offshore Carbon Storage Resource Assessment Project (FE0026087) is part of the U.S. Department of Energy (U.S. DOE) National Energy Technology Laboratory's (NETL) Carbon Storage program to improve the effectiveness and reduce the costs of carbon dioxide (CO_2) storage implementation. The objectives of the Mid-Atlantic U.S. Offshore Carbon Storage Resource Assessment Project are to 1) complete a systematic carbon storage resource assessment of the offshore mid-Atlantic coastal region from the Georges Bank Basin (GBB) through the Long Island Platform to the southern Baltimore Canyon Trough (BCT), 2) define key input parameters to reduce uncertainty for offshore resource assessment and efficiency estimates, 3) examine risk factors, and 4) engage industry and regulatory stakeholders through development of a road map to assist future project planning and implementation.

This work fits into DOE's larger effort to develop carbon capture and storage (CCS) as an option for future investment in a low-carbon energy development pathway. To support development of CCS applications, it is important that the U.S. develop a detailed geologic assessment of the carbon storage capacity on a regional basis. The Northeast and Mid-Atlantic regions have challenging onshore geology that make carbon storage limited to small isolated areas with limited capacity. In contrast, the offshore sediments on the continental shelf are ideal for carbon storage. Identifying commercial ready storage sites are critical for deployment of advanced capture technologies. This project establishes the basis for future CCS development in the offshore environment when the market conditions are appropriate.

The project will provide DOE a comprehensive examination of potential storage resource and data integration study for an area of the offshore not previously characterized for carbon storage. This Task 2 deliverable provides an interim report on developing a regional stratigraphic framework to evaluate the deep saline formations and caprocks. This effort includes data compilation and synthesis; construction of a digital database of logs and geophysical data; correlation of seismic data with well log data; construction of the geologic framework via interpretation of porosity and mineralogy using well log data and core data; and construction of new formation maps and geologic cross-sections.

For many large CO_2 point sources along the U.S. Atlantic Coast, significant potential for carbon storage lies in offshore geologic formations. The project is using existing data to answer questions about potential storage opportunities. Much of the geologic information was derived from 44 deep exploratory wells and seismic surveys completed during the 1970s and 1980s. A significant effort was made to create electronic versions of paper logs, well reports, and core laboratory reports, as the data quality and format varied widely. The project databases to storage, manage, analyze and distribute information have been built. Work flows for both geologic and seismic data synthesis and analysis have been developed and will continue to be elaborated and refined. Sequence stratigraphic analysis has been especially useful to determine variations in lithology and lateral correlations across the study area. In areas without well data, existing seismic data has been used to build the framework. Preliminary results suggest the presence of laterally continuous sandstone formations and seals that offer significant potential storage capacity. Prospective storage resource estimates will be developed for detailed study areas and extrapolated to the larger regional stratigraphic framework to complete the carbon storage resource assessment for the region.

1.0 Introduction

1.1 Project Background

The Mid-Atlantic U.S. Offshore Carbon Storage Resource Assessment Project (FE0026087) is part of the U.S. Department of Energy (U.S. DOE) National Energy Technology Laboratory's (NETL) Carbon Storage program to improve the effectiveness and reduce the costs of carbon dioxide (CO_2) storage implementation. This project aims to develop an informative picture of offshore storage potential and viable geologic storage options for the mid-Atlantic U.S. (Figure 1-1).

The objectives of this project are to 1) complete a systematic carbon storage resource assessment of the Mid-Atlantic Offshore study area; 2) define key input parameters to reduce uncertainty for offshore resource assessment and efficiency estimates; 3) examine risk factors that may impact storage resource estimates; and 4) engage industry and regulatory stakeholders through development of a road map to assist future project planning and implementation.

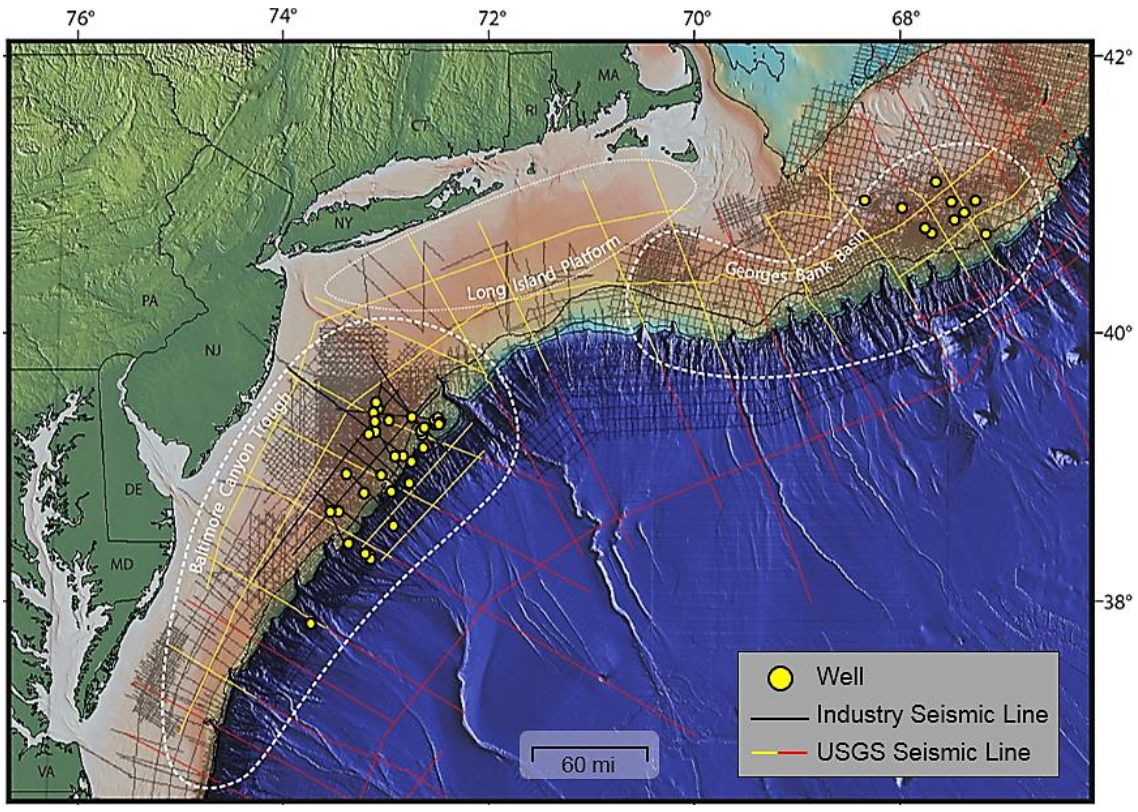

Figure 1-1. Map of the Mid-Atlantic Offshore Carbon Storage Resource Assessment Project study area showing outlines of the three main subregions with the locations of wells and seismic lines.

Note: Dashed lines approximate the subregion outlines based on the 5-km structural contour.

This study will gather and integrate data from a variety of sources: geologic samples from research borehole cores, Continental Offshore Stratigraphic Test (COST) wells, and petroleum exploration wells; analog data from onshore coastal plain studies; and publicly available seismic survey data. The anticipated outcomes include a regional-scale storage resource assessment for areas of the mid-Atlantic not previously characterized, and volumetric storage resource estimates for geographically expansive offshore geologic units. In addition, the Project Team will review and update guidance on efficiency factors for offshore resource assessment and best practices for site selection criteria.

The project is led by Battelle in Columbus, Ohio. The Project Team includes the state geological surveys of Maryland, Delaware, and Pennsylvania; the United States Geological Survey; Rutgers University; Harvard University; and Lamont-Doherty Earth Observatory (LDEO) at Columbia University. In addition, the Texas Bureau of Economic Geology and Virginia Department of Mines, Minerals, & Energy serve as technical advisors to the Project Team.

1.2 Geologic Background and Overall Approach

The Mid-Atlantic Offshore study area encompasses nearly 171,000 square kilometers (km^2) along the mid-Atlantic states of Virginia, Maryland, Delaware, New York, New Jersey, and Pennsylvania (see Figure 1-1). The study area comprises three major subregions: Georges Bank Basin (GBB), Long Island Platform, and Baltimore Canyon Trough (BCT). The project study area extends from within 10 kilometers (km) to 300 km offshore, encompassing the inner continental shelf to portions of the continental slope. Water depths in the mid-Atlantic continental shelf grade gently from zero depth along the shoreline to the depths of 100 to 200 meters (m) at the continental slope. Along the continental slope, water depths plummet more than 2,000 m into the North Atlantic Basin.

The Mid-Atlantic U.S. passive continental margin contains thick (2- to 16-km) post-rift (upper Lower Jurassic and younger) sediments in the offshore basins and thinner (0- to 2.4-km) uppermost Jurassic to Holocene sediment in the onshore coastal plain in the Salisbury Embayment (e.g., Grow and Sheridan, 1988). Rifting occurred during the Late Triassic to earliest Jurassic (230 to 198 million years ago [Ma]) followed by extrusion of Early Jurassic seaward dipping basalts. Seafloor spreading began prior to the Callovian (~165 Ma; Middle Jurassic) (e.g., Grow and Sheridan, 1988), with the likely opening beginning off Georgia ca. 200 Ma and progressing northward off the mid-Atlantic margin by ca. 180 Ma (Withjack et al., 1998). This south-to-north “zipper” onset of seafloor spreading is associated with a diachronous post-rift unconformity that separates active “rift-stage” deposits from more passive margin “drift-stage” deposits that accumulated in an ever-widening and deepening basin open to the ocean. Post-rift history was generally dominated by passive simple thermoflexural subsidence and loading (Steckler and Watts, 1982; Grow and Sheridan, 1988; Kominz et al., 1998). Subsidence began offshore in the Early Jurassic and progressively moved onshore from the Late Jurassic to Early Cretaceous (ca. 150 to 125 Ma) as a thermoflexural response to increasing crustal rigidity (Watts, 1981; Grow and Sheridan, 1988; Olsson et al., 1988). The region has provided an excellent record of relative sea-level changes (e.g., Olsson et al., 1988; Miller et al., 2005), though glacial isostatic adjustments complicate the Pliocene and younger record (e.g., Peltier,

1998; Raymo et al., 2011) and deposition has been impacted by mantle-based dynamic topography changes (Moucha et al., 2008; Rowley et al., 2011).

The offshore basins contain a thick succession of Paleogene to Jurassic sedimentary rocks above crystalline basement that lies at depths of 5 to 15 km. The sedimentary rocks consist of layers of mudstone, shales, sandstone, carbonates, and evaporites that dip to the east-southeast toward the continental slope (Libby-French, 1984). The sedimentary rocks overlie deeper rift basin strata, Early Jurassic flows and sills associated with the Central Atlantic Magmatic Province, continental crust, and oceanic crust. Younger quaternary clay, siltstone, and sand overlie the Paleogene-Triassic sedimentary rocks, with ocean sediments present at the ocean floor. Local structures such as igneous intrusions, salt diapirs, growth faults, and escarpments are present in portions of the Mid-Atlantic Offshore study area (Figure 1-2).

Previous work indicates that sandstone formations in this region have porosities of 25% and permeabilities greater than 100 millidarcys (mD) (e.g., Amato and Bebout, 1980; Slater, 2010). Case studies from the northern Newark basin (onshore New York Metropolitan area) suggest that storage mechanisms at this candidate CO_2 storage site may translate to analog Mesozoic rift basins offshore in the Long Island Platform (e.g., Post and Coleman, 2015). This suggests an extremely large capacity for potential storage of CO_2 in the Mid-Atlantic Offshore study area.

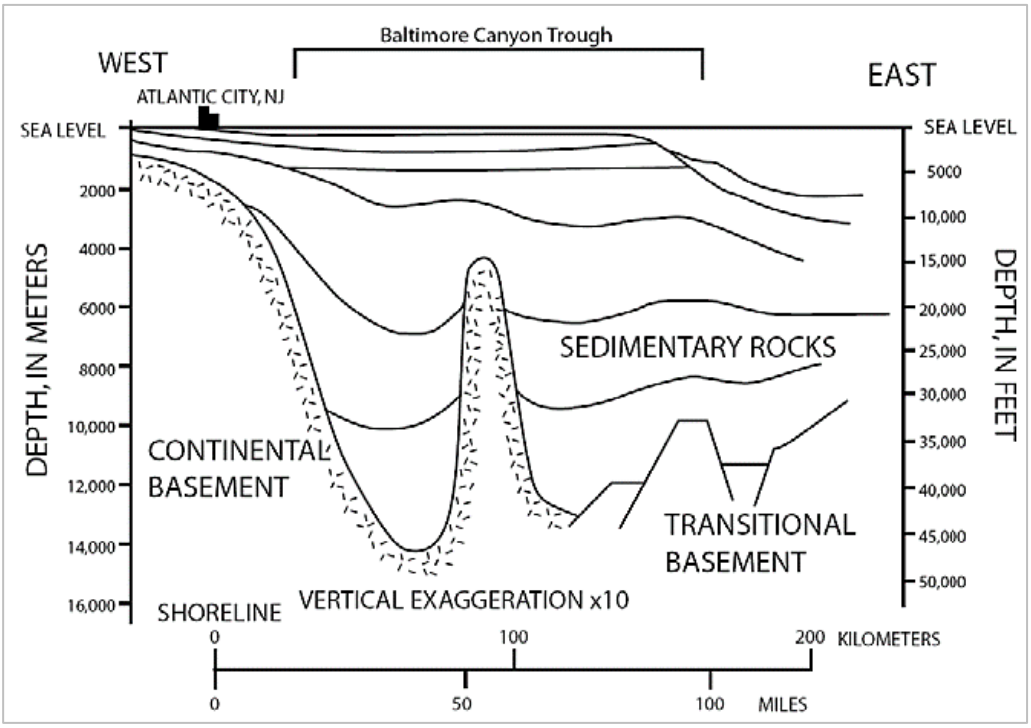

Figure 1-2. Generalized cross-section for the study area (source: Slater et al., 2010, modified after Scholle, 1977).

Preliminary investigation of storage resource near a geologic structure known as the Great Stone Dome (GSD) in the northern BCT suggests that as much as 5.9 gigatons (Gt) of CO_2 could be stored and structurally trapped at this location. Further work is required to integrate all seismic, core, and well-log data available in the study area to calculate and refine Prospective Storage Resource estimates for Mid-Atlantic Offshore deep saline formations.

1.3 Regional Stratigraphic Framework Objectives

A detailed regional geologic framework encompassing the BCT, the Long Island Platform, and the GBB is being constructed through well log analysis and correlations integrated with core data and seismic interpretation to create regional maps that are continuous across political boundaries. The sequence stratigraphic framework developed for the study area will provide enhanced predictability of potential storage zones in the region (Miller et al., 2013). Areas within the regional framework will be selected for more detailed evaluation based on data availability and storage reservoir quality. This research is focused on defining the geologic framework for CO_2 storage in the Mid-Atlantic Offshore study area through the tasks, objectives, and methods listed in Table 1-1.

Table 1-1. Summary of stratigraphic framework task objectives.

Task (Section)	Objectives	Methods
Data compilation (Section 2)	Acquire information on geologic formations, geotechnical rock properties, geologic structures, and petrophysical properties	Identify data sources; collect well data, seismic survey data, geophysical well logs, rock core test data, and previous research on Mid-Atlantic Offshore geology
Digital database construction (Section 3)	Review, classify, and organize information into database	Systematically review data, QA/QC data, transfer information into online GIS system
Correlation of seismic data with well log data (Section 4)	Calibrate seismic data to geophysical logs to convert time horizons to depth	Use V-D functions updated from Mountain et al. (2010) and Klitgord et al. (1994)
Characterization of geologic carbon storage zones (Section 5)	Depict the distribution, thickness, extent, and nature of deep rock layers in terms of CO_2 storage potential	Develop geologic structure maps, cross-sections, and interpretation of porosity, mineralogy for deep rock layers

QA/QC = quality assurance/quality control; GIS = geographic information system; V-D = velocity-depth.

2.0 Data Compilation

2.1 Data Types and Sources

Much of the geologic information gathered for the Mid-Atlantic Offshore Carbon Storage Resource Assessment is derived from 44 deep exploratory wells and seismic surveys completed during the 1970s and 1980s. Lack of hydrocarbon resources and restrictions on offshore exploration have limited acquisition of additional, newer subsurface data.

Datasets and inventories have been integrated from industry, governmental, and academic repositories specializing in offshore data collection and analysis, with over 30 years of data acquisition and some newly available/reprocessed datasets from LDEO, the Delaware Geological Survey (DGS), the United States Geological Survey (USGS), and the Bureau of Ocean Energy Management (BOEM).

Existing seismic, well log, and core data have been compiled to facilitate subsurface modeling and calculation of CO_2 storage potential. In addition to well reports, a literature review was performed to collect reports, papers, etc., containing information pertinent to the study. Key formation properties such as area, thicknesses, porosities, and in-situ fluid conditions will be quantified to conduct a regional-scale pore volume assessment for offshore storage targets of interest (Figure 2-1).

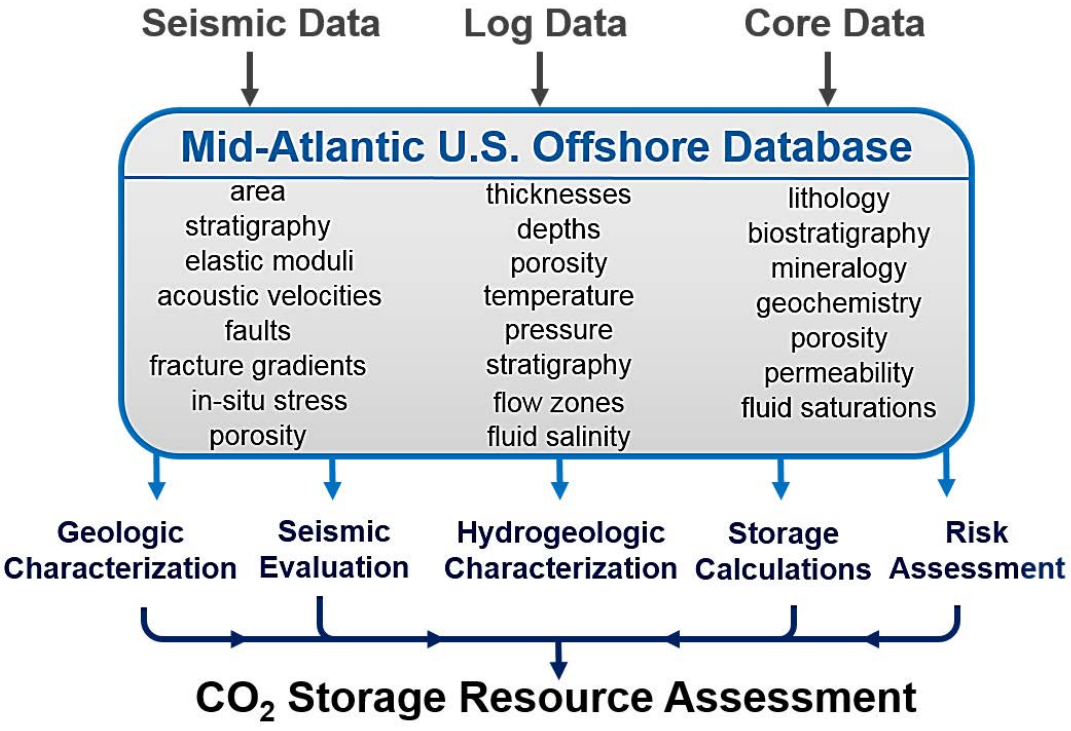

Figure 2-1. Key formation properties to be derived from compiled seismic, log, and core data for the offshore CO_2 storage resource assessment.

To date, approximately 2,000 km of seismic data from the 1980s have undergone high-resolution reprocessing, and over 1,500,000 feet of log data have been (re)digitized from the set of 2,294 available raster logs. Team members from the Pennsylvania Geological Survey have retrieved and scanned over twenty (20) well logs and technical reports from microfiche containing information for six wells in the study area. In addition to seismic and log data compilation, the DGS team has led the effort to inventory over 2,296 samples of core, and compile over 25,000 entries of hydrogeologic property data (e.g., porosity, permeability, grain density, water saturation) for 6,640 individual samples. A master inventory list of available log files, core samples, core data, and seismic ties for the 44 wells in the study area is provided in Appendix A.

2.2 Well Log Data

Existing raster log files, paper logs, and digital Log ASCII Standard [LAS]) log files were compiled from holdings at DGS, USGS, the National Oceanic and Atmospheric Administration (NOAA), and the BOEM geological and geophysical database (https://www.boem.gov/Resource-Evaluation-Data). This inventory consisted of the initial set of well logs used for geologic analysis and was the primary dataset of well logs. The set of logs from various sources was integrated and inventoried to identify data gaps in priority log types and select raster logs to be digitized. The outcome of this effort was to ensure that digital gamma ray (GR), neutron porosity (NPHI), bulk density (RHOB), and sonic log (DT) data were available for all 44 wells in the study area. In total, over 2,294 well logs were compiled for the 44 wells in the study area (Appendix A). A list of all priority logs available in digital format for each well is provided in Appendix B.

Well information and log files (digital and raster) for the 44 wells in the study area have been imported into a Petra® database developed for the project. The Petra® database is being used for compilation, quality assurance/quality control (QA/QC), petrophysical analysis, and mapping of petrophysical properties for the potential storage zones and caprocks. Table 2-1 provides a description of the priority logs pertinent to the hydrologic properties data collection and testing.

LAS files are structured ASCII text files containing log curve data and header information that can be imported into petrophysical software suites such as Petra® for advanced geophysical analysis. This function maintains the data in digital form while archiving the well logs for future use. Paper copies of well log data from the BOEM or the DGS Outer Continental Shelf (OCS) Sample Repository were obtained and converted into raster format using scanning equipment owned and operated by the Pennsylvania Geologic Survey.

All undigitized raster image files are calibrated to ensure proper accuracy of the digital data stored. An example of this process is shown in Figure 2-2. The calibration process includes the straightening of images (often paper logs get contorted during the scanning process), the registration of depth markers (as noted by the horizontal red line in Figure 2-2), and the input of scales for each unique log type and measurement range. Once an image is calibrated, the log curve lines are manually or automatically selected within the software package, and the digital curves are output to an LAS file type to be stored for further use.

Table 2-1. Wireline data used for Carbon Storage Resource Assessment.

Log Code	Description	Data Uses
GR	Gamma Ray	Used to correlate formation tops and intraformational sedimentary sequences across the study area. The GR log is also used to calculate net-thicknesses.
NPHI	Neutron Porosity	Used to estimate total porosity.
RHOB	Bulk Density	Used to estimate total porosity.
RT	Resistivity	Used to identify different patterns in the formations, such as coarsening upward, fining upward, and serrated, which are indicative of different lithologies and depositional environments. RT is used in conjunction with GR, RHOB, and NPHI to help select formation tops and bottoms.
DT	Sonic	Used to analyze sonic log wave velocity responses and examine travel times across these formations to further characterize the nature of porosity and other geomechanical properties of the formations of interest.
TEMP	Formation Temperature	Measures the temperature gradient of the formation and fluids in a well. The temperature gradient is used to estimate CO_2 density at reservoir conditions.
PRS	Formation Pressure	Used to derive a pressure gradient for a well and estimate CO_2 density at reservoir conditions. Sources of data are production logs and formation test data.
CALI	Caliper	Measures the diameter of the borehole. This is used for quality control to understand changes in the borehole which could impact log responses.

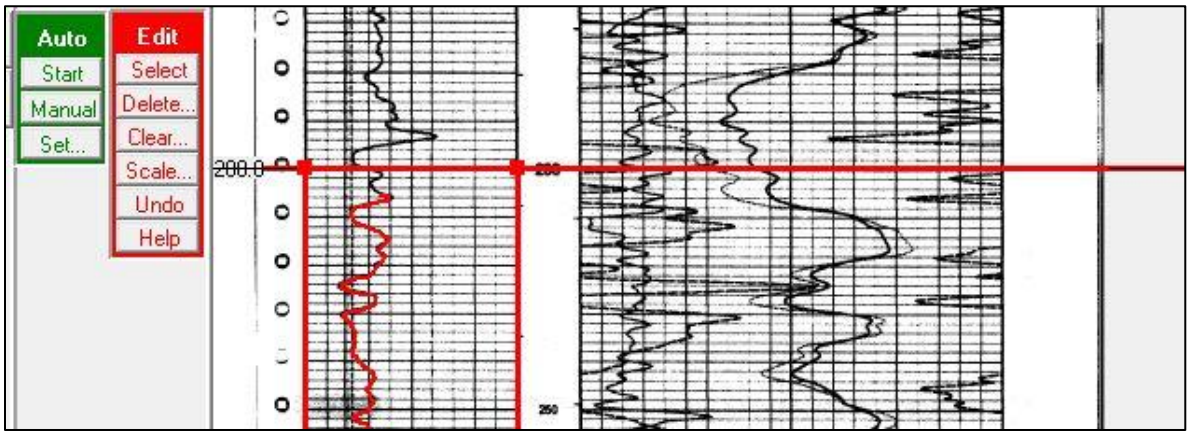

Figure 2-2. Image taken from the Petra® log digitization module showing the process of converting a raster log (electronic image file) into a digital log curve.

Digital well logs were acquired from both BOEM and USGS repositories. Well logs already available in LAS format were directly uploaded into Petra®.

All digital logs to be used in petrophysical and storage resource calculations, including GR, NPHI, RHOB, and DT logs, underwent a consistent QA/QC procedure consisting of the following steps:

- Logs were clipped to removed erroneous data at the beginning and end of log curves.
- Log data segmented over different depth intervals of a well were spliced together to create continuous (in most cases) composite curves.
- Log curves for all wells were resampled to an equal to step rate of 0.5 feet (ft) to facilitate petrophysical calculations in Petra®.
- All log porosities were transformed to decimal units (rather than percent).
- The data statistics (e.g., minimum, maximum, mean) of each log curve were calculated for every well to identify outliers in the dataset. When these logs were identified, the data were compared with data in the original LAS file as well as the raster (image/TIF) log to determine and correct the problem, if possible. If the data could not be corrected, the log curve was removed from the Petra® database
- GR curves with varying signal intensities were normalized using a type well in each study area subregion (BCT: Exxon 684-1; GBB: COST G-1) to better enable net thickness calculations to be carried out via use of the industry standard cutoff of 75 GAPI (American Petroleum Institute gamma ray units). This cutoff distinguishes sandstones (GR <75 GAPI) from clay-bearing (e.g., shale) non-reservoir rocks (GR >75 GAPI) (Slatt, 2006).

The Pennsylvania team has retrieved and scanned over twenty (20) well logs and technical reports from microfiche containing information for six wells in the study area. The database of digitized well logs has been updated and maintained on the project's online file sharing platform Box (see Section 3). Log data will be compared to and calibrated with core data from each well prior to calculation of petrophysical properties such as porosity and net thickness.

2.3 Geologic Sample Data

The initial effort involved completing the inventory of the DGS OCS Sample Repository collection to determine specific material available for this study. This collection represents an agglomeration of numerous collections over the course of more than a decade with a variety of states or organization and preservation. This step involved an item-by-item inventory to identify specific samples at specific depths available for analysis. The inventory includes raw samples, such as cores, washed cuttings, and unwashed cuttings, as well as prepared sample material, such as thin sections, micropaleontologic slides, and washed micropaleontology and heavy mineral sample residues. Materials were repackaged as necessary to ensure sample integrity for analytical work. This effort included:

- Itemized sample inventory of conventional and sidewall core (SWC) material (485 core + SWC boxes)
- Itemized sample inventory of prepared materials (thin sections, micropaleontology slides, vials) (1,014 boxes of prepared samples)
- Itemized sample inventory of washed cuttings (1,915 boxes)
- Itemized sample inventory of unwashed cuttings (390 boxes)

The sample inventory has been updated and maintained on Box. Appendix C contains the spreadsheet of the physical samples available for the study area. Sample descriptions, porosity, permeability, mineralogical, and stratigraphic data from existing paper and microfilm records, scientific publications, and federal and company reports were compiled into a master spreadsheet of hydrologic properties data and QC checked by the team. With over 9,000 individual depth entries, repeatable automated approaches to identifying data gaps are helpful. The DGS investigated and defined processes for applying database querying capabilities using Microsoft (MS) Access for the Data Gap Analysis (Figure 2-3).

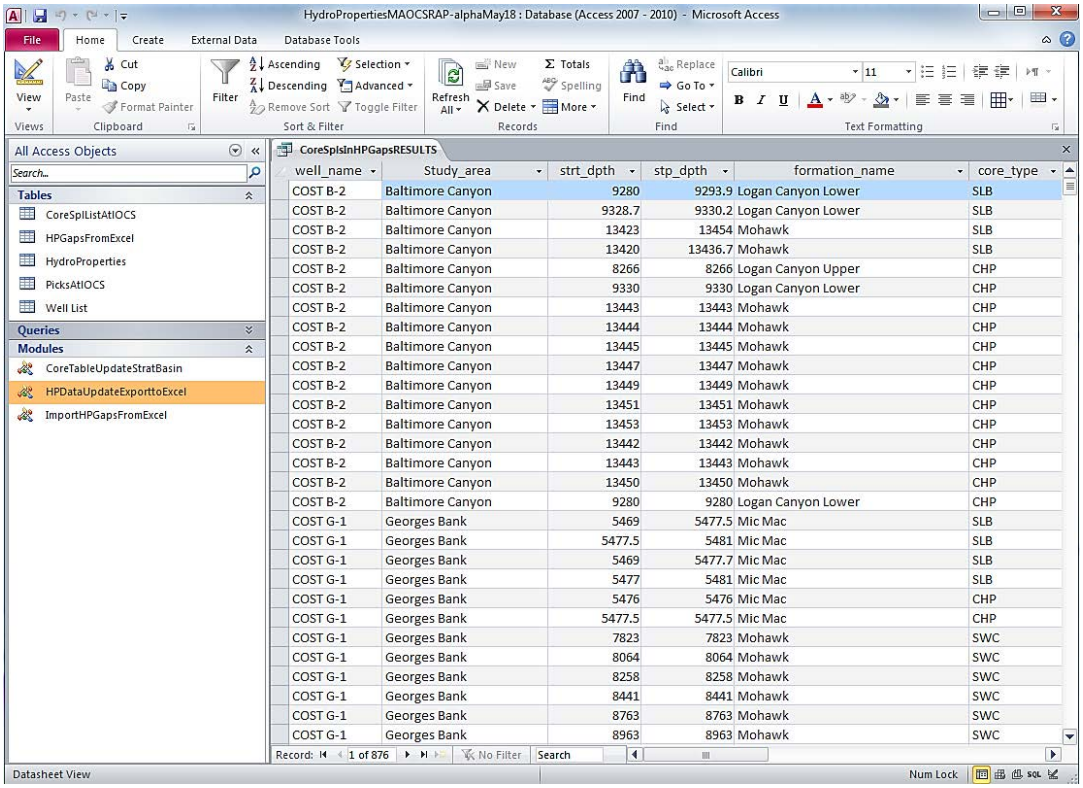

well_name	Study_area	strt_dpth	stp_dpth	formation_name	core_type
COST B-2	Baltimore Canyon	9280	9293.9	Logan Canyon Lower	SLB
COST B-2	Baltimore Canyon	9328.7	9330.2	Logan Canyon Lower	SLB
COST B-2	Baltimore Canyon	13423	13454	Mohawk	SLB
COST B-2	Baltimore Canyon	13420	13436.7	Mohawk	SLB
COST B-2	Baltimore Canyon	8266	8266	Logan Canyon Upper	CHP
COST B-2	Baltimore Canyon	9330	9330	Logan Canyon Lower	CHP
COST B-2	Baltimore Canyon	13443	13443	Mohawk	CHP
COST B-2	Baltimore Canyon	13444	13444	Mohawk	CHP
COST B-2	Baltimore Canyon	13445	13445	Mohawk	CHP
COST B-2	Baltimore Canyon	13447	13447	Mohawk	CHP
COST B-2	Baltimore Canyon	13449	13449	Mohawk	CHP
COST B-2	Baltimore Canyon	13451	13451	Mohawk	CHP
COST B-2	Baltimore Canyon	13453	13453	Mohawk	CHP
COST B-2	Baltimore Canyon	13442	13442	Mohawk	CHP
COST B-2	Baltimore Canyon	13443	13443	Mohawk	CHP
COST B-2	Baltimore Canyon	13450	13450	Mohawk	CHP
COST B-2	Baltimore Canyon	9280	9280	Logan Canyon Lower	CHP
COST G-1	Georges Bank	5469	5477.5	Mic Mac	SLB
COST G-1	Georges Bank	5477.5	5481	Mic Mac	SLB
COST G-1	Georges Bank	5469	5477.7	Mic Mac	SLB
COST G-1	Georges Bank	5477	5481	Mic Mac	SLB
COST G-1	Georges Bank	5476	5476	Mic Mac	CHP
COST G-1	Georges Bank	5477.5	5477.5	Mic Mac	CHP
COST G-1	Georges Bank	7823	7823	Mohawk	SWC
COST G-1	Georges Bank	8064	8064	Mohawk	SWC
COST G-1	Georges Bank	8258	8258	Mohawk	SWC
COST G-1	Georges Bank	8441	8441	Mohawk	SWC
COST G-1	Georges Bank	8763	8763	Mohawk	SWC
COST G-1	Georges Bank	8963	8963	Mohawk	SWC

Figure 2-3. Screenshot of the MS Access database containing hydrogeologic sample data.

During the sample and analysis planning workshop held at the DGS sample repository on May 10, 2017, available samples were fully evaluated and selected for four wells and a preliminary sample evaluation was performed for three additional wells during this workshop. This included an examination of whole core and SWC samples, chips, and slices at intervals of interest where data gaps had been identified via the MS Access database query to determine if a sufficient quantity of the sample was available for further analyses. A total of 29 samples were selected for sample analyses, and an additional 25 samples were identified for potential analysis. A flow chart summarizing the selection criteria is shown in Figure 2-4. This figure outlines the process through which sample material was selected for analysis. The initial samples selected for analysis are presented in Table 2-2.

Moving forward, another round of sample selection will be undertaken to finalize the sample selection set. This process will involve applying the workflow to the remaining core samples identified in the formations of interest. Once a full assessment of viable sample material is completed, the core samples will be shipped to a commercial laboratory and the PGS for testing and analysis.

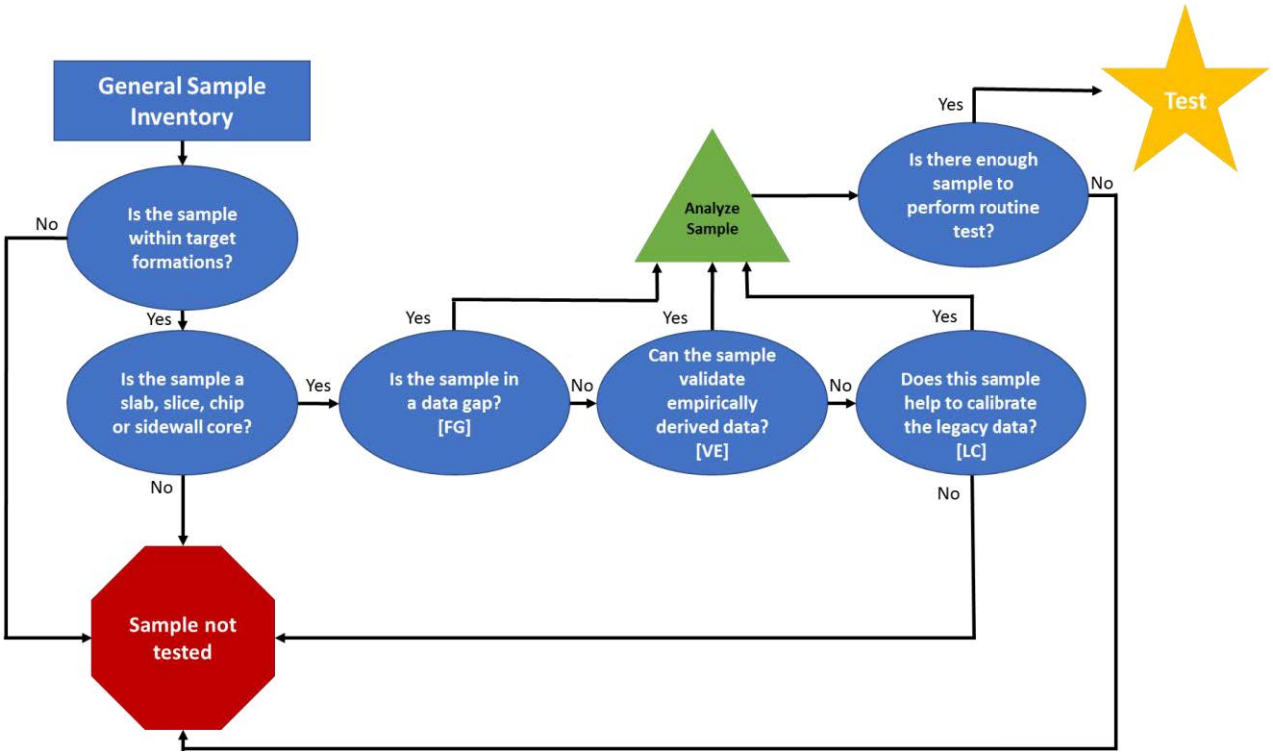

Figure 2-4. Flow chart for selection of samples for routine porosity, permeability, and grain density analysis.

Table 2-2. Core samples selected for routine analysis.

Well ID	Basin	Core Type	Depth (ft)	Sample Points	No. of Samples	Formation	Utility
Selected Sample Locations							
COST G1	GBB	Slab	5469 - 5481	1 sandstone & 1 shale; (5473.5 & TBD)	2	Mic Mac	VE
COST G1	GBB	Slab	9980 - 10003	Every ~5 ft (9985, 9990, 9995, etc.)	3	Mohawk	VE
COST B2	BCT	Slab[a]	5030 - 5031.5	1 representative sample	1	Wyandot	LC
COST B2	BCT	Slab	8238 - 8266	Every ~5 ft (8240, 8245, 8250, etc.)	6	U. Logan Canyon	LC
COST B2	BCT	Slab[b]	9280 - 9330.2	Every ~10 ft (9280, 9290, 9300, etc.)	5	L. Logan Canyon	LC
Mobil 544-1	GSD	SWC	5211	5211	1	Dawson Canyon	FG
Mobil 544-1	GSD	SWC	5435	5435	1	Dawson Canyon	FG
Mobil 544-1	GSD	SWC	5962	5962	1	Dawson Canyon	FG
Mobil 544-1	GSD	SWC	6260	6260	1	Logan Canyon	FG
Mobil 544-1	GSD	SWC	6420	6420	1	Logan Canyon	FG
Mobil 544-1	GSD	SWC	6579	6579	1	Logan Canyon	FG
Mobil 544-1	GSD	SWC	6696	6696	1	Logan Canyon	FG
Mobil 544-1	GSD	SWC[a]	6798	6798	1	Logan Canyon	FG
Mobil 544-1	GSD	SWC	7096	7096	1	Logan Canyon	FG
Mobil 544-1	GSD	SWC	7258	7258	1	Naskapi	FG
Mobil 544-1	GSD	SWC	8497	8497	1	Missisauga	FG
Mobil 544-1	GSD	SWC	9039	9039	1	Missisauga	LC
Potential Sample Locations							
COST G2	GBB	Slab	8736 - 8787.3	Every ~10 ft (8740, 8250, 8260, etc.)	Up to 5	Mohawk	VE, LC
COST B3	BCT	SWC	6260	6260	1	Dawson Canyon	FG
COST B3	BCT	SWC	7040	7040	1	Dawson Canyon	FG
COST B3	BCT	SWC	7640	7640	1	Dawson Canyon	FG
COST B3	BCT	SWC	8382	8382	1	U. Logan Canyon	FG
COST B3	BCT	SWC	9750	9750	1	Naskapi	FG
COST B3	BCT	SWC/ Slab	9900-11600	TBD[c]	Up to 3	Missisauga	VE
COST B3	BCT	SWC/ Slab	12400-15700	TBD[c]	Up to 3	Mohawk	VE
Exxon 684-1	BCT	Chip	9420 - 9455	TBD[c]	Up to 3	Naskapi	LC
Exxon 684-1	BCT	Chip	12119-12700	TBD[c]	Up to 3	Mic Mac	LC
Exxon 684-1	BCT	Chip	12700-16185	TBD[c]	Up to 3	Mohawk	LC

FG = Fills data gap; VE = validates empirical data; LC = legacy data comparison; TBD = to be determined.

[a] Selected also for SEM and XRD.

[b] XRF performed at 9,286 to 9,288 ft.

[c] Plugs/chips will be selected at the laboratory based on best physical condition. Point depths are for guidance purposes only. More than three samples may be sent.

Rock sample properties to be evaluated include lithology, porosity, permeability, and mineralogy. In addition, other sample analyses are being considered to support geologic characterization, seismic data evaluation, and risk assessment tasks. The ability to acquire in-situ measurements of bulk-rock composition and/or acoustic properties using hand-held portable instruments is being explored. Bulk-rock geochemistry of core samples via X-ray fluorescence (XRF) may be used to quantitatively determine lithology and provide insight into potential formation reactivity with CO_2 during and after injection. Data related to acoustic rock properties may be calibrated and correlated with seismic data to facilitate geomechanical analysis for risk assessment. One challenge with using historical oil and gas exploration data for geologic storage site characterization is the lack of pressure entry data (characterizing caprock integrity was not the objective of exploration). If possible, a few samples of caprock material will be selected to undergo mercury injection capillary pressure (MICP) analysis to obtain more refined porosity and permeability values (i.e., threshold values less than 0.001 mD) for these tighter formations.

2.4 Seismic Survey Data

Seismic evaluation involves acquiring publicly available seismic data, digitizing seismic data where necessary, loading all digital data into a seismic analysis program, conducting seismic interpretation of major seismic packages, and integrating seismic data with structural and/or stratigraphic interpretation and well data. These existing multichannel seismic (MCS) data will be used to map the regional offshore stratigraphy and to address deeper targets in the areas of interest. The well-log and seismic-survey data will be used to construct regional maps and cross-sections of the candidate reservoirs and caprock formations. Seismic data are especially useful for correlating and characterizing stratigraphic units in areas with no deep wells, such as the Long Island Platform.

One significant aspect of this study is the reprocessing of 4,000 km of seismic profiles to apply modern techniques to enhance resolution (Figure 2-5). LDEO identified target regions for the USGS legacy seismic data totaling 4,000 km of two-dimensional (2D) lines, which were shared with the Project Team for review and comment. Seismic lines were selected for reprocessing based on: 1) key project targets and best-quality seismic lines for further analysis and 2) location and quality of available metadata needed for seismic reprocessing. The seismic data processing company Absolute Imaging is under subcontract to LDEO and provided seismic processing products: e.g., gain correction, filtering, and pre-stack time migration (PSTM) on all selected USGS legacy data. To date, approximately 3,000 km of 2D seismic lines within the target study region have been reprocessed and delivered to LDEO for QA/QC. LDEO has completed its assessment of 2,000 km lines of reprocessed USGS legacy seismic data and delivered the reprocessed data to all project participants.

In addition to legacy and reprocessed USGS lines, recently released seismic data from BOEM and seismic data recently made available through the National Archive for Marine Seismic Surveys (NAMSS) are being used to greatly augment the seismic data set (Figures 2-6 and 2-7). Much of the seismic data from offshore surveys occurs along the slope and farther offshore than what is being studied in this research because of excessive water depths.

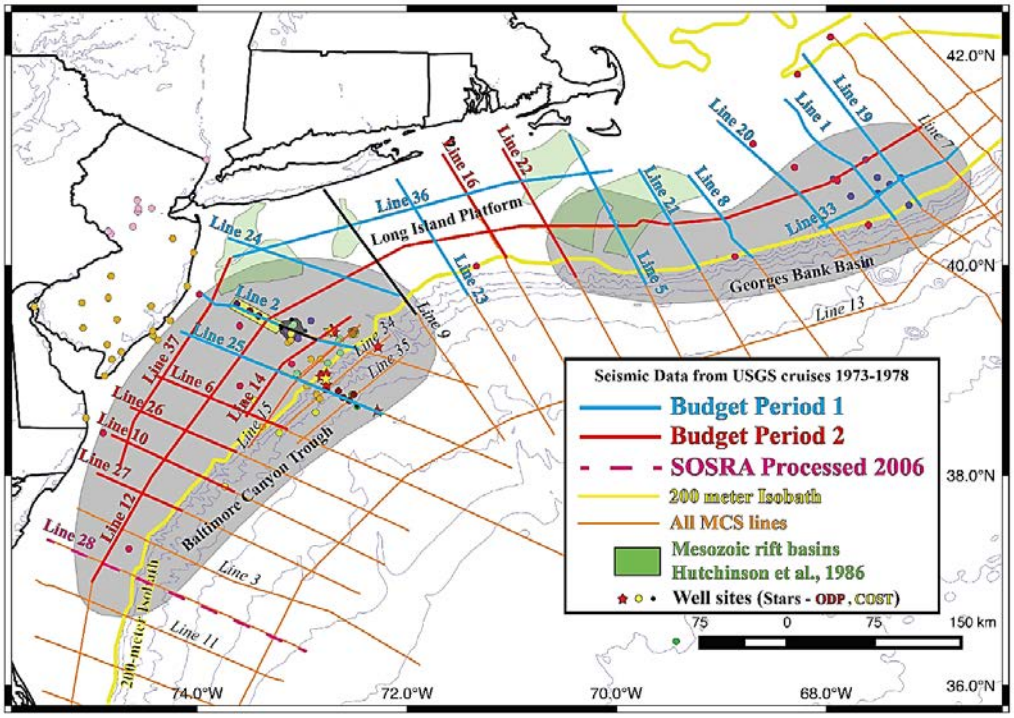

Figure 2-5. Study area map showing the reprocessing plan for legacy seismic data.

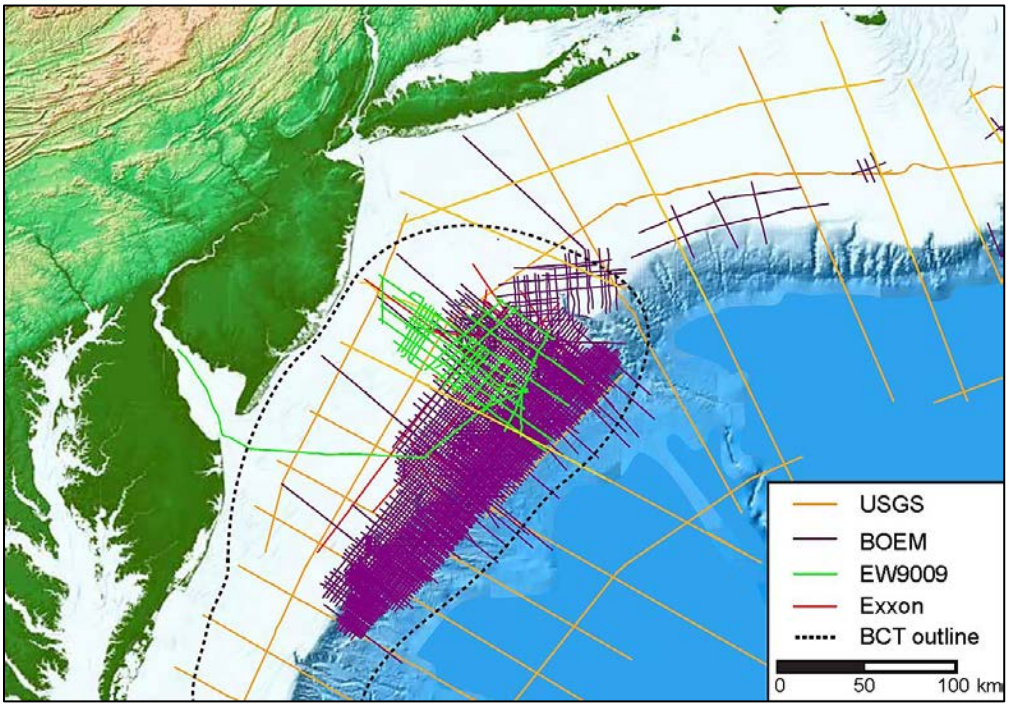

Figure 2-6. Location map showing seismic data recently released by BOEM for the BCT.

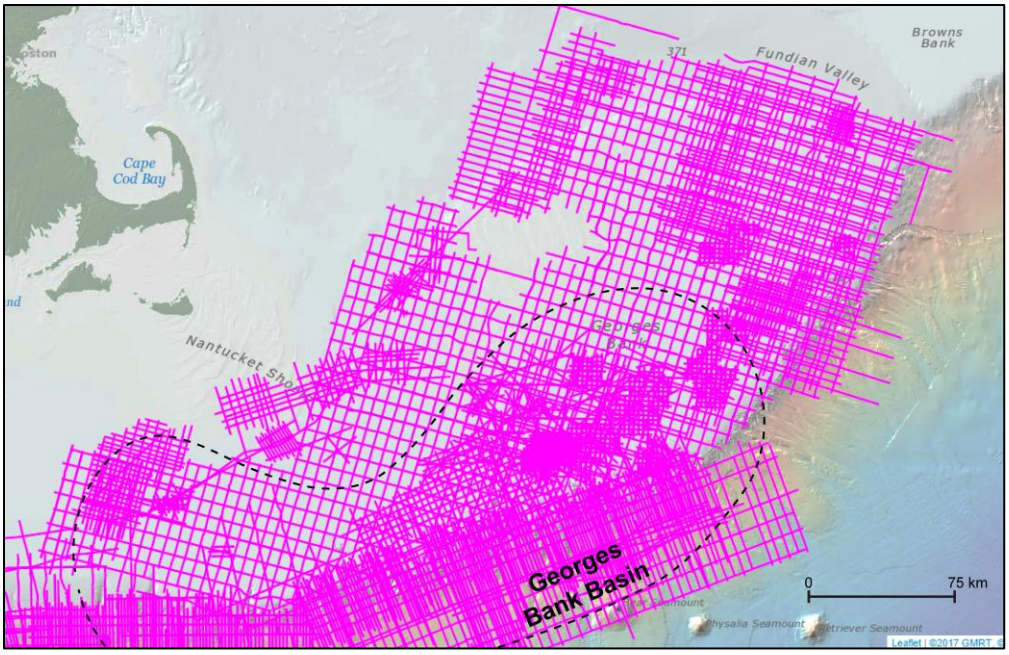

Figure 2-7. Location map showing seismic data acquired by BOEM for the GBB and recently made available through the NAMSS (Triezenberg et al., 2016).

Thirty-two seismic lines were acquired, covering the north and mid-Atlantic U.S. continental margin from GBB through the BCT. These lines were collected by USGS from 1973 to 1978 and are available in the Society of Exploration Geophysicists (SEG) "Y" format from the USGS online data holdings. An additional 21 seismic profile lines, collected by the Federal Institute for Geosciences and Natural Resources in 1979, were digitally scanned from paper records for conversion to SEG Y.

In addition to the existing seismic dataset, high-resolution three-dimensional (3D) seismic data from the National Science Foundation (NSF)-funded cruise 1510 of the R/V *Marcus G. Langseth* may be available to the project team for analysis. Rutgers is one of three collaborative institutions in the NSF-funded project (along with Dalhousie University and the University of Texas at Austin). In compliance with NSF rules, the data will be fully available two years after delivery. Before then, release of the data is at the discretion of the team of co-investigators. While collected primarily for 3D shallower objectives (<1 second [s] two-way travel time [TWTT], <1 km), data quality for deeper objectives appears to be excellent and should prove to be very useful in evaluating the storage potential for the landward portion of the GSD. The R/V Langseth 3D cruise was the largest PCable deployment yet attempted by industry or research (24 simultaneous streamers), and towing characteristics of the array proved to be more complex than anticipated. The first preparation of a full PSTM volume has revealed that streamer locations must be recalculated. That process is still under way.

2.5 Literature

A comprehensive literature review was undertaken at the onset of this project to fully catalog and incorporate the current understanding of the geologic framework of this study area into this

project. A full bibliography of all references collected to date is in Appendix D, which is subdivided into key categories for reference. This process is ongoing and will include reference to published material produced from the work completed under this project

The geology and storage potential for onshore coastal plain targets was recently reviewed by Miller et al. (2017). Offshore oil and gas potential for the BCT was reviewed following industry activity in the late 1970s and early 1980s by Libby-French (1984) and Prather (1991), providing a baseline for delineating reservoir and caprock potential. These prior offshore studies took a classic lithostratigraphic approach. This project is applying a sequence stratigraphic approach to evaluate the continuity of reservoirs and caprocks. Preliminary results from this project indicate that previous correlations have documented the first-order distribution but that they are incorrect in detail.

3.0 Database Construction

3.1 Overview of Project Databases

The Project Team has worked collaboratively to build and maintain a database of non-proprietary data on the geology of the Mid-Atlantic Offshore study area. Six main databases are being used to store, manage, analyze, and distribute information compiled and generated as part of the data compilation effort: 1) Box, 2) ArcGIS online (AGOL), 3) Petra®, 4) IHS Kingdom®, 5) Petrel®, and 6) MS Access. Table 3-1 provides a summary of each database and its application in this project.

This section focuses on the format, organization, and data integration challenges associated with Box, the primary platform used for storing and sharing all information and data associated with the project. Integration of the various datasets into a geospatial framework using the AGOL database is also discussed.

Table 3-1. Overview of the databases used to store, manage, analyze, and share data compiled and generated as part of the Mid-Atlantic U.S. Offshore Storage Resource Assessment project.

Database	Description	Primary Data Type(s)	Project Application
Box	Cloud-based content management and file sharing platform	All project files and data	Main database for storing, managing, sharing, and retrieving all project data, electronic files, and inventories
ArcGIS Online	Cloud-based mapping platform and geographic information system	Geospatial	Integrate and display spatial distribution/availability of well, core, log, and seismic data, and inventories
Petra®	Well and log data management and analysis software	Well, Log, Petrophysical	Log data QC and petrophysical analysis
IHS Kingdom®	Well and seismic data management and interpretation software	Seismic	Seismic data storage, interpretation, and log-seismic correlations
Petrel®	Well and log data database and seismic analysis software	Seismic	Seismic data storage, interpretation, and log-seismic correlations
MS Access	Relational database management system	Core, Hydrogeologic	Core and hydrogeologic data QC, querying, and cross-referencing

3.2 Box Database Format

Box is a cloud-based content management and file-sharing platform that offers unlimited storage and upload of electronic files of any format, with a file Preview module that supports over 120 file types (Box.com, 2017). Box serves as the central repository for the data compiled and generated by the Mid-Atlantic Offshore Storage Resource Assessment team due to the site's file versatility and comprehensive list of collaboration tools, access controls, and file tracking features. The Mid-Atlantic Offshore project files and data are saved primarily as image files, tabulated spreadsheet data, document and text files, and LAS file format, with all files searchable on Box by name and extension (Figure 3-1).

Data management and file sharing are facilitated by a collaborative online workspace that allows real-time and concurrent editing of files via online applications included with site access, and file activity tracking. File updates and edits are managed with automatic versioning and version controls that allow access to all previous file versions and file restoration.

Access to the project's Box database is limited to project team members, with owner-controlled invitations, user access restrictions, and file expiration dates. File security is also managed on Box via user authentication and file encryption during upload, download, and storage (Box.com, 2017).

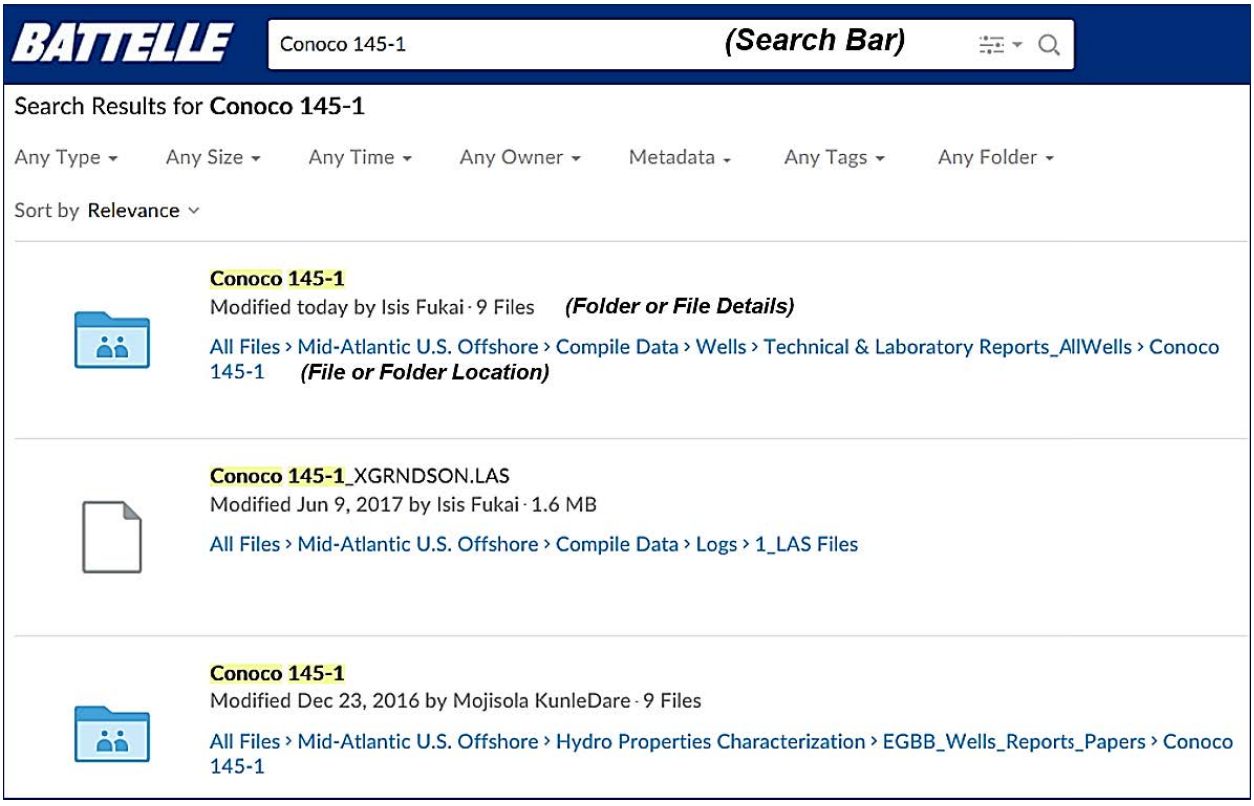

Figure 3-1. Screenshot showing the search feature on Box using the Conoco 145-1 well as an example.

3.3 Box Organization/Data Fields

Information, files, and data comprising the Mid-Atlantic Offshore Carbon Storage Resource Assessment Project database is organized into eight main topical folders on Box: Compile Data, Compile Literature, Deliverables, Hydrogeological Properties Characterization, Meeting Materials, Storage Resource Calculations, Tech Transfer, and Outreach (Figure 3-2). The two main folders for storing and accessing original source project data are the Compile Data and the Compile Literature folders.

3.3.1 Compile Data Folder

The project's main datasets and inventory files are stored in the Compile Data folder, organized into seven subfolders based on data type: Biostratigraphy Reports and Data, CO_2 Sources & Emissions; Cores, Cuttings, Rock Samples; Logs; Seismic; Stratigraphic Tops; and Wells (Figure 3-3).

The Compile Data folder also contains a Master Database Inventory spreadsheet that contains detailed well information along with lists/counts of all data available for each well in the Mid-Atlantic Offshore study area, including log data, core data, core samples, technical reports, and information on whether the well can be used as a seismic tie. A file directory denoting where each data file can be located on Box is also included in the master inventory. The Master Database Inventory spreadsheet is included in Appendix A.

Figure 3-2. Screenshot showing project folder organization on Box, including folder name, modification date, and file count.

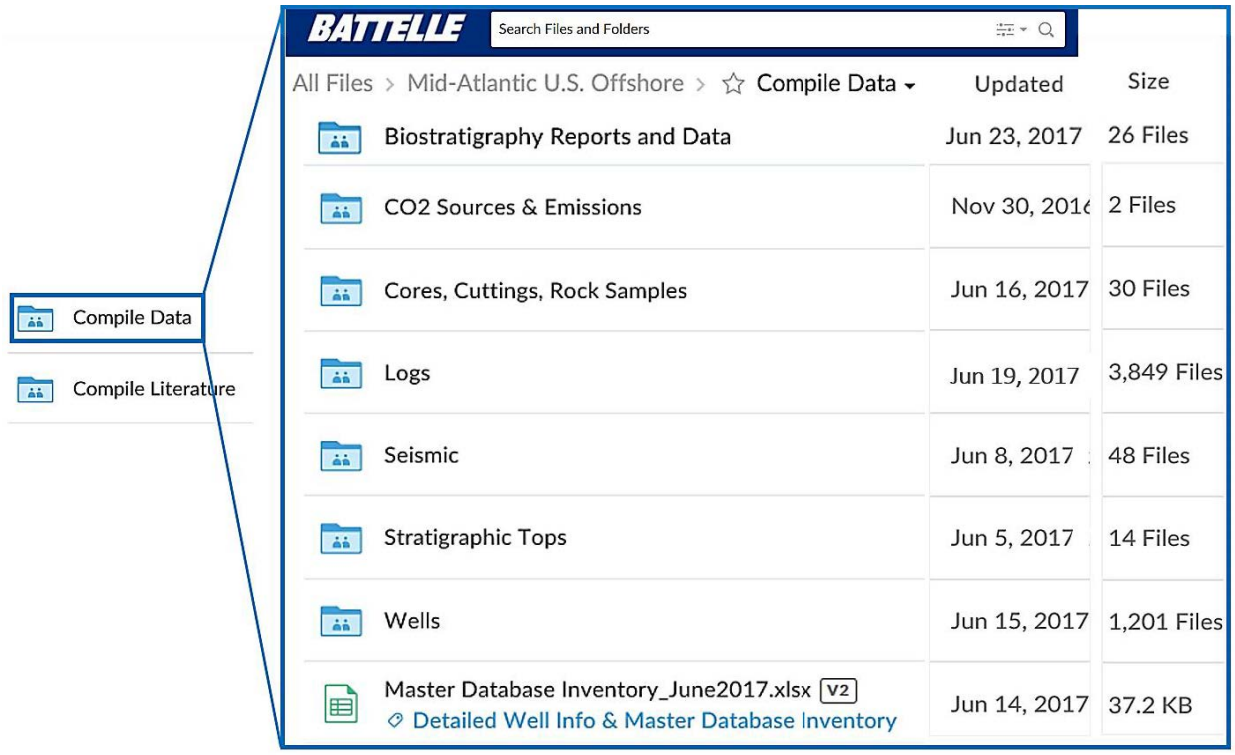

Figure 3-3. Screenshot showing the project data organized into six main subfolders within the Compile Data folder.

All information compiled on biostratigraphy and palynology in the offshore study area is saved in the Biostratigraphy Reports and Data subfolder in Compile Data. This includes twenty-six PDF files for approximately 20 wells in the study area. This information is being used in sequence stratigraphic correlations.

The CO_2 Sources & Emissions subfolder contains CO_2 emission data from all stationary point sources in the U.S. released by the US. Environmental Protection Agency's (EPA) Greenhouse Gas Reporting Program (EPA, 2015; 2016). The CO_2 emission data are mapped alongside the locations of wells and potential storage formations in the Mid-Atlantic Offshore study area to conduct a preliminary assessment of source-sink potential in the region.

Inventories of all offshore core and cutting samples housed at DGS are stored in the Cores, Cuttings, Rock Samples subfolder in the Compile Data folder (Figure 3-4). Core and cutting data (including porosity, permeability, fluid saturation, and grain densities) that were compiled as part of Task 2 Hydrogeologic Properties Characterization are also saved in this folder. These sample inventories and core data are being used to quantify reservoir and seal properties, calibrate log data, identify data gaps in the study area, and select samples for additional analysis for the Sampling and Analysis Plan.

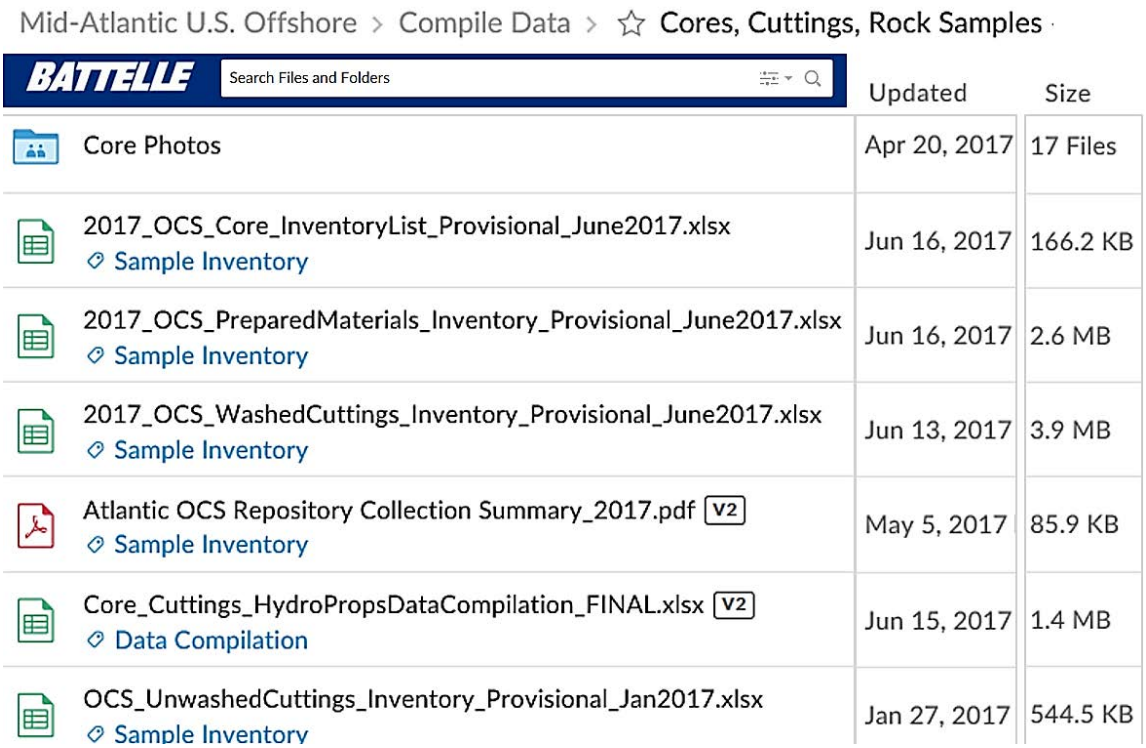

Figure 3-4. Screenshot showing the organization of the Cores, Cuttings, Rock Samples folder on Box.

Note: The file contains core photographs, sample inventory files, and a file of tabulated core and cuttings data (e.g., porosity, permeability, grain density) compiled as part of the Hydrogeologic Properties Characterization task.

The Log subfolder includes all LAS (digital) and raster (image) logs available for the study area, along with a summary inventory of all log types available for each well and uploaded into the project Petra® database (Figure 3-5). All digital log curves available in the study area are saved in one of two LAS files created for each well. One file contains GR, NPHI, RHOB, and DT curves (denoted as “X” curves in the filename) that have undergone the QA/QC procedures described in Section 2.2, and will be used for petrophysical and storage resource calculations. All other digital log curves available for each well are saved in a second LAS file. LAS filenames consist of the well name followed by the QA/QC log curve name (e.g., Conoco 145_XGRNDSON.las) or “AllOtherLogs” (e.g., Conoco 145-1_AllOtherLogs.las) for easy search and retrieval (Figure 3-6). A detailed LAS file inventory is also included in the LAS file folder along with all LAS filenames and every curve included in that file for a specific well.

The raster file folder (see Figure 3-5) follows a similar format as the LAS file folder. The raster file folder contains all 1,489 raster files for 42 wells in the study area and a detailed file inventory listing the raster filename and log curves associated with each image file. Logs and checkshot (CS) data used for seismic integration and time-to-depth conversions are also compiled in a designated subfolder called USGS Seismic Well Tie Logs (see Figure 3-5).

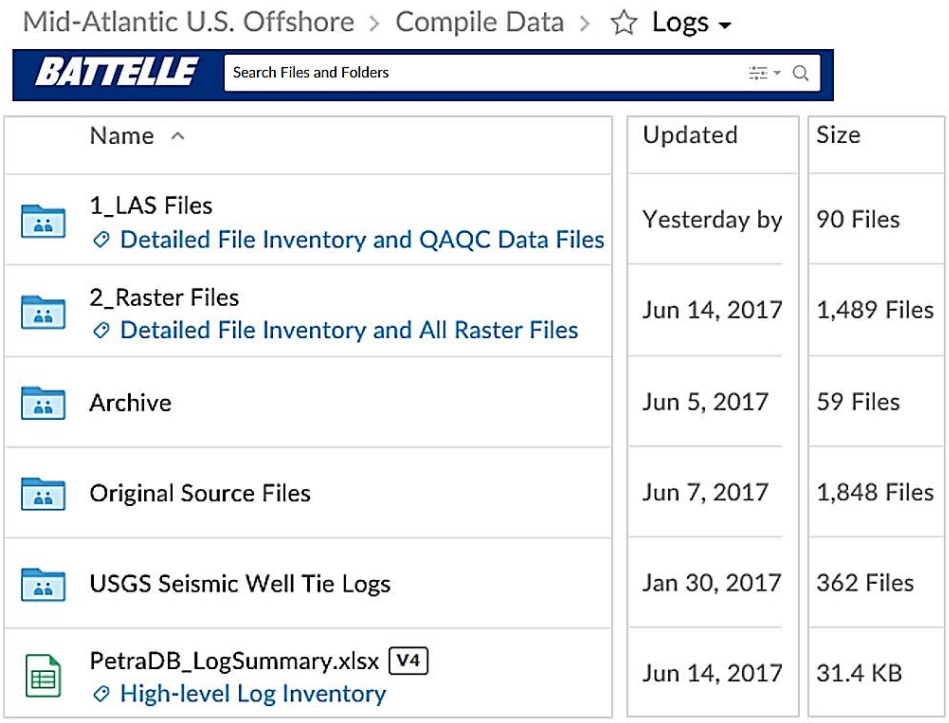

Figure 3-5. Screenshot showing the organization of the project's Logs folder containing a high-level summary inventory of all available log types for each well uploaded into the project's Petra® database, as well as folders containing the actual LAS (digital) and raster (image files) for all wells in the study area.

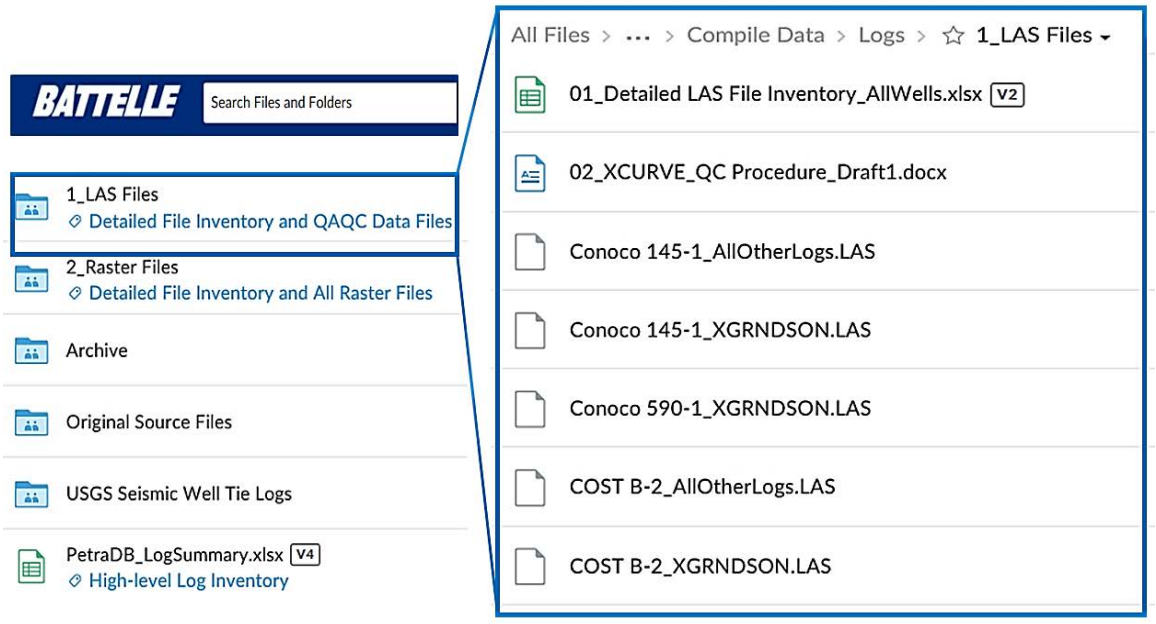

Figure 3-6. Screenshot showing the organization of the project's LAS files in the Logs folder containing all LAS files and a detailed inventory of all LAS filenames and curves available for each well in the study area.

An inventory of all seismic lines available in the study area, as well as those being reprocessed to higher resolution via the use of modern techniques, is saved in the Seismic folder on Box (see Figure 3-3) for team members to access. However, because of the large size of SEG Y files associated with seismic data, the raw and interpreted seismic data are temporarily being stored and managed on IHS Kingdom® and Petrel® software at LDEO, Rutgers, and USGS until team members finalize interpretations and processing. Once the legacy seismic data are reprocessed, interpreted, and ready for distribution, image files of the lines will be uploaded to Box and the SEG Y data will be distributed to the team. The first 2,000 km lines of reprocessed data have been distributed; the second 2,000 km lines will be distributed to the team in the next phase of the project. Seismic data will then be used to constrain formation geometry, continuity, and geologic structures in the study area.

The Stratigraphic Tops folder (see Figure 3-3) includes top and base picks for the entire Mesozoic interval of interest in the study area. This includes lithostratigraphic tops, biostratigraphic tops, and chronostratigraphic tops. These structural tops and bases have been used to define the regional sequence stratigraphic framework in the study area, infer depositional environments of potential reservoirs and caprocks, and define the zones for calculating key formation properties that will be used for storage resource calculations, such as net thickness and porosity.

3.3.2 Compile Literature Folder

All literature, reports, and publications related to Mid-Atlantic Offshore geology and subsurface resources are saved in the Compile Literature folder (Figure 3-7). The Compile Literature folder contains 96 files that are organized into six subfolders based on Mid-Atlantic study area subregions, other offshore regions, offshore CO_2 storage resource assessments, and general/overview studies. These reports provide reference material and information from previous and ongoing studies that is shared with the project team to help develop the regional stratigraphic framework for offshore CO_2 storage in the Mid-Atlantic Offshore study area. A detailed list of all literature, reports, and publications compiled for the project is provided in Appendix D.

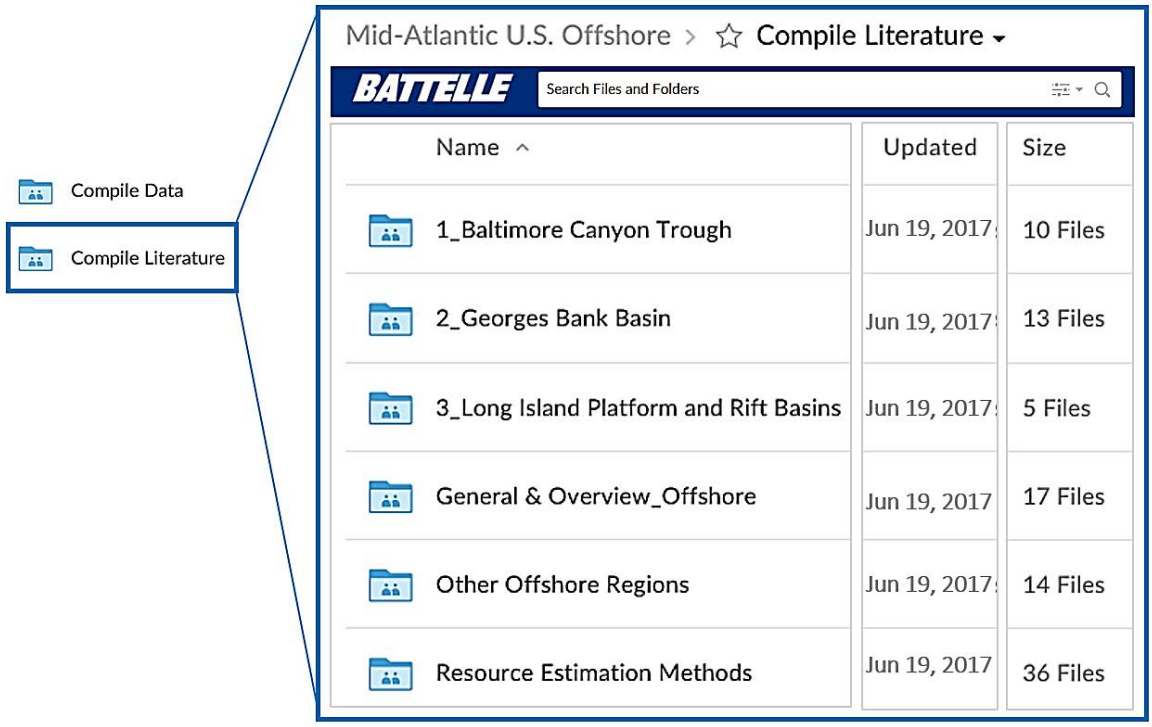

Figure 3-7. Screenshot showing the contents of the Compile Literature folder on the project's Box site, with literature, reports, and publications organized into six topical subfolders.

3.4 ArcGIS Online

The Maryland Geological Survey created an AGOL (ESRI, Inc.) map to facilitate data inventory and information transfer for the project. AGOL is a collaborative web-based geographic information system for creating and sharing maps, layers, and data. Data layers can readily be uploaded/downloaded from a graphical user interface and displayed with custom annotation and symbology.

Current layers on the Mid-Atlantic Offshore project map include a preliminary well list (as of June 2016), BOEM Atlantic Planning Areas, the 8G line, shipping lanes, maritime limits and boundaries, total greenhouse gas emissions in the mid-Atlantic region (2014), Atlantic Marine Sanctuaries, and bathymetry (Figure 3-8). Additional data to be added to the project map include the traces of all reprocessed seismic lines, locations of wells and exploratory drill holes (Ocean Drilling Program) in the study area, and the number and type of geophysical log data, core samples, core data, and drill cuttings associated with each well/hole.

Information can be accessed in the map model in both summary and detailed table format for a specific well or map item of interest, with links to core/log datasets and technical reports provided for download (Figure 3-9).

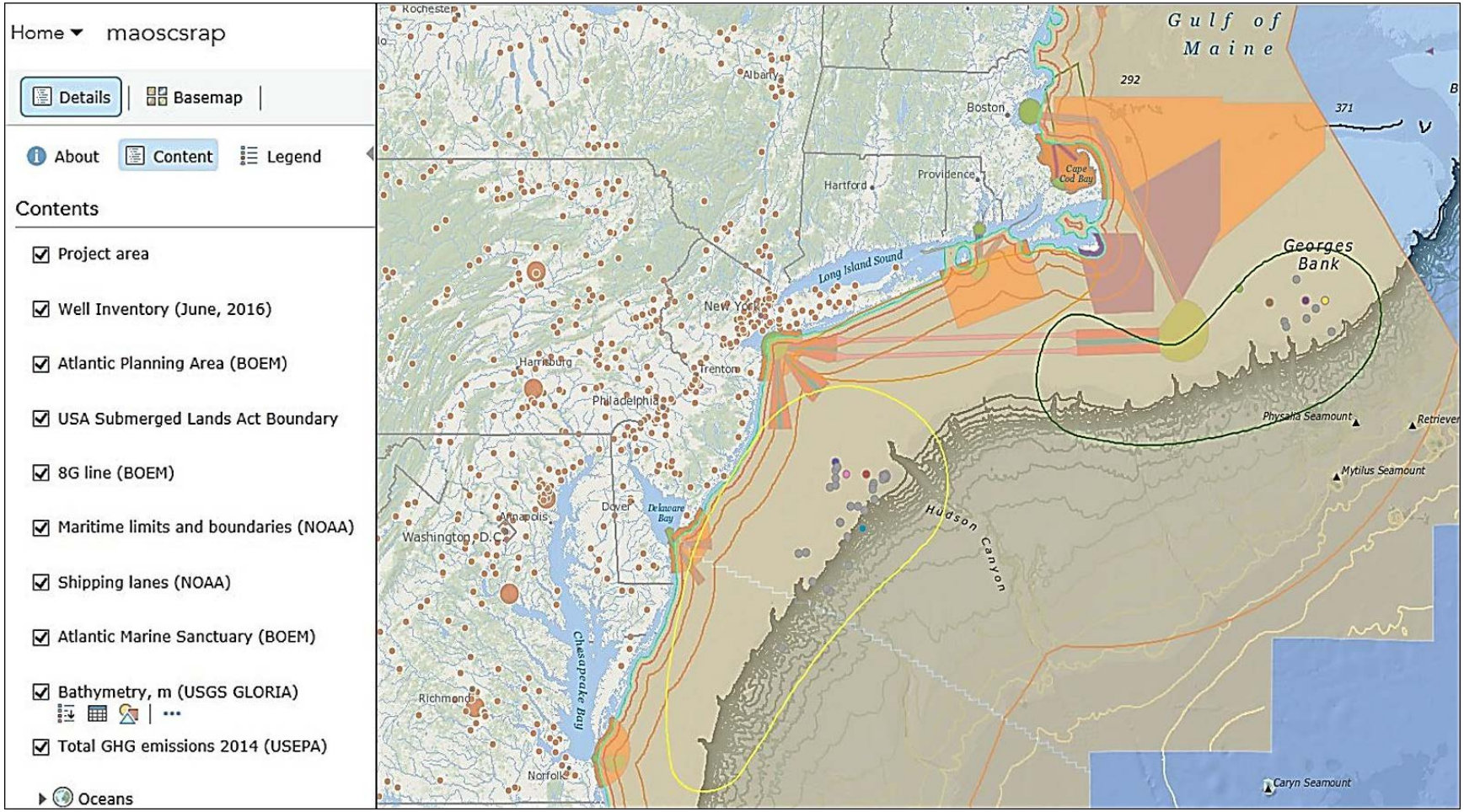

Figure 3-8. AGOL map developed for the Mid-Atlantic Offshore project showing the map layers and distribution of data/data types currently uploaded in the database.

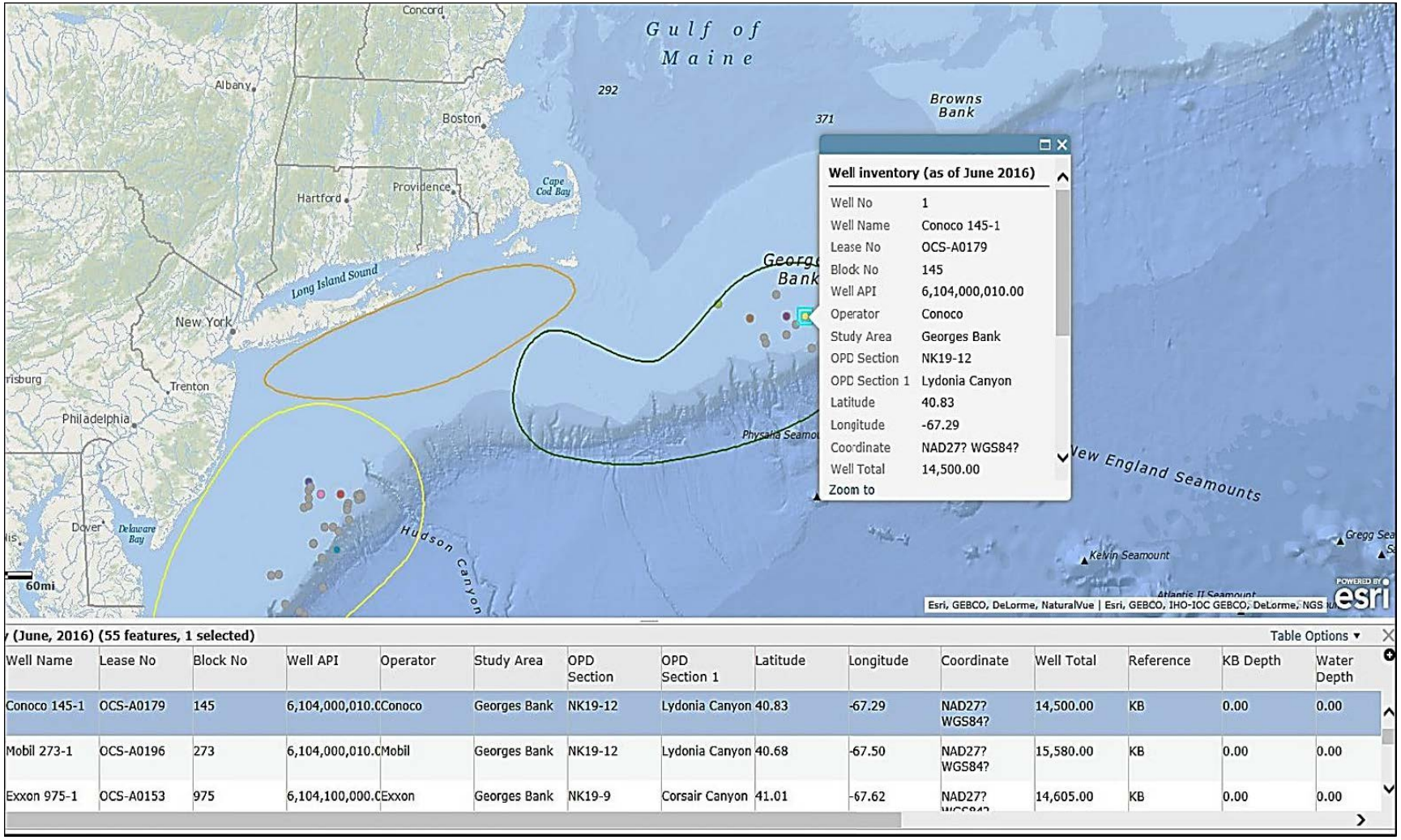

Well Name	Lease No	Block No	Well API	Operator	Study Area	OPD Section	OPD Section 1	Latitude	Longitude	Coordinate	Well Total	Reference	KB Depth	Water Depth
Conoco 145-1	OCS-A0179	145	6,104,000,010.0	Conoco	Georges Bank	NK19-12	Lydonia Canyon	40.83	-67.29	NAD27? WGS84?	14,500.00	KB	0.00	0.00
Mobil 273-1	OCS-A0196	273	6,104,000,010.0	Mobil	Georges Bank	NK19-12	Lydonia Canyon	40.68	-67.50	NAD27? WGS84?	15,580.00	KB	0.00	0.00
Exxon 975-1	OCS-A0153	975	6,104,100,000.0	Exxon	Georges Bank	NK19-9	Corsair Canyon	41.01	-67.62	NAD27?	14,605.00	KB	0.00	0.00

Figure 3-9. User interface of the Mid-Atlantic Offshore project map showing information display and retrieval on AGOL.

4.0 Correlation of Seismic Data with Well Log Data

4.1 Background

The objective of this task is correlation of seismic data with well log data using velocity-depth (V-D) functions updated from Mountain et al. (2010) and Klitgord et al. (1994). The well-log and seismic-survey data will be used to construct regional maps of the candidate reservoirs and caprock formations and to develop cross sections. A summary of wells and available velocity/CS data and log data used to perform well ties is provided in Table 4-1. Figure 4-1 shows the locations of wells in the BCT and the GBB that have been tied to seismic data, as well as the wells that are currently untied.

Table 4-1. Summary of wells used for seismic ties and available chronostratigraphic data, velocity/CS data, and log data for the Mid-Atlantic Offshore study area.

Well ID	Subregion	Chrono-stratigraphy	VSP / CS	RHOB	DT	Seismic tie
Exxon 133-1	GBB	✓	✓	✓	✓	ISWT
Conoco 145-1	GBB	✓	✓	✓	✓	ISWT
Tenneco 187-1	GBB	✓	✓	✓	✓	ISWT
Mobil 273-1	GBB	✓	✓	✓	✓	ISWT
Mobil 312-1	GBB	✓	✓	✓	✓	ISWT
Shell 357-1	GBB	✓	Partial	✓	✓	ISWT
Shell 410-1	GBB	✓	✓		✓	Son. Cal.
Exxon 975-1	GBB	✓	✓	✓	✓	ISWT
COST G-1	GBB	✓	✓	✓	✓	ISWT
COST G-2	GBB	✓	✓	✓	✓	ISWT
Mobil 17-2	BCT	✓	✓	✓	✓	ISWT
Murphy 106-1	BCT	✓	✓		✓	Son. Cal.
Shell 272-1	BCT	✓		✓	✓	
Shell 273-1	BCT				✓	
Shell 372-1	BCT	✓	✓	✓	✓	ISWT
Tenneco 495-1	BCT	✓	✓	✓	✓	ISWT
Exxon 500-1	BCT	✓	✓	✓	✓	ISWT
Mobil 544-1	BCT	✓	✓	✓	✓	ISWT
Shell 586-1	BCT	✓	✓	✓	✓	ISWT
Shell 587-1	BCT	✓	✓		✓	Son. Cal.
Conoco 590-1	BCT	✓	✓	✓	✓	ISWT
Texaco 598-1	BCT	✓	✓	✓	✓	ISWT
Exxon 599-1	BCT	✓	✓	✓	✓	
Shell 632-1	BCT	✓	✓	✓	✓	CS
Texaco 642-1	BCT	✓		✓	✓	
Tenneco 642-2	BCT	✓	✓	✓	✓	ISWT
Tenneco 642-3	BCT		✓	✓	✓	ISWT
Homco 676-1	BCT	✓		✓	✓	
Exxon 684-1	BCT	✓	✓	✓	✓	ISWT
Exxon 684-2	BCT	✓	✓	✓	✓	ISWT
Gulf 718-1	BCT	✓		✓	✓	

Well ID	Subregion	Chrono-stratigraphy	VSP / CS	RHOB	DT	Seismic tie
Exxon 728-1	BCT			✓	✓	
Exxon 816-1	BCT		✓	✓	✓	CS
Homco 855-1	BCT	✓		✓	✓	
Gulf 857-1	BCT	✓	✓	✓	✓	ISWT
Exxon 902-1	BCT	✓	✓	✓	✓	ISWT
Shell 93-1	BCT	✓	✓	✓	✓	ISWT
COST B-2	BCT	✓	✓	✓	✓	ISWT
COST B-3	BCT	✓	✓	✓	✓	ISWT

ISWT = integrated seismic well tie; CS = checkshot; Son. Cal. = sonic calibration.

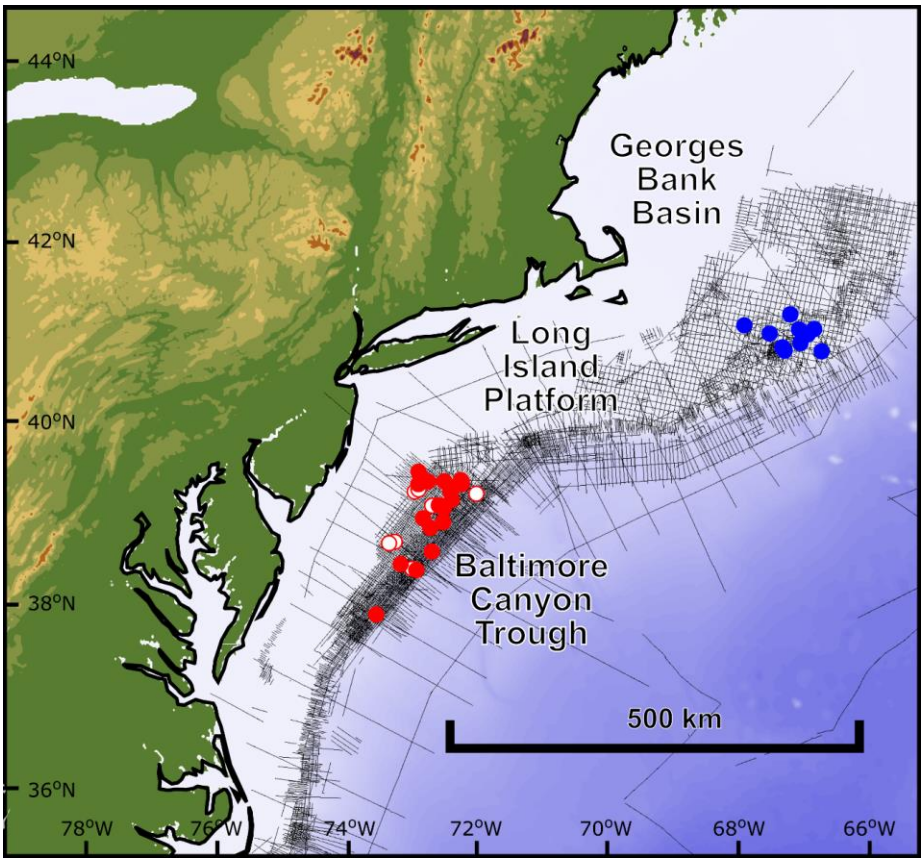

Figure 4-1. Map showing the locations of wells that have been tied to seismic data (solid colored circles) in the BCT (red) and the GBB (blue), as well as the wells that are currently untied (white circles).

Note: The black lines represent USGS and industry seismic lines.

4.2 V-D Function Methodology

Log data from exploration wells (measured in feet below Kelly Bushing [KB]) were projected onto seismic sections (measured in TWTT in seconds from sea level) by developing a regional V-D function. CS surveys are potentially the most accurate method to transfer data from depth to time on individual wells, but such data are often lacking and may be inaccurate. Therefore, a regional V-D function was developed by combining the following functions:

1) a function from the top 800 milliseconds (ms) (~1 km) of sediments calculated by Mountain et al. (2010) using stacking velocities (Vrms) examined at 22 common depth point (CDP) gathers along Oc270 MCS line 229 (Figure 4-2) (a composite Vrms versus travel time relationship was obtained and the Dix (1955) equation applied to obtain a V-D function) and

2) a V-D function similarly obtained from the deeper section (>800 ms) using stacking velocities from USGS MCS data, smoothing the velocities, removing geologically improbable velocity variations, and applying the Dix (1955) equation to obtain interval velocities and a regional V-D function (Klitgord et al., 1994) (Figure 4-2).

To ensure a reliable correlation, the accuracy of the conversion of the seismic data (in TWTT) to depth was checked against values obtained from well velocity surveys at the well locations. The Mountain et al. (2010) and Klitgord et al. (1994) V-D functions were spliced into one curve and then interpolated to consistent travel time intervals of 0.1 s (Figure 4-2).

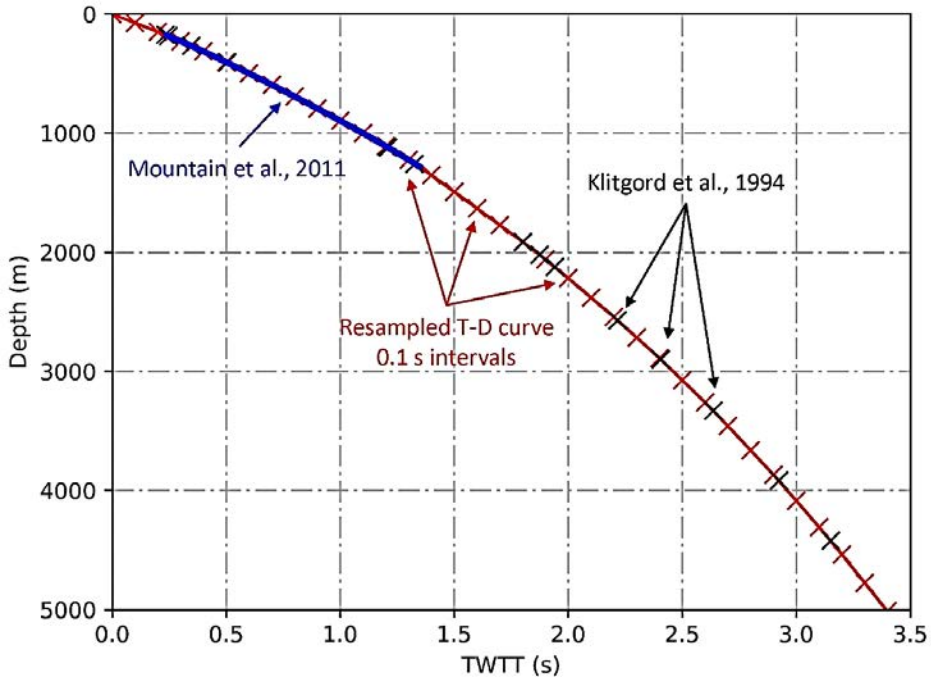

Figure 4-2. Plot of TWTT versus depth showing a regional V-D function developed by integrating the top 800 ms from Mountain et al. (2010) with the deeper function of Klitgord et al. (1994).

4.3 Preliminary Results

4.3.1 GBB Seismic-Well Log Correlations

Accurate ages of the seismic reflectors were determined by tying the seismic data to industry wells in the GBB (Figure 4-3). The tying procedure was based on available CS data and DT and RHOB logs (see Table 4-1). The procedure included calibration of sonic velocities using the CS data to form a high-resolution time-depth relationship. Where available, synthetic seismograms were constructed to evaluate seismic-well ties. In total, 10 wells were tied to seismic data in the GBB (Figure 4-3).

4.3.2 BCT Seismic-Well Log Correlations

A similar method was followed to correlate seismic and well-log data in the BCT. In total, 21 wells were tied to seismic data in the BCT (Figure 4-4). In addition, newly released seismic data collected by industry in the 1970s and 1980s contributed to improved data density and quality offshore New Jersey, enhancing the ability to identify seismic sequence boundaries in Cretaceous reflections in the northern BCT.

In addition to the regional assessment of the seismic data (e.g., Figure 4-4), localized reflector terminations were recognized and interpreted in the northern BCT. Three preliminary seismic sequence boundaries (Middle Cretaceous 1, 2, and 3 [MK1, MK2, and MK3]) have been traced above a Barremian unconformity (Lippert, 1983) and below the major Top Cretaceous (Upper Cretaceous [UK1]) reflector using reflector terminations near the GSD (Figure 4-5). The seismic profiles have been tied to wells using checkshots, vertical seismic profiles, and synthetic seismograms. When tied, these middle Cretaceous reflections show good correlation to sequence boundaries (Logan Canyon 1, 2 and 3 [LC1, LC2, and LC3]) identified in gamma logs (within 100 ft (33 meters [m]).

The reflections traced also follow patterns seen in the logs. For instance, the gamma log shows that the LC1 sequence diminishes slope-ward. Similarly, MK1 can be traced throughout the northern BCT, but pinches out when approaching the shelf/slope margin (Figure 4-6). Future analysis will further constrain the time-depth relationship between all wells in the northern BCT, and allow correlation between potential sequence boundaries seen in the seismic data and those identified in the well logs.

Well data from the southern BCT have been projected onto the seismic data obtained from the NAMSS) (Figure 4-7) (Triezenberg et al., 2016). Biostratigraphic interpretations and geophysical log data facilitated correlations among wells guided by the seismic profiles connecting Shell 272-1, Shell 273-1, Mobil 17-2, and Tenneco 495-1. The biostratigraphic picks that bound or fall within these sedimentary packages mapped by the seismic profiles provide preliminary chronostratigraphic assignment. The seismic sections were interpreted using stratal terminations to guide tracings and identify the significant seismic surfaces. In all, 10 distinct horizons and stratal packages have been mapped, many of which may be sequence boundaries. In the deeper section (below 2.5 to 3 s TWTT), correlation of strata is more difficult due to the reduction in resolvable vertical detail.

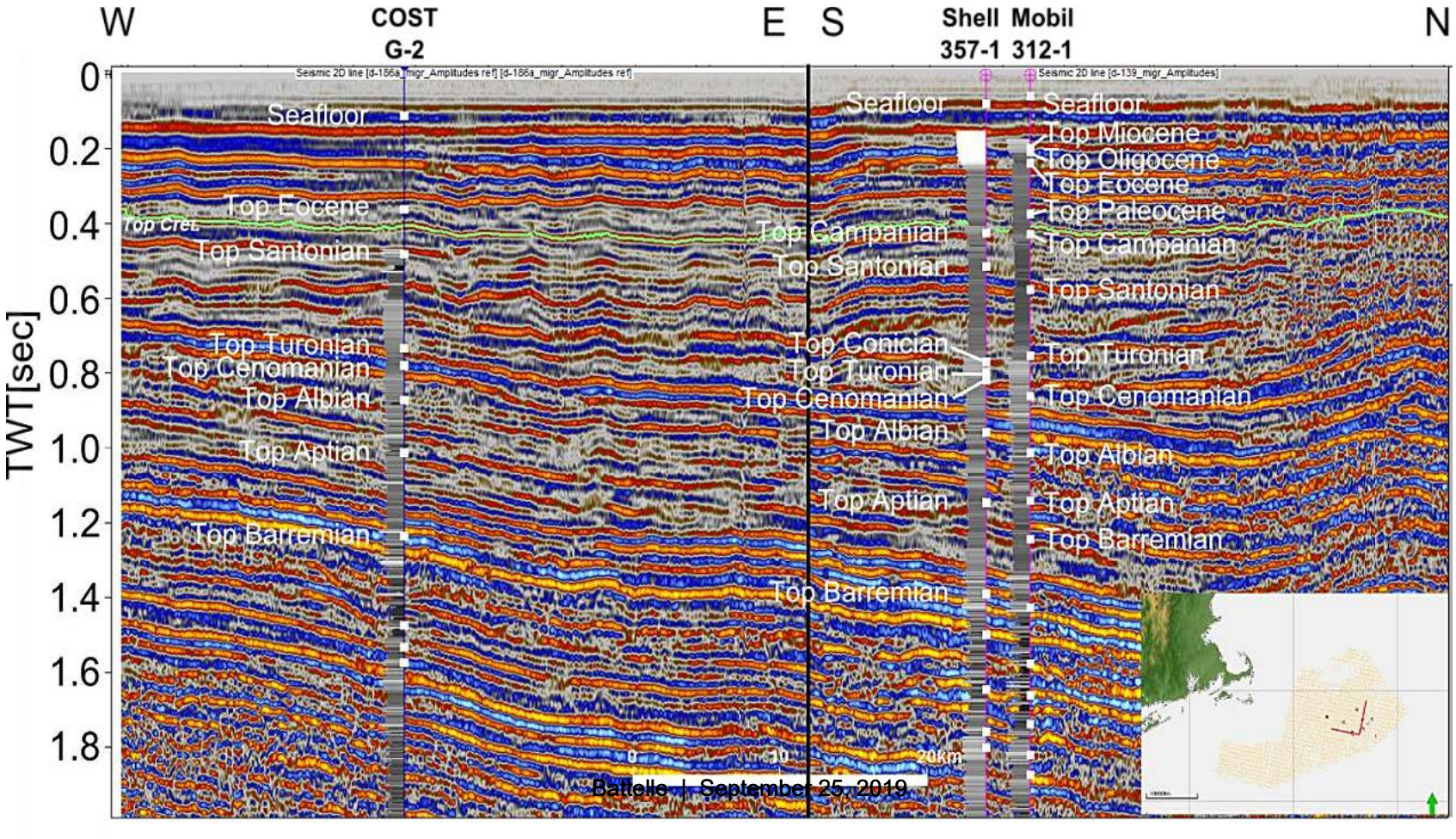

Figure 4-3. Seismic correlation of GR logs and well tops from COST G-2, Shell 357-1, and Mobil 312-1 wells in the GBB projected on a composite seismic section in GBB.

Note: The section is composed of BOEM MCS seismic data. Green line marks the UK1 reflector. Seismic data are in TWTT (s) on y-axis.

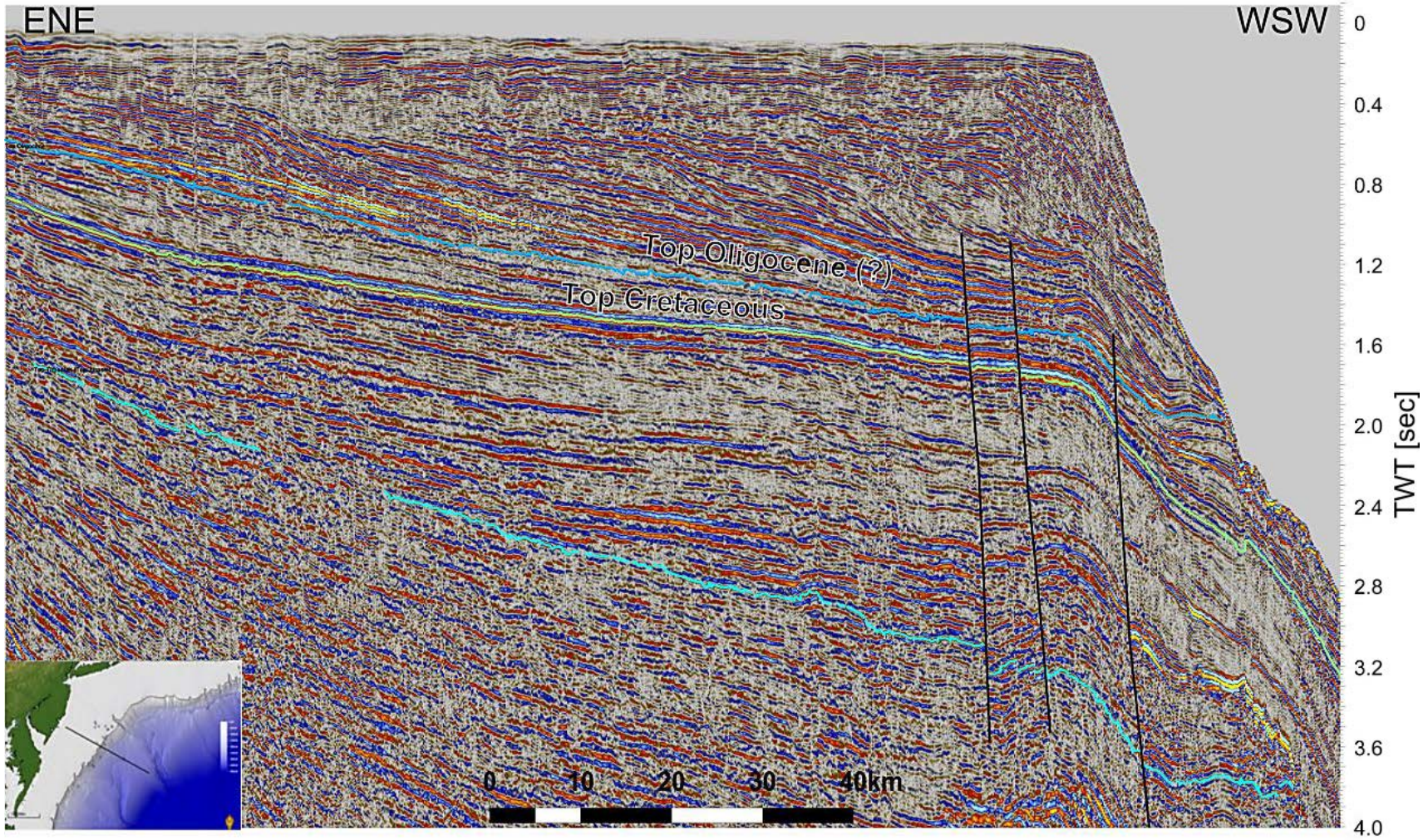

Figure 4-4. Interpreted line 25 across BCT (green line marks the UK1 reflector).

Note: Seismic data are in TWTT (s) on y-axis.

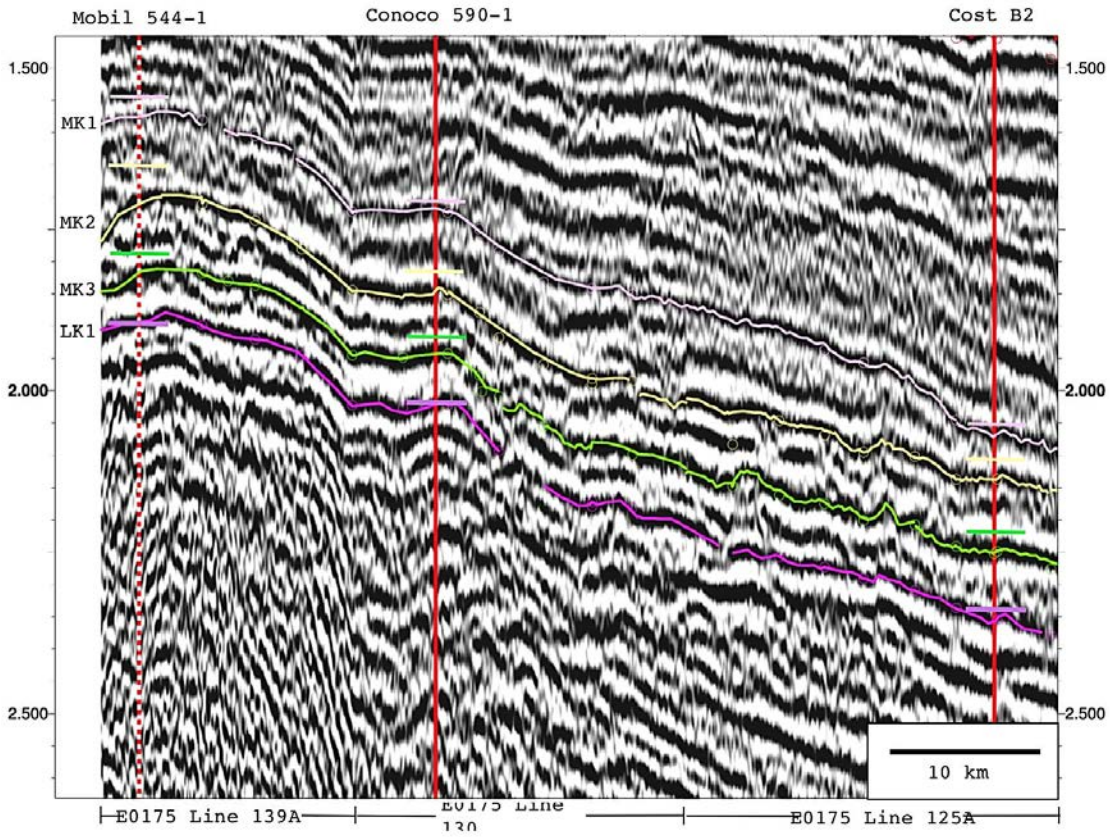

Figure 4-5. Preliminary correlation of seismic and well log data from the Mobil 544-1, Conoco 590-1, and COST B-2 wells near the GSD using BOEM MCS seismic data.

Note: Purple, yellow, and green lines represent interpreted sequence boundaries (MK1, MK2, MK3, LK1) and red lines represent well traces. Seismic data are in TWTT (s) on y-axis.

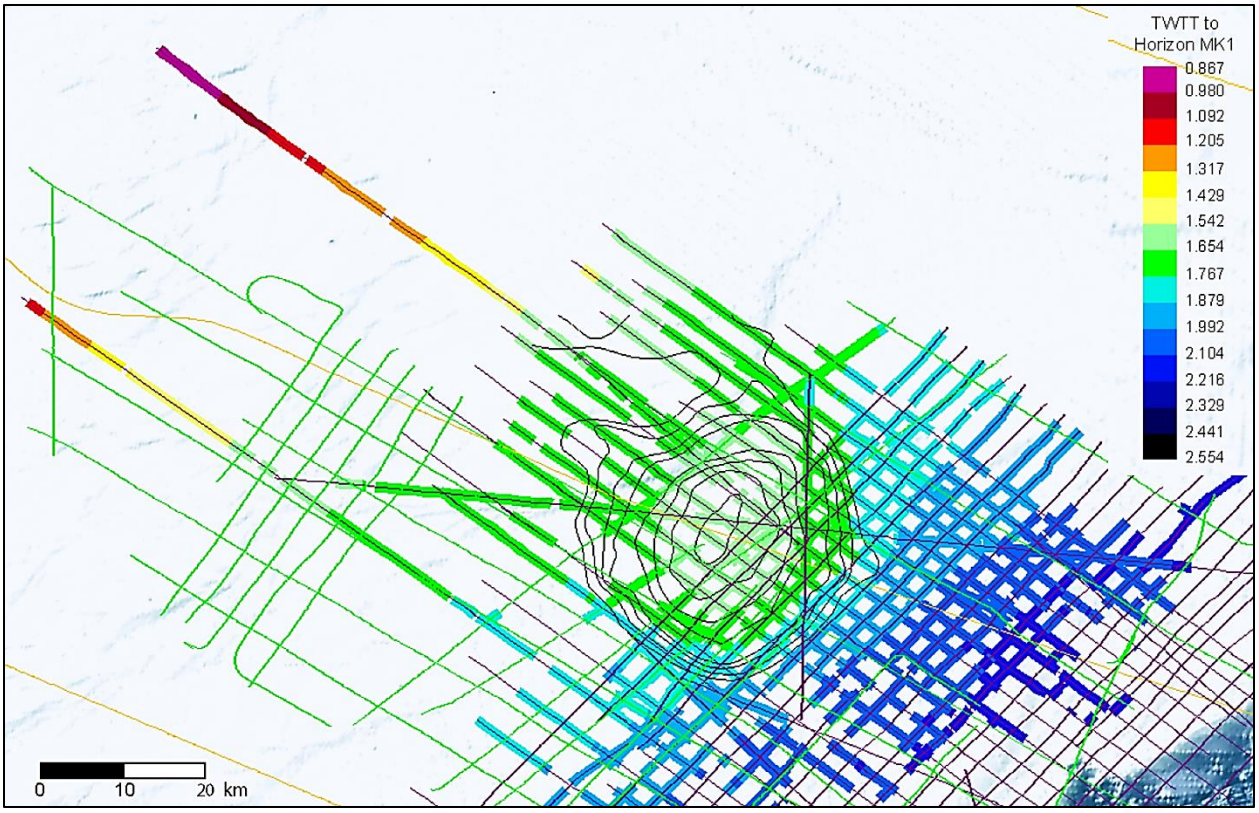

Figure 4-6. Preliminary map of the top of the LC1 sequence near the GSD interpreted from the top of the MK1 seismic sequence.

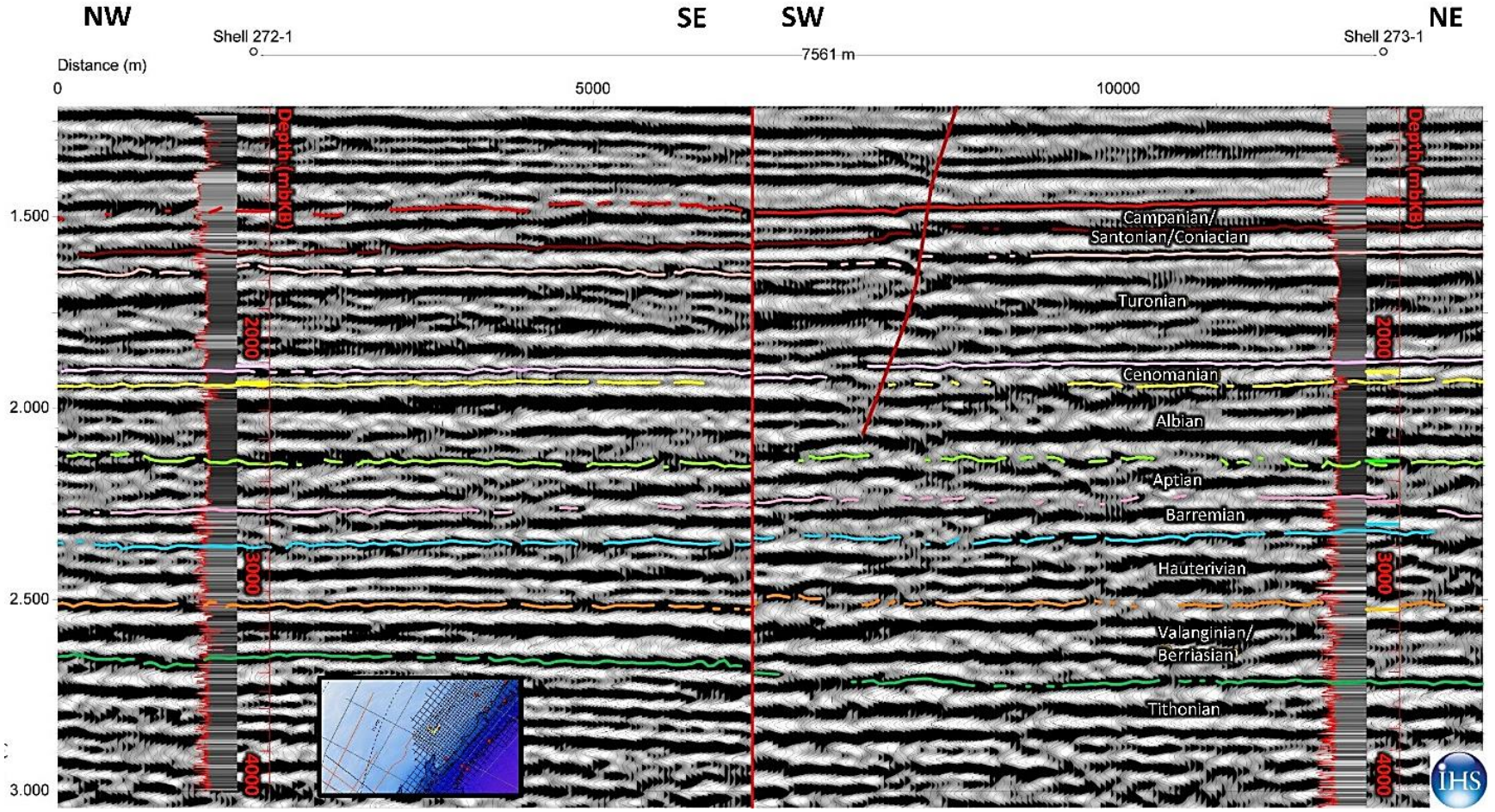

Figure 4-7. Projection of log data (originally in feet below KB) from the Shell 272-1 and Shell 273-1 wells, in acoustic TWTT (y-axis) on a seismic section consisting of the a-207 and a-142 seismic lines obtained from NAMSS (Triezenberg et al., 2016).

Note: Interpreted biostratigraphic horizons used to preliminarily assign and map chronological packages of sediments are also shown. Seismic data are in TWTT (s) on y-axis.

Correlations from Shell 272-1 and Shell 273-1 were conducted using geophysical logs, biostratigraphic interpretations, and seismic reflection profiles. The data show a seismic correlation of a sandy unit, indicated by low GR log values, that generally corresponds with the biostratigraphic pick of the top of the Albian in both the Shell 272-1 and Shell 273-1 wells. This sand correlates to the Highstand Systems Tract (HST) of the Logan Canyon 2 (LC2) sequence in the northern BCT (Miller et al., 2017). The undifferentiated shale below this sand has been identified by Libby-French (1984) as the Naskapi unit, and it comprises the equivalent of the LC2 partim and the Logan Canyon 3 (LC3) partim sequences of Miller et al. (in review). The boundary between these two stratal packages can be tentatively identified by the biostratigraphic pick of the Aptian top. This surface can be correlated between the wells using the seismic data. The base of the LC3 (Miller et al., in review), which corresponds to the top of the Missisauga (Libby-French, 1984), is marked by a serrated gamma log pattern that is characteristic of tidal/estuarine to fluvial coastal plain deposits and a proximal position within the basin compared to the overlying LC3. In Shell 273-1, the biostratigraphic pick interpreted as the top of the Barremian corresponds with the top of the Missisauga formation, and can be relatively confidently traced across the seismic section to the Shell 272-1 well.

Correlations of other seismic surfaces between Shell 272-1 and Shell 273-1 are based on loop correlations connecting these wells with Mobil 17-2 and/or Tenneco 495-1. Specifically, Turonian biostratigraphic tops can be traced from Mobil 17-2 to Tenneco 495-1 through Shell 272-1, with stratal terminations within this package indicating a basin-ward, deltaic progradation of sediments during this time. A reflector that was originally identified as the Cretaceous-Paleogene (K/Pg) boundary bounds the Campanian, Santonian, and/or Coniacian strata below it. The Hauterivian reflector tracks with the overlying Barremian horizon; these coupled surfaces identify the top of the Missisauga formation. Coarse correlations of Early Cretaceous Valanginian and Berriasian strata are made through loop correlations of biostratigraphic markers in the Shell 273-1 and Mobil 17-2 wells. Similarly, a top Jurassic Tithonian biostratigraphic pick was made in Tenneco 495-1 and Mobil 17-2 and is traced around the seismic grid. These preliminary seismic correlations are strongly supported by well log correlations and suggest that seismic correlations of major surfaces in the southern BCT will be feasible in the next phase of the project.

5.0 Characterization of Geologic Storage Zones

5.1 Stratigraphic Framework Overview

Characterization of offshore deep saline formations for potential geologic storage of CO_2 involves interpreting hydrogeologic and geophysical properties to estimate subsurface pore volumes available for storage. Subsurface information on properties that control the distribution and movement of fluids, such as stratigraphy, lithology, porosity, and permeability, are being extracted from borehole geophysical logs, seismic data, and core data. Biostratigraphic and sedimentological data also will provide information to improve age control and characterization of depositional environments for offshore formations. Using sample material available at the DGS OCS Sample Repository, Cretaceous-age sands of the BCT and GBB will be evaluated for planktonic foraminiferal, pollen, and dinocyst biostratigraphy to evaluate continuity of potential reservoirs and caprock.

Geologic characterization involves construction of new formation maps (e.g., structural, isopach, porosity), dip-sections, age-correlation charts, and geologic cross-sections that delineate geologic sequestration units in the BCT, the Long Island Platform, and the GBB. These maps will provide a critical picture of the regional stratigraphic framework and the distribution of deep saline formations (mostly sands and sandstones) suitable for offshore CO_2 storage, as well as the nature and quality of the caprocks.

Two approaches have been used for stratigraphic correlations: 1) lithostratigraphic interpretation that involves correlating log signatures as lithologic boundaries based on the largely bivariate signal of sand versus shale in the offshore siliciclastic rocks (e.g., Libby-French,1984), and 2) sequence stratigraphic correlations involving the integration of biostratigraphy with well logs on a basinal scale to identify sequence boundaries. The sequence stratigraphic framework developed for the study area will provide enhanced predictability of potential storage zones in the region (Miller et al., 2013).

5.1.1 Lithostratigraphic Approach

A methodology was developed to guide the selection of lithostratigraphic formation tops and bases from well log signatures. These tops and bases were used to define formation zones to which existing core data points and samples have been assigned as part of the data gap analysis (see Section 2.3). These lithostratigraphic tops will also be used to define the zones of interest for petrophysical and storage resource calculations. Intervals picked include those deep saline formations of interest for CO_2 storage, such as the Logan Canyon and Missisauga formations, as well as formations with potential to act as regional seals, such as the Dawson Canyon, Naskapi, and Mic-Mac (Table 5-1).

Table 5-1. Summary of the major lithostratigraphic picks for the study area.

Chronologic Age	Seal or Reservoir	Formation Name[a]
Upper Cretaceous	Seal	Dawson Canyon
	Reservoir	Logan Canyon
Lower Cretaceous	Seal	Naskapi
	Reservoir	Missisauga
	Seal	Mic Mac
Upper Jurassic	Reservoir	Mohawk
	Base/Seal	Mohican / Iroquois

a. Units based on Libby-French (1984).

A combination of four well logs was used to pick lithostratigraphic formation tops and bases: 1) GR, 2) resistivity (RT), 3) RHOB, and 4) NPHI. These four logs provide petrophysically meaningful information for well correlation and subsurface analysis. Zones of clean sandstone or carbonate have a low GR reading, as can be observed in the Logan Canyon sand, whereas shale and clay-bearing intervals, such as the Dawson Canyon and Naskapi shale, show higher GR responses because they typically contain relatively high amounts of radioactive elements such as uranium, thorium, and potassium. In addition to the GR log, the RT log was used to identify depositional patterns, such as coarsening upward, fining upward, and serrated signatures, indicative of specific lithologies and depositional environments.

The cross-over observed between the RHOB and NPHI logs was used to distinguish sands and sandstones (potential reservoirs) from mud and shale units (non-reservoir, confining units). An NPHI curve to the left of the RHOB curve on the log track was interpreted as an indication of the presence of shaley formations, whereas the presence of the RHOB curve to the left of the NPHI curve suggests the presence of a sandy formation. This is because, in general, shaley formations have higher NPHI than sandstones due to higher amounts of clay-bound water, and sandy formations have lower RHOB due to higher pore volumes and quartz content. Moreover, RHOB and NPHI logs can be compared to detect natural gas in formations, because the presence of gas increases the apparent porosity seen by RHOB but decreases the apparent porosity NPHI log, yielding a "gas crossover".

5.1.2 Sequence Stratigraphic Approach

Sequence stratigraphy refers to correlation of rock units based on tracing of unconformities (sequence boundaries) and of flooding surfaces (especially transgressive surfaces [TSs] and maximum flooding surfaces [MFSs]), then inferring depositional systems within these strata surfaces. Sequence stratigraphic analysis was completed to better define the nature and

distribution of target CO_2 storage intervals and caprocks. This analysis is especially useful to determine variations in lithology and lateral correlations across the OCS study area.

In the northern BCT, GR logs and seismic data were used to prepare sequence stratigraphic interpretations and correlations for the GSD and OCS, focusing on the Logan Canyon Sands, a series of Aptian to lower Cenomanian sands first identified and correlated by Libby-French (1984). Libby-French identified the upper Logan Canyon and lower Logan Canyon sands separated by the Sable Shale and correlated them through 26 wells in the northern BCT. Similarly, Seker (2012) constructed well log cross sections for 11 wells along the OCS and Hlavaty et al. (2012) did the same for 6 wells across the GSD. These studies took a largely lithostratigraphic approach, though all tried to honor available biostratigraphy.

Well log correlations were refined by integrating GR log data with biostratigraphy within a sequence stratigraphic framework that shows the Logan Canyon is actually three sand bodies associated with three distinct sequences. Numerical values from GR logs were plotted with gray-scaled shadings such that the highest gamma values are black and the lowest are light gray, with shades of gray in between proportional to the gamma log values. This approach yields optimal visualization of well log stacking patterns, with the presumption that the gamma logs in these sandstones and mudstones reflect primarily sand versus mud content. Correlations of Logan Canyon sequences are based on reinterpretations of lithology from geophysical logs and on biostratigraphy obtained from BOEM's data repository for the Atlantic margin.

Age control uses planktonic foraminifera, calcareous nannofossils, and palynomorph biostratigraphy (pollens, spores, dinoflagellates) from original industry paleontology reports. The biostratigraphy was revised to acknowledge modern understanding of species ranges, specifically for the Aptian, and preference for Albian and Early Cenomanian tops is given to species which are encountered in at least two wells. However, some of the interpretations that were reported as chronostratigraphic tops were not compatible with log correlations, and select foraminiferal, nannofossil, and palynomorph highest occurrences (HOs) were instead used from 12 exploratory wells. The ages of HOs were determined using GTS2012 (Gradstein et al., 2012) for correlation with global bioevents. Within the Logan Canyon sands, four main bioevents were identified in each well and correlated across the margin. The scarcity of biomarkers in the older stratigraphic succession (below the Aptian) made it difficult to obtain an accurate age estimate; therefore, this study was restricted to the Aptian-to-Cenomanian Logan Canyon sequences. The revised lithologic tops based on sequence boundaries align well with biostratigraphic tops.

5.2 Geologic Interpretations

Well log transects for the northern BCT and the GBB are nearly complete for their targeted formations.

Well Log Transects Across the Northern BCT

Well logs spanning two geological targets were examined in detail in the northern BCT (Figure 5-1), including:

- Fault closures and traps on the middle shelf associated with the GSD, a large, Early Cretaceous mafic igneous intrusion/dike swarm. Seven dry wells were drilled on- and off-structure, and it is thought that igneous emplacement thoroughly fractured the section, destroyed potential traps, and enabled hydrocarbons to escape (Prather, 1991). These porous rocks were then sealed by thick Upper Cretaceous to Paleogene shales. The combination of porous reservoirs and good caprocks combined with the absence of hydrocarbons makes the GSD an ideal carbon storage target.
- Structures on the middle shelf and OCS, which yielded natural gas in 5 of 21 wells in sandstones and limestones at Texaco 598-1, Exxon 599-1, Texaco 642-1 and -3, and Tenneco 642-2, with a small amount of oil in thermally immature Albian sandstone in the latter well at 2,500 m (Prather, 1991).

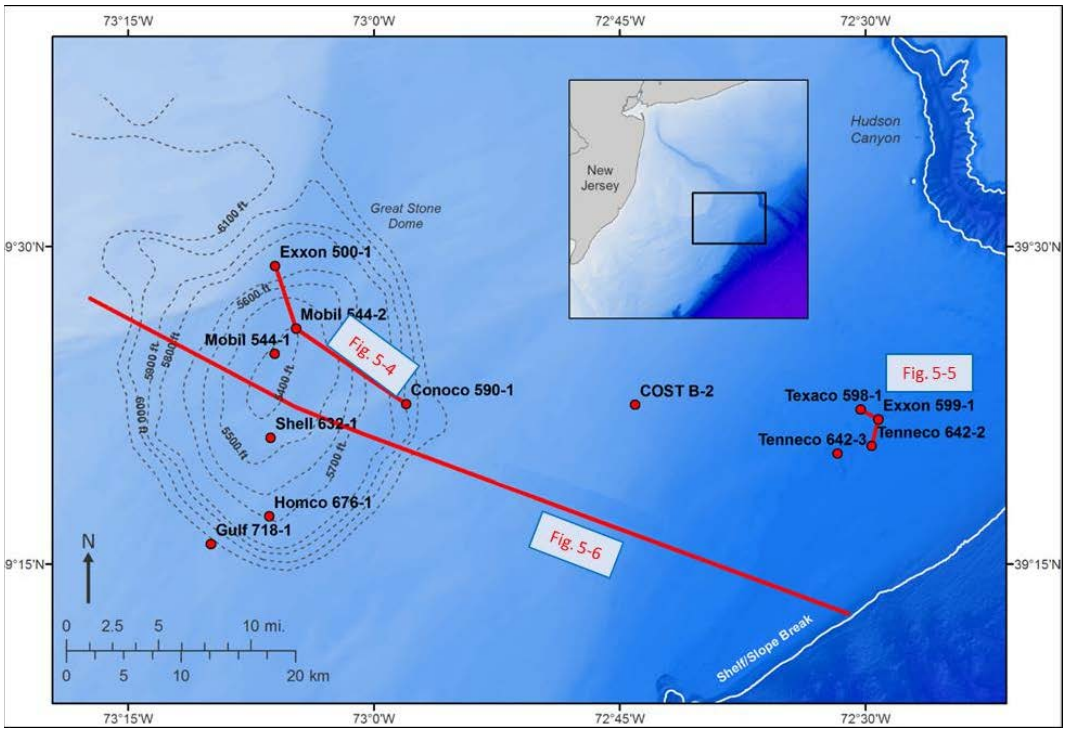

Figure 5-1. Shaded generalized bathymetric location map of the GSD with structural contours to basement after Prather (1991) and the 12 exploration wells discussed here (Miller et al., in review).

Geologic interpretations of the well logs for the northern BCT reinforce previous geological interpretations of excellent reservoirs and seals in this basin. The COST B-2 well is among the most intensely studied offshore wells, and though few cores were collected at this site, there is an especially complete set of logs. Examination of B-2 cores at DGS and integration of core descriptions and core photographs with GR logs (Figure 5-2) provide new insights into environments of deposition and sequences in the Logan Canyon Formation. Core 2, acquired from 9,285 to 9,330 ft (below KB) (2,712.5 to 2,726.4 meters below sea floor [mbsf][1]) from the COST B-2 well captured a partial sequence including the upper part of a Transgressive Systems Tract (TST), MFS, and the lower part of a HST of the LC3 sequence. Sedimentological features indicating a marine setting include the following succession from the base upwards:

1) Massive to laminated sandstone with *Ophiomorpha* burrows, indicating deposition in shoreface (likely upper shoreface) environments, are overlain by transgressive siltstones deposited in deeper shoreface to offshore environments; two parasequences occur in this TST (Figure 5-2);
2) Laminated black shales deposited in offshore environments are associated with a gamma log peak and represent the MFS at 9,316.5 ft (2,722.1 mbsf);
3) Trough cross laminations (Figure 5-2); sand-filled mud cracks; tidal bundles, including what appear to be neap (thinly laminated) and spring (thickly laminated) tidal bundles and exposure surfaces (Figure 5-2); lenticular beds; and soft sediment deformation features all indicate deposition in tidal mudflats of the lower HST. Two parasequences are indicated by a shallowing upward trend with exposure surfaces overlain by deeper siltstones associated with the flooding surface (Figure 5-2).

Placing the core-log observations into a full sequence stratigraphic context delineates three sequence boundaries in the Logan Canyon at COST B-2 (Figure 5-2). Stacking patterns are a way to extend the interpretation of lithofacies beyond the cored interval using well logs, particularly GR and Spontaneous Potential (SP). Black arrows are shown next to the log data to indicate the inferred fining direction within each parasequence.

The LC3 sequence is the lowermost of the three Logan Canyon sequences (Figure 5-3) (sequences are numbered with 1 at the top). As shown in Figure 5-3, the basal LC3 sequence boundary is placed at 9,745 ft below KB (2,852.8 mbsf) at a sharp change from a regressive HST below to a flooding surface at the base of a series of four parasequences that progressively coarsen up to a TS at 9,585 ft below KB (2,804.0 mbsf). The overlying TST consists of three fining-upward parasequences, culminating in the MFS at 9,316 ft below KB (2,722.0 mbsf). The uppermost unit of LC3 is the HST comprising five coarsening-upward parasequences; blocky sands in the uppermost one may represent a falling stage systems tract (FSST).

[1] Feet below KB are used as logging units to ensure compatibility with previous studies (e.g., Scholle, 1980; Libby-French, 1984); depths converted to meters below seafloor are provided for ease of comparison with seismic profiles.

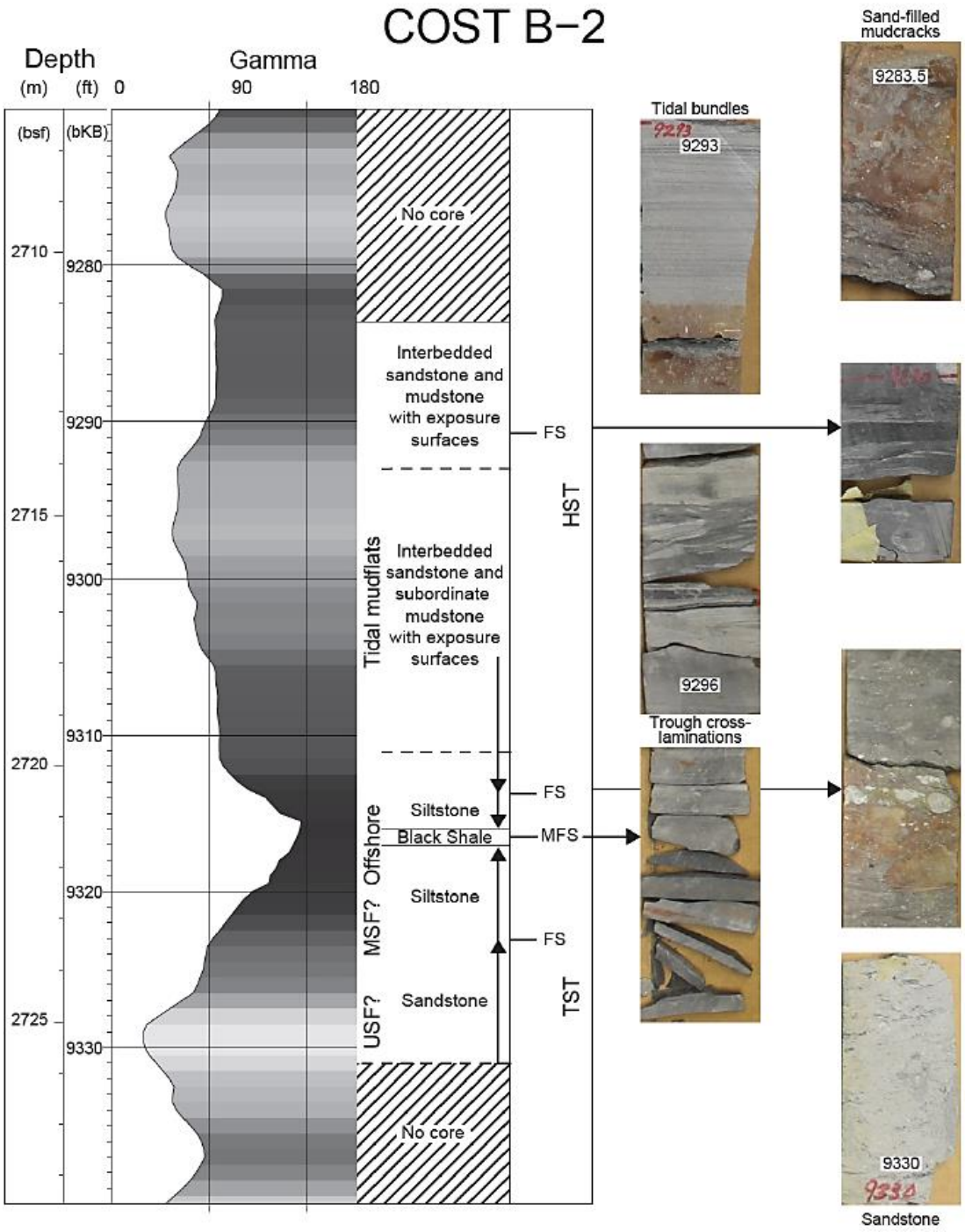

Figure 5-2. Sequence stratigraphic interpretation based on correlation of GR log data with core data from the COST B-2 well.

Note: High GR values are shaded black to dark gray and are indicative of muds or shales; medium GR values appear gray for muddy sands or sandstones or for finely interbedded units of mud/shale and sand/sandstone. FS = flooding surface; TS = transgressive surface; MFS = Maximum Flooding Surface; TST = Transgressive Systems Tract; HST = Highstand Systems Tract (Miller et al., in review).

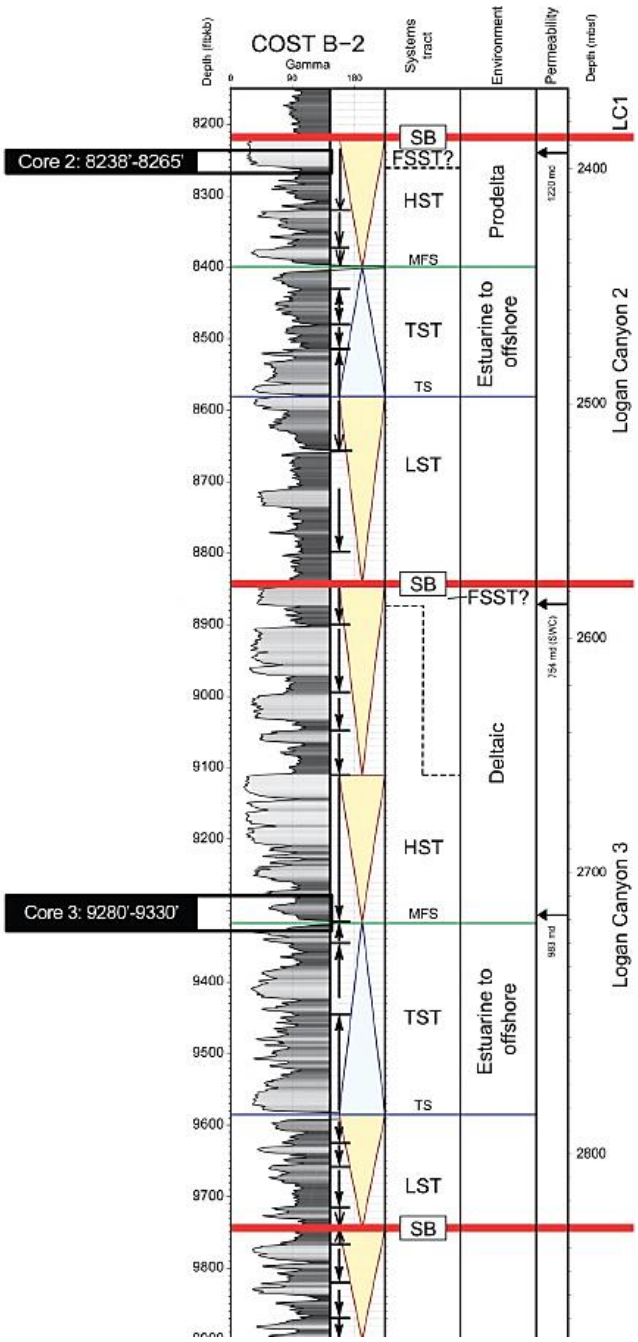

Figure 5-3. COST B-2 stratigraphic section. Low GR values appear light gray to white and are indicative of clean sands.

Note: Parasequences are represented by black arrows point in the fining direction and are bounded by flooding surfaces that are shown as horizontal lines. Large triangles are yellow for coarsening-upward, and blue for fining-upward systems tracts, and have been identified by parasequence trends (stacking patterns) and GR log spikes (often Maximum Flooding Surfaces (MFS) or Transgressive Surfaces (TS). Red lines are sequence boundaries (SB). LC1 = Logan Canyon 1 sequence (Miller et al., in review).

Several lines of evidence indicate that the HST consists of deltaic deposits, most likely at the delta front. This is based on the trend of upsection shoaling supported by descriptions of alternating porous clean sandstones, coals/lignites with calcareous shales, and shaley limestones deposited in recurring tidal flat environments (Scholle, 1977). The log patterns at COST B-2 display classic river/wave-dominated deltaic stacking (Van Wagoner et al., 1990) where sand intervals thicken upward, percent sand increases upward, and there are sharp upper contacts with abrupt shifts to finer-grained facies at flooding surfaces (parasequence boundaries).

The LC3 as defined here is partly equivalent to the lower Logan Canyon sand of Libby-French (1984), though the lower Lowstand Systems Tract (LST) shales below 9,680 ft (2,833.0 mbsf) were placed by the latter in the Sable Shale, illustrating the differences between a sequence stratigraphic and lithostratigraphic approach. This sequence is Aptian based on the HO of the dinoflagellate cysts *Cerbia tabulata* in the MFS at 9,316.5 ft (2,722.1 mbsf), with an age of ~118 Ma. This is the thickest of the Logan Canyon sequences at COST B-2 and is the most sand-prone, with porous (~30%) permeable sandstones (754 mD at 8,870 ft [2,704.3 mbsf] and 983 mD at 9,305 ft [2,836.9 mbsf]) measured at COST B-2.

The LC2 basal sequence boundary is placed at 8,845 ft (2,696.6 mbsf). The base of the sequence consists of shales that coarsen upwards to sands in two parasequences. The TS is placed at a thin shale at 8,582 ft (2,616.5 mbsf) that represents a change in stacking from coarsening up to fining up. Parasequences above this are poorly defined by lithofacies but aggrade upward to a distinct gamma maximum at the MFS at 8,400 ft (2,578.4 mbsf). The HST consists of three coarsening-upward parasequences, culminating in a blocky, porous, very permeable sand (26.5% and 1,220 mD at 8,240 ft [2,512.2 mbsf]) that may be a falling stage systems tract (FSST). The shales in the LST were assigned to the Sable Shale by Libby-French (1984) and the sands above to the upper Logan Canyon by Libby-French (1984). The sequence is entirely within the Albian, as indicated by the HO of *F. washitensis, P. buxtor,* and *P. cretacea* at 8,200 ft (2,500.0 mbsf). The blocky sands have previously been identified as a potential target for carbon storage (D. Schrag, personal communication, 2012).

The LC1 sequence at COST B-2 lacks the thick sands that are present updip on the GSD (Figure 5-4), but is similar to the downdip OCS wells that also lack sands (Figure 5-5). Nevertheless, sufficient sands and stacking patterns are preserved to infer a coarsening-upward LST, a fining-upward TST, a MFS, and two coarsening-upward parasequences in the HST. The LC1 sequence was assigned to the Dawson Canyon Shale by Libby-French (1984), again emphasizing the difference between lithostratigraphic correlations and sequence stratigraphic correlations. The LC1 sequence is the lowermost Cenomanian based on the HO of *F. washitensis* at 7,930 ft (2,299.4 mbsf).

The procedures outlined for the COST B-2 well were applied to the seven wells spanning the GSD and four wells on the OCS (Figures 5-4 through 5-6). For clarity, the well log interpretation focuses on two wells on the GSD (Exxon 500 and Mobil 544-2 just off-structure) and one on its flanks (Conoco 590-1) in a downbasin dip transect. Sequences are discussed from the lowest (LC3) upsection.

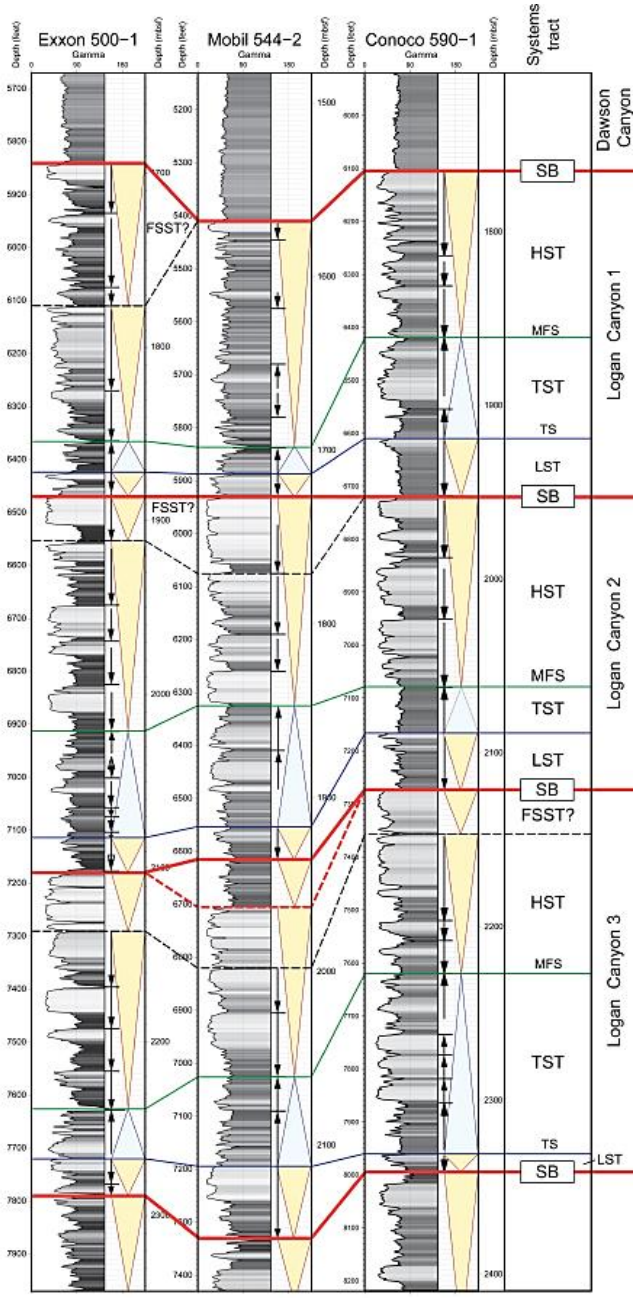

Figure 5-4. Example of well logs for the Logan Canyon Sands in the dip transect across the GSD. Depth (feet) is hung on the top of the Albian (Miller et al., in review).

Note: See Figure 5-2 and 5-3 captions for legend and abbreviations. Cross section location shown in Figure 5-1.

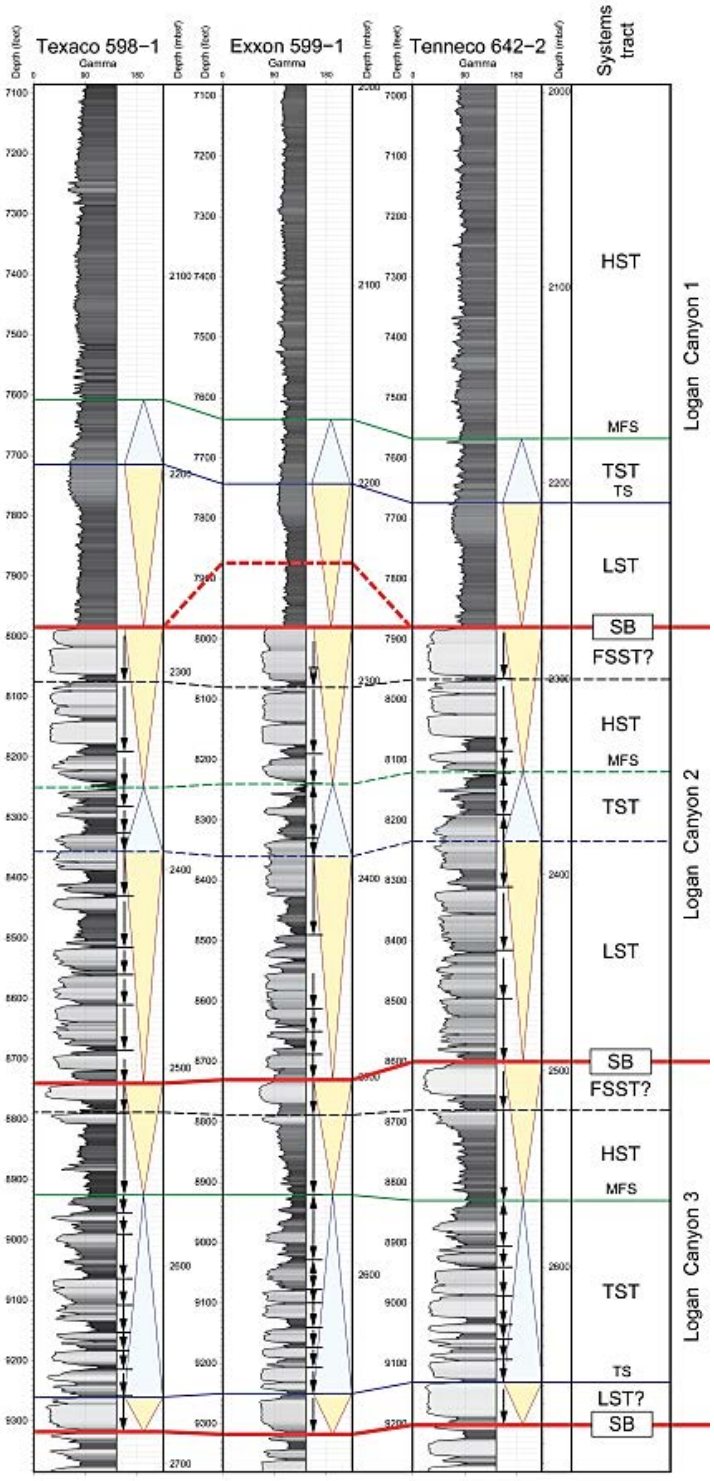

Figure 5-5. Example of well logs for the Logan Canyon Sands across the OCS.

Note: See Figure 5-2 and 5-3 captions for legend and abbreviations. Cross section location shown in Figure 5-1.

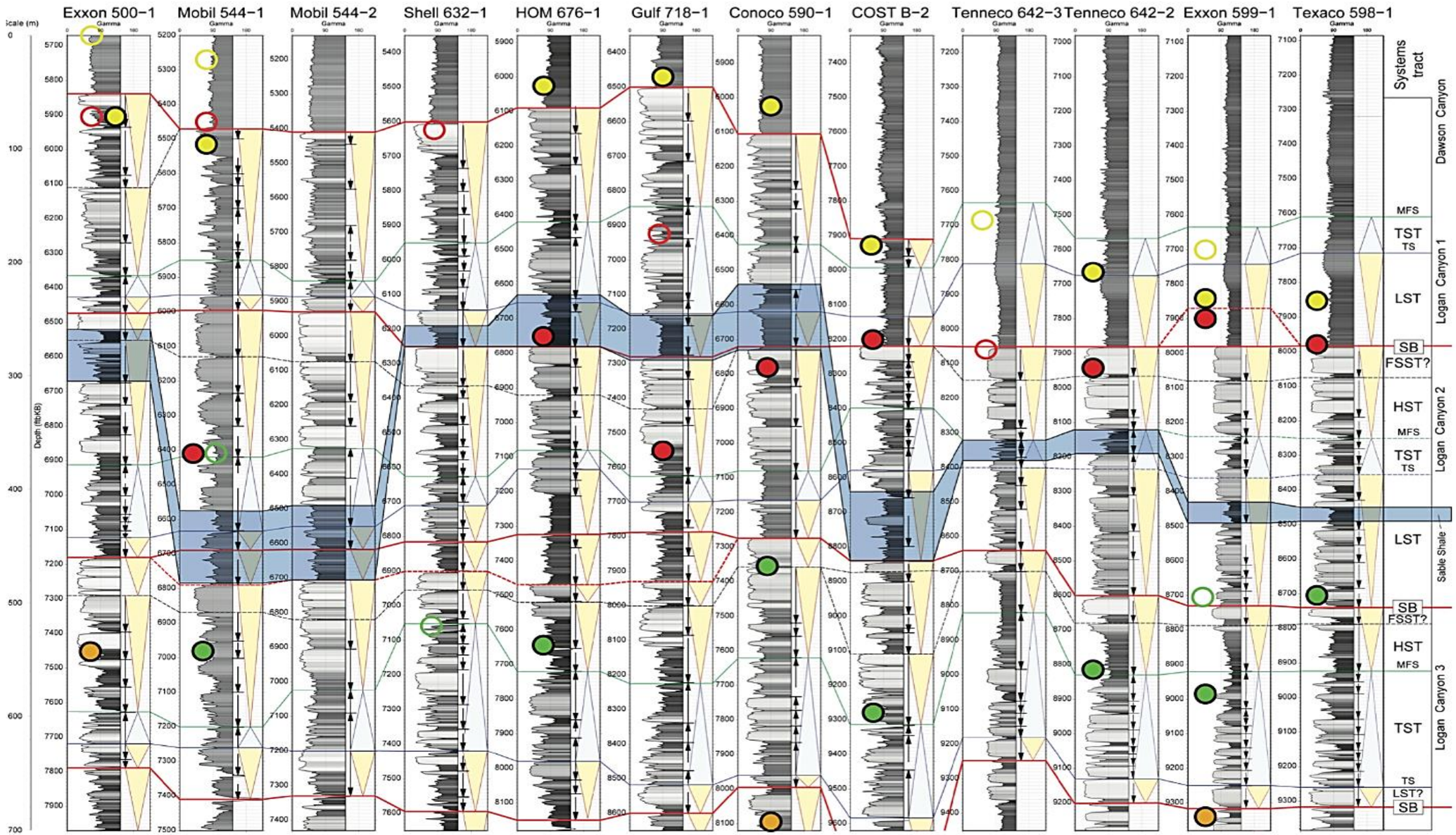

Figure 5-6. Well log transect from the GSD to the OCS showing biostratigraphic data.

Note: Logs are hung on the top of the Albian (red line). Blue-shaded zone is the correlation of the Sable Shale of Libby-French (1984) originally thought to separate the upper Logan and lower Logan Canyon sands. See Figure 5-2 and 5-3 captions for additional legend explanations and abbreviations (Miller et al., in review). Cross section location shown in Figure 5-1.

As at the COST B-2 well, the LC3 sequence is the most sand-prone sequence that is described on the dip transect and throughout the GSD (Figure 5-4). The LST of the LC3 is identified by one to three coarsening-upward parasequences and the LST thin downdip across the GSD (Figure 5-4). The TSTs consist of one to five fining-upward parasequences that thin and decrease in number onto the GSD structure (Figure 5-4). The HST consist of several coarsening-upward parasequences and are relatively continuous in thickness (Figure 5-4). Blocky sands at the top may be a FSST. The precise top of sequence LC3 is uncertain at Mobil 544-2 (Figure 5-4) as well as at four other wells on the GSD (Figure 5-6). There is a coarsening-upward shale unit on top of blocky sand at all the GSD wells that could be tied to either the LC3 or as part of the LST of an overlying sequence. As at COST B-2, the log data of the HST and FSST all show classic river/wave-dominated deltaic stacking patterns with the sand intervals thickening and increasing in percent sand upward, with sharp upper contacts and abrupt shifts to finer-grained facies. These sands have the potential to be excellent reservoirs for carbon storage. Well log correlations suggest that the high porosities and permeabilities measured at COST B-2 (Scholle, 1977) will be similar to these wells at the GSD for these HST/FSST sands, and that the overlying sequence boundary and attendant mudstones provide a reliably intact confining unit. Though it has not been confirmed that individual sand beds are traceable, the sequence stratigraphic framework allows one to confidently predict thick, sand-prone zones just below the overlying sequence boundary.

The overlying LC2 sequence has features similar to LC3. It also is sand-prone, beginning with a shale-rich LST that thins onto the GSD but thickens downdip at Conoco 590-1 and further into the basin. In contrast to the LC3, the LC2 TST thickens onto the GSD. The HST again remains relatively constant in thickness and displays similar river/wave-dominated deltaic gamma log stacking patterns, not only on the GSD (Figure 5-4) but also across the shelf to the COST B-2 well and the OCS (Figures 5-5, 5-6). Peak permeabilities (>1,000 mD) were measured in the porous, blocky sands at the top of the sequence at COST B-2, and similarly high values apply to the wells at the GSD. There is some variability in the continuity and thickness of these sands (e.g., there are five to seven sand zones on the GSD wells) (Figure 5-4) and storage capabilities may thus vary from well to well. But like the LC3, the LC2 sequence is an excellent candidate for carbon storage. These HST sands were generally included with the upper Logan Canyon on the GSD. However, as shown on Figure 5-6, the Sable Shale defined by Libby-French (1984) (separating the upper and lower Logan Canyon) was placed both above and below the basal LC1 sequence boundary as interpreted (though the Sable Shale is generally the LST of the overlying LC1 sequence on the GSD); this placement highlights ambiguities in tracing the shale. Problems associated with tracing individual sand and shale units were avoided by keying in on the stacking patterns and sequence boundaries.

The LC1 is sand-prone on the GSD and transitions into shale out into the basin. On the GSD, the LC1 has a thin LST that thickens downdip, whereas the TST thickens downdip to Conoco 590-1 and is lost in the shale downdip from that. The HST is again relatively constant in thickness, but is not as sand-rich as the underlying sequences. Sands zones are also less correlatable in the LC1 than in the sequences below. The LC1 sequence is capped by thick Dawson Canyon shales that provide an apparently impermeable seal for the underlying sandstones (Libby-French, 1984). It is interesting to note that the Cenomanian sands of the LC1 sequence pinch out by the COST B-2 well and are generally retrogradational compared to the

underlying LC2 and LC3 sands. The “shaling out” of the sequence meant that previous studies have correlated the LC1 updip with the LC2 sands downdip. This miscorrelation could only be avoided by the use of sequence stratigraphy integrated with biostratigraphy.

Seven wells have been analyzed following a transect across the OCS; three are along a dip profile and are interpreted in Figure 5-5; the other four are shown in the Figure 5-6. In all cases, sequences LC3 and LC2 are sand-prone and LC1 is shale-prone, as is the case at COST B-2.

The LC3 sequence has a thin LST on the OCS that is thicker at COST B-2 and many of the GSD wells, though it is sandier downdip. The TST is thick and sandy and fines up to the MFS across the OCS. The HST is distinctly more shaley than at COST B-2, except for a blocky sand at its top.

The LC2 sequence has a very thick LST on the OCS that thins toward COST B-2 and further onto the GSD (Figure 5-5, 5-6). It consists of four to five blocky parasequences that do not readily correlate from well to well (Figure 5-5). The TST is thin at all wells (Figure 5-5). The HST is moderately and relatively uniform in thickness and consists of blocky sands, particularly at the top of the sequence that may be the FSST (Figure 5-5). The HST appears to be an excellent reservoir on the OCS (as it is farther landward over the GSD) and is a potential target for carbon storage.

As previously noted, the LC1 sequence is predominantly shale. A thick LST is indicated by a coarsening upsection at all of the OCS wells (Figure 5-5). The TST appears to be thin at all wells, though the MFS is poorly defined (as is the upper sequence boundary).

Well Log Transects Across the Eastern GBB

The first efforts to characterize the deep saline formations in the eastern GBB took a conventional lithostratigraphic approach, focusing on the Logan Canyon and Missisauga Formations. Future work may include the deeper Mohawk Formation, although initial inspection suggests that the sands are less contiguous. A well-log cross section was constructed linking reservoir sands and confining units based on the lithostratigraphic approach used by Libby-French (1984) (Figure 5-7) (Graham et al., 2016).

Sequences and parasequences have been identified using color-scale displays of the gamma logs within the Logan Canyon, Naskapi, and Missisauga Formations in the eastern GBB. Stacking trends in gamma logs from the COST G-1 and COST G-2 wells were analyzed for sequence stratigraphy (Figure 5-8). The color scale illustrates fining- and coarsening-upward packages that can be used to define TSTs (fining upward) and LSTs and HSTs (both coarsening upward). Potential flooding surfaces were identified as zones associated with high gamma log values recorded amidst lower gamma log values. These log changes indicate a change in sediment composition and depositional environment. The stacking patterns on logs can be used to determine trends in the depositional patterns of individual wells, which can then be correlated to similar stacking patterns at nearby wells, and correlated across entire basins, as was conducted in the BCT (Miller et al., in review).

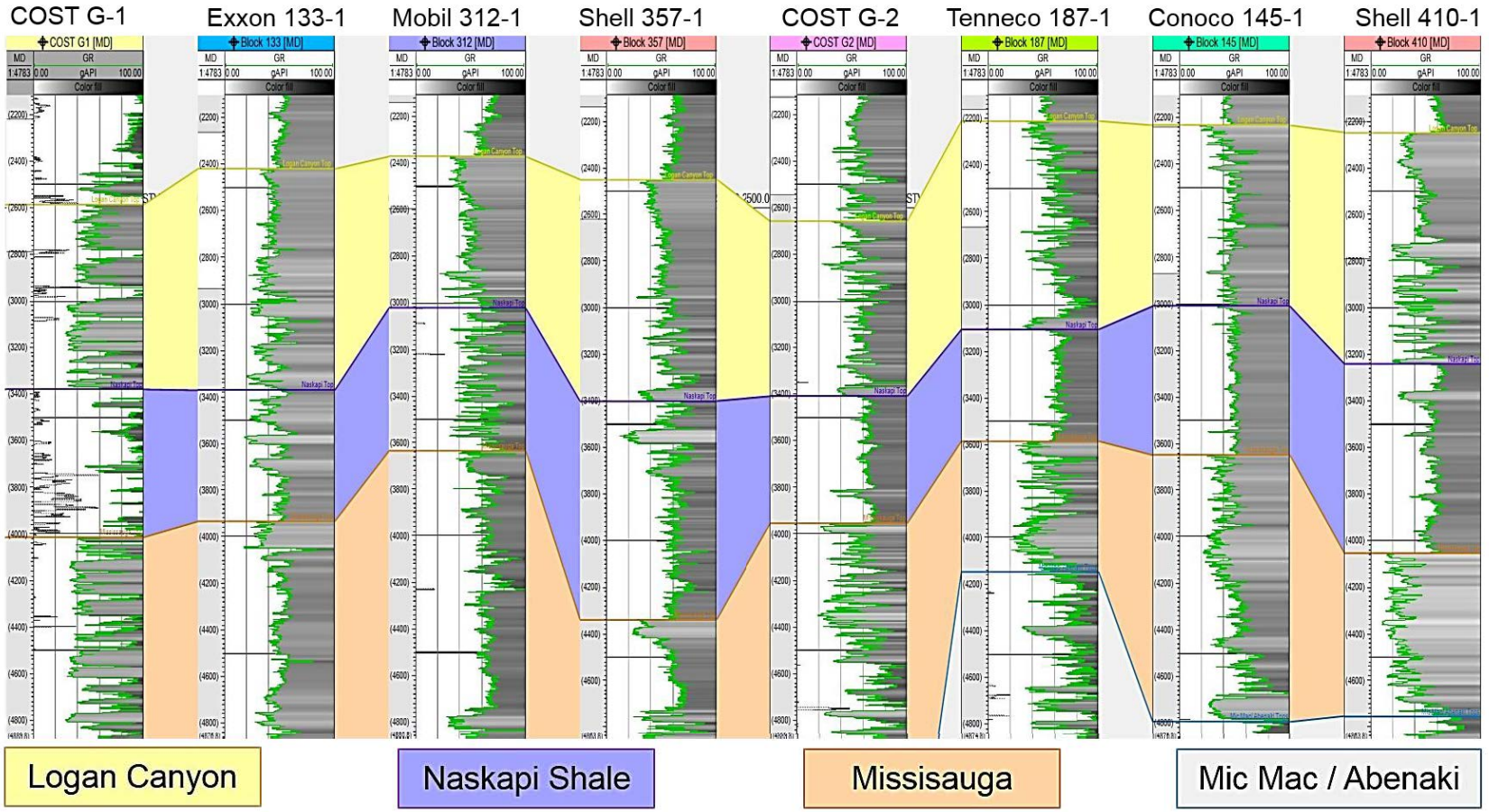

Figure 5-7. Grayscale-shaded well log cross-section in the GBB showing lithostratigraphic interpretation based on Libby-French (1984).

Note: High GR values are shaded black to dark gray and indicate muds-shales; low GR values appear white and indicate clean sands; medium GR values appear gray for muddy sands-sandstones, finely interbedded muds and shales, and sands-sandstones. The GR curve is shaded green. Lithologic formations are denoted by color bands between well logs: the Logan Canyon Formation is yellow, the Naskapi Formation is purple, and the Missisauga Formation is orange. Depth (feet) is hung on 2,500 feet below KB.

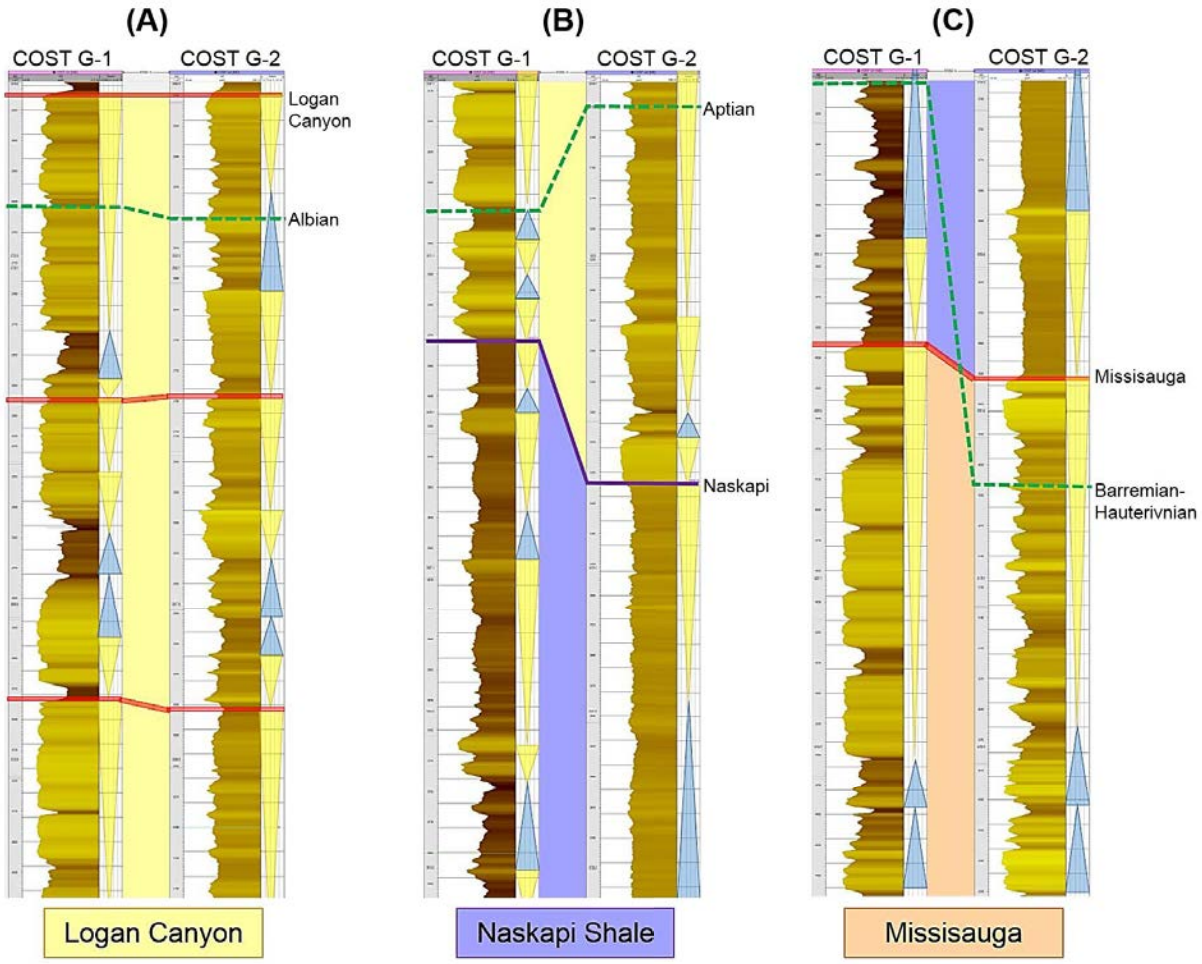

Figure 5-8. Yellow-brown shaded well log cross section showing sequence stratigraphic interpretation and lithostratigraphic interpretation of the COST G-1 and COST G-2 wells from (A) the Logan Canyon, to (B) the Naskapi, and (C) the Missisauga formation.

Note: High GR values are shaded brown to dark brown and indicate muds-shales; low GR values appear yellow and indicate clean sands; medium GR values appear yellow-brown for muddy sands-sandstones, finely interbedded muds and shales, and sands-sandstones. Large triangles are yellow for coarsening-upward systems tracts and blue for fining-upward systems tracts; they have been identified by parasequence trends and spikes in the GR logs. Sequence boundaries are marked by red lines. Lithologic tops (e.g., Logan Canyon, Naskapi Shale, Missisauga) are denoted by colors between well logs. Sequence stratigraphic tops are represented by dotted green line. Lithologic ages shown in depth are taken from Amato and Bebout (1980). Depth (feet) is hung from the top of the Logan Canyon.

Initial results from the eastern GBB to the COST G-1 and COST G-2 wells (see Figure 5-8) show strong sequence stratigraphic correlation not only between these two wells, but also to sequences identified in the BCT. The “Logan Canyon 2” sequence in the BCT (Miller et al., in review) is almost identical to the second sequence identified in the eastern GBB, and the LC1 and LC3 sequences are also readily evident.

Sequence stratigraphy and seismic data correlation will continue to be applied across the rest of the wells in the eastern GBB in order to determine a more exact lithologic correlation, both across this basin and with the BCT. A preliminary attempt at this effort is shown in Figure 5-9, which is consistent within biostratigraphic constraints. The final results will help us to determine the suitability of the likely geologic storage targets in the eastern GBB by improving understanding of the continuity of target formations, lithologic changes in formation character across the basin, and the nature and continuity of confining shales.

This preliminary assessment also show that lithostratigraphic correlations from previous work may be misleading in delineating storage zones and confining units (e.g., the placement of the Sable Shale of Libby-French (1984), shown on Figure 5-7, is not the same shale across the basin changes with respect to biostratigraphic and sequence stratigraphic boundaries). Source rocks for petroleum are poorly developed in the basin, and although there is natural gas in the OCS wells, it was not deemed economical (Prather, 1991). However, the situation is favorable for carbon storage, which requires good seals that avoid leakage along faults or into existing exploration wells.

Porosity and Permeability Discussion

Within the BCT, the Logan Canyon sands are excellent candidates for storage. They are porous (~30%), very permeable (~1,000 mD), and interconnected sandstone reservoirs capped by shale seals. The reservoir extends at least from the GSD to the OCS, a distance of ~60 km. The Logan Canyon sequences show little evidence for faulting and have few well penetrations (versus storage in previous exploration targets). The Logan Canyon sequences examined here are suitable for storage from the GSD to the OCS, though the OCS sites are perhaps less desirable due to the presence of gas in the underlying Missisauga sands (Prather, 1991; Seker, 2012).

Preliminary evaluation of potentially suitable saline sand reservoirs in the eastern GBB included the Logan Canyon, Missisauga, and Mohawk formations:

- **Logan Canyon Formation**: Defined in the Scotian Basin and correlated to the BCT (Scholle and Wenkam, 1982), the Logan Canyon Sands (Cenomanian to Albian; possibly Aptian) in the eastern GBB appear to be thick and porous as they are in the BCT. The sands are thick (typically 100 to 300 ft) and blocky, separated by thin shale beds. The upper appear to be marine, though the lower part appears to be deltaic (delta front) (Amato and Bebout, 1980). Porosities range from 24% to 33%, with permeabilities ranging from ~300 to approaching 2,900 mD based on discrete measurements (Amato and Bebout, 1980). The shallower depth of this reservoir in the eastern GBB (2,500 to 3,400 ft) versus the BCT (~ 6,000 to 8,000 ft near the GSD and 8,000 to 10,000 ft nearer to the shelf edge) may suggest a cost advantage but also a disadvantage, because this is at the upper depth limit for supercritical sequestration and the confining beds are not as thick as in the BCT.

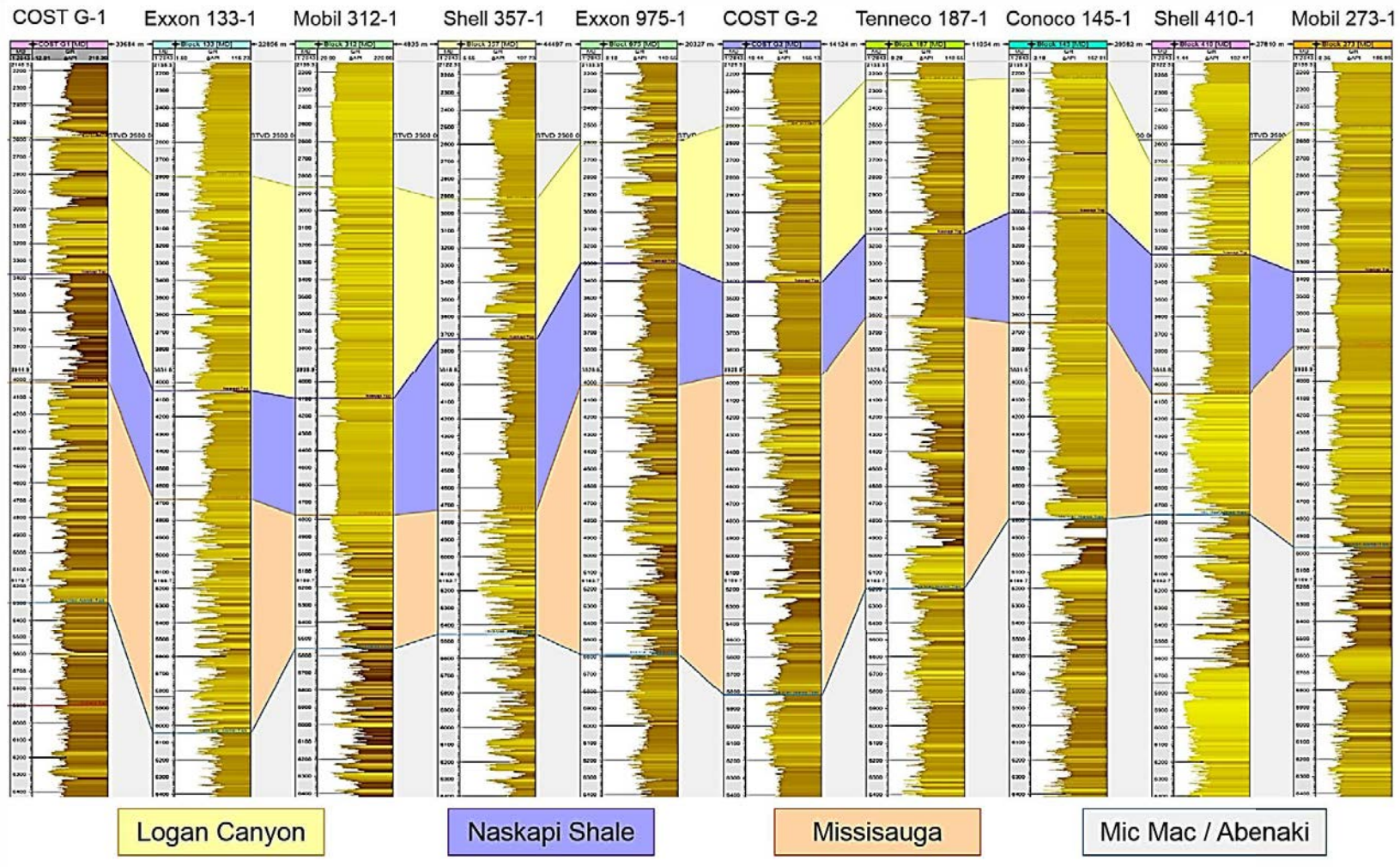

Figure 5-9. Yellow-brown shaded well log cross-section of GR logs and lithostratigraphic interpretation of all ten wells in the GBB.

Note: See notes for Figure 5-8 for explanation of GR log shading. Lithologic formations are denoted by colors between well logs. Depth (feet) is hung on 2500 feet below KB.

- **Missisauga Formation**: Defined in the Scotian Basin and correlated to the BCT and eastern GBB (Scholle and Wenkam, 1982), the Missisauga Formation (Barremian-Berriasian) appears also to be porous, generally blocky sands (typically 70 to 200 ft) and shales with a suitable burial depth (~3,900 to 5,700 ft). There appear to be numerous transgressions and regressions, with coaly shales bracketing marine-marginal marine sands. The sands have typical porosities of 25% to 30% with sparse permeability measurements (~200 to over 1,000 mD). Initial examination of this unit suggests that it is not suitable for CCS in the outer shelf region of the BCT due to the presence of common natural gas (Seker, 2012), but it may be a good target for the eastern GBB. It appears to be confined by the Naskapi Shale, which is ~500 ft thick at COST G-1 and G-2 wells.
- **Mohawk Formation:** Defined in the Scotian Basin and correlated to the BCT, the Mohawk Formation (Oxfordian-Kimmeridgian) (~6,000 to 10,000 ft) appears to be intercalated sands and silts that could be a suitable target.

Units below 10,000 ft have not yet been studied in detail, due in part to low porosities noted by Scholle and Wenkam (1982). As noted in the COST G-1 and G-2 reports (Amato and Bebout, 1980), reservoir characteristics “deteriorate drastically below 10,000 ft where limestone, dolomites, and anhydrites are the dominant lithologies.” There are low porosities in these lithologies drilled off-structure at COST G-1 and G-2, though there may be fracture porosities on structures (Amato and Bebout, 1980).

Rutgers is developing a method for calculating porosity and mineralogy using three common well logs (GR, RHOB, and NPHI). For example, COST B-2 is a well with a complete suite of logs, as well as laboratory-measured porosity and mineralogy (as solid mineral fraction). The method is based on two sets of “filters”: the mathematical filter and the mineralogical filter. The former ensures that the mineral fractions add up to 100%, and the latter makes use of the probabilities of the co-occurrence of mineral groups and diagenetic mineral zonation according to depth (e.g., the four minerals of each solution have to be from the same mineral group, have cations and anions with the same value of valence, and have to be in a range of depth where those minerals can coexist).

Over the past three months, the following improvements were made to the porosity model:

- Variations in the physical properties of the drilling mud were introduced into the model, which improved the model-observation correlation substantially.
- The age and depth dependence of the average mineral composition of sedimentary rocks were introduced, which further improved the model-observation correlation (Figure 5-10) (R2 value is increased from 0.25 to 0.88 compared to classic petrophysical methods).

Further work will use more local knowledge of sedimentary rock composition and its variations with age and depth, which should further improve the method. The method may then be applied to estimate the storage capacity in the off-shore sediments.

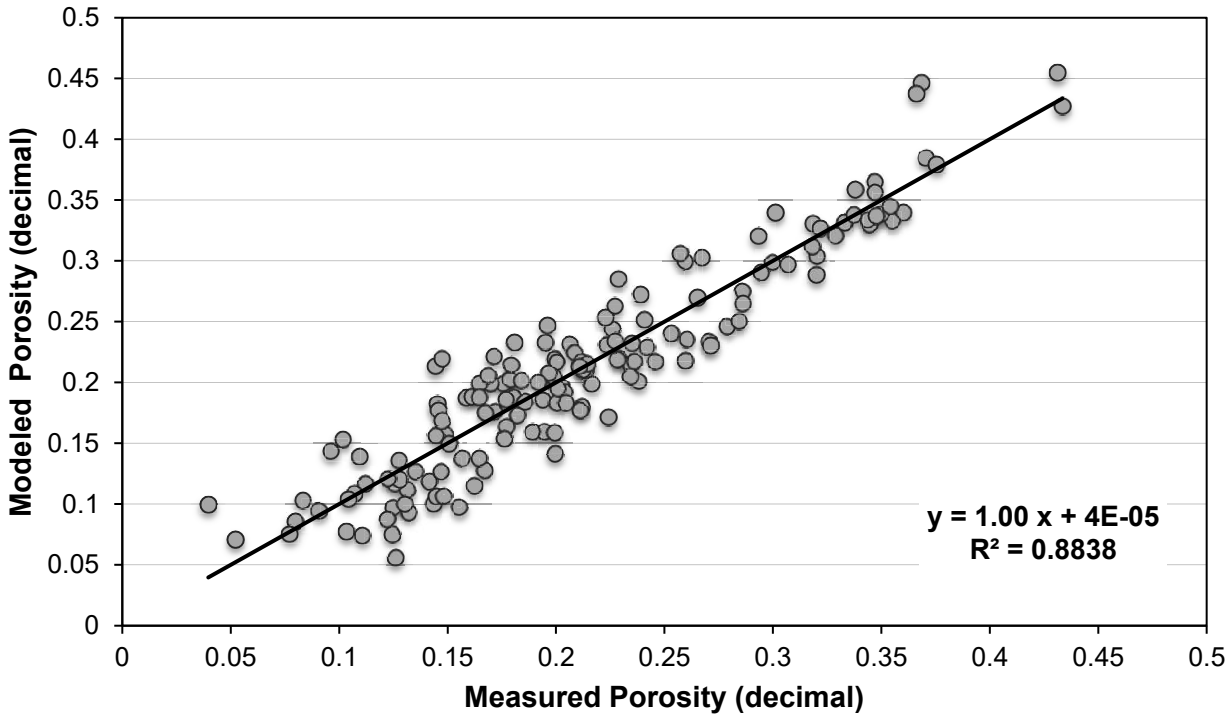

Figure 5-10. Modeled effective porosity against laboratory measured effective porosity, with model inputs being GR, NPHI, and RHOB logs, and the probability of occurrence of any mineral with depth and age compiled from literature.

Note: The model also corrects for drilling fluid contamination (Romero, Master's thesis in preparation).

5.3 Formation Mapping

Formation mapping is being conducted to define the tops, bases, and petrophysical properties of potential deep saline storage zones to be considered in the storage resource calculations. Well data available in the detailed study areas will be extrapolated to the larger regional framework to complete the carbon storage resource assessment for the region. Formation maps showing thickness and area of potential storage zones will be generated using seismic reflection data in large portions of the study area that are not constrained by well data. Interpretation of the seismic data is constrained by well control points. Figure 5-11 shows the process flow for constructing TWTT structural maps.

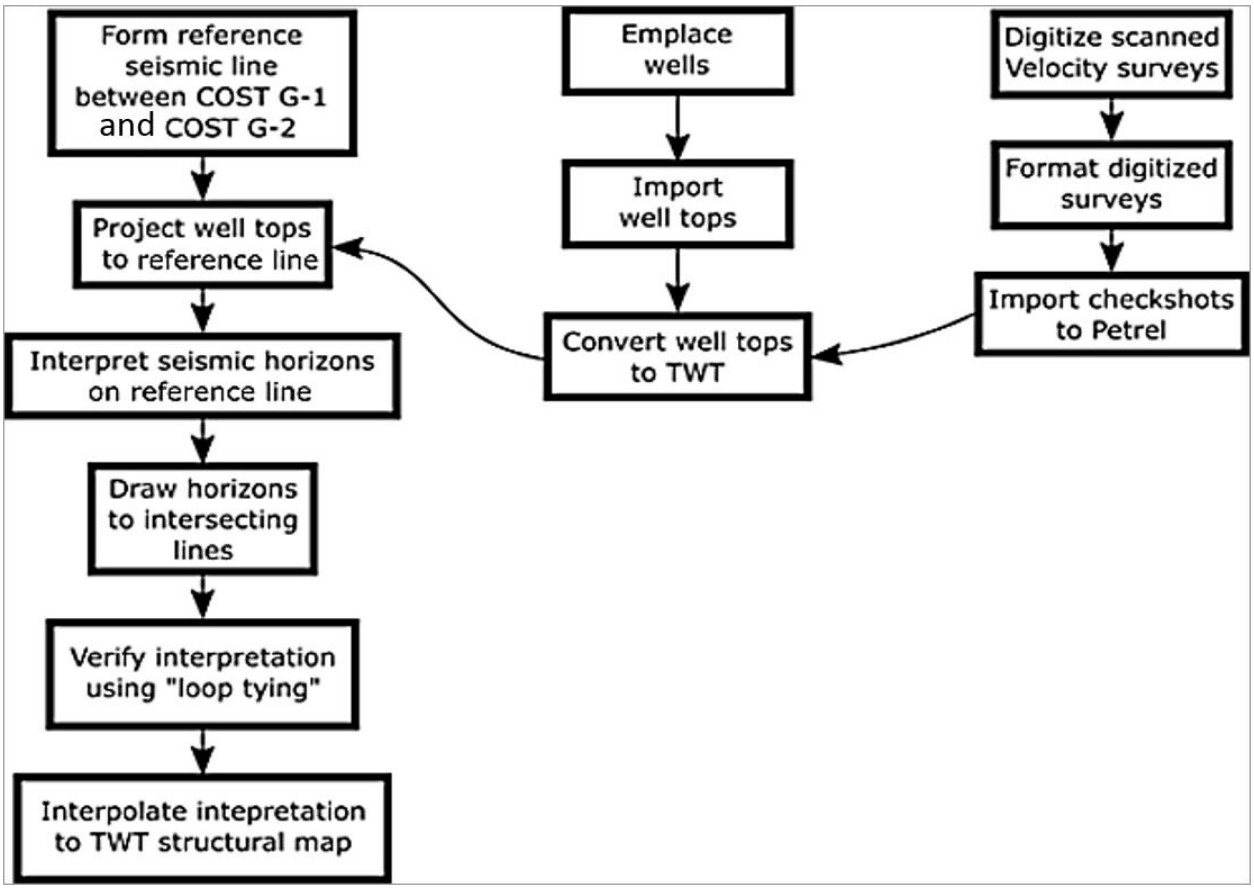

Figure 5-11. Process flow for building TWTT structural maps; the well-depth ties are a component of this chart.

Figure 5-12 shows an example of TWTT structural maps constructed for the GBB based on ~270 time-migrated seismic reflection lines. The following procedure was used to build the TWTT structural maps:

1. Create a reference composite seismic section between wells.
2. Interpret chronostratigraphically significant horizons on the reference line based on previous work.
3. Extend the interpretation by drawing seismic horizons from the reference composite line into other seismic lines. Horizon drawing was done from one seismic line to an intersecting line, and verified by "loop-tying" the horizon back to the original line. Interpretation was done using seismic attributes, including "Structural smoothing" and "Remove bias", and Petrel built-in horizon auto-tracking algorithms.
4. Create TWTT structural maps by interpolating and extrapolating the interpreted horizons inside a defined polygon.

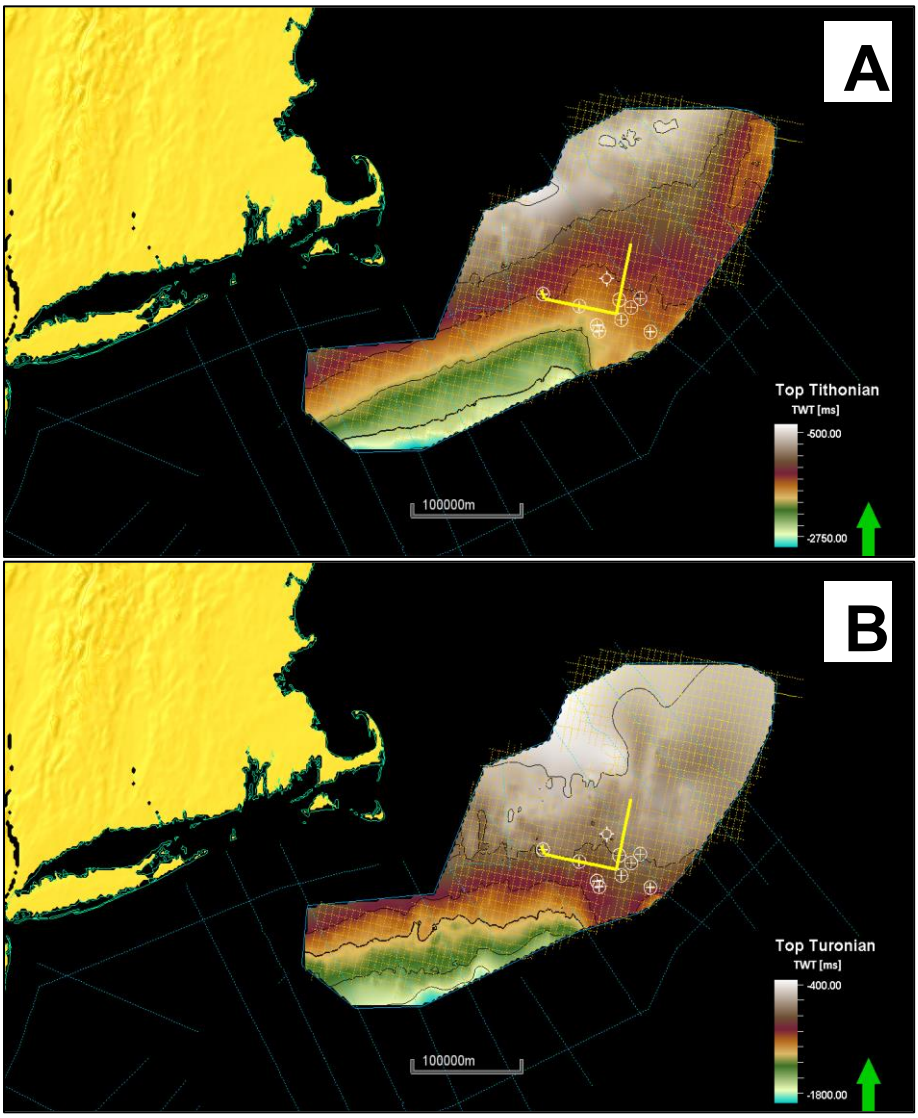

Figure 5-12. Example of a TWTT structural map for the GBB showing (A) the top of the Tithonian (Top Jurassic) and (B) the top of the Turonian.

Note: Composite line location is marked by a bold yellow line; wells are illustrated as white circles.

Following a similar procedure, a regional UK1 TWTT structural map was constructed (Figure 5-13) based on a set of newly released industry seismic data together with USGS legacy seismic lines. The top of the Cretaceous structural map was constructed by following a prominent reflector, which was traced in GBB and BCT (Figure 4-4). Wells on both marginal segments indicate it to be of latest Cretaceous age. The reflector is topped by Tertiary strata and is interpreted as a regional unconformity based on reflectors terminations and paleontological data. The interpretation grid was interpolated to form a continuous surface stretching from BCT to GBB (Figure 5-13).

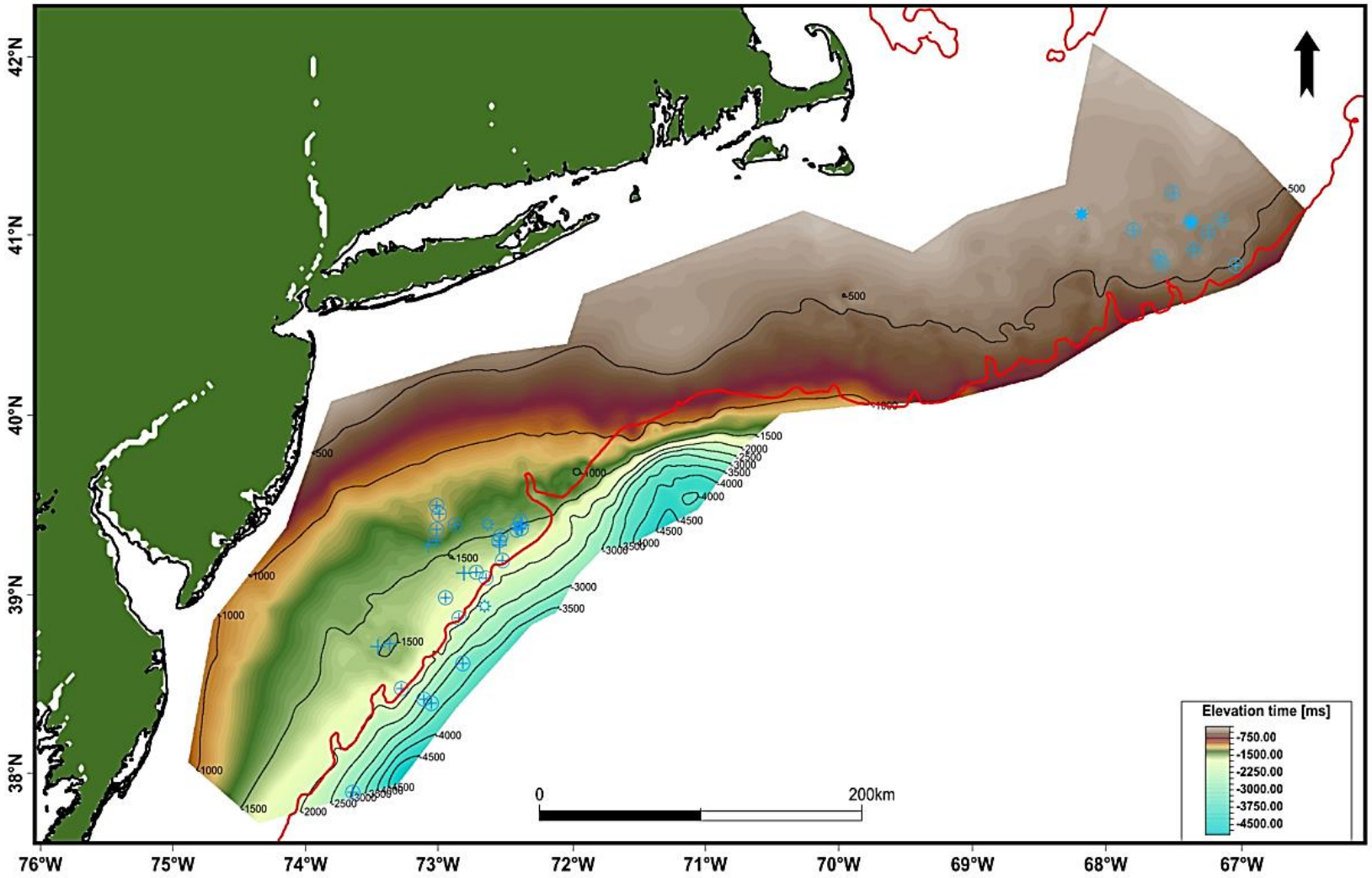

Figure 5-13. TWTT structural map of the UK1 reflector between the northern BCT and GBB.

Note: Red contour marks the -200 meter isobath. Blue crosses are locations of COST and industry wells.

The available data provide promising indicators of thick sediments with potential for stratigraphic traps and rift basins with potential for mineralized storage. In the next phase of the project, one important activity will be to use the reprocessed seismic data to improve the delineation of rift basins and the target sand reservoirs (e.g., Logan Canyon and Missisauga) and complete correlations across the study area. Because the level of data availability and quality is not the same in all areas, there will be various scales of investigation (regional, sub-basin formation-scale, and local).

6.0 Conclusions

The Mid-Atlantic U.S. Offshore Carbon Storage Resource Assessment project is conducting a comprehensive examination of potential storage resource and data integration study for an offshore area not previously characterized for carbon storage. The Mid-Atlantic Offshore study area encompasses nearly 171,000 km^2 and extends from within 10 km to 300 km offshore. DOE is developing CCS as an option for future investment in a low-carbon energy development pathway. One important aspect of this larger effort is to develop detailed geologic assessments of the carbon storage capacity on a regional basis. Identifying commercial ready storage sites are critical for deployment of advanced capture technologies. This project is investigating potential carbon storage resources to improve capacity estimates and to contribute to best practices for carbon storage.

6.1 Data Compilation/Database Construction

The project team identified data sources and collected well data, seismic survey data, geophysical well logs, rock core test data, and previous research on Mid-Atlantic Offshore geology. Much of the geologic information gathered for the carbon storage resource assessment was derived from 44 deep exploratory wells and seismic surveys completed during the 1970s and 1980s. Lack of hydrocarbon resources and restrictions on offshore exploration have limited acquisition of additional, newer subsurface data.

A significant effort was made to create electronic versions of paper logs, well reports, and core laboratory reports, as the data quality and format varied widely. Well logs, for example, were available as paper logs, raster images, and/or LAS files, and it was necessary to convert all well log data into the LAS format. In addition, the physical samples located at the DGS required inventorying as well as sample preservation. Well reports were compiled to provide information acquired on geologic formations, geotechnical rock properties, geologic structures, and petrophysical properties. A subset of the seismic data was selected for reprocessing to enhance resolution in target areas and to assist the correlation of rock layers in areas with no deep wells.

Data integration and collaborative web-based tools were used to create and share maps, layers, and data. Information from each sample/data inventory has been integrated into a master well inventory file and entered into three main project databases to facilitate activities such as cross-comparison of data sets, QA/QC processes, data analysis, subsurface modeling and mapping, and development of the sampling and analysis plan. These ongoing activities will continue throughout the project as new information becomes available and data are analyzed.

6.2 Geologic Storage Zones and Seals

Well log data are being interpreted for mineralogy, porosity, and permeability to augment the geologic framework. Well log cross sections provide a critical regional picture of 1) the distribution of strata (mostly sands and sandstones) potentially suitable for sequestration, and 2) the nature and quality of the caprock. The data are being used to create regional cross sections (along strike and along dip) and age-correlation charts. Initial formation maps and cross sections have been developed for the GBB, and these products are being refined through

correlation with seismic data. Newly reprocessed USGS seismic data resulting from Task 3 are being imported and interpreted into Petrel®. Legacy seismic data have been acquired for the subregion, including over 400 additional seismic lines.

Sequence stratigraphic analysis was completed to better define the nature and distribution of target CO_2 storage intervals and caprocks. In the BCT, the well log data have been registered by facies analysis of conventional core from the COST B-2 well, and the biostratigraphic correlations (e.g., Aptian-Albian, Albian, earliest Cenomanian, and later Cenomanian units) have been updated. This analysis is especially useful to determine variations in lithology and lateral correlations across the OCS study area. The biostratigraphic correlations help refine the placement of sequence boundaries in gamma logs showing that lithologic breaks are consistent with hiatuses between the dated units. Conventional core analysis from the COST B-2 well has also allowed for calibration of gamma log observations to reveal transgressive units and facilitate correlation of a MFS to the adjacent wells. The same process is being applied to the 10 wells in the GBB.

In areas without well data, such as the Long Island Platform and parts of the GBB and southern BCT, seismic data will be used to build the framework. Formation mapping was completed to connect seismic data with well control points. The application of modern processing techniques to historic seismic data will provide enhanced resolution of deep structures. Work flows for both geologic and seismic data synthesis and analysis have been developed and will continue to be expanded and refined.

6.3. Implications for the Mid-Atlantic Offshore Storage Resource Assessment

For many large CO_2 point sources along the U.S. Atlantic Coast, significant potential for carbon storage lies in offshore geologic formations. Work under the Midwest Regional Carbon Sequestration Partnership (MRCSP) indicates that several sandstone formations in this region have porosities greater than 25% and permeabilities greater than 100 mD. Preliminary investigation of GSD in the northern BCT suggests that as much as 5.9 Gt of CO_2 could be stored and trapped at this location alone. This suggests an extremely large capacity for potential storage of CO_2 in the Mid-Atlantic Offshore study area.

The project is using existing data to answer questions about potential storage opportunities. Storage resource estimates will be developed for detailed study areas and extrapolated to the larger regional framework to complete the carbon storage resource assessment for the region. This task will involve the use of the structural tops and bottoms, reservoir properties, pore volume estimates, and storage efficiency factors to calculate the Prospective Storage Resource of offshore formations of interest. Future work includes conducting additional sampling and analysis of existing core, completing the reprocessing of 4,000 km of seismic lines, and finalizing the sequence stratigraphic and regional correlation. Depending on the characteristics of the formations and on the richness of data sets that can be compiled for each reservoir, a hierarchical approach will be applied to improve the accuracy of the storage resource estimates. One significant outcome of this research will be the development of an integrated database for the study area. Ultimately, the datasets and files generated by this study will be made available through the U.S. DOE Energy Data Exchange platform.

7.0 References

Amato, R. and Babout, J. (eds.), 1980, Geologic and Operational Summary, COST No. G-1 Well, Georges Bank Area, North Atlantic OCS. USGS Open-File Report 80-268.

Box.com. Full Feature Index. ©2017. https://www.box.com/products-and-features

Dix, C. H. (1955). Seismic velocities from surface measurements: Geophysics, 20, 68–86.

EPA (2015, Aug 8). Greenhouse Gas Reporting Program 2014 Dataset. Available at: https://www.epa.gov/ghgreporting/ghg-reporting-program-data-sets

EPA (2016, Aug 13). Greenhouse Gas Reporting Program 2015 Dataset. Available at: https://www.epa.gov/ghgreporting/ghg-reporting-program-data-sets

Gradstein, F. M., Ogg, J. G., Schmitz, M., and Ogg, G. (2012). The Geologic Time Scale 2012 2-Volume Set, vol. 1–2: Oxford, Elsevier BV, p. 1176.

Graham, S., Miller, K. G., Mountain, G.S., and Lombardi, C. (2016). Potential for carbon capture and storage (CCS) in the eastern Georges Bank Basin, offshore Massachusetts: Geological Society of America Abstracts with Programs, v. 48, n. 7, doi: 10.1130/abs/2016AM-287229.

Grow, J. A., and Sheridan, R. E. (1988). U.S. Atlantic continental margin: A typical Atlantic-type or passive continental margin, *in* Sheridan, R.E., Grow, J.A., eds., The Atlantic Continental Margin: Boulder, Colorado, Geological Society of America, Geology of North America, v. 1-2, p. 1-7.

Hlavaty, C. L., Kopp, R. E., Miller, K. G., Browning, J. V., Reinfelder, Y. F., Mountain, G. S., and Slater, B. (2012). Carbon sequestration beneath the New Jersey continental shelf: An assessment of the geological and socio-political factors: Geological Society of America Abstracts with Programs, v. 44, p. 239.

Klitgord, K. D., Poag, C., Schneider, C., and North, L. (1994). Geophysical database of the East Coast of the United States northern Atlantic margin--cross sections and gridded database (Georges Bank Basin, Long Island Platform, and Baltimore Canyon Trough), 2331-1258.

Kominz, M. A., Miller, K. G., and Browning, J. V. (1998). Long-term and short-term global Cenozoic sea-level estimates: Geology, v. 26, p. 311-314.

Libby-French, J. (1984). Stratigraphic framework and petroleum potential of northeastern Baltimore Canyon trough, Mid-Atlantic outer continental shelf: AAPG Bulletin, v. 68, no. 1, p. 50-73.

Lippert, R.H. 1983. The Great Stone Dome – A compaction structure, in A.W. Bally. ed., Seismic expression of structural styles – a picture and work atlas. AAPG Studies in Geology 15, v.1, 13-1 to 13-4.

Miller, K.G., Kominz, M.A., Browning, J.V., Wright, J.D., Mountain, G.S., Katz, M.E., Sugarman, P.J., Cramer, B.S., Christie-Blick, N., and Pekar, S.F., 2005, The Phanerozoic record of global sea-level change: Science, v. 310, p. 1293-1298.

Miller, K.G., Mountain, G.S., Browning, J.V., Katz, M.E., Monteverde, D.H., Sugarman, P.J., Ando, H., Bassetti, M.A., Bjerrum, C.J., Hodgson, D., Hesselbo, S., Karakaya, S., Proust, J.-N., and Rabineau, M. (2013). Testing sequence stratigraphic models by drilling Miocene foresets on the New Jersey shallow shelf: Geosphere, v. 9, p. 1236-1256, doi: 10.1130/GES00884.1

Miller, K.G., Browning, J.V., Sugarman, P.J., Monteverde, Andreasen, D.C., Lombardi, C., Thornburg, J, Reinfelder, Y., and Kopp, RE. (2017). Lower to mid-Cretaceous sequence stratigraphy and characterization of CO2 storage potential in the Mid-Atlantic U.S. Coastal Plain. Journal of Sedimentary Research, 87, pp. 609-629.

Miller, K. G., Lombardi, C. J., Browning, J. V. Schmelz, W. J., Gallegos, G., and Mountain, G. S. (in review). Back to Basics of Sequence Stratigraphy: Early Miocene and Mid Cretaceous examples from the New Jersey paleoshelf.

Moucha, R., Forte, A. M., Mitrovica, J. X., Rowley, D. B., Quere, S., Simmons, N. A., and Grand, S. P. (2008). Dynamic topography and long–term sea level variations: there is no such thing as a stable continental platform: Earth and Planetary Science Letters, v. 271, p. 101–108.

Mountain, G. S., Proust, J.-N., McInroy, D., and Cotterill, C., and the Expedition 313 Scientists (2010). Proceedings of the Integrated Ocean Drilling Program, Expedition 313: Tokyo, Integrated Ocean Drilling Program Management International, Inc., doi:10.2204/iodp.proc .313.2010.

Olsson, R. K., Gibson, T. G., Hansen, H. J., and Owens, J. P. (1988). Geology of the northern Atlantic coastal plain: Long Island to Virginia, *in* Sheridan, R. E., Grow, J. A., eds., The Atlantic Continental Margin: Boulder, Colorado, Geological Society of America, Geology of North America, v. 1-2, p. 87-105.

Peltier, W. R. (1998). Postglacial variations in the level of the sea: Implications for climate dynamics and solid-Earth geophysics: Reviews of Geophysics, v. 36, p. 603-689.

Post, P. J., and Coleman, J. L., Jr. (2015). Mesozoic rift basins of the U.S. central Atlantic offshore: comparisons with onshore basins, analysis, and potential petroleum prospectivity, *in* GCSSEPM Foundation 34th Annual Perkins-Rosen Research Conference, Houston, Texas, p. 1-93.

Prather, B. E. (1991). Petroleum geology of the Upper Jurassic and Lower Cretaceous, Baltimore Canyon Trough, western North Atlantic Ocean: American Association of Petroleum Geologists Bulletin, v. 75, p. 258-277.

Raymo, M.E., Mitrovica, J.X., O'Leary, M.J., DeConto, R.M., and Hearty, P.J. (2011). Departures from eustasy in Pliocene sea-level records: Nature Geoscience, v. 4, p. 328-332.

Romero, P. (in preparation). Estimating Formation Porosity and Mineralogy Using Three Common Geophysical Logs (Gamma Ray, Density, Neutron Porosity). Master's thesis in final preparation.

Rowley, D. B., Forte, A. M., Moucha, R. R., Mitrovica, J. X., Simmons, N. A., and Grand, S. P. (2011). Dynamic Topography Change of the Eastern U.S. since 4 Ma: Implications for Sea Level and Stratigraphic Architecture of Passive Margins: Science, v. 340, p. 1563-1563.

Scholle, P.A., ed. (1977). Geological studies on the COST No. B-2 well, U.S. mid-Atlantic outer continental shelf area: U.S. Geological Circular 750, 71 p.

Scholle, P.A., ed. (1980). Geological studies of the COST No. B-3 well, United States mid-Atlantic continental slope area: U.S. Geological Survey Circular 833, 132 p.

Seker, Z. (2012). Cretaceous well-log and sequence stratigraphic correlation of the outer continental shelf and upper slope off of New Jersey: [M.S. thesis]: Rutgers University, 155 p.

Slater, B., Stolorow, A., and Smith, L. (2010). Potential for Supercritical Carbon Sequestration in the Offshore Bedrock Formations of the Baltimore Canyon Trough, *in* AAPG Eastern Section Meeting, Kalamazoo, Michigan, AAPG.

Slatt, R. M. (2006). Stratigraphic Reservoir Characterization for Petroleum Geologists, Geophysicists, and Engineers. Ed. John Cubit. Handbook of Petroleum Exploration and Production 6, 237-239.

Steckler, M.S. and Watts, A.B. (1982). Subsidence history and tectonic evolution of Atlantic-type continental margins, in Scrutton, R.A., ed., Dynamics of Passive Margins, AGU Geodynamic Ser., 6, p. 184-196.

Triezenberg, P., Hart, P., and Childs, J. (2016). National Archive of Marine Seismic Surveys (NAMSS): a USGS Data Website of Marine Seismic Reflection Data within the US Exclusive Economic Zone (EEZ): US Geological Survey Data Release (2016) http://dx. doi. org/10.5066, F7930R7P.

Van Wagoner, J. C., Mitchum, R. M., Campion, K. M., and Rahmanian, V. D. (1990). Siliciclastic sequence stratigraphy in well logs, cores, and outcrops: Concepts for high-resolution correlation of time and facies: AAPG Methods in Exploration Series 7, 55 p.

Watts, A. B. (1981). The U.S. Atlantic continental margin; Subsidence history, crustal structure, and thermal evolution, *in* Bally, A.W., ed., Geology of passive continental margins: History, structure, and sedimentologic record. American Association of Petroleum Geologists Education Course Note Series 19:1–75.

Withjack, M.O., Schlische, R.W., and Olsen, P.E., (1998). Diachronous rifting, drifting, and inversion on the passive margin of central eastern North America: An analog for other passive margins: American Association of Petroleum Geologists Bulletin, v. 82, p. 817-835.

Appendix A
Master Database Inventory

Appendix A

Master database inventory for the Mid-Atlantic Offshore Carbon Storage Resource Assessment Project showing detailed well information and all data associated with each well.

Well ID	API No.	Sub-region	Lease	Block	OPD no.	BOEM OPD Section	Lat.[1]	Long.[1]	TD (ft)	TVD (ft)	KB (ft)	Water Depth (ft)	Completion Date	LAS File Count[2]	Raster File Count[3]	Core Sample Count[4]	Cuttings Count[4]	Thin Section Count[4]	Core Data[4]	Seismic Tie	Technical Reports[5]
Conoco 145-1	6104000007	GBB	OCS-A0179	145	NK19-12	Lydonia Canyon	40.833	-67.285	14,500	14,398	85	300	8/25/1982	2	45	9	1,373	125	✓		✓
Conoco 590-1	6110500007	BCT	OCS-A0024	590	NJ18-3	Hudson Canyon	39.376	-72.967	12,000	11,908	73	242	6/7/1978	2	44		1,126	123	✓	✓	✓
COST B-2	6110500001	BCT	----	594	NJ18-3	Hudson Canyon	39.376	-72.734	16,043	16,039	90	298	2/28/1976	2	95	92	3,690	127	✓	✓	✓
COST B-3	6110400002	BCT	----	66	NJ18-6	Wilmington Canyon	38.917	-72.773	15,820	15,820	42	2,686	1/24/1979	2	70	299	2,427	246	✓	✓	✓
COST G-1	6106200001	GBB	----	79	NK19-11	Hydrographer Canyon	40.931	-68.305	16,071	16,071	98	157	7/27/1976	2	69	39	2,868	160	✓	✓	✓
COST G-2	6104000001	GBB	----	141	NK19-12	Lydonia Canyon	40.836	-67.508	21,874	21,874	79	272	8/6/1977	2	83	105	4,129	527	✓	✓	✓
Exxon 133-1	6104000002	GBB	OCS-A0170	133	NK19-12	Lydonia Canyon	40.818	-67.934	14,118	14,100	85	225	11/24/1981	2	52	73	1,560	114	✓	✓	✓
Exxon 500-1	6110500016	BCT	OCS-A0009	500	NJ18-3	Hudson Canyon	39.485	-73.101	12,253	12,253	79	204	9/28/1979	2	42		812	64	✓	✓	✓
Exxon 599-1	6110500019	BCT	OCS-A0029	599	NJ18-3	Hudson Canyon	39.364	-72.487	17,121	17,121	82	442	11/2/1980	2	54	70	1,905	105	✓		✓
Exxon 684-1	6110500002	BCT	OCS-A0046	684	NJ18-3	Hudson Canyon	39.303	-72.642	17,620	17,615	38	399	12/23/1978	2	83	509	1,935	107	✓	✓	✓
Exxon 684-2	6110500010	BCT	OCS-A0046	684	NJ18-3	Hudson Canyon	39.279	-72.653	16,800	16,759	78	417	7/15/1979	2	62	7	1,742	123	✓	✓	✓
Exxon 728-1	6110500022	BCT	OCS-A0052	728	NJ18-3	Hudson Canyon	39.255	-72.653	15,205	15,205	83	433	7/5/1981	2	36		1,595	78	✓		✓
Exxon 816-1	6110500020	BCT	OCS-A0055	816	NJ18-3	Hudson Canyon	39.168	-72.635	17,753	17,753	82	461	5/7/1981	2	9		2,000	248	✓		✓
Exxon 902-1	6110500013	BCT	OCS-A0065	902	NJ18-3	Hudson Canyon	39.07	-72.754	15,968	15,889	72	433	4/15/1979	2	48	29	1,017	132	✓	✓	✓
Exxon 975-1	6104100001	GBB	OCS-A0153	975	NK19-9	Corsair Canyon	41.007	-67.622	14,605	14,605	83	209	3/10/1982	2	36	15	1,532	189	✓	✓	✓
Gulf 718-1	6110500005	BCT	OCS-A0048	718	NJ18-3	Hudson Canyon	39.266	-73.166	12,813	12,800	74	204	3/31/1979	2	48		1,369	56	✓		✓
Gulf 857-1	6110500008	BCT	OCS-A0059	857	NJ18-3	Hudson Canyon	39.105	-72.824	18,554	18,552	73	349	1/29/1979	2	75		996	192	✓	✓	✓
Homco 676-1	6110500006	BCT	OCS-A0042	676	NJ18-3	Hudson Canyon	39.288	-73.107	12,500	12,500	96	220	9/22/1978	2	59		1,430	67	✓		✓
Homco 855-1	6110500012	BCT	OCS-A0057	855	NJ18-3	Hudson Canyon	39.106	-72.914	17,505	17,505	100	290	2/8/1979	2	57		1,589	90	✓		✓
Mobil 17-1	6110400004	BCT	OCS-A0075	17	NJ18-6	Wilmington Canyon	38.968	-73.049	1,200	1,200	83	260	1/24/1979	2	14		1,656				✓
Mobil 17-2	6110400005	BCT	OCS-A0075	17	NJ18-6	Wilmington Canyon	38.968	-73.049	13,992	13,975	83	260	5/14/1979	2	61	76	250	73	✓	✓	✓
Mobil 273-1	6104000008	GBB	OCS-A0196	273	NK19-12	Lydonia Canyon	40.684	-67.503	15,580	15,578	89	301	9/13/1982	2	35		1,399	111		✓	✓
Mobil 312-1	6104000004	GBB	OCS-A0200	312	NK19-12	Lydonia Canyon	40.658	-67.765	20,000	19,977	89	259	6/27/1982	2	61		1,953	142		✓	✓
Mobil 544-1	6110500003	BCT	OCS-A0015	544	NJ18-3	Hudson Canyon	39.416	-73.101	17,449	17,449	84	220	12/29/1978	2	83	96	1,826	94	✓	✓	✓
Mobil 544-2	6110500023	BCT	OCS-A0015	544	NJ18-3	Hudson Canyon	39.436	-73.079	8,312	8,312	47	220	10/1/1981	2	31		476				✓
Murphy 106-1	6110400008	BCT	OCS-A0081	106	NJ18-6	Wilmington Canyon	38.853	-72.955	18,405	18,401	98	412	5/29/1980	2			2,096	123	✓	✓	✓
Shell 272-1	6110400003	BCT	OCS-A0096	272	NJ18-6	Wilmington Canyon	38.702	-73.54	13,500	13,500	84	217	2/19/1979	2	33		1,338	79	✓		✓

Well ID	API No.	Sub-region	Lease	Block	OPD no.	BOEM OPD Section	Lat.[1]	Long.[1]	TD (ft)	TVD (ft)	KB (ft)	Water Depth (ft)	Completion Date	LAS File Count[2]	Raster File Count[3]	Core Sample Count[4]	Cuttings Count[4]	Thin Section Count[4]	Core Data[4]	Seismic Tie	Technical Reports[5]
Shell 273-1	6110400001	BCT	OCS-A0097	273	NJ18-6	Wilmington Canyon	38.716	-73.456	17,500	17,500	84	235	12/16/1978	2	58	69	2,662	89	✓		✓
Shell 357-1	6104000006	GBB	OCS-A0210	357	NK19-12	Lydonia Canyon	40.614	-67.745	19,427	19,398	72	265	9/27/1982	2	130		1,982	144	✓	✓	✓
Shell 372-1	6110400011	BCT	OCS-A0317	372	NJ18-6	Wilmington Canyon	38.6	-72.937	11,631	11,631	48	6,952	7/9/1984	2	81	41	451	57	✓	✓	✓
Shell 410-1	6104000003	GBB	OCS-A0218	410	NK19-12	Lydonia Canyon	40.573	-67.209	15,568	15,556	72	381	3/31/1982	2	74		1,698	141	✓	✓	✓
Shell 586-1	6110400010	BCT	OCS-A0336	586	NJ18-6	Wilmington Canyon	38.405	-73.218	16,000	16,000	48	5,838	5/22/1984	2	72	62	2,749	98	✓	✓	✓
Shell 587-1	6110400009	BCT	OCS-A0337	587	NJ18-6	Wilmington Canyon	38.381	-73.164	14,500	14,470	48	6,448	12/21/1983	2		72	1,810	72	✓	✓	✓
Shell 632-1	6110500009	BCT	OCS-A0032	632	NJ18-3	Hudson Canyon	39.35	-73.105	14,000	14,000	84	205	7/14/1978	2	50	17	1,077	91	✓	✓	✓
Shell 93-1	6110300001	BCT	OCS-A0370	93	NJ18-9	Baltimore Rise	37.893	-73.736	17,740	17,740	48	5,013	11/4/1984	2	75	55	1,227	78	✓	✓	✓
Tenneco 187-1	6104000005	GBB	OCS-A0182	187	NK19-12	Lydonia Canyon	40.771	-67.389	18,127	18,127	83	300	8/21/1982	2	81		2,016	133	✓	✓	✓
Tenneco 495-1	6110400007	BCT	OCS-A0131	495	NJ18-6	Wilmington Canyon	38.466	-73.378	18,300	18,300	88	355	10/11/1979	2	71		2,217	93	✓	✓	✓
Tenneco 642-2	6110500014	BCT	OCS-A0038	642	NJ18-3	Hudson Canyon	39.343	-72.494	18,400	18,400	88	443	6/10/1979	2	63		2,396	154	✓	✓	✓
Tenneco 642-3	6110500018	BCT	OCS-A0038	642	NJ18-3	Hudson Canyon	39.337	-72.529	16,475	16,475	80	446	10/14/1980	2	50		1,844	90	✓		✓
Texaco 598-1	6110500004	BCT	OCS-A0028	598	NJ18-3	Hudson Canyon	39.372	-72.505	15,025	15,025	82	432	8/26/1978	2	88	140	1,519	32	✓	✓	✓
Texaco 598-2	6110500011	BCT	OCS-A0028	598	NJ18-3	Hudson Canyon	39.372	-72.531	17,708	17,642	82	421	3/20/1979	2	7		2,173	88	✓		✓
Texaco 598-3	6110500017	BCT	OCS-A0028	598	NJ18-3	Hudson Canyon	39.382	-72.5	16,103	16,103	78	425	5/25/1980	2	5		1,242	100	✓		✓
Texaco 598-4	6110500021	BCT	OCS-A0028	598	NJ18-3	Hudson Canyon	39.361	-72.508	16,050	16,050	78	435	3/24/1981	2	2		1,608	87	✓		✓
Texaco 642-1	6110500015	BCT	OCS-A0038	642	NJ18-3	Hudson Canyon	39.348	-72.515	17,807	17,797	82	450	12/1/1979	2	2	421	1,386	52	✓		✓
													SUM:	**88**	**2,294**	**2,296**	**76,146**	**5,094**	**-**	**-**	**-**
													Well counts:	**44**	**42**	**21**	**44**	**42**	**40**	**28**	**44**

1. Latitudes (Lat.) and longitudes (Long.) are in NAD27
2. LAS log file location (Box): Compile Data>Logs>1_LAS Files
3. Raster log file location (Box): Compile Data>Logs>2_Raster Files
4. Sample inventories, and tabulated core data file location (Box): Compile Data>Cores, Cuttings, Rock Samples
5. Technical reports file location (Box): Compile Data>Wells>Technical & Laboratory Reports_AllWells

Appendix B
Inventory List of Priority Logs in Digital Format

Appendix B

Inventory list of all priority logs available in digital format for each well in the study area.

Well ID	Sub-region[1]	Priority Log Types[2]						
		GR	NPHI	RHOB	DT	RT	TEMP	PRS
Conoco 590-1	BCT	✓	✓	✓	✓	✓	✓	✓
COST B-2	BCT	✓	✓	✓	✓	✓	✓	✓
COST B-3	BCT	✓	✓	✓	✓	✓		
Exxon 500-1	BCT	✓	✓	✓	✓	✓		
Exxon 599-1	BCT	✓	✓	✓	✓	✓		✓
Exxon 684-1	BCT	✓	✓	✓	✓	✓	✓	
Exxon 684-2	BCT	✓	✓	✓	✓	✓		
Exxon 728-1	BCT	✓	✓	✓	✓	✓		✓
Exxon 816-1	BCT	✓	✓	✓	✓	✓		
Exxon 902-1	BCT	✓	✓	✓	✓	✓		
Gulf 718-1	BCT	✓	✓	✓	✓			✓
Gulf 857-1	BCT	✓	✓	✓	✓			✓
Homco 676-1	BCT	✓	✓	✓	✓	✓		✓
Homco 855-1	BCT	✓	✓	✓	✓	✓		✓
Mobil 17-1	BCT	✓			✓	✓		
Mobil 17-2	BCT	✓	✓	✓	✓	✓		
Mobil 544-1	BCT	✓	✓	✓	✓	✓		✓
Mobil 544-2	BCT	✓	✓	✓		✓		✓
Murphy 106-1	BCT	✓	✓	✓	✓	✓		
Shell 272-1	BCT	✓	✓	✓	✓	✓		
Shell 273-1	BCT	✓	✓	✓	✓	✓		
Shell 372-1	BCT	✓	✓	✓	✓	✓		
Shell 586-1	BCT	✓	✓	✓	✓	✓		
Shell 587-1	BCT	✓			✓	✓		
Shell 632-1	BCT	✓	✓	✓	✓	✓		
Shell 93-1	BCT	✓	✓	✓	✓	✓		
Tenneco 495-1	BCT	✓	✓	✓	✓	✓		✓
Tenneco 642-2	BCT	✓	✓	✓	✓	✓		✓
Tenneco 642-3	BCT	✓	✓	✓	✓	✓		✓
Texaco 598-1	BCT	✓	✓	✓	✓	✓		✓
Texaco 598-2	BCT	✓	✓	✓	✓	✓		
Texaco 598-3	BCT	✓	✓	✓	✓	✓		
Texaco 598-4	BCT	✓	✓	✓	✓	✓		
Texaco 642-1	BCT	✓	✓	✓	✓	✓		
Conoco 145-1	GBB	✓	✓	✓	✓	✓	✓	✓
COST G-1	GBB	✓	✓	✓	✓	✓	✓	✓
COST G-2	GBB	✓	✓	✓	✓	✓	✓	✓
Exxon 133-1	GBB	✓	✓	✓	✓	✓		
Exxon 975-1	GBB	✓	✓	✓	✓	✓	✓	

Well ID	Sub-region[1]	Priority Log Types[2]						
		GR	NPHI	RHOB	DT	RT	TEMP	PRS
Mobil 273-1	GBB	✓	✓	✓	✓	✓		✓
Mobil 312-1	GBB	✓	✓	✓	✓	✓		✓
Shell 357-1	GBB	✓	✓	✓	✓	✓		✓
Shell 410-1	GBB	✓	✓	✓	✓	✓		✓
Tenneco 187-1	GBB	✓	✓	✓	✓	✓		✓
Well Count		**44**	**42**	**42**	**43**	**42**	**7**	**22**

1. BCT: Baltimore Canyon Trough; GBB: Georges Bank Basin

2. GR: gamma ray, NPHI: neutron porosity, RHOB: bulk density, DT: sonic, RT: resistivity, TEMP: formation temperature, PRS: formation pressure

Appendix C
Inventory of Physical Samples

Appendix C

Inventory of all physical samples, including core material, thin-sections, and washed cuttings, available to the Project Team for sampling and analysis.

Well ID	Core Sample Count	Thin Section Count	Cuttings Count
Conoco 145-1	9	125	1,373
Conoco 590-1		123	1,126
COST B-2	92	127	3,690
COST B-3	299	246	2,427
COST G-1	39	160	2,868
COST G-2	105	527	4,129
Exxon 133-1	73	114	1,560
Exxon 500-1		64	812
Exxon 599-1	70	105	1,905
Exxon 684-1	509	107	1,935
Exxon 684-2	7	123	1,742
Exxon 728-1		78	1,595
Exxon 816-1		248	2,000
Exxon 902-1	29	132	1,017
Exxon 975-1	15	189	1,532
Gulf 718-1		56	1,369
Gulf 857-1		192	996
Homco 676-1		67	1,430
Homco 855-1		90	1,589
Mobil 17-1			1,656
Mobil 17-2	76	73	250
Mobil 273-1		111	1,399
Mobil 312-1		142	1,953
Mobil 544-1	96	94	1,826
Mobil 544-2			476
Murphy 106-1		123	2,096
Shell 272-1		79	1,338
Shell 273-1	69	89	2,662
Shell 357-1		144	1,982
Shell 372-1	41	57	451
Shell 410-1		141	1,698
Shell 586-1	62	98	2,749
Shell 587-1	72	72	1,810
Shell 632-1	17	91	1,077
Shell 93-1	55	78	1,227
Tenneco 187-1		133	2,016
Tenneco 495-1		93	2,217
Tenneco 642-2		154	2,396
Tenneco 642-3		90	1,844
Texaco 598-1	140	32	1,519

Well ID	Core Sample Count	Thin Section Count	Cuttings Count
Texaco 598-2		88	2,173
Texaco 598-3		100	1,242
Texaco 598-4		87	1,608
Texaco 642-1	421	52	1,386
Grand Total	**2,296**	**5,094**	**76,146**

Appendix D
Bibliography

Appendix D

A full bibliography of all references collected to date, subdivided into key categories.

Baltimore Canyon Trough

Benson. R. N. (1984). Structure Contour Map of Pre-Mesozoic Basement, Landward Margin of Baltimore Canyon Trough: Delaware Geological Survey Miscellaneous Map Series No. 2, scale 1:500,000, 2 sheet(s).

Libby-French, J. (1984). Stratigraphic Framework and Petroleum Potential of Northeastern Baltimore Canyon Trough, Mid-Atlantic Outer Continental Shelf: The AAPG Bulletin, v. 68, p. 50-73.

Mountain, G., Proust, J. N., and Expedition 313 Science Party (2010). The New Jersey Margin Scientific Drilling Project (IODP Expedition 313): Untangling the Record of Global and Local Sea-Level Changes: Scientific Drilling, v. 10, p. 26-34.

MRCSP (2011). Preliminary Characterization of CO_2 Sequestration Potential in New Jersey and The Offshore Coastal Region: Report DE-FC26-05NT42589.

Scholle, P. A. (1977). Geologic Studies on the COST No. B-2 well, U.S. Mid-Atlantic Outer Continental Shelf Area: U.S. Geologic Survey, Report 750.

Sheridan, R. E., Olsson, R. K., and Miller, J. J. (1991). Seismic Reflection and Gravity Study of Proposed Taconic Suture Under the New Jersey Coastal Plain: Implications for Continental Growth: Geologic Society of America Bulletin, v. 103, p. 402.

Slater, B., Stolorow, A., and Smith, L. (September 28, 2010). Potential for Supercritical Carbon Sequestration in the Offshore Bedrock Formations of the Baltimore Canyon Trough, *in* AAPG Eastern Section Meeting, Kalamazoo, Michigan, AAPG.

Slater, B., Stolorow, A., Smith, L., and Mountain, G. (2011). MRCSP Phase III Offshore Sequestration Potential & TriCarb Project Update.

Smith, M. A., Amato, R. V., Furbush, M. A., Pert, D. M., Nelson, M. E., Hendrix, J. S., Tamm, L. C., Wood, G., and Shaw, D. R. (1976). Geological and Operational Summary, COST No. B-2 Well, Baltimore Canyon Trough Area, Mid-Atlantic OCS: U.S. Department of the Interior Geological Survey, Report 76-774.

General & Overview Offshore

Batum, M., Outer Continental Shelf Sub-Seabed CO_2 Sequestration Authorities and Research: Bureau of Ocean Energy Management.

Bureau of Ocean Energy Management, 2010, Outer Continental Shelf: Official Protraction Diagrams, Atlantic Coast, scale NAD83, 1 sheet(s).

House, K., Schrag, D., Oates, P., Miegs, L., and Haggerty, R. CO_2 Sequestration and Reactive Transport.

International Energy Agency (2016). International Workshop on Offshore Geologic CO_2 Storage: Carbon Sequestration Leadership Forum, Report 2016/TR2.

Jansa, L. F. (1981). Mesozoic Carbonate Platforms and Banks of the Eastern North American Margin: Marine Geology, v. 44, p. 97.

Meckel, T. A., Hovorka, S. D., Trevino, R., Smyth, R., and Romanak, K. (2014). Toward an International Program for Offshore Storage of CO_2: International Initiative for CCS sub-sea (iCCSc): Energy Procedia, v. 63, p. 5015.

Post, P. J., Klazynski, R. J., Klocek, E. S., Riches, T. J., and Li, K. (2016). Inventory of Technically and Economically Recoverable Hydrocarbon Resources of the Atlantic Outer Continental Shelf as of January 1, 2014: U.S. Department of the Interior, Bureau of Ocean Energy Management, Report BOEM 2016-071.

Reid, J. C., DePoy, E. A., and Taylor, K. B. (September 2012). Preliminary Carbon Dioxide (CO_2) Sequestration Characterization, Dare, Tyrrell and Hyde Counties, North Carolina, *in* AAPG Eastern Section meeting, Cleveland, Ohio, AAPG.

Reid, J. C., and Taylor, K. B. (2013). Mesozoic Rift Basin - Onshore North Carolina and South-Central Virginia, U.S.A.: Deep River and Dan River - Danville Total Petroleum Systems (TPS) and Assessment Units (AU) for Continuous Gas Accumulation: North Carolina Geological Survey, Report Openfile 2013-01.

Reid, J. M., Reid, J. A., Jenkins, C. J., Hastings, S. J., Williams, S. J., and Poppe, L. J. (2005). usSEABED: Atlantic Coast Offshore Surficial Sediment Data Release: U.S.G.S. Data Series 2005-118, v. 1.0.

Shrag, D. P., et al. (2009). Storage of Carbon Dioxide in Offshore Sediments: Science, v. 325, p. 1658.

Smyth, R. C., Carr, D. L., Hovorka, S. D., Coleman, S., Breton, C. A., and Miller, E. N. (2011). Continued Evaluation of Potential for Geologic Storage of Carbon Dioxide in the Southeastern United State: The University of Texas at Austin, Bureau of Economic Geology, Report GCCC Digital Publication Series #11-26.

Smyth, R. C., Hovorka, S. D., Meckel, T., Breton, C., Paine, J. G., Hill, G. R., Herzog, H., Zhang, H., and Li, W. (2008). Potential Sinks for Geologic Storage of Carbon Dioxide Generated by Power Plants in North and South Carolina: Gulf Coast Carbon Center, Report Final.

Smyth, R. C., Thomas, P. G., and Heiligenstein, C. (2014) Concerning Offshore Geologic Storage of Carbon Dioxide in the U.S.A. Energy Procedia, v. 63, p. 5822.

Stetson, H. C. (1949). The Sediments and Stratigraphy of the East Coast Continental Margin; Georges Bank to Norfolk Canyon: Physical Oceanography and Meteorology, v. 11.

Vidas, H., Hugman, B., Chikkatur, A., and Venkatesh, B. (2012). Analysis of the Costs and Benefits of CO_2 Sequestration on the U.S. Outer Continental Shelf: U.S. Department of the Interior, Bureau of Ocean Energy Management, Report BOEM 2012-100.

Georges Bank Basin

Amato, R. V., and Bebout, J. W. (1980). Geologic and Operational Summary, COST No. G-1 Well, Georges Bank Area, North Atlantic OCS: U.S. Geologic Survey, Report Open-File Report 80-268.

Amato R. V., and Bebout, J. W. (1980). Portion of U.S.G.S. Seismic Line 77-1 Showing Relationship of COST No. G-1 Major Lithologic Units to Seismic Reflectors: Open-File Report 80-268, 1 sheet(s).

Amato R. V., and Bebout, J. W. (1980). Stratigraphic Column and Summary Chart of Geologic Data, COST No. G-1 Well, U.S. North Atlantic Continental Margin: Open-File Report 80-268, 1 sheet(s).

Core Laboratories Inc. (1982). Conventional Core Analysis: Conoco 145-1: Report OCS-A-0179 No. 1.

Edson, G. M., Olson, D. L., and Petty, A. J. (2000). Conoco Lydonia Canyon Block 145 No. 1 Well: U.S. Department of the Interior, Report MMS 2000-034.

Edson, G. M., Olson, D. L., and Petty, A. J. (2000). Georges Bank Petroleum Exploration: U.S. Department of the Interior, Report MMS 2000-031.

Neff, J. M., Bothner, M. H., Maciolek, N. J., and Grassle, J. F. (1989). Impacts of Exploratory Drilling for Oil and Gas on the Benthic Environment of Georges Bank: Marine Environmental Research, v. 27, p. 77.

Poppe, L. J. (1990). Lithology and X-ray Mineralogy of the Conoco 145-1 Well, U.S. North Atlantic Outer Continental Shelf: U.S. Dept. of the Interior, Geological Survey, Report Open-File Report 90-255.

Poppe, L. J., Poag, C. W., and Stanton, R. W. (1992). Mid-Mesozoic (Mid-Jurassic to Early Cretaceous) evolution of the Georges Bank Basin, U.S. North Atlantic Outer Continental Shelf: Sedimentology of the Conoco 145-1 Well: Sedimentary Geology, v. 75, p. 171.

Poppe, L. J., Poag, C. W., and Stanton, R. W. (1991). Stratigraphy, Lithology, and Paleoenvironments of the Conoco 145-1 Well, Georges Bank Basin, U.S. North Atlantic Outer Continental Shelf: Geologic Society of America, v. 23, no. 1, p. 117.

Scholle P. A., Krivoy, H. L., and Hennessy, J. L. (1980). Summary Chart of Geological Data from the COST No. G-1 Well, U.S. North-Atlantic Outer Continental Shelf: Oil and Gas Investigations Chart OC-104, 1 sheet(s).

Scholle, P. A., and Wenkam, C. R. (1982). Geological Studies of the COST Nos. G-1 and G-2 Wells, United States North Atlantic Outer Continental Shelf: U.S. Geological Survey, Report Circular 861.

Smith, D., and Post, P. J. (2016). Atlantic Well Folio: Georges Bank Basin: Bureau of Ocean Energy Management, Report BOEM 2016-026.

Long Island Platform and Rift Basins

Coleman, J. L., Post, P. J., and Milici, R. C. (2015). Assessment of the Oil and Natural Gas Potential of the East Coast Mesozoic Synrift Basins, Onshore and State Waters of the United States, *in* GCSSEPM Foundation 34th Annual Perkins-Rosen Research Conference, Houston, Texas, p. 96-194.

Goldberg, D. S., Kent, D. V., and Olsen, P. E. (2010). Potential on-shore and off-shore reservoirs for CO_2 sequestration in Central Atlantic magmatic province basalts: PNAS, v. 107, p. 1327-1332.

Post, P. J., and Coleman, J. L. (2015). Mesozoic rift basins of the U.S. central Atlantic offshore: comparisons with onshore basins, analysis, and potential petroleum prospectivity, *in* GCSSEPM Foundation 34th Annual Perkins-Rosen Research Conference, Houston, Texas, p. 1-93.

Withjack, M. O., Schlische, R. W., and Olsen, P. E. (1998). Diachronous Rifting, Drifting, and Inversion on the Passive Margin of Central Eastern North America: An Analog for Other Passive Margins: The AAPG Bulletin, v. 82, p. 817-835.

Other Offshore Regions

Delprat-Jannaud, F., Korre, A., Shi, J. Q., McConnell, B., Arvanitis, A., Boavida, D., Car, M., Gastine, M., Grunnaleite, I., Bateman, K., Poulsen, N., Sinayuc, C., Vahakuopus, T., Vercelli, S., and Wokcicki, A. (2013). State-of-the-Art review of CO_2 Storage Site Selection and Characterization Methods: Report CGS Europe Report No. D3.3.

Hagen, S. (2012). Sleipner: Knowledge sharing in CCS projects, Mobile, Alabama, Statoil. May 16-17.

Heinemann, N., Wilkinson, M., Pickup, G. E., Haszeldine, R. S., and Cutler, N. A. (2011). CO_2 Storage in the Offshore UK Bunter Sandstone Formation: International Journal of Greenhouse Gas Control, v. 6, p. 210.

Holler, S., and Viebahn, P. (2011). Assessment of CO_2 Storage Capacity in Geological Formations of Germany and Northern Europe: Energy Procedia, v. 4, p. 4897.

Jin, M., Pickup, G. E., Mackay, E., Todd, A., Monaghan, A., and Naylor, M. (2010). Static and Dynamic Estimates of CO_2 Storage Capacity in Two Saline Formations in the UK, *in* SPE Europec/EAGE Annual Conference and Exhibition, Barcelona, Spain, SPE International, 14-17 June 2010.

Lindeberg, E., Vuillaume, J., and Ghaderi, A. (2009). Determination of the CO_2 Storage Capacity of the Utsira Formation: Energy Procedia, v. 1, p. 2777.

Lothe, A. E., Emmel, B., Grover, A., and Bergmo, P. E. (2014). CO_2 Storage Modelling and Capacity Estimation for the Trondelag Platform, Offshore Norway - Using a Basin Modelling Approach: Energy Procedia, v. 63, p. 3648.

Meckel, T. (2014). Carbon Capture and Offshore Storage in the Gulf of Mexico, *in* Coastal Resilience: The Environment, Infrastructure, and Human Systems, New Orleans, Louisiana, Golf Coast Carbon Center. 23 May 2014.

Meckel, T. A., Trevino, R., Carr, D. L., Nicholson, A., and Wallace, K. (2013). Offshore CCS in the northern Gulf of Mexico and the significance of regional structural compartmentalization: Energy Procedia, v. 37, p. 4526.

Riis, F., and Halland, E. (2014). CO_2 storage atlas of the Norwegian Continental shelf: Methods used to evaluate capacity and maturity of the CO_2 storage potential: Energy Procedia, v. 63, p. 5258.

Schumann, D., Detschke, E., and Pietzner, K. (2014). Public perception of CO_2 offshore storage in Germany: regional differences and determinants: Energy Procedia, v. 63, p. 7096.

Tanase, D. (2013). Tomakomai CCS Demonstration Project in Japan: Energy Procedia, v. 37.

Tew, B. H., Armbrecht, C., Eugene, D. W., Hills, D., Duncan, I., Moody, J., Pashin, J. C., Sams, K., Hwang, L., Rogers, S. M., Esposito, R., Carpenter, S., and Meckel, T. (2013). Preliminary Evaluation of Offshore Transport and Geologic Storage of Carbon Dioxide: National Energy Technology Laboratory, Report DE-FC26-05NT42590.

Tucker, O., Garnham, P., Wood, P., Berlang, W., and Susanto, I. (2013). Development of an offshore monitoring plan for a commercial CO_2 storage pilot: Energy Procedia, v. 37, p. 4317.

Resource Estimation Methods

Andersen, O., Lie, K., and Nilsen, H. M. (2016). An Open-Source Toolchain for Simulation and Optimization of Aquifer-Wide CO_2 Storage: Energy Procedia, v. 86, p. 324.

Anthonsen, K. L., Frykman, P., and Nielsen, C. M. (2016). Mapping of the CO_2 storage potential in the Nordic region: Geologic Survey of Denmark and Greenland Bulletin, v. 35, p. 87.

Bachu, S. (2015). Review of CO_2 storage efficiency in deep saline aquifers: International Journal of Greenhouse Gas Control, v. 40, p. 188.

Bachu, S. (2008). Phase III Final Report Comparison between Methodologies Recommended for Estimation of CO_2 Storage Capacity in Geological Media: Carbon Sequestration Leadership Forum, Report CSLF-T-2008-04.

Bachu, S., Bonijoly, D., Bradshaw, J., Burruss, R., Christensen, N. P., Holloway, S., and Mathiassen, O. M. (2007). Phase II Final Report from the Task Force for Review and

Identification of Standards for CO_2 Storage Capacity Estimation: Carbon Sequestration Leadership Forum, Report CSLF-T-2007-04.

Bachu, S., Bonijoly, D., Bradshaw, J., Burruss, R., Holloway, S., Christensen, N. P., and Mathiassen, O. M. (2007). CO_2 storage capacity estimation: Methodology and haps: International Journal of Greenhouse Gas Control, v. 1, p. 430.

Blondes, M. S., Brennan, S. T., Merrill, M. D., Buursink, M. L., Warwick, P. D., Cahan, S. M., Cook, T. A., Corum, M. D., Craddock, W. H., DeVera, C. A., Drake, R. M., Drew, L. J., Freeman, P. A., Lohr, C. D., Olea, R. A., Roberts-Ashby, T. L., Slucher, E. R., and Varela, B. A. (2013). National Assessment of Geologic Carbon Dioxide Storage Resources - Methodology Implementation: U.S. Geologic Society, Report Open-File Report 2013-1055.

Bradshaw, J., Bachu, S., Bonijoly, D., Burruss, R., Christensen, N. P., and Mathiassen, O. M. (2005). Phase I Final Report from the Task Force for Review and Identification of Standards for CO_2 Storage Capacity Measurement: Carbon Sequestration Leadership Forum, Report CSLF-T-2005-09.

Bradshaw, J., Bachu, S., Bonijoly, D., Burruss, R., Holloway, S., Christensen, N. P., and Mathiassen, O. M. (2007). CO_2 storage capacity estimation: issue and development of standards: International Journal of Greenhouse Gas Control, v. 1, p. 62-68.

Brennan, S. T., Burruss, R. C., Merrill, M. D., Freeman, P. A., and Ruppert, L. F. (2010). A Probabilistic Assessment Methodology for the Evaluation of Geologic Carbon Dioxide Storage: U.S. Geologic Survey, Report Open-File Report 2010-1127.

Celia, M. A., Bachu, S., Nordbotten, J. M., and Bandilla, K. W. (2015). Status of CO_2 storage in deep saline aquifers with emphasis on modeling approaches and practical simulations: Water Resources Research, v. 51.

Frailey, S. M. (2013). Estimating CO_2 plume size: A correlation for site screening: International Journal of Greenhouse Gas Control, v. 13, p. 230.

Frailey, S. M. (2009). Methods for Estimating CO_2 Storage in Saline Reservoirs: Energy Procedia, v. 1, p. 2769.

Goodman, A. (2015). Resource Assessment Methods for CO_2 Storage in Geologic Formations, *in* Carbon Storage R&D Project Review Meeting, Pittsburgh, PA, National Energy Technology Laboratory. 18-20 August 2015.

Goodman, A. (2012). Comparison of CO_2 Storage Resource Methodologies, *in* Carbon Storage R&D Project Review Meeting Developing the Technologies and Building the Infrastructure for CCUS, Pittsburgh, PA, National Energy Technology Laboratory. 21-23 August 2012.

Goodman, A., Bromhal, G., Strazisar, B., Rodosta, T., Guthrie, W. F., Allen, D., and Guthrie, G. (2013). Comparison of methods for geologic storage of carbon dioxide in saline formations: International Journal of Greenhouse Gas Control, v. 18, p. 329.

Goodman, A., Hakala, A., Bromhal, G., Deel, D., Rodosta, T., Frailey, S., Small, M., Allen, D., Romanov, V., Fazio, J., Huerta, N., McIntyre, D., Kutchko, B., and Guthrie, G. (2011). U.S. DOE methodology for the development of geologic storage potential for carbon dioxide at the national and regional scale: International Journal of Greenhouse Gas Control, v. 5, p. 952.

Goodman, A., Sanguinito, S., and Levine, J.S. (2016). Prospective CO_2 saline resource estimation methodology: Refinement of existing US-DOE-NETL methods based on data availability: International Journal of Greenhouse Gas Control, v. 54, p. 242.

Gorecki, C. D., Ayash, S. C., Liu, G., Braunberger, J. R., and Dotzenrod, N. W. (2015). A comparison of volumetric and dynamic CO_2 storage resource and efficiency in deep saline formations: International Journal of Greenhouse Gas Control, v. 42, p. 213.

Gorecki, C. D., Sorensen, J., Bremer, J., Ayash, S. C., Knudsen, D., Holubnyak, Y., Smith, S., Steadman, E., and Harju, J. (2009). Development of Storage Coefficients for Carbon Dioxide Storage in Deep Saline Formations: International Energy Agency, Report No. 2009/13.

Heidug, W. (2013). Methods to assess geologic CO_2 storage capacity: status and best practice: International Energy Agency, Report Workshop Report 2013.

Hurtado, A., Eguilior, S., Maldonado, R., and Recreo, F. (2016). Perturbative studies to calculate the permeability and porosity of a CO_2 storage formation in a data shortage context: Energy Procedia, v. 86, p. 432.

Jones, K. B., and Blondes, M. S. (2015). Carbon Dioxide Storage in Unconventional Reservoirs Workshop: Summary of Recommendations: U.S. Geologic Survey, Report Open-File Report 2015-1079.

Lie, K.-A., Nilsen, H. M., Anderson, O., and Moyner, O. (2014). A simulation workflow for large-scale CO_2 storage in the Norwegian North Sea, *in* 14th European Conference on the Mathematics of Oil Recovery, Catania, Sicily, Italy, ECMOR. 8-11 September 2014.

Popova, O., Small, M., Thomas, A. C., McCoy, S. T., and Karimi, B. (2012). CO_2 Storage Resource Assessment Methodologies: Current Status and Comparative Analysis, *in* AAPG Annual Convention and Exhibition, Long Beach, CA, AAPG. 22-25 April 2012.

Roberts-Ashby, T. L., and Ashby, B. (2016). A method for examining the geospatial distribution of CO_2 storage resources applied to the Pre-Punta Gorda Composite and Dollar Bay reservoirs of the South Florida Basin, U.S.A. Marine and Petroleum Geology, v. 77, p. 141.

Steele-MacInnis, M., Capobianco, R. M., Dilmore, R., Goodman, A., Guthrie, G., Rimstidt, J. D., and Bodnar, R. J. (2013)., Volumetrics of CO_2 Storage in Deep Saline Formations: Environmental Science & Technology, v. 47, p. 79.

Thibeau, S., Bachu, S., Birkholzer, J., Holloway, S., Neele, F., and Zhou, Q. (2014). Using Pressure and Volumetric Approaches to Estimate CO_2 Storage Capacity in Deep Saline Aquifers: Energy Procedia, v. 63, p. 5294.

U.S. DOE NETL (2015). Carbon Utilization and Storage Atlas, Fifth Edition. U.S. Department of Energy, Office of Fossil Energy, National Energy Technology Laboratory.

U.S. DOE NETL. (2013). Best Practices for: Site Screening, Site Selection, and Initial Characterization for Storage of CO_2 in Deep Geologic Formations: U.S. Department of Energy, National Energy Technology Laboratory, Report DOE/NETL-2013/1605.

Zhou, Q., Birkholzer, J. T., Tsang, C. F., and Rutqvist, J. (2008). A Method for Quick Assessment of CO_2 Storage Capacity in Closed and Semi-Closed Saline Formations: Lawrence Berkeley National Laboratory, p. 45.

Attachment B: High Resolution File: Age depth plot using the First Appearance Datum (FAD) determined by the graphic correlation analysis

Figure 10

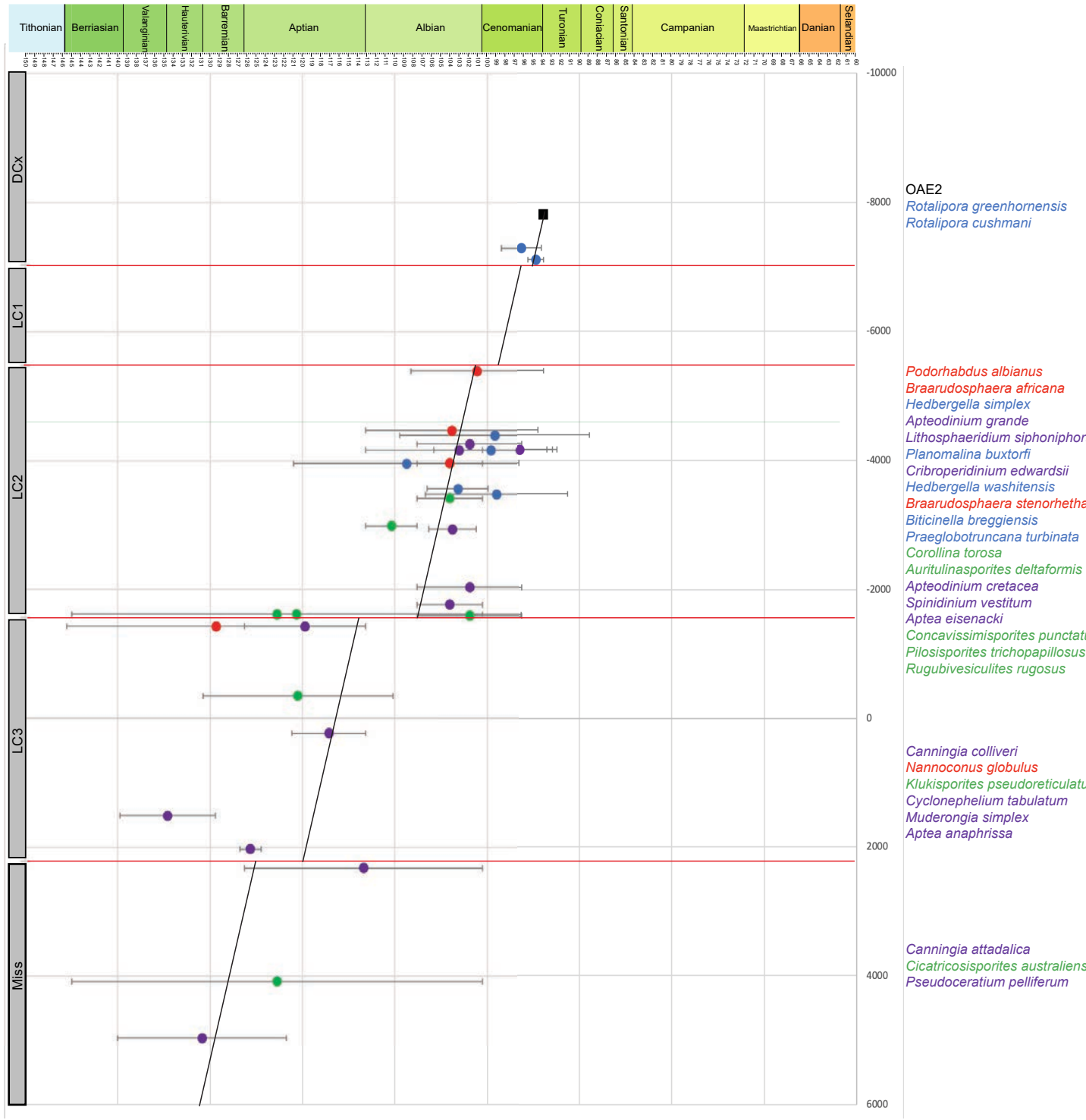
Tithonian
Berriasian
Valanginian
Hauterivian
Barremian
Aptian
Albian
Cenomanian
Turonian
Coniacian
Santonian
Campanian
Maastrichtian
Danian
Selandian
DCx
LC1
LC2
LC3
Miss
-10000
-8000
-6000
-4000
-2000
0
2000
4000
6000
OAE2
Rotalipora greenhornensis
Rotalipora cushmani
Podorhabdus albianus
Braarudosphaera africana
Hedbergella simplex
Apteodinium grande
Lithosphaeridium siphoniphor
Planomalina buxtorfi
Cribroperidinium edwardsii
Hedbergella washitensis
Braarudosphaera stenorhetha
Biticinella breggiensis
Praeglobotruncana turbinata
Corollina torosa
Auritulinasporites deltaformis
Apteodinium cretacea
Spinidinium vestitum
Aptea eisenacki
Concavissimisporites punctat
Pilosisporites trichopapillosus
Rugubivesiculites rugosus
Canningia colliveri
Nannoconus globulus
Klukisporites pseudoreticulatu
Cyclonephelium tabulatum
Muderongia simplex
Aptea anaphrissa
Canningia attadalica
Cicatricosisporites australiens
Pseudoceratium pelliferum

Attachment C: High Resolution File: Well-log interpretation compilation for 29 of the 34 deep-penetrating wells in the BCT

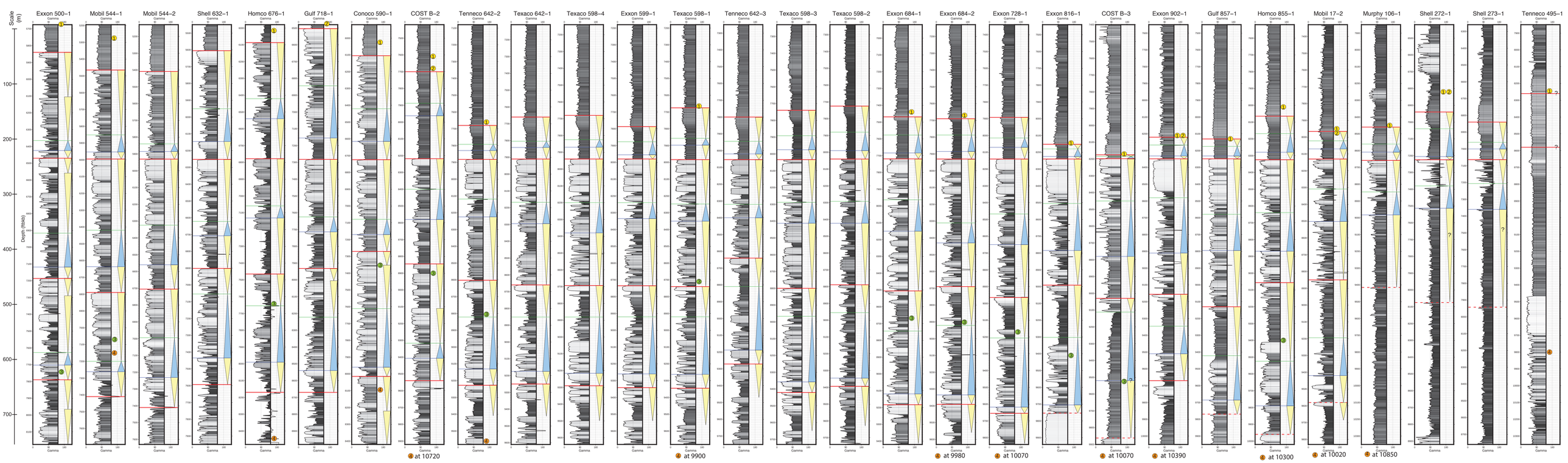
Scale (m)
Depth (thdo)
100
200
300
400
500
600
700
Exxon 500–1
Mobil 544–1
Mobil 544–2
Shell 632–1
Homco 676–1
Gulf 718–1
Conoco 590–1
COST B–2
Tenneco 642–2
Texaco 642–1
Texaco 598–4
Exxon 599–1
Texaco 598–1
Tenneco 642–3
Texaco 598–3
Texaco 598–2
Exxon 684–1
Exxon 684–2
Exxon 728–1
Exxon 816–1
COST B–3
Exxon 902–1
Gulf 857–1
Homco 855–1
Mobil 17–2
Murphy 106–1
Shell 272–1
Shell 273–1
Tenneco 495–1
Gamma
at 10720
at 9900
at 9980
at 10070
at 10070
at 10390
at 10300
at 10020
at 10850

Attachment D: Summary of Geologic Data from Three Core Holes Drilled Through the Potomac Group in the Coastal Plain Of Cecil County, Maryland.

Department of Natural Resources
Resource Assessment Service
MARYLAND GEOLOGICAL SURVEY
Richard A. Ortt, Jr., Director

REPORT OF INVESTIGATIONS NO. 87

SUMMARY OF GEOLOGIC DATA FROM THREE CORE HOLES DRILLED THROUGH THE POTOMAC GROUP IN THE COASTAL PLAIN OF CECIL COUNTY, MARYLAND

by

Heather A. Quinn

DNR Publication No. 12-051419-149

September 2019

CONTENTS

APPENDICES

FIGURES

TABLES

PLATES

ABBREVIATIONS AND ACRONYMS USED IN THIS REPORT

bls	below land surface
cm	centimeter
DNR	Maryland Department of Natural Resources
DGS	Delaware Geological Survey
Fm (or fm)	Formation (formation); capitalized for formal stratigraphic name
ft	feet
ft bls	feet below land surface
GIS	geographic information system
km	kilometer
m	meter
mi	mile
MDE	Maryland Department of the Environment
MGS	Maryland Geological Survey
NAD 83	North American Datum of 1983
NAVD 88	North American Vertical Datum of 1988
QA/QC	quality assurance/quality control
WMA	Wildlife Management Area
USGS	U.S. Geological Survey
ybp	years before present

SUMMARY OF GEOLOGIC DATA FROM THREE CORE HOLES DRILLED THROUGH THE POTOMAC GROUP IN THE COASTAL PLAIN OF CECIL COUNTY, MARYLAND

ABSTRACT

Three core holes were drilled to gain additional insight into the stratigraphic and hydrogeologic framework of the Potomac Group, which contains important water-bearing units in the coastal plain of Cecil County, Maryland. Core holes were located on the Elk Neck peninsula (CE Cd 91) and the west and east sides of the Town of Elkton (CE Be 155 and CE Bf 156, respectively). Each hole was continuously cored through coastal plain sediments into variably weathered crystalline basement rock. Geophysical logs were run in each hole to obtain additional information on geologic and hydrogeologic properties. Analyses of fossil pollen and spores were performed on core samples primarily to obtain information on the ages of the strata and assist with correlation. This report presents lithologic descriptions of the cores, compilations of the geophysical logs, results of the palynological analyses, and summarizes data collection, compilation and interpretive activities conducted.

The Potomac Group is present in the Coastal Plain Province of Maryland, Delaware and New Jersey and appears to extend some distance off-shore. In many areas of the Maryland Coastal Plain, the Potomac Group can be divided into three formations – Patapsco, Arundel and Patuxent Formations, in descending order – within which are several aquifers and confining units. In the upper Chesapeake Bay area, including portions of Cecil County, these formations and the related aquifers and confining units are not as well-defined or as clearly distinguishable from each other as they are in the central and southern (western shore) portions of the Maryland Coastal Plain.

Information obtained from these core holes helped fill data gaps on the east side of the Chesapeake Bay between Turkey Point and the Maryland-Delaware line. As a result, previous conflicting stratigraphic and hydrostratigraphic correlations in the area and the assumptions in the interpretive techniques used could be evaluated. Data collected and analyzed for this project underscore the geologic complexity of the Potomac Group even over relatively short distances and emphasize the importance of palynology as a key component to be used with other geologic and geophysical data in correlating strata. Results of this study yielded some significant new information about, and greater understanding of, the subsurface geology and hydrogeology of the area.

The thickness of the coastal plain sediments differs among the core holes, ranging from approximately 489 feet at central Elk Neck peninsula to approximately 200 feet or less near Elkton. Within the Potomac Group, the lateral extent of a particular water-bearing sand interval can vary greatly. Notably a 40-foot-thick sand recorded at depth in a well about 0.52 miles from CE Cd 91 on the Elk Neck peninsula appears to be absent in CE Cd 91, yet a shallower, approximately 50-foot-thick, sandy interval is present in both. There is also considerable variation among the three core holes in the type of basement rock and the thickness of saprolite and weathering of the basement rock below the Potomac Group.

Stratigraphic correlations made in this study, supported by palynological data, suggest that the upper portion of the Potomac Group (the Patapsco Formation) in the Elkton area lies directly on weathered basement rocks and the older portions of the Potomac Group are absent there. In contrast, in the central part of Elk Neck a relatively thick interval (possibly 48 to 100 feet or more) of the older portion of the Potomac Group (Patuxent-Arundel Formations) is present above basement rock and is overlain by the Patapsco Formation. This differs significantly from some previous interpretations and indicates that the Patuxent-Arundel interval extends farther updip in the subsurface of central part of the Cecil County. In addition, the boundary between palynological Zones II and III (within the Patapsco Formation) may be higher in the subsurface below the Elk Neck peninsula than indicated in previous interpretations for that area.

Palynological information from these three core holes suggests that stratigraphic correlations within the Potomac Group that are completed primarily using geophysical logs – especially where logs are widely separated and lack

age-datum control – need to be revisited. Often no single geologic investigative method or technique is sufficient to define or refine the stratigraphy (or hydrostratigraphy) of the Potomac Group sediments so multiple lines of evidence are needed. Because stratigraphic relations play a role in developing a hydrostratigraphic framework and aquifer models, which in turn are used to estimate aquifer recharge and groundwater resources, errors in the extent and relation of strata can have an impact on groundwater resource assessments.

INTRODUCTION

The Potomac Group includes important aquifers in the coastal plain of the Mid-Atlantic region. Aquifers within the Potomac Group are heavily used in northeastern and southern Maryland, northern Delaware and southern New Jersey. The geology of the Potomac Group is complex. Uncertainties in regional correlation of aquifers exist largely due to the complex three-dimensional configuration of the sand units, and also because of the limited availability of palynological data (fossil plant spores and pollen) to assist in determining ages and stratigraphic relations of these non-marine strata. Water availability and water quality are increasingly critical issues in policy decisions in Maryland, Delaware, and New Jersey. Population growth and periodic occurrence of drought conditions have highlighted the need for a better understanding of the aquifers in the region to support water resource management. For this reason, several core holes were completed in northeastern Maryland to collect core for lithologic and palynologic analysis as well as geophysical data.

PURPOSE AND SCOPE

This report provides data and results from geological investigations conducted on three core holes drilled and cored through the Potomac Group in the coastal plain of Cecil County, Maryland. Data include a summary of drilling activities, detailed lithologic descriptions, core photographs, geophysical logs, and palynologic analyses. In addition, some regional cross sections are provided which incorporate data from these core holes with others previously completed in the region.

The objective of this work was to clarify the geologic and aquifer framework in the outcrop/subcrop area of the Potomac Group in Cecil County, Maryland, and potentially resolve some of the differing regional interpretations and correlations. The core sites selected and the core analyses planned had the potential to fill data gaps by providing palynological age data as well as additional lithologic and geophysical data in areas where previous workers had shown differing cross sections and extrapolated correlations through parts of the Potomac Group.

LOCATION OF STUDY AREA

The study area is near the northern limit of the Coastal Plain Province in Cecil County, Maryland (fig. 1). Core hole locations are shown on Figure 2 and Plate 1. Core hole CE Cd 91 was drilled at the Department of Natural Resources, Black Hill Ranger Station located on the south side of McKinneytown Road on the Elk Neck peninsula in Cecil County, Maryland. Core hole CE Be 155 was located on the western side of Elkton, Maryland, near the town's wastewater treatment facility. CE Bf 156 was located on the eastern side of Elkton, on a town property. Geographic coordinates and approximate land surface elevation for these core holes are provided in Table 1.

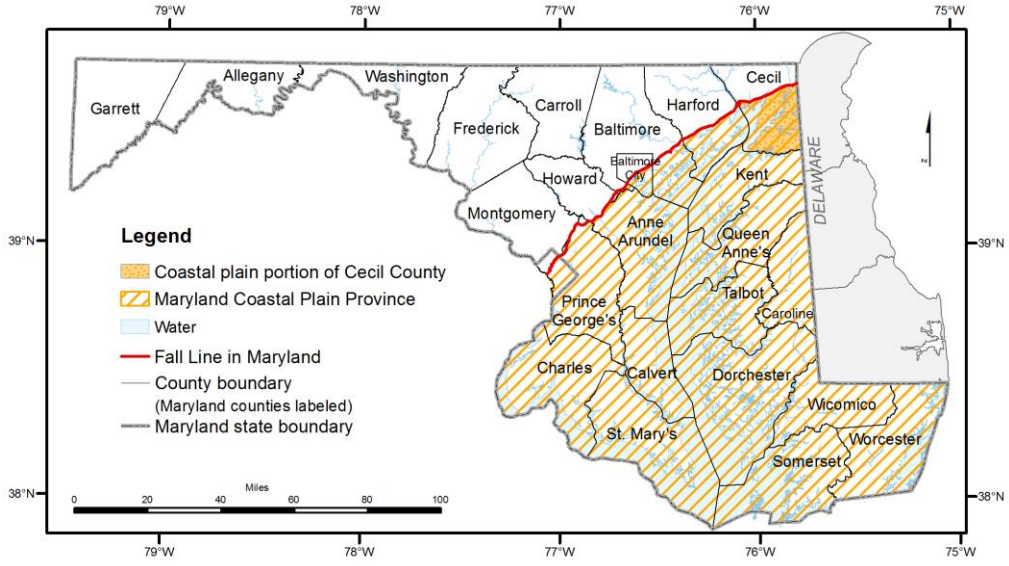

Figure 1. Extent of the Coastal Plain Province in Maryland and within Cecil County.

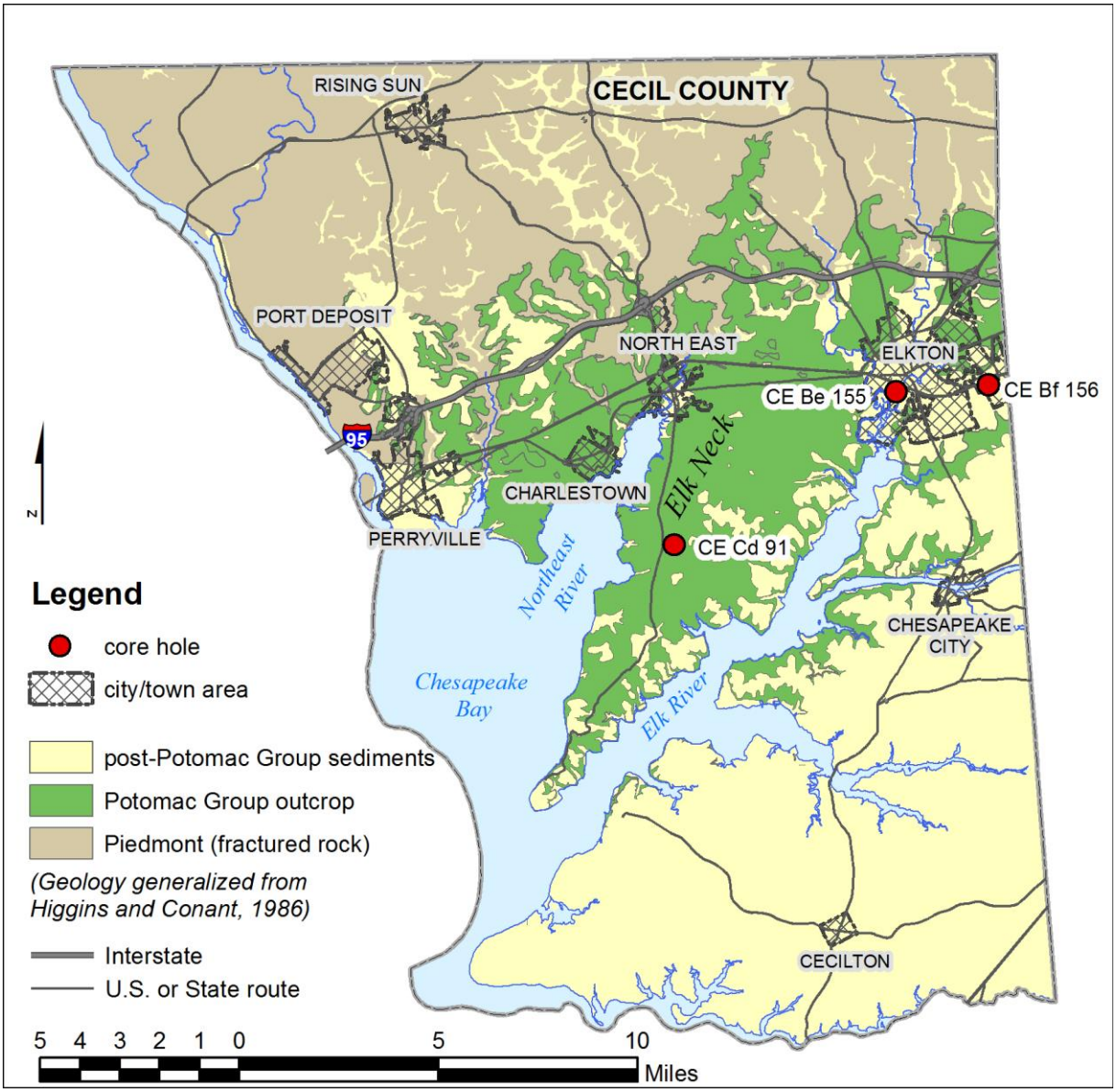

Figure 2. Location of Maryland Geological Survey core holes and general outcrop area of the Potomac Group in Cecil County, Maryland (generalized from Higgins and Conant, 1986).

Table 1. Core hole coordinates and elevations.

Core hole ID	Latitude (degrees, minutes, seconds; NAD 83)	Longitude (degrees, minutes, seconds; NAD 83)	Land Surface Elevation (feet NAVD 88)
CE Cd 91	39° 32’ 42.78”	75° 56’ 35.16”	+175
CE Be 155	39° 36’ 00.30”	75° 50’ 15.40”	+21
CE Bf 156	39° 36’ 08.01”	75° 47’ 36.50”	+79

ACKNOWLEDGEMENTS

Many people and government agencies contributed to the work summarized in this report. The coring was part of two projects investigating the complex hydrostratigraphy of the Potomac Group in parts of Cecil County. The first project focused on the central part of Elk Neck; the second focused on the area around the Town of Elkton, Maryland.

Work related to coring at the Black Hill Ranger Station was funded in part by the Maryland Department of the Environment (MDE). The Maryland Department of Natural Resources (DNR), Forest Service, provided site access and a temporary water supply for drilling at the ranger station site. Coordination provided by Shawn Day, DNR Forest Ranger, facilitated completion of the field work. Drilling and coring at the Black Hill Ranger Station were performed by the U.S. Geological Survey (USGS) including Eugene Cobbs III, Mike Green, and Jeffrey Grey. Work related to coring in Elkton, Maryland, was funded in part by the USGS National Cooperative Geologic Mapping Program, Award No. G11AC20406, fiscal year 2011.

The work related to the compilation and analysis of data from these core holes and integration of this data with previous work on the hydrostratigraphy of the Potomac Group in the region was supported in part by the U.S. Department of Energy through grants to Battelle under the Mid-Atlantic U.S. Offshore Carbon Storage Resource Assessment Project (DOE Project – DE-FE0026087). (The views and conclusions contained in this document are those of the author and should not be interpreted as necessarily representing the official policies, either expressed or implied, of the U.S. Government.)

The Maryland Geological Survey (MGS) greatly appreciates the assistance of the Town of Elkton, Maryland, in securing access to two properties and a temporary water supply for the drilling of the Elkton core holes. In particular, coordination provided by Lewis George, Town Administrator, and Daniel Handley, Director of the Department of Public Works, helped expedite the field work.

The MGS is grateful to the Delaware Geological Survey (DGS) for their cooperation and assistance with many aspects of this project. The DGS performed the drilling/coring at the two Elkton sites led by Paul "Steve" McCreary. The DGS also completed the geophysical logging of all three boreholes and processing of samples for palynological analysis. In particular, the MGS acknowledges Peter P. McLaughlin Jr., for his efforts in coordinating the geophysical logging and palynologic sample preparation of this project as well as field support. The MGS wishes to thank the many DGS geologists and staff who provided field and laboratory assistance including Kelvin Ramsey, Jaime Tomlinson, and Charles T. Smith.

Several geologists, currently or formerly, of the MGS also contributed to the field work discussed in this report, including Andrew Staley, David Drummond, Owen McKain, Ben Allen, Katherine Burgy, Lindsay Keeney and David Bolton. Dr. Gilbert J. Brenner, consulting palynologist, provided analysis of pollen samples on the core samples.

The manuscript was reviewed by David Andreasen, Andrew Staley and Richard Ortt of the MGS; Peter P. McLaughlin, Jr., of the DGS; and Jesse D. Thornburg of Temple University.

GEOLOGIC BACKGROUND AND PREVIOUS INVESTIGATIONS

OVERVIEW

The Potomac Group sediments are the oldest of the Coastal Plain deposits in Maryland. From the Fall Line, where the Potomac Group pinches out, the unit increases in thickness down dip to the east and southeast to more than 4,000 ft at Ocean City (Hansen and Doyle, 1982; Hansen, 1984). Potomac Group sediments crop out along the Fall line from Virginia to Delaware in an arcuate band that is widest in central Maryland. In Cecil County, Potomac Group sediments are exposed at or near the surface over much of the area between the Fall Line and the Elk River (Higgins and Conant, 1986, 1990). In the upper Chesapeake Bay area, the Potomac Group sediments lie on a basement of variably weathered Paleozoic and older metamorphic and igneous rocks. The top of the unit is an unconformity and, where it is not exposed at the land surface, the Potomac Group is overlain by Upper Cretaceous sediments of the Magothy or Merchantville Formations or by Neogene to Quaternary sediments.

GENERAL LITHOLOGIES

Sediments of the Potomac Group are a complex mosaic of multicolored silts, clays, sands and gravelly sands. The sediments were first described and erected as a geologic formation by McGee (1886a, b) to characterize the sands and iron-ore clays lying on crystalline basement rock in Maryland, Virginia, and the District of Columbia. Numerous workers have noted that lithologies tend to vary rather rapidly both horizontally and vertically in many areas of Maryland (e.g., Glaser 1969, Hansen 1972, Otton and Mandle, 1984). Higgins and Conant (1990) note that in Cecil County, Maryland, Potomac Group sands and gravels are mostly quartzose and locally micaceous. Finer lithologies have variable proportions of silts and clays, occur in a wide variety of colors, and are commonly mottled and variegated (e.g., Jordan, 1962; Glaser, 1969; Higgins and Conant, 1990; McKenna and others, 2004). Clays have been shown to be predominantly kaolinite with lesser illite (Higgins and Conant, 1990). Plant-derived materials, including lignitic beds and charcoal, are common.

LITHOFACIES AND DEPOSITIONAL ENVIRONMENTS

Potomac Group sediments have been interpreted as an array of fluvial-deltaic deposits that accumulated as part of a broad alluvial plain (e.g., Glaser, 1969; Hansen, 1969; Jordan, 1983). It has been recognized that in some areas sands are more massive and extensive suggestive of a wide braided stream system with shifting channels whereas in other areas sand bodies are more discrete with fining-upward sequences suggestive of more channelized variably meandering streams (Hansen, 1969). In the northern Maryland and Delaware area (the vicinity of the study area) Potomac Group sediments have been interpreted as alluvial (continental), largely fluviatile, in origin with depositional environments including floodplains, swamps/marshes, river banks/levees and river channels (Owens, 1969; Higgins and Conant, 1990).

More recently, work in northern Delaware and southwestern New Jersey (Fort Mott area) has led to the interpretation that the dominant depositional environment for Potomac Group sediments in this area was an anastomosing river system (McKenna and others, 2004; Sugarman and others, 2004, 2005; Zullo 2012). An anastomosing river consists of two or more interconnected, low gradient, channels that have relatively stable banks and bars (as compared to braided rivers). Channels are separated by floodplains which include natural levees and wetlands (e.g., backswamps, oxbow lakes) and new channels are generally thought to be formed by avulsion (e.g., Smith and Smith, 1980; Makaske, 2001). Makaske (2001) considered anastomosing river systems to include multiple channel belts in which any individual belt may include braided, meandering or straight channels.

McKenna and others (2004) identified five lithofacies and corresponding interpreted depositional environments in the Potomac Group sediments of northern Delaware. Three facies were predominantly sands: amalgamated sands, thick sands, and thin sands (interpreted as amalgamated channels, isolated channels, and crevasse splay/proximal levee, respectively); two facies were fine grained: interlaminated sand and silt (interpreted as distal levee/floodplain) and mottled silts and clays (interpreted as weathered floodplain with paleosols). In a subsequent study near the Chesapeake and Delaware Canal, Zullo (2012) identified lithologies that were similar, in part, with those of McKenna and others (2004), however, her interpretations of some depositional environments differed slightly and were not completely a one-to-one match to the same lithologies. Zullo's six lithofacies were paleosols, lake, frequently flooded lake/abandoned channel, splay/levee, fluvial channel and splay channel. During the time span represented by the Potomac Group, multiple phases of deposition, avulsion and erosion have been interpreted to have produced the complex geologic deposit.

Identification and recognition of lithofacies and their depositional relationships have the potential to provide better understanding into possible spatial distribution of lithologies and hydrogeologic characteristics. Many workers have identified representative borehole geophysical log patterns associated with particular lithofacies and fluvial cycles of deposition determined from core and/or cuttings (e.g., Hansen 1968; Hansen, 1969; Edwards and Hansen, 1969; Woodruff, 1976; McKenna and others, 2004; Sugarman and others, 2005; Zullo 2012). Thus these geophysical log patterns, as a reflection of lithofacies relationships, may allow insights into subsurface architecture when lithologic information is limited or not available. Zullo (2012) was able to recognize four lithofacies in seismic data as well as discontinuities and valley incision events not recognizable in available data from boreholes

typically spaced too far apart. Both McKenna and others (2004) and Zullo (2012) note the discontinuous nature of individual sand bodies and limitations to the extent of larger sand packages, describing the distribution of the Potomac Group sands in New Castle County, Delaware, as a "labyrinth style of heterogeneity".

LITHOSTRATIGRAPHY

In Maryland, the Potomac Group includes four formations, which in descending order from youngest to oldest, are: the Patapsco, Arundel, Patuxent and Waste Gate. The Waste Gate Formation, which pinches out in the subsurface south of Cecil County and is not known to contain freshwater, is not included in this study. The division of the Potomac Group into the Patuxent, Arundel, and Patapsco Formations (and corresponding aquifer units) is best developed in the Baltimore-Washington D.C. corridor. In areas to the northeast around the upper Chesapeake Bay, including the study area, this subdivision is not as well developed or as clearly discernable and often these strata are referred to either as the Patuxent-Arundel Formations (undivided) and the Patapsco Formation (e.g., Edwards and Hansen, 1979); or just the Potomac Group (undivided) (e.g., Owens, 1969; Higgins and Conant, 1990).

In Delaware and New Jersey, lithologies are similar enough through the unit that they cannot be mapped separately and one lithostratigraphic unit is recognized: the Potomac Formation (e.g., Jordan, 1962, 1983; Owens and others, 1998; Benson, 2006). Some recent studies in Delaware and New Jersey, however, have used an informal, three-part subdivision for the Potomac Formation -- a Potomac I, II, and III (upward; oldest to youngest) in New Jersey (e.g., Sugarman and others, 2005; Thornburg and others, 2019), and a Potomac A, B, and C (downward; youngest to oldest) in Delaware (e.g., Benson, 2006; He and Andres, 2011). These three-part subdivisions are not identical to the formations (or hydrogeologic units) as defined in Maryland. In Delaware, for example, the three-part subdivision of Benson (2006) was intended to represent essentially time-stratigraphic units and was used in a groundwater-flow model (although subdivisions do not represent aquifer and confining units).

BIOSTRATIGRAPHY AND AGE

The age of the Potomac Group has been based mainly on plant fossils, primarily pollen and spores, and correlation to marine and non-marine sections in other areas. Overall, the Potomac Group is considered to range in age from Early Cretaceous (Berremian at base of the Waste Gate Formation) to early Late Cretaceous (Cenomanian at the top of the Patapsco Formation) (Hansen and Doyle, 1982; Hansen , 1984). For the Potomac Group units present in the northern part of the Delmarva Peninsula, fossil spores and pollen indicate deposition during the parts of the Early Cretaceous (Aptian, Albian) and Late Cretaceous (Cenomanian), stages that range in age from about 125 to 94 million years ago (Doyle and Robbins, 1977; Hochuli and others, 2006; McLaughlin, 2006).

Brenner (1963) first established two major microfloral (spores and pollen) zones (Zones I and II) and several subzones within Zone II based on outcrop and subsurface samples of Potomac Group sediments from Maryland. Microflora from the Patuxent and Arundel Formations samples were nearly identical and therefore Zone I corresponded to the Patuxent and Arundel Formations undivided; the base of Zone II corresponded with the base of the Patapsco Formation. Within Zone II, Brenner was able to identify Subzones A and B and within Subzone B, a further subdivision into Subzone B-1 and B-2 in some areas. Brenner indicated that the major change in microflora from Zone I to II suggested a disconformity although the relatively low frequency of new forms in Subzone IIA suggested that the time gap represented by the disconformity may not be great.

Subsequent investigations have both added to and modified the Potomac Group pollen zones and subzones and their ages. Within Zone I, additional differences in pollen assemblages found in the lower and upper parts of the zone (associated with the Patuxent and Arundel Formations, respectively) have been noted (Doyle and Hickey 1976; Doyle and Robbins 1977; Doyle 1992). Hochuli and others (2006) compared Potomac sections and palynology with other Cretaceous sections, mainly in Europe. They also recognized a lower Zone I and an upper Zone I that are likely separated by a disconformity corresponding to the boundary between the Patuxent and Arundel Formations and the Aptian and early Albian ages, respectively.

Palynological zones within the Patapsco Formation were expanded by Doyle and Hickey (1976) and Doyle and Robbins (1977). They recognized Subzone IIC (formerly part of Brenner's IIB) and

Zone III within the youngest portion of the Potomac Group, which includes the "Elk Neck Beds" (of Wolfe and Pakiser, 1971) of the Patapsco Formation in northeastern Maryland. Hansen and Edwards (1979) found that in several core holes in the upper Chesapeake Bay, Subzone IIA palynomorphs were rarely found and samples from intervals between Zone I and Subzone IIB were often non-fossiliferous; thus boundary between Zone I and II was poorly constrained locally.

More recent work has revised the ages of some of zones for the Patapsco Formation in Maryland. Hochuli and others (2006) considered pollen of Subzone IIC to be early Cenomanian. Thus, per Hochuli and others (2006) the boundary between Early and Late Cretaceous falls between Subzones IIB and IIC. Subsequent work by Horikx and others (2016) suggest that the boundary between Early and Late Cretaceous occurs within Subzone IIC. Some comparisons of pollen and spore zones, ages and geologic units are shown in Tables 2 and 3.

Table 2. Potomac Group spore-pollen zones and comparison of assigned ages.

Zones and Subzones	**Age** *(Doyle and Robbins, 1977)*	**Age (revised)** *(Hochuli and others., 2006)*	**Age (revised)** *(Horikx and others., 2016)*
Zone III	early Cenomanian	early Cenomanian	early Cenomanian
Subzone IIC	latest Albian		latest Albian to early Cenomanian
Subzone IIB	middle and early late Albian	middle to late Albian	middle to late Albian
Subzone IIA	early to middle Albian		middle Albian
Upper Zone I	Aptian to early Albian	early Albian	early Albian
Lower Zone I	Barremian to Aptian	Aptian	Aptian

Table 3. Relationship of spore-pollen zones to Potomac Group strata in Maryland.

Time-Rock Units			**Spore-Pollen**	**Maryland Rock Units**	
System	Series	Stage	Zones and Subzones *(as modified by Horikx et al, 2016)*	Group	Formation
Cretaceous	Upper Cretaceous	Cenomanian-lower	Zone III	Potomac	*Elk Neck beds (Patapsco)*
			Subzone IIC		Patapsco
	Lower Cretaceous	Albian-upper			
			Subzone IIB		
		Albian-middle	Subzone IIA		
		Albian-lower	Zone I-upper		Arundel
		Aptian	Zone 1-lower		Patuxent *(where differentiated)*

TIME-STRATIGRAPHIC UNITS

In portions of Delaware, Maryland and New Jersey, Benson (2006) devised a time-stratigraphic framework that attempted to correlate depositionally contemporaneous Potomac Formation (Group) facies/strata with the ultimate goal of improving predictions of hydraulic connectivity between potential aquifer sands and overall aquifer architecture. Benson (2006) summarized the approaches and views of previous workers regarding the overall stratification, correlation and time-lines of equivalent deposition within the Potomac Formation as: (1) largely parallel to the basement unconformity (e.g., Jordan, 1968; Sundstrom and Pickett, 1967); or (2) largely parallel to a regional unconformity at the top of the Potomac Formation/Group (e.g., Spoljaric, 1967). Benson (2006) pursued a third approach with

deposition/stratification largely parallel to a key time-line datum.

In this approach, Benson (2006) used a distinct "shale to sand" contact just above the microfloral boundary between Subzone IIC and Zone III (and recognizable on geophysical logs) as a key marker and time-line datum. [It should be noted that he referred to this shale-sand contact as the Lower and Upper Cretaceous (LK-UK) datum, however, according to age revisions by Hochuli and others (2006) the LK-UK boundary occurs between microfloral Subzones IIB and IIC; and per Horicks and others (2016) the datum occurs within Subzone IIC.] Control boreholes that penetrated to basement and had related palynological data, lithologic data, and geophysical logs were used to identify initial marker beds above and below the LK-UK datum that were stratigraphically consistent in position and considered correlatable on geophysical logs. Then the geophysical markers beds (silt-clay kicks) were used to extrapolate matches to other geophysical logs. The extrapolations were tested on some local logs in Delaware (associated with palynological data) and then applied regionally (including a number of logs without associated palynological data). Several cross sections were extended into Maryland.

The underlying assumption of Benson (2006) is that each silt-clay marker bed represents a widespread, floodplain deposit (often a paleosol) that formed nearly synchronously so these marker beds are essentially time lines that define time-stratigraphic units. It is also assumed that time-equivalent silt-clay markers can be recognized correctly in logs without palynologic or other age data. Cross section K-K' of Benson (2006, plate 3) shows the older Zone I portions (Patuxent-Arundel Formations) of the Potomac Group pinching out in the subsurface under the Elk Neck peninsula. However, in other parts of Maryland, including northwest Cecil County and Harford County, the older Zone I portion has been reported to be exposed at the surface (Brenner 1963; Wolf and Pakiser, 1971). Therefore, it seems plausible that older portions of the Potomac Group may be more extensive in the subsurface of Cecil County, Maryland, than as interpreted by Benson (2006). Given the distance over which some the extrapolations by Benson (2006) were made and the known complexity of the Potomac Group strata, this present study sought to find additional data to evaluate the concept and correlations previously presented.

HYDROSTRATIGRAPHY

In Maryland, the Patuxent and Patapsco Formations include important aquifer units and multi-aquifer systems as well as confining or semi-confining units; the Arundel Formation, also referred to as the Arundel Clay, is considered a confining unit (Hansen 1972; Andreasen and others, 2013). In some areas, particularly south of the Baltimore area, the Patapsco Formation includes two distinct aquifers called the Lower and Upper Patapsco aquifers (Mack and Achmad, 1986; Andreasen and others, 2013). Individual sands within an aquifer or aquifer system may be separated by clays and commonly thin, pinch out, or grade into silt and clay, resulting in a number of discontinuous sand bodies.

Edwards and Hansen (1979) made some tentative correlations between Maryland formations in the upper Chesapeake Bay area and the informal hydrologic subdivisions of Sundstrom and others (1967) in Delaware using, in part, palynological zones of two Delaware wells by Doyle and Robbins (1997). In particular, Edwards and Hansen (1979) noted the presence of a thick clay-silt bed characteristically associated with palynological Subzone IIC in the upper Patapsco Formation that might serve as both an effective regional stratigraphic marker bed in the upper Chesapeake Bay area and an effective confining bed between the upper and lower hydrologic zones of Sundstrom and others (1967).

Subsequently, in Cecil County, Otton and others (1988) defined an upper and a lower Potomac aquifer separated by a confining unit. In this three-part subdivision, the lower Potomac aquifer included beds of microfloral Zones I, IIA and IIB (thus encompassing strata in the Patuxent-Arundel and portions of the Patapsco Formations). The middle Potomac confining unit included fine-grained sediments mainly associated with microfloral Subzone IIC but could extend to portions of Zone III; and the upper Potomac aquifer included sandy beds of microfloral Zone III. Otton and others (1988) noted that their lower Potomac aquifer in Cecil County roughly corresponds to the lower Potomac aquifer of Martin (1984) in New Castle County, Delaware, where Martin identified three Potomac aquifers (lower, middle and upper) with intervening confining units for groundwater modeling. [It is noted, however that subdivisons and correlations of Martin (1984) are inconsistent with correlations of Benson, 2006].

In Delaware, more recent groundwater models for the Potomac Formation were developed for parts of New Castle County (U.S. Army Corps of Engineers, 2004, 2007; He and Andres, 2011) using the Potomac A, B, and C (downward; youngest to oldest) subdivisions developed from the time-stratigraphic work of Benson (2006). As Benson noted, these subdivisions are essentially time-stratigraphic units and do not strictly represent aquifers and confining units. Benson indicated, however, that such a subdivision might allow for a better identification of aquifer quality sands that were genetically related at the time of deposition and therefore possibly better connected hydrologically. Thus the subdivision could help determine the lateral connectivity of aquifers more accurately. The subdivisions (and resulting models) also have significant implications regarding aquifer recharge (i.e., direct recharge from connection to the surface was limited to the uppermost sands). In Benson's study area (northern Delaware and Cecil County, Maryland), older portions of the Potomac Group were shown to thin by onlap and ultimately pinch out in the subsurface between basement and younger Potomac Group strata. In terms of aquifer characteristics this would allow only direct recharge to shallow aquifer sands in this area and preclude direct recharge from the surficial aquifer to deeper Potomac aquifer sands. In general, in the hydrogeologic model derived from Benson's framework, Potomac A appears to include palynological Zone III and younger parts of the formation; Potomac B correlates largely with Subzone IIC; and Potomac C includes most sediments from the base of Subzone IIC to basement.

In the future, a more robust use of long-term monitoring of groundwater levels and correlation of water levels with withdrawals may help determine the hydraulic connectivity of strata. Regional groundwater-level data can be used to develop potentiometric contour maps that may help identify distinct aquifers, as well as potential recharge and discharge relationships. Groundwater level responses to pumping tests and longer-term withdrawals may identify which layers are hydraulically isolated from one another or, conversely, hydraulically connected.

METHODS AND MATERIALS

DRILLING, CORING AND LOGGING

Continuous coring techniques were used at all three sites although the nature of the sediments – including very sandy intervals as well as intermittent ironstone and occasional gravels – made collection of 100 percent of the cored interval essentially impossible. Core material recovered was measured in feet (ft) and all depths of drilling were recorded in ft below land surface. Coring began about 4 to 5 ft below the land surface. Recovery ranged from zero to slightly more than 100 percent in individual core intervals but averaged about 60 percent in core hole CE-Cd-91, about 47 percent in CE Be 155 and about 67 percent in CE Bf 156. In general, the depth of the core recovered was standardized so that the top of each core was assigned to the top of each run unless noted otherwise in detailed lithologic logs (see Appendices A, B, C). Core diameter was approximately 2.25 inches.

Core hole CE Cd 91 (permit CE-95-2880) was drilled on the Elk Neck peninsula at the Department of Natural Resources, Black Hill Ranger Station. The USGS Geologic Division's Eastern Drilling Team performed the drilling from July 9 through July 22, 2009, using a hydraulic rotary rig equipped with a wire-line coring system. The borehole was drilled to a depth of 590 ft. The hole was continuously cored from 5 to 590 ft with approximately 350 ft of core recovered.

Two core holes were drilled in Elkton, Maryland, where depth to basement rock was known to be approximately 200 ft or less. The work was conducted cooperatively with the Delaware Geological Survey. Drilling and coring were performed using the Delaware Geological Survey's hydraulic rotary rig equipped with wire-line coring system. Staff from both the Maryland and Delaware geological surveys provided field support.

The Elkton sites were located on the east and west sides of town, approximately 2.5 miles apart (Plate 1). Core hole CE Bf 156, located on the east side of Elkton, was drilled to a total depth of 200 ft between October 17 and 19, 2011 under permit CE-10-0116. The hole was continuously cored from depths of 4 to 200 ft with approximately 125 ft of core recovered. Core hole CE Be 155, drilled under permit CE-10-0115 on the western side of Elkton from October 24 through 26, 2011, had a total depth of nearly 203 ft

(202.83 ft). The hole was continuously cored from depths of 4 to 202.83 ft with approximately 93 ft recovered.

In general, cores were gently cleaned on-site to remove drilling mud. MGS geologists measured and described core in the field. Lithologic color was recorded with wet core matched and coded to Munsell Soil Color Charts (version 2000, revised). Once descriptions were complete, the core was packaged for storage. Core was cut as needed to fit into 2-ft sections. Each section was enclosed in a strip of plastic sheeting fitted into each channel of a waxed cardboard core box. Each box could hold up to 10 ft of core in five 2-ft segments. Labeled wooden blocks were used to mark top and bottom of core within the core boxes. Boxes were labeled by borehole identifier and depth interval and/or core run. Core was photographed both as boxed and as needed in closer view during the core description process to record distinctive characteristics of particular intervals/features.

Geophysical logging was completed in each of the three core holes by the DGS. Geophysical logs included natural gamma radiation, single-point resistance, and resistivity (16-inch normal, 64-inch normal and 48-inch lateral) in all three boreholes. Spontaneous potential logs were successfully completed in CE Cd 91 and CE Be 155. Spontaneous potential and fluid resistivity logs were also run in CE Cd 156. In CE Cd 91, initially a natural gamma tool was run inside the drilling rods to provide a record of nearly the full length of the hole in case of hole collapse; and subsequently, in the open borehole, a natural gamma and induction tool was also used. The induction tool provides conductivity and converted resistivity of the surrounding rock/sediment within about 10 to 50 inches from the borehole and is not sensitive to borehole fluid. The normal-resistivity logs are most effective in formations with high electrical resistivities (low conductivity); in contrast, the induction log is generally more effective in formations with high electrical conductivity (low resistivity). The suite of wireline geophysical logs obtained in each hole provides a continuous record of rock and fluid properties. It is recognized, however, that minor differences between geophysical log depth and core depth may occur due to depth justification related to core intervals that were incomplete, disturbed, or stretched/expanded, and/or the effect on the logging from slight cable stretching or borehole factors affecting the equipment. In addition, some borehole geophysical logs do not extend to the total reported depth drilled due to the inherent properties tool length/sensor distribution and, in part, from borehole instability (presumably some infilling and/or collapse). At the completion of logging, each borehole was properly abandoned (grouted and sealed).

PALYNOLOGICAL SUBSAMPLING AND PROCESSING

Core subsamples for palynological analysis were selected from lithologies most likely to yield pollen and/or spores. Samples consisted mainly of gray clays or silty clays without mottling and without an overwhelming abundance of charcoal or lignite (specifically, intervals potentially unaffected by oxidation and/or bioturbation and without the excessive material that makes sample preparation difficult). Core subsampling was conducted with Peter P. McLaughlin Jr., of the DGS and DGS completed the sample processing.

Thirteen intervals were selected from CE Cd 91 core for processing; three intervals yielded no organic residue. Slides were made from processed material from the remaining 10 intervals. Similarly, six of the eight subsamples selected from CE Be 155 and five of the nine subsamples from CE Bf 156 contained adequate pollen to generate slides for analysis. A summary of the subsampled intervals and the processing results are provided in Appendix D, Table D-1. A set of the resulting slides were submitted to Gilbert J. Brenner, consulting palynologist, for analysis.

RESULTS OF PROJECT DRILLING/SAMPLING

Detailed core descriptions and records of recovery for CE Cd 91, CE Be 155 and CE Bf 156 are provided in the Appendices A, B, and C, respectively, along with photographs of boxed core and summary diagrams. Records of recovery and lithology for each core interval were generally aligned by default to the top of the interval drilled and therefore, where recovery was incomplete, the depths of some lithologic descriptions within a particular interval may not precisely reflect the true depth within the cored

interval (i.e., missing material may not be from the base of the cored interval). Where adjustments were made to realign recovered core within a particular cored interval based on field data or geophysical log information, this is noted in the record of detailed core descriptions in Appendices A, B and C. The report of the palynological analyses by Gilbert J. Brenner for Potomac Group samples from all three cores is provided in Appendix D.

SUMMARY OF CE Cd 91 (ELK NECK CORE HOLE)

A diagram showing a generalized lithologic column for CE Cd 91 with recovery, select borehole geophysical logs (gamma ray, single-point resistance, induction-conductivity, and 16- and 64-inch normal resistivity logs) and palynological samples and zones is provided in Appendix A, Plate A-1. Total depth drilled was 590 ft. Recovery was approximately 60 percent. Geophysical logs extend to depths of 568.5 ft or slightly less. Photographs of boxed core are provided in Table A-1. A detailed lithologic log, recorded largely in the field is provided in Table A-2. A summary of the palynological results is provided in Table 4.

CE Cd 91 Basement Rock and Saprolite

In borehole CE Cd 91, approximately 101 ft of weathered rock and saprolite were encountered between depths of approximately 590 and 489 ft. The lowermost 10-ft interval (590 to 580 ft) is slightly weathered mica gneiss, mainly gray and white with some distinctively greenish (possibly epidote-rich) intervals. Where banding is apparent it is often dipping at about 45 degrees. From depths of 580 to

Table 4. Summary of palynological analyses[1] of core subsamples from CE Cd 91.

Sample Number	From depth (ft)	To depth (ft)	Sample ID	Stage	Palyno-zone	Geologic Unit	Paleoecology	Pollen Recovery	Paleoclimate
1	17.5	17.6	106487	Lower Cenomanian	III	Upper Patapsco	non-marine, deltaic	poor	subtropical humid
2	20.0	20.1	106488	Lower Cenomanian	III	Upper Patapsco	non-marine, deltaic	poor	subtropical humid
3	76.85	77.0	106489	Albian	IIB	Patapsco	non-marine, deltaic	poor	subtropical humid
4	110.0	110.15	106490					essentially barren	
5	123.0	123.1	106491	Albian	IIB2	Patapsco	non-marine, deltaic	poor	subtropical humid
6	161.3	161.4	106492					*[no analysis]*[2]	
7	271.5	271.6	106493	Albian	IIB	Patapsco	non-marine, deltaic	fair	subtropical humid
8	281.7	281.8	106494	Albian	IIB	Patapsco	non-marine, deltaic	very poor	subtropical humid
9	331.2	331.3	106495					*[no analysis]* [2]	
10	338.5	338.6	106496					*[no analysis]* [2]	
11	384.3	384.5	106497	Aptian	I	Patuxent-Arundel	non-marine, deltaic	very poor	subtropical humid
12	390.8	390.9	106498					essentially barren	
13	441.0	441.2	106499	Aptian	I	Patuxent-Arundel	non-marine, deltaic	good	subtropical humid

[1] Based on final report from Dr. Gilbert Brenner, consulting palynologist; see Appendix D.
[2] Inadequate pollen in processing phase; no slide prepared for analysis (see Table D-1).

570 ft, the gneiss appears more weathered with a highly fractured/weathered interval occurring about 576 ft.

A distinct color change from gray and white to predominantly brownish hues occurs at a depth of approximately 570 ft. From depths of 570 to 490 ft, the core is characterized by intervals of reddish brown, yellowish brown, grayish brown, white, and light gray, severely weathered rock (possibly schist, which in a few places appears to retain faint foliation and/or relict banding) and saprolite. The saprolite tends to be clayey to silty and micaceous with abundant fine-gravel-sized quartz and lithic fragments. On the natural gamma log, a strong negative deflection is recorded at about 494 to 492 ft; to a lesser extent, there is a corresponding increase in resistivity on the short (16-inch) normal resistivity log. In the core at approximately this depth there is an interval of very soft to soft, sandy, gravelly, clay-silt that includes a thin (about 0.6-inch- /1.5-cm-thick) dipping layer of concentrated smokey quartz fragments. A couple feet of highly weathered rock and saprolite occur above this interval.

CE Cd 91 Potomac Group

The boundary between the saprolite and the Patuxent-Arundel Formations appears to occur at a depth of about 489 ft (an approximate elevation of -314 ft NAVD 88) where there is a change in texture from the faint layering of the saprolite to the poorly sorted, micaceous, gravelly, sandy clay to muddy sand. Overall, however, the transition from saprolite to Patuxent-Arundel sediments is not very distinct and appears to be somewhat gradational with the lowermost Patuxent sediments containing material that appears to be derived from saprolite and weathered basement rock.

From the base of the Potomac Group at 489 ft up to an approximate depth of 463 ft, there are a series of variably sandy to silty clays with lesser clayey sands and silts. In general, these sediments are weakly to moderately mottled in subdued shades of red, gray, tan, and white, although there is a distinctive interval of white silt (approximate depths of 469 to 467 ft) in sharp contact with an underlying medium bed (0.85-ft- /26-cm-thick) of dark red, sandy clay in which mottling is minimal. For the most part, sediments from this interval appear to be consistent with the mottled silts and clays facies of McKenna and others (2004) which is interpreted as ancient weathered floodplain deposits with paleosols.

Sediments between depths of approximately 463 and 442 ft are mainly sandy. Geophysical log patterns show a general fining-upward sequence followed by a coarsening-upward sand. Within the lower fining-upward sequence (463 to 450 ft) there are smaller fining-upward cycles. Core from the lower sequence is very micaceous, predominantly light gray and ranges from sand and gravel at the base to laminated (horizontal to inclined) and/or cross-laminated, variably silty, very fine to fine sands at the top. The overlying sands from approximately 450 to 442 ft coarsen upward and are mainly light gray, variably silty to clayey and subtly laminated. Overall sands in this interval (463 to 442 ft) appear to share characteristics of thin sands facies of McKenna and others (2004) (e.g., sand intervals generally less than 10 ft thick, coarse to very fine grain sizes, generally fining upward). McKenna and others (2004) interpreted the depositional environment of this facies as crevasse splay/proximal levee. Zullo (2012) identified a similar splay/levee facies, which included both fining and coarsening-upward sequences.

Two thin beds of distinctive clays – a lower, dark bluish gray, silty clay with minor mottling/burrowing and an overlying laminated, red and gray, silty clay – occur between depths of 442 and 439 ft. A palynological sample from the dark bluish gray clay at depths of approximately 441 ft was identified as Zone I. The dark gray, mottled clay, which contains minor amounts of fine, black, carbonaceous particles and fine sand, suggests deposition in some poorly drained, low energy interfluvial environment such as back swamp or lake/pond (Smith and Smith, 1980). In contrast, the laminated (inclined but parallel) red and gray mud suggest exposure to an oxidizing paleoenvironment not subject to rooting and/or burrowing. While many laminated mudstones have been associated with quiescent slackwater environments such as abandoned channels and floodplains (episodic deposition from floods), some recent flume studies suggest laminated muds may be deposited in some flowing conditions (e.g., Schieber and Yawar, 2009; Yawar and Schieber, 2017). Thus the gray and red laminated muds may reflect deposition in flowing water followed by subaerial weathering.

The silty clays are overlain by another fining-upward sandy sequence (439 to 424 ft), within which are two smaller fining-upward sequences. Overall, sediments are characterized by variably silty to clayey, very fine- to medium-grained sands that are thinly bedded, generally color banded (pale red and tan mainly

toward the bottom; light gray and yellowish brown toward the top) and occasionally mottled. In the lower sandier portion, tiny mica flakes are common in some intervals. A few yellow-brown (limonite?) cemented laminations are present in the upper few feet and tan, coarse-sand-sized spherules (probably siderite) are common in some intervals. The term sphaerosiderite is used here to refer to these tan spherules that appear to be roughly millimeter-scale, spherical aggregates of siderite crystals. The overall irregular, but generally fining-upward pattern of the geophysical logs is similar to the thin sands lithofacies of McKenna and others (2004) interpreted as crevasse splay/proximal levee depositional environments; but it is also possible that sediments in this interval represent deposits of several paleoenvironments (for example, a small channel-fill sand at the base overlain by various floodplain deposits) and pedogenesis.

The increasingly clayey and fine-grained sands grade upward into multicolored, mottled clays and clay-silts that occur between depths of approximately 424 and 394 ft. The mottled clay-silts contain many features characteristic of paleosols facies of Zullo (2012) including root-like structures, abundant tan sphaerosiderite in places, some dark gray and red hematite nodules and cement, and occasionally black carbonaceous/charcoal fragments.

Interlayered to interlaminated carbonaceous sands occur between depths of approximately 394 to 381 ft. These sediments are characterized by micaceous, dark to medium gray, very fine to fine sands that are variably silty to clayey and contain fine, black, carbonaceous particles throughout. Black carbonaceous particles are also occasionally concentrated in laminated layers and a very thin bed of charcoal/lignitized or carbonized wood occurs at the base of the interval that forms a sharp contact with the underlying mottled clays. This interval has some characteristics of the splay levee facies of Zullo (2018) in which very fine to fine sand dominates, charcoal is common and some intervals are interlaminated with silt and clay. Zullo notes this splay/level facies has similarities to both the interlaminated sand and silt facies (interpreted as interpreted as distal levee/floodplain) and the thin sand facies (interpreted as crevasse splay/proximal levee) of McKenna and others (2004). An irregular geophysical log pattern is common to these facies. A palynological sample from depths of 384.5 to 384.4 ft was identified as Zone I.

The contact between the carbonaceous sands and the overlying silts and clays is fairly sharp (within core run 62 at an approximate depth of 381 ft). At the bottom of this interval there is a bed of very stiff, gray clay-silt that is faintly wavy laminated to mottled. Overlying this bed are variably sandy, silty clays that extend up to approximately 359 ft. These sandy, silty clays are weakly to strongly mottled and multicolored. In a few intervals, coarse sand-sized spherules, both tan and red (sphaerosiderite and hematite), are abundant (depths of 372 to 370 ft, for example), however, red spherules may be only hematite oxidation rims over sphaerosiderite as was reported by Sugarman and others (2004) in Potomac Formation paleosol deposits at Fort Mott, New Jersey. Hematite rimmed siderite may be the result of initial soil development in more poorly drained conditions followed by improved drainage and oxidizing conditions (Kraus, 1999).

Recovery was very poor in the 360- to 350-ft interval due to a cobble stuck in the end of the core barrel, but material recovered consisted of silt-clay and gravel. The geophysical log patterns suggest the gravelly interval occurs between depths of about 359 to 355 ft and that it was overlain by a muddy (silt-clay) interval from depths of approximately 355 to 347 ft.

The overlying 10-ft interval between depths 347 and 339 ft generally fines upward but includes a few smaller fining-upward cycles. The base of the interval is a sandy gravel that grades upward to sandy, silt-clay which is mainly light gray but mottled/stained in light yellowish- to olive-brown colors (depths of about 347 to 343 ft); the subsequent small fining-upward cycles grade from clayey, silty, fine to coarse sands to sandy silt-clays (approximately 343 to 339 ft).

A series of predominantly muddy sediments dominates from depths of about 339 and 289 ft. While many of the clay-silts are dominated by yellowish red hues, the intensity and strength varies considerably. Between depth of 339 and 320 ft there are two distinct silt-clay intervals: a lower, weakly mottled clay-silt (339 to 329 ft) (subtle grays, grayish brown and reddish gray colors) that has sharp upper contact with an overlying very stiff, generally mottled, reddish clay (329 to 320 ft) which contains sand-sized red and white/tan spherules and minor black carbonaceous material particularly concentrated toward the base. Two palynological samples from the lower clay-silt (samples from 338.6 to 338.5 ft and 331.3 to 331.2 ft) were found to be

barren. Strongly mottled and multicolored, variably sandy, silts and clays interlayered with a few beds of mainly gray, silty, clayey fine sands occur between depths of 320 and 294 ft. Coarse-sand-sized spherules are common; sphaerosiderite is dominant but red, presumably hematite, spherules are also present. A stiff, mottled, red and light gray clay occurs between 294 and 289 ft which has a slightly higher gamma signature than the underlying silts and clays. Overall, these mottled silts, clays and muddy fine sands appear consistent with lithofacies interpreted as weathered floodplain deposits with paleosols (McKenna and others, 2004).

Gray, variably sandy, silts and clays are present between depths of 289 and 275 ft. These sediments vary from mottled to interlayered or interlaminated (convoluted, wavy and horizontal) and contain charcoal and carbonaceous particles in a few limited intervals. The convoluted to wavy layers in the lower part of the interval suggest possible soft-sediment deformation. The medium to dark gray color, clay-rich sediments with lesser fine sandy silts and carbonaceous material suggests a generally low energy, reducing, interfluvial environment with limited influx of fine sandy to silty sediments such as back swamp or lake/pond (Smith and Smith, 1980). This interval has some characteristics of the frequently flooded lake/abandoned channel lithofacies of Zullo (2018) with sand more common toward the lower portions recovered and increasingly stiff clay upward. Geophysical logs show a more varying zig-zag pattern with and overall trend of increased resistivity and lower gamma upward suggesting more variation in lithology than appeared in recovered material. A sample from approximately 282 ft (281.8 to 281.7 ft) was the lowest identified palynological Subzone IIB sample in the core. A slightly shallower sample (corresponding to a depth of 278.4 to 278.3 ft) from an interval of very stiff, silty clay, also contained palynomorphs identified as Subzone IIB.

A thin fragmented layer of ironstone and partially cemented sand occurs at the base of a bed of sand that geophysical logs suggest is approximately 4 ft thick (depths of 275 to 271 ft). Recovery was poor. Ironstone and cemented sands are black to dark reddish brown; the limited material recovered from the very top of the sandy interval was fine to coarse grained, very clayey, and light brownish gray in color. An interval of silty clay exists between depths of about 271 to 264 ft. Color varies from mottled light gray and white at the base to white to mottled red, reddish gray and white. Intervals of dark red-brown nodules of hematite occur toward the top.

In CE Cd 91, the thickest interval of predominantly sandy sediments occurs between depths of approximately 264 to 210 ft. In this interval there are two sandy sections separated by about seven feet of interlayered finer sediments. The lower sandy interval (from 264 to 248 ft) is characterized by multicolored (dark reddish brown, black, brown and orange-brown) sand and iron-cemented sand. This lower sandy section is overlain by interlayered silty clays, sands and ironstone. Silty clays are mainly white and pale brown to yellowish brown but a few thin beds of clay adjacent to ironstone are also purplish. The overlying upper sandy section from depths of 241 to 210 ft is characterized by light gray to red, sands that are mainly medium- to coarse-grained, but range in grain size from very coarse to fine, with small fining-upward and occasionally coarsening-upward cycles on the scale of a few feet. The natural gamma log displays an overall blocky pattern from approximately 264 to 210 ft; however, the resistance and resistivity logs, while generally high signals, tend to show more irregular patterns with an overall fining-upward trend in the upper half. The lower sands tend to be more consistently fine to medium grained as well as significantly iron cemented, whereas the upper sand is more variable in grain size and distribution which may account for some of the difference in the log patterns. Overall, the sediments appear to be a fluvial channel deposit that shares characteristics with the amalgamated sand facies of McKenna and others (2004) interpreted as amalgamated channel depositional environment (e.g., sand interval 30 to 70 ft thick with internal fining-upward packages on the order of 3 to 10 ft; sharp base, abrupt top; mostly fine to medium sand and less common coarse and very coarse sand; blocky geophysical log pattern).

Between depths of 210 and 200 ft are irregularly interlaminated to interlayered sands and silt-clays, primarily white to light gray and yellow brown in color. A few thin layers of red and tan spherules are present. The overlying interval is a distinctive 1.6 ft of light gray, red, pale red, and yellow, laminated to wavy laminated, silty clay. The laminated clay is overlain by a partially mottled silty clay that grades up into an thick interval of increasingly mottled and variegated (reds and white) silty clay up to a depth of about 165 ft. Some intervals include hematite nodules, wavy laminations and paleosol structures (e.g., root traces, infilled cracks).

A thin (less than 1-ft-thick) bed of brown sand bearing lignite and minor pyrite lies at the base of a thick weakly mottled, gray and brown clay that extends up to about 159 ft depth. The gray clays grade into increasing reddish and then intensely mottled to wavy laminated, red and white silty clays that extend up to 129 ft where they grade into a very weakly mottled, light gray and pale red, silty clay. Dark red-brown spherules to nodules (presumably hematite) occur throughout the mottled clays.

A medium to dark gray, variably sandy, silty clay occurs from approximately 124 to 103 ft. The clay includes a minor amount of black, carbonaceous fragments and a few dark reddish brown ironstone fragments and nodules. The lower contact, which is a distinct color change (from the underlying red and white clays), is fairly sharp although a subtly mottled appearance and some burrow-like structures are most apparent in the lower foot (124 to 123 ft). This clay seems to be a floodplain deposit in a more poorly drained area. It may correspond to the more silty to clayey components of the interlaminated sand and silt facies of McKenna and others (2004). A palynological sample from 123 ft contained Subzone IIB2 palynomorphs.

Interbedded to interlaminated brown, variably silty sand and medium to dark gray, silty clays occur from depths of approximately 103 to 70 ft. The geophysical log patterns are generally irregular. These sediments appear to be similar to the interlaminated sand and silt facies of McKenna and others (2004), interpreted as a distal levee/floodplain depositional environment. A palynological sample from depths of 77.0 to 76.85 ft was the highest sample identified as Subzone IIB.

A light gray, variably silty, very fine- to fine-grained sand occurs from about 70 to 62 ft. This sand has some faint laminations/cross laminations and a few pyrite grains. Overall the sediments fine upward. This interval may be comparable part of a thin sands facies of McKenna and others (2004) interpreted as a crevasse splay/proximal levee depositional environment.

From depths of 62 to 45 ft, mottled and occasionally laminated to wavy laminated, red and light gray, variably sandy clay occurs. Tan and red, sand-sized spherules and occasional red nodules (hematite and sphaerosiderite) are abundant in places. There are numerous apparent paleosol structures (e.g., root structures and infilled cracks).

The geophysical logs suggest that the interval between depths of 45 and 20.3 ft may include interlayered silt-clays and sandier intervals, however, recovery was intermittent and presumably was poor in the sandier intervals of which there are little represented in the core. Much of the recovered core at these depths contained variably sandy and silty clays mottled in red and light gray with paleosol structures, some tan sphaerosiderite, and to a greater extent, red hematite spherules, and rare pyrite. There were two intervals of mainly light gray, variably silty clay that contained trace, irregular, black, hair-like manganese (?) strands. Some portions were very weakly mottled to faintly wavy laminated.

Silty clays recovered between depths of 20.3 and about 14.4 ft were mainly medium to dark gray with black, carbonaceous fragments occurring throughout and occasionally concentrated in thin layers or laminae. The silty clays vary from subtly mottled toward the base to layered and/or bioturbated toward the top. Two palynological samples from this interval (depths of 20.1 to 20.0 ft and 17.6 to 17.5 ft) contain Zone III palynomorphs. The dark muddy sediment with abundant charcoal, faint mottling to lamination, possible bioturbation in areas suggests a low energy environment; the concentration of carbonaceous material in layers suggests periodic input along the lines of the frequently flooded lake/abandoned channel lithofacies of Zullo (2018) or possibly a backswamp facies.

The dark gray, carbonaceous silty clay appears to be overlain by a convoluted, possibly bioturbated, brown, silt and clay. A thin bed of siltstone (estimated from drilling conditions to be about 0.5 ft thick) occurs between 14 and 12 ft. Otherwise most of this interval is missing. Overlying sediments from 12 to 5 ft depths are coarse-to fine-grained, brownish yellow sands and gravelly sands. Gravelly sands are more common toward the base. The interval from 5 ft to land surface was not cored. Surficial sediments in the immediate site area were mapped as the Potomac Group, however, in the vicinity, thin remnants of the Pensauken(?) formation have been mapped (Higgins and Conant, 1986).

SUMMARY OF CE Be 155 (WESTERN ELKTON CORE HOLE)

A diagram showing a generalized lithologic column for CE Be 155 with recovery, select borehole geophysical logs (gamma ray, single-point resistance, and 16- and 64-inch normal resistivity logs) and

palynological samples and zones is provided in Appendix B, Plate B-1. Total depth drilled was 202.83 ft. Recovery was approximately 47 percent. Geophysical logs extend to depths up to 202.4 ft. Photographs of boxed core are provided in Table B-1. A detailed lithologic log, recorded largely in the field is provided in Table B-2. A summary of the palynological results of the subsamples from the Potomac Group is provided in Table 5.

CE Be 155 Basement Rock and Saprolite

In core hole CE Be 155, the deepest material recovered (202.83 to 202.3 ft) appeared to be severely weathered basement rock. Fragments of rock and thin semi-indurated layers suggest basement rock may be a muscovite, biotite, quartz gneiss. Material recovered from depths of 202.3 to 170.7 ft appears to be saprolite with some rock fragments; recovery in this interval was generally poor. Saprolite recovered varies from clayey, silty sand to clay-silt; one clay-silt layer had a talc-like feel when fresh. In general, saprolite is light to medium gray or greenish gray and micaceous.

CE Be 155 Potomac Group

In core hole CE Be 155, the contact between the base of Potomac Group strata and saprolite is interpreted to occur at a depth of about 171 ft (an approximate elevation of -150 ft NAVD 88), at the sharp contact between a light greenish gray interval of mica, silt-clay, sand-sized quartz grains (interpreted as saprolite) and an overlying grayish brown sand (interpreted as Potomac Group). The thickness of basal sandy interval is estimated to be about 4 ft from a combination of material recovered and the geophysical log pattern.

The contact between the basal Potomac sand and the overlying sequence of predominantly clays is estimated to occur at a depth of 167 ft from the geophysical log pattern. A cobble-sized piece of smokey quartz stuck in the drill shoe limited full recovery in core run spanning depths of 170 to 165 ft. The predominantly clayey intervals extend from the top of the quartz cobble up to approximately 151 ft. The lowermost portion (approximately 167 to 159 ft) is a mottled to convoluted, yellowish brown and gray, clay that is increasingly sandy upward and grades into to a thin bed of clayey, silty sand. From depths of approximately 159 to 155, silty clays are weakly mottled shades of red, reddish brown, and dark gray with coarse-sand-sized red and, to a lesser extent, tan spherules and nodules of hematite and presumably siderite. Limited material recovered between 155 and 151 ft indicates there are clayey sediments with a thin iron-cemented layer present. Sediments in this interval appear to be consistent with variably weathered floodplain deposits.

Table 5. Summary of palynological analyses[1] of core subsamples from CE Be 155.

Sample Number	From depth (ft)	To depth (ft)	Sample ID	Stage	Palyno-zone	Geologic Unit	Paleoecology	Pollen Recovery	Paleoclimate
1	77.7	77.85	110501					*[no analysis]* [2]	
2	82.10	82.25	110502					*[no analysis]* [2]	
3	86.85	87.0	110503					barren	
4	92.50	92.65	110504[3]	Albian	IIB-2	Upper Patapsco	Tree fern forest, non-marine, deltaic	poor	subtropical humid
5	128.20	128.35	110505					barren	
6	132.55	132.7	110506	Albian	IIB-2	Patapsco	Non-marine, deltaic	fair	subtropical humid
7	138.05	138.15	110507					barren	
8	140.0	140.15	110508	Albian	IIB-2	Patapsco	Non-marine, deltaic	good	subtropical humid

[1] Based on final report from Dr. Gilbert Brenner, consulting palynologist; see Appendix D.
[2] Inadequate pollen in processing phase; no slide prepared for analysis (see Table D-1).
[3] Depth of sample 110504 based upon drilling record of estimated position of the recovered core material within core run.

An interval of sand occurs from depths of 151 to 140.85 ft. The limited material recovered indicates sands range in grain size from coarse to fine but may be primarily fine to medium grained. Sands are wavy laminated to color banded (light yellowish brown with brown and gray). Sands grade up into thin interval of wavy interlaminated to interlayered silt-clay and sand which is topped by a very thin iron-cemented layer. A very thin bed (0.1 ft) of soft, gray, silty clay occurs above the cemented sand. The upper contact of the soft clay with the overlying very firm clay is sharp. The gamma log pattern is a low, fairly smooth, cylindrical or blocky shape common to fluvial channels with fairly uniform deposition; resistivity logs show corresponding increases.

A very firm, very dark to dark gray, silty clay spans depths of approximately 140.5 to 138.2 ft corresponding with a gamma spike and, to a lesser extent, a corresponding decrease in the signal on the resistance and resistivity logs. A palynological sample from a depth of approximately 140 ft was determined to contain Subzone IIB-2 palynomorphs. This is the deepest sample submitted for palynological analysis in CE Be 155. The subsequent interval (depths of 138.2 to about 122 ft) is characterized by interlayered silt-clays, very fine to fine sands, and carbonaceous material (carbonized wood/charcoal/lignite). Black woody fragments occur throughout in addition to being concentrated in thin beds. While most of the carbonaceous material appears to be charcoal, a few layers are more peat-like, including an interval at the top where there is a gamma peak. Sands are variably silty to clayey. Both sands and silt-clays tend to be mottled and medium to dark gray. Overall, layers tend to be inclined except toward the top of the interval, where the sediments are interlaminated and nearly horizontal. Pyrite is present at a depth of about 129 ft. Three samples were submitted for palynological analyses within depths of 138.2 to about 122 ft but only one had sufficient palynomorphs to analyze. The palynological sample from a depth of approximately 132.6 ft was determined to represent palynological Subzone IIB-2. Sediments from depths of 140.5 to about 122 ft share some characteristics of Zullo's (2012) frequently flooded lake/abandoned channel facies with medium to dark gray colors and presence of pyrite suggesting reducing environments, interlayered fine sands with the silt-clays suggesting some periodic inputs of sands and carbonaceous material by flooding into to a floodplain lake/abandoned channel or backswamp environment.

Geophysical logs indicate a sand interval occurs between depths of 122 and 111 ft. The gamma log pattern is fairly low and cylindrical/blocky with resistivity logs showing a corresponding peak. Recovered core material is limited but suggests sediments in this interval are mainly light gray sands that are variably gravelly and contain some silt-clay clasts and ironstone. The sediments and geophysical log pattern are consistent with characteristics of a fluvial channel deposit. Immediately above this sand are two thin but distinct layers: an interval of wavy laminated to mottled, red-brown and gray, clayey silts with hematite spherules/nodules (about 0.6 ft thick) suggesting a paleosol and a muddy, gravelly, coarse-grained sand (about 0.4 ft thick).

Sediments between depths of 110 and 100 ft are interlayered to wavy laminated and mottled, silt-clay and very fine to fine sands. Sediments have yellowish hue (iron stained?) from about 110 to 104.5 ft and several thin iron-cemented laminae occur in this interval. There is a sharp change in color at about 104.5 ft and sediments above are gray and lack cemented laminae. A bed of gray, very fine to fine sand occurs between depths of 103 and 100 ft. This sand is slightly silty to clayey and contains a few fragments of lignite and/or possibly charcoal. There is a low gamma signal opposite this sand bed. Sediments between depths of approximately 110 and 100 ft have some characteristics of the splay/levee facies of Zullo (2012) (silt and clay interbedded with very fine to fine sand; typically gray to light gray color; some intervals with laminations or small scale cross-stratification; some silt-clay intervals are burrowed; charcoal is common). Zullo (2012) notes that her splay/levee facies includes some characteristics of both the interlaminated sand and silt and the thin sands lithofacies of McKenna and others (2004). The very fine to fine sand appearing as a distinct short decrease in gamma value amidst higher gamma ray values on the geophysical logs (depths of 103 to 100 ft) may correspond to the separate splay channel facies of Zullo (2012).

Between depths of 100 and 70 ft, sediments are predominantly weakly mottled to faintly laminated, silty clays. The color varies from medium to dark grays at the base to increasingly brown and then reddish brown toward the top. In the uppermost foot, the clays are variegated light gray and pinkish brown. Fragments of lignite and/or charcoal are particularly common in the dark gray to brown intervals;

occasionally lignite/charcoal is concentrated in a thin layer. A palynology sample from 90.65 to 90.5 ft was identified as Subzone IIB-2. Three palynology samples between depths of 87 and 77 ft (where clays are increasingly brown to reddish brown) were barren. These silty clays appear to be floodplain deposits that transition from a more reducing depositional environment of the dark colored clay-silts toward the base (possibly akin the proximal floodplain paleosol subset of Zullo, 2012) to a more oxidizing environment of the reddish clays toward the top. Thus the variations in these clays appear to reflect influences of the environment of deposition and subsequent pedogenesis including post-depositional variations in drainage/water table, as recognized in many Potomac paleosols (e.g., Thornburg and others, 2019).

Fragments of black and reddish brown ironstone at the top of the core run from 75 to 70 ft may be from the 70-to-65-ft interval where recovery was poor. Geophysical logs along with limited core suggest that between depths of approximately 70 and 64 ft there are 6 ft of light gray sands that first coarsen upward and then fine upward and grade into an interval of sandy, clayey silts that extend from depths of about 64 to about 58 ft, based on the gamma log signal. In general, the silts are very pale brown/tan with some orangey brown, inclined, thin bands/laminations and faint mottling. Red hematite spherules and nodules are present in a thin interval at a depth of approximately 61 ft. The interval from approximately 70 to 64 ft may represent a splay channel with subsequent pedogenesis.

The stratigraphic assignment of sediments between depths of about 58 and 19 ft are uncertain. They are tentatively placed in the Potomac Group but may represent a younger unit. Approximately 32 ft of sand occur between depths of about 58 to 26 ft. The limited core recovered from this interval is characterized by white to very pale brown/tan, fine to medium sands with trace silt-clay toward the bottom and trace fine gravel toward the top. The gamma log has a low, cylindrical/blocky pattern with a sharp base and abrupt top that would be consistent with the pattern seen in the amalgamated sand facies of McKenna and others (2004). It is not clear, however, why the resistance and resistivity logs also have relatively low signals although perhaps surface water quality/characteristics have influenced groundwater (e.g., proximity to oligohaline Elk Neck River). Nevertheless, resistivity logs do show a slight increase in signal upward which suggests sands coarsen and/or less clay-silt lessens upward. Laminated to thinly bedded, clayey silts and very fine to fine silty sands are present from depths of approximately 26 to 19 ft. The interval is color banded with light gray dominant and lesser orangey tan to brown.

CE Be 155 Lowland deposits (former Talbot Formation)

The surficial unit at this site is the coarse-grained facies of the Lowland deposits. The informal name Lowland deposits is used for deposits formerly mapped as Talbot Formation (Higgins and Conant, 1986), a name currently in disuse. Higgins and Conant (1986) considered these deposits fluvial in origin and Quaternary in age. In the core, the base of this unit is interpreted to occur at a depth of 19 ft (+2 ft NGVD), at the base of a gravel layer. Core material recovered between depths of 19 and about 9 ft are mainly subrounded gravels and brown sands. Interlayered fine- to coarse-grained sands and clayey silts occur from 9 to 4 ft. Sediments are generally micaceous with some relatively large flakes in some sands.

SUMMARY OF CE Bf 156 (EASTERN ELKTON CORE HOLE)

A diagram showing a generalized lithologic column for CE Bf 156 with recovery, select borehole geophysical logs (gamma ray, single-point resistance, and 16- and 64-inch normal resistivity logs) and palynological samples and zones is provided in Appendix C, Plate C-1. Total depth drilled was 200 ft. Recovery was approximately 64 percent. Geophysical logs extend to depths up to 199.7 ft. Photographs of boxed core are provided in Table C-1. A detailed lithologic log, recorded largely in the field is provided in Table C-2. A summary of the palynological results of CE Bf 156 samples from the Potomac Group is provided in Table 6.

CE Bf 156 Basement Rock and Saprolite

In core CE Bf 156, nearly 30 ft of weathered rock and saprolite were encountered between depths of 200 and 170.4 ft. Core from depths of 200 to 175 ft was very light to dark green, variably weathered and variably indurated basement rock. Presumably this material is part of the gabbro and serpentinite unit mapped in outcrop at Grays Hill by Higgins and Conant (1986) approximately 0.5 miles north of the drill site. The weathered basement rock appears to

Table 6. Summary of palynological analyses[1] of core subsamples from CE Bf 156.

Sample Number	From depth (ft)	To depth (ft)	Sample ID	Stage	Palyno-zone	Geologic Unit	Paleoecology	Pollen Recovery	Paleoclimate
1	40.05	40.2	110489	Lower Cenomanian	IIC-III	Upper Patapsco	non-marine, deltaic	poor	subtropical; humid
2	71.35	71.5	110490	Albian	IIB	Upper Patapsco	non-marine, deltaic	poor	subtropical; humid
3	75.05	75.2	110491					essentially barren	
4	80.0	80.15	110492	Albian	IIB	Upper Patapsco	non-marine, deltaic	poor	subtropical; humid
5	86.6	86.75	110493					*[no analysis]* [2]	
6	92.1	92.2	110494					*[no analysis]* [2]	
7	96.45	96.55	110495					*[no analysis]* [2]	
8	160.0	160.15	110496					*[no analysis]* [2]	
9	163.9	164.0	110497	Albian	II	Patapsco	non-marine, deltaic	poor	subtropical; humid

[1] Based on final report from Dr. Gilbert Brenner, consulting palynologist; see Appendix D.
[2] Inadequate pollen in processing phase; no slide prepared for analysis (see Table D-1).

grade upward into a light gray to greenish gray clay-silt saprolite. Recovery in the interval between 175 and 170.4 was poor (less than 1 ft recovered). Saprolite is estimated to be only a few ft thick from the geophysical logs.

CE Bf 156 Potomac Group

In core hole CE Bf 156, the contact between the top of saprolite and the base of Potomac Group strata is interpreted to occur at a depth of approximately 170.4 ft (corresponding to an elevation of -91.4 ft NAVD 88), where the resistivity and resistance logs show a marked increase. Core recovered from the 170.4-to-166.9-ft interval, although limited, shows a distinct change in lithology from silty clay of the uppermost saprolite to basal gravel overlain by tan to orangey brown sands (Potomac Group). The gravel may represent a lag deposit associated with newly avulsed fluvial channel. The sands (from depths of 170.2 to 166.9 ft), while only several feet thick, coarsen and fine repeatedly, generally coarsening upward from a fine to medium sand to a coarse sand with fine gravel, then fining upward to a laminated and cross-laminated slightly clayey and silty, fine to medium sand, and ultimately coarsening again. The geophysical logs show an increase in resistance/resistivity and a decrease in gamma signal opposite this sandy interval. A very thin ironstone crust at an approximate depth of 167.3 ft marks an abrupt color change from an orangey brown color below to medium gray above within the uppermost fine to coarse sand. With the range in sand grain sizes, thin beds, and fining-upward cycles, these sands share some characteristics with the thin sands facies (crevasse splay/proximal levee deposits) of McKenna and others (2004). Zullo (2012) notes fining- and coarsening-upward intervals may reflect progradation and abandonment, respectively, of a splay or levee, however, in contrast to McKenna and others (2004) the grain size of sediments in the splay-level facies of Zullo (2012) do not exceed fine sand. The fine- to coarse-grained sands in CE Bf 156 are more consistent with grain sizes in Zullo's fluvial channel facies.

The basal gravel and sands are overlain by several feet of gray, interlayered and bioturbated(?)/ convoluted clayey silts, fine sands, and sandy, silty clays (approximate depths of 167 to 163 ft) grading up to an interval of medium gray, faintly mottled, slightly sandy, silty clays with a few thin laminations of silty fine sand (depths 163 to 158 ft). A sample from a depth of approximately 164 ft contained Zone II (Albian age) palynomorphs. A second sample from a depth of 160 ft did not contain sufficient

palynomorphs for analysis. Geophysical logs and limited core recovered between 158 and 151 ft suggest the interval is characterized by interlayered silty sands and sandy, clay-silts.

A 46-ft-thick sand sequence occurs from depths of approximately 151 to 105 ft. The lower 18 ft (approximate depths of 151 to 133 ft) are tan to pale yellow, fine- to coarse-grained sands with minor ironstone and silt-clay. Sands from approximate depths of 133 to 120 ft are generally very pale brown, faintly laminated to bedded, fine to medium sands. Sands from 120 to 105 ft show increasing effects of iron staining upward. These sands are characterized as multicolored (reds, browns, orange, black), mainly fine to medium grained and contain thin iron-cemented layers toward the top. Overall, the gamma log over this 46-ft shows a relatively low, smooth, blocky pattern which would be expected of quartz-dominated sands with few fines and micas. It is not clear, however, why the response of the resistance/resistivity logs is rather subdued compared to other sands in this borehole; possibly groundwater in these sands have a higher concentration of total dissolved solids than other intervals. The low, blocky/cylindrical gamma signal, thickness of the overall sand interval, predominantly fine to medium grain size, occasional cross-lamination to cross bedding is suggestive of the amalgamated sand facies of McKenna and others (2004).

There is a sharp gamma peak between depths of 105 and 103 ft. Recovery in this interval was limited but includes a clayey silt that may correspond to this peak. Sediments recovered between 105 and 99 ft are variegated, wavy interlaminated sands, silt-clays and ironstone/iron-cemented sand laminae.

Between depths of approximately 99 and 42 ft there are a variety of interlayered sands and silt-clays with a range of weathering, iron staining, and iron cementation. In some intervals sandy beds are more dominant and in others finer grained sediments are more common. The lowermost 18 ft (depths from 99 to 81 ft) are irregularly interbedded and interlaminated tan to yellow, fine sands and gray silty clays. Three samples submitted for palynological processing from the 97 to 86 ft interval did not contain sufficient palynomorphs for analysis. The interval from 81 to about 70.2 ft has an increase in clay beds compared the interval below and sediments are characterized by interlayered gray, silty clay and gray fine sand. Palynological samples from approximately depths of 80 and 71 ft were found to contain Subzone IIB (Albian age) palynomorphs; the sample from a depth of 75 ft was essentially barren. The geophysical log pattern from depths of 99 to 70.2 ft is irregular but shows a slight decrease in resistance and resistivity opposite the more clayey section (81 to 70.2 ft). In the overlying interval (depths from approximately 70.2 to 42 ft), sandy layers are more prevalent and overall the interval appears to be modified by pedogenenis. The increase in sand layers is reflected in an increase in resistance/resistivity and slight decrease in gamma log signatures. This interval is characterized by interlayered, multicolored (yellow, red, tan, orangey brown, very light gray), fine sands and silty clays with some thin layers (laminae to thin beds) of dark reddish brown to black, ironstone and partially cemented sands. The sands first coarsen upward (from very fine and fine grained to fine and medium grained) and then fine upward (to very fine to fine grained with an increase in clay and silt). There is a corresponding increase and subsequent decrease recorded in the resistance and resistivity logs. A thin layer (about 0.25 ft) of brown ironstone is present at a depth of approximately 53 ft. Toward the top (approximate depths of 45 to 46 ft), sand-sized spherules of siderite/sphaerosiderite(?), predominantly tan to light gray in color, were abundant in a bed of light gray, clayey, silty, very fine to fine sand.

Overall, the interlayered sands and silt-clays display some characteristics of the splay/levee facies of Zullo (2012) which, in turn, has some characteristics of both the interlaminated sand and silt facies and the thin sands facies of McKenna and others (2004). In this core, the lower interval (99 to 70.2 ft) appears most similar to the interlaminated sand and silt facies (distal levee/floodplain deposits) of McKenna (2004) with thin beds, predominance of fine sediments (silty clay and fine sand), and irregular log pattern. The upper interval (70.2 to 42 ft) shares characteristics with the thin sands facies (crevasse splay/proximal levee) of McKenna and others (2004) with the irregular log pattern, individual sands typically 1 to 3 ft or less, and very fine to medium grain size. This interval also shows the coarsening-upward and fining-upward trends of the splay/levee facies of Zullo (2012). Notably, however, charcoal -- a characteristic of the facies of both McKenna and others (2004) and Zullo (2012) – appears to be absent. In fact, in the entire core material recovered from CE Bf 156, charcoal and lignite are nearly absent.

The interval from approximate depths of 42 to 33 ft is dominated by mottled to layered silty clays and

clayey silts with fewer sandy layers. Colors are rather subdued reddish and yellowish browns and light to medium grays. One palynological sample from an approximate depth of 40 ft (an approximate elevation of + 39 NAVD 88) is assigned to Zone IIC-III, suggesting a lower Cenomanian stage (Upper Cretaceous).

CE Bf 156 Pensauken Formation

The surficial unit at the site has been mapped as the Pensauken Formation (Higgins and Conant, 1986). While Higgins and Conant (1990) note that the composition of the Pensauken Formation varies across Cecil County. Gravels and sandy gravels are typical of the lower part of this formation; sands and loams are more characteristic of the upper part of the unit. The Pensauken Formation is considered to be of fluvial origin and possibly Miocene in age (Higgins and Conant, 1990). In the core, the base of this unit is set at depth of approximately 33 ft (+46 ft NAVD 88), based on core materials and geophysical logs, which indicate gravel and gravelly sands lie above an interval of mottled red-brown, brownish yellow and light gray, silty clays and clayey silts interpreted as the Potomac Group. Recovery in the core run from depths of 35 to 25 ft, which spans the contact, was poor because several pieces of coarse gravel were found to be blocking the barrel. Sands recovered from depths of 25 ft and above tend to be orangey brown to brownish yellow with some iron cemented particles and thin layers. Sands vary from intervals that are mainly fine to medium grained to gravelly and medium to coarse grained.

DISCUSSION

Multiple methods of data collection and investigation were key to gaining a more comprehensive understanding of strata underlying at each location. Core recovered from all three core holes varied in terms of overall recovery and suitability for palynological analysis. In many sandy intervals, core recovery was poor. Intervals containing good characteristics for pollen/spore preservation and extraction (i.e., gray clays and silts without an overabundance of carbonized woody materials or mottling suggestive of bioturbation) were fairly limited. Nevertheless, recovered core provided lithologic information to compare with geophysical logs and material for pollen-spore subsampling. Geophysical logs provided continuous information for the borehole, filling in information on lithologies where core recovery was low. Pollen analyses provided some data to tie specific core intervals to particular ages and a stratigraphic framework.

In addition to the results from the three core holes presented in this study, additional information was reviewed from previously published data (Edwards and Hansen, 1979; Overbeck and others, 1958; Wiley and others, 1987, Higgins and Conant 1990) and driller's logs. An effort was made to collect information on boreholes and/or wells that were drilled to basement, geophysically logged and/or those that were subsampled for paleontologic or palynological analyses. Summary data for other key core holes used in this study are provided in Appendix E. Using these data along with information from the project core holes, two cross-sections were constructed and are shown on Plate 2. Line A-B trends northwest to northeast along the Elk Neck Peninsula; line B-C is a short west-to-east trending line that passes through Elkton. These cross sections correspond to portions of section lines J-J' and K-K' of Benson (2006). Even with the addition of the three cores from this study, correlations shown on Plate 2 are considered tentative because the distance between many boreholes is still significant and the boundaries between palynological zones are not tightly constrained.

BASEMENT ROCK

Basement rock type, extent of weathering, and depth was different at each site. At core hole CE Cd 91 on the Elk Neck peninsula, basement rock appears to be mica gneiss which in some intervals had a slightly greenish cast when freshly cored (approximately 20 ft penetrated). Saprolite and severely weathered basement rock are about 81 ft thick. The elevation of the contact between saprolite and the Potomac Group at CE Cd 91 is approximately -314 ft NAVD 88. Basement rock at the site of the western Elkton core hole CE Be 155 appeared to be a severely weathered micaceous gneiss or schist (less than 1 ft penetrated); the overlying saprolite is about 32 ft thick. At the site of eastern Elkton core hole, CE Bf 156, basement rock is serpentinite and/or gabbro that had a distinctive teal green color when freshly cored (approximately 25 ft penetrated); saprolite is thin (estimated to be about 5 ft thick). As anticipated, the elevation of the contact between saprolite and the

Potomac Group is slightly lower at CE Be 155 (approximately -149.5 ft NAVD 88) than at CE Bf 156 (approximately -91.4 ft NAVD 88), which is in the vicinity of Grays Hill where gabbro and serpentinite crop out.

POTOMAC GROUP

Potomac Group Lithologies and Lithofacies Comparisons

The Potomac Group is more than three times as thick at CE Cd 91 as it is at the core hole locations in Elkton. The Potomac Group lithologies in these three core holes represent a variety of non-marine coastal plain deposits. Based upon a combination of core material and geophysical logs, many lithologies share characteristics with specific lithofacies of McKenna and others (2004) and/or Zullo (2012) in the Potomac Group of northern Delaware. In some cases, however, lithologies do not share all traits identified as characteristic of a particular lithofacies identified in the Delaware studies and a few intervals in the Maryland cores do not seem to correlate clearly to a single lithofacies of either McKenna and others (2004) or Zullo (2012).

The relative dominance of particular lithofacies differs at each location. In general in CE Cd 91, there are significant intervals of the mottled silts and clays lithofacies that suggest weathered floodplain deposition with paleosols in oxidizing conditions. This lithofacies is present but less common in the Elkton cores. These clay-silts are mottled and/or color banded, commonly in hues of red, red-brown, yellow-brown, light gray, and/or white. The intensity of the color mottling varies from strong to weak. Rootlike structures are common in some intervals. The clay-silts are variably sandy. Some intervals contain tan sphaerosiderite; some intervals include red hematite spherules/nodules; some intervals include both. The presence of siderite/sphaerosiderite in paleosols suggests some portion of soil development in waterlogged or poorly drained conditions, whereas the presence of ferric nodules suggests some portion of soil development in well-drained, oxidizing conditions (Retallack, 1988; Kraus, 1999). The presence of both suggests some fluctuations in the water table over time (Kraus, 1999). The geophysical log pattern is characterized by relatively high but irregular gamma signal and relatively low resistivity.

In addition to the oxidized weathered floodplain silts and clays, there are also relatively thick intervals (greater than 20 ft thick) of medium to dark gray and to a lesser extent brown, faintly mottled, silty clays suggestive of floodplain deposition in more poorly drained, reducing environments. These clays include minor charcoal or lignite and occasional burrows. In general, these clay-silts occur vertically adjacent to oxidized paleosols or an interval of sediments that seems to match the interlaminated sand and silt lithofacies (distal levee/floodplain) of McKenna and others (2004). These medium to dark gray clay-silts seem most characteristic of backswamp deposits (silty mud and muddy silt with variable organic debris) of Smith and Smith (1980) and the dark gray, clays and silts of the lake lithofacies of Zullo (2012). Core examples include clay-silts in CE Cd 91 between approximate depths of 124 and 103 ft and in CE Be 155 between approximate depths of 100 and 87 ft. No similarly thick interval of this medium to dark gray clay-silt was found in CE Bf 156. These clays and silts tend to have a similar geophysical log signature to those of the weathered floodplain deposits (i.e., relatively high, irregular gamma and low resistivity).

Sediments that appear to correspond to the interlaminated sand and silt lithofacies (distal levee/floodplain paleoenvironment) of McKenna and others (2004) were present in all three cores. In the project cores these sediments are characterized by interbedded to interlaminated medium to dark gray, silty clays and gray or brown, variably silty sand. Charcoal, lignite and/or carbonaceous particles were sometimes abundant in these sediments in CE Be 155 and CE Cd 91. In contrast, charcoal and lignite were nearly absent in CE Bf 156.

All three cores also appeared to have lithologic intervals that shared characteristics of the thin sands lithofacies (crevasse splay/proximal levee depositional environment) of McKenna and others (2004) and the partially similar, but distinct, splay/ levee facies of Zullo (2012), which is generally characterized as finer grained but still sand-dominant. Natural levee deposits are characterized as laminated fine sand and silt; crevasse splay deposits may coarsen upward from the base and the fine upward toward the top and can range in grain size from silt to coarse sand with very fine gravel (Makaske, 2001). In project cores, the sediments that appear to fall in these categories are generally very fine to fine sands that are interbedded to interlaminated with silts and clays and, to a lesser extent, variably silty, fine to

medium sands with coarse sand and fine gravel. Laminations tend to be wavy, sometimes discontinuous, and vary from angled to horizontal. In many of these intervals iron staining and cementation has occurred; occasionally layers of ironstone are present. More rarely tan sphaeroderite is present. Examples include CE Cd 91 between depths of 70 and 62 ft; CE Be 155 at depths of 110 to 104 ft, 65 to 62 ft; and 25 to 20 ft; and a rather thick interval in CE Bf 156 between 70.2 to 42 ft.

A couple of the more unique lithologies encountered in the project cores appear to potentially correspond to a couple lithofacies described by Zullo (2012). These included an interval of interlayered to interlaminated, medium to dark gray silt-clays, very fine to fine sands, and black carbonaceous material present in CE Be 155 (depths of approximately 140 ft to 122 ft) that shares characteristics with Zullo's (2012) frequently flooded lake/abandoned channel facies. Also in core CE Be 155, there is a thin interval (3 ft or less at approximate depths of 103 to 100 ft) of very fine to fine sand that may to correspond to Zullo's splay channel lithofacies.

Relatively thick sand intervals were encountered in all three cores, however core recovery was often limited in these sections. The material recovered and the geophysical log patterns did not always neatly match the characteristics of the thick sands (isolated channels) or the amalgamated sands (amalgamated channels) of McKenna and others (2004). Nevertheless some comparisons can be made.

In general, the thick sands facies (isolated channels) of McKenna and others (2004) consists of individual 5- to 20-ft-thick sands within 10- to 30-ft-thick, fining-upward packages. In CE Cd 91, there are two sand intervals that appear to share many of the characteristics of the thick sand lithofacies. These sands are about 12 to 15 ft thick (approximate depths of 463 to 451 ft and 439 to 424 ft). Sands are mainly fine to medium grained grading up to clayey, silty, fine sands. Each sand interval displays an overall fining-upward trend within which are smaller fining-upward cycles. They display almost identical geophysical log patterns that are generally bell-shaped. In core CE Be 155, there are two sand intervals that also appear to share some characteristics with the thick sands lithofacies of McKenna and others (2004). These sands are about 10 ft thick (approximately depths of 111 to 122 ft and 141 to 151 ft). Geophysical log patterns, however, are more blocky than bell shaped although limited core recovered does suggest coarser material was present at the base of each.

In each of the three project cores, an interval of sand on the order of 30 to 55 ft was encountered that shares many characteristics of the amalgamated sands lithofacies of McKenna and others (2004). In CE Cd 91 and CE Bf 156 these intervals include several stacked sands. Within these stacked sands there are some fining-upward intervals on the order of 3 to 10 ft; and occasionally some coarsening upward. Sands range in grain size from coarse to fine but medium to fine sands are most common; occasionally sands are slightly silty. In some intervals sediments exhibit planar parallel to cross laminations or bedding and many of these sands have iron staining or cementation. In CE Be 155 there is a 32-ft-thick sand interval. Material recovered across this interval is tan, fine to medium sand with trace amounts of silt and clay toward the base and trace amounts of coarse sand and fine gravel toward the top.

The gamma logs for these 30- to 55-ft-thick sands in all three boreholes, had a cylindrical/blocky pattern with a fairly sharp base, abrupt top, and low, generally smooth, signal throughout. This would be expected from relatively clean, quartz-dominated, fluvial sands without significant clay minerals. The resistance and resistivity log patterns for these intervals varied. In CE Cd 91, resistivity responses were relatively high but blocky to irregular, apparently reflecting the effect of variation in grain size, cementation and occasional muddier layers on the electrical resistivity. In both CE Be 155 and CE Bf 156, resistance and resistivity logs showed little to no increase opposite these sands yet other sands in these boreholes did generate increased responses. The sands are located in two different positions in the respective boreholes. In CE Bf 156, the approximately 46-ft sand interval occurred toward the base of the Potomac Group sediments and the single-point resistance and 16- and 64-inch normal resistivity logs show virtually no increase within the sand interval. Data from the spontaneous potential and fluid resistivity logs (not included here), show a positive deflection opposite the basal sand (and a negative deflection opposite the higher sand) on the spontaneous potential curve and a very slight gradual increase in fluid resistivity from the base to the top of the borehole on the fluid resistivity curve in up-hole run. These patterns suggest that in CE Bf 156 there was more conductive borehole fluid at depth and that in the lower sand, the formation water had a lower ionic concentration ("fresher") than the borehole fluid (in contrast to the

upper interval where borehole fluid had a lower ionic concentration than the formation water). In CE Be 155, the roughly 32-ft sand interval occurred toward the top of the borehole (possibly even a younger sand than the Potomac Group). The single-point resistance log showed virtually no increase opposite the entire sand interval whereas the normal resistivity logs, which also had a very low response toward the base of the sand, did show a slight increase upward. The spontaneous potential log in CE Be 155 showed essentially no deflection near the base of the sand and a slight negative deflection upward (essentially mirroring the 16-inch normal resistivity curve). The variation in the spontaneous potential and normal resistivity logs may indicate a slight upward coarsening of sand and/or decrease in clay silt or a change in water quality. The overall subdued response in this sand interval may be due to overall water quality that differed from deeper sands at this location. McKenna and other (2004) characterized the geophysical log patterns for the amalgamated sands lithofacies as blocky, but in the boreholes for this project only the gamma logs consistently displayed this pattern.

Fine-grained overbank deposits are dominant in the model of an anastomosing river system which has been suggested for the Potomac Group in the study area and northern Coastal Plain portions of Delaware and New Jersey (e.g., McKenna and other 2004; Sugarman and others, 2004; Zullo, 2012). Makaske (2001) estimated that in subrecent and ancient anastomosing systems, overbank deposits account for 45 to 90 percent of the fluvial deposits. For channels in modern anastomosing river systems, Makaske (2001) reported some width/depth ratios that ranged from 13 to 17 in temperate humid environments and 10 to 28 in tropical humid environments. For comparison, Makaske (2001) compiled width/thickness ratios of 16 “interpreted subrecent and ancient anastomosing river systems”. He found ratios ranged from 2 to 1000, although the majority (14 of the 16 reported) had width/thickness ratios of 165 or less. Makaske reasoned that the greater width/thickness ratios reported in the ancient anastomosing river systems compared to width/depth ratios of modern systems may be the result of several factors. Factors include lateral channel migration over time during deposition resulting in lateral accretion, laterally connected sandy sediments of crevasse splays or natural levees mistaken as channel fill, and where borehole or other geophysical logs were widely spaced some apparent connections of separate channel deposits. Many authors have emphasized that not all overbank deposits are fine grained and not all channel-fill sediments are coarse grained, therefore some care needs to be taken in assessing lithofacies and characterizing depositional environments (Smith and Smith,1980; Miall, 1982; Bridge, 1985; Makaske 2001).

Seismic work by Zullo (2012) in Delaware near the Chesapeake and Delaware Canal indicated fluvial sand bodies in the Potomac Group had an apparent average width of 568.9 ft (173.4 m) and thickness of 35.1 ft (10.7 m). The maximum channel width was 2,708 ft (826 m) and the maximum extent of laterally connected fluvial channels was about 0.9 mi (1.5 km); however, only about 27 percent of the sand bodies encountered displayed contact with other sand bodies on the seismic lines. Zullo (2012) reported an average of the (apparent) width/thickness ratios of the fluvial channel sands was 17.3. This is within the range of width/depth ratios compiled by Makaske (2001) for modern anastomosing rivers in temperate and tropical, humid environments, and toward the lower end of the reported ancient width-to-thickness ratios.

The variability of lithologies, particularly Potomac Group sands, over relatively short distances is apparent when comparing core hole CE Cd 91 with the previously drilled and logged CE Cd 53, which lies only about 0.52 mi (0.84 km) away (Plates 1 and 2). A significant 40-ft-thick sand shown in geophysical logs for CE Cd 53 at depths between about 360 and 320 ft (approximate elevations of -226 to -186 to ft NAVD 88) is apparently absent in the core from CE Cd 91 where lithologies at roughly comparable elevations are predominantly muddy (Plate 2, Line A-B). In contrast, thick intervals of sands at a shallower, but roughly comparable, elevations appear to be present in the subsurface at both locations. This sandy interval in CE Cd 91 (depths of 264 to 210 ft) has characteristics that suggest the sands may be represent an amalgamated channels lithofacies. While some workers have suggested that amalgamated channels may produce widespread, relatively clean stacked sand across broad fluvial valleys on the order of 3 mi (5 km) (and therefore have the potential to produce relatively high yielding aquifers), work by Zullo (2012) noted above indicates the width of channels in the Potomac Group in the vicinity is much smaller. Zullo’s work suggests that the sand interval in CE Cd 91 (depths of 264 to 210 ft; approximate elevations of -89 to -35 ft NAVD 88) and the upper sand in CE Cd 53 (depths of about 238 to 176 ft; approximate elevations of -104 to -42 ft NAVD 88) are not likely to be depositionally

related as part of one broad channel section unless they are connected along a thalweg, but these sands are within the range of multiple, laterally connected fluvial channels and could potentially be hydraulically connected.

The two core holes drilled in Elkton (CE Be 155 and CE Bf 156) are separated by a distance of about 2.5 miles and an elevation difference of about 58 ft. These two core holes tend to have a greater proportion of sandier lithologies overall than that in CE Cd 91, although both CE Be 155 and CE Bf 156 still appear to have considerable overbank deposits. Both of these Elkton core holes had relatively few intervals of mottled clays and silts (interpreted as weathered floodplain with paleosols), however, an interval of this lithofacies occurs near the top of these two cores as well as in CE Cd 91. Despite some similarities and their relative proximity, there are notable contrasts and variation in lithofacies between the two Elkton core holes. For example, the charcoal/lignite-rich backswamp/lake/abandoned channel deposits present in CE Be 155 are absent in CE Cf 156. In addition, the distribution of likely channel sands is quite different in the two core holes.

Given the "point location" of a core (versus an outcrop or seismic survey) and the variability within any single lithofacies, there are inherent limits to the certainty of any facies determination as applied to a particular core and subsequent extrapolation to a paleoenvironment geospatially. Comparison with the work of by McKenna and others (2004) and Zullo (2012) on Potomac Formation lithofacies of northern Delaware suggests that the lithofacies recognized in those works can generally be recognized in the core material in this study. In CE Cd 91, the dominance of the overbank silty to clayey sediments relative to channel sand seems consistent with the anastomosing fluvial system concept which they propose. The generally sandier sediments, albeit with still considerable thicknesses of overbank fines, in the Elkton cores, may reflect greater proximity to the ancient channels where lithologies that appear to be representative of natural levee, crevasse splay deposits and proximal floodplain would be likely be deposited. However it is also recognized that many of the lithologies encountered do not uniquely define an anastomosing fluvial system given the vast scale of such a system which may include both meandering and braided streams. In addition, in core without data to ascertain ages of sediments it is difficult to know to what extent lithofacies are roughly contemporaneous (and thus potentially depositionally or hydrologically related) with similar deposits in other cores or locations.

Potomac Group Palynological Results and Correlations

In the Potomac Group samples from the three cores in this project, pollen and spore recovery varied from none to good and included palynomorphs from Zones/Subzones I, IIB, IIC, III (tabs. 4, 5, 6 and Appendix D). No samples were identified as palynological Subzone IIA. Brenner (Appendix D) considered the palynological assemblages to represent a subtropical humid paleoclimate.

In the subsurface of the Elk Neck peninsula, the boundary between palynological Zones I and II (Patuxent-Arundel Formations and Patapsco Formation) is not well constrained. Across the depths where the Zone I - II boundary occurs, relatively few samples from core holes in the area have been subject to palynological analysis and, of those that have, few were found to contain dateable palynological information in that interval and even fewer samples were found to contain Subzone IIA palynomorphs. It is not clear if the rarity of Subzone IIA, as well as palynomorphs overall in uppermost Zone I and lower Zone II is largely a function of limited suitable lithologies to analyze (i.e., age-correlative material could be present though possibly not a lithology likely to preserve pollen or spores and/or not sampled) or if intervals representing that time are absent altogether in some locations (i.e., nondeposition or post depositional erosion locally).

In some areas of Maryland (i.e., Southern Maryland and Harford County), the uppermost sediments of Zone I age are clays identified as Arundel Formation or Patuxent-Arundel Formations (undifferentiated) and the base of the Patapsco, including Subzone IIA, is a sand or sandy interval (e.g., Hansen, 1968; Powars, 1997). However, due to the similarity in lithologies found in the Patuxent-Arundel and Patapsco Formations, it can be difficult to determine the boundary without additional palynological data. In the vicinity of this study, core hole CE Dc 2 at Turkey Point (southwestern tip of the Elk Neck peninsula) was one of the few to contain Zone IIA palynomorphs, although limited Zone I and no Subzone IIB palynomorphs were found in samples from that core (Edwards and Hansen, 1979). It should be noted that Edwards and Hansen (1979) grouped Subzone IIA sediments with Zone I sediments in some cross sections (including the cross-section

along Elk Neck peninsula) because Subzone IIA palynomorphs were identified in only one sample from one core and the sample came from a layer they interpreted to be part of a fining-upward sequence that appeared conformable with sediments considered to be fluvial sequences containing Zone I palynomorphs. Some data for the Turkey Point core hole CE Cd 2 from Edwards and Hansen (1979) is summarized on Plate 2 and in Appendix E of this report.

In CE Cd 91, Brenner identified two palynological samples as Zone I (Appendix D). These samples contained pollen and spores more common in Zone I than Zone II and neither sample contained of spores and pollen restricted to Zone II. The shallower sample was from a depth of about 384 ft, approximately 105 ft above the contact with underlying saprolite. This sample had very poor palynomorph recovery. The deeper sample (from a depth of 441 ft, approximately 48 feet above the contact with saprolite) had good recovery. Following the revised age zonations of Horikx and others (2016), Zone I ranges from Aptian to early Albian age. Brenner (Appendix D) notes that the palynomorph assemblage present in the deeper sample appears characteristic of a cooling phase that that typically begins in upper Zone I.

In CE Cd 91, the boundary between palynological Zones I and II appears to occur within a roughly 100-ft interval between depths of the highest Zone I sample (approximately 384.5 ft) and lowest Subzone IIB sample (approximately 281.8 ft). Sediments in this interval (between samples with dateable palynomorphs) are predominantly red, yellow, brown, and light gray, mottled clay-silts that are interpreted as weathered floodplain deposits with syn- or post-depositional oxidation and thus not likely to preserve pollen and spores. Two samples from depths of approximately 338 and 331 ft were submitted for palynological processing but were devoid of suitable material to analyze.

There are several relatively thin intervals of variably gravelly and sandy deposits (depths of 347 to 343 ft and 359 to 355 ft) that may represent the sand-on-clay contact that is common at the Patuxent-Arundel to Patapsco boundary in many places. However, recovery in these intervals was poor, making it difficult to assess the nature of the contacts and internal structure of the sediments. Additionally, there is a thick interval (nearly 50 ft) of mottled silt-clays above these sands that may be representative of either the Patuxent-Arundel Formations (undifferentiated) or the Patapsco Formation.

Therefore, no division is made between Zone I and Subzone IIA (if present) in CE Cd 91. Tentatively, the base of Subzone IIB is placed at the base of an interval of mottled to convoluted/wavy laminated, dark gray, silty clay and fine sandy, silt (containing the deepest Subzone IIB sample) which lies above a stiff, mottled, reddish brown and light gray clay with a slightly higher gamma deflection. The contact between these clays was not captured in the core recovered but is estimated to occur at a depth of about 289 ft based upon the geophysical log pattern.

In the two Elkton cores, none of the samples contained palynomorphs older than Subzone IIB so it seems that Patuxent-Arundel Formations are probably absent at these two locations. Core from CE Be 155, the western Elkton site, contained significant amounts of charcoal, lignite and woody material which limited some of the intervals suitable for pollen sampling. The three samples with viable pollen and/or spores were interpreted as Subzone IIB-2 corresponding to an Albian age and the Patapsco Formation. These samples were taken from depths ranging from approximately 140 to 90 ft (-119 ft to -69 ft NAVD 88). Three shallower samples from CE Be 155 between depths of 87 and 77 ft were barren.

In CE Bf 156, the eastern Elkton corehole, three samples between depths of approximately 164 and 71.4 ft were identified as Zone II or Subzone IIB. One sample from CE Bf 156 (at a depth 40.2 to 40.05 ft) contained palynomorphs identified as Zone IIC-III and designated as lower Cenomanian by Brenner (Appendix D). If the sample represents the lower Cenomanian then the boundary between the Lower Creatceous (Albian) and Upper Cretaceous (Cenomanian) at this location occurs between depths of 71.4 and 40.2 ft (+7.6 to +38.8 ft NAVD 88).

Comparison of palynological data from the three cores in this study with the correlations shown by Benson (2006) indicate that in some areas the previous correlations need to be reviewed and revised. The two Elkton core hole sites for this project essentially lie along portions of cross-section lines J and K of Benson (2006) in the vicinity of CE Bf 82 and CE Bf 81. Core hole CE Cd 91 lies along section line K-K' (of Benson, 2006), near CE Cd 53. All of these boreholes are shown on Plates 1 and 2 of this study.

Most significantly, palynological analyses from CE Cd 91 indicated material in this core contained pollen and spores from Zones I, IIB/IIB-2, and III which allows for some comparison with correlations on Elk Neck by Benson (2006). The distribution of the CE Cd 91 palynological data is shown on Plates 2 and A-1 of this report. It appears that there is Zone I material corresponding the Patuxent-Arundel Formations at the base of the Potomac Group at this location (perhaps 48 ft to possibly more than 100 ft in thickness). Correlation lines shown in Benson (2006), derived primarily from geophysical logs (i.e., without corresponding palynological data), suggested material of this age would be absent in this area.

In addition, data from the current study indicate that the Subzone IIC-Zone III boundary and the Albian-Cenomanian boundary are much higher in the section in central part of Elk Neck peninsula than is suggested by the position of Benson's LK-UK datum at CE Cd 53. Benson (2006) indicated that his LK-UK datum is associated with a shale-to-sand kick just above the Subzone IIC and Zone III boundary. Without the benefit of palynological data, Benson (2006, Plate 3, cross-section K-K') placed his LK-UK datum at a small clay-sand kick at a depth of about 209 ft in CE Cd 53. Based upon an approximate ground surface elevation of +134 ft, Benson's LK-UK datum would be at an elevation of about -75 ft NAVD 88 in CE Cd 53.

At CE Cd 91, located about 0.52 miles away, the clay-sand kick corresponding to Benson's LK-UK datum pick at CE Cd 53 would place Benson's LK-UK datum within the lower part of the Subzone IIB interval. In CE Cd-91 the shallowest subsample found to contain Subzone IIB palynomorphs was at a depth of approximately 77 ft. No pollen samples were identified as Subzone IIC, but the deepest sample containing Zone III was from a depth of approximately 20 ft. With a land surface elevation of approximately +175 ft NAVD 88 at CE Cd 91, this would mean that the actual LK-UK boundary would fall within elevations of about +98 ft and +155 ft which is considerably higher than Benson's datum pick.

Similarly, in Elkton, Benson (2006, Plate 3, section lines K-K' and J-J') shows his LK-UK datum to occur at an approximate depth of 130 ft in CE Bf 82. With an estimated land surface elevation of about +70 ft NAVD 88 this would place his LK-UK datum at an elevation of about -60 ft NAVD 88. CE Bf 82 is located about 1.62 miles west of CE Bf 156 and about 0.94 miles southeast of CE Be 155 (Plates 1 and 2 this report). A comparison of data from these boreholes suggests either the clay-to-sand contact selected by Benson (2006) as the LK-UK datum position at CE Bf 82 is too deep (if indeed the clay-to-sand datum is supposed to be one associated with, and possibly slightly above, the Subzone IIC-Zone III boundary) or is older than, and not contemporaneous with, the datum as identified in Delaware (because it appears to fall within Subzone IIB in the Elkton area).

From these data comparisons it appears that some of the correlations of Benson (2006) that extend from Delaware into Maryland in the vicinity of the Elk Neck peninsula and Elkton are incorrect and need to shift significantly. At least some of the clays that were thought to be recognizable and roughly time-equivalent key marker beds in geophysical logs from Maryland boreholes are not likely to be time-equivalent to the marker bed clays identified in Delaware boreholes with palynological data. Therefore, the correlation lines (as extended into Maryland) do not connect roughly time-correlative floodplain surfaces as Benson (2006) presumed, and the at least some of the clays (or shale "kicks") thought to be correlative seem unlikely to represent synchronously deposited, areally extensive, floodplain deposits (confining layers).

However, Benson (2006) and other previous workers (Edwards and Hansen, 1979; Otton and others, 1988) have recognized a thick clayey interval that typically is associated with palynological Subzone IIC in the upper Chesapeake Bay area. This suggests that this clay interval may represent floodplain sediments that were deposited nearly synchronously (geologically) and therefore may function as a widespread confining layer within the Potomac Group hydrostratigraphic framework. In CE Bf 156 there is an interval of clay identified as Zone IIC-III. There are silt-clays present in cores CE Cd 91 between intervals identified as Subzone IIB and Zone III, though these silt-clays have not been analyzed for pollen or spores. If silt-clays in these intervals are at least in part correlative to Subzone IIC then there may be a rather widespread nearly synchronously deposited silty-clay [although the silt-clays corresponding to Subzone IIC appear occur at elevations higher in the subsurface under the Elk Neck and Elkton sites than suggested in some of the extrapolations into Maryland shown by Benson (2006)]. It is not clear if any Potomac Group sediments younger than Subzone IIB are present at CE Be 155.

Overall, data from this study show how difficult it can be to unequivocally correlate log patterns/clay "kicks" within the Potomac Group. As a consequence, the underlying assumption that correlated clay "kicks" are accurately correlated and represent continuous (confining) layers resulting from a particular sequence of ancient flooding may not be valid. In addition, the changes in correlation as a result of data in this study may affect hydrologic models and estimates of aquifer recharge and confining unit continuity.

Results from this study emphasize the need for, and benefit of, multiple lines of investigation for correlation, particularly within the Potomac Group. Optimally, these include a method to age-date the strata, such as paleontologic/palynologic data, as well as geophysical logs, lithologic data, seismic lines and regional hydraulic data. Often, all of these data are not available at each site; sometimes the best available data is a geophysical log from a borehole or well. However, with limited data, there is potential for misinterpretation and miscorrelation especially where data are fairly widely spaced. This suggests that the limitations and/or the tentative nature of some correlations and extrapolations should be clearly identified, particularly when results are directly applicable to resource management.

SUMMARY AND CONCLUSIONS

Core holes drilled through coastal plain sediments into basement rock on the Elk Neck peninsula and on the east and west sides of Elkton in Cecil County, Maryland, revealed some of the regional variability of the Potomac Group and underlying basement rock in the vicinity. Borehole geophysical logs also illustrate the lithologic variability. Comparison of geophysical logs with core lithologies and palynology, however, underscore the importance of multiple sources of data for correlation and the challenge of relying heavily on geophysical logs alone for correlation in the Potomac Group.

The Potomac Group lies on variably weathered basement rock. On the Elk Neck peninsula at CE Cd 91, basement rock is a mica gneiss, which is overlain by about 81 ft of severely weathered basement rock and saprolite. On the western side of Elkton at CE Bf 155, a severely weathered mica gneiss or schist is overlain by about 32 ft of saprolite. On the eastern side of Elkton at CE Bf 156, basement rock is serpentinite/gabbro with only a few feet of saprolite. The contact between the saprolite and the Potomac Group was deepest under the Elk Neck peninsula and shallowest on the east side of Elkton (approximately -314 ft NAVD 88 at CE Cd 91 and -91.4 ft NAVD 88 at CE Bf 156).

Pollen and spore recovery from Potomac Group core samples varied. Nevertheless, palynological data from these sites provides some age dates to assist in correlating sediments. In the Elkton area, data from CE Bf 156 (eastern Elkton site) indicated that the probable contact between palynological Zone IIC-III and Subzone IIB occurs between depths of 71 and 40 ft (an approximate elevation range of +8 to +39 ft NAVD 88). Using the revised ages Horikx and others (2016), which suggest the boundary between the Lower Cetaceous (Albian) and Upper Cretaceous (Cenomanian) would occur within Subzone IIC, it seems likely that the boundary would occur within this interval. Palynological results from the samples below a depth of 71 ft are identified as from Zone II or IIB of Albian age, corresponding to the Patapsco Formation. Results of palynological data from CE Be 155 (western Elkton site) indicate that sediments between depths of 140 and 90 ft (between -119 and -69 NAVD 88) are of Subzone IIB-2, Albian age, corresponding to the Patapsco Formation. These data suggest that in the Elkton area, older Patuxent-Arundel age (Zone I) sediments are likely to be absent.

Palynological samples from core hole CE Cd 91 (Elk Neck site) included spores and pollen from Zones/Subzones I, IIB/IIB-2 and III. Based on limited sample data, Zone I material is present at the base of the Potomac Group (corresponding to Aptian age and the Patuxent-Arundel Formations, undivided). The thickness of the Zone I interval is poorly constrained but it may be may be 48 feet to possibly more than 100 ft thick. This appears to be quite different from an earlier interpretation (Benson, 2006) which suggests the Patuxent-Arundel Formations (palynological Zone I) would be absent at this location on the Elk Neck peninsula. In addition, data from both CE Cd 91 and CE Bf 156 indicate that a key clay-silt marker bed (presumed confining unit) associated with palynological Subzone IIC and the Lower Cretaceous (Albian)-Upper Cretaceous

(Cenomanian) boundary, is likely to be higher in the section (where present) along Elk Neck peninsula and the Elkton area than estimated by Benson (2006). Both of these changes in correlation affect the overall stratigraphic framework and potentially the hydrostratigraphic framework and should be taken into account in modeling groundwater or reservoir characteristics in the area.

Results of this study suggest some previous correlations need to be reviewed and additional work needs to be done to evaluate the stratigraphic and hydrostratigraphic relationships of the Potomac Group strata and aquifers in parts of Cecil County. In the Potomac Group, understanding the distribution of high quality aquifer facies and their connectivity (hydrostratigraphy) is complicated by the significant lateral and vertical facies variations. This study underscores the difficulty of interpreting the original genetic relations of units across distances without corroborating data to tie ages to sediments. Stratigraphic correlations in the Potomac Group that are based largely on geophysical logs without the independent biostratigraphic or other age-dating information (or in the case of hydrostratigraphic correlations without additional data to assess aquifer connectivity or isolation) probably should be conveyed as more provisional than is typically implied.

REFERENCES

Andreasen, D.C., Staley, A. W., and Achmad, G., 2013, Maryland Coastal Plain aquifer information system: hydrogeologic framework: Maryland Geological Survey Open-File Report No. 12-02-20, 121 p.

Benson, R.N., 2006, Internal Stratigraphic Correlation of the Subsurface Potomac Formation, New Castle County, Delaware, and adjacent areas in Maryland and New Jersey: Delaware Geological Survey Report of Investigations No. 71, 15 p.

Brenner, G.J., 1963, The spores and pollen of the Potomac Group of Maryland: Maryland Geological Survey Bulletin 27, 215 p.

Bridge, J. S., 1985, Paleochannel patterns inferred from alluvial deposits: a critical evaluation: Journal of Sedimentary Petrology, vol. 55, no. 4, p. 579-589.

Doyle, J.A., 1992, Revised palynological correlations of the lower Potomac Group (USA) and the Cocobeach sequence of Gabon (Barremian-Aptian): Cretaceous Research, vol. 13, p. 339-349.

Doyle, J.A., and Hickey, L.J., 1976, Pollen and leaves from the mid-Cretaceous Potomac Group and their bearing on early angiosperm evolution, *in* Beck, C.B., ed., Origin of the angiosperms. New York, Columbia University Press, New York, p. 139-206.

Doyle, J.A., and Robbins, E.I., 1977, Angiosperm pollen zonation of the continental Cretaceous of the Atlantic Coastal Plain and its application to deep wells in the Salisbury Embayment: Palynology, vol. 1, p. 43-78.

Edwards, J.J., Jr. and Hansen, H.J., 1979**,** New data bearing on the structural significance of the upper Chesapeake Bay magnetic anomaly: Maryland Geological Survey Report of Investigations No. 30, 44 p.

Glaser, J.D., 1969, Petrology and origin of Potomac and Magothy (Cretaceous) sediments, middle Atlantic Coastal Plain: Maryland Geological Survey Report of Investigations No. 11, 102 p.

Hansen, H.J., 1968, Geophysical log cross-section network of the Cretaceous sediments of Southern Maryland: Maryland Geological Survey Report of Investigations No. 7, 46 p.

_____, 1969, Depositional environments of subsurface Potomac Group in southern Maryland: American Association of Petroleum Geologists Bulletin, vol. 53, p. 1923-1937.

_____, 1972, A user's guide for the artesian aquifers of the Maryland coastal plain, Part Two: Aquifer characteristics: Maryland Geological Survey Open-File Report 72-02-1,123 p.

_____, 1984, Hydrogeologic characteristics of the Waste Gate Formation, a new subsurface unit of the Potomac Group underlying the eastern Delmarva Peninsula: Maryland Geological Survey Information Circular 39, 22 p..

Hansen, H.J., and Doyle, J.A., 1982, Waste Gate Formation: Maryland Geological Survey Open File Report 82-02-1, 87 p.

He, C., and Andres, A.S., 2011, Simulation of groundwater flow in southern New Castle County, Delaware: Delaware Geological Survey Report of Investigations No. 77, 12 p.

Hickey, L.J., 1984, Summary and implications of the fossil plant record of the Potomac Group, *in*

Frederiksen, N.O., and Krafft, K., eds., Cretaceous and Tertiary Stratigraphy, Paleontology, and Structure, Southwestern Maryland and Northeastern Virginia: American Association of Stratigraphic Palynologists Field Trip Volume and Guidebook, p. 213-248.

Higgins, M.W., and Conant, L.C. 1986, Geologic Map of Cecil County, Maryland: Maryland Geological Survey, scale 1:62500.

_____, 1990, The Geology of Cecil County, Maryland: Maryland Geological Survey Bulletin 37, 181 p.

Hochuli, P.A., Heimhofer, U., Burla, S., and Weissert, H., 2006, Timing of early angiosperm radiation: recalibrating the classical section: Journal of the Geological Society of London, vol. 163, p. 587-594.

Horikx, M., Hochuli, P.A., Feist-Burkhardt, S., and Heimhofer, U., 2016, Albanian angiosperm, pollen from shallow marine strata in the Lusitanian Basin, Portugal: Timing of early angiosperm radiation: recalibrating the classical section: Review of Palaeobotany and Palynology, vol 228, p. 67-92.

Jordan, R.R., 1962, Stratigraphy of the Sedimentary Rocks of Delaware: Delaware Geological Survey, Bulletin 9, 51 p.

_____, 1968, Observations on the distribution of sands within the Potomac Formation of northern Delaware: Southeastern Geology, vol. 9, p. 77-85.

_____, 1983, Stratigraphic Nomenclature of nonmarine Cretaceous rocks of the inner margin of Coastal Plain in Delaware and adjacent states, Delaware Geological Survey Report of Investigations 37, 43 p.

Kraus, B., 1999, Paleosols in clastic sedimentary rocks: their geologic applications: Earth-Science Reviews 47, p. 41-70.

Makaske, M.J., 2001, Anastomosing rivers: a review of their classification, origin and sedimentary products: Earth-Science Reviews 53, p. 149-196.

Martin, M.M., 1984, Simulated ground-water flow in the Potomac aquifers, New Castle County, Delaware: U.S. Geological Survey Water-Resources Investigation Report 83-4007, 85 p. [https://pubs.usgs.gov/wri/1984/4007/report.pdf, accessed 4/6/2018]

McKenna, T.E., McLaughlin, P.P. and Benson, R.N., 2004, Characterization of the Potomac aquifer, an extremely heterogeneous system in the Atlantic Coastal Plain of Delaware: Delaware Geological Survey Open File Report 45.

McGee, J W, 1886a, Geological formations underlying Washington and vicinity: Report of the Health Officer of the District of Columbia for the year ending June 30, 1985, p. 19-21, 23-25.

_____, 1886b, Geological formations underlying Washington and vicinity: American Journal of Science, 3rd ser., v. 31, p. 473-474.

McLaughlin, P.P., 2006, Preliminary report on the palynology of the Potomac Formation of Delaware, *in* Benson, R.N., Internal stratigraphic correlation of the subsurface Potomac Formation, New Castle County, Delaware, and adjacent areas in Maryland and New Jersey, Delaware Geological Survey Report of Investigations No. 71, p. 9-15.

Miall, A.D., 1982, Analysis of fluvial depositional systems: American Association of Petroleum Geologists, Education Course Note Series No. 20, 75 p.

Munsell Color (Firm), 2000 revised (washable edition), Munsell Soil Color Charts: with Genuine Munsell Color Chips: Grand Rapids, MI: Munsell Color.

Otton, E.G., and Mandle, R. J., 1984, Hydrogeology of the upper Chesapeake Bay areas, Maryland, with emphasis on aquifers in the Potomac Group: Maryland Geological Survey Report of Investigations No. 39, 62p.

Otton, E.G., Willey, R.E., McGregor, R.A., Achmad, G., Hiortdahl, S.N., and Gerhart, J.M., 1988, Water resources and estimated effects of ground-water development, Cecil County, Maryland: Maryland Geological Survey Bulletin 34, 133

Overbeck, R. M., Slaughter, T. H., and Hulme, A. E., 1958, Water Resources of Cecil, Kent, and Queen Anne's Counties: Maryland Department of Geology, Mines, and Water Resources: Maryland Geological Survey Bulletin 21, 478 p.

Owens, J. P., 1969, Coastal Plain rocks of Harford County, *in* Southwick, D.L., Owens J.P., and Edwards, J. Jr., The Geology of Harford County, Maryland: Baltimore, Maryland Geological Survey, p. 77-103.

Owens, J. P., Sugarman, P. J., Sohl, N. F., Parker, R. A., Houghton, H. F., Volkert, R. A., Drake, Avery A., Jr., and Orndorff, R.C., 1998, Bedrock Geologic Map of Central and Southern New Jersey: New Jersey Geological

Survey Geologic Map I-2540-B, scale 1:100,000.

Powars, D.S., 1997, Stratigraphy and geophysical logs from a corehole drilled to bedrock at Robins Point, J-Field, Edgewood area, Aberdeen Proving Ground, Maryland: U.S. Geological Survey Open File Report 97-357, 68 p.

Retallack, G. J., 1988, Field recognition of paleosols: Geological Society of America Special Paper 216, p. 1-20.

Smith, D.G. and Smith, N.D., 1980, Sedimentation in anastomosed river systems: Examples from alluvial valleys near Banff, Alberta: Journal of Sedimentary Petrology, 50: 157-164.

Spoljaric, N., 1967, Quantitative lithofacies analyses of Potomac Formation, Delaware: Delaware Geological Survey Report of Investigations No. 12, 26 p.

Schieber, J., and Yawar, Z., 2009, A new twist on mud deposition – mud ripples in experiment and rock record: The Sedimentary Record, vol. 7, no. 2, p. 4-8.

Sugarman, P.J., Miller, K.G., Browning, J.V., Kulpecz, A.A., McLaughlin, P.P., and Monteverde, D.H., 2005, Hydrostratigraphy of the New Jersey coastal plain: Sequences and facies predict continuity of aquifers and confining units: Stratigraphy, vol. 2, p. 259-275.

Sugarman, P.J., Miller, K.G., McLaughlin, P.P., Jr., Browning, J.V., Hernandez, J., Monteverde, D., Uptegrove, J., Baxter, S.J., McKenna, T.E., Andres, A.S., Benson, R.N., Ramsey, K.W., Keyser, T., Katz, M.E., Kahn, A., Friedman, A., Wojtko, M., Feigenson, M.D., Olsson, R.K., Brenner, G., Self-Trail, J.M., and Cobbs, G., III, 2004, Fort Mott Site, *in* Miller, K.G., Sugarman, P.J., Browning, J.V., et al., eds., Proceedings of the Ocean Drilling Program, Initial Reports, Volume 174AX (Suppl.): College Station, TX, Ocean Drilling Program, p. 1-50. doi:10.2973/odp.proc.ir.174axs.105.2004. [http://www-odp.tamu.edu/publications/174AXSIR/chap_04/chap_04.htm, accessed 1/31/2019.

Sundstrom, R.W. and Pickett, T.E., 1967, The availability of ground water from the Potomac Formation in the Chesapeake and Delaware Canal area, Delaware: Newark, University of Delaware Water Resources Center, 95 p.

Thornburg, J.D, Miller K.G., Browning, J.V., and Wright, J.D., 2019, Mid-Cretaceous paleopedology and landscape reconstruction of the Mid-Atlantic U.S. Coastal Plain: Journal of Sedimentary Research, v. 98, p. 253-272.

U.S. Army Corps of Engineers (USACE), 2004, Conceptual hydrogeologic model summary of upper New Castle County, Delaware: U.S Army Corps of Engineers Philadelphia District, March 2004, 39 p.

_____, 2007, Updated draft groundwater model production run report, upper New Castle County, Delaware: U.S Army Corps of Engineers Philadelphia District, February 2007, 26 p.

Wiley, R.E., McGregor, R.A., de Grouchy, J., and Tompkins, M.D., 1987, Hydrologic data for Cecil County, Maryland: Maryland Geological Survey Basic Data Report No. 16, 150 p.

Wolfe, J.A. and Pakiser, H.M., 1971, Stratigraphic interpretations of some Cretaceous microfossil floras of the Middle Atlantic States: U.S. Geological Survey Professional Paper 750-B, p. B35-B-47.

Woodruff, K.D., 1976, Selected logging data and examples of geophysical logs for the coastal plain of Delaware: Delaware Geological Survey Report of Investigations No. 25, 40 p.

Yawar, Z, and Schieber, J., 2017, On the origin of silt laminae in laminated shares: Sedimentary Geology, vol. 360, p 22-34.

Zullo, C.C., 2012, Seismic imaging and hydrogeologic characterization of the Potomac Formation in northern New Castle County, Delaware: Doctoral dissertation, University of Delaware, Newark, Delaware, 239 p.

PLATES

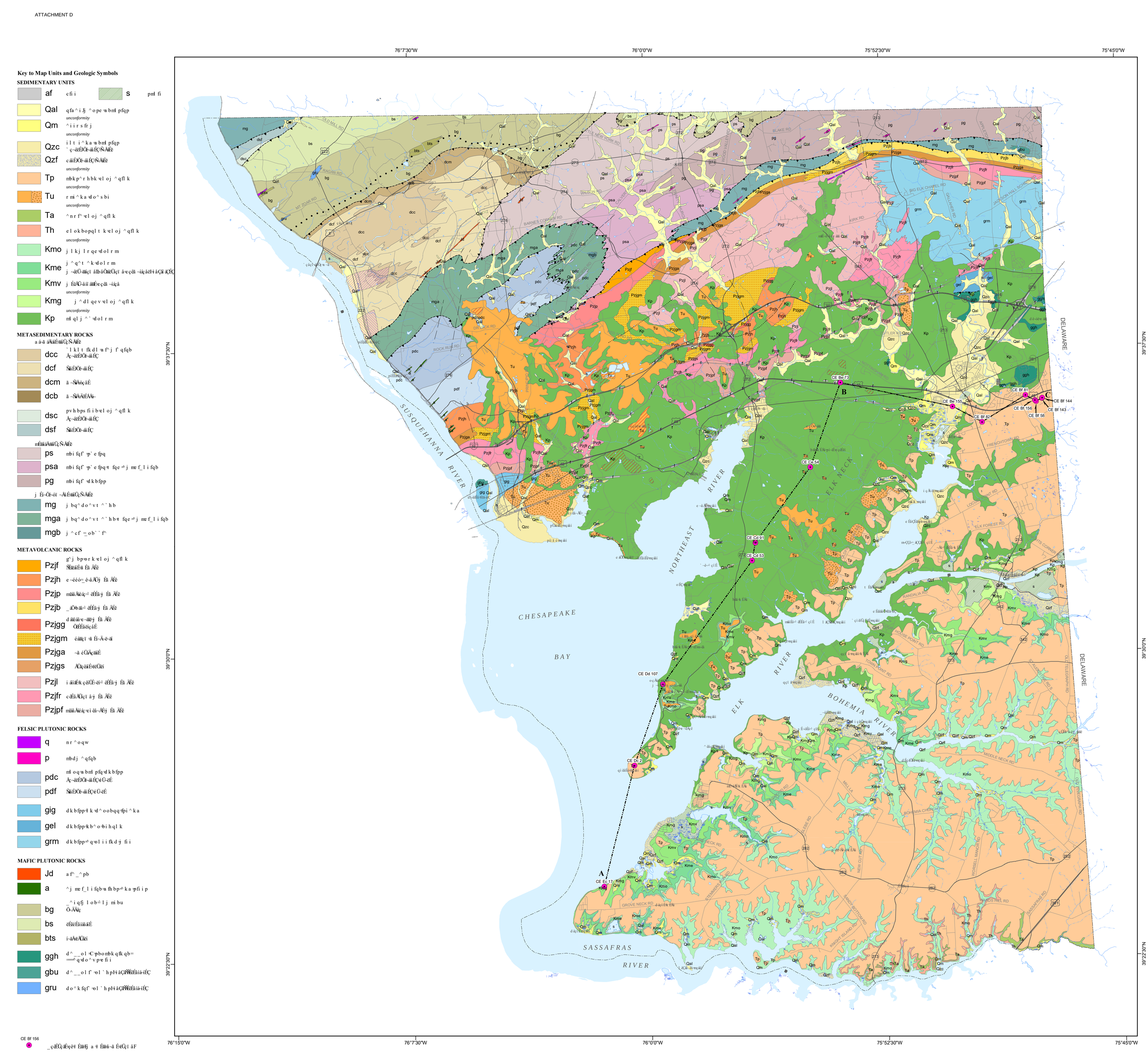

Key to Map Units and Geologic Symbols

SEDIMENTARY UNITS

- af — cfii
- s — pmlfi
- Qal — qfa^ijj ^ope¬abmlpfqp *unconformity*
- Qm — ^iirsfrj *unconformity*
- Qzc — ilt i^ka¬abmlpfqp
- Qzf — cÃÉÖÖé-ãíÉÇÑÁíÉè *unconformity*
- Tp — mbkp^rhbk¬elojˆqflk *unconformity*
- Tu — rmi^ka¬dlo^sbi *unconformity*
- Ta — ^nrf^¬eljoˆqflk
- Th — elokbopqltk¬eljoˆqflk *unconformity*
- Kmo — jlkjlrqe¬dolrm
- Kme — j^q^t^k¬dolrm j ¬èéÜ-ãíçî âlbâÜíèÜçî å¬eçêã ~íáçâêl÷åçãíáÇíÉ
- Kmv — j ÍèÄÜ-âíí ãíÉ¬eçêã ~íáçâ *unconformity*
- Kmg — j^dlqev¬eljoˆqflk *unconformity*
- Kp — mlqljˆ`¬dolrm

METASEDIMENTARY ROCKS

aá-ã áÑáÉ¬ãíÜçÑÁíÉè

- dcc — `lklt fkdl¬afˆjf qfqb Æç-èéÐÖé-ãíÉÇ
- dcf — ÑíÉÐÖé-ãíÉÇ
- dcm — ã ~ÑÁÆèçåÉ
- dcb — ã ~ÑÁÆÃéÉÁÃã-
- dsc — pvhbpsfiib¬eljo j ^qflk Æç-èéÐÖé-ãíÉÇ
- dsf — ÑíÉÐÖé-ãíÉÇ

mÉãíãÁãíÜçÑÁíÉè

- ps — mbifqfˆ¬p`efpq
- psa — mbifqfˆ¬p`efpq¬tfqe≠jmæf_lifqb
- pg — mbifqfˆ¬dkbfpp

jÉí-ÖÉ-óî ~ÁíÉ¬ãíÜçÑÁíÉè

- mg — jbq^do^vt^`hb
- mga — jbq^do^vt^`hb¬tfqe≠jmæf_lifqb
- mgb — j^cf=ob``fˆ

METAVOLCANIC ROCKS

g^jbp¬ork¬eljoˆqflk Ñëëãíëã íã ÁÉè

- Pzjf — e~éé ó=_é-ãÁÜj íã ÁÉè
- Pzjh — e~éé ó=_é-ãÁÜj íã ÁÉè
- Pzjp — méãÁéé ç≠ëÉÉã÷j íã ÁÉè
- Pzjb — _óÖbãñ≠ëÉÉã÷j íã ÁÉè
- Pzjgg — dæéãíé¬ãëë÷j íã ÁÉè Öëÿÿãíëíçåé
- Pzjgm — éãâçî ¬ã íë–Á-é-ãí
- Pzjga — ~ã éÜíÁçãíÉ
- Pzjgs — ÁÜíçéãíÉ¬ëëÜëi
- Pzjl — iãíãÉk çëíÜÉ-ëí≠ëÉÉã÷j íã ÁÉè
- Pzjfr — cëÉãÁÜíçî ãj íã ÁÉè
- Pzjpf — méãÁéé ç¬ei éã~ÁÉ÷j íã ÁÉè

FELSIC PLUTONIC ROCKS

- q — nr^oqw
- p — mbdj ^qfqb
- pdc — ml oq¬abml pfq¬dkbfpp Æç-èéÐÖé-ãíÉÇéÜ-ëÉ
- pdf — ÑíÉÐÖé-ãíÉÇéÜ-ëÉ
- gig — dkbfpp¬lk¬d^oobqq¬fpi^ka
- gel — dkbfpp¬kb^o¬bihqlk
- grm — dkbfpp≠q¬eliifkdj fii

MAFIC PLUTONIC ROCKS

- Jd — afˆ_^pb
- a — ^jmæf_lifqb¬afhbp≠ka¬pfiip
- bg — _^iqfj lob≠ljmibu Ö-ÄÁç
- bs — efëéfãíáãáÉ
- bts — í-ãÁéÁÜëí
- ggh — d^__olí¬pbombkqfkqb= ==^q¬dlo^vpæfii
- gbu — d^__olfˆ¬olˆhpÍ¬ãÇãÑëfãíáí-íÉÇ
- gru — dlo^kfqfˆ¬olˆhpÍ¬ãÇãÑëfãíáí-íÉÇ

CE Bf 156 — _çëÜçãÉçëî ÍãñÍj a ¬í Íãñâ-ã Íé¬ëÜçî ãF

B / A — ` ôçëë-ëÉÁíçã-ãíÉ

bñÁ¬í ~íÉÇÖÉ-ÇÉÇ¬éÉ-JñíÍãíãÍ Í÷ã çì åí¬çÑ =ã ~éé ÍÇÖÉçÇÖÁí åã-Ü-e-ÁÉíã-éíã çì ÍÇ

Contacts

dfçãçÖÁÁçåí-ÁÍ =éé ç ñã ~íÉÖÉ-Ç-íçã-ã¬çéñÑëÉÇ

Faults

çç÷-ãíÑ¬ã-ãíÍëíçã Á-íçã-ÁëÍ-ãíó¬ëéÑëÁÍÇ¬ãíãÍé-íÍÍëíW çÜçëíÇ-ëÜÇíî ÜÉÍëíÑëÍÇÇçëíÜî ÜÉÍëÁçÁÉ-ãÍÇÑ¬íëíã÷Í ëÜÇíî ÜÉÍëíÇÍãíóçéñëíãÍëíã -ó¬ÁÉ÷íÍëíçã-ÁÉÑ

- q Üã ëí÷Ñí ãÍ =íÉÍÜçã÷íéé ÍëíãÍ
- ^ ñã-íÉ-ÁÉ÷Í= ÖbñãÜÍãÍëíçã-íÍÇ =Íã çÇÑÁÇ÷Ñó= éé ÍãÍçã-ÜÍãÍëíçã-íÍÇÑíÇÉF
- ^ ñã-íÉ-ÁÉ÷Íro çÁí≠ Ü ëÁÜÍãÍëíçã-íÍÇÑíÇ

Folds

çç÷-ãíÑ¬ã-ãíÉ-ÁëÍ-ãíÁíçã-ÁëÍ-ãíó¬ëéÑëÁÍÇ¬ãíãÍé-íÍÍëíW Ç-íÜÇî ÜÉÍëíÉ¬ëéçñã ~íÉÖçíÇî ÜÉÍëÁçÁÉ-ãÍÇÑ¬íëíã÷Í ëÜÇíî ÜÉÍëíÇÍãíóçéñëíãÍëíã -ó¬ÁÉ÷íÍëíçã-ÁÉÑ

- ^ ñã-íÉ-ÁÉ÷Í= ÖbñãÜÍãÍëíçã-íÍÇÑíÇ =Íã çÇÑÁÇ÷Ñó= éé ÍãÍçã-ÜÍãÍëíçã-íÍÇÑíÇÉF
- ^ ñã-íÉ-ÁÉ÷Íro çÁí≠ Ü ëÁÜÍãÍëíçã-íÍÇÑíÇ

CE Be 73 — B — CE Cd 54 — CE Cd 91 — CE Cd 53 — CE Dd 107 — CE Dc 2 — CE Ec 17 — A

CE Be 155 — CE Bf 82 — CE Bf 81 — CE Bf 144 — CE Bf 143 — CE Bf 156 — CE Bf 58 — C

STATE OF MARYLAND
j ~ëáíã÷Í Íþ ~ãëíó
Governor

a bmˆoqj bkq¬Í çˆk^qro^i¬obplro` bp
gçÜí¬o¬Ked ëãÑÑãí
Secretary

MARYLAND DEPARTMENT OF NATURAL RESOURCES

pÁ-ãÉ¬ÑÑÇÍÍÑÑÑM

1 0.5 0 1 2 3 4 Miles
5,000 0 5,000 10,000 15,000 20,000 Feet
1 0.5 0 1 2 Kilometers

`ç åíçì êÍãíÍëí-ã¬ÑÑÑj Íífëëë

`ì ëëÍãíã-é¬éçëÉÁíçåW j ~ëáíãÇpí-íÉ¬ñ-íÉ÷ç ç ëÇÑí-íÉpçëÍã-ÉÑÜÍÍÍëíÉF ==Éoçåëçåí-ãa ~ã ÁëÍ÷ç åÑëçã-ãí÷ç åáÑÑÑÜÑÖÇçÍãÁëÍÑÉÍãÁÉ¬ëéëÍã F ==Éoçëãçåí-ãa ~íí ã Wëçëíó^ ã ÍëÁ÷á¬a ~íí ã ÑÜPF

d fçÖé-éÜÁÁçéçÑí-íÉ÷ëÍãíãí ÇÍÍçåÖñí ÇÍÍ÷é¬íRÇ ãíÍëã ~ãëëÜçî á¬íí÷Á¬Á¬Ãí=

kçíÉWëÇçéÍãíÉëÜçî á¬ççÉë¬çí÷éÍëéÍëÍãí÷Á çåëëëíÍãí÷ í ëëíÁ¬ãÇ¬íí ã K

_~ëÉã ~é÷Á çáíÉÇ=ãÇÍÑíé-ÁÍÇÑëçã W

r ÍçÑëÍçåçÖÁ÷ãpí ëíÍë÷Erpd pFW =k ~íçå÷ãe óÇçåçÖÁa ~í-ëÍ÷Éke a FÍÜÇÖÉíëçã íçåÍ÷Ñçé-ÜçÖÇçÉ-éÜÁÑÑí ëÍë÷ÍñÁëí÷ëÍëÉÁ÷éçëíçåëçÑëÜçëÍãíÉ ==k ç a ~ÜÇÖÉíëçã íçå÷Ç-í-ëÍ÷ÖÍãÍë-ãíó÷ÇÍÍ ÉçëÍÇ=í-ÑWQMMÑNWDMMÉÁ-ëÉ =qçéçÖé-éÜÁÉPMñ-SMã áíí íÉ÷ëÍëÍë÷ÉÑWMMMÉÁ-ëÉFÇÖÑ-ãíÜÍëÍ÷éÜ-éÜë÷Ea í dÉÑÑ÷éçéçÖé-éÜõ ==mçëíçåëçÑw÷çëà÷b ~ëíÍt ãñ ãÜçå÷t ÍëíÍa çí Íë÷t Íëí=åÖ=~íáíí çëÍëÍëÉÇ÷íÉÇNUPJNUQ ==^ëÉçî åÍ÷çéçÖé-éÜÁÑÑí ëÍë÷ëÍ÷á-íáí÷ëÇã ÑÑÑMMMMç÷NÜÍÑMMÉÁ-ëÉ =d fçÖé-éÜÁÁk ~ã Íë÷íáÑçëã ~íçå÷póëíã ÷Edk fpF¢í-Á-ëÍ÷ÑçÁ íí ë÷ãÑÍëí ëÍëÍëã-Á÷á-ã Íë÷ëÇî å

j ~ëöí-åÇd fçåçÖÁ÷ãpí ëíÍë÷Ej dpF= =pÜçëÍãíÉ÷íÉÁçéÑëÍ÷ÉÑÜÇÜÑMÑ÷ÍÜÇÖÉíëçã íçå÷ãÑçéÍëÍÁéçëíçåëçÑëÜçëÍãíÉ

k ~íçå÷ãe ÖëÁ íë÷ãñ ~ÖÍëö÷méçÖé-ã ÷Ek^ fnF= ==k ~íí ë÷ãÁçåçéÑã ÍÍÉ÷ÖMÑãñ ~ÖÍëöÍÑçÇÖñëö-íçå÷çÑëÍëÁéçëíçåëçÑëÜçëÍãíÉ

j ~ëöí-åÇpí-íÉ÷ëÖÜ ~ö÷ç ÇÍ ãñëíé-íçå÷Ej a Jpe^FW =j a ¤ çéÍë÷íÍ Í÷ÉåÍÍëíãÉm÷çÖé-ã Í÷É åÍÍëíãÉm÷çÖé-ã Í÷É Áíí÷ç íãíó÷íÁÍëíÉÇMMÑÑÑçÍë÷éëçëí-íçå÷ÑëíëÍë ==í ëëÖñ-íçÇ÷í-ëÍ÷ÇÍÍ ÉçëÍÇ=í-ÑWQMMÉÁ-ëÉ

bëíã ~íÉÇÖMMÜã ~ÖÍëÍãÁ÷çëÜÇÉÁíã-íçå÷Éëéçëñã ~íÉ÷ÁëíÍëçÑÁçíåíÉÇÑWNÇÖÉÍëÍÉ÷PSã ãíÍëÍÉ÷í Íëí Ëçç÷ÇÍÍëíãíÉ÷Á ëëÍãíã ~ÖÍëÍãÁÇÉÁíã-íçå÷ëÍÉWÜíëWí ï ï íÇÖÇ¥ç~íÇçí ÍÖÇçã ~Öí çÇÍëíëã ÉÁíã-íçå÷ëëÉF

Plate 1. Locations of cross sections A-B and B-C shown on geologic map of Cecil County, Maryland (modified from Higgins and Conant 1986)

Plate 2.
Cross sections A-B and B-C.

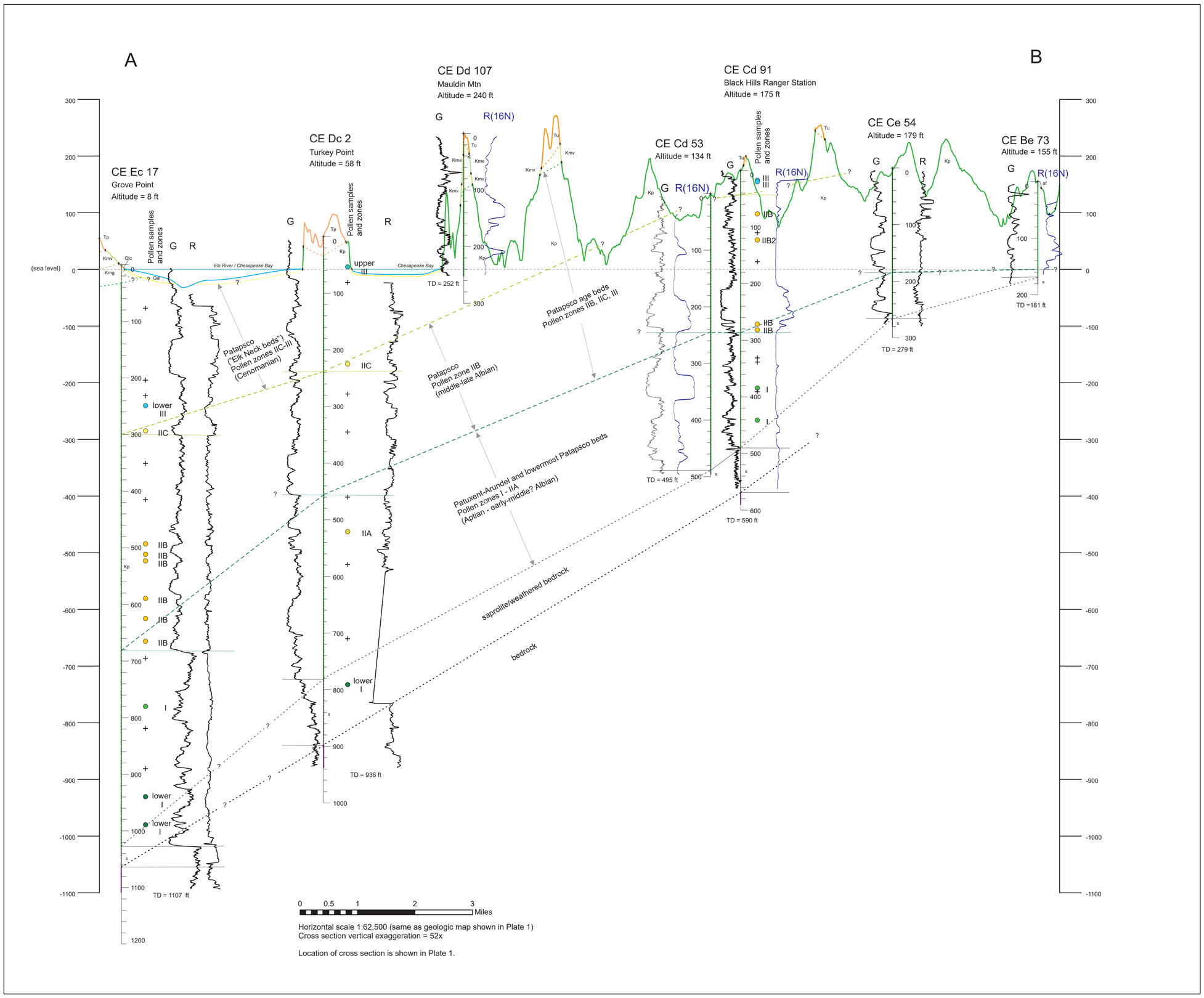

Cross section A-B.

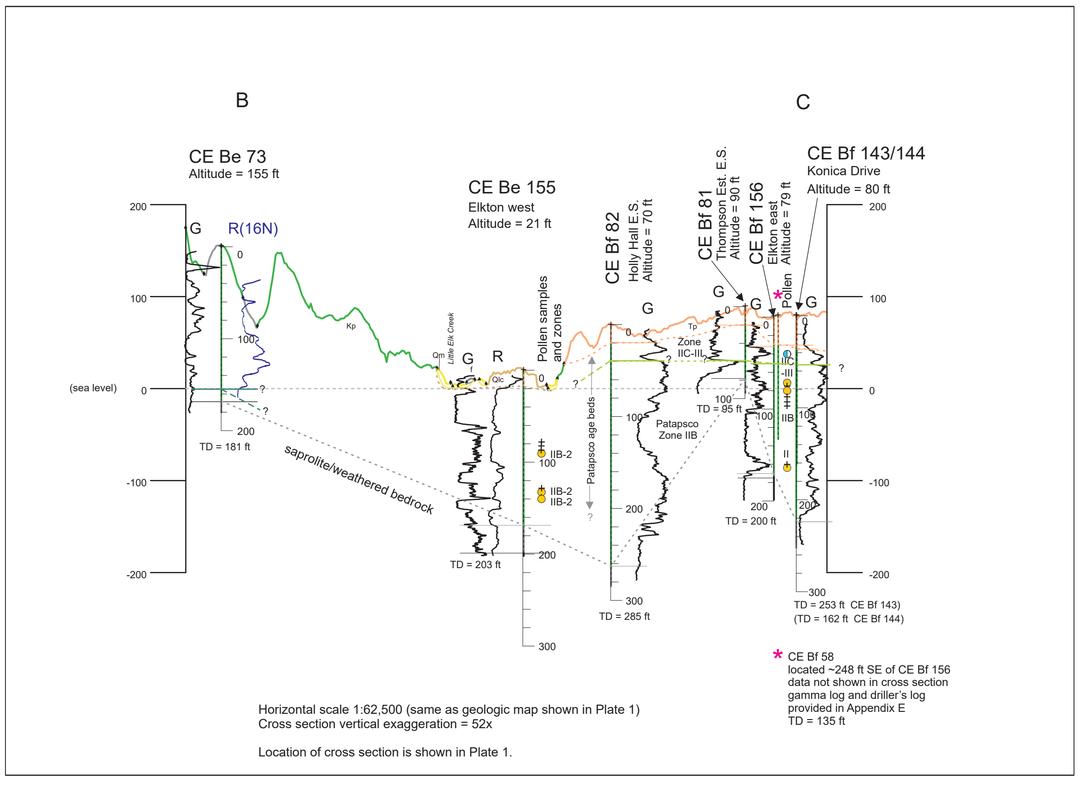

Cross section B-C.

Plate 2. Cross sections A-B and B-C.

Legend for Figures

Pollen Samples & Zones

- upper III
- lower III
- IIC-III
- IIC
- IIB/IIB-2
- II
- IIA
- I
- lower I
- \+ barren or not dateable

Geophysical Logs

- G Gamma log
- R Single point resistance log
- R(16N) Resistivity log (16-inch normal)

Correlation Lines (within Potomac Group)
Queried where datum or correlation is speculative

- Estimated Lower-Upper Cretaceous boundary
- Estimated base of Patapsco palynological Subzone IIB (middle Albian)

Geologic Unit Contacts and Symbols
(Contacts approximately located; dashed where inferred in subsurface)

- f artificial fill
- Qal/Qm Quaternary alluvium or marsh deposits
- Qlc Quaternary lowland deposits, coarse-grained facies
- Tp Pensuaken Formation
- Tu Upland deposits
- Kme Marshalltown/Englishtown Formations, undivided
- Kmv Merchantville Formation
- Kmg Magothy Formation
- Kp Potomac Group
- s Top of saprolite/weathered bedrock
- Top of bedrock

APPENDIX A

CE Cd 91 Summary Diagram, Core Photographs and Detailed Lithologic Descriptions

Plate A-1

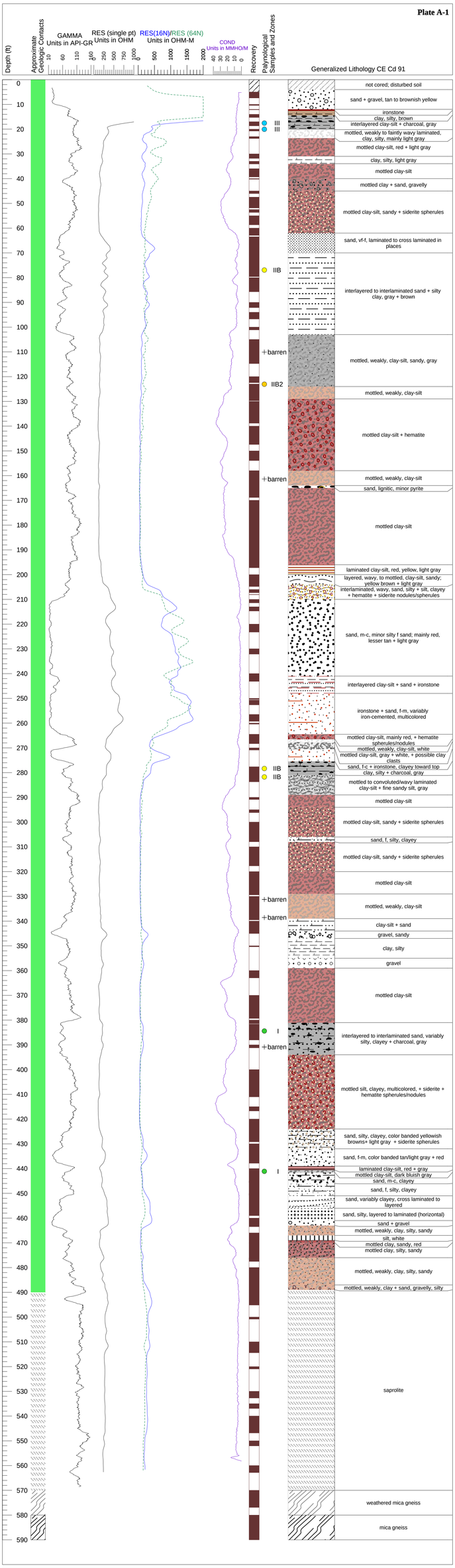

Geologic Units
Potomac
weathered rock
saprolite
bedrock

Core Recovery
core
not cored
none

f = fine
m = medium
c = coarse

Plate A-1. Summary of data collected from borehole CE Cd 91.

Table A-1. Photographs of CE Cd 91 core.

	
CE Cd 91 Core Box 1 (spans depths of approximately 5 to 23 ft)	CE Cd 91 Core Box 2 (spans depths of approximately 23 to 40 ft)
	
CE Cd 91 Core Box 3 (spans depths of approximately 40 to 56 ft)	CE Cd 91 Core Box 4 (spans depths of approximately 56 to 65 ft)

Table A-1. Photographs of CE Cd 91 core -- Continued.

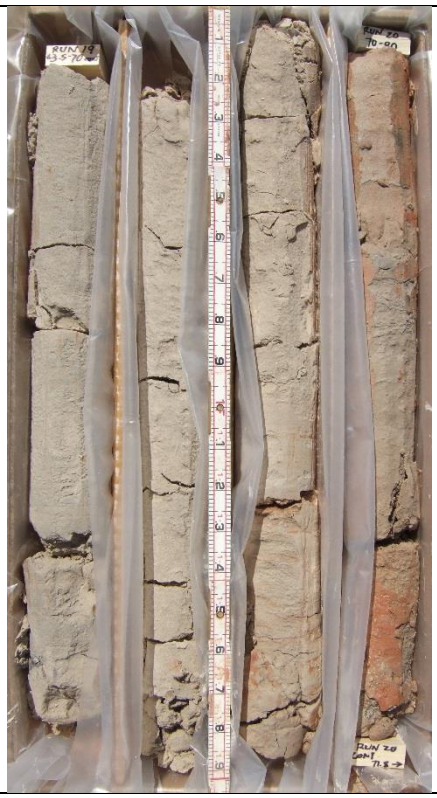	
CE Cd 91 Core Box 5 (spans depths of approximately 65 to 72 ft)	CE Cd 91 Core Box 6 (spans depths of approximately 72 to 79 ft)
	
CE Cd 91 Core Box 7 (spans depths of approximately 79 to 90 ft)	CE Cd 91 Core Box 8 (spans depths of approximately 90 to 105 ft)

Table A-1. Photographs of CE Cd 91 core -- Continued.

	
CE Cd 91 Core Box 9 (spans depths of approximately 105 to 110 ft)	CE Cd 91 Core Box 10 (spans depths of approximately 110 to 123 ft)
	
CE Cd 91 Core Box 11 (spans depths of approximately 123 to 130 ft)	CE Cd 91 Core Box 12 (spans depths of approximately 130 to 138 ft)

Table A-1. Photographs of CE Cd 91 core -- Continued.

	
CE Cd 91 Core Box 13 (spans depths of approximately 138 to 146 ft)	CE Cd 91 Core Box 14 (spans depths of approximately 146 to 158 ft)
	
CE Cd 91 Core Box 15 (spans depths of approximately 158 to 165 ft)	CE Cd 91 Core Box 16 (spans depths of approximately 165 to 172 ft)

Table A-1. Photographs of CE Cd 91 core -- Continued.

	
CE Cd 91 Core Box 17 (spans depths of approximately 172 to 179 ft)	CE Cd 91 Core Box 18 (spans depths of approximately 179 to 187 ft)
	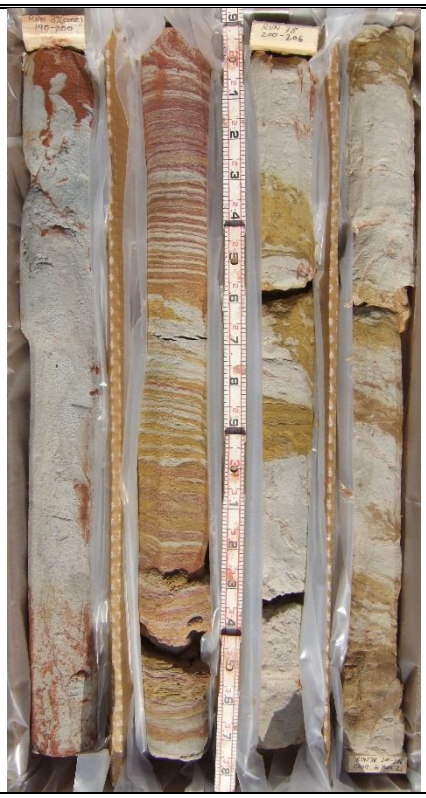
CE Cd 91 Core Box 19 (spans depths of approximately 187 to 194 ft)	CE Cd 91 Core Box 20 (spans depths of approximately 194 to 204 ft)

Table A-1. Photographs of CE Cd 91 core -- Continued.

	
CE Cd 91 Core Box 21 (spans depths of approximately 204 to 222 ft)	CE Cd 91 Core Box 22 (spans depths of approximately (222 to 251 ft)
	
CE Cd 91 Core Box 23 (spans depths of approximately 251 to 261 ft)	CE Cd 91 Core Box 24 (spans depths of approximately 261 to 280 ft)

Table A-1. Photographs of CE Cd 91 core -- Continued.

	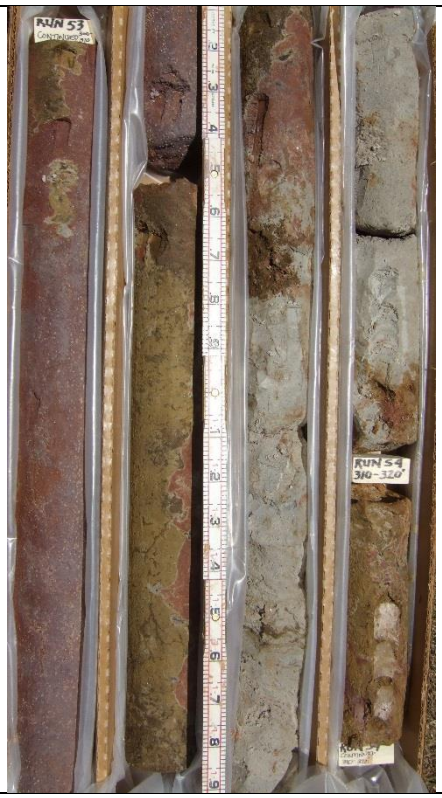
CE Cd 91 Core Box 25 (spans depths of approximately 280 to 302 ft)	CE Cd 91 Core Box 26 (spans depths of approximately 302 to 311 ft)
	
CE Cd 91 Core Box 27 (spans depths of approximately 311 to 320 ft)	CE Cd 91 Core Box 28 (spans depths of approximately 320 to 328 ft)

Table A-1. Photographs of CE Cd 91 core -- Continued.

	
CE Cd 91 Core Box 29 (spans depths of approximately 328 to 335 ft)	CE Cd 91 Core Box 30 (spans depths of approximately 335 to 355 ft)
	
CE Cd 91 Core Box 31 (spans depths of approximately 355 to 371 ft)	CE Cd 91 Core Box 32 (spans depths of approximately 371 to 378 ft)

Table A-1. Photographs of CE Cd 91 core -- Continued.

	
CE Cd 91 Core Box 33 (spans depths of approximately 378 to 385 ft)	CE Cd 91 Core Box 34 (spans depths of approximately 385 to 404 ft
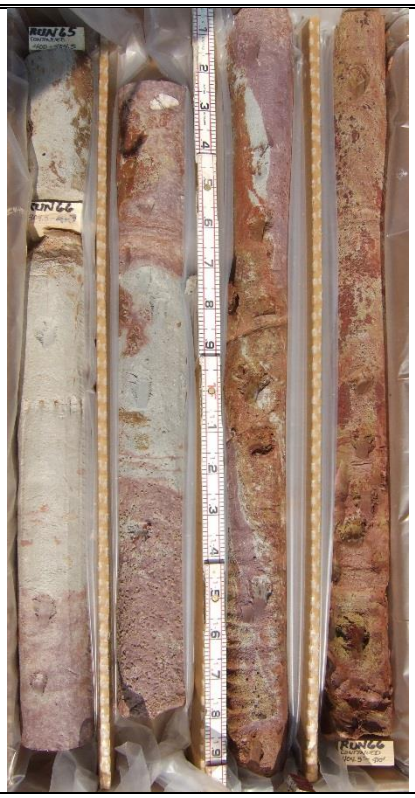	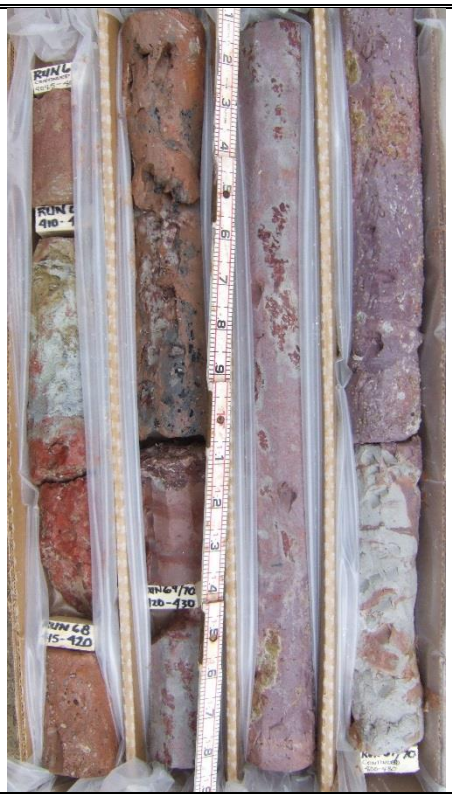
CE Cd 91 Core Box 35 (spans depths of approximately 404 to 410 ft)	CE Cd 91 Core Box 36 (spans depths of approximately 410 to 424 ft)

Table A-1. Photographs of CE Cd 91 core -- Continued.

	
CE Cd 91 Core Box 37 (spans depths of approximately 424 to 432 ft)	CE Cd 91 Core Box 38 (spans depths of approximately 432 to 442 ft)
	
CE Cd 91 Core Box 39 (spans depths of approximately 442 to 448 ft)	CE Cd 91 Core Box 40 (spans depths of approximately 448 to 455 ft)

Table A-1. Photographs of CE Cd 91 core -- Continued.

	
CE Cd 91 Core Box 41 (spans depths of approximately 455 to 463 ft)	CE Cd 91 Core Box 42 (spans depths of approximately 463 to 472 ft)
	
CE Cd 91 Core Box 43 (spans depths of approximately 472 to 481 ft)	CE Cd 91 Core Box 44 (spans depths of approximately 481 to 489 ft)

Table A-1. Photographs of CE Cd 91 core -- Continued.

	
CE Cd 91 Core Box 45 (spans depths of approximately 489 to 500 ft)	CE Cd 91 Core Box 46 (spans depths of approximately 500 to 530 ft)
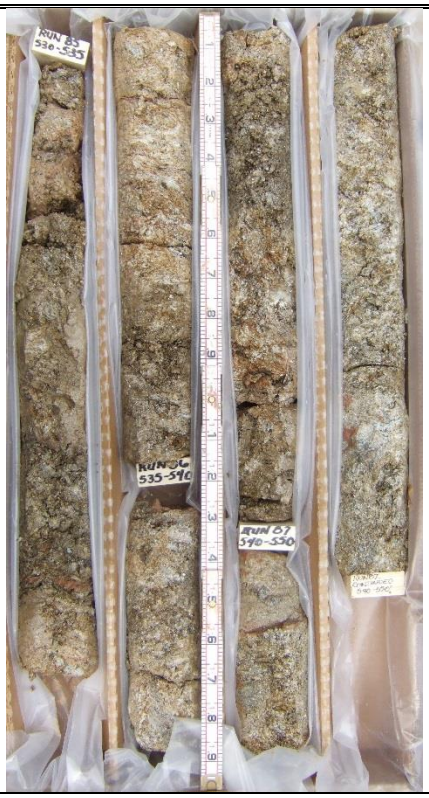	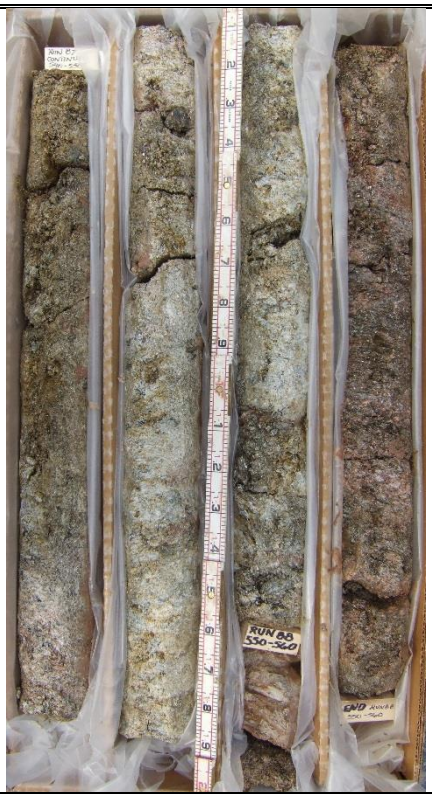
CE Cd 91 Core Box 47 (spans depths of approximately 530 to 542 ft)	CE Cd 91 Core Box 48 (spans depths of approximately 542 to 560 ft)

Table A-1. Photographs of CE Cd 91 core -- Continued.

CE Cd 91 Core Box 49
(spans depths of approximately 560 to 574 ft)

CE Cd 91 Core Box 50
(spans depths of approximately 574 to 584 ft)

CE Cd 91 Core Box 51
(spans depths of approximately 584 to 590 ft)

Table A-2. Description of core from CE Cd 91.

[Explanation of codes at end of table.]

Core run	Interval drilled depth in ft		Amount recovered (ft)	Core intervals ft in core run*		Lithologic description**
	from	to		from	to	
	0	5	n/a	n/a	n/a	Not cored: disturbed soil
1	5	10	2.40	0.00	0.10	Sand, fine to coarse, gravelly; brownish yellow (10 YR 6/6)
				0.10	0.50	Sand, fine to medium; pale brown (10YR 7/4); trace black carbonaceous particles
				0.50	0.95	Sand, medium to coarse; little gravel; brownish yellow (10YR 6/6)
				0.95	1.40	Sand, fine to medium; pale brown (10YR 7/4); trace black carbonaceous particles
				1.40	2.10	Sand, medium to coarse, gravelly; very pale brown (10YR 7/4)
				2.10	2.40	Sand, coarse, silty; very pale brown (10YR 7/4)
2	10	12	0.40	0.00	0.35	Sand, medium to coarse, gravelly; brownish yellow (10 YR 6/6)
				0.35	0.40	Sands, laminated (~0.02 ft [0.6 cm] thick): fine to medium, silty, light brownish yellow (10YR 6/4); medium to coarse, gravelly, reddish brown (5YR 4/3); fine to medium, silty, brownish yellow (10YR 6/6)
3	12	14	0.15	0.00	0.15	Siltstone/ironstone; dark reddish brown (5YR 3/3) and reddish brown (5YR 5/4) (color banded); (drilling suggests ~0.5 ft thick)
4	14	17	1.25	0	0.55	Silt-clay, gravelly, soft; brown (10YR 5/3); (possible uphole material)
				0.55	0.85	Clay, silty; stiff; dark gray (2.5Y 4/1); black carbonaceous layer at 0.7 ft; plus fine particles throughout
				0.85	1.25	Clay, silty; stiff; mottled colors: gray (2.5 YR 5/1) and light gray (2.5YR 7/1); black carbonaceous/woody material in intervals at 1 to 1.1 ft and 1.22 to 1.24 ft)
5	17	20	1.65	0	0.77	Clay, silty; mottled dark gray (2.5Y 4/1) and very dark gray (2.5Y 3/1)
				0.77	1.65	Clay, silty; dark gray (2.5Y4/1); black carbonaceous particles throughout and concentrated at 1.25 to 1.30 ft and 1.5 to 1.65 ft)
6	20	23	0.75	0	0.20	Clay, silty, little to trace sand, very fine to fine; grayish brown (10 YR 5/2); black carbonaceous particles; vaguely laminated; distinct but undulating contact with below; (possible uphole material)
				0.20	0.75	Clay, silty, stiff; gray (10YR 6/1); faintly wavy laminated
7	23	27	0.77	0	0.60	Clay, silty; faintly mottled to wavy laminated, grays (10YR 6/1) (10Y/R 5/1); thin hair-like black manganese(?)-filled cracks; sharp contact with material below
				0.60	0.77	Clay, silty; moderately stiff; light gray (10YR 7/1) with reddish brown (5 YR 4/4) undulating layer near top and in wisps/flecks throughout
				0.77	4.00	*no recovery*
8	27	30	0.00	0	0	*no recovery; (stopped to troubleshoot drilling and set temporary casing)*
9	30	33	1.80	0	0.60	Clay, slightly silty; soft; mottled light gray (10YR 7/1), reddish brown (5YR 5/4)
				0.60	0.90	Clay, slightly silty; stiff; mottled gray (10YR 6/1) and weak red (10R 5/4); undulating color-change contact with below
				0.90	1.80	Clay, slightly silty; gray (10YR 6/1); trace irregular, thin (hair-like) black manganese (?) "strands"
10	33	36	1.05	0	1.05	Clay, slightly silty (similar to above); gray (7.5YR 6/1) with trace, irregular, thin (hair-like), black manganese(?) in upper 0.8 ft; gray and weak red (10R 4/4) in lower 0.1 ft
11	36	40	3.30	0	3.05	Clay, slightly silty, fine sandy; mottled light gray (2.5Y 7/1), pale red (10R 6/2), purplish-red/red (10R 4/6); with tan and dark red spherules (iron cemented?; 0.5-1.0 mm); red infilled cracks/roots(?); pyrite at 3 ft; grades into below
				3.05	3.30	Clay, silty, fine sandy; mainly light gray (2.5 YR 7/1)

Table A-2. Description of core from CE Cd 91 -- Continued.

[Explanation of codes at end of table.]

Core run	Interval drilled depth in ft		Amount recovered (ft)	Core intervals ft in core run*		Lithologic description**
	from	to		from	to	
12	40	45	0.20	0	0.20	Clay, sandy, with little fine gravel, angular to well rounded; stiff; mottled to wavy laminated color: dusky red (10R 4/4), weak red (10R 5/3), light gray (10YR 7/1)
				0.2	5.00	*no recovery- driller reported similar drilling resistance (stiff clay) over entire 5-ft interval; geophysical logs suggest sandy upper half*
13	45	47.5	1.00	0	0.80	Clay, sandy , fine; stiff; mottled dusky red (10R 3/4), weak red (10R 4/4) and light gray (10YR 7/1); with scattered tan to red granules/spherules and paleosol structures; infilled cracks/roots(?) dusky red (10R 3/4) to brown 7.5YR 4/4).
				0.8	1.00	Clay, sandy, fine; stiff; mottled dusky red (10R 3/4), red (10R 5/6) and light gray (10YR 7/1); more spherules/granules than above.
14	47.5	50	2.40	0	1.90	Clay, sandy, fine; stiff; mottled dusky to weak reds (10R 3/4 - 4/4) and light gray (10YR 7/1); with tan to red granules/spherules (abundant toward top) and paleosol structures; infilled cracks/roots(?)
				1.9	2.20	Similar to above but laminated and few spherules
				2.2	2.40	Similar to upper 1.9 ft except few granules/spherules
15	50	52.5	1.80	0	1.00	Clay, sandy, fine to coarse; moderately stiff; mainly mottled weak red (10R 5/4), minor olive brown (2.5YR 4/3); abundant spherules; irregular boundary with below
				1	1.80	Clay; stiff; mottled light gray (10YR 7/1, weak red 10R 5/4 and minor dusky red (10R 3/4); infilled cracks, paleosol structures; few spherules
16	52.5	55	1.10	0	1.10	Clay; stiff; wavy laminated: light gray (10YR 7/1), pale red (10R 7/4) and dusky red (10R 3/4); infilled cracks, paleosol structures; light gray and dark red spherules coarser than uphole (coarse to v coarse sand-sized) and iron cemented clasts; clasts and coarse spherules typically composed of cemented fine-medium grains of sand
17	55	60	3.65	0	1.90	Clay, sandy, fine; stiff; mottled to wavy banded coloration: weak to dusky red (10R 5/4 -3/4), light gray (10YR 7/1); infilled cracks; abundant light gray medium-coarse sand-sized spherules/nodules to angular clasts
				1.9	2.30	Clay, sandy, fine; stiff; intense, wavy banded coloration: dusky red (10R 3/4), pale red (10R 6/4), light gray (10YR 7/1) ; fewer spherules/clasts
				2.3	3.65	Clay, sandy, fine; mottled, banded to wavy laminated colors: weak red (10R 5/4), light gray (10 YR 7/1), lt olive brown (2.5Y 5/6), reddish brown (5YR 5/4); abundant, very coarse sand-sized spherules/clasts toward top of interval, variable in size and abundance downward
18	60	63.5	2.90	0	1.90	Clay, sandy, fine; stiff; mottled to laminated weak red (10R 5/4), light gray (10YR 7/1), lt olive brown (2.5Y 5/6); dusky red (10R 3/4) infilled cracks; light gray, coarse sand-sized spherules/clasts common
				1.9	2.90	Sand, very fine to fine, silty; well sorted; sub-rounded (fines upward); light gray (10YR 7/1)
19	63.5	70	6.40	0	0.70	Sand, very fine to fine, silty; well sorted; subrounded; light gray (10YR
				0.7	6.40	Sand, very fine to fine; well sorted; subrounded; light gray (10YR 7/1); pyrite grains (medium-coarse sand-sized) at 2.7 ft of run; faint lamination/cross-lamination esp. in basal 0.6 ft (weak red color)
20	70	80	9.60	0	3.40	Sand, fine to medium, subrounded to subangular; gray (10YR 6/1)
				3.4	5.00	Clay and Sand, interbedded (beds 0.08-0.17ft [2.4-5.2 cm] thick); clay very dark gray (10YR 3/1); sand as above
				5	6.80	Sand, fine to medium, subrounded to subangular; gray (10YR 6/1)
				6.8	7.90	Clay and Sand, laminated to interbedded (mm to 5.2 cm thick); clay very dark gray (10YR 3/1); sand as above
				7.9	9.60	Sand, fine to medium, subrounded to subangular; gray (10YR 5/1)

Table A-2. Description of core from CE Cd 91 -- Continued.

[Explanation of codes at end of table.]

Core run	Interval drilled depth in ft		Amount recovered (ft)	Core intervals ft in core run*		Lithologic description**
	from	to		from	to	
21	80	90	5.70	0	1.00	Sand, fine to medium, subrounded to subangular; gray (10YR 6/1)
				1	1.50	Clay, silty and Sand, very fine to fine, silty, irregularly laminated to thinly bedded; stiff; dark gray (10YR 5/1- 4/1)
				1.5	2.50	Sand, very fine to medium, subrounded to subangular; with silt-clay laminations increasing downward; gray (10YR 6/1); lignite particles concentrated in basal 0.2 ft
				2.5	4.50	Clay, silty to very fine sandy; stiff; dark gray (10YR 5/1- 4/1); faintly laminated by fine carbonaceous particles and slight variations in sand content.
				4.5	5.70	Sand, very fine to medium; subrounded to rounded; gray (10YR 5/1-6/1); carbonaceous particles throughout and concentrated at top and base of interval
22	90	94	2.10	0	0.70	Clay, slightly sandy, fine; gray (10YR 6/1)
				0.7	1.80	Sand, fine to medium; well sorted; subangular to subrounded; brown (7.5YR 5/2)
				1.8	2.10	Clay and Sand, fine, interbedded (~0.08-0.17 ft [2.4-5.2 cm] thick); (clay) gray (10YR 6/1) and (sand) brown (7.5YR 5/2)
23	94	100	2.70	0	0.20	Clay; gray (7.5YR 5/1)
				0.2	0.30	Sand, fine; light brown (7.5YR 6/4)
				0.3	0.80	Clay; dark gray (7.5YR 4/1)
				0.8	1.35	Sand, fine, clayey; subangular; light brown (7.5YR 6/4)
				1.35	1.70	Clay, sandy; gray (7.5YR 4/1)
				1.7	2.30	Sand, fine; light brown (7.5YR 6/4); trace carbonaceous particles
				2.3	2.70	Clay, sandy; dark gray (7.5YR 4/1)
24	100	105	1.15	0	0.40	Sand, fine, clayey; brown (7.5YR 5/3) and gray (7.5YR 5/1)
				0.4	0.60	Sand, fine, and black carbonaceous material
				0.6	0.90	Sand, fine, slightly silty; gray (7.5 YR 4/1 to 5/1) to brown (7.5YR 5/3); trace fine carbonaceous particles
				0.9	1.15	Clay-silt, sandy, fine; dark gray to gray (7.5YR 4/1-5/1)
25	105	110	5.00	0	1.50	Clay, silty; dark gray (7.5YR 4/1)
				1.5	2.20	Clay, sandy, fine; dark gray to gray (7.5YR 4/1-5/1); with a couple gravel-sized nodules of dark red-brown ironstone (up to 4 cm)
				2.2	5.00	Clay, silty; dark gray to gray (7.5YR 4/1-5/1); with bits of carbonaceous material between 2.7 and 3.5 ft of run; few dark red-brown ironstone nodules/fragments (up to 10 mm)
26	110	120	4.70	0	0.20	Clay, silty, dark gray to gray (10YR 4/1-5/1)
				0.2	4.70	Sand, very fine to fine, silty, clayey; gray (10YR 5/1-6/1); few gravel-sized dark reddish brown ironstone fragments/nodules *(note: core as photographed has a thin clayey rind; center of core is sandy)*
27	120	123	2.40	0	2.30	Clay-silt, sandy and Sand, very fine to fine, silty to clayey, firm; gradationally interbedded (0.1 to 0.8 ft); dark gray/reddish gray (10YR 4/1-10R 5/1) to gray (10YR 5/1); trace lignite/carbonaceous particles; few dark reddish brown nodules/fragments of ironstone; *(note: core as photographed has a thin clayey rind; center of core varies)*

Table A-2. Description of core from CE Cd 91 -- Continued.

[Explanation of codes at end of table.]

Core run	Interval drilled depth in ft		Amount recovered (ft)	Core intervals ft in core run*		Lithologic description**
	from	to		from	to	
28	123	130	6.70	0	1.10	Clay; mottled very dark gray to gray (10YR 3/1-4/1) with minor tan, burrow-like structures; basal contact fairly sharp
				1.1	4.65	Clay; mottled mainly gray to light gray (7.5YR 6/1 to 7/1) with some pale red; little to trace red -brown (iron oxide/cemented) nodules/spherules
				4.65	4.95	Clay-silt, slightly sandy, very fine; very thinly bedded and color banded; upper and lower layers ~0.05 ft (1.5 cm) thick, angled, light gray (7.5 YR 7/1); center layer very wavy laminated/disturbed, pale red with light gray
				4.95	5.90	Clay sandy; faintly mottled mainly light gray (7.5 YR 7/1), less pale red; with red-brown spherules/nodules abundant at top and decreasing downward
				5.9	6.70	Clay, sandy; light gray to white (7.5YR 7/1-8/1) at top with increasing mottling with red (10R 4/6) toward bottom.
29	130	140	8.80	0	8.80	Clay, silty; mottled to undulating layers of white to light gray (7.5YR 8/1 - 7/1) and red (10R 4/6) (paleosol structures?); with red nodules/ spherules; two distinct dipping factures in core at about 4.3 ft and 5 ft
30	140	150	7.40	0	1.80	Clay; mottled gray (7.5 YR 5/1) and red (10R 4/6); trace red-brown nodules (1-3 mm)
				1.8	5.10	Clay; mottled to wavy laminated, light gray to white (10YR 7/1-8/1) and red 10R 4/6; increasing red-brown nodules with depth; *[core twisted/corkscrewed via drilling process (high mud pressure) between about 3.5 and 5 ft of run]*
				5.1	5.50	Clay; mottled to wavy laminated; mainly red (10R 4/6) and less light gray (10YR 7/1)
				5.5	6.20	Clay, as above but with first appearance of white /tan spherules/nodules (1-2 mm) along with fewer red-brown nodules
				6.2	7.40	Clay, wavy bedded to laminated and mottled light-gray to white (10YR 7/1 8/1) and red (10R 4/6); white/tan and red-brown spherules/nodules
31	150	158	3.90	0	1.20	Clay; mottled light gray to white (10YR 7/1-8/1 and red (10R 4/6); trace tan and red-brown spherules
				1.2	1.35	Clay; wavy laminated light gray (10YR 7/1) and red to purplish (dusky) red (10R 4/6 - 3/4); trace spherules
				1.35	1.60	Clay; mottled light gray to white (10YR 7/1-8/1 and red (10R 4/6); trace tan and red-brown spherules
				1.6	2.40	Clay; wavy laminated light gray (10YR 7/1) and red to purplish (dusky) red (10R 4/6 - 3/4); trace spherules
				2.4	3.50	Clay; mottled red 10R 4/6) with less gray to light gray (10 YR 6/1-7/1); trace tan and red-brown spherules
				3.5	3.90	Clay; mottled weak red (10R4/4) and reddish gray (10R 5/1)
32	158	160	2.00	0	0.40	Clay; mottled red 10R4/6 and gray (10YR 6/1)
				0.4	0.60	Clay; alternately laminated and faintly mottled, gray (10YR 6/1) and red to weak red (10R 4/6-4/4)
				0.6	2.00	Clay; mottled gray (10YR 5/1-6/1) with less red-weak to red (10R 5/6-5/4); trace red-brown nodules/spherules; diagonal break/fracture in core at about 1.6 ft
33	160	164.5	4.50	0	3.00	Clay; mottled dark gray (7.5YR 4/1) and brown (7.5YR 4/4-5/4); trace reddish brown nodules in upper portion.
				3	3.80	same as above (clay, mottled) but with occasional thin layers and particles of black, carbonaceous? particles
				3.8	4.25	Clay, silty, with very fine sand increasing downward (grades into sand below); faintly mottled; gray (7.5YR 5/1), brown (7.5YR 4/2); dark gray (7.5YR 4/1)
				4.25	4.50	Sand, very fine to fine, clayey, silty; gray (7.5YR 5/1), dar gray (7.5YR 4/1); black carbonaceous particles

Table A-2. Description of core from CE Cd 91 -- Continued.

[Explanation of codes at end of table.]

Core run	Interval drilled depth in ft		Amount recovered (ft)	Core intervals ft in core run*		Lithologic description**
	from	to		from	to	
34	164.5	170	4.80	0	0.50	Sand, fine to medium; gray (10YR 5/1) to dark yellowish brown (10YR 4/4), lignitic, minor pyrite
				0.5	4.80	Clay, silty, trace very fine sand; mainly mottled but with laminated and wavy laminated intervals; stiff; dusky red (10R 3/4), light gray (10YR 7/1), reddish brown (2.5 YR 5/4); trace dark red nodules
35	170	180	10.00	0	10.00	Clay, silty, slightly sandy; mottled with distinct paleosol(?) structures; stiff; weak red (10R 5/2), light gray (10YR 7/1), dark red (10R 3/6); white/tan and red-brown spherules/nodules
36	180	190	10.00	0	9.00	Clay, silty; mottled with distinct paleosol(?) structures; stiff; weak red (10R 5/2), light gray (10YR 7/1), dark red (10R 3/6), olive yellow (2.5Y 6/8) but mainly reddish in upper 6.5 feet and more variegated weak red and light gray below.
				9	10.00	Clay, silty, wavy lamimated and mottled; stiff; weak red (10R 5/2), light gray (10YR 7/1), dark red (10R 3/6); dark red-brown nodules and
37	190	200	7.20	0	3.00	Clay, silty; alternating mottled and wavy laminated; stiff; weak red (10R 5/2), light gray (10YR 7/1), dark red (10R 3/6)
				3	5.10	Clay, sandy, fine; light gray (7.5YR 7/1); a few small (coarse-sand-sized) nodules of pyrite between 3.8 and 4.1 ft
				5.1	5.60	Clay, silty; mottled; weak red (10R 5/2), light gray (10YR 7/1), dark red (10R 3/6)
				5.6	7.20	Clay, silty; laminated to wavy laminated; light gray and weak red (10R 5/4) grading down to light gray, yellow (10YR 7/8), pale red (10R 6/3)
38	200	206	4.80	0	3.80	Clay-silt, sandy, fine; mottled; light gray (10YR 7/1), yellow (10YR 7/8), light olive brown (2.5YR 5/3); cobble (cut) at base (~3.8 ft)
				3.8	4.80	Sand, fine-medium, silty and Silt, clayey, thinly bedded to wavy laminated; sand is yellowish brown (10YR 5/6), silt white to light gray (10YR 8/1-7/1); thin layers of red, tan (hematite/siderite?) spherules/nodules at 4.15 ft and 4.6 ft
39	206	208	1.30	0	1.30	Similar to above with weak red, partially cemented silty sand at 0.40 - 0.42 ft
40	208	210	0.10	0	0.10	*Essentially no recovery* - Silt, clayey, sandy; mottled; light gray to white (10YR 7/1-8/1), yellowish brown (10YR 5/6)
41	210	213	1.40	0	0.20	Clay, slightly silty; firm; white to light gray (10YR 8/1-7/1)
				0.2	0.30	Clay, silty; red (10R 5/6); red spherules and thin ironstone at base
				0.3	1.30	Sand, fine to medium; red (2.5YR 5/6)
				1.3	1.40	Sand, silty, clayey; mottled; light red (2.5YR 6/6) and white to light gray (10YR 8/1-7/1)
42	213	220	1.30	0	1.30	Sand, medium to coarse, trace fine gravel, angular to subangular; mainly very pale brown (10YR 7/3) grades to light reddish brown (2.5YR 6/4) *(note: drilling fluid stained some of sand light red)*
43	220	230	3.20	0	2.30	Sand, medium to coarse; trace clay; overall reddish; grains mainly very pale brown to light gray (10YR 7/3-7/2) or clear; grades into coarser
				2.3	2.60	Sand, medium to coarse, some fine gravel, angular to subangular; overall light reddish brown to red (2.5YR 6/4-5/6) but grains mainly very pale brown to light gray (10YR 7/3-7/2) or clear
				2.6	3.20	Sand, medium to coarse fines downward to Sand, fine, slightly silty; bedded to laminated; color grades from red and light reddish brown (2.5YR 5/6-6/4) to very pale brown (10YR 7/3) and reddish yellow (7.5YR 6/6)

Table A-2. Description of core from CE Cd 91 -- Continued.

[Explanation of codes at end of table.]

Core run	Interval drilled depth in ft		Amount recovered (ft)	Core intervals ft in core run*		Lithologic description**
	from	to		from	to	
44	230	240	2.10	0	1.85	Sand, medium, little coarse; light brown 7.5 YR 6/4
				1.85	2.10	Sand fine to medium, variably silty, laminated to thinly bedded, color banded "pink" tan (5YR 7/4), strong brown (7.5YR 5/6); reddish yellow (7.5YR 6/6); iron-cemented sand at base
45	240	250	3.10	0	0.37	Sand, coarse to very coarse, some medium sand and fine gravel; overall reddish brown with individual grains white, clear, tan; gray iron-cemented sand at top and base;
				0.37	0.40	Clay, purplish and white
				0.4	0.44	Ironstone to iron-cemented sand; brown (7.5 YR 4/4)
				0.44	1.00	Clay, silty, and Silt, clayey; laminated to cross laminated; white (10YR 8/1), very pale brown (10YR 8/3); yellowish brown (10YR 5/6), stong brown 7.5YR 5/6.
				1	1.75	Sand, fine to medium; white at top to red (2.5YR 5/6); iron cemented lamination at 1.45 ft interval depth
				1.75	2.45	Clay, silty; laminated; white, pale brown and strong brown
				2.45	2.75	Sand, fine to coarse; strong brown 7.5YR 5/6, iron cemented sands toward base as clasts
				2.75	3.10	Clay, purplish to weak red 10R 5/3; thin layer of black to yellowish red (5YR 4/6) Iron-cemented sand at ~2.93 ft and at base
46	250	256.5	2.30	0	0.40	Sand, fine to medium, clayey; variably iron-cemented; dark reddish brown (5YR 3/3 - 2.5/2)
				0.4	*0.70*	*no recovery -interval lost coming out of barrel; presumably sand*
				0.7	2.60	Sand, fine to medium; variably iron-cemented and Ironstone; strong brown (7.5YR 4/6-5/6), dark reddish brown (5YR 3/3 - 2.5/2) and black
47	256.5	260	2.75	0	1.30	Iron-cemented sand, fine to medium; brown, dark reddish brown (5YR 3/3 - 2.5/2), white, black
				1.3	1.45	Sand, fine to medium, trace silt, clay (uncemented); purplish to weak red (10R 4/4)
				1.45	2.75	Iron-cemented sand, fine to medium; brown, dark reddish brown to black; few irrigular blebs of semi-consolidated sand with trace silt/clay
48	260	270	4.20	0	0.40	Similar to above
						Note: geophysical log suggests missing sandy interval to ~264.5 ft
				0.4	0.90	Clay; plastic; thinly bedded to mottled; mainly white to light gray, lesser red to pale red (10R 5/6-6/2); interval with dark red (siderite/hematite?) spherules at ~0.7ft
				0.9	2.60	Clay, variably silty; very stiff; mottled; reddish gray 10R 5/1), red (10R 4/4); intervals with dark red (siderite/hematite?) spherules
				2.6	3.70	Clay, silty; very stiff; white to light gray (10YR 8/1)
				3.7	4.20	Clay, silty, little fine sand; very stiff; mottled; gray (5YR 5/1) and white (10YR 8/1)
49	270	280	3.20	0	0.55	Clay clasts(?) in fine sandy clay matrix; clasts light gray (10YR 7/1), light yellowish brown (10YR 6/4); matrix light brownish gray (10YR 6/2)
				0.55	0.70	Sand, fine to coarse and Clay, trace fine gravel; light brownish gray (10YR 6/2)
				0.7	0.85	Ironstone and cemented sand; black, dark reddish brown
						Note: geophysical log suggests missing sandy interval to ~277.5 ft
				0.85	1.15	Clay and Silt; irregularly layered; thin layer of coarse sand at base; grayish brown (10YR 5/2) and yellowish brown (10YR 5/6)
				1.15	3.20	Clay, silty; very stiff; faintly mottled to laminated; mainly dark gray (5YR 4/1); few tan siltier laminations; black carbonaceous material toward base (2.7 ft and down) *(Note: pollen sample from this interval)*

Table A-2. Description of core from CE Cd 91 -- Continued.

[Explanation of codes at end of table.]

Core run	Interval drilled depth in ft		Amount recovered (ft)	Core intervals ft in core run*		Lithologic description**
	from	to		from	to	
50	280	290	3.70	0	0.60	Silt and fine Sand, slightly clayey; laminated to mottled; gray to dark gray (10YR 5/1-4/1); black carbonaceous particles
				0.6	0.85	Clay, silty; dark gray (10YR 4/1); black carbonaceous material concentrated in few thin layers
				0.85	1.00	Silt and fine Sand, slightly clayey; (wavy) laminated; gray to dark gray(10YR 5/1-4/1); black carbonaceous particles concentrated in one lamination
				1	3.70	Clay, slightly silty; faintly mottled to thinly bedded and wavy laminated toward base; dark gray to very dark gray (10YR 4/1-3/1); minor black carbonaceous particles
51	290	295	0.85	0	0.55	Clay; moderately stiff; mottled; light gray (10YR 7/1) and reddish brown (10YR 4/4)
				0.55	0.85	Clay; stiff; mainly reddish brown (10 YR 4/4)
52	295	300	1.13	0	0.05	As above
				0.05	1.13	Clays, variably silty (siltier toward base); stiff; variably mottled, laminated and thinly bedded; highly variegated colors: gray (10YR 6/1), yellowish brown (10YR 5/4), reddish brown (2.5YR 4/4), weak red (10R 4/3), reddish gray (10R 5/1); white spherules (coarse sand sized) below ~ 0.5 ft.
53	300	310	7.92	0	1.90	Clay, silty, trace fine sand; stiff; mottled with paleosol(?) and/or burrowing pattern; mainly red (2.5YR 4/6) with brown and light yellowish brown (2.5Y 6/4); trace white coarse-sand-sized spherules; fine mica flakes; grades into underlying interval
				1.9	3.60	Clay-Silt, variable sand, fine to coarse; very stiff; faintly mottled; weak red (10R 5/3) and reddish gray (10R 5/1); white coarse sand-sized spherules
				3.6	5.60	Clay, silty, trace fine sand; very stiff; mottled with paleosol(?) and/or burrowing pattern; light yellowish brown (2.5Y 6/4); red (2.5YR 4/6) with brown (10YR 4/3), minor light gray (10 YR 7/1); trace white coarse-sand-sized spherules
				5.6	5.73	Part Silt, sandy, fine to coarse brown (10YR 4/3) and part Clay, silty; stiff; light gray (10YR7/1), continues downward
				5.73	6.30	Silt-Clay, sandy, fine-grained with increasing sand downward; very stiff to stiff; faint mottles and occasional laminations; light gray to gray (10YR 7/1-6/1); minor light olive brown (2.5Y 5/3)
				6.3	7.45	Sand, fine, silty, clayey; stiff; faint mottles and occasional wavy laminations; light gray to gray (10YR 7/1-6/1); minor light olive brown (2.5Y 5/3); fine mica particles
				7.45	7.92	Silt-Clay, trace sand; very stiff; mottled toward base on interval; mainly light gray (10YR 7/1), lesser dark yellowish brown (10YR 4/4) and red
54	310	320	7.66	0	6.60	Clay, silty, slightly sandy, very fine to fine; mottled; yellowish brown (10YR 5/4), weak red (10R 5/3), reddish gray (10R5/1), minor brown (10YR 4/3); white and red spherules (siderite?)
				6.6	7.00	Clay-Silt with increasing fine sand downward; otherwise similar to above
				7	7.66	Sand, fine, clayey, silty; mottled but mainly light gray (10YR 7/1) less dark brown (10YR 5/3), light yellowish brown (2.5 YR 6/4); sand-sized spherules mainly tan; fine mica particles
55	320	330	9.40	0	7.50	Clay, variably silty, stiff to very stiff; generally mottled; reddish brown (2.5YR 4/4) brown (7.5 YR 4/4), minor thin streaks and blebs of light gray; some white and red spherules; minor black carbonaceous material toward base
				7.5	9.30	Similar to above but with increase in medium to coarse sand and spherules, white, red; some black carbonaceous material to ~ 8.2 ft
				9.3	9.40	Clay, slightly silty; plastic; dark gray (7.5YR 4/1)

Table A-2. Description of core from CE Cd 91 -- Continued.

[Explanation of codes at end of table.]

Core run	Interval drilled depth in ft		Amount recovered (ft)	Core intervals ft in core run*		Lithologic description**
	from	to		from	to	
56	330	340	9.50	0	5.00	Clay, silty; faintly mottled, dark reddish gray (5YR 4/1) and light bluish gray (gley2 7/1); grades into underlying interval
				5	5.45	Silt-Clay; mottled, bluish gray (gley2 6/1), greenish gray (gley 1 5/1) dark reddish gray (5YR 4/1); grades into underlying interval
				5.45	7.30	Clay silty with increasing silt downward; mainly dark reddish gray (10YR 4/1); some fine mica particles
				7.3	8.00	Silt, sandy fine, trace clay; gray to grayish brown (10YR 5/1-5/2); fine mica particles
				8	8.90	Clay, silty; dark reddish gray (5 YR 4/2)
				8.9	9.50	Sand, fine to coarse, clayey; mottled; multicolored - light bluish gray (approx. gley 2 7/1), gray (10YR 5/1), brown (10YR 4/3)
57	340	350	5.00	0	3.00	Silt-Clay, sandy coarsening downward to Sand, fine to coarse, silty, clayey, trace fine gravel; variably mottled; mainly gray (10YR 6/1) grading down to multicolored light olive brown (2.5YR 5/4), gray to light gray (10YR 6/1-7/1); weak red (10R 5/3)
				3	4.85	Silt-Clay, sandy coarsening downward to Sand, fine to medium, slightly silty, clayey, trace fine gravel; variably mottled; light olive brown (2.5YR 5/4) and light gray (10YR 7/1) grading downward to light gray gray (10YR 7/1)
				4.85	5.00	Gravel, sandy; subrounded to subangular; mainly white or translucent gray quartz with multicolored (light gray, weak red, dark gray) sand matrix
58	350	360	0.35	0	0.35	Silt-Clay and Gravel, fine to coarse, subrounded to subangular; gray (10YR 6/1) with white to tan gravel *(gravel stuck in end of barrel so material as recovered may not be representative of interval)*
59	360	370	2.95	0	0.35	Clay, silty; light gray (7.5YR 7/1) and dark gray (10 YR 4/1; distinct break with next interval *(this may be remnant of previous run)*
				0.35	2.95	Clay, slightly silty with silt increasing downward; faintly mottled reddish gray (10R 5/1 and gray (7.5R 6/1) to distinctly gray and dusky red (10R 3/3) in lower foot
60	370	372	2.00	0	1.80	Clay, silty, sandy, fine to coarse; very stiff and dry; mottled; weak red (10R 4/3) Gray (10YR 6/1) and yellowish brown (10YR 5/4); abundant dark red and tan iron-rich spherules
				1.8	2.00	Sand, fine, silty, clayey; mottled; light gray (7.5YR 7/1) and weak red (10R 4/4)
61	372	380	7.30	0	2.45	Clay, silty, sandy, fine; stiff; mottled; light gray to gray (2.5Y 7/1-6/1), weak reds (10R 5/2-4/4), yellowish brown (10YR 5/4)
				2.45	2.60	Clay, silty; moderately stiff; laminated to thinly bedded; gray and light olive brown (2.5Y 5/4)
				2.6	4.40	Clay-Silt, slightly sandy; mottled; yellowish brown (10YR 5/4), red (10R 4/6), light gray (2.5Y 7/2) --overall yellowish cast; abundant spherules (red, tan)
				4.4	5.50	Clay-Silt; mottled; multicolored: weak red (10R 5/3-5/4), olive brown (2.5 Y 4/4), red to dark red (2.5 YR 4/6-3/6) (color change from above); fine mica flakes
				5.5	7.73	Clay-Silt as above but color change to grays (2.5Y 6/1-5/1)
62	380	381.65	1.40	0	0.40	Clay and Sand, fine; soft; clay mainly yellowish brown and sand gray; micaceous (sand); *may be up hole material*
				0.4	0.95	Clay-Silt; very stiff; wavy laminated to faintly mottled; gray to dark gray (10YR 5/4-4/1)
				0.95	1.40	Sand, very fine to fine; laminated; gray (10YR 6/1); micaceous

Table A-2. Description of core from CE Cd 91 -- Continued.

[Explanation of codes at end of table.]

Core run	Interval drilled depth in ft		Amount recovered (ft)	Core intervals ft in core run*		Lithologic description**
	from	to		from	to	
63	~381.65	390	6.38	0	2.30	Sand, fine; gray (10YR 6/1); micaceous; flecks of black carbonaceous material
				2.3	3.55	Sand, fine; gray to dark gray (10YR 5/1-4/1); micaceous; increase in black carbonaceous material with concentrations in few thin layers at 2.3 to 2.35 ft
				3.55	6.38	Sand, fine, variably silty, clayey (in intervals); dark gray (10YR 4/1); micaceous; increase in carbonaceous particles and concentrated in laminations to thin beds at 4 to 4.1 ft, and 6.15 to 6.38 ft; some mottling (possible burrowing)(light gray sand) between 5 and 6 ft
64	390	400	1.20	0	1.10	similar to above; 0.05 ft carbonaceous layer at base
				1.1	1.20	Clay, slightly silty; very stiff; irregular color laminations gray(2.5Y 6/1) and light yellowish brown (10YR 6/4)
65	400	404.5	5.00	0	2.30	Clay-Silt, trace fine sand; overall fairly plastic and soft; mainly light gray (10YR 7/1 to 2.5Y 7/1) with periodic intervals of stiff mottled red, yellowish brown and gray
				2.3	4.50	Clay-Silt, variably sandy, fine to medium; stiff; mottled; mainly light gray (10YR 7/1 to 2.5Y 7/1) with brown (7.5YR 4/3) and flecks of dark red (10R 3/6); *note core interval stretched so recovery greater than drilled interval*
66	404.5	410	7.50	0	1.67	Clay-Silt; grades downward from light gray (2.5Y 7/1) to mottled with weak red (10R 5/2) to multicolored with reddish brown (2.5YR 4/4) and yellowish brown 10YR 4/4
				1.67	1.80	Clay, silty, plastic, slighty crinkly laminated; multicolored as above
				1.8	2.30	Clay-Silt, sandy, mainly light gray (10YR 6/1)
				2.3	2.95	Clay, silty, mottled; weak red (10R 5/2) with minor gray; abundant coarse-sand-sized tan (siderite?) spherules or spherulitic aggregates
				2.95	7.5 (really 5.50 without stretch)	Clay-Silt, variably sandy; distinctly mottled (paleosol structures?); variegated weak red, pale brown to light yellowish brown (10YR 6/3-6/4), light (bluish) gray (Gley1 7/1), red (10R 4/6); dark red (hematite?) spherules to nodules throughout with heaviest concentration at 5 to 5.7 ft*; note: core stretched between ~ 3 and 7 ft so recovery length greater than depth interval cored*
67	410	415	1.00	0	0.20	Clay-Silt, sandy fine; mottled; yellowish brown and light gray (Gley1 7/1)
				0.2	0.45	Clay-Silt and Sand, fine to coarse; light gray to gray (bluish) (Gley1 7/1-
				0.45	1.00	Clay; extermely stiff; dry; mottled; reds (10R 4/6 -4/8) and light gray (10YR 7/1); few dark red (siderite/hematite?) spherules/spherulitic
68	415	420	1.70	0	1.45	Clay; very soft, plastic; mottled/mixture; multicolored (gray to very dark gray, dusky red (10R 3/2) ; some red and tan nodules (siderite?); bits of black carbonaceous material; *note: some of this material may be mixture of uphole material*
				1.45	1.70	Clay; stiff ot very stiff, mottled to layered; dusky red (10R 3/2- 3/3), weak red (10R 4/2-4/3), minor gray (10YR 6/1); some dark red (siderite/hematite?) nodules espeically toward top
69/70	420	430	9.17	0	3.34	Clay, slightly silty; mottled (paleosol structures); multicolored but grades downward from weak red (10R 4/2) to dusky red (10 3/2) with lesser amounts of yellowish brown (10YR 5/4), dark red (10R 3/6), gray 5YR 5/1); below 2 ft (with change in red color) abundant tan coarse-sand-sized spherulitic aggregates (siderite?)
				3.34	3.85	Clay, silty, sandy, very fine; mottled; mainly gray (10YR 6/1), minor reds
				3.85	9.17	Sand, very fine to fine, clayey, silty; slightly mottled to thinly bedded toward bottom; light gray (2.5Y 7/1), light olive brown (2.5Y 5/4); some tan, coarse-sand-sized, spherulitic aggregates (siderite?)

Table A-2. Description of core from CE Cd 91 -- Continued.

[Explanation of codes at end of table.]

Core run	Interval drilled depth in ft		Amount recovered (ft)	Core intervals ft in core run*		Lithologic description**
	from	to		from	to	
71	430	440	7.80	0	0.30	Sand, medium, slightly silty; light gray (5YR 7/1)
				0.30	3.00	Sand, fine to medium, variably clayey; mottled to bedded; variegated at top (red, gray, tan) to color banded light gray and pale yellow (2.5Y 7/3), yellowish brown (10YR 5/4); some indurated layers at 0.95-1.15 ft, 1.7-1.8 ft with yellow brown (10YR 5/4) (limonite?) cement; tan spherules (siderite?)
				3.00	7.10	Sand, fine to medium; slightly mottled to layered; light gray and pinkish gray (5YR 7/2-6/2), some layers of darker reddish brown (5YR 5/4); some intervals and laminations (2-10 mm) with abundant very fine to fine sand-sized black grains; spherules to nodules (limonite?) between 3.5 to 4.1 ft and 5.1 to 5.5 ft; tiny mica flakes in places
				7.1	7.80	Sand, fine, variably clayey with more clay toward top of interval; brown (10YR 5/3) with reddish clay
72	440	445	5.70	0	0.60	Clay, silty; laminated; light gray (10R 7/1) and dusky red (10R 3/3); few (siderite?) spherules on surface *(possibly not in place)* ; distinct contact with below
			(>100%)	0.6	1.55	Clay, silty; with minor patches of fine sand and/or black lignite; mottled to swirling pattern; bluish gray to dark bluish gray (Gley 2 5/5PB and 3/10B);
				1.55	3.80	Sand, medium to coarse, slightly clayey; bedded to laminated; slightly bluish gray (Gley 2 6/5B); some laminations with very fine black grains abundant
				3.8	5.70	Sand, medium, trace coarse, slightly clayey; faintly laminated; light bluish gray (Gley 2 7/5PB) and pale yellow (2.5YR 7/3)
73	445	450	5.80	0	1.55	Sand, fine to medium, some coarse; faintly bedded to laminated and occasional mottling; light bluish gray (Gley 2 7/5B), pinkish gray (5YR 7/2)
			(>100%)	1.55	3.50	Sand as above but clayey, increase in pinkish gray mottling
				3.5	4.40	Sand, fine, silty, clayey; no layering; nearly white (Gley 1 8/N); increase in mica content
				4.4	5.80	Sand, fine to medium, silty; mottled increasingly downward; white to light gray, pinkish gray (5YR 7/2); very micaceous
74	450	460	9.00	0	0.50	Sand, very fine, silty, clayey; little mottling; mainly nearly white with lesser dark reddish brown (5YR 4/4); micaceous
				0.5	2.65	Sand, very fine to fine, slightly clayey; some thin beds to laminations (more clayey); light bluish gray (Gley 2 7/10B); abundant muscovite (bigger particles than above); sparse fine black grains; grades into underlying interval
				2.65	6.60	Sand, very fine to medium, variably clayey; thin beds and laminations; light and dark gray; darker layers due to concentrations of very fine black grains; abundant muscovite, fairly coarse size; thin clayey interval at ~ 4.65 to 4.85 ft
				6.6	7.10	Sand, medium to coarse, slightly silty; interlayered gray and reddish brown (5YR 5/4); micaceous
				7.1	8.30	Sand very fine to fine, slightly silty; laminated (~ 1- 3 mm); overall gradation from med to light gray with depth but lighter and darker gray laminations throughout; latter with concentrations of very fine black grains; lighter layers siltier; abundant fairly coarse-grained muscovite
				8.3	9.00	Sand, medium to coarse, slighty silty; grades downward from light gray and dark reddish brown to all brown (5YR 4/6)

Table A-2. Description of core from CE Cd 91 -- Continued.

[Explanation of codes at end of table.]

Core run	Interval drilled depth in ft		Amount recovered (ft)	Core intervals ft in core run*		Lithologic description**
	from	to		from	to	
75	460	466	3.45	0	0.60	Sand, very fine to fine; reddish brown (5YR 5/3) grading downward to light bluish gray (Gley 2 8/5PB) then interlayered with a darker gray at base of interval; abundant muscovite
				0.6	2.80	Sand, fine to coarse, variably gravelly and Gravel, sandy; thinly interbedded; some fining up; gravel subrounded to subangular; light reddish brown to reddish brown, light to medium grays; gravel mostly quartz; thin layer of iron (pyrite?) cemented grains at top; some muscovite
				2.8	3.45	Clay, silty, sandy, very fine; massive; light gray; very fine black grains interspersed thoughout
76	466	470	4.10	0	0.25	Clay, faintly mottled, mainly weak red (10R 5/3) to yellowish toward base; very fine black grains interspersed throughout
				0.25	0.90	Sand, very fine to fine, clayey with trace gravel (may not be in situ); faintly mottled; mainly gray (7.5 YR 6/1) with lesser yellowish to pinkish
				0.9	3.25	Silt, slightly sandy; occasional mottles; mainly white (Gley 1 8/N) with minor yellowish gray, light gray (Gley 1 7/N), pink (5YR 7/3)
				3.25	4.10	Clay, very sandy, slightly mottled; abrupt color change from above: mainly dark red (10R 3/6) minor light gray (10R 7/1); sand mostly quartz, clear; fine black grains
77	470	476	6.9 (>100%)	0	6.90	Clay, silty sandy, very fine to fine; mottled; multicolored: upper mainly light gray (Gley 1 7/N) and reds (10R 3/6 to 5/4), central light yellowish brown (10YR 6/5), dusky red (10 R 3/4) and grays, bottom mainly light gray
78	476	480	1.50	0	1.50	Clay, sandy grading down to Sand, fine to coarse, clayey; faintly mottled; mainly bluish gray (Gley 2 6/5PB) with some light reddish brown (2.5 YR 6/4), brownish yellow (10YR 6/6)
79	480	490	10.40 (>100%)	0	1.20	Clay; mottled; dusky red and brownish yellow
				1.2	3.10	Clay, silty, sandy, very fine to fine; mottled to color banded: weak reds and brownish yellow in upper interval to mainly light gray to light bluish gray (Gley 2 7/5PB) with minor brownish yellow and dusky red in lower portion; very fine muscovite
				3.1	6.20	Sand, very fine to coarse, silty, clayey; mottled; light gray, brownish yellow, pale red to red (2.5 YR 7/2-5/6); micaceous, fine-grained
				6.2	7.90	Clay, sandy, very fine to fine; increasing sand downward, pinkish gray (5YR 6/2) to weak red (2.5YR 5/2); grades into underlying sand
				8.1	9.80	Clay, sandy, gravelly and Sand, very fine to coarse, silty, clayey, gravelly; gravels angular to very angular; poorly sorted; mottled; multicolored: grays, yellows, reds; gravels include quartz and lithic fragments up to 2 cm; contact with underlying saprolite not very distinct
				9.8	10.40	Saprolite: clay-silt, gravel with lithic pieces (weathered schist?); distinct horizontal layering (relict schistose structure?); multicolored: grays, greenish gray, yellows, reddish browns; abundant mica; possible chlorite

Table A-2. Description of core from CE Cd 91 -- Continued.

[Explanation of codes at end of table.]

Core run	Interval drilled depth in ft		Amount recovered (ft)	Core intervals ft in core run*		Lithologic description**
	from	to		from	to	
80	490	500	5.10	0	2.30	Saprolite - highly weathered schist; soft; banding (relict) about 30-70 degrees from horizontal; multicolored: earthly yellows, browns, blue-grays, white, dark purplish brown, reds; contains quartz crystals, abundant muscovite in blocks and small sheets, unweathered feldspar(?), chlorite(?) staurolite(?), garnet(?); interval of concentrated muscovite blocks and sheets toward base; irregular basal contact
				2.3	2.85	Clay-silt and Gravel (highly to completely weathered rock?), very soft; very pale brown (10YR 7/4) with thin (1-2 mm) irregular streaks of reddish brown (2.5YR 4/4); fine muscovite; gravel includes quartz and lithic pieces; lower contact irregular
				2.85	3.50	Clay-silt (weathered feldspar?), gravelly, sandy; soft; weakly and irregularly layered; white (Gley 1 8/10Y) with few reddish brown streaks of clay; abundant fine muscovite, coarse-sand- to fine-gravel-sized quartz; layer of smoky quartz (1.5 cm thick) near bottom dipping about 70 degrees; lower contact irregular, dipping about 70 degrees
				3.5	5.10	Saprolite - highly weathered schist as in upper 0-2.3 ft interval but banding is not as apparent
81	500	510	0.80	0	0.45	Clay-silt, gravelly, sandy; mixed reddish brown (2.5YR 5/4) and white; *note: interval may be uphole material; not in place*
				0.45	0.80	Saprolite - highly weathered schist as in previous run; pieces of smokey quartz up to 3 cm; banding seems to dip about 45 degrees
82	510	512	1.90	0	0.70	Saprolite - highly weathered schist as in previous run
				0.7	1.30	Weathered schist (more rock-like than above); fine foliation dipping about 60 degrees; light gray to white with pale yellow and black; bleb of black mineral about 1 cm near top
				1.3	1.90	Weathered schist; color change to darker yellowish brown with some blackish layers 1-2 cm thick; some rock fragments at bottom of interval (amphibole?)
83	512	520	2.40	0	0.10	Rock, black, hard (amphibole?)
				0.1	1.70	Weathered schist; some banding appears to dip about 70-80 degrees; top 0.2 ft fairly hard and similar to lower part of previous run; otherwise softer and color more varied: yellow, brown, white, gray, reddish brown; white material in 1.0-1.3 ft interval is soft
				1.7	204.00	Highly weathered schist(?); soft; faint schistose foliation; colors similar to above; possibly slough(?)
84	520	530	0.95	0	0.65	Highly weathered schist; soft; faint foliation dipping about 45 degrees; mostly yellowish brown 0-0.3 ft, gray 0.3-0.65 ft; abundant muscovite
				0.65	0.95	Highly weathered schist; very soft; no discernable foliation; grayish white with yellow-brown streaks.
85	530	535	2.70	0	0.50	Mix of saprolite and slough/mud?
				0.5	2.70	Saprolite (mica schist/gneiss? highly to completely weathered to sand-silt with fine gravel-sized pieces of schist/gneiss and some "ghost" pieces); soft; vaguely foliated in some intervals; overall color varies from light yellowish brown (10YR 6/4) to light olive brown-olive brown (2.5Y 5/4-4/4) to brown-grayish brown (10YR 5/4-5/3) with flecks of light gray, dark brown, black, white.
86	535	540	1.90	0	1.90	Saprolite, similar to above

Table A-2. Description of core from CE Cd 91 -- Continued.

[Explanation of codes at end of table.]

Core run	Interval drilled depth in ft		Amount recovered (ft)	Core intervals ft in core run*		Lithologic description**
	from	to		from	to	
87	540	550	6.80	0	0.20	Mix of saprolite and sloughed material?
				0.2	3.10	Saprolite similar to previous runs but overall lighter in color; soft to medium hard; some coarse -sand to gravel-sized smokey quartz
				3.1	3.90	Saprolite similar to above but overall darker in color
				3.9	6.25	Saprolite similar to above; largely soft with few firmer intervals; overall lighter in color than above
				6.25	6.80	Saprolite, darker than above with larger but friable fragments of mica schist/gneiss, abundant silvery mica and dark gray particles.
88	550	560	2.05	0	0.20	Sloughed material? (clay-silt partly laminated red and gray)
				0.2	2.05	Saprolite (highly weathered mica schist/gneiss); firm and friable to moderately hard; dark gray (7.5 YR 4/1) to red (2.5 YR 4/6) with lesser white and yellowish brown (10YR 5/4); coarse-sand- to fine-gravel-sized lithic fragments and smokey quartz
89	560	570	2.80	0	1.85	Saprolite (mica schist/gneiss? highly to completely weathered to sand-silt with fine gravel-sized lithic fragments and smokey quartz); soft to moderately hard; vaguely foliated about 45 degree dip between 1.2-1.7 ft; color generally darkens downward; pale brown (10 YR 6/3), gray (10YR 5/1), reddish brown, brown with minor pinkish white (10R 8/2) and white; two subrounded pebbles of smokey quartz at top of interval approximately 2 cm in length.
				1.85	2.60	Saprolite similar to above but no foliation dicernable and color change to dominantly pinkish white to reddish brown (2.5YR 5/3)
				2.6	2.80	Saprolite (highly weathered mica schist/gneiss); light bluish gray (gley 2 8/1-7/1 5PB)
90	570	575		0	0.35	Weathered mica gneiss; vaguely foliated/banded; black, dark gray and white; white intervals highly weathered (former feldspar?); lower contact sharp
				0.35	5.00	Weathered mica schist/gneiss (chlorite?, biotite, muscovite, schist/gneiss); vaguely foliated in some intervals; distinct color change from above: greenish gray (gley 1 6/1 - 5/1 5G) to dark gray with lesser white (weathered feldspar?) and pale red/pink; some smokey quartz
91	575	580	1.90	0	0.90	Similar to above
				9	1.90	Highly weathered and fragmented mica schist/gneiss (lithic fragments of greenish gray mica schist/gneiss with soft whitish and pinkish silt-clay); may be partially sloughed material
92	580	590	10.00	0	10.00	Mica gneiss; variably friable to hard; some foliation/banding, foliation in upper 4 ft dips about 45 degrees; greenish gray and gray, with white, black, pink; some distinctly greenish intervals; includes quartz (clear to smokey), muscovite, biotite, few tiny garnets (variably weathered), epidote(?).

* Interval recovered is shown aligned with top of drilled interval unless drilling conditions or other information indicate otherwise.

** Color codes are based on wet sample matched to Munsell Soil Color Chart, 2000 (revised)

APPENDIX B

CE Be 155 Summary Diagram, Core Photographs and Detailed Lithologic Descriptions

Plate B-1

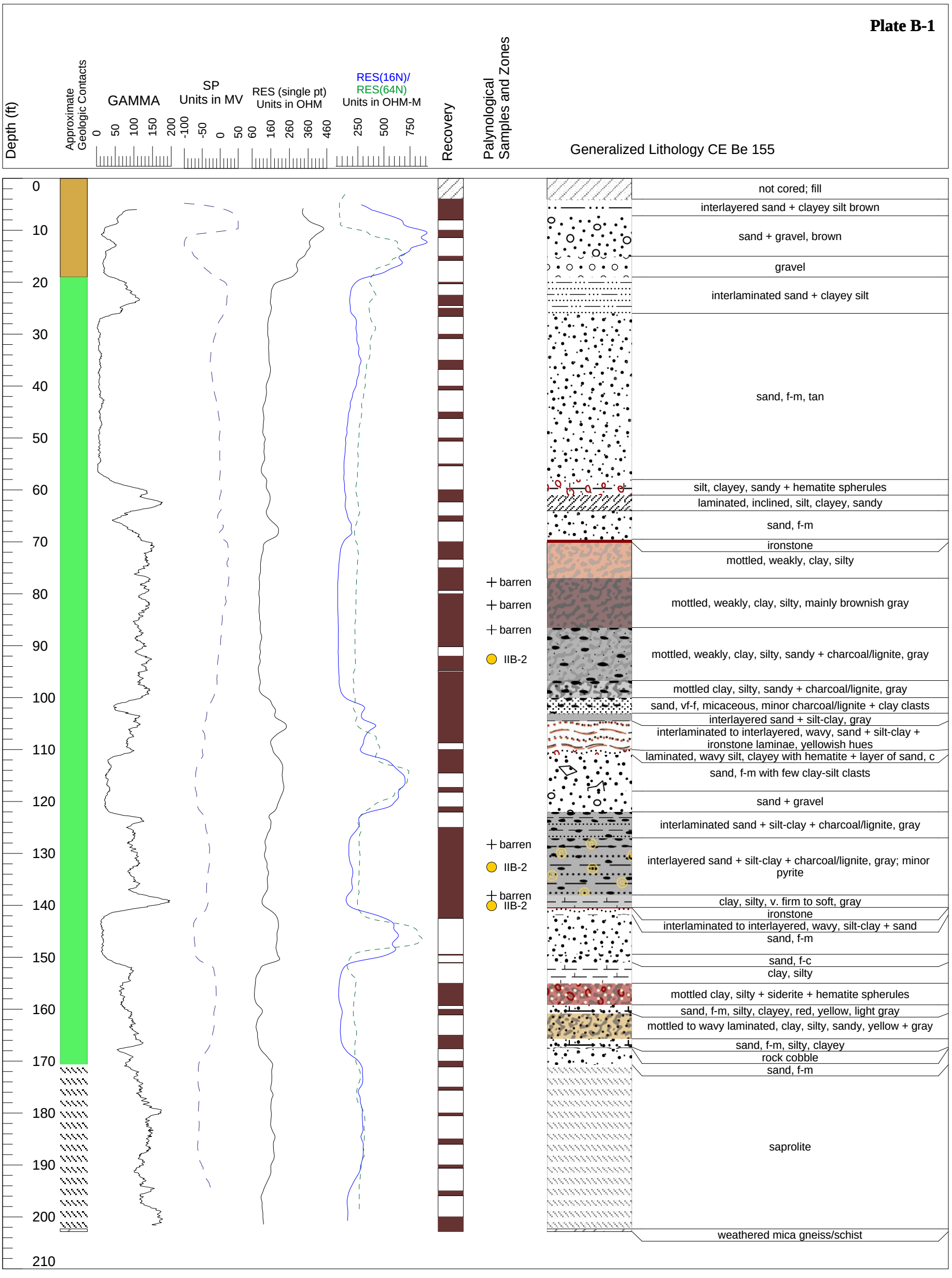

Plate B-1. Summary of data collected from borehole CE Be 155.

Table B-1. Photographs of CE Be 155 core.

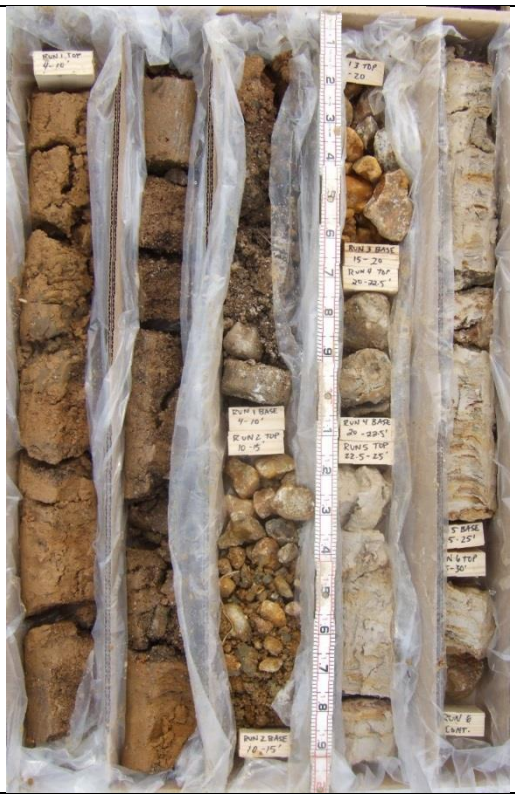	
CE Be 155 Core Box 1 (spans depths of approximately 4 to 26 ft)	CE Be 155 Core Box 2 (spans depths of approximately 26 to 61 ft)
	
CE Be 155 Core Box 3 (spans depths of approximately 61 to 78 ft)	CE Be 155 Core Box 4 (spans depths of approximately 78 to 87 ft)

Table B-1. Photographs of CE Be 155 core -- Continued.

	
CE Be 155 Core Box 5 (spans depths of approximately 87 to 98 ft)	CE Be 155 Core Box 6 (spans depths of approximately 98 to 107 ft)
	
CE Be 155 Core Box 7 (spans depths of approximately 107 to 126 ft)	CE Be 155 Core Box 8 (spans depths of approximately 126 to 134 ft)

Table B-1. Photographs of CE Be 155 core -- Continued.

CE Be 155 Core Box 8a
(Core close up showing pyrite at depth of ~130 ft)

CE Be 155 Core Box 9
(spans depths of approximately 134 to 155 ft)

CE Be 155 Core Box 10
(spans depths of approximately 155 to 170.5 ft)

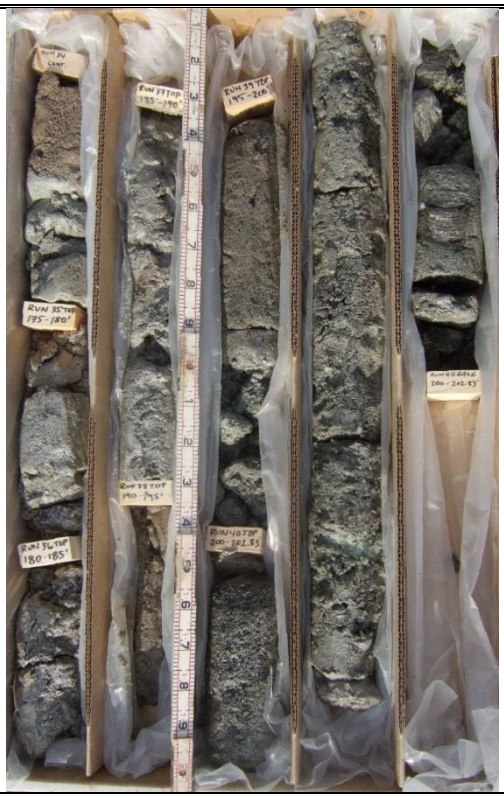

CE Be 155 Core Box 11
(spans depths of approximately 170.5-202.83 ft)

Table B-2. Description of core from CE Bf 155.

[Explanation of codes at end of table.]

Core run	Interval drilled depth in ft		Amount recovered feet	Core intervals ft within core run*		Lithologic description**
	from	to		from	to	
	0	4	n/a			Dug; not cored; (fill)
1	4	10	4	0.00	1.24	Silt, clayey; trace fine sand; disturbed; very soft; brown (7.5YR 4/4)
				1.24	2.60	Sand, fine to coarse; silty, clayey; micaceous; layered; brown (7.5YR 4/4) and dark brown (7.5YR 3/4)
				2.60	2.85	Sand, fine to coarse, and gravel; silty, clayey; micaceous; brown (7.5YR 4/4)
				2.85	3.20	Silt, clayey; strong brown (7.5YR 5/6)
				3.20	4.00	Sand, fine to coarse; gravelly; silty, clayey; micaceous (large flakes); mainly brown (7.5YR 4/4); gravels white, tan
2	10	15	1.4	0.00	1.00	Gravel, fine to coarse; mostly subrounded; few fractured/subangular; mostly tan, quartz; few other rock fragments
				1.00	1.40	Sand, fine to coarse, and Gravel; color varies from strong brown (7.5YR 5/6) to pale yellow (2.5Y 7/3)
3	15	20	0.8	0.00	0.80	Gravel, fine to coarse; mostly subrounded; some subangular or fractured; tan to orangy tan; quartz and other rock fragments
4	20	22.50	0.3	0.00	0.30	Poor recovery; cobble jammed in core barrel; (geophysics suggests similar to subsequent interval below: silt, clayey, sandy)
5	22.50	25	2	0.00	2.00	Silt, clayey and Sand, very fine; faintly laminated; very pale gray (10YR 8/1) and strong brown with darker reddish to purplish brown laminations at 23.1 ft, 23.9 ft, 24.1 ft
6	25	30	1.6	0.00	0.15	Poor recovery; material similar to last interval recovered (may not be in place)
				0.15	1.40	Laminated sand, very fine to fine, silty, and silt, clayey; sandy; yellow (10YR 7/6) to very pale gray (color banded within sandy or silty intervals); and occasional clay-silt purplish
				1.40	1.60	Sand, very fine to medium; trace fine gravel and coarse sand; tan very pale blown (10YR 7/3)
7	30	35	0.85	0.00	0.85	Sand, fine to medium; trace fine gravel and silt; very pale brown (10YR 7/3); very loose
8	35	40	1.8		1.80	Sand, fine to medium; trace coarse sand; very pale brown to white (10YR 8/2 -8/1); very loose
9	40	45	0.75		0.75	Sand, fine to medium; white (10YR 8/1); trace mica; very loose
10	45	50	1.25	0.00	1.25	Sand, fine to medium; very pale brown (10YR 8/2); tiny mica flakes; very loose
11	50	55	0.6	0.00	0.60	Sand, fine to medium; trace silt-clay; very pale brown (10YR 8/2); tiny mica flakes; very loose
12	55	60	0.37	0.00	0.37	Sand, fine to medium; trace silt-clay; very pale brown (10YR 8/2); tiny mica flakes; very loose
13	60	65	2.3	0.00	0.45	Silt, clayey; trace sand, very fine; mostly very pale brown; gravel embedded at top may be from uphole
				0.45	0.77	Silt, clayey, sandy, very fine; mottled very pale brown, strong brown and red-brown; hematite spherules at 60.73 ft
				0.77	1.90	Silt, clayey, sandy, very fine to fine; sand content increases downward; very pale brown (10YR 7/2) with laminations of strong brown; tiny mica flakes
				1.90	2.30	Sand, very fine to fine; trace silt and clay; white (10YR 8/1); tiny mica flakes

Table B-2. Description of core from CE Be 155 -- Continued.

[Explanation of codes at end of table.]

Core run	Interval drilled depth in ft		Amount recovered feet	Core intervals ft within core run*		Lithologic description**
	from	to		from	to	
14	65	70	1		1.00	Sand, fine to medium; trace coarse sand; light gray (10YR 7/1-7/2); tiny mica flaces present; very loose
15	70	75	3.35	0.00	0.10	Ironstone/cemented sand; dark reddish brown to black
				0.10	0.30	Clay, silty; light gray (7.5YR 7/1)
				0.30	1.30	Clay, silty; brown to light pinkish brown (10YR 5/3); thin light gray laminations toward base of interval
				1.30	1.60	Clay, silty; mottled brown and light gray; firm yet plastic
				1.60	3.30	Clay, silty, brown to reddish brown (5YR 4/4) toward base of interval; firm yet plastic
16	75	80	4.35	0.00	2.30	Clay, silty; faintly laminated with very fine micas in some layers; reddish brown (5YR 4/3) with some gray and reddish layers; firm; grades downward to mottled
				2.30	4.35	Clay, silty; very fine mica flakes; laminated to mottled dark gray (5YR 4/1) and dark reddish gray (5YR 4/2); firm
17	80	85	5	0.00	5.00	Clay, silty; slightly sandy, very fine with mica flakes; laminated to mottled brown and dark gray (7.5YR 4/2 - 4/1); few black charcoal fragments toward base
18	85	90	5.2	0.00	0.90	Clay, silty, slightly sandy, very fine to fine; micaceous; laminated to mottled brown and dark gray (7.5YR 4/2 - 4/1)
				0.90	1.40	Clay, silty, sandy, very fine to fine; micaceous; mottled (brownish) dark gray (7.5YR 4/1) with white (sand)
				1.40	2.00	Clay, silty; slightly sandy, very fine, with mica flakes; laminated to mottled (brownish) dark gray (7.5YR 4/1); abundant black charcoal fragments
				2.00	3.05	Clay, silty, slightly sandy, very fine to fine; micaceous; laminated to mottled dark gray (7.5YR 4/1)
				3.05	3.20	Clay, silty, sandy, very fine to fine; micaceous; mottled dark gray (7.5YR 4/1) with white (sand)
				3.20	3.50	Clay, silty; slightly sandy, very fine with mica flakes; laminated to mottled dark gray (7.5YR 4/1); abundant black charcoal fragments
				3.50	3.90	Clay, silty, slightly sandy, very fine to fine; micaceous; laminated to mottled dark gray (7.5YR 4/1)
				3.90	5.00	Clay, silty; slightly sandy, very fine; mica bearing; laminated to mottled dark gray (7.5YR 4/2 - 4/1); abundant black charcoal fragments
19	90	95	2.8	*0.00*	*2.00*	*no recovery; drilled easily as if possibly void and/or sandy; geophysics suggest similar to above with possible slight increase in sand content*
				2.00	4.50	Clay, silty, slightly sandy, very fine to fine; mica bearing; mainly gray (7.5YR 5/1); black charcoal fragments
				4.50	4.80	Charcoal/lignite; minor light gray sandy, silty clay
20	95	100	5	0.00	1.70	Clay, silty, slightly sandy, fine with micas; dark grayish brown (10YR 4/2); fine black charcoal/lignite fragments
				1.70	3.20	Interlayered clay-silt and sand, fine to medium; with micas; gray; fine black charcoal/lignite fragments
				3.20	5.00	Clay, silty; fine mica flakes; mottled dark gray and lighter gray; fine black charcoal/lignite fragments

Table B-2. Description of core from CE Be 155 -- Continued.

[Explanation of codes at end of table.]

Core run	Interval drilled depth in ft		Amount recovered feet	Core intervals ft within core run*		Lithologic description**
	from	to		from	to	
21	100	105	5.1	0.00	0.15	Clay, silty, slightly sandy, very fine; fine mica flakes; gray (10YR 6/1)
				0.15	3.40	Sand, very fine to fine; slightly silty to clayey; fine mica flakes; gray (10YR 6/1); few black charcoal/lignite fragments
				3.40	3.60	Silt-clay; trace very fine sand; micas; dark gray (10YR 4/1)
				3.60	4.00	Sand, very fine to fine, clayey, silty; fines increasing downward;gray (10YR 6/1)
				4.00	4.22	Silt-clay; trace very fine sand; dark gray (10YR 4/1)
				4.22	4.52	Sand, very fine to fine; gray
				4.52	4.62	Sand, very fine to fine with micas; abrupt color change to brownish yellow (10YR 6/6)
				4.62	4.70	Ironstone/cemented sand; dark reddish brown
				4.70	5.10	Sand, very fine to fine, silty, clayey; laminated; orange brown (sand) and gray (clay-silt); mica-bearing
22	105	110	3.6	0.00	3.40	Sand, very fine to fine; strong brown (7.5YR 5/8) with laminations of clay-silt, light gray (7.5YR 7/1); thin ironstone/hardpan at core intervals 1.27ft, 1.53ft, 1.9ft, 1.95ft
				3.40	3.60	Cobble, quartz
23	110	115	4.5	0.00	0.30	Sand, coarse, and gravel, fine, clayey, silty; angular to subangular gravel fragments; multicolored (white, tan, gray) gravels; light gray clay-silt
				0.30	0.55	Silt, clayey; laminated (wavy) with Sand, fine to medium; gray
				0.55	0.90	Silt, clayey; laminated (wavy/convoluted) with Sand, very fine to medium; red brown and gray; hematite nodules
				0.90	4.50	Sand very fine to fine; micas; light gray 10YR 7/2); few clasts of clay-silt
24	115	125	1.3			*Note: geophysics suggest missing sandy interval to ~117.3 ft*
				0.00	0.70	Sand, fine to medium, slightly clayey, silty; light gray (10YR 7/1)
				0.70	1.20	Gravel, fine to coarse and Sand, fine to coarse; white to clear
						Note: geophysics suggest missing sandy interval to ~118.2-121.03 ft
				1.20	1.27	Ironstone/cemented sand; dark gray
				1.27	1.30	Peat(?), dark brown to black; may be from deeper in drilled interval
						no recovery; geophysics suggest 122.03-125-ft is similar to below
25	125	130	5.1	0.00	2.00	Laminated silt-clay, dark gray (10YR 4/1); sand, very fine to fine, gray (10YR 5/1); black charcoal/lignite fragments; micas
				2.00	2.50	Interlayered black woody material/lignite and silt-clay, dark gray (10YR 5/1); micas
				2.50	2.90	Laminated silt-clay, dark gray (10YR 4/1); sand, very fine to fine, gray (10YR 5/1); and black woody material/lignite; micas
				2.90	3.05	Black woody material/lignite
				3.05	3.40	Silt-clay, dark gray (10YR 5/1); few black woody fragments micas
				3.40	3.60	Black woody material/lignite
				3.60	4.90	Laminated silt-clay, dark gray (10YR 4/1); sand, very fine to fine, gray (10YR 5/1); and black woody material/lignite; pyrite cubes near base; micas
				4.90	5.10	Black woody material/lignite

Table B-2. Description of core from CE Be 155 -- Continued.

[Explanation of codes at end of table.]

Core run	Interval drilled depth in ft		Amount recovered feet	Core intervals ft within core run*		Lithologic description**
	from	to		from	to	
26	130	135	4.95	0.00	1.40	Interlayered black woody material/lignite and silt-clay, dark gray (10YR 5/1); micas
				1.40	3.20	Silt-clay, variably sandy, very fine to fine, dark gray to gray ((10YR 4/1-5/1); and black wood/lignite fragments; micas
				3.20	3.30	Sand, very fine to fine, gray (10YR 4/1); micas; few black woody fragments
				3.30	3.40	Black woody material/lignite
				3.40	3.60	Sand, very fine to fine, gray (10YR 4/1); micas; few black woody fragments
				3.60	3.90	Silt-clay, dark gray (10YR 5/1); few black woody fragments micas
				3.90	4.30	Sand, very fine to fine, silty to clayey, gray (10YR 4/1); micas; few black woody fragments
				4.30	4.50	Black woody material/lignite
				4.50	4.62	Sand, very fine to fine, silty to clayey, gray (10YR 4/1); micas; few black woody fragments
				4.62	5.00	Silt-clay, slightly sandy; dark gray (10YR 5/1)
27	135	140	5	0.00	0.30	Interlayered silt-clay and sand very fine to fine, dark gray to gray (10YR 4/-5/1); micas; black woody material in thin layers and fragments
				0.30	0.40	Black woody material/lignite
				0.40	1.30	Interlayered silt-clay and sand very fine to fine, dark gray to gray (10YR 4/-5/1); micas; black woody material in thin layers and fragments
				1.30	1.40	Black woody material/lignite
				1.40	3.20	Interlayered silt-clay and sand very fine to fine, dark gray to gray (10YR 4/-5/1); micas; black woody material in thin layers and fragments
				3.20	5.00	Clay, silty; dark gray and gray (10YR 4/1-5/1), very firm
28	140	149.42	2.5	0.00	0.35	Clay, silty; very dark gray (10YR 3/1), very firm
				0.35	0.45	Clay, silty; gray and yellowish brown, soft
				0.45	0.52	Ironstone/cemented sand; dark reddish brown
				0.52	0.85	Silt-clay and sand, fine to medium; multicolored (white, yellowish brown, reddish brown, tan); convoluted layers
				0.85	2.00	Sand, fine-medium; trace silt-clay; multi-colored: yellowish red (5YR 5/8), very pale brown (10YR 8/4-7/4), light yellowish brown (10YR 6/4)
				2.00	2.50	Sand, fine-medium, (coarser than above)
29	149.42	149.57	0.15	0.00	0.15	Sand, fine-coarse; slightly silty to clayey; strong brown to very pale brown (difficulty in drilling)
30	150	155	0.08			*Difficulty drilling; recovered amount presumed not at top; geophysics suggest < 1 ft would be sand or gravel)*
				0	0.08	Essentially no recovery; (~1 inch of gray clay and hardpan from 5-ft interval presumably not at 150 ft) geophysics suggest ~4 ft of clay possible
31	155	160	4.3	0.00	3.95	Clay, silty; mottled dark reddish brown (weak red 10R 4/4) and dark gray (5YR 4/1); some coarse-sand-sized particles possibly siderite; mica-bearing
				3.95	4.15	Clay, silty; mottled weak red (10R 4/3) and gray to yellowish brown at base of interval; some coarse-sand-sized particles possibly siderite/hematite; possible mineralization fronts (dark red surrounded by yellowish brown then lt gray); mica bearing
				4.15	4.30	Sand very fine to fine, silty, clayey; mica-bearing; mulitcolored: gray, yellowish brown, red

Table B-2. Description of core from CE Be 155 -- Continued.

[Explanation of codes at end of table.]

Core run	Interval drilled depth in ft		Amount recovered feet	Core intervals ft within core run*		Lithologic description**
	from	to		from	to	
32	160	165.00	1.1	0.80	0.80	Sand, fine to medium, silty, clayey; mainly light gray (gley1 7/1); micaceous
				1.00	1.00	Clay, silty, sandy; mottled to wavy laminated; yellowish brown and light gray
				1.10	1.10	Clay, silty, slightly sandy, mottled to wavy laminated, yellowish brown
33	165	170	2.6	0.00	0.70	Clay, silty, slightly sandy, fine to medium, mottled to wavy laminated, yellowish brown (olive brown 2.5Y 4/3) and gray (2.5Y 5/1); micaceous
				0.70	2.30	Sand, fine to medium, silty, clayey; gray (2.5Y 5/1) micaceous; firm
				2.30	2.60	Quartz rock (stuck in end of shoe)
34	170	175	1.1	0.00	0.70	Sand, fine to medium, grayish brown (10YR 5/2); micas; distinct contact with interval below
				0.70	1.10	Sand, fine to medium, silty, clayey; very micaceous (micas very soft; weathering to clay); greenish gray to gray (gley1 6/1-6) (weathered mica schist?)
35	175	180	0.6	0.00	0.60	similar to cored interval above; possibly weathered mica schist?; quartz stone with pyrite at base
36	180	185	0.5	0.00	0.10	Rock fragments -- smokey quartz, black biotite(?)
				0.10	0.50	Weathered mica?: Clay-silt; (talc-like feel) silvery gray, soft
37	185	190	1	0.00	1.00	Weathered mica/chlorite schist(?): clay-silt, silvery gray, with rock fragments -- smokey quartz, black biotite/amphibole; very micaceous; very soft
38	190	195	0.6	0.00	0.60	Essentially no recovery -- appears likely to be material from up-hole (sand, fine to medium; micaceous, gray 2.5Y 5/1)
39	195	200	0.9	0.00	0.60	Essentially no recovery -- appears likely to be material from up-hole
				0.60	0.90	Weathered chlorite/mica schist(?): Clay-silt, sandy, fine to medium; talc-like; silvery gray; very soft; few greenish rock fragments (poor recovery)
40	200	202.83	2.95	0.00	0.20	Mica, biotite, quartz gneiss or schist; indurated
				0.20	2.30	Weathered rock(?) -- rock fragments mixed with clay-like matrix; piece of chlorite(?) very light green rock framents at 1.8-1.9 ft
				2.30	2.55	Rock framents of mica, biotite/amphibole gneiss or schist?
				2.55	2.95	Fragments of biotite quartz gneiss; flecks of pyrite; dark gray to green; one fragment with large crystal or "phenocryst"

* Interval recovered is shown aligned with top of drilled interval unless drilling conditions or other information indicate otherwise.

** Color codes are based on wet sample matched to Munsell Soil Color Chart, 2000 (revised)

APPENDIX C

CE Bf 156 Summary Diagram, Core Photographs and Detailed Lithologic Descriptions

Plate C-1

Depth (ft) | Approximate Geologic Contacts | GAMMA (-10, 40, 90, 140) | RES (single pt) Units in OHM (20, 120, 220) | RES(16N)/RES(64N) Units in OHM-M (-40, 160, 360, 560) | Recovery | Palynological Samples and Zones | Generalized Lithology CE Bf 156

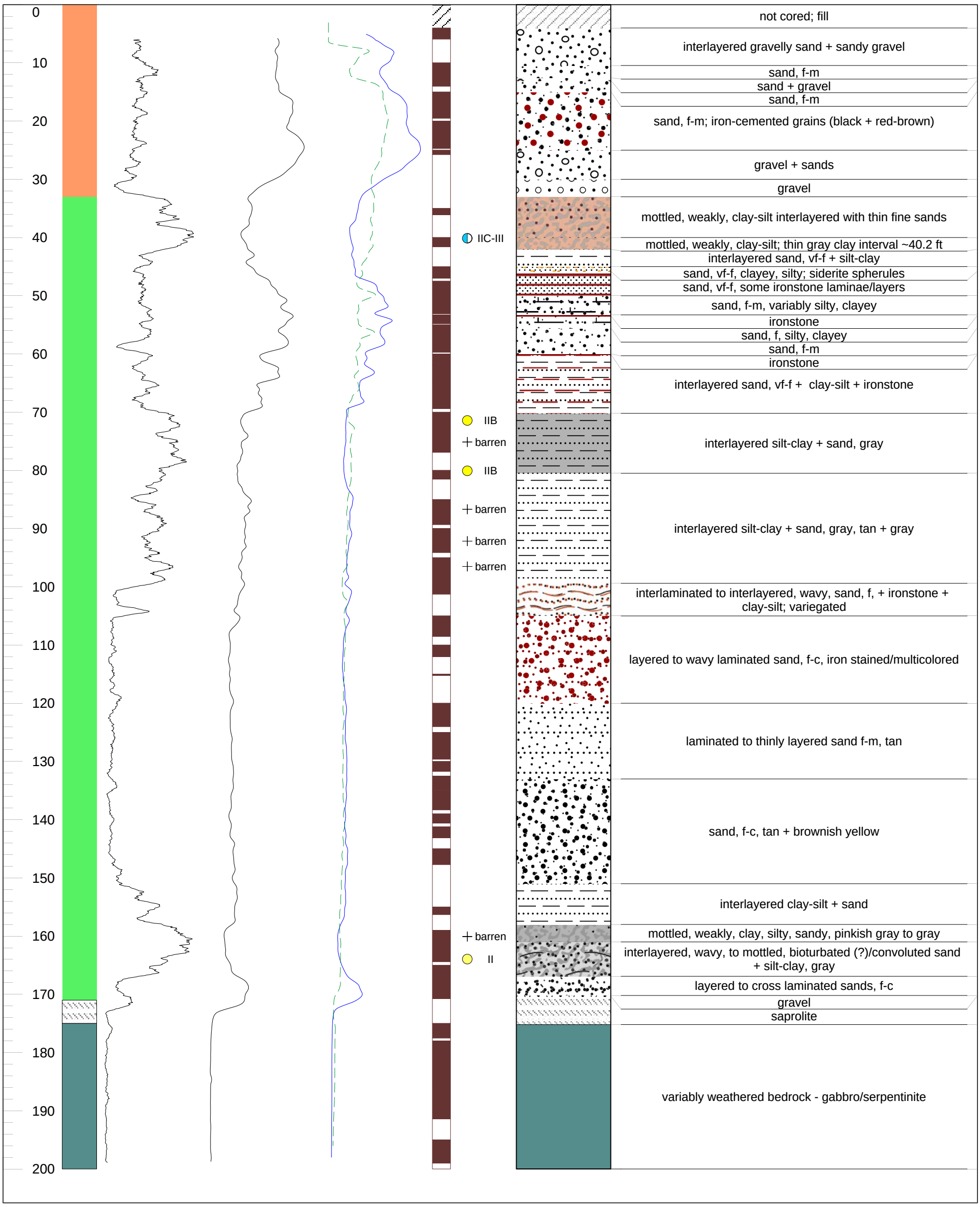

Geologic Units
- Pensauken
- Potomac
- saprolite/weathered rock
- saprolite
- bedrock

Core Recovery
- core
- not cored
- none

Grain size abbreviations
f = fine
m = medium
c = coarse

Plate C-1. Summary of data collected at borehole CE Bf 156

Table C-1. Photographs of CE Bf 156 core.

	
CE Bf 156 Core Box 1 (spans depths of approximately 4 to 18 ft)	CE Bf 156 Core Box 2 (spans depths of approximately 18 to 40 ft)
	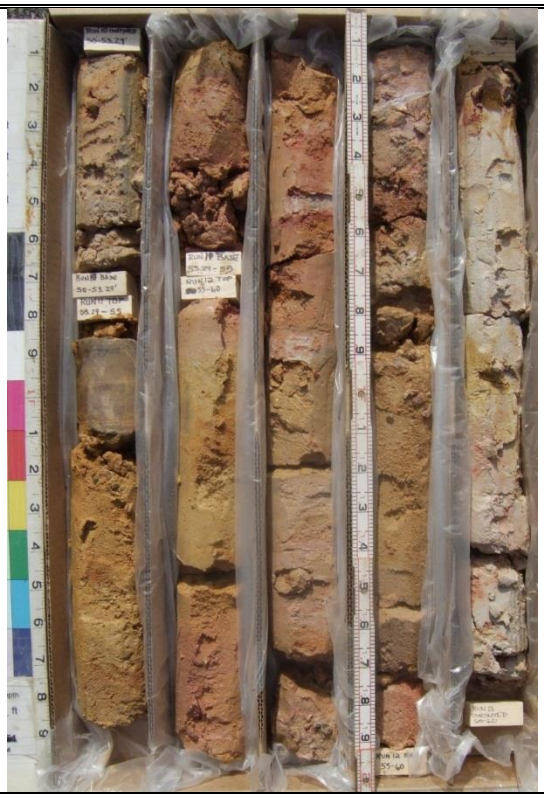
CE Bf 156 Core Box 3 (spans depths of approximately 40 to 52 ft)	CE Bf 156 Core Box 4 (spans depths of approximately 52 to 61.5 ft)

Table C-1. Photographs of CE Bf 156 core -- Continued.

	
CE Bf 156 Core Box 5 (spans depths of approximately 61.5 to 70 ft)	CE Bf 156 Core Box 6 (spans depths of approximately 70 to 85 ft)
	
CE Bf 156 Core Box 7 (spans depths of approximately 85 to 95 ft)	CE Bf 156 Core Box 8 (spans depths of approximately 95 to 107 ft)

Table C-1. Photographs of CE Bf 156 core -- Continued.

	
CE Bf 156 Core Box 9 (spans depths of approximately 107 to 125 ft)	CE Bf 156 Core Box 10 (spans depths of approximately 125 to 135 ft)
	
CE Bf 156 Core Box 11 (spans depths of approximately 135 to 147 ft)	CE Bf 156 Core Box 12 (spans depths of approximately 147-165 ft)

Table C-1. Photographs of CE Bf 156 core -- Continued.

CE Bf 156 Core Box 13
(spans depths of approximately165 to 178 ft)

CE Bf 156 Core Box 13a
(close up of core box including 170-175 ft interval)

CE Bf 156 Core Box 14
(spans depths of approximately 178 to 187 ft)

CE Bf 156 Core Box 15
(spans depths of approximately 187-200 ft)

Table C-2. Description of core from CE Bf 156.

[Explanation of codes at end of table.]

Core run	Interval depth in ft		Amount recovered feet	Core intervals ft within core run*		Lithologic description**
	from	to		from	to	
	0	1				Not cored: fill, gravel
	1	4				Not cored: fill (sand, fine to coarse, clayey, silty)
1	4	10	1.90	0.00	0.12	Sand, little silt-clay; trace gravel; strong brown (7.5YR 5/6)
				0.12	0.54	Sand, fine to coarse, and Gravel, little silt-clay; strong brown (7.5YR 5/6); black ironstone at interval base
				0.54	1.90	Sand, fine to coarse, little gravel; trace fines; color gradation from strong brown (7.5YR 5/6) to very pale brown (10YR 7/6)
2	10	15	4.00	0.00	0.45	Sand, medium-coarse, and Gravel, subrounded; interlayered
				0.45	2.60	Sand, fine to medium; trace fines; subtly laminated; brownish yellow (10YR 6/6) and very pale brown (10YR 7/4)
				2.60	3.10	Sand, fine to coarse, and Gravel; subrounded, brownish yellow (10YR6/6) (sand) with white and brownish pebbles
				3.10	4.00	Sand, fine to medium; brownish yellow (10YR 6/6)
3	15	20	4.50	0.00	3.10	Sand, fine to medium; trace fines; faintly laminated brownish yellow (10Y6/6) to yellowish brown (10YR 5/6); occasional reddish brown, iron-cemented sand grains/hematite(?)
				3.10	5.00	Sand, fine to medium; trace fines; strong brown 7.5YR 5/6; black ellipsoidal grains (iron cemented sand particles?)
4	20	25	4.70	0.00	1.52	Sand, fine to medium; trace coarse sand, gravel and fines; faintly laminated brownish yellow (10Y6/6) to yellowish brown (10YR 5/6); black ellipsoidal grains (iron-cemented sand particles?)
				1.52	1.62	Silty, clayey and Gravel
				1.62	1.92	Sand, fine to coarse, and broken chert(?) pebble(s)
				1.92	2.10	Sand, fine to coarse; gravelly; trace fines; reddish yellow (7.5 YR 6/6) with cemented sphere of "white" sand (very pale gray 7.5YR 8/1)
				2.10	4.47	Sand, fine to medium; trace coarse sand and fines; faintly laminated brownish yellow (10Y7/6) to yellowish brown (10YR 5/6); black ellipsoidal grains (iron-cemented sand particles?)
5	25	35	0.75	0.00	0.75	Gravel, fine to coarse; subrounded and broken; brown, purplish, white
6	35	40	1.10	0.00	0.12	Silt, clayey; light brown (7.5YR 6/3)
				0.12	0.40	Silt, clayey; mottled brownish yellow (10YR 6/6) and light gray (10YR 7/1)
				0.40	0.70	Silt, clayey; variegated (light brown, brownish yellow and light gray); bedding disturbed (possible artifact of drilling?)
				0.70	0.85	Silt, clayey; gray (10YR 5/1)
				0.85	1.10	Sand, fine to medium with laminations of silty clay; light gray (10YR 7/1), very pale brown (19YR 7/4) and yellowish brown (10YR 5/8)
7	40	45	1.60	0.00	0.20	Clay, silty; brown (7.5YR 5/2); a few gravel fragments (possibly from up-hole)
				0.20	0.70	Clay, silty, yellowish brown (10YR 5/4); (interval disturbed; possibly slightly compressed in coring process)
				0.70	2.10	Clay, silty, brown (7.5YR 5/4)
				2.10	2.70	Sand, very fine to fine, silty; light gray (10YR 7/1)

Table C-2. Description of core from CE Bf 156 -- Continued.

[Explanation of codes at end of table.]

Core run	Interval depth in ft		Amount recovered	Core intervals ft within core run*		Lithologic description**
	from	to	feet	from	to	
8	45	48	2.00	0.00	0.90	Sand, very fine to fine; clayey, silty; round grains/crystals of siderite (?); light gray (10YR 7/1); mica bearing
				0.90	1.25	Sand, very fine to fine, clayey, silty; laminated, light gray (10YR 7/1) and light yellowish brown (10YR 6/4); mica bearing
				1.25	1.45	Sand, very fine to fine, trace silt-clay; light gray (10YR 7/2) and brownish yellow (10YR 6/8); mica bearing
				1.45	1.52	Sand, very fine to fine, trace silt-clay; reddish yellow (7.5YR 6/8); mica bearig
				1.52	1.80	Ironstone, dark reddish brown (5YR 3/3-3/4); fragmented (possibly from drilling?)
				1.80	2.00	Sand, very fine to fine, trace silt-clay; reddish yellow (7.5YR 6/8); mica bearing
9	48	50	2.50	0.00	0.80	Sand, very fine to fine, little to trace silt-clay (few clay-silt laminations); reddish yellow (7.5YR 7/6) and light gray; mica bearing
				0.80	0.95	Ironstone, fragmented
				0.95	2.35	Sand, very fine to fine; trace silt-clay; light gray (10YR 7/1) to reddish yellow (7.5YR 7/6); mica bearing
				2.35	2.36	Ironstone, thin layers
				2.36	2.50	Sand, very fine to fine, little to trace silt-clay; light gray (10YR 7/1) to reddish yellow (7.5YR 7/6); mica bearing
10	50	53.29	3.10	0.00	2.30	Sand, fine to medium, slightly silty, clayey; reddish brown (7.5YR 6/6) mottled downward to tan "pink" (7.5YR 7/4); black layers (iron?); mica bearing
				2.30	2.35	Gravel, fine; thin layer
				2.35	2.55	Clay, silty, sandy, fine, pinkish gray (7.5YR 6/2)
				2.55	3.10	Sand, fine; tan "pink" (7.5YR 7/4)
11	53.29	55	1.50	0.00	0.25	Ironstone
				0.25	1.10	Sand, fine; silty, clayey, reddish yellow (7.5YR 6/6); mica bearing
				1.10	1.50	Sand, fine, silty, clayey, light red (2.5YR 6/6)
12	55	60	4.70	0.00	0.60	Sand, fine, slightly silty to clayey; mainly yellow (10YR 7/6)
				0.60	1.25	Sand, fine to medium, slightly silty to clayey; light reddish brown (2.5 YR 6/4)
				1.25	2.55	Sand, fine to medium, slightly silty, clayey interbedded with thin layers of Silt-Clay; clays mostly gray; sands reddish browns, yellow browns; mica bearing
				2.55	2.80	Sand, fine to medium; trace fines; multicolored; mica bearing
				2.80	3.10	Sand, fine to medium, silty, clayey; light reddish brown (2.5YR7/6)
				3.10	3.65	Sand, fine-medium; trace coarse sand, silt and clay; mainly yellow (10YR 7/6) and light reddish brown (2.5YR 7/6); mica bearing
				3.65	3.70	Ironstone
				3.70	4.70	Sand, fine-medium; trace coarse sand, silt and clay; mainly yellow (10YR 7/6) and light reddish brown (2.5YR 7/6); mica bearing
13a	60	62	1.90	0.00	0.20	Ironstone; dark reddish brown
				0.20	1.90	Sand, very fine to fine, silty, clayey; multicolored: light gray 10YR 7/2), light reddish brown (5YR 6/4), yellowish brown (10YR 5/6)

Table C-2. Description of core from CE Bf 156 -- Continued.

[Explanation of codes at end of table.]

Core run	Interval depth in ft		Amount recovered	Core intervals ft within core run*		Lithologic description**
	from	to	feet	from	to	
13b	62	65	3.00	0.00	0.05	Clay, silty; variegated very pale brown (10YR 8/2) and light reddish brown (2.5 YR 6/4)
				0.05	0.10	Ironstone, dark reddish brown
				0.10	1.03	Sand, very fine to fine, slightly silty, clayey; mottled mainly brownish yellow (10YR 6/6) and light gray
				1.03	1.07	Sand, very fine to medium
				1.07	1.25	Ironstone, thin layers; with fine sand
				1.25	1.80	Sand, very fine to fine, slightly silty, clayey; mottled; mainly brownish yellow (10YR 6/6) and light gray
				1.80	2.80	Sand, very fine to fine, slightly silty, clayey; mottled; similar to above but darker colors
				2.80	3.00	Ironstone, thin layers; interlayered with fine Sand, reddish-yellow
14	65	70	4.40	0.00	0.20	Ironstone, dark reddish brown
				0.20	0.71	Thinly interbedded silt, clayey and sand, very fine to fine; clays reddish brown and gray; sands brownish yellow
				0.71	1.80	Sand, very fine to fine; color grades downward from reddish yellow (7.5YR 6/8) to yellow (10YR 7/6)
				1.80	2.30	Silt, clayey, sandy, very fine to fine; gray and reddish brown; semi-cemented sands at 1.95 and 2.25
				2.30	3.40	Sand, fine, color grades from brownish yellow to yellow (10YR 7/6)
				3.40	3.80	Thinly interbedded clay-silt, and sand, fine; clays gray; sands brownish yellow
				3.80	4.40	Sand, fine; trace silty-clay; brownish yellow (10YR 6/6) and reddish yellow (5YR 6/6)
15	70	80	6.90	0.00	1.20	Thinly interbedded clay, silty and sand, fine, silty, clayey; mostly dark gray; mica bearing
				1.20	2.85	Clay, silty; dark gray (10YR 4/1); black charcoal(?) at 71.8 ft; mica bearing
				2.85	3.77	Thinly interbedded clay, silty, and sand, fine; dark gray (10YR 4/1); mica bearing
				3.77	4.45	Sand, fine; gray (10YR 5/1); mica bearing
				4.45	4.97	Clay, silty; dark gray (10YR 4/1); mica bearing
				4.97	5.02	Sand, fine; gray (10YR 5/1); mica bearing
				5.02	5.70	Clay, silty; dark gray (10YR 4/1); mica bearing
				5.70	6.35	Clay, silty, variably sandy interlayered with Sand, fine; dark gray (10YR 4/1); mica bearing
				6.35	6.55	Silt, clayey, sandy; dark gray (10YR 4/1); mica bearing
				6.55	6.65	Ironstone; black
				6.65	6.69	Sand, fine; light brownish gray (10yr 6/2); mica bearing
16	80	85	1.50	0.00	0.50	Clay, silty, slightly sandy, very fine; dark gray (10YR 4/1); micas
				0.50	1.50	Thinly interbedded sand, fine and silt-clay; pale brown (10YR 6/2)(sand) and dark gray (10YR 4/1) (clay); micas
17	85	90	4.30	0.00	1.25	Sand, fine; pale brown (10YR 6/2); faintly laminated in lower 0.35 ft of interval); micas
				1.25	1.62	Thinly interbedded sand, fine, and silt-clay; brown (10YR 5/3) sand; grayish brown (10YR5/2) clay
				1.62	1.85	Clay, silty; grayish brown (10YR 5/2)
				1.85	2.75	Sand, fine; mainly pale brown (10YR 6/2)
				2.75	4.30	Clay, silty with thin layers sand; dark grayish brown (10YR 4/2) and pale brown (10YR 6/2)

Table C-2. Description of core from CE Bf 156 -- Continued.

[Explanation of codes at end of table.]

Core run	Interval depth in ft		Amount recovered feet	Core intervals ft within core run*		Lithologic description**
	from	to		from	to	
18	90	95	4.10	0.00	1.50	Clay, silty with layers of sand, fine; dark gray (10YR 4/1) and very pale gray 10YR 7/3)
				1.50	1.80	Sand, fine; pale brown 10YR4/3
				1.80	2.40	Clay, silty with thin layers of sand, fine; dark gray (10YR 4/1) and (sands) very pale gray (10YR 7/3) to reddish yellow (7.5YR 6/8)
				2.40	3.55	Sand, fine; clasts of gray silt-clay; thin iron-cemented red layer neat top of interval; color fades downward from strong brown (10YR 5/8) to yellow (10YR7/6)
				3.55	4.10	Silt, clayey with thin layers of sand, fine; dark gray (10YR 4/1) and (sands) very pale gray (10YR 7/3)
19	95	100	5.00	0.00	0.30	Clay, silty, thin sandy layers; mottled gray and pale brown
				0.30	0.75	Sand, fine; very pale brown (10YR 7/4) to reddish yellow (7.5YR 6/6)
				0.75	1.55	Clay, silty laminated and thinly layered with sand, fine; gray and very pale brown
				1.55	1.85	Sand, fine; pinkish gray (7.5YR 6/2)
				1.85	3.00	Clay, silty, with thin layers of sand, fine; pale brown
				3.00	3.43	Sand fine; multicolored
				3.43	4.45	Clay, silty, with thin layers of sand, fine; dark gray (10YR 4/1) and pale brown (10YR 6/2)
				4.45	4.50	Ironstone, dark reddish brown, angled in core
				4.50	4.85	Sand, fine, thin semi-cemented crusts and silt laminations, wavy; variegated color
				4.85	4.95	Silt, clayey with thin sand layers, wavy; dark gray (10YR 4/1) and reddish yellow
				4.95	5.00	Ironstone, red (10R 4/6)
20	100	105	1.50	0.00	0.20	Ironstone; red and black laminated; (appears as cemented clay-silt)
				0.20	0.25	Laminated sand, silty and clay-silt; reddish yellow and gray
				0.25	0.45	Clay, silty; yellowish brown (10YR 5/4)
				0.45	0.75	Sand, fine, little silt-clay; with thin ironstone layers at 100.45, 100.55 and 100.65 ft); mica bearing
				0.75	0.91	Thinly interbedded sand, fine and clay-silt; reddish brown (5YR5/4, tan and gray; mica bearing
				0.91	1.25	Silt, clayey, multicolored wavy layers red, gray and orange-brown
				1.25	1.50	Sand, fine; mottled colors: weak red (purplishish red) (10R 4/4), red (orangey red) (2.5YR 5/6); mica bearing
21	105	110	3.50	0.00	0.70	Sand, fine to medium; trace silt, clay; multicolored: yellowish red (5YR 5/6), red (10R 4/8), dusky red (10R 3/2) reddish brown (5YR 4/4)
				0.70	3.50	Sand, medium; some fine sand; multicolored to banded: red, gray, brown, tan,
22	110	115	2.00	0.00	1.10	Sand, fine to coarse; trace silt, clay; light reddish brown (5YR 6/40; very loose (clean, uncemented)
				1.10	2.00	Sand, fine to medium, some silt-clay, multicolored invervals: light brown (7.5YR 6/4), light yellowish brown (10YR 6/4), very pale brown (10YR 8/3) yellow 10YR 7/6
23	115	120	0.22	0.00	0.22	Poor recovery; clay silt and sand, fine to very coarse, little fine gravel

Table C-2. Description of core from CE Bf 156 -- Continued.

[Explanation of codes at end of table.]

Core run	Interval depth in ft		Amount recovered feet	Core intervals ft within core run*		Lithologic description**
	from	to		from	to	
24	120	125	4.00	0.00	4.00	Sand, fine to medium, trace silt and clay; subtle bedding to laminations, mainly very pale brown 10YR 7/3 with strong brown (7.5YR4/6) interval at 2.95 to 3.1ft
25	125	130	4.60	0.00	4.60	Sand, fine to medium; mainly very pale brown (10YR 7/3); occasional faint layering/bedding orange- brown; mica bearing
26	130	133	1.70	0.00	1.70	Sand, fine to medium; mainly very pale brown (10YR 7/3); occasional faint layering/bedding orange- brown; mica bearing
27	133	135	2.40	0.00	1.82	Sand, fine to medium; very pale brown (10YR 7/3) to brownish yellow (10YR 6/6)
				1.82	1.94	Silt, clayey, little sand, very fine; very pale brown (10YR 8/3), thinly laminated, few dark red nodules (hematite?)
				1.94	2.50	Sand, fine to medium; very pale brown (10YR 7/3) to brownish yellow (10YR 6/6)
28	135	139	3.30	0.00	2.00	Sand, fine to medium; very pale brown; purplish (weak red 10YR 5/3) at 135.3 ft and semi-cemented half layers at 135.45 ft
				2.00	2.90	Sand, fine to coarse but mainly medium grained; mainly yellow (10YR 3/3)
				2.90	3.30	Sand, fine to coarse but increased medium-coarse grains; color banding very pale brown (10YR 8/4) to yellow (10YR 7/8)
29	139	141.21	1.60	0.00	0.90	Sand, fine to coarse, trace fines; light yellowish brown (10YR 6/4)
				0.90	1.60	Sand, fine to medium, trace fines (finer than above), very pale brown (10 YR 8/4) laminated toward lower part of interval
30	141.21	145	1.91	0.00	0.60	Sand, fine to coarse, trace fines; sand includes apparent quartzite fragments
				0.60	0.70	Sand, fine to medium, silty, clayey; top and bottom of interval is strong brown (7.5YR 5/8) center is lighter (10YR 7/8)
				0.70	1.00	Sand, fine to coarse, trace fines; color grades from strong brown (10YR 5/8) to very pale brown (10YR 7/3)
				1.00	1.91	Sand, fine to medium; little silt, clay, trace coarse sand; very densely packed; mainly tan (pale yellow 2.5Y 8/3)
31	145	150	2.70	0.00	2.50	Sand, medium to coarse, trace fine sand; grains subrounded to angular; very loose; very pale brown (10YR 7/4)
				2.50	2.70	Sand, fine to coarse, silty, clayey; iron cemented fragments toward base; color layered very pale brown to strong browns
32	150	155	0.00			no recovery *(some material may be in next run)*
33	155	159	1.30	0.00	0.20	Clay, silty, sandy, fine; little gravel
				0.20	0.83	Thinly interbedded sand, fine to medium and silt-clay; light gray and orange-brown
				0.83	1.50	Clay, silty; little sand, very fine to fine, gray 7.5YR 5/1; very plastic
33a	159	160	1.00	0.00	1.00	Clay, silty; pinkish gray (7.5YR 6/2); faint mottling; plastic
34	160	165	4.40	0.00	1.00	Clay, silty; faintly mottled pinkish gray (7.5YR 6/2) to gray; plastic
				1.00	2.72	Clay, silty, little sand, very fine to fine; faint mottles and some laminae of silty, fine sand; gray to dark gray; micaceous; firmer than above
				2.72	3.40	Clay, silty, sandy; similar to above with increase in sand and mottled lighter gray color, few lignite(?) fragments; micaceous
				3.40	3.90	Clay, silty with sand, very fine to fine, in burrows(?)/convoluted thin layers; gray; micaceous
				3.90	4.40	Clay, silty with sand, very fine to fine in thin wavy layers (possibly burrowed?), micaceous

Table C-2. Description of core from CE Bf 156 -- Continued.

[Explanation of codes at end of table.]

Core run	Interval depth in ft		Amount recovered feet	Core intervals ft within core run*		Lithologic description**
	from	to		from	to	
35	165	170	5.00	0.00	1.90	Silt, clayey, interlayered with sand very fine to fine, silty; burrowed or slumped/convoluted bedding in places; gray; micaceous
				1.90	2.60	Sand, fine to coarse, silty; gray until ironstone at 2.3 ft then strong brown (7.5YR 5/8); coarse mica flakes
				2.60	3.20	Sand, fine to medium; little clay, silty; thinly laminated/cross-laminated; micaceous
				3.20	4.25	Sand, fine to coarse, little silt, clay; variably strong brown (7.5YR 5/8) to reddish yellow (7.5YR 5/6); micaceous
				4.25	4.35	Sand, coarse, and Gravel
				4.35	5.00	Sand, fine to coarse, reddish yellow (7.5YR 5/6); micaceous
36	170	175	0.75	0.00	0.20	Sand, fine to medium, trace fines, faintly laminated
				0.20	0.40	Gravel (quartz)
				0.40	0.50	Saprolite(?); clay-silt, tan and white; mottled
				0.50	0.75	Saprolite; clay-silt, light gray to greenish gray
37	175	178	2.50	0.00	0.20	Saprolite; clay, light gray (may be from above)
				0.20	2.60	Weathered serpentinite and/or gabbro; mottled teal green with light whitish green in places (gley1 5/2 and 4/2); very firm to soft
38	178	185	7.00	0.00	6.50	Weathered serpentinite and/or gabbro; mottled dark teal green (gley1 4/2) with whitish green in places (gley 1 7/1)
				6.50	7.00	Weathered rock; gray, almost "salt and pepper" grains
39	185	195	6.40	0.00	6.40	Weathered serpentinite and/or gabbro, variably indurated (clayey to nearly rock); various shades of teal green, dark to light
40	195	200	4.00	0.00	1.00	Broken bits or weathered rock, same as above
				1.00	4.00	Weathered rock with increasing induration; mainly dark teal/greenish gray to 2.6 ft then lighter greenish gray

* Interval recovered is shown aligned with top of drilled interval unless drilling conditions or other information indicate otherwise.

** Color codes are based on wet sample matched to Munsell Soil Color Chart, 2000 (revised)

APPENDIX D

Palynology - Subsample Summary and
Palynological Report by Gilbert J. Brenner

Table D-1. Summary of sample selection and processing for palynological analysis.

Borehole ID	Sample ID	Sample Depth Interval (ft bls)	Processing Notes	General lithologic description *(color of wet sample matched to Munsell soil color chart, 2000 edition)*
CE Cd 91	106487	17.5 - 17.6	1 slide	Clay, silty; dark gray to very dark gray (2.5Y 4/1 - 2.5Y 3/1) mottled
CE Cd 91	106488	20.0 - 20.1	3 slides	Clay-silt, slightly sandy very fine to fine grained; grayish brown (10YR 5/2); flecks of black carbonaceous material throughout; vaguely laminated; sample just below interval of concentrated lignite/carbonaceous material
CE Cd 91	106489	76.85 - 77.0	1 slide	Interbedded clay, dense, very dark gray (10YR 3/1) and sand, very fine-fine-grained, gray (10YR 6/1); bedding 0.5-1.0 cm thick
CE Cd 91	106490	110.0 - 110.15	1 slide	Clay, silty; very dark gray (10YR 3/1)
CE Cd 91	106491	123.0 - 123.1	1 slide	Clay, dark gray (10YR 4/1); burrow-like structures
CE Cd 91	106492	161.3 – 161.4	barren (0 slides)	Clay, dark gray (7.5 YR 4/1) and brown (7.5 YR 4/4)
CE Cd 91	106493	271.5 - 271.6 (278.5 - 278.6*)	1 slide	Clay, silty; dark gray (5YR 4/1) very stiff; fine mica flakes present
CE Cd 91	106494	281.7 - 281.8	1 slide	Clay, slightly silty; dark gray (10 YR 4/1); slightly mottled
CE Cd 91	106495	331.2 - 331.3	barren (0 slides)	Clay, silty; dark reddish gray (5R 4/2), very stiff; occasionally mottled color with bluish gray (GLEY2 7/10B); mica flakes
CE Cd 91	106496	338.5 - 338.6	barren (0 slides)	Clay, silty; dark reddish gray (5YR 4/2) very stiff; mica flakes
CE Cd 91	106497	384.3 - 384.5	1 slide	Sand, fine-grained, dark gray (10YR 4/1), micaceous, flecks of black carbonaceous material
CE Cd 91	106498	390.8 - 390.9	4 slides	Sand, fine-grained, clayey, silty; gray (10YR 5/1) stiff, micaceous; just above carbonaceous/lignitic layer
CE Cd 91	106499	441.0 - 441.2	1 slide	Clay, silty; variably sandy, vaguely variegated swirling pattern of very dark bluish gray and bluish gray (GLEY2 3/10B and GLEY2 5/5PB); lignite/carbonaceous material in places
* Depth of CE Cd 91 sample 106493 within borehole is about 278.5 - 278.6 ft based upon comparison of core recovered (material within core run) with geophysical logs; original sample depth assumed core recovered was aligned to top.				
CE Be 155	110501	77.7 - 77.85	inadequate pollen (0 slides)	Clay, silty; very fine mica flakes; laminated to mottled dark gray (5YR 4/1) and dark reddish gray (5YR 4/2); firm
CE Be 155	110502	82.1 - 82.25	inadequate pollen (0 slides)	Clay, silty; slightly sandy, very fine with mica flakes; laminated to mottled brown and dark gray (7.5YR 4/2 - 4/1)
CE Be 155	110503	86.85 – 87.0		Clay, silty; slightly sandy, very fine with mica flakes; laminated to mottled (brownish) dark gray (7.5YR 4/1); abundant black charcoal/lignite fragments
CE Be 155	110504	90.5 - 90.65 (92.5-92.65**)		Clay, silty, slightly sandy, very fine to fine; mica bearing; mainly gray (7.5YR 5/1); black charcoal/lignite fragments
CE Be 155	110505	128.2 - 128.35		Silt-clay, dark gray (10YR 5/1); few black woody fragments; micas
CE Be 155	110506	132.55 - 132.7		Silt-clay, variably sandy, very fine to fine, dark gray to gray (10YR 4/1-5/1); and black wood/lignite fragments; micas
CE Be 155	110507	138.05 - 138.15		Clay, silty; dark gray and gray (10YR 4/1-5/1), very firm
CE Be 155	110508	140.0 - 140.15		Clay, silty; very dark gray (10YR 3/1), very firm
* Depth of CE Be 155 sample 1110504 within borehole is about 92.5-92.65 ft; based on drilling record (top 2 ft of 90-95 ft core run not recovered); original sample depth reported based upon measurement from top of core recovered.				

Table D-1. Summary of sample selection and processing for palynological analysis – Continued.

Borehole ID	Sample ID	Sample Depth Interval (ft bls)	Processing Notes	General lithologic description *(color of wet sample matched to Munsell soil color chart, 2000 edition)*
CE Bf 156	110489	40.05 - 40.2		Clay, silty; brown (7.5YR 5/2)
CE Bf 156	110490	71.35 - 71.5		Clay, silty; dark gray (10YR 4/1); mica bearing
CE Bf 156	110491	75.05 - 75.2		Clay, silty; dark gray (10YR 4/1); mica bearing
CE Bf 156	110492	80.0 - 80.15		Clay, silty, slightly sandy, very fine; dark gray (10YR 4/1); micas
CE Bf 156	110493	86.6 - 86.75	inadequate pollen (0 slides)	Clay, silty; grayish brown (10YR 5/2)
CE Bf 156	110494	92.1 - 92.2	inadequate pollen (0 slides)	Clay, silty with thin layers of sand, fine; dark gray (10YR 4/1) and (sands) very pale gray (10YR 7/3) to reddish yellow (7.5YR 6/8)
CE Bf 156	110495	96.45 - 96.55	inadequate pollen (0 slides)	Clay, silty laminated and thinly layered with sand, fine; gray and very pale brown
CE Bf 156	110496	160.0 - 160.15	inadequate pollen (0 slides)	Clay, silty, little sand, very fine to fine sand; with laminations of silty, fine sand; micaceous
CE Bf 156	110497	163.9 – 164.0		Clay, silty with sand, very fine to fine in thin wavy layers (possibly burrowed?), micaceous

Appendix D. Summary report on the palynology of the Potomac Group samples from cores CE Cd 91, CE Be 155, and CE Bf 156.

by

Gilbert J. Brenner
State University of New York (at New Paltz)

CORE CE Cd 91

Fifteen processed slides from nine sample intervals were submitted for analysis, however, slides from two sample intervals (depths 110.0 to 110.15 feet and 390.8 to 390.9 feet) were essentially barren of palynomorphs. The remaining 10 slides from eight sample intervals of core CE Cd 91 were analyzed for their palynological content. The organic residue in most of the slides was mostly compost of carbonized plant debris. Palynomorphs in most of the slides were not abundant, but there were enough index forms found to make palynozone determinations.

Depth: 17.5-17.6 feet
Stage Determination: Lower Cenomanian
Palynozone: III
Stratigraphic Unit: Upper Patapsco
Paleoecology: Non-Marine, Deltaic
Palynological Recovery: Poor
Climate: Subtropical humid

Palynomorphs	Known Palynological Zone Range ACP	Frequency
Alisporites bilateralis Rouse	I - III	R
Apendicisporites potomacensis Brenner	I - II	R
Araurcariacites australis (Cookson)	I - III	R
Cicatricosisporites patapscoensis Brenner	*IIA - III	C
Cicatricosisporites subrotundus	*IIB - III	R
Cingulatisporites eukirchensoides D & S	I - III	R
Concavissimisporites variverrucatus (Couper)	I - II	R
Cyathidites minor Couper	Widespread	C
Densoisporites perinatus Couper	I – II	R
Gleicheniidites senonicus Ross	I – III	A
Podocarpidites potomacensis Brenner	II-III	C
Taurocusporites reduncus (Bolkhovitina)	I-II	R

Discussion: This sample has poor palynomorph recovery with mostly carbonized tracheal fragments present. There are no angiospem pollen present that date this sample to Zone III; however, the sample below this at 20.0-20.1 feet does have some angiosperms grains that are restricted to Zone III. Some of the spore species present at 17.5-17.6 feet range from Zone II-III. Abundant grains of Gleicheniidites senonicus suggest a nearby forest rich in tree ferns.

R, Rare (less than 1%); O, Occasional (1-5%); C, Common (6-10%); A, Abundant (greater than 10%);
* = Restricted Range that dates sample; ACP = Atlantic Coastal Plain

Appendix D. Continued

Core CE Cd 91--Continued

Depth: 20.0-20.1 feet
Stage Determination: Lower Cenomanian
Palynozone: III
Stratigraphic Unit: Upper Patapsco
Paleoecology: Non-Marine, Deltaic
Palynological Recovery: Poor
Climate: Subtropical humid

Palynomorphs	Known Palynological Zone Range ACP	Frequency
Angiosperms		
Tricolpopollenites micromunus Brenner	IIA - III	R
Tricolporopollenites distinctus G & P	*IIC - III	R
Tricolporopollenites sp. B Doyle	*III	R
Spores		
Appendicisporites potomacensis Brenner	I - II	R
Cicatricosisporites spp.	I - III	R

Discussion: Phytomorph fragments of tracheids and leaf cutin dominate the sample. Some rare grains of angiosperm pollen date this sample as Lower Cenomanian, Zone III, which is uppermost Patapsco (formerly Raritan in the old literature). The Raritan of New Jersey is younger and missing in the Elk Neck area.

Depth: 76.85-77.0 feet
Stage Determination: Albian
Palynozone: IIB
Stratigraphic Unit: Patapsco
Paleoecology: Non-Marine, Deltaic
Palynological Recovery: Poor
Climate: Subtropical humid

Palynomorphs	Known Palynological Zone Range ACP	Frequency
Angiosperms		
Tricolpopollenites micromunus G&P	*II - III	R
Spores and Pollen		
Appendicisporites potomacensis Brenner	I - II	R
Alisporites bilateralis Rouse	I - III	R
Matonisporites excavatus Brenner	*IIB	R
Podocarpidites radiatus Brenner	I - II	R
Taurocusporites segmentatus Stover	*II	O

R, Rare (less than 1%); O, Occasional (1-5%); C, Common (6-10%); A, Abundant (greater than 10%);
* = Restricted Range that dates sample; ACP = Atlantic Coastal Plain

Appendix D. Continued

Core CE Cd-91—Continued

Depth: 110.0-110.15 feet Barren of Palynomorphs

Depth: 123.0-123.1 feet
Stage Determination: Albian
Palynozone: IIB2
Stratigraphic Unit: Patapsco
Paleoecology: Non-Marine, Deltaic
Palynological Recovery: Poor
Climate: Subtropical humid

Palynomorphs	Known Palynological Zone Range ACP	Frequency
Angiosperms		
Tricolpites crassimurus G & P	II	R
Spores and Pollen		
Appendicisporites potomacensis Brenner	I - II	R
Apiculatisporites babsae Brenner	II	R
Densoisporites perinatus Couper	I - II	R
Neoraistrickia robusta Brenner	*IIB	R
Podocarpidites radiatus Brenner	I - II	R
Rugubvesiculatus reductus Pierce	*IIB2	R

Depth: 271.5-271.6 feet
Stage Determination: Albian
Palynozone: IIB
Stratigraphic Unit: Patapsco
Paleoecology: Non-Marine, Deltaic
Palynological Recovery: Fair
Climate: Subtropical humid

Palynomorphs	Known Palynological Zone Range ACP	Frequency
Appendicisporites potomacensis Brenner	I - II	O
Neoraistrickia robusta Brenner	*IIB	R
Pilosisporites trichopapillosus (Thiergart)	I - II	R

Discussion: The easily recognizable spore Neoraistrickia robusta places this sample in Zone IIB.

R, Rare (less than 1%); O, Occasional (1-5%); C, Common (6-10%); A, Abundant (greater than 10%);
* = Restricted Range that dates sample; ACP = Atlantic Coastal Plain

Appendix D. Continued

Core CE Cd-91—Continued

Depth: 281.7-281.8 feet
Stage Determination: Albian
Palynozone: IIB
Stratigraphic Unit: Patapsco
Paleoecology: Non-Marine, Deltaic
Palynological Recovery: Very Poor
Climate: Subtropical humid

Palynomorphs	Known Palynological Zone Range ACP	Frequency
Angiosperm		
Clavatipollenites hughesii	I - II	R
Spores		
Appendicisporites tricornatatus W & G	I - II	C
Apiculatisporites babsae	II	R
Converrucosisporites platyverrucosis Brenner	I - II	O
Densoisporites microrugulatus Brenner		
Ephedripites patapscoensis Brenner	*IIB	R
Foveotriletes subtriangulatus Brenner	I - II	O
Taurocusporites segmentatus Stover	*II	A
Taurocusporites reduncus (Bolkhovitina)	I - II	R
Taurocusporites spackmani Brenner	*IIB	O

Depth: 384.3-384.5 feet
Stage Determination: Aptian
Palynozone: I
Stratigraphic Unit: Patuxent-Arundel equivalent
Paleoecology: Non-Marine, Deltaic
Palynological Recovery: Very Poor
Climate: Subtropical humid

Palynomorphs	Known Palynological Zone Range ACP	Frequency
Abietineaepollenites sp.	Not restricted	R
Classopollis torosus	More common in Zone I	R
Cicatricosisporites aralica	I - II, More common in Zone I	O
Cicatricosisporites spp.	More Common in Zone I	C
Exesipollenites tumulusBalme	More Common in Zone I	O
Shizosporis reticulatus C & D	I - II	R

Discussion: This sample has very poor palynomorph recovery. None of the Zone II spores and pollen restricted to Zone II are found in this sample. As in the better sample recovery, the assemblage is more typical of Zone I.

R, Rare (less than 1%); O, Occasional (1-5%); C, Common (6-10%); A, Abundant (greater than 10%);
* = Restricted Range that dates sample; ACP = Atlantic Coastal Plain

Appendix D. Continued

Core CE Cd-91—Continued

Depth: 390.8-390.9 feet Barren of Palynomorphs

Depth: 441.0-441.2 feet
Stage Determination: Aptian
Palynozone: Upper Zone I
Stratigraphic Unit: Patuxent-Arundel equivalent
Paleoecology: Non-Marine, Deltaic
Palynological Recovery: Good
Climate: Subtropical humid

Palynomorphs	Known Palynological Zone Range ACP	Frequency
Abietineaepollenites sp.	Not restricted	C
Alisporites bilateralia	Not restricted	A
Appendicisporites potomacensis Brenner	I - II	R
Cicatricosisporites aralica	I - II, More common in Zone I	C
Cicatricosisporites australensis	I - II, More common in Zone I	C
Decussosporites microreticulatus Brenner	I - II	R
Exesipollenites tumulus Balme	More Common in Zone I	O
Podocarpidites potomacensis Brenner	I - III	C
Podocarpidites radiatus Brenner	II - III	C

Discussion: This sample contains a well-preserved palynoflora, but no spores are found that are indicative of Zone II as are found from 271.5-271.6 feet and higher. The palynomorph assemblage in this sample has a high percentage of bisaccate pollen typical of the pollen Pinaceae. This usually represents a cooling phase that begins in the Potomac Group starting in Upper Zone I and into Zone II.

R, Rare (less than 1%); O, Occasional (1-5%); C, Common (6-10%); A, Abundant (greater than 10%);
* = Restricted Range that dates sample; ACP = Atlantic Coastal Plain

Appendix D. Continued

CORES CE Be 155 AND CE Cf 156

Processed slides from six core samples from CE Be 155 and five core samples from CE Bf 156 in Cecil County were submitted for analysis; however, four sample intervals (noted below) were essentially barren of palynomorphs. The remaining samples were analyzed for their palynological content.

Palynomorph assemblages were not rich in species or abundant in number, but some index forms were found in several of the samples from the two coreholes. Low palynomorph recovery required that all slides be scanned at 1000x magnification. Most of the preserved plant residue consisted of degraded and carbonized plant debris, lignified tracheids, leaf cutin, fragments of cutinized plant vessels and charcoal, etc. All of the samples are non-marine with no evidence of any marine influence.

Core CE Be 155

Analysis of Corehole CE Be 155: The best palynomorph recovery was from the core at 140.0-140.15 feet (sample 110508). Several palynospecies in this core sample are restricted to Palynozone IIB of the Patapsco Formation. None of the core samples above this depth in Corehole CE Be 155 contain the more advanced tricolpates and tricolporate palynospecies that were found in Corehole CE Bf 156 at 40.05-40.20 feet (sample 110489).

Depth: 86.85-87.0 feet (110503) Barren

Depth: 90.5-90.65 feet (110504)
Stage Determination: Albian
Palynozone: Zone IIB-2, based on position within corehole above cores at 140.0-140.15 feet to 132.55-132.70 feet.
Stratigraphic Unit: Upper Patapsco
Paleoecology: Tree Fern Forest, Non-Marine, Deltaic
Palynological Recovery: Poor
Climate: Subtropical humid

Palynomorphs	Known Palynological Zone Range ACP	Frequency
Angiosperms		
Clavatipollenites minutus Brenner	I – III, Most common in IIB-C	C
Liliacidites dividuus(Pierce) Brenner	*II	O
Gymnosperms		
Alisporites bilateralia Rouse	I - III	R
Classopollis torosus (Reissinger)	Cretaceous	R
Entylissa nitidus Balme	I - II	R
Exesipollenites tumulus Balme	I - II	O
Monosulcites eparkros Brenner	I - II	R
Podocarpidites radiatus Brenner	I - III	C

R, Rare (less than 1%); O, Occasional (1-5%); C, Common (6-10%); A, Abundant (greater than 10%);
* = Restricted Range that dates sample; ACP = Atlantic Coastal Plain

Appendix D. Continued

Core CE Be 155—Continued

Depth: 90.5-90.65 feet (110504)—Continued

	Known Palynological Zone Range ACP	Frequency
Spores		
Cicatricosisporites aralica (Bolkhovitina)	I - III	C
Cicatricosisporites hallei Delcourt & Sprumont	I - III	C
Cingulatisporites sp.	I - II	R
Converrucosisporites proxigranulatus Brenner	I - II	O
Cyathidites minor Couper	Not Restricted	C
Gleicheniidites senonicus Ross	I - III	C
Laevigatsporites gracilis Wilson & Webster	Not Restricted	R
Lycopodiacidites intraverrucosus Brenner	I - II	R
Lycopdiacidites trianularis Brenner	I - II	R
Taurocusporites reduncus (Bolkhovitina)	I - II	O

Depth: 128.2-128.35 feet (110505) Barren

Depth: 132.55-132.7 feet (110506)
Stage Determination: Albian
Palynozone: Subzone B2 of Palynozone II
Stratigraphic Unit: Patapsco
Paleoecology: Non-Marine, Deltaic
Palynological Recovery: Fair
Climate: Subtropical humid

Palynomorphs	Known Palynological Zone Range ACP	Frequency
Angiosperms(Rare)		
Clavatipollenites minutus Brenner	I – III, Most common in IIB-C	C
Gymnosperms		
Abietineaepollenites sp.	Not restricted	R
Alisporites bilateralia Rouse	I - III	R
Araurcariacites australis (Cookson)	I - III	R
Classopollis torosus (Reissinger)	Cretaceous	O
Exesipollenites tumulus Balme	I & II	O
Rugubivesiculites reductus Pierce	*IIB	R
Spores		
Cicatricosisporites australensis	I - II	C
Cingulatisporites eukirchensoides Delcourt & Sprumont	I – II, More common in II	R
Concavissimisorites variverrucatus (Couper)	I - II	R
Cyathidites minor Couper	Not Restricted	C
Lycopodiacidites intraverrucosus Brenner	I - II	R

R, Rare (less than 1%)**;** O, Occasional (1-5%); C, Common (6-10%); A, Abundant (greater than 10%);
* = Restricted Range that dates sample; ACP = Atlantic Coastal Plain

Appendix D. Continued

Core CE Be 155—Continued

Depth: 132.55-132.7 feet (110506)—Continued

Spores--Continued	Known Palynological Zone Range ACP	Frequency
Peromonolites allenensis Brenner	I - II	R
Pilosisporites trichopapillosus (Thiergart)	I - II	R
Psilatriletes circumundulatus Brenner	I - II, More common in II	R
Taurocusporites reduncus (Bolkhovitina)	I - II	R

Discussion: A single grain of Rugubivesiculites reductus places this sample in palynozone IIB.

Depth: 138.05-138.15 feet (110507) Barren

Depth: 140.0-140.15 feet (110508)
Stage Determination: Albian
Palynozone: Subzone B2 of Palynozone II
Stratigraphic Unit: Patapsco
Paleoecology: Non-Marine, Deltaic
Palynological Recovery: Good
Climate: Subtropical humid

Palynomorphs	Known Palynological Zone Range ACP	Frequency
Angiosperms (Rare)		
Clavatipollenites hughesii Couper	I - II	R
Clavatipollenites minutus Brenner	I – III, More common in IIB-C	R
Gymnosperms		
Circulina parva Brenner	I - II	R
Classopollis torosus (Reissinger)	Cretaceous	A
Ephedripites multicostatus Brenner	I - II	R
Exesipollenites tumulus Balme	I & II	C
Laricoidites gigantus Brenner	I - II	O
Spores		
Cicatricosisporites brevilaesuratus Couper	I - II	R
Cicatricosisporites subrotundis Brenner	*IIB	R
Cyathidites minor Couper	Not Restricted	C
Gleicheniidites apilobatus Brenner	I - II	R
Laevigatsporites gracilis Wilson & Webster	Not Restricted	R
Monosulcites chaloneri Brenner	*II	R
Monosulcites eparkros Brenner	I & II	R
Taurocusporites spackmani Brenner	*IIB	R
Trilobosporites humilus Delcourt & Sprumont	I - II	R

Discussion: Two palynomorph species in this sample are restricted to Subzone B of Zone II.

R, Rare (less than 1%); O, Occasional (1-5%); C, Common (6-10%); A, Abundant (greater than 10%);
* = Restricted Range that dates sample; ACP = Atlantic Coastal Plain

Appendix D. Continued

Core CE Bf 156

Depth: 40.05-40.2 feet (110489)
Stage Determination: Lower Cenomanian
Palynozone: IIC-III
Stratigraphic Unit: Upper Patapsco-Lowermost Raritan of Cecil County, Maryland
Paleoecology: Non-Marine, Deltaic
Palynological Recovery: Poor
Climate: Subtropical humid

Palynomorphs	Known Palynological Zone Range ACP	Frequency
Angiosperms		
Tricolporopollenites sp. A Doyle	*III	C
Tricolpites crassimurus (Groot and Penny)	*III	R
Tricolpites hemejci Pactova	*III	R
Tricolpites parvulus Groot & Penny	*IIB	R
Tricolpites sp. B Doyle	*IIB	R
Gymnosperms		
Araurcariacites australis (Cookson)	I - III	R
Podocarpidites potomacensis Brenner	II - III	R
Spores		
Cyathidites minor Couper	Widespread	C
Gleicheniidites senonicus Ross	I - III	A

Discussion: While this sample has sparse palynomorph recovery, with mostly carbonized tracheal fragments present, there are several grains of tricolpate and tricolporate pollen that are restricted to Palynozones IIC and III. These species are not known to occur in Palynozone IIB. Frequent grains of Gleicheniidites senonicus and Cyathidites minor suggests a nearby forest rich in tree ferns and herbaceous flowering plants.

Depth: 71.35-71.5 feet (110490)
Stage Determination: Albian
Palynozone: Zone IIB
Stratigraphic Unit: Upper Patapsco
Paleoecology: Non-Marine, Deltaic
Palynological Recovery: Poor
Climate: Subtropical humid

Palynomorphs	Known Palynological Zone Range ACP	Frequency
Angiosperms		
Clavatipollenites minutus Brenner	I – III, Most common in IIB-C	C

R, Rare (less than 1%)**;** O, Occasional (1-5%); C, Common (6-10%); A, Abundant (greater than 10%);
* = Restricted Range that dates sample; ACP = Atlantic Coastal Plain

Appendix D. Continued

Core CE Bf 156--Continued

Depth: 71.35-71.5 feet (110490)--Continued

Palynomorphs	Known Palynological Zone Range ACP	Frequency
Gymnosperms		
Abietineaepollenites sp.	Not Restricted	R
Alisporites bilateralia Rouse	Not Restricted	C
Araurcariacites australis (Cookson)	I - III	R
Phyllocladidies microreticulatus Brenner	I - II	O
Spores		
Cicatricosisporites hallei	I - III	C
Converrucosisporites proxigranulatus Brenner	I - II	O
Densoisporites perinatus Couper	I - II	R
Gleicheniidites senonicus Ross	I - III	C
Taurocusporites reduncus (Bolkhovitina)	I - II	R

Depth: 75.05-75.2 feet (110491) Essentially barren except for a few non-diagnostic spores

Depth: 80.0-80.15 feet (110492)
Stage Determination: Albian
Palynozone: Zone IIB/ Based on position within corehole above core at 163.9-164.0 feet
Stratigraphic Unit: Upper Patapsco
Paleoecology: Non-Marine, Deltaic
Palynological Recovery: Poor
Climate: Subtropical humid

Palynomorphs	Known Palynological Zone Range ACP	Frequency
Angiosperms		
Clavatipollenites minutus Brenner	I – III, Most common in IIB-C	R
Gymnosperms		
Podocarpidites radiatus Brenner	I - II	R
Spores		
Peromonolites allenensis Brenner	I - II	R
Cicatricosisporites hallei Delcourt & Sprumont	I - III	C
Cyathidites minor Couper	Not restricted	R

R, Rare (less than 1%); O, Occasional (1-5%); C, Common (6-10%); A, Abundant (greater than 10%);
* = Restricted Range that dates sample; ACP = Atlantic Coastal Plain

Appendix D. Continued

Core CE Bf-156—Continued

Depth: 163.9-164.0 feet (110497)
Stage Determination: Albian
Palynozone: Zone II
Stratigraphic Unit: Patapsco
Paleoecology: Non-Marine, Deltaic
Palynological Recovery: Poor, few palynomorphs found.
Climate: Subtropical humid

Palynomorphs	Known Palynological Zone Range ACP	Frequency
Gymnosperms		
Classopollis torosus sp (Bolkhovitina)	I - III	R
Podocarpidites radiatus Brenner	I - II	R
Spores		
Apiculatisporites babsae Brenner	*II	R
Cicatricosisporites australensis (Cookson)	I - II	O
Concavissimisorites variverrucatus (Cooper)	I - II	R
Densoisporites perinatus Couper	I - II	R
Taurocusporites reduncus (Bolkhovitina)	I - II	O

Discussion: Few palynomorphs. Two specimens of Apiculatisporites babsae place this sample in palynozone II. This form is not found in palynozone I.

R, Rare (less than 1%); O, Occasional (1-5%); C, Common (6-10%); A, Abundant (greater than 10%);
* = Restricted Range that dates sample; ACP = Atlantic Coastal Plain

APPENDIX E

Select Data from Additional Wells and Boreholes

Borehole ID: CE Be 73

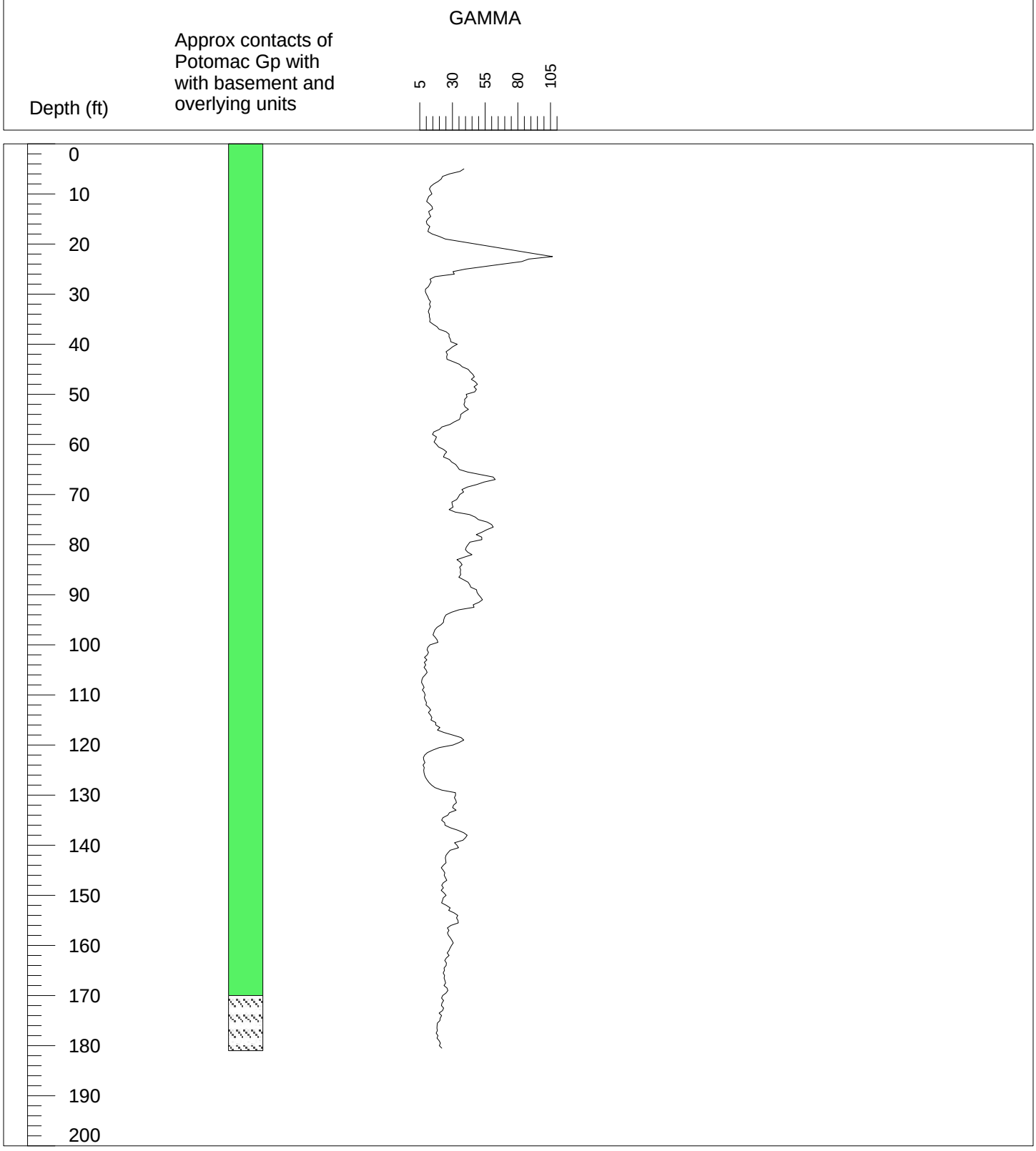

Potomac

saprolite/weathered rock

For additonal details, including detailed descriptions of cuttings and limited core, see:
Otton and others, 1988.

ATTACHMENT D
Borehole ID: CE Bf 143

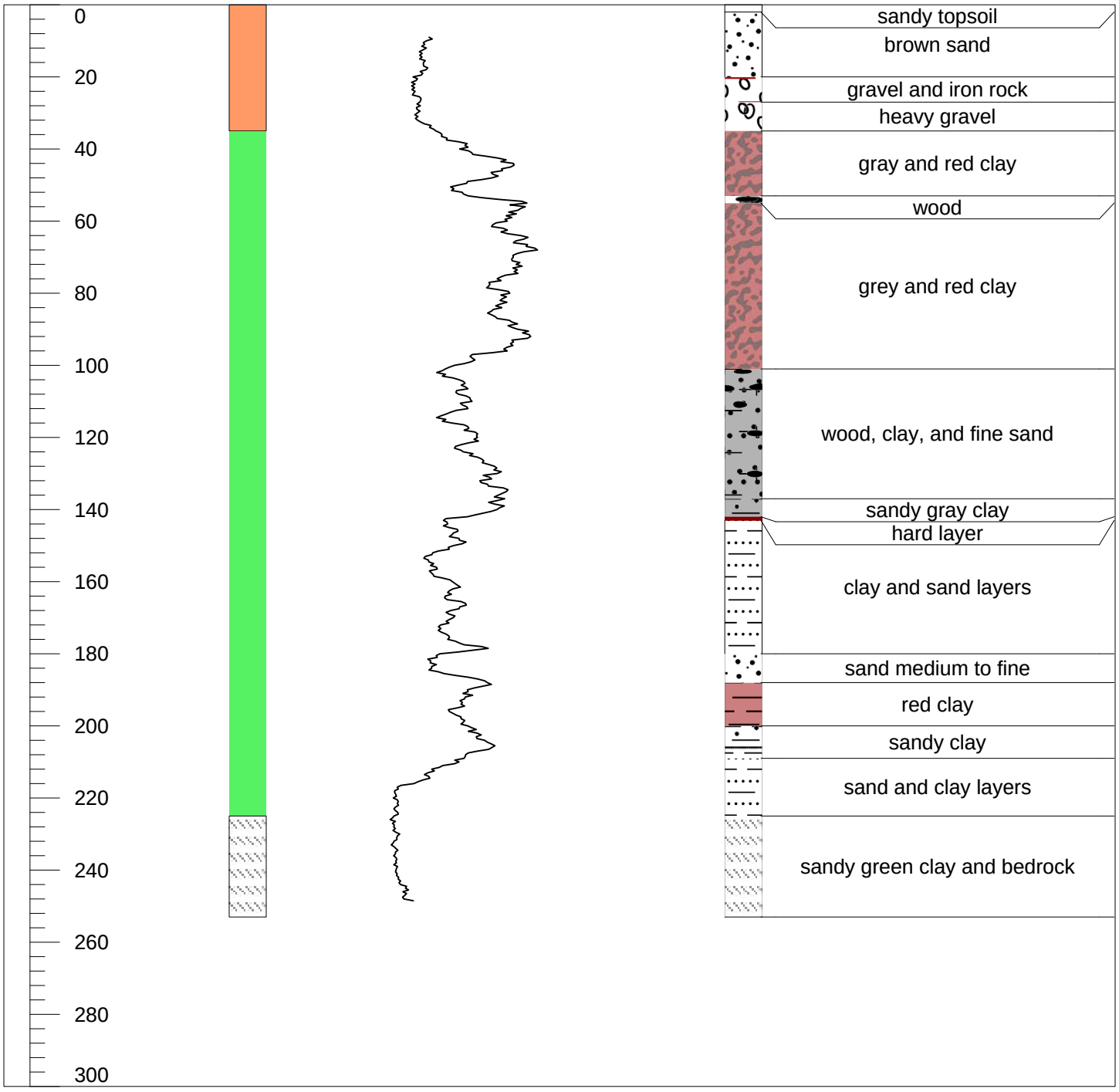

Pensauken
Potomac
saprolite/weathered rock

Borehole ID: CE Bf 144

(Close to Well CE Bf 143; share a geophysical log)

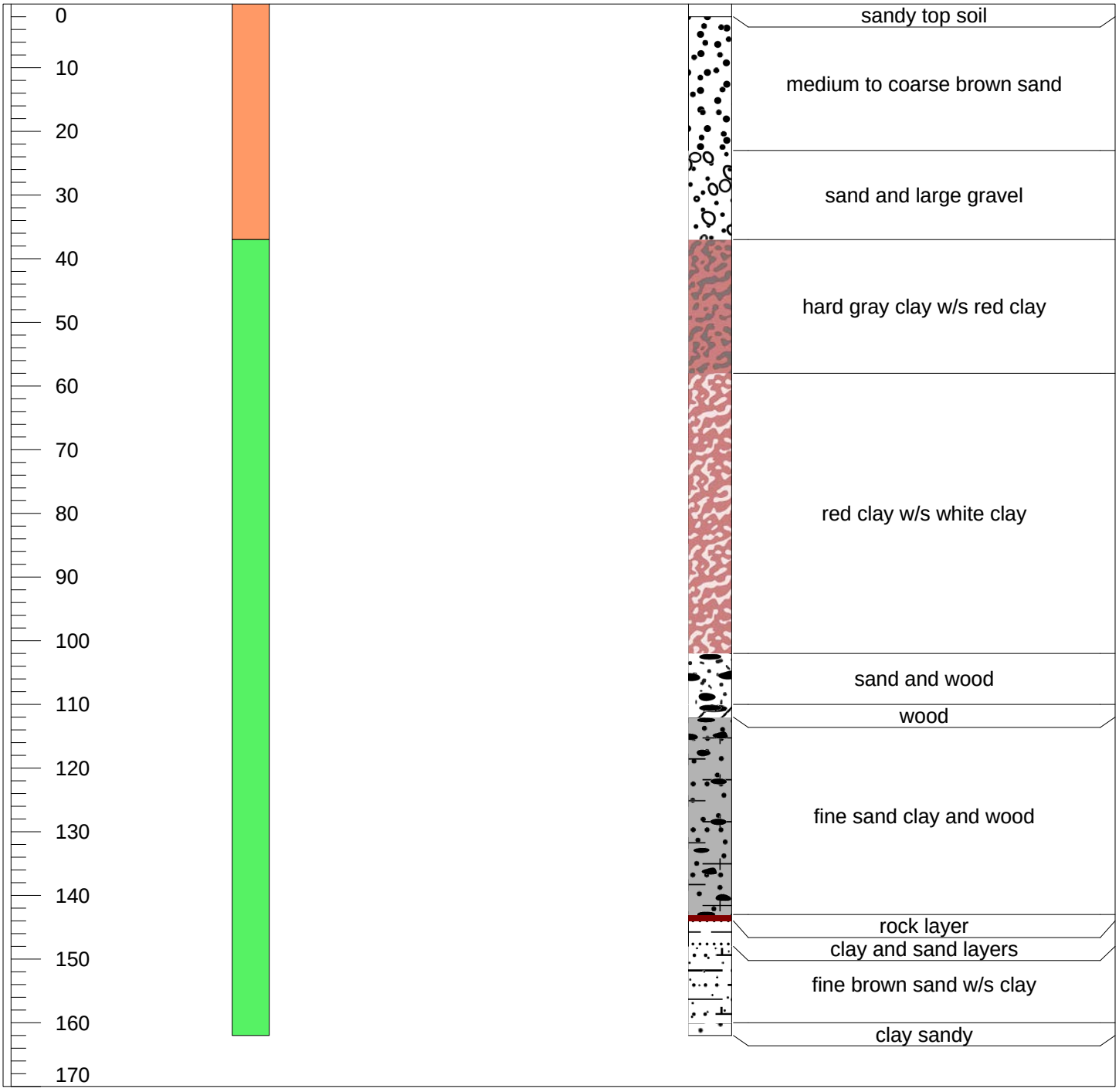

Pensauken

Potomac

Borehole ID: CE BI 58

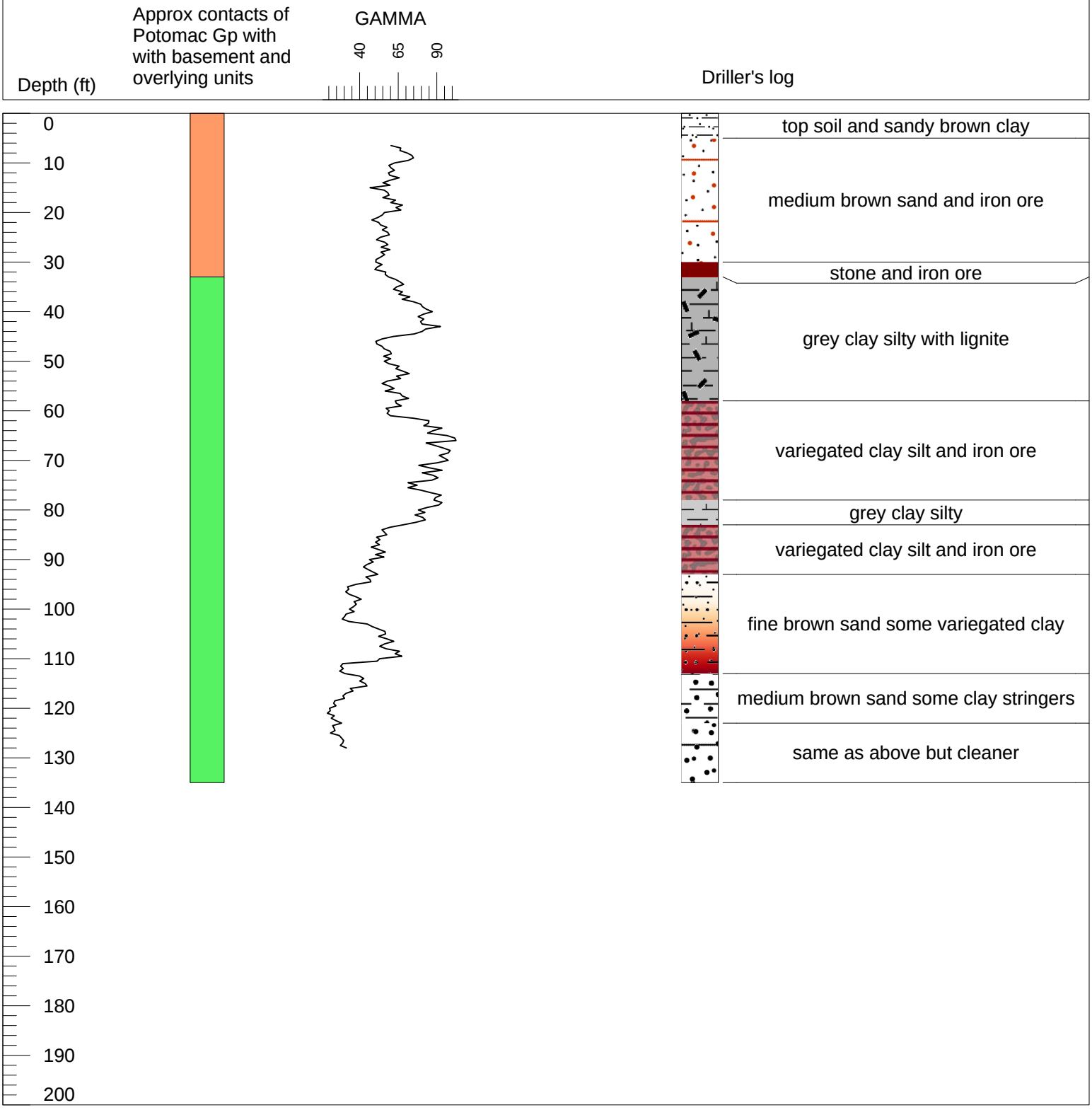

ATTACHMENT D
Borehole ID : CE Bf 81

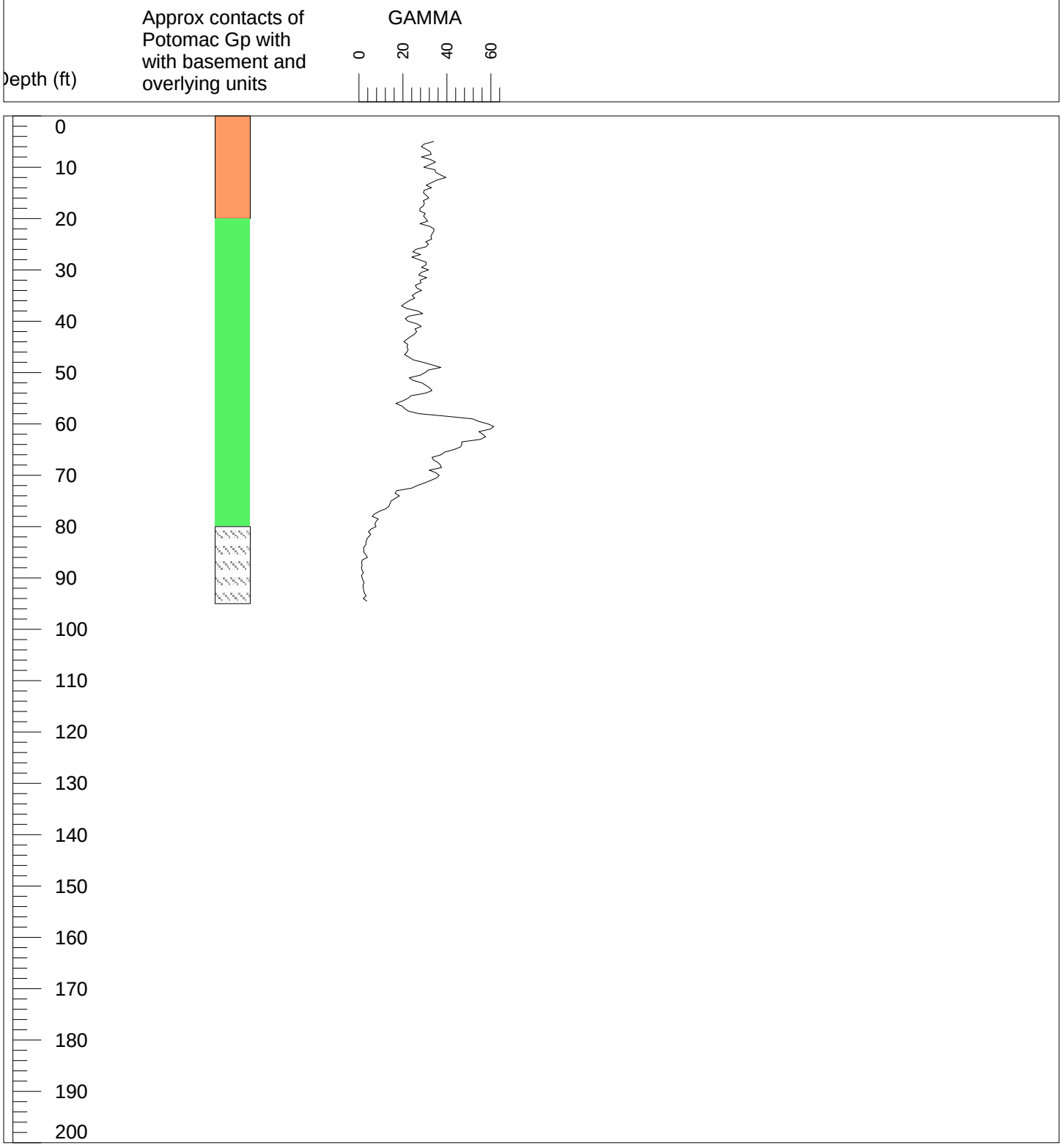

Pensauken
Potomac
saprolite/weathered rock

For additonal details, including detailed descriptions of cuttings and limited core, see:
Otton and others, 1988.

ATTACHMENT D
Borehole ID: CE Bf 82

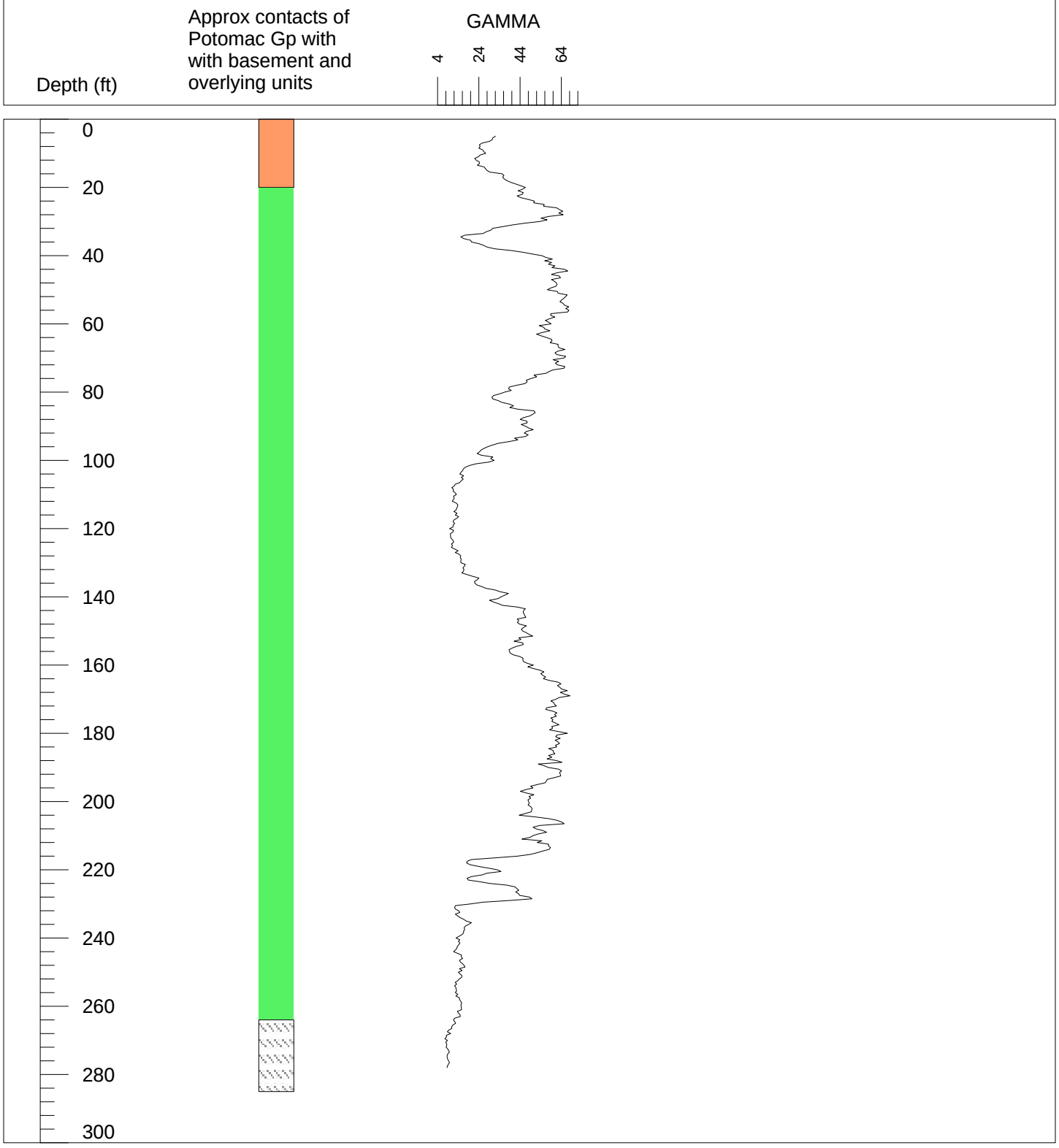

Pensauken
Potomac
saprolite/weathered rock

For additonal details, including detailed descriptions of cuttings and limited core, see:
Otton and others, 1988.

ATTACHMENT D
Borehole ID: CE Cd 53

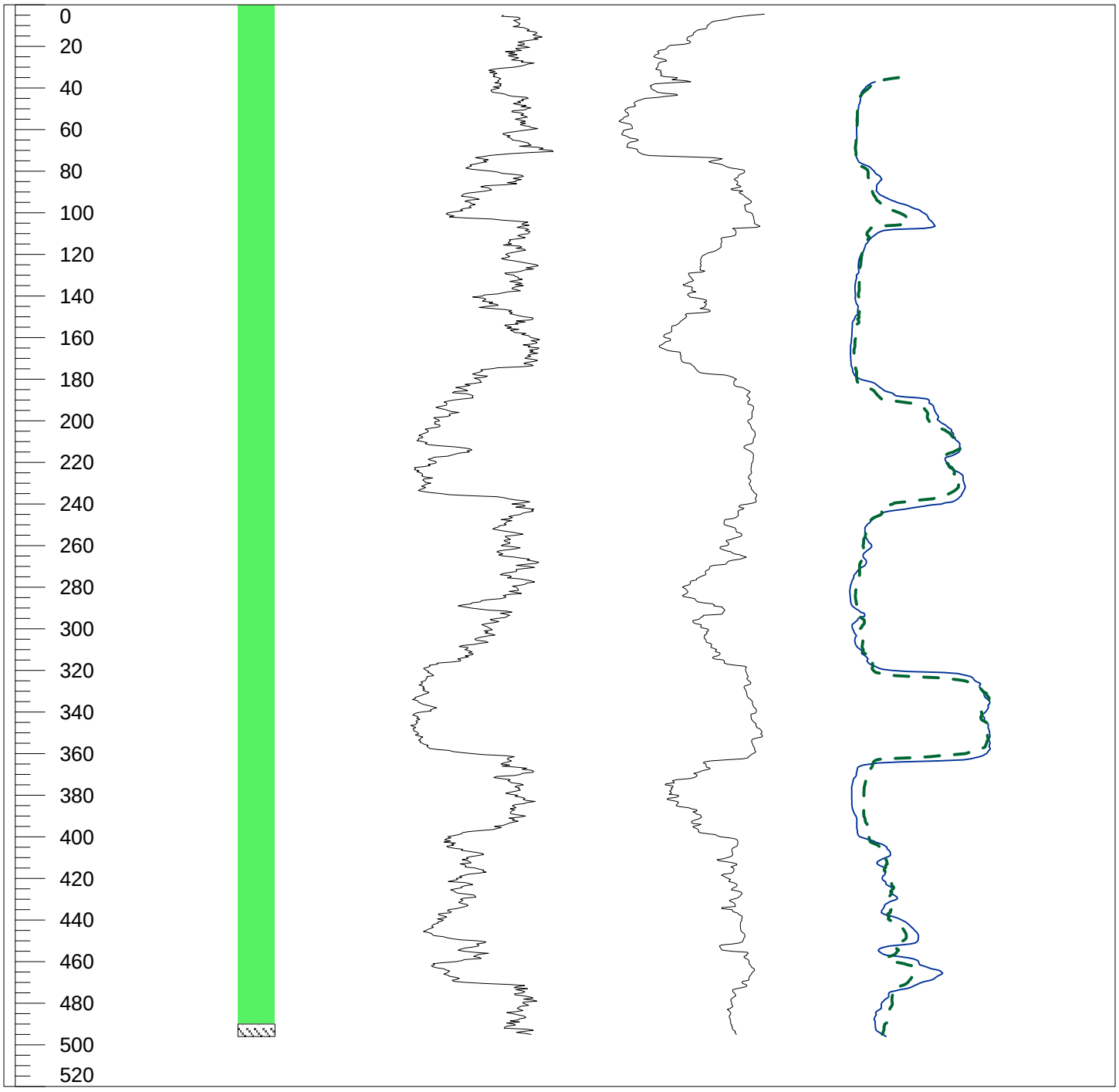

Potomac

saprolite/weathered rock

For additonal details, including detailed descriptions of cuttings and limited core, see:
Otton and others, 1988.

Borehole ID: CE Ce 54

Approx contacts of Potomac Gp with with basement and overlying units

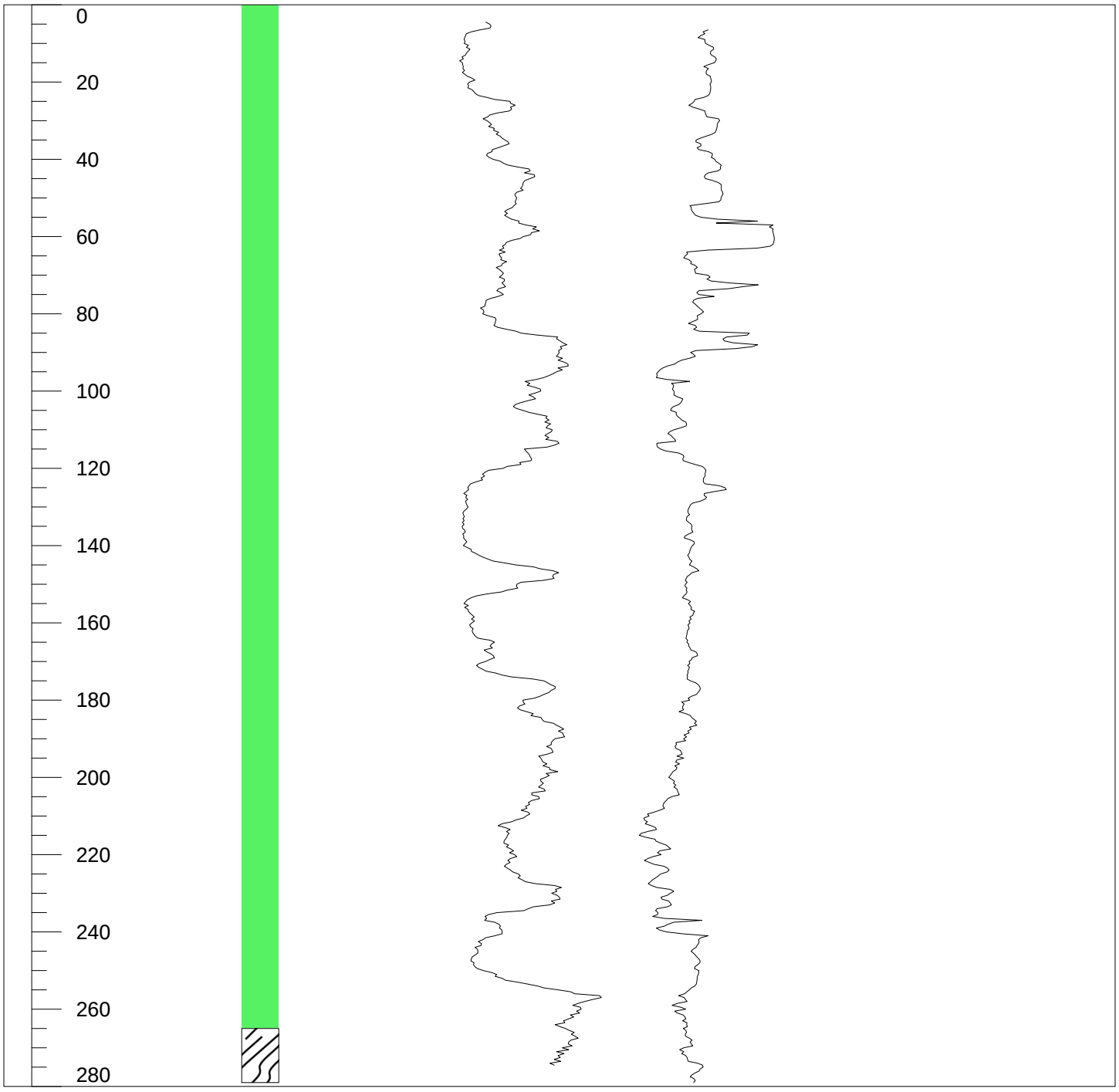

Potomac Group

saprolite/weathered rock

For additonal details, including detailed descriptions of cuttings and limited core, see:
Otton and others, 1988.

ATTACHMENT D

Borehole ID: CE Dc 2

Turkey Point

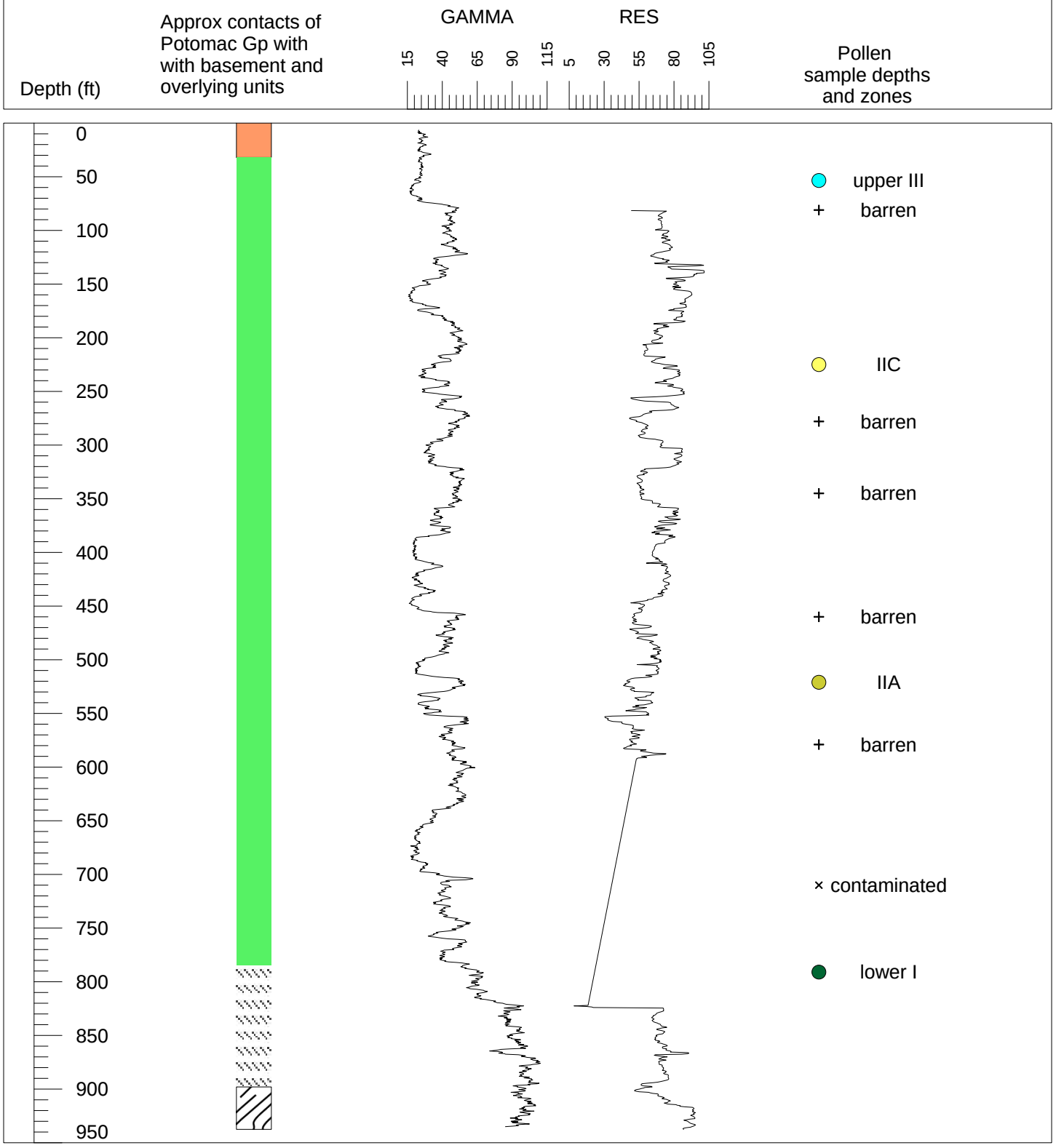

Pensauken ?

Potomac

saprolite/weathered bedrock

bedrock

For additonal details, see:
Edwards and Hansen, 1979
D-113

ATTACHMENT D
Borehole Ce Dd 107
Mauldin Mountain

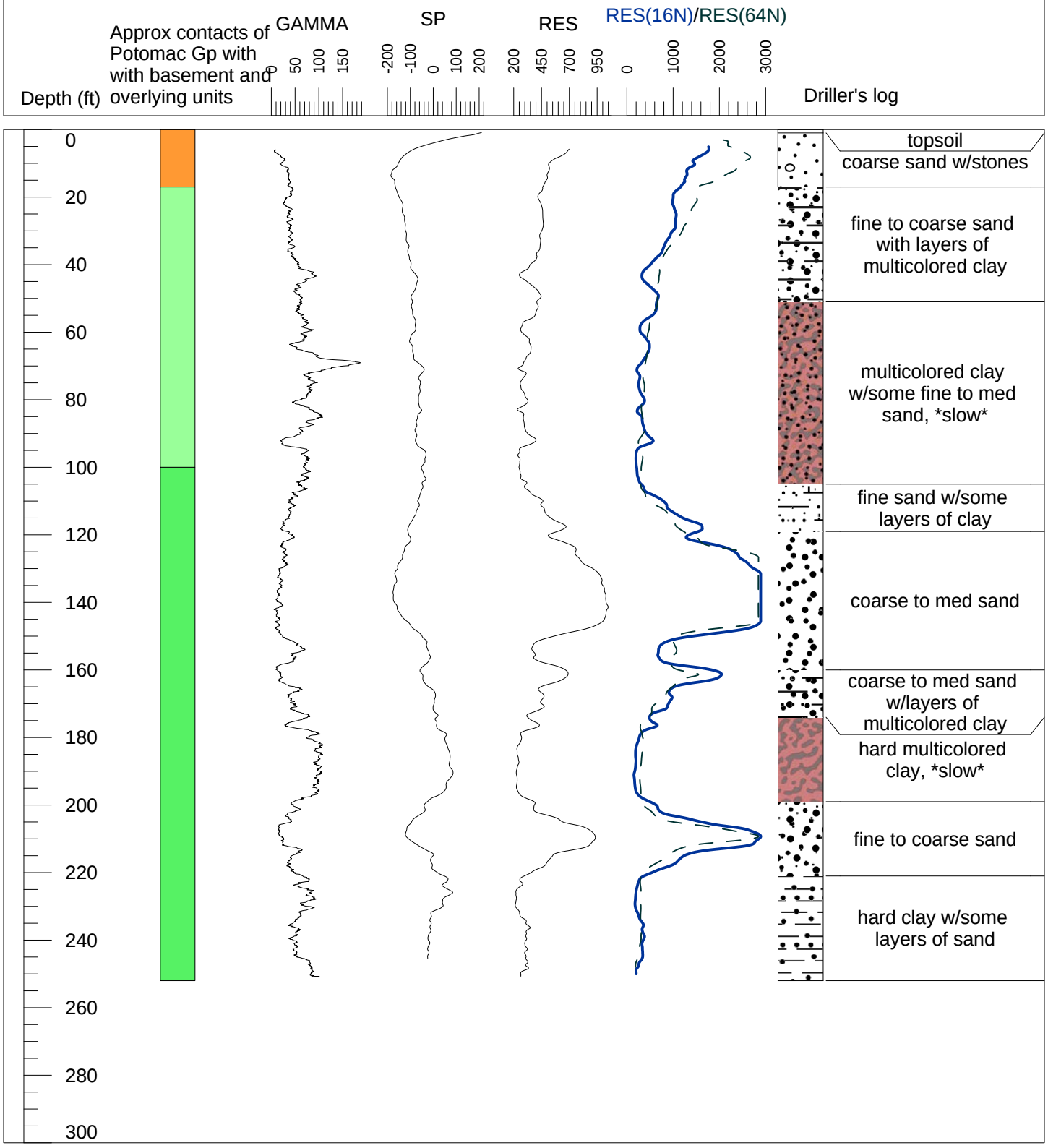

Upland gravel
Cretaceous post Potomac
Potomac

Borehole ID: CE Ec 17

Grove Point

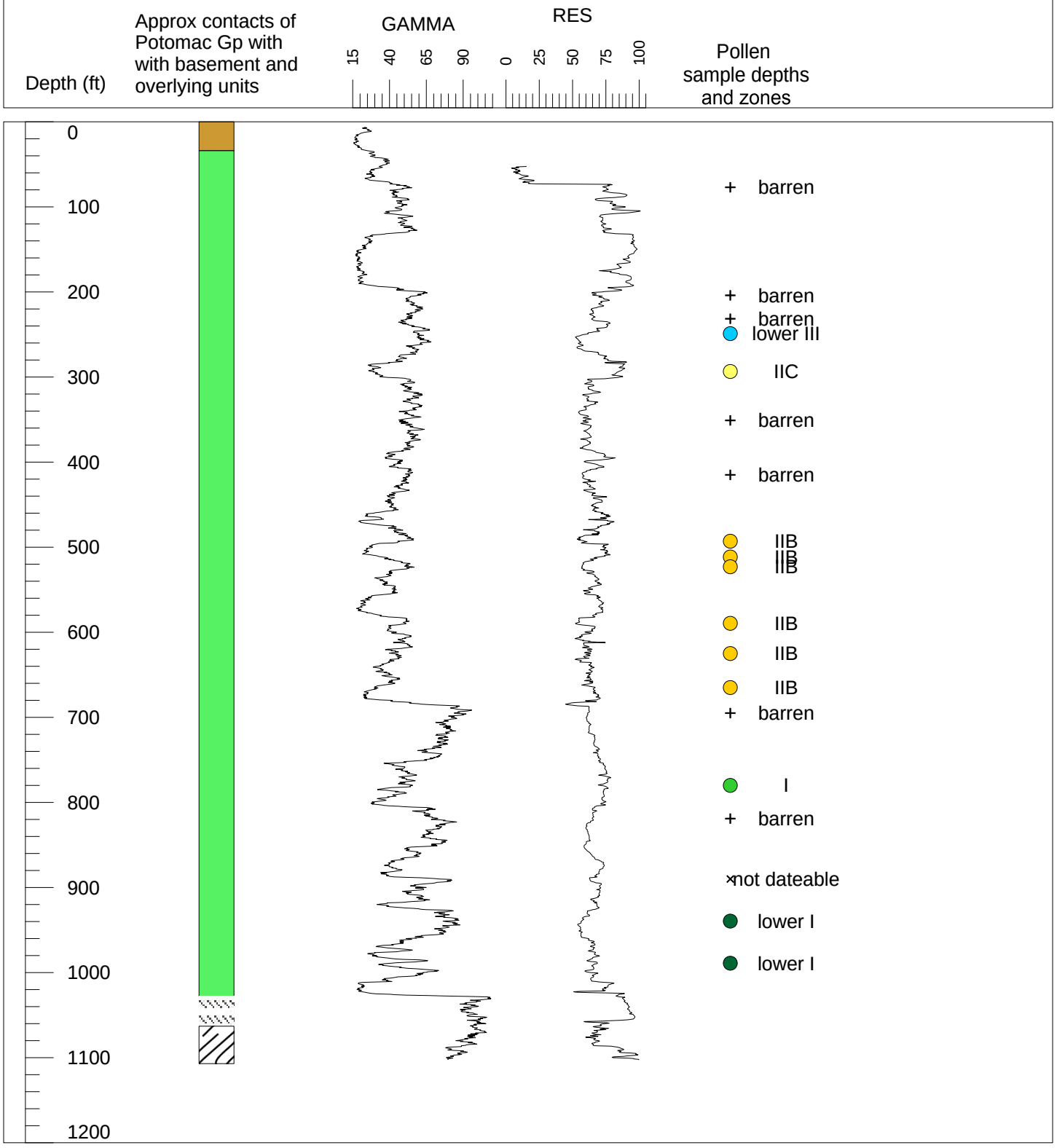

Lowland deposits (former Talbot)

Potomac

saprolite/weathered bedrock

bedrock

For additonal details, see:
Edwards and Hansen, 1979

Larry Hogan
Governor

Jeannie Haddaway-Riccio
Secretary

Boyd K. Rutherford
Lt. Governor

A message to Maryland's citizens

The Maryland Department of Natural Resources (DNR) seeks to balance the preservation and enhancement of the living and physical resources of the state with prudent extraction and utilization policies that benefit the citizens of Maryland. This publication provides information that will increase your understanding of how DNR strives to reach that goal through the earth science assessments conducted by the Maryland Geological Survey.

MARYLAND DEPARTMENT OF NATURAL RESOURCES
Resource Assessment Service
Tawes State Office Building
580 Taylor Avenue
Annapolis, Maryland 21401
Toll free in Maryland: 877-620-8DNR
Out of State call: 410-260-8021
TTY users: Call via the Maryland Relay
Internet Address: dnr.Maryland.gov

MARYLAND GEOLOGICAL SURVEY
2300 St. Paul Street
Baltimore, Maryland 21218
Telephone Contact Information: 410-554-5500
Internet Address: mgs.md.gov

DNR Publication No. 12-051419-149
September 2019

Attachment E: Full Seismic Reprocessing Report from Absolute Imaging Inc.

Creating a
seismic image that is absolutely clear

absolute IMAGING

COLUMBIA UNIVERSITY

East Coast USA (NY)
Phase 2
Lines 6,10,12,14,16,22,26,27 and 37

September 15th, 2017

Creating a seismic image that is absolutely clear

absolute IMAGING

Location Map

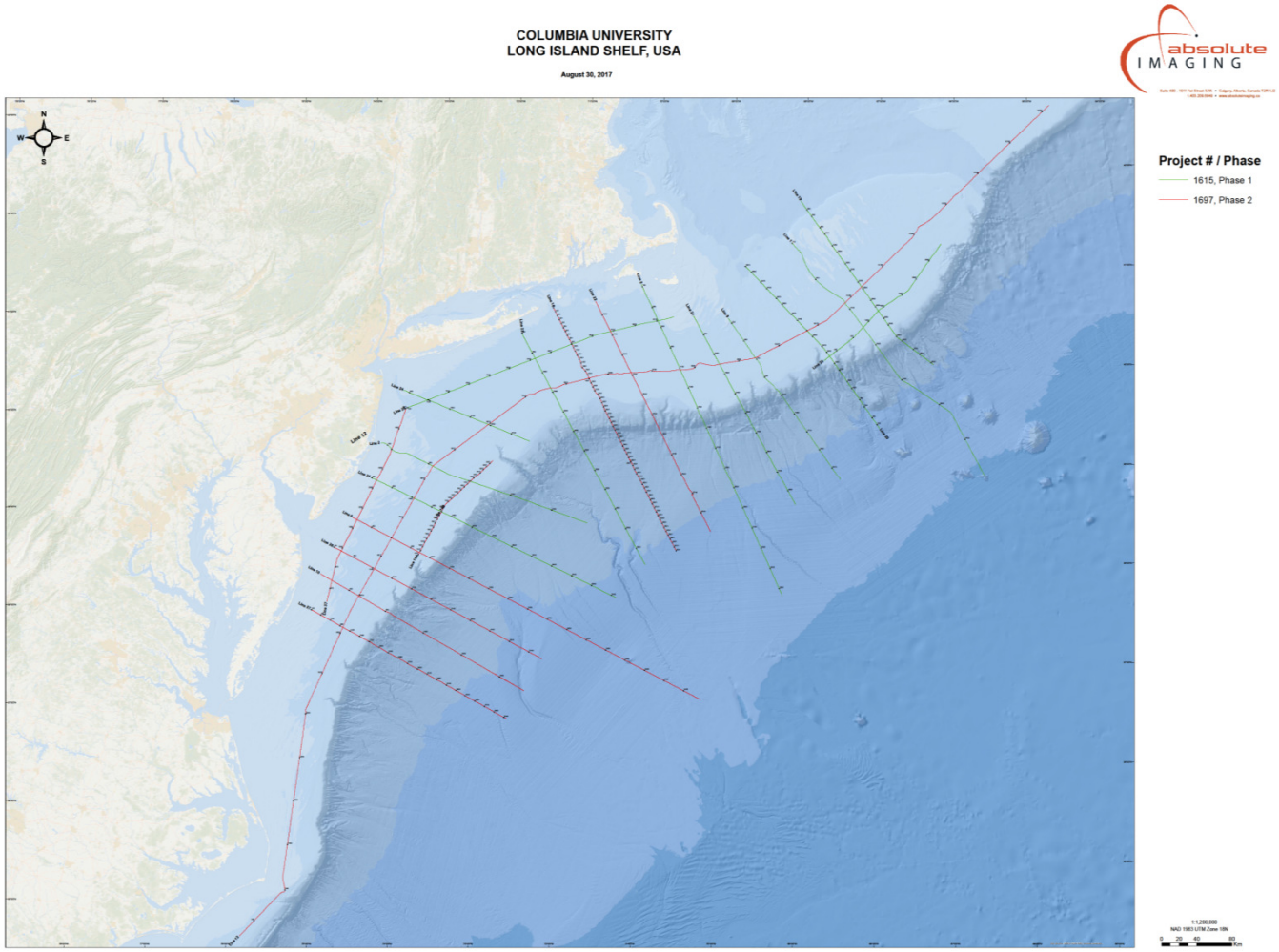

absolute IMAGING

Line List

Priority	Line #	Original line length	Length to Process (km)	Proposed Length to Process (km) including Gaps	SP Range Total	SP Range To Process	Proposed SP Range Including Gaps
1	12	240	940	214	101-4897	101-3950	101-4400
2	6	384	107	120	210-4035	210-1410	210-1410
3	10	254	152	128	101-1504	101-1250	101-1504
4	14	352	140	127	A:1001-2261 B:1001-2491	A:1001-2261 B:1001-2491	1001-2261 1001-2491
5	16	306	~310	123	1-6201	1-2400	1-2400
6	22	154	294	107	909-6701	909-3900	909-3900
7	26	378	270	104	101-5474	149-4871	101-4871
8	27	154	256	152	233-5311	233-1925	233-1925
9	37	239	240	115	101-4871	101-4871	101-4871

Location Map Showing Processing Extents

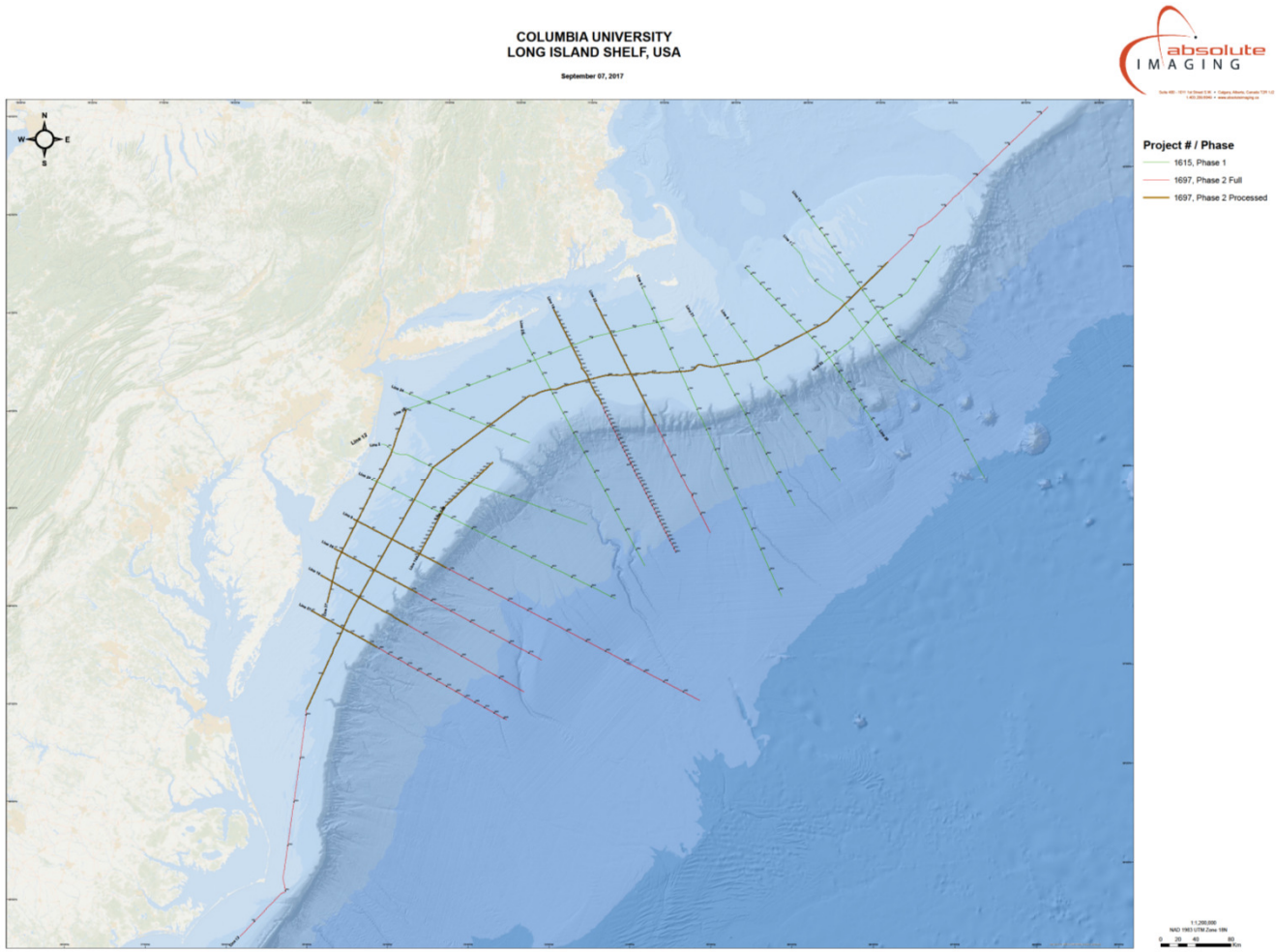

absolute IMAGING

Acquisition Parameters Line 6

- Acquisition Date: September 1974
- Data Acquired By: Digicon Inc Crew 511
- Data Acquired For: USGS
- Shooting Orientation: South East
- Instrument: DFS III
- Recording Channels: 48
- Filter: 8-62 Hz
- Sample Rate: 4 ms
- Record Length: 12.25 seconds
- Airgun Source: 1700 cubic inches
- Gun Depth: 9 meters
- Shotpoint Interval: 50 meters
- Group Interval: 50 meters
- Near offset: 350 meters
- Far Offset : 3900meters
- Streamer Depth: 18 meters
- Nominal Fold: 36

absolute IMAGING

Acquisition Parameters Line 10

- Acquisition Date: November 1975
- Data Acquired By: Digicon Inc Crew 511
- Data Acquired For: USGS
- Shooting Orientation: South East
- Instrument: DFS III
- Recording Channels: 48
- Filter: 8-18/124 Hz
- Sample Rate: 2 ms
- Record Length: 12.25 seconds
- Airgun Source: 1700 cubic inches
- Gun Depth: 9 meters
- Shotpoint Interval: 50 meters
- Group Interval: 50 meters
- Near offset: 350 meters
- Far Offset : 3900meters
- Streamer Depth: 18 meters
- Nominal Fold: 36

absolute IMAGING

Acquisition Parameters: Line 12

- Acquisition Date: October 1975
- Data Acquired By: Digicon Inc.
- Data Acquired For: USGS
- Shooting Orientation: South West/North East
- Instrument: DFS III
- Recording Channels: 48
- Filter: 8/18-124/Out Hz/Oct
- Sample Rate: 2 ms
- Record Length: 7/10 seconds
- Airgun Source: 1260 PSI
- Gun Depth: 9.1 meters
- Shotpoint Interval: 50 meters
- Group Interval: 50/100 meters
- Near offset: 350 meters
- Far Offset : 3900 meters
- Streamer Depth: 9.1 meters
- Nominal Fold: 36

absolute IMAGING

Acquisition Parameters Line 14, 16

- Acquisition Date: September 1977
- Data Acquired By: Teledyne Exploration
- Data Acquired For: USGS
- Shooting Orientation: South East
- Instrument: DFS IV
- Recording Channels: 48
- Filter: Out-Auto Hz
- Sample Rate: 2 ms
- Record Length: 12 seconds
- Airgun Source: 2000 PSI
- Gun Depth: 6.4 meters
- Shotpoint Interval: 50 meters
- Group Interval: 50 meters
- Near offset: 350 meters
- Far Offset : 3900 meters
- Streamer Depth: 12 meters
- Nominal Fold: 36

absolute IMAGING

Acquisition Parameters Line 22, 26, 27, 37

- Acquisition Date: June 1978
- Data Acquired By: Geophysical Services Inc Party 2912
- Data Acquired For: USGS
- Shooting Orientation: South East
- Instrument: DFS IV
- Recording Channels: 48
- Filter: 8/18-62 Hz
- Sample Rate: 4 ms
- Record Length: 12.25 seconds
- Airgun Source: 2000 Cubic inches
- Gun Depth: 9 meters
- Shotpoint Interval: 50 meters
- Group Interval: 50 meters
- Near offset: 376(Varying) meters
- Far Offset : 3900 meters
- Streamer Depth: 12 meters
- Nominal Fold: 24/30

absolute IMAGING

Processing Flow

1. Reformat (10 sec & 2 ms)
2. Interpolate channels 25-48 from 100m to 50m
3. Geometry Creation & QC
4. Trace Editing
5. Shot & Channel Scaling (to balance amplitudes across section)
6. Brute Velocity Analysis (2000m)
7. Erratic Noise Suppression (TFD & FX Median Filter in shot domain)
8. Predictive Deconvolution
9. Designature (Zero phasing)
10. Coherent Noise Suppression (SWNA in shot domain)
11. WB Demultiple (SRME)
12. Random Noise Suppression (Cadzow in shot domain)
13. Shot & Channel Scaling (to balance amplitudes across section)
14. Final Velocity Analysis (1000m)
15. Isotropic PSTM Velocity Analysis (500m)
16. Kirchhoff Pre Stack Time Migration output to gathers
17. High Resolution Radon Demultiple (HRRT)
18. Mute
19. CDP Bin Sharing Stack
20. Dip Scan (to suppress high angle noises)
21. Time & Spatial Variant Filter
22. Time Variant Scaling - Expanding window (500ms rolling window with 50% overlapping)
23. Static Shift (gun & cable correction)
24. SEG-Y output (10 sec & 2 ms)

absolute IMAGING

Noise Suppression Techniques

TFD Noise Removal (TFD)

- The TFD noise removal tool performs noise suppression and sub-spectral balancing using sample wise median thresholding within frequency sub-bands in the time-frequency space. This tool will attenuate noise bursts, spikes, air blasts and other noise within the frequencies of interest.

FX Median Filter

- Seismic ensembles are scanned frequency by frequency within overlapping time gates, for amplitudes which differ by more than a specifiable amount from the characteristic amplitude as determined by the local **median** of the amplitudes within a group of traces centered on the trace currently under consideration. If such an anomalous amplitude is found, it is replaced by the local median amplitude.

absolute IMAGING

Interpolation Technique

Fourier Trace Interpolation

- Fourier Trace Interpolation uses the Fast Fourier Transform method to interpolate seismic wavefields from spacitally recorded sampling to a finer spatial sampling.

- In this project, the 48 original traces in a shot are used to generate 24 interpolated traces, then the original traces and interpolated traces are merged to form a new interpolated shot with 72 traces.

absolute IMAGING

Noise Suppression Techniques

Surface Wave Noise Attenuation (SWNA)

- This process applies what is variously called Low Frequency Array Filtering to 3D shot gathers. Essentially this means that a frequency dependent trace mix is applied for the purpose of attenuating noise due to near surface waves. Such energy can be attenuated significantly by summing adjacent traces in the frequency-space domain over a distance corresponding to the wavelength of the surface wave.

Cadzow Random Noise Attenuation

- Eigen Image or Cadzow filtering performs matrix-rank reduction on constant frequency slices. The filter strength is determined by the rank – the number of decomposed images that are summed together to create the noise suppressed image. The smaller the rank, the harsher the filter.

absolute IMAGING

Demultiple Techniques

Predictive Deconvolution

- The recorded seismic signal may be considered as the convolution of the source signal with the instruments, the geophones, and the response of the Earth. The Earth response includes some undesirable effects, such as reverberation, attenuation, and ghosting. The objective of deconvolution is to extract the reflectivity component of the seismic trace by removing the effects of the seismic wavelet, including short-period multiples by designing and applying inverse filters.

- In statistical deconvolution no information about the wavelet is known, so we must derive information about the wavelet from the data itself, specifically from the **autocorrelation** of the data.

- Predictive deconvolution uses information from the earlier part of the seismic trace to predict and deconvolve the latter part of the trace. Predictive deconvolution 'predicts' the repetitive element within the seismic trace (multiples, ringing etc.) and generates an operator (of a specific length) which will remove them, leaving only the random element i.e. the reflection series.

absolute IMAGING

Demultiple Techniques

Surface Related Multiple Elimination (SRME)

- SRME provides an effective way of estimating all surface-related multiples for adequately sampled and properly prepared 2D marine data. Surface-related multiple elimination (SRME) uses the recorded seismic data to predict and iteratively subtract the multiple series. The key advantage of SRME is that it needs no subsurface information whatsoever. The multiples are completely predicted from the data. 2D SRME can deal with all kinds of surface-related 2D multiples, provided all relevant data are recorded within the aperture and offset limitations of the survey line.

The basic steps in the sequence are:

1. SRME Regularization to regularize geometry (the spatial sampling) within each shot record, starting ensuring the spatial sampling (offset interval) between traces is a constant increment.
2. SRME Macro to estimate or “model” the multiples.
3. SRME Un-Regularization to restore the “modeled multiple” records to the same spatial sampling as the original recorded shots.
4. SRME Match Filter to design and apply a match filter that matches the modeled multiples to the recorded shots.
5. SRME Adaptive Subtraction to “fine tune” the match between pairs of traces (estimated multiple trace and original recorded trace), then subtract the multiple trace from the original trace.

absolute IMAGING

Demultiple Techniques

High Resolution Radon Transform (HRRT) Demultiple

- Uses the Radon transform to perform noise attenuation (usually the attenuation of multiples). It discriminates signal from noise by move-out of seismic events that have been fit to a family of curves – parabolic, hyperbolic or linear.

- Typically, the signal is muted in the Radon domain, then the noise is inverse transformed back to offset-time. This predicted noise is then subtracted from the input data to leave an estimate of the signal. Other muting strategies are possible with this tool.

absolute IMAGING

Raw w Geometry (Line 12 Segment G)

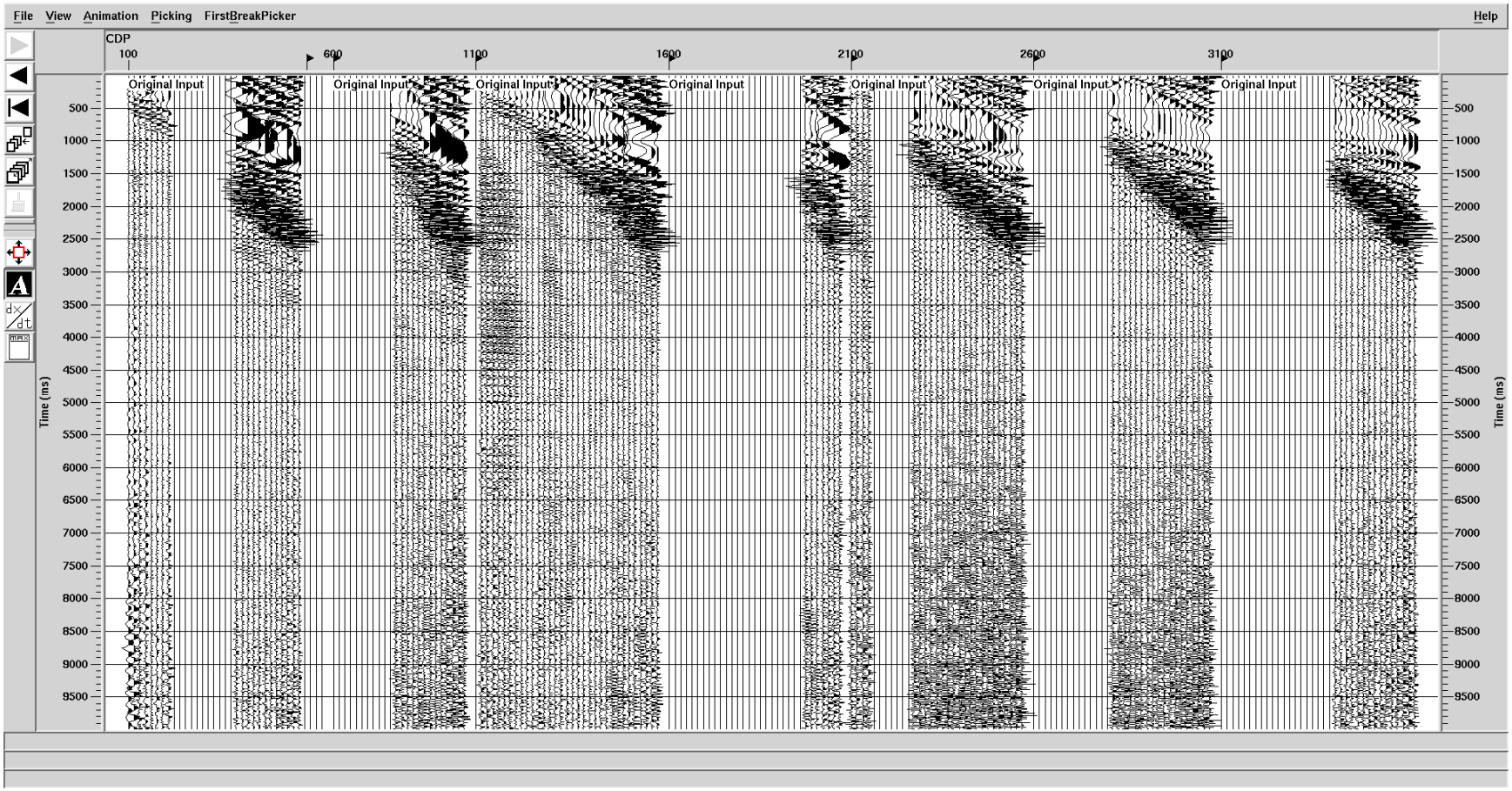

absolute IMAGING

Interpolation (Line 12 Segment G)

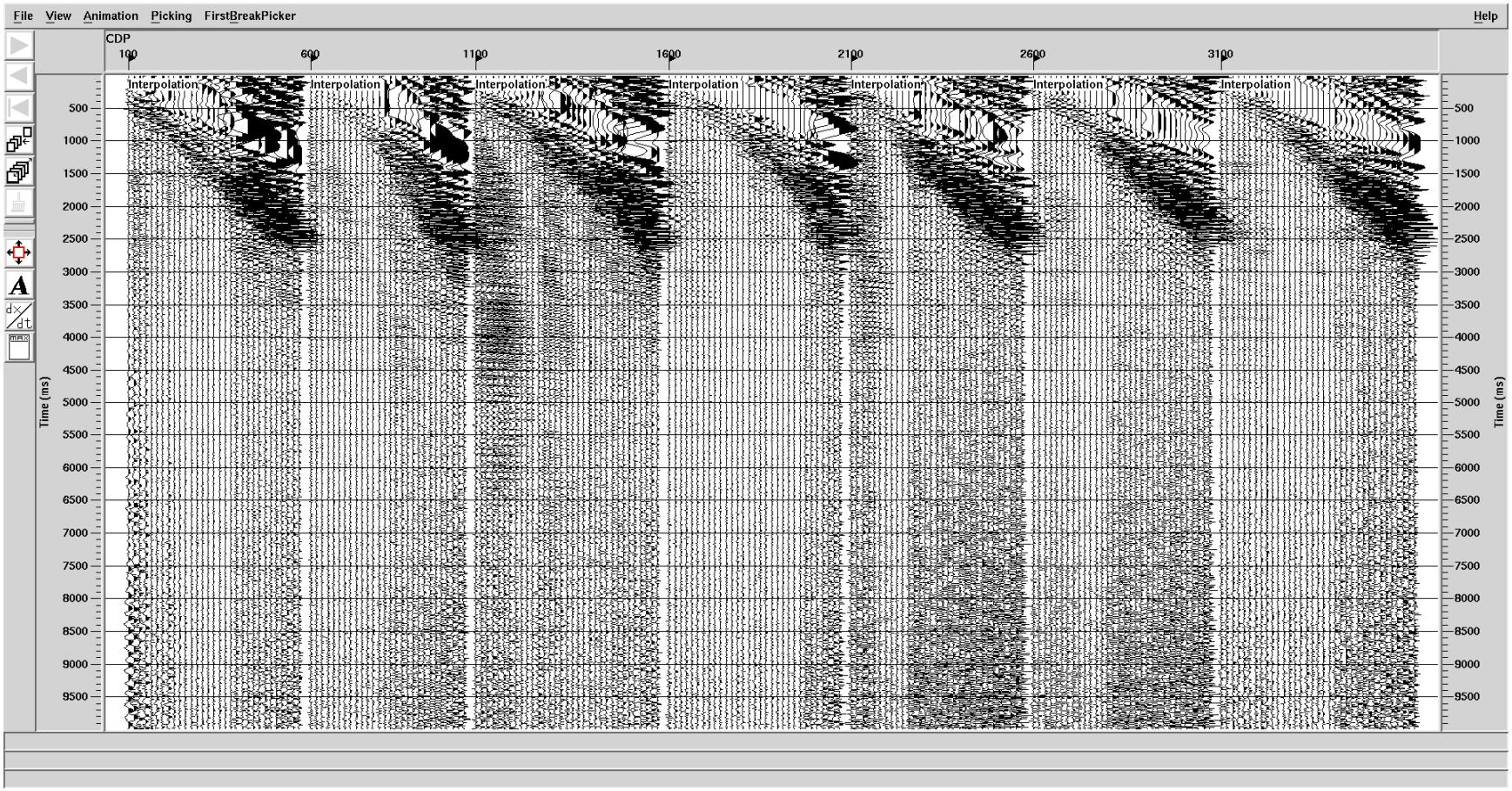

absolute IMAGING

SC Scaling (Line 12 Segment G)

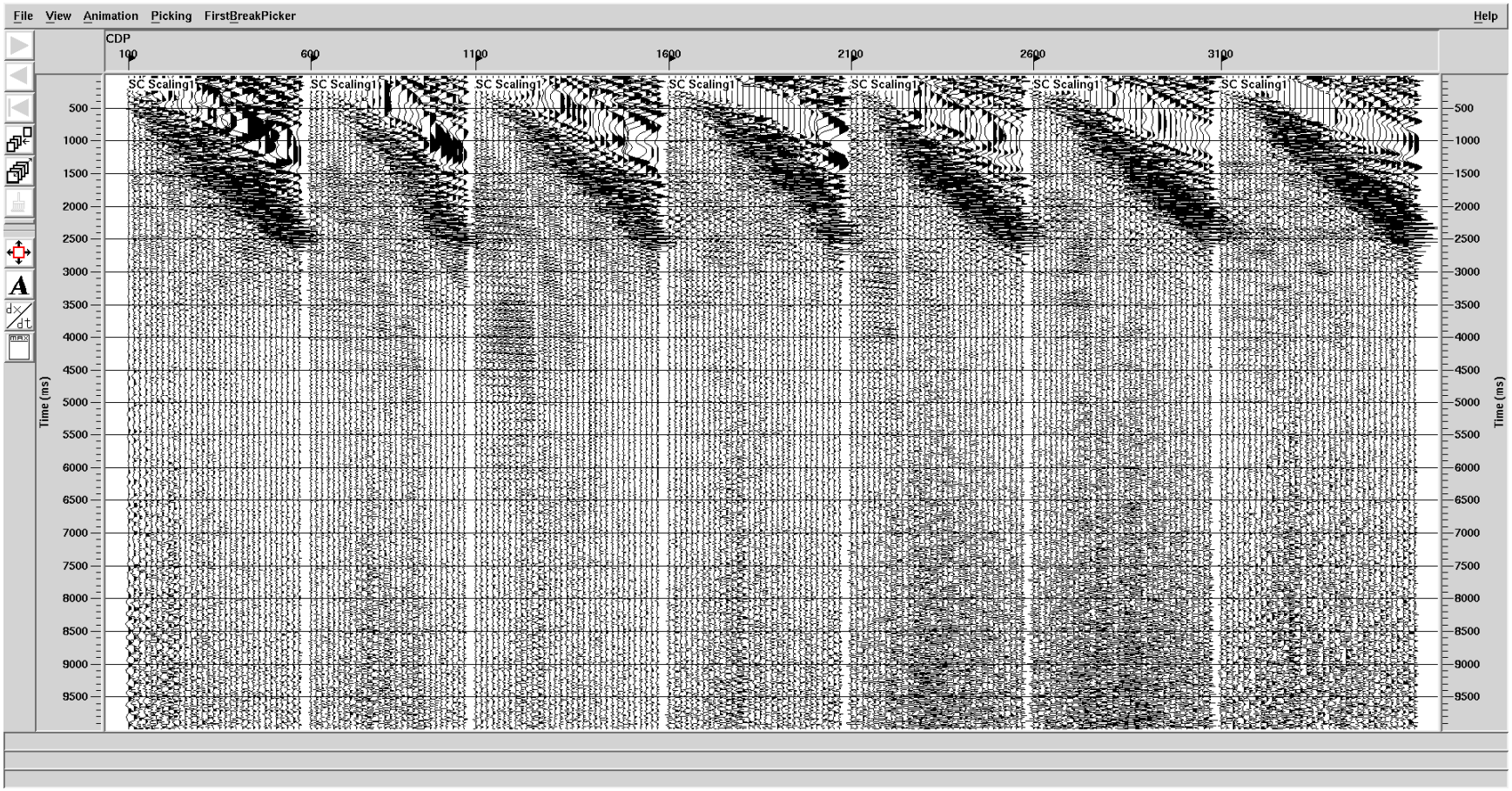

absolute IMAGING

Median Filter (Line 12 Segment G)

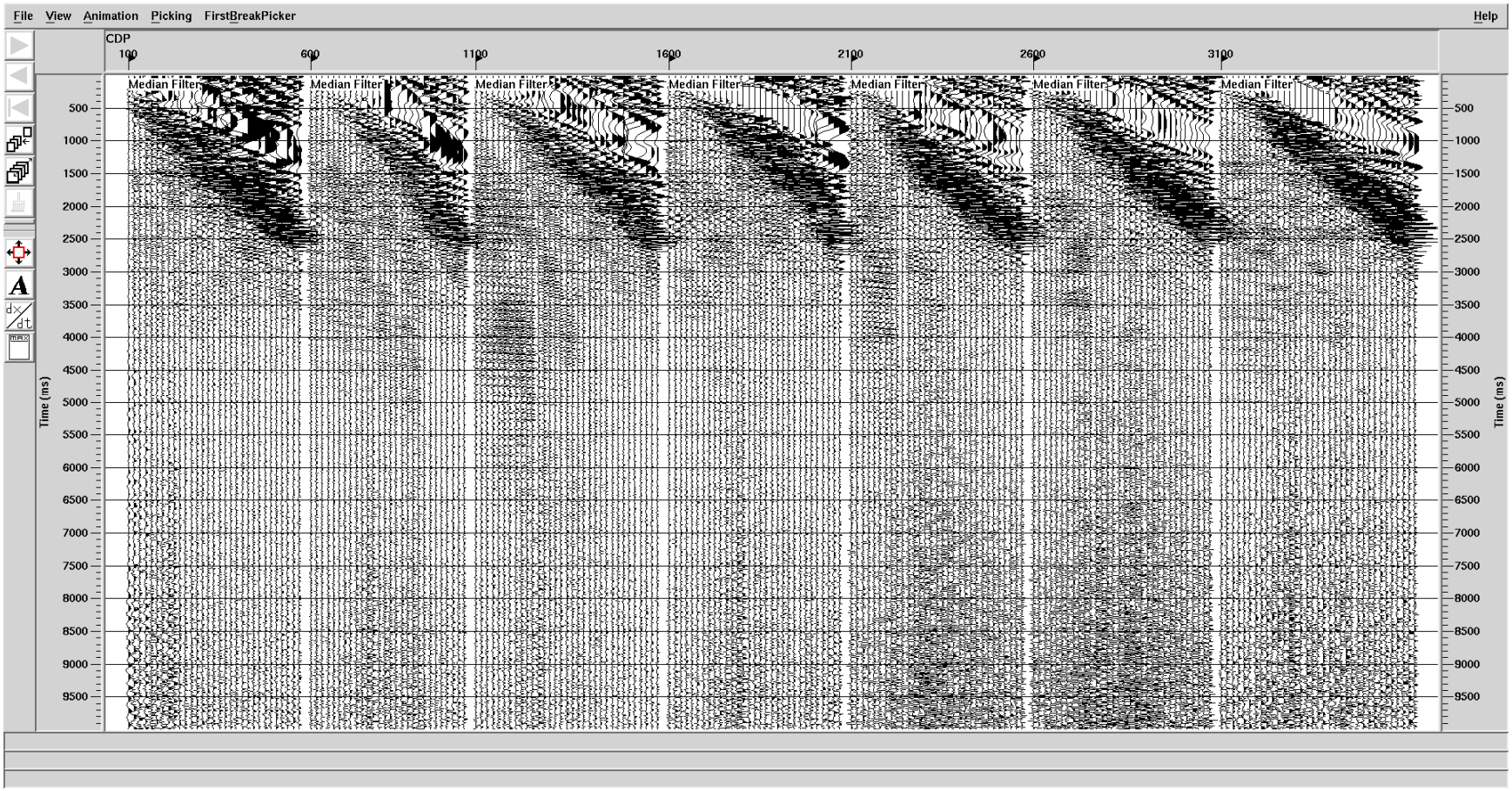

absolute IMAGING

Predictive Decon (Line 12 Segment G)

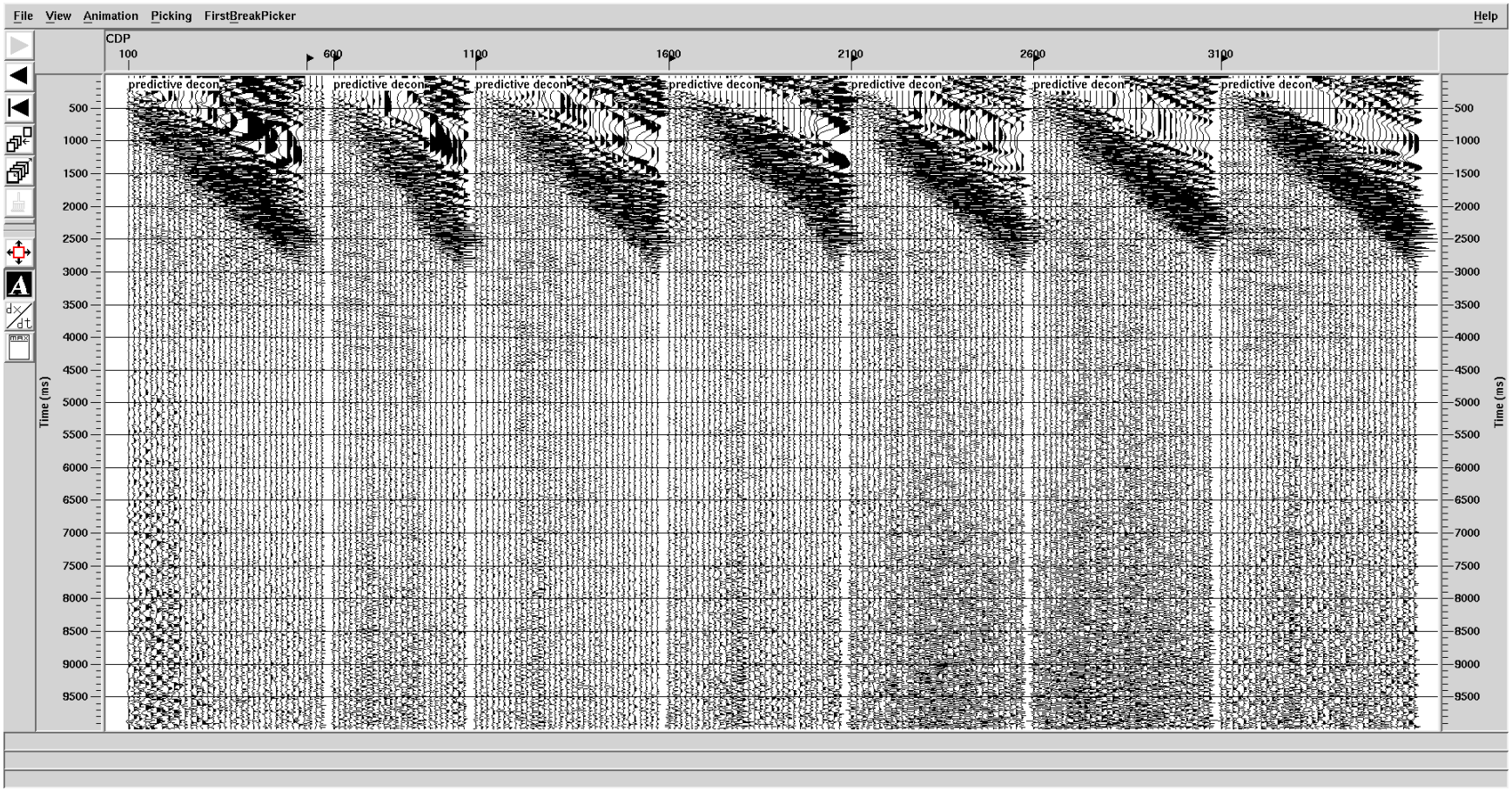

Creating a seismic image that is absolutely clear

absolute IMAGING

Designature (Line 12 Segment G)

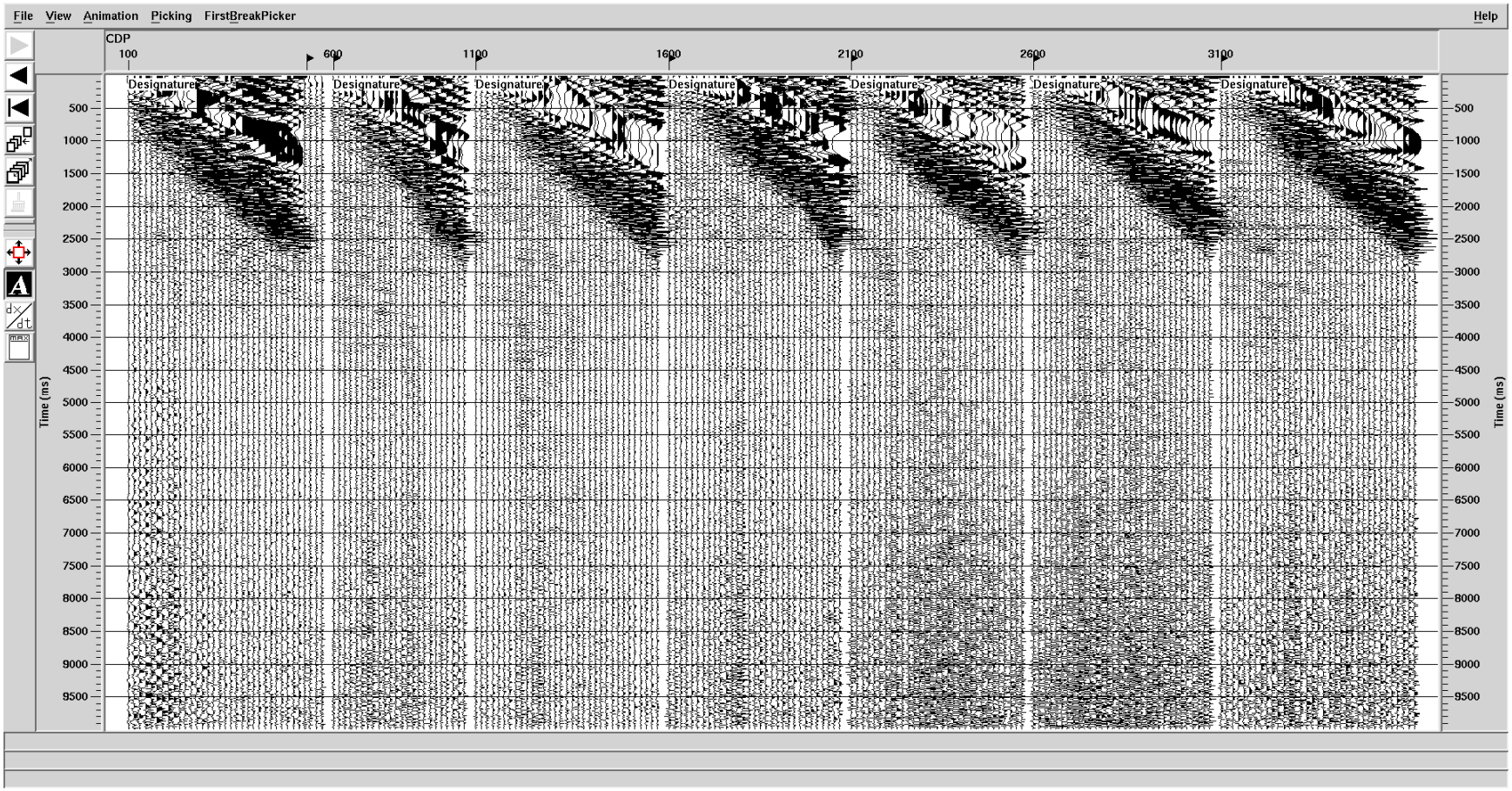

absolute IMAGING

SWNA (Line 12 Segment G)

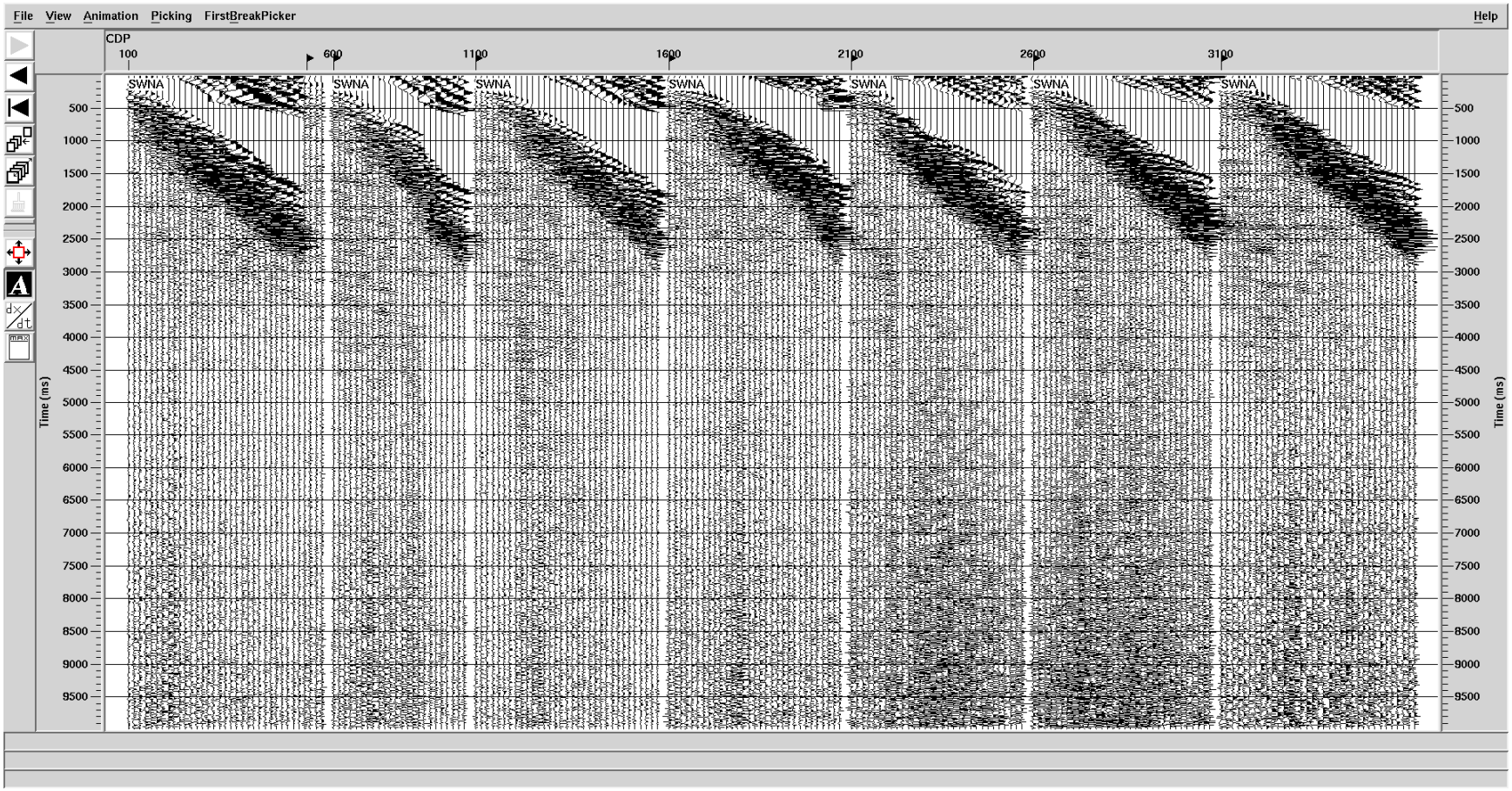

absolute IMAGING

SRME (Line 12 Segment G)

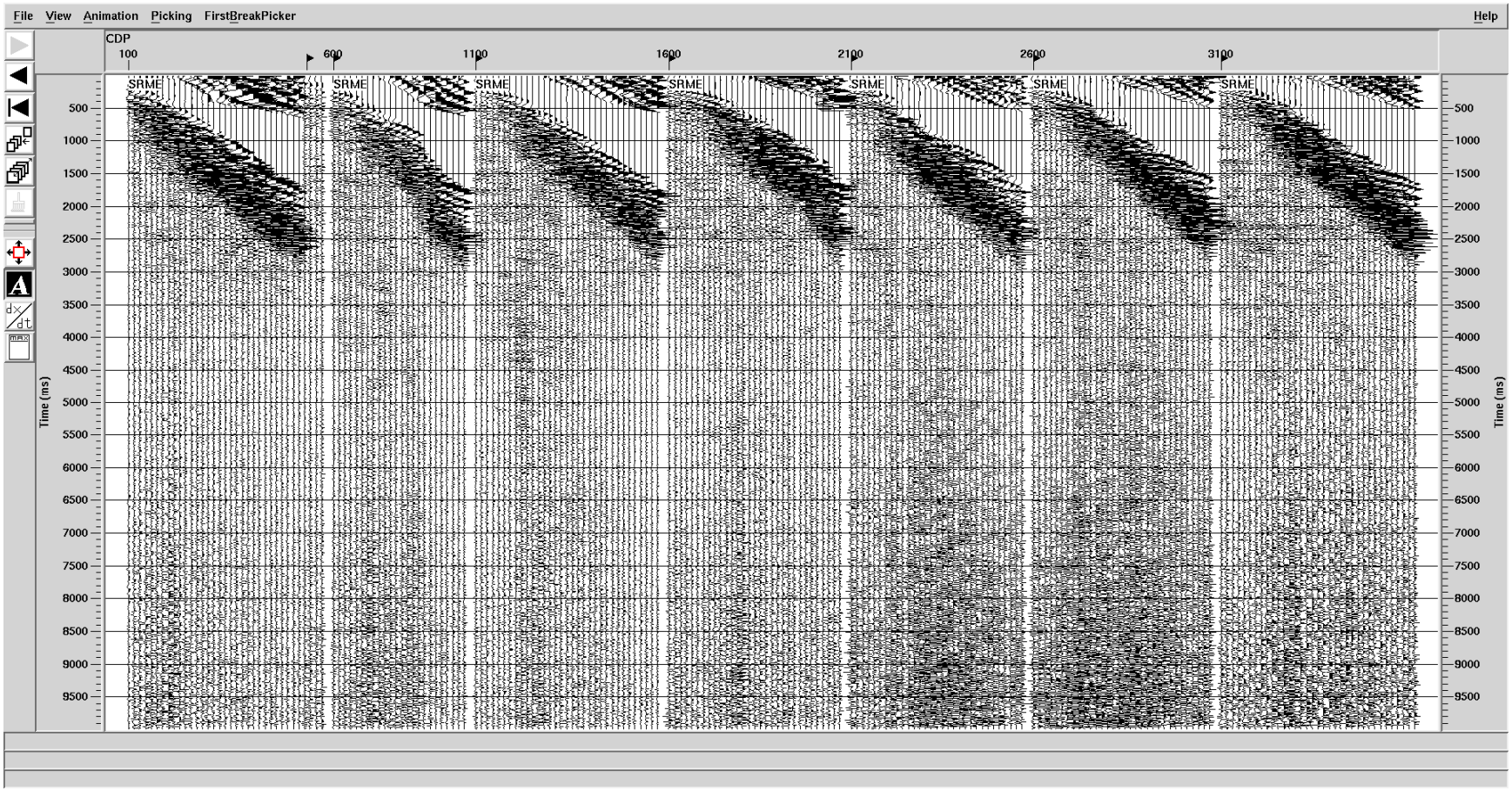

absolute IMAGING

Cadzow (Line 12 Segment G)

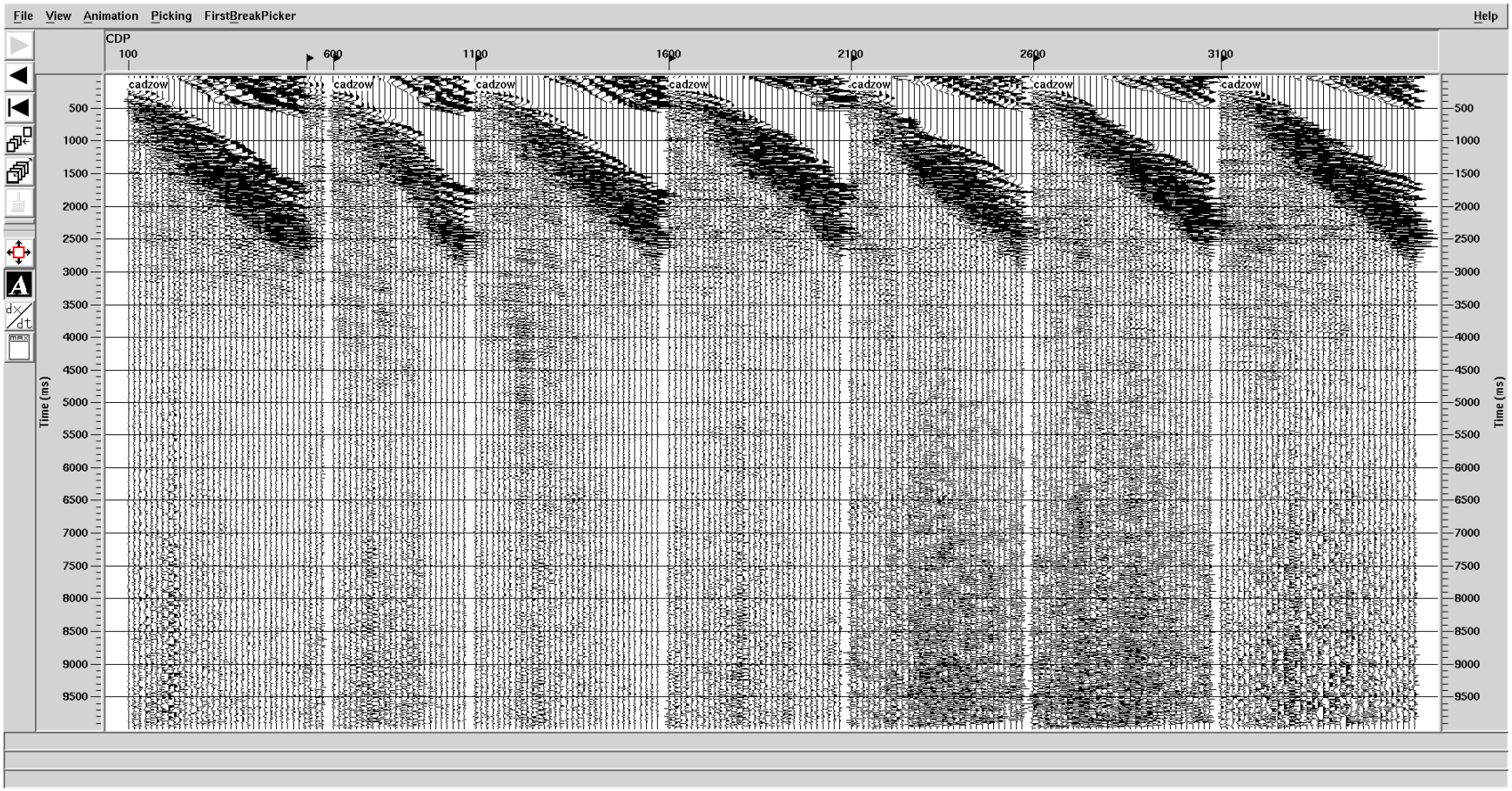

absolute IMAGING

Radon (Line 12 Segment G)

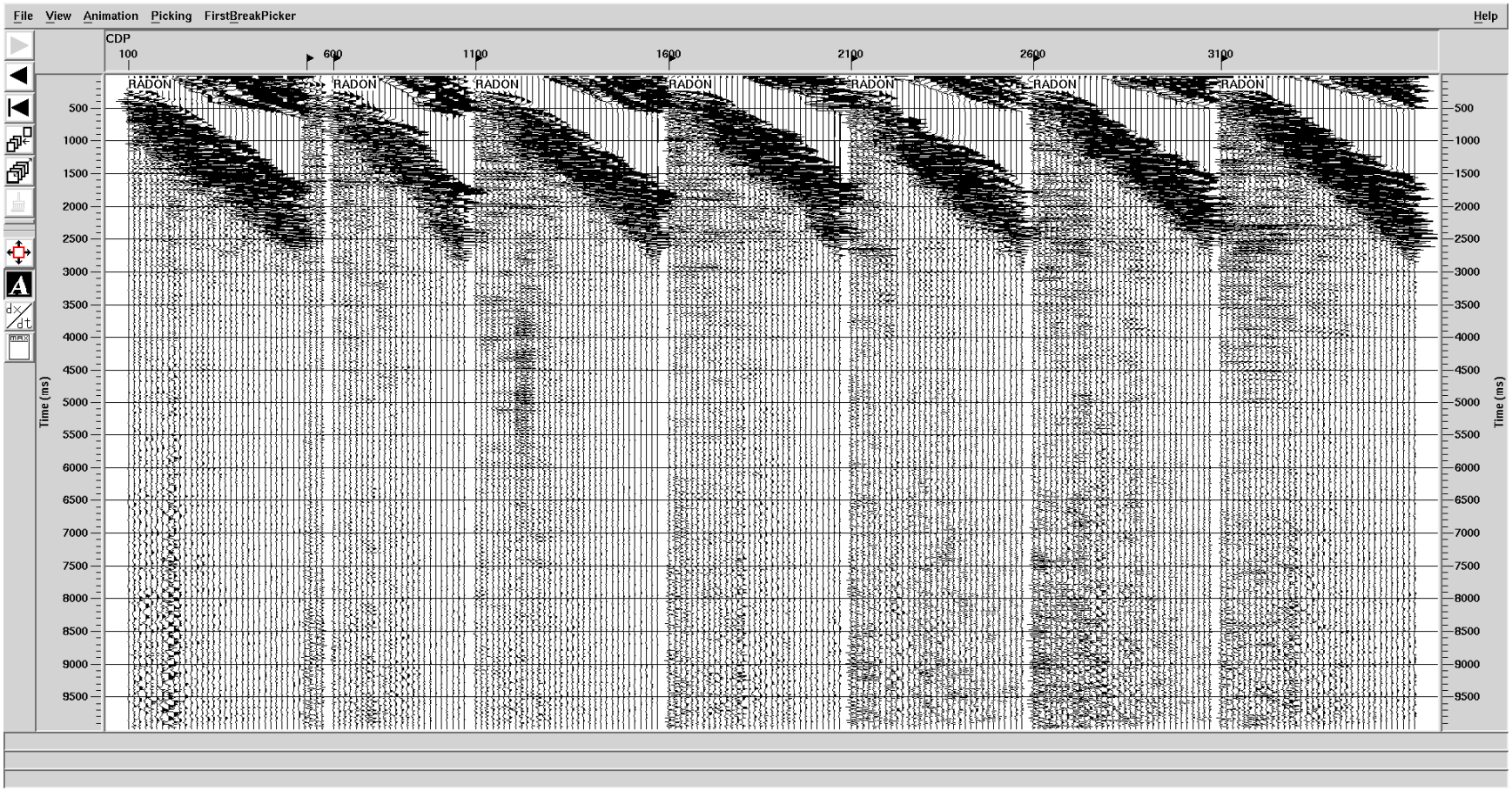

absolute IMAGING

SC Scaling (Line 12 Segment G)

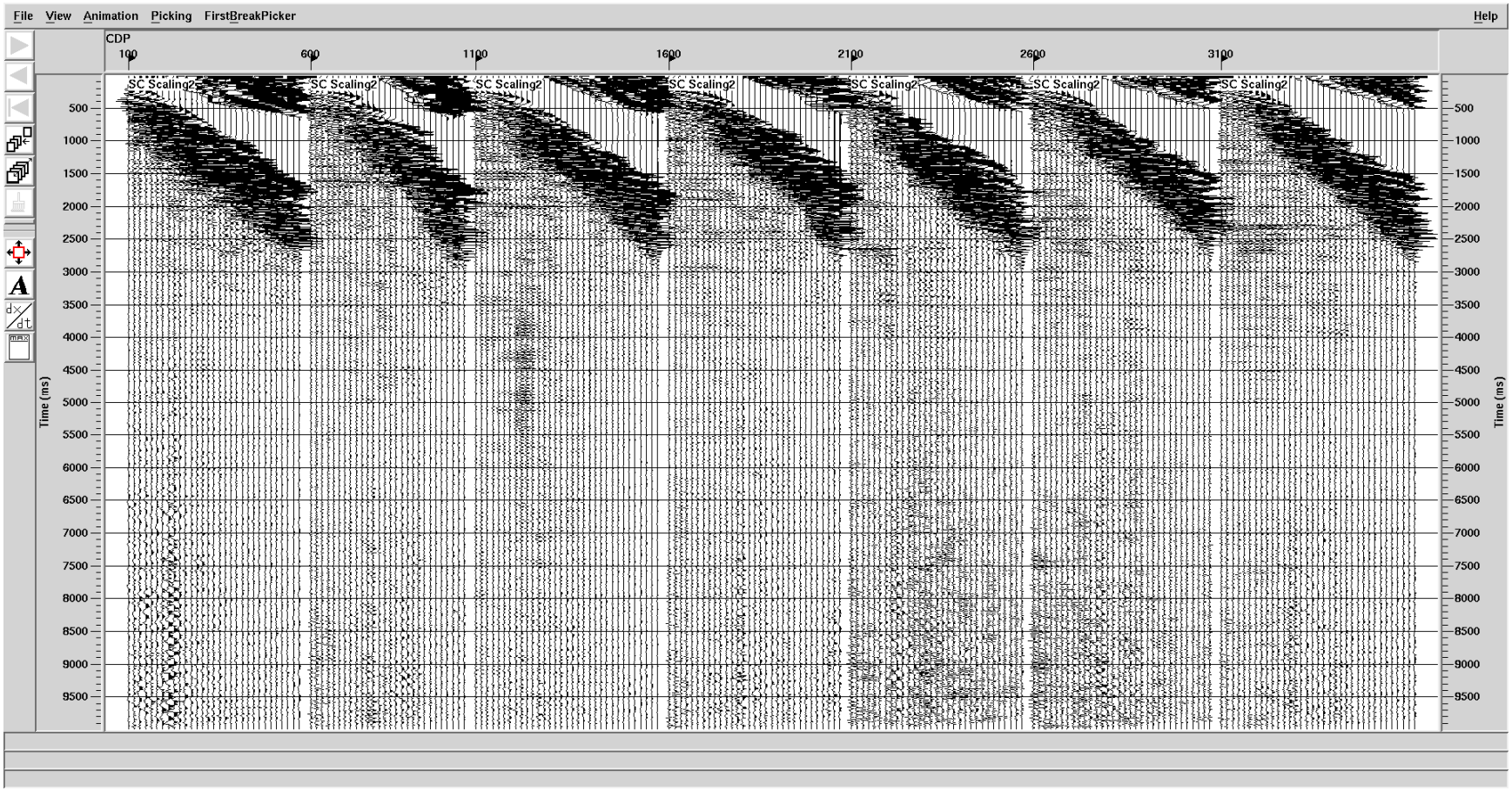

absolute IMAGING

Raw w Geometry (Line 12 Segment G)

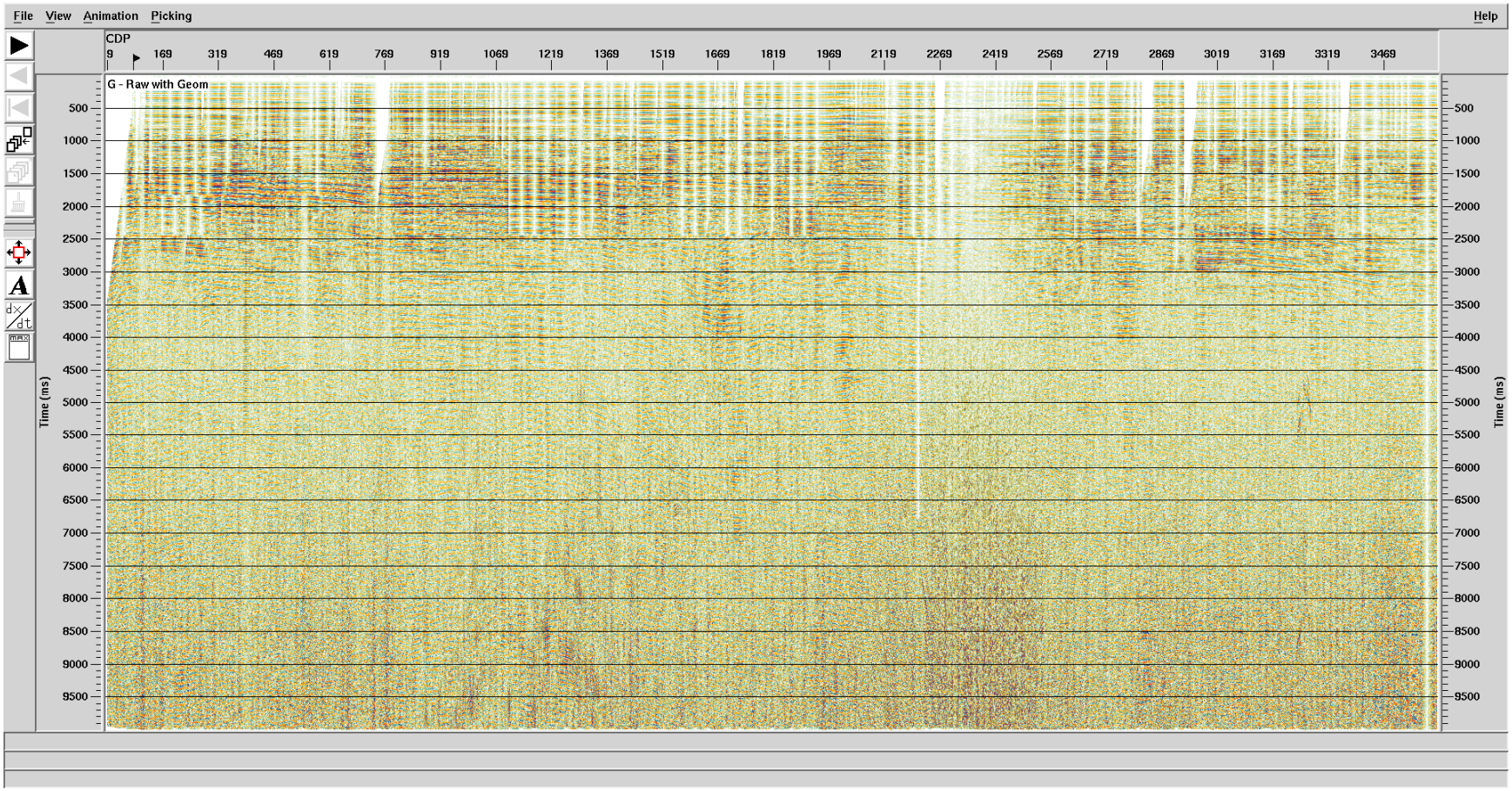

absolute IMAGING

Interpolation (Line 12 Segment G)

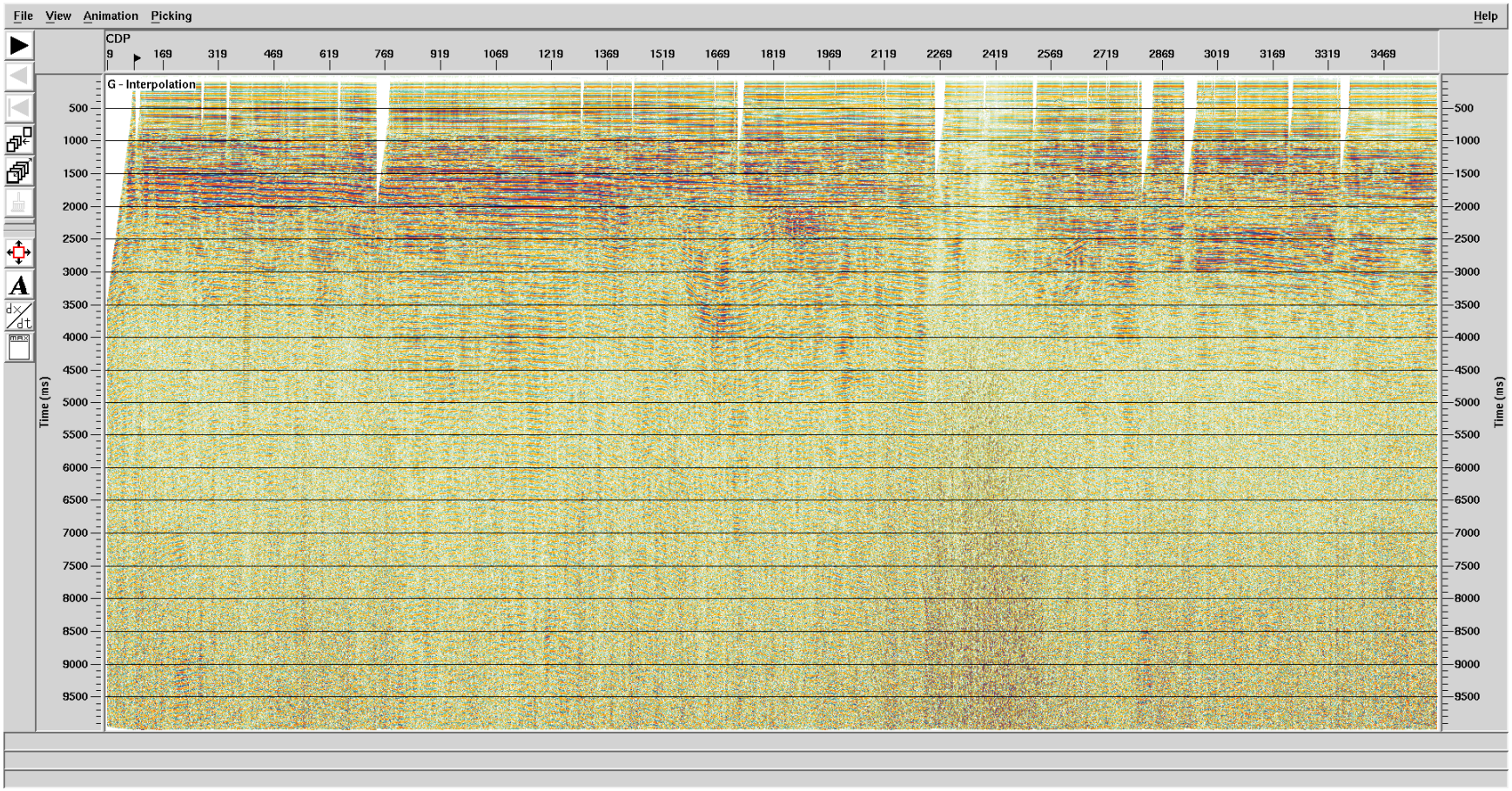

absolute IMAGING

SC Scaling (Line 12 Segment G)

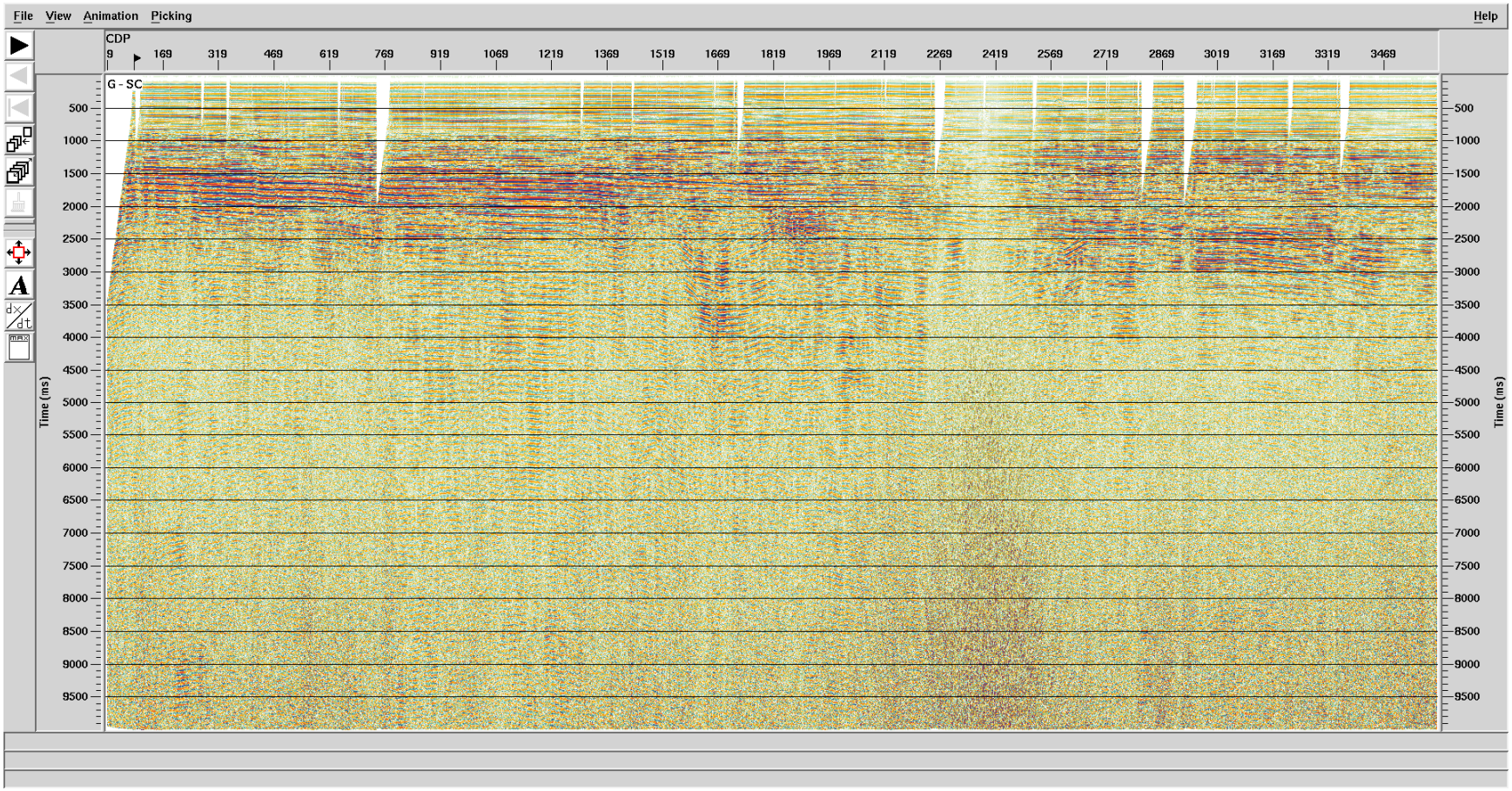

absolute IMAGING

Median Filter (Line 12 Segment G)

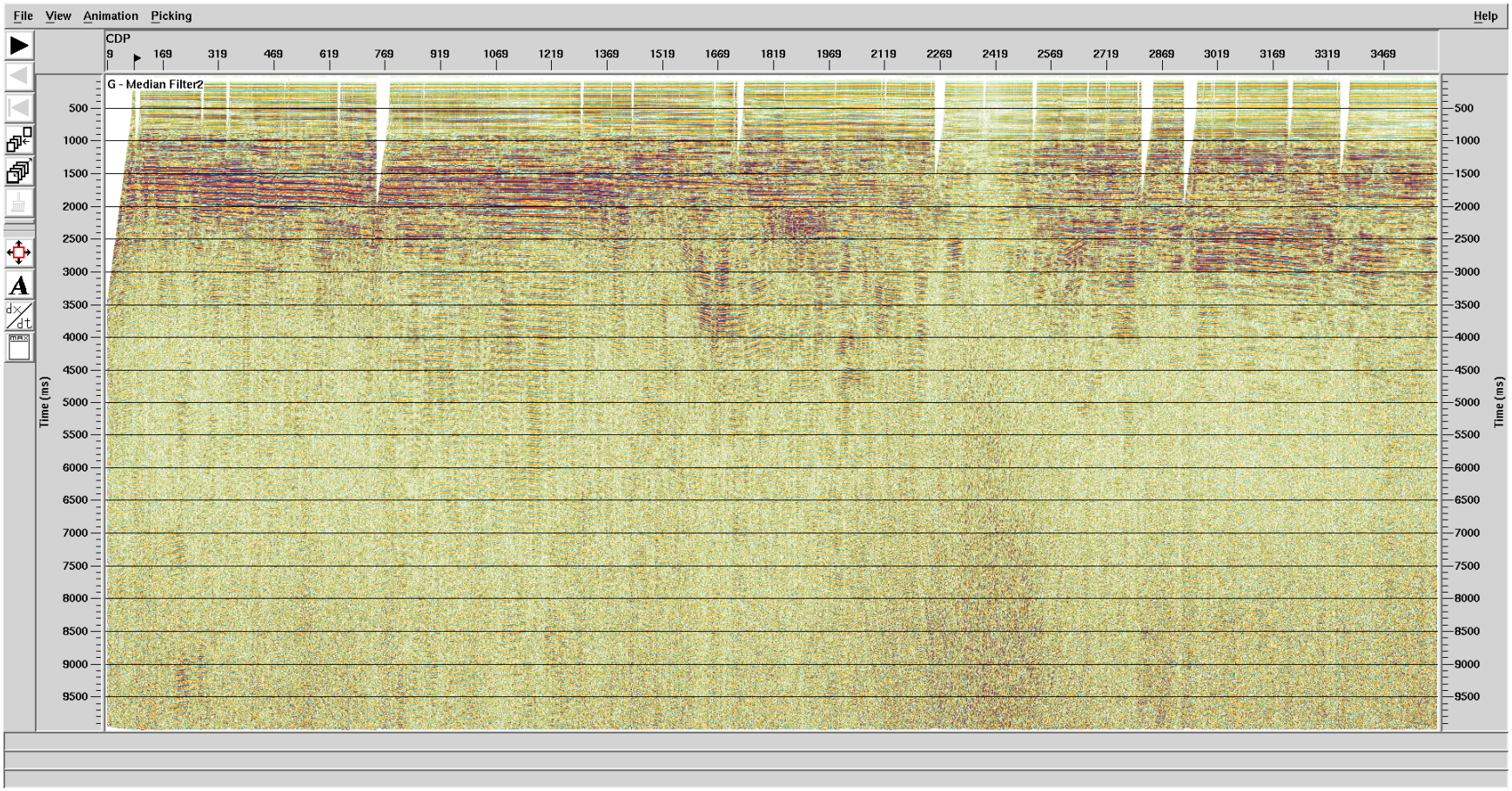

absolute IMAGING

Predictive Decon (Line 12 Segment G)

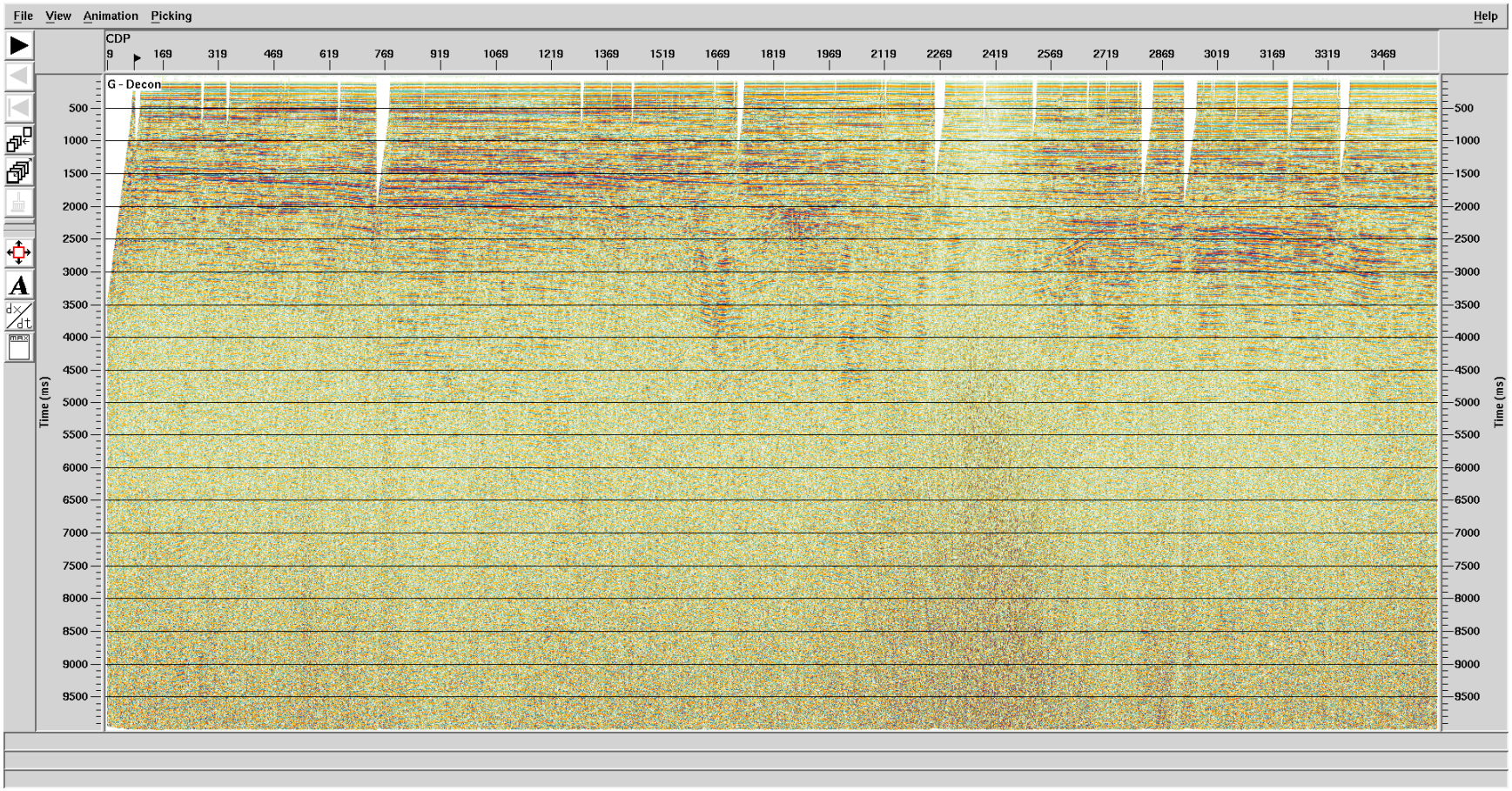

absolute IMAGING

Designature (Line 12 Segment G)

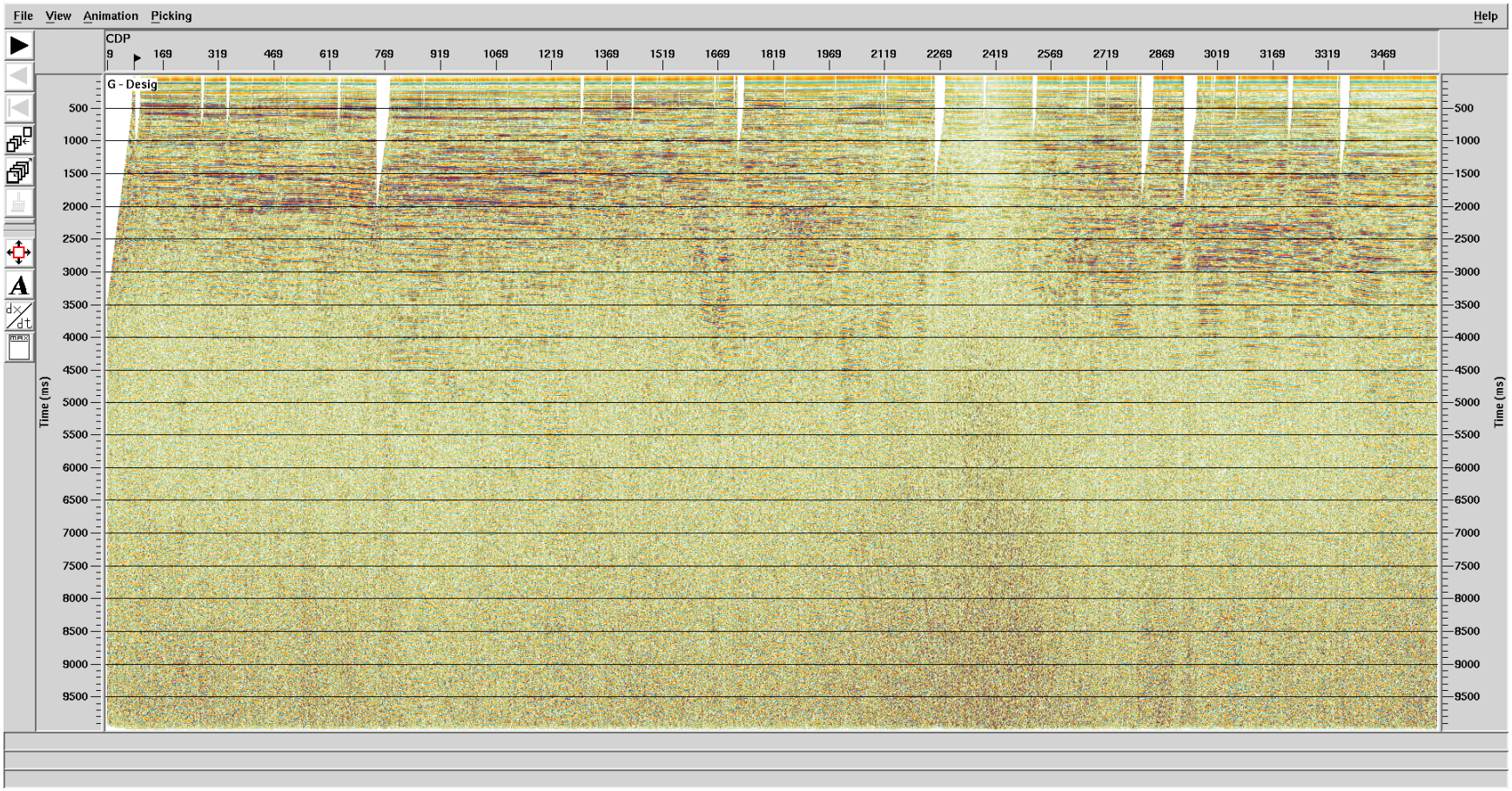

absolute IMAGING

SWNA (Line 12 Segment G)

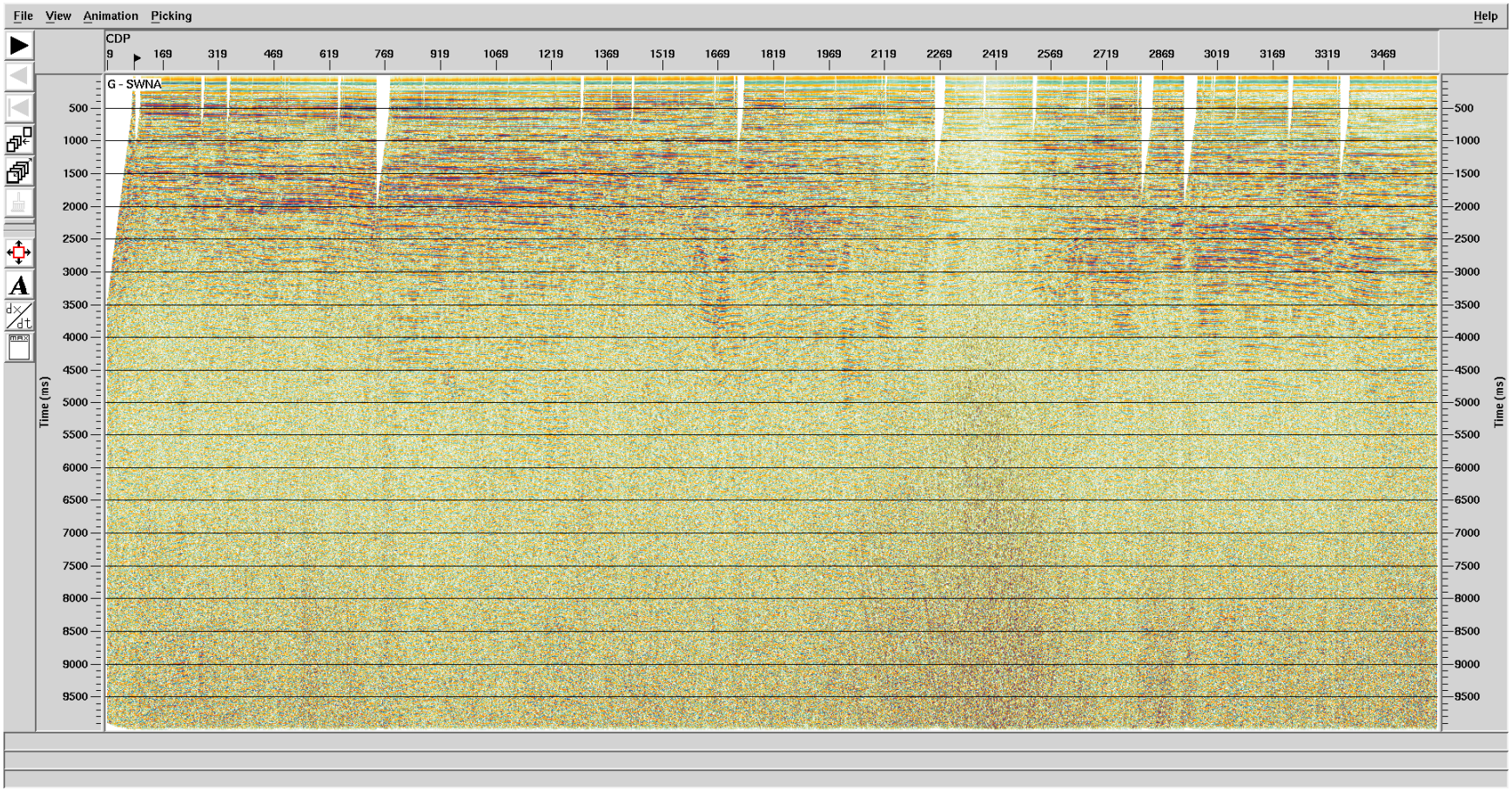

absolute IMAGING

SRME (Line 12 Segment G)

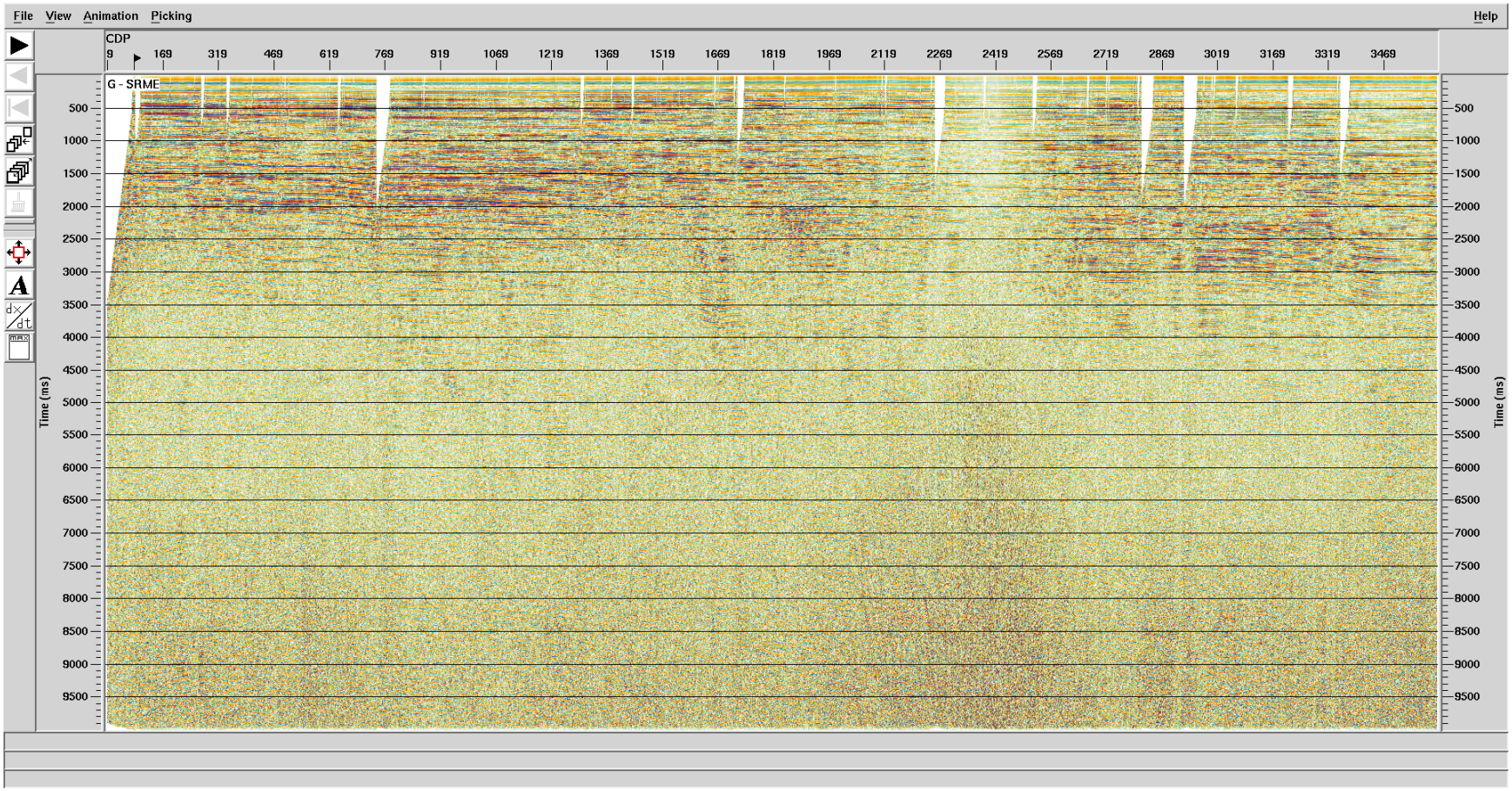

absolute IMAGING

Cadzow (Line 12 Segment G)

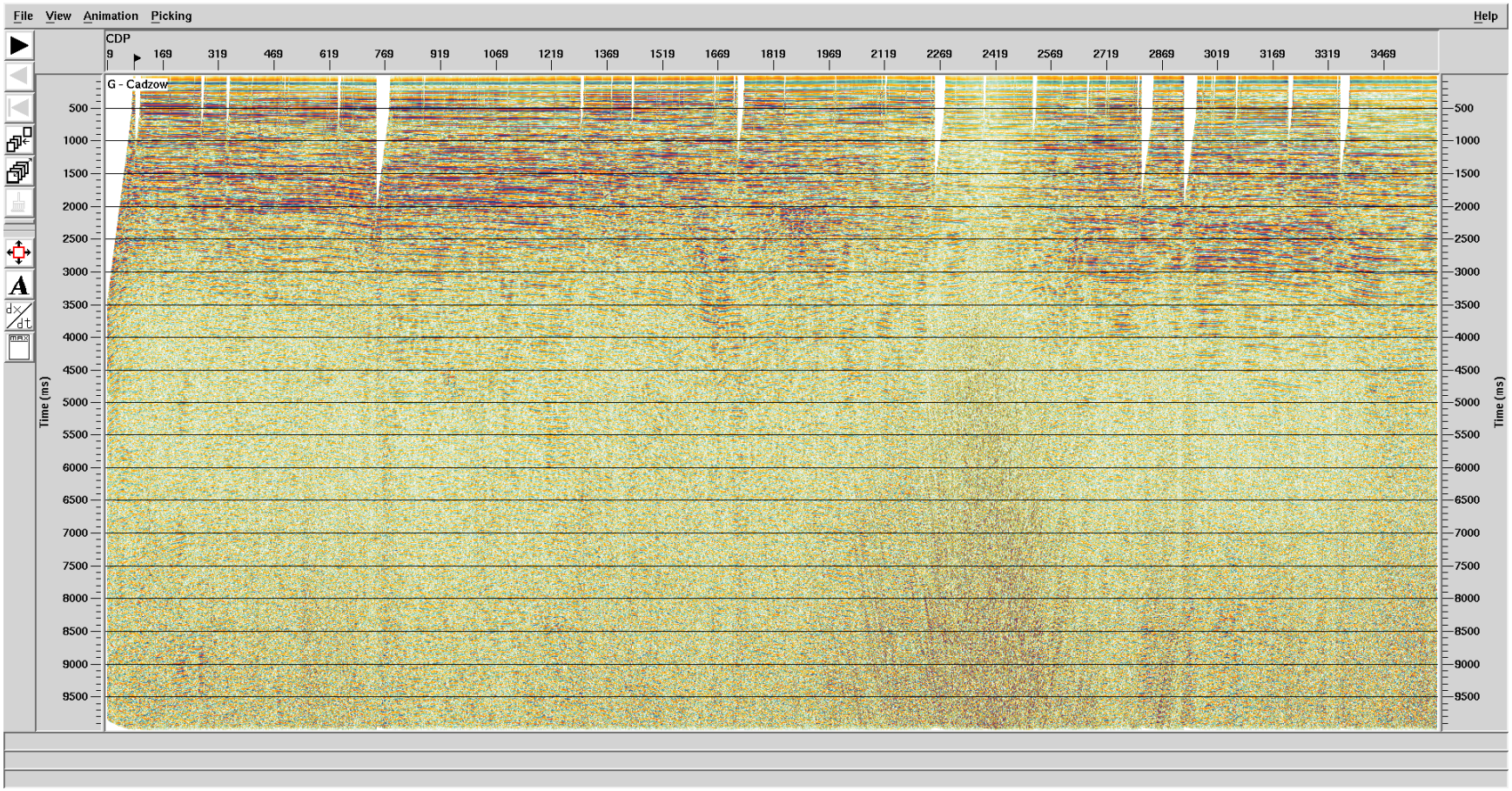

absolute IMAGING

Radon (Line 12 Segment G)

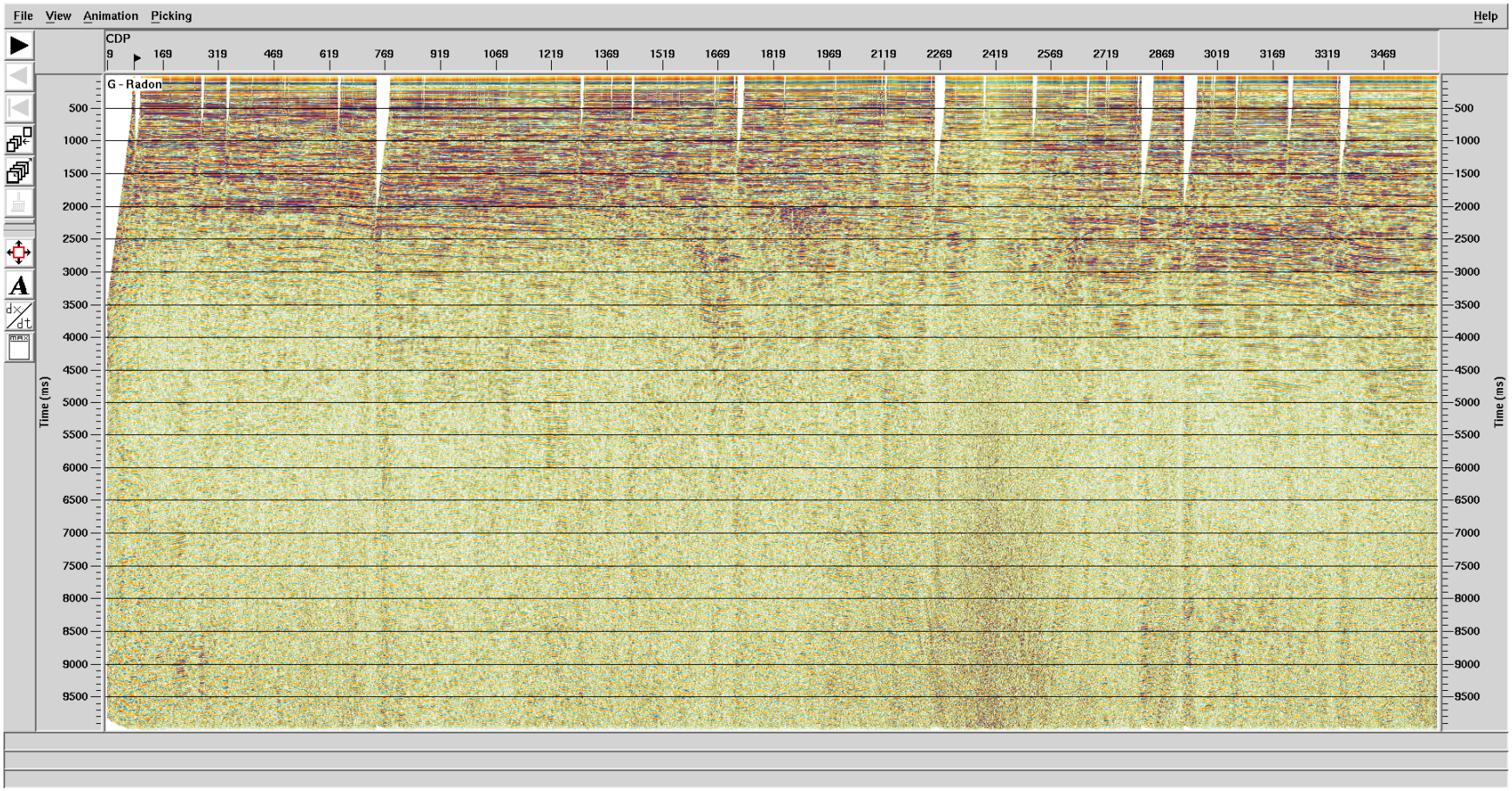

absolute IMAGING

SC Scaling (Line 12 Segment G)

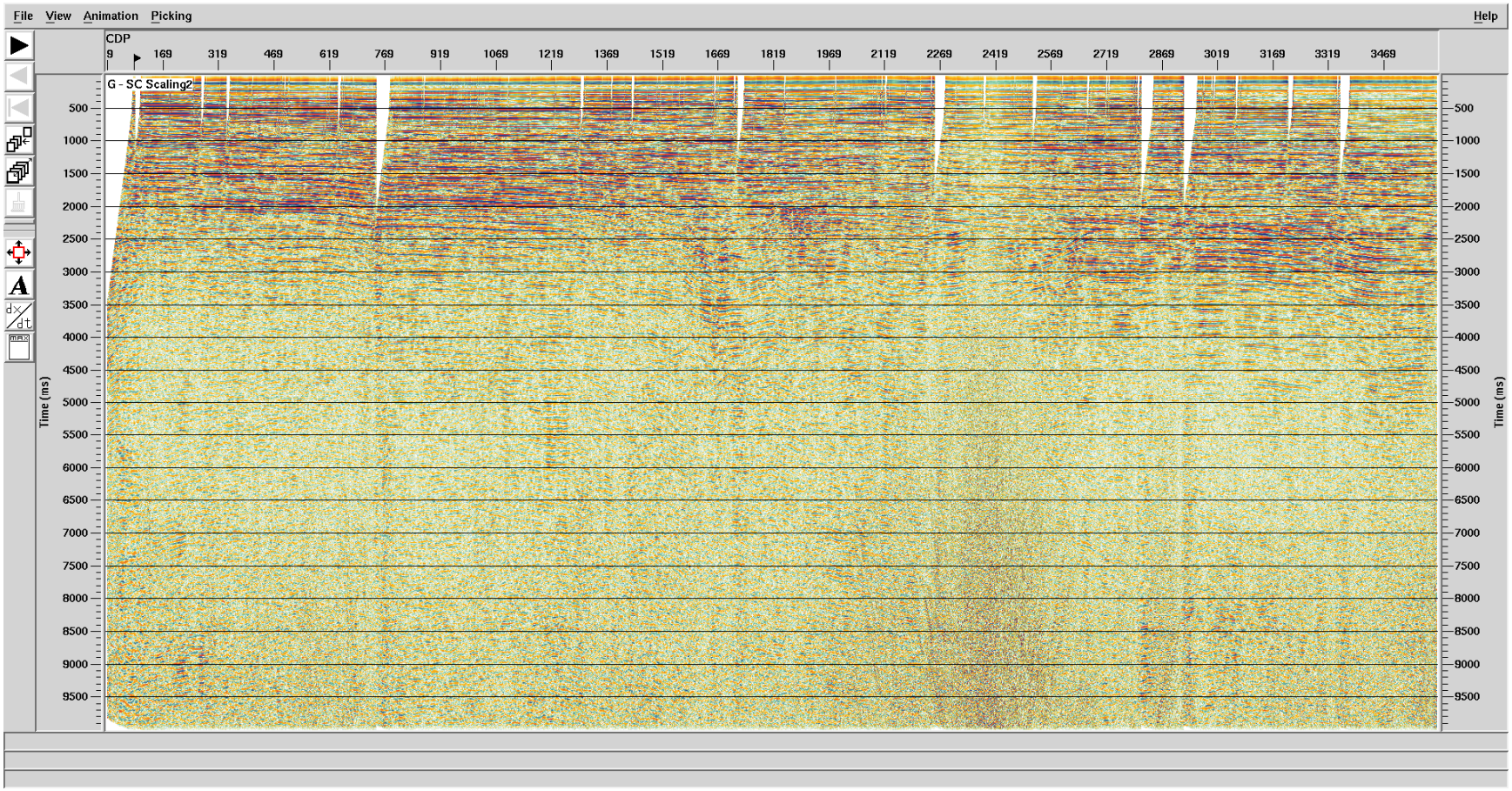

absolute IMAGING

Final Stack (Line 12 Segment G)

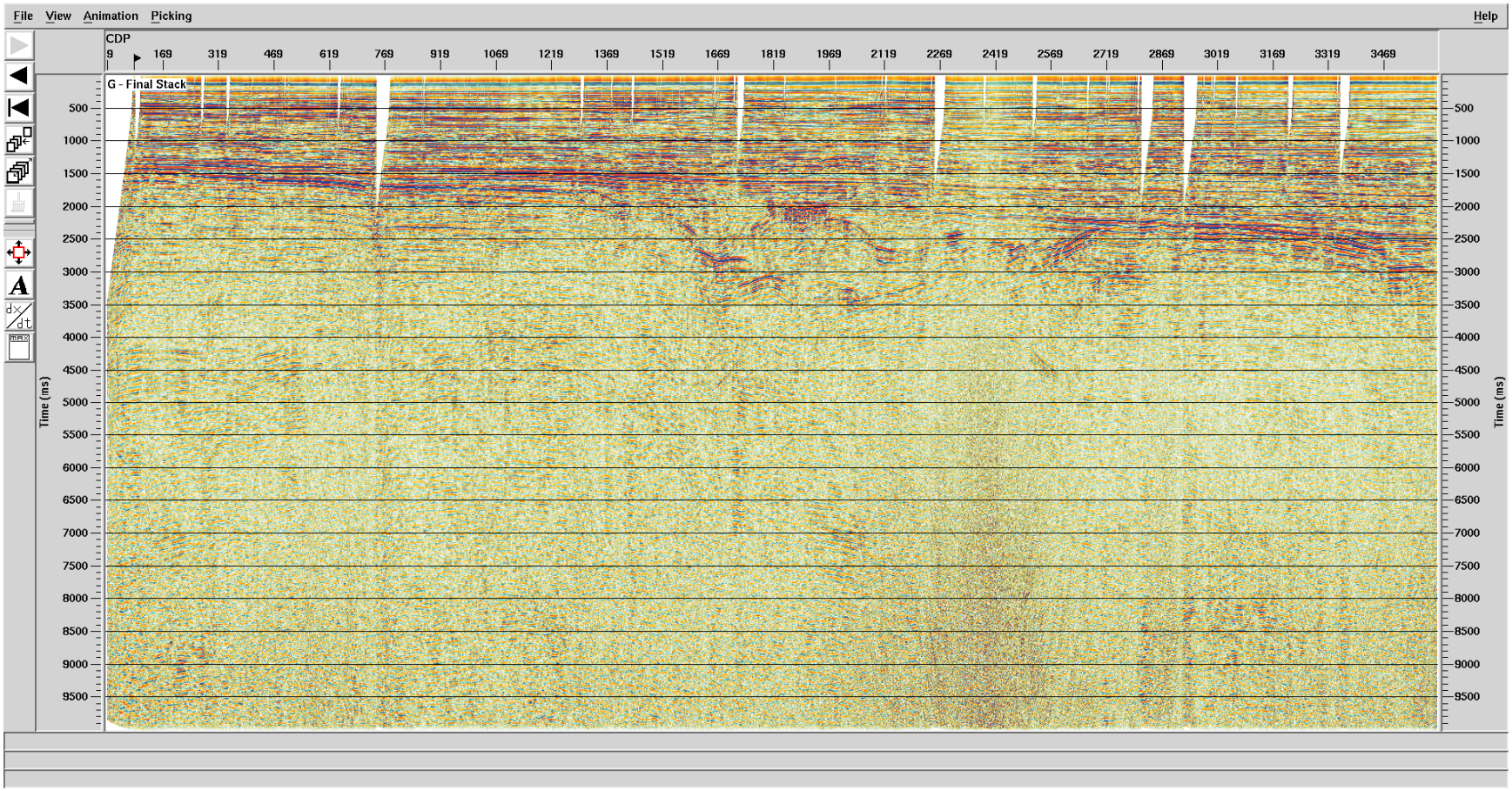

absolute IMAGING

Brute Velocity (Line 12 Segment G)

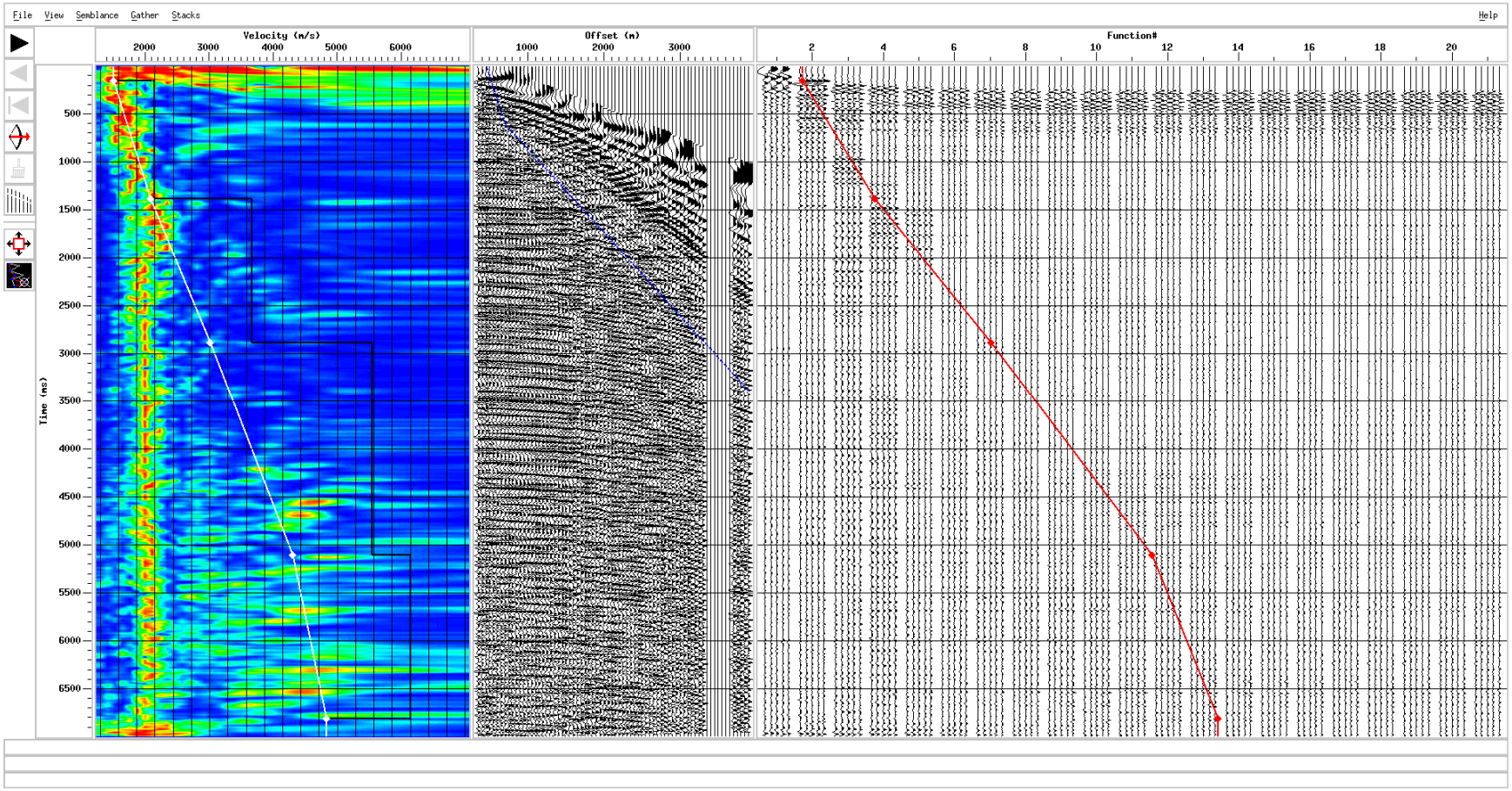

absolute IMAGING

Final Velocity (Line 12 Segment G)

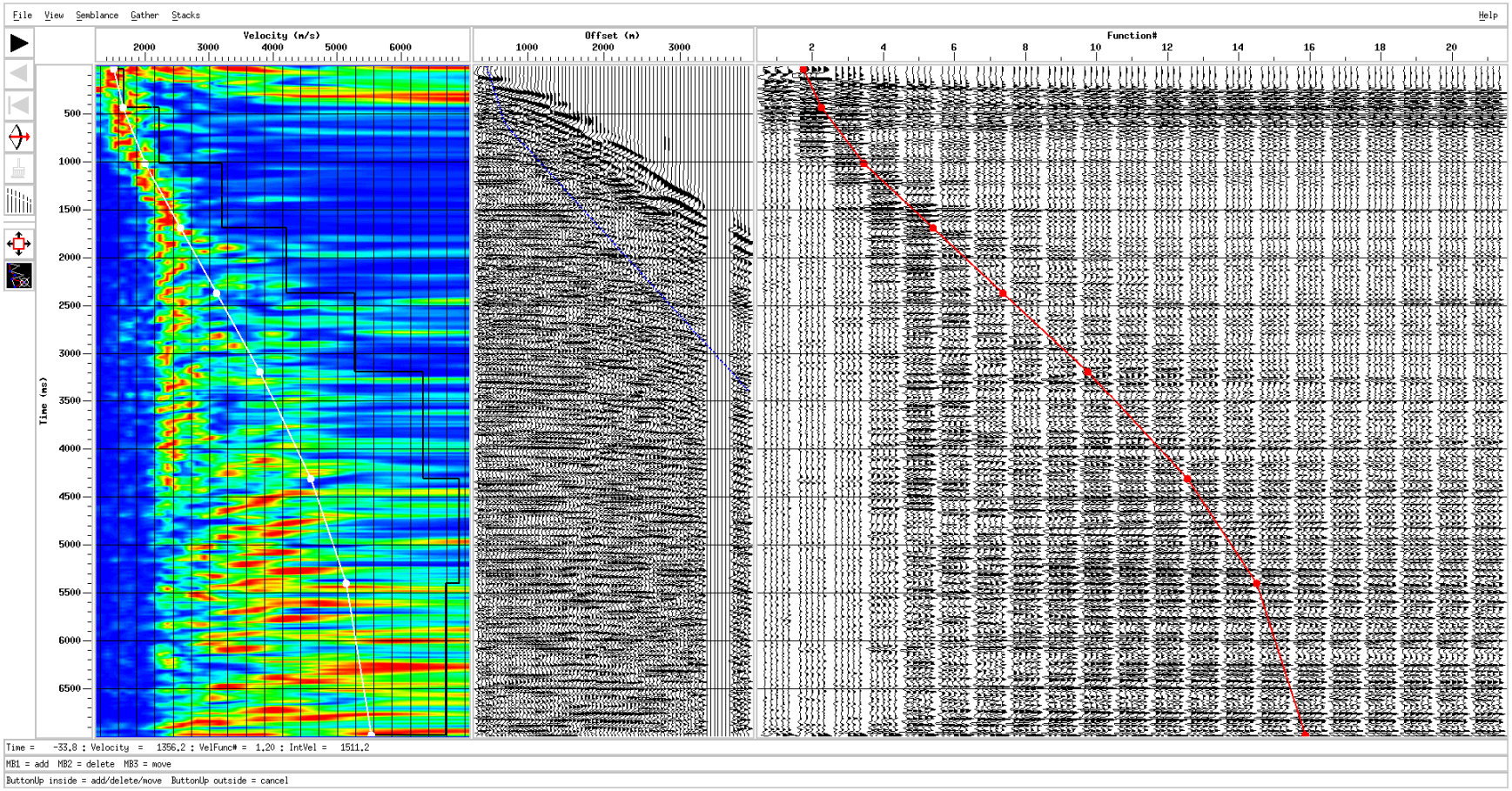

absolute IMAGING

Brute Velocity (Line 12 Segment G)

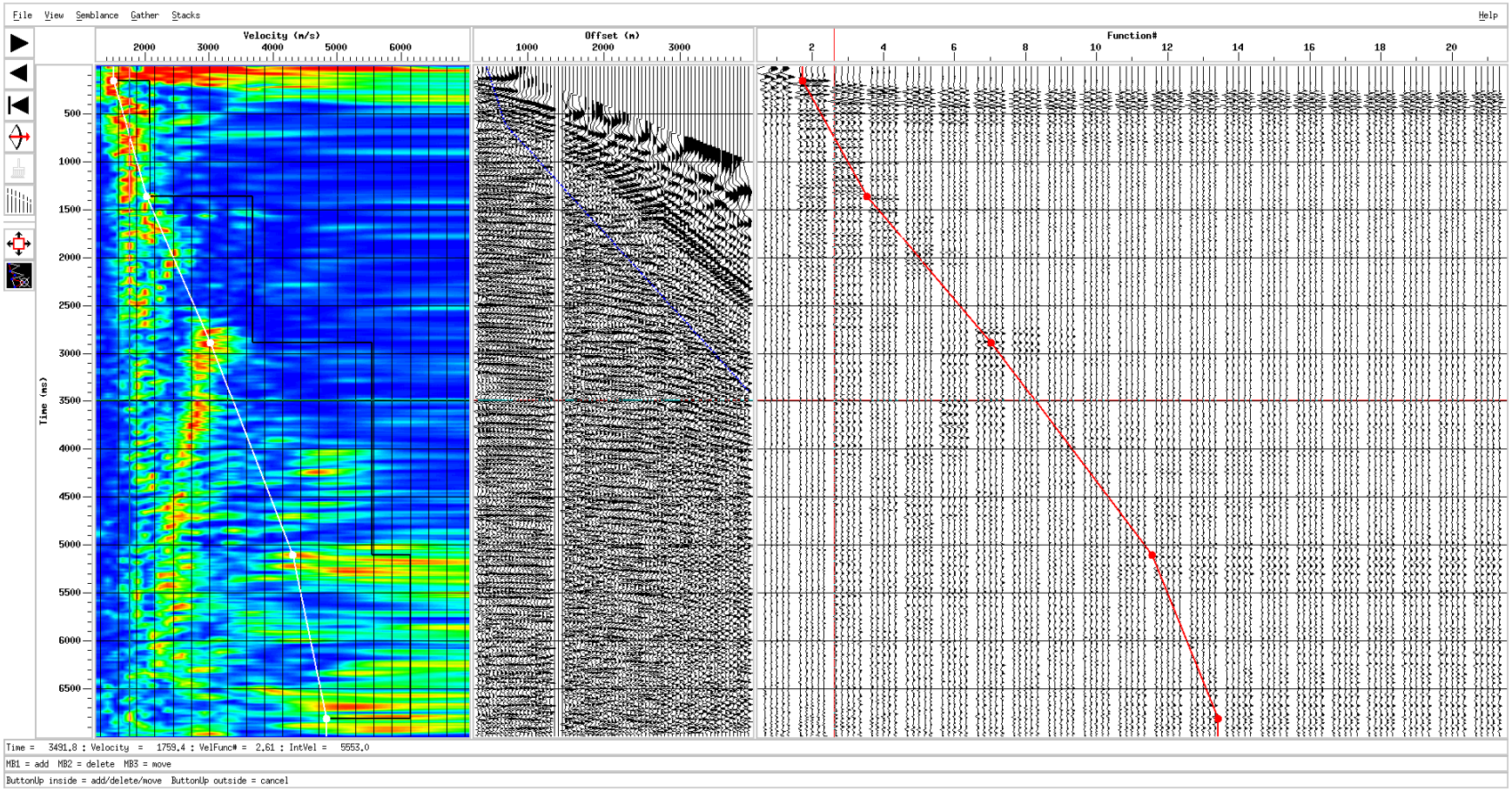

absolute IMAGING

Final Velocity (Line 12 Segment G)

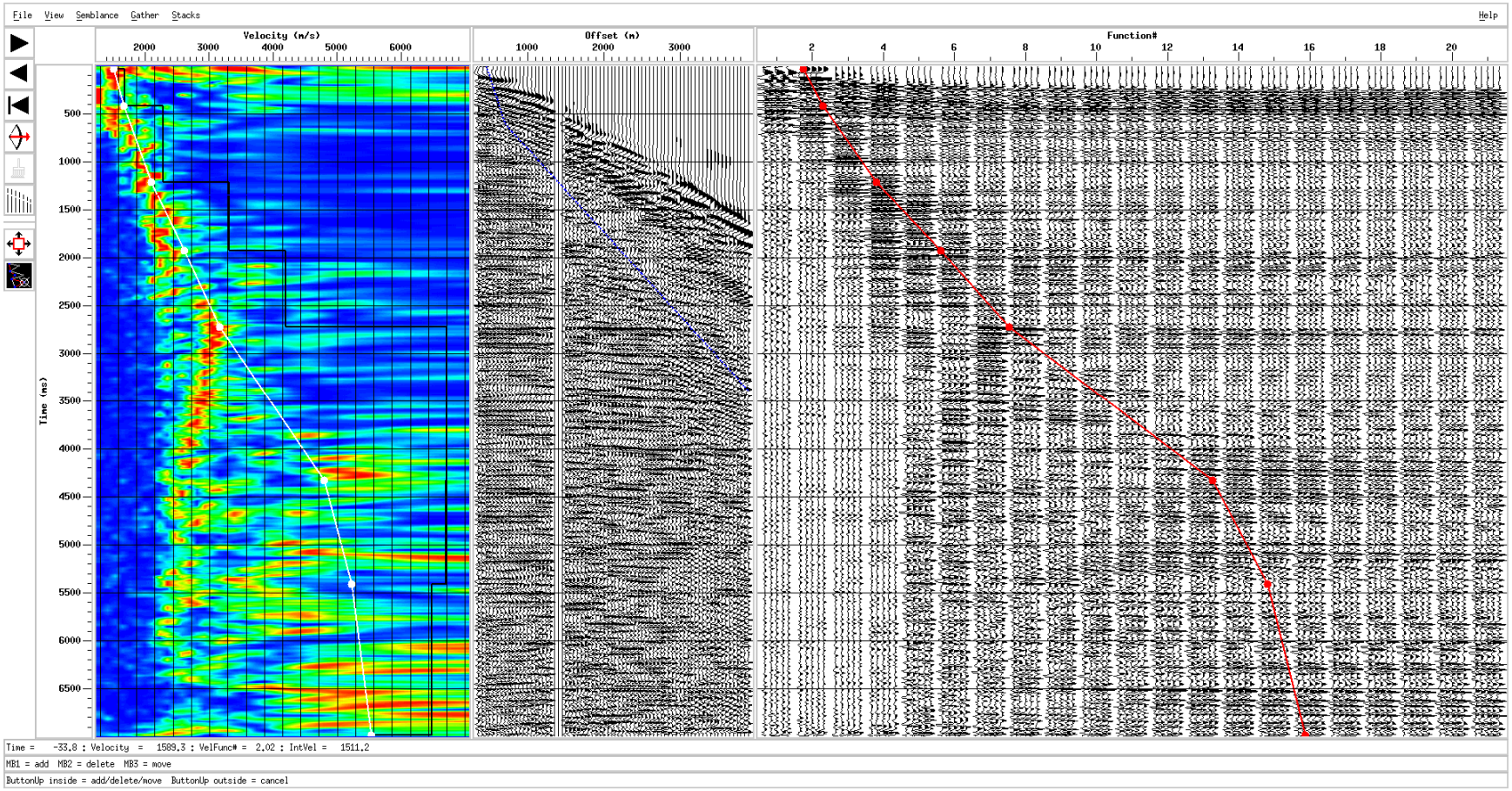

absolute IMAGING

Brute Velocity (Line 12 Segment G)

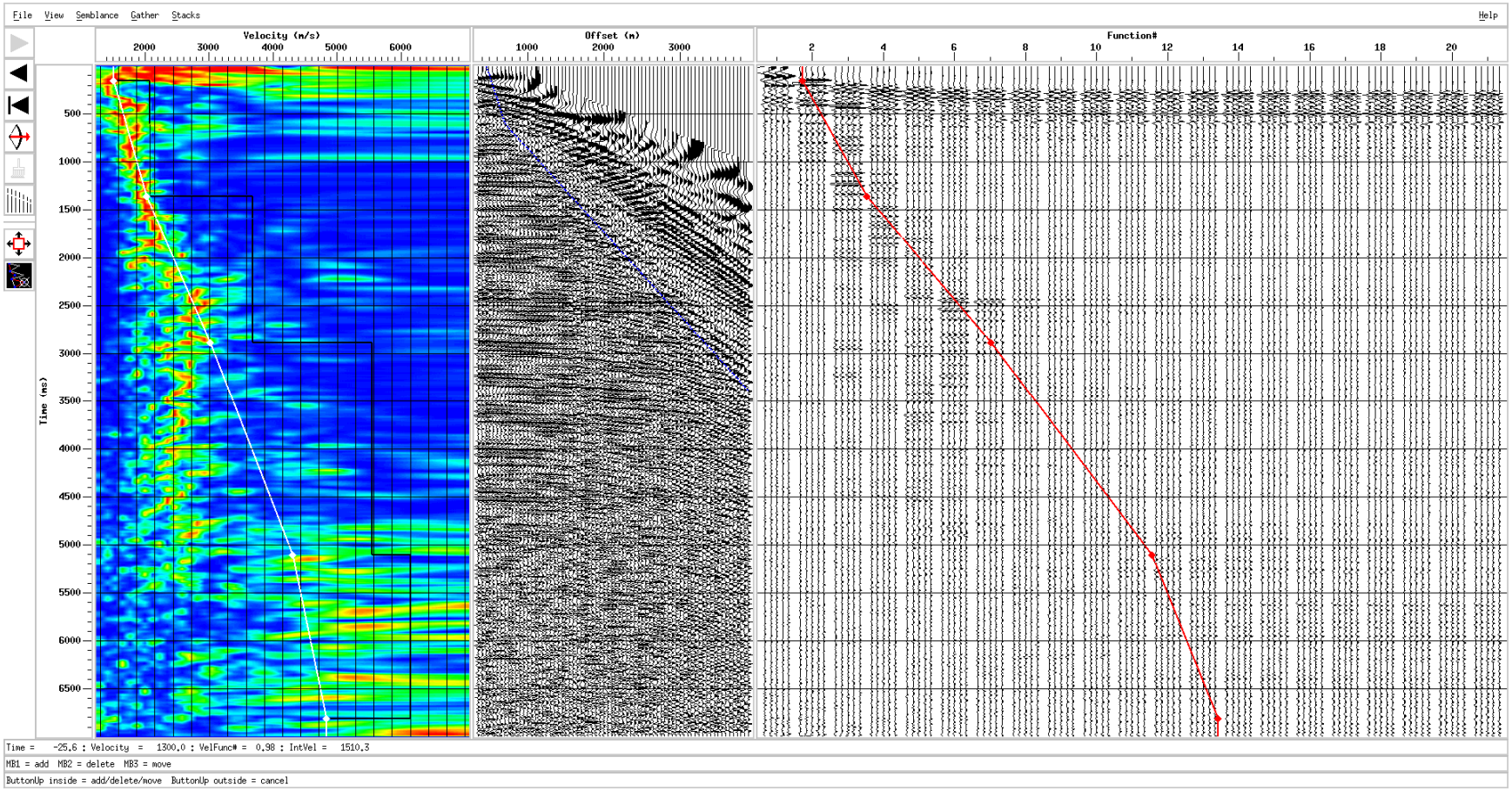

absolute IMAGING

Final Velocity (Line 12 Segment G)

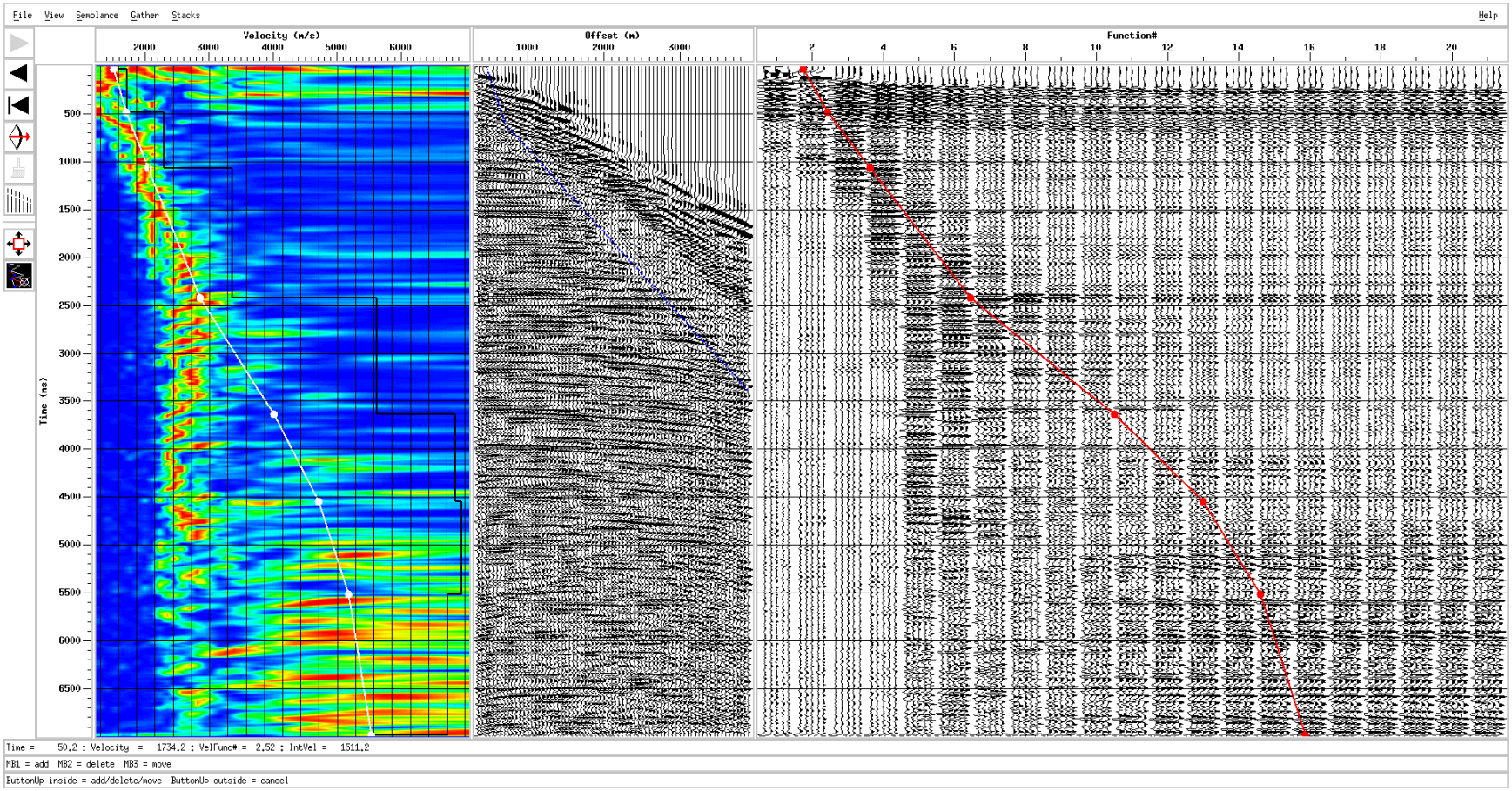

absolute IMAGING

Final Merged Stack (Line 12 Segment G)

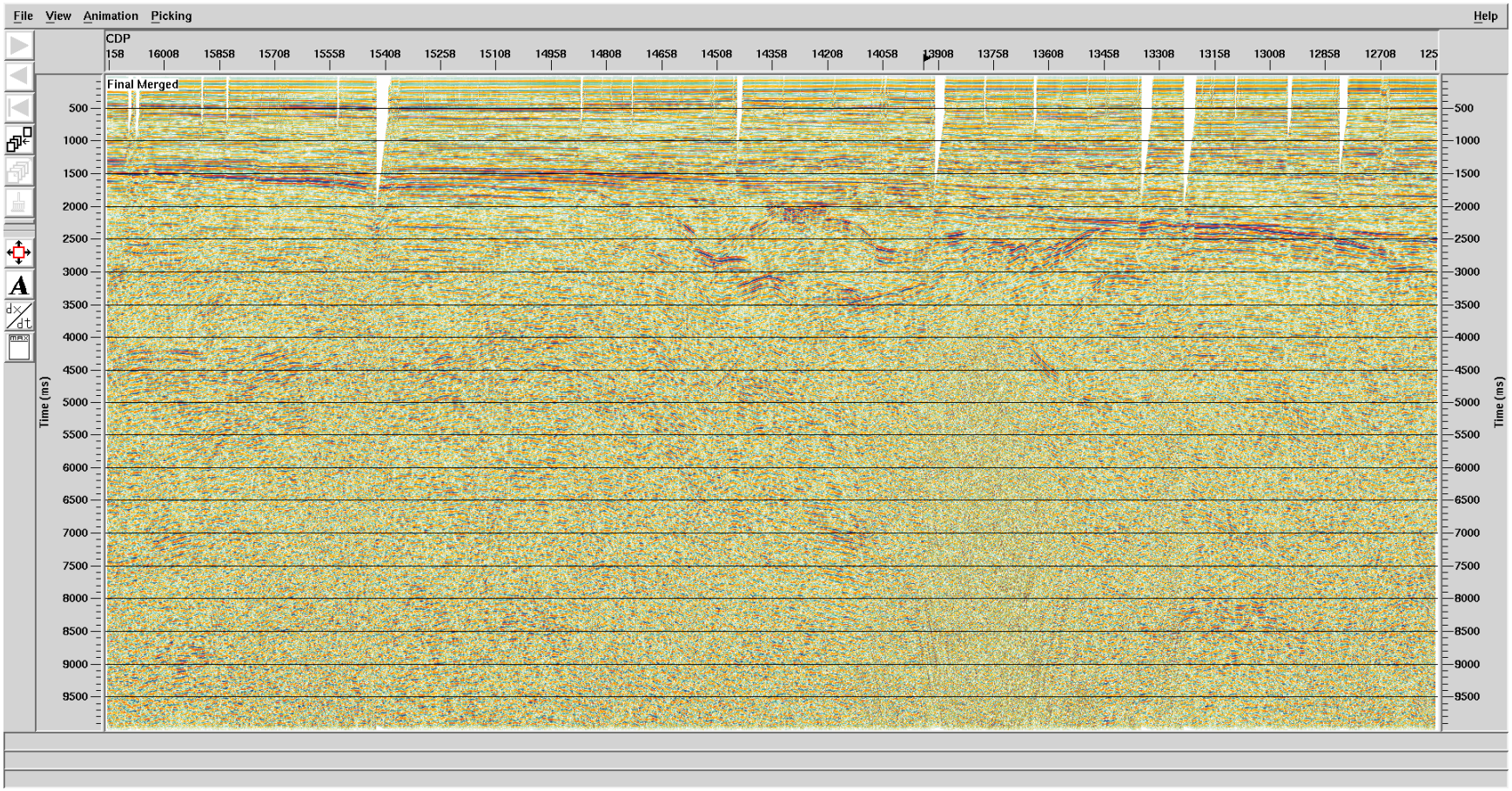

absolute IMAGING

Final Merged Binshare Stack (Line 12 Segment G)

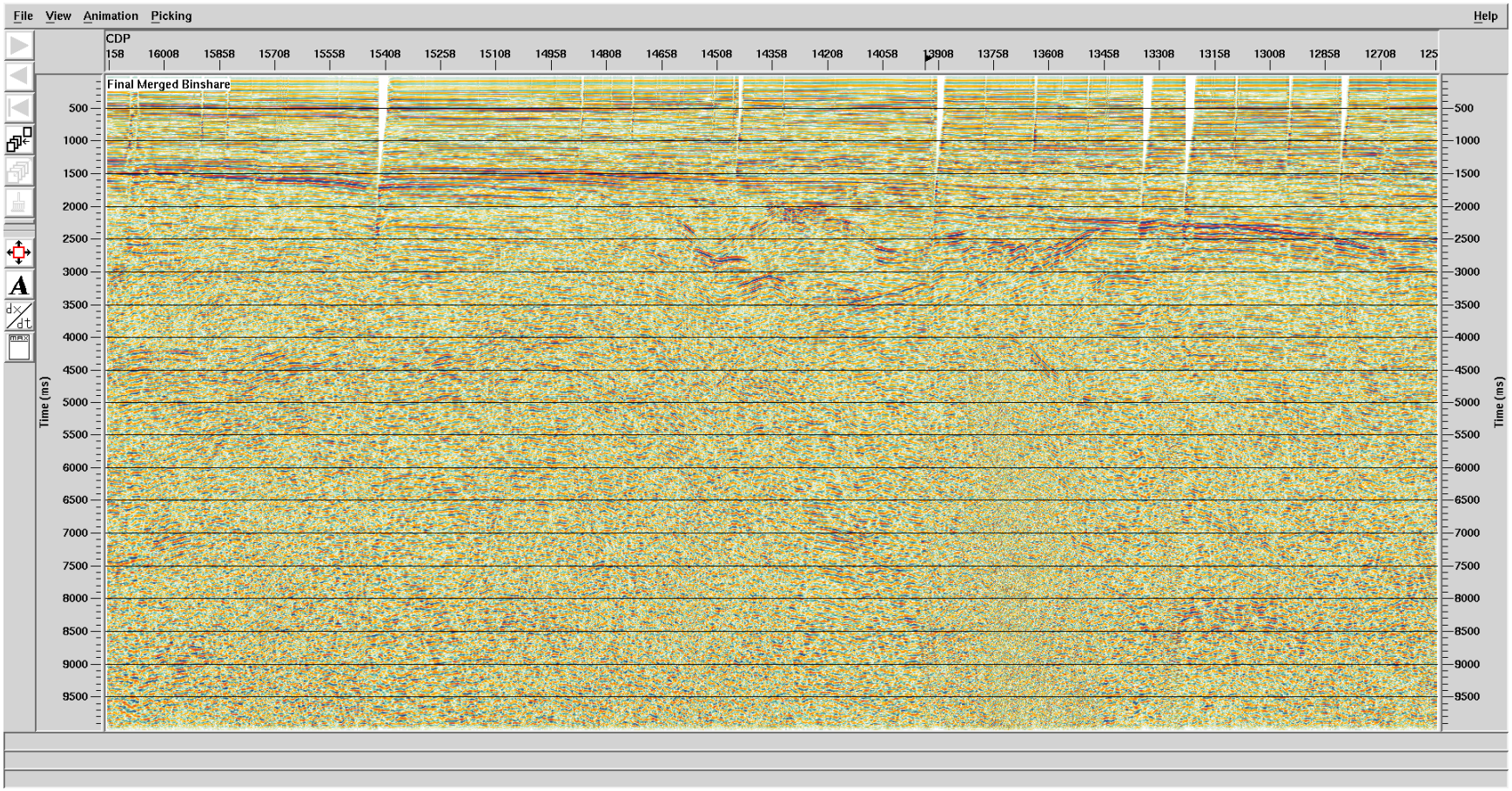

absolute IMAGING

Final PSTM Velocity (Line 12 Segment G)

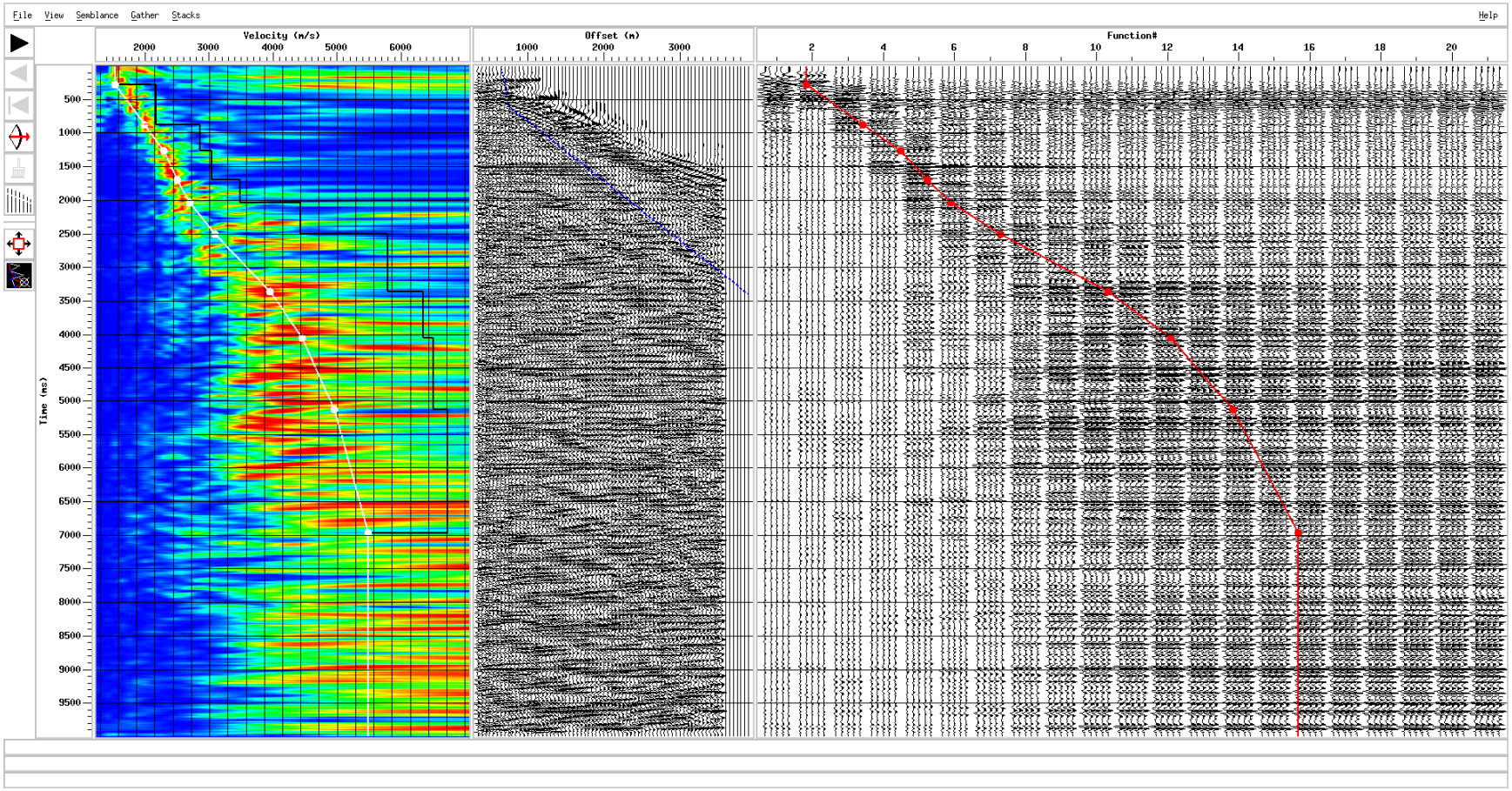

absolute IMAGING

Final PSTM Velocity (Line 12 Segment G)

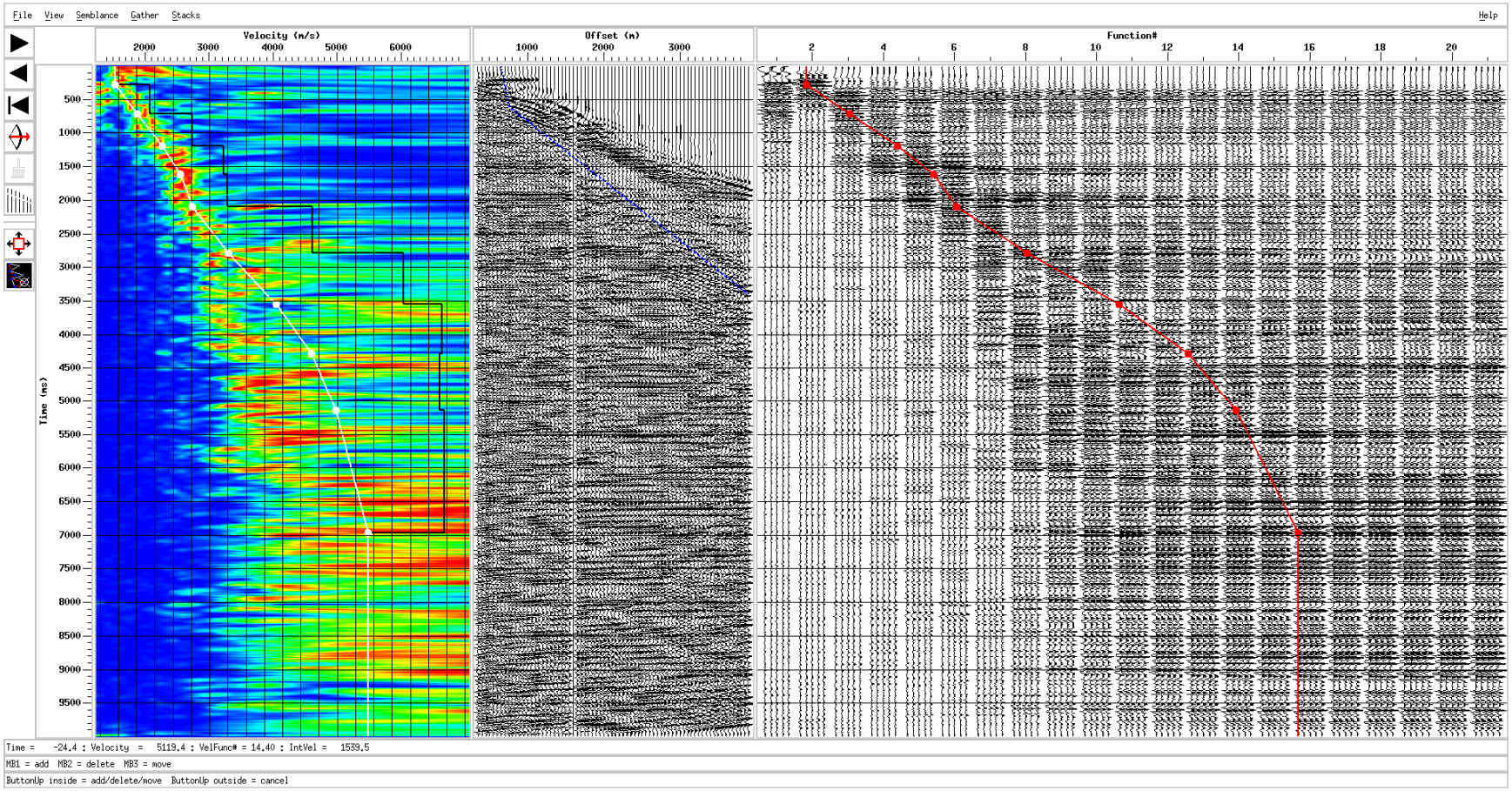

absolute IMAGING

Final PSTM Velocity (Line 12 Segment G)

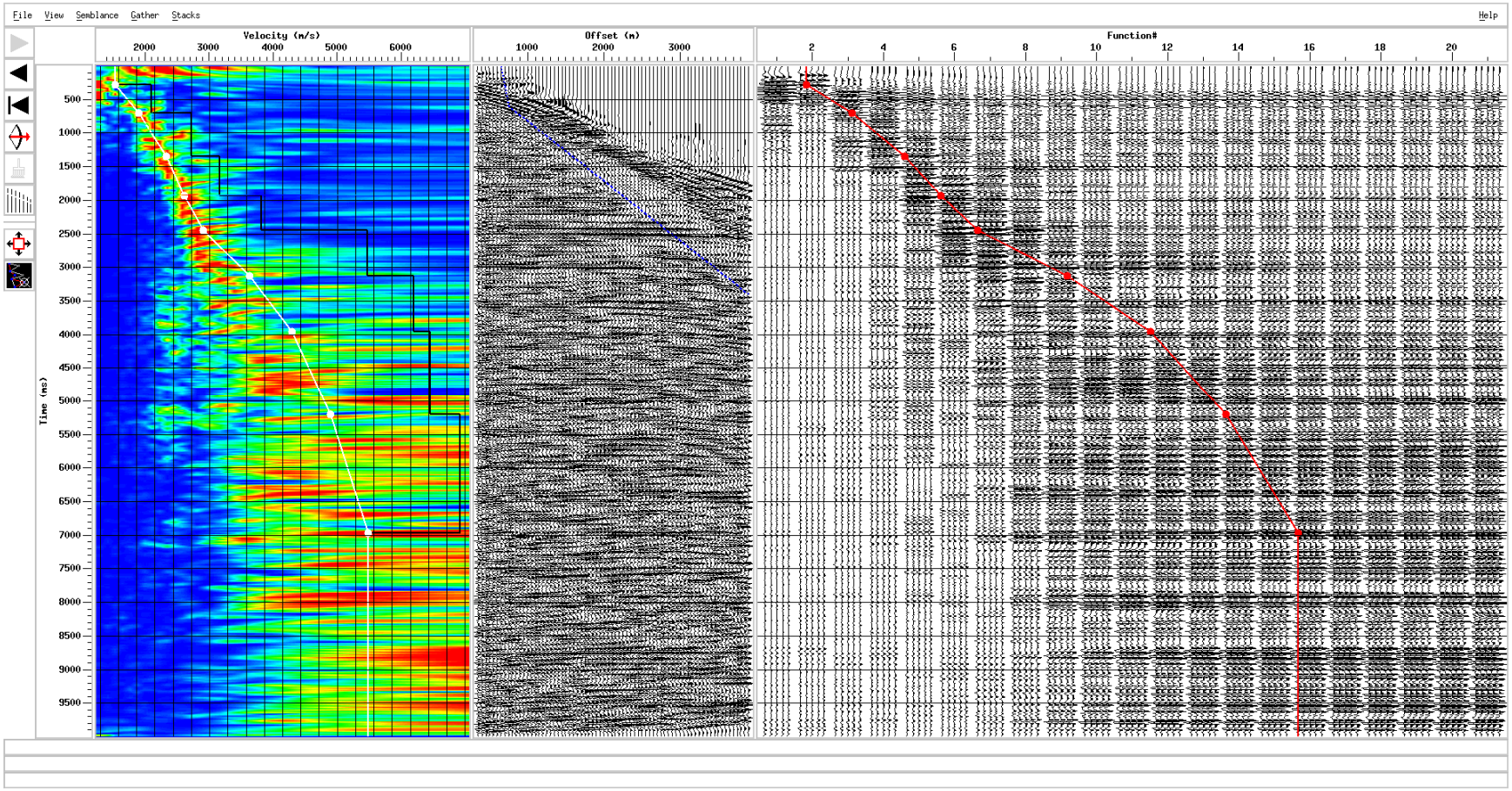

Creating a seismic image that is absolutely clear

absolute IMAGING

Final Merged Binshare POM (Line 12 Segment G)

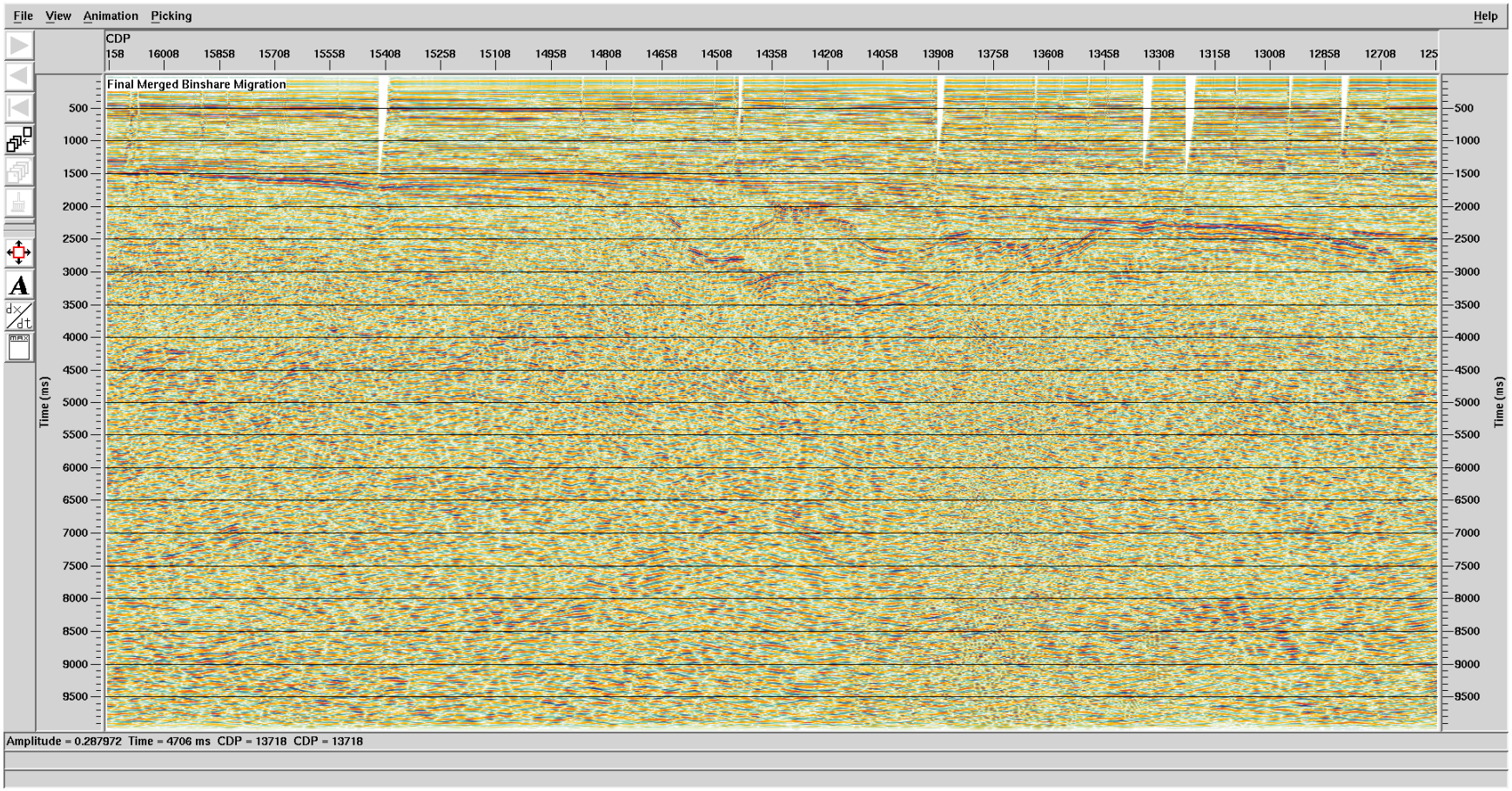

absolute IMAGING

Final PSTM (Line 12 Segment G)

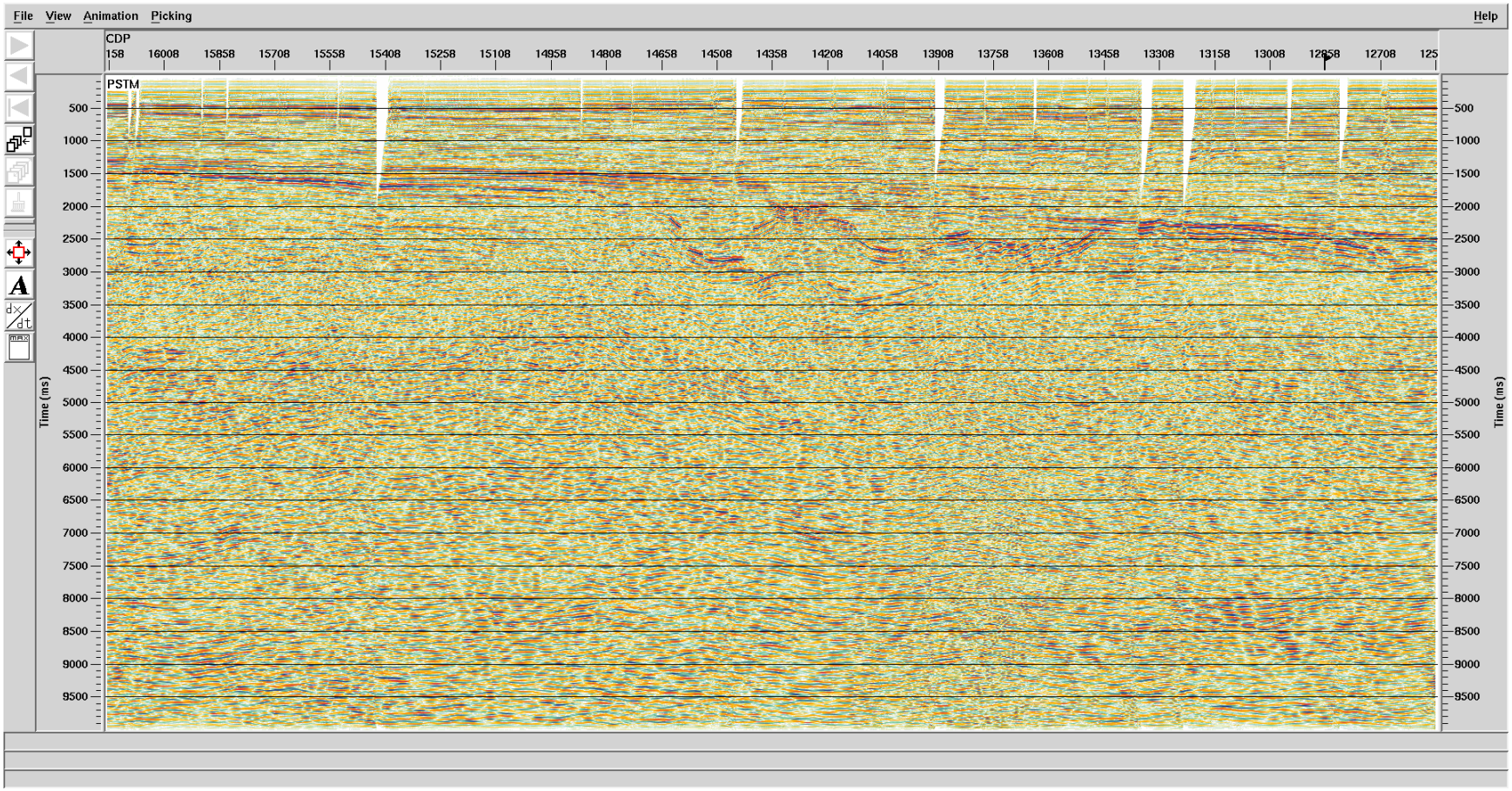

HRRT Demultiple Post PSTM – Modelled Multiples

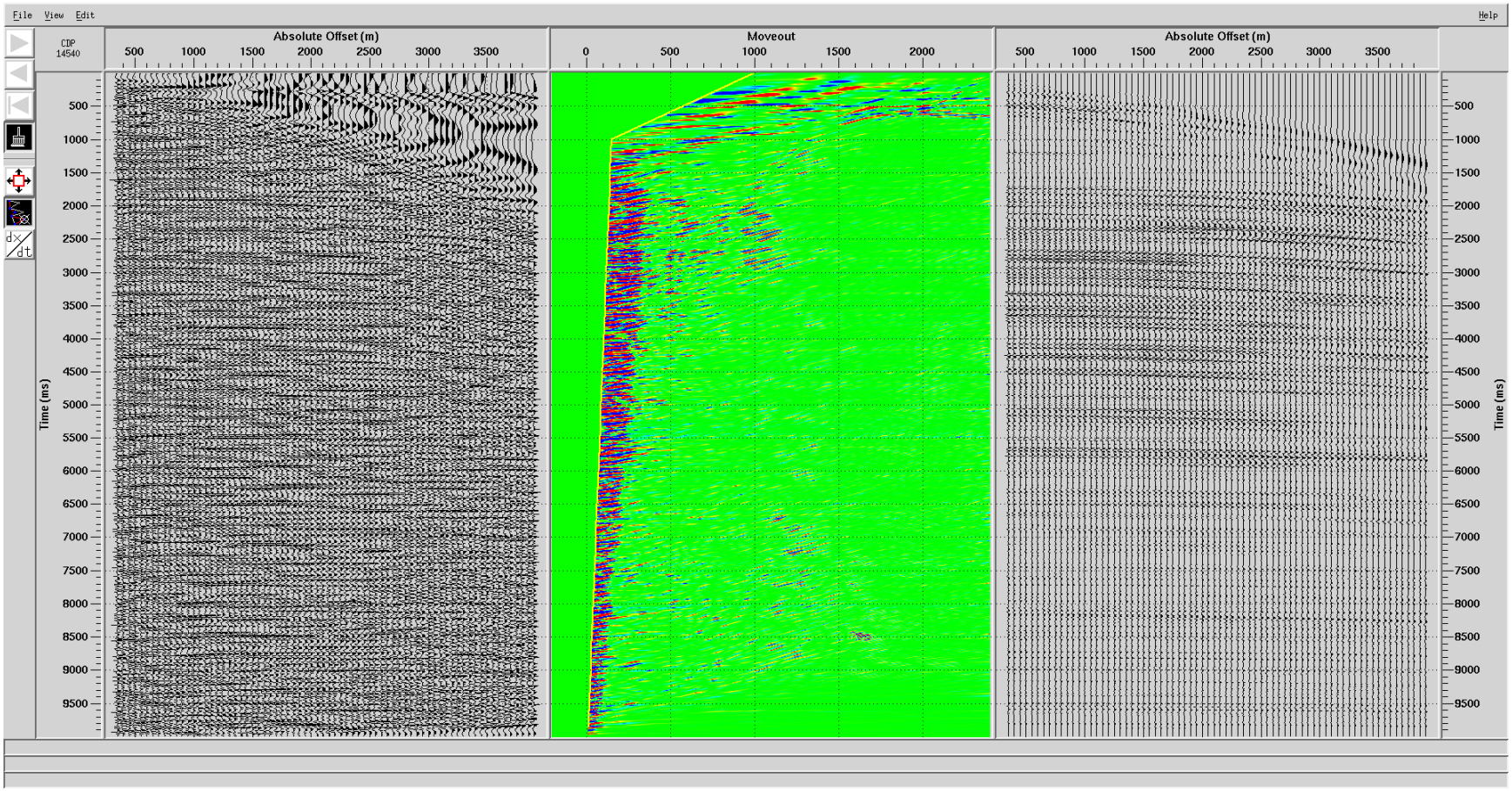

HRRT Demultiple Post PSTM – Output

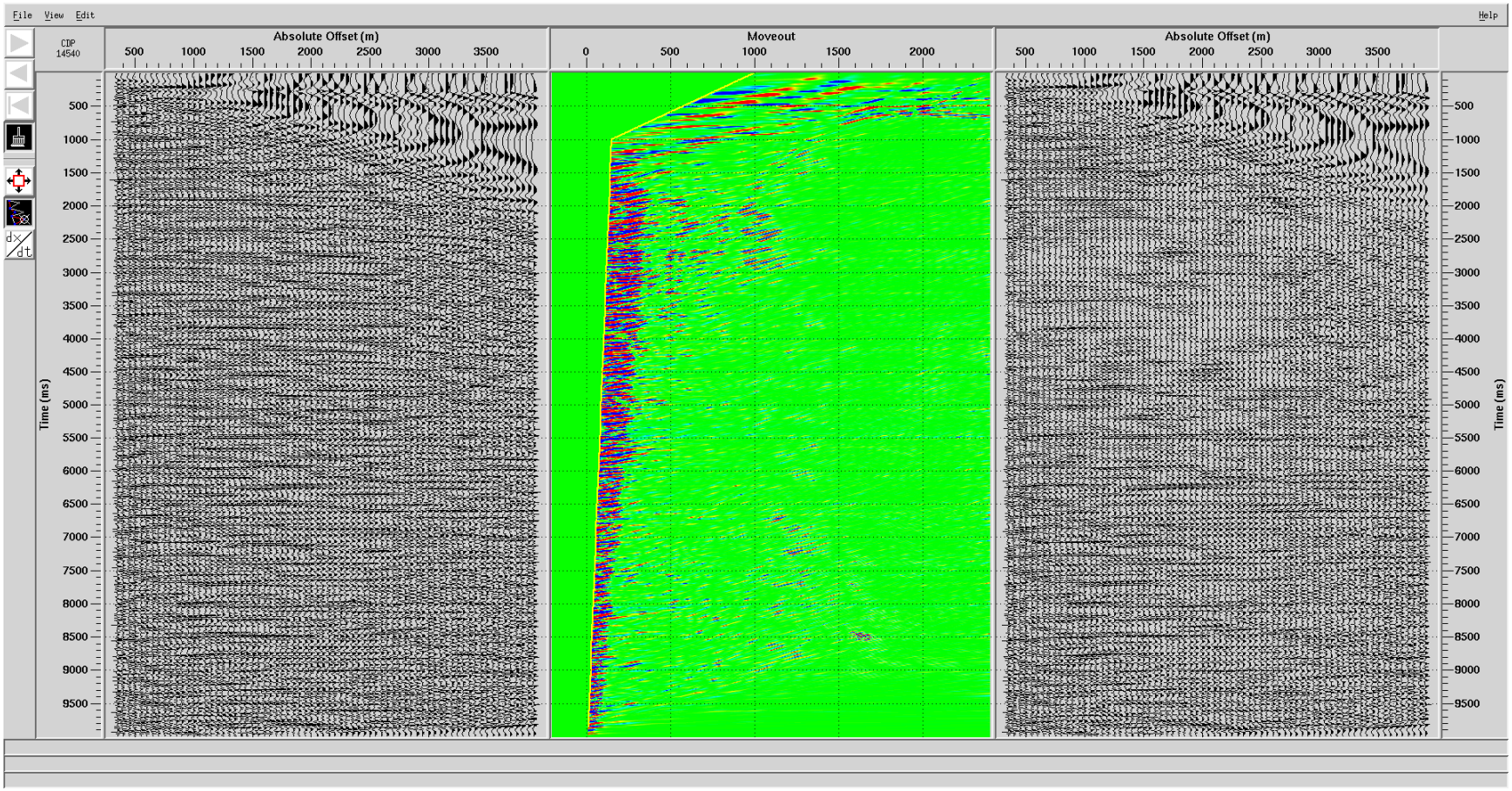

Creating a seismic image that is absolutely clear

absolute IMAGING

Final PSTM + HRRT Radon (Line 12 Segment G)

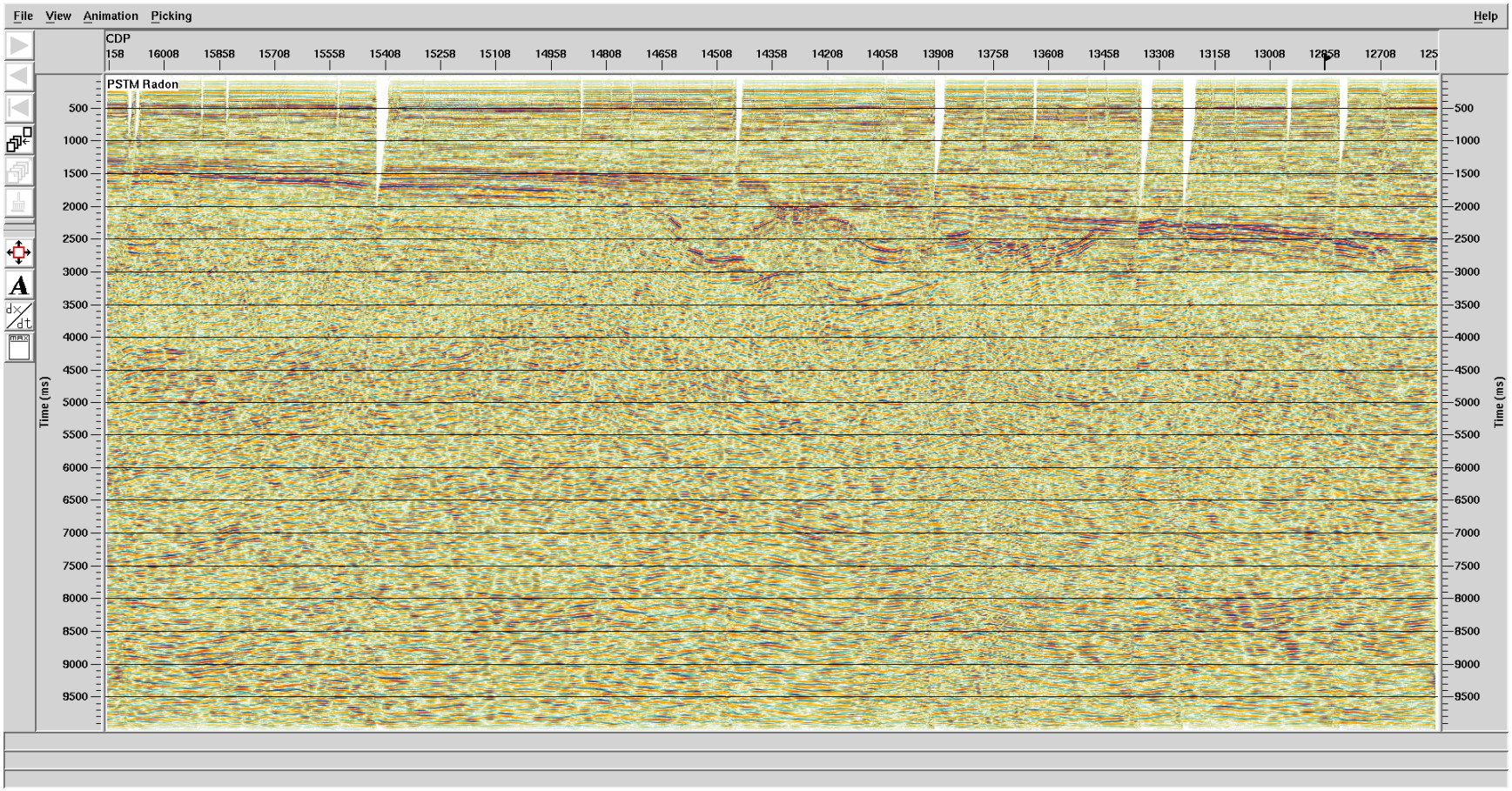

Creating a seismic image that is absolutely clear

absolute IMAGING

Final PSTM + HRRT Radon + Binshare + Dipscan (Line 12 - G)

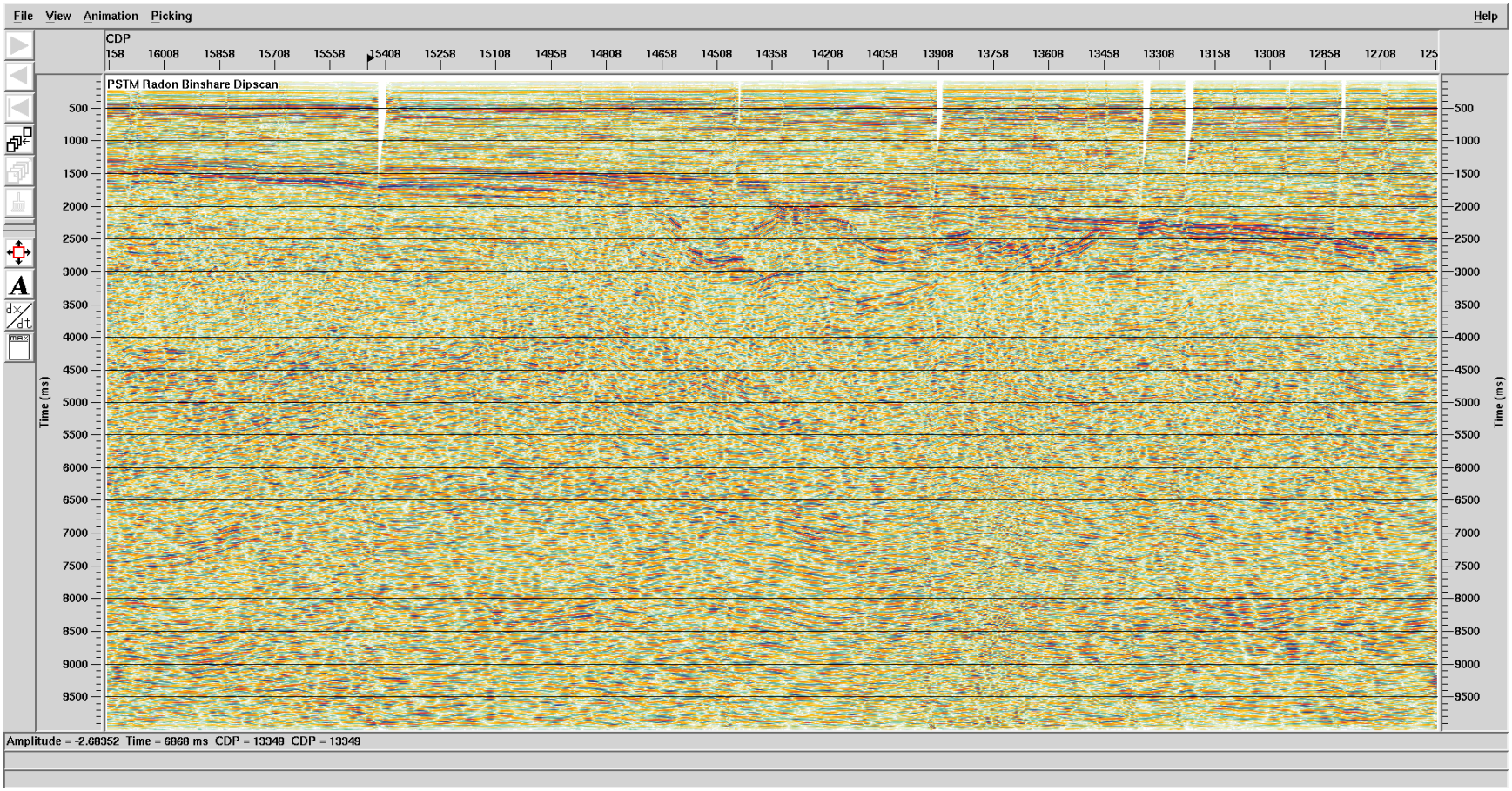

absolute IMAGING

Final PSTM + HRRT Radon + Binshare + Dipscan (Line 12)

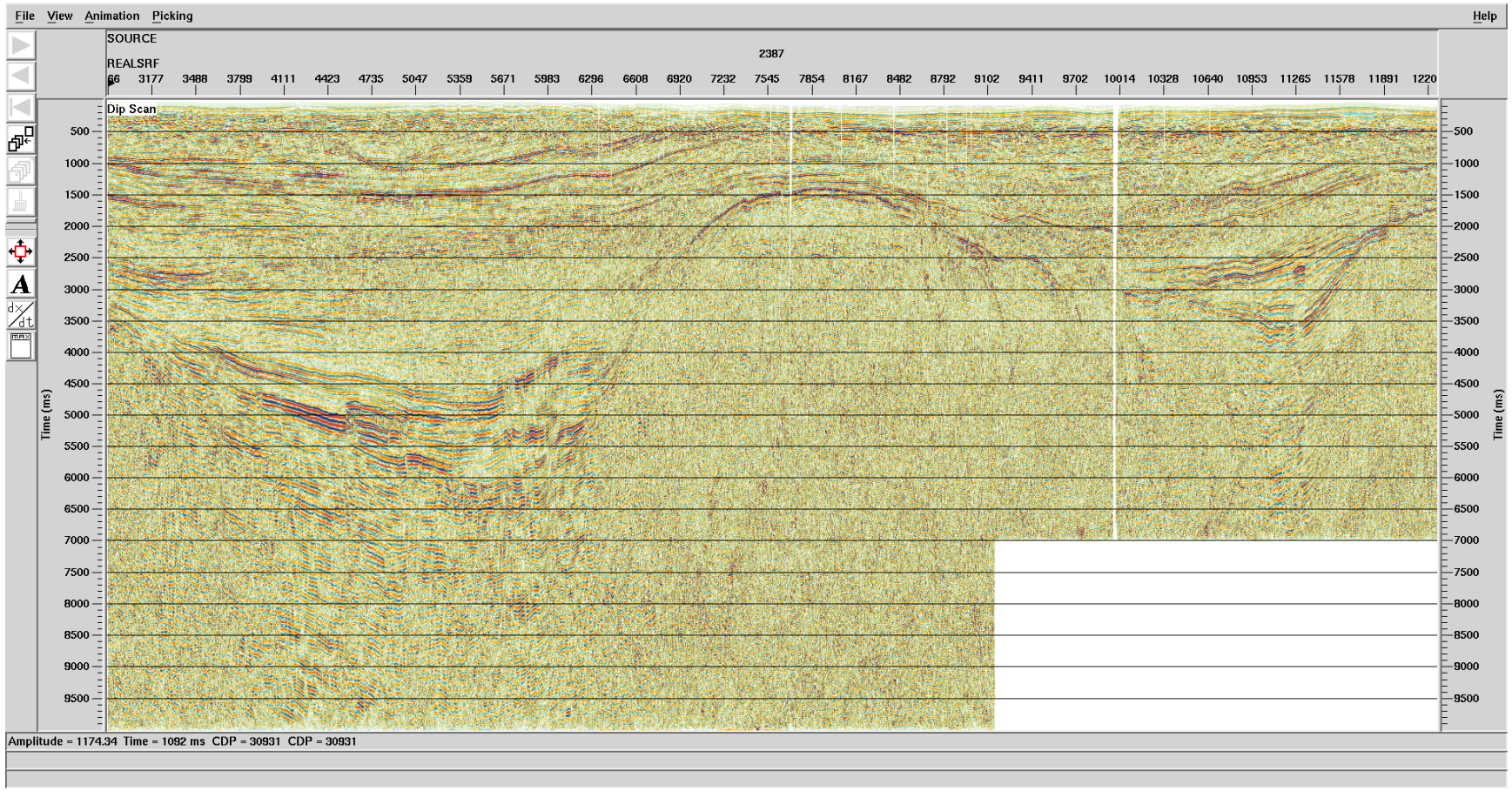

absolute IMAGING

Final PSTM + HRRT Radon + Binshare + Dipscan (Zoom)

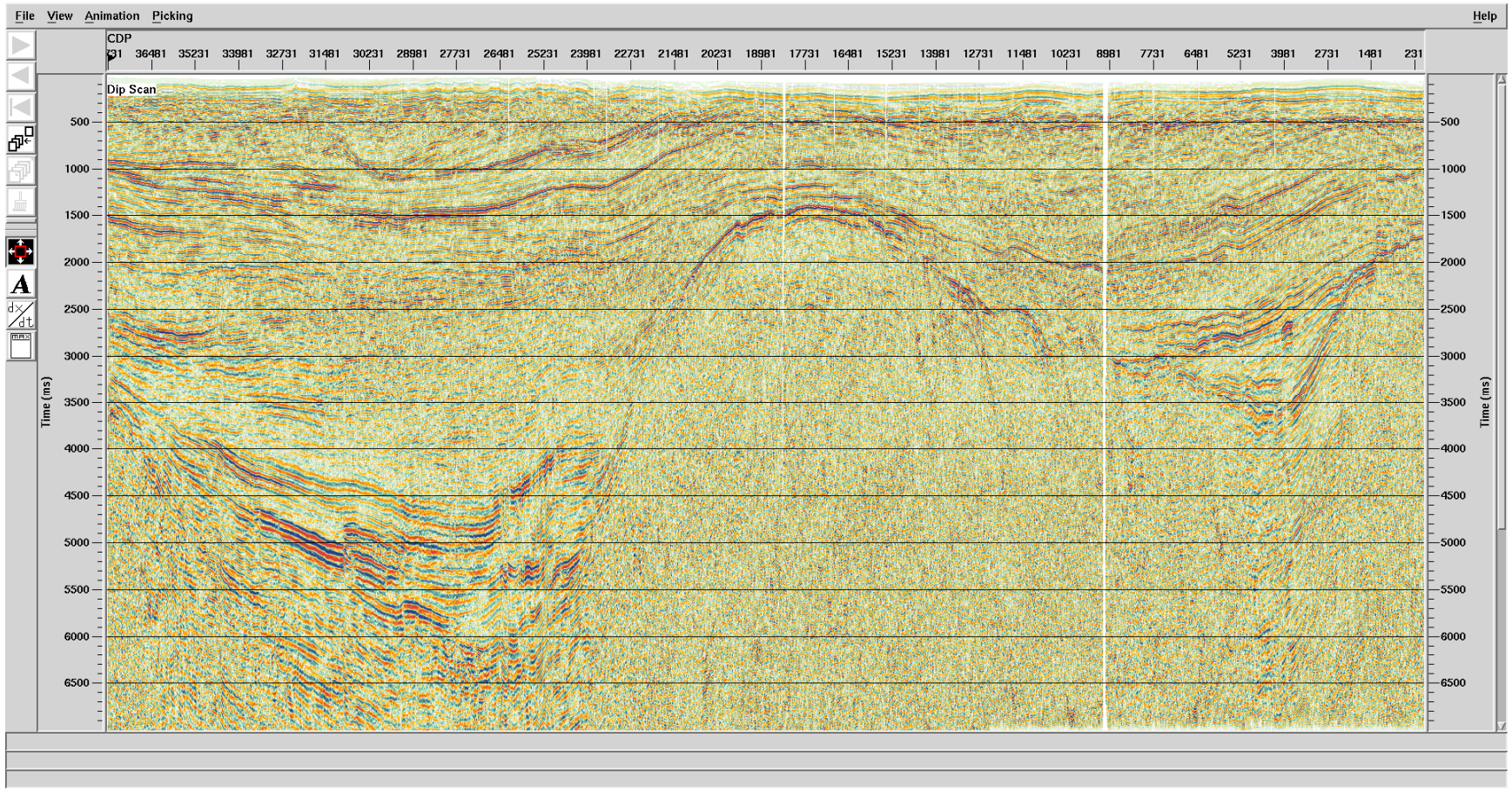

absolute IMAGING

Final PSTM: Line 6

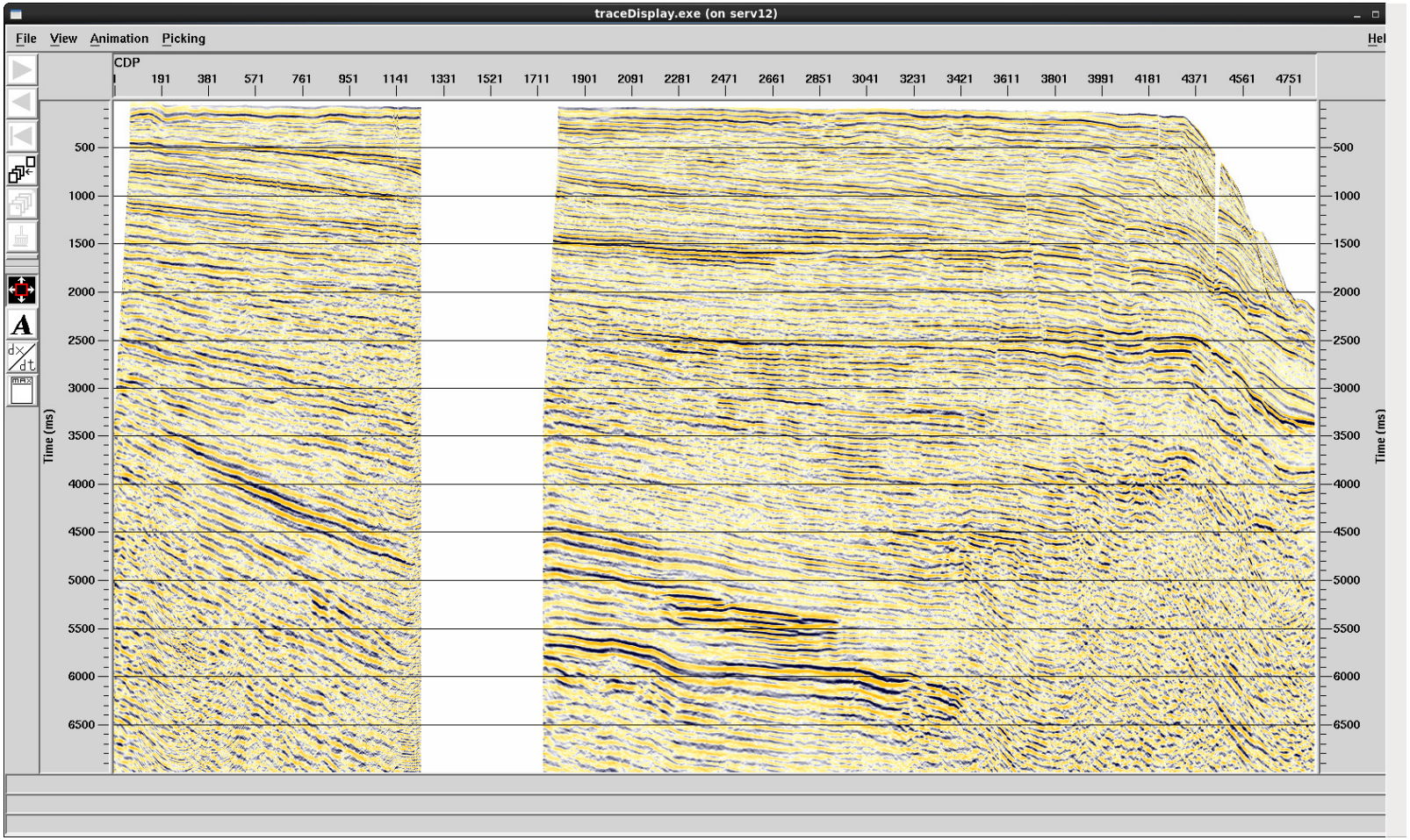

absolute IMAGING

Final PSTM RMS Velocities: Line 6

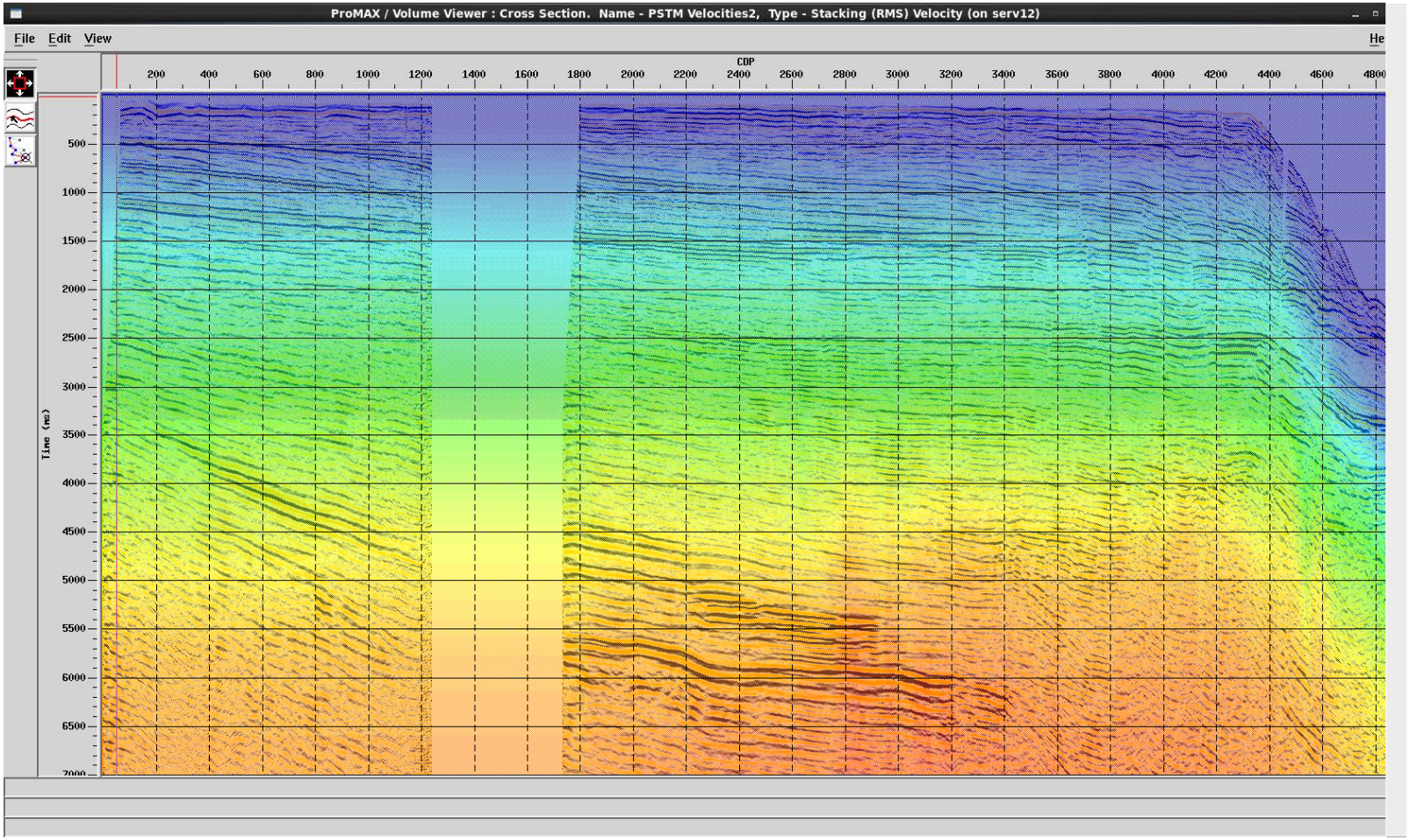

Final PSTM Interval Velocities: Line 6

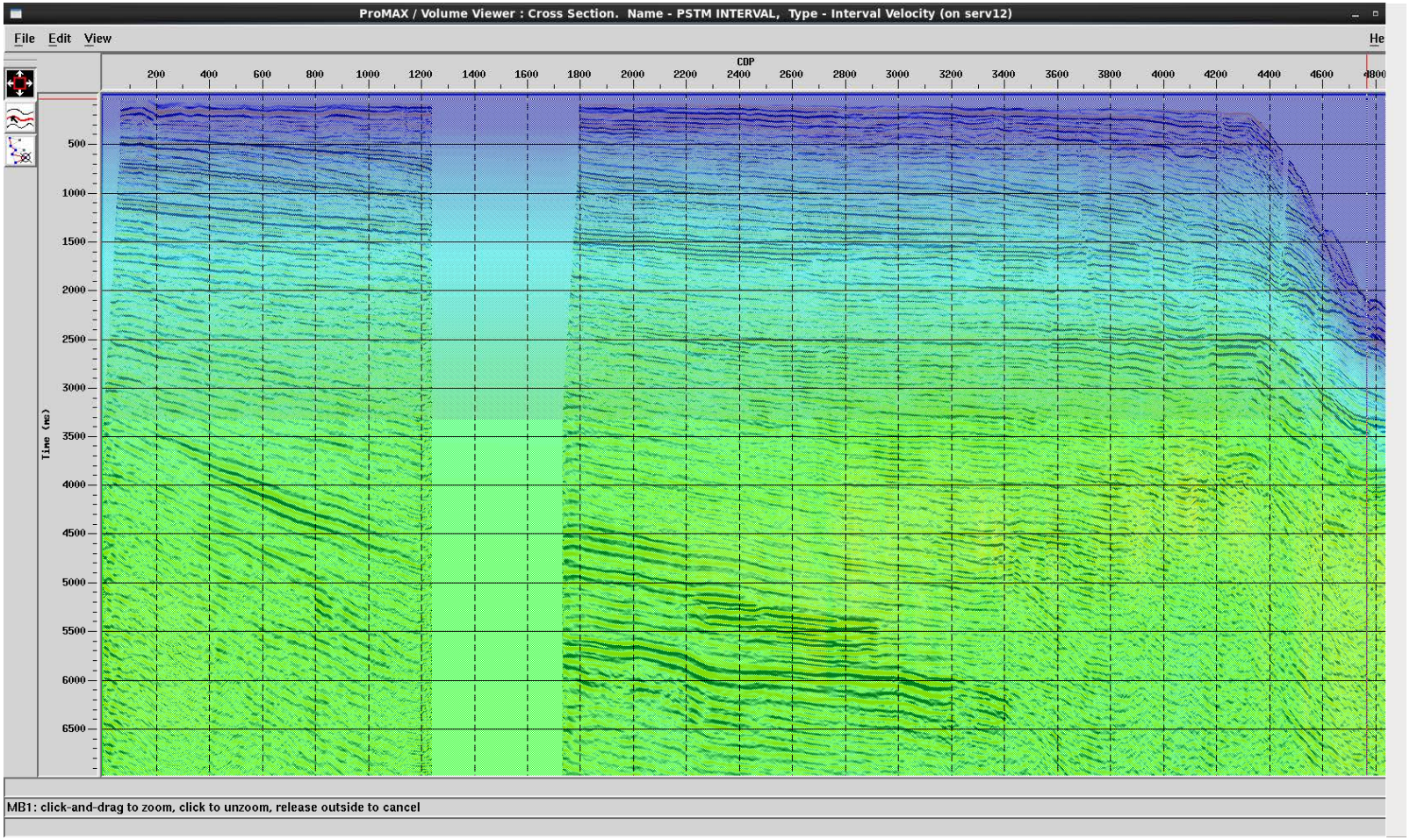

Final PSTM: Line 10

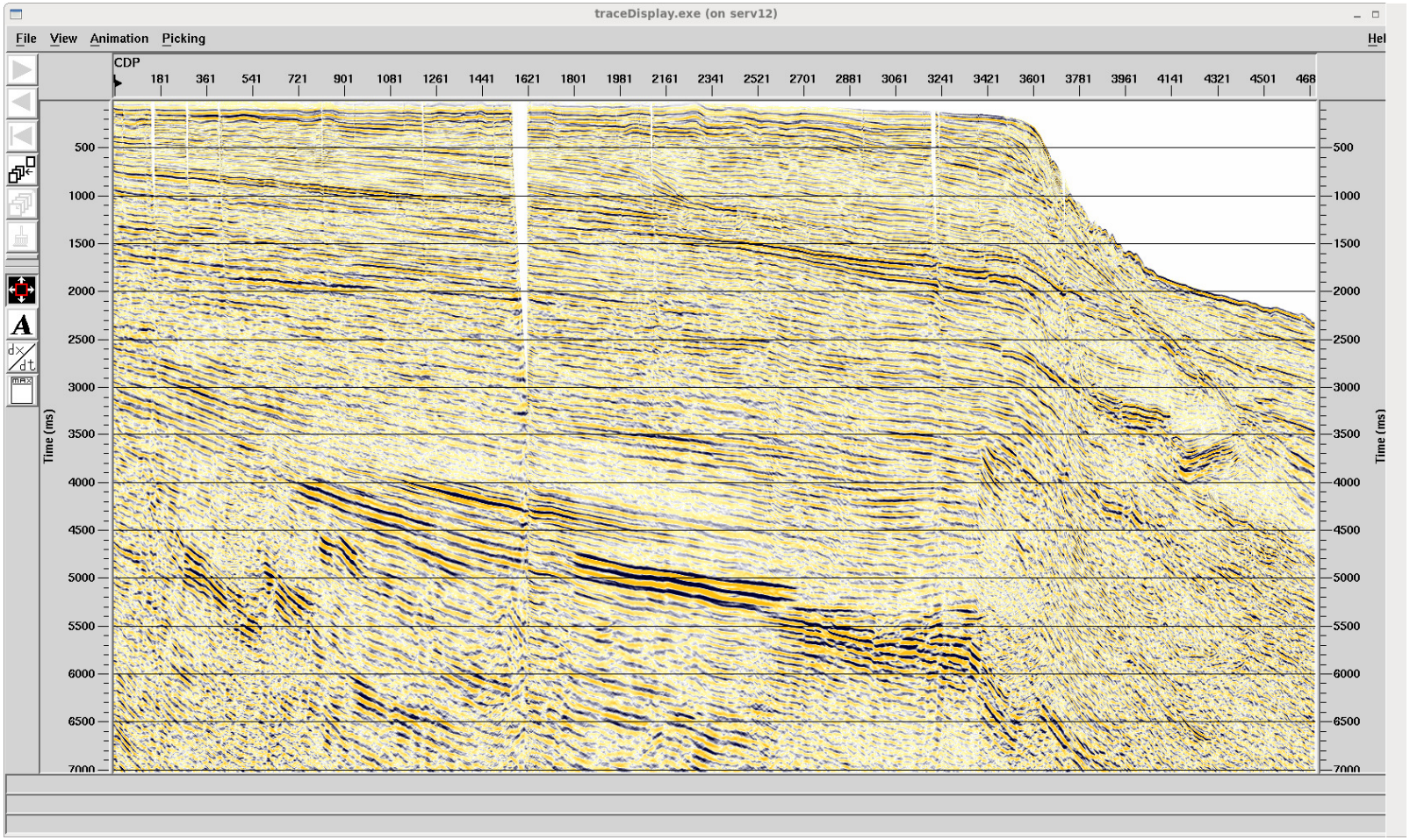

absolute IMAGING

Final PSTM RMS Velocities: Line 10

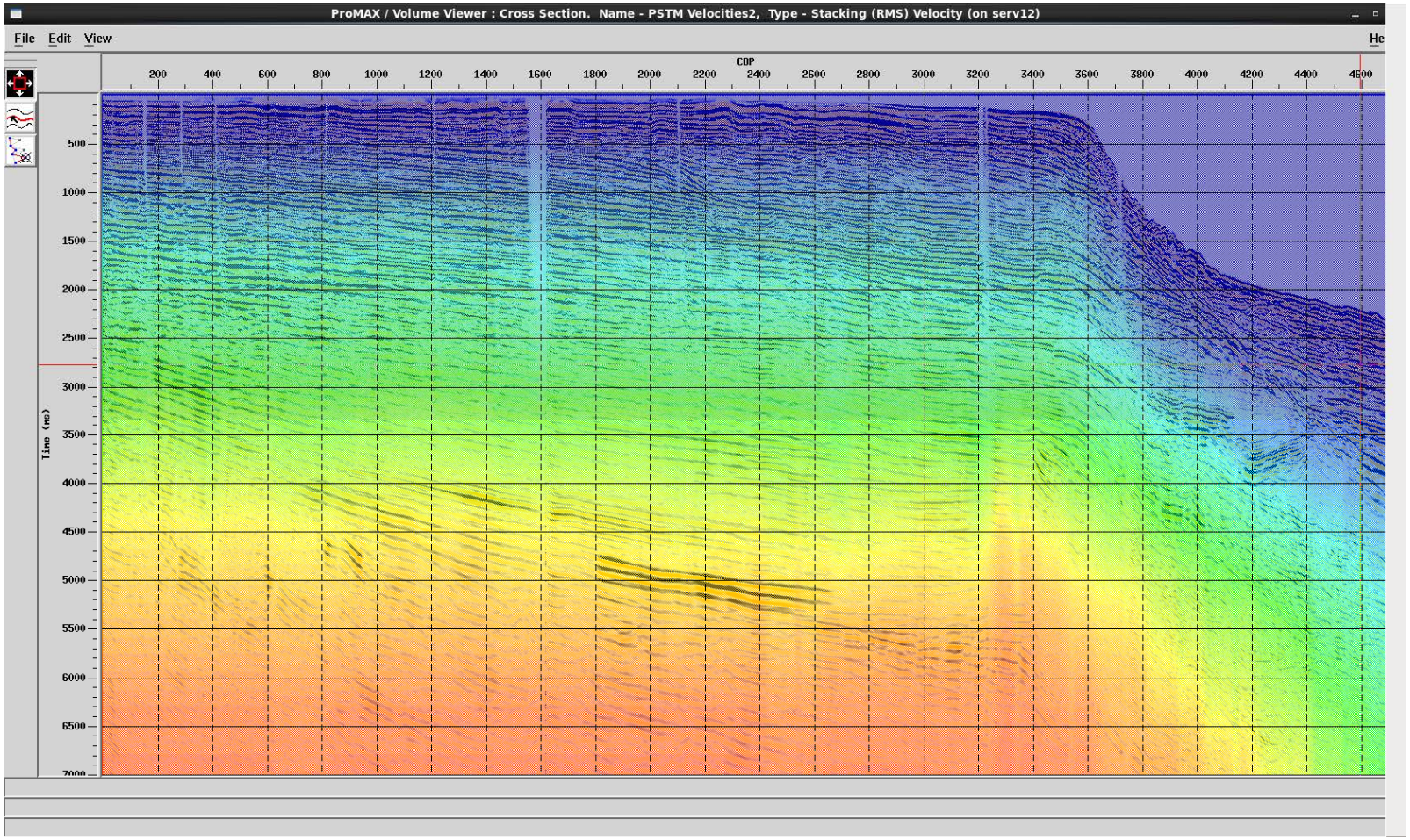

absolute IMAGING

Final PSTM Interval Velocities: Line 10

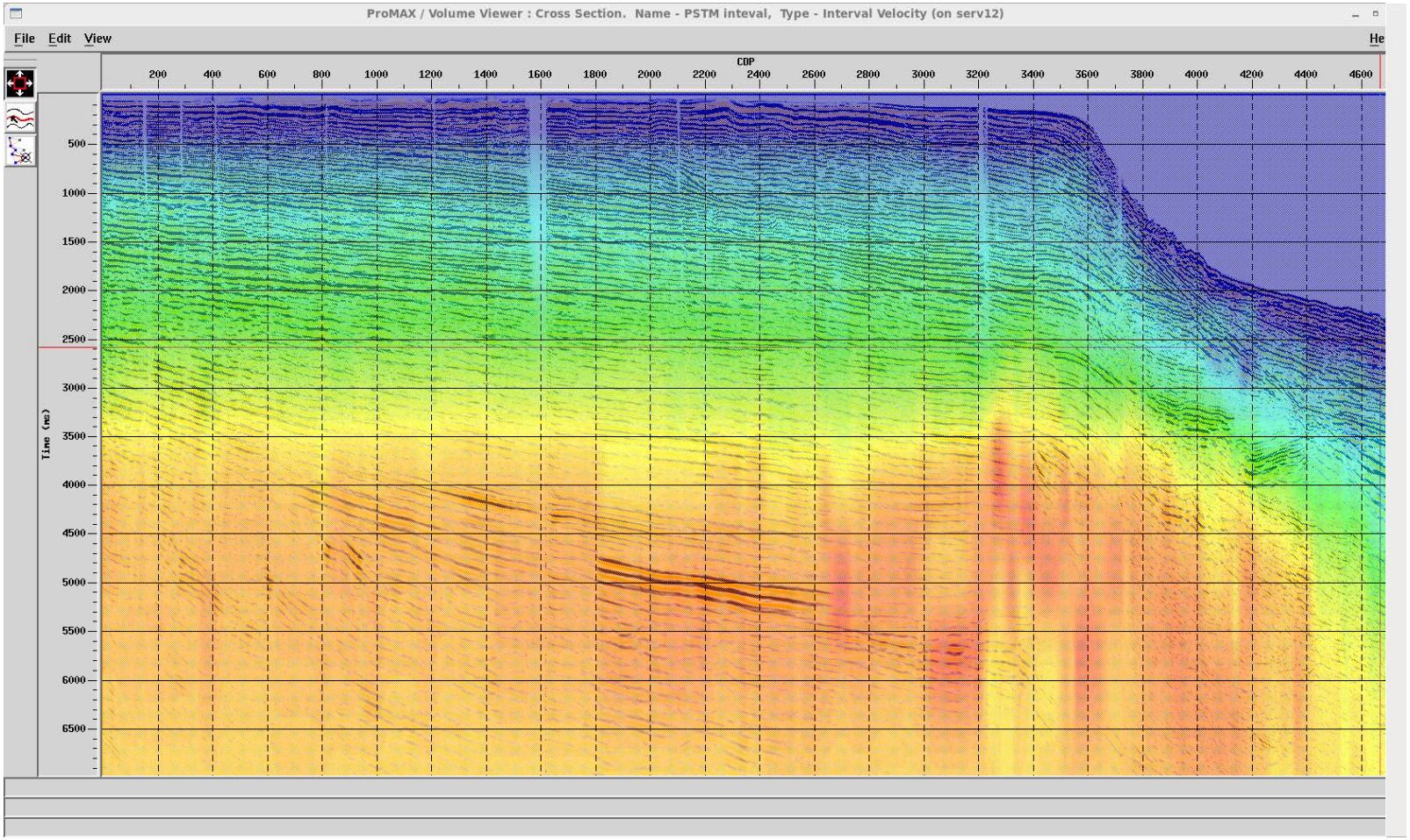

absolute IMAGING

Final PSTM: Line 12

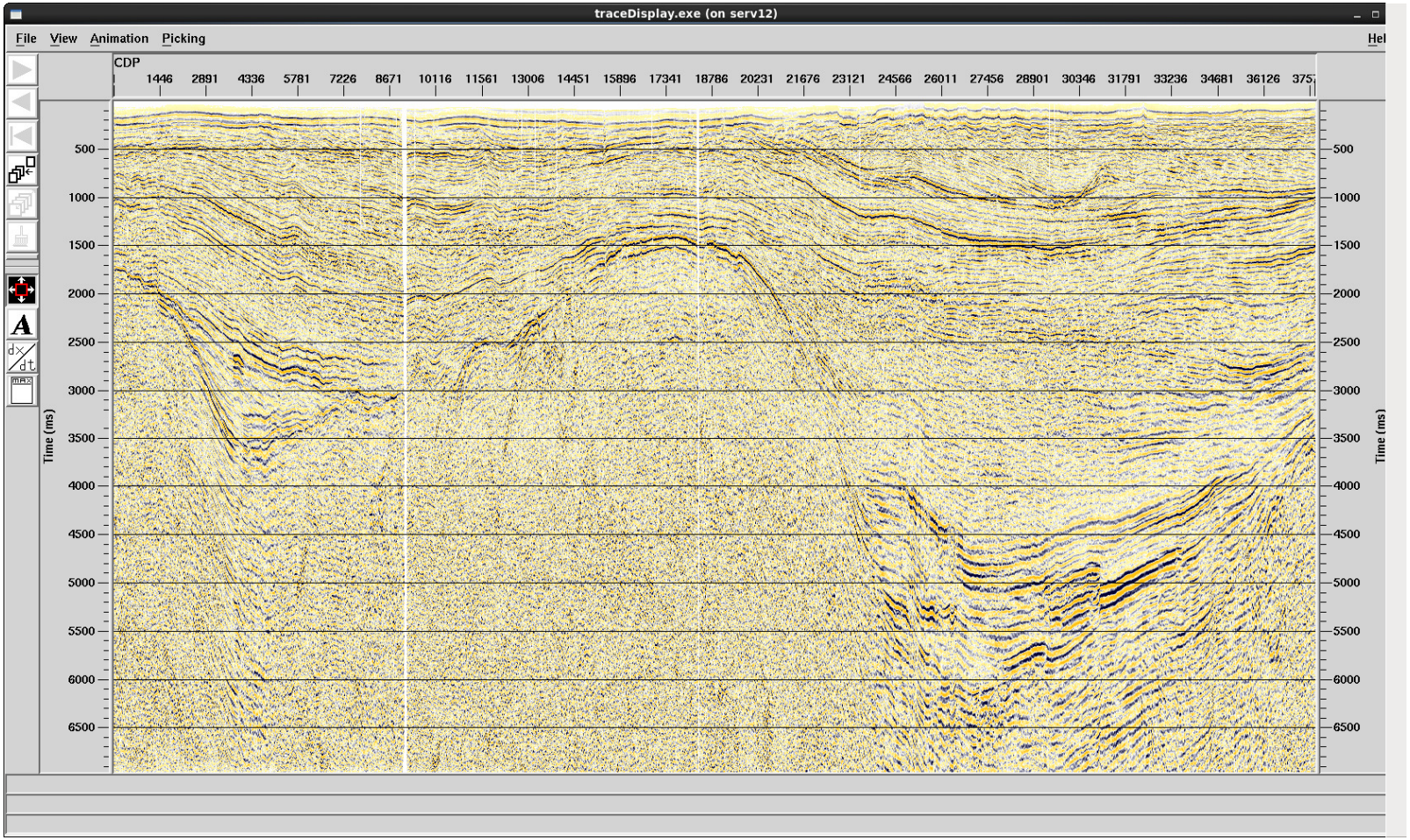

absolute IMAGING

Final PSTM RMS Velocities: Line 12

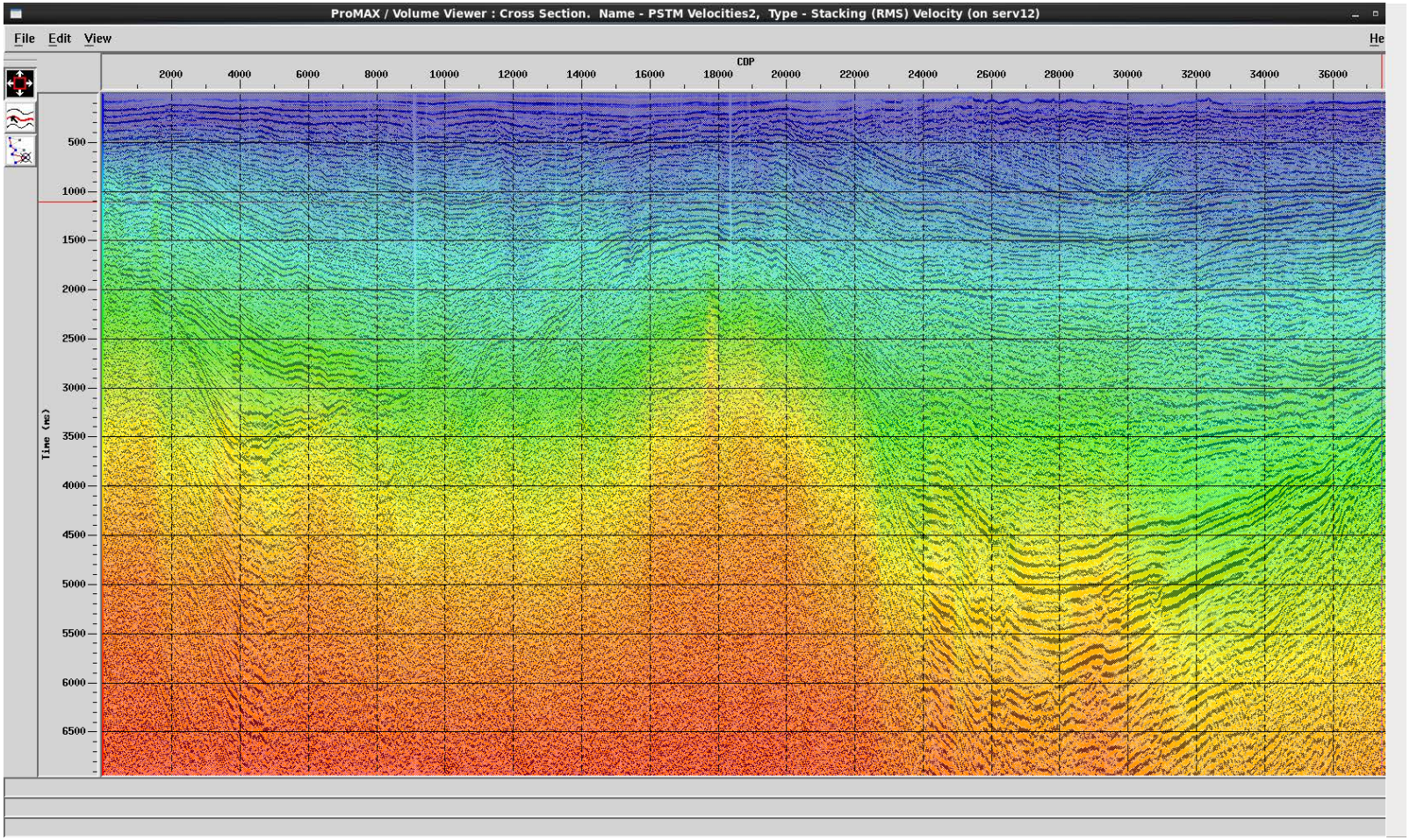

absolute IMAGING

Final PSTM Interval Velocities: Line 12

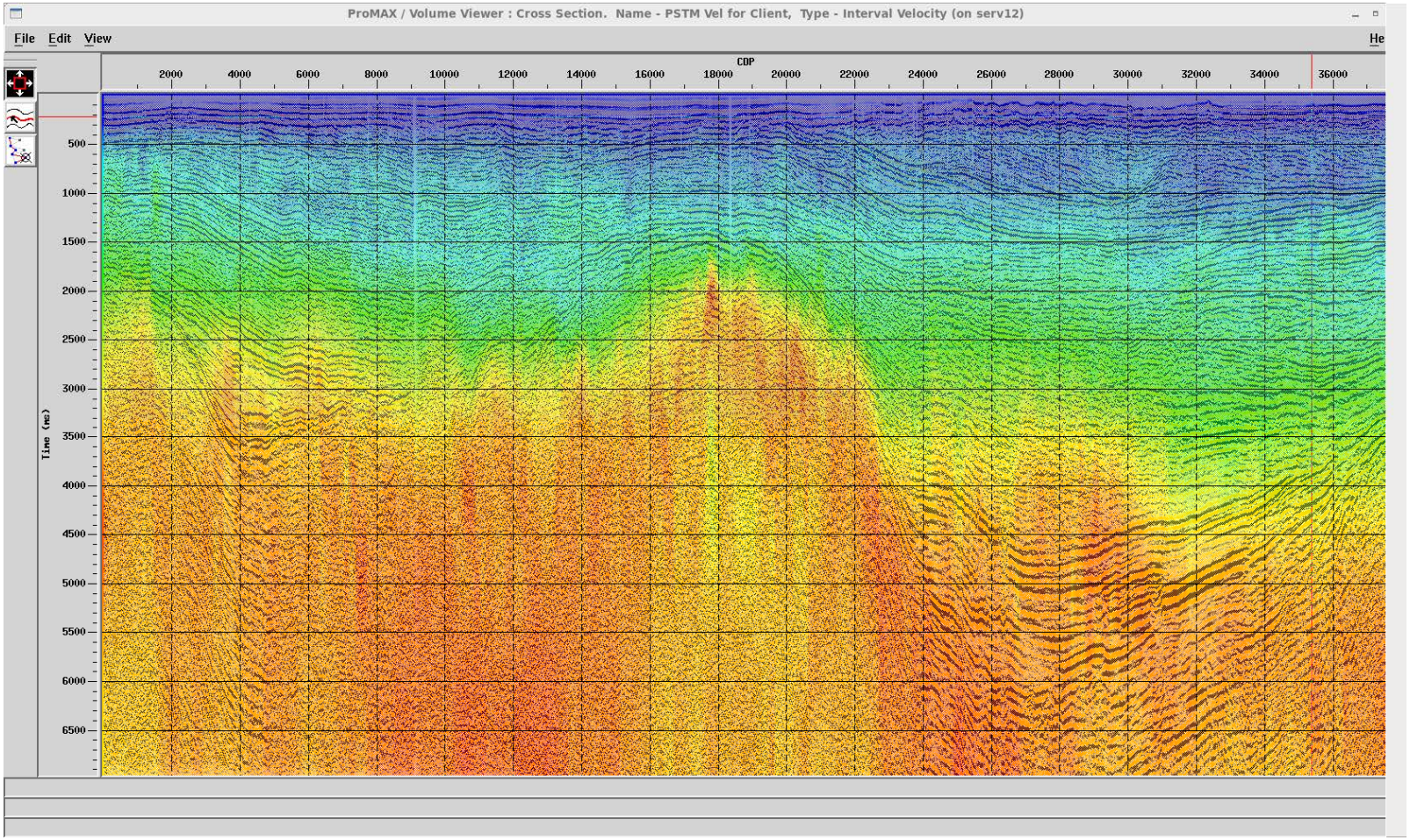

absolute IMAGING

Final PSTM: Line 14

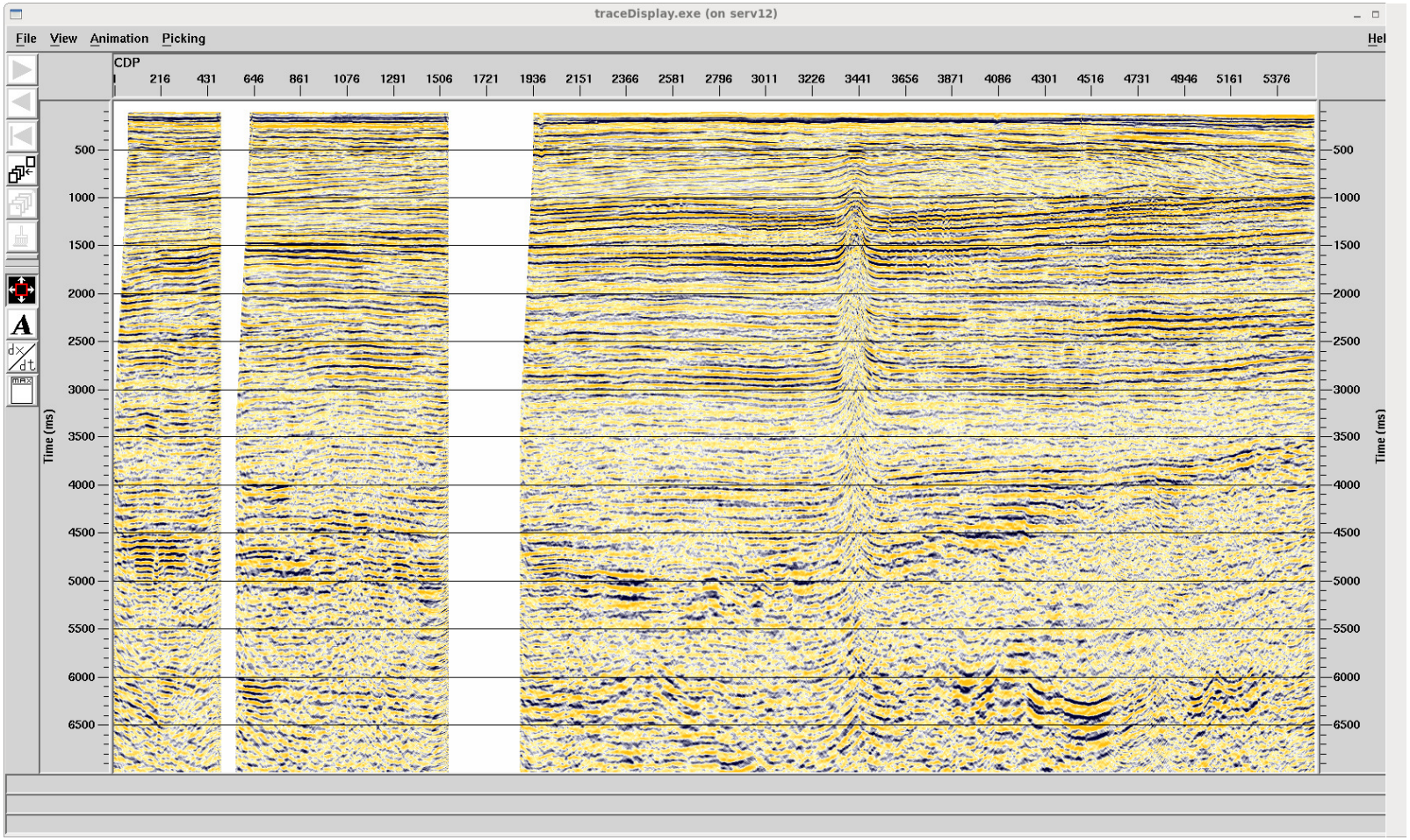

absolute IMAGING

Final PSTM RMS Velocities: Line 14

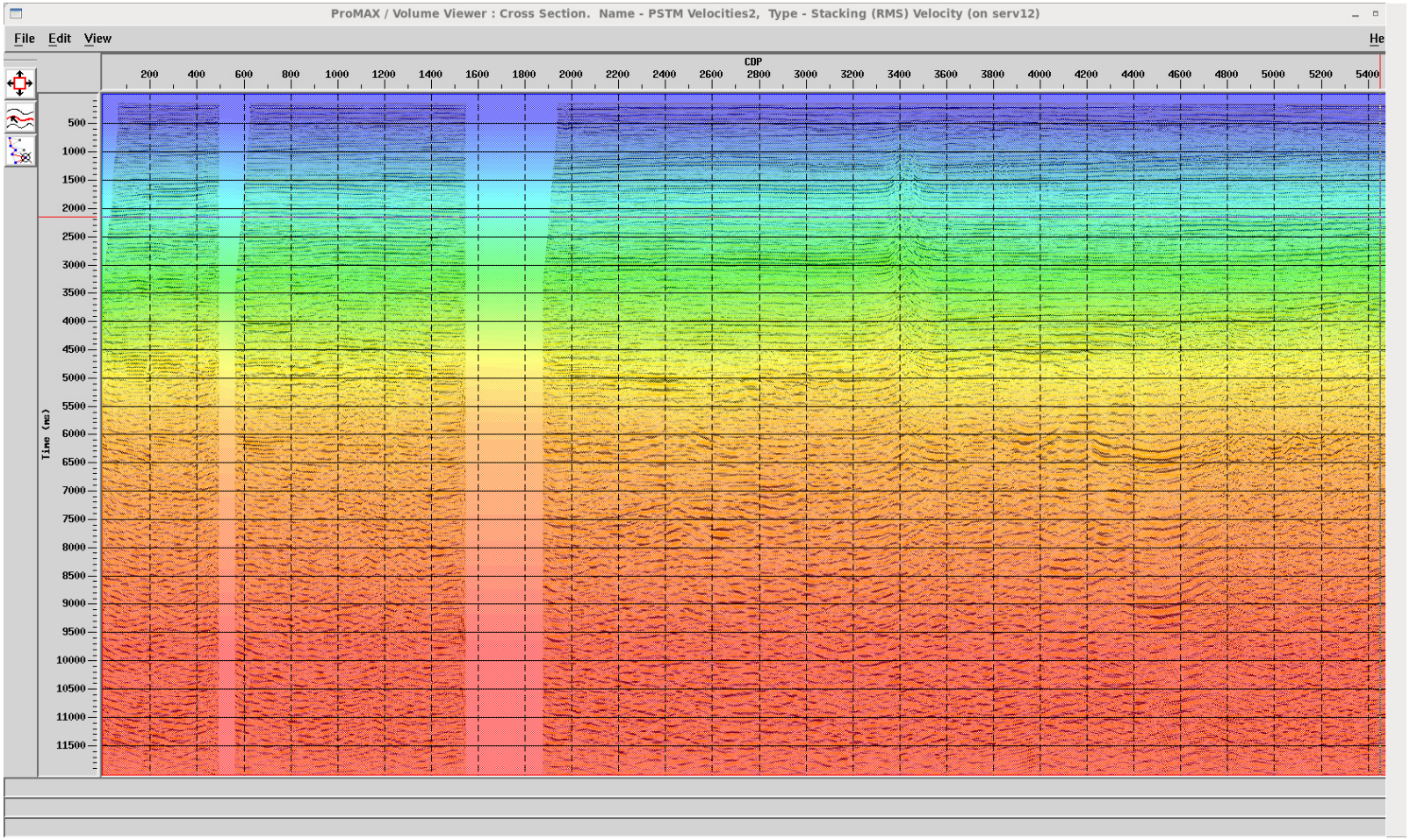

absolute IMAGING

Final PSTM Interval Velocities: Line 14

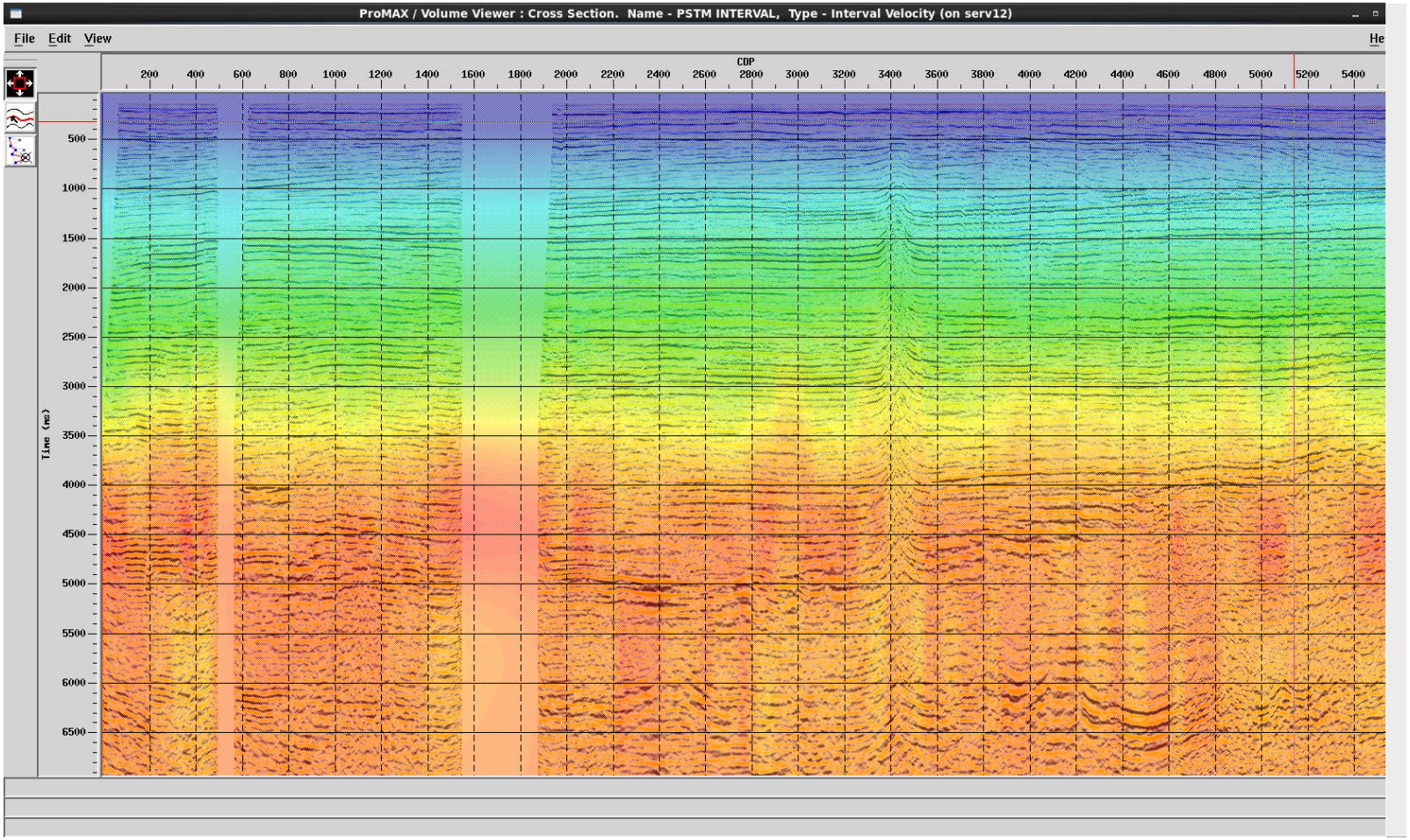

absolute IMAGING

Final PSTM: Line 16

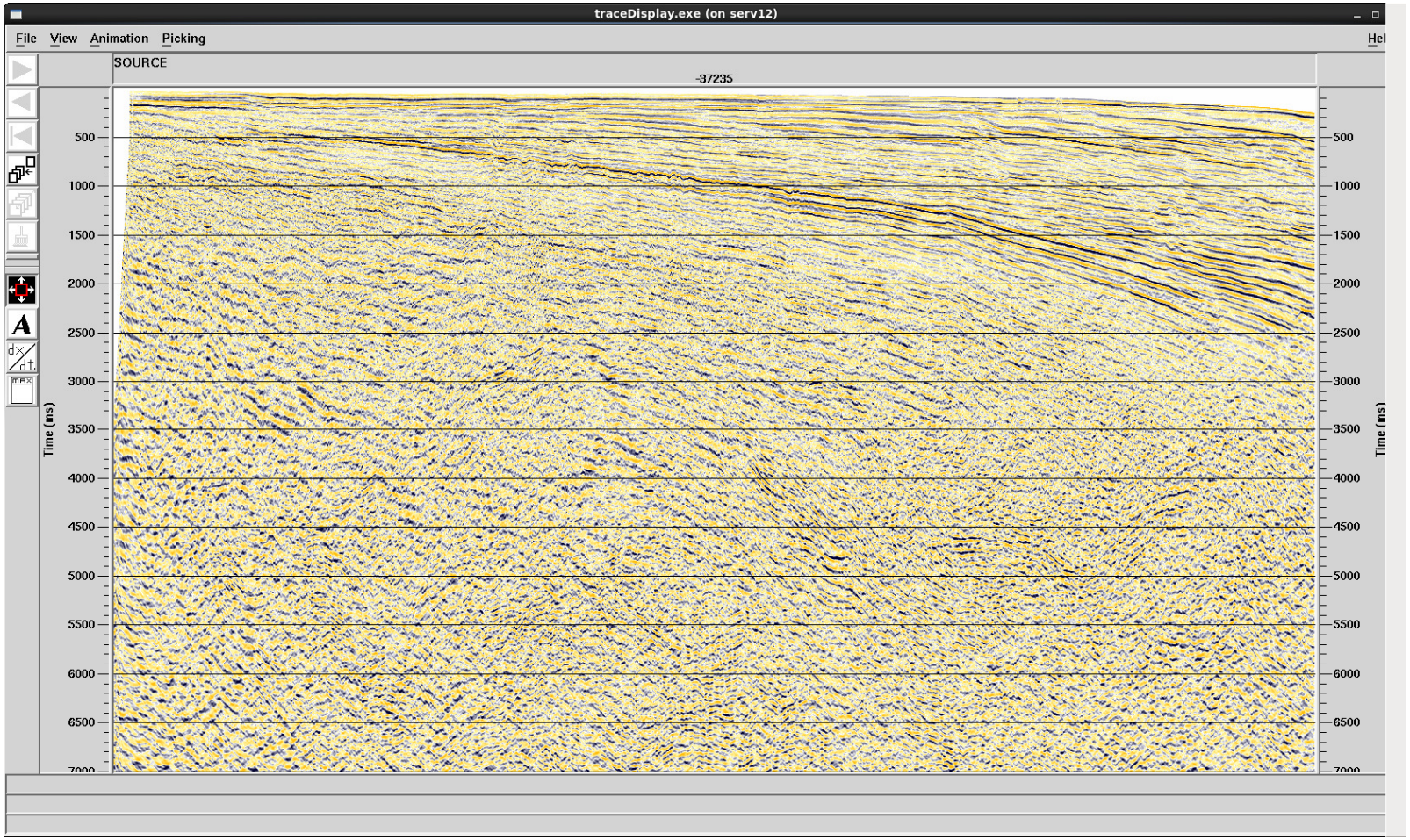

Final PSTM RMS Velocities: Line 16

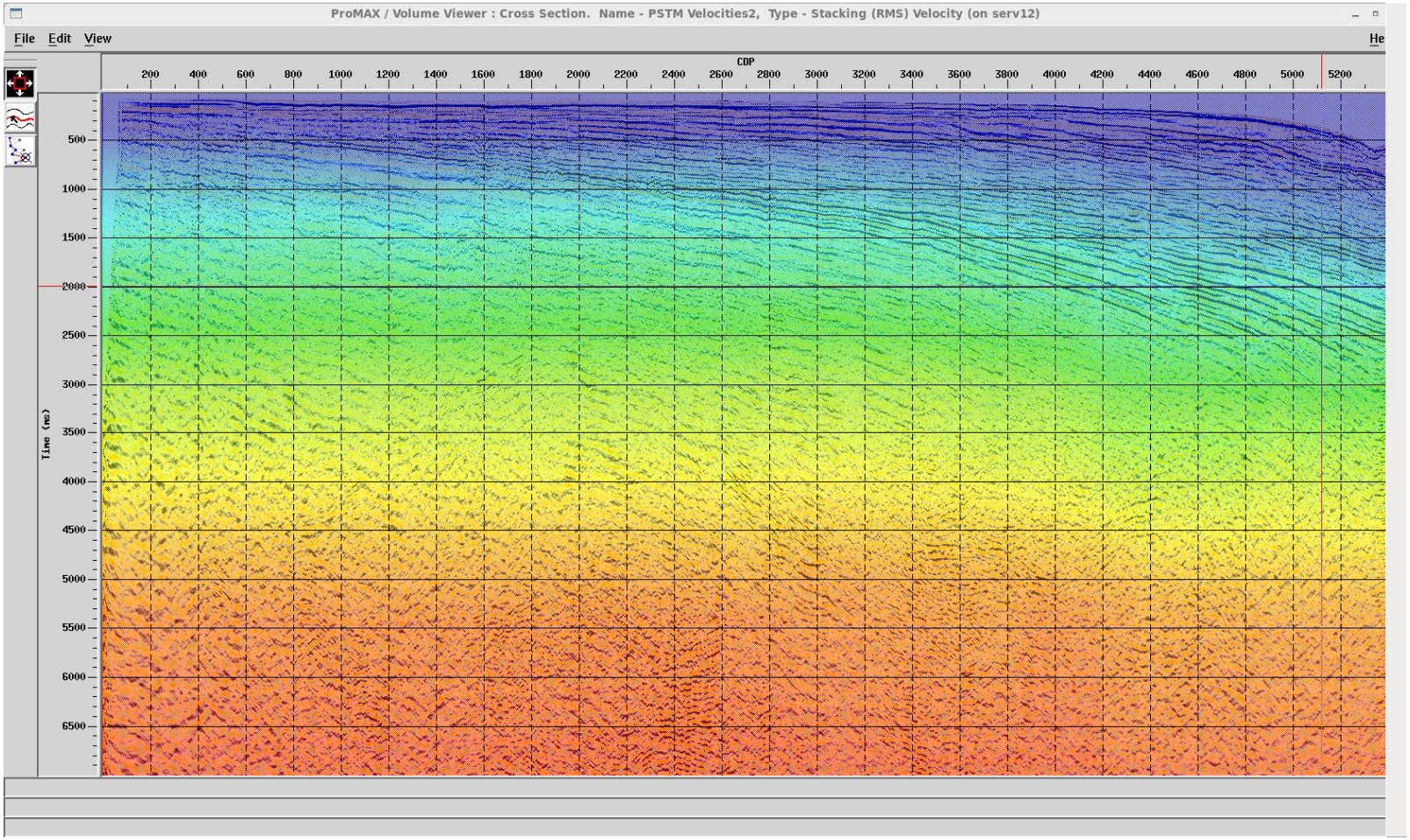

absolute IMAGING

Final PSTM Interval Velocities: Line 16

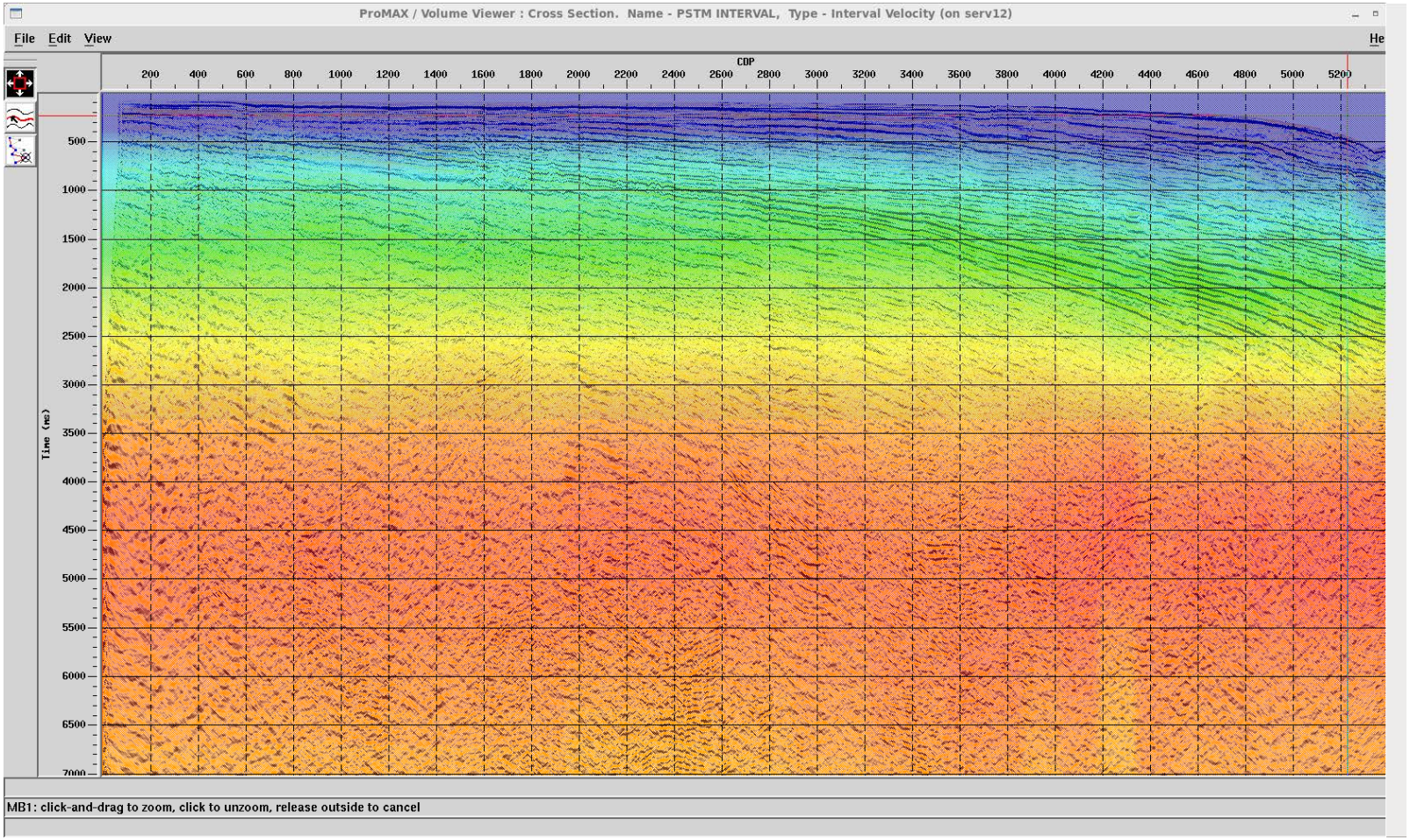

absolute IMAGING

Final PSTM: Line 22

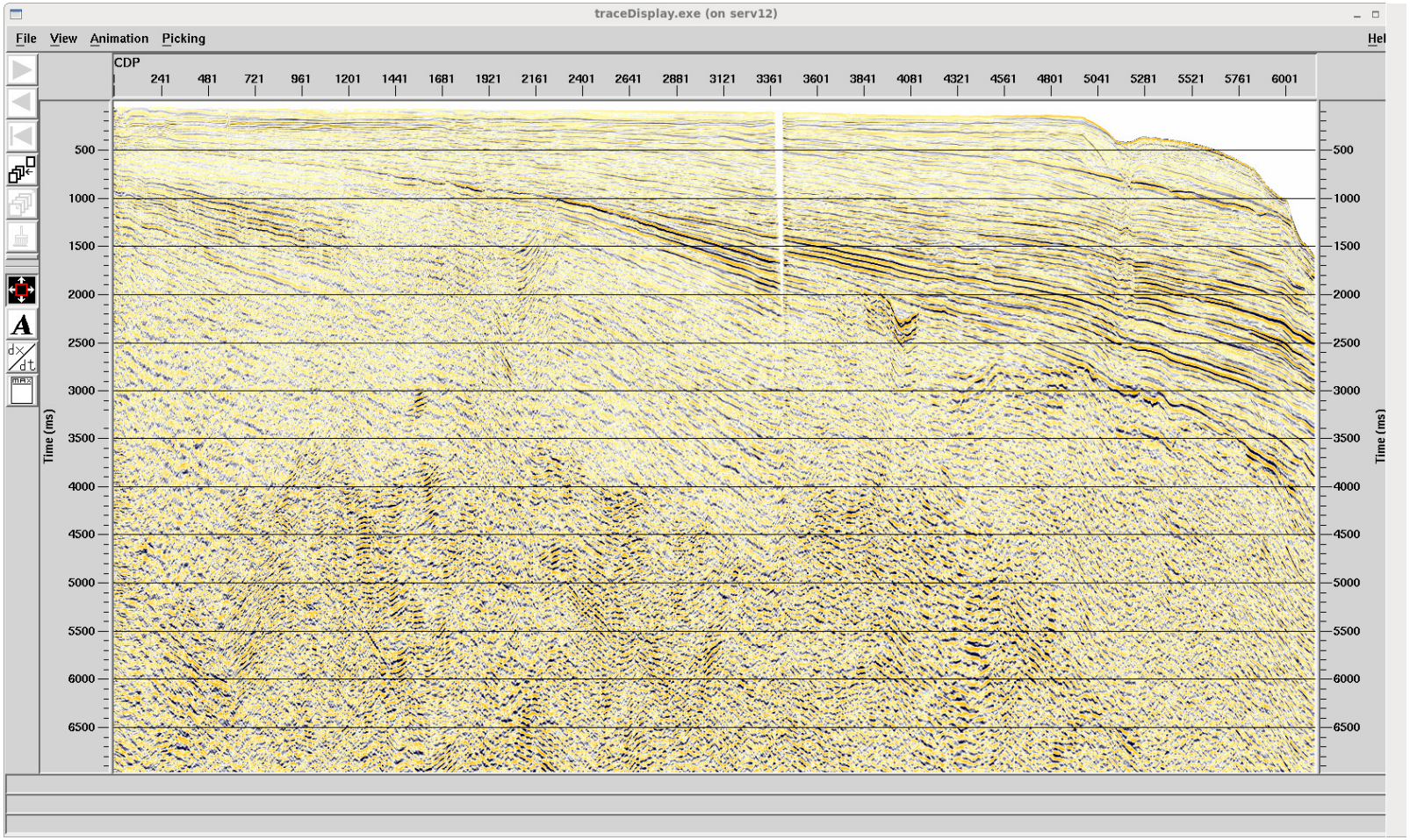

absolute IMAGING

Final PSTM RMS Velocities: Line 22

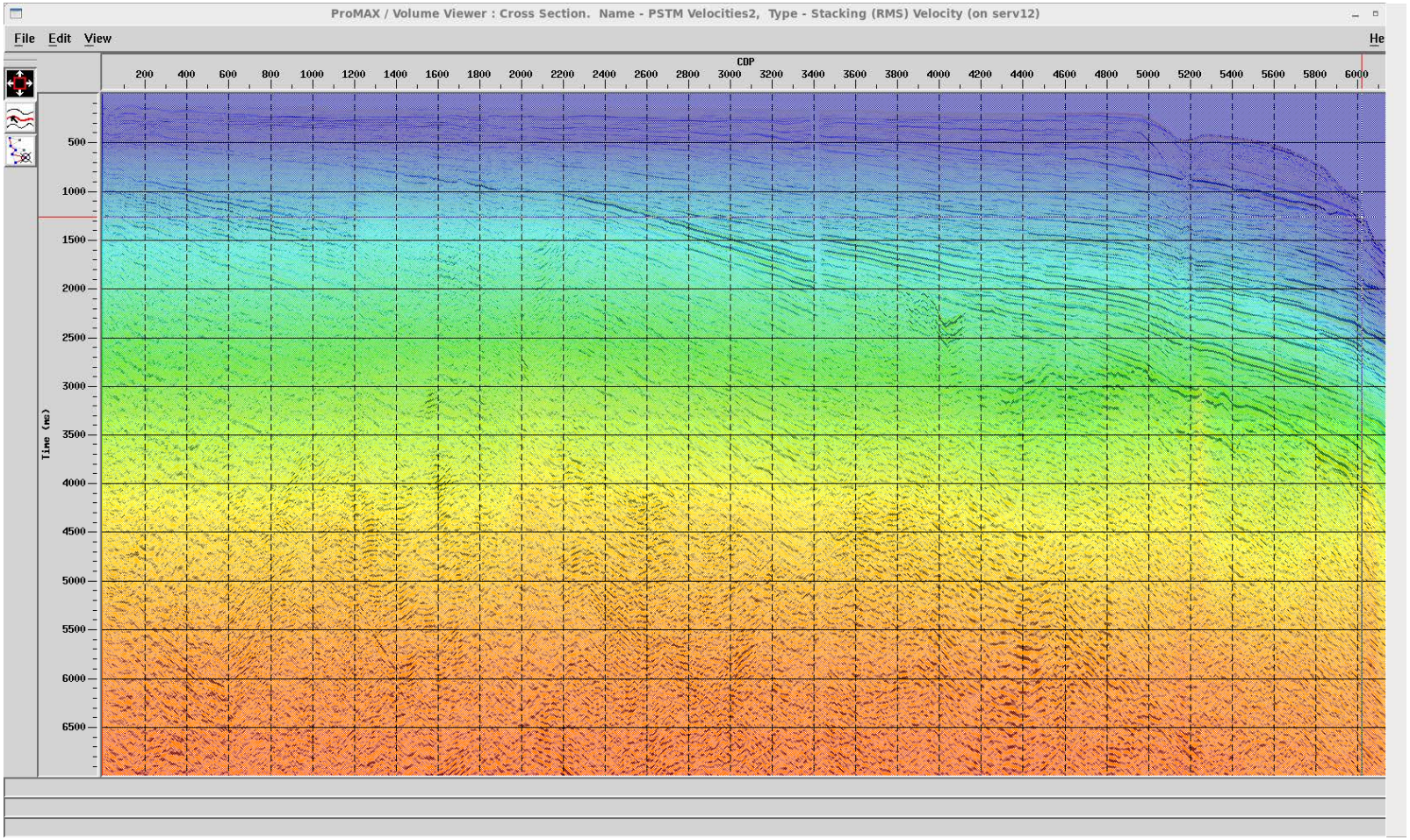

absolute IMAGING

Final PSTM Interval Velocities: Line 22

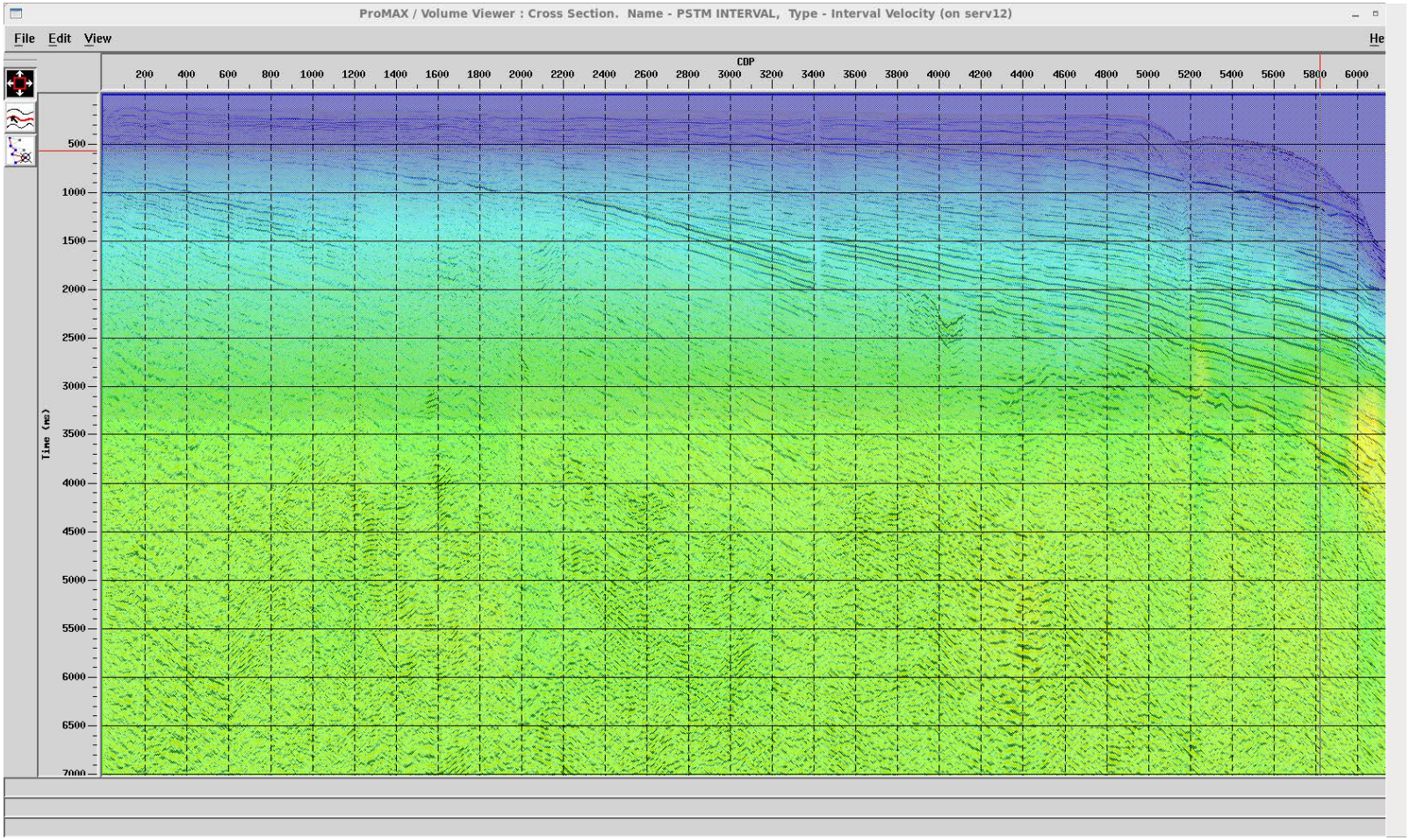

absolute IMAGING

Final PSTM: Line 26

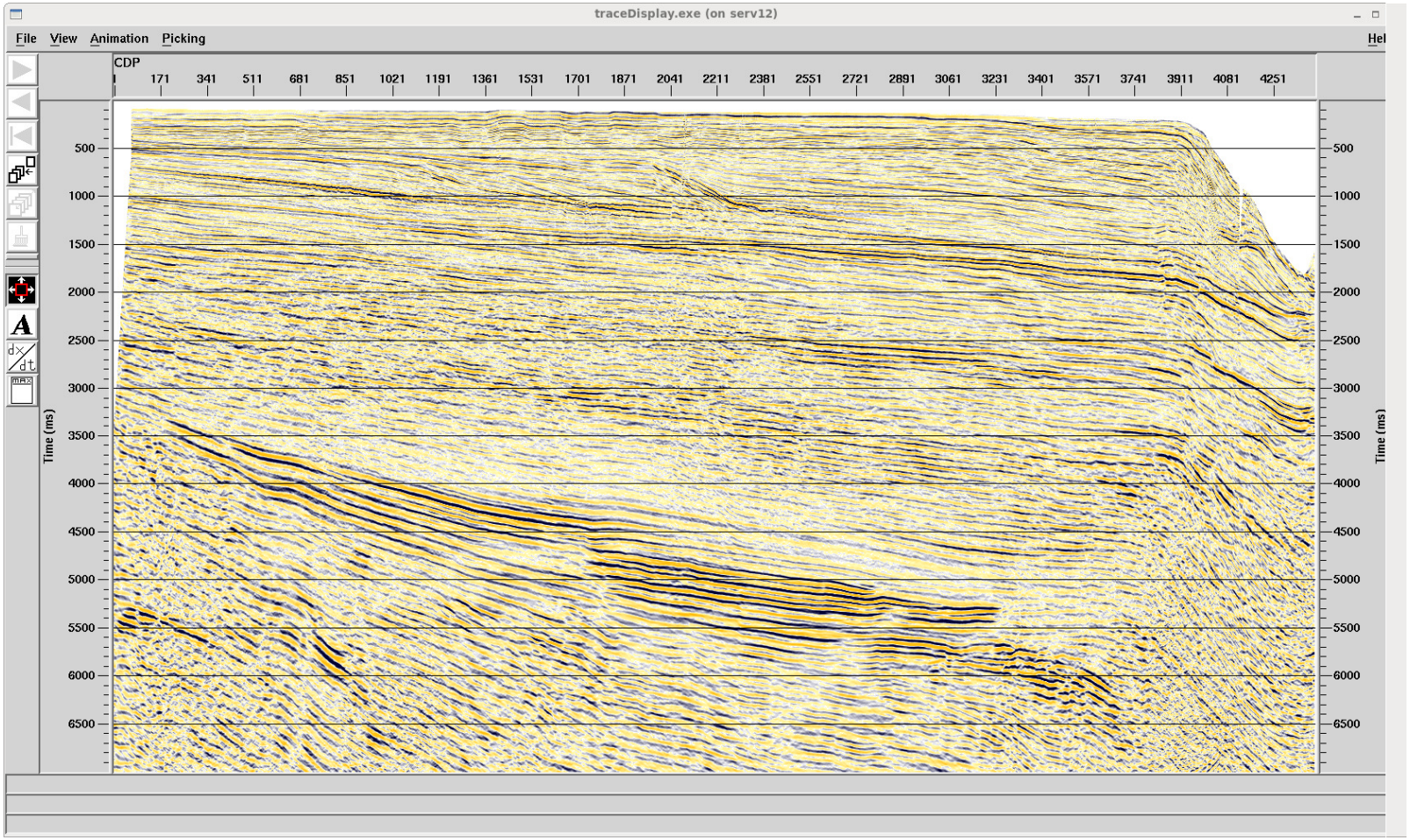

absolute IMAGING

Final PSTM RMS Velocities: Line 26

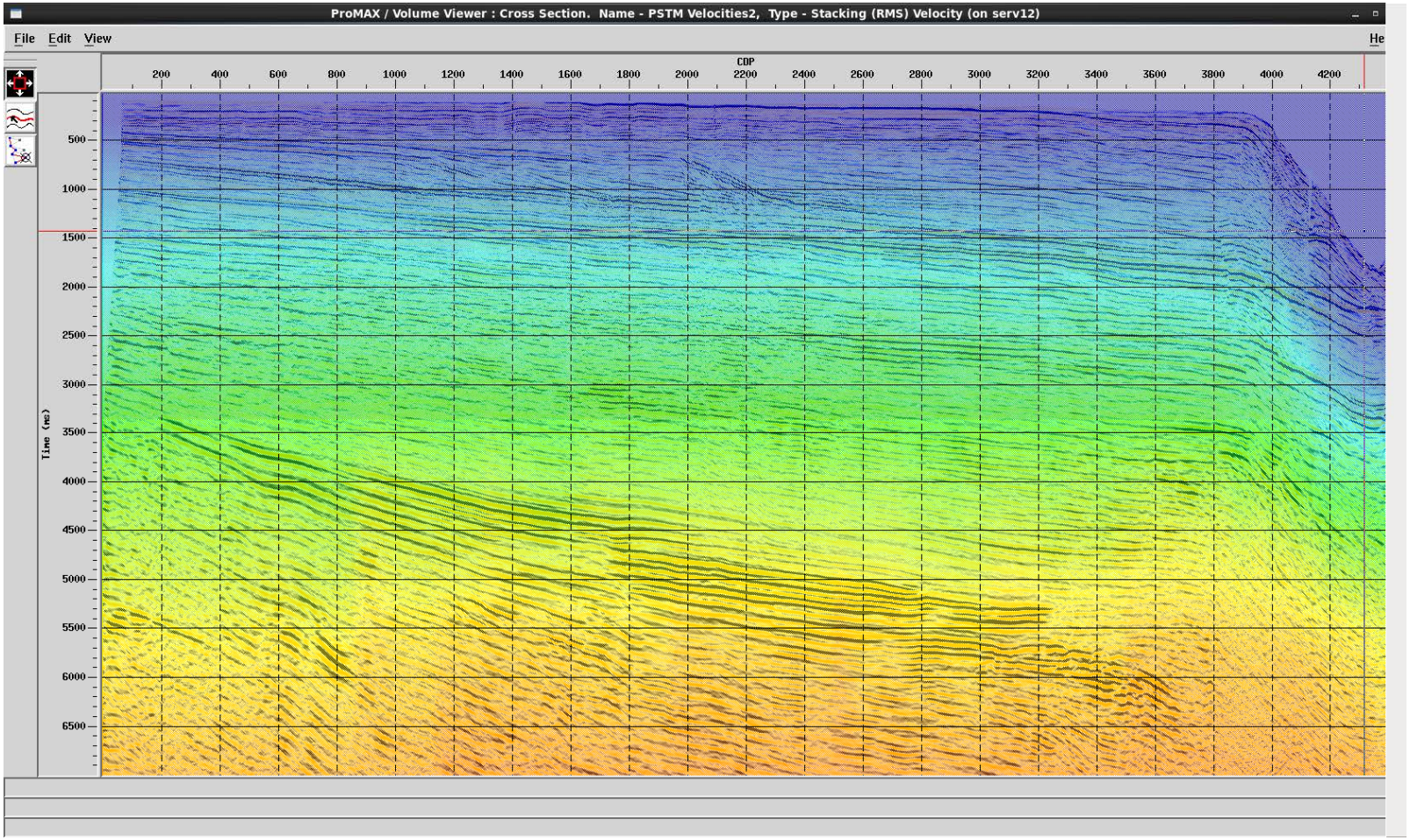

absolute IMAGING

Final PSTM Interval Velocities: Line 26

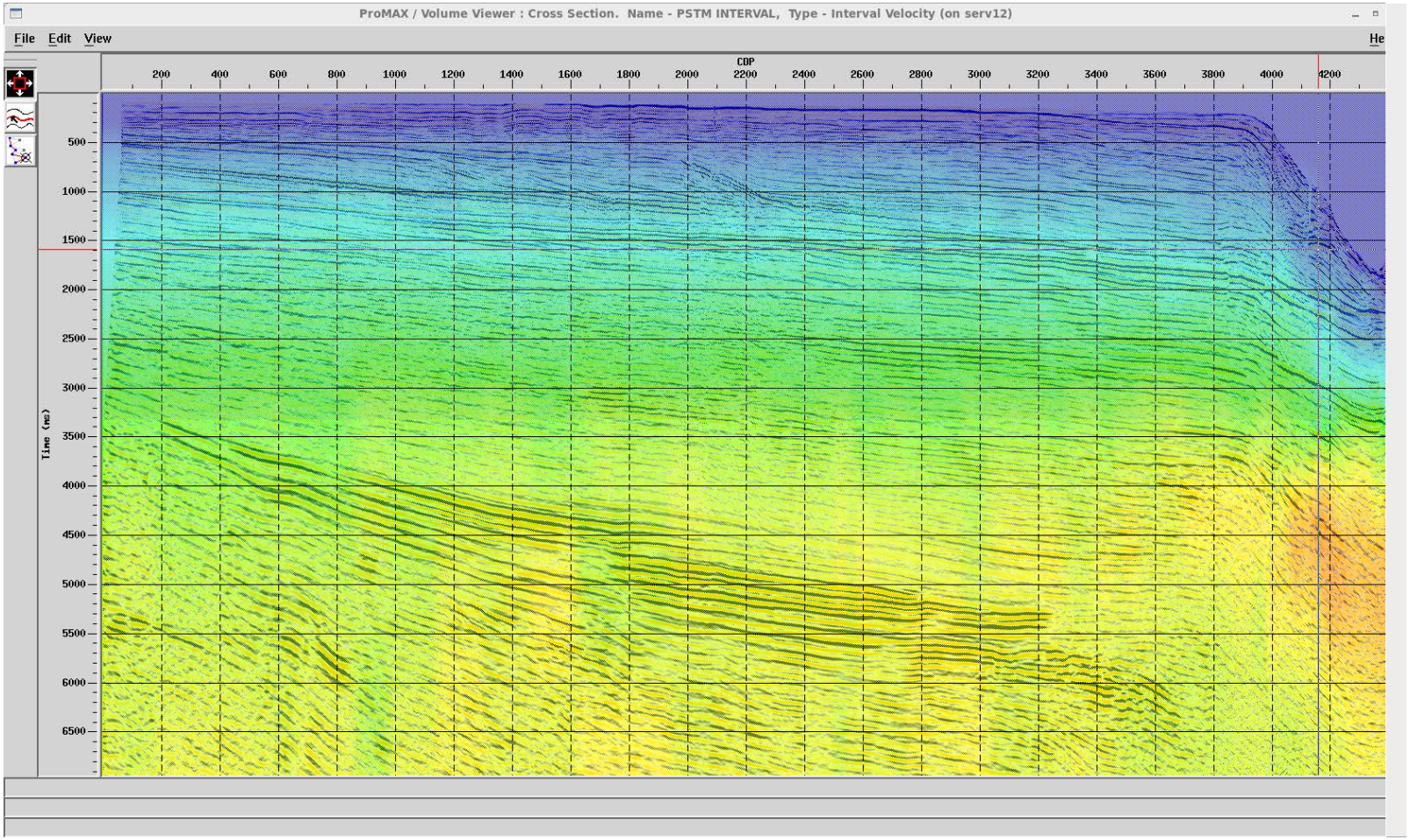

absolute IMAGING

Final PSTM: Line 27

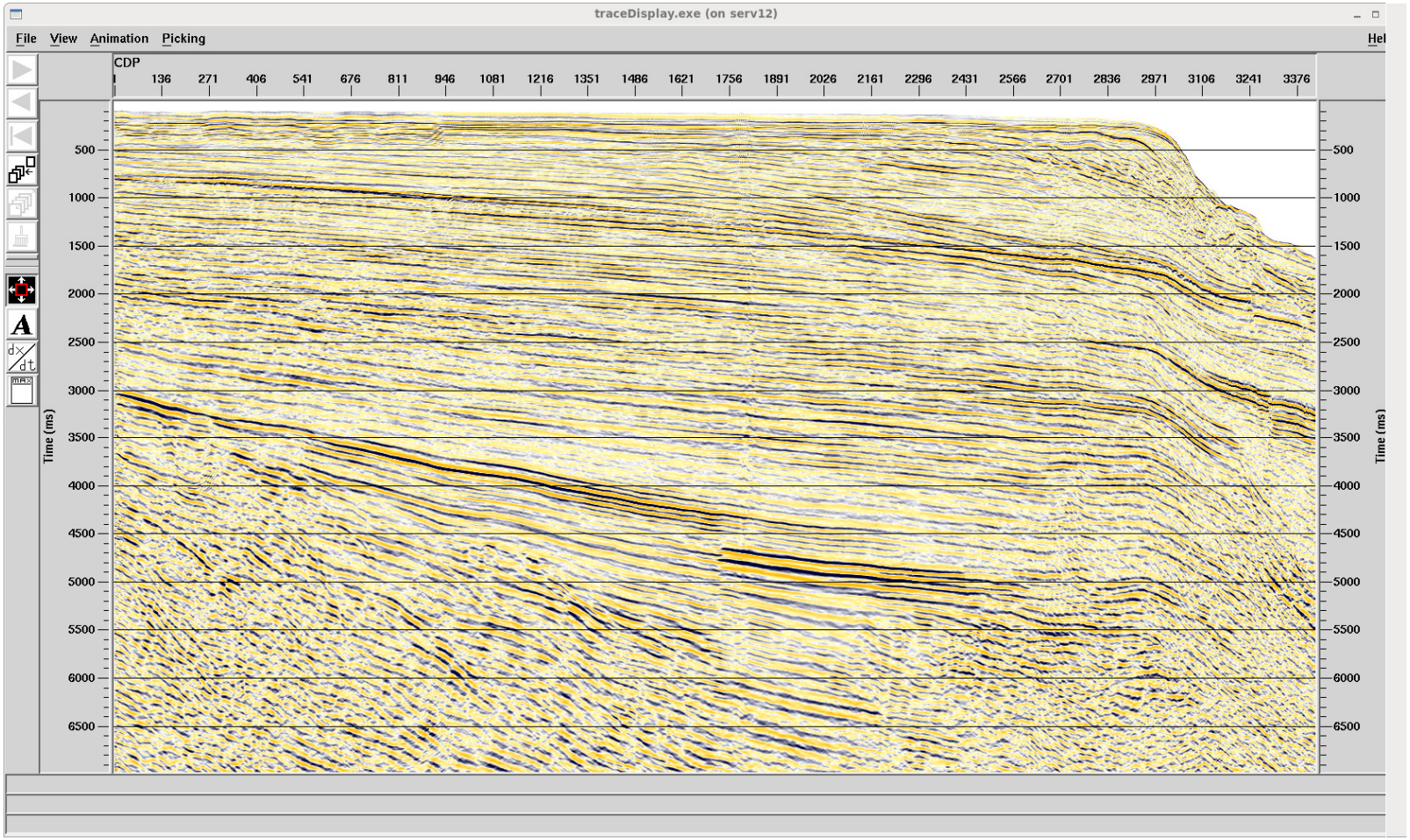

absolute IMAGING

Final PSTM RMS Velocities: Line 27

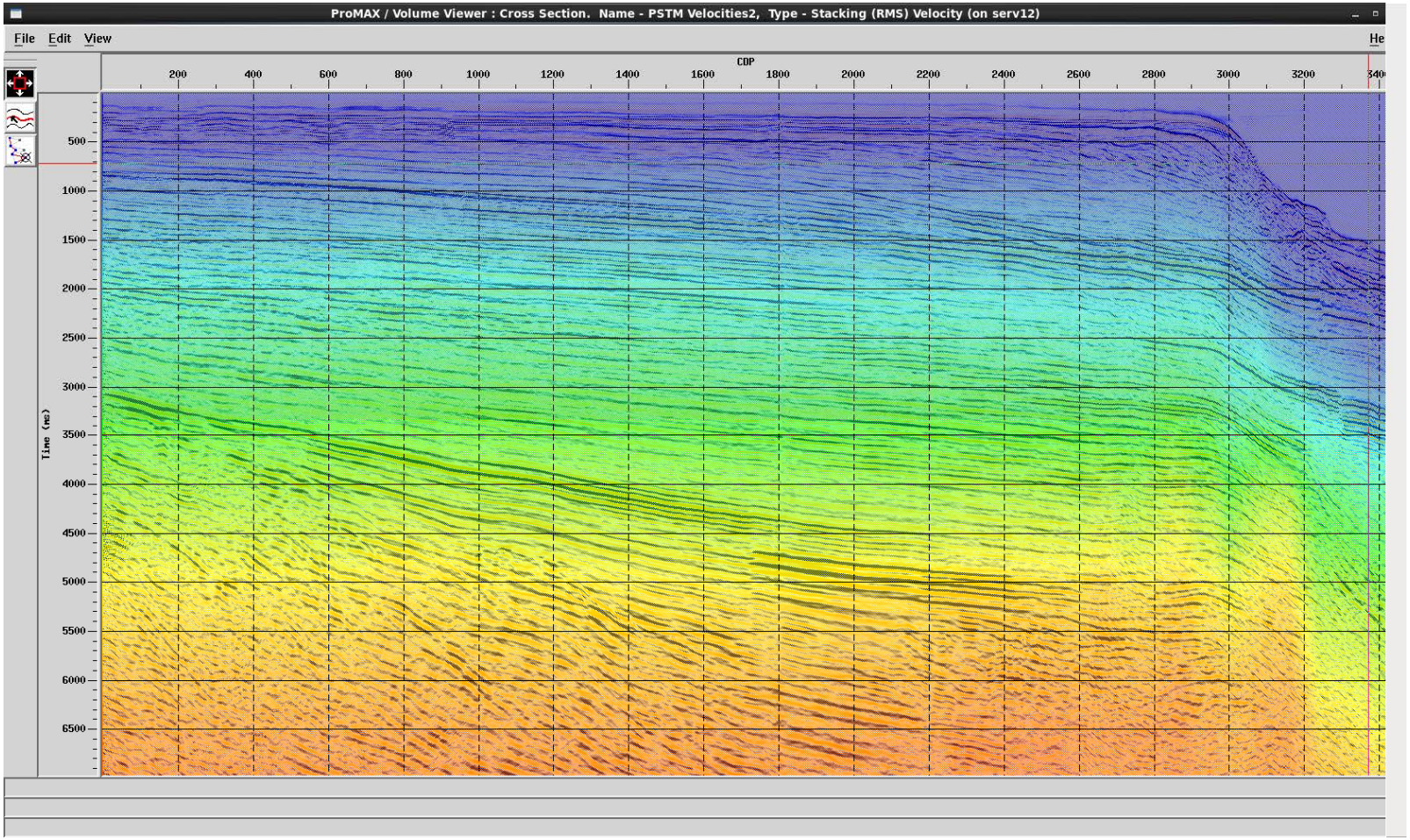

absolute IMAGING

Final PSTM Interval Velocities: Line 27

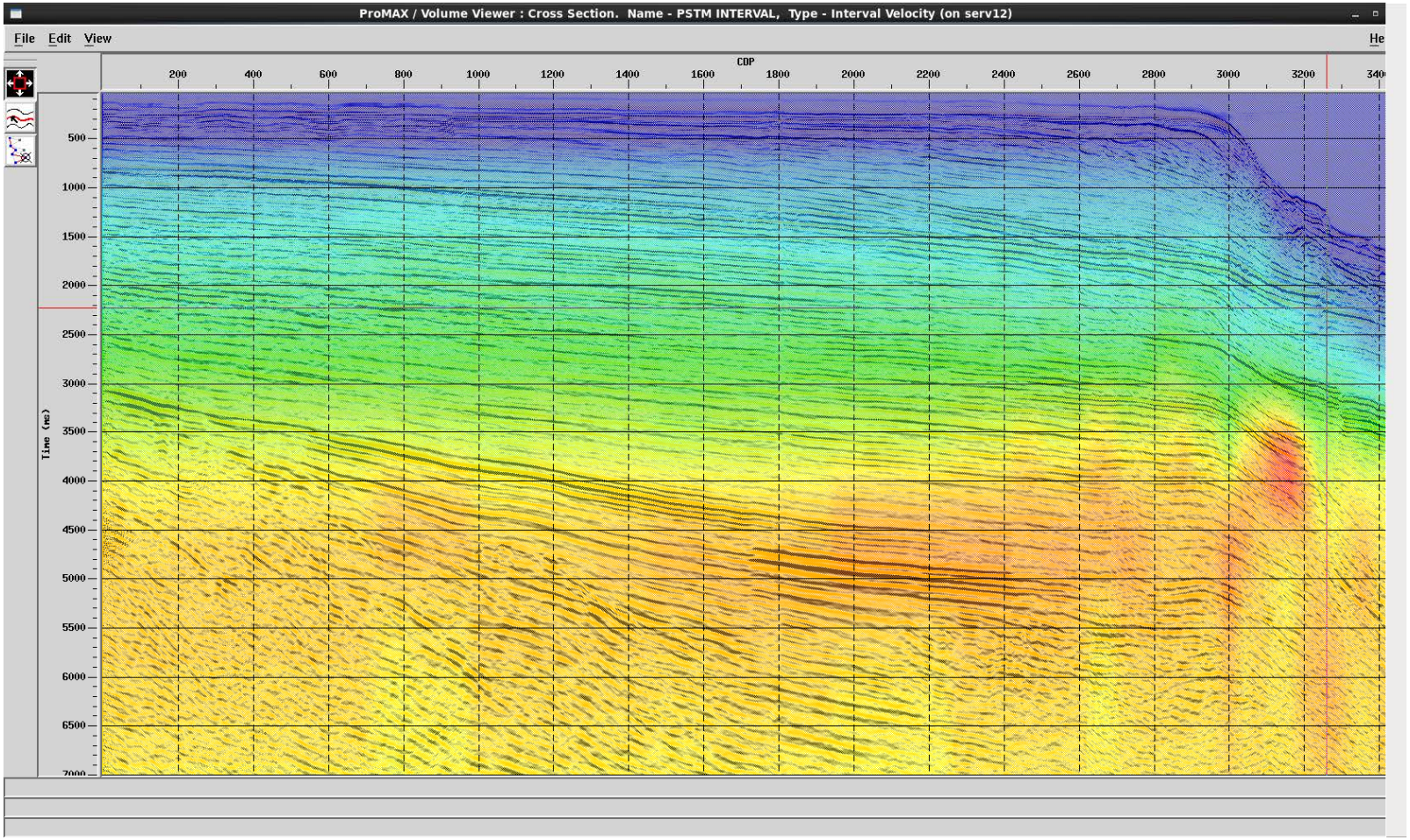

absolute IMAGING

Final PSTM: Line 37

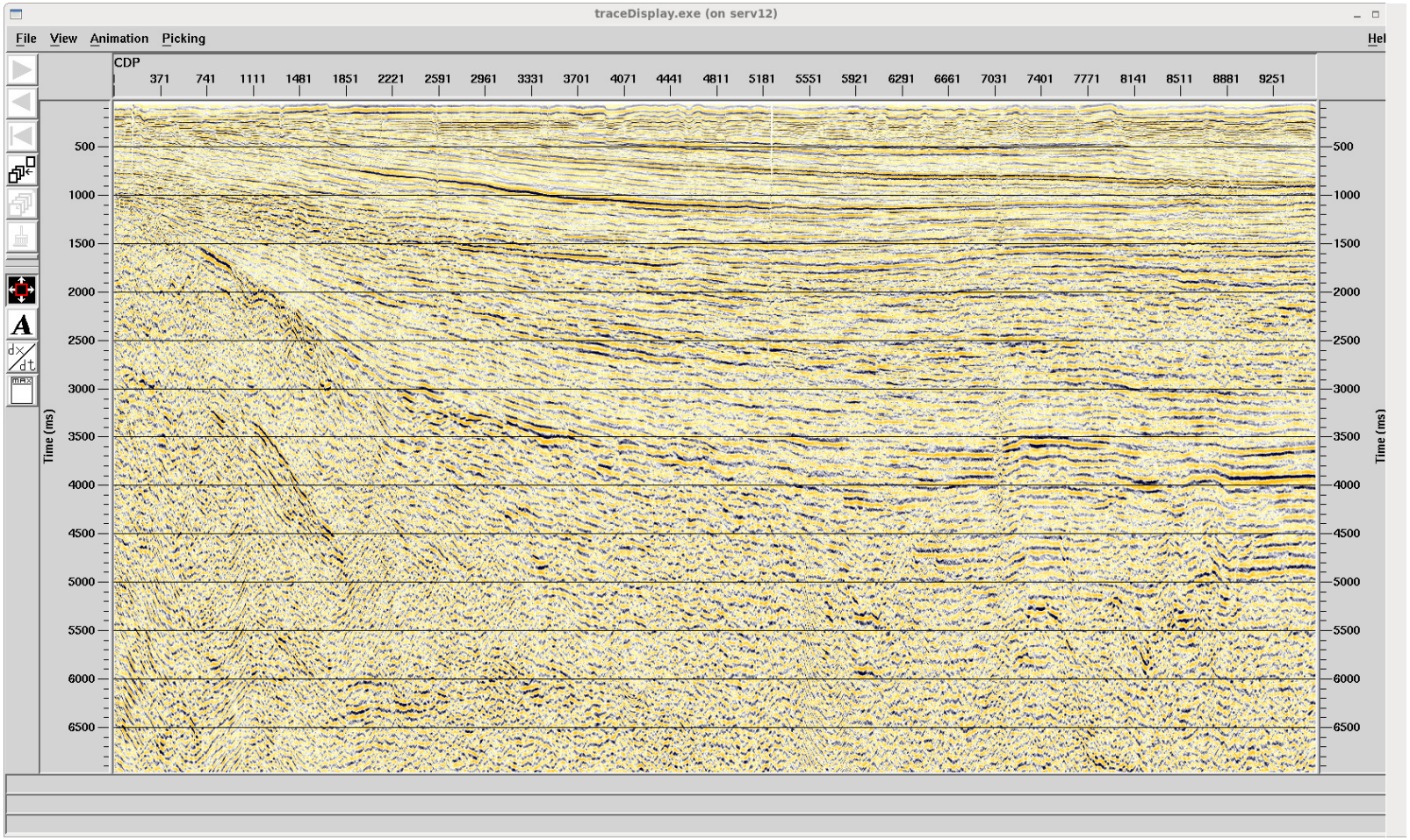

absolute IMAGING

Final PSTM RMS Velocities: Line 37

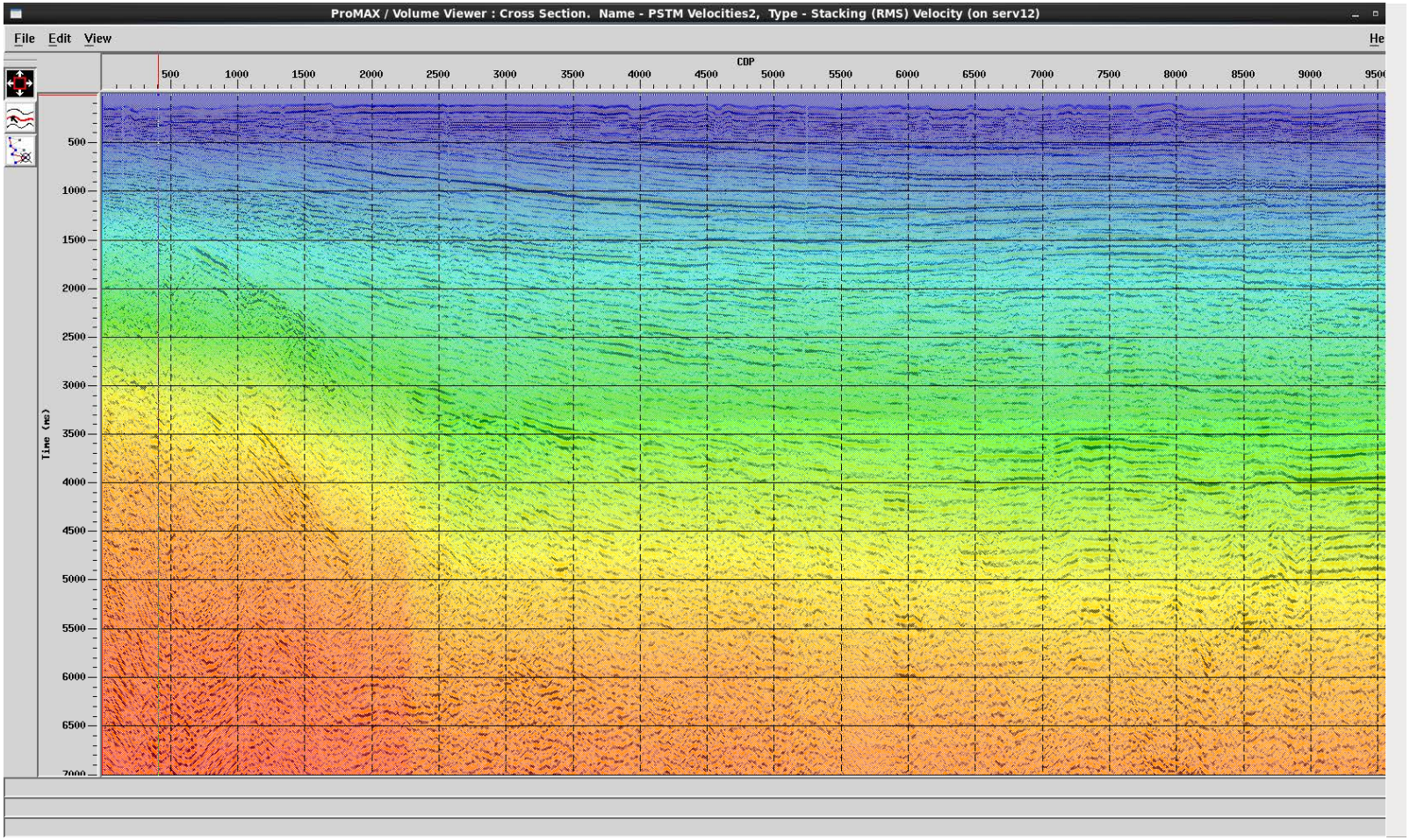

absolute IMAGING

Final PSTM Interval Velocities: Line 37

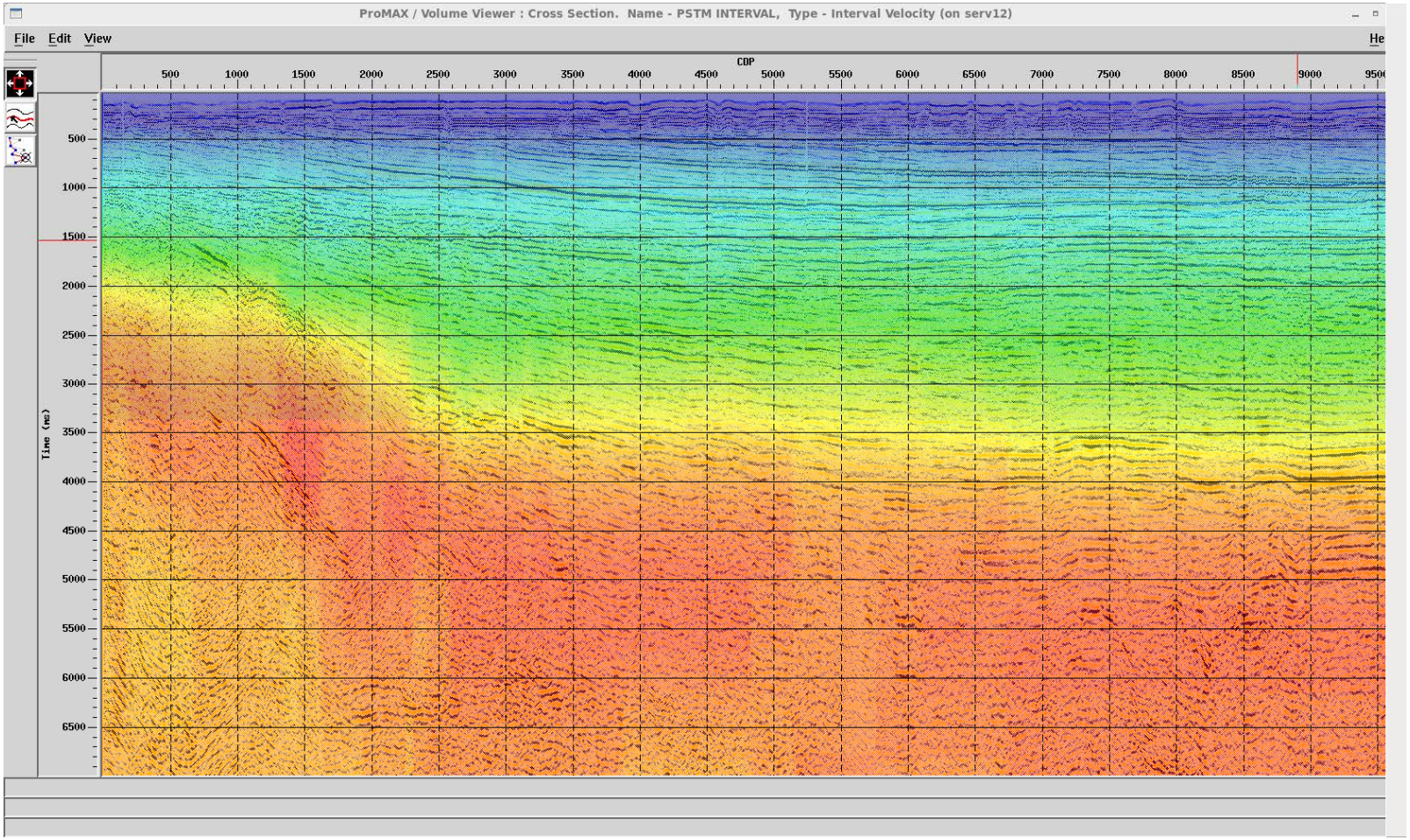

absolute IMAGING

Tying Data

General comments on project line ties and procedure using Lintal

- Generally Modern Marine Data of the same vintage ties quite well and does not in general suffer from the statics issues that Land Data does and bulks applied to the lines are generally a result in differences in the initial time delays inherent in the Acquisition differences.
- The lines included in this project were shot by multiple contractors during the 1970's, using a variety of equipment and recording systems. The acquisition parameters, data quality and lack of supporting documentation all may be contributing factors to properly correlating the ties.
- Using the Lintal Software all the tie points in a project are reviewed and a cross correlation is calculated over a set window. In this case that window was set between 800 and 2200 ms. The processor can then allow the program to suggest relative bulks and phase corrections for each line. From this baseline the processor uses their experience to make further adjustments.
- Phase changes were limited to a polarity flip, or 180 degrees. Given the differing acquisition contactors, cables and recording systems, some phase differences might be expected.
- Generally all the ties demonstrate a good correlation with the exception of a couple of ties which seem to suffer from poorer data quality at the tie locations.
- There are several tie points that exist in areas where at least one line has data missing. This can be seen in the ties between lines 12-8, 33-1 and 14-2 ties.
- Line 12 was used as a base line and all lines were then tied to this, followed by adding the additional cross lines, 33, 36, 37 and 14.

absolute IMAGING

Lintal Line Tie Map

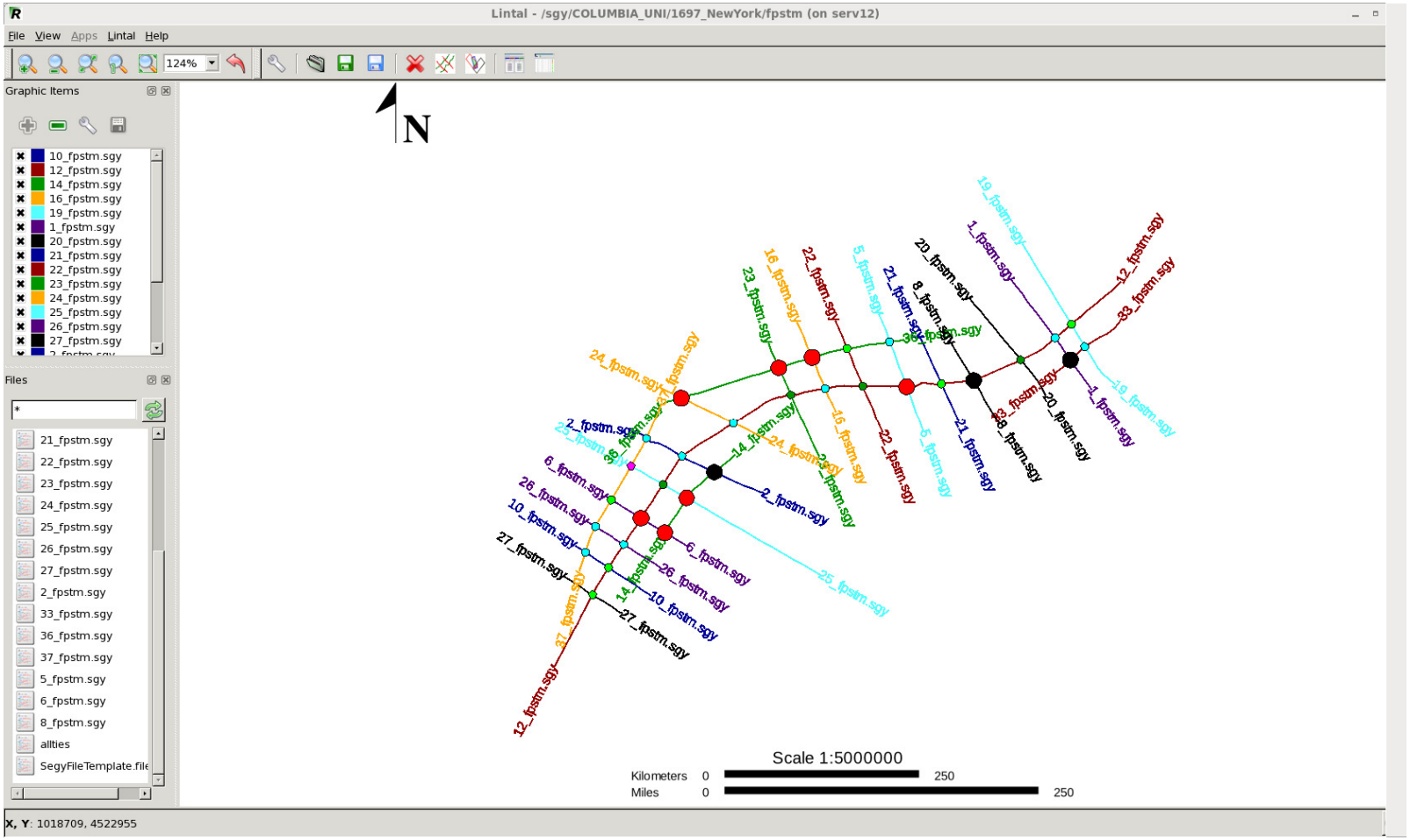

absolute IMAGING

Applied Time and Phase adjustments

Line #	Time Shift	Phase Shift
1	-29	180
2	2	0
5	-4	180
6	17	180
8	0	0
10	-5	0
12	0	0
14	-25	0
16	-36	0
19	-44	0
20	-13	0
21	-4	180
22	-50	0
23	-25	0
24	-75	0
25	-72	0
26	-13	0
27	-36	0
33	-47	0
36	-42	0
37	-44	0

absolute IMAGING

Line 12 Ties with Lines 1 and 19

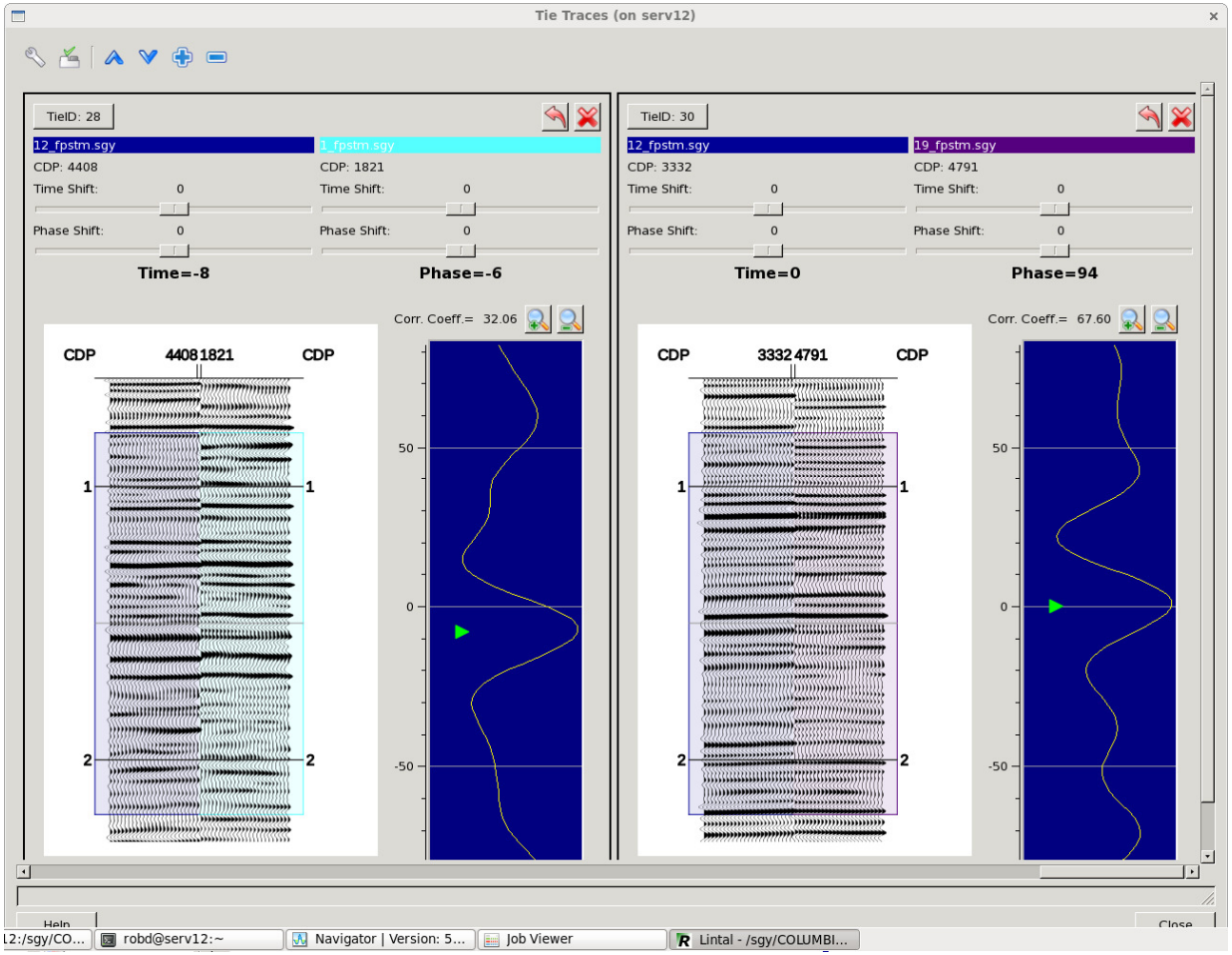

absolute IMAGING

Line 12 Ties with Lines 8 and 20

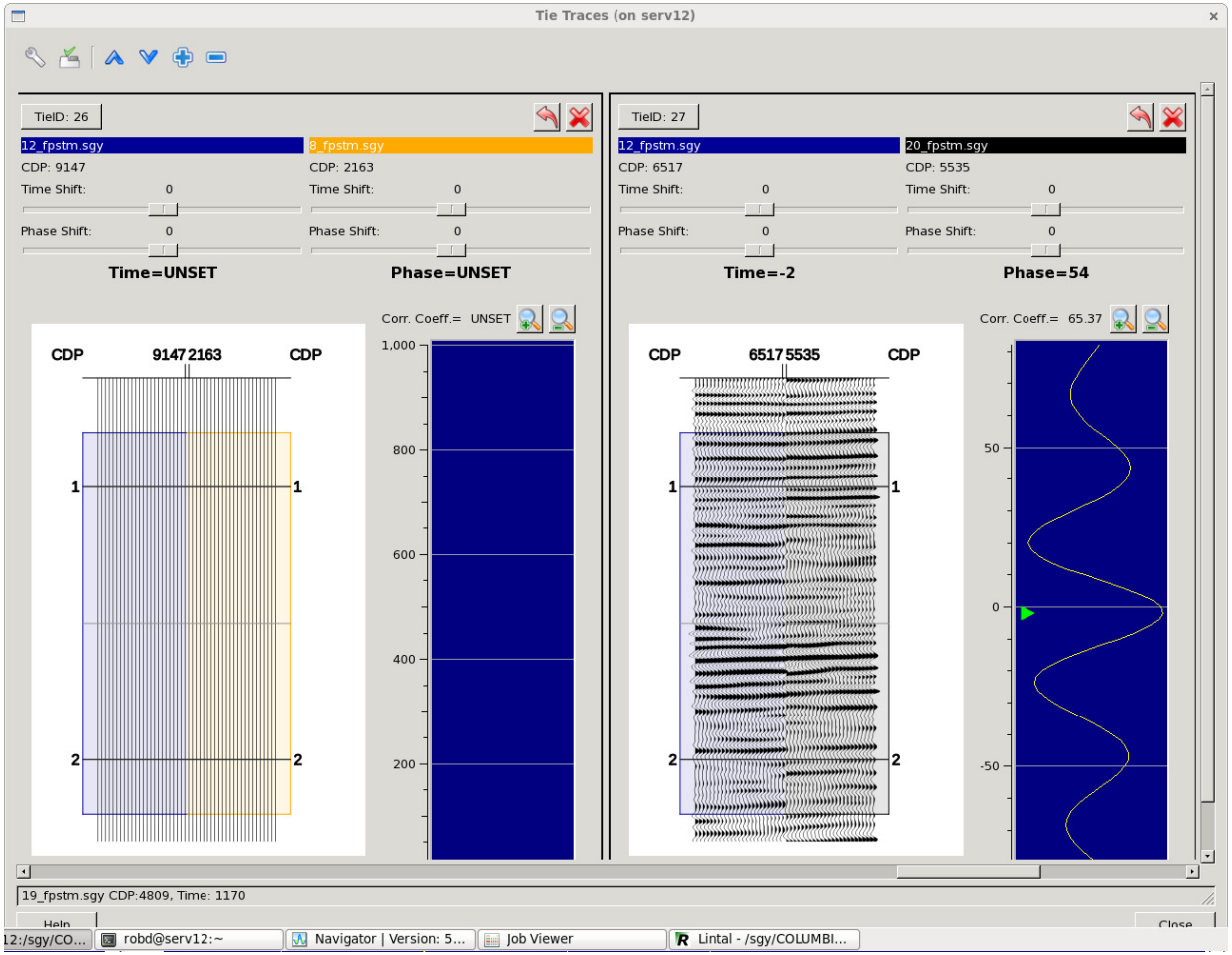

absolute IMAGING

Line 12 Ties with Lines 5 and 21

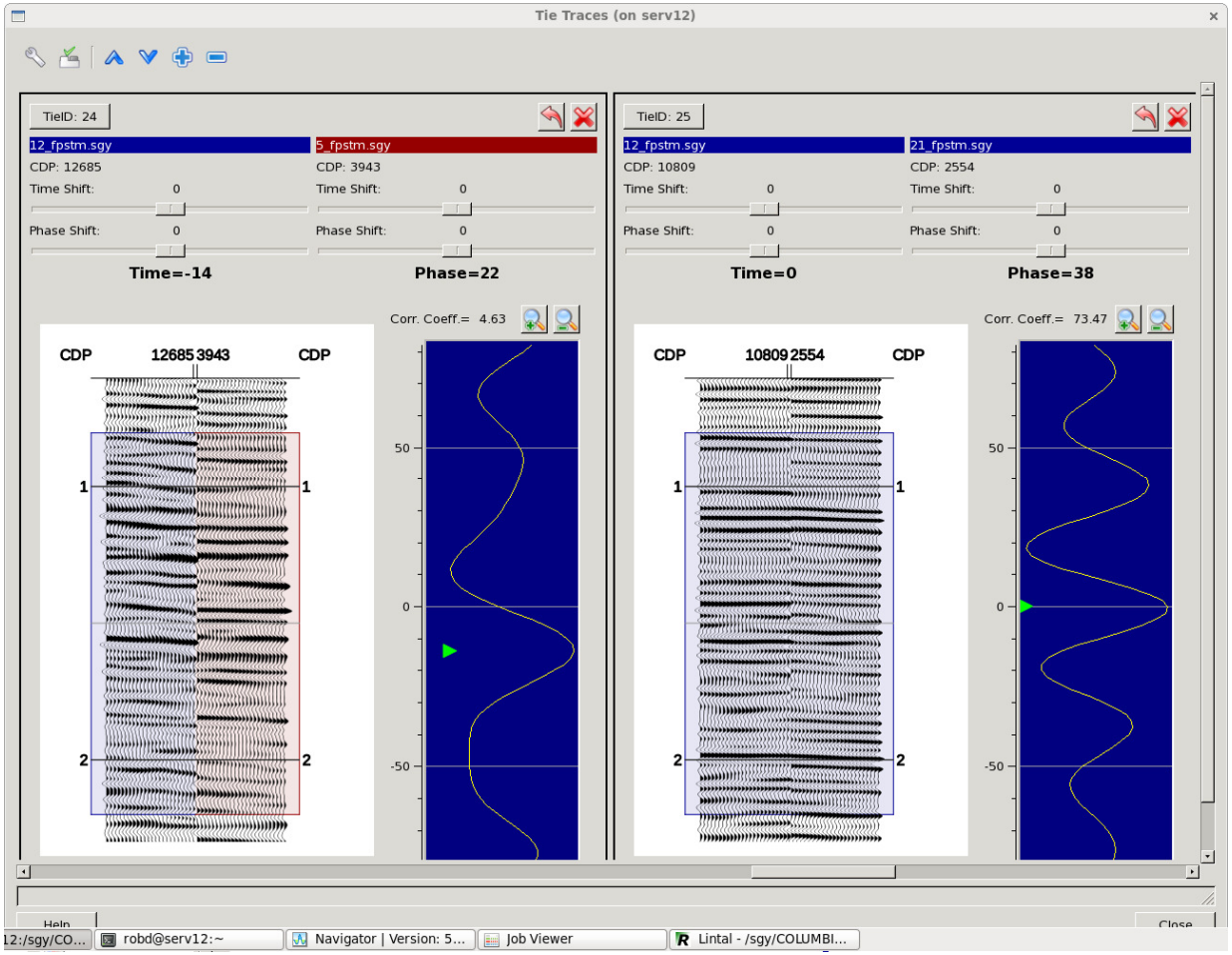

absolute IMAGING

Line 12 Ties with Lines 16 and 22

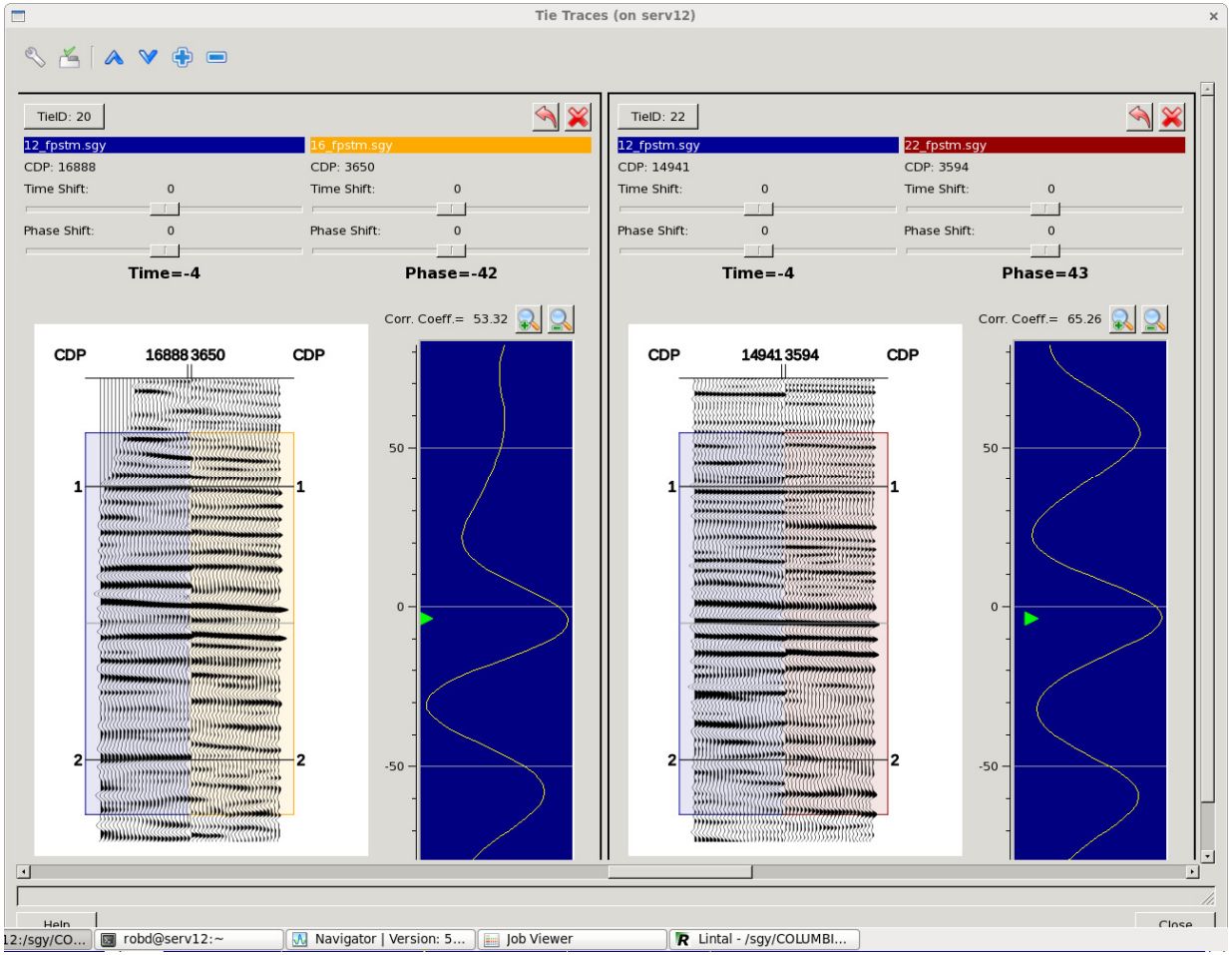

Line 12 Ties with Lines 24 and 23

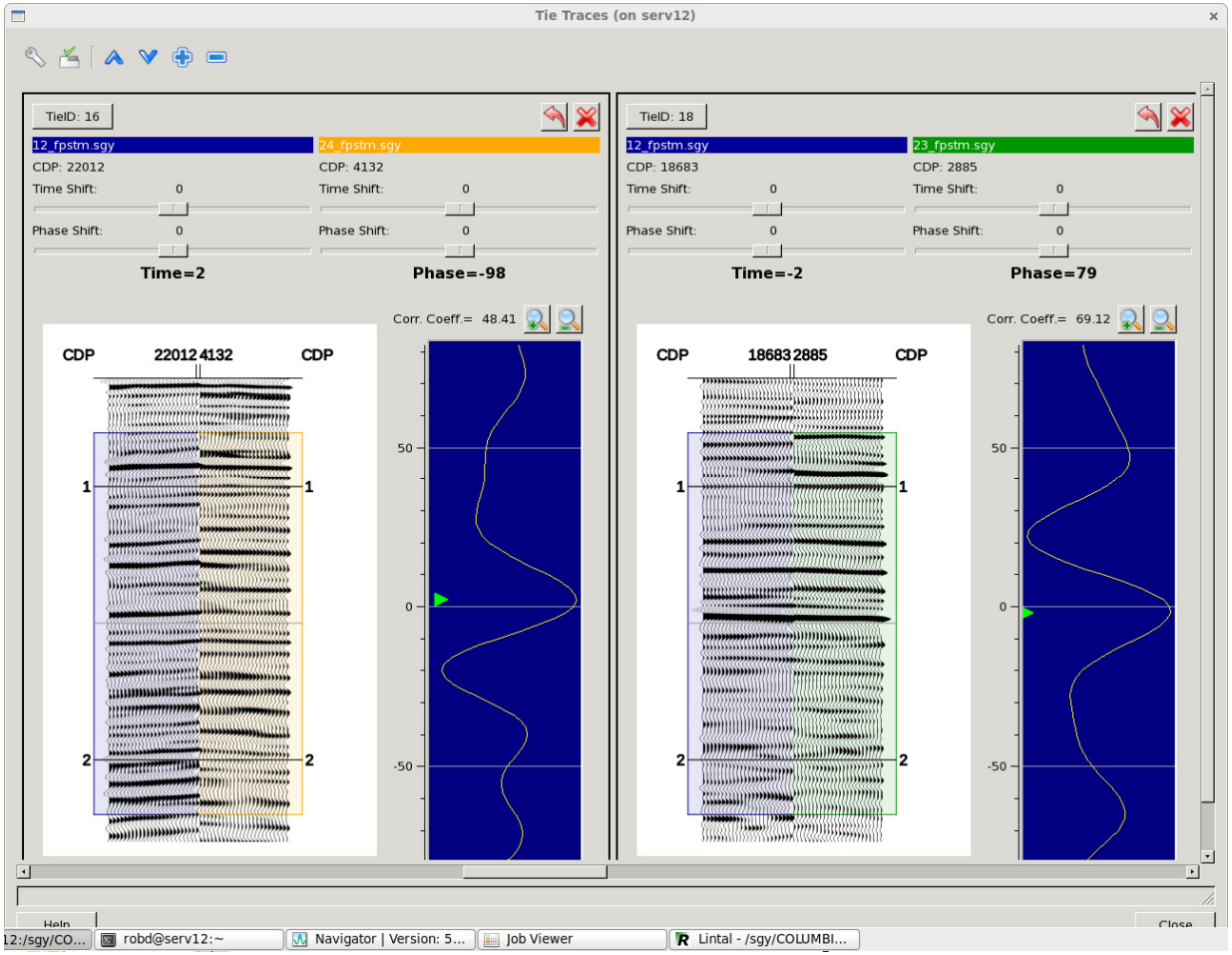

absolute IMAGING

Line 12 Ties with Lines 25 and 2

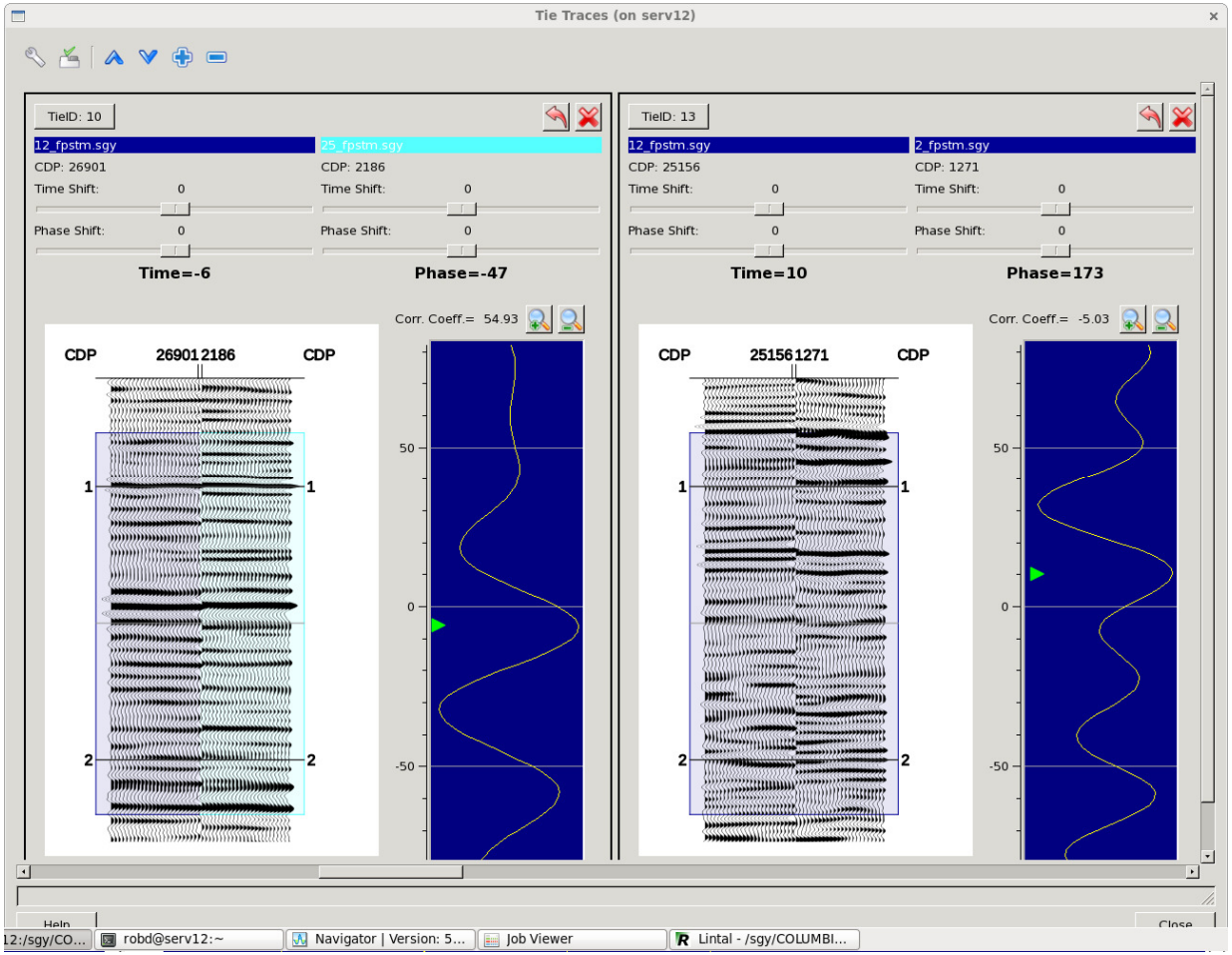

absolute IMAGING

Line 12 Ties with Lines 26 and 6

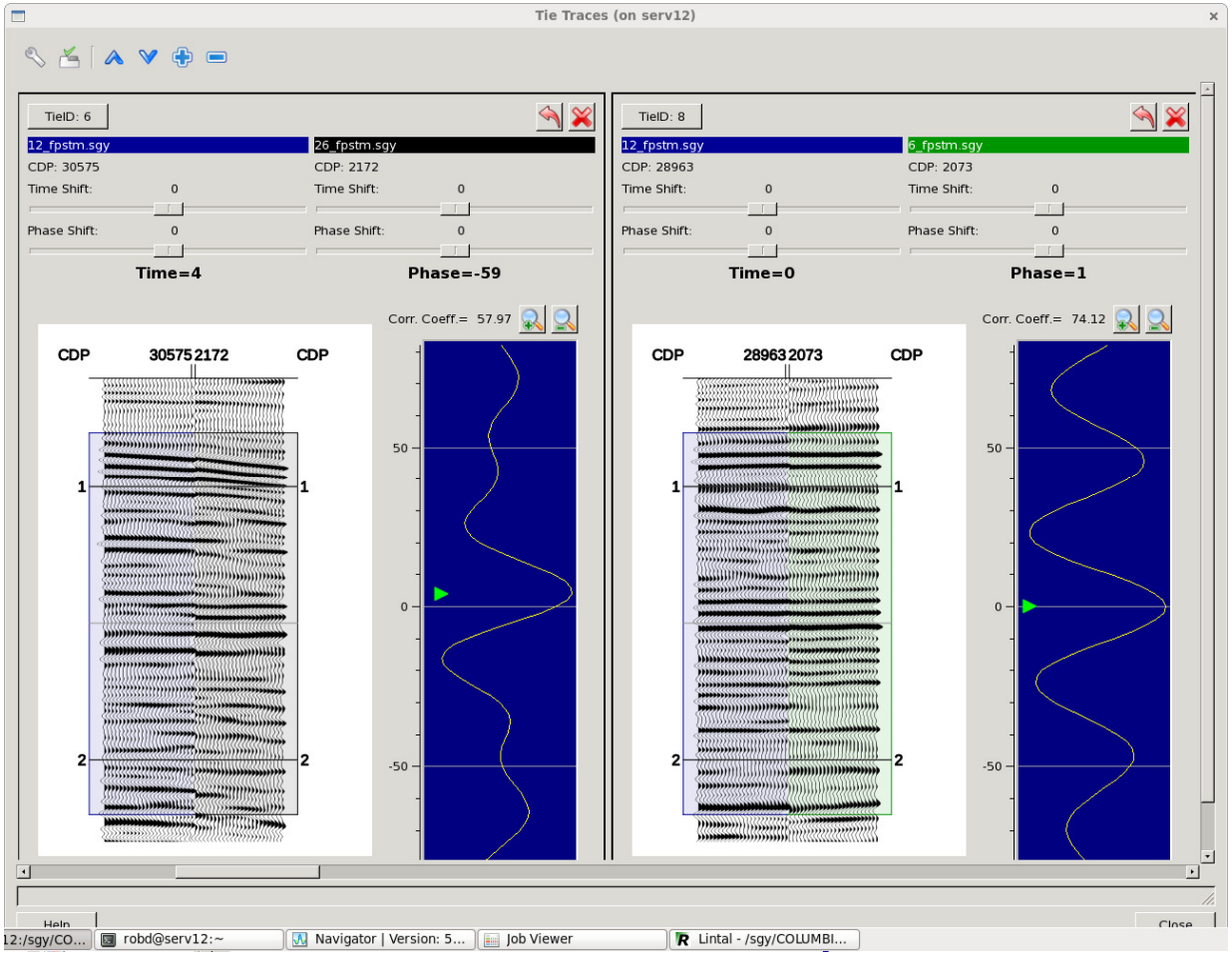

absolute IMAGING

Line 12 Ties with Lines 27 and 10

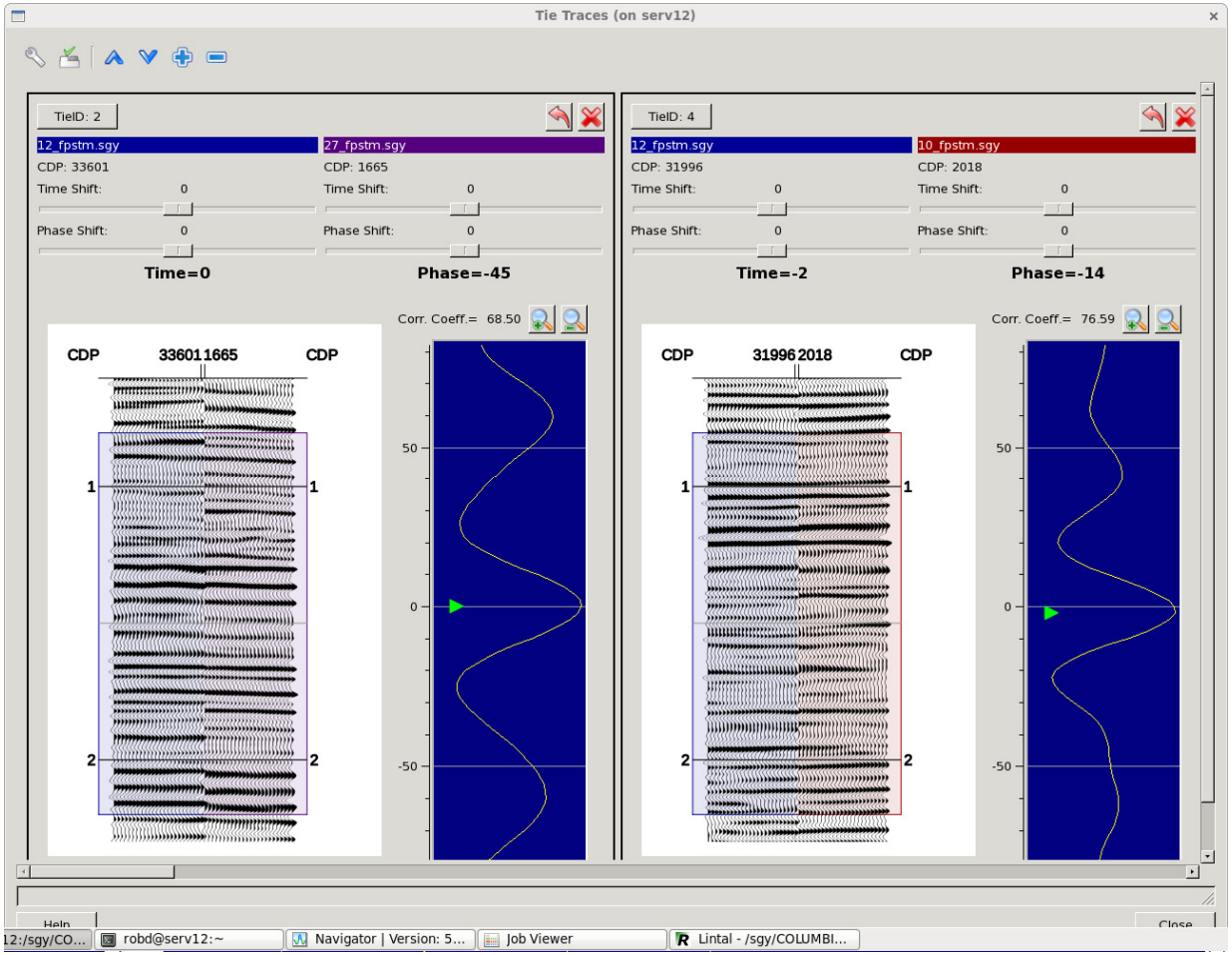

absolute IMAGING

Line 37 Ties with Lines 26 and 6

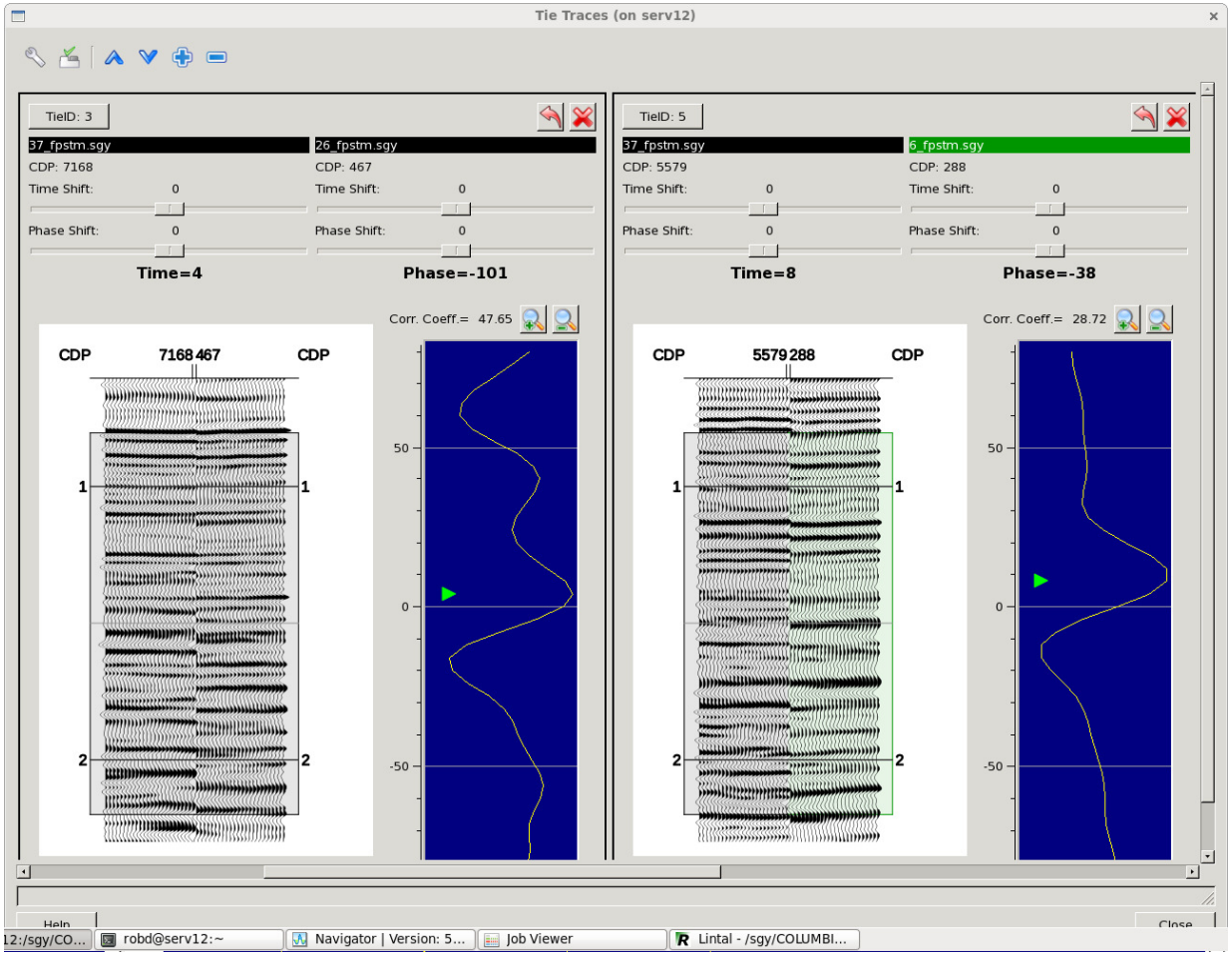

absolute IMAGING

Line 37 Ties with Lines 10 and 26

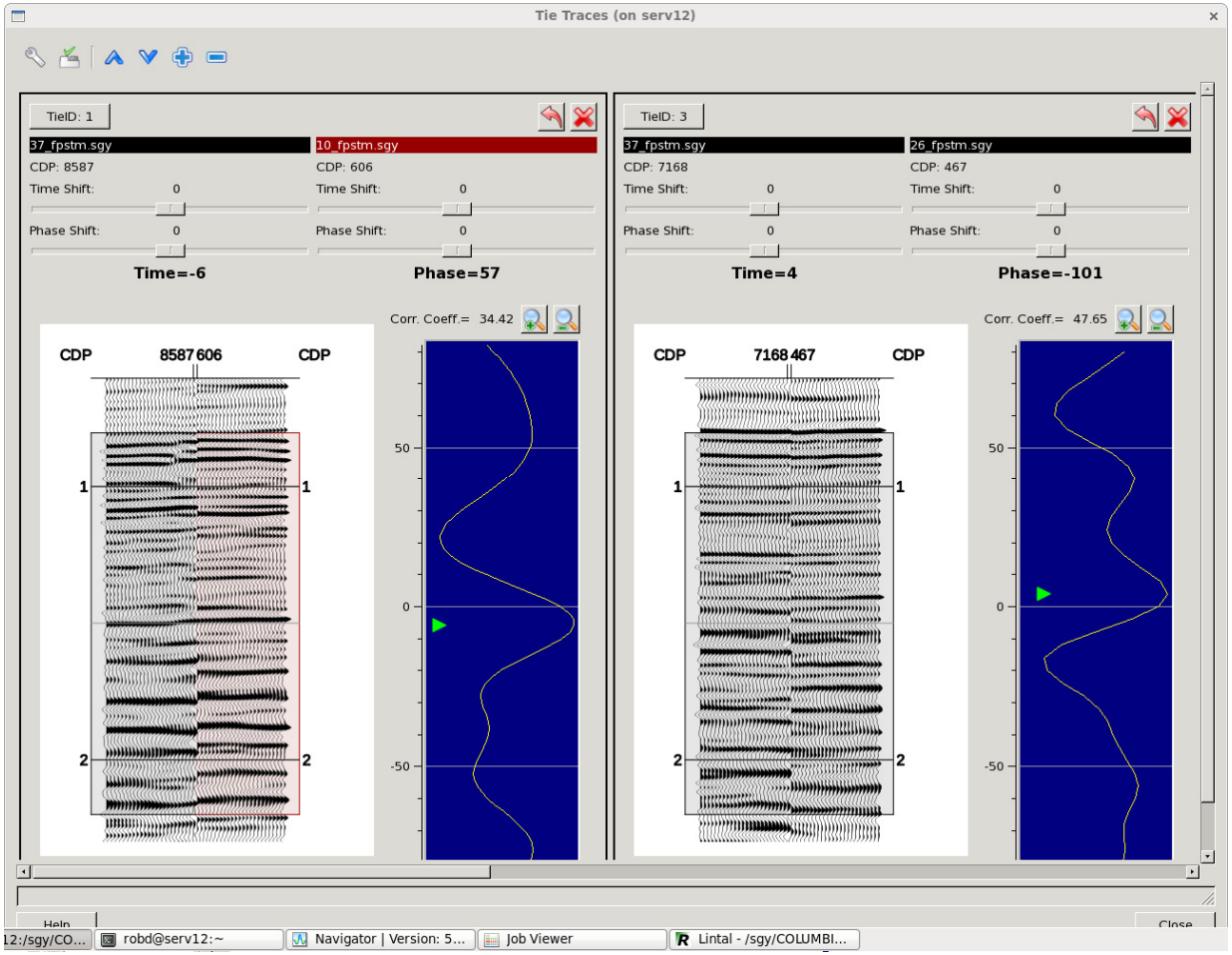

absolute IMAGING

Line 14 Ties with Lines 25 and 2

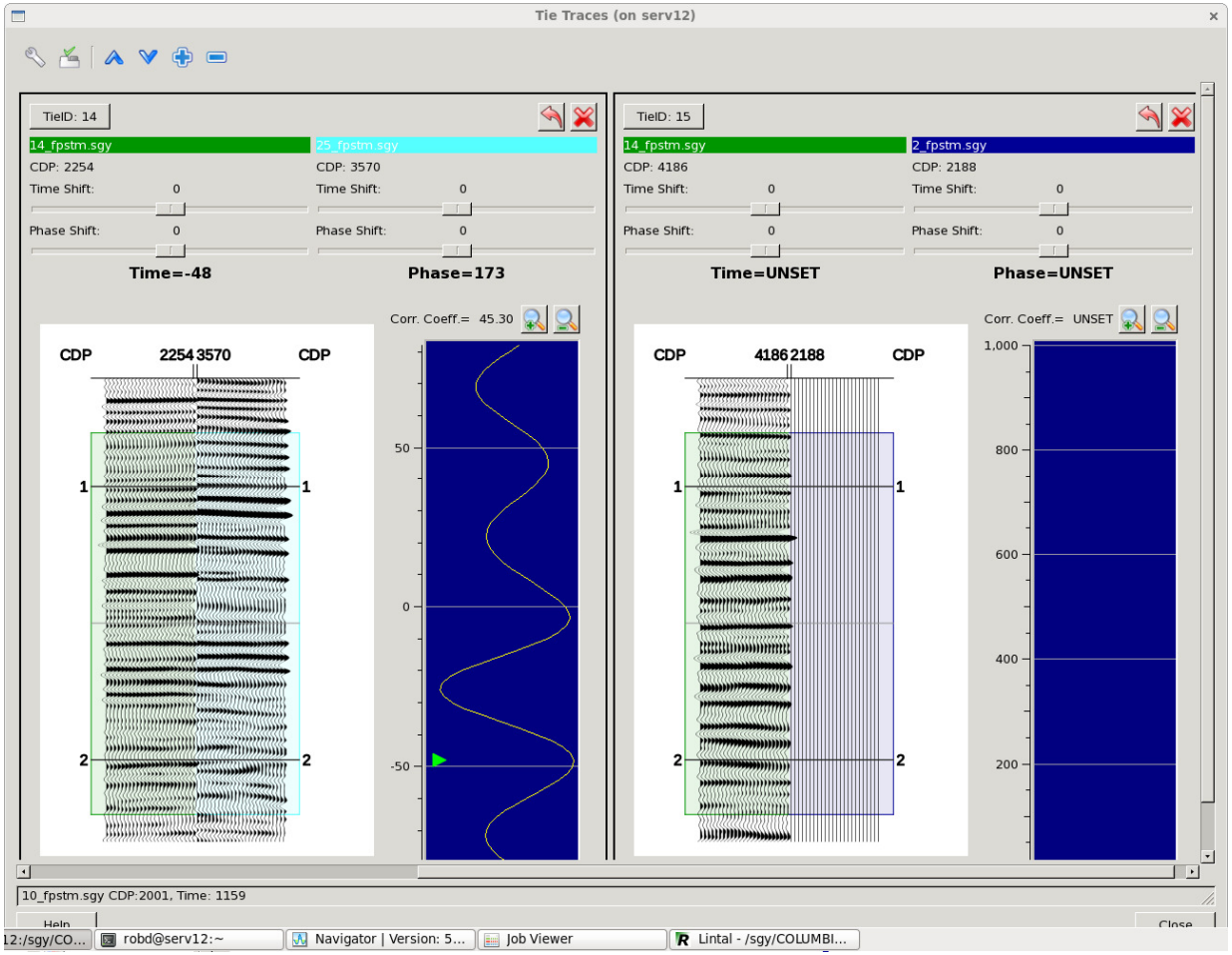

Line 14 Ties with Lines 6 and 25

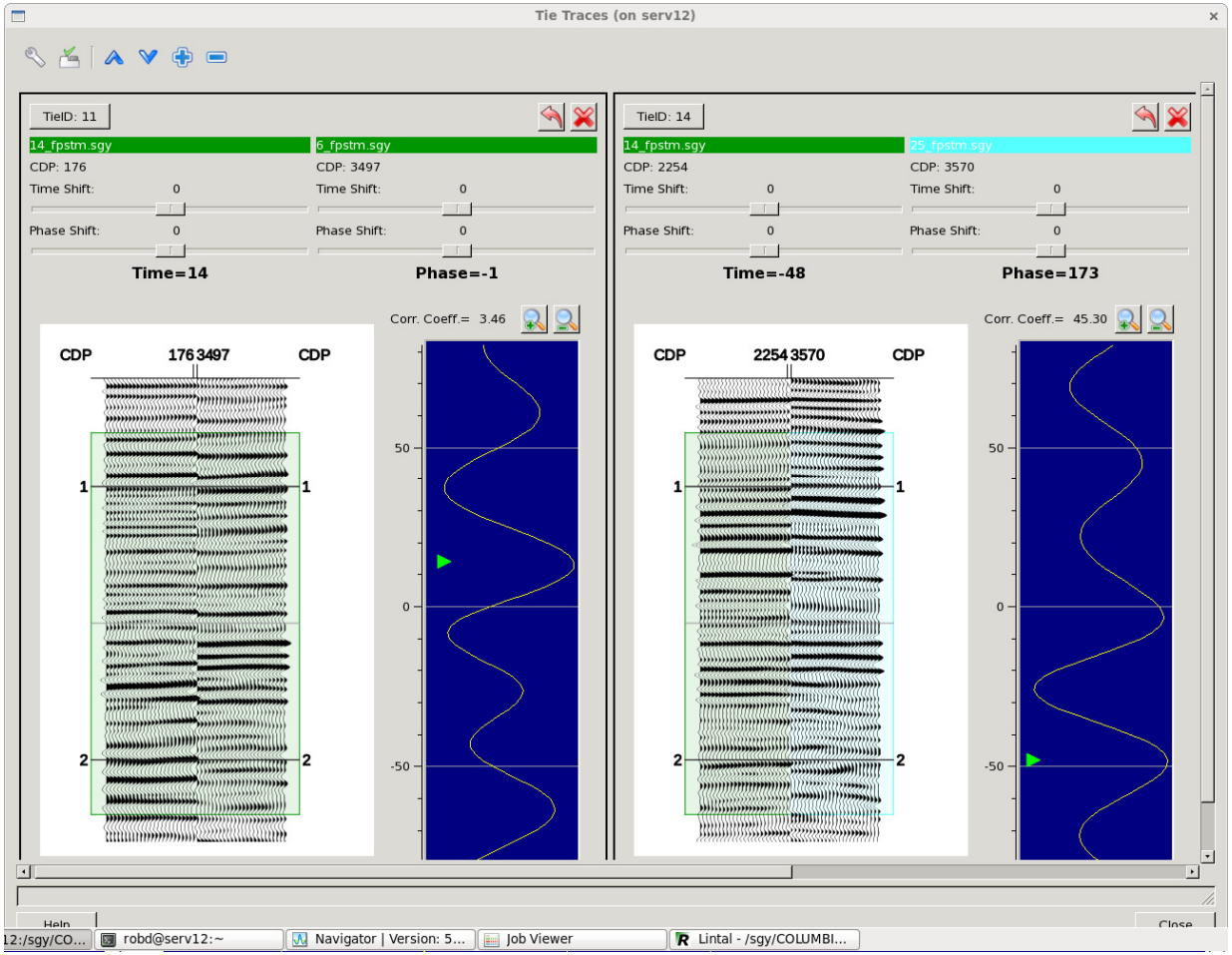

Line 36 Ties with Lines 22 and 5

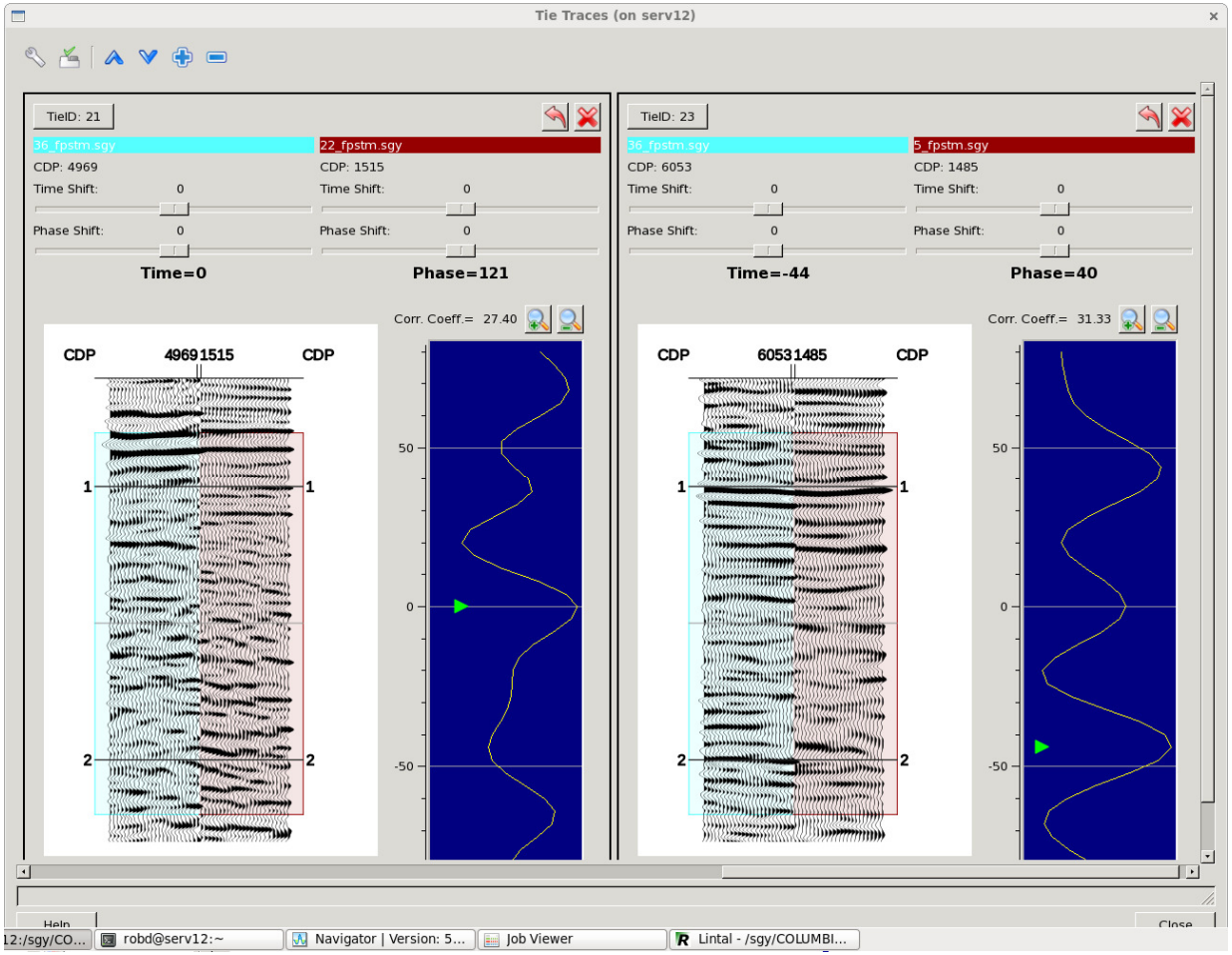

absolute IMAGING

Line 36 Ties with Lines 24 and 23

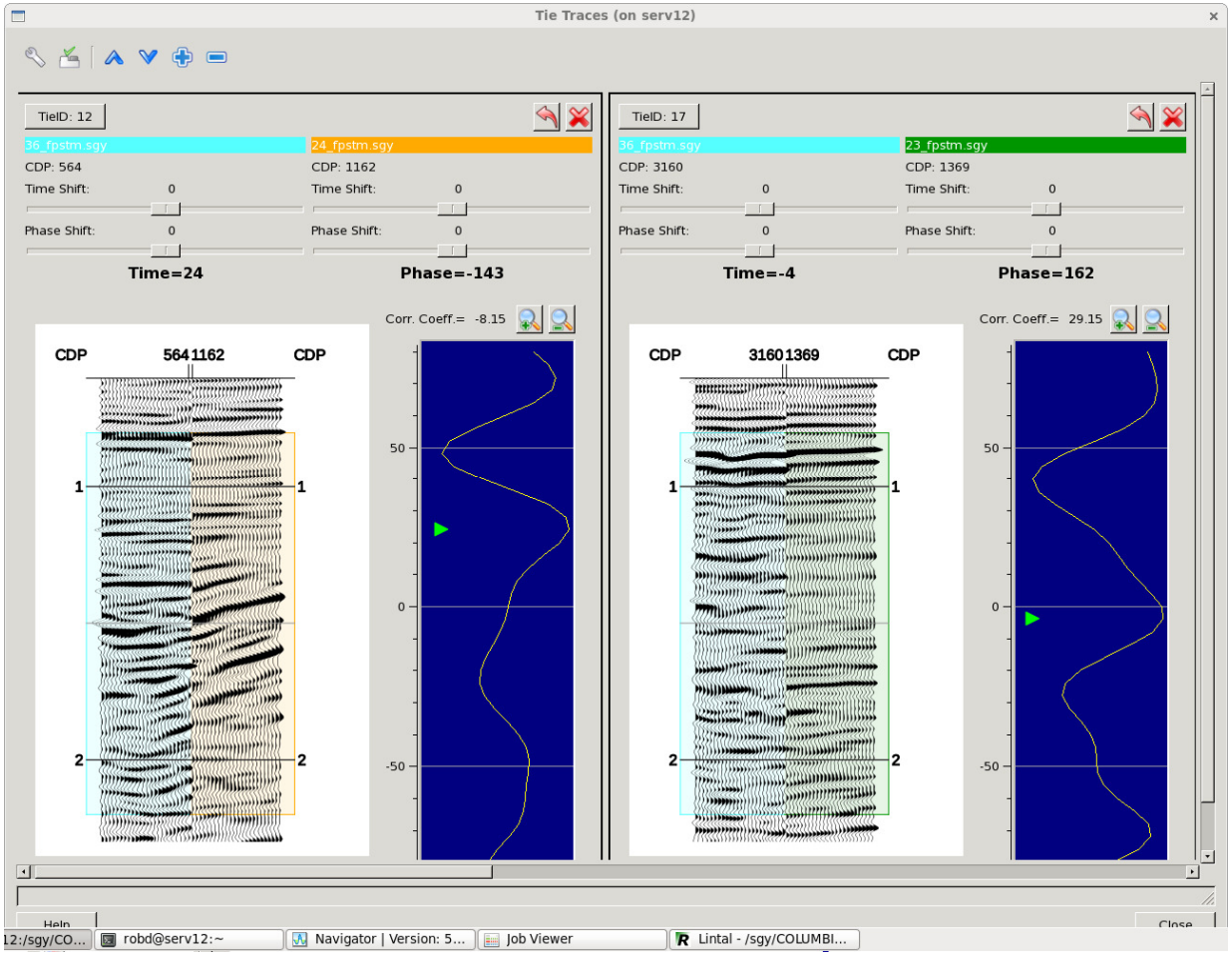

absolute IMAGING

Line 33 Ties with Lines 1 and 19

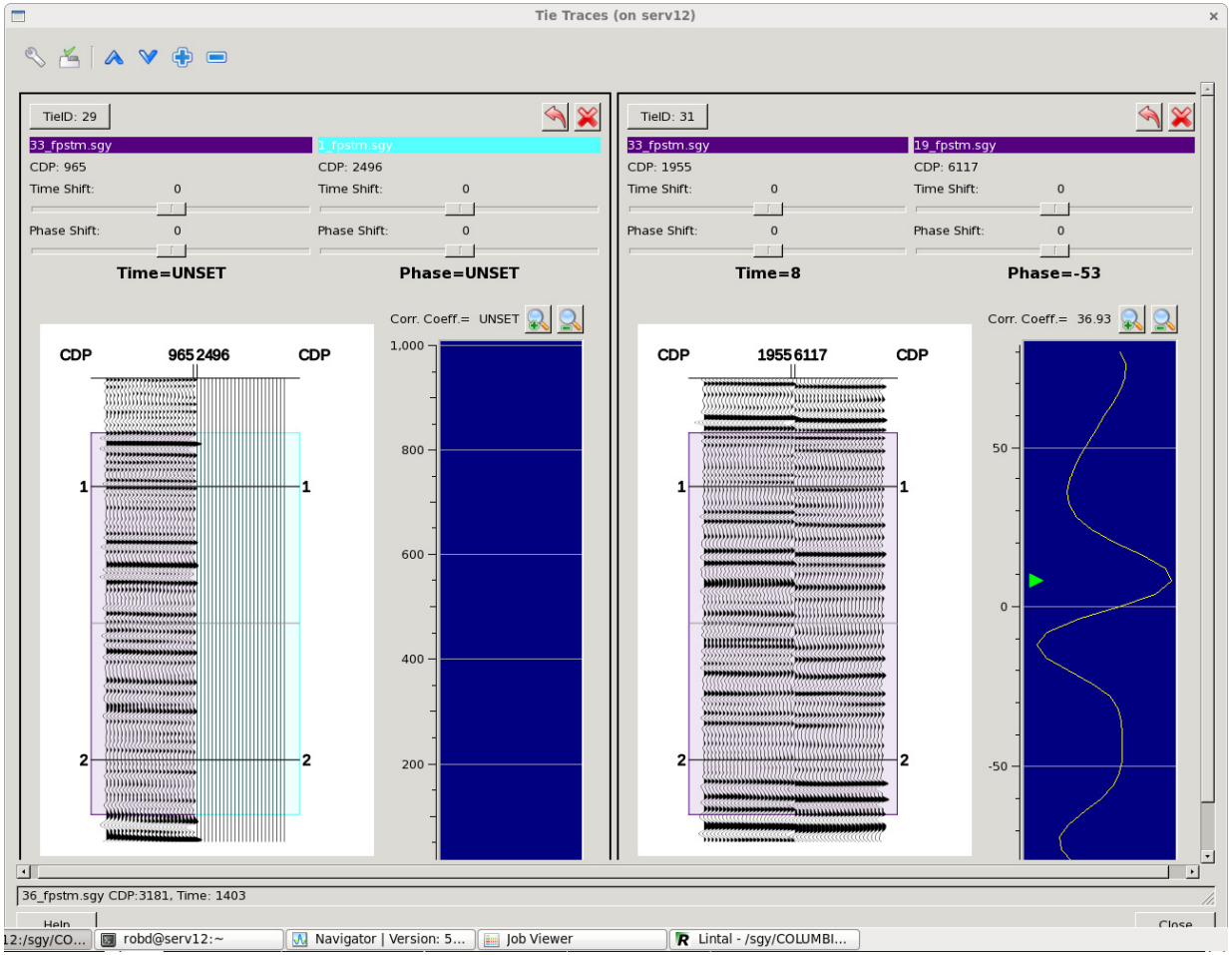

Contact Information

Absolute Imaging Inc.
Suite 400, 1011 – 1st Street SW
Calgary, AB, T2R 1J2
www.absoluteimaging.ca

Elvis Floreani, P. Geoph.
Principal | President
403.209.6851
elvis@absoluteimaging.ca

Nick Nikic
Manager, Marine Processing & Depth Imaging
1.403.806.6371
nick@absoluteimaging.ca

Daniel Wang
Special Project Geophysicist
403.806.6738
daniel@absoluteimaging.ca

Robert Dack
Senior Processing Geophysicist
403.817.2098
robd@absoluteimaging.ca

Absolute Imaging: Seismic Processing Summary

Contents

Client:	Columbia University
Area:	New York,USA
Disc:	ftp
AI Project:	1615
Disc Format:	ISO 9660
Data Format:	SEGY, IBM 32 bit floating point
Data Type:	Pre Stack Time Migration
Data Length:	7 sec
Sample Interval:	4 ms
Time of 1st Sample:	0
Location:	UTM Zone: 19 NAD: 83
Processed by:	Absolute Imaging Inc. September 2016

Line Number	Shotpoint Range	CDP Range	Live CDP#
1	101.0 - 1850.0	1 - 3388	3097
2	101.0 - 1860.0	1 - 3515	2529
5	185.0 - 1750.0	1 - 6386	6374
8	151.0 - 1310.0	1 - 4717	2929
19	101.0 - 4400.0	2 - 8547	8546
20	1780.0 - 4875.0	3339 - 9561	6223
21	210.0 - 2480.0	26 - 4639	4614
23	361.0 - 3501.0	25 - 6358	6334
24	487.0 - 3558.0	1 - 6197	6068
25	430.0 - 6-50.0	1 - 11423	11423
33	769.0 - 3879.0	1 - 4295	4295
36	67.0 - 6499.0	1 - 6408	6408

BYTE LOCATIONS:

SP	Byte 17-20
CDP	Byte 21-24
UTMX	Byte 73-76
UTMY	Byte 77-80

Directory Structure	Stack Types
\1615- New York	
\fpstm	Filtered/Scaled Pre Stack Time Migration
\pstm	Pre Stack Time Migration
\stk	Structure Stack
\pstm_rms	Pre Stack Time Migration RMS Velocities
\pstm_int	Pre Stack Time Migration Interval Velocities
\pstm_gathers	Pre Stack Time Migration gathers

Attachment F: Task 4 Topical Report – Task 4 Hydrologic Properties Data Package Report

Please note – the Task 4 Topical Report references the following Appendices within the Report. Only appendices D and E are included in this PDF. Appendices A-C, F-H are all Excel Files and can be found on the EDX Website.

Appendix A: DGS OCS Repository Inventory Spreadsheet
Appendix B: Hydrologic Properties Data Spreadsheet
Appendix C: Samples and Analyses Summary Spreadsheet
Appendix D: Core Hydro Properties Analysis Report from Core Labs
Appendix E: Petrographic Analysis Report from Pennsylvania Geological Survey
Appendix F: XRF Analysis Report from Pennsylvania Geological Survey
Appendix G: XRD Analysis Report from Pennsylvania Geological Survey
Appendix H: SEM-EDS Analysis Report from Pennsylvania Geological Survey

Mid-Atlantic U.S. Offshore Carbon Storage Resource Assessment Project

Task 4 Hydrologic Properties Data Package Report

MID-ATLANTIC U.S. OFFSHORE
CARBON STORAGE RESOURCE
ASSESSMENT PROJECT

DOE Award Number DE-FE0026087

Prepared by:
Battelle
505 King Avenue
Columbus, OH 43201
Principal Investigator: Dr. Neeraj Gupta
Project Manager: Ms. Lydia Cumming

Prepared for:
The U.S. Department of Energy
National Energy Technology Laboratory
Project Manager: Mr. William O'Dowd

April 30, 2018

Disclaimer

Acknowledgments

This material is based upon work supported by the Department of Energy under Award Number DE-FE0026087. The Project Team is led by Battelle and includes the state geological surveys of Delaware, Maryland, and Pennsylvania; United States Geological Survey (USGS); Lamont-Doherty Earth Observatory at Columbia University (LDEO); and Rutgers University. Harvard University, Texas Bureau of Economic Geology, and Virginia Department of Mines, Minerals, & Energy serve as technical advisors.

Dr. Neeraj Gupta was the Battelle Principal Investigator for the Mid-Atlantic U.S. Offshore Carbon Storage Resource Assessment Project and Ms. Lydia Cumming provided project management and technical coordination between team members. Drs. Peter McLaughlin and Mojisola KunleDare at the Delaware Geological Survey were responsible for coordinating and implementing the work completed for the Task 4 report. These Task 4 report authors are especially thankful for support relating to Task 4, including: the sample analysis and well log digitization efforts led by Ms. Kristin Carter and Mr. Brian Dunst at the Pennsylvania Geological Survey and management of the ArcGIS online database by Mr. Andrew Stanley and Mr. David Andreasen at the Maryland Geological Survey. Project team members also contributing to this report included Dr. Stephen Shank (Pennsylvania Geological Survey), Ms. Kimberly Baldwin and Mr. William Schmelz (Rutgers) and Mr. Andrew Burchwell, Ms. Isis Fukai, and Mr. Joel Sminchak (Battelle).

Table of Contents

List of Tables

Page

List of Figures

Page

List of Appendices

The following appendices are contained in a separate file (**Task 4 Report Appendices.ZIP**) submitted as part of the data package report

Appendix A: DGS OCS Repository Inventory Spreadsheet
Appendix B: Hydrologic Properties Data Spreadsheet
Appendix C: Samples and Analyses Summary Spreadsheet
Appendix D: Core Hydro Properties Analysis Report from Core Labs
Appendix E: Petrographic Analysis Report from Pennsylvania Geological Survey
Appendix F: XRF Analysis Report from Pennsylvania Geological Survey
Appendix G: XRD Analysis Report from Pennsylvania Geological Survey
Appendix H: SEM-EDS Analysis Report from Pennsylvania Geological Survey

Acronyms & Abbreviations

AMCOR	Atlantic Margin Coring
BCT	Baltimore Canyon Trough
BOEM	Bureau of Ocean Energy Management
CO_2	Carbon dioxide
COST	Continental Offshore Stratigraphic Test
DGS	Delaware Geological Survey
EDS	Energy Dispersive X-ray Spectroscopy
GBB	George's Bank Basin
IOPD	Integrated Ocean Drilling Program
LDEO	Lamont-Doherty Earth Observatory
MAOCSRAP	Mid-Atlantic Offshore Carbon Storage Resource Assessment Project
MMS	Minerals Management Service
NPHI	Neutron Porosity
OCS	Outer Continental Shelf
ODP	Ocean Drilling Program
PaGS	Pennsylvania Geological Survey
RHOB	Bulk Density
SEM	Scanning Electron Microscopy
USGS	United States Geological Society
XRD	X-ray Diffraction
XRF	X-ray Fluorescence

Executive Summary

The Mid-Atlantic U.S. Offshore Carbon Storage Resource Assessment Project (FE0026087) is part of the U.S. Department of Energy (U.S. DOE) National Energy Technology Laboratory's (NETL) Carbon Storage program to improve the effectiveness and reduce the costs of carbon dioxide (CO_2) storage implementation. The objectives of the Mid-Atlantic U.S. Offshore Carbon Storage Resource Assessment Project are to (1) complete a systematic carbon storage resource assessment of the offshore mid-Atlantic coastal region from the Georges Bank Basin (GBB) through the Long Island Platform to the southern Baltimore Canyon Trough (BCT), (2) define key input parameters to reduce uncertainty for offshore resource assessment and efficiency estimates, (3) examine risk factors, and (4) engage industry and regulatory stakeholders through development of a road map to assist future project planning and implementation.

This report presents a summary of the hydrogeological data package for the Mid-Atlantic U.S. Offshore Carbon Storage Resource Assessment Project study area. The data package includes geotechnical information on the deep wells in the offshore that penetrate the Cretaceous or deeper formations. The database will be used to calculate carbon storage resources by defining the extent and boundaries between stratigraphic and flow units and estimating the properties of the rocks within these layers.

The data compilation effort involved reviewing publicly available data and records. A significant effort was made to create electronic version of paper logs, well reports, and core laboratory reports. An item-by-item inventory was carried out in the DGS Atlantic OCS Sample Repository to identify specific samples at specific depths available for analysis. A team of DGS workers assessed the entire collection of available materials and created an updated Excel-spreadsheet inventory of boxes and containers in the collection. This assessment was followed by a detailed inventory of each item in the boxes; every core section, envelope or bag of cuttings samples, microscope slide, and prepared sample residue was logged into the detailed Excel-spreadsheet inventory. The inventory effort took approximately 18 months, from January 2016 through June 2017. Information was tabulated in a database summarizing the well API number, location, logging data, depths, and available sample data. This database will facilitate the integration of total porosity curves for each well generated from logs with core data for calculating petrophysical properties to be used in storage resource calculations.

The review of the geological data compiled from the 44 exploratory wells located within the study area helps provide an understanding of the nature of the rock units in the offshore. The model boundaries will be limited by the availability of data. The wells were drilled in the 1970s and 1980s, and the quality and quantity of data varies. Also, the wells are not evenly distributed in the study area. Consequently, areas up to several hundred square miles have no data points. The seismic data evaluation task, which is being conducted in parallel, is defining sequence boundaries that will help extend the units identified in the wells to areas without well coverage.

1.0 Introduction

1.1 Project Overview

The objectives of the Mid-Atlantic U.S. Offshore Carbon Storage Resource Assessment Project are to (1) complete a systematic carbon storage resource assessment of the offshore mid-Atlantic coastal region from the Georges Bank Basin (GBB) through the Long Island Platform to the southern Baltimore Canyon Trough (BCT), (2) define key input parameters to reduce uncertainty for offshore resource assessment and efficiency estimates, (3) examine risk factors, and (4) engage industry and regulatory stakeholders through development of a road map to assist future project planning and implementation. The Project Team will establish a regional framework for offshore geologic carbon dioxide (CO_2) storage by accomplishing the following tasks:

- Define the geologic characteristics of candidate storage zones and caprocks (Task 2)
- Use seismic data to better define the continuity of storage zones and caprocks (Task 3)
- Catalog the hydrologic properties of mid-Atlantic offshore formations (Task 4)
- Determine appropriate efficiency parameters that will represent the net effective pore volume and Prospective Storage Resource specific to offshore lithologies (Task 5)
- Examine risk factors related to offshore storage (Task 6)
- Communicate with industry and other stakeholders about the future prospects for offshore storage in the mid-Atlantic (Task 7)
- Ensure that results and lessons learned are transferred to industry and other stakeholders (Task 8)

This study will gather and integrate data from a wide variety of sources, including geologic samples from research boreholes, Continental Offshore Stratigraphic Test (COST) wells, and petroleum exploration wells in four regions: (1) the GBB; (2) the BCT; (3) the Long Island Platform; and 4) onshore coastal plain studies to provide analog data.

The offshore Mid-Atlantic study area encompasses 170,000 square kilometers (km^2) along the Mid-Atlantic States of Virginia, Maryland, Delaware, New York, New Jersey, and Pennsylvania (Figure 1). The project study area consists of three major subregions: GBB, Long Island Platform, and BCT. The project study area extends from within 10 km to 300 km offshore, encompassing the outer continental shelf and portions of the continental slope. Water depths in the mid-Atlantic continental shelf grade gently from zero depth along the shoreline to depths of 100 to 200 meters (m) at the continental slope. Along the continental slope, water depths plunge more than 2,000 m into the North American Basin.

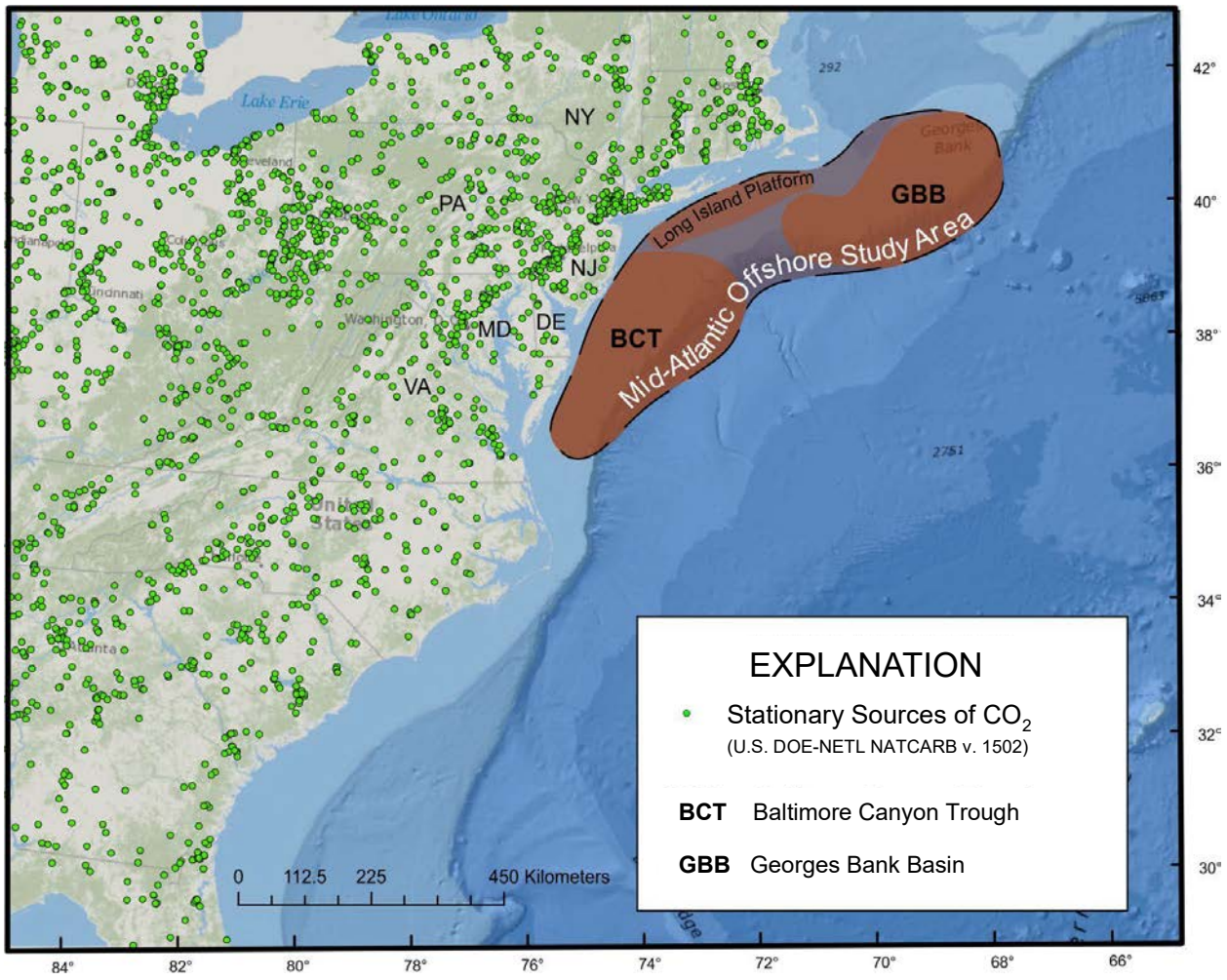

Figure 1. Map of the study area and large point sources of CO_2.

A number of oil and gas companies as well as the COST, the United States Geological Survey (USGS) Atlantic Margin Coring (AMCOR) project, the Ocean Drilling Program (ODP), and the Integrated Ocean Drilling Program (IODP) have drilled this area. A large amount of data, including wireline logs, cores, cuttings, and seismic surveys, was collected, and much of it is available for additional study. Previous work indicates that several sandstone formations in this region have porosities greater than 25% and permeabilities greater than 100 millidarcies (mD). This suggests an extremely large capacity for potential storage of CO_2.

1.2 Hydrologic Properties: Objectives and Approach

The objective of the hydrologic property analysis conducted for this project was to assemble a comprehensive dataset from mid-Atlantic Outer Continental Shelf (OCS) wells that will support two of the project's main goals: to assess pore space available for CO_2 storage and to characterize potential storage zones and confining caprocks. This task involved compiling information on all available existing samples and data, as well as generating new data from new laboratory analyses.

Analysis of hydrologic properties requires data on lithology, mineralogy, porosity, and permeability derived from sample analyses and geophysical logs. The project team first identified all available, relevant existing well samples and data, most of which are housed at the

Delaware Geological Survey (DGS) OCS Sample Repository. Following this review, a comprehensive inventory was made of the sample materials at the DGS. Next, an inventory was made of relevant reports and publications that contain reservoir quality data for the mid-Atlantic OCS wells drilled in the 1970s and 1980s. Those legacy reservoir data were compiled in a database that facilitates hydrologic characterization and resource assessment of OCS formations of interest. With the data compiled, gaps in existing data coverage were identified in intervals of interest; additionally, legacy data points with notable hydrologic properties (i.e., very high permeability) were identified as candidates for validation. Finally, sample materials were selected from the data gaps and validation candidates and sent to vendor and partner laboratories for analysis of hydrologic properties and composition.

The data inventory work was complemented by an inventory of geophysical logs available from the mid-Atlantic OCS wells. This effort involved comparing existing digitized log files to scanned logs available from the Bureau of Ocean Energy Management (BOEM) and to logs available on paper and microfilm in the DGS OCS repository. Key log types were digitized from each well. The digitized logs allow for calibration of geophysical log data with rock-core-based hydrologic property data, as well as for stratigraphic analysis and well-log correlation.

2.0 Hydrologic Properties: Data Collection and Compilation

The collection of existing hydrologic property data was focused on samples and reports housed at the DGS OCS Sample Repository. This task involved compiling information on all available existing samples and data and generating new data from new laboratory analyses. The collection inventory work included compilation of the type, number, stratigraphic and spatial distribution of cores, cuttings, and prepared sample materials. The collection of legacy hydrologic property data included mining of proprietary and published reports in DGS files as well as public records and the literature. Details of the data collection effort are explained below in Sections 2.1 and 2.2.

2.1 DGS OCS Sample Collection Inventory

A detailed inventory of the DGS Atlantic OCS Sample Repository collection was carried out to identify specific materials available for this study. The DGS Atlantic OCS sample collection represents an agglomeration of numerous samples from wells drilled on the U.S. Atlantic OCS between 1975 and 1984; these samples exist in a variety of states of organization and preservation. The collection includes raw samples such as cores, washed cuttings, and unwashed cuttings, as well as prepared sample materials such as thin sections and micropaleontologic slides.

2.1.1 Inventory Methods

An item-by-item inventory was carried out in the DGS Atlantic OCS Sample Repository to identify specific samples at specific depths available for analysis. A team of DGS workers assessed the entire collection of available materials and created an updated Excel-spreadsheet inventory of boxes and containers in the collection. This assessment was followed by a detailed inventory of each item in the boxes; every core section, envelope or bag of cuttings samples, microscope slide (thin section and micropaleontology), and prepared sample residue (micropaleontology and geochemical) was logged into the detailed Excel-spreadsheet inventory. The inventory effort took approximately 18 months, from January 2016 through June 2017, with between one and four staff members working on it at any time during this period.

The inventory work also allowed for an assessment of the condition of the samples. Materials in deteriorating packaging and most immediately at risk were repackaged to ensure sample integrity for analytical work.

The sample inventory is tabulated in a master spreadsheet file composed of numerous worksheets that contain summary data and detailed inventories for each class of sample material. The inventory spreadsheets are maintained on the online file-sharing platform Box. Throughout the project, the inventories were updated to account for sample loans and new prepared sample returns resulting from those loans. A copy of the repository inventory spreadsheet can be found in Appendix A.

2.1.2 Inventory Results

The extensive inventory effort made for this project has resulted in a highly detailed, comprehensive listing of every item for each sample type in the collection. The total number of

inventoried items potentially applicable to this project is approximately 100,000. Table 1 summarizes the numbers of the most relevant sample types.

Of most importance are the core samples, which allow precisely located analyses of hydrologic properties and composition in potential storage and sealing units. Core sample types in the collection include large core slabs as well as smaller slices and chips taken from the cores. The number of core chips in the collection is large, totaling more than 1,700.

Cuttings are the most numerous sample type in the collection (mostly washed but many unwashed as well). More than 76,000 individual washed cuttings sample envelopes and bags were inventoried. The coverage of washed cuttings from the OCS wells is extensive, but these materials have the disadvantage of being composed of smaller pieces and commonly suffering from some degree of mixing of materials from outside designated depth range of a sample. They are expected to be less useful for analysis of hydrologic properties than the cores.

2.2 OCS Existing Data Compilation

A significant “data mining” effort was undertaken to obtain existing relevant geologic data from public records, published reports, and the literature. These data were generated during and shortly after the exploratory drilling in the Atlantic OCS in the 1970s and 1980s to evaluate the petroleum geology associated with the exploration targets. These data were compiled for this project to characterize important physical properties of the CO_2 storage reservoirs and caprock formations. A complete inventory was essential both to assess available hydrologic property data for the Atlantic OCS wells and to identify data gaps where additional analyses may be warranted.

Table 1. Summary of physical samples available for this study at the DGS OCS sample repository.

Project area	Well name	Washed cutting	SWC	Conventional core			Thin sections		
				Chip	Slab	Slice	Cutting	SWC	Conv. cores
Georges Bank	Conoco 145-1	1373			9		98		27
Baltimore Canyon	Conoco 590-1	1126					123		
Baltimore Canyon	COST B-2	3690		84	8		100		27
Baltimore Canyon	COST B-3	2427	44	130	11	114	86	72	88
Georges Bank	COST G-1	2868	37	16	23		59	56	45
Georges Bank	COST G-2	4129		25	80		129	55	394
Georges Bank	Exxon 133-1	1560		73			114		
Baltimore Canyon	Exxon 500-1	812					125	2	
Baltimore Canyon	Exxon 599-1	1905		70			105		
Baltimore Canyon	Exxon 684-1	1935		509			107		
Baltimore Canyon	Exxon 684-2	1742		7			82	28	13
Baltimore Canyon	Exxon 728-1	1595					78		

Table 1 (cont.). Summary of physical samples available for this study at the DGS OCS sample repository.

Project area	Well name	Washed cutting	SWC	Conventional core			Thin sections		
				Chip	Slab	Slice	Cutting	SWC	Conv. cores
Baltimore Canyon	Exxon 902-1	1017		29			82	37	13
Georges Bank	Exxon 975-1	1532		15			185		4
Baltimore Canyon	Gulf 718-1	1369					56		
Baltimore Canyon	Gulf 857-1	996					82	110	
Baltimore Canyon	Homco 676-1	1430					67		
Baltimore Canyon	Homco 855-1	1589					90		
Baltimore Canyon	Mobil 17-1	1656							
Baltimore Canyon	Mobil 17-2	250	76				73		
Georges Bank	Mobil 273-1	1399					111		
Georges Bank	Mobil 312-1	1953					142		
Baltimore Canyon	Mobil 544-1	1826	96				94		
Baltimore Canyon	Mobil 544-2	476							
Baltimore Canyon	Murphy 106-1	2096					123		
Baltimore Canyon	Shell 272-1	1338					79		
Baltimore Canyon	Shell 273-1	2662	24	45			89		
Georges Bank	Shell 357-1	1982					144		
Baltimore Canyon	Shell 372-1	451		41			17		40
Georges Bank	Shell 410-1	1698					141		
Baltimore Canyon	Shell 586-1	2749		10	11	41	47		51
Baltimore Canyon	Shell 587-1	1810		30	5	37	34		38
Baltimore Canyon	Shell 632-1	1077		17			91		
Baltimore Canyon	Shell 93-1	1227		55			98		
Georges Bank	Tenneco 187-1	2016					133		
Baltimore Canyon	Tenneco 495-1	2217					118		

Table 1 (cont.). Summary of physical samples available for this study at the DGS OCS sample repository.

Project area	Well name	Washed cutting	SWC	Conventional core			Thin sections		
				Chip	Slab	Slice	Cutting	SWC	Conv. cores
Baltimore Canyon	Tenneco 642-3	1844					90		
Baltimore Canyon	Texaco 598-1	1519		140			32		
Baltimore Canyon	Texaco 598-2	2173					88		
Baltimore Canyon	Texaco 598-3	1242					100		
Baltimore Canyon	Texaco 598-4	1608					87		
Baltimore Canyon	Texaco 642-1	1386		421			52		
	TOTALS	76146	277	1717	147	192	3933	416	904

SWC = sidewall core; Conv. core = conventional core.

2.2.1 Data Compilation Methods

The data mining effort was a major task. Mining of the legacy data was led by DGS staff and conducted in collaboration with staff from Battelle, the Maryland Geological Survey, and the Pennsylvania Geological Survey (PaGS). The project team searched files and literature for relevant reservoir-related data on the petroleum geology of the Atlantic OCS wells. Numerous reports and publications were identified and collected from a number of sources, including hard copies of proprietary reports in DGS files, microfilm copies of reports available at the DGS, digital copies (PDF) of reports available from the Minerals Management Service (MMS), government publications (USGS, MMS), and open literature. Sample descriptions and porosity, permeability, mineralogical, and stratigraphic data were compiled into a master spreadsheet of hydrologic properties and subjected to quality control checks by the team.

2.2.2 Data Compilation Results

The data mining effort resulted in the compilation of a master spreadsheet of hydrologic properties records from more than 9,000 individual sample/observation depths in 42 wells. These data were compiled in an Access database and derivative Excel spreadsheets and are provided in Appendix B of this report. The hydrologic property database includes more than 4,800 porosity measurements and more than 4,200 permeability measurements within the defined interval of interest for this study for hydrologic properties, between the top of the Dawson Canyon unit and the bottom of the Mohawk unit (Table 2).

A close review of the data reveals a number of values that are somewhat anomalous compared to other values in the same intervals. Cases where permeability values are unusually high are of special interest. These data points were highlighted for possible verification to determine whether the data are reproducible. Damaged sample materials, poor analytical work, and/or outdated techniques are other possible sources of data quality problems to be considered. In addition, evaluation of the distribution of the data can reveal “data gaps” in intervals of potential interest for carbon storage where additional analyses may be warranted. These cases are considered further in Section 3.

Table 2. Summary of counts of mined legacy hydrologic data in the stratigraphic interval of interest (Dawson Canyon to Mohawk).

Project area	Well name	Porosity count	Permeability count
Baltimore Canyon	Conoco 590-1	69	69
Baltimore Canyon	COST B-2	418	267
Baltimore Canyon	COST B-3	183	154
Baltimore Canyon	Exxon 500-1	65	65
Baltimore Canyon	Exxon 599-1	196	196
Baltimore Canyon	Exxon 684-1	562	562
Baltimore Canyon	Exxon 684-2	163	163
Baltimore Canyon	Exxon 728-1	18	18
Baltimore Canyon	Exxon 816-1	63	63
Baltimore Canyon	Exxon 902-1	81	81
Baltimore Canyon	Gulf 718-1	35	35
Baltimore Canyon	Gulf 857-1	60	60
Baltimore Canyon	Homco 676-1	5	5
Baltimore Canyon	Homco 855-1	57	57
Baltimore Canyon	Mobil 17-2	16	16
Baltimore Canyon	Mobil 544-1	176	163
Baltimore Canyon	Murphy 106-1	117	114
Baltimore Canyon	Shell 272-1	134	134
Baltimore Canyon	Shell 273-1	350	320
Baltimore Canyon	Shell 372-1	149	101
Baltimore Canyon	Shell 586-1	127	99
Baltimore Canyon	Shell 587-1	105	97
Baltimore Canyon	Shell 632-1	202	202
Baltimore Canyon	Shell 93-1	8	1
Baltimore Canyon	Tenneco 495-1	70	70
Baltimore Canyon	Tenneco 642-2	169	107
Baltimore Canyon	Tenneco 642-3	202	202
Baltimore Canyon	Texaco 598-1	90	90
Baltimore Canyon	Texaco 598-2	33	33
Baltimore Canyon	Texaco 598-3	129	129
Baltimore Canyon	Texaco 598-4	129	129
Baltimore Canyon	Texaco 642-1	108	108
Georges Bank	Conoco 145-1	53	36
Georges Bank	COST G-1	138	125
Georges Bank	COST G-2	153	140
Georges Bank	Exxon 133-1	11	2
Georges Bank	Exxon 975-1	65	9
Georges Bank	Mobil 273-1	25	
Georges Bank	Mobil 312-1	25	
Georges Bank	Shell 357-1	33	
Georges Bank	Shell 410-1	4	
Georges Bank	Tenneco 187-1	24	1
	TOTALS	**4820**	**4223**

3.0 Sample Selection

The distribution of available data on rock properties and hydrologic characteristics was analyzed in detail to find data gaps (where no data are available) and to identify existing data where verification or calibration would be beneficial. These intervals of interest were identified as potential targets for new sample analyses. The availability of sample materials in these data gaps was assessed using a series of data queries in Microsoft Access and Microsoft Excel as well as graphically by viewing plots of data versus well logs in Petra®.

3.1 Data Gap Assessment Methodology

Due to the large number of data line entries, repeatable automated approaches were used to identify data gaps. The DGS investigated and defined processes for applying Microsoft Access querying capabilities and Microsoft Excel sorting functions for the data gap analysis (Figure 2).

The data gap analysis involves three primary datasets: (1) hydrologic property data compiled from mining of well reports and publications; (2) stratigraphic picks for the wells that are used to frame the interval of interest (Task Set 2); and (3) a detailed item-by-item inventory of sample holdings in the DGS OCS Sample Repository. Three sets of tasks cross-reference these datasets, which are described below.

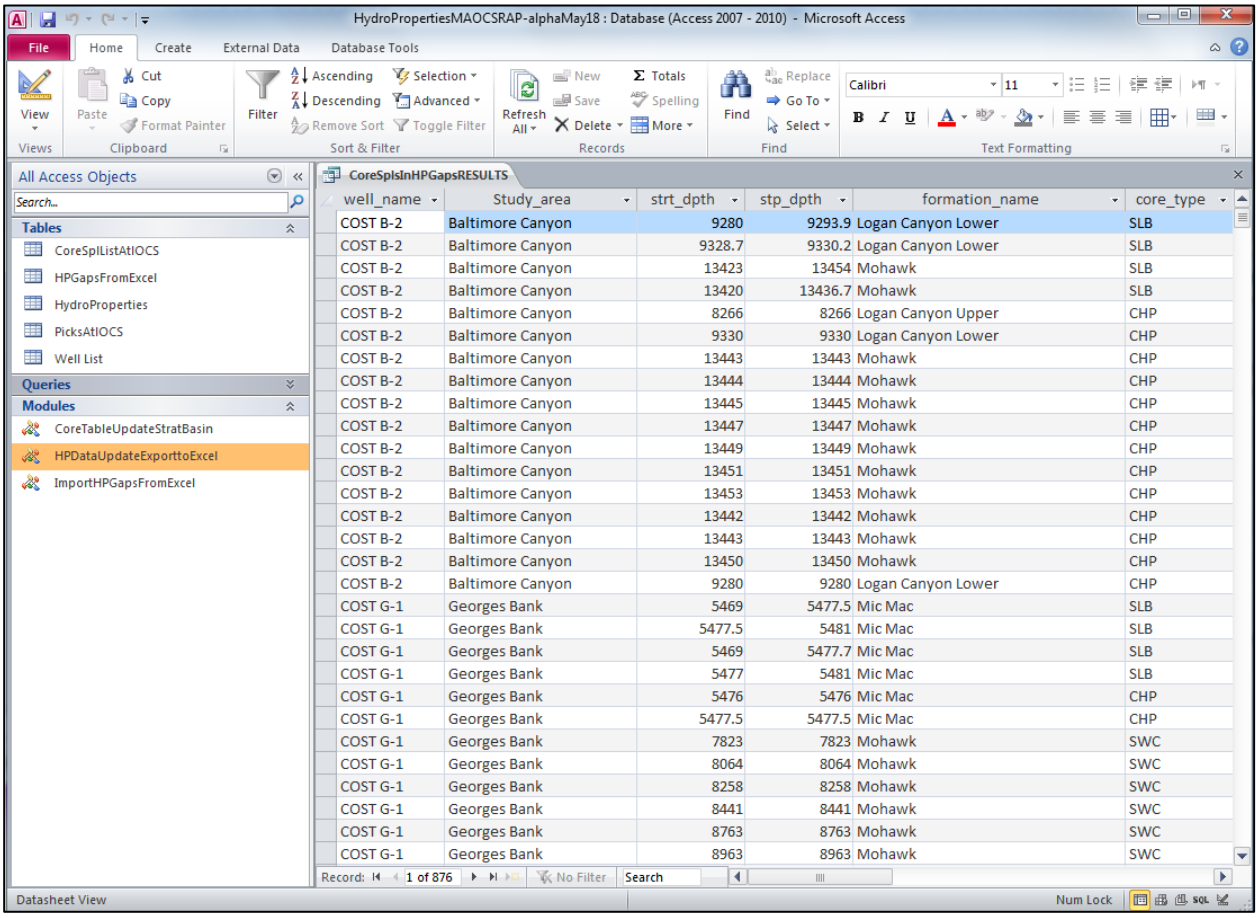

Figure 2. Screenshot of the Access database containing all compiled hydrogeologic sample data.

Task Set 1 utilizes Microsoft Access (and Microsoft Visual Basic for Applications code) to generate a list of compiled hydrologic property data (porosity, permeability, grain density) in the defined stratigraphic interval of interest for this project (Table 3). This is done (using the compiled hydrologic property data and stratigraphic picks data) by assigning each data point to its stratigraphic interval. The current definition of the interval of interest is between the top of the Dawson Canyon and the base of the Mohawk.

Task Set 2 utilizes Microsoft Excel (and Microsoft Visual Basic for Applications code) to analyze the distribution of hydrologic property data produced in Task Set 1 and create a list of gaps in the data coverage.

Task Set 3 utilizes Microsoft Access (and Microsoft Visual Basic for Applications code) to compare the data gaps identified in Task Set 2 to the itemized core sample inventory. Based on this comparison, a list of samples available for laboratory analyses was created to further evaluate porosity and/or permeability in the stratigraphic interval of interest (Table 3).

Table 3. Summary of counts and types of core samples available within data gaps in the stratigraphic interval of interest (Dawson Canyon to Mohawk).

Project area	Well name	Sample type	Interval of interest					
			Dawson Canyon	Logan Canyon	Naskapi	Mississauga	Mic Mac	Mohawk
Georges Bank Basin	COST G-1	CHIP					2	
		SLAB					4	
		SWC						7
		SLAB						4
Baltimore Canyon Trough	COST B-2	CHIP		3				10
		SLAB	2	2				2
	COST B-3	CHIP				2		14
		SLAB				1	1	2
		SLC				1		9
		SWC	3	4		4	2	18
	Exxon 684-1	CHIP					105	247
	Exxon 684-2	CHIP						1
	Mobil 17-2 [a]	SWC		5	1	4	27	15
	Mobil 544-1	SWC	6	24	1	9	5	10
	Shell 273-1	CHIP		1				
	Shell 586-1	SLAB		1			2	
		SLC		1			1	
	Shell 587-1	CHIP					1	
		SLAB		3			1	
		SLC		1			1	
	Shell 632-1	CHIP				1		
	Texaco 598-1	CHIP						7

SWC = sidewall core
a. Insufficient material remaining for routine analyses.

3.2 Sample Selection Methodology

The data gap analysis provided a basis for sample selection. The criteria for sample selection included the following requirements and decision factors:

Criterion 1. Fills a data gap (FG). Where possible, samples were selected to fill gaps in existing porosity, permeability, and grain density data.

Criterion 2. Helps to verify empirically derived permeability values (VE). Existing permeability data for sidewall cores may be verified by obtaining new measured values on corresponding conventional core samples and/or remaining sidewall core materials, where available.

Criterion 3. Helps to calibrate existing legacy data (LC). Samples were also selected to examine changes in permeability in the sample material over time and help calibrate porosity log data.

The DGS hosted three workshops to select samples for hydrologic property analyses based on these criteria. At these workshops, sampling strategies were discussed, sample priorities were determined, and cores were examined to make final sample selections. The first workshop, which focused on planning of sampling and analysis, was held on May 10, 2017. The sampling analysis plan was designed to evaluate hydrologic properties using several analytical methods on samples from the same depth. This allowed direct comparison of data obtained from different types of laboratory measurements and thin-section analysis.

During sampling workshops held on July 13 and July 31, 2017, the project team evaluated sample materials available in intervals targeted for new analyses. Conventional core slabs, chips, and slices and sidewall core samples were examined to determine if a sufficient quantity of the sample was available. A flow chart summarizing the selection criteria is shown in Figure 3. In total, 75 sample points from 17 wells were selected. A list of selected samples is presented in Table 4. Figures 4 and 5 show the location maps for wells from which samples were selected.

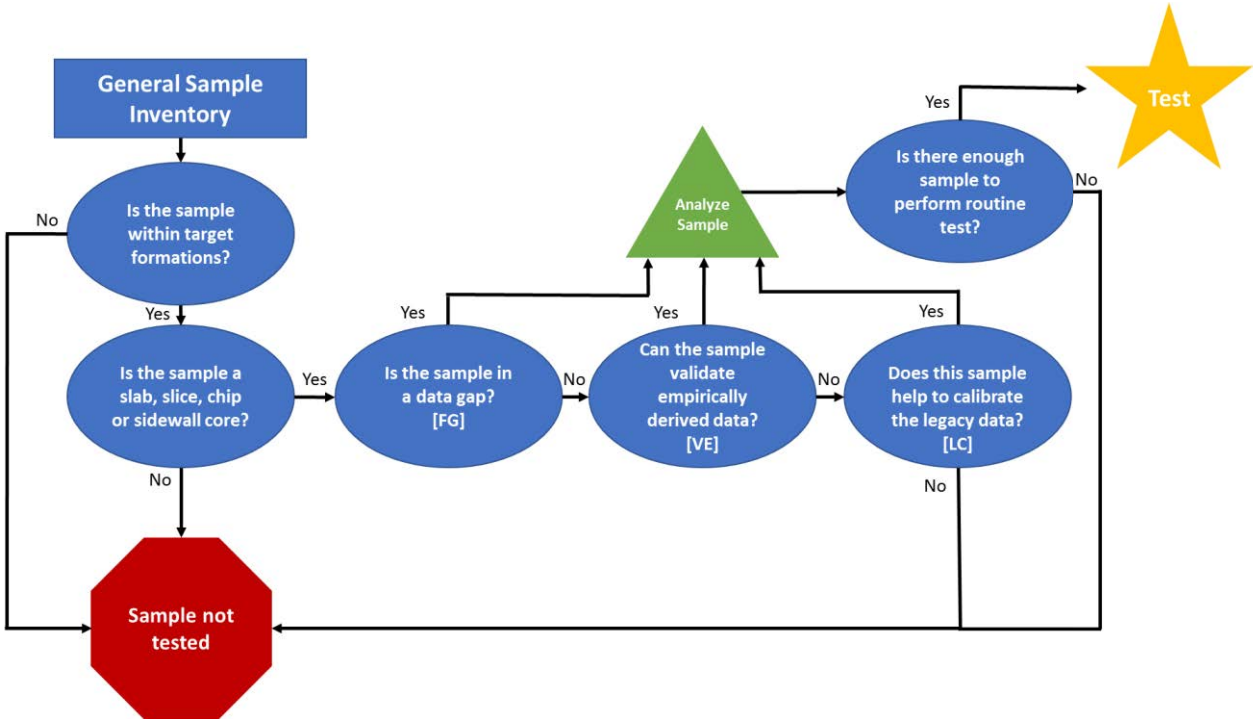

Figure 3. Flow chart for routine porosity, permeability, and grain density sample selection.

Table 4. Summary of samples selected for new hydrologic property analysis.

Study area	Well	Formation	Depth (ft)	Samples	Sample type	Selection criteria
BCT	COST B-2	Dawson Canyon	5030.2	5030-2a, 5030-2b	Slab	LC
BCT	COST B-2	Logan Canyon	8241	8241-1, 8241-2	Slab	LC
BCT	COST B-2	Logan Canyon	8244	8244	Slab	LC
BCT	COST B-2	Logan Canyon	8247	8247	Slab	LC
BCT	COST B-2	Logan Canyon	8250	8250	Slab	LC
BCT	COST B-2	Logan Canyon	8251.8	8251	Slab	LC
BCT	COST B-2	Logan Canyon	9286.5	9286	Slab	LC
BCT	COST B-2	Logan Canyon	9302	9302	Slab	LC
BCT	COST B-2	Logan Canyon	9305.4	9305-1	Slab	LC
BCT	COST B-2	Logan Canyon	9330.2	9330-2	Slab	LC
BCT	COST B-2	Logan Canyon	8239.5	8239, 8239-2	Slab	LC
BCT	COST B-2	Logan Canyon	8242	8242	Slab	LC
BCT	COST B-2	Logan Canyon	8249	8249	Slab	LC
BCT	COST B-2	Logan Canyon	9289.3	9289-1	Slab	LC
BCT	COST B-2	Logan Canyon	9304.4	9304-2	Slab	LC
BCT	COST B-3	Dawson Canyon	7640	7640	SWC	FG
BCT	COST B-3	Logan Canyon	8382	8382	SWC	FG
BCT	COST B-3	Logan Canyon	9750	9750	SWC	FG
BCT	COST B-3	Mississauga	9931.6	9931	Slab	VE
BCT	COST B-3	Mississauga	9932	9932	Slab	VE
BCT	COST B-3	Mississauga	11042	11042	Slab	VE
BCT	COST B-3	Mississauga	11050.8	11050-3	Slab	VE
BCT	COST B-3	Mississauga	11054	11054	Slab	VE
BCT	COST B-3	Dawson Canyon	6260	6260	SWC	FG
BCT	COST B-3	Dawson Canyon	7040	7040	SWC	FG
BCT	COST B-3	Mississauga	9934	9934	Slab	VE
BCT	COST B-3	Mic Mac	12581.9	12581.9	Slab	VE
GBB	COST G-1	Mississauga	5473	5473	Slab	VE
GBB	COST G-1	Mississauga	5480-5481	5480-1, 5480-2	Slab	VE
GBB	COST G-1	Mohawk	10001.3	10001-1, 10001-2	Slab	VE
GBB	COST G-1	Mississauga	5471	5471	Chip	VE
GBB	COST G-1	Mohawk	9992.8	9992, 9993	Slab	VE
GBB	COST G-2	Mohawk	8753.7	8753	Slab	VE, LC
GBB	COST G-2	Mohawk	8756	8756-1, 8756-2	Slab	VE, LC
BCT	Exxon 684-1	Naskapi	9438	9438	Chip	LC
BCT	Exxon 684-1	Naskapi	9439	9439	Chip	LC
BCT	Exxon 684-1	Mic Mac	12137	12137	Chip	LC
BCT	Exxon 684-1	Mic Mac	12199	12199	Chip	LC
BCT	Exxon 684-1	Mohawk	12767	12767	Chip	LC
BCT	Exxon 684-1	Mohawk	12802	12802	Chip	LC
BCT	Exxon 684-1	Naskapi	9440	9440	Chip	LC

Table 4 (cont.). Summary of samples selected for new hydrologic property analysis.

Study area	Well	Formation	Depth (ft)	Samples	Sample type	Selection criteria
BCT	**Exxon 684-1**	Naskapi	9441	9441	Chip	LC
BCT	**Exxon 684-1**	Mic Mac	12204	12204	Chip	LC
BCT	**Exxon 684-1**	Mohawk	12729	12729	Chip	LC
BCT	**Mobil 544-1**	Dawson Canyon	5211	5211	SWC	FG
BCT	**Mobil 544-1**	Dawson Canyon	5435	5435	SWC	FG
BCT	**Mobil 544-1**	Logan Canyon	5962	5962	SWC	FG
BCT	**Mobil 544-1**	Logan Canyon	6260	6260	SWC	FG
BCT	**Mobil 544-1**	Logan Canyon	6420	6420	SWC	FG
BCT	**Mobil 544-1**	Logan Canyon	6579	6579	SWC	FG
BCT	**Mobil 544-1**	Logan Canyon	6696	6696	SWC	FG
BCT	**Mobil 544-1**	Logan Canyon	6798	6798	SWC	FG
BCT	**Mobil 544-1**	Logan Canyon	7096	7096	SWC	FG
BCT	**Mobil 544-1**	Logan Canyon	7258	7258	SWC	FG
BCT	**Mobil 544-1**	Mississauga	8497	8497	SWC	FG
BCT	**Mobil 544-1**	Mississauga	9039	9039	SWC	LC
BCT	**Exxon 684-2**	Mohawk	15242	15242	Chip	VE, LC
BCT	**Shell 273-1**	Logan Canyon	7010	7010	Chip	VE, LC
BCT	**Shell 273-1**	Logan Canyon	7077	7077	Chip	VE, LC
BCT	**Shell 586-1**	Logan Canyon	9058-9058.7	9058-9058.7	Slab	VE, LC
BCT	**Shell 632-1**	Dawson Canyon	4594.5	4594.5	Chip	VE, LC
BCT	**Shell 632-1**	Logan Canyon	6278.8	6278.8	Chip	VE, LC
BCT	**Shell 632-1**	Mississauga	8083.1	8083.1	Chip	VE, LC
BCT	**Shell 93-1**	Mississauga	9937	9937	Chip	VE, LC
BCT	**Texaco 598-1**	Mohawk	12840.5	12480-12481	Chip	VE, LC
BCT	**Texaco 598-1**	Mohawk	13271-13272	13271-13272	Chip	VE, LC
BCT	**Texaco 598-1**	Mohawk	13275-13276	13275-13276	Chip	VE, LC
BCT	**Texaco 642-1**	Mic Mac	12444	12444	Chip	VE, LC
BCT	**Texaco 642-1**	Mohican / Iroquois	15608	15608	Chip	VE, LC
BCT	**Exxon 599-1**	Mohawk	12386.5	12386.5	Chip	VE, LC
BCT	**Exxon 599-1**	Mohawk	12403	12403	Chip	VE, LC
BCT	**Shell 372-1**	Logan Canyon	10872.9-10873.2	10872.9-10873.2	Chip	VE, LC
BCT	**Shell 587-1**	Logan Canyon	11554.9	11555	Slab	VE, LC
BCT	**Shell 587-1**	Logan Canyon	11555.2	11555	Slab	VE, LC
BCT	**Conoco 145-1**	Mohican / Iroquois	9226	9226	Slab	VE, LC

GBB = Georges Bank Basin, BCT = Baltimore Canyon Trough.
SWC = sidewall core.
FG = Fills data gap, VE= validates empirical data, LC= legacy data comparison.

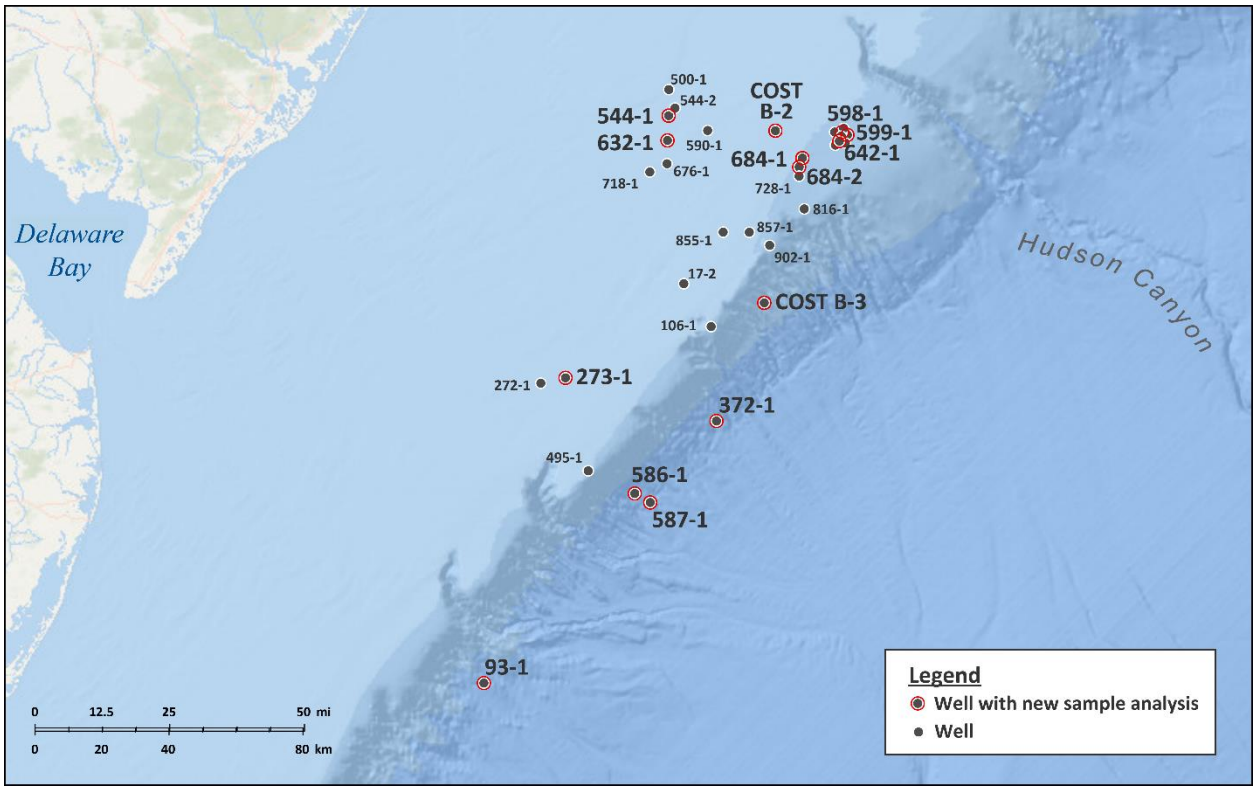

Figure 4. Wells with sample material for routine analyses in the BCT.

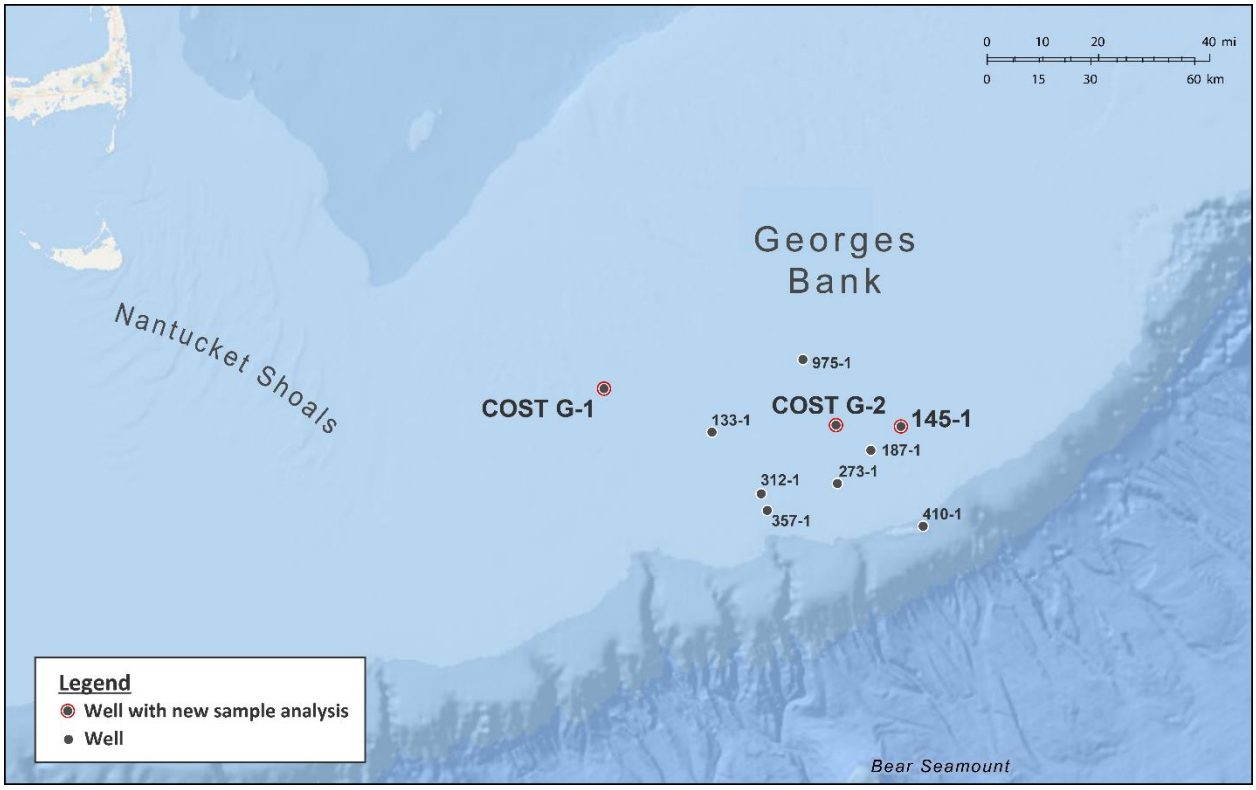

Figure 5. Wells with sample material for routine analyses in the GBB.

4.0 Laboratory Sample Analysis

This section describes the laboratory analyses conducted on sample materials from 17 wells in the mid-Atlantic OCS. Table 5 summarizes the analyses carried out for each well; the full list is presented in a Sample and Analyses Summary spreadsheet (Appendix C). A full compilation of the results discussed in this section can be found in Appendices D through H.

Table 5. Summary of new analyses by well.

Well name	Permeability		Porosity (plug)	Grain density (plug)	Thin section	XRF	XRD	SEM
	(probe)	(plug)						
Conoco 145-1					1	1	1	
COST B-2	17	15	15	15	18	15	17	5
COST B-3	12	6	6	6	13	13	13	4
COST G-1	8	4	4	4	7	5	6	2
COST G-2	3	2	2	2	2	2	2	
Exxon 599-1	2	1	1	1	3	4	3	
Exxon 684-1	10	4	4	4	10	10	8	4
Exxon 684-2	1	1	1	1	1	1		
Mobil 544-1	12	1	1	1	12	11	12	1
Shell 273-1	2				2	2	1	
Shell 372-1	2				2	1	1	
Shell 586-1	2	1	1	1	1	1	1	1
Shell 587-1	1				1	1	1	
Shell 632-1	3	1	1	1	3	3	3	
Shell 93-1	1				1	1	1	
Texaco 598-1	3	3	3	3	3	3	3	1
Texaco 642-1	2	1	1	1	2	2	2	
Totals	**81**	**40**	**40**	**40**	**82**	**76**	**75**	**18**

XRF = X-ray fluorescence; XRD = X-ray diffraction; SEM = scanning electron microscopy.

4.1 Laboratory Methods

Laboratory analyses included measurement of hydrologic properties and analysis of sample composition. The hydrologic properties of the selected sample materials were assessed by measuring porosity, permeability, and grain density. Thin sections were used to evaluate porosity and to identify the mineral composition of the selected samples. Three types of instrumental analyses were performed to identify and characterize the framework grains, matrix, cements and porosity properties: X-ray fluorescence (XRF), X-ray diffraction (XRD), and scanning electron microscopy (SEM). While the different techniques have strengths and limitations, they ultimately complement each other for a comprehensive characterization of sample materials. For example, the XRF only has a small (~8mm diameter) sample contact surface so only provides data for the point of analysis, whereas the XRD provides average mineralogical information on a powdered sample. However, the XRD cannot detect amorphous or poorly crystalline material, whereas the XRF can provide elemental composition of such materials. Additionally, SEM analysis provides information on the crystalline nature of minerals, pore space geometry, and cement conditions of the samples.

4.1.1 Hydrologic Property Measurements

Porosity, permeability, and grain density measurements were made by Core Laboratories of Houston, Texas, on the samples selected for analysis. Core Laboratories inspected the sample materials and cut core plugs in each sample deemed suitable at the best location considering sample condition. Core plugs could not be obtained for many samples due to small size or poor condition. Permeability measurements were made on all samples submitted using a Pressure-Decay Profile Permeameter. Exact probe permeability measurement points were selected at the laboratory based on the best sample condition. Porosity, permeability, and grain density were measured on core plugs using an automated Core Measurement System (CMS-300™) instrument. The types of analyses carried out on the plugs are summarized in Table 6. Results of the analyses were reported by Core Laboratories to the DGS and disseminated to the project team via the project data-sharing portal on Box.

Table 6. Summary of analytical methods used for the collection of new hydrologic property data.

Analysis	Technique	Instrument	Sample type	Notes
Porosity	Boyle's law	Automated Core Measurement System (CMS-300™)	1-inch core plug, sidewall cores	Archimedes bulk volume method used where sample unsuitable for measurement at stress
Permeability	Boyle's law	Automated Core Measurement System (CMS-300™)	1-inch core plug, sidewall cores	CMS permeability to air, Klinkenberg permeability using helium, nitrogen used for permeability less than 0.1 mD (unsteady state)
Permeability	Pressure Decay Profile (PDPK)	Pressure – Decay Profile Permeameter (PDPK)	Core, slabs, slices, chips, sidewall cores	PDPK permeability to air using nitrogen
Grain Density	Boyle's law	Automated Core Measurement System (CMS-300™)	1-inch core plug, sidewall cores	Grain volume measured by Boyle's law; grain density calculated from measurement and weight on dried plug samples

4.1.2 Thin-Section Preparation and Analysis

Upon completion of the hydrologic property analyses by Core Laboratories, remaining samples materials were returned to the DGS. These materials were next shipped to Wagner Petrographic for thin-section preparation. The samples were impregnated with blue epoxy and thin-section slides were prepared. One-half of each prepared slide was stained for potassium feldspar, plagioclase feldspar, and calcite, and the thin section was covered with a coverslip. Eighty new thin sections, plus two previously prepared thin sections from the DGS repository, were sent to the PaGS for petrographic analysis of mineralogy and porosity. Petrographic analysis of these thin sections included the preparation of standard point counts, visual descriptions of porosity, and photomicrographs. In general, point-count analyses followed the Gazzi-Dickinson method for the measurement of framework grains and matrix spaces. Because the purpose of this work was also to describe the nature and extent of porosity in these samples, ten specific pore types were also included as matrix space categories in the point counts. Each count targeted a minimum of 400 points to ensure 95 percent confidence. Those thin sections with counts of less than 400 either did not have a large enough area to perform a full count or were made up of very fine-grained material with indeterminable mineral content.

Photomicrograph images were collected to document mineralogical composition, cementing materials, and porosity conditions.

4.1.3 X-ray Fluorescence (XRF)

XRF analysis was carried out onsite at the DGS by PaGS staff to determine quantitative bulk-rock geochemistry. Measurements were made using a handheld portable Thermo Scientific Niton™ XL3t GOLDD+ handheld analyzer. The first two batches were analyzed on July 13 and July 20, 2017, prior to sample shipment to Core Laboratories. The last batch was analyzed on December 5, 2017, after samples were returned from Core Laboratories and before shipment to Wagner Petrographic. The Thermo Scientific handheld analyzer was used to analyze 76 rock core samples. Analyses were conducted using the built-in TestAllGeo calibration. This program analyzes different suites of elements in four separate groups. Total analytical time was 150 seconds. Larger samples were analyzed three times, and the average was calculated by the XRF instrument and reported. Most small samples (chips and sidewall cuttings) were analyzed only once. The analyzer window and shielded stand were blown clean with a camera blower brush between samples.

4.1.4 X-ray Diffraction analysis (XRD)

Semi-quantitative estimates of the bulk mineralogy of 75 rock core samples were determined using X-ray powder diffraction. The analyses were run using a PANalytical Empyrean X-ray diffractometer. The samples were loaded in 16-mm-diameter back-packed sample holders that were mounted in a sample spinner.

Analyses were performed with PANalytical HighScore Plus software and the ICDD PDF-4 database. Replicate analyses of nine samples were run as a test of precision. Semi-quantitative results were interpreted using the Rietveld method, which utilizes the whole X-ray pattern to find agreement between observed patterns and the published crystal structure data of the minerals through least-squares analyses. Quantities are then calculated based on these analyses. This method can account for such factors as preferred orientation and peak shape that can present problems in dealing with layered silicate minerals. The HighScore Plus software enabled the programming of an automated Rietveld procedure that took these factors into account and was therefore able to provide a level of precision sufficient for classifying the lithologies that were encountered.

4.1.5 Scanning Electron Microscope (SEM)

Bulk mineralogy and porosity characteristics underwent further evaluation at the PaGS. Remaining billets from thin-section preparation were analyzed using a Hitachi S-2600N SEM with backscatter electron (BSE) and energy dispersive spectroscopy (EDS) detectors. The EDS system was manufactured by Gresham Scientific Instruments (now Teledyne e2v), and Quartz Imaging software was used for data acquisition and display. The SEM analysis produced individual and composite geochemical maps displaying distribution of aluminum (Al), calcium (Ca), iron (Fe), potassium (K), magnesium (Mg), sodium (Na), oxygen (O), sulfur (S), and silicon (Si). Operating conditions are reported with the images. Two maps each were created per sample. As well, images showing high resolution crystalline texture and pore-space geometry were taken. Most samples were polished to improve image quality.

4.2 Laboratory Sample Analyses

4.2.1 Core Hydrologic Properties

Seventy-four depth points were identified for analysis where core materials were available, including conventional core slabs, chips, slices, and sidewall cores. One-inch core plugs were cut for 40 samples of those materials and analyzed for porosity, permeability, and grain density by Core Laboratories. A total of 81 probe permeameter measurements were made at 75 depth points, six of which had duplicate measurements made on the same sample. Full descriptions of the results as well as methods, procedures, and inputs can be found in the final analysis report (Appendix D).

The 40 core plugs were tested with the automated CMS-300™ and yielded permeabilities to air ranging from 0.004 to 318 mD, Klinkenberg permeabilities ranging from 0.001 to 286 mD, porosities ranging from 3.40 to 30.3%, and grain densities ranging from 2.609 to 2.750 grams per cubic centimeter (g/cm^3). Average values measured from the core plug analysis are shown in Table 7.

Eighty-one sample points were selected for permeability measurements with the Pressure-Decay Profile Permeameter (PDPK); seventy-seven sample points yielded results. Measured probe permeabilities ranged from 0.0922 to 2810 mD. Table 8 shows averages of the permeability values for each well by formation as measured with the probe permeameter and compares them to permeability measurements obtained from the core plugs by the CMS instrument. Where possible, probe permeameter measurements were taken at the same depth point, or otherwise at the closest point, as the core plugs measured with the CMS instrument to allow for comparison of results from these methods. As the averages on Table 8 indicate, permeabilities measured with the probe permeameter (PDPK) are overall significantly higher than those measured from the core plugs using the CMS instrument.

Variations in the absolute values obtained by different methods for the same sample can be attributed to inherent differences between, and limitations of, each method. Sample quality issues such as fractured or chipped samples, sample failure during testing, or plugs being too short to conform to boot material also affect specific samples and are identified in the analytical report submitted by Core Laboratories (Appendix D). These factors have been taken into consideration when selecting which values are most representative of hydrologic properties at each sample point. Intrinsic variations attributable to geological factors, such as lithofacies, mineralogy, and depositional environment, are being further investigated with the accompanying, ongoing stratigraphic, petrographic, and mineralogical analyses to further characterize the potential storage targets and seals.

Table 7. Average values of new hydrologic properties by well and formation measured from core plugs.

Basin	Well / formation	No. of measure-ments	Average porosity (%)	Average Klinkenberg permeability K_α (mD)	Average permeability to air K_{air} (mD)	Average grain density (g/cm^3)
BCT	**COST B-2**	**15**				
	Dawson Canyon	1	19.51	71.29	85.75	2.69
	Logan Canyon	14	18.17	21.86	27.11	2.71
BCT	**COST B-3**	**6**				
	Mississauga	5	16.33	38.67	45.55	2.69
	Mic Mac	1	8.80	0.25	0.34	2.71
GBB	**COST G-1**	**4**				
	Mississauga	2	21.66	146.16	161.94	2.70
	Mohawk	2	6.47	0.15	0.18	2.70
GBB	**COST G-2**	**2**				
	Mohawk	2	18.85	18.23	22.38	2.67
BCT	**Exxon 599-1**	**1**				
	Mohawk	1	17.26	124.53	199.60	2.64
BCT	**Exxon 684-1**	**4**				
	Mic Mac	2	3.76	0.04	0.06	2.65
	Mohawk	1	17.20	66.37	79.23	2.64
	Naskapi	1	27.21	N/A	N/A	2.69
BCT	**Exxon 684-2**	**1**				
	Mohawk	1	10.90	N/A	N/A	2.68
BCT	**Mobil 544-1**	**1**				
	Dawson Canyon	1	N/A	N/A	N/A	N/A
BCT	**Shell 586-1**	**1**				
	Logan Canyon	1	17.01	0.40	0.57	2.71
BCT	**Shell 632-1**	**1**				
	Mississauga	1	18.50	N/A	N/A	2.69
BCT	**Texaco 598-1**	**3**				
	Mohawk	3	17.17	44.36	75.95	2.67
BCT	**Texaco 642-1**	**1**				
	Mohican / Iroquois	1	3.39	0.09	0.16	2.68

N/A= Result unobtainable for various reasons; see laboratory report in Appendix D.

Table 8. Average values of new measured permeability analyses from probe permeameter and core plug CMS permeability measurements for comparison.

Basin	Well / formation	No. of measurements		Average pressure decay profile permeability K_a (PDPK) (mD)	Average Klinkenberg permeability K_α (CMS) (mD)	Average permeability to air K_{air} (CMS) (mD)
		(PDPK)	(CMS)			
BCT	**COST B-2**	**17**	**15**			
	Dawson Canyon	2	1	501.65	71.29	85.75
	Logan Canyon	15	14	428.95	21.86	27.11
BCT	**COST B-3**	**12**	**6**			
	Dawson Canyon	3		0.26		
	Mississauga	6	5	219.61	38.67	45.55
	Logan Canyon	2		185.00		
	Mic Mac	1	1	0.51	0.25	0.34
GBB	COST G-1	**8**	**4**			
	Mississauga	4	2	555.26	146.16	161.94
	Mohawk	4	2	9.55	0.15	0.18
GBB	**COST G-2**	**3**	**2**			
	Mohawk	3	2	54.17	18.23	22.38
BCT	**Exxon 599-1**	**2**	**1**			
	Mohawk	2	1	1710.00	124.53	199.60
BCT	**Exxon 684-1**	**10**	**3**			
	Mic Mac	3	2	7.34	0.04	0.06
	Naskapi	4		1945.00		
	Mohawk	3	1	386.77	66.37	79.23
BCT	**Exxon 684-2**	**1**				
	Mohawk	1		11.60		
BCT	**Mobil 544-1**	**12**				
	Dawson Canyon	2		277.00		
	Logan Canyon	8		470.12		
	Mississauga	2		6.53		
BCT	**Shell 273-1**	**2**				
	Dawson Canyon	2		166.37		
BCT	**Shell 372-1**	**2**				
	Logan Canyon	2		34.84		
BCT	**Shell 586-1**	**2**	**1**			
	Logan Canyon	2	1	17.20	0.40	0.57
BCT	**Shell 587-1**	**1**				
	Logan Canyon	1		1.80		
BCT	**Shell 632-1**	**3**				
	Dawson Canyon	1		372.00		
	Logan Canyon	1		3.28		
	Mississauga	1		23.80		
BCT	**Shell 93-1**	**1**				
	Mississauga	1		1320.00		

Table 8 (cont.). Average values of new measured permeability analyses from probe permeameter and core plug CMS permeability measurements for comparison.

Basin	Well / formation	No. of measurements		Average pressure decay profile permeability K_a (PDPK) (mD)	Average Klinkenberg permeability K_α (CMS) (mD)	Average permeability to air K_{air} (CMS) (mD)
		(PDPK)	(CMS)			
BCT	**Texaco 598-1**	**3**	**3**			
	Mohawk	3	3	131.57	44.36	75.95
BCT	**Texaco 642-1**	**2**	**1**			
	Mic Mac	1	1	0.11		
	Mohican/Iroquois	1		30.60	0.09	0.16

These new porosity and permeability data are generally consistent with the legacy data compiled for this project. They confirm that reservoir-quality porosity and permeability values occur in many of the stratigraphic units of the Atlantic OCS, including previously identified reservoir targets of the Logan Canyon and Mississauga Formations. However, in some cases, significantly different measurements may occur in the same unit within a few feet of each other. For example, in the Logan Canyon Formation, in the COST B-2 well, the 11% porosity and permeability below 1 mD at 9286.0 feet (ft) contrasts with 25.5% and 41 to 56 mD at 9289.15 ft; in the Mississauga Formation, in the COST B-3 well, porosity is 24% and permeability 25 to 29 mD at 9932 ft, contrasting with less than 4% porosity and permeability below 0.01 mD at 9934 ft. (see Appendix D and Table 14). Such variations within these units result in the more modest average hydrologic properties shown in Tables 7 through 9; they also underscore the fact that these units are heterogeneous and that the stratigraphic and areal variations in hydrologic properties need to be taken into consideration in resource calculations (see also the discussion in Section 4.3). By the same token, the Naskapi and Mic Mac Formations are considered and evaluated as sealing units, but the occurrence of a high porosity (27.21%) sandstone in the Naskapi Formation at 9438 ft in the Exxon 684-1 well with high legacy permeability (768 mD) and new probe permeability (1890 mD) values (see Appendix D and Table 14) suggests that these units may also be heterogeneous and that they would be best evaluated locally for their importance as seals.

Average porosity and permeability values for the study area for each unit are shown in Table 9. The unit averages of the new data in Tables 8 and 9 obscure the degree of variation within those formations. For example, in the Logan Canyon and Mississauga Formations, the new permeabilities vary from less than 1 mD to more than 1 darcy (the latter from probe permeameter measurements, which are higher than core plug CMS measurements at the same depth). However, full results can be obtained from the final analysis report (Appendix D). Scatter plots of these full results (Figures 6 through 9) show that the new data are generally in agreement with the legacy data (as noted earlier), probe permeability measurements were significantly higher than core plug permeability measurements, and several 1-Darcy level values in the legacy data were not reproduced (e.g., COST G-1 at 5473 ft, COST B-2 at 9305.4 ft, and Texaco 598-1 at 13275 ft).

Table 9. Average values of all measured porosity and permeability by formation for new sample analyses.

Formation	Average pressure decay profile permeability K_a (PDPK) (mD)	Average Klinkenberg permeability K_α (mD)	Average permeability to air K_{air} (mD)	Average porosity (%)
Dawson Canyon	226.28	71.29	85.75	19.51
Logan Canyon	341.04	20.43	25.34	18.10
Naskapi	1945.00			27.21
Mississauga	349.68	74.50	84.35	17.93
Mic Mac	4.53	0.11	0.15	5.44
Mohawk	231.82	40.08	61.31	14.75
Mohican/Iroquois	30.60	0.09	0.16	3.39

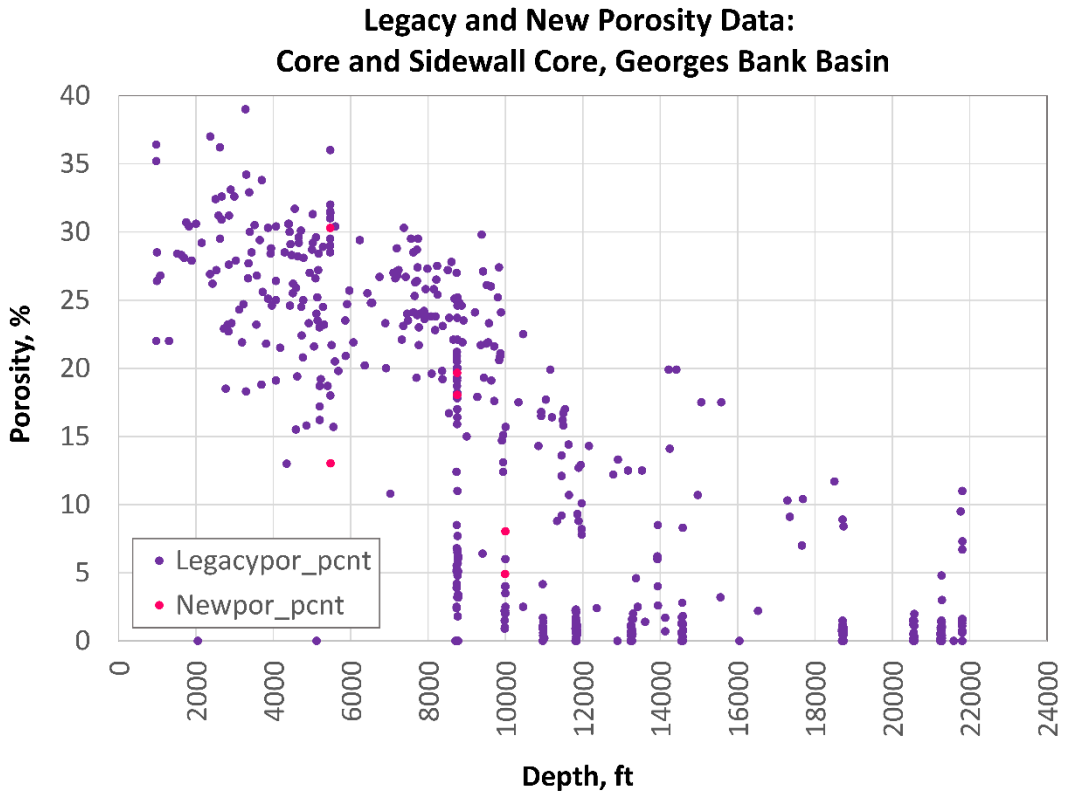

Figure 6. Georges Bank Basin porosity data, new and legacy data.

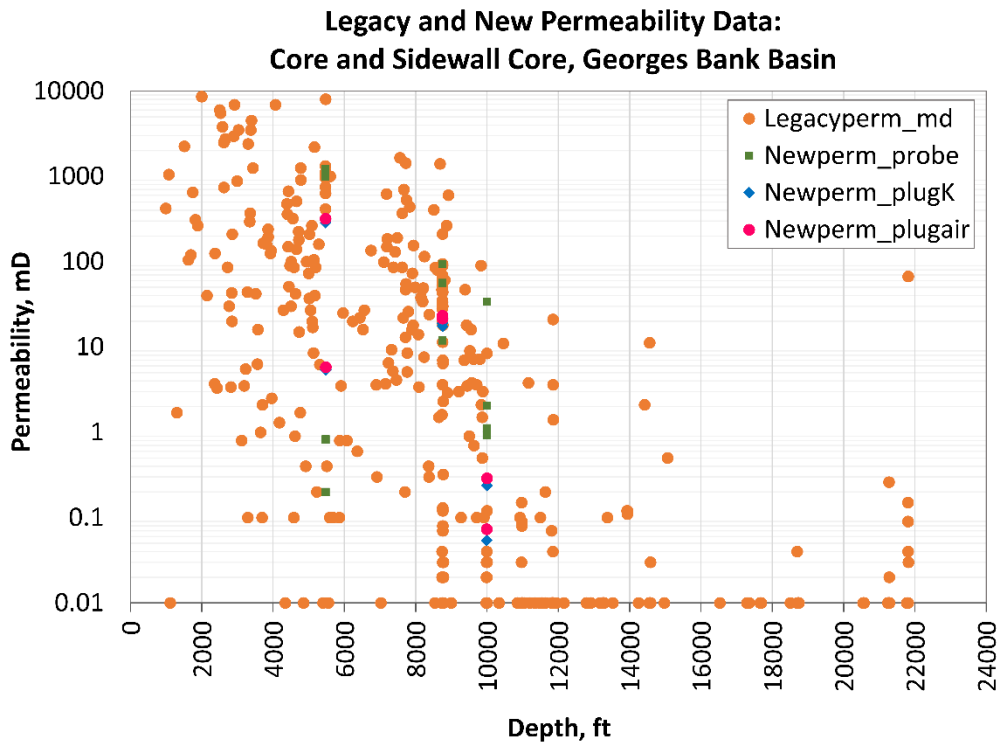

Figure 7. Georges Bank Basin permeability data, new and legacy data.

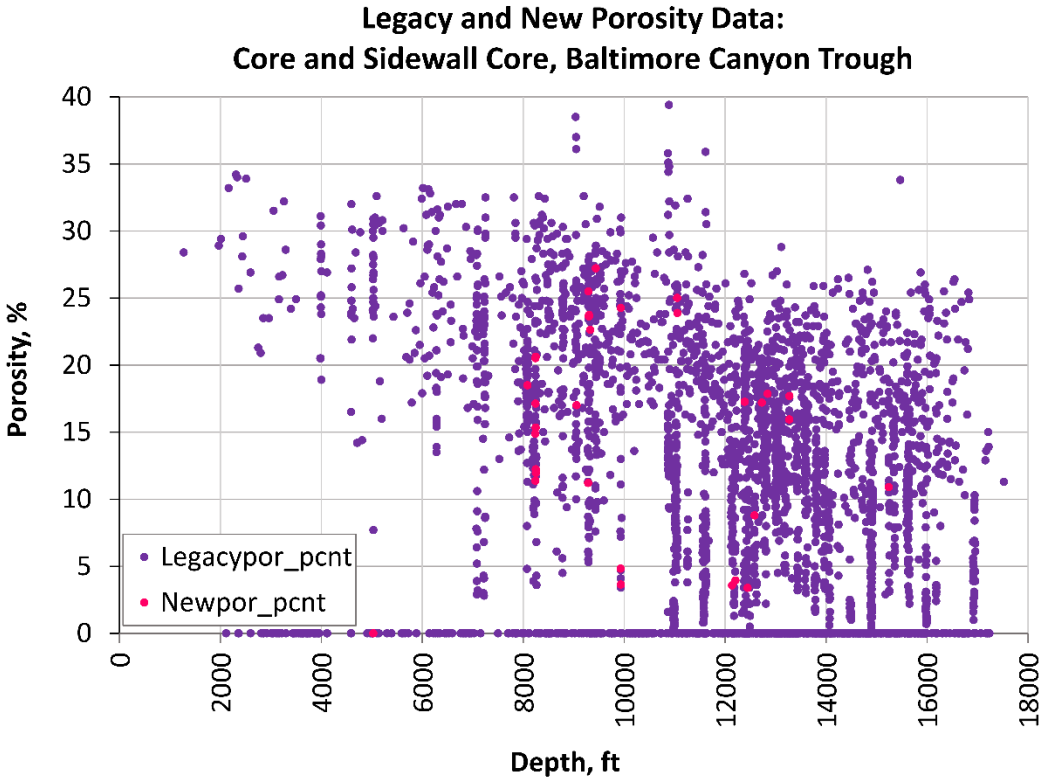

Figure 8. Baltimore Canyon Trough porosity data, new and legacy data.

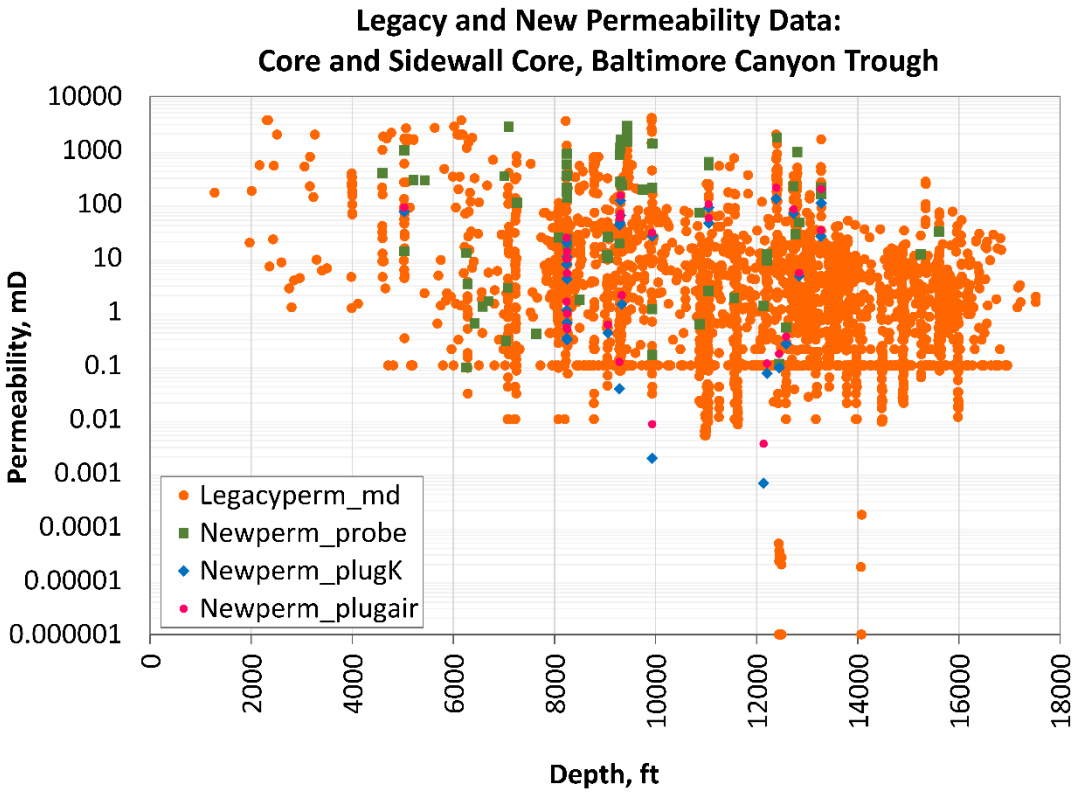

Figure 9. Baltimore Canyon Trough permeability data, new and legacy data.

4.2.2 Petrographic Analysis

Petrographic analysis of porosity and mineralogy was conducted on 82 standard thin sections from 17 different wells by the PaGS. Thin-section locations targeted various depths and lithologies in these wells to assess various potential reservoir and caprock characteristics. Most of these thin sections were impregnated with blue epoxy (to facilitate pore observations) and half-stained for calcite, plagioclase, and potassium feldspar (to facilitate mineral and matrix identification). Porosity point counts (a proxy for volumetric porosity as a percentage) were prepared for each thin section as part of the petrographic analysis, including total porosity estimates and percentages of ten different porosity types, as shown in Table 10. For most of the relatively porous (>10%) samples, the largest component of the porosity volumes was intergranular porosity, commonly followed by grain/cement dissolution porosity. Comparison of the new, laboratory-measured porosity data to the thin-section-based porosity measurements shows that the laboratory measurements are much higher than the thin-section-based porosity estimates (e.g., COST B-2, 8239-8251 ft).The thin-section porosity and laboratory porosity measurements yield comparable numbers in some intervals, with the laboratory measurements overall slightly higher (e.g., COST B-3, 11050.8 ft; COST B-2, 5030.2 ft), most commonly in those samples with high percentage of visible porosity (macroporosity) such as intergranular and dissolution porosity (see also discussion in Section 4.3). Thin-section analytical results were used to determine which samples warranted further scrutiny using SEM techniques (see next section). The individual thin-section reports are included as Appendix E. Figures 10, 11, and 12 are examples of the observations made on framework grains, matrix, cementation, and porosity which allow for a more robust assessment and characterization of potential storage targets and caprocks. Original source image files will be made available, in addition to the workbooks, on the NETL EDX virtual data library for carbon storage science at the conclusion of the project.

Table 10. Summary of petrography results showing total porosity and distribution of porosity types.

Well	Depth (ft)	Thin section		Total porosity (%)	Porosity type									
		Stain	Billet no.		Inter-granular	Intra-granular	Inter-crystalline	Moldic	Grain/cement dissolution	Clay/mica framework	Organic matter	Vug	Channel	Fracture
COST G-1	5471	**Y**	**H32**	22.8	13.5			0.8	7.3			1.0		0.3
COST G-1	5473	**Y**	**H33**	19.0	11.2			1.0	6.3			0.5		
COST G-1	5480-5481 (5480.6)	**N**	**H34**	0.0										
COST G-1	5480.6		**DGS**	0.0										
COST G-1	9992	**N**	**H35**	0.0										
COST G-1	9992.8	**N**	**H36**	0.0										
COST G-1	10001.3	**N**	**H37**	0.5									0.5	
COST G-2	8753.7	**Y**	**H38**	11.7	5.5			0.2	5.5				0.5	
COST G-2	8756	**Y**	**H39**	11.1	5.7			0.2	5.2					
COST B-2	5030.2	**Y**	**H1**	15.6	8.7			2.9	4.1					
COST B-2	8239	**Y**	**H2**	9.7	4.4	0.7		1.5	2.9					0.2
COST B-2	8239.5	**Y**	**H3**	7.8	4.6	0.2		0.2	2.4					0.2
COST B-2	8241	**Y**	**H4**	4.5	3.0				1.3					0.3
COST B-2	8242	**Y**	**H5**	9.7	5.8	0.2		0.5	2.7					0.5
COST B-2	8244	**Y**	**H6**	5.8	4.3				1.4					
COST B-2	8247	**Y**	**H7**	3.8	2.1	0.9		0.5						0.2
COST B-2	8248.9	**Y**	**H8**	5.4	3.7	0.5			1.2					
COST B-2	8249	**Y**	**H9**	2.4	1.0	0.7		0.2	0.5					
COST B-2	8250	**Y**	**H10**	5.9	3.1	0.7			1.7					0.5
COST B-2	8251	**Y**	**H11**	2.7	1.2	0.2			1.0					0.2
COST B-2	9286.5	**Y**	**H12**	1.4					1.4					
COST B-2	9289.3	**Y**	**H13**	8.9	4.3			2.2	2.4					
COST B-2	9302	**Y**	**H14**	15.4	7.9	0.2		2.2	4.1			1.0		
COST B-2	9304.4	**Y**	**H15**	16.0	9.3	0.3		2.3	3.5			0.5		0.3
COST B-2	9305.4	**N**	**H16**	10.3	5.9			0.7	3.5					0.2
COST B-2	9330	**Y**	**H17**	6.9	4.1				2.9					
COST B-2	9330.2	**Y**	**H18**	8.9	4.1	0.5			4.1			0.2		
COST B-3	6260	**N**	**H19**	0.0										
COST B-3	7040	**N**	**H20**	0.5					0.2				0.2	
COST B-3	7640	**N**	**H21**	2.6				0.5					2.1	
COST B-3	8382	**Y**	**H22**	11.7	6.7				5.0					
COST B-3	9750	**N**	**H23**	0.9					0.2				0.7	
COST B-3	9931.6	**Y**	**H24**	0.0										
COST B-3	9932	**Y**	**H25**	5.1	2.7				2.4					

Table 10 (cont.). Summary of petrography results showing total porosity and distribution of porosity types.

Well	Depth (ft)	Thin section		Total porosity (%)	Porosity type									
		Stain	Billet no.		Inter-granular	Intra-granular	Inter-crystalline	Moldic	Grain/cement dissolution	Clay/mica framework	Organic matter	Vug	Channel	Fracture
COST B-3	9934	**Y**	**H26**	0.7				0.2	0.5					
COST B-3	11050.8	**Y**	**H28**	22.9	13.4				9.2			0.2		
COST B-3	11051-11052	**N**	**H29**	3.0	1.0				1.5				0.5	
COST B-3	11054	**Y**	**H30**	17.9	10.5			0.5	6.7			0.2		
COST B-3	12581.9	**Y**	**H31**	2.0									2.0	
Mobil 544-1	5211	**N**	**H50**	3.3						3.3				
Mobil 544-1	5435	**N**	**H51**	3.5						0.5				3.1
Mobil 544-1	5962	**N**	**H52**	0.9				0.9						
Mobil 544-1	6260	**N**	**H53**	5.3				0.5		3.7				1.1
Mobil 544-1	6420	**N**	**H54**	0.0										0.0
Mobil 544-1	6579	**N**	**H55**	9.3						7.8				1.5
Mobil 544-1	6696	**N**	**H56**	2.8						1.5				1.3
Mobil 544-1	6798	**Y**	**H57**	11.7	1.1		10.2	0.4						
Mobil 544-1	7096	**Y**	**H58**	16.2	10.6		5.1	0.5						
Mobil 544-1	7258	**Y**	**H59**	17.8	17.5			0.3						
Mobil 544-1	8497	**Y**	**H60**	0.0										
Mobil 544-1	9039	**Y**	**H61**	17.2	9.0		0.4	7.8						
Exxon 684-1	9438	**Y**	**H40**	15.4	12.0		0.8	0.8	1.8					
Exxon 684-1	9439	**Y**	**H41**	21.6	20.2			0.7	0.7					
Exxon 684-1	9440	**Y**	**H42**	19.3	17.6			0.7	1.0					
Exxon 684-1	9441	**Y**	**H43**	20.4	18.9			0.4	1.1					
Exxon 684-1	12137	**N**	**H44**	0.5										0.5
Exxon 684-1	12199	**Y**	**H45**	5.7	2.1		3.5							0.0
Exxon 684-1	12204	**N**	**H46**	0.3										0.3
Exxon 684-1	12729	**Y**	**H47**	9.5	6.9		1.7	0.9						
Exxon 684-1	12767	**Y**	**H48**	10.0	7.9		0.9	1.1						
Conoco 145-1	9226	**Y**	**H62**	0.0										
Exxon 684-2	15242	**Y**	**H63**	3.7	1.7		1.7	0.2						
Shell 273-1	7010	**Y**	**H64**	5.7						5.7				
Shell 273-1	7077	**Y**	**H65**	0.5				0.5						
Shell 586-1	9058-9058.7	**Y**	**H67**	5.7	2.4			3.3						
Shell 632-1	4594.5	**Y**	**H69**	23.7	23.7									

Table 10 (cont.). Summary of petrography results showing total porosity and distribution of porosity types.

Well	Depth (ft)	Thin section		Total porosity (%)	Porosity type									
		Stain	Billet no.		Inter-granular	Intra-granular	Inter-crystalline	Moldic	Grain/cement dissolution	Clay/mica framework	Organic matter	Vug	Channel	Fracture
Shell 632-1	6278.8	**Y**	**H70**	5.1				3.8	1.3					
Shell 93-1	9937	**Y**	**H72**	31.6	31.3			0.2						
Texaco 598-1	12840-12841	**Y**	**H73**	10.0	4.6		1.0	2.4	2.0					
Texaco 598-1	13271-13272	**Y**	**H74**	12.7	6.4		3.2	1.7	1.5					
Texaco 598-1	13275-13276	**Y**	**H75**	10.3	7.4		1.0	1.0	1.0					
Texaco 642-1	12444	**Y**	**H76**	0.7										0.7
Texaco 642-1	15608	**N**	**H77**	21.3	18.8			2.5						
Exxon 599-1	12386	**Y**	**H78**	10.6	8.3		0.4	1.8						
Exxon 599-1	12387	**Y**	**H79**	12.6	11.2		0.5	1.0						
Exxon 599-1	12403	**Y**	**H80**	12.9	11.4		0.2	1.2						
Shell 372-1	10872.9-10873.2	**N**	**H66**	1.6										1.6
Shell 372-1	10872.9-10873.2		**DGS**	0.0										
Shell 587-1	11555	**Y**	**H68**	1.5				1.0	0.2					0.2

COST B-2 - 9305.4 ft. Logan Canyon

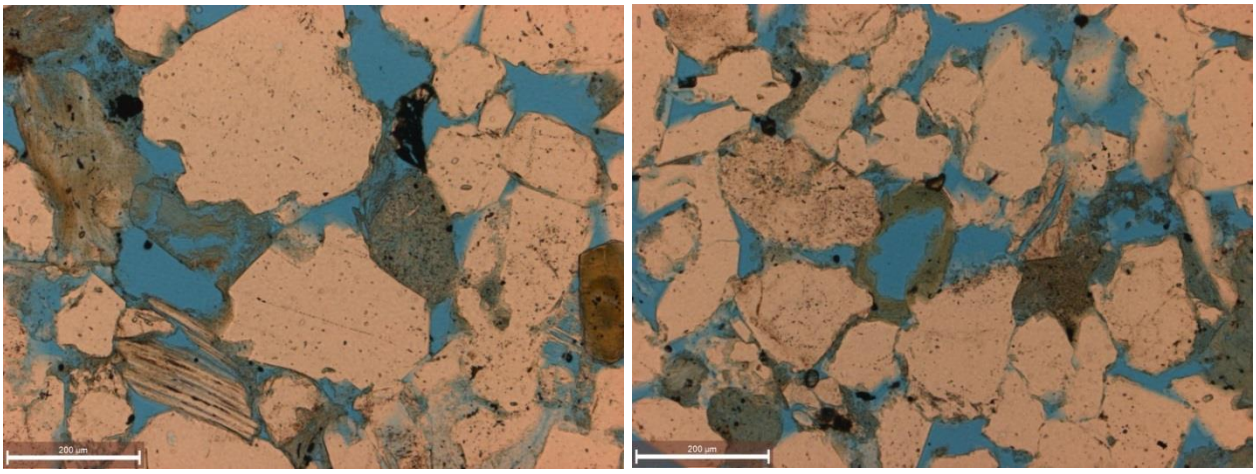

Intergranular and dissolution porosity (left); intergranular, moldic and dissolution porosity

Figure 10. Photomicrographs from potential sandstone storage target in COST B-2 well showing different porosity types.

COST B-2- 8242 ft. Logan Canyon

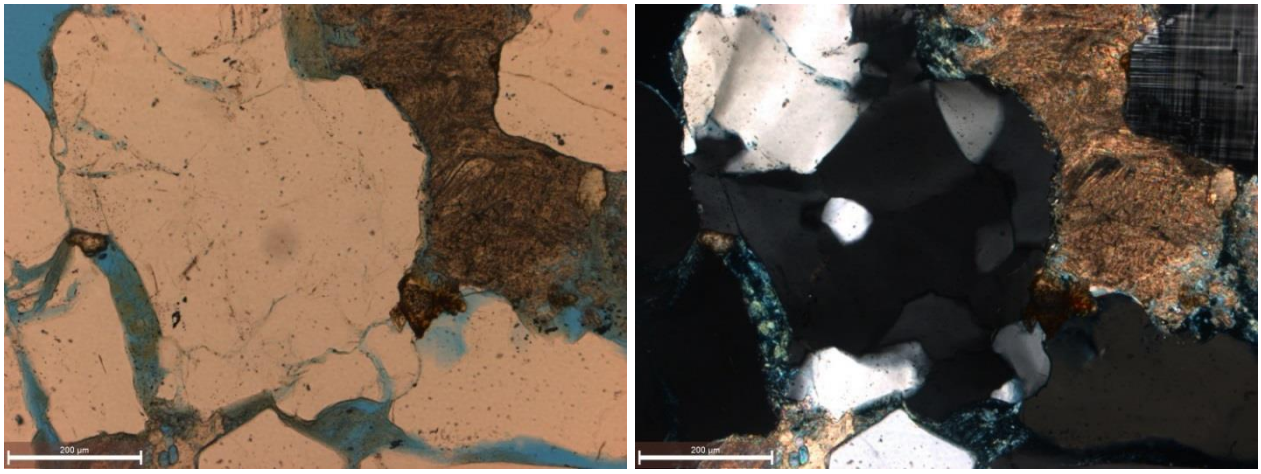

Plane polarized light (left) and Crossed Nicols

Figure 11. Photomicrographs from potential sandstone storage target in COST B-2 well showing framework grains, cement, matrix minerals and pore spaces.

MOBIL 544-1-6420 ft. Logan Canyon shale

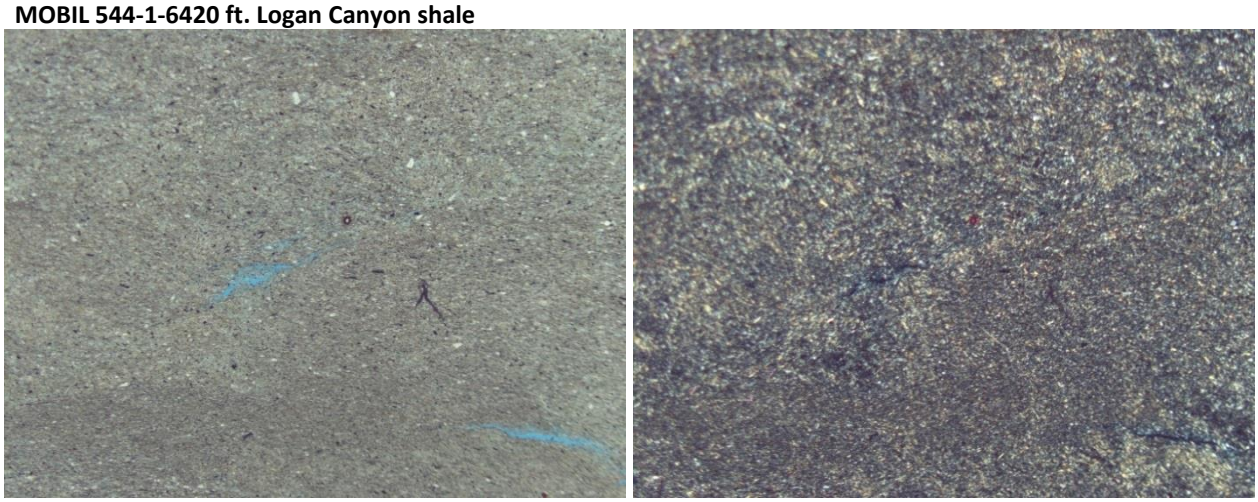

2.5 x Field of View ~ 5 mm **Plane polarized light (left) and Crossed Nicols (right)**

MOBIL 544-1-6696 ft. Logan Canyon calcareous siltstone

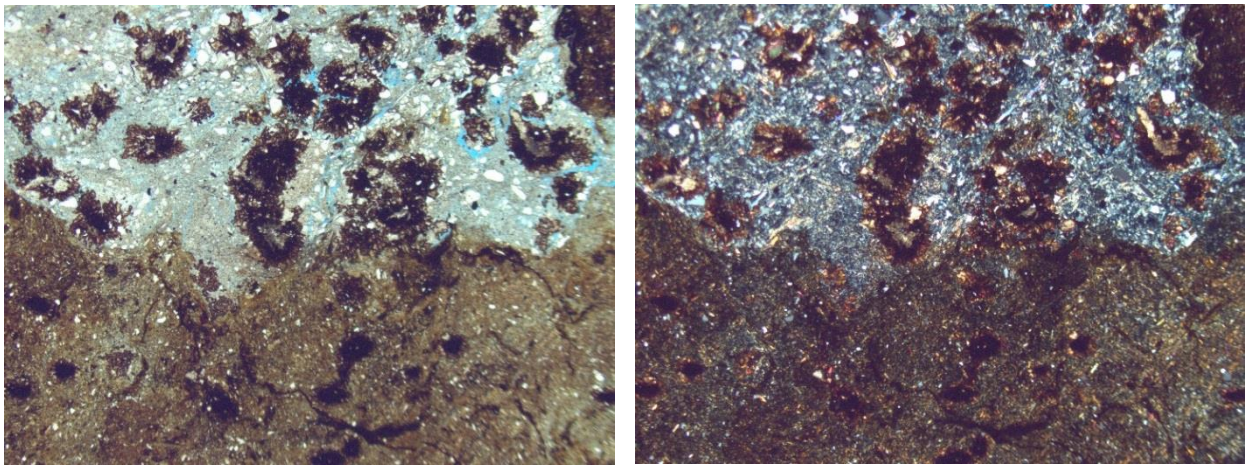

2.5 x Field of View ~ 5 **Plane polarized light (left) and Crossed Nicols (right)**

Figure 12. Photomicrographs showing two different tight lithologies associated with potential baffles within the storage zone.

4.2.3 X-ray Fluorescence

The XRF analysis allows for bulk compositional analysis to quantify the bulk concentrations of major, minor, and trace elements. Analytical results presented include the major, minor, and trace elements that may yield reliable results. The results for the heavier elements are generally better; however, the analyzer cannot detect sodium. The results from the major minerals from the 76 rock core samples analyzed are presented in Table 11. Spreadsheets of the full analysis and data are included in Appendix F.

Given the limitations of the different mineralogical and geochemical analysis methods used for this project (XRF, XRD, SEM), the results from each method are used to complement each other and correlated with petrography in their application to better understanding the hydrologic property data.

Where absolute values may vary between the results obtained from XRF and XRD analysis, generally the relative values agree in the identification of siliciclastic, carbonate and mixed lithologies from high values of SiO_2 and CaO respectively. Samples with potentially high carbonate cement and clayey matrix content can also be identified from high content of CaO and Al_2O_3.

For example, XRF results for the Conoco 145-1 sample at 9226 ft correlate with the XRD and petrographic results and complement each other in characterizing the sample as a calcite-cemented calcareous sandstone. This helps to validate the legacy data from this interval of 3% porosity and <0.01mD permeability.

These XRF results add to the data available to make detailed comparisons between results from different analytical methods on samples from the same or close depths and in validating and interpreting both legacy and new data.

4.2.4 X-ray Diffraction

The XRD analysis provides for bulk mineral analysis, to quantify the bulk mineralogical content (percentages of quartz + feldspar, carbonate, and clay).

Table 14 shows the average of the percentage quantities of the mineral compositions obtained for each unit sampled per well. The results identify carbonate, siliciclastic and mixed lithologies and also give indications of where carbonate cements and clay minerals may have an effect on reservoir properties as indicated by high content of calcite and dolomite and kaolinite, chlorite and mica group minerals respectively, in those samples.

Regional and stratigraphic variations in lithofacies can also be quickly identified. For example, the Logan Canyon Formation sample from Shell 586-1 consists of 100% calcite, whereas in the Shell 632-1 the sample form the Logan Canyon is siliciclastic, consisting of 61% quartz, a high content of calcite (38%) suggests a high content of carbonate grains and cement which correlates with the observations made from petrographic analysis. When correlated with the petrographic analysis and combined with the XRF and SEM analysis, these observations will be used to validate and interpret the hydrologic properties measured in the laboratory. They provide additional data to enable detailed investigations of the properties of the potential storage resources and caprocks.

Spreadsheets of the full analysis and replicate analysis data are included in Appendix G.

Table 11. Summary of results of XRF analysis showing major minerals.

Sample/lab ID	Depth (ft)	Mineral (wt%)								
		SiO_2	TiO_2	Al_2O_3	FeO	MnO	MgO	CaO	K_2O	P_2O_5
CONOCO 145-1 AVG	9226	25.28	0.12	2.87	0.59	0.05	1.38	41.72	0.67	0.05
COST B2 5030.2 AVG	5030.2	53.92	0.07	1.85	2.55	0.03	0.88	18.7	0.71	0.28
COST B2 8239.5 AVG	8239.5	55.84	0.04	2.3	2.87	0.03	0.93	19.31	0.46	0.29
COST B2 8241 AVG	8241	49.9	0.05	3.23	4.81	0.05	1.35	19.89	0.54	0.14
COST B2 8241 b AVG	8241	52.56	0.05	3.13	3.45	0.04	1.22	20.23	0.77	0.1
COST B2 8242 AVG	8242	60.42	0.11	3.96	5.45	0.04	1.2	12.08	0.8	0.28
COST B2 8244 AVG	8244	49.63	0.07	2.96	4.75	0.04	0.52	20.04	0.6	0.21
COST B2 8247 AVG	8247	47.21	0.05	2.31	3.23	0.05	0.86	26.12	0.58	0.14
COST B2 8250 AVG	8250	59.05	0.09	3	4.07	0.04	0.44	14.55	0.8	0.21
COST B2 8251.8 AVG	8251.8	51.57	0.09	3.38	3.81	0.04	0.68	21.05	0.82	0.24
COST B2 9286.5 AVG	9286.5	61.62	0.18	4.13	2.19	0.05	1.47	16.85	0.9	0.15
COST B2 9289.3 AVG	9289.3	70.82	0.27	5.2	2.54	0.02	0.86	1.13	1.21	0.22
COST B2 9302 AVG	9302	71.79	0.33	5.2	2.31	0.02	0.97	1.88	1.28	0.12
COST B2 9304 AVG	9304	64.87	0.49	5.85	2.7	0.03	1.27	2.69	1.14	0.14
COST B2 9330.2 AVG	9330.2	60.26	1.48	10.1	4.06	0.03	1.35	1.41	1.55	0.85
COST B3 6260	6260	25.14	0.16	6.16	2.33	0.04	2.05	31.41	1.11	0.44
COST B3 7040	7040	44.77	0.75	19.45	5.47	0.05	2.24	1.89	2.33	0.18
COST B3 7640	7640	50.35	0.77	16.8	4.96	0.05	1.87	1.33	2.45	0.17
COST B3 8382	8382	54.86	0.94	14.95	5.81	0.04	1.92	0.7	2.88	0.15
COST B3 9750	9750	38.43	0.86	15.8	5.77	0.03	1.58	6.81	2.33	0.15
COST B3 11042 AVG	11042	49.15	1.08	23.27	5.67	0.04	2.54	1.32	2.85	0.17
COST B3 11049.5 AVG	11049.5	73.71	0.57	5.6	1.27	0.02	1.28	1.54	1.49	0.05
COST B3 11050.8 AVG	11050.8	69.42	0.4	6.35	2.18	0.02	0.72	1.37	1.71	0.26
COST B3 11051.5 AVG	11051.5	76.44	0.42	5.39	0.72	0.02	0.95	0.78	1.43	0.09
COST B3 11054 AVG	11054	75.34	0.56	5.4	1.18	0.02	0.84	0.99	1.46	0.02
COST B3 12581.9 AVG	12581.9	10.39	0.05	1.37	0.62	0.04	1.67	54.97	0.2	0.15
COST B3 9931.6 AVG	9931.6	37.26	0.18	2.63	1.95	0.05	1.55	36.56	0.69	0.79
COST B3 9932 AVG	9932	37.38	0.1	2.48	2.25	0.05	0.78	35.83	0.69	1.74
COST B3 9934 AVG	9934	50.98	0.08	2.43	1.68	0.04	0.9	28.05	0.81	0.2
COST G1 10001.3 AVG	10001.3	69.05	0.59	8.59	2.1	0.04	1.6	6.26	1.44	0.74
COST G1 5471 AVG	5471	61.06	0.9	13.08	1.4	0.02	0.89	0.14	2.33	0.13
COST G1 5473 AVG	5473	61.43	0.54	11.49	0.46	0.02	0.85	0.93	2.08	0.2
COST G1 5480.6 AVG	5480.6	42.84	0.92	19.17	6.03	0.06	1.98	7.6	1.85	0.9
COST G1 9992.8 AVG	9992.8	44.32	0.2	5.77	0.53	0.08	1.15	27.14	1.19	0.34
COST G1 9992.8b AVG	9992.8	44.34	0.34	5.71	0.61	0.08	1.25	27.17	1.09	0.14
COST G2 8753.7 AVG	8753.7	70.56	0.38	7.39	2.06	0.06	0.92	1.82	1.26	0.17
COST G2 8756 AVG	8756	70.78	0.31	7.44	1.68	0.09	1.15	2.69	1.24	0.18
EXXON 599-1 AVG	12386	60.11	0.15	8.63	0.25	0.01	1.35	0.9	1.33	0.06
EXXON 599-1 AVG	12386.5	77.26	0.08	6.29	0.16	0.01	0.47	0.75	1.27	0.08
EXXON 599-1 AVG	12387	64	0.21	8.56	0.63	0.02	0.97	0.48	1.38	0.09
EXXON 599-1 AVG	12403	68.94	0.16	6.53	0.34	0.02	1.06	0.72	1.08	0.19

Table 11 (cont.). Summary of results of XRF analysis showing major minerals.

Sample/lab ID	Depth (ft)	Mineral (wt%)								
		SiO_2	TiO_2	Al_2O_3	FeO	MnO	MgO	CaO	K_2O	P_2O_5
EXXON 684-1 12137	12137	56.07	1.11	21.62	6.62	0.06	1.78	0.6	2.37	0.46
EXXON 684-1 12199	12199	71.08	0.28	11.47	0.83	0.02	0.31	0.24	1.79	0.25
EXXON 684-1 12204	12204	46.28	0.93	17.34	8.38	0.04	2.25	1.58	2.1	0.32
EXXON 684-1 12729	12729	69.29	0.17	9.66	0.28	0.01	0.48	0.15	2.08	0.05
EXXON 684-1 12767	12767	68.67	0.37	8.23	0.16	0.01	0.32	0.16	1.42	0.11
EXXON 684-1 12802	12802	68.63	0.24	10.37	0.31	0.01	0.54	0.1	1.22	0.06
EXXON 684-1 9438	9438	76.81	0.58	6.28	0.28	0.01	0.51	0.39	1.3	0.09
EXXON 684-1 9439	9439	72.69	0.1	3.47	0.49	0.01	0.26	0.37	1	0.05
EXXON 684-1 9440	9440	61.19	0.17	6.7	1.51	0.02	0.54	0.94	0.78	0.09
EXXON 684-1 9441	9441	59.58	0.38	6.44	2.93	0.07	0.65	1.02	1.02	0.09
MOBIL 544-1 5211	5211	35.34	0.66	15.12	7.28	0.05	1.6	2.94	2.28	0.14
MOBIL 544-1 5435	5435	34.31	0.57	12.89	4.87	0.03	1.73	12.21	2.12	0.22
MOBIL 544-1 6260	6260	49.46	0.67	5.27	6.93	0.01	0	0.04	0.82	0.39
MOBIL 544-1 6420	6420	53.12	1.32	23.93	2.78	0.03	1.73	0.16	2.62	0.15
MOBIL 544-1 6579	6579	59.14	1.55	17.48	0.65	0.02	0.54	0.13	1.93	0.46
MOBIL 544-1 6696	6696	72.74	0.69	20.32	4.67	0.05	1.03	0.36	2.44	0.24
MOBIL 544-1 6798	6798	65.08	0.19	10.05	0.31	0.01	0.28	0.03	1.76	0.09
MOBIL 544-1 7096	7096	69.96	2.1	7.96	2.07	0.06	0.86	0.11	1.03	0.15
MOBIL 544-1 7258	7258	67.43	0.3	9.93	0.79	0.01	0.77	0.13	1.26	0.23
MOBIL 544-1 8497	8497	33.77	1.83	27.09	5.93	0.22	2.69	11.1	1.37	0.68
MOBIL 544-1 9039	9039	53.29	0.58	11.98	5.12	0.1	1.92	2.47	1.83	0.28
SHELL 273-1 AVG	7010	53.56	1	11.18	6.18	0.05	1.54	1.45	2.34	0.44
SHELL 273-1 AVG	7077	43.5	0.58	9.94	4.79	0.08	1.82	19.2	1.6	0.13
SHELL 372-1 AVG	11555	3.66	0.03	1.14	0.12	0.04	0	60.89	0.14	0.01
SHELL 372-1 AVG	10872.9-10873.2	43.56	0.62	16.73	6.16	0.05	2.46	13.38	2.07	0.28
SHELL 586-1 AVG	9058-9058.7	4.24	0.06	1.91	0.35	0.05	0.76	58.75	0.31	0.1
SHELL 632-1 AVG	4594.5	57.84	0.81	9.95	3.26	0.05	1.14	1.52	1.2	0.59
SHELL 632-1 AVG	6278.8	36.59	0.09	4.75	8.48	0.05	0.72	20.22	0.71	0.17
SHELL 632-1 AVG	8083.1	70.58	0.21	8.77	1.12	0.03	0.81	1.66	1.66	0
SHELL 93-1 AVG	9937	51.28	0.66	12.34	3.1	0.03	1.43	4.08	1.84	0.16
Texaco 598-1 AVG	12840.5	66.2	0.34	10.19	2.73	0.02	1.28	0.5	1.4	0.12
Texaco 598-1 AVG	13271-13272	79.13	0.08	6.24	1.19	0.01	1.48	0.39	0.26	0.03
Texaco 598-1 AVG	13275-13276	77.17	0.07	4.57	1.18	0.04	1.6	1.01	0.18	0
Texaco 642-1 AVG	12444	69.64	0.84	13.64	2.83	0.06	1.96	4.28	2.08	0
Texaco 642-1 AVG	15608	59.71	0.51	11.92	3.02	0.02	4.32	1.17	1.55	0.12

AVG = Average of three readings.

Table 12. Average percentages of quantity of bulk minerals present in XRD samples by stratigraphic unit.

Well	Bulk Mineral (Av. %)														
	Quartz	Plagioclase	K feldspar	Mica group	Chlorite group	Kaolinite	Calcite	Dolomite	Aragonite	Ankerite	Siderite	Gypsum	Pyrite	Rutile	Anatase
Conoco 145-1															
Mohican / Iroquois	31.0	12		1		2	54.0								
COST B-2															
Logan Canyon	68.8		7.0	2.5	6.17	1.25	24.57								
Dawson Canyon	61.0	1	1.0				39.0								
COST B-3															
Dawson Canyon	40.3	1		15.3	22		29.7	1							
Mississauga	62.4	1	3.63	6.4	19	13.4	21.3						2		
Mic Mac	7.0						93.0								
Logan Canyon	52.0		22	7	20										
COST G-1															
Mississauga	64.0		10.5	6.3		15.3	22.0	1	1						
Mohawk	40.7	12.7	1.5	8.0	16	1.0	35.0								
COST G-2															
Mohawk	67.5	24.5	5.0	2.0		4.5	1.0								
Exxon 599-1															
Mic Mac	92.0	1.0	3.0	1.0		6.0									
Exxon 684-1															
Mic Mac	38.0	10.5	3.5	17.3	10	30.7							5		
Mohawk	79.0	5.7	4.3	1.0		5.7	15.0								
Naskapi	95.5		9.0	1.0										1	
Mobil 544-1															
Dawson Canyon	34.5	3.0	2.0	23.0	13.5	17.0	15.5				4	2			
Mississauga	34.0	11.0		20.0		33.0		19.5			3.5				2
Logan Canyon	66.75	1.5	4.5	11.5	16	18.71	30.0			1	4.0		1		
Shell 273-1															
Logan Canyon	69.0		16.0	6.0		6.0	3.0								
Shell 372-1															
Logan Canyon	26.0			10.0		26.0	36.0	1					3		
Shell 586-1															
Logan Canyon							100.0								
Shell 587-1															
Logan Canyon							100.0								
Shell 632-1															
Dawson Canyon	100.0			1.0											
Logan Canyon	61.0					2.0	38.0	1							
Mississauga	91.0			9.0		1.0									
Shell 93-1															
Mississauga	62.0	32.0		1.0		6.0							1		
Texaco 598-1															
Mohawk	76.7	8.0	3.5	6.0		12.0									
Texaco 642-1															
Mic-Mac	59.0		1.0	16.0		20.0	5.0								
Mohican / Iroquois	56.0	30.0	4.0	2.0	6.0		2.0								

4.2.5 Scanning Electron Microscopy (SEM)

Eighteen billets from seven wells were analyzed using the SEM with BSE and EDS detectors (Table 13). Photomicrographs with corresponding descriptions and EDS spectra were produced, which may be used to identify mineralogy and for high-resolution imaging of pore geometries and textural relationships in samples. They can also be used to semi-quantitatively determine the chemical composition of a sample. The EDS analysis produced individual and composite geochemical maps displaying distribution of aluminum (Al), calcium (Ca), iron (Fe), potassium (K), magnesium (Mg), sodium (Na), oxygen (O), sulfur (S), and silicon (Si).

Table 13. Samples used in SEM-EDS analysis.

Well name	Depth (ft)
COST B-2	5030.2
	8242
	8251
	9286.5
	9305.4
COST B-3	6260
	7040
	9750
	9931.6
COST G-1	5473
	10001.3
Exxon 684-1	9438
	9440
	12137
	12204
Mobil 544-1	6798
Shell 586-1	9058-9058.7
Texaco 598-1	13271-13272

Figures 13 and 14 show sample images of BSE analysis results and composite element maps from EDS analysis for the COST B-2 and COST B-3 wells, highlighting properties such as composition, porosity, and cementation. The results identify the different lithologies of the samples and the composition of matrix and cement. This is invaluable in facilitating detailed comparisons between results from different analytical methods and to understanding the relationship of composition to measured porosity and permeability values. Excel workbooks containing the BSE images, individual element maps, composite element maps, spectra, and instrument settings for each sample are saved to the project data sharing portal on Box and are

attached to this report as Appendix H. Original source image files will be made available, in addition to the workbooks, on EDX at the conclusion of the project.

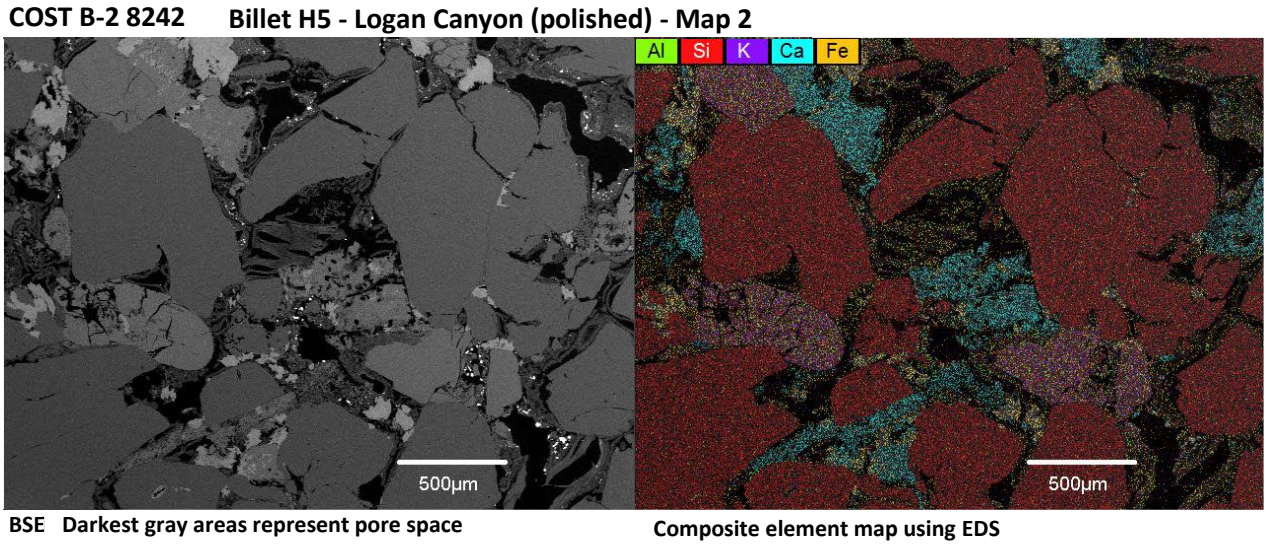

Figure 13. Sample SEM results from potential sandstone storage target in COST B-2 well.

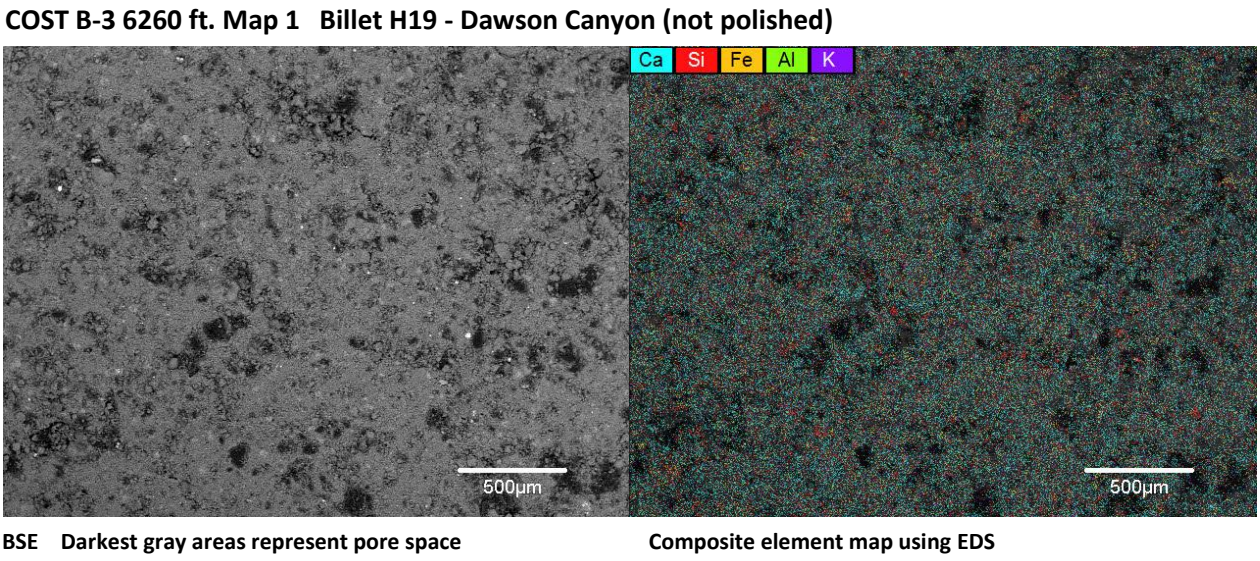

Figure 14. Sample SEM results from calcareous potential caprock in the COST B-3 well.

4.3 Integration of New and Legacy Hydrologic Property Data

Work has been completed on the integration of the new analytical results with the mined legacy data spreadsheets, formatting for the Access database, and import into the Access database. Stratigraphic picks have been revised, and the current picks were used to assign the hydrologic property data values to the appropriate defined potential storage units for resource calculations and potential caprock units for characterization. It is important to note that the analytical results provided in the appendices (i.e., Appendix D, E, F, G and H) have formation names assigned based on the stratigraphic picks that were available at the time of sampling. As a result, there

will be differences in the formations assigned to some samples in the reports and in the tables in this report. Current stratigraphic picks for each sample can be found in Table 4 and also in Appendix C, which contains a comparison of the provisional and current stratigraphic picks.

This integration process will also involve assessing and validating each value through cross-comparison of mined legacy data with new data from all the studies performed. This effort will involve scrutinizing data values from core plug analysis (40 analysis points each for permeability, porosity, and grain density), probe permeability (81 analysis points), petrographic analysis (82 analysis points), and mineralogical and geochemical analyses (76 XRF analysis points, 75 XRD analysis points, and 18 SEM analysis points). These data will be combined with the stratigraphic and petrophysical analyses. This large volume of data available, both from mined legacy data and new data generated specifically for this project, can be applied, compared, and cross-correlated to allow for a robust interpretation and application of the data to storage resource assessments. An integration workshop will be held to accomplish this task.

Results from intervals designated as high priority for further analysis during sample selection due to variability in the range of available values or lack of measured values will be prioritized. For example, a wide range of permeability values was observed over closely spaced sample intervals in the legacy data from the COST B-2 well, core 2 (8238 to 8265 ft) and core 3 (9280 to 9330 ft), as shown in the plot by Rutgers (Figure 15).

Initial results verify the observed variability; the new measurements are shown in Figures 16 and 17 and in Table 14. However, the more robust core plug measurements did not reproduce the highest permeability values (>1000 mD) at corresponding or close sample points, suggesting that these values will need to be scrutinized further when integrating all the available data. These steps—analysis, cross-validation, and integration of analyses results—will prove to be crucial in the utilization of all the data for the remaining project tasks.

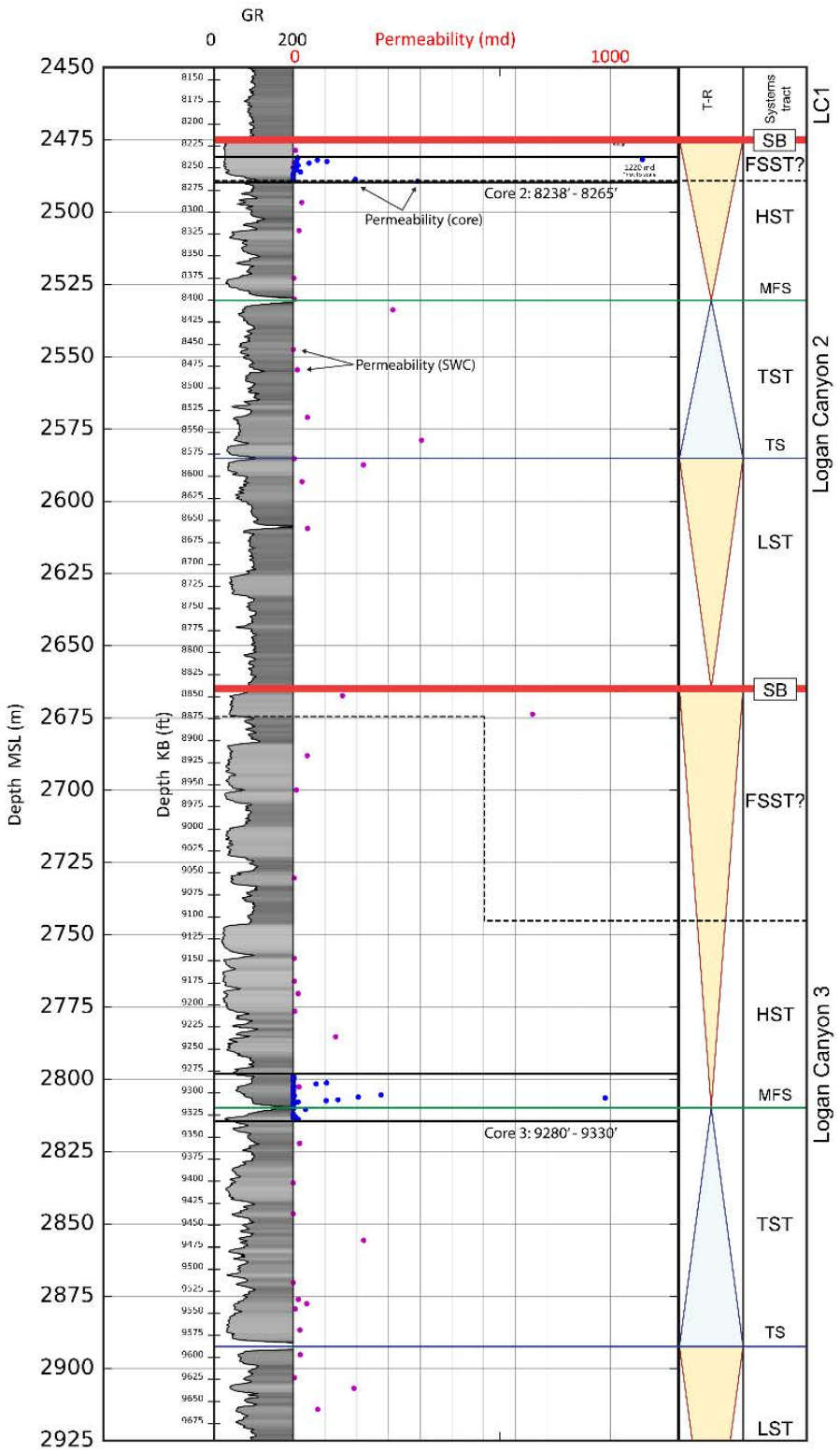

Figure 15. Stratigraphic column and permeability in the Logan Canyon Formation in the COST B-2 well (courtesy Rutgers University team).

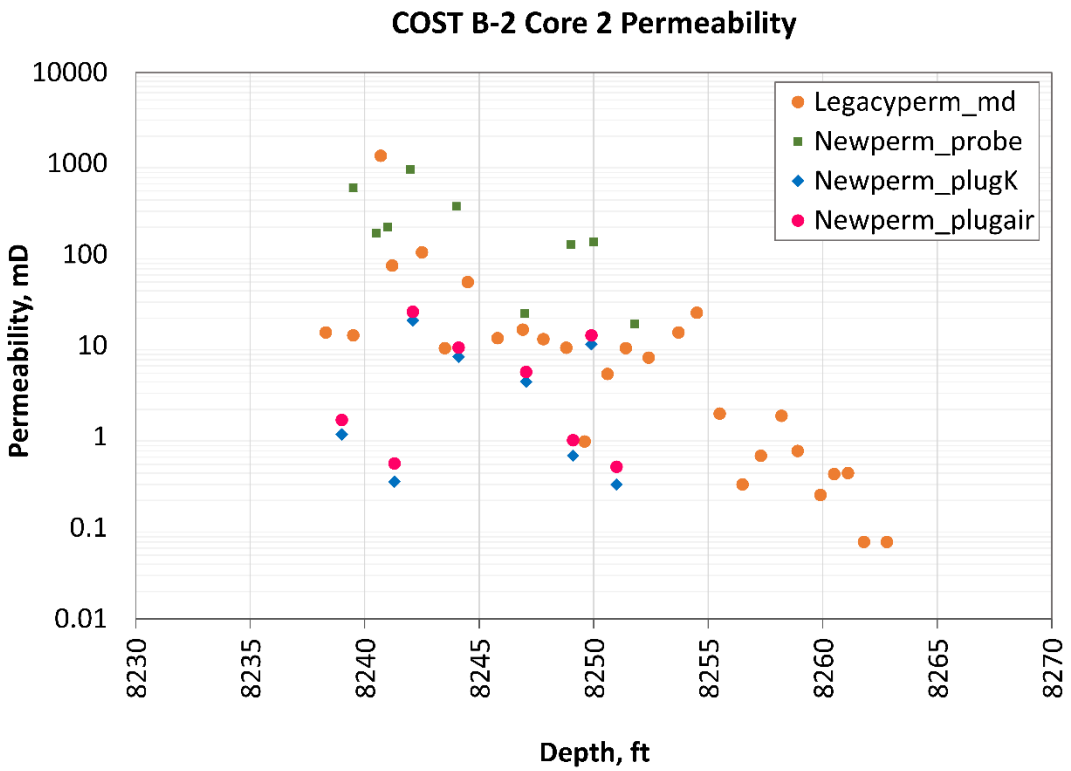

Figure 16. Comparison of legacy permeability data with new permeability measurements collected for this study, COST B-2 well, Core 2, 8238-8265 ft.

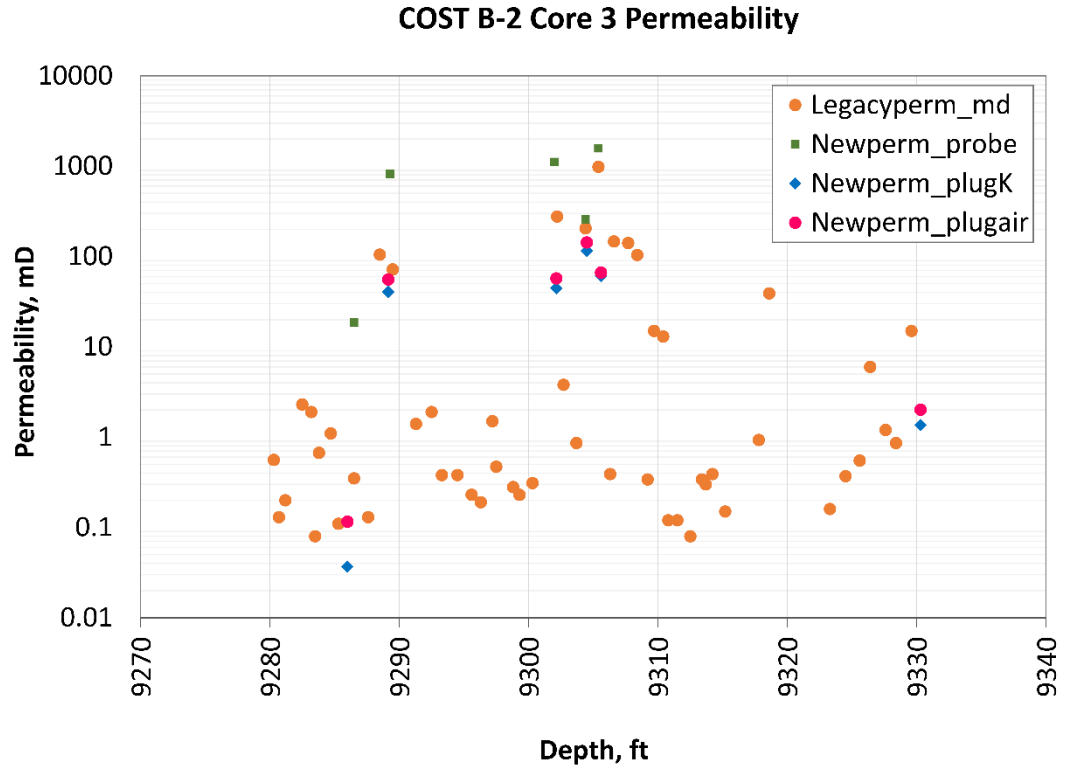

Figure 17. Comparison of legacy permeability data with new permeability measurements collected for this study, COST B-2 well, Core 3, 9280-9330 ft.

Table 14 also shows that the sidewall core samples that were selected to fill gaps in the COST B-3 and Mobil 544-1 wells (as these were the only samples available in the gaps) could only be analyzed for probe permeability. These results will have to be supplemented with the petrography and mineralogical analysis in determining the hydrologic properties to use in those intervals.

Some observations can be made from the data in Table 14 which can inform how these data are applied for resource calculations as well as other project tasks as noted in Section 4.4. Generally, thin section porosity estimates are lower than measured porosity, which may be due to the fact that point counting only accounts for visible porosity. This suggests that microporosity may have a significant effect on the hydrologic properties of the units. Several samples (e.g., COST G-1 5471 ft, COST B-3 11050.8 ft and Shell 632-1 4594.5 ft) where macroporosity dominates show closer correlation between measured and thin section porosity values. This correlation is not observed where microporosity may be an important factor e.g. COST B-2 8247 ft. (Figure 18). See Table 10 and Table 14 for absolute values of porosity and porosity types.

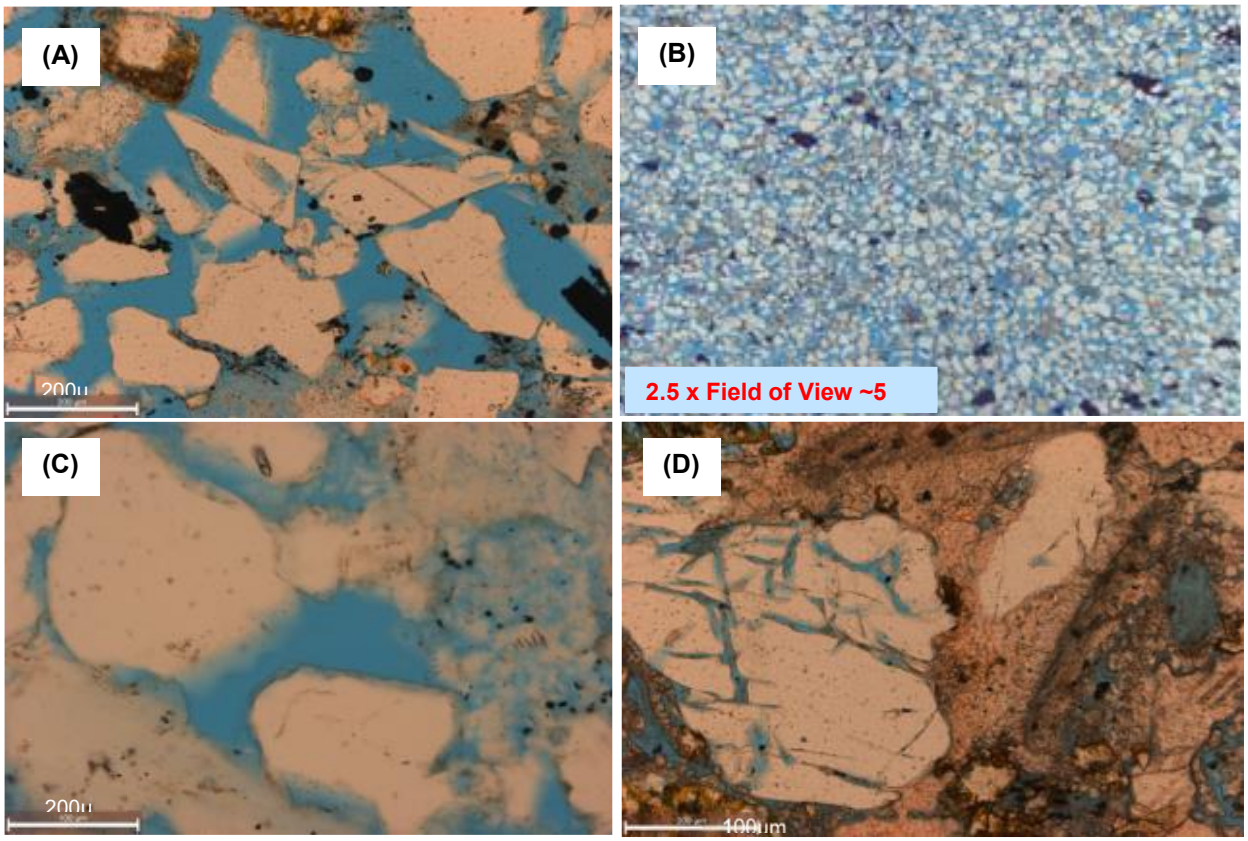

Figure 18. Photomicrographs showing (A) COST G-1 (at 5471 ft) intergranular and dissolution porosity; (B) Shell 632-1 (at 4594.5 ft) intergranular porosity; (C) COST B-3 (at 11050.8 ft) intergranular and dissolution porosity; and (D) COST B-2 (at 8247 ft) intergranular porosity

Table 14. Comparison of legacy and new hydrologic property data for the analyzed samples.

Well	Sample selection criteria/utility	Depth (ft)	Sample type	Thin section		Core porosity		Core permeability				Grain density		Notes
				Billet no.	Porosity	Legacy	New - plug	Legacy	New - probe	New - plugK	New - plugair	Legacy	New-plug	
COST G-1	VE	5471	Slab/Chip	**H32**	22.8	29.00		753.0	1000.00			2.66		
COST G-1	VE	5473	Slab	**H33**	19.0	32.00	30.29	1120.0	1220.00	286.8886	318.0758	2.67	2.66	
COST G-1	VE	5480-5481 (5480.6)	Slab	**H34**	0.0	29.50	13.03		0.827; 0.2	5.4259	5.8077	2.66	2.73	Plug measurements at 5480.4; Legacy value is average of 7 samples btw 5469-5489
COST G-1	VE	5480.6	Slab	**DGS**	0.0	29.50			0.827; 0.2	5.4259	5.8077	2.66	2.73	Plug measurements at 5480.4
COST G-1	VE	9992	Slab	**H35**	0.0	2.20	4.91	0.0		0.0542	0.0731	2.67	2.70	Legacy at 9992.5; New at 9992.05
COST G-1	VE	9992.8	Slab	**H36**	0.0			0.0	1.12; 0.929			2.67		Legacy at 9992.5
COST G-1	VE	10001.3	Slab	**H37**	0.5	4.00	8.04	0.0		0.2385	0.2889	2.66	2.70	Legacy at 10001, plug at 10001.1
COST G-1	VE	10001.3	Slab	**H37**	0.5	2.50		0.0	2.06; 34.1			2.66	2.70	
COST G-2	VE, LC	8753.7	Slab	**H38**	11.7	20.00	19.66	211.0	94.20	18.9728	23.1783	2.68	2.67	plug at 8753.0
COST G-2	VE, LC	8753.7	Slab	**H38**		23.70		19.0				***2.61***		SWC at 8753.0, empirical K
COST G-2	VE, LC	8756	Slab	**H39**	11.1	18.20	18.05	90.0	56.4; 11.9	17.4784	21.5809	2.67	2.67	Legacy at 8755.95
COST B-2	LC	5030.2	Slab	**H1**	15.6	24.70	19.51		990.00	71.2945	85.7541	2.68	2.69	plug at 5030.3
COST B-2	LC	8239	Slab	**H2**	9.7		14.87			1.0608	1.5325		2.72	
COST B-2	LC	8239.5	Slab	**H3**	7.8	16.20	14.87	13.0	542.00	1.0608	1.5325	2.69	2.72	plug at 8239
COST B-2		8240.7				26.50		1220.0				2.66		* Legacy value of interest
COST B-2	LC	8241	Slab	**H4**	4.5	18.60	11.37	76.0	202.00	0.3212	0.5098	2.70	2.71	Legacy at 8241.2, plug at 8241.3; *critical sample
COST B-2	LC	8242	Slab	**H5**	9.7	23.10	20.52	106.0	861.00	18.9339	23.5900	2.69	2.71	Legacy at 8242.5, plug at 8242.1
COST B-2	LC	8244	Slab	**H6**	5.8	19.70	17.13	50.0	338.00	7.5665	9.5247	2.67	2.70	legacy at 8244.5; plug at 8244.1
COST B-2	LC	8244	Slab	**H6**		***23.30***		***2.8***				***2.75***		SWC
COST B-2	LC	8247	Slab	**H7**	3.8	18.50	15.33	15.0	22.50	4.0261	5.1510	2.70	2.71	Legacy at 8246.9; plug at 8247.05
COST B-2	LC	8248.9	Slab	**H8**	5.4	18.60		9.5				2.71		Legacy at 8248.8
COST B-2	LC	8249	Slab	**H9**	2.4	11.70	12.23	0.9	130.00	0.6217	0.9173	2.69	2.70	Legacy at 8249.6;plug at 8249.1
COST B-2	LC	8250	Slab	**H10**	5.9	17.40	20.62	4.9	137.00	10.3738	12.9812	2.71	2.74	Legacy at 8250.6; plug at 8249.9
COST B-2	LC	8251	Slab	**H11**	2.7	18.20	11.96	9.4	17.30	0.2989	0.4692	2.70	2.71	Legacy at 8251.4; probe at 8251.8
COST B-2	LC	9286.5	Slab	**H12**	1.4	8.70	11.21	0.4	18.50	0.0368	0.1159	2.69	2.70	Plug at 9286
COST B-2	LC	9289.3	Slab	**H13**	8.9	25.30	25.49	72.0	825.00	40.5881	55.6171	2.66	2.67	Legacy at 9289.5; plug at 9289.15
COST B-2	LC	9302	Slab	**H14**	15.4	27.40	23.62	277.0	1110.00	44.5984	57.4080	2.69	2.75	Legacy at 9302.2; plug at 9302.15
COST B-2	LC	9304.4	Slab	**H15**	16.0	23.70	23.74	205.0	257.00	115.3904	143.3522	2.66	2.68	Plug at 9304.5
COST B-2	LC	9305.4	Slab	**H16**	10.3	28.10	23.71	983.0	1580.00	60.8881	66.3801	2.67	2.68	Plug at 9305.6; *critical sample
COST B-2	LC	9330	Slab	**H17**	6.9	24.40		15.0				2.68		Legacy at 9329.6; *critical sample
COST B-2	LC	9330.2	Slab	**H18**	8.9	24.40	22.62	15.0	223.00	1.3633	2.0134	2.68	2.70	Legacy at 9329.6; plug at 9330.3; *critical sample
COST B-3	FG	6260	SWC	**H19**	0.0				0.09					
COST B-3	FG	7040	SWC	**H20**	0.5				0.29					
COST B-3	FG	7640	SWC	**H21**	2.6				0.39					
COST B-3	FG	8382	SWC	**H22**	11.7				N/A					
COST B-3	FG	9750	SWC	**H23**	0.9				185.00					
COST B-3	VE	9931.6	Slab	**H24**	0.0	4.10	4.82	0.0	0.16	<LOD	<LOD	2.70	2.71	Plug at 9931
COST B-3	VE	9932	Slab	**H25**	5.1	23.00	24.27	2292.0	198.00	25.3676	29.1006	2.74	2.74	
COST B-3	VE	9934	Slab	**H26**	0.7	3.40	3.64	0.0	1.11	0.0019	0.0081	2.69	2.69	Legacy at 9934.5

Table 14 (cont.). Comparison of legacy and new hydrologic property data for the analyzed samples.

Well	Sample selection criteria/utility	Depth (ft)	Sample type	Thin section		Core porosity		Core permeability				Grain density		Notes
				Billet no.	Porosity	Legacy	New - plug	Legacy	New - probe	New - plugK	New - plugair	Legacy	New-plug	
COST B-3	VE	11050.8	Slab	**H28**	22.9	25.70	25.01	236.0	514.00	85.0208	98.2190	2.65	2.66	Legacy at 11050.2; plug at 11050
COST B-3	VE	11051-11052	SLS	**H29**	3.0	24.00		142.0				2.65		Legacy at 11051.2
COST B-3	VE	11054	Slab	**H30**	17.9	25.70	23.89	222.0	602.00	44.2948	54.8612	2.66	2.67	Legacy at 11053.7; plug at 11054.1
COST B-3	VE	12581.9	Slab	**H31**	2.0	9.70	8.80	47.0	0.51	0.2509	0.3425	2.71	2.71	Legacy core fractured, legacy K at 12581.0 is 0.02mD
Mobil 544-1	FG	5211	SWC	**H50**	3.3				279.00					
Mobil 544-1	FG	5435	SWC	**H51**	3.5				275.00					
Mobil 544-1	FG	5962	SWC	**H52**	0.9				N/A					
Mobil 544-1	FG	6260	SWC	**H53**	5.3				12.30					
Mobil 544-1	FG	6420	SWC	**H54**	0.0				0.60					
Mobil 544-1	FG	6579	SWC	**H55**	9.3				1.24					
Mobil 544-1	FG	6696	SWC	**H56**	2.8				1.56					
Mobil 544-1	FG	6798	SWC	**H57**	11.7				N/A					
Mobil 544-1	FG	7096	SWC	**H58**	16.2				2700.00					Sample failed during measurement
Mobil 544-1	FG	7258	SWC	**H59**	17.8				105.00					
Mobil 544-1	FG	8497	SWC	**H60**	0.0				1.66					
Mobil 544-1	LC	9039	SWC	**H61**	17.2				11.40					
Exxon 684-1	LC	9438	Chip	**H40**	15.4	24.50	27.21	768.0	1890.00	N/A	N/A		2.69	Legacy at 9438-9439
Exxon 684-1	LC	9439	Chip	**H41**	21.6	26.10		1865.0	2810.00					Legacy at 9439-9440
Exxon 684-1	LC	9440	Chip	**H42**	19.3	28.90		1005.0	1440.00					Legacy at 9440-9441
Exxon 684-1	LC	9441	Chip	**H43**	20.4	25.00		1754.0	1640.00					Legacy at 9441-9442
Exxon 684-1	LC	12137	Chip	**H44**	0.5	N/A	3.58	N/A	1.27	0.0006	0.0035	N/A	2.69	No legacy analysis on shale
Exxon 684-1	LC	12199	Chip	**H45**	5.7	10.90		4.2	8.96			2.69		Legacy at 12199-12200
Exxon 684-1	LC	12204	Chip	**H46**	0.3	6.60	3.94	<0.1	11.80	0.0710	0.1081	2.66	2.61	Legacy at 12204-12204.5
Exxon 684-1	LC	12729	Chip	**H47**	9.5	20.10	17.20	332.0	212.00	66.3663	79.2340	2.73	2.64	Legacy at 12729-12730
Exxon 684-1	LC	12767	Chip	**H48**	10.0	16.60		18.0	27.30			2.68		Legacy at 12767-12768
Exxon 684-1	LC	12802	Chip	**H49**	14.6	18.30		949.0	921.00			2.68		Legacy at 12802-12803
Conoco 145-1	VE, LC	9226	Slab	**H62**	0.0	3.00		<0.01						Thin section only
Exxon 684-2	VE, LC	15242	Chip	**H63**	3.7	13.10	10.90	1.3	11.60			2.67	2.68	
Shell 273-1	VE, LC	7010	Chip	**H64**	5.7				330.00					
Shell 273-1	VE, LC	7077	Chip	**H65**	0.5	6.40		0.0	2.74					Legacy values from sample 7077-7078
Shell 586-1	VE, LC	9058-9058.7	Slab/chip	**H67**	5.7	17.00	17.01	0.5	24.40	0.3975	0.5702	2.70	2.71	2 probe at 9058-9058.7, new core at 9058.3, legacy at 9058.0
Shell 586-1	VE, LC	9058-9058.7	Slab/chip	**H67**	5.7	17.00	17.01	0.5	10.00	0.3975	0.5702	2.70	2.71	2 probe at 9058-9058.7, new core at 9058.3, legacy at 9058.0
Shell 632-1	VE, LC	4594.5	Chip	**H69**	23.7	24.80		39.0	372.00					Legacy at 4594-4595
Shell 632-1	VE, LC	6278.8	Chip	**H70**	5.1	18.30		1.1	3.28					
Shell 632-1	VE, LC	8083.1	Chip	**H71**	10.3	17.50	18.50	8.3	23.80				2.69	Legacy at 8083-8084
Shell 93-1	VE, LC	9937	Chip	**H72**	31.6		27.00	105.0	1320.00					Legacy at 9935 from SWC, empirical K
Texaco 598-1	VE, LC	12840-12841	Chip	**H73**	10.0	17.30	17.86	4.9	45.70	4.5450	5.2236	2.66		New poroperm at 12840.5

Table 14 (cont.). Comparison of legacy and new hydrologic property data for the analyzed samples.

Well	Sample selection criteria/utility	Depth (ft)	Sample type	Thin section		Core porosity		Core permeability				Grain density		Notes
				Billet no.	Porosity	Legacy	New - plug	Legacy	New - probe	New - plugK	New - plugair	Legacy	New-plug	
Texaco 598-1	VE, LC	13275-13276	Chip	**H75**	10.3	18.40	17.69	1590.0	151.00	103.4680	190.0954	2.68		New core plug data at 13275
Texaco 642-1	VE, LC	12444	Chip	**H76**	0.7	3.39			0.11	0.0908	0.1637	2.68		Legacy K from close core samples reported as <0.1 (<LOD)
Texaco 642-1	VE, LC	12444	Chip	**H76**	0.7	22.50		14.0						SWC, empirical K
Texaco 642-1	VE, LC	15608	Chip	**H77**	21.3	19.30		4.0	30.60			2.67		
Exxon 599-1	VE, LC	12386	Chip	**H78**	10.6	17.90	17.26	1953.0		124.5270	199.5965		2.64	Legacy at 12386-12386.4: New at 13286.5
Exxon 599-1	VE, LC	12386	Chip	**H78**	10.6	15.20	17.26	314.0		124.5270	199.5965		2.64	Legacy at 12386.6-12387: New at 13286.5
Exxon 599-1	VE, LC	12387	Chip	**H79**	12.6	19.30	17.26	126.0		124.5270	199.5965			New at 13286.5
Exxon 599-1	VE, LC	12403	Chip	**H80**	12.9	18.30		408.0	1710.00					Legacy at 12402-12403
Exxon 599-1	VE, LC	12403	Chip	**H80**	12.9	18.60		1436.0	1710.00					Legacy at 12403-12404
Shell 372-1	VE, LC	10872.9-10873.2	Chip	**H66**	1.6	16.10		24.6	0.584; 69.1			2.78		Legacy at 10872 on fractured plug; 2 probe measurements
Shell 372-1	VE, LC	10872.9-10873.2	Chip	**H66**	1.6	14.20		2.2	0.584; 69.1			2.76		Legacy at 10873 on fractured plug
Shell 372-1	VE, LC	10872.9-10873.2	Chip	**DGS**	0.0	16.10		24.6	0.584; 69.1			2.78		Legacy at 10872 on fractured plug
Shell 372-1	VE, LC	10872.9-10873.2	Chip	**DGS**	0.0	14.20		2.2	0.584; 69.1			2.76		Legacy at 10873 on fractured plug
Shell 587-1	VE, LC	11555	Slab/chip	**H68**	1.5	7.90		10.1	1.80			2.707		New probe data at 11554.9

* SWC = sidewall core; FG = fills data gap, VE = validates empirical data, LC = legacy data comparison; LOD = limit of detection.
Note: Sidewall core measurements in bold italics; N/A = not available.

4.4 Future Applications of Hydrologic Property Data

The large volume of hydrologic property data assembled for the project are being used primarily to characterize potential storage resources as well as potential caprock units. However, the interdisciplinary nature of the research effort requires the integration of data generated from the different tasks.

These data will be applied to other tasks as needed, such as stratigraphic analysis, well log calibration and characterization, seismic inversion, and risk assessment; the results will be integrated to validate and /or update previous and ongoing interpretation. One application could be to use legacy data to extend the calibration of neutron and density logs to porosity values. For example, new analysis from the Shell 586-1 well on a limestone sample from 9058.3 ft returned the same values as the legacy values from 9058.0 ft, with both yielding porosities of 17% and grain densities of 2.7. This reproducibility of the values gives confidence for their application to log/porosity calibration, especially when a limestone matrix is used. Similarly comparable results are seen in several sandstone samples. For example, new analyses from 8756 ft in the COST G-2 well yielded a porosity of 18% and a grain density of 2.67, essentially the same as legacy data from 8755.95 ft. The reproducibility of measurements suggests that the compiled data can be used for log porosity calibration when a sandstone matrix is used.

It is important to note that the formations provided in this report and appendices are based on provisional picks that may be revised as the seismic data evaluation and storage resource calculation tasks progress. A lithostratigraphic approach was developed to guide the selection of formation tops and bases from well log signatures. These tops and bases were used to define formation zones to which existing core data points and samples have been assigned as part of the data gap analysis. However, the sequence stratigraphy is being used to correlate rock units across the study area, using seismic data where well data are not available. Thus, another activity will be to assign hydrologic property data to sequence stratigraphic-based rock units by correlating the lithostratigraphic-based intervals to the sequence stratigraphic-based intervals.

5.0 Conclusions

The objective of the hydrologic property analyses conducted for this project was to assemble a comprehensive dataset from mid-Atlantic OCS wells that will support two of the project's main goals: to assess pore space available for CO_2 storage and to characterize the physical properties of potential storage zones and confining caprocks. Data were compiled on the porosity, permeability, and composition of sample materials. Work involved a comprehensive compilation of existing data from well reports and other publications as well as generation of new data from new laboratory analyses. The use of multiple methodologies for analysis of porosity, permeability, and sample composition allows for the understanding of rock properties at different scales and from different physical measures. Porosity was measured by laboratory tests of core plugs and examination of thin sections. Permeability was measured by laboratory measurements of core plugs and probe permeameter measurements on sample surfaces. Composition was measured using XRD of powdered samples, XRF measurements on sample surfaces, SEM of small sample surfaces, and examination of thin sections.

A large volume (more than 9,000 individual entries) of legacy hydrologic property data was assembled by mining well reports, documents, and published material. Gaps in the compiled data within the stratigraphic intervals of interest (Dawson Canyon to Mohawk) were assessed using an automated method built into an Access database. This process was also used to assess the availability of samples at the DGS OCS repository to enable new analyses to be carried out to fill gaps in data coverage and validate existing data where applicable.

A series of workshops were held to plan sample analyses and to select samples. Seventy-five sample points from 17 wells were selected for analysis. Porosity, permeability, and grain density measurements carried out by a commercial laboratory yielded important new data that filled in gaps in legacy data coverage and provided new analyses to verify legacy data of special interest. Petrographic, mineralogical, and geochemical analyses conducted at the PaGS generated additional porosity and compositional data that can be used to understand the relationship of hydrologic properties and mineralogy of samples. In total, the new analyses provided 40 new data points for permeability, porosity, and grain density from core plug samples, 81 points of permeability measurement from probe permeameter analyses, 82 points with new porosity and mineralogy data measured in thin sections, and a large dataset of new instrumental measurements of sample mineralogy and geochemistry (76 XRF analysis points, 75 XRD analysis points, and 18 SEM analysis points). The new hydrologic property data have been integrated with existing legacy data in an Access database.

Overall, the results confirm that the most promising storage resources are in the Logan Canyon and Mississauga Formations and that the Naskapi and Mic Mac Formations are locally important as seals. The results also show that the units are heterogeneous, with stratigraphic and areal (geographic) variations in lithologies and hydrologic properties observed. These variations must be taken into consideration in the assessment of each unit.

Comparison of the data obtained using different analytical methods for measuring hydrologic properties and composition also shows the importance of understanding the strengths and weaknesses of each method, particularly relating to sample size, sampling resolution, and the physical means of measurement. Different sources of porosity and permeability measurements provide different means of characterizing the hydrologic properties of the formations. Some measurement methods estimate the properties of a larger volume of rock (for example, on core plugs) that give a better average character, whereas other methods (such as probe

permeameter) provide measurements on a small point area on a surface. The multiple datasets can be compared to each other for a more comprehensive understanding of the rock properties.

The results of these analyses provide a basis for improved understanding of the potential storage resource and caprock units. Where legacy data were reproduced, the existing data were validated, which allows for confident application to other tasks such as well log calibration and risk assessment. Where there are discrepancies, results from multiple analyses allow for scrutiny and validation of property values. Calibration of sample-based hydrologic property measurements to geophysical log data can be extended spatially in future work through the relationship of geophysical log data to seismic character.

The large volume of both mined legacy data and new analytical data compiled for this project task, combined with stratigraphic and petrophysical analyses conducted for other project tasks, allows for a robust interpretation of hydrologic properties of the subsurface formations of the Atlantic OCS, resulting in insights that can ultimately be applied to the assessment of carbon storage resource volumes present in the study area.

Mid-Atlantic U.S. Offshore Carbon Storage Resource Assessment Project

MID-ATLANTIC U.S. OFFSHORE
CARBON STORAGE RESOURCE
ASSESSMENT PROJECT

DOE Award Number DE-FE0026087

THIN SECTION REPORTS

March 2018

Thin Section Reports Index

	Well	Depth (ft.)	Sample Type	Thin Section - Stained	Thin Section - Not Stained	Thin Section - Billet No.
1.	**COST G-1**	5471	Slab/Chip	**X**		**H32**
2.	**COST G-1**	5473	Slab	**X**		**H33**
3.	**COST G-1**	5480.6	Slab		**X**	**H34**
4.	**COST G-1**	5480.6	Slab			**DGS**
5.	**COST G-1**	9992	Slab		**X**	**H35**
6.	**COST G-1**	9992.8	Slab		**X**	**H36**
7.	**COST G-1**	10001.3	Slab		**X**	**H37**
8.	**COST G-2**	8753.7	Slab	**X**		**H38**
9.	**COST G-2**	8756	Slab	**X**		**H39**
10.	**COST B-2**	5030.2	Slab	**X**		**H1**
11.	**COST B-2**	8239	Slab	**X**		**H2**
12.	**COST B-2**	8239.5	Slab	**X**		**H3**
13.	**COST B-2**	8241	Slab	X		**H4**
14.	**COST B-2**	8242	Slab	**X**		**H5**
15.	**COST B-2**	8244	Slab	**X**		**H6**
16.	**COST B-2**	8247	Slab	**X**		**H7**
17.	**COST B-2**	8248.9	Slab	**X**		**H8**
18.	**COST B-2**	8249	Slab	**X**		**H9**
19.	**COST B-2**	8250	Slab	**X**		**H10**
20.	**COST B-2**	8251	Slab	**X**		**H11**
21.	**COST B-2**	9286.5	Slab	**X**		**H12**
22.	**COST B-2**	9289.3	Slab	**X**		**H13**
23.	**COST B-2**	9302	Slab	**X**		**H14**
24.	**COST B-2**	9304.4	Slab	**X**		**H15**
25.	**COST B-2**	9305.4	Slab		**X**	**H16**
26.	**COST B-2**	9330	Slab	**X**		**H17**
27.	**COST B-2**	9330.2	Slab	**X**		**H18**
28.	**COST B-3**	6260	Sidewall core		**X**	**H19**
29.	**COST B-3**	7040	Sidewall core		**X**	**H20**
30.	**COST B-3**	7640	Sidewall core		**X**	**H21**
31.	**COST B-3**	8382	Sidewall core	**X**		**H22**
32.	**COST B-3**	9750	Sidewall core		**X**	**H23**
33.	**COST B-3**	9931.6	Slab	**X**		**H24**
34.	**COST B-3**	9932	Slab	**X**		**H25**
35.	**COST B-3**	9934	Slab	**X**		**H26**
36.	**COST B-3**	11042	Slab	**X**		**H27**
37.	**COST B-3**	11050.8	Slab	**X**		**H28**
38.	**COST B-3**	11051-11052	SLS		**X**	**H29**
39.	**COST B-3**	11054	Slab	**X**		**H30**
40.	**COST B-3**	12581.9	Slab	**X**		**H31**
41.	**Mobil 544-1**	5211	Sidewall core		**X**	**H50**
42.	**Mobil 544-1**	5435	Sidewall core		**X**	**H51**

Thin Section Reports Index

	Well	Depth (ft.)	Sample Type	Thin Section - Stained	Thin Section - Not Stained	Thin Section - Billet No.
43.	Mobil 544-1	5962	Sidewall core		X	H52
44.	Mobil 544-1	6260	Sidewall core		X	H53
45.	Mobil 544-1	6420	Sidewall core		X	H54
46.	Mobil 544-1	6579	Sidewall core		X	H55
47.	Mobil 544-1	6696	Sidewall core		X	H56
48.	Mobil 544-1	6798	Sidewall core	X		H57
49.	Mobil 544-1	7096	Sidewall core	X		H58
50.	Mobil 544-1	7258	Sidewall core	X		H59
51.	Mobil 544-1	8497	Sidewall core	X		H60
52.	Mobil 544-1	9039	Sidewall core	X		H61
53.	Exxon 684-1	9438	Chip	X		H40
54.	Exxon 684-1	9439	Chip	X		H41
55.	Exxon 684-1	9440	Chip	X		H42
56.	Exxon 684-1	9441	Chip	X		H43
57.	Exxon 684-1	12137	Chip		X	H44
58.	Exxon 684-1	12199	Chip	X		H45
59.	Exxon 684-1	12204	Chip		X	H46
60.	Exxon 684-1	12729	Chip	X		H47
61.	Exxon 684-1	12767	Chip	X		H48
62.	Exxon 684-1	12802	Chip	X		H49
63.	Exxon 684-2	15242	Chip	X		H63
64.	Conoco 145-1	9226	Slab	X		H62
65.	Shell 273-1	7010	Chip	X		H64
66.	Shell 273-1	7077	Chip	X		H65
67.	Shell 372-1	10872.9-10873.2	Chip		X	H66
68.	Shell 372-1	10872.9-10873.2	Chip			DGS
69.	Shell 586-1	9058-9058.7	Slab/Chip	X		H67
70.	Shell 587-1	11555	Slab/Chip	X		H68
71.	Shell 632-1	4594.5	Chip	X		H69
72.	Shell 632-1	6278.8	Chip	X		H70
73.	Shell 632-1	8083.1	Chip	X		H71
74.	Shell 93-1	9937	Chip	X		H72
75.	Texaco 598-1	12840-12841	Chip	X		H73
76.	Texaco 598-1	13271-13272	Chip	X		H74
77.	Texaco 598-1	13275-13276	Chip	X		H75
78.	Texaco 642-1	12444	Chip	X		H76
79.	Texaco 642-1	15608	Chip		X	H77
80.	Exxon 599-1	12386	Chip	X		H78
81.	Exxon 599-1	12387	Chip	X		H79
82.	Exxon 599-1	12403	Chip	X		H80

Thin Section Analysis Report

Sample ID: COST G-1
Sample Condition: standard rectangular size
Formation Name: Mic-Mac
Depth (ft): 5471 ft
Lithology: Sandstone

Date of Analysis: 2/26/2018
Analyzed by: Kristin M. Carter
Point Count Step Size 0.4 mm
Number of Counts 400

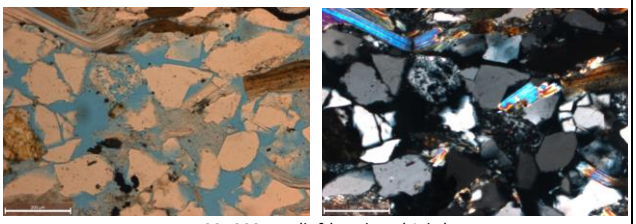

no32_0001 PL (left) and XN (right)

All scale bars are 200 um, unless otherwise noted

Texture - Qualitative Assessment

Approximate Average Grain Size (mm): 0.2
Grain Sorting: moderately well sorted
Grain Rounding: angular to subrounded

Composition - Modal Analysis Data

Framework

Mineral Grains	Total	Percent
Quartz		**22.5**
Monocrystalline	87	21.8
Polycrystalline	3	0.8
Chert		
Feldspar		**33.8**
Plagioclase	113	28.3
Microcline	3	0.8
K-Feldspar	19	4.8
Carbonate		**0.0**
Calcite		
Dolomite		

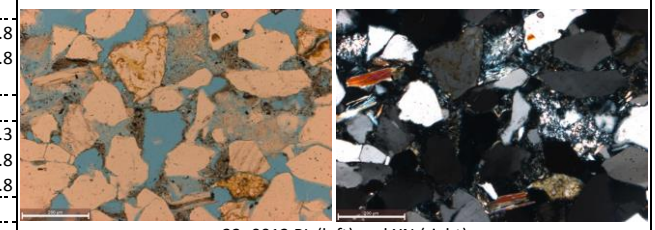

no32_0012 PL (left) and XN (right)

Lithic Grains	Total	Percent
		0.0
Metamorphic		
Sedimentary		
Volcanic		

Accessory Minerals	Total	Percent
		2.3
Rutile		
Tourmaline		
Zircon		
Opaques	9	2.3

Matrix Spaces

Cement	Total	Percent
		0.0
Quartz		
K-Feldspar		
Calcite		
Dolomite/Ankerite		
Iron Oxide		

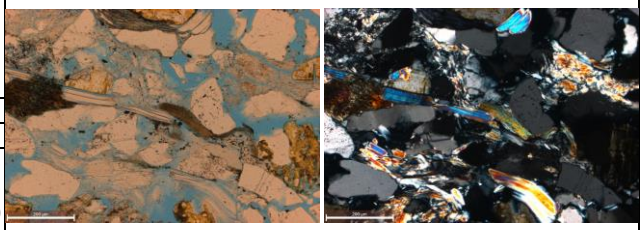

no32_0011 PL (left) and XN (right)

Matrix	Total	Percent
Clay Minerals		**18.8**
Clay Minerals (not individually identifiable)	45	11.3
Muscovite	18	4.5
Biotite	4	1.0
Chlorite		
Glauconite		
Illite	8	2.0

Porosity	Total	Percent
		22.8
Intergranular	54	13.5
Intragranular		
Intercrystalline		
Moldic	3	0.8
Grain/Cement Dissolution	29	7.3
Clay/Mica Framework		
Organic Matter		
Vug	4	1.0
Channel		
Fracture	1	0.3
	Total	**100.0**

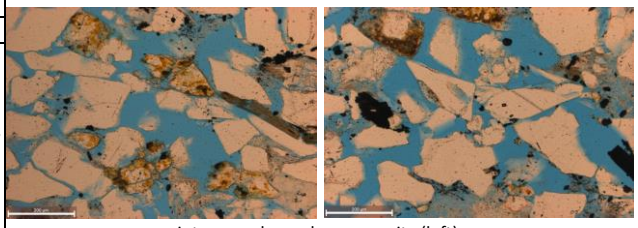

intergranular and vug porosity (left);
intergranular and dissolution porosity (right)
no32_0006 PL (left) and no32_0008 PL (right)

Back to Index

Thin Section Analysis Report

Sample ID: COST G-1
Sample Condition: standard rectangular size
Formation Name: Mic-Mac
Depth (ft): 5473 ft
Lithology: Sandstone

Date of Analysis: 2/28/2018
Analyzed by: Kristin M. Carter
Point Count Step Size 0.4 mm
Number of Counts 411

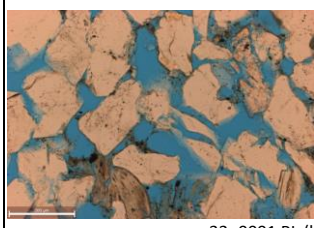
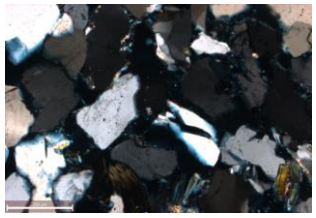

no33_0001 PL (left) and XN (right)

All scale bars are 200 um, unless otherwise noted

Texture - Qualitative Assessment

Approximate Average Grain Size (mm): 0.2
Grain Sorting: moderately well sorted
Grain Rounding: angular to subrounded

Composition - Modal Analysis Data

Framework

Mineral Grains	Total	Percent
Quartz		**18.2**
Monocrystalline	71	17.3
Polycrystalline	4	1.0
Chert		
Feldspar		**39.9**
Plagioclase	130	31.6
Microcline	6	1.5
K-Feldspar	28	6.8
Carbonate		**0.2**
Calcite	1	0.2
Dolomite		

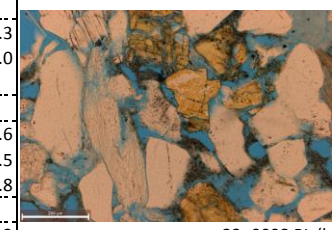
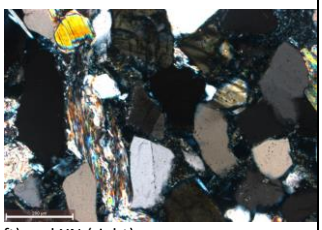

no33_0008 PL (left) and XN (right)

Lithic Grains	Total	Percent
		0.0
Metamorphic		
Sedimentary		
Volcanic		

Accessory Minerals	Total	Percent
		0.7
Rutile		
Tourmaline	1	0.2
Zircon		
Opaques	2	0.5

Matrix Spaces

Cement	Total	Percent
		0.0
Quartz		
K-Feldspar		
Calcite		
Dolomite/Ankerite		
Iron Oxide		

Matrix	Total	Percent
Clay Minerals		**21.9**
Clay Minerals (not individually identifiable)	68	16.5
Muscovite	13	3.2
Biotite	2	0.5
Chlorite		
Glauconite		
Illite	7	1.7

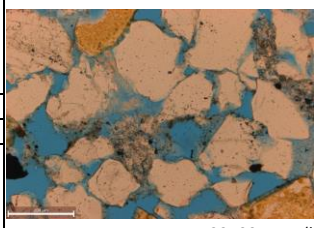
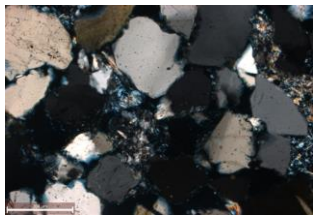

no33_0014 PL (left) and XN (right)

Porosity	Total	Percent
		19.0
Intergranular	46	11.2
Intragranular		
Intercrystalline		
Moldic	4	1.0
Grain/Cement Dissolution	26	6.3
Clay/Mica Framework		
Organic Matter		
Vug	2	0.5
Channel		
Fracture		
	Total	**100.0**

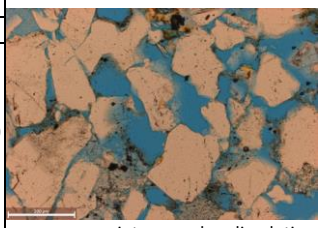
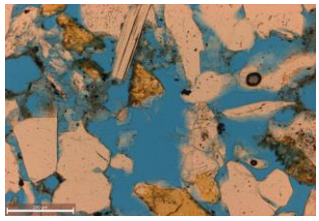

intergranular, dissolution and moldic porosity (left);
vug, moldic and dissolution porosity (right)
no33_0006 PL (left) and no33_0010 PL (right)

Back to Index

Thin Section Analysis Report

Sample ID: COST G-1
Sample Condition: rectangular, two pieces
Formation Name: Mic-Mac
Depth (ft): 5480-5481 (5480.6) ft
Lithology: Siltstone

Date of Analysis: 2/28/2018
Analyzed by: Kristin M. Carter
Point Count Step Size 0.3 mm
Number of Counts 407

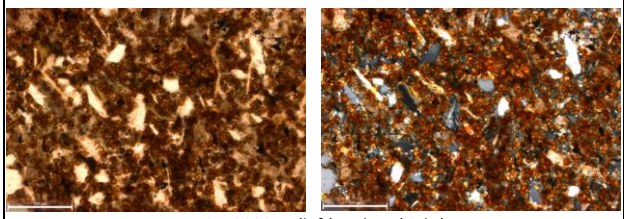

no34_0009 PL (left) and XN (right)

All scale bars are 100 um, unless otherwise noted

Texture - Qualitative Assessment

Approximate Average Grain Size (mm): 0.05
Grain Sorting: poorly to moderately well sorted
Grain Rounding: angular to subrounded

Composition - Modal Analysis Data

Framework

Mineral Grains	Total	Percent
Quartz		**6.9**
Monocrystalline	28	6.9
Polycrystalline		
Chert		
Feldspar		**5.7**
Plagioclase	22	5.4
Microcline	1	0.2
K-Feldspar		
Carbonate		**1.0**
Calcite	4	1.0
Dolomite		

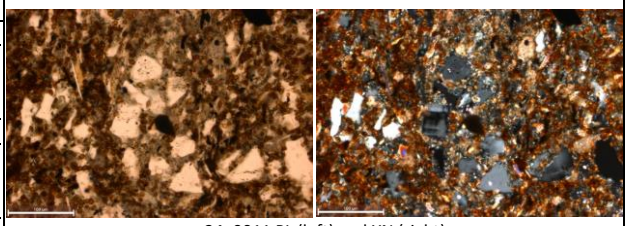

no34_0011 PL (left) and XN (right)

Lithic Grains	Total	Percent
		0.0
Metamorphic		
Sedimentary		
Volcanic		

Accessory Minerals	Total	Percent
		2.9
Rutile		
Tourmaline		
Zircon		
Opaques	12	2.9

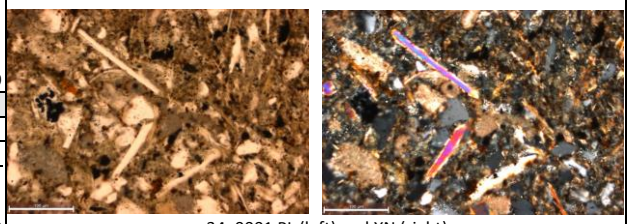

no34_0001 PL (left) and XN (right)

Matrix Spaces

Cement	Total	Percent
		23.6
Quartz		
K-Feldspar		
Calcite	4	1.0
Dolomite/Ankerite		
Iron Oxide	92	22.6

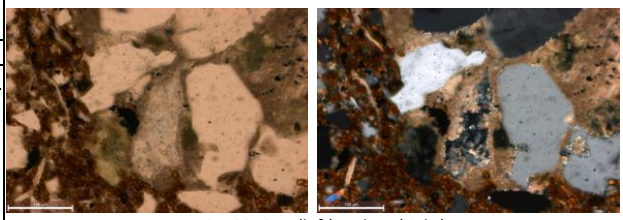

no34_0010 PL (left) and XN (right)

Matrix	Total	Percent
Clay Minerals		**60.0**
Clay Minerals (not individually identifiable)	221	54.3
Muscovite	11	2.7
Biotite	9	2.2
Chlorite	3	0.7
Glauconite		
Illite		

Porosity	Total	Percent
		0.0
Intergranular		
Intragranular		
Intercrystalline		
Moldic		
Grain/Cement Dissolution		
Clay/Mica Framework		
Organic Matter		
Vug		
Channel		
Fracture		
	Total	**100.0**

Back to Index

Thin Section Analysis Report

Sample ID: COST G-1
Sample Condition: rectangular, two pieces
Formation Name: Mic-Mac
Depth (ft): 5480.6 ft
Lithology: Siltstone

Date of Analysis: 3/2/2018
Analyzed by: Kristin M. Carter
Point Count Step Size 0.3 mm
Number of Counts 407

Texture - Qualitative Assessment

Approximate Average Grain Size (mm): 0.05
Grain Sorting: poorly sorted
Grain Rounding: angular to subrounded

Composition - Modal Analysis Data

Framework

Mineral Grains	Total	Percent
Quartz		**10.3**
Monocrystalline	41	10.1
Polycrystalline	1	0.2
Chert		
Feldspar		**5.2**
Plagioclase	21	5.2
Microcline		
K-Feldspar		
Carbonate		**4.4**
Calcite	18	4.4
Dolomite		

Lithic Grains	Total	Percent
		0.0
Metamorphic		
Sedimentary		
Volcanic		

Accessory Minerals	Total	Percent
		4.7
Rutile		
Tourmaline		
Zircon		
Opaques	19	4.7

Matrix Spaces

Cement	Total	Percent
		2.7
Quartz		
K-Feldspar		
Calcite	10	2.5
Micrite	1	0.2
Dolomite/Ankerite		
Iron Oxide		

Matrix	Total	Percent
Clay Minerals		**72.7**
Clay Minerals (not individually identifiable)	283	69.5
Muscovite	5	1.2
Biotite	1	0.2
Chlorite	6	1.5
Glauconite		
Illite	1	0.2

Porosity	Total	Percent
		0.0
Intergranular		
Intragranular		
Intercrystalline		
Moldic		
Grain/Cement Dissolution		
Clay/Mica Framework		
Organic Matter		
Vug		
Channel		
Fracture		
	Total	**100.0**

Pre-Existing Delaware Geological Survey Thin Section

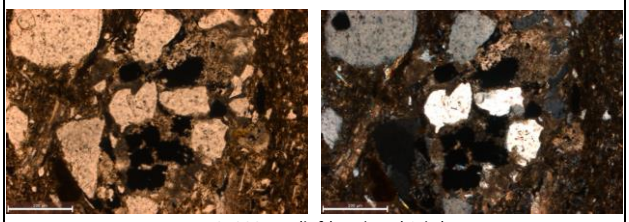

no40_0004 PL (left) and XN (right)

All scale bars are 200 um, unless otherwise noted

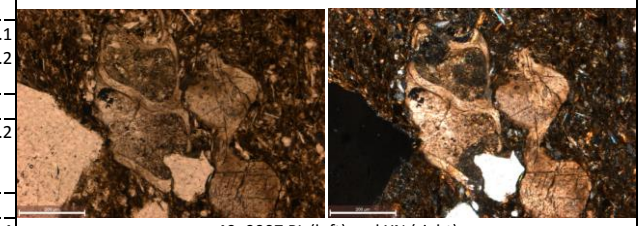

no40_0007 PL (left) and XN (right)

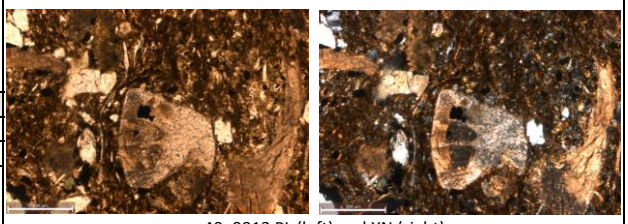

no40_0013 PL (left) and XN (right)

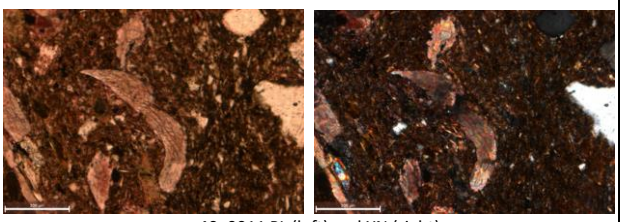

no40_0011 PL (left) and XN (right)

Back to Index

Thin Section Analysis Report

Sample ID: COST G-1
Sample Condition: standard rectangular size
Formation Name: Mohawk
Depth (ft): 9992 ft
Lithology: Sandstone

Date of Analysis: 2/28/2018
Analyzed by: Kristin M. Carter
Point Count Step Size 0.3 mm
Number of Counts 401

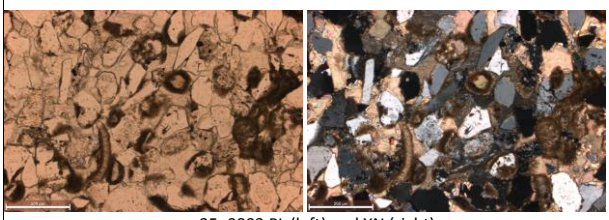

no35_0003 PL (left) and XN (right)

All scale bars are 200 um, unless otherwise noted

Texture - Qualitative Assessment

Approximate Average Grain Size (mm): 0.1
Grain Sorting: moderately well sorted
Grain Rounding: mostly subrounded

Composition - Modal Analysis Data

Framework

Mineral Grains	Total	Percent
Quartz		**16.7**
Monocrystalline	64	16.0
Polycrystalline	3	0.7
Chert		
Feldspar		**22.7**
Plagioclase	86	21.4
Microcline	5	1.2
K-Feldspar		
Carbonate		**5.2**
Calcite		
Micritized Oolites	21	5.2
Dolomite		

Lithic Grains	Total	Percent
		0.0
Metamorphic		
Sedimentary		
Volcanic		

Accessory Minerals	Total	Percent
		1.2
Rutile		
Tourmaline		
Zircon		
Opaques	5	1.2

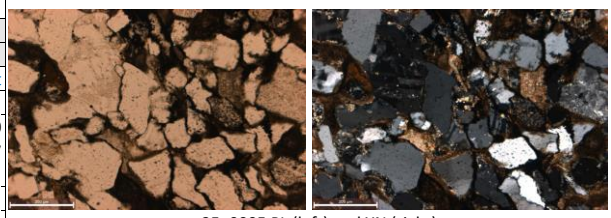

no35_0005 PL (left) and XN (right)

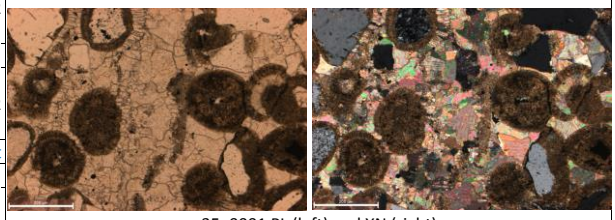

no35_0001 PL (left) and XN (right)

Matrix Spaces

Cement	Total	Percent
		52.6
Quartz		
K-Feldspar		
Calcite	127	31.7
Micrite	61	15.2
Dolomite/Ankerite		
Iron Oxide	23	5.7

Poikilotopic calcite cement in places

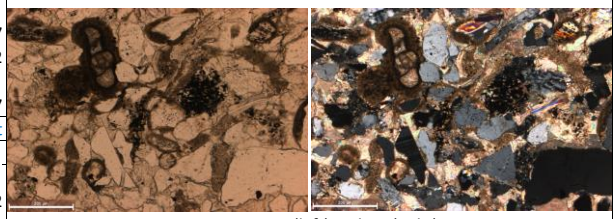

no35_0012 PL (left) and XN (right)

Matrix	Total	Percent
Clay Minerals		**1.5**
Clay Minerals (not individually identifiable)		
Muscovite	1	0.2
Biotite	1	0.2
Chlorite		
Glauconite		
Illite	4	1.0

Porosity	Total	Percent
		0.0
Intergranular		
Intragranular		
Intercrystalline		
Moldic		
Grain/Cement Dissolution		
Clay/Mica Framework		
Organic Matter		
Vug		
Channel		
Fracture		
	Total	**100.0**

Back to Index

Thin Section Analysis Report

Sample ID: COST G-1
Sample Condition: standard rectangular size
Formation Name: Mohawk
Depth (ft): 9992.8 ft
Lithology: Sandstone

Date of Analysis: 2/28/2018
Analyzed by: Kristin M. Carter
Point Count Step Size 0.3 mm
Number of Counts 417

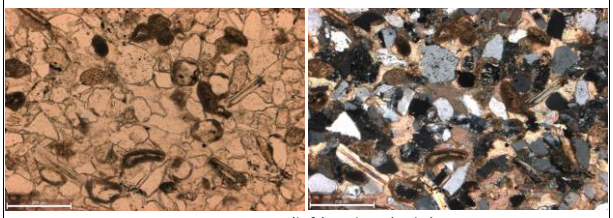

no36_0002 PL (left) and XN (right)

All scale bars are 200 um, unless otherwise noted

Texture - Qualitative Assessment

Approximate Average Grain Size (mm): 0.1
Grain Sorting: well sorted
Grain Rounding: mostly subrounded

Composition - Modal Analysis Data

Framework

Mineral Grains	Total	Percent
Quartz		**21.3**
Monocrystalline	89	21.3
Polycrystalline		
Chert		
Feldspar		**18.5**
Plagioclase	76	18.2
Microcline	1	0.2
K-Feldspar		
Carbonate		**2.9**
Calcite		
Micrite-Coated Grains	12	2.9
Dolomite		

Lithic Grains	Total	Percent
		0.0
Metamorphic		
Sedimentary		
Volcanic		

Accessory Minerals	Total	Percent
		2.4
Rutile		
Tourmaline		
Zircon		
Opaques	10	2.4

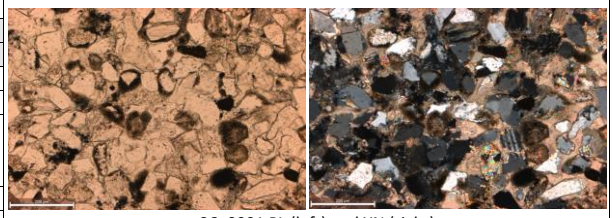

no36_0001 PL (left) and XN (right)

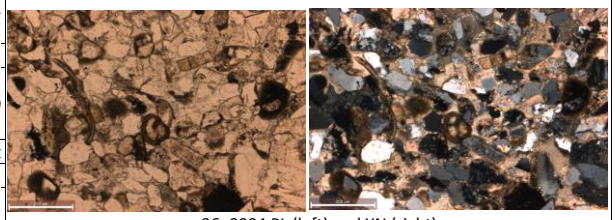

no36_0004 PL (left) and XN (right)

Matrix Spaces

Cement	Total	Percent
		54.2
Quartz		
K-Feldspar		
Calcite	197	47.2
Micrite	29	7.0
Dolomite/Ankerite		
Iron Oxide		

Poikilotopic calcite cement in places

Matrix	Total	Percent
Clay Minerals		**0.7**
Clay Minerals (not individually identifiable)		
Muscovite	3	0.7
Biotite		
Chlorite		
Glauconite		
Illite		

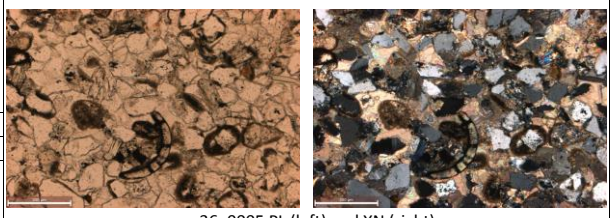

no36_0005 PL (left) and XN (right)

Porosity	Total	Percent
		0.0
Intergranular		
Intragranular		
Intercrystalline		
Moldic		
Grain/Cement Dissolution		
Clay/Mica Framework		
Organic Matter		
Vug		
Channel		
Fracture		
	Total	**100.0**

Back to Index

Thin Section Analysis Report

Sample ID: COST G-1
Sample Condition: standard rectangular slide
Formation Name: Mohawk
Depth (ft): 10,001.3 ft
Lithology: Sandstone

Date of Analysis: 2/28/2018
Analyzed by: Kristin M. Carter
Point Count Step Size 0.3 mm
Number of Counts 426

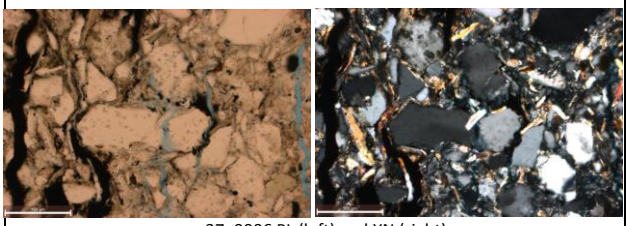

no37_0006 PL (left) and XN (right)

All scale bars are 100 um, unless otherwise noted

Texture - Qualitative Assessment

Approximate Average Grain Size (mm): 0.1
Grain Sorting: poorly to moderately sorted
Grain Rounding: angular to subrounded

Composition - Modal Analysis Data

Framework

Mineral Grains	Total	Percent
Quartz		**17.6**
Monocrystalline	73	17.1
Polycrystalline	2	0.5
Chert		
Feldspar		**23.0**
Plagioclase	97	22.8
Microcline	1	0.2
K-Feldspar		
Carbonate		**0.0**
Calcite		
Dolomite		

Lithic Grains	Total	Percent
		0.0
Metamorphic		
Sedimentary		
Volcanic		

Accessory Minerals	Total	Percent
		6.8
Rutile		
Tourmaline		
Zircon		
Opaques	29	6.8

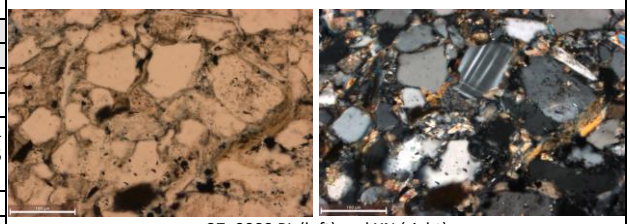

no37_0009 PL (left) and XN (right)

Matrix Spaces

Cement	Total	Percent
		7.5
Quartz		
K-Feldspar		
Calcite	30	7.0
Micrite	2	0.5
Dolomite/Ankerite		
Iron Oxide		

Matrix	Total	Percent
Clay Minerals		**44.6**
Clay Minerals (not individually identifiable)	154	36.2
Muscovite	13	3.1
Biotite	16	3.8
Chlorite		
Glauconite		
Illite	7	1.6

Porosity	Total	Percent
		0.5
Intergranular		
Intragranular		
Intercrystalline		
Moldic		
Grain/Cement Dissolution		
Clay/Mica Framework		
Organic Matter		
Vug		
Channel	2	0.5
Fracture		
	Total	**100.0**

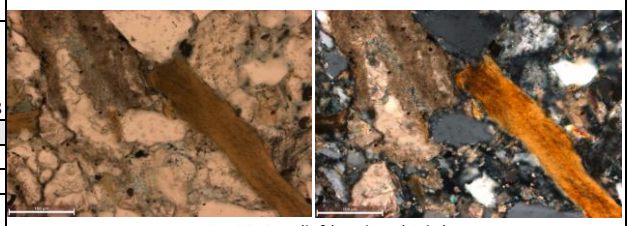

no37_0010 PL (left) and XN (right)

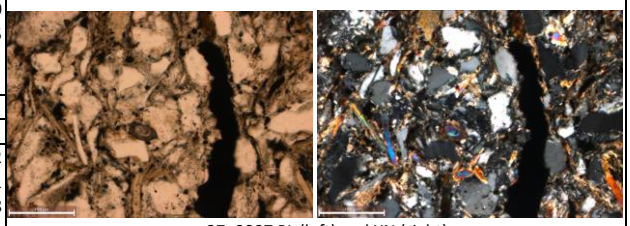

no37_0007 PL (left) and XN (right)

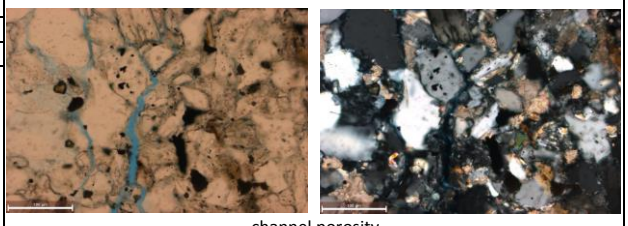

channel porosity
no37_0004 PL (left) and XN (right)

Back to Index

Thin Section Analysis Report

Sample ID: COST G-2
Sample Condition: standard rectangular size
Formation Name: Mohawk
Depth (ft): 8753.7 ft
Lithology: Sandstone

Date of Analysis: 3/2/2018
Analyzed by: Kristin M. Carter
Point Count Step Size 1.0 mm
Number of Counts 403

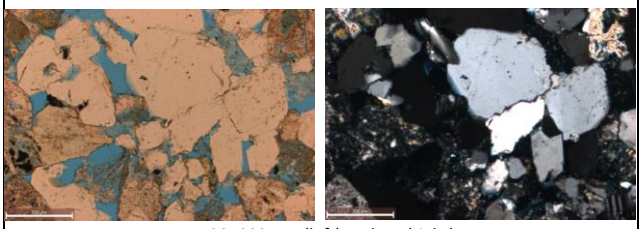

no38_0001 PL (left) and XN (right)

All scale bars are 200 um, unless otherwise noted

Texture - Qualitative Assessment

Approximate Average Grain Size (mm): 0.2
Grain Sorting: moderately well sorted
Grain Rounding: subangular to subrounded

Composition - Modal Analysis Data

Framework

Mineral Grains	Total	Percent
Quartz		**18.4**
Monocrystalline	57	14.1
Polycrystalline	17	4.2
Chert		
Feldspar		**47.9**
Plagioclase	192	47.6
Microcline	1	0.2
K-Feldspar		
Carbonate		**0.0**
Calcite		
Dolomite		

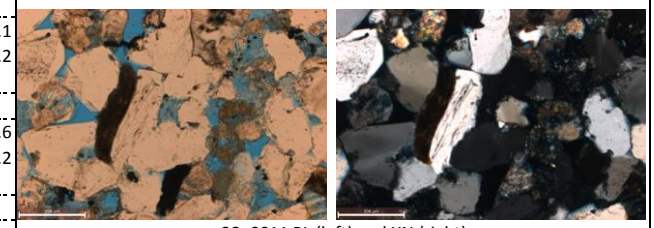

no38_0011 PL (left) and XN (right)

Lithic Grains	Total	Percent
		0.0
Metamorphic		
Sedimentary		
Volcanic		

Accessory Minerals	Total	Percent
		1.2
Rutile		
Tourmaline		
Zircon		
Opaques	5	1.2

Matrix Spaces

Cement	Total	Percent
		1.5
Quartz		
K-Feldspar		
Calcite	6	1.5
Dolomite/Ankerite		
Iron Oxide		

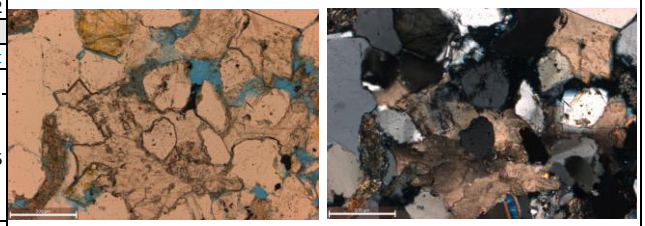

no38_0003 PL (left) and XN (right)

Matrix	Total	Percent
Clay Minerals		**19.4**
Clay Minerals (not individually identifiable)	60	14.9
Muscovite	1	0.2
Biotite	1	0.2
Chlorite	3	0.7
Glauconite		
Illite	13	3.2

Porosity	Total	Percent
		11.7
Intergranular	22	5.5
Intragranular		
Intercrystalline		
Moldic	1	0.2
Grain/Cement Dissolution	22	5.5
Clay/Mica Framework		
Organic Matter		
Vug		
Channel	2	0.5
Fracture		
	Total	**100.0**

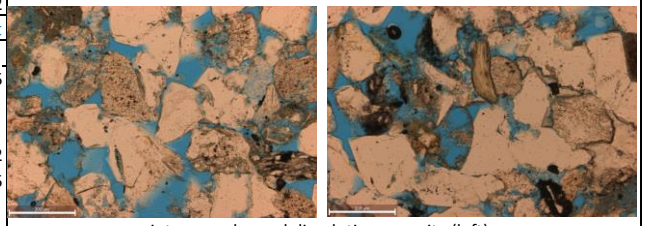

intergranular and dissolution porosity (left);
moldic and intergranular porosity (right)
no38_0006 PL (left) and no38_0010 PL (right)

Back to Index

Thin Section Analysis Report

Sample ID: COST G-2
Sample Condition: standard rectangular size
Formation Name: Mohawk
Depth (ft): 8756 ft
Lithology: Sandstone

Date of Analysis: 3/2/2018
Analyzed by: Kristin M. Carter
Point Count Step Size 1.0 mm
Number of Counts 405

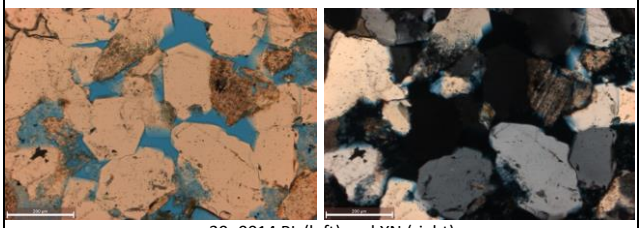

no39_0014 PL (left) and XN (right)

All scale bars are 200 um, unless otherwise noted

Texture - Qualitative Assessment

Approximate Average Grain Size (mm): 0.3
Grain Sorting: moderately well sorted
Grain Rounding: angular to subrounded

Composition - Modal Analysis Data

Framework

Mineral Grains	Total	Percent
Quartz		**25.9**
Monocrystalline	93	23.0
Polycrystalline	12	3.0
Chert		
Feldspar		**36.3**
Plagioclase	141	34.8
Microcline	6	1.5
K-Feldspar		
Carbonate		**0.5**
Calcite	2	0.5
Dolomite		

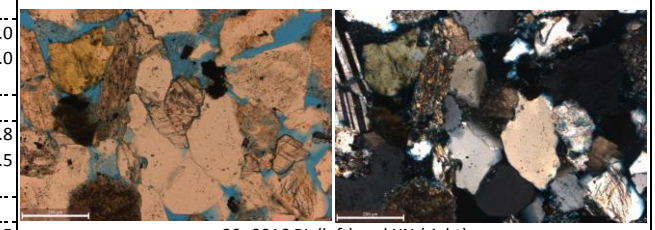

no39_0016 PL (left) and XN (right)

Lithic Grains	Total	Percent
		0.0
Metamorphic		
Sedimentary		
Volcanic		

Accessory Minerals	Total	Percent
		0.7
Rutile		
Tourmaline		
Zircon		
Opaques	3	0.7

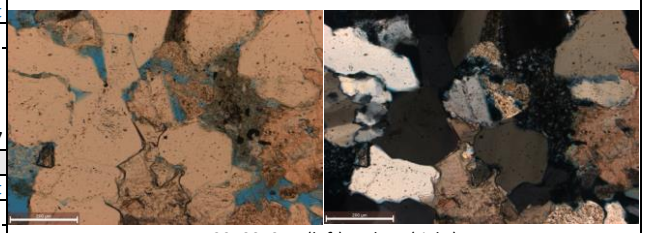

no39_0010 PL (left) and XN (right)

Matrix Spaces

Cement	Total	Percent
		4.4
Quartz		
K-Feldspar		
Calcite	18	4.4
Dolomite/Ankerite		
Iron Oxide		

Matrix	Total	Percent
Clay Minerals		**21.0**
Clay Minerals (not individually identifiable)	62	15.3
Muscovite	1	0.2
Biotite		
Chlorite		
Glauconite		
Illite	22	5.4

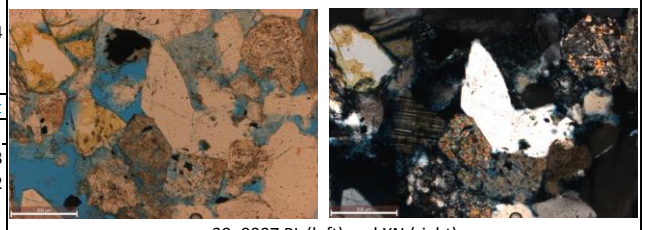

no39_0007 PL (left) and XN (right)

Porosity	Total	Percent
		11.1
Intergranular	23	5.7
Intragranular		
Intercrystalline		
Moldic	1	0.2
Grain/Cement Dissolution	21	5.2
Clay/Mica Framework		
Organic Matter		
Vug		
Channel		
Fracture		
	Total	**100.0**

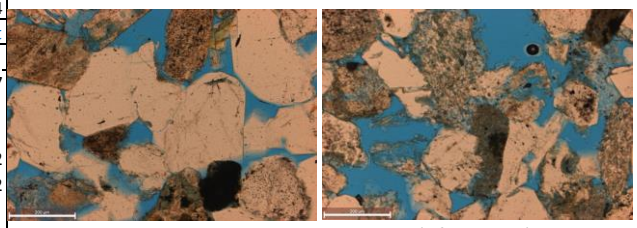

intergranular and dissolution porosity (left and right)
no39_0005 PL (left) and no39_0019 PL (right)

Back to Index

Thin Section Analysis Report

Sample ID: COST B-2
Sample Condition: standard rectangular size
Formation Name: Wyandot
Depth (ft): 5030.2 ft
Lithology: Sandstone

Date of Analysis: 2/9/2018
Analyzed by: Kristin M. Carter
Point Count Step Size 1.0 mm
Number of Counts 416

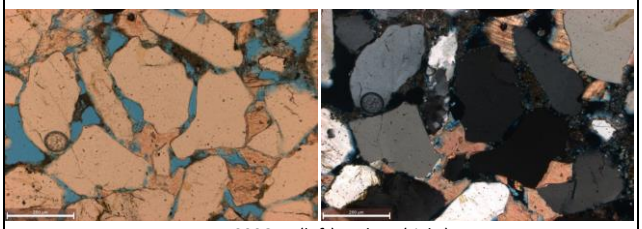

no1_0006 PL (left) and XN (right)

All scale bars are 200 um, unless otherwise noted

Texture - Qualitative Assessment

Approximate Average Grain Size (mm): 0.2
Grain Sorting: moderately well sorted
Grain Rounding: subangular to subrounded

Composition - Modal Analysis Data

Framework

Mineral Grains	Total	Percent
Quartz		**57.2**
Monocrystalline	236	56.7
Polycrystalline	2	0.5
Chert		
Feldspar		**5.5**
Plagioclase	11	2.6
Microcline	2	0.5
K-Feldspar	10	2.4
Carbonate		**2.4**
Calcite	10	2.4
Dolomite		

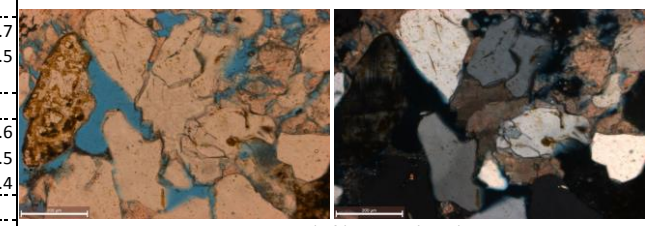

no1_0011 PL (left) and XN (right)

Lithic Grains	Total	Percent
		0.0
Metamorphic		
Sedimentary		
Volcanic		

Accessory Minerals	Total	Percent
		0.0
Rutile		
Tourmaline		
Zircon		
Opaques		

Matrix Spaces

Cement	Total	Percent
		19.0
Quartz		
K-Feldspar		
Calcite	67	16.1
Dolomite/Ankerite		
Iron Oxide	12	2.9

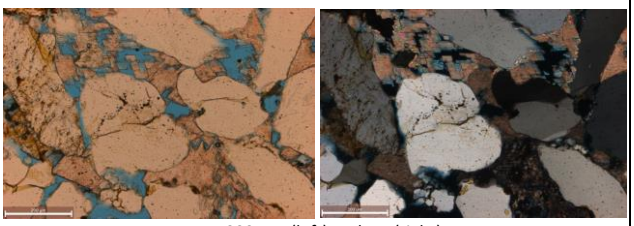

no1_0007 PL (left) and XN (right)

Matrix	Total	Percent
Clay Minerals		**0.2**
Clay Minerals (not individually identifiable)		
Muscovite	1	0.2
Biotite		
Chlorite		
Glauconite		
Illite		

Porosity	Total	Percent
		15.6
Intergranular	36	8.7
Intragranular		
Intercrystalline		
Moldic	12	2.9
Grain/Cement Dissolution	17	4.1
Clay/Mica Framework		
Organic Matter		
Vug		
Channel		
Fracture		
	Total	**100.0**

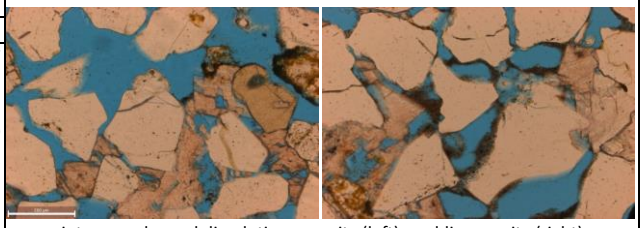

intergranular and dissolution porosity (left); moldic porosity (right)
no1_0010 PL (left) and no1_0001 PL (right)

Back to Index

Thin Section Analysis Report

Sample ID: COST B-2
Sample Condition: standard, two pieces
Formation Name: Upper Logan Canyon
Depth (ft): 8239 ft
Lithology: Sandstone

Date of Analysis: 2/9/2018
Analyzed by: Kristin M. Carter
Point Count Step Size 1.0 mm
Number of Counts 412

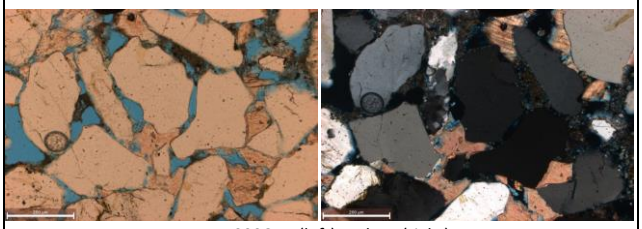

no1_0006 PL (left) and XN (right)

All scale bars are 200 um, unless otherwise noted

Texture - Qualitative Assessment

Approximate Average Grain Size (mm): 0.6
Grain Sorting: poorly sorted
Grain Rounding: subangular to subrounded

Composition - Modal Analysis Data

Framework

Mineral Grains	Total	Percent
Quartz		**54.9**
Monocrystalline	202	49.0
Polycrystalline	24	5.8
Chert		
Feldspar		**4.6**
Plagioclase	13	3.2
Microcline	1	0.2
K-Feldspar	5	1.2
Carbonate		**4.9**
Calcite	20	4.9
Dolomite		

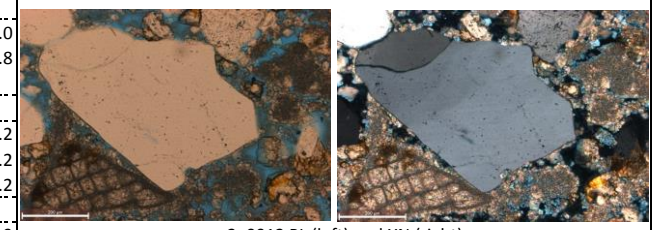

no2_0012 PL (left) and XN (right)

Lithic Grains	Total	Percent
		0.0
Metamorphic		
Sedimentary		
Volcanic		

Accessory Minerals	Total	Percent
		0.0
Rutile		
Tourmaline		
Zircon		
Opaques		

Matrix Spaces

Cement	Total	Percent
		19.4
Quartz		
K-Feldspar		
Calcite	74	18.0
Dolomite/Ankerite		
Iron Oxide	6	1.5

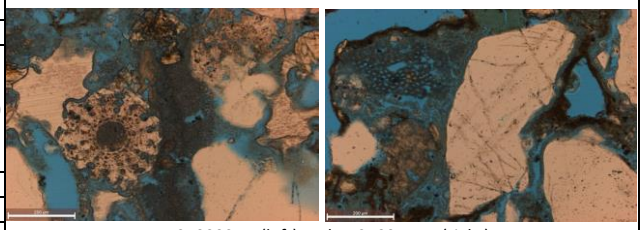

no2_0009 PL (left) and no2_0011 PL (right)

Matrix	Total	Percent
Clay Minerals		**6.6**
Clay Minerals (not individually identifiable)	27	6.6
Muscovite		
Biotite		
Chlorite		
Glauconite		
Illite		

Porosity	Total	Percent
		9.7
Intergranular	18	4.4
Intragranular	3	0.7
Intercrystalline		
Moldic	6	1.5
Grain/Cement Dissolution	12	2.9
Clay/Mica Framework		
Organic Matter		
Vug		
Channel		
Fracture	1	0.2
	Total	**100.0**

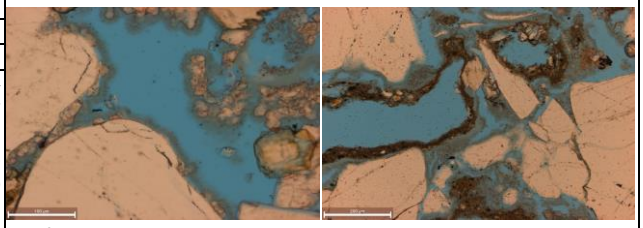

left scale bar - 100 um

intergranular porosity (left); moldic and dissolution porosity (right)

no2_0002 PL (left) and no2_0004 PL (right)

Back to Index

Thin Section Analysis Report

Sample ID: COST B-2
Sample Condition: standard rectangular size
Formation Name: Upper Logan Canyon
Depth (ft): 8239.5 ft
Lithology: Sandstone

Date of Analysis: 2/12/2018
Analyzed by: Kristin M. Carter
Point Count Step Size 1.0 mm
Number of Counts 412

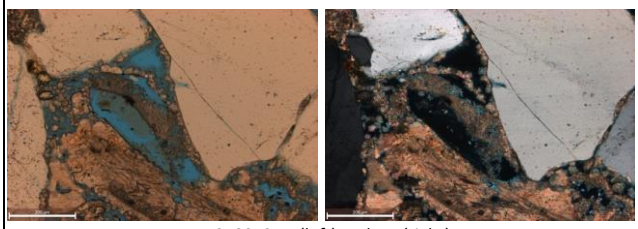

no3_0012 PL (left) and XN (right)

All scale bars are 200 um, unless otherwise noted

Texture - Qualitative Assessment

Approximate Average Grain Size (mm): 0.8
Grain Sorting: poorly sorted
Grain Rounding: subangular to subrounded

Composition - Modal Analysis Data

Framework

Mineral Grains	Total	Percent
Quartz		**51.2**
Monocrystalline	176	42.7
Polycrystalline	35	8.5
Chert		
Feldspar		**2.7**
Plagioclase		
Microcline	1	0.2
K-Feldspar	10	2.4
Carbonate		**10.7**
Calcite	44	10.7
Dolomite		

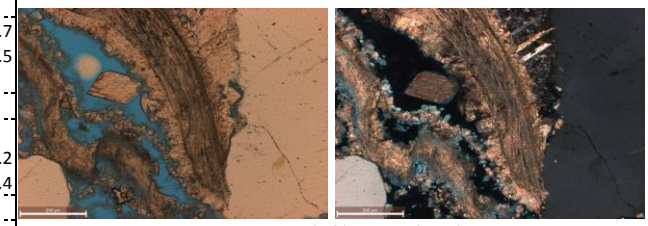

no3_0004 PL (left) and XN (right)

Lithic Grains	Total	Percent
		0.0
Metamorphic		
Sedimentary		
Volcanic		

Accessory Minerals	Total	Percent
		0.0
Rutile		
Tourmaline		
Zircon		
Opaques		

Matrix Spaces

Cement	Total	Percent
		23.3
Quartz		
K-Feldspar		
Calcite	95	23.1
Dolomite/Ankerite		
Iron Oxide	1	0.2

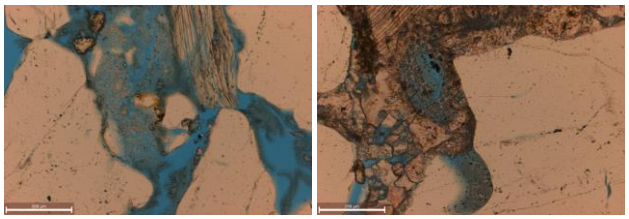

no3_0007 PL (left) and no3_0010 PN (right)

Matrix	Total	Percent
Clay Minerals		**4.4**
Clay Minerals (not individually identifiable)	17	4.1
Muscovite		
Biotite		
Chlorite	1	0.2
Glauconite		
Illite		

Porosity	Total	Percent
		7.8
Intergranular	19	4.6
Intragranular	1	0.2
Intercrystalline		
Moldic	1	0.2
Grain/Cement Dissolution	10	2.4
Clay/Mica Framework		
Organic Matter		
Vug		
Channel		
Fracture	1	0.2
	Total	**100.0**

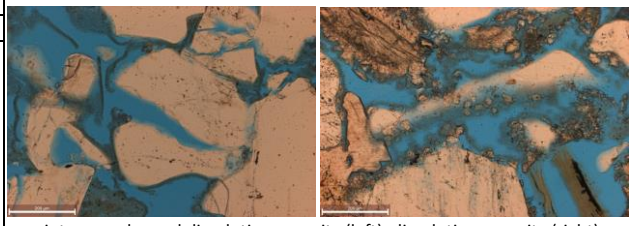

intergranular and dissolution porosity (left); dissolution porosity (right)
no3_0005 PL (left) and no3_0008 PL (right)

Back to Index

Thin Section Analysis Report

Sample ID: COST B-2
Sample Condition: standard rectangular size
Formation Name: Upper Logan Canyon
Depth (ft): 8241 ft
Lithology: Sandstone

Date of Analysis: 2/12/2018
Analyzed by: Kristin M. Carter
Point Count Step Size 1.0 mm
Number of Counts 400

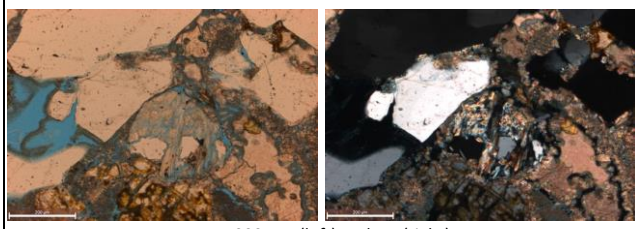

no4_0004 PL (left) and XN (right)

All scale bars are 200 um, unless otherwise noted

Texture - Qualitative Assessment

Approximate Average Grain Size (mm): 0.5
Grain Sorting: poorly sorted
Grain Rounding: angular to subrounded

Composition - Modal Analysis Data

Framework

Mineral Grains	Total	Percent
Quartz		**50.3**
Monocrystalline	162	40.5
Polycrystalline	39	9.8
Chert		
Feldspar		**2.5**
Plagioclase		
Microcline	5	1.3
K-Feldspar	5	1.3
Carbonate		**11.3**
Calcite	45	11.3
Dolomite		

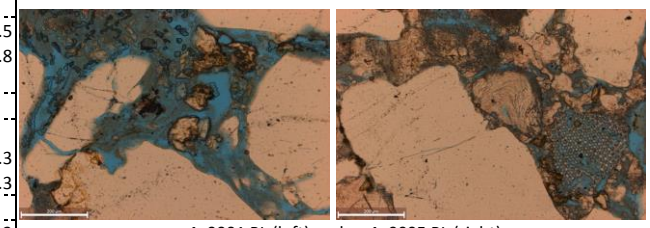

no4_0001 PL (left) and no4_0005 PL (right)

Lithic Grains	Total	Percent
		0.0
Metamorphic		
Sedimentary		
Volcanic		

Accessory Minerals	Total	Percent
		0.0
Rutile		
Tourmaline		
Zircon		
Opaques		

Matrix Spaces

Cement	Total	Percent
		26.5
Quartz		
K-Feldspar		
Calcite	98	24.5
Dolomite/Ankerite		
Iron Oxide	8	2.0

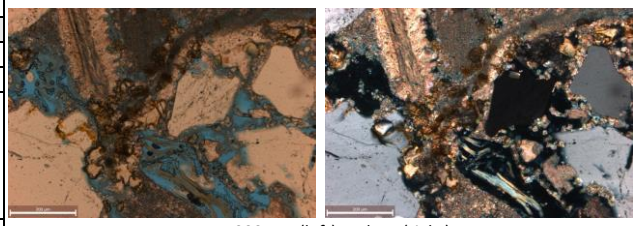

no4_0007 PL (left) and XN (right)

Matrix	Total	Percent
Clay Minerals		**5.0**
Clay Minerals (not individually identifiable)	17	4.3
Muscovite		
Biotite		
Chlorite	1	0.3
Glauconite		
Illite	2	0.5

Porosity	Total	Percent
		4.5
Intergranular	12	3.0
Intragranular		
Intercrystalline		
Moldic		
Grain/Cement Dissolution	5	1.3
Clay/Mica Framework		
Organic Matter		
Vug		
Channel		
Fracture	1	0.3
	Total	**100.0**

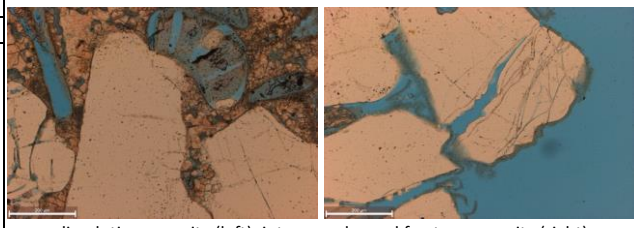

dissolution porosity (left); intergranular and fracture porosity (right)
no4_0002 PL (left) and no4_0011 PL (right)

Back to Index

Thin Section Analysis Report

Sample ID: COST B-2
Sample Condition: standard rectangular size
Formation Name: Upper Logan Canyon
Depth (ft): 8242 ft
Lithology: Sandstone

Date of Analysis: 2/12/2018
Analyzed by: Kristin M. Carter
Point Count Step Size 1.0 mm
Number of Counts 412

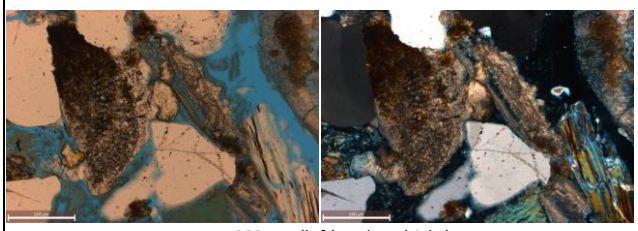

no5_0005 PL (left) and XN (right)

All scale bars are 200 um, unless otherwise noted

Texture - Qualitative Assessment

Approximate Average Grain Size (mm): 0.6
Grain Sorting: poorly sorted
Grain Rounding: subangular to subrounded

Composition - Modal Analysis Data

Framework

Mineral Grains	Total	Percent
Quartz		**54.1**
Monocrystalline	205	49.8
Polycrystalline	18	4.4
Chert		
Feldspar		**1.5**
Plagioclase	2	0.5
Microcline	2	0.5
K-Feldspar	2	0.5
Carbonate		**8.3**
Calcite	34	8.3
Dolomite		

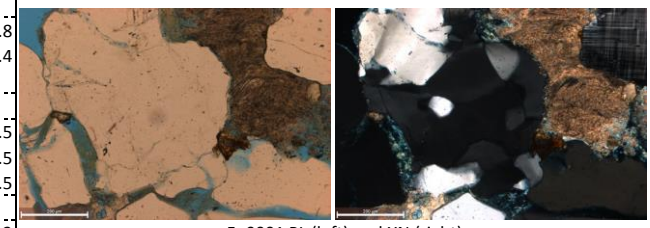

no5_0001 PL (left) and XN (right)

Lithic Grains	Total	Percent
		0.0
Metamorphic		
Sedimentary		
Volcanic		

Accessory Minerals	Total	Percent
		0.0
Rutile		
Tourmaline		
Zircon		
Opaques		

Matrix Spaces

Cement	Total	Percent
		14.3
Quartz		
K-Feldspar		
Calcite	51	12.4
Dolomite/Ankerite		
Iron Oxide	8	1.9

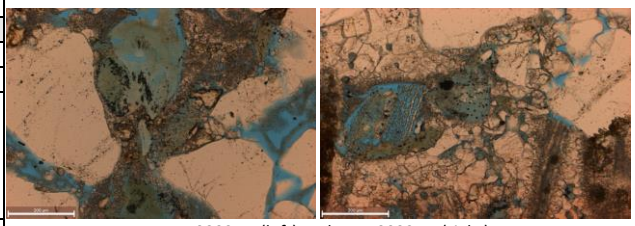

no5_0003 PL (left) and no5_0009 PL (right)

Matrix	Total	Percent
Clay Minerals		**12.1**
Clay Minerals (not individually identifiable)	47	11.4
Muscovite		
Biotite	2	0.5
Chlorite		
Glauconite		
Illite	1	0.2

Porosity	Total	Percent
		9.7
Intergranular	24	5.8
Intragranular	1	0.2
Intercrystalline		
Moldic	2	0.5
Grain/Cement Dissolution	11	2.7
Clay/Mica Framework		
Organic Matter		
Vug		
Channel		
Fracture	2	0.5
	Total	**100.0**

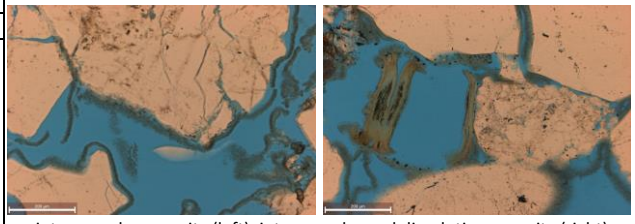

intergranular porosity (left); intergranular and dissolution porosity (right)
no5_0004 PL (left) and no5_0008 PL (right)

Back to Index

Thin Section Analysis Report

Sample ID: COST B-2
Sample Condition: standard rectangular size
Formation Name: Upper Logan Canyon
Depth (ft): 8244 ft
Lithology: Sandstone

Date of Analysis: 2/13/2018
Analyzed by: Kristin M. Carter
Point Count Step Size 1.0 mm
Number of Counts 416

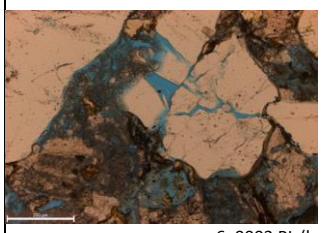
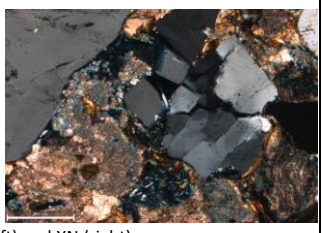

no6_0003 PL (left) and XN (right)

All scale bars are 200 um, unless otherwise noted

Texture - Qualitative Assessment

Approximate Average Grain Size (mm): 0.6
Grain Sorting: moderately sorted
Grain Rounding: subangular to subrounded

Composition - Modal Analysis Data

Framework

Mineral Grains	Total	Percent
Quartz		**44.5**
Monocrystalline	174	41.8
Polycrystalline	11	2.6
Chert		
Feldspar		**3.6**
Plagioclase	2	0.5
Microcline	3	0.7
K-Feldspar	10	2.4
Carbonate		**19.2**
Calcite	80	19.2
Dolomite		

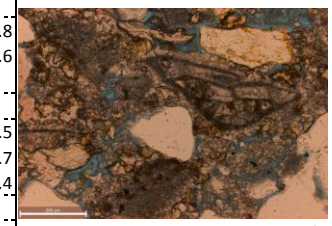
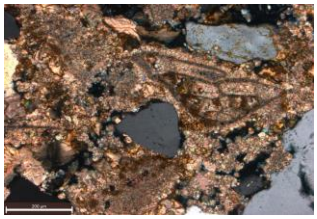

no6_0002 PL (left) and XN (right)

Lithic Grains	Total	Percent
		0.0
Metamorphic		
Sedimentary		
Volcanic		

Accessory Minerals	Total	Percent
		0.0
Rutile		
Tourmaline		
Zircon		
Opaques		

Matrix Spaces

Cement	Total	Percent
		20.0
Quartz		
K-Feldspar		
Calcite	81	19.5
Dolomite/Ankerite		
Iron Oxide	2	0.5

Matrix	Total	Percent
Clay Minerals		**7.0**
Clay Minerals (not individually identifiable)	23	5.5
Muscovite	1	0.2
Biotite	2	0.5
Chlorite		
Glauconite		
Illite	3	0.7

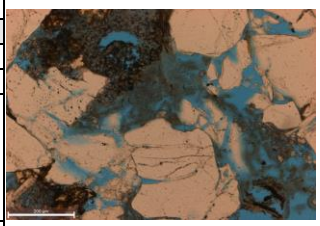
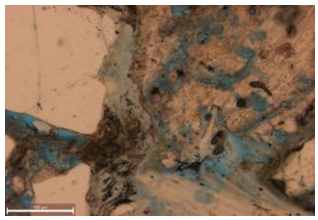

right scale bar - 100 um

no6_0007 PL (left) and no6_0010 PL (right)

Porosity	Total	Percent
		5.8
Intergranular	18	4.3
Intragranular		
Intercrystalline		
Moldic		
Grain/Cement Dissolution	6	1.4
Clay/Mica Framework		
Organic Matter		
Vug		
Channel		
Fracture		
	Total	**100.0**

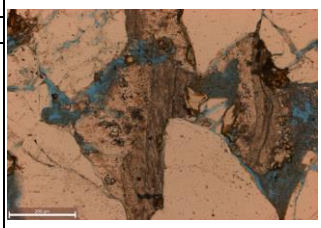
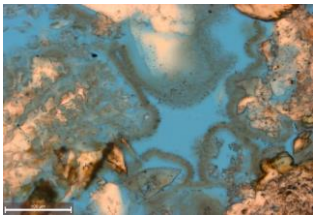

right scale bar - 100 um

dissolution and intergranular porosity (left and right)
no6_0004 PL (left) and no6_0011 PL (right)

Back to Index

Thin Section Analysis Report

Sample ID: COST B-2
Sample Condition: standard rectangular size
Formation Name: Upper Logan Canyon
Depth (ft): 8247 ft
Lithology: Sandstone

Date of Analysis: 2/13/2018
Analyzed by: Kristin M. Carter
Point Count Step Size 1.0 mm
Number of Counts 422

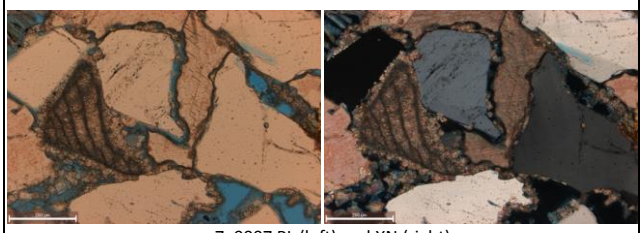

no7_0007 PL (left) and XN (right)

All scale bars are 200 um, unless otherwise noted

Texture - Qualitative Assessment

Approximate Average Grain Size (mm): 0.4
Grain Sorting: poorly sorted
Grain Rounding: angular to subrounded

Composition - Modal Analysis Data

Framework

Mineral Grains	Total	Percent
Quartz		**44.5**
Monocrystalline	172	40.8
Polycrystalline	16	3.8
Chert		
Feldspar		**4.5**
Plagioclase	2	0.5
Microcline	8	1.9
K-Feldspar	9	2.1
Carbonate		**15.9**
Calcite	67	15.9
Dolomite		

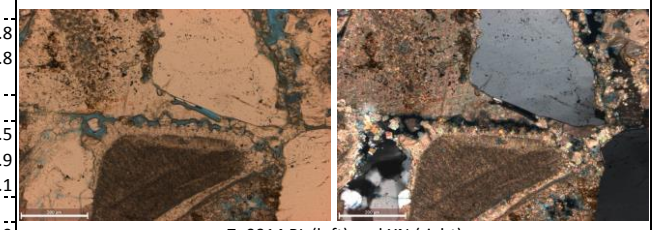

no7_0014 PL (left) and XN (right)

Lithic Grains	Total	Percent
		0.0
Metamorphic		
Sedimentary		
Volcanic		

Accessory Minerals	Total	Percent
		0.0
Rutile		
Tourmaline		
Zircon		
Opaques		

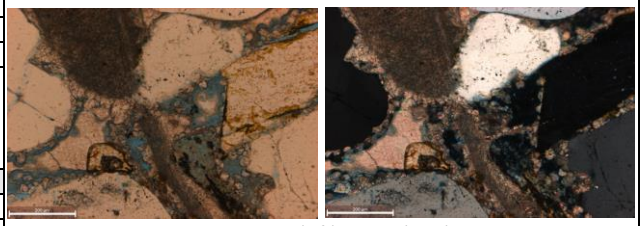

no7_0002 PL (left) and XN (right)

Matrix Spaces

Cement	Total	Percent
		24.6
Quartz	1	0.2
K-Feldspar		
Calcite	100	23.7
Dolomite/Ankerite		
Iron Oxide	3	0.7

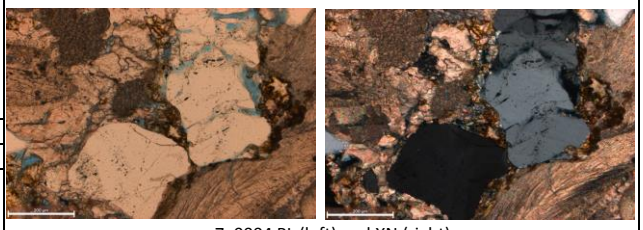

no7_0004 PL (left) and XN (right)

Matrix	Total	Percent
Clay Minerals		**6.6**
Clay Minerals (not individually identifiable)	21	5.0
Muscovite	2	0.5
Biotite	4	0.9
Chlorite		
Glauconite		
Illite	1	0.2

Porosity	Total	Percent
		3.8
Intergranular	9	2.1
Intragranular	4	0.9
Intercrystalline		
Moldic	2	0.5
Grain/Cement Dissolution		
Clay/Mica Framework		
Organic Matter		
Vug		
Channel		
Fracture	1	0.2
	Total	**100.0**

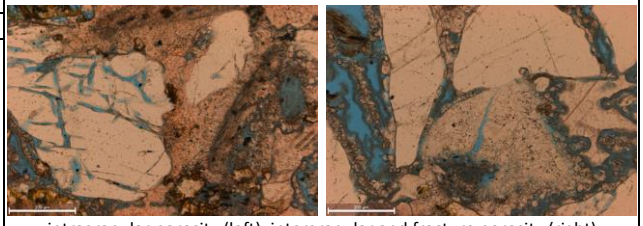

intragranular porosity (left); intergranular and fracture porosity (right)
no7_0003 PL (left) and no7_0008 PL (right)

Back to Index

Thin Section Analysis Report

Sample ID: COST B-2
Sample Condition: standard rectangular size
Formation Name: Upper Logan Canyon
Depth (ft): 8248.9 ft
Lithology: Sandstone

Date of Analysis: 2/13/2018
Analyzed by: Kristin M. Carter
Point Count Step Size 1.0 mm
Number of Counts 408

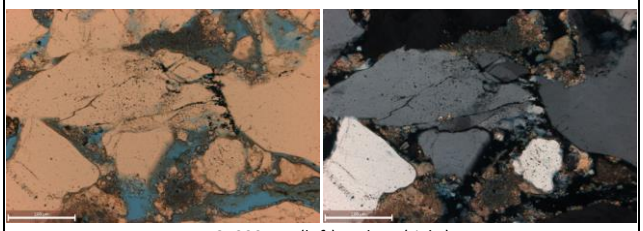

no8_0007 PL (left) and XN (right)

All scale bars are 200 um, unless otherwise noted

Texture - Qualitative Assessment

Approximate Average Grain Size (mm): 0.5
Grain Sorting: poorly sorted
Grain Rounding: subangular to subrounded

Composition - Modal Analysis Data

Framework

Mineral Grains	Total	Percent
Quartz		**52.5**
Monocrystalline	186	45.6
Polycrystalline	28	6.9
Chert		
Feldspar		**4.2**
Plagioclase	4	1.0
Microcline	5	1.2
K-Feldspar	8	2.0
Carbonate		**14.0**
Calcite	57	14.0
Dolomite		

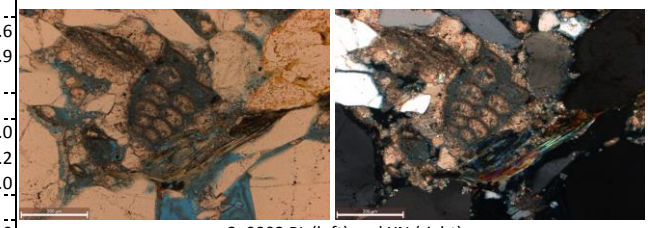

no8_0002 PL (left) and XN (right)

Lithic Grains	Total	Percent
		0.0
Metamorphic		
Sedimentary		
Volcanic		

Accessory Minerals	Total	Percent
		0.0
Rutile		
Tourmaline		
Zircon		
Opaques		

Matrix Spaces

Cement	Total	Percent
		16.9
Quartz	2	0.5
K-Feldspar		
Calcite	64	15.7
Dolomite/Ankerite		
Iron Oxide	3	0.7

Matrix	Total	Percent
Clay Minerals		**7.1**
Clay Minerals (not individually identifiable)	24	5.9
Muscovite		
Biotite	4	1.0
Chlorite		
Glauconite		
Illite	1	0.2

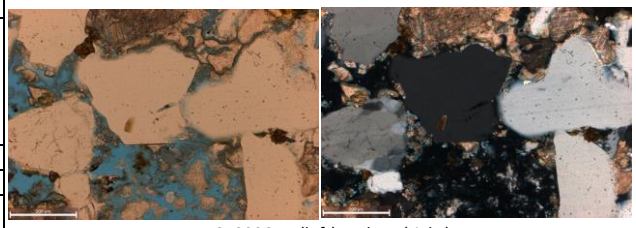

no8_0006 PL (left) and XN (right)

Porosity	Total	Percent
		5.4
Intergranular	15	3.7
Intragranular	2	0.5
Intercrystalline		
Moldic		
Grain/Cement Dissolution	5	1.2
Clay/Mica Framework		
Organic Matter		
Vug		
Channel		
Fracture		
	Total	**100.0**

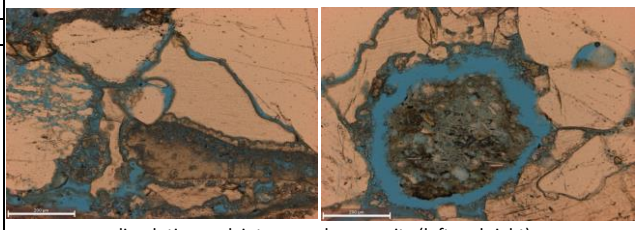

dissolution and intergranular porosity (left and right)
no8_0010 PL (left) and no8_0011 PL (right)

Back to Index

Thin Section Analysis Report

Sample ID: COST B-2
Sample Condition: standard rectangular size
Formation Name: Upper Logan Canyon
Depth (ft): 8249 ft
Lithology: Sandstone

Date of Analysis: 2/15/2018
Analyzed by: Kristin M. Carter
Point Count Step Size 1.0 mm
Number of Counts 412

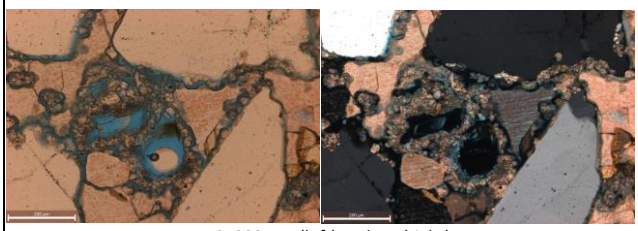

no9_0004 PL (left) and XN (right)

All scale bars are 200 um, unless otherwise noted

Texture - Qualitative Assessment

Approximate Average Grain Size (mm): 0.5
Grain Sorting: poorly sorted
Grain Rounding: subangular to subrounded

Composition - Modal Analysis Data

Framework

Mineral Grains	Total	Percent
Quartz		**52.9**
Monocrystalline	205	49.8
Polycrystalline	13	3.2
Chert		
Feldspar		**3.4**
Plagioclase	2	0.5
Microcline	7	1.7
K-Feldspar	5	1.2
Carbonate		**19.7**
Calcite	81	19.7
Dolomite		

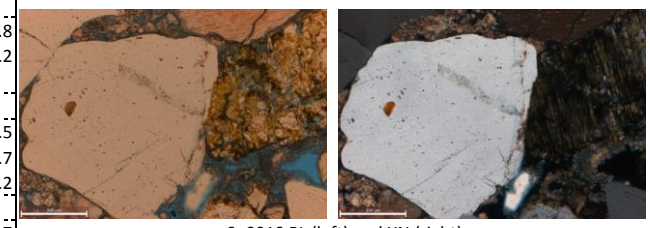

no9_0010 PL (left) and XN (right)

Lithic Grains	Total	Percent
		0.0
Metamorphic		
Sedimentary		
Volcanic		

Accessory Minerals	Total	Percent
		0.2
Rutile		
Tourmaline		
Zircon		
Opaques	1	0.2

Matrix Spaces

Cement	Total	Percent
		16.7
Quartz	1	0.2
K-Feldspar		
Calcite	67	16.3
Dolomite/Ankerite		
Iron Oxide	1	0.2

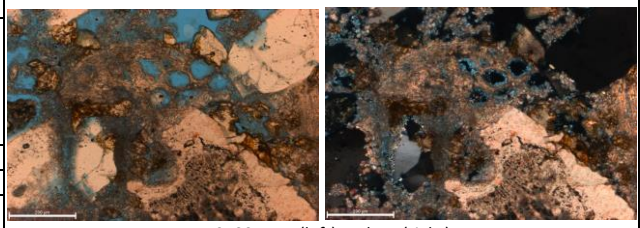

no9_0011 PL (left) and XN (right)

Matrix	Total	Percent
Clay Minerals		**4.6**
Clay Minerals (not individually identifiable)	14	3.4
Muscovite	2	0.5
Biotite	3	0.7
Chlorite		
Glauconite		
Illite		

Porosity	Total	Percent
		2.4
Intergranular	4	1.0
Intragranular	3	0.7
Intercrystalline		
Moldic	1	0.2
Grain/Cement Dissolution	2	0.5
Clay/Mica Framework		
Organic Matter		
Vug		
Channel		
Fracture		
	Total	**100.0**

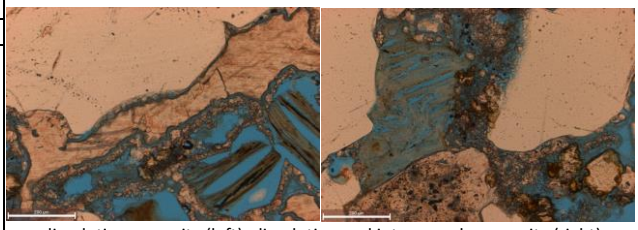

dissolution porosity (left); dissolution and intergranular porosity (right)
no9_0007 PL (left) and no9_0015 PL (right)

Back to Index

Thin Section Analysis Report

Sample ID: COST B-2
Sample Condition: standard rectangular size
Formation Name: Upper Logan Canyon
Depth (ft): 8250 ft
Lithology: Sandstone

Date of Analysis: 2/15/2018
Analyzed by: Kristin M. Carter
Point Count Step Size 1.0 mm
Number of Counts 423

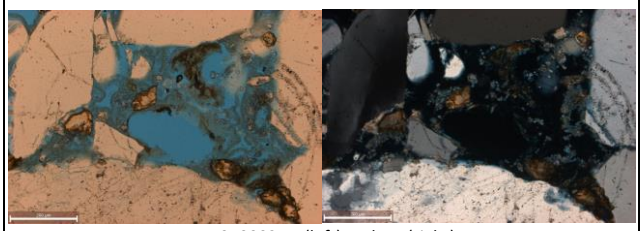

no10_0003 PL (left) and XN (right)

All scale bars are 200 um, unless otherwise noted

Texture - Qualitative Assessment

Approximate Average Grain Size (mm): 0.5
Grain Sorting: poorly sorted
Grain Rounding: subangular to subrounded

Composition - Modal Analysis Data

Framework

Mineral Grains	Total	Percent
Quartz		**53.7**
Monocrystalline	215	50.8
Polycrystalline	11	2.6
Chert	1	0.2
Feldspar		**5.7**
Plagioclase	8	1.9
Microcline	9	2.1
K-Feldspar	7	1.7
Carbonate		**10.2**
Calcite	43	10.2
Dolomite		

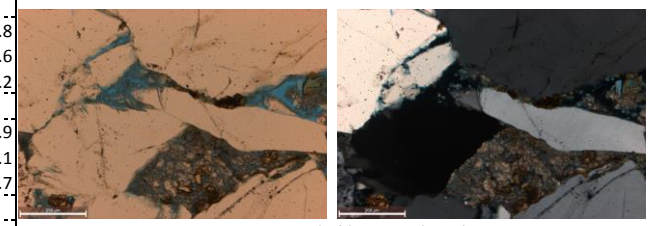

no10_0005 PL (left) and XN (right)

Lithic Grains	Total	Percent
		0.0
Metamorphic		
Sedimentary		
Volcanic		

Accessory Minerals	Total	Percent
		0.0
Rutile		
Tourmaline		
Zircon		
Opaques		

Matrix Spaces

Cement	Total	Percent
		14.9
Quartz	1	0.2
K-Feldspar		
Calcite	59	13.9
Dolomite/Ankerite		
Iron Oxide	3	0.7

Matrix	Total	Percent
Clay Minerals		**9.7**
Clay Minerals (not individually identifiable)	29	6.9
Muscovite	4	0.9
Biotite	7	1.7
Chlorite		
Glauconite		
Illite	1	0.2

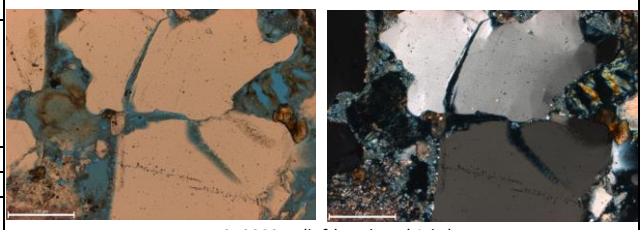

no10_0002PL (left) and XN (right)

Porosity	Total	Percent
		5.9
Intergranular	13	3.1
Intragranular	3	0.7
Intercrystalline		
Moldic		
Grain/Cement Dissolution	7	1.7
Clay/Mica Framework		
Organic Matter		
Vug		
Channel		
Fracture	2	0.5
	Total	**100.0**

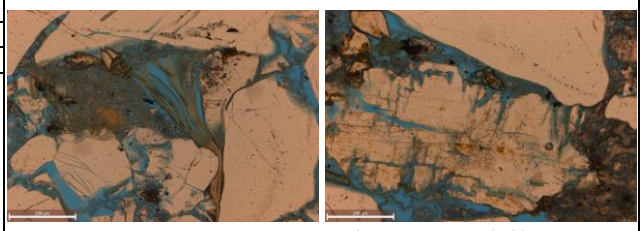

intergranular, dissolution and fracture porosity (left);
dissolution and intergranular porosity (right)
no10_0001 PL (left) and no10_0004 PL (right)

Back to Index

Thin Section Analysis Report

Sample ID: COST B-2
Sample Condition: standard rectangular size
Formation Name: Upper Logan Canyon
Depth (ft): 8251 ft
Lithology: Sandstone

Date of Analysis: 2/15/2018
Analyzed by: Kristin M. Carter
Point Count Step Size 1.0 mm
Number of Counts 413

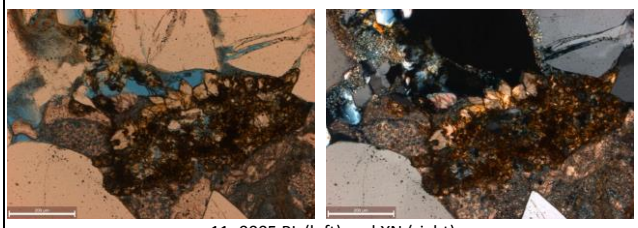

no11_0005 PL (left) and XN (right)

All scale bars are 200 um, unless otherwise noted

Texture - Qualitative Assessment

Approximate Average Grain Size (mm): 0.5
Grain Sorting: moderately sorted
Grain Rounding: angular to subrounded

Composition - Modal Analysis Data

Framework

Mineral Grains	Total	Percent
Quartz		**52.3**
Monocrystalline	206	49.9
Polycrystalline	10	2.4
Chert		
Feldspar		**3.9**
Plagioclase		
Microcline	3	0.7
K-Feldspar	13	3.1
Carbonate		**12.8**
Calcite	53	12.8
Dolomite		

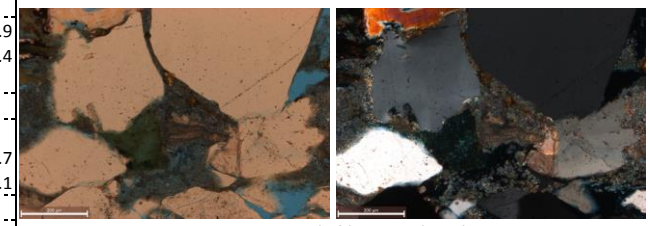

no11_0003 PL (left) and XN (right)

Lithic Grains	Total	Percent
		0.0
Metamorphic		
Sedimentary		
Volcanic		

Accessory Minerals	Total	Percent
		0.0
Rutile		
Tourmaline		
Zircon		
Opaques		

Matrix Spaces

Cement	Total	Percent
		21.8
Quartz	1	0.2
K-Feldspar		
Calcite	85	20.6
Dolomite/Ankerite		
Iron Oxide	4	1.0

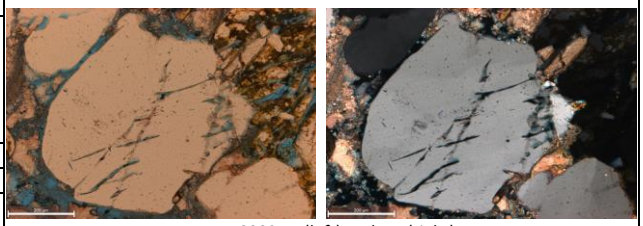

no11_0002 PL (left) and XN (right)

Matrix	Total	Percent
Clay Minerals		**6.5**
Clay Minerals (not individually identifiable)	19	4.6
Muscovite	3	0.7
Biotite	5	1.2
Chlorite		
Glauconite		
Illite		

Porosity	Total	Percent
		2.7
Intergranular	5	1.2
Intragranular	1	0.2
Intercrystalline		
Moldic		
Grain/Cement Dissolution	4	1.0
Clay/Mica Framework		
Organic Matter		
Vug		
Channel		
Fracture	1	0.2
	Total	**100.0**

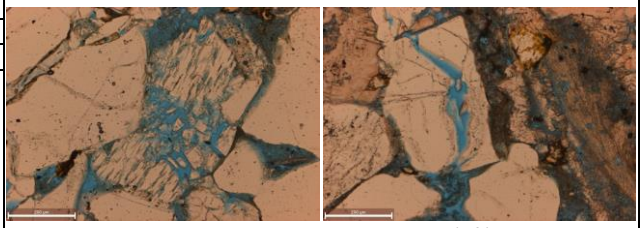

intergranular and dissolution porosity (left)
fracture and intergranular porosity (right)
no11_0001 PL (left) and no11_0004 PL (right)

Back to Index

Thin Section Analysis Report

Sample ID: COST B-2
Sample Condition: standard rectangular size
Formation Name: Lower Logan Canyon
Depth (ft): 9286.5 ft
Lithology: Sandstone

Date of Analysis: 2/16/2018
Analyzed by: Kristin M. Carter
Point Count Step Size 1.0 mm
Number of Counts 420

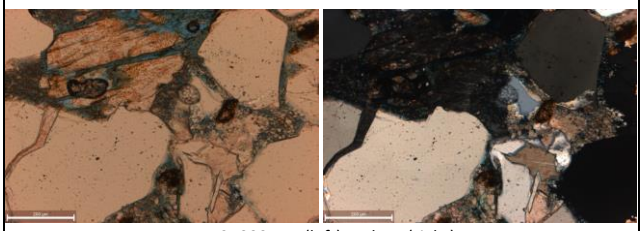

no12_0001 PL (left) and XN (right)

All scale bars are 200 um, unless otherwise noted

Texture - Qualitative Assessment

Approximate Average Grain Size (mm): 0.5
Grain Sorting: poorly sorted
Grain Rounding: subangular to subrounded

Composition - Modal Analysis Data

Framework

Mineral Grains	Total	Percent
Quartz		**54.8**
Monocrystalline	208	49.5
Polycrystalline	22	5.2
Chert		
Feldspar		**3.1**
Plagioclase	5	1.2
Microcline	6	1.4
K-Feldspar	2	0.5
Carbonate		**11.2**
Calcite	47	11.2
Dolomite		

no12_0003 PL (left) and XN (right)

Lithic Grains	Total	Percent
		0.0
Metamorphic		
Sedimentary		
Volcanic		

Accessory Minerals	Total	Percent
		0.2
Rutile		
Tourmaline		
Zircon		
Opaques	1	0.2

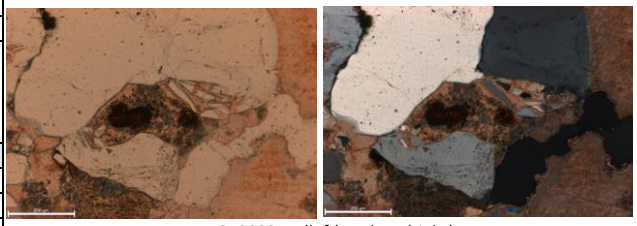

no12_0009 PL (left) and XN (right)

Matrix Spaces

Cement	Total	Percent
		23.8
Quartz		
K-Feldspar		
Calcite	83	19.8
Dolomite/Ankerite		
Iron Oxide	17	4.0

Matrix	Total	Percent
Clay Minerals		**5.5**
Clay Minerals (not individually identifiable)	17	4.0
Muscovite	5	1.2
Biotite		
Chlorite	1	0.2
Glauconite		
Illite		

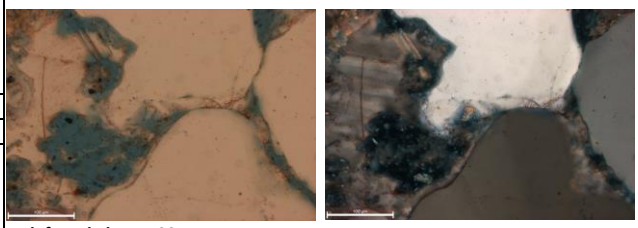

left scale bar - 100 um

no12_0006 PL (left) and XN (right)

Porosity	Total	Percent
		1.4
Intergranular		
Intragranular		
Intercrystalline		
Moldic		
Grain/Cement Dissolution	6	1.4
Clay/Mica Framework		
Organic Matter		
Vug		
Channel		
Fracture		
	Total	**100.0**

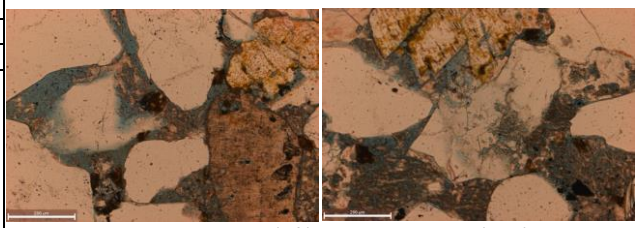

dissolution porosity (left); dissolution porosity (right)
no12_0014 PL (left) and no12_0015 PL (right)

Back to Index

Thin Section Analysis Report

Sample ID: COST B-2
Sample Condition: standard rectangular size
Formation Name: Lower Logan Canyon
Depth (ft): 9289.3 ft
Lithology: Sandstone

Date of Analysis: 2/16/2018
Analyzed by: Kristin M. Carter
Point Count Step Size 1.0 mm
Number of Counts 417

Texture - Qualitative Assessment

Approximate Average Grain Size (mm): 0.4
Grain Sorting: moderately well sorted
Grain Rounding: subangular to subrounded

Composition - Modal Analysis Data

Framework

Mineral Grains	Total	Percent
Quartz		**52.5**
Monocrystalline	204	48.9
Polycrystalline	15	3.6
Chert		
Feldspar		**4.8**
Plagioclase	11	2.6
Microcline	2	0.5
K-Feldspar	7	1.7
Carbonate		**0.0**
Calcite		
Dolomite		

Lithic Grains	Total	Percent
		0.0
Metamorphic		
Sedimentary		
Volcanic		

Accessory Minerals	Total	Percent
		1.0
Rutile		
Tourmaline		
Zircon		
Opaques	4	1.0

Matrix Spaces

Cement	Total	Percent
		11.0
Quartz	2	0.5
K-Feldspar		
Calcite	1	0.2
Dolomite/Ankerite		
Iron Oxide	43	10.3

Matrix	Total	Percent
Clay Minerals		**21.8**
Clay Minerals (not individually identifiable)	84	20.1
Muscovite	2	0.5
Biotite	2	0.5
Chlorite	3	0.7
Glauconite		
Illite		

Porosity	Total	Percent
		8.9
Intergranular	18	4.3
Intragranular		
Intercrystalline		
Moldic	9	2.2
Grain/Cement Dissolution	10	2.4
Clay/Mica Framework		
Organic Matter		
Vug		
Channel		
Fracture		
	Total	**100.0**

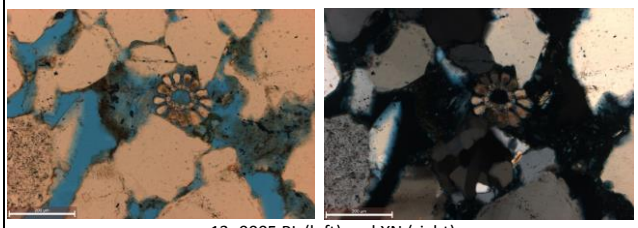

no13_0005 PL (left) and XN (right)

All scale bars are 200 um, unless otherwise noted

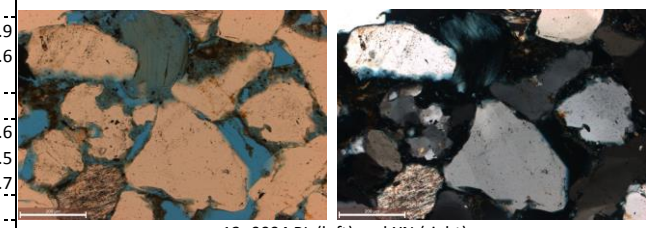

no13_0004 PL (left) and XN (right)

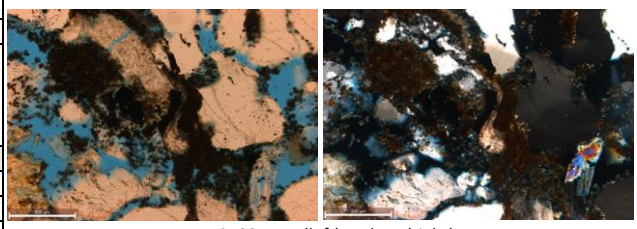

no13_0014 PL (left) and XN (right)

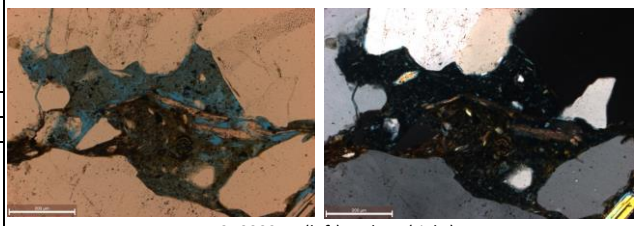

no13_0002 PL (left) and XN (right)

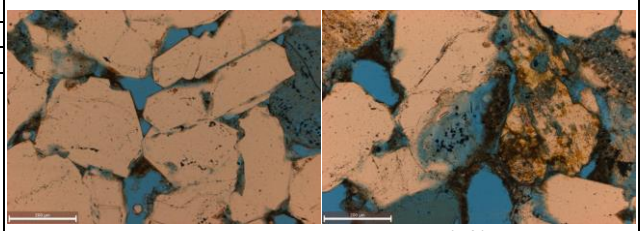

intergranular and dissolution porosity (left);
dissolution and moldic porosity (right)
no13_0012 PL (left) and no13_0015 PL (right)

Back to Index

Thin Section Analysis Report

Sample ID: COST B-2
Sample Condition: standard rectangular size
Formation Name: Lower Logan Canyon
Depth (ft): 9302 ft
Lithology: Sandstone

Date of Analysis: 2/16/2018
Analyzed by: Kristin M. Carter
Point Count Step Size 1.0 mm
Number of Counts 416

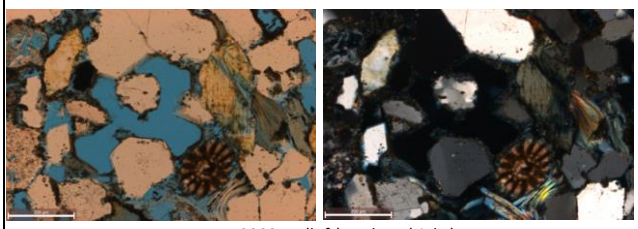

no14_0008 PL (left) and XN (right)

All scale bars are 200 um, unless otherwise noted

Texture - Qualitative Assessment

Approximate Average Grain Size (mm): 0.4
Grain Sorting: moderately sorted
Grain Rounding: angular to subrounded

Composition - Modal Analysis Data

Framework

Mineral Grains	Total	Percent
Quartz		**46.6**
Monocrystalline	187	45.0
Polycrystalline	7	1.7
Chert		
Feldspar		**7.9**
Plagioclase	14	3.4
Microcline	7	1.7
K-Feldspar	12	2.9
Carbonate		**2.9**
Calcite	12	2.9
Dolomite		

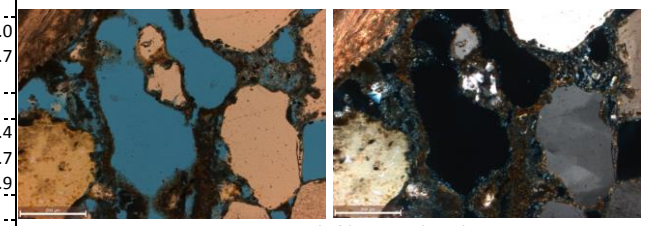

no14_0009 PL (left) and XN (right)

Lithic Grains	Total	Percent
		0.0
Metamorphic		
Sedimentary		
Volcanic		

Accessory Minerals	Total	Percent
		0.5
Rutile		
Tourmaline	1	0.2
Zircon		
Opaques	1	0.2

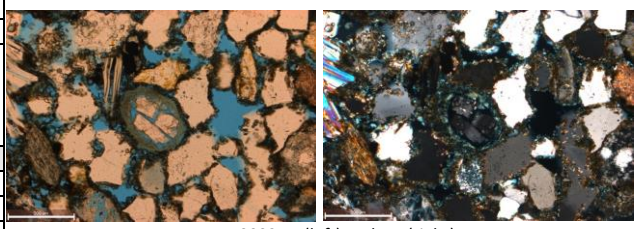

no14_0003 PL (left) and XN (right)

Matrix Spaces

Cement	Total	Percent
		7.5
Quartz		
K-Feldspar		
Calcite	4	1.0
Dolomite/Ankerite		
Iron Oxide	27	6.5

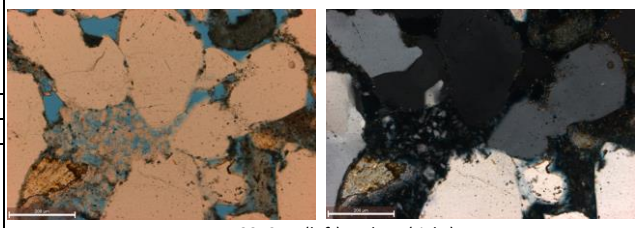

no14_0012 PL (left) and XN (right)

Matrix	Total	Percent
Clay Minerals		**19.2**
Clay Minerals (not individually identifiable)	58	13.9
Muscovite	7	1.7
Biotite	2	0.5
Chlorite	11	2.6
Glauconite		
Illite	2	0.5

Porosity	Total	Percent
		15.4
Intergranular	33	7.9
Intragranular	1	0.2
Intercrystalline		
Moldic	9	2.2
Grain/Cement Dissolution	17	4.1
Clay/Mica Framework		
Organic Matter		
Vug	4	1.0
Channel		
Fracture		
	Total	**100.0**

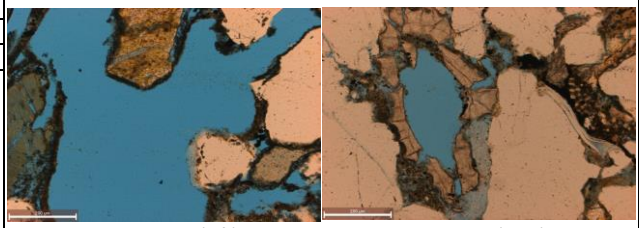

vug porosity (left); moldic and dissolution porosity (right)
no14_0004 PL (left) and no14_0006 PL (right)

Back to Index

Thin Section Analysis Report

Sample ID: COST B-2
Sample Condition: standard rectangular size
Formation Name: Lower Logan Canyon
Depth (ft): 9304.4 ft
Lithology: Sandstone

Date of Analysis: 2/16/2018
Analyzed by: Kristin M. Carter
Point Count Step Size 1.0 mm
Number of Counts 400

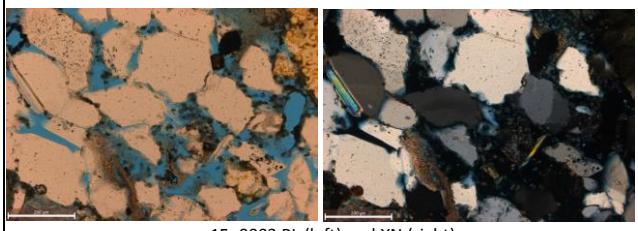

no15_0003 PL (left) and XN (right)

All scale bars are 200 um, unless otherwise noted

Texture - Qualitative Assessment

Approximate Average Grain Size (mm): 0.3
Grain Sorting: moderately well sorted
Grain Rounding: angular to subrounded

Composition - Modal Analysis Data

Framework

Mineral Grains	Total	Percent
Quartz		**49.8**
Monocrystalline	192	48.0
Polycrystalline	7	1.8
Chert		
Feldspar		**3.0**
Plagioclase	8	2.0
Microcline	4	1.0
K-Feldspar		
Carbonate		**1.5**
Calcite	6	1.5
Dolomite		

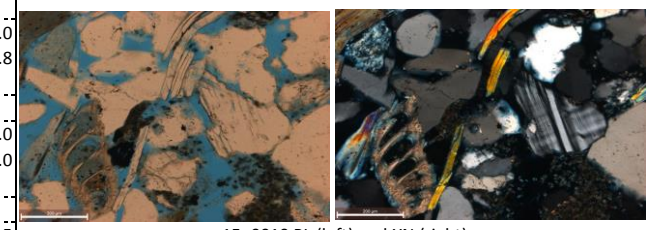

no15_0010 PL (left) and XN (right)

Lithic Grains	Total	Percent
		0.0
Metamorphic		
Sedimentary		
Volcanic		

Accessory Minerals	Total	Percent
		1.3
Rutile		
Tourmaline		
Zircon		
Opaques	5	1.3

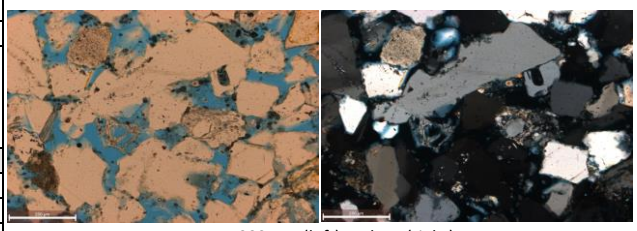

no15_0005 PL (left) and XN (right)

Matrix Spaces

Cement	Total	Percent
		11.3
Quartz	2	0.5
K-Feldspar		
Calcite	4	1.0
Dolomite/Ankerite		
Iron Oxide	39	9.8

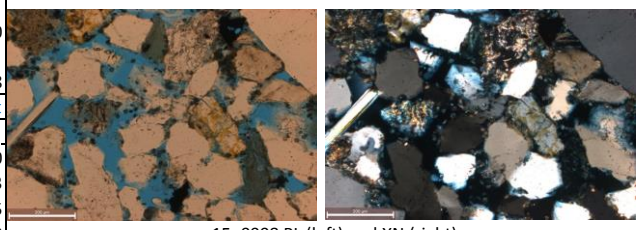

no15_0008 PL (left) and XN (right)

Matrix	Total	Percent
Clay Minerals		**17.3**
Clay Minerals (not individually identifiable)	44	11.0
Muscovite	5	1.3
Biotite	6	1.5
Chlorite	8	2.0
Glauconite		
Illite	6	1.5

Porosity	Total	Percent
		16.0
Intergranular	37	9.3
Intragranular	1	0.3
Intercrystalline		
Moldic	9	2.3
Grain/Cement Dissolution	14	3.5
Clay/Mica Framework		
Organic Matter		
Vug	2	0.5
Channel		
Fracture	1	0.3
	Total	**100.0**

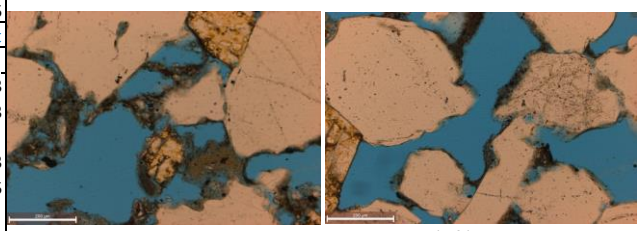

intergranular and moldic porosity (left);
vug and intergranular porosity (right)
no15_0001 PL (left) and no15_0006 PL (right)

Back to Index

Thin Section Analysis Report

Sample ID: COST B-2
Sample Condition: standard rectangular size
Formation Name: Lower Logan Canyon
Depth (ft): 9305.4 ft
Lithology: Sandstone

Date of Analysis: 2/16/2018
Analyzed by: Kristin M. Carter
Point Count Step Size 1.0 mm
Number of Counts 426

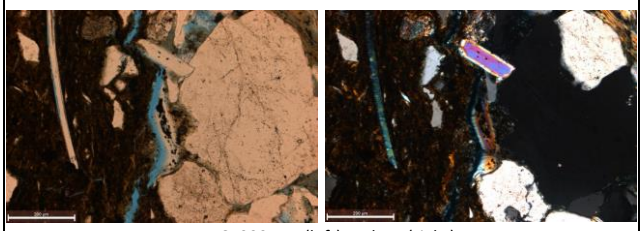

no16_0005 PL (left) and XN (right)
All scale bars are 200 um, unless otherwise noted

Texture - Qualitative Assessment

Approximate Average Grain Size (mm): 0.4
Grain Sorting: poorly sorted
Grain Rounding: subangular to subrounded

Composition - Modal Analysis Data

Framework

Mineral Grains	Total	Percent
Quartz		**41.1**
Monocrystalline	171	40.1
Polycrystalline	4	0.9
Chert		
Feldspar		**4.0**
Plagioclase	14	3.3
Microcline	2	0.5
K-Feldspar	1	0.2
Carbonate		**2.1**
Calcite	9	2.1
Dolomite		

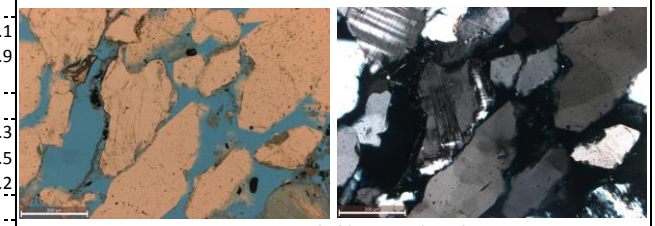

no16_0002 PL (left) and XN (right)

Lithic Grains	Total	Percent
		0.0
Metamorphic		
Sedimentary		
Volcanic		

Accessory Minerals	Total	Percent
		4.2
Rutile		
Tourmaline		
Zircon		
Opaques	18	4.2

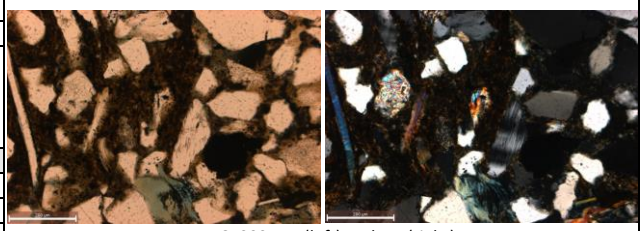

no16_0004 PL (left) and XN (right)

Matrix Spaces

Cement	Total	Percent
		20.2
Quartz		
K-Feldspar		
Calcite	4	0.9
Dolomite/Ankerite		
Iron Oxide	82	19.2

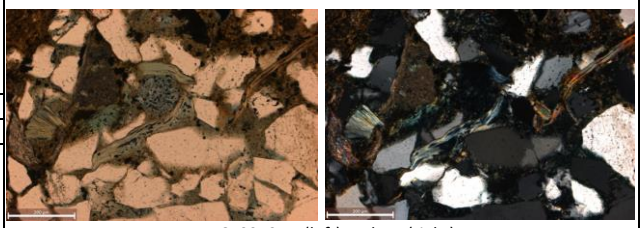

no16_0010 PL (left) and XN (right)

Matrix	Total	Percent
Clay Minerals		**18.1**
Clay Minerals (not individually identifiable)	45	10.6
Muscovite	9	2.1
Biotite	9	2.1
Chlorite	5	1.2
Glauconite		
Illite	9	2.1

Porosity	Total	Percent
		10.3
Intergranular	25	5.9
Intragranular		
Intercrystalline		
Moldic	3	0.7
Grain/Cement Dissolution	15	3.5
Clay/Mica Framework		
Organic Matter		
Vug		
Channel		
Fracture	1	0.2
	Total	**100.0**

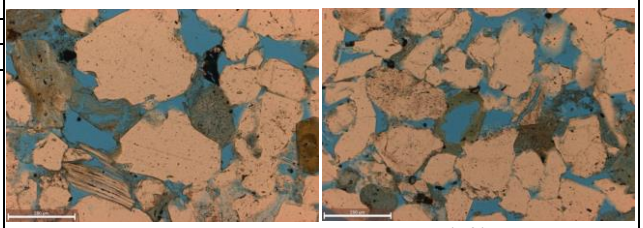

intergranular and dissolution porosity (left);
intergranular, moldic and dissolution porosity (right)
no16_0011 PL (left) and no16_0012 PL (right)

Back to Index

Thin Section Analysis Report

Sample ID: COST B-2
Sample Condition: half the standard size
Formation Name: Lower Logan Canyon
Depth (ft): 9330 ft
Lithology: Sandstone

Date of Analysis: 2/20/2018
Analyzed by: Kristin M. Carter
Point Count Step Size 0.3 mm
Number of Counts 419

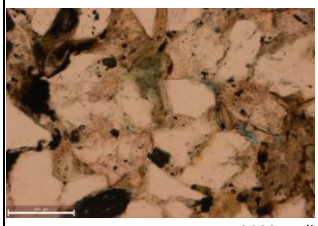
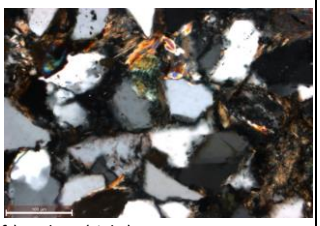

no17_0003 PL (left) and XN (right)

All scale bars are 100 um, unless otherwise noted

Texture - Qualitative Assessment

Approximate Average Grain Size (mm): 0.1
Grain Sorting: well sorted
Grain Rounding: angular to rounded

Composition - Modal Analysis Data

Framework

Mineral Grains	Total	Percent
Quartz		**46.3**
Monocrystalline	190	45.3
Polycrystalline	4	1.0
Chert		
Feldspar		**14.6**
Plagioclase	40	9.5
Microcline	3	0.7
K-Feldspar	18	4.3
Carbonate		**0.2**
Calcite	1	0.2
Dolomite		

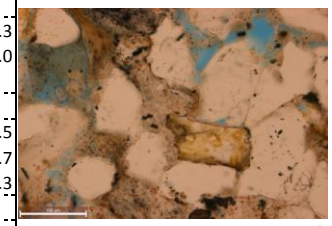
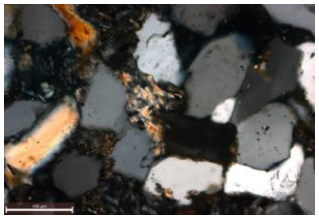

no17_0014 PL (left) and XN (right)

Lithic Grains	Total	Percent
		0.0
Metamorphic		
Sedimentary		
Volcanic		

Accessory Minerals	Total	Percent
		6.4
Rutile		
Tourmaline	1	0.2
Zircon		
Opaques	26	6.2

Matrix Spaces

Cement	Total	Percent
		3.3
Quartz		
K-Feldspar		
Calcite		
Dolomite/Ankerite		
Iron Oxide	14	3.3

Matrix	Total	Percent
Clay Minerals		**22.2**
Clay Minerals (not individually identifiable)	23	5.5
Muscovite	18	4.3
Biotite	9	2.1
Chlorite	29	6.9
Glauconite		
Illite	14	3.3

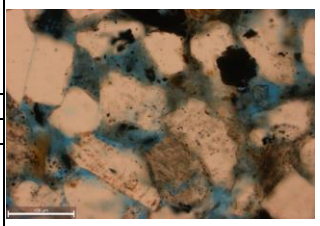
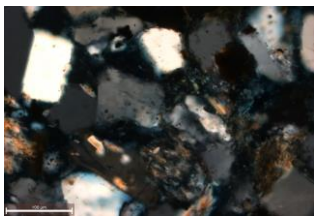

no17_0015 PL (left) and XN (right)

Porosity	Total	Percent
		6.9
Intergranular	17	4.1
Intragranular		
Intercrystalline		
Moldic		
Grain/Cement Dissolution	12	2.9
Clay/Mica Framework		
Organic Matter		
Vug		
Channel		
Fracture		
	Total	**100.0**

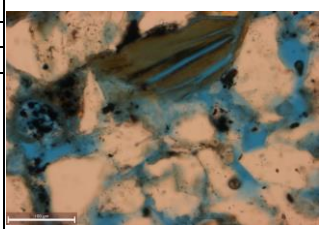
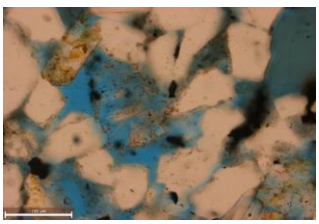

intergranular and dissolution porosity (left and right)
no17_0007 PL (left) and no17_0009 PL (right)

Back to Index

Thin Section Analysis Report

Sample ID: COST B-2
Sample Condition: standard rectangular size
Formation Name: Lower Logan Canyon
Depth (ft): 9330.2 ft
Lithology: Sandstone

Date of Analysis: 2/20/2018
Analyzed by: Kristin M. Carter
Point Count Step Size 0.3 mm
Number of Counts 417

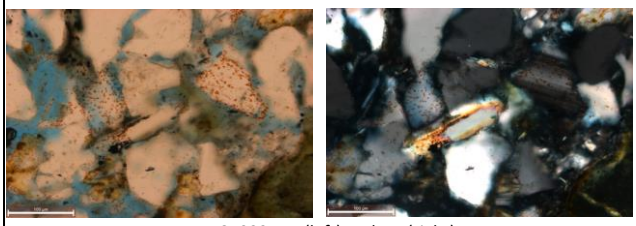

no18_0001 PL (left) and XN (right)
All scale bars are 100 um, unless otherwise noted

Texture - Qualitative Assessment

Approximate Average Grain Size (mm): 0.1
Grain Sorting: well sorted
Grain Rounding: angular to rounded

Composition - Modal Analysis Data

Framework

Mineral Grains	Total	Percent
Quartz		**36.5**
Monocrystalline	149	35.7
Polycrystalline	3	0.7
Chert		
Feldspar		**15.1**
Plagioclase	50	12.0
Microcline	1	0.2
K-Feldspar	12	2.9
Carbonate		**0.2**
Calcite	1	0.2
Dolomite		

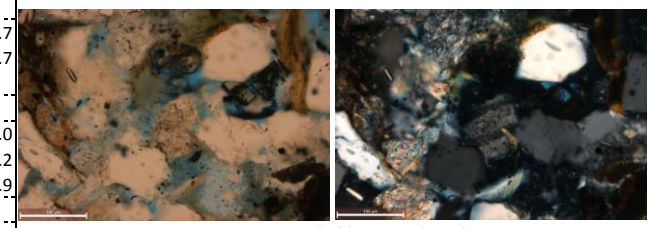

no18_0011 PL (left) and XN (right)

Lithic Grains	Total	Percent
		0.0
Metamorphic		
Sedimentary		
Volcanic		

Accessory Minerals	Total	Percent
		7.2
Rutile		
Tourmaline		
Zircon		
Opaques	30	7.2

Matrix Spaces

Cement	Total	Percent
		1.4
Quartz		
K-Feldspar		
Calcite		
Dolomite/Ankerite		
Iron Oxide	6	1.4

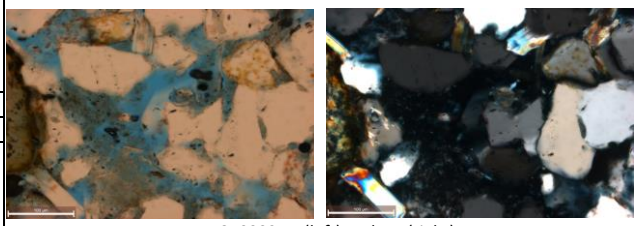

no18_0002 PL (left) and XN (right)

Matrix	Total	Percent
Clay Minerals		**30.7**
Clay Minerals (not individually identifiable)	65	15.6
Muscovite	8	1.9
Biotite	10	2.4
Chlorite	35	8.4
Glauconite		
Illite	10	2.4

Porosity	Total	Percent
		8.9
Intergranular	17	4.1
Intragranular	2	0.5
Intercrystalline		
Moldic		
Grain/Cement Dissolution	17	4.1
Clay/Mica Framework		
Organic Matter		
Vug	1	0.2
Channel		
Fracture		
	Total	**100.0**

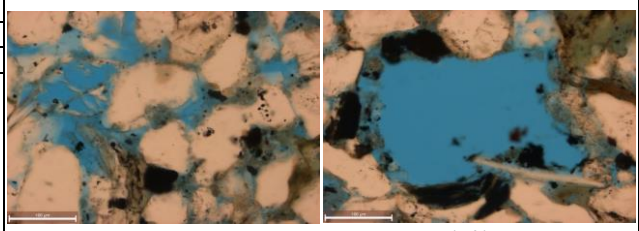

intergranular and dissolution porosity (left);
vug and dissolution porosity (right)
no18_0009 PL (left) and no18_0010 PL (right)

Back to Index

Thin Section Analysis Report

Sample ID: COST B-3
Sample Condition: circular sidewall core
Formation Name: Dawson Canyon
Depth (ft): 6260 ft
Lithologic Classification: Limestone

Date of Analysis: 2/20/2018
Analyzed by: Kristin M. Carter
Point Count Step Size 0.3 mm
Number of Counts 405

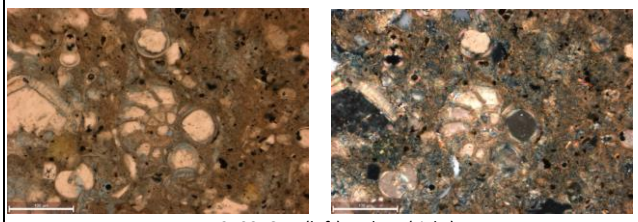

no19_0016 PL (left) and XN (right)

All scale bars are 100 um, unless otherwise noted

Texture - Qualitative Assessment

Approximate Average Grain Size (mm): 0.1
Grain Sorting: well sorted
Grain Rounding: subrounded to rounded

Composition - Modal Analysis Data

Framework

Mineral Grains	Total	Percent
Quartz		**2.5**
Monocrystalline	10	2.5
Polycrystalline		
Chert		
Feldspar		**1.0**
Plagioclase	4	1.0
Microcline		
K-Feldspar		
Carbonate		**24.0**
Calcite	97	24.0
Dolomite		

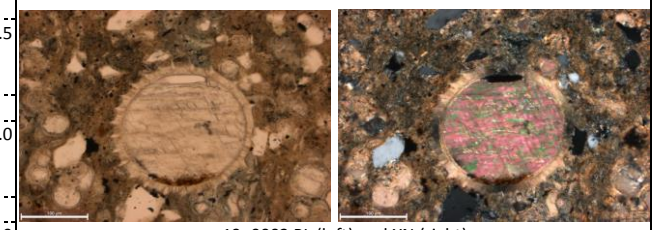

no19_0002 PL (left) and XN (right)

Lithic Grains	Total	Percent
		0.0
Metamorphic		
Sedimentary		
Volcanic		

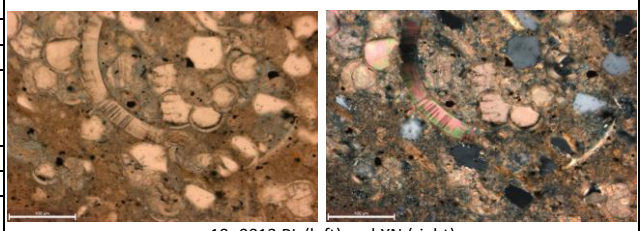

no19_0013 PL (left) and XN (right)

Accessory Minerals	Total	Percent
		2.5
Rutile		
Tourmaline		
Zircon	1	0.2
Opaques	9	2.2

Matrix Spaces

Cement	Total	Percent
		26.2
Quartz		
K-Feldspar		
Calcite	106	26.2
Dolomite/Ankerite		
Iron Oxide		

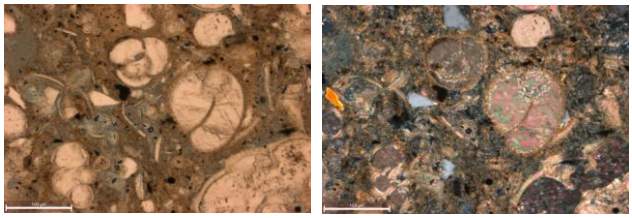

no19_0005 PL (left) and XN (right)

Matrix	Total	Percent
Clay Minerals		**44.0**
Clay Minerals (not individually identifiable)	163	40.2
Muscovite	5	1.2
Biotite	4	1.0
Chlorite	6	1.5
Glauconite		
Illite		0.0

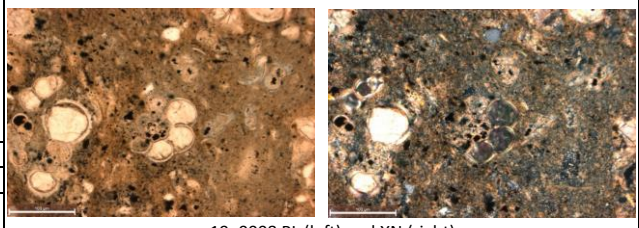

no19_0008 PL (left) and XN (right)

Porosity	Total	Percent
		0.0
Intergranular		
Intragranular		
Intercrystalline		
Moldic		
Grain/Cement Dissolution		
Clay/Mica Framework		
Organic Matter		
Vug		
Channel		
Fracture		
	Total	**100.0**

Back to Index

Thin Section Analysis Report

Sample ID: COST B-3
Sample Condition: circular sidewall core
Formation Name: Dawson Canyon
Depth (ft): 7040 ft
Lithology: Siltstone

Date of Analysis: 2/20/2018
Analyzed by: Kristin M. Carter
Point Count Step Size 0.3 mm
Number of Counts 407

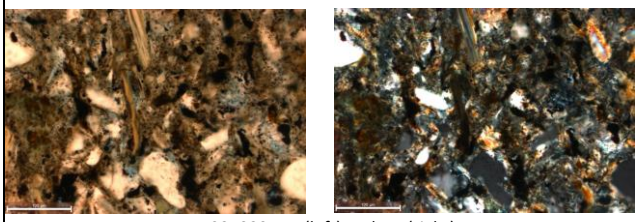

no20_0001 PL (left) and XN (right)

All scale bars are 100 um, unless otherwise noted

Texture - Qualitative Assessment

Approximate Average Grain Size (mm): <0.1
Grain Sorting: moderately well sorted
Grain Rounding: subangular to subrounded

Composition - Modal Analysis Data

Framework

Mineral Grains	Total	Percent
Quartz		**12.0**
Monocrystalline	49	12.0
Polycrystalline		
Chert		
Feldspar		**8.4**
Plagioclase	34	8.4
Microcline		
K-Feldspar		
Carbonate		**0.7**
Calcite	3	0.7
Dolomite		

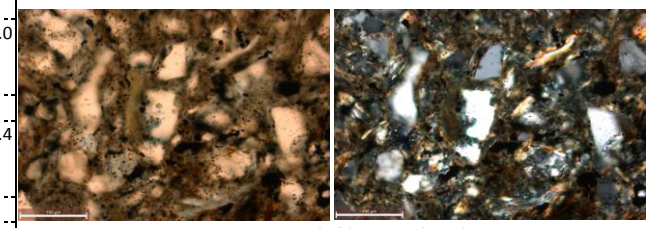

no20_0004 PL (left) and XN (right)

Lithic Grains	Total	Percent
		0.0
Metamorphic		
Sedimentary		
Volcanic		

Accessory Minerals	Total	Percent
		8.8
Rutile		
Tourmaline	1	0.2
Zircon		
Opaques	35	8.6

Matrix Spaces

Cement	Total	Percent
		1.0
Quartz		
K-Feldspar		
Calcite		
Dolomite/Ankerite		
Iron Oxide	4	1.0

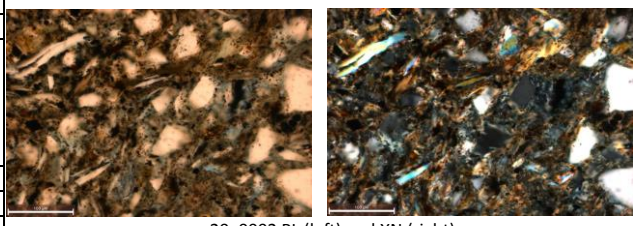

no20_0002 PL (left) and XN (right)

Matrix	Total	Percent
Clay Minerals		**68.6**
Clay Minerals (not individually identifiable)	224	55.0
Muscovite	28	6.9
Biotite	13	3.2
Chlorite	5	1.2
Glauconite		
Illite	9	2.2

Porosity	Total	Percent
		0.5
Intergranular		
Intragranular		
Intercrystalline		
Moldic		
Grain/Cement Dissolution	1	0.2
Clay/Mica Framework		
Organic Matter		
Vug		
Channel	1	0.2
Fracture		
	Total	**100.0**

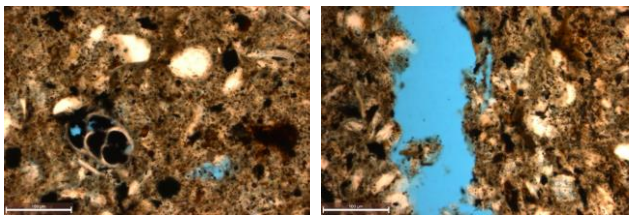

dissolution porosity (left); channel porosity (right)
no20_0007 PL (left) and no20_0009 PL (right)

Back to Index

Thin Section Analysis Report

Sample ID: COST B-3
Sample Condition: circular sidewall core
Formation Name: Dawson Canyon
Depth (ft): 7640 ft
Lithology: Siltstone

Date of Analysis: 2/21/2018
Analyzed by: Kristin M. Carter
Point Count Step Size 0.3 mm
Number of Counts 429

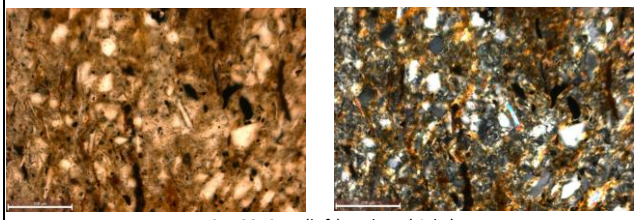

no21_0012 PL (left) and XN (right)

All scale bars are 100 um, unless otherwise noted

Texture - Qualitative Assessment

Approximate Average Grain Size (mm): 0.05
Grain Sorting: moderately well sorted
Grain Rounding: subangular to subrounded

Composition - Modal Analysis Data

Framework

Mineral Grains	Total	Percent
Quartz		**0.9**
Monocrystalline	4	0.9
Polycrystalline		
Chert		
Feldspar		**3.7**
Plagioclase	16	3.7
Microcline		
K-Feldspar		
Carbonate		**0.0**
Calcite		
Dolomite		

Lithic Grains	Total	Percent
		0.0
Metamorphic		
Sedimentary		
Volcanic		

Accessory Minerals	Total	Percent
		6.8
Rutile		
Tourmaline		
Zircon		
Opaques	29	6.8

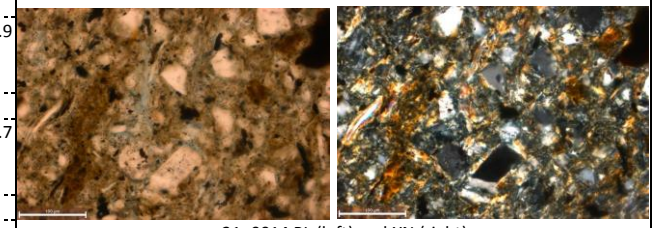

no21_0014 PL (left) and XN (right)

Matrix Spaces

Cement	Total	Percent
		6.3
Quartz		
K-Feldspar		
Calcite		
Dolomite/Ankerite		
Iron Oxide	27	6.3

Matrix	Total	Percent
Clay Minerals		**79.7**
Clay Minerals (not individually identifiable)	330	76.9
Muscovite	6	1.4
Biotite	4	0.9
Chlorite	2	0.5
Glauconite		
Illite		

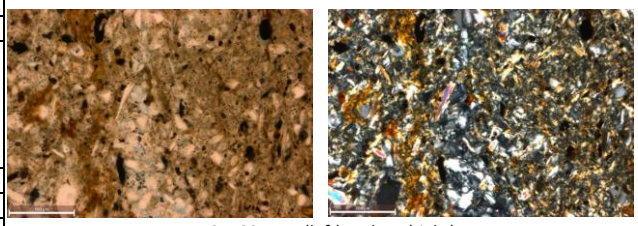

no21_0011 PL (left) and XN (right)

Porosity	Total	Percent
		2.6
Intergranular		
Intragranular		
Intercrystalline		
Moldic	2	0.5
Grain/Cement Dissolution		
Clay/Mica Framework		
Organic Matter		
Vug		
Channel	9	2.1
Fracture		
	Total	**100.0**

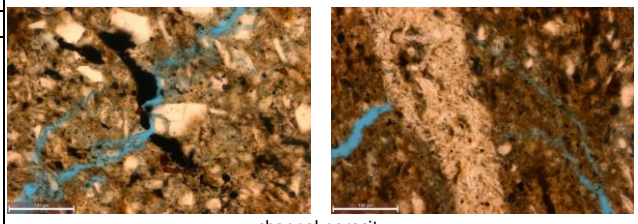

channel porosity
no21_0006 PL (left) and no21_0007 PL (right)

Back to Index

Thin Section Analysis Report

Sample ID: COST B-3
Sample Condition: two rock pieces/half slide
Formation Name: Upper Logan Canyon
Depth (ft): 8382 ft
Lithology: Sandstone

Date of Analysis: 2/21/2018
Analyzed by: Kristin M. Carter
Point Count Step Size 0.3 mm
Number of Counts 402

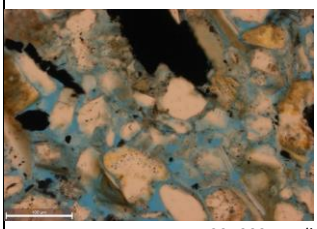
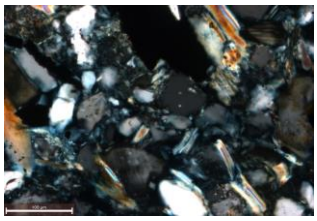

no22_0007 PL (left) and XN (right)

All scale bars are 100 um, unless otherwise noted

Texture - Qualitative Assessment

Approximate Average Grain Size (mm): 0.1
Grain Sorting: moderately well sorted
Grain Rounding: angular to subrounded

Composition - Modal Analysis Data

Framework

Mineral Grains	Total	Percent
Quartz		**12.2**
Monocrystalline	48	11.9
Polycrystalline	1	0.2
Chert		
Feldspar		**25.6**
Plagioclase	74	18.4
Microcline		
K-Feldspar	29	7.2
Carbonate		**0.0**
Calcite		
Dolomite		

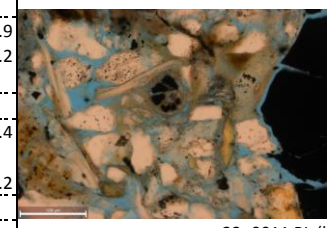
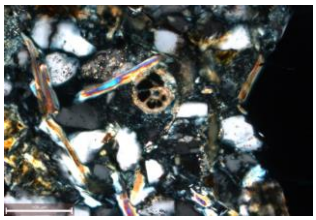

no22_0011 PL (left) and XN (right)

Lithic Grains	Total	Percent
		0.0
Metamorphic		
Sedimentary		
Volcanic		

Accessory Minerals	Total	Percent
		7.5
Rutile		
Tourmaline		
Zircon		
Opaques	30	7.5

Matrix Spaces

Cement	Total	Percent
		0.2
Quartz		
K-Feldspar		
Calcite		
Dolomite/Ankerite		
Iron Oxide	1	0.2

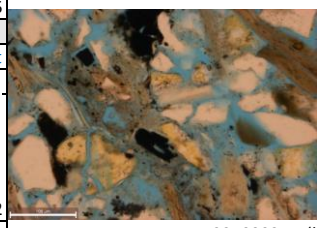
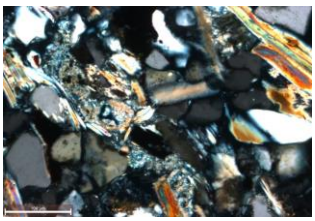

no22_0003 PL (left) and XN (right)

Matrix	Total	Percent
Clay Minerals		**42.8**
Clay Minerals (not individually identifiable)	77	19.2
Muscovite	18	4.5
Biotite	61	15.2
Chlorite	12	3.0
Glauconite		
Illite	4	1.0

Porosity	Total	Percent
		11.7
Intergranular	27	6.7
Intragranular		
Intercrystalline		
Moldic		
Grain/Cement Dissolution	20	5.0
Clay/Mica Framework		
Organic Matter		
Vug		
Channel		
Fracture		
	Total	**100.0**

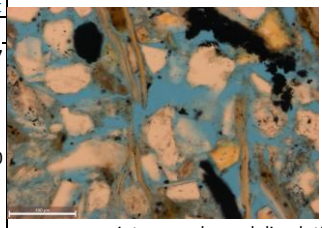
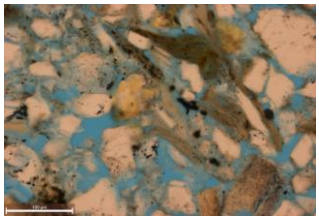

intergranular and dissolution porosity (left and right)
no22_0002 PL (left) and no22_0004 PL (right)

Back to Index

Thin Section Analysis Report

Sample ID: COST B-3
Sample Condition: corroded sidewall core
Formation Name: Naskapi
Depth (ft): 9750 ft
Lithology: Siltstone

Date of Analysis: 2/21/2018
Analyzed by: Kristin M. Carter
Point Count Step Size 0.3 mm
Number of Counts 425

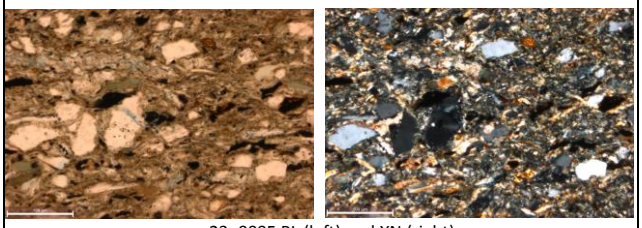

no23_0005 PL (left) and XN (right)

All scale bars are 100 um, unless otherwise noted

Texture - Qualitative Assessment

Approximate Average Grain Size (mm): <0.05
Grain Sorting: moderately well sorted
Grain Rounding: subangular to subrounded

Composition - Modal Analysis Data

Framework

Mineral Grains	Total	Percent
Quartz		**4.0**
Monocrystalline	17	4.0
Polycrystalline		
Chert		
Feldspar		**11.1**
Plagioclase	46	10.8
Microcline	1	0.2
K-Feldspar		
Carbonate		**0.9**
Calcite	4	0.9
Dolomite		

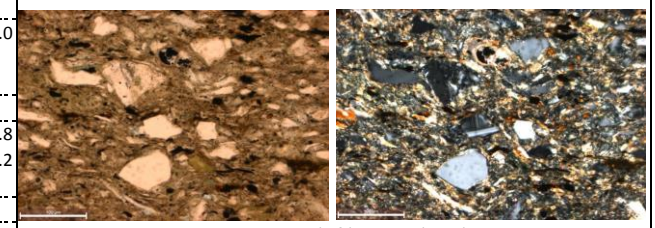

no23_0002 PL (left) and XN (right)

Lithic Grains	Total	Percent
		0.0
Metamorphic		
Sedimentary		
Volcanic		

Accessory Minerals	Total	Percent
		5.4
Rutile		
Tourmaline		
Zircon		
Opaques	23	5.4

Matrix Spaces

Cement	Total	Percent
		1.2
Quartz		
K-Feldspar		
Calcite	5	1.2
Dolomite/Ankerite		
Iron Oxide		

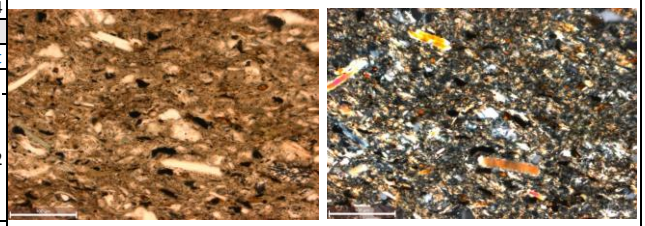

no23_0003 PL (left) and XN (right)

Matrix	Total	Percent
Clay Minerals		**76.5**
Clay Minerals (not individually identifiable)	301	70.8
Muscovite	13	3.1
Biotite	5	1.2
Chlorite	6	1.4
Glauconite		
Illite		

Porosity	Total	Percent
		0.9
Intergranular		
Intragranular		
Intercrystalline		
Moldic		
Grain/Cement Dissolution	1	0.2
Clay/Mica Framework		
Organic Matter		
Vug		
Channel	3	0.7
Fracture		
	Total	**100.0**

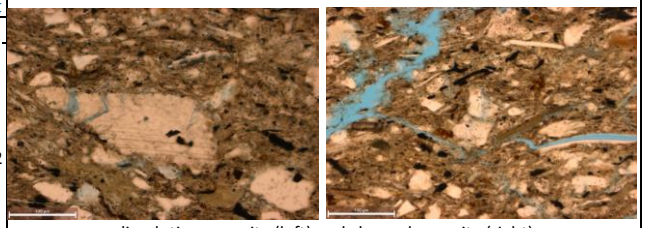

dissolution porosity (left) and channel porosity (right)
no23_0004 PL (left) and no23_0010 PL (right)

Back to Index

COST B-3 9931.6 ft

Thin Section Analysis Report

Sample ID: COST B-3
Sample Condition: standard rectangular size
Formation Name: Mississauga
Depth (ft): 9931.6 ft
Lithology: Sandstone

Date of Analysis: 2/21/2018
Analyzed by: Kristin M. Carter
Point Count Step Size 0.4 mm
Number of Counts 404

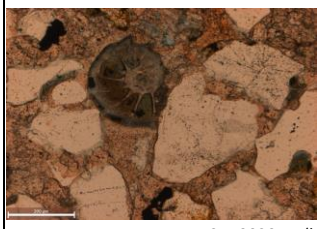
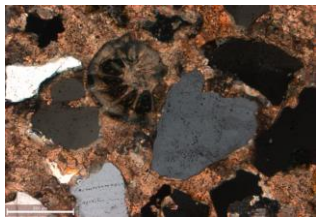

no24_0020 PL (left) and XN (right)

All scale bars are 200 um, unless otherwise noted

Texture - Qualitative Assessment

Approximate Average Grain Size (mm): 0.3
Grain Sorting: moderately well sorted
Grain Rounding: angular to subrounded

Composition - Modal Analysis Data

Framework

Mineral Grains	Total	Percent
Quartz		**24.0**
Monocrystalline	89	22.0
Polycrystalline	8	2.0
Chert		
Feldspar		**15.1**
Plagioclase	36	8.9
Microcline	2	0.5
K-Feldspar	23	5.7
Carbonate		**4.7**
Calcite	19	4.7
Dolomite		

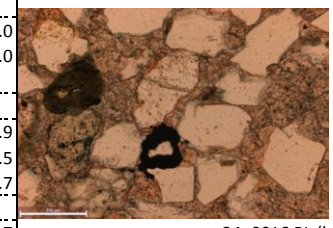
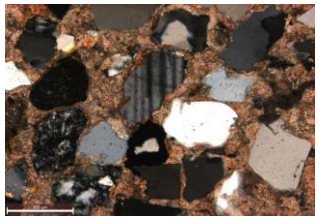

no24_0016 PL (left) and XN (right)

Lithic Grains	Total	Percent
		0.0
Metamorphic		
Sedimentary		
Volcanic		

Accessory Minerals	Total	Percent
		3.2
Rutile		
Tourmaline		
Zircon		
Opaques	13	3.2

Poikilotopic calcite cement

Matrix Spaces

Cement	Total	Percent
		48.5
Quartz		
K-Feldspar		
Calcite	196	48.5
Dolomite/Ankerite		
Iron Oxide		

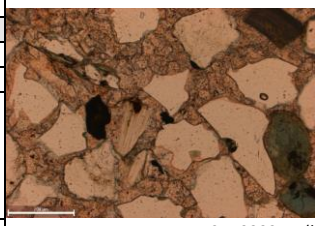
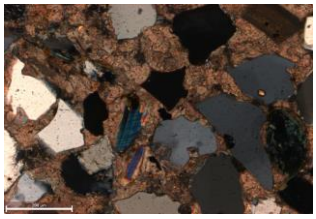

no24_0002 PL (left) and XN (right)

Matrix	Total	Percent
Clay Minerals		**4.5**
Clay Minerals (not individually identifiable)		
Muscovite	3	0.7
Biotite	2	0.5
Chlorite	13	3.2
Glauconite		
Illite		

some 'glauconite' pellets, but no glauconite found in XRD work

Porosity	Total	Percent
		0.0
Intergranular		
Intragranular		
Intercrystalline		
Moldic		
Grain/Cement Dissolution		
Clay/Mica Framework		
Organic Matter		
Vug		
Channel		
Fracture		
	Total	**100.0**

minor porosity observed, but not in point count

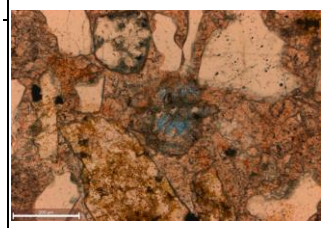
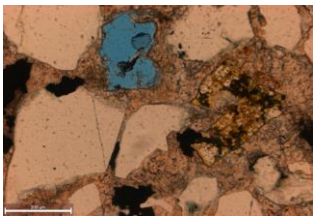

dissolution porosity (left) and moldic porosity (right)
no24_0013 PL (left) and no24_0014 PL (right)

Back to Index

Thin Section Analysis Report

Sample ID: COST B-3
Sample Condition: standard rectangular size
Formation Name: Mississauga
Depth (ft): 9932 ft
Lithology: Sandstone

Date of Analysis: 2/21/2018
Analyzed by: Kristin M. Carter
Point Count Step Size 0.4 mm
Number of Counts 412

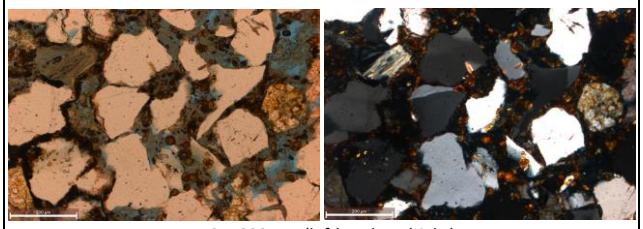

no25_0001 PL (left) and XN (right)

All scale bars are 200 um, unless otherwise noted

Texture - Qualitative Assessment

Approximate Average Grain Size (mm): 0.3
Grain Sorting: moderately well to well sorted
Grain Rounding: angular to subrounded

Composition - Modal Analysis Data

Framework

Mineral Grains	Total	Percent
Quartz		**20.1**
Monocrystalline	81	19.7
Polycrystalline	2	0.5
Chert		
Feldspar		**35.4**
Plagioclase	134	32.5
Microcline	1	0.2
K-Feldspar	11	2.7
Carbonate		**0.0**
Calcite		
Dolomite		

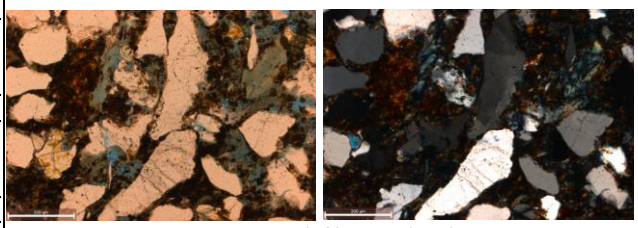

no25_0005 PL (left) and XN (right)

Lithic Grains	Total	Percent
		0.0
Metamorphic		
Sedimentary		
Volcanic		

Accessory Minerals	Total	Percent
		10.0
Rutile		
Tourmaline		
Zircon	1	0.2
Opaques	40	9.7

Matrix Spaces

Cement	Total	Percent
		12.1
Quartz		
K-Feldspar		
Calcite	2	0.5
Dolomite/Ankerite		
Iron Oxide	48	11.7

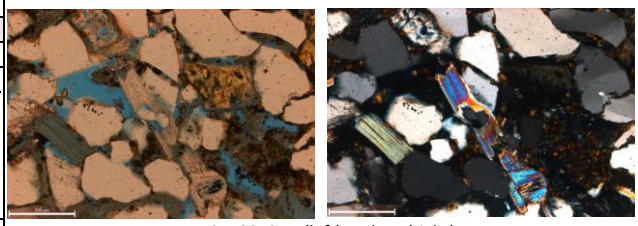

no25_0010 PL (left) and XN (right)

Matrix	Total	Percent
Clay Minerals		**17.2**
Clay Minerals (not individually identifiable)	54	13.1
Muscovite	5	1.2
Biotite		
Chlorite	11	2.7
Glauconite		
Illite	1	0.2

Porosity	Total	Percent
		5.1
Intergranular	11	2.7
Intragranular		
Intercrystalline		
Moldic		
Grain/Cement Dissolution	10	2.4
Clay/Mica Framework		
Organic Matter		
Vug		
Channel		
Fracture		
	Total	**100.0**

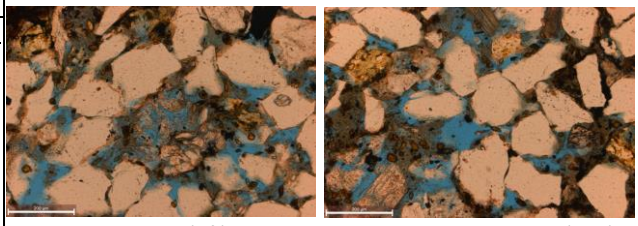

dissolution porosity (left) and intergranular and dissolution porosity (right)
no25_0002 PL (left) and no25_0013 PL (right)

Back to Index

Thin Section Analysis Report

Sample ID: COST B-3
Sample Condition: standard rectangular size
Formation Name: Mississauga
Depth (ft): 9934 ft
Lithology: Sandstone

Date of Analysis: 2/23/2018
Analyzed by: Kristin M. Carter
Point Count Step Size 1.0 mm
Number of Counts 404

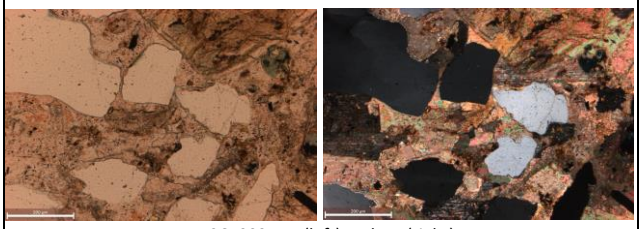

no26_0001 PL (left) and XN (right)

All scale bars are 200 um, unless otherwise noted

Texture - Qualitative Assessment

Approximate Average Grain Size (mm): 0.3
Grain Sorting: poorly sorted
Grain Rounding: subangular to subrounded

Composition - Modal Analysis Data

Framework

Mineral Grains	Total	Percent
Quartz		**24.0**
Monocrystalline	78	19.3
Polycrystalline		
Chert	19	4.7
Feldspar		**13.9**
Plagioclase	39	9.7
Microcline	9	2.2
K-Feldspar	8	2.0
Carbonate		**4.0**
Calcite	16	4.0
Dolomite		

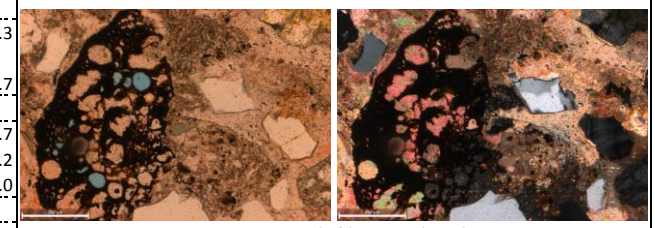

no26_0013 PL (left) and XN (right)

Lithic Grains	Total	Percent
		0.0
Metamorphic		
Sedimentary		
Volcanic		

Accessory Minerals	Total	Percent
		2.0
Rutile		
Tourmaline		
Zircon	2	0.5
Opaques	6	1.5

Poikilotopic calcite cement

Matrix Spaces

Cement	Total	Percent
		53.2
Quartz		
K-Feldspar		
Calcite	212	52.5
Dolomite/Ankerite		
Iron Oxide	3	0.7

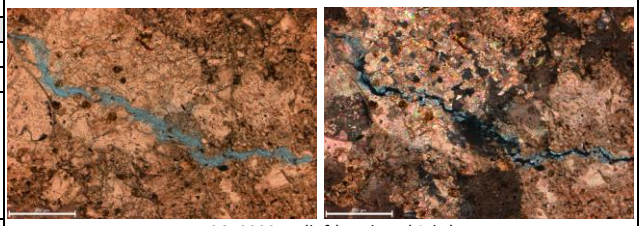

no26_0022 PL (left) and XN (right)

Matrix	Total	Percent
Clay Minerals		**2.2**
Clay Minerals (not individually identifiable)		
Muscovite	1	0.2
Biotite		
Chlorite	8	2.0
Glauconite		
Illite		

Porosity	Total	Percent
		0.7
Intergranular		
Intragranular		
Intercrystalline		
Moldic	1	0.2
Grain/Cement Dissolution	2	0.5
Clay/Mica Framework		
Organic Matter		
Vug		
Channel		
Fracture		
	Total	**100.0**

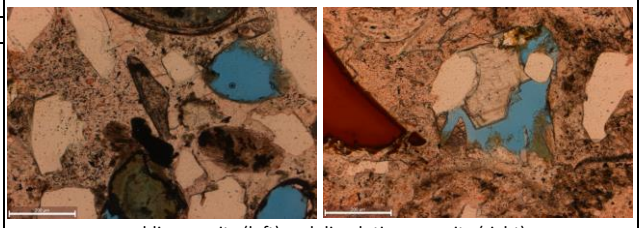

moldic porosity (left) and dissolution porosity (right)
no26_0009 PL (left) and no26_0011 PL (right)

Back to Index

Thin Section Analysis Report

Sample ID: COST B-3
Sample Condition: rectangular, three pieces
Formation Name: Mississauga
Depth (ft): 11,042 ft
Lithology: Siltstone

Date of Analysis: 2/23/2018
Analyzed by: Kristin M. Carter
Point Count Step Size 0.3 mm
Number of Counts 403

Texture - Qualitative Assessment

Approximate Average Grain Size (mm): 0.05
Grain Sorting: moderately well sorted
Grain Rounding: subangular to subrounded

Composition - Modal Analysis Data

Framework

Mineral Grains	Total	Percent
Quartz		**3.0**
Monocrystalline	12	3.0
Polycrystalline		
Chert		
Feldspar		**10.4**
Plagioclase	41	10.2
Microcline	1	0.2
K-Feldspar		
Carbonate		**0.5**
Calcite	2	0.5
Dolomite		

Lithic Grains	Total	Percent
		0.0
Metamorphic		
Sedimentary		
Volcanic		

Accessory Minerals	Total	Percent
		11.4
Rutile		
Tourmaline		
Zircon		
Opaques	46	11.4

Matrix Spaces

Cement	Total	Percent
		1.2
Quartz		
K-Feldspar		
Calcite	4	1.0
Dolomite/Ankerite		
Iron Oxide	1	0.2

Matrix	Total	Percent
Clay Minerals		**73.4**
Clay Minerals (not individually identifiable)	256	63.5
Muscovite	25	6.2
Biotite	15	3.7
Chlorite		
Glauconite		
Illite		

Porosity	Total	Percent
		0.0
Intergranular		
Intragranular		
Intercrystalline		
Moldic		
Grain/Cement Dissolution		
Clay/Mica Framework		
Organic Matter		
Vug		
Channel		
Fracture		
	Total	**100.0**

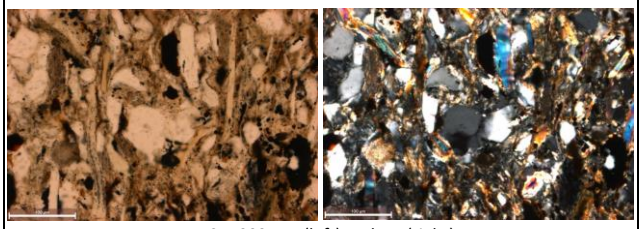

no27_0001 PL (left) and XN (right)

All scale bars are 100 um, unless otherwise noted

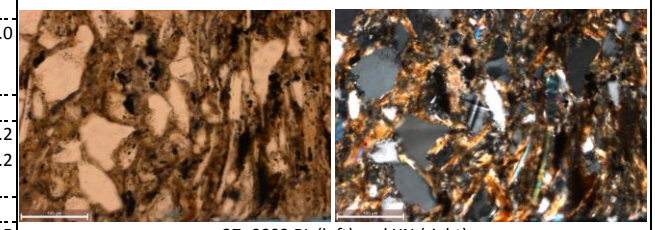

no27_0002 PL (left) and XN (right)

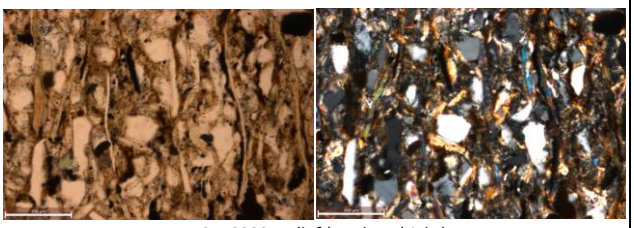

no27_0008 PL (left) and XN (right)

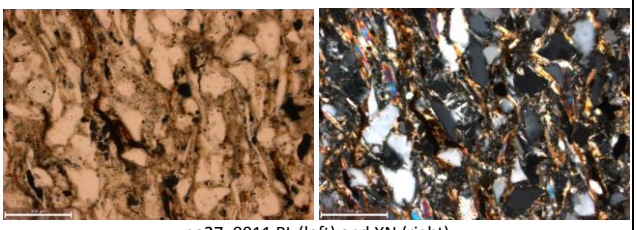

no27_0011 PL (left) and XN (right)

Back to Index

Thin Section Analysis Report

Sample ID: COST B-3
Sample Condition: standard rectangular size
Formation Name: Mississauga
Depth (ft): 11,050.8 ft
Lithology: Sandstone

Date of Analysis: 2/23/2018
Analyzed by: Kristin M. Carter
Point Count Step Size 0.3 mm
Number of Counts 424

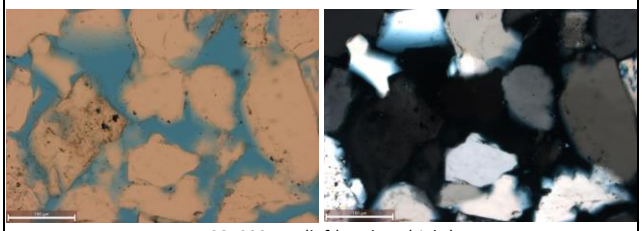

no28_0001 PL (left) and XN (right)

All scale bars are 100 um, unless otherwise noted

Texture - Qualitative Assessment

Approximate Average Grain Size (mm): 0.1
Grain Sorting: well to moderately well sorted
Grain Rounding: subangular to subrounded

Composition - Modal Analysis Data

Framework

Mineral Grains	Total	Percent
Quartz		**30.9**
Monocrystalline	124	29.2
Polycrystalline	7	1.7
Chert		
Feldspar		**31.1**
Plagioclase	124	29.2
Microcline	8	1.9
K-Feldspar		
Carbonate		**0.5**
Calcite	2	0.5
Dolomite		

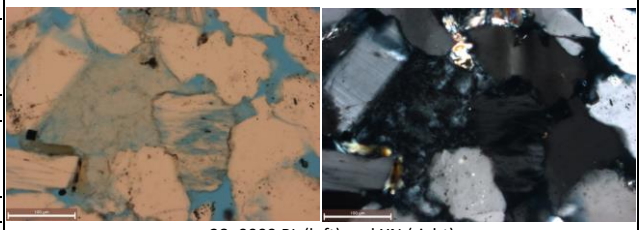

no28_0009 PL (left) and XN (right)

Lithic Grains	Total	Percent
		0.0
Metamorphic		
Sedimentary		
Volcanic		

Accessory Minerals	Total	Percent
		0.7
Rutile	1	0.2
Tourmaline		
Zircon	1	0.2
Opaques	1	0.2

Matrix Spaces

Cement	Total	Percent
		0.2
Quartz		
K-Feldspar		
Calcite	1	0.2
Dolomite/Ankerite		
Iron Oxide		

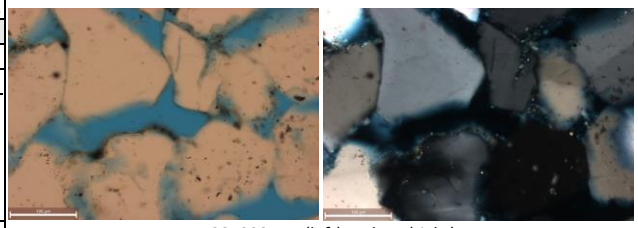

no28_0004 PL (left) and XN (right)

Matrix	Total	Percent
Clay Minerals		**13.7**
Clay Minerals (not individually identifiable)	34	8.0
Muscovite	8	1.9
Biotite	4	0.9
Chlorite		
Glauconite		
Illite	12	2.8

Porosity	Total	Percent
		22.9
Intergranular	57	13.4
Intragranular		
Intercrystalline		
Moldic		
Grain/Cement Dissolution	39	9.2
Clay/Mica Framework		
Organic Matter		
Vug	1	0.2
Channel		
Fracture		
	Total	**100.0**

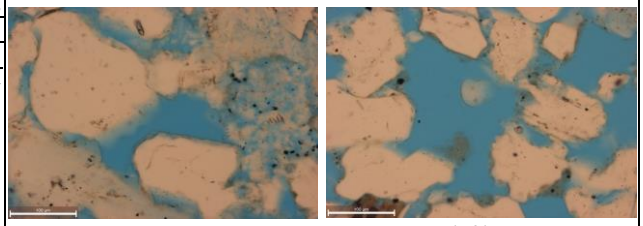

intergranular and dissolution porosity (left);
vug and dissolution porosity (right)
no28_0007 PL (left) and no28_0008 PL (right)

Back to Index

COST B-3 11,051-11,052 ft

Thin Section Analysis Report

Sample ID: COST B-3
Sample Condition: smaller rectangular size
Formation Name: Mississauga
Depth (ft): 11,051 - 11,052 ft
Lithology: Sandstone*

Date of Analysis: 2/23/2018
Analyzed by: Kristin M. Carter
Point Count Step Size 1.0 mm
Number of Counts 402

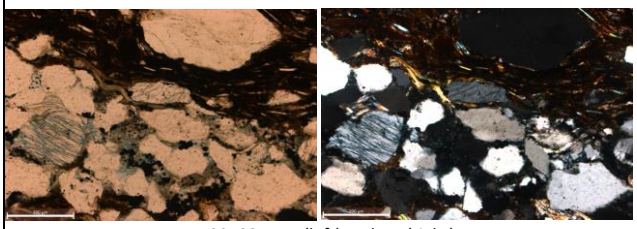

no29_0014 PL (left) and XN (right)

All scale bars are 200 um, unless otherwise noted

*parts of slide are characterized as siltstone, other as sandstone

Texture - Qualitative Assessment

Approximate Average Grain Size (mm): 0.3
Grain Sorting: poorly sorted
Grain Rounding: subangular to subrounded

Composition - Modal Analysis Data

Framework

Mineral Grains	Total	Percent
Quartz		**20.4**
Monocrystalline	70	17.4
Polycrystalline	12	3.0
Chert		
Feldspar		**11.7**
Plagioclase	44	10.9
Microcline	3	0.7
K-Feldspar		
Carbonate		**0.7**
Calcite	3	0.7
Dolomite		

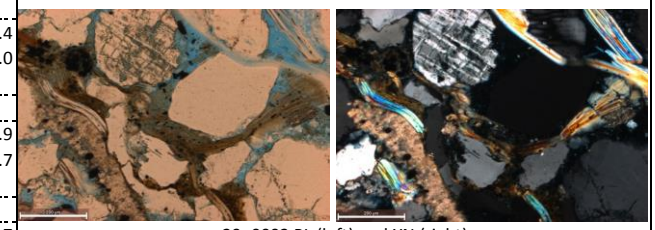

no29_0002 PL (left) and XN (right)

Lithic Grains	Total	Percent
		0.0
Metamorphic		
Sedimentary		
Volcanic		

Accessory Minerals	Total	Percent
		13.7
Rutile		
Tourmaline		
Zircon		
Opaques	55	13.7

Matrix Spaces

Cement	Total	Percent
		0.2
Quartz		
K-Feldspar		
Calcite	1	0.2
Dolomite/Ankerite		
Iron Oxide		

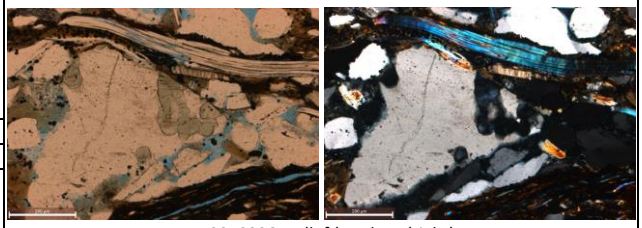

no29_0006 PL (left) and XN (right)

Matrix	Total	Percent
Clay Minerals		**50.2**
Clay Minerals (not individually identifiable)	166	41.3
Muscovite	13	3.2
Biotite	13	3.2
Chlorite	5	1.2
Glauconite		
Illite	5	1.2

Porosity	Total	Percent
		3.0
Intergranular	4	1.0
Intragranular		
Intercrystalline		
Moldic		
Grain/Cement Dissolution	6	1.5
Clay/Mica Framework		
Organic Matter		
Vug		
Channel	2	0.5
Fracture		
	Total	**100.0**

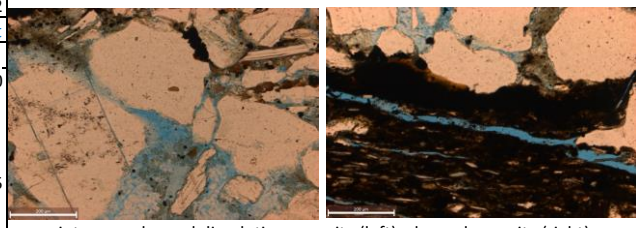

intergranular and dissolution porosity (left); channel porosity (right)
no29_0004 PL (left) and no29_0008 PL (right)

Back to Index

Thin Section Analysis Report

Sample ID: COST B-3
Sample Condition: standard rectangular size
Formation Name: Mississauga
Depth (ft): 11,054 ft
Lithology: Sandstone

Date of Analysis: 2/26/2018
Analyzed by: Kristin M. Carter
Point Count Step Size 0.4 mm
Number of Counts 430

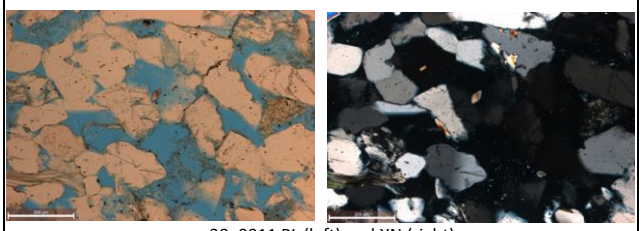

no30_0011 PL (left) and XN (right)

All scale bars are 200 um, unless otherwise noted

Texture - Qualitative Assessment

Approximate Average Grain Size (mm): 0.2
Grain Sorting: moderately to poorly sorted
Grain Rounding: subangular to subrounded

Composition - Modal Analysis Data

Framework

Mineral Grains	Total	Percent
Quartz		**30.0**
Monocrystalline	126	29.3
Polycrystalline	3	0.7
Chert		
Feldspar		**34.7**
Plagioclase	143	33.3
Microcline	6	1.4
K-Feldspar		
Carbonate		**0.7**
Calcite	3	0.7
Dolomite		

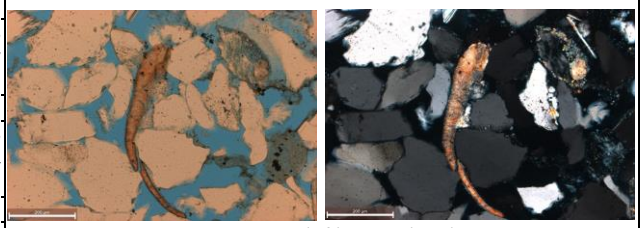

no30_0010 PL (left) and XN (right)

Lithic Grains	Total	Percent
		0.0
Metamorphic		
Sedimentary		
Volcanic		

Accessory Minerals	Total	Percent
		1.2
Rutile		
Tourmaline	1	0.2
Zircon		
Opaques	4	0.9

Matrix Spaces

Cement	Total	Percent
		0.5
Quartz		
K-Feldspar		
Calcite	2	0.5
Dolomite/Ankerite		
Iron Oxide		

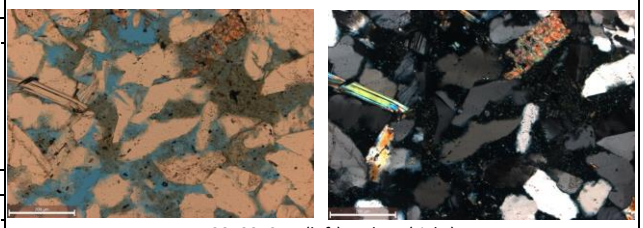

no30_0013 PL (left) and XN (right)

Matrix	Total	Percent
Clay Minerals		**15.1**
Clay Minerals (not individually identifiable)	50	11.6
Muscovite	10	2.3
Biotite	1	0.2
Chlorite	3	0.7
Glauconite		
Illite	1	0.2

Porosity	Total	Percent
		17.9
Intergranular	45	10.5
Intragranular		
Intercrystalline		
Moldic	2	0.5
Grain/Cement Dissolution	29	6.7
Clay/Mica Framework		
Organic Matter		
Vug	1	0.2
Channel		
Fracture		
	Total	**100.0**

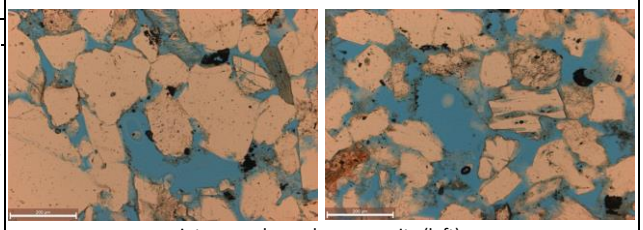

intregranular and vug porosity (left);
moldic and dissolution porosity (right)
no30_0004 PL (left) and no30_0016 PL (right)

Back to Index

Thin Section Analysis Report

Sample ID: COST B-3
Sample Condition: circular sidewall core
Formation Name: Mohawk
Depth (ft): 12,581.9 ft
Lithology: Limestone*

Date of Analysis: 2/26/2018
Analyzed by: Kristin M. Carter
Point Count Step Size 1.0 mm
Number of Counts 401

Texture - Qualitative Assessment

Approximate Average Grain Size (mm): 0.4
Grain Sorting: poorly sorted
Grain Rounding: angular to subrounded

Composition - Modal Analysis Data

Framework

Mineral Grains	Total	Percent
Quartz		**5.7**
Monocrystalline	23	5.7
Polycrystalline		0.0
Chert		
Feldspar		**0.7**
Plagioclase	1	0.2
Microcline		
K-Feldspar	2	0.5
Carbonate		**50.1**
Micrite	201	50.1
Dolomite		

Lithic Grains	Total	Percent
		0.0
Metamorphic		
Sedimentary		
Volcanic		

Accessory Minerals	Total	Percent
		0.7
Rutile		
Tourmaline		
Zircon		
Opaques	3	0.7

Matrix Spaces

Cement	Total	Percent
		40.1
Quartz		
K-Feldspar		
Calcite	161	40.1
Dolomite/Ankerite		
Iron Oxide		

Matrix	Total	Percent
Clay Minerals		**0.5**
Clay Minerals (not individually identifiable)	1	0.2
Muscovite	1	0.2
Biotite		
Chlorite		
Glauconite		
Illite		

Porosity	Total	Percent
		2.0
Intergranular		
Intragranular		
Intercrystalline		
Moldic		
Grain/Cement Dissolution		
Clay/Mica Framework		
Organic Matter		
Vug		
Channel	8	2.0
Fracture		
	Total	**100.0**

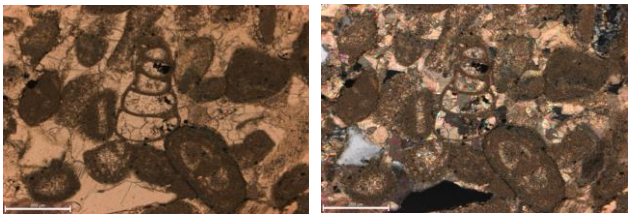

no31_0023 PL (left) and XN (right)

All scale bars are 200 um, unless otherwise noted

*many grains are completely or partially micritized

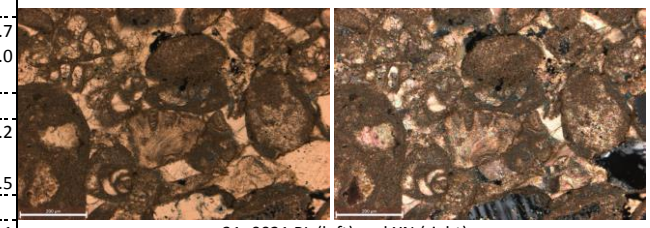

no31_0021 PL (left) and XN (right)

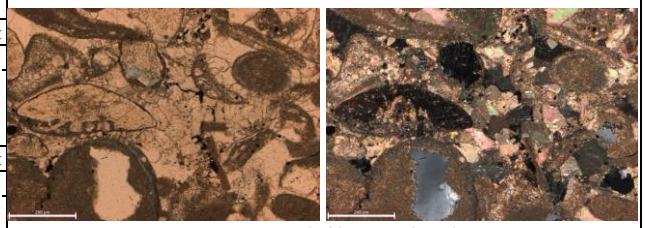

no31_0026 PL (left) and XN (right)

Poikilotopic calcite cement in places

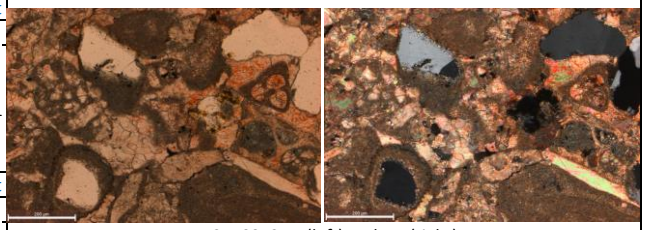

no31_0013 PL (left) and XN (right)

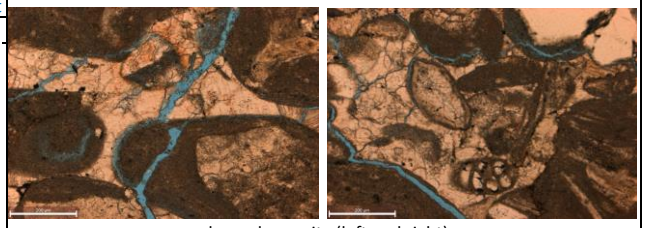

channel porosity (left and right)

no31_0005 PL (left) and no31_0010 PL (right)

Back to Index

Thin Section Analysis Report

Sample ID: MOBIL 544-1-5211
Sample Condition: 22x16 mm, large voids
Formation Name: Dawson Canyon
Depth (ft): 5211
Lithology: siltstone

Date of Analysis: 3/19/2018
Analyzed by: S. Shank
Point Count Step Size 0.4 mm
Number of Counts 456

Texture - Qualitative Assessment

Approximate Average Grain Size (mm): <0.1 (quartz grains)
Grain Sorting:
Grain Rounding: angular to subrounded

Composition - Modal Analysis Data

Framework

Mineral Grains	Total	Percent
Quartz		**6.1**
Monocrystalline	28	6.1
Polycrystalline		0.0
Chert		
Feldspar		**1.8**
Plagioclase	1	0.2
Microcline		
K-Feldspar	7	1.5
Carbonate		**0.0**
Calcite		
Dolomite		

Lithic Grains	Total	Percent
		0.0
Metamorphic		
Sedimentary		
Volcanic		

Accessory Minerals	Total	Percent
		0.4
Rutile		
Tourmaline		
Zircon		
Opaques	2	0.4

Matrix Spaces

Cement	Total	Percent
		14.7
Quartz		
K-Feldspar		
Calcite	53	11.6
Dolomite/Ankerite		
Iron Oxide	14	3.1

Matrix	Total	Percent
Clay Minerals		**73.7**
Clay Minerals (not individually identifiable)	336	73.7
Muscovite		
Biotite		
Chlorite		
Glauconite		
Illite		

Porosity	Total	Percent
		3.3
Intergranular		
Intragranular		
Intercrystalline		
Moldic		
Grain/Cement Dissolution		
Clay/Mica Framework	15	3.3
Organic Matter		
Vug		
Channel		
Fracture		
	Total	**100.0**

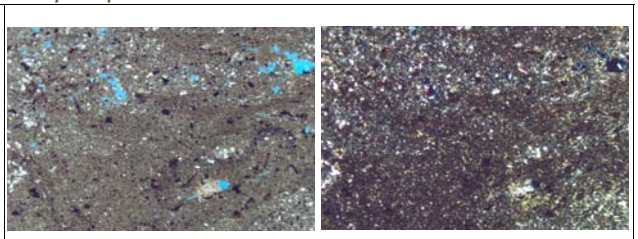

2.5 x Field of View ~5 mm
patchy distribution of quartz, larger voids-not primary?

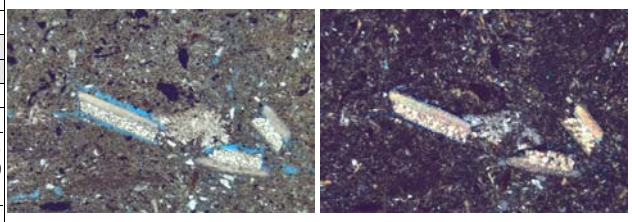

5 x Field of View ~3 mm
shell fragment with adjacent porosity, some porosity in matrix

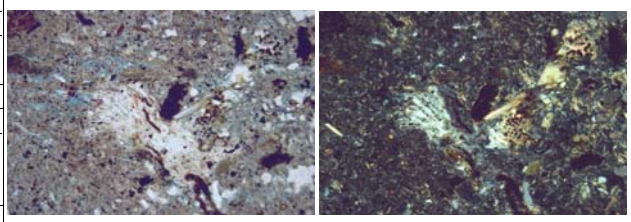

10x Field of View ~1 mm
gypsum, some porosity in matrix clays

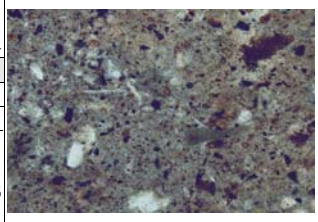

20x Field of View ~0.5 mm
close up of matrix

Back to Index

Thin Section Analysis Report

Sample ID: MOBIL 544-1-5435
Sample Condition: 25 mm round, fractured
Formation Name: Dawson Canyon
Depth (ft): 5435
Lithology: siltstone

Date of Analysis: 3/19/2018
Analyzed by: S. Shank
Point Count Step Size 0.4 mm
Number of Counts 425

Fractures
Matrix composed of clays and calcite

Texture - Qualitative Assessment

Approximate Average Grain Size (mm): <0.1 (quartz grains)
Grain Sorting:
Grain Rounding: angular to subrounded

Composition - Modal Analysis Data

Framework

Mineral Grains	Total	Percent
Quartz		**3.3**
Monocrystalline	14	3.3
Polycrystalline		
Chert		
Feldspar		**0.0**
Plagioclase		
Microcline		
K-Feldspar		
Carbonate		**16.0**
Calcite	50	11.8
Shell/fossil	18	4.2
Lithic Grains	**Total**	**Percent**
		0.0
Metamorphic		
Sedimentary		
Volcanic		
Accessory Minerals	**Total**	**Percent**
		1.6
Rutile		
Tourmaline		
Gypsum	5	1.2
Opaques	2	0.5

Matrix Spaces

Cement	Total	Percent
		3.3
Quartz		
K-Feldspar		
Calcite		
Dolomite/Ankerite		
Iron Oxide	14	3.3
Matrix	**Total**	**Percent**
Clay Minerals		**72.2**
Clay Minerals & Calcite	307	72.2
Muscovite		
Biotite		
Chlorite		
Glauconite		
Illite		
Porosity	**Total**	**Percent**
		3.5
Intergranular		
Intragranular		
Intercrystalline		
Moldic		
Grain/Cement Dissolution		
Clay/Mica Framework	2	0.5
Organic Matter		
Vug		
Channel		
Fracture	13	3.1
	Total	**100.0**

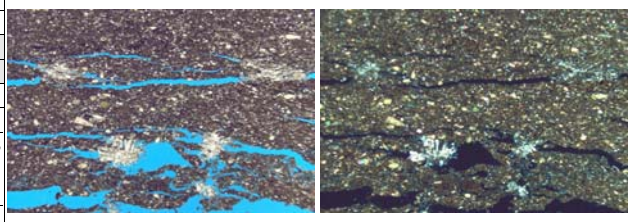

2.5 x Field of View ~ 5 mm
Fractures with secondary? gypsum

10x Field of View ~1 mm
Distinct calcite grains and fossil shell

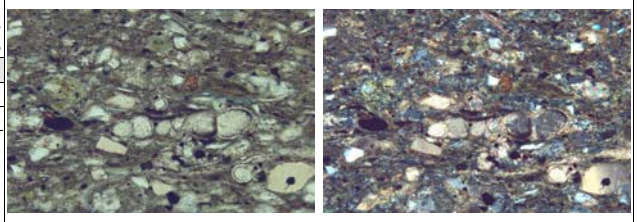

20x Field of View ~0.5 mm
distinct calcite grains and fossil shells

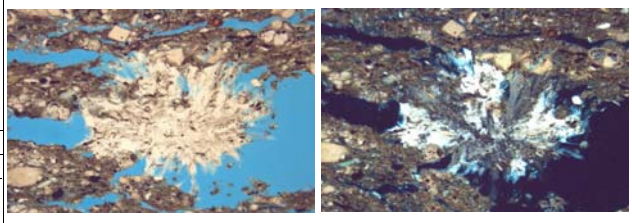

10x Field of View ~1 mm
Close up of gypsum
Gypsum appears to be restricted to secondary fractures

Back to Index

Thin Section Analysis Report

Sample ID: MOBIL 544-1-5962
Sample Condition: 3 small fragments, 13x13 mm
Formation Name: Dawson Canyon
Depth (ft): 5962
Lithology: glauconitic sandy limestone

Date of Analysis: 3/19/2018
Analyzed by: S. Shank
Point Count Step Size 1.0 mm
Number of Counts 116

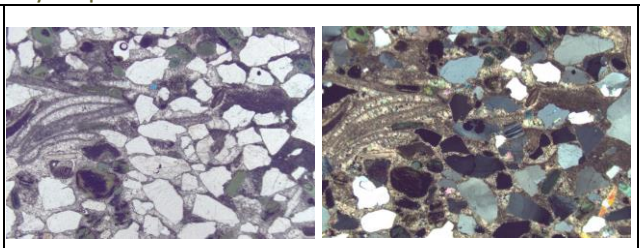

2.5 x Field of View ~ 5 mm
Quartz grains, "glauconite" pellets and shell fragments in calcite matrix
Minimal porosity

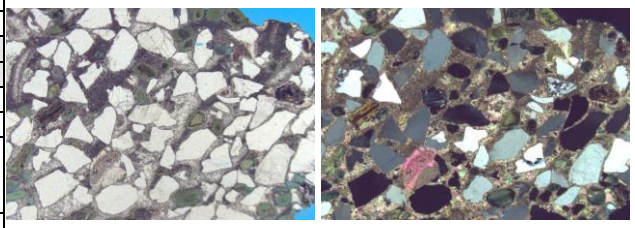

2.5 x Field of View ~ 5 mm

Texture - Qualitative Assessment

Approximate Average Grain Size (mm): 0.5
Grain Sorting: moderate
Grain Rounding: angular to subangular

Composition - Modal Analysis Data

Framework

Mineral Grains	Total	Percent
Quartz		**38.8**
Monocrystalline	40	34.5
Polycrystalline	5	4.3
Chert		
Feldspar		**2.6**
Plagioclase		
Microcline	1	0.9
K-Feldspar	2	1.7
Carbonate		**0.0**
Calcite		
Dolomite		

Lithic Grains	Total	Percent
		0.0
Metamorphic		
Sedimentary		
Volcanic		

Accessory Minerals	Total	Percent
		0.0
Rutile		
Tourmaline		
Zircon		
Opaques		

Matrix Spaces

Cement	Total	Percent
		45.7
Quartz		
K-Feldspar		
Calcite	53	45.7
Dolomite/Ankerite		
Iron Oxide		

Matrix	Total	Percent
Clay Minerals		**12.1**
Clay Minerals (not individually identifiable)		
Muscovite		
Biotite		
Chlorite		
Glauconite	14	12.1
Illite		

Porosity	Total	Percent
		0.9
Intergranular		
Intragranular		
Intercrystalline		
Moldic	1	0.9
Grain/Cement Dissolution		
Clay/Mica Framework		
Organic Matter		
Vug		
Channel		
Fracture		
	Total	**100.0**

Back to Index

Thin Section Analysis Report

Sample ID: MOBIL 544-1-6260
Sample Condition: 20 mm round, poor
Formation Name: Dawson Canyon
Depth (ft): 6260
Lithology: siltstone

Date of Analysis: 3/19/2018
Analyzed by: S. Shank
Point Count Step Size 0.4 mm
Number of Counts 437

Texture - Qualitative Assessment

Approximate Average Grain Size (mm): <0.1 (quartz grains)
Grain Sorting: poor
Grain Rounding: angular to subrounded

Composition - Modal Analysis Data

Framework		
Mineral Grains	Total	Percent
Quartz		**27.5**
Monocrystalline	120	27.5
Polycrystalline		
Chert		
Feldspar		**1.6**
Plagioclase	7	1.6
Microcline		
K-Feldspar		
Carbonate		**0.0**
Calcite		
Shell/fossil		
Lithic Grains	Total	Percent
		0.0
Metamorphic		
Sedimentary		
Volcanic		
Accessory Minerals	Total	Percent
		9.8
Rutile		
Tourmaline		
Gypsum		
Opaques	43	9.8
Matrix Spaces		
Cement	Total	Percent
		3.2
Quartz		
K-Feldspar		
Calcite		
Dolomite/Ankerite		
Iron Oxide	14	3.2
Matrix	Total	Percent
Clay Minerals		**52.6**
Clay Minerals (not individually identifiable)	228	52.2
Muscovite	2	0.5
Biotite		
Chlorite		
Glauconite		
Illite		
Porosity	Total	Percent
		5.3
Intergranular		
Intragranular		
Intercrystalline		
Moldic	2	0.5
Grain/Cement Dissolution		
Clay/Mica Framework	16	3.7
Organic Matter		
Vug		
Channel		
Fracture	5	1.1
	Total	**100.0**

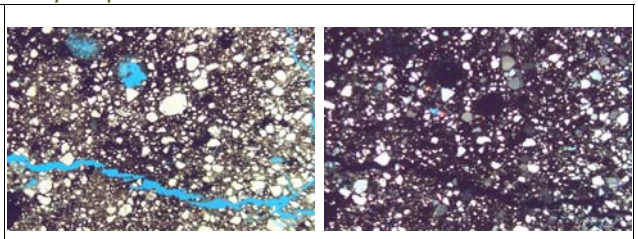

2.5 x Field of View ~5 mm
Fractures and patchy (moldic) porosity

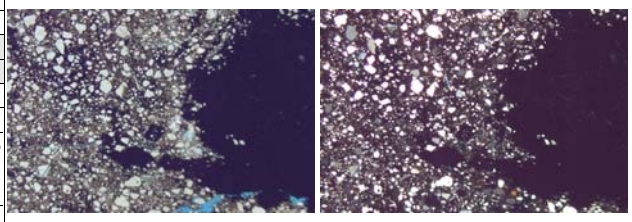

2.5 x Field of View ~5 mm
Large opaque mass (iron sulfide)

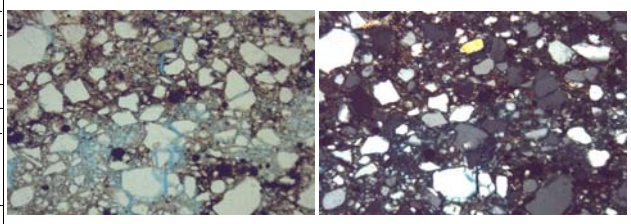

10x Field of View ~1 mm
Patchy matrix porosity
Poorly cemented

Back to Index

Thin Section Analysis Report

Sample ID: MOBIL 544-1-6420
Sample Condition: 20 mm round
Formation Name: Dawson Canyon
Depth (ft): 6420
Lithology: shale

Date of Analysis: 3/19/2018
Analyzed by: S. Shank
Point Count Step Size 0.8 mm
Number of Counts 314

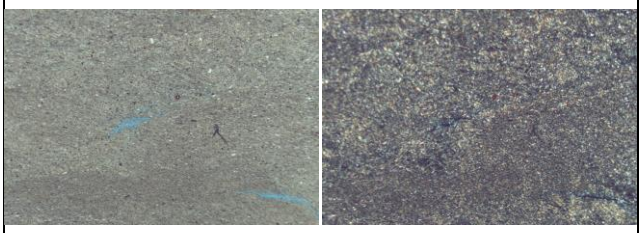

2.5 x Field of View ~ 5 mm
Extremely fine-grained
Some wispy discontinuous fractures

Texture - Qualitative Assessment

Approximate Average Grain Size (mm): <<0.1
Grain Sorting:
Grain Rounding:

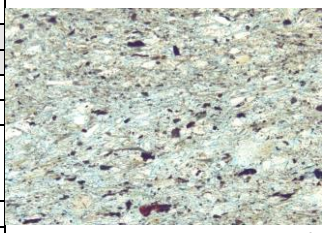

20x Field of View ~0.5 mm
Poorly cemented, pervasive microporosity shown by blue tint
Pervasive micropores too small to count under microscope

Composition - Modal Analysis Data

Framework

Mineral Grains	Total	Percent
Quartz		**1.3**
Monocrystalline	4	1.3
Polycrystalline		
Chert		
Feldspar		**0.0**
Plagioclase		
Microcline		
K-Feldspar		
Carbonate		**0.0**
Calcite		
Shell/fossil		

Lithic Grains	Total	Percent
		0.0
Metamorphic		
Sedimentary		
Volcanic		

Accessory Minerals	Total	Percent
		0.3
Rutile		
Tourmaline		
Gypsum		
Opaques	1	0.3

Matrix Spaces

Cement	Total	Percent
		0.0
Quartz		
K-Feldspar		
Calcite		
Dolomite/Ankerite		
Iron Oxide		

Matrix	Total	Percent
Clay Minerals		**98.4**
Clay Minerals (not individually identifiable)	309	98.4
Muscovite		
Biotite		
Chlorite		
Glauconite		
Illite		

Porosity	Total	Percent
		0.0
Intergranular		
Intragranular		
Intercrystalline		
Moldic		
Grain/Cement Dissolution		
Clay/Mica Framework		
Organic Matter		
Vug		
Channel		
Fracture		0.0
	Total	**100.0**

Back to Index

Thin Section Analysis Report

Sample ID: MOBIL 544-1-6579
Sample Condition: 20 mm round
Formation Name: Dawson Canyon
Depth (ft): 6579
Lithology: siltstone

Date of Analysis: 3/19/2018
Analyzed by: S. Shank
Point Count Step Size 0.8 mm
Number of Counts 335

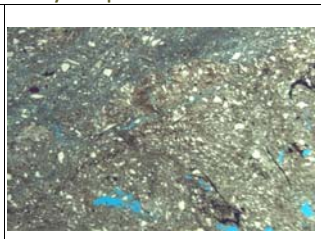

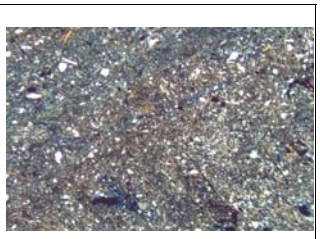

2.5 x Field of View ~ 5 mm
Patchy distribution of quartz and clays
Porosity in thin fractures and voids

Texture - Qualitative Assessment

Approximate Average Grain Size (mm): <0.1 (quartz grains)
Grain Sorting: poor
Grain Rounding: angular to subrounded

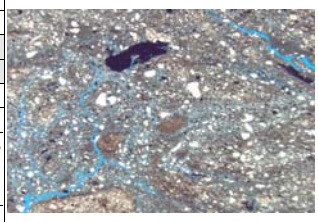

2.5 x Field of View ~ 5 mm
Fractures and patchy matrix porosity

Composition - Modal Analysis Data

Framework

Mineral Grains	Total	Percent
Quartz		**11.3**
Monocrystalline	38	11.3
Polycrystalline		
Chert		
Feldspar		**0.0**
Plagioclase		
Microcline		
K-Feldspar		
Carbonate		**0.0**
Calcite		
Shell/fossil		

Lithic Grains	Total	Percent
		0.0
Metamorphic		
Sedimentary		
Volcanic		

Accessory Minerals	Total	Percent
		0.6
Rutile		
Tourmaline		
Gypsum		
Opaques	2	0.6

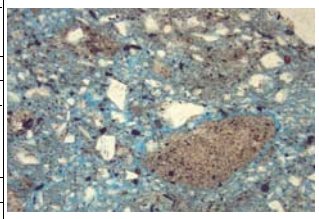

10x Field of View ~1 mm
Poorly cemented, locally pervasive microporosity

Matrix Spaces

Cement	Total	Percent
		0.6
Quartz		
K-Feldspar		
Calcite		
Dolomite/Ankerite		
Iron Oxide	2	0.6

Matrix	Total	Percent
Clay Minerals		**78.2**
Clay Minerals (not individually identifiable)	262	78.2
Muscovite		
Biotite		
Chlorite		
Glauconite		
Illite		

Porosity	Total	Percent
		9.3
Intergranular		
Intragranular		
Intercrystalline		
Moldic		
Grain/Cement Dissolution		
Clay/Mica Framework	26	7.8
Organic Matter		
Vug		
Channel		
Fracture	5	1.5
	Total	**100.0**

Back to Index

Thin Section Analysis Report

Sample ID: MOBIL 544-1-6696
Sample Condition: 20 mm round
Formation Name: Dawson Canyon
Depth (ft): 6696
Lithology: calcareous siltstone

Date of Analysis: 3/19/2018
Analyzed by: S. Shank
Point Count Step Size 0.8 mm
Number of Counts 389

Texture - Qualitative Assessment

Approximate Average Grain Size (mm): 0.1 (quartz grains)
Grain Sorting: poor
Grain Rounding: angular to subrounded

Composition - Modal Analysis Data

Framework		
Mineral Grains	Total	Percent
Quartz		**6.9**
Monocrystalline	27	6.9
Polycrystalline		
Chert		
Feldspar		**0.0**
Plagioclase		
Microcline		
K-Feldspar		
Carbonate		**13.1**
Siderite/Calcite	51	13.1
Shell/fossil		
Lithic Grains	Total	Percent
		0.0
Metamorphic		
Sedimentary		
Volcanic		
Accessory Minerals	Total	Percent
		0.3
Rutile		
Tourmaline		
Gypsum		
Opaques	1	0.3
Matrix Spaces		
Cement	Total	Percent
		4.9
Quartz		
K-Feldspar		
Calcite		
Dolomite/Ankerite		
Iron Oxide	19	4.9
Matrix	Total	Percent
Clay Minerals		**72.0**
Clay Minerals (not individually identifiable)	280	72.0
Muscovite		
Biotite		
Chlorite		
Glauconite		
Illite		
Porosity	Total	Percent
		2.8
Intergranular		
Intragranular		
Intercrystalline		
Moldic		
Grain/Cement Dissolution		
Clay/Mica Framework	6	1.5
Organic Matter		
Vug		
Channel		
Fracture	5	1.3
	Total	**100.0**

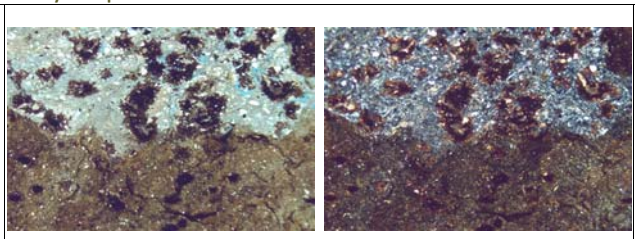

2.5 x Field of View ~ 5 mm
Highly variable mineralogy and porosity
Iron oxide stained siderite aggregates

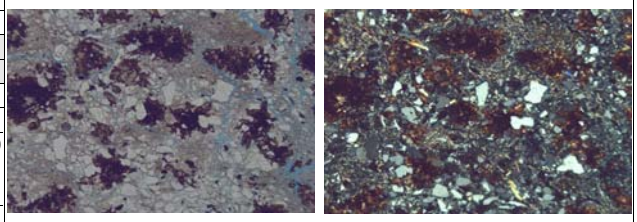

2.5 x Field of View ~ 5 mm
Quartz and siderite rich
Porosity in veins and fractures and around quartz

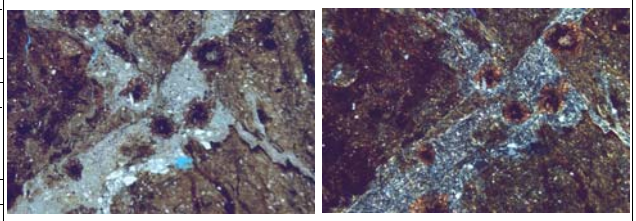

5x Field of View ~3 mm
Highly heterogeneous mineralogy and porosity

Back to Index

Thin Section Analysis Report

Sample ID: MOBIL 544-1-6798
Sample Condition: 3 small fragments
Formation Name: Dawson Canyon
Depth (ft): 6798
Lithology: sandstone

Date of Analysis: 3/19/2018
Analyzed by: S. Shank
Point Count Step Size 0.8 mm
Number of Counts 266

Texture - Qualitative Assessment

Approximate Average Grain Size (mm): 0.2
Grain Sorting: poor
Grain Rounding: angular to subrounded

Composition - Modal Analysis Data

Framework

Mineral Grains	Total	Percent
Quartz		**39.5**
Monocrystalline	103	38.7
Polycrystalline	2	0.8
Chert		
Feldspar		**4.1**
Plagioclase		
Microcline		
K-Feldspar	11	4.1
Carbonate		**0.0**
Calcite		
Dolomite		

Lithic Grains	Total	Percent
		0.0
Metamorphic		
Sedimentary		
Volcanic		

Accessory Minerals	Total	Percent
		2.6
Rutile		
Tourmaline		
Zircon		
Opaques	7	2.6

Matrix Spaces

Cement	Total	Percent
		11.7
Quartz	29	10.9
K-Feldspar		
Calcite		
Dolomite/Ankerite		
Iron Oxide	2	0.8

Matrix	Total	Percent
Clay Minerals		**30.5**
Clay Minerals (not individually identifiable)	47	17.7
Muscovite	4	1.5
Kaolinite	30	11.3
Chlorite		
Glauconite		
Illite		

Porosity	Total	Percent
		11.7
Intergranular	3	1.1
Intragranular		
Intercrystalline	27	10.2
Moldic	1	0.4
Grain/Cement Dissolution		
Clay/Mica Framework		
Organic Matter		
Vug		
Channel		
Fracture		
	Total	**100.0**

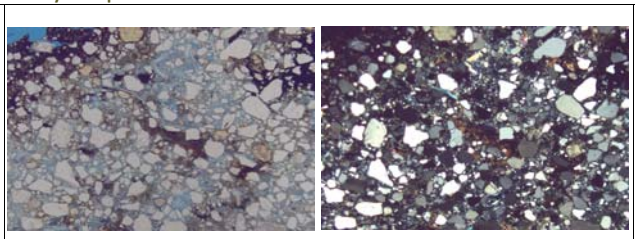

2.5 x Field of View ~5 mm
Quartz sandstone with abundant interstitial clays & quartz

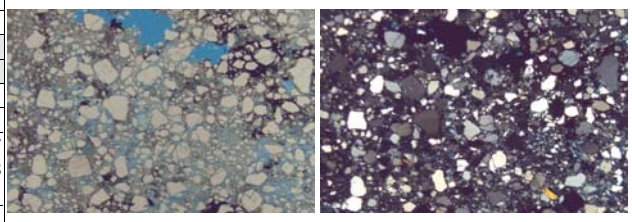

2.5x Field of View ~ 5 mm
Quartz sandstone with abundant interstitial clays & quartz

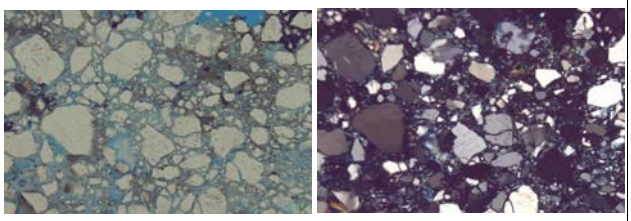

5x Field of View ~2.5 mm
Quartz sandstone with abundant interstitial clays & quartz

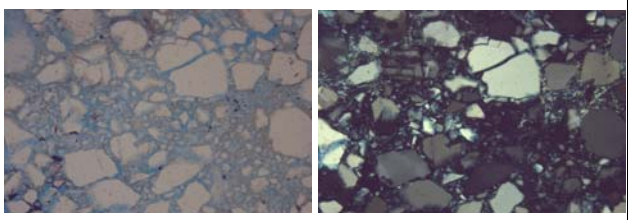

5x Field of View ~2.5 mm
Quartz grains look fractured

Back to Index

Thin Section Analysis Report

Sample ID: MOBIL 544-1-7096
Sample Condition: several small fragments
Formation Name: Dawson Canyon
Depth (ft): 7096
Lithology: sandstone

Date of Analysis: 3/20/2018
Analyzed by: S. Shank
Point Count Step Size 0.8 mm
Number of Counts 432

Texture - Qualitative Assessment

Approximate Average Grain Size (mm): 0.15
Grain Sorting: poor
Grain Rounding: angular to subrounded

Composition - Modal Analysis Data

Framework

Mineral Grains	Total	Percent
Quartz		**50.7**
Monocrystalline	212	49.1
Polycrystalline	7	1.6
Chert		
Feldspar		**4.4**
Plagioclase		
Microcline		
K-Feldspar	19	4.4
Carbonate		**0.0**
Calcite		
Dolomite		

Lithic Grains	Total	Percent
		0.0
Metamorphic		
Sedimentary		
Volcanic		

Accessory Minerals	Total	Percent
		10.6
Garnet		
Tourmaline	2	0.5
Zircon	1	0.2
Opaques	43	10.0

Matrix Spaces

Cement	Total	Percent
		2.5
Quartz	11	2.5
K-Feldspar		
Calcite		
Dolomite/Ankerite		
Iron Oxide		0.0

Matrix	Total	Percent
Clay Minerals		**15.5**
Clay Minerals (not individually identifiable)	28	6.5
Muscovite	2	0.5
Kaolinite	37	8.6
Chlorite		
Glauconite		
Illite		

Porosity	Total	Percent
		16.2
Intergranular	46	10.6
Intragranular		
Intercrystalline	22	5.1
Moldic	2	0.5
Grain/Cement Dissolution		
Clay/Mica Framework		
Organic Matter		
Vug		
Channel		
Fracture		
	Total	**100.0**

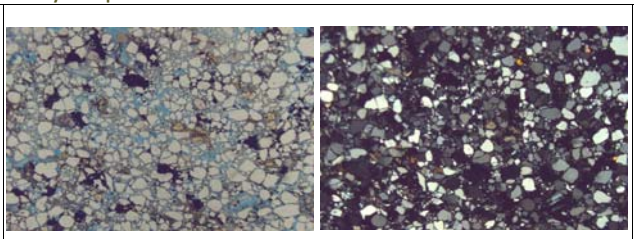

2.5 x Field of View ~5 mm
Quartz sandstone with abundant opaques, interstitial clays & quartz

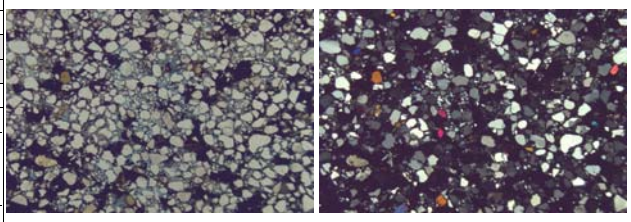

2.5x Field of View ~ 5 mm
Relatively common tourmaline, zircon, trace garnet

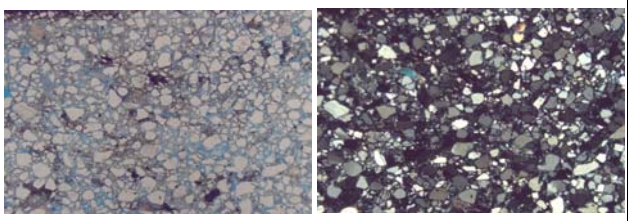

2.5x Field of View ~ 5 mm
Variable mineralogy - minor opaques

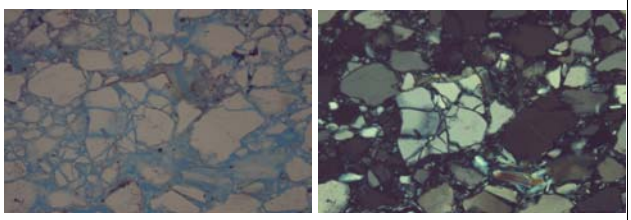

10x Field of View ~1 mm
Quartz grains look extensivelyfractured

Back to Index

Thin Section Analysis Report

Sample ID: MOBIL 544-1-7258
Sample Condition: 20 mm round
Formation Name: Dawson Canyon
Depth (ft): 7096
Lithology: sandstone

Date of Analysis: 3/20/2018
Analyzed by: S. Shank
Point Count Step Size 0.8 mm
Number of Counts 348

Texture - Qualitative Assessment

Approximate Average Grain Size (mm): 0.15
Grain Sorting: poor
Grain Rounding: angular to subrounded

Composition - Modal Analysis Data

Framework

Mineral Grains	Total	Percent
Quartz		**63.5**
Monocrystalline	216	62.1
Polycrystalline	5	1.4
Chert		
Feldspar		**3.2**
Plagioclase	3	0.9
Microcline	1	0.3
K-Feldspar	7	2.0
Carbonate		**0.0**
Calcite		
Dolomite		

Lithic Grains	Total	Percent
		0.0
Metamorphic		
Sedimentary		
Volcanic		

Accessory Minerals	Total	Percent
		0.6
Garnet		
Tourmaline		
Zircon		
Opaques	2	0.6

Matrix Spaces

Cement	Total	Percent
		0.0
Quartz		
K-Feldspar		
Calcite		
Dolomite/Ankerite		
Iron Oxide		

Matrix	Total	Percent
Clay Minerals		**14.9**
Clay Minerals (not individually identifiable)	52	14.9
Muscovite		
Kaolinite		
Chlorite		
Glauconite		
Illite		

Porosity	Total	Percent
		17.8
Intergranular	61	17.5
Intragranular		
Intercrystalline		
Moldic	1	0.3
Grain/Cement Dissolution		
Clay/Mica Framework		
Organic Matter		
Vug		
Channel		
Fracture		
	Total	**100.0**

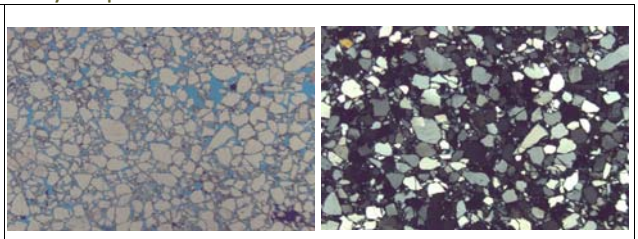

2.5 x Field of View ~5 mm
Quartz sandstone with abundant intergranular porosity

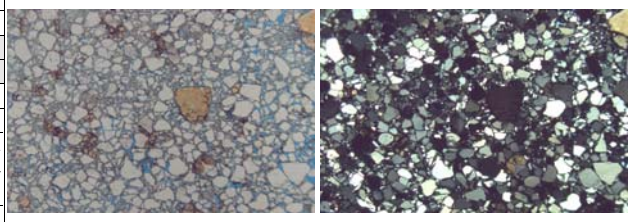

2.5x Field of View ~ 5 mm
Relatively fresh feldspars

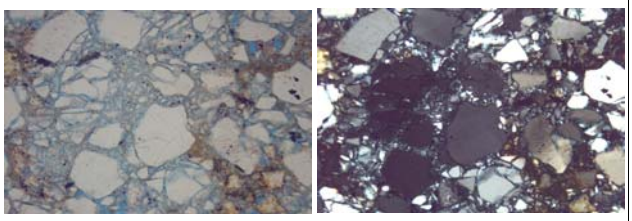

10x Field of View ~1 mm
Quartz appears to be locally crushed

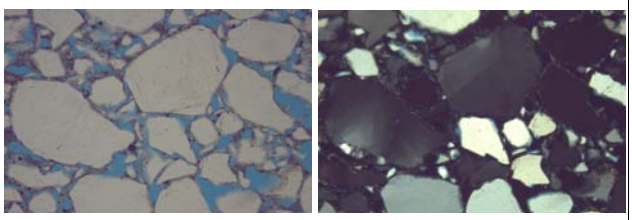

10x Field of View ~1 mm
cryptocrystalline material rims quartz grains

Back to Index

Thin Section Analysis Report

Sample ID: MOBIL 544-1-8497
Sample Condition: two fragments
Formation Name: Mississauga
Depth (ft): 8497
Lithology: porphyritic andesite

Date of Analysis: 3/20/2018
Analyzed by: S. Shank
Point Count Step Size
Number of Counts 0

Texture - Qualitative Assessment

Approximate Average Grain Size (mm):
Grain Sorting:
Grain Rounding:

Composition - Modal Analysis Data

Framework

Mineral Grains	Total	Percent
Quartz		0.0
Monocrystalline		
Polycrystalline		
Chert		
Feldspar		0.0
Plagioclase		
Microcline		
K-Feldspar		
Carbonate		0.0
Calcite		
Dolomite		

Lithic Grains	Total	Percent
		0.0
Metamorphic		
Sedimentary		
Volcanic		

Accessory Minerals	Total	Percent
		0.0
Garnet		
Tourmaline		
Zircon		
Opaques		

Matrix Spaces

Cement	Total	Percent
		0.0
Quartz		
K-Feldspar		
Calcite		
Dolomite/Ankerite		
Iron Oxide		

Matrix	Total	Percent
Clay Minerals		0.0
Clay Minerals (not individually identifiable)		
Muscovite		
Kaolinite		
Chlorite		
Glauconite		
Illite		

Porosity	Total	Percent
		0.0
Intergranular		
Intragranular		
Intercrystalline		
Moldic		
Grain/Cement Dissolution		
Clay/Mica Framework		
Organic Matter		
Vug		
Channel		
Fracture		
	Total	**0.0**

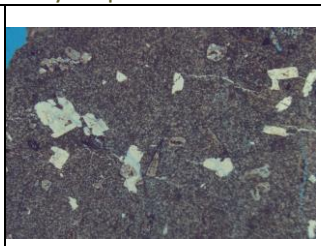
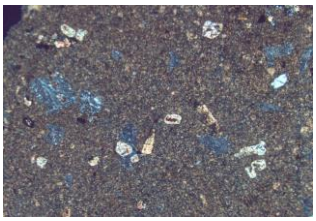

2.5x Field of View ~5 mm
Original mineralogy altered to extremely fine-grained clays and carbonate
Distinctive texture retained

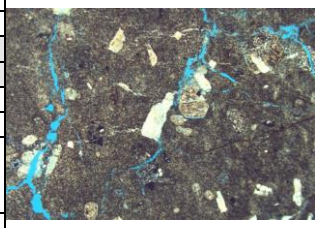

2.5x Field of View ~ 5 mm
Abundant fractures

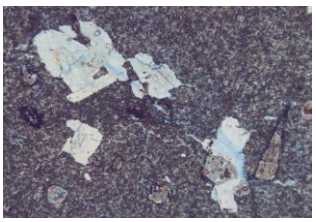
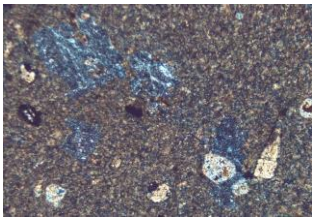

5x Field of View ~3 mm
Distinctive porphyrtic texture
Relict plagioclase and hornblende phenocrysts

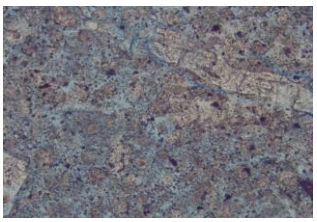

20x Field of View ~0.5 mm
Extensive microporosity

Back to Index

Thin Section Analysis Report

Sample ID: MOBIL 544-1-9039
Sample Condition: several small fragments
Formation Name: Mississauga
Depth (ft): 9039
Lithology: sandstone

Date of Analysis: 3/20/2018
Analyzed by: S. Shank
Point Count Step Size 0.8 mm
Number of Counts 244

Texture - Qualitative Assessment

Approximate Average Grain Size (mm): 0.15
Grain Sorting: poor
Grain Rounding: angular to subrounded

Composition - Modal Analysis Data

Framework

Mineral Grains	Total	Percent
Quartz		**35.2**
Monocrystalline	77	31.6
Polycrystalline	9	3.7
Chert		
Feldspar		**9.8**
Plagioclase	24	9.8
Microcline		
K-Feldspar		
Carbonate		**0.0**
Calcite		
Dolomite		

Lithic Grains	Total	Percent
		0.0
Metamorphic		
Sedimentary		
Volcanic		

Accessory Minerals	Total	Percent
		1.2
Garnet		
Tourmaline		
Zircon		
Opaques	3	1.2

Matrix Spaces

Cement	Total	Percent
		0.8
Quartz		
K-Feldspar		
Calcite		
Dolomite/Ankerite		
Iron Oxide	2	0.8

Matrix	Total	Percent
Clay Minerals		**35.7**
Clay Minerals (not individually identifiable)	50	20.5
Muscovite	4	1.6
Kaolinite	33	13.5
Chlorite		
Glauconite		
Illite		

Porosity	Total	Percent
		17.2
Intergranular	22	9.0
Intragranular		
Intercrystalline	1	0.4
Moldic	19	7.8
Grain/Cement Dissolution		
Clay/Mica Framework		
Organic Matter		
Vug		
Channel		
Fracture		
	Total	**100.0**

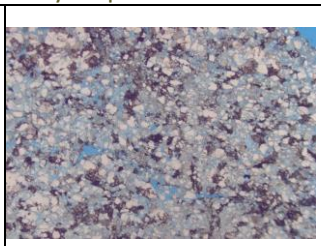
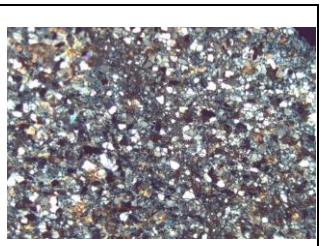

2.5 x Field of View ~5 mm
Sandstone with abundant intergranular porosity and intergranular clays
Thin section appears to somewhat thin (<30 microns)

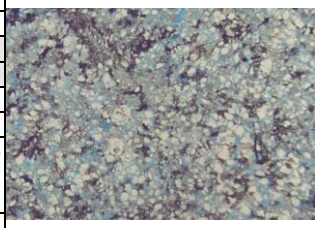
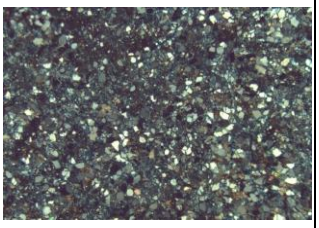

2.5x Field of View ~ 5 mm

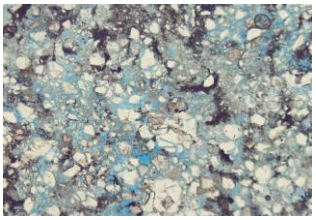
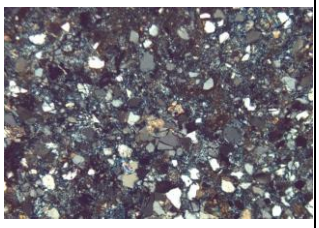

5x Field of View ~3 mm
Quartz appears to be locally fractured

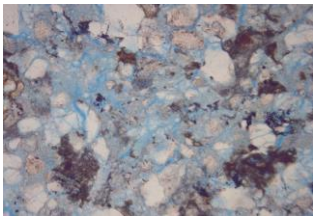
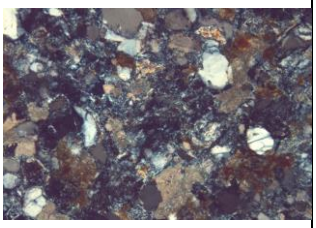

10x Field of View ~1 mm
Relatively common plagioclase, common dissolution

Back to Index

Thin Section Analysis Report

Sample ID: EXXON 684-1
Sample Condition: chip size 20x18 mm
Formation Name: Naskapi
Depth (ft): 9,438 ft
Lithology: Sandstone

Date of Analysis: 2/15/2018
Analyzed by: S. Shank
Point Count Step Size 1.0 mm
Number of Counts 493


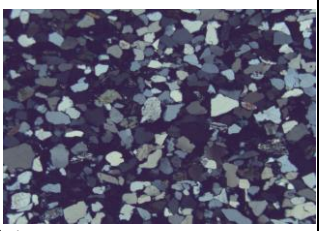

2.5 x Field of View ~ 5 mm

Abundant intergranular porosity

Texture - Qualitative Assessment

Approximate Average Grain Size (mm): 0.2
Grain Sorting: moderate
Grain Rounding: rounded to angular

Composition - Modal Analysis Data

Framework

Mineral Grains	Total	Percent
Quartz		**69.6**
Monocrystalline	331	67.1
Polycrystalline	12	2.4
Chert		
Feldspar		**5.1**
Plagioclase	4	0.8
Microcline	2	0.4
K-Feldspar	19	3.9
Carbonate		**0.0**
Calcite		
Dolomite		

Lithic Grains	Total	Percent
		0.0
Metamorphic		
Sedimentary		
Volcanic		

Accessory Minerals	Total	Percent
		0.0
Rutile		
Tourmaline		
Zircon		
Opaques		

Matrix Spaces

Cement	Total	Percent
		0.0
Quartz		
K-Feldspar		
Calcite		
Dolomite/Ankerite		
Iron Oxide		

Matrix	Total	Percent
Clay Minerals		**9.9**
Clay Minerals (not individually identifiable)	27	5.5
Kaolinite	22	4.5
Muscovite		
Biotite		
Chlorite		
Glauconite		

dark cryptocrystalline material

Porosity	Total	Percent
		15.4
Intergranular	59	12.0
Intragranular		
Intercrystalline	4	0.8
Moldic	4	0.8
Grain/Cement Dissolution	9	1.8
Clay/Mica Framework		
Organic Matter		
Vug		
Channel		
Fracture		
	Total	**100.0**


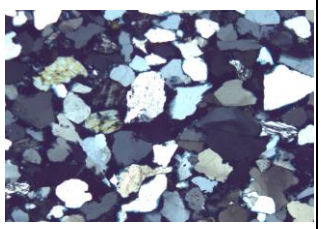

5x Field of View ~3 mm

Intergranular porosity with some interstitial white patches of kaolinite.
Some dissolution of K-feldspar visible.
Some intercrystalline microporosity between kaolinite.
Quartz grains often rimmed by cryptocrystalline brown material.

Back to Index

Thin Section Analysis Report

Sample ID: EXXON 684-1
Sample Condition: chip size 24x20 mm
Formation Name: Naskapi
Depth (ft): 9439 ft
Lithology: Sandstone

Date of Analysis: 2/20/2018
Analyzed by: S. Shank
Point Count Step Size 1.0 mm
Number of Counts 421

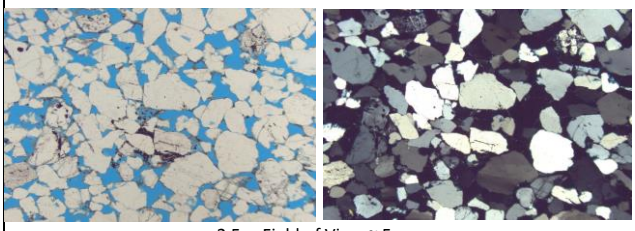

2.5 x Field of View ~ 5 mm

Abundant intergranular porosity

Texture - Qualitative Assessment

Approximate Average Grain Size (mm): 0.5
Grain Sorting: moderate
Grain Rounding: subrounded to angular

Composition - Modal Analysis Data

Framework

Mineral Grains	Total	Percent
Quartz		**66.7**
Monocrystalline	262	62.2
Polycrystalline	19	4.5
Chert		
Feldspar		**4.3**
Plagioclase	1	0.2
Microcline	4	1.0
K-Feldspar	13	3.1
Carbonate		**0.0**
Calcite		
Dolomite		

Lithic Grains	Total	Percent
		0.0
Metamorphic		
Sedimentary		
Volcanic		

Accessory Minerals	Total	Percent
		1.2
Rutile		
Tourmaline	1	0.2
Zircon		
Opaques	4	1.0

Matrix Spaces

Cement	Total	Percent
		0.7
Quartz	3	0.7
K-Feldspar		
Calcite		
Dolomite/Ankerite		
Iron Oxide		

Matrix	Total	Percent	
Clay Minerals		**5.5**	
Clay Minerals (not individually identifiable)	22	5.2	dark cryptocrystalline material
Kaolinite			
Muscovite	1	0.2	
Biotite			
Chlorite			
Glauconite			

Porosity	Total	Percent
		21.6
Intergranular	85	20.2
Intragranular		
Intercrystalline		
Moldic	3	0.7
Grain/Cement Dissolution	3	0.7
Clay/Mica Framework		
Organic Matter		
Vug		
Channel		
Fracture		
Total	**100.0**	

Back to Index

EXXON 684-1 9440 ft

Thin Section Analysis Report

Sample ID: EXXON 684-1
Sample Condition: chip 32x20 mm
Formation Name: Naskapi
Depth (ft): 9440 ft
Lithology: sandstone

Date of Analysis: 2/20/2018
Analyzed by: S. Shank
Point Count Step Size 1.0 mm
Number of Counts 410

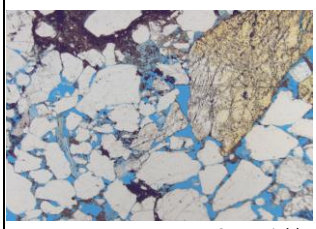
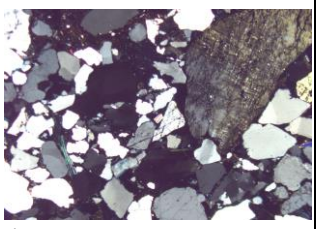

2.5 x Field of View ~ 5 mm
Interganular porosity, relatively fresh feldspar
Some intergranular dark material, trace kaolinite

Texture - Qualitative Assessment

Approximate Average Grain Size (mm): 0.75
Grain Sorting: poor
Grain Rounding: angular to subrounded

Composition - Modal Analysis Data

Framework

Mineral Grains	Total	Percent
Quartz		**64.4**
Monocrystalline	235	57.3
Polycrystalline	29	7.1
Chert		
Feldspar		**8.0**
Plagioclase	2	0.5
Microcline	15	3.7
K-Feldspar	16	3.9
Carbonate		**0.0**
Calcite		
Shell/fossil		

Lithic Grains	Total	Percent
		0.0
Metamorphic		
Sedimentary		
Volcanic		

Accessory Minerals	Total	Percent
		2.4
Rutile		
Tourmaline		
Zircon		
Opaques	10	2.4

Matrix Spaces

Cement	Total	Percent
		0.0
Quartz		
K-Feldspar		
Calcite		
Dolomite/Ankerite		
Iron Oxide		

Matrix	Total	Percent
Clay Minerals		**5.9**
Clay Minerals (not individually identifiable)	21	5.1
Kaolinite	3	0.7
Muscovite		
Biotite		
Chlorite		
Glauconite		

Porosity	Total	Percent
		19.3
Intergranular	72	17.6
Intragranular		
Intercrystalline		
Moldic	3	0.7
Grain/Cement Dissolution	4	1.0
Clay/Mica Framework		
Organic Matter		
Vug		
Channel		
Fracture		
Total		100.0

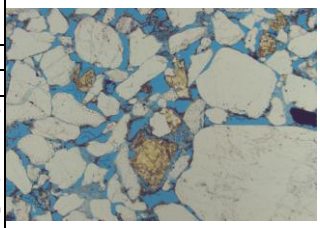
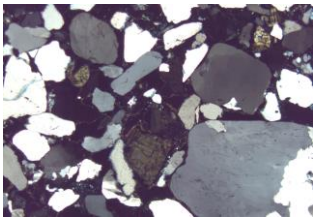

2.5 x Field of View ~ 5 mm

Back to Index

Thin Section Analysis Report

Sample ID: EXXON 684-1
Sample Condition: round 25 mm
Formation Name: Naskapi
Depth (ft): 9441 ft
Lithology: Sandstone

Date of Analysis: 2/22/2018
Analyzed by: S. Shank
Point Count Step Size 1.0 mm
Number of Counts 460

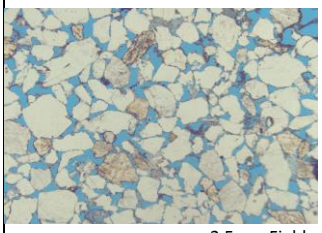
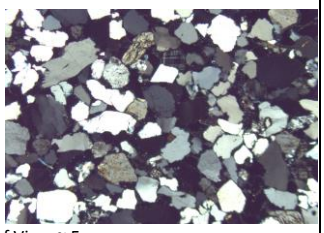

2.5 x Field of View ~ 5 mm
Extensive intergranular porosity with minimal cement or matrix

Texture - Qualitative Assessment

Approximate Average Grain Size (mm): 0.5
Grain Sorting: well
Grain Rounding: angular to subrounded

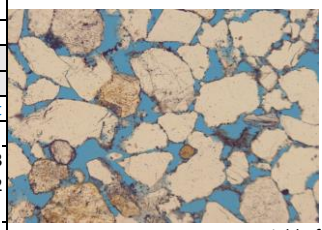
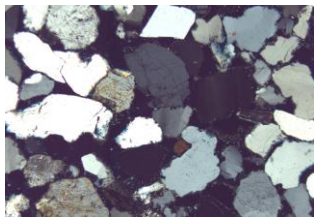

5 x Field of View ~3 mm
Extensive intergranular porosity with minimal cement or matrix

Composition - Modal Analysis Data

Framework

Mineral Grains	Total	Percent
Quartz		**70.4**
Monocrystalline	314	68.3
Polycrystalline	10	2.2
Chert		
Feldspar		**5.2**
Plagioclase	2	0.4
Microcline	4	0.9
K-Feldspar	18	3.9
Carbonate		**0.0**
Calcite		
Shell/fossil		

Lithic Grains	Total	Percent
		0.0
Metamorphic		
Sedimentary		
Volcanic		

Accessory Minerals	Total	Percent
		0.2
Rutile		
Tourmaline		
Zircon		
Opaques	1	0.2

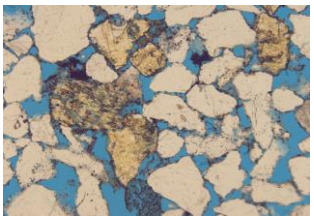

5x Field of View ~3 mm
Feldspar dissolution

Matrix Spaces

Cement	Total	Percent
		0.0
Quartz		
K-Feldspar		
Calcite		
Dolomite/Ankerite		
Iron Oxide		

Matrix	Total	Percent
Clay Minerals		**3.7**
Clay Minerals (not individually identifiable)	17	3.7
Kaolinite		
Muscovite		
Biotite		
Chlorite		
Glauconite		

dark cryptocrystalline material

Porosity	Total	Percent
		20.4
Intergranular	87	18.9
Intragranular		
Intercrystalline		
Moldic	2	0.4
Grain/Cement Dissolution	5	1.1
Clay/Mica Framework		
Organic Matter		
Vug		
Channel		
Fracture		
	Total	100.0

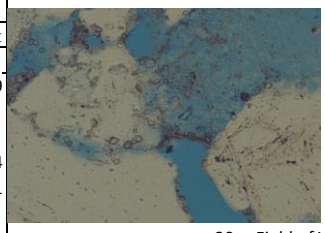
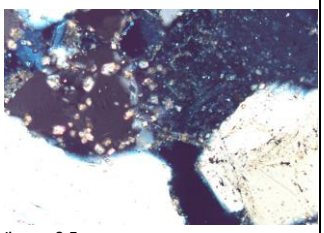

20x Field of View ~0.5 mm
Small calcite rhombs along grain margins
Trace clays and kaolinite in intergranular pores

Back to Index

Thin Section Analysis Report

Sample ID: EXXON 684-1
Sample Condition: chip 25x10 mm
Formation Name: Mic-Mac
Depth (ft): 12,137 ft
Lithology: Siltstone

Date of Analysis: 2/22/2018
Analyzed by: S. Shank
Point Count Step Size 0.4 mm
Number of Counts 404

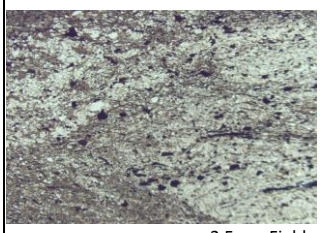
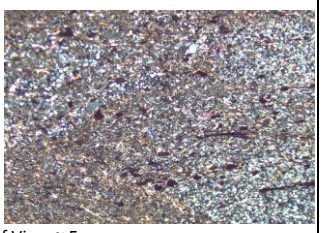

2.5 x Field of View ~ 5 mm
Patchy distribution of quartz, and light and darker clays

Texture - Qualitative Assessment

Approximate Average Grain Size (mm): <0.015 mm
Grain Sorting:
Grain Rounding: angular to subrounded

Composition - Modal Analysis Data

Framework

Mineral Grains	Total	Percent
Quartz		**18.3**
Monocrystalline	74	18.3
Polycrystalline		
Chert		
Feldspar		**0.2**
Plagioclase	1	0.2
Microcline		
K-Feldspar		
Carbonate		**0.0**
Calcite		
Shell/fossil		

Lithic Grains	Total	Percent
		0.0
Metamorphic		
Sedimentary		
Volcanic		

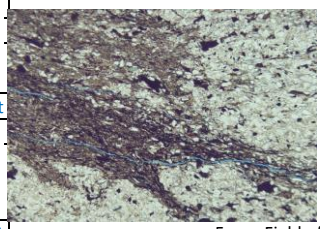
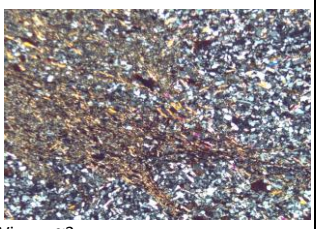

5 x Field of View ~3 mm
Thin discontinuous fractures

Accessory Minerals	Total	Percent
		1.2
Rutile		
Tourmaline		
Zircon		
Opaques	5	1.2

Matrix Spaces

Cement	Total	Percent
		0.0
Quartz		
K-Feldspar		
Calcite		
Dolomite/Ankerite		
Iron Oxide		

Matrix	Total	Percent
Clay Minerals		**79.7**
Clay Minerals (not individually identifiable)	318	78.7
Kaolinite		
Muscovite	4	1.0
Biotite		
Chlorite		
Glauconite		

dark cryptocrystalline material

Porosity	Total	Percent
		0.5
Intergranular		
Intragranular		
Intercrystalline		
Moldic		
Grain/Cement Dissolution		
Clay/Mica Framework		
Organic Matter		
Vug		
Channel		
Fracture	2	0.5
	Total	100.0

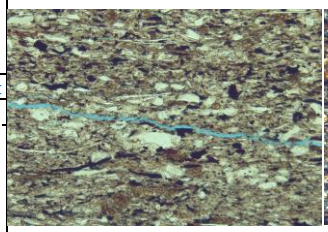
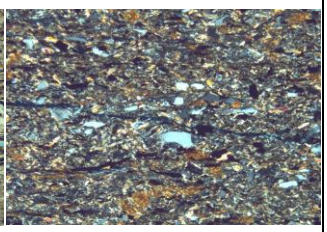

20x Field of View ~0.5 mm
Close up of fracture and matrix

Back to Index

Thin Section Analysis Report

Sample ID: EXXON 684-1
Sample Condition: chip 35x20 mm
Formation Name: Mic-Mac
Depth (ft): 12,199 ft
Lithology: Sandstone

Date of Analysis: 2/22/2018
Analyzed by: S. Shank
Point Count Step Size 1 mm
Number of Counts 423

Texture - Qualitative Assessment

Approximate Average Grain Size (mm): 0.4
Grain Sorting: moderate
Grain Rounding: angular to subrounded

Composition - Modal Analysis Data

Framework

Mineral Grains	Total	Percent
Quartz		**56.0**
Monocrystalline	228	53.9
Polycrystalline	9	2.1
Chert		
Feldspar		**6.9**
Plagioclase	1	0.2
Microcline	2	0.5
K-Feldspar	26	6.1
Carbonate		**0.0**
Calcite		
Shell/fossil		

Lithic Grains	Total	Percent
		0.0
Metamorphic		
Sedimentary		
Volcanic		

Accessory Minerals	Total	Percent
		0.9
Rutile		
Tourmaline		
Zircon		
Opaques	4	0.9

Matrix Spaces

Cement	Total	Percent
		4.0
Quartz	17	4.0
K-Feldspar		
Calcite		
Dolomite/Ankerite		
Iron Oxide		

Matrix	Total	Percent
Clay Minerals		**26.5**
Clay Minerals (not individually identifiable)	22	5.2
Kaolinite	78	18.4
Muscovite	12	2.8
Biotite		
Chlorite		
Glauconite		

Porosity	Total	Percent
		5.7
Intergranular	9	2.1
Intragranular		
Intercrystalline	15	3.5
Moldic		
Grain/Cement Dissolution		
Clay/Mica Framework		
Organic Matter		
Vug		
Channel		
Fracture		0.0
	Total	100.0

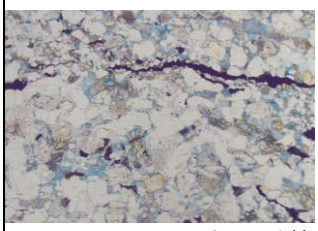
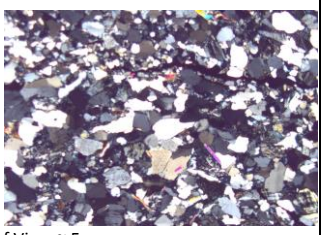

2.5 x Field of View ~ 5 mm
Overgrowths in quartz and abundant kaolinite in pores

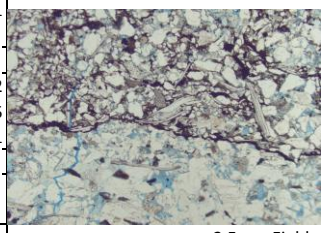
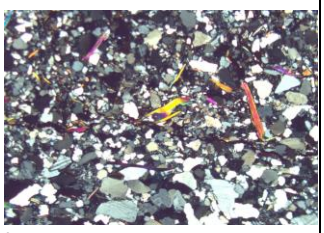

2.5 x Field of View ~ 5 mm
Compositional variation

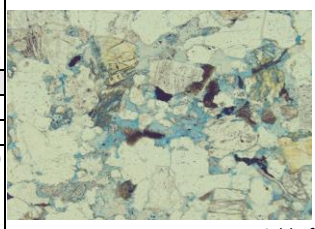
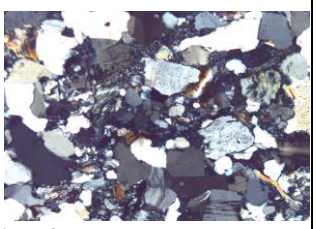

5x Field of View ~3 mm
overgrowths on quartz grains
dissolution of feldspars
dark cryptocrystalline material

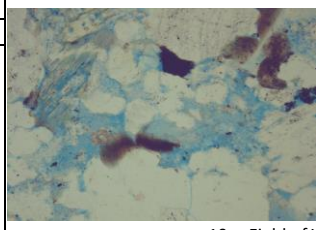
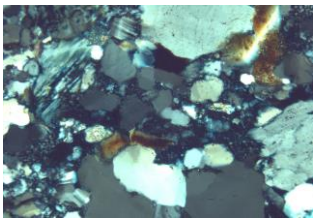

10x Field of View ~1.25 mm
overgrowths on quartz grains
dissolution of feldspars

Back to Index

Thin Section Analysis Report

Sample ID: EXXON-684-1
Sample Condition: chip 20x18 mm, broken
Formation Name: Mic-Mac
Depth (ft): 12,204 ft
Lithology: Siltstone

Date of Analysis: 2/25/2018
Analyzed by: S. Shank
Point Count Step Size 1 mm
Number of Counts 393

Texture - Qualitative Assessment

Approximate Average Grain Size (mm): 0.03
Grain Sorting: poor
Grain Rounding: subangular to angular

Composition - Modal Analysis Data

Framework

Mineral Grains	Total	Percent
Quartz		**15.5**
Monocrystalline	61	15.5
Polycrystalline		
Chert		
Feldspar		**8.9**
Plagioclase	35	8.9
Microcline		
K-Feldspar		
Carbonate		**0.0**
Calcite		
Shell/fossil		

Lithic Grains	Total	Percent
		0.0
Metamorphic		
Sedimentary		
Volcanic		

Accessory Minerals	Total	Percent
		9.2
Rutile		
Tourmaline		
Zircon		
Opaques	36	9.2

Matrix Spaces

Cement	Total	Percent
		0.0
Quartz		
K-Feldspar		
Calcite		
Dolomite/Ankerite		
Iron Oxide		

Matrix	Total	Percent
Clay Minerals		**66.2**
Clay Minerals (not individually identifiable)	250	63.6
Kaolinite		
Muscovite	8	2.0
Biotite		
Chlorite	2	0.5
Glauconite		

Porosity	Total	Percent
		0.3
Intergranular		
Intragranular		
Intercrystalline		
Moldic		
Grain/Cement Dissolution		
Clay/Mica Framework		
Organic Matter		
Vug		
Channel		
Fracture	1	0.3
	Total	100.0

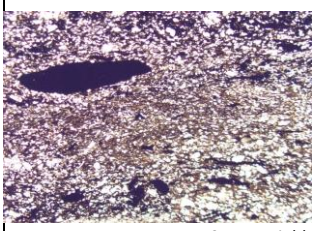
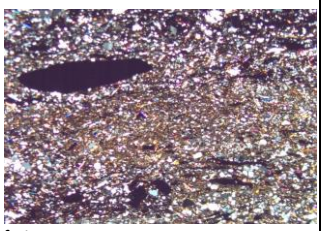

2.5 x Field of View ~ 5 mm

Abundant opaques

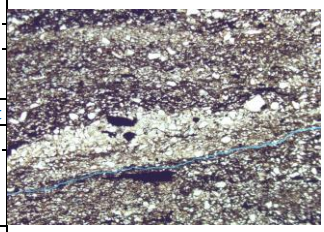
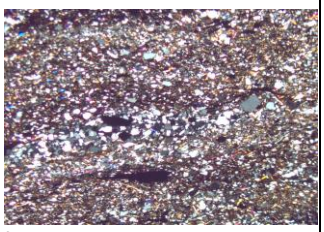

2.5 x Field of View ~ 5 mm

Thin, discontinuous fracture

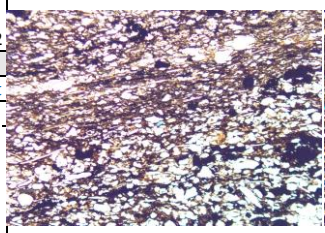
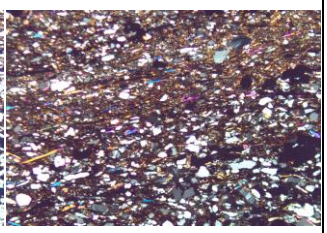

5x Field of View ~3 mm

dark cryptocrystalline material

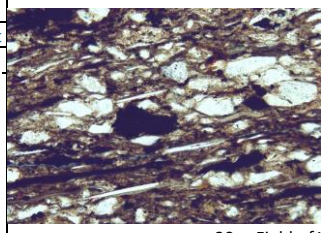
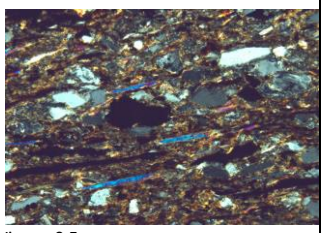

20x Field of View ~0.5 mm

Quartz, feldspar grains in dark matrix

Close up of thin, discontinuous fracture

Back to Index

Thin Section Analysis Report

Sample ID: EXXON 684-1
Sample Condition: chip 22x18 mm
Formation Name: Mohawk
Depth (ft): 12,729 ft
Lithology: feldspathic sandstone

Date of Analysis: 2/25/2018
Analyzed by: S. Shank
Point Count Step Size 1 mm
Number of Counts 462

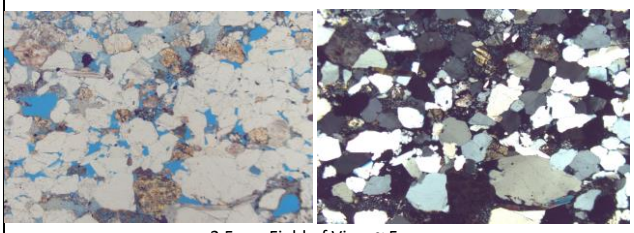

2.5 x Field of View ~ 5 mm

Moderate porosity, common feldspars

Texture - Qualitative Assessment

Approximate Average Grain Size (mm): 0.75
Grain Sorting: well to moderate
Grain Rounding: subrounded to subangular

Composition - Modal Analysis Data

Framework

Mineral Grains	Total	Percent
Quartz		**59.1**
Monocrystalline	254	55.0
Polycrystalline	19	4.1
Chert		
Feldspar		**14.3**
Plagioclase	35	7.6
Microcline	8	1.7
K-Feldspar	23	5.0
Carbonate		**0.0**
Calcite		
Shell/fossil		

Lithic Grains	Total	Percent
		0.0
Metamorphic		
Sedimentary		
Volcanic		

Accessory Minerals	Total	Percent
		0.2
Rutile		
Tourmaline		
Zircon		
Opaques	1	0.2

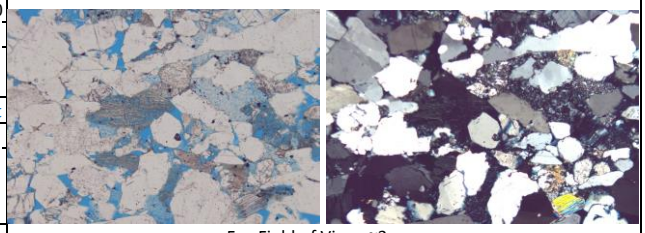

5x Field of View ~3 mm

Feldspar dissolution, kaolinite in pore spaces

Prismatic quartz in center

Matrix Spaces

Cement	Total	Percent
		7.1
Quartz	32	6.9
K-Feldspar		
Calcite		
Dolomite/Ankerite		
Iron Oxide	1	0.2

Matrix	Total	Percent
Clay Minerals		**9.7**
Clay Minerals (not individually identifiable)	5	1.1
Kaolinite	34	7.4
Muscovite	6	1.3
Biotite		
Chlorite		
Glauconite		

Porosity	Total	Percent
		9.5
Intergranular	32	6.9
Intragranular		
Intercrystalline	8	1.7
Moldic	4	0.9
Grain/Cement Dissolution		
Clay/Mica Framework		
Organic Matter		
Vug		
Channel		
Fracture		

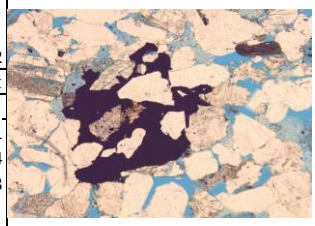

5x Field of View ~3 mm

opaque cement

Total 100.0

Back to Index

Thin Section Analysis Report

Sample ID: EXXON 684-1
Sample Condition: chip 35x13 mm
Formation Name: Mohawk
Depth (ft): 12,279 ft
Lithology: sandstone

Date of Analysis: 2/27/2018
Analyzed by: S. Shank
Point Count Step Size 1 mm
Number of Counts 442

Texture - Qualitative Assessment

Approximate Average Grain Size (mm): 0.5
Grain Sorting: well to moderate
Grain Rounding: subrounded to subangular

Composition - Modal Analysis Data

Framework

Mineral Grains	Total	Percent
Quartz		**67.0**
Monocrystalline	287	64.9
Polycrystalline	9	2.0
Chert		
Feldspar		**7.7**
Plagioclase	13	2.9
Microcline	6	1.4
K-Feldspar	15	3.4
Carbonate		**0.0**
Calcite		
Shell/fossil		

Lithic Grains	Total	Percent
		0.0
Metamorphic		
Sedimentary		
Volcanic		

Accessory Minerals	Total	Percent
		0.5
Rutile		
Tourmaline		
Zircon		
Opaques	2	0.5

Matrix Spaces

Cement	Total	Percent
		7.7
Quartz	30	6.8
K-Feldspar		
Calcite	3	0.7
Dolomite/Ankerite		
Iron Oxide	1	0.2

Matrix	Total	Percent
Clay Minerals		**7.2**
Clay Minerals (not individually identifiable)	6	1.4
Kaolinite	26	5.9
Muscovite		
Biotite		
Chlorite		
Glauconite		

Porosity	Total	Percent
		10.0
Intergranular	35	7.9
Intragranular		
Intercrystalline	4	0.9
Moldic	5	1.1
Grain/Cement Dissolution		
Clay/Mica Framework		
Organic Matter		
Vug		
Channel		
Fracture		
	Total	100.0

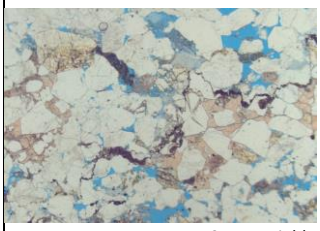
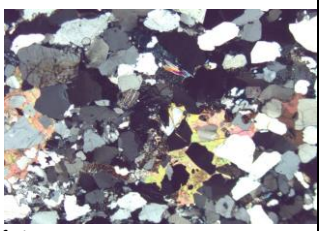

2.5 x Field of View ~ 5 mm
Moderate porosity, uncommon calcite cement
stylolite

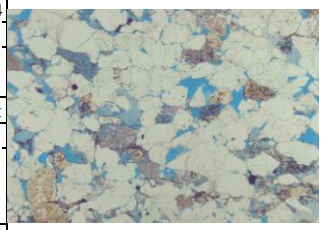
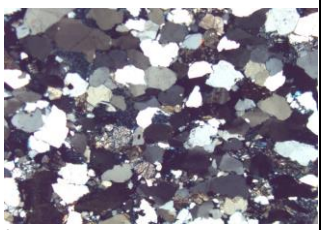

2.5 x Field of View ~ 5 mm
Moderate intergranular porosity
Feldspar dissolution, kaolinite in pores

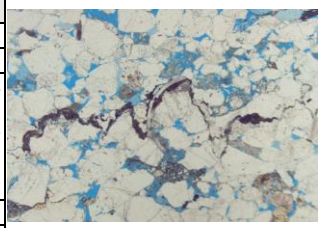
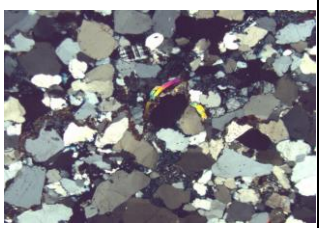

2.5 x Field of View ~ 5 mm
stylolite

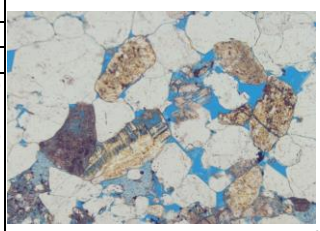
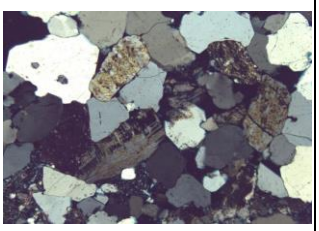

5 x Field of View ~3 mm
feldspar dissolution
kaolinite and dark clays in pores

Back to Index

Thin Section Analysis Report

Sample ID: EXXON 684-1
Sample Condition: chip 33x18 mm
Formation Name: Mohawk
Depth (ft): 12,802 ft
Lithology: sandstone

Date of Analysis: 2/27/2018
Analyzed by: S. Shank
Point Count Step Size 1 mm
Number of Counts 403

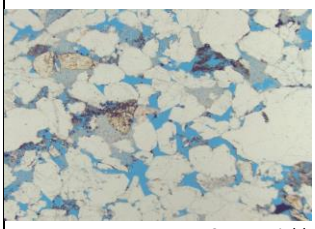
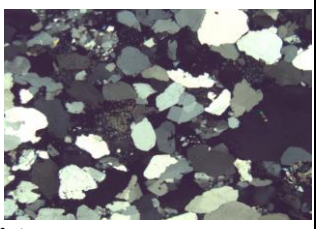

2.5 x Field of View ~ 5 mm
Moderate porosity, common kaolinite

Texture - Qualitative Assessment

Approximate Average Grain Size (mm): 0.5
Grain Sorting: well to moderate
Grain Rounding: subrounded to subangular

Composition - Modal Analysis Data

Framework

Mineral Grains	Total	Percent
Quartz		**68.0**
Monocrystalline	250	62.0
Polycrystalline	24	6.0
Chert		
Feldspar		**2.7**
Plagioclase	2	0.5
Microcline	2	0.5
K-Feldspar	7	1.7
Carbonate		**0.0**
Calcite		
Shell/fossil		

Lithic Grains	Total	Percent
		1.0
Metamorphic	3	0.7
Sedimentary	1	0.2
Volcanic		

Accessory Minerals	Total	Percent
		0.7
Rutile		
Tourmaline		
Zircon	1	0.2
Opaques	2	0.5

Matrix Spaces

Cement	Total	Percent
		2.7
Quartz	11	2.7
K-Feldspar		
Calcite		
Dolomite/Ankerite		
Iron Oxide		

Matrix	Total	Percent
Clay Minerals		**10.2**
Clay Minerals (not individually identifiable)	1	0.2
Kaolinite	40	9.9
Muscovite		
Biotite		
Chlorite		
Glauconite		

Porosity	Total	Percent
		14.6
Intergranular	54	13.4
Intragranular		
Intercrystalline	4	1.0
Moldic	1	0.2
Grain/Cement Dissolution		
Clay/Mica Framework		
Organic Matter		
Vug		
Channel		
Fracture		
Total		100.0

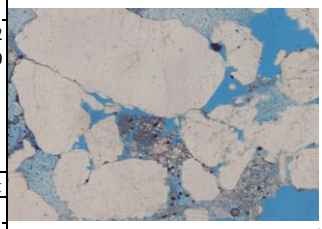
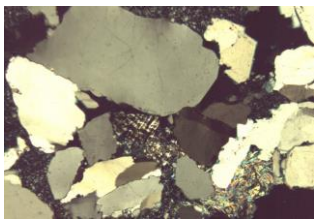

5 x Field of View ~3 mm
Feldspar dissolution, kaolinite in pores

Back to Index

Thin Section Analysis Report

Sample ID: EXXON 684-2
Sample Condition: chip 22x15 mm
Formation Name: Mohawk
Depth (ft): 15,242 ft
Lithology: calcareous sandstone

Date of Analysis: 2/28/2018
Analyzed by: S. Shank
Point Count Step Size 1 mm
Number of Counts 410

Texture - Qualitative Assessment

Approximate Average Grain Size (mm): 0.75
Grain Sorting: poor
Grain Rounding: rounded to angular

Composition - Modal Analysis Data

Framework

Mineral Grains	Total	Percent
Quartz		**59.8**
Monocrystalline	208	50.7
Polycrystalline	37	9.0
Chert		
Feldspar		**2.0**
Plagioclase	1	0.2
Microcline		
K-Feldspar	7	1.7
Carbonate		**0.0**
Calcite		
Shell/fossil		
Lithic Grains	**Total**	**Percent**
		4.6
Metamorphic	1	0.2
Sedimentary	18	4.4
Volcanic		
Accessory Minerals	**Total**	**Percent**
		0.2
Rutile		
Tourmaline		
Zircon		
Opaques	1	0.2

Matrix Spaces

Cement	Total	Percent
		9.5
Quartz	18	4.4
K-Feldspar		
Calcite	21	5.1
Dolomite/Ankerite		
Iron Oxide		
Matrix	**Total**	**Percent**
Clay Minerals		**20.2**
Clay Minerals (not individually identifiable)	11	2.7
Kaolinite	67	16.3
Muscovite	5	1.2
Biotite		
Chlorite		
Glauconite		
Porosity	**Total**	**Percent**
		3.7
Intergranular	7	1.7
Intragranular		
Intercrystalline	7	1.7
Moldic	1	0.2
Grain/Cement Dissolution		
Clay/Mica Framework		
Organic Matter		
Vug		
Channel		
Fracture		
	Total	100.0

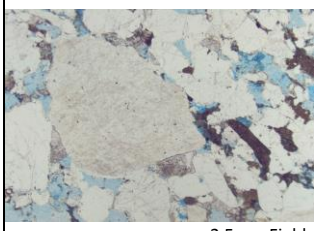
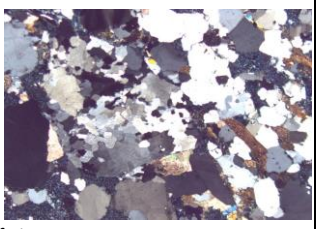

2.5 x Field of View ~ 5 mm
limited porosity, abundant kaolinite

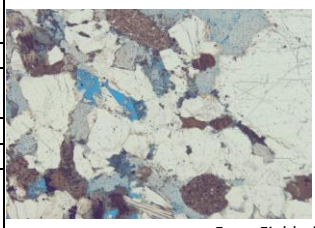
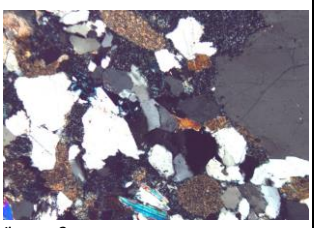

5 x Field of View ~3 mm
rounded brown shale clasts

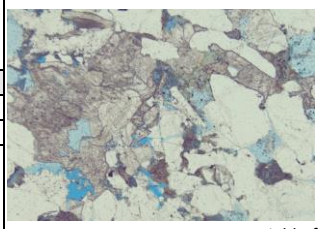
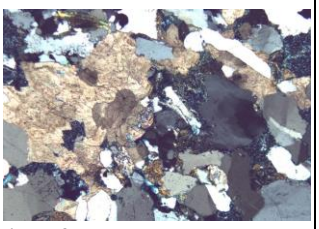

5 x Field of View ~3 mm
calcite cement

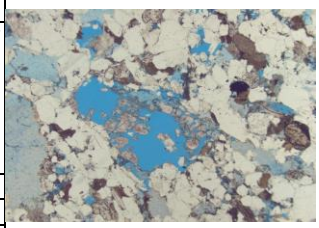
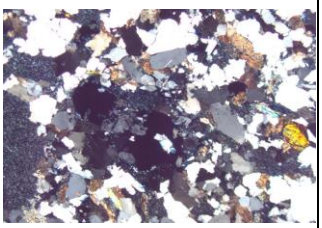

2.5 x Field of View ~ 5 mm
Feldspar dissolution, kaolinite in pores

Back to Index

CONOCO 145-1 9226 ft

Thin Section Analysis Report

Sample ID: CONOCO 145-1
Sample Condition:
Formation Name: Mohawk
Depth (ft): 9226 ft
Lithology: Calcareous sandstone

Date of Analysis: 3/7/2018
Analyzed by: S. Shank
Point Count Step Size 1.0 mm
Number of Counts 417

Texture - Qualitative Assessment

Approximate Average Grain Size (mm): 0.2
Grain Sorting: well
Grain Rounding: rounded to angular

Composition - Modal Analysis Data

Framework

Mineral Grains	Total	Percent
Quartz		**25.9**
Monocrystalline	82	19.7
Polycrystalline	26	6.2
Chert		
Feldspar		**8.4**
Plagioclase	22	5.3
Microcline		
K-Feldspar	13	3.1
Carbonate		**4.3**
Calcite	13	3.1
Shell/fossil	5	1.2

Lithic Grains	Total	Percent
		0.0
Metamorphic		
Sedimentary		
Volcanic		

Accessory Minerals	Total	Percent
		0.2
Rutile		
Tourmaline		
Zircon		
Opaques	1	0.2

Matrix Spaces

Cement	Total	Percent
		24.2
Quartz		
K-Feldspar		
Calcite	98	23.5
Dolomite/Ankerite		
Iron Oxide	3	0.7

Matrix	Total	Percent
Clay Minerals		**36.9**
Clay Minerals (not individually identifiable)	154	36.9
Kaolinite		
Muscovite		
Biotite		
Chlorite		
Glauconite		

Porosity	Total	Percent
		0.0
Intergranular		
Intragranular		
Intercrystalline		
Moldic		
Grain/Cement Dissolution		
Clay/Mica Framework		
Organic Matter		
Vug		
Channel		
Fracture		
	Total	100.0

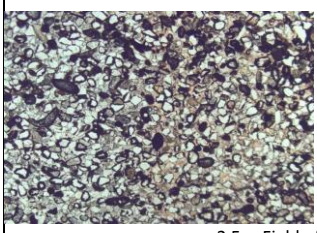
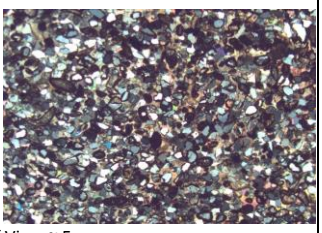

2.5 x Field of View ~ 5 mm
Grains often rimmed by cryptocrystalline brown material
Calcite cement

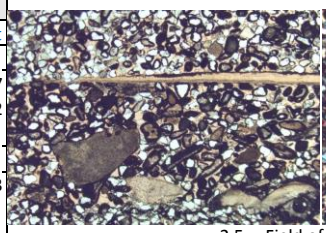
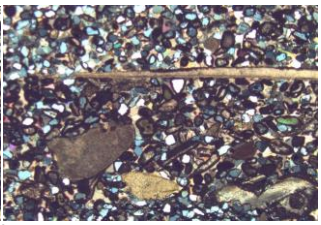

2.5 x Field of View ~ 5 mm
Abundant fossil material

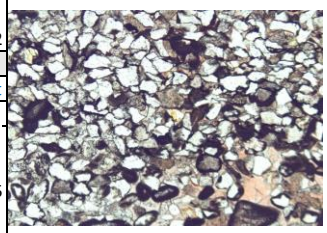
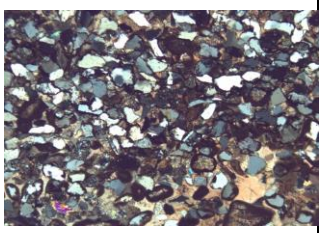

5x Field of View ~3 mm
fine and coarse calcite cement
dark cryptocrystalline material

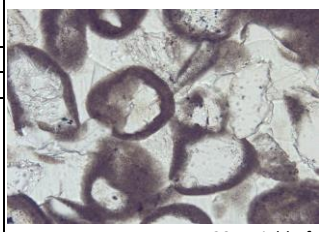
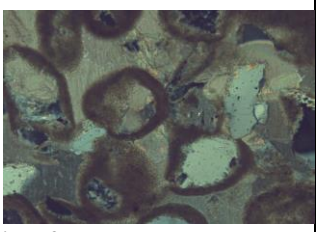

20x Field of View ~0.5 mm
Quartz and carbonate grains rimmed by cryptocrystalline material
Calcite cement

Back to Index

Thin Section Analysis Report

Sample ID: SHELL 273-1-7010
Sample Condition: 35x15mm
Formation Name: Dawson Canyon
Depth (ft): 7010
Lithology: clay-rich sandstone

Date of Analysis: 2/28/2018
Analyzed by: S. Shank
Point Count Step Size 1 mm
Number of Counts 406

Texture - Qualitative Assessment

Approximate Average Grain Size (mm): 0.1 (quartz grains)
Grain Sorting: moderate
Grain Rounding: angular

Composition - Modal Analysis Data

Framework

Mineral Grains	Total	Percent
Quartz		**31.0**
Monocrystalline	126	31.0
Polycrystalline		
Chert		
Feldspar		**7.4**
Plagioclase	20	4.9
Microcline		
K-Feldspar	10	2.5
Carbonate		**2.2**
Calcite	4	1.0
Fossil/shell	5	1.2
Lithic Grains	**Total**	**Percent**
		0.0
Metamorphic		
Sedimentary		
Volcanic		
Accessory Minerals	**Total**	**Percent**
		1.5
Garnet		
Tourmaline		
Zircon		
Opaques	6	1.5

Matrix Spaces

Cement	Total	Percent
		2.0
Quartz		
K-Feldspar		
Calcite	6	1.5
Dolomite/Ankerite		
Iron Oxide	2	0.5
Matrix	Total	Percent
Clay Minerals		**50.2**
Clay Minerals (not individually identifiable)	202	49.8
Muscovite	2	0.5
Kaolinite		
Chlorite		
Glauconite		
Illite		
Porosity	Total	Percent
		5.7
Intergranular		
Intragranular		
Intercrystalline		
Moldic		
Grain/Cement Dissolution		
Clay/Mica Framework	23	5.7
Organic Matter		
Vug		
Channel		
Fracture		
	Total	**100.0**

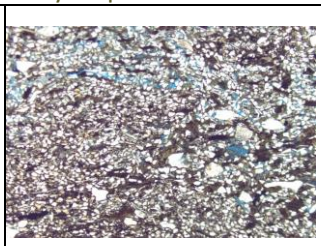

2.5 x Field of View ~5 mm
Thin discontinuous veins

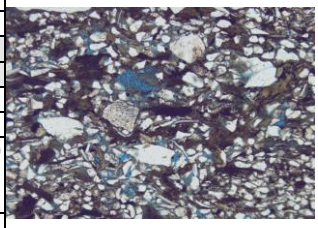

2.5 x Field of View ~5 mm
Minor porosity between clays and quartz grains, rare moldic

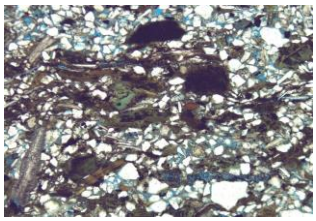

5x Field of View ~3 mm
Minor porosity between clays and quartz grains

Back to Index

Thin Section Analysis Report

Sample ID: SHELL 273-1-7077
Sample Condition: 25 mm round
Formation Name: Dawson Canyon
Depth (ft): 7077
Lithology: calcareous sandstone

Date of Analysis: 2/28/2018
Analyzed by: S. Shank
Point Count Step Size 1 mm
Number of Counts 404

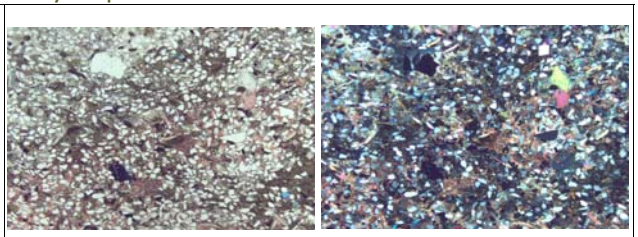

2.5 x Field of View ~5 mm
Quartz grains in calcite cement
Trace moldic porosity (plucked grains?)

Texture - Qualitative Assessment

Approximate Average Grain Size (mm): 0.1 (quartz grains)
Grain Sorting: moderate
Grain Rounding: angular to subrounded

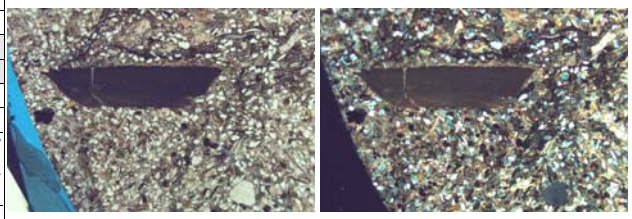

5x Field of View ~3 mm
Shell fragment

Composition - Modal Analysis Data

Framework		
Mineral Grains	Total	Percent
Quartz		**30.9**
Monocrystalline	120	29.7
Polycrystalline	5	1.2
Chert		
Feldspar		**4.7**
Plagioclase	5	1.2
Microcline	12	3.0
K-Feldspar	2	0.5
Carbonate		**0.0**
Calcite		
Fossil/shell		
Lithic Grains	Total	Percent
		0.0
Metamorphic		
Sedimentary		
Volcanic		
Accessory Minerals	Total	Percent
		1.0
Garnet		
Tourmaline		
Zircon		
Opaques	4	1.0

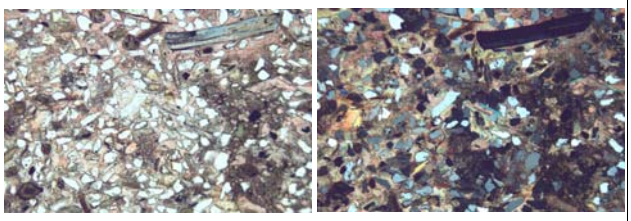

5x Field of View ~3 mm

Matrix Spaces			
Cement	Total	Percent	
		48.8	
Quartz			
K-Feldspar			
Calcite	197	48.8	
Dolomite/Ankerite			
Iron Oxide			
Matrix	Total	Percent	
Clay Minerals		**14.1**	
Clay Minerals (not individually identifiable)	36	8.9	
Muscovite			
Biotite/Chlorite	21	5.2	Biotite grains altering to chlorite
Chlorite			
Glauconite			
Illite			
Porosity	Total	Percent	
		0.5	
Intergranular			
Intragranular			
Intercrystalline			
Moldic	2	0.5	plucked grains?
Grain/Cement Dissolution			
Clay/Mica Framework			
Organic Matter			
Vug			
Channel			
Fracture			
	Total	**100.0**	

Back to Index

Thin Section Analysis Report

Sample ID: SHELL 372-1
Sample Condition: 30x20 mm, fractured
Formation Name: N/A
Depth (ft): 10872.9-10873.2
Lithology: calcareous siltstone

Date of Analysis: 3/5/2018
Analyzed by: S. Shank
Point Count Step Size 1 mm
Number of Counts 432

Texture - Qualitative Assessment

Approximate Average Grain Size (mm): 0.05 (quartz grains)
Grain Sorting: poor
Grain Rounding: rounded to subangular

Composition - Modal Analysis Data

Framework

Mineral Grains	Total	Percent
Quartz		**8.1**
Monocrystalline	30	6.9
Polycrystalline	5	1.2
Chert		
Feldspar		**0.7**
Plagioclase	3	0.7
Microcline		
K-Feldspar		
Carbonate		**6.3**
Calcite	25	5.8
Fossil/shell	2	0.5
Lithic Grains	**Total**	**Percent**
		0.0
Metamorphic		
Sedimentary		
Volcanic		
Accessory Minerals	**Total**	**Percent**
		1.6
Garnet		
Tourmaline		
Zircon		
Opaques	7	1.6

Matrix Spaces

Cement	Total	Percent
		15.0
Quartz		
K-Feldspar		
Calcite	65	15.0
Dolomite/Ankerite		
Iron Oxide		
Matrix	Total	Percent
Clay Minerals		**66.7**
Clay Minerals (not individually identifiable)	285	66.0
Muscovite	3	0.7
Biotite/Chlorite		
Chlorite		
Glauconite		
Illite		
Porosity	Total	Percent
		1.6
Intergranular		
Intragranular		
Intercrystalline		
Moldic		
Grain/Cement Dissolution		
Clay/Mica Framework		
Organic Matter		
Vug		
Channel		
Fracture	7	1.6
	Total	**100.0**

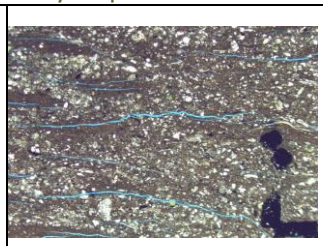
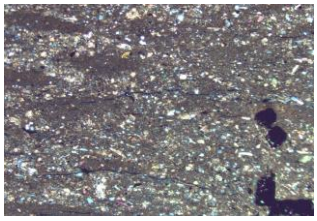

2.5 x Field of View ~5 mm
Common thin, discontinuous fractures

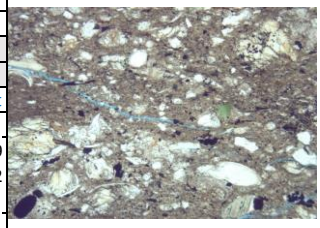
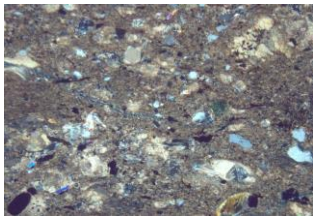

10x Field of View ~1 mm
Close up of fracture

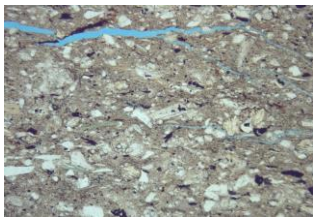
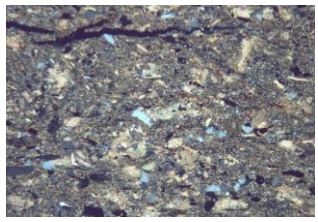

10x Field of View ~1 mm
Close up of fracture
Abundant carbonate grains and in matrix

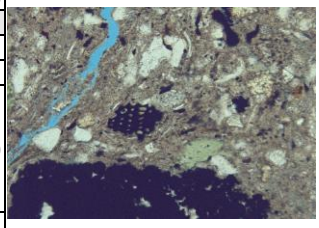
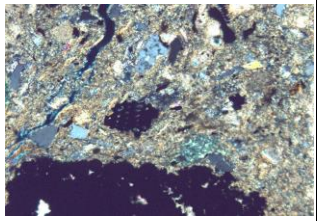

20x Field of View ~0.5 mm
sulfide? replacement of fossil

Does not include large fracture in section

Back to Index

MID-ATLANTIC U.S. OFFSHORE CARBON STORAGE RESOURCE ASSESSMENT PROJECT

DGS
SHELL 372-1 10,872.9-10,873.2 ft

Thin Section Analysis Report

Sample ID: SHELL 372-1
Sample Condition: standard rectangular slide
Formation Name:
Depth (ft): 10,872.9-10,873.2 ft
Lithology: Siltstone

Date of Analysis: 3/5/2018
Analyzed by: Kristin M. Carter
Point Count Step Size 0.3 mm
Number of Counts 407

Texture - Qualitative Assessment

Approximate Average Grain Size (mm): 0.05
Grain Sorting: poorly sorted
Grain Rounding: angular to subrounded

Composition - Modal Analysis Data

Framework

Mineral Grains	Total	Percent
Quartz		**1.7**
Monocrystalline	7	1.7
Polycrystalline		
Chert		
Feldspar		**5.7**
Plagioclase	23	5.7
Microcline		
K-Feldspar		
Carbonate		**11.1**
Calcite	45	11.1
Dolomite		

Lithic Grains	Total	Percent
		0.0
Metamorphic		
Sedimentary		
Volcanic		

Accessory Minerals	Total	Percent
		12.8
Rutile		
Tourmaline		
Zircon		
Opaques	52	12.8

Matrix Spaces

Cement	Total	Percent
		13.8
Quartz		
K-Feldspar		
Calcite	56	13.8
Dolomite/Ankerite		
Iron Oxide		

Matrix	Total	Percent
Clay Minerals		**55.0**
Clay Minerals (not individually identifiable)	199	48.9
Muscovite	5	1.2
Biotite	3	0.7
Chlorite	5	1.2
Glauconite		
Illite	12	2.9

Porosity	Total	Percent
		0.0
Intergranular		
Intragranular		
Intercrystalline		
Moldic		
Grain/Cement Dissolution		
Clay/Mica Framework		
Organic Matter		
Vug		
Channel		
Fracture		
	Total	**100.0**

Pre-Existing Delaware Geological Survey Thin Section

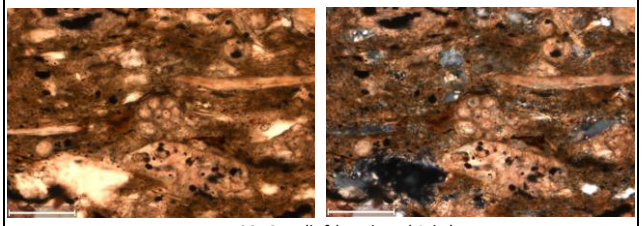

no41_0016 PL (left) and XN (right)

All scale bars are 100 um, unless otherwise noted

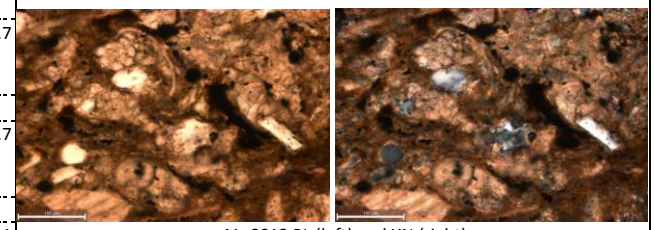

no41_0012 PL (left) and XN (right)

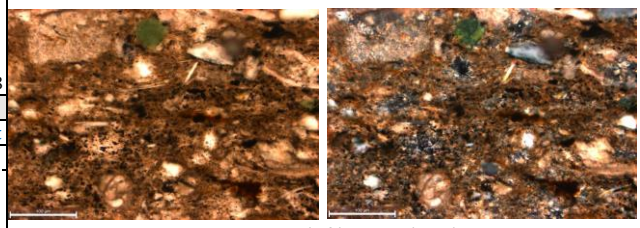

no41_0004 PL (left) and XN (right)

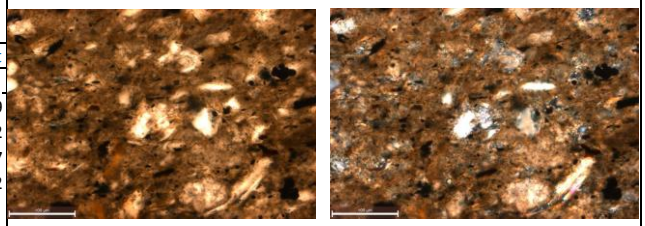

no41_0019 PL (left) and XN (right)

Back to Index

Thin Section Analysis Report

Sample ID: SHELL 586-1-9058-9058.7
Sample Condition: 32x20 mm
Formation Name: Logan Canyon
Depth (ft): 9058-9058.7
Lithology: oolitic limestone

Date of Analysis: 3/5/2018
Analyzed by: S. Shank
Point Count Step Size 1 mm
Number of Counts 420

Texture - Qualitative Assessment

Approximate Average Grain Size (mm):
Grain Sorting:
Grain Rounding:

Composition - Modal Analysis Data

Framework

Mineral Grains	Total	Percent
Quartz		**0.0**
Monocrystalline		
Polycrystalline		
Chert		
Feldspar		**0.0**
Plagioclase		
Microcline		
K-Feldspar		
Carbonate		**42.1**
Calcite (oolites)	128	30.5
Fossil/shell	49	11.7

Lithic Grains	Total	Percent
		0.0
Metamorphic		
Sedimentary		
Volcanic		

Accessory Minerals	Total	Percent
		0.0
Garnet		
Tourmaline		
Zircon		
Opaques		

Matrix Spaces

Cement	Total	Percent
		52.1
Quartz		
K-Feldspar		
Calcite	219	52.1
Dolomite/Ankerite		
Iron Oxide		

Matrix	Total	Percent
Clay Minerals		**0.0**
Clay Minerals (not individually identifiable)		
Muscovite		
Biotite/Chlorite		
Chlorite		
Glauconite		
Illite		

Porosity	Total	Percent
		5.7
Intergranular	10	2.4
Intragranular		
Intercrystalline		
Moldic	14	3.3
Grain/Cement Dissolution		
Clay/Mica Framework		
Organic Matter		
Vug		
Channel		
Fracture		0.0
	Total	**100.0**

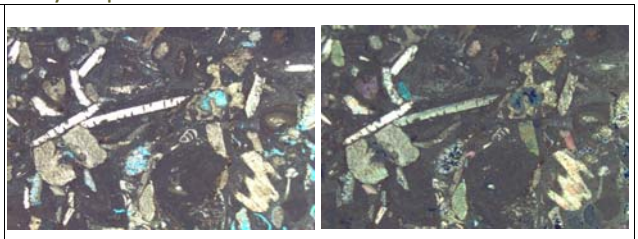

2.5 x Field of View ~5 mm
Abundant fossil fragments
Minor moldic porosity

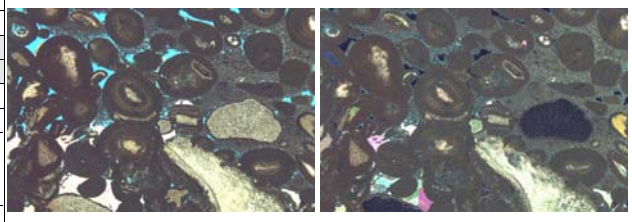

2.5 x Field of View ~5 mm

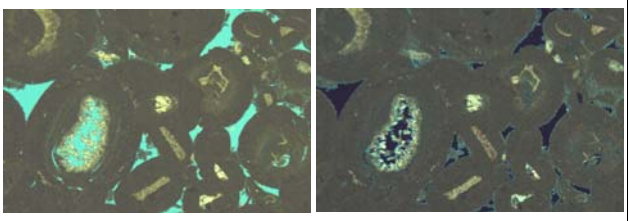

5x Field of View ~3 mm
Porosity between oolites and within oolites

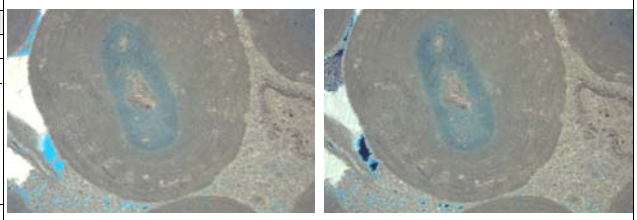

10x Field of View ~1 mm
Microporosity in oolites and cement

or cement dissolution?

Back to Index

Thin Section Analysis Report

Sample ID: SHELL 587-1-11555
Sample Condition: 25 mm round
Formation Name: N/A
Depth (ft): 11555
Lithology: limestone

Date of Analysis: 3/5/2018
Analyzed by: S. Shank
Point Count Step Size 1 mm
Number of Counts 406

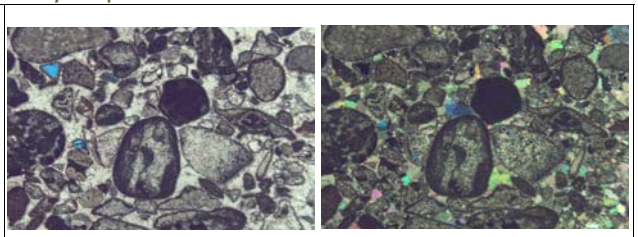

2.5 x Field of View ~5 mm
Abundant fossil fragments
Minor moldic porosity

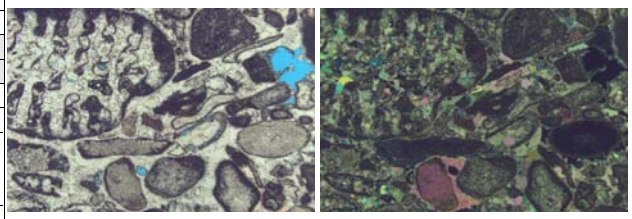

2.5 x Field of View ~5 mm
Abundant fossil fragments
Minor moldic porosity

Texture - Qualitative Assessment

Approximate Average Grain Size (mm):
Grain Sorting:
Grain Rounding:

Composition - Modal Analysis Data

Framework

Mineral Grains	Total	Percent
Quartz		**0.0**
Monocrystalline		
Polycrystalline		
Chert		
Feldspar		**0.0**
Plagioclase		
Microcline		
K-Feldspar		
Carbonate		**52.0**
Calcite (oolites, shell fragments)	211	52.0

Lithic Grains	Total	Percent
		0.0
Metamorphic		
Sedimentary		
Volcanic		

Accessory Minerals	Total	Percent
		0.0
Garnet		
Tourmaline		
Zircon		
Opaques		

Matrix Spaces

Cement	Total	Percent
		46.6
Quartz		
K-Feldspar		
Calcite	189	46.6
Dolomite/Ankerite		
Iron Oxide		

Matrix	Total	Percent
Clay Minerals		**0.0**
Clay Minerals (not individually identifiable)		
Muscovite		
Biotite/Chlorite		
Chlorite		
Glauconite		
Illite		

Porosity	Total	Percent
		1.5
Intergranular		
Intragranular		
Intercrystalline		
Moldic	4	1.0
Grain/Cement Dissolution	1	0.2
Clay/Mica Framework		
Organic Matter		
Vug		
Channel		
Fracture	1	0.2
	Total	**100.0**

Back to Index

Thin Section Analysis Report

Sample ID: SHELL 632-1-4594.5
Sample Condition: 27x20 mm
Formation Name: Dawson Canyon
Depth (ft): 4594.5
Lithology: sandstone

Date of Analysis: 3/5/2018
Analyzed by: S. Shank
Point Count Step Size 1 mm
Number of Counts 417

Texture - Qualitative Assessment

Approximate Average Grain Size (mm): 0.1
Grain Sorting: well
Grain Rounding: angular to subrounded

Composition - Modal Analysis Data

Framework

Mineral Grains	Total	Percent
Quartz		**52.3**
Monocrystalline	199	47.7
Polycrystalline	19	4.6
Chert		
Feldspar		**6.5**
Plagioclase	21	5.0
Microcline		
K-Feldspar	6	1.4
Carbonate		**0.0**
Calcite		
Fossil/shell		

Lithic Grains	Total	Percent
		0.0
Metamorphic		
Sedimentary		
Volcanic		

Accessory Minerals	Total	Percent
		0.5
Garnet		
Tourmaline		
Zircon		
Opaques	2	0.5

Matrix Spaces

Cement	Total	Percent
		8.4
Quartz		
K-Feldspar		
Calcite		
Dolomite/Ankerite		
Iron Oxide	35	8.4

Matrix	Total	Percent
Clay Minerals		**8.6**
Clay Minerals (not individually identifiable)	34	8.2
Muscovite	2	0.5
Kaolinite		
Chlorite		
Glauconite		
Illite		

Porosity	Total	Percent
		23.7
Intergranular	99	23.7
Intragranular		
Intercrystalline		
Moldic		
Grain/Cement Dissolution		
Clay/Mica Framework		
Organic Matter		
Vug		
Channel		
Fracture		
	Total	**100.0**

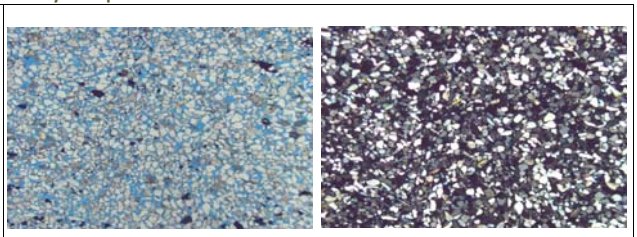

2.5 x Field of View ~5 mm
Sandstone with abundant intergranular porosity

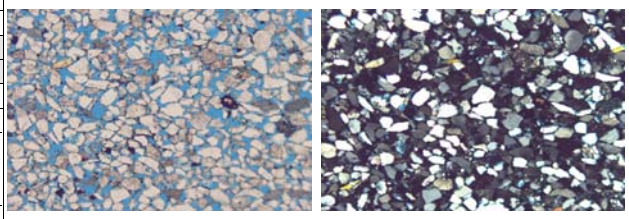

5x Field of View ~3 mm
Fairly common plagioclase

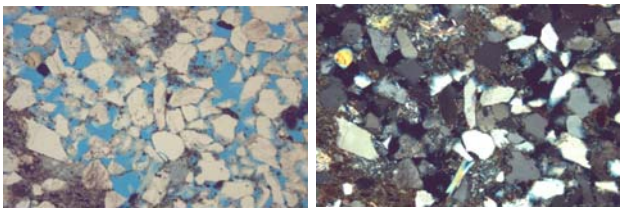

10x Field of View ~1 mm
Locally common interstitial clay

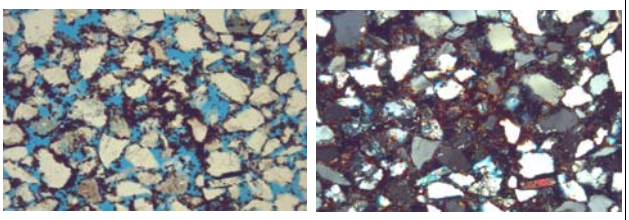

10x Field of View ~1 mm
Locally abundant iron oxide around quartz grains

Back to Index

Thin Section Analysis Report

Sample ID: SHELL 632-1-6278.8
Sample Condition: 30x20 mm
Formation Name: Logan Canyon
Depth (ft): 6278.8
Lithology: glauconitic sandy limestone

Date of Analysis: 3/6/2018
Analyzed by: S. Shank
Point Count Step Size 1 mm
Number of Counts 450

Texture - Qualitative Assessment

Approximate Average Grain Size (mm): 0.5
Grain Sorting: moderate
Grain Rounding: angular to subrounded

Composition - Modal Analysis Data

Framework

Mineral Grains	Total	Percent
Quartz		**31.1**
Monocrystalline	125	27.8
Polycrystalline	15	3.3
Chert		
Feldspar		**1.6**
Plagioclase		
Microcline	2	0.4
K-Feldspar	5	1.1
Carbonate		**0.2**
Calcite		
Fossil/shell	1	0.2

Lithic Grains	Total	Percent
		0.0
Metamorphic		
Sedimentary		
Volcanic		

Accessory Minerals	Total	Percent
		0.4
Garnet		
Tourmaline		
Zircon		
Opaques	2	0.4

Matrix Spaces

Cement	Total	Percent
		44.4
Quartz		
K-Feldspar		
Calcite	165	36.7
Dolomite/Ankerite		
Iron Oxide	35	7.8

Matrix	Total	Percent
Clay Minerals		**17.1**
Clay Minerals (not individually identifiable)	3	0.7
Muscovite		
Kaolinite		
Chlorite	9	2.0
Glauconite	65	14.4
Illite		

Porosity	Total	Percent
		5.1
Intergranular		
Intragranular		
Intercrystalline		
Moldic	17	3.8
Grain/Cement Dissolution	6	1.3
Clay/Mica Framework		
Organic Matter		
Vug		
Channel		
Fracture		
	Total	**100.0**

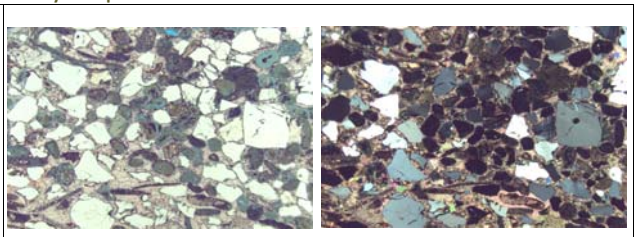

2.5 x Field of View ~5 mm
Dissolution of glauconite, common shell fragments

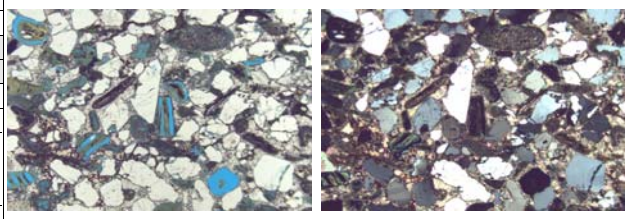

2.5 x Field of View ~5 mm
Dissolution of glauconite

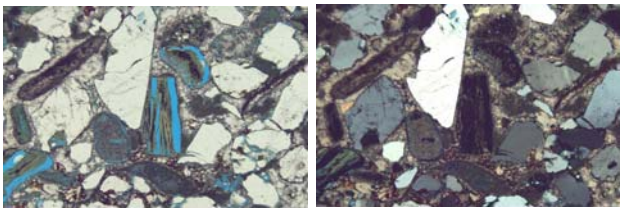

5x Field of View ~3 mm

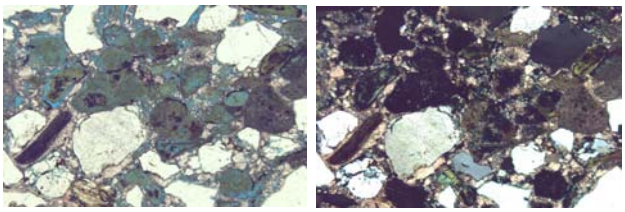

5x Field of View ~3 mm

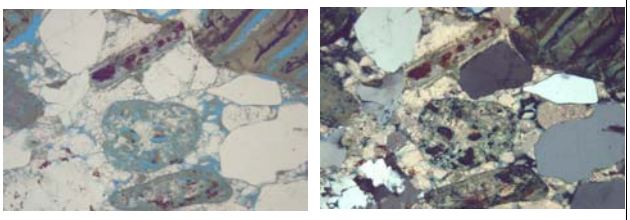

10x Field of View ~1 mm

Back to Index

Thin Section Analysis Report

Sample ID: SHELL 632-1-8083.1
Sample Condition: 25 mm round
Formation Name: Mississauga
Depth (ft): 8083.1
Lithology: sandstone

Date of Analysis: 3/6/2018
Analyzed by: S. Shank
Point Count Step Size 1 mm
Number of Counts 377

Texture - Qualitative Assessment

Approximate Average Grain Size (mm): 0.4
Grain Sorting: moderate
Grain Rounding: subrounded to subangular

Composition - Modal Analysis Data

Framework		
Mineral Grains	Total	Percent
Quartz		**63.9**
Monocrystalline	199	52.8
Polycrystalline	42	11.1
Chert		
Feldspar		**0.0**
Plagioclase		
Microcline		
K-Feldspar		
Carbonate		**0.0**
Calcite		
Fossil/shell		
Lithic Grains	Total	Percent
		0.0
Metamorphic		
Sedimentary		
Volcanic		
Accessory Minerals	Total	Percent
		0.8
Garnet		
Tourmaline		
Zircon		
Opaques	3	0.8
Matrix Spaces		
Cement	Total	Percent
		7.7
Quartz	17	4.5
K-Feldspar		
Calcite	11	2.9
Dolomite/Ankerite		
Iron Oxide	1	0.3
Matrix	Total	Percent
Clay Minerals		**17.2**
Clay Minerals (not individually identifiable)	34	9.0
Muscovite	2	0.5
Kaolinite	29	7.7
Chlorite		
Glauconite		
Illite		
Porosity	Total	Percent
		10.3
Intergranular	19	5.0
Intragranular		
Intercrystalline		
Moldic		
Grain/Cement Dissolution	20	5.3
Clay/Mica Framework		
Organic Matter		
Vug		
Channel		
Fracture		
	Total	**100.0**

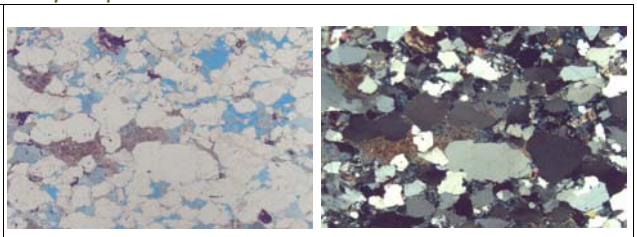

2.5 x Field of View ~5 mm
Moderate porosity with intergranular clays and kaolinite
Overgrowths on quartz but difficult to distinguish

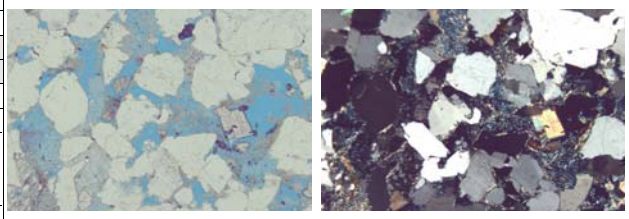

5x Field of View ~3 mm
calcite rhomb in pore, feldspar dissolution

5x Field of View ~3 mm
metamorphic rock fragment

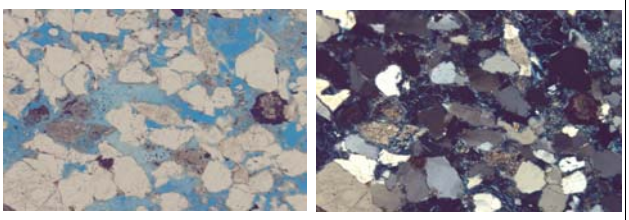

5x Field of View ~3 mm
prismatic quartz in pore, abundant kaolinite and clay

Back to Index

Thin Section Analysis Report

Sample ID: SHELL 93-1-9937
Sample Condition: 35x15 mm
Formation Name: Mississauga
Depth (ft): 9937
Lithology: feldspathic sandstone

Date of Analysis: 3/2/2018
Analyzed by: S. Shank
Point Count Step Size 1 mm
Number of Counts 402

Texture - Qualitative Assessment

Approximate Average Grain Size (mm): 0.2
Grain Sorting: well
Grain Rounding: angular

Composition - Modal Analysis Data

Framework

Mineral Grains	Total	Percent
Quartz		**31.1**
Monocrystalline	113	28.1
Polycrystalline	12	3.0
Chert		
Feldspar		**10.7**
Plagioclase	17	4.2
Microcline	1	0.2
K-Feldspar	25	6.2
Carbonate		**0.5**
Calcite		
Fossil/shell	2	0.5

Lithic Grains	Total	Percent
		0.0
Metamorphic		
Sedimentary		
Volcanic		

Accessory Minerals	Total	Percent
		0.2
Garnet		
Tourmaline		
Zircon		
Opaques	1	0.2

Matrix Spaces

Cement	Total	Percent
		2.0
Quartz		
K-Feldspar		
Calcite	6	1.5
Dolomite/Ankerite		
Iron Oxide	2	0.5

Matrix	Total	Percent
Clay Minerals		**23.9**
Clay Minerals (not individually identifiable)	93	23.1
Muscovite	3	0.7
Kaolinite		
Chlorite		
Glauconite		
Illite		

Porosity	Total	Percent
		31.6
Intergranular	126	31.3
Intragranular		
Intercrystalline		
Moldic	1	0.2
Grain/Cement Dissolution		
Clay/Mica Framework		
Organic Matter		
Vug		
Channel		
Fracture		
	Total	**100.0**

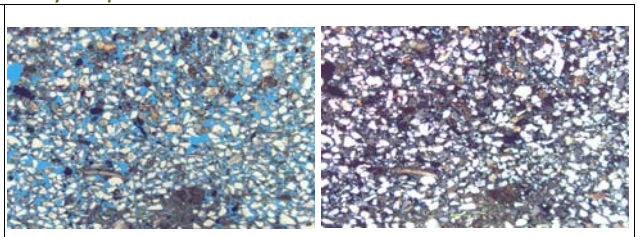

2.5 x Field of View ~5 mm
Sandstone with abundant intergranular porosity and intergranular clays

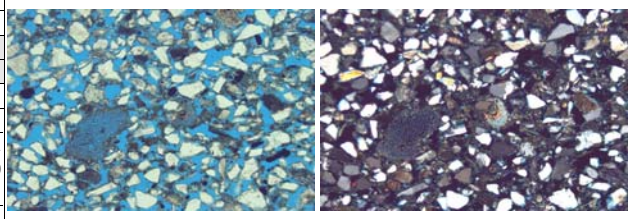

5x Field of View ~3 mm
Common fossil fragments

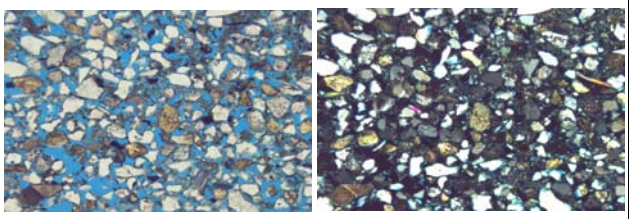

5x Field of View ~3 mm
Common feldspar

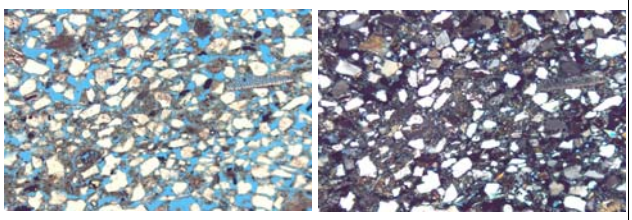

5x Field of View ~3 mm
Common fossil fragments

Back to Index

Thin Section Analysis Report

Sample ID: TEXACO 598-1-12840-12841
Sample Condition: 32x20 mm
Formation Name: Mohawk
Depth (ft): 12840-12841
Lithology: arkose

Date of Analysis: 3/7/2018
Analyzed by: S. Shank
Point Count Step Size 1 mm
Number of Counts 409

Texture - Qualitative Assessment

Approximate Average Grain Size (mm): 0.2
Grain Sorting: well to moderate
Grain Rounding: subrounded

Composition - Modal Analysis Data

Framework		
Mineral Grains	Total	Percent
Quartz		**52.3**
Monocrystalline	173	42.3
Polycrystalline	41	10.0
Chert		
Feldspar		**12.7**
Plagioclase	39	9.5
Microcline	1	0.2
K-Feldspar	12	2.9
Carbonate		**0.0**
Calcite		
Fossil/shell		
Lithic Grains	Total	Percent
		0.0
Metamorphic		
Sedimentary		
Volcanic		
Accessory Minerals	Total	Percent
		0.7
Garnet		
Tourmaline		
Zircon		
Opaques	3	0.7
Matrix Spaces		
Cement	Total	Percent
		6.1
Quartz	25	6.1
K-Feldspar		
Calcite		
Dolomite/Ankerite		
Iron Oxide		
Matrix	Total	Percent
Clay Minerals		**18.1**
Clay Minerals (not individually identifiable)	22	5.4
Muscovite	5	1.2
Kaolinite	47	11.5
Chlorite		
Glauconite		
Illite		
Porosity	Total	Percent
		10.0
Intergranular	19	4.6
Intragranular		
Intercrystalline	4	1.0
Moldic	10	2.4
Grain/Cement Dissolution	8	2.0
Clay/Mica Framework		
Organic Matter		
Vug		
Channel		
Fracture		
	Total	**100.0**

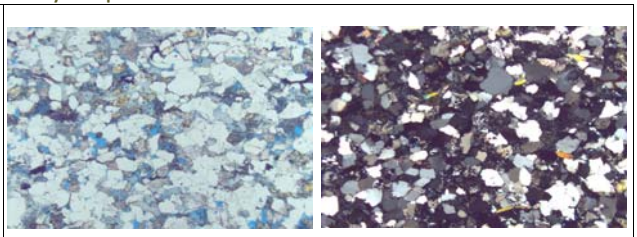

2.5 x Field of View ~5 mm
Moderate intergranular porosity, abundant clays in pores
Fairly extensive feldspar dissolution

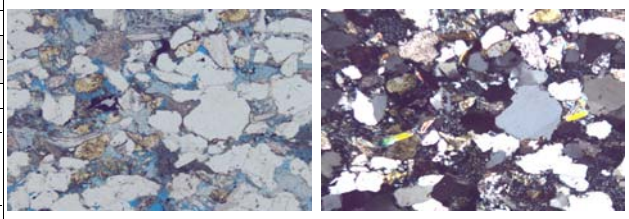

5x Field of View ~3 mm
Close up of feldspar dissolution, abundant clays

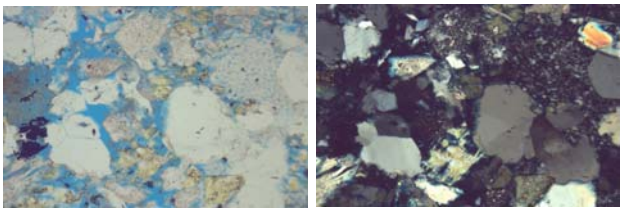

10x Field of View ~1 mm
Prismatic quartz in pores
Close up of feldspar dissolution, abundant clays

Back to Index

Thin Section Analysis Report

Sample ID: TEXACO 598-1-13271-13272
Sample Condition: 28x18 mm
Formation Name: Mohawk
Depth (ft): 13271-13272
Lithology: sandstone

Date of Analysis: 3/7/2018
Analyzed by: S. Shank
Point Count Step Size 1 mm
Number of Counts 409

Texture - Qualitative Assessment

Approximate Average Grain Size (mm): 0.5
Grain Sorting: moderate
Grain Rounding: subrounded

Composition - Modal Analysis Data

Framework		
Mineral Grains	Total	Percent
Quartz		**62.3**
Monocrystalline	221	54.0
Polycrystalline	34	8.3
Chert		
Feldspar		**2.4**
Plagioclase	9	2.2
Microcline		
K-Feldspar	1	0.2
Carbonate		**0.0**
Calcite		
Fossil/shell		
Lithic Grains	**Total**	**Percent**
		0.0
Metamorphic		
Sedimentary		
Volcanic		
Accessory Minerals	**Total**	**Percent**
		0.2
Garnet		
Tourmaline		
Zircon		
Opaques	1	0.2
Matrix Spaces		
Cement	**Total**	**Percent**
		4.4
Quartz	16	3.9
K-Feldspar		
Calcite	2	0.5
Dolomite/Ankerite		
Iron Oxide		
Matrix	**Total**	**Percent**
Clay Minerals		**17.8**
Clay Minerals (not individually identifiable)	21	5.1
Muscovite	3	0.7
Kaolinite	49	12.0
Chlorite		
Glauconite		
Illite		
Porosity	**Total**	**Percent**
		12.7
Intergranular	26	6.4
Intragranular		
Intercrystalline	13	3.2
Moldic	7	1.7
Grain/Cement Dissolution	6	1.5
Clay/Mica Framework		
Organic Matter		
Vug		
Channel		
Fracture		
	Total	**100.0**

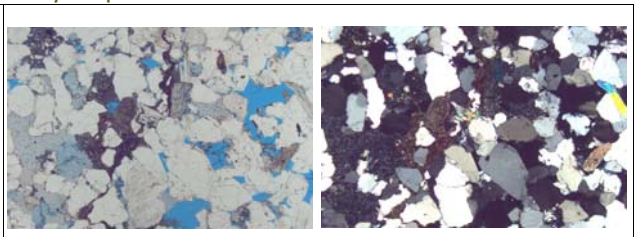

2.5 x Field of View ~5 mm
Moderate intergranular porosity, abundant clays in pores
Extensive feldspar dissolution

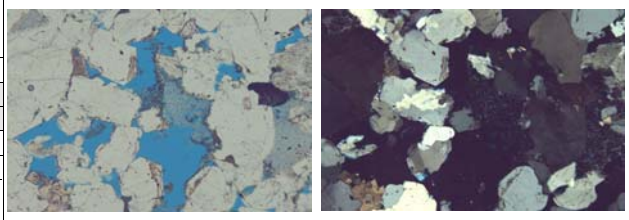

5x Field of View ~3 mm
Close up of pore with calcite, clays, prismatic quartz

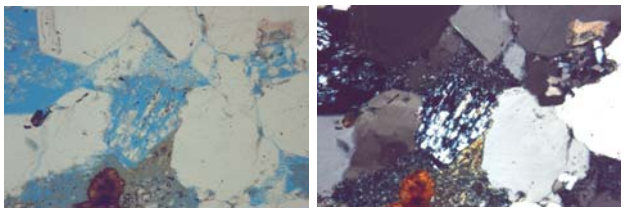

10x Field of View ~1 mm
Prismatic quartz in pores
Close up of feldspar dissolution, clays

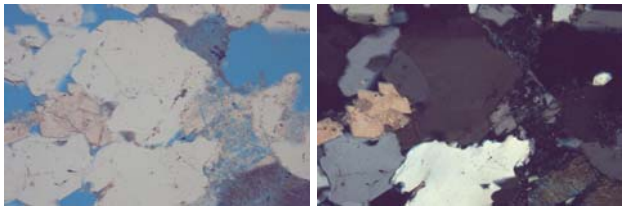

10x Field of View ~1 mm
Calcite, plagioclase dissolution

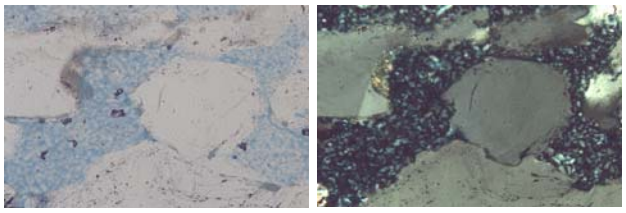

20x Field of View ~0.5 mm
kaolinite in pore with intercrystalline porosity

Back to Index

Thin Section Analysis Report

Sample ID: TEXACO 598-1-13275-13276
Sample Condition: 30x15 mm fragment
Formation Name: Mohawk
Depth (ft): 13275-13276
Lithology: sandstone

Date of Analysis: 3/8/2018
Analyzed by: S. Shank
Point Count Step Size 1 mm
Number of Counts 417

Texture - Qualitative Assessment

Approximate Average Grain Size (mm): 0.7
Grain Sorting: moderate
Grain Rounding: subrounded

Composition - Modal Analysis Data

Framework		
Mineral Grains	Total	Percent
Quartz		**67.9**
Monocrystalline	246	59.0
Polycrystalline	37	8.9
Chert		
Feldspar		**1.0**
Plagioclase	3	0.7
Microcline		
K-Feldspar	1	0.2
Carbonate		**0.0**
Calcite		
Fossil/shell		
Lithic Grains	Total	Percent
		0.0
Metamorphic		
Sedimentary		
Volcanic		
Accessory Minerals	Total	Percent
		1.0
Garnet		
Tourmaline		
Zircon		
Opaques	4	1.0
Matrix Spaces		
Cement	Total	Percent
		4.1
Quartz	14	3.4
K-Feldspar		
Calcite	2	0.5
Siderite/Dolomite/Ankerite	1	0.2
Iron Oxide		
Matrix	Total	Percent
Clay Minerals		**15.8**
Clay Minerals (not individually identifiable)	42	10.1
Muscovite	1	0.2
Kaolinite	23	5.5
Chlorite		
Glauconite		
Illite		
Porosity	Total	Percent
		10.3
Intergranular	31	7.4
Intragranular		
Intercrystalline	4	1.0
Moldic	4	1.0
Grain/Cement Dissolution	4	1.0
Clay/Mica Framework		
Organic Matter		
Vug		
Channel		
Fracture		
	Total	**100.0**

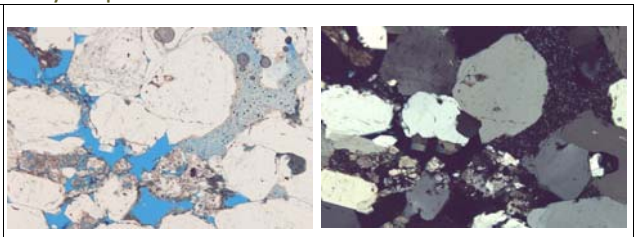

2.5 x Field of View ~5 mm
Moderate intergranular porosity, abundant clays in pores
Feldspar dissolution

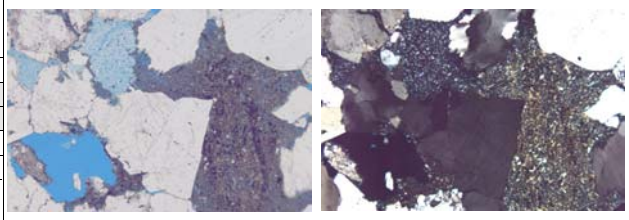

2.5 x Field of View ~5 mm
Dark clay in pore

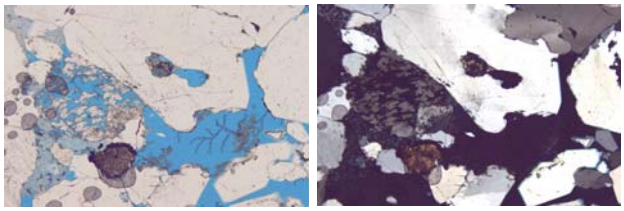

2.5 x Field of View ~5 mm
Close up of feldspar dissolution, clays
Prismatic quartz

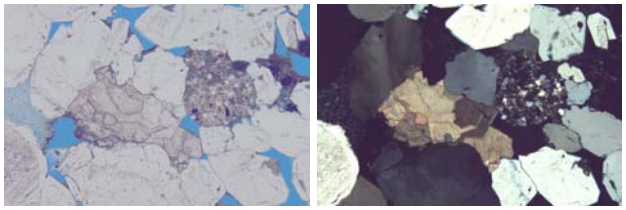

2.5 x Field of View ~5 mm
Calcite in pore

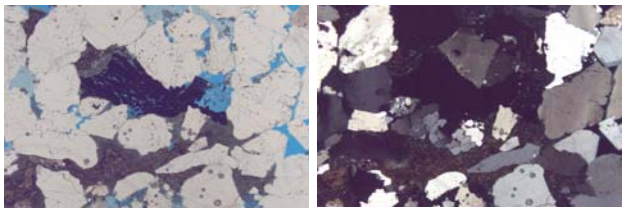

20x Field of View ~0.5 mm
sulfide in pore

Back to Index

Thin Section Analysis Report

Sample ID: TEXACO 642-1-12444
Sample Condition: 30x20 mm
Formation Name: Mic-Mac
Depth (ft): 12444
Lithology: calcareous siltstone

Date of Analysis: 3/9/2018
Analyzed by: S. Shank
Point Count Step Size 1 mm
Number of Counts 415

Texture - Qualitative Assessment

Approximate Average Grain Size (mm): <0.05 (quartz grains)
Grain Sorting: moderate
Grain Rounding: subangular

Composition - Modal Analysis Data

Framework		
Mineral Grains	Total	Percent
Quartz		**36.9**
Monocrystalline	153	36.9
Polycrystalline		
Chert		
Feldspar		**3.4**
Plagioclase	8	1.9
Microcline		
K-Feldspar	6	1.4
Carbonate		**0.5**
Calcite		
Fossil/shell	2	0.5
Lithic Grains	Total	Percent
		0.0
Metamorphic		
Sedimentary		
Volcanic		
Accessory Minerals	Total	Percent
		4.6
Garnet		
Tourmaline		
Zircon		
Opaques	19	4.6
Matrix Spaces		
Cement	Total	Percent
		11.6
Quartz		
K-Feldspar		
Calcite	48	11.6
Dolomite/Ankerite		
Iron Oxide		
Matrix	Total	Percent
Clay Minerals		**42.4**
Clay Minerals (not individually identifiable)	164	39.5
Muscovite	12	2.9
Kaolinite		
Chlorite		
Glauconite		
Illite		
Porosity	Total	Percent
		0.7
Intergranular		
Intragranular		
Intercrystalline		
Moldic		
Grain/Cement Dissolution		
Clay/Mica Framework		
Organic Matter		
Vug		
Channel		
Fracture	3	0.7
	Total	**100.0**

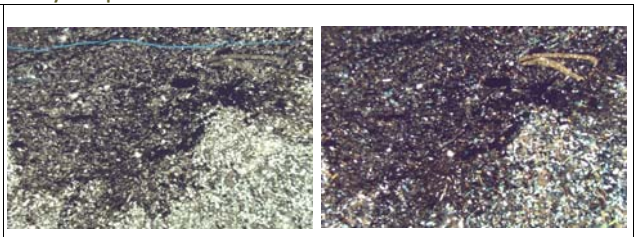

2.5x Field of View ~5 mm
Patchy quartz & calcite distribution, thin discontinuous fracture

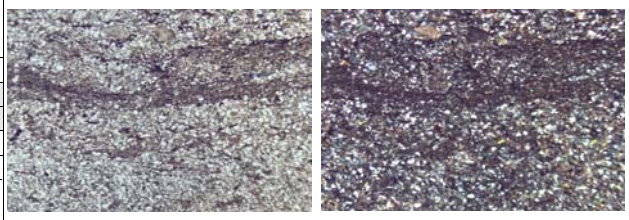

2.5x Field of View ~5 mm
Small fossil fragments, very thin fractures

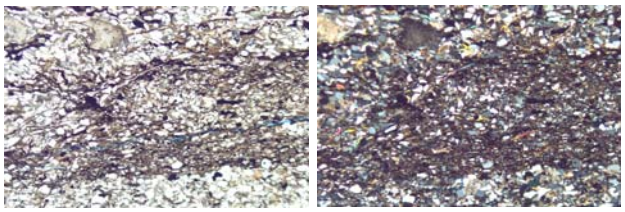

5x Field of View ~3 mm
Close up of above

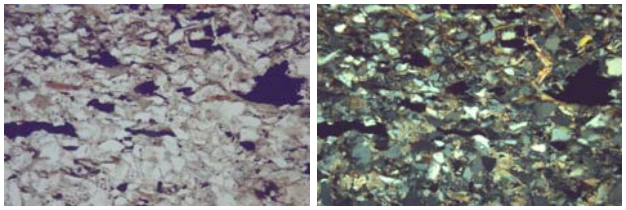

10x Field of View ~1 mm
Close up of quartz grains in clay matrix

Back to Index

Thin Section Analysis Report

Sample ID: TEXACO 642-1-15608
Sample Condition: 25 mm round
Formation Name: Mohawk
Depth (ft): 15608
Lithology: arkose

Date of Analysis: 3/9/2018
Analyzed by: S. Shank
Point Count Step Size 0.4 mm
Number of Counts 399

Texture - Qualitative Assessment

Approximate Average Grain Size (mm): 0.2
Grain Sorting: well
Grain Rounding: angular to subrounded

Composition - Modal Analysis Data

Framework

Mineral Grains	Total	Percent
Quartz		**50.1**
Monocrystalline	185	46.4
Polycrystalline	15	3.8
Chert		
Feldspar		**20.3**
Plagioclase	50	12.5
Microcline	11	2.8
K-Feldspar	20	5.0
Carbonate		**0.0**
Calcite		
Fossil/shell		

Lithic Grains	Total	Percent
		0.5
Metamorphic		
Sedimentary	2	0.5
Volcanic		

Accessory Minerals	Total	Percent
		0.8
Garnet		
Tourmaline		
Zircon		
Opaques	3	0.8

Matrix Spaces

Cement	Total	Percent
		2.0
Quartz	6	1.5
K-Feldspar		
Calcite	2	0.5
Dolomite/Ankerite		
Iron Oxide		

Matrix	Total	Percent
Clay Minerals		**5.0**
Clay Minerals (not individually identifiable)	20	5.0
Muscovite		
Kaolinite		
Chlorite		
Glauconite		
Illite		

Porosity	Total	Percent
		21.3
Intergranular	75	18.8
Intragranular		
Intercrystalline		
Moldic	10	2.5
Grain/Cement Dissolution		
Clay/Mica Framework		
Organic Matter		
Vug		
Channel		
Fracture		
	Total	**100.0**

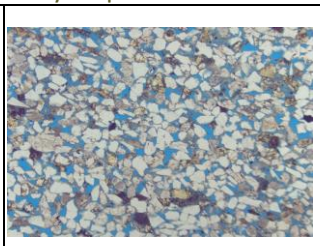
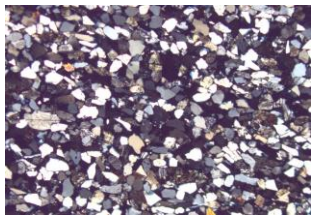

2.5 x Field of View ~5 mm
Abundant porosity with little clay

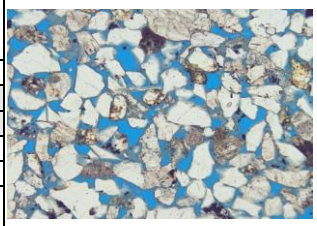
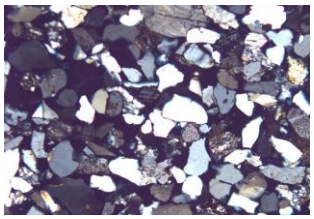

5x Field of View ~3 mm
Abundant relatively fresh feldspar

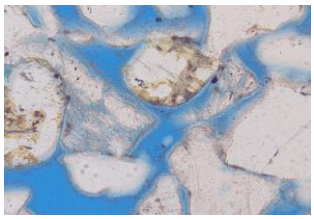
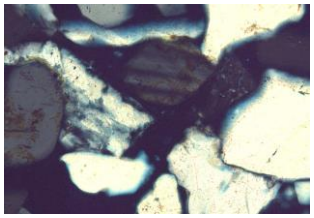

20x Field of View ~0.5 mm
Some plagioclase dissolution

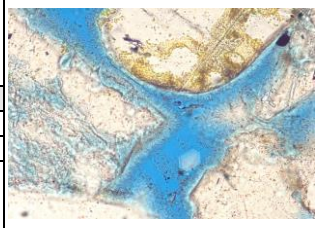

40x Field of View ~0.25 mm
Fuzzy rinds on mineral grains

Back to Index

Thin Section Analysis Report

Sample ID: EXXON 599-1
Sample Condition: chip size 35x21 mm
Formation Name: Mic-Mac
Depth (ft): 12,386 ft
Lithology: Sandstone

Date of Analysis: 2/28/2018
Analyzed by: S. Shank
Point Count Step Size 1.0 mm
Number of Counts 445

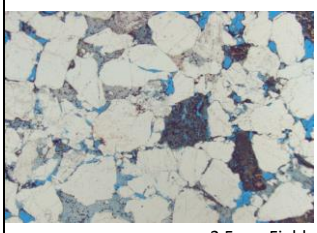
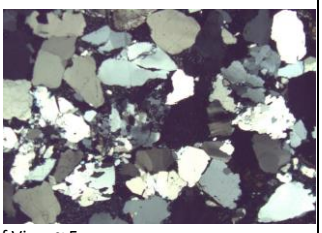

2.5 x Field of View ~ 5 mm
Quartz grains with quartz overgrowths (hard to distinguish)
Abundant kaolinite and dark material in intergranular pores

Texture - Qualitative Assessment

Approximate Average Grain Size (mm): 0.75
Grain Sorting: well
Grain Rounding: subangular to subrounded

Composition - Modal Analysis Data

Framework

Mineral Grains	Total	Percent
Quartz		**73.9**
Monocrystalline	285	64.0
Polycrystalline	44	9.9
Chert		
Feldspar		**4.7**
Plagioclase	1	0.2
Microcline		
K-Feldspar	20	4.5
Carbonate		**0.0**
Calcite		
Shell/fossil		

Lithic Grains	Total	Percent
		0.2
Metamorphic	1	0.2
Sedimentary		
Volcanic		

Accessory Minerals	Total	Percent
		0.0
Rutile		
Tourmaline		
Zircon		
Opaques		

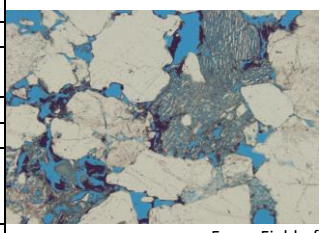
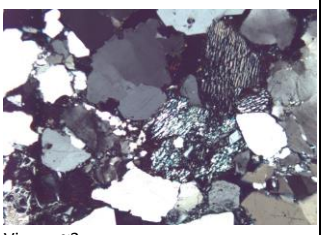

5 x Field of View ~3 mm
Extensive feldspar dissolution and clays filling in pores
Irregular shape of quartz due to overgrowths

Matrix Spaces

Cement	Total	Percent
		0.0
Quartz		
K-Feldspar		
Calcite		
Dolomite/Ankerite		
Iron Oxide		

Matrix	Total	Percent
Clay Minerals		**10.6**
Clay Minerals (not individually identifiable)	22	4.9
Kaolinite	25	5.6
Muscovite		
Biotite		
Chlorite		
Glauconite		

dark cryptocrystalline material

Porosity	Total	Percent
		10.6
Intergranular	37	8.3
Intragranular		
Intercrystalline	2	0.4
Moldic	8	1.8
Grain/Cement Dissolution		
Clay/Mica Framework		
Organic Matter		
Vug		
Channel		
Fracture		
	Total	100.0

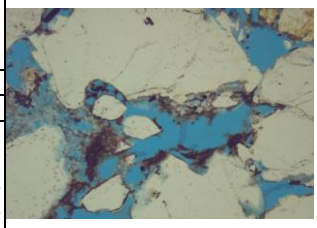

10x Field of View ~1.5 mm
Quartz overgrowths with prismatic quartz crystal in pores

Back to Index

Thin Section Analysis Report

Sample ID: EXXON 599-1
Sample Condition: chip size 35x15 mm
Formation Name: Mic-Mac
Depth (ft): 12,387 ft
Lithology: Sandstone

Date of Analysis: 2/28/2018
Analyzed by: S. Shank
Point Count Step Size 1.0 mm
Number of Counts 412

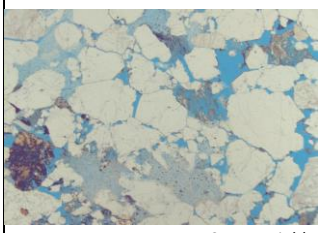
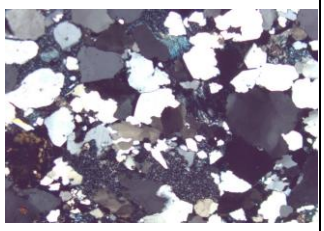

2.5 x Field of View ~ 5 mm
Quartz grains with quartz overgrowths (hard to distinguish)
Abundant kaolinite in intergranular pores

Texture - Qualitative Assessment

Approximate Average Grain Size (mm): 0.6
Grain Sorting: moderate
Grain Rounding: subrounded to subangular

Composition - Modal Analysis Data

Framework

Mineral Grains	Total	Percent
Quartz		**70.4**
Monocrystalline	261	63.3
Polycrystalline	29	7.0
Chert		
Feldspar		**4.1**
Plagioclase	1	0.2
Microcline	1	0.2
K-Feldspar	11	2.7
Carbonate		**0.5**
Calcite	2	0.5
Shell/fossil		

Lithic Grains	Total	Percent
		0.2
Metamorphic		
Sedimentary	1	0.2
Volcanic		

Accessory Minerals	Total	Percent
		0.0
Rutile		
Tourmaline		
Zircon		
Opaques		

Matrix Spaces

Cement	Total	Percent
		1.9
Quartz	8	1.9
K-Feldspar		
Calcite		
Dolomite/Ankerite		
Iron Oxide		

Matrix	Total	Percent
Clay Minerals		**10.2**
Clay Minerals (not individually identifiable)	5	1.2
Kaolinite	35	8.5
Muscovite	2	0.5
Biotite		
Chlorite		
Glauconite		

Porosity	Total	Percent
		12.6
Intergranular	46	11.2
Intragranular		
Intercrystalline	2	0.5
Moldic	4	1.0
Grain/Cement Dissolution		
Clay/Mica Framework		
Organic Matter		
Vug		
Channel		
Fracture		
	Total	100.0

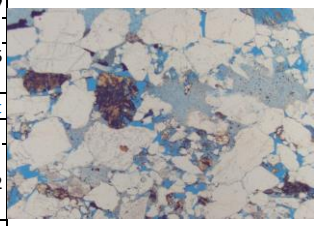

2.5 x Field of View ~ 5 mm
Quartz grains with quartz overgrowths (hard to distinguish)
Abundant kaolinite in intergranular pores

dark cryptocrystalline material

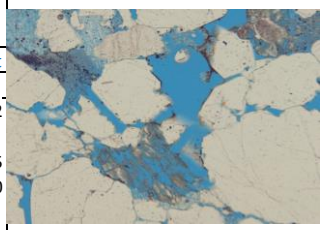
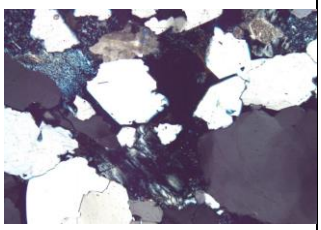

5x Field of View ~3 mm
Quartz overgrowths with angular quartz crystal faces in pores
Extensive dissolution of feldspars

Back to Index

Thin Section Analysis Report

Sample ID: EXXON 599-1
Sample Condition: chip size 35x13 mm
Formation Name: Mic-Mac
Depth (ft): 12,403 ft
Lithology: Sandstone

Date of Analysis: 2/28/2018
Analyzed by: S. Shank
Point Count Step Size 1.0 mm
Number of Counts 404

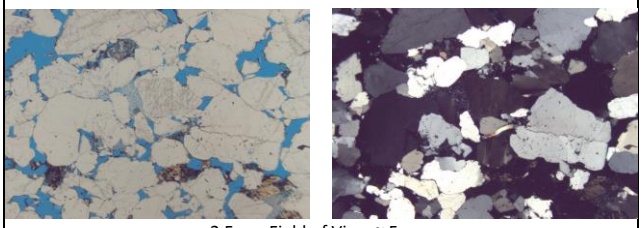

2.5 x Field of View ~ 5 mm
Quartz grains with quartz overgrowths (hard to distinguish)
Abundant kaolinite in intergranular pores

Texture - Qualitative Assessment

Approximate Average Grain Size (mm): 0.75
Grain Sorting: well
Grain Rounding: subangular to subrounded

Composition - Modal Analysis Data

Framework

Mineral Grains	Total	Percent
Quartz		**73.8**
Monocrystalline	277	68.6
Polycrystalline	21	5.2
Chert		
Feldspar		**2.0**
Plagioclase	3	0.7
Microcline		
K-Feldspar	5	1.2
Carbonate		**0.0**
Calcite		
Shell/fossil		

Lithic Grains	Total	Percent
		0.0
Metamorphic		
Sedimentary		
Volcanic		

Accessory Minerals	Total	Percent
		0.0
Rutile		
Tourmaline		
Zircon		
Opaques		

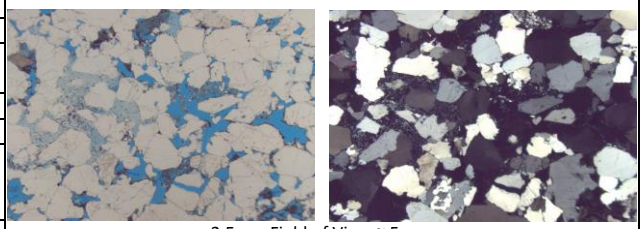

2.5 x Field of View ~ 5 mm
Quartz grains with quartz overgrowths (hard to distinguish)
Abundant kaolinite in intergranular pores

Matrix Spaces

Cement	Total	Percent
		3.0
Quartz	11	2.7
K-Feldspar		
Calcite		
Dolomite/Ankerite		
Iron Oxide	1	0.2

Matrix	Total	Percent	
Clay Minerals		**8.4**	
Clay Minerals (not individually identifiable)	7	1.7	dark cryptocrystalline material
Kaolinite	25	6.2	
Muscovite	2	0.5	
Biotite			
Chlorite			
Glauconite			

Porosity	Total	Percent
		12.9
Intergranular	46	11.4
Intragranular		
Intercrystalline	1	0.2
Moldic	5	1.2
Grain/Cement Dissolution		
Clay/Mica Framework		
Organic Matter		
Vug		
Channel		
Fracture		
Total		100.0

Back to Index

ADVANCED CORE ANALYSIS STUDY

Delaware Geological Survey, University of Delaware

CO_2 Storage Resource Assessment Project

FINAL REPORT

Submitted to:

Delaware Geological Survey, University of Delaware

December 21, 2017

Performed by:

Core Laboratories
Petroleum Services Division
6316 Windfern
Houston, Texas 77040

HOU-1703089

Core Laboratories
6316 Windfern Road
Houston, Texas 77040 USA
Tel: 713-328-2673
Fax: 713-328-2197
www.corelab.com

December 21, 2017

Delaware Geological Survey, University of Delaware
DGS Building, 257 Academy Street
Newark, DE 19716-7501

Attention: Mojisola A. KunleDare, PhD

Subject: Delaware Geological Survey, University of Delaware
CO_2 Storage Resource Assessment Project
File: HOU-1703089

Dear Dr. KunleDare,

Presented in this report are the final results of the Core Analysis measurements performed on core plug samples from various wells as part of a CO_2 Storage Resource Assessment project.

We appreciate the opportunity to be of service to Delaware Geological Survey, University of Delaware with this study and look forward to working with you on future projects. If you have any questions concerning this report, please do not hesitate to contact us.

Sincerely,

Joel Henderson

Joel Henderson
Laboratory Supervisor
Petroleum Services Division
Houston, Texas
(713) 328-6047
Joel.Henderson@corelab.com

CLB Listed NYSE

Delaware Geological Survey, University of Delaware
CO_2 Storage Resource Assessment Project

Table of Contents

SUMMARY AND DISCUSSION

The Houston Advanced Technology Center of Core Laboratories were requested to test eighty-one (81) sample points (slabs, chips, slices and sidewall core samples) and forty (40) plugs (drilled samples) from multiple wells for petrophysical analysis. The eighty-one sample points were tested using the Pressure – Decay Profile Permeameter (PDPK) and the forty (40) drilled plug samples were tested using the automated Core Measurement System (CMS-300™). Each test method provides permeability analysis, but differences in methodology do affect final results. Details of each method are described below.

Pressure – Decay Profile Permeameter (PDPK)

Profile, or Probe, Permeability measurements were performed on the core samples with "as received" fluid saturations in place. Profile permeability was measured using Core Laboratories' PDPK by flowing nitrogen gas through a portion of the sample. A probe was seated on the surface of the core as nitrogen under pressure was allowed to decay through the probe and into the core surface. The decay of the initial pressure was monitored versus time and permeability to air was then calculated automatically using the pressure decay versus time data.

The resulting permeability to air ranged from 0.0922 to 2810 millidarcies, however, only seventy-seven (77) samples were actually tested. From the sample depths selected, sample 19 (8382.00 feet) from the Cost B-3 well was unsuitable for PDPK testing and no material was available for Sample 53 (5962 feet) and sample 58 (6798 feet) from the Mobil 544-1 well and from Sample 77 (12386.50 feet) from the Exxon 599-1 well. Also, sample 59 (7096.00 feet), from the Mobil 544-1 well, failed during testing so permeability results may be inaccurate for this sample.

Automated Core Measurement System (CMS-300™)

The forty (40) 1-inch diameter plugs that were drilled using nitrogen gas were cleaned by Soxhlet extraction, using cycles of chloroform/methanol azeotrope and methanol, until the samples were salt free. The samples were dried in a convection oven and then the automated CMS-300™ was used to determine porosity and unsteady-state permeability. The data collected by the CMS-300™ allows determination of pore volume and porosity using Boyle's Law, Klinkenberg permeability (K_{inf}), the gas slippage factor to helium (b_{He},psi) the Forcheimer inertial resistance ("turbulence") factor beta (β, ft), and Alpha (α). The terms b, β and α can have significant effects on permeability calculations for tight cores (see procedures for explanation of terms).

For operation of the CMS-300 system each dried core plug was automatically loaded into a core holder from a carousel and 800 psi net confining stress was applied. Pressurized helium was discharged into one end of the sample from a reference cell and vented to the atmosphere from the other end. The pressure decay was monitored with time. Examination of the test results show that the Klinkenberg permeabilities ranged from 0.001 to 286 millidarcies and permeabilities to air ranged from 0.004 to 318 millidarcies. The porosities ranged from 3.40 to 30.3 percent.

Comparison of Results

A review of the data show different permeability results for PDPK and CMS-300 measurements.

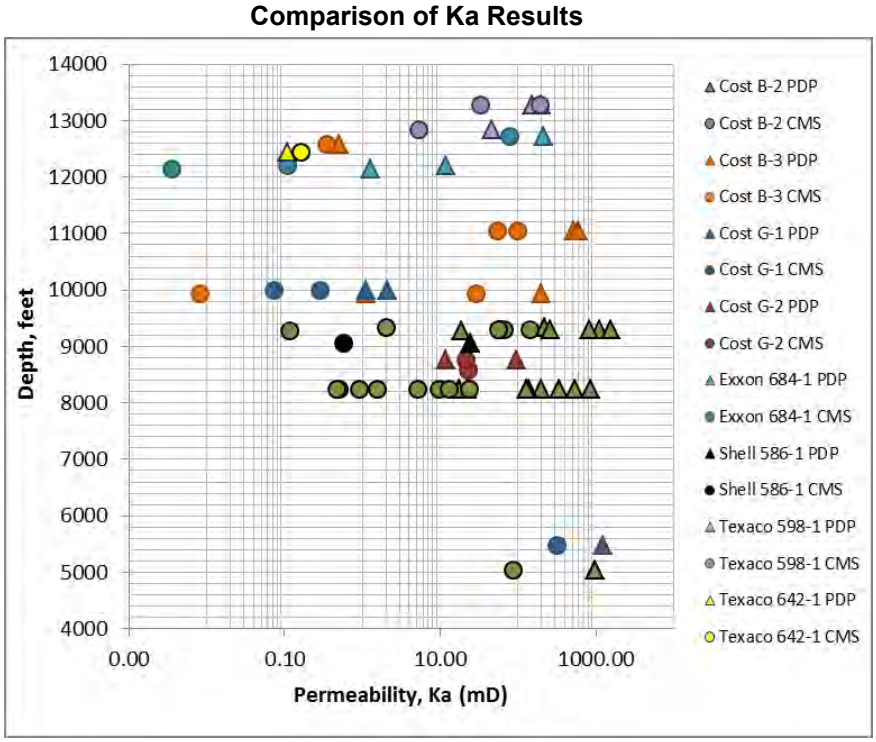

The samples appear to have some clays associated within the pore space. Clay morphology can be altered depending on how the samples were preserved or handled. Platy clays (montmorillite or chlorite booklets) generally show no damage, but smectite or illite types of clays often cause permeability issues. Further analysis would be necessary to identify clay types.

Some difference can also be attributed to the plug permeability and the probe permeability methodology. Most core plugs are taken in the horizontal direction, parallel to the bedding direction, to provide the better permeability values. The samples tested with probe permeability may have duplicate permeability values when compared to CMS measurements, unless the measurement was determined at a point that is not in the preferred bedding direction. In cases where bedding direction was ambiguous, measurements could have been determined perpendicular to preferred bedding direction, resulting in lower permeability values. Also, if samples were very friable, there may have been an insufficient seal from the probe permeability equipment, which can cause permeability variation. Lastly, the grain size and sandstone cements will affect permeability values. Variability in the depositional environment can produce variability in the permeability.

If further analysis is required, we recommend investigating the mineralogy with SEM and thin section analyses. It is possible that differences in rock fabric, mineralogy, or pore throat systems are affecting these results. Experience with other formations has demonstrated that changes in these properties from well to well, even within the same field, are not unusual.

TEST SCHEDULE SUMMARY

Company: Delaware Geological Survey, University of Delaware
CO_2 Storage Resource Assessment Project

File: HOU-1703089

Sample Number	Well	Formation	Depth, feet	Profile Permeability to Gas - PDPK	Basic Properties - CMS-300 (plugs)
1	COST B-2	Wyandot	5030.20	X	
P-1	COST B-2	Wyandot	5030.30		X
2	COST B-2	Wyandot	5031.20	X	
P-11	COST B-2	U. Logan Canyon	8239.00		X
12	COST B-2	U. Logan Canyon	8239.50	X	
13	COST B-2	U. Logan Canyon	8240.50	X	
3	COST B-2	U. Logan Canyon	8241.00	X	
P-2	COST B-2	U. Logan Canyon	8241.30		X
14	COST B-2	U. Logan Canyon	8242.00	X	
P-12	COST B-2	U. Logan Canyon	8242.10		X
4	COST B-2	U. Logan Canyon	8244.00	X	
P-3	COST B-2	U. Logan Canyon	8244.10		X
5	COST B-2	U. Logan Canyon	8247.00	X	
P-4	COST B-2	U. Logan Canyon	8247.05		X
15	COST B-2	U. Logan Canyon	8249.00	X	
P-13	COST B-2	U. Logan Canyon	8249.10		X
P-5	COST B-2	U. Logan Canyon	8249.90		X
6	COST B-2	U. Logan Canyon	8250.00	X	
P-6	COST B-2	U. Logan Canyon	8251.00		X
7	COST B-2	U. Logan Canyon	8251.80	X	
P-7	COST B-2	L. Logan Canyon	9286.00		X
8	COST B-2	L. Logan Canyon	9286.50	X	
P-14	COST B-2	L. Logan Canyon	9289.15		X
16	COST B-2	L. Logan Canyon	9289.30	X	
9	COST B-2	L. Logan Canyon	9302.00	X	
P-8	COST B-2	L. Logan Canyon	9302.15		X
17	COST B-2	L. Logan Canyon	9304.40	X	
P-15	COST B-2	L. Logan Canyon	9304.50		X
10	COST B-2	L. Logan Canyon	9305.40	X	
P-9	COST B-2	L. Logan Canyon	9305.60		X
11	COST B-2	L. Logan Canyon	9330.20	X	
P-10	COST B-2	L. Logan Canyon	9330.30		X
26	COST B-3	Dawson Canyon	6260.00	X	
27	COST B-3	Dawson Canyon	7040.00	X	
18	COST B-3	Dawson Canyon	7640.00	X	
19	COST B-3	U. Logan Canyon	8382.00	X	
20	COST B-3	Naskapi	9750.00	X	
P-16	COST B-3	Mississauga	9931.00		X
21	COST B-3	Mississauga	9931.60	X	
22	COST B-3	Mississauga	9932.00	X	
P-17	COST B-3	Mississauga	9932.00		X

TEST SCHEDULE SUMMARY

Company: Delaware Geological Survey, University of Delaware
CO_2 Storage Resource Assessment Project

File: HOU-1703089

Sample Number	Well	Formation	Depth, feet	Profile Permeability to Gas - PDPK	Basic Properties - CMS-300 (plugs)
28	COST B-3	Mississauga	9934.00	X	
P-20	COST B-3	Mississauga	9934.00		X
23	COST B-3	Mississauga	11042.00	X	
P-18	COST B-3	Mississauga	11050.00		X
24	COST B-3	Mississauga	11050.80	X	
25	COST B-3	Mississauga	11054.00	X	
P-19	COST B-3	Mississauga	11054.10		X
29	COST B-3	Mohawk	12581.90	X	
P-21	COST B-3	Mohawk	12581.90		X
35	COST G-1	Mic-Mac	5471.00	X	
30	COST G-1	Mic-Mac	5473.00	X	
P-22	COST G-1	Mic-Mac	5473.00		X
P-23	COST G-1	Mic-Mac	5480.40		X
P-25	COST G-1	Mohawk	9992.05		X
36	COST G-1	Mohawk	9992.80	X	
37	COST G-1	Mohawk	9992.80	X	
P-24	COST G-1	Mohawk	10001.10		X
33	COST G-1	Mohawk	10001.30	X	
34	COST G-1	Mohawk	10001.30	X	
31	COST G-1	Mic-Mac	5480.00 - 5481.00	X	
32	COST G-1	Mic-Mac	5480.00 - 5481.00	X	
P-26	COST G-2	Mohawk	8573.00		X
38	COST G-2	Mohawk	8753.70	X	
39	COST G-2	Mohawk	8756.00	X	
40	COST G-2	Mohawk	8756.00	X	
P-27	COST G-2	Mohawk	8756.00		X
77	Exxon 599-1	Mic Mac	12386.50	X	
P-38	Exxon 599-1	Mic Mac	12386.50		X
78	Exxon 599-1	Mic Mac	12403.00	X	
41	Exxon 684-1	Naskapi	9438.00	X	
P-28	Exxon 684-1	Naskapi	9438.00		X
42	Exxon 684-1	Naskapi	9439.00	X	
47	Exxon 684-1	Naskapi	9440.00	X	
48	Exxon 684-1	Naskapi	9441.00	X	
43	Exxon 684-1	Mic-Mac	12137.00	X	
P-29	Exxon 684-1	Mic-Mac	12137.00		X
44	Exxon 684-1	Mic-Mac	12199.00	X	
49	Exxon 684-1	Mic-Mac	12204.00	X	
P-30	Exxon 684-1	Mic-Mac	12204.00		X
50	Exxon 684-1	Mohawk	12729.00	X	
P-31	Exxon 684-1	Mohawk	12729.00		X

TEST SCHEDULE SUMMARY

Company: Delaware Geological Survey, University of Delaware
CO_2 Storage Resource Assessment Project

File: HOU-1703089

Sample Number	Well	Formation	Depth, feet	Profile Permeability to Gas - PDPK	Basic Properties - CMS-300 (plugs)
45	Exxon 684-1	Mohawk	12767.00	X	
46	Exxon 684-1	Mohawk	12802.00	X	
63	Exxon 684-2	Mohawk	15242.00	X	
P-39	Exxon 684-2	Mohawk	15242.00		X
51	Mobil 544-1	Dawson Canyon	5211.00	X	
P-32	Mobil 544-1	Dawson Canyon	5211.00		X
52	Mobil 544-1	Dawson Canyon	5435.00	X	
53	Mobil 544-1	Dawson Canyon	5962.00	X	
54	Mobil 544-1	Dawson Canyon	6260.00	X	
55	Mobil 544-1	Dawson Canyon	6420.00	X	
56	Mobil 544-1	Dawson Canyon	6579.00	X	
57	Mobil 544-1	Dawson Canyon	6696.00	X	
58	Mobil 544-1	Dawson Canyon	6798.00	X	
59	Mobil 544-1	Dawson Canyon	7096.00	X	
60	Mobil 544-1	Naskapi	7258.00	X	
61	Mobil 544-1	Mississauga	8497.00	X	
62	Mobil 544-1	Mississauga	9039.00	X	
64	Shell 273-1	Dawson Canyon	7010.00	X	
65	Shell 273-1	Dawson Canyon	7077.00	X	
79	Shell 372-1		10872.90 - 10873.20	X	
80	Shell 372-1		10872.90 - 10873.20	X	
P-33	Shell 586-1	Logan Canyon	9058.30		X
66	Shell 586-1	Logan Canyon	9058.00 - 9058.70	X	
67	Shell 586-1	Logan Canyon	9058.00 - 9058.70	X	
81	Shell 587-1		11554.90	X	
68	Shell 632-1	Dawson Canyon	4594.50	X	
69	Shell 632-1	Logan Canyon	6278.80	X	
70	Shell 632-1	Mississauga	8083.10	X	
P-40	Shell 632-1	Mississauga	8083.10		X
71	Shell 93-1	Mississauga	9937.00	X	
72	Texaco 598-1	Mohawk	12840.50	X	
P-34	Texaco 598-1	Mohawk	12840.50		X
P-35	Texaco 598-1	Mohawk	13271.00		X
P-36	Texaco 598-1	Mohawk	13275.00		X
73	Texaco 598-1	Mohawk	13271.00 - 13272.00	X	
74	Texaco 598-1	Mohawk	13275.00 - 13276.00	X	
75	Texaco 642-1	Mic Mac	12444.00	X	
P-37	Texaco 642-1	Mic Mac	12444.00		X
76	Texaco 642-1	Mohawk	15608.00	X	

Note: "P-" indicates drilled 1-inch PLUG sample

Petrophysical Properties

Profile Permeameter Analysis
CMS-300TM Conventional Plug Analysis

University of Delaware
Various Wells

CL File No.: 201703089
Date: 11/14/17
Analyst(s): JDH-IM

PROFILE PERMEAMETRY ANALYSIS PROTOCOL

Permeability

Multiple chunk samples from various wells were received. Probe permeability was determined on all available samples.

An o-ring tipped probe was seated on the surface of the core. A reference cell was filled with nitrogen gas to a predetermined pressure.

Once equilibrated, the pressure was allowed to decay through the probe and into the core surface. A decay of the initial pressure was monitored versus time. Permeability was then calculated using the pressure decay versus time data.

Sample Preparation

After PDPK measurements, 40 pieces of core material were identified and drilled for 1-inch diamter plug samples.

University of Delaware
Various Wells

CL File No.: 201703089
Date: 11/14/17
Analyst(s): JDH-LA

PROFILE PERMEABILITY MEASUREMENTS

No	Well	Formation	Depth	Ka (mD)	Footnote
1	COST B-2	Wyandot	5030.2	990	
2	COST B-2	Wyandot	5031.2	13.3	
3	COST B-2	U. Logan Canyon	8241	202	
4	COST B-2	U. Logan Canyon	8244	338	
5	COST B-2	U. Logan Canyon	8247	22.5	
6	COST B-2	U. Logan Canyon	8250	137	
7	COST B-2	U. Logan Canyon	8251.8	17.3	
8	COST B-2	L. Logan Canyon	9286.5	18.5	
9	COST B-2	L. Logan Canyon	9302	1110	
10	COST B-2	L. Logan Canyon	9305.4	1580	
11	COST B-2	L. Logan Canyon	9330.2	223	
12	COST B-2	U. Logan Canyon	8239.5	542	
13	COST B-2	U. Logan Canyon	8240.5	171	
14	COST B-2	U. Logan Canyon	8242	861	
15	COST B-2	U. Logan Canyon	8249	130	
16	COST B-2	L. Logan Canyon	9289.3	825	
17	COST B-2	L. Logan Canyon	9304.4	257	
18	COST B-3	Dawson Canyon	7640	0.388	
19	COST B-3	U. Logan Canyon	8382	NA	(1)
20	COST B-3	Naskapi	9750	185	
21	COST B-3	Mississauga	9931.6	0.158	
22	COST B-3	Mississauga	9932	198	
23	COST B-3	Mississauga	11042	2.4	
24	COST B-3	Mississauga	11050.8	514	
25	COST B-3	Mississauga	11054	602	
26	COST B-3	Dawson Canyon	6260	0.0922	
27	COST B-3	Dawson Canyon	7040	0.286	
28	COST B-3	Mississauga	9934	1.11	
29	COST B-3	Mohawk	12581.9	0.506	
30	COST G-1	Mic-Mac	5473	1220	
31	COST G-1	Mic-Mac	5480-5481	0.827	
32	COST G-1	Mic-Mac	5480-5481	0.2	
33	COST G-1	Mohawk	10001.3	2.06	
34	COST G-1	Mohawk	10001.3	34.1	
35	COST G-1	Mic-Mac	5471	1000	
36	COST G-1	Mohawk	9992.8	1.12	
37	COST G-1	Mohawk	9992.8	0.929	
38	COST G-2	Mohawk	8753.7	94.2	
39	COST G-2	Mohawk	8756	56.4	
40	COST G-2	Mohawk	8756	11.9	
41	Exxon 684-1	Naskapi	9438	1890	
42	Exxon 684-1	Naskapi	9439	2810	
43	Exxon 684-1	Mic-Mac	12137	1.27	
44	Exxon 684-1	Mic-Mac	12199	8.96	

University of Delaware
Various Wells

CL File No.: 201703089
Date: 11/14/17
Analyst(s): JDH-LA

PROFILE PERMEABILITY MEASUREMENTS

No	Well	Formation	Depth	Ka (mD)	Footnote
45	Exxon 684-1	Mohawk	12767	27.3	
46	Exxon 684-1	Mohawk	12802	921	
47	Exxon 684-1	Naskapi	9440	1440	
48	Exxon 684-1	Naskapi	9441	1640	
49	Exxon 684-1	Mic-Mac	12204	11.8	
50	Exxon 684-1	Mohawk	12729	212	
51	Mobil 544-1	Dawson Canyon	5211	279	
52	Mobil 544-1	Dawson Canyon	5435	275	
53	Mobil 544-1	Dawson Canyon	5962	NA	(2)
54	Mobil 544-1	Dawson Canyon	6260	12.3	
55	Mobil 544-1	Dawson Canyon	6420	0.604	
56	Mobil 544-1	Dawson Canyon	6579	1.24	
57	Mobil 544-1	Dawson Canyon	6696	1.56	
58	Mobil 544-1	Dawson Canyon	6798	NA	(2)
59	Mobil 544-1	Dawson Canyon	7096	2700	(3)
60	Mobil 544-1	Naskapi	7258	105	
61	Mobil 544-1	Mississauga	8497	1.66	
62	Mobil 544-1	Mississauga	9039	11.4	
63	Exxon 684-2	Mohawk	15242	11.6	
64	Shell 273-1	Dawson Canyon	7010	330	
65	Shell 273-1	Dawson Canyon	7077	2.74	
66	Shell 586-1	Logan Canyon	9058-9058.7	24.4	
67	Shell 586-1	Logan Canyon	9058-9058.7	10	
68	Shell 632-1	Dawson Canyon	4594.5	372	
69	Shell 632-1	Logan Canyon	6278.8	3.28	
70	Shell 632-1	Mississauga	8083.1	23.8	
71	Shell 93-1	Mississauga	9937	1320	
72	Texaco 598-1	Mohawk	12840.5	45.7	
73	Texaco 598-1	Mohawk	13271-13272	198	
74	Texaco 598-1	Mohawk	13275-13276	151	
75	Texaco 642-1	Mic Mac	12444	0.107	
76	Texaco 642-1	Mohawk	15608	30.6	
77	Exxon 599-1	Mic Mac	12386.5	NA	(2)
78	Exxon 599-1	Mic Mac	12403	1710	
79	Shell 372-1	N/A	10872.9-10873.2	0.584	
80	Shell 372-1	N/A	10872.9-10873.2	69.1	
81	Shell 587-1	N/A	11554.9	1.8	

Footnotes

(1) Sample unsuitable for profile permeability testing.

(2) No material available for testing.

(3) Sample failed during measurement, results may not be accurate.

University of Delaware
Various Wells

CL File No.: 201703089
Date: 11/14/17
Analyst(s): JDH-IM

CMS-300 CONVENTIONAL PLUG ANALYSIS PROTOCOL

Sample Preparation
1.0" diameter plugs were drilled with nitrogen gas and trimmed into right cylinders with a diamond-blade trim saw.
All sample trims were archived.

Core Extraction
Plugs selected for routine core analysis were placed in a Soxhlet extraction unit cycling between a chloroform / methanol (87:13) azeotrope and methanol until hydrocarbon and salt free.

Sample Drying
Samples were oven dried at 240° F to weight equilibrium (+/- 0.001 g).

Porosity
Porosity was determined using Boyle's Law technique by measuring grain volume at ambient conditions & pore volume at indicated net confining stresses (NCS)

Grain Density
Grain density values were calculated by direct measurement of grain volume and weight on dried plug samples.
Grain volume was measured by Boyle's Law technique.

Permeability
Permeability to air was measured on each sample using unsteady-state method at indicated NCS.

Fluid Saturations
Fluid saturations were determined by the Dean Stark technique using the following fluid properties:

Brine	1.032 g/cc (50000 ppm TDS)
Oil	0.845 g/cc (36° API)

University of Delaware
Various Wells

CL File No.: 201703089
Date: 11/14/17
Analyst(s): JDH-IM

EXPLANATION OF CMS-300 TERMS "b", "Beta, and "Alpha"

K_∞	=	Equivalent non-reactive liquid permeability, corrected for gas slippage, mD
K_{air}	=	Permeability to Air, calculated using K_∞ and b, mD
b	=	Klinkenberg slip factor, psi
β (Beta)	=	Forcheimer inertial resistance factor, ft^{-1}
α (Alpha)	=	A factor equal to the product of Beta and K_∞. This factor is employed in determining the pore level heterogeneity index, H_i.
H_i	=	$\log_{10}(\alpha\phi/RQI)$ α, microns = $3.238E^{-9}\ \beta K_\infty$
Ø	=	Porosity, fraction
RQI	=	Reservoir Quality Index, microns
RQI	=	$0.0314(K/\phi)^{0.5}$

For further information please refer to:

Jones, S.C.: "Two-Point Determination of Permeability and PV vs. Net Confining Stress" SPE Formation Evaluation (March 1988) 235-241.

Jones S.C.: "A Rapid Accurate Unsteady-State Klinkenberg Permeameter," Soc. Pet. Eng. J. (Oct. 1972) 383-397.

Jones, S.C.: "Using the Inertial Coefficient, β, To Characterize Heterogeneity in Reservoir Rock: SPE 16949 (September 1987).

Amaefule, J.O.; Kersey, D.G.; Marschall, D.M.; Powell, J.D.; Valencia, L.E.; Keelan, D.K.: "Reservoir Description: A Practical Synergistic Engineering and Geological Approach Based on Analysis of Core Data,: SPE Technical Conference (Oct. 1988) SPE 18167.

University of Delaware
Various Wells

CL File No.: 201703089
Date: 11/14/17
Analyst(s): JDH-IM

CMS-300 CONVENTIONAL PLUG ANALYSIS

Drilled Plug Sample Number	Well Name	Formation	Depth (ft)	Net Confining Stress (psig)	Porosity (%)	Permeability		b(air) psi	Beta ft(-1)	Alpha (microns)	Grain Density (g/cm^3)	Footnote
						Klinkenberg (md)	Kair (md)					
P-1	COST B-2	Wyandot	5030.30	800	19.51	71.3	85.8	3.48	2.99E+08	6.88E+01	2.693	(3)
P-2	COST B-2	U. Logan Canyon	8241.30	800	11.37	.321	.510	13.83	3.30E+11	3.36E+02	2.711	(3)
P-3	COST B-2	U. Logan Canyon	8244.10	800	17.13	7.57	9.52	5.01	4.13E+09	1.01E+02	2.696	(3)
P-4	COST B-2	U. Logan Canyon	8247.05	800	15.33	4.03	5.15	5.61	1.01E+10	1.31E+02	2.712	
P-5	COST B-2	U. Logan Canyon	8249.90	800	20.62	10.4	13.0	4.78	1.93E+09	6.45E+01	2.735	(3)
P-6	COST B-2	U. Logan Canyon	8251.00	800	11.96	.299	.469	13.48	2.19E+11	2.08E+02	2.706	(3)
P-7	COST B-2	L. Logan Canyon	9286.00	800	11.21	.037	.116	58.54	4.99E+11	5.80E+01	2.703	(3)
P-8	COST B-2	L. Logan Canyon	9302.15	800	23.62	44.6	57.4	5.05	4.29E+08	6.18E+01	2.750	(3)
P-9	COST B-2	L. Logan Canyon	9305.60	800	23.71	60.9	66.4	1.56	2.96E+08	5.81E+01	2.685	(3)
P-10	COST B-2	L. Logan Canyon	9330.30	800	22.62	1.36	2.01	10.24	7.24E+09	3.19E+01	2.704	(3)
P-11	COST B-2	U. Logan Canyon	8239.00	800	14.87	1.06	1.53	9.70	2.35E+10	8.01E+01	2.724	(3)
P-12	COST B-2	U. Logan Canyon	8242.10	800	20.52	18.9	23.6	4.52	1.37E+09	8.39E+01	2.711	(3)
P-13	COST B-2	U. Logan Canyon	8249.10	800	12.23	.622	.917	10.73	9.49E+10	1.89E+02	2.702	(3)
P-14	COST B-2	L. Logan Canyon	9289.15	800	25.49	40.6	55.6	6.54	5.38E+08	7.07E+01	2.669	
P-15	COST B-2	L. Logan Canyon	9304.50	800	23.74	115	143	4.07	1.59E+08	5.91E+01	2.682	(3)
P-16	COST B-3	Mississauga	9931.00	800	4.82	NA	NA	NA	NA	NA	2.715	(2)
P-17	COST B-3	Mississauga	9932.00	800	24.27	25.4	29.1	2.66	6.32E+08	5.17E+01	2.735	(3)
P-18	COST B-3	Mississauga	11050.00	800	25.01	85.0	98.2	2.65	1.61E+08	4.43E+01	2.660	(3)
P-19	COST B-3	Mississauga	11054.10	800	23.89	44.3	54.9	4.20	3.34E+08	4.79E+01	2.666	(3)
P-20	COST B-3	Mississauga	9934.00	800	3.64	.002	.008	109.69	3.12E+15	1.90E+04	2.692	(3)
P-21	COST B-3	Mohawk	12581.90	800	8.80	.251	.343	8.75	2.90E+12	2.36E+03	2.712	(3)
P-22	COST G-1	Mic-Mac	5473.00	800	30.29	287	318	1.76	4.45E+07	4.13E+01	2.662	
P-23	COST G-1	Mic-Mac	5480.40	800	13.03	5.43	5.81	1.39	3.52E+10	6.19E+02	2.729	(1)
P-24	COST G-1	Mohawk	10001.10	800	8.04	.238	.289	5.09	7.99E+12	6.17E+03	2.701	(3)
P-25	COST G-1	Mohawk	9992.05	800	4.91	.054	.073	9.27	2.61E+12	4.57E+02	2.701	(3)

University of Delaware
Various Wells

CL File No.: 201703089
Date: 11/14/17
Analyst(s): JDH-IM

CMS-300 CONVENTIONAL PLUG ANALYSIS

Drilled Plug Sample Number	Well Name	Formation	Depth (ft)	Net Confining Stress (psig)	Porosity (%)	Permeability		b(air) psi	Beta ft(-1)	Alpha (microns)	Grain Density (g/cm^3)	Footnote
						Klinkenberg (md)	Kair (md)					
P-26	COST G-2	Mohawk	8573.00	800	19.66	19.0	23.2	4.08	1.37E+09	8.42E+01	2.672	(3)
P-27	COST G-2	Mohawk	8756.00	800	18.05	17.5	21.6	4.34	1.52E+09	8.59E+01	2.670	(3)
P-28	Exxon 684-1	Naskapi	9438.00	Ambient	27.21	NA	NA	NA	NA	NA	2.685	(5)
P-29	Exxon 684-1	Mic-Mac	12137.00	800	3.58	.001	.004	157.87	4.97E+16	1.04E+05	2.690	(3)
P-30	Exxon 684-1	Mic-Mac	12204.00	800	3.94	.071	.108	13.61	4.32E+11	9.94E+01	2.609	(3)
P-31	Exxon 684-1	Mohawk	12729.00	800	17.20	66.4	79.2	3.34	2.92E+08	6.28E+01	2.645	(3)
P-32	Mobil 544-1	Dawson Canyon	5211.00	NA	NA	NA	NA	NA	NA	NA	NA	(6)
P-39	Exxon 684-2	Mohawk	15242.00	Ambient	10.90	NA	NA	NA	NA	NA	2.680	(5)
P-33	Shell 586-1	Logan Canyon	9058.30	800	17.01	.398	.570	10.10	3.48E+11	4.48E+02	2.709	(3)
P-40	Shell 632-1	Mississauga	8083.10	Ambient	18.50	NA	NA	NA	NA	NA	2.695	(5)
P-34	Texaco 598-1	Mohawk	12840.50	800	17.86	4.55	5.22	2.99	7.23E+09	1.06E+02	2.662	(3)
P-35	Texaco 598-1	Mohawk	13271.00	800	15.94	25.1	32.5	5.41	3.91E+08	3.17E+01	2.659	(3)
P-36	Texaco 598-1	Mohawk	13275.00	800	17.69	103	190	14.17	1.42E+08	4.75E+01	2.676	(3)
P-37	Texaco 642-1	Mic Mac	12444.00	800	3.39	.091	.164	20.56	1.37E+11	4.02E+01	2.677	(3)
P-38	Exxon 599-1	Mic Mac	12386.50	800	17.26	125	200	10.12	9.86E+07	3.98E+01	2.644	(3)

Footnotes :

(1) : Denotes fractured or chipped sample. Permeability and/or porosity may be optimistic.

(2) : Sample permeability below the measurement range of CMS-300 equipment at indicated net confining stress (NCS). Data unavailable.

(3) : Denotes very short sample, porosity may be optimistic due to lack of conformation of boot material to plug surface.

(5) : Denotes sample unsuitable for measurement at stress. Porosity determined using Archimedes bulk volume at ambient conditions.

(6) : Denotes sample failed during cleaning, no measurements possible.

Areas shaded to highlight separate wells.

Permeability greater than 0.1 mD measured using helium gas. Permeability less than 0.1 mD measured using nitrogen gas. All b values converted to b (air)

Attachment G: Task 5 Topical Report – Carbon Storage Resource Assessment Topical Report

Mid-Atlantic U.S. Offshore Carbon Storage Resource Assessment Project

Carbon Storage Resource Assessment Topical Report

MID-ATLANTIC U.S. OFFSHORE CARBON STORAGE RESOURCE ASSESSMENT PROJECT

DOE Award Number DE-FE0026087

Prepared by:

Battelle
505 King Avenue
Columbus, OH 43201-2696
Principal Investigator: Dr. Neeraj Gupta
Project Manager: Ms. Lydia Cumming

Prepared for:

The U.S. Department of Energy
National Energy Technology Laboratory
Program Manager: Mr. William O'Dowd

October 12, 2018

Disclaimer

This report was prepared as an account of work sponsored by an agency of the United States Government. Neither the United States Government, nor any agency thereof, nor any of their employees, makes any warranty, express or implied, or assumes any liability or responsibility for the accuracy, completeness, or usefulness of any information, apparatus, product, or process disclosed, or represents that its use would not infringe privately owned rights. Reference herein to any specific commercial product, process, or service by trade name, trademark, manufacturer, or otherwise does not necessarily constitute or imply its endorsement, recommendations, or favoring by the United States Government or any agency thereof. The views and the opinions of authors expressed herein do not necessarily state or reflect those of the United States Government or any agency thereof.

This technical summary report contains preliminary findings related to project progress and should not be considered final.

Acknowledgements

This material is based upon work supported by the Department of Energy under Award Number DE-FE0026087. The Project Team is led by Battelle and includes the state geological surveys of Delaware, Maryland, and Pennsylvania; United States Geological Survey (USGS); Lamont-Doherty Earth Observatory (LDEO) at Columbia University; Rutgers University. Harvard University; Texas Bureau of Economic Geology; and Virginia Department of Mines, Minerals, & Energy serve as technical advisors.

Battelle was responsible for the overall project execution, including project management and technical analysis. Dr. Neeraj Gupta was the Battelle Principal Investigator for this work and Ms. Lydia Cumming provided project management and technical coordination between team members. The Task 5 leader is Ms. Isis Fukai. Other Battelle Project Team members contributing to this report include Ms. Priya Ravi Ganesh, Dr. Heather McCarren, and Ms. Laura Keister.

Guidance on petrophysical calculation methods and mineralogical/geochemical data used for characterization of storage reservoir lithologies was provided by team members at the Pennsylvania Geological Survey (Ms. Kristin Carter, Mr. Brian Dunst, and Dr. Steve Shank). Correlation of seismic data with well log and biostratigraphy data for characterization of stratigraphic sequences was performed by Rutgers University (Dr. Kenneth Miller, Mr. William [John] Schmelz, Ms. Kimberly Baldwin, Mr. Stephen Graham, Ms. Leslie Jordan, and Dr. Gregory Mountain) and USGS (Dr. Uri ten Brink and Mr. Guy Lang [Haifa University]). Seismic inversion was performed by Dr. Will Fortin (LDEO). Petrophysical analysis relied on laboratory data prepared in previous tasks by team members at the Delaware Geological Survey (Drs. Mojisola KunleDare and Peter McLaughlin). Task 5 analysis also benefited from map data management and ArcGIS work by the Maryland Geological Survey (Mr. Andrew Stanley, Mr. David Andreasen, Ms. Heather Quinn, and Mr. Richard Ortt) and research performed by the Bureau of Ocean Energy Management and offshore drilling programs along the Mid-Atlantic from the 1970s to 1980s.

Table of Contents

List of Figures

Page

List of Tables

Acronyms and Abbreviations

2D	Two-dimensional
3D	Three-dimensional
API	American Petroleum Institute
BCT	Baltimore Canyon Trough
CCS	Carbon Capture and Storage
CMP	Common mid-point
CO_2	Carbon Dioxide
COST	Continental Offshore Stratigraphic Test
CSLF	Carbon Sequestration Leadership Forum
DPHI	Density Porosity Log
DT	Sonic Log
EDX	NETL Energy Data eXchange
ft	Foot
gAPI	American Petroleum Institute Gamma Ray Unit
GBB	Georges Bank Basin
GR	Gamma Ray
GSD	Great Stone Dome
Gt	Gigatonne
IEAGHG	International Energy Agency Greenhouse Gas
KB	Kelly Bushing
km	Kilometer
LDEO	Lamont-Doherty Earth Observatory
LK#	Lower Cretaceous Sequence Number
m	Meter
mD	Millidarcy
MK#	Middle Cretaceous Sequence Number
ms	Millisecond
Mt	Megatonne
NETL	National Energy Technology Laboratory
NPHI	Neutron Porosity
OCS	Outer Continental Shelf
Pa	Pascal
PE	Photo-electric
PHI	Porosity
psi	Pounds per Square Inch
QA/QC	Quality Assurance/Quality Control
RHOB	Bulk Density
SLA	Submerged Lands Act
SPE-SRMS	Society of Petroleum Engineers Storage Resources Management System
TD	Total Depth (measured)
TVD	Total Vertical Depth
U.S. DOE	U.S. Department of Energy
UJ#	Upper Jurassic Sequence Number
UK#	Upper Cretaceous Sequence Number
USGS	United States Geological Survey
Vp	Primary-wave velocity
Vs	Secondary-wave velocity
XRD	X-ray Diffraction
XRF	X-ray Fluorescence

Executive Summary

The Mid-Atlantic U.S. Offshore Carbon Storage Resource Assessment Project (FE0026087) is part of the United States Department of Energy (DOE) National Energy Technology Laboratory's (NETL) Carbon Storage program to improve the effectiveness and reduce the costs of carbon dioxide (CO_2) storage implementation. The objectives of the Mid-Atlantic U.S. Offshore Carbon Storage Resource Assessment Project are to: 1) complete a systematic carbon storage resource assessment of the offshore Mid-Atlantic coastal region from the Georges Bank Basin (GBB) through the Long Island Platform to the southern Baltimore Canyon Trough (BCT); 2) define key input parameters to reduce uncertainty for offshore resource assessment and efficiency estimates; 3) examine risk factors; and 4) engage industry and regulatory stakeholders through development of a road map to assist future project planning and implementation.

This work fits into DOE's larger effort to develop carbon capture and storage (CCS) as an option for future investment in low-carbon energy. To support development of CCS applications, it is important that the United States develop a detailed geologic assessment of the carbon storage resources on a regional basis. Identifying commercial-ready storage sites is critical for deployment of advanced CO_2 capture technologies. The project will help to establish the foundation for future CCS development in the offshore environment when the market conditions are appropriate.

This Task 5 deliverable provides an interim report on the CO_2 storage resource calculation workflow and results. Regional-scale prospective CO_2 storage resources have been estimated for three potential deep saline storage zones to establish preliminary, screening-level constraints on the geologic storage resources available in the Mid-Atlantic offshore study region. Results of the regional analysis were used to delineate a selected area for refinement of storage resource estimates via dynamic injection and storage simulation.

Factors evaluated in previous tasks (e.g., Task 2, 4, and 6) such as basin age/maturity, and sediment lithification were used to establish screening criteria to identify offshore sub-region(s) with suitable conditions for storage resource calculations. Sandstone sequences in Middle Cretaceous (MK1-3), Lower Cretaceous (LK1), and Upper Jurassic (UJ1) strata were identified as three potential deep saline storage zones. A comprehensive data integration process involving iterative comparison and correlation of core, log, and seismic data was conducted to quantify and map petrophysical properties, pore volumes, and storage efficiency values for the MK1-3, LK1, and UJ1 storage zones.

The key outcomes for Task 5 include the following:

- Formation-specific storage efficiency probability values were calculated, with geologic storage efficiency factors exhibiting a range of 0.10 - 0.58 (P10-P90) based on the combined net-to-total pore volume dataset from the three offshore storage zones. Low and high probability values ranging from 0.09 to 0.26, respectively, were estimated for displacement efficiency factors based on the distribution of results from regional dynamic simulations in the MK1-3 zone.
- Regional prospective storage resources were calculated and mapped, and results from the three storage zones range from 37 gigatonnes (Gt) to 403 Gt of CO_2 (Table ES-1). Figure ES-1 shows the regional prospective storage resource map (P50) for the MK1-3 zone. Storage resources greater than 2.4 megatonnes (Mt) CO_2/km^2 are observed in the northern Baltimore Canyon Trough (BCT) near the Great Stone Dome (GSD) structure.

- Simplified dynamic reservoir simulation performed for a selected area near the GSD suggests 45 Mt to 51 Mt of CO_2 could potentially be stored at the end of 30 years for the specific injection scenario (single injection well in one 51-meter (m)-thick reservoir interval within the MK1-3 zone) and pressure constraints evaluated.

Table ES-1. High (P90), median (P50), and low (P10) values of prospective CO_2 storage resource estimates for the three offshore storage zones of interest.

Storage Zone	Total Prospective Storage Resources (Gt)		
	P10	P50	P90
MK1-3	37	148	378
LK1	59	178	403
UJ1	54	153	355

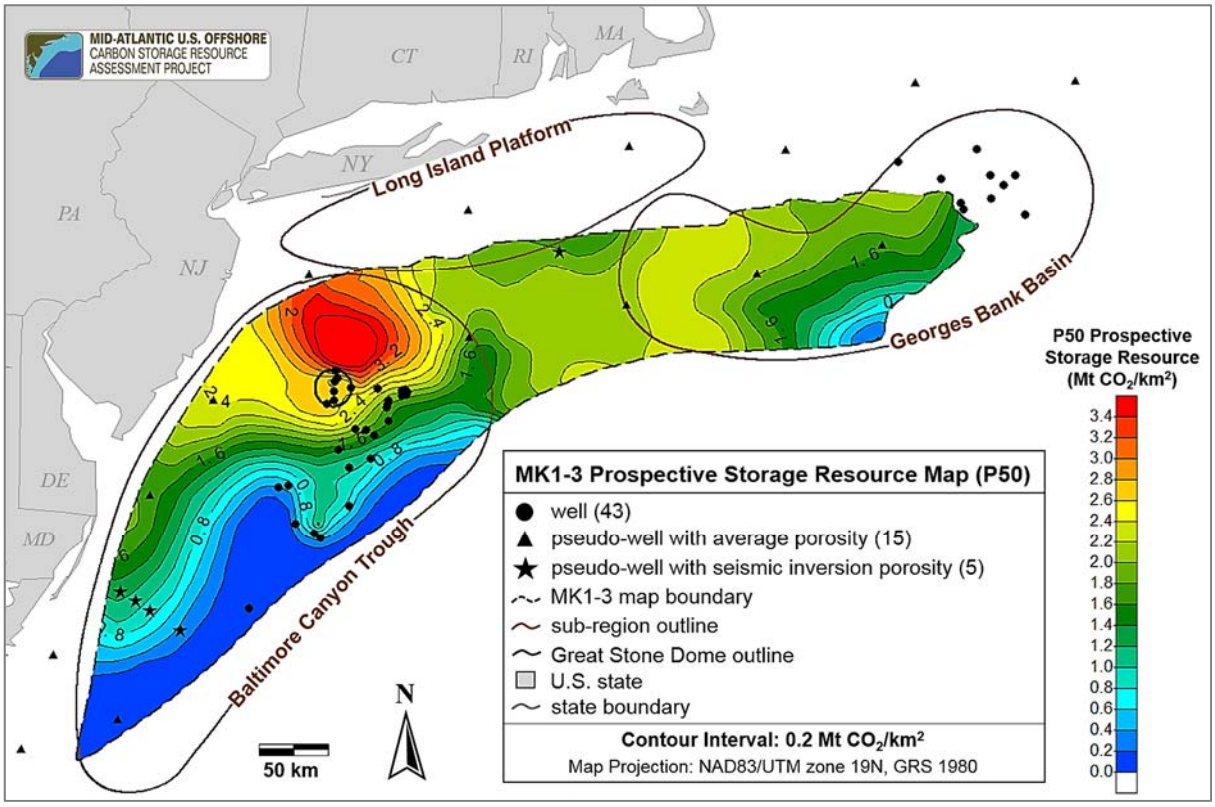

Figure ES-1. Map showing prospective storage resource estimates in Mt CO_2 per square kilometer (km^2) for MK1-3.

The report concludes with recommendations for future research. Additional subsurface data acquisition and analysis is needed to reduce uncertainty and data gaps within the offshore study region. Development of a three-dimensional (3D) static earth model would help to better characterize the geospatial variability of accessible pore volumes, reservoir injectivity, caprock/confining mechanisms, and estimated storage resources in the selected area of the northern BCT. Additional analysis should also consider potential regulatory issues, storage site requirements, and affected communities in the Mid-Atlantic region.

1.0 Introduction

1.1 Project Overview

The Mid-Atlantic U.S. Offshore Carbon Storage Resource Assessment Project (FE0026087) is part of the United States Department of Energy (DOE) National Energy Technology Laboratory's (NETL) Carbon Storage program to improve the effectiveness and reduce the costs of carbon dioxide (CO_2) storage implementation. This project aims to develop an informative picture of offshore storage potential and viable geologic storage options for the Mid-Atlantic United States (Figure 1).

The objectives of this project are to: 1) complete a systematic carbon storage resource assessment of the Mid-Atlantic offshore study area; 2) define key input parameters to reduce uncertainty for offshore resource assessment and efficiency estimates; 3) examine risk factors that may impact storage resource estimates; and 4) engage industry and regulatory stakeholders through development of a road map to assist future project planning and implementation.

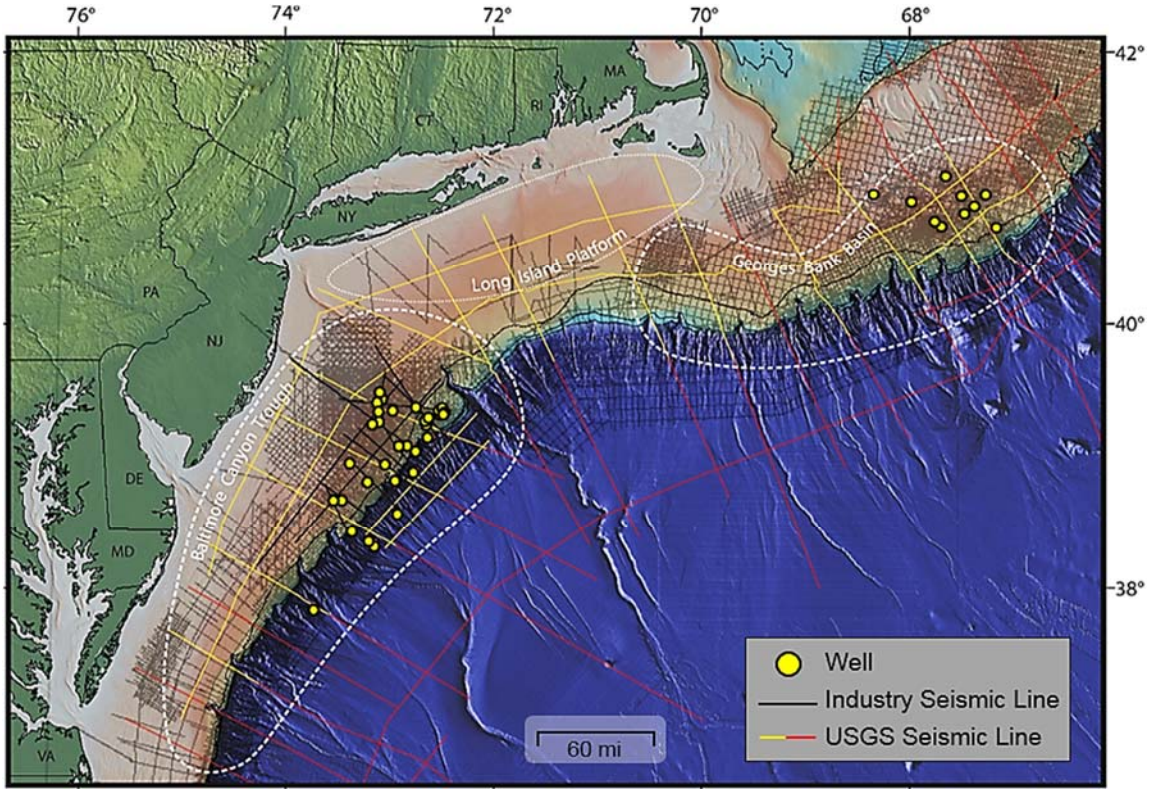

Figure 1. Map of the Mid-Atlantic Offshore Carbon Storage Resource Assessment Project study area showing outlines of the three main sub-regions with the locations of wells and seismic lines.

Note: Dashed lines approximate the sub-region outlines based on minimum of 5-kilometer (km) sediment thickness.

This study involves compilation and integration of data from a variety of sources, including: geologic samples from research boreholes and Continental Offshore Stratigraphic Test (COST) wells, and petroleum exploration wells; analog data from onshore coastal plain studies; and publicly available seismic survey data.

The anticipated outcomes include a regional-scale storage resource assessment for areas of the Mid-Atlantic not previously characterized, and storage resource estimates for geographically expansive offshore geologic units, including site selection criteria, offshore-specific storage efficiency factors, and refined storage estimates for a selected area using dynamic reservoir simulation methods.

The project is led by Battelle in Columbus, Ohio. The Project Team includes the state geological surveys of Maryland, Delaware, and Pennsylvania; the United States Geological Survey (USGS)/Haifa University; Rutgers University; and Lamont-Doherty Earth Observatory (LDEO) at Columbia University. In addition, team members from Harvard University, the Texas Bureau of Economic Geology, and the Virginia Department of Mines, Minerals, & Energy serve as technical advisors to the Project Team.

1.2 Study Area and Geologic Background

The Mid-Atlantic offshore study area encompasses nearly 171,000 km^2 along the Mid-Atlantic states of Virginia, Maryland, Delaware, New York, New Jersey, and Pennsylvania (see Figure 1). The study area comprises three major sub-regions: Georges Bank Basin (GBB), Long Island Platform, and Baltimore Canyon Trough (BCT). The project study area extends from within 10 kilometers (km) to 300 km offshore, encompassing the inner continental shelf to portions of the continental slope. Water depths in the Mid-Atlantic continental shelf grade gently from zero depth along the shoreline to the depths of 100 to 200 meters (m) at the shelf edge. Along the continental slope, water depths increase to more than 2,000 m into the North Atlantic Basin.

The Mid-Atlantic U.S. passive continental margin contains thick (2 to 16 km) post-rift Lower Jurassic and younger sediments in offshore basins, and thinner (0 to 2.4 km) uppermost Jurassic to Holocene sediments on the onshore coastal plain (e.g., Grow and Sheridan, 1988). Rifting occurred during the Late Triassic to earliest Jurassic (230 to 198 million years ago [Ma]) followed by extrusion of Early Jurassic seaward dipping basalts. A south-to-north onset of seafloor spreading is associated with a diachronous post-rift unconformity that separates active “rift-stage” deposits from more passive margin deposits that accumulated in an ever-widening and deepening basin open to the ocean. Subsidence began offshore in the Early Jurassic and progressively moved onshore from the Late Jurassic to Early Cretaceous (ca. 150 to 125 Ma) as a thermo-flexural response to increasing crustal rigidity (Watts, 1981; Grow and Sheridan, 1988; Olsson et al., 1988). The region has a well-preserved record of relative sea-level changes (e.g., Olsson et al., 1988; Miller et al., 2005).

The Mid-Atlantic offshore basins contain a thick succession of Jurassic to Paleogene sedimentary rocks above crystalline basement that lie at depths of 5 to 15 km. The sedimentary rocks of interest as caprocks and storage zones consist of Jurassic and Cretaceous-age mudstone/shale and sandstone sequences that generally dip to the east-southeast toward the continental slope (Libby-French, 1984). Previous studies have identified porous and permeable sandstone units in Middle Cretaceous, Lower Cretaceous, and Upper Jurassic sequences at depths ranging from approximately 800 to 4000 m (e.g., Amato and Bebout,1980; Scholle, 1977; Slater 2010; New Jersey Geological Survey, 2011). This interval is overlain by Upper Cretaceous mudstone and shale that extends regionally across the study area and is considered to be a potential caprock.

Structural and stratigraphic traps have been identified in each offshore basin area via analysis of 2-dimensional (2D) seismic lines and sequence stratigraphic relationships (e.g., Scholle, 1977; Schlee, 1980; Brown et al., 2011; New Jersey Geological Survey, 2011). In the northern BCT, structural closures form above an Early Cretaceous igneous intrusion called the Great Stone Dome (GSD) and structural highs interpreted as broad grabens and/or deeply buried reef

deposits atop carbonate platforms (e.g., Schlee et al., 1976; Poag, 1978; Jansa and Pe-Piper, 1988). In the northeastern GBB, the structure of Lower Cretaceous and Upper Jurassic strata is dominated by the Yarmouth Arch, with beds dipping away from the NW-SE oriented axis of the arch (Smith et al., 1976; Savva et al., 2016). An additional feature is the presence of buried Mesozoic rift basins largely in the Long Island Platform (Olsen, 1997; Hutchinson, 1986). Case studies from the northern Newark basin (onshore New York Metropolitan area) suggest that storage mechanisms at this onshore basin may translate to analog Mesozoic rift basins offshore in the Long Island Platform (e.g., Post and Coleman, 2015).

Preliminary static storage resource estimates reported in previous work suggest significant storage potential in Cretaceous-age sandstones in the northern BCT (Cumming et al., 2017; New Jersey Geological Survey, 2011). Previous dynamic simulation studies report total injection rates as high as 6 Mt of CO_2 per year achieved in Cretaceous sediments via eight injection wells in the northern BCT (Brown et al., 2011).

1.3 Task 5 Objectives

Storage resource assessment is a critical component of the site screening and characterization process necessary to advance development of deep geologic resources for CO_2 storage in a region. Regional static volumetric CO_2 storage estimates and simplified dynamic models are useful for delineating prospective storage targets at the basin or sub-basin scale, and therefore play a key role in the initial stages of site screening and selection for a geologic CO_2 storage project (Frailey, 2013; DOE-NETL, 2013; Gorecki et al., 2015).

Prospective CO_2 storage resource estimates were calculated using static volumetric and dynamic methods to establish screening-level constraints on the regional-scale CO_2 storage potential of deep saline formations in the Mid-Atlantic offshore sub-regions. Results from each sub-region were used to delineate selected areas to refine static prospective resource estimates and conduct dynamic simulations of CO_2 injection and storage performance for zones of interest.

Task 5 has been divided into three main technical efforts: 1) data integration and physical property mapping; 2) regional-scale storage resource calculations; and 3) local-scale storage resource calculation refinement. This task involved integration of core, log, biostratigraphic, and seismic data to define the structural and stratigraphic framework of storage zones and caprocks, storage reservoir petrophysical properties, and pore volume estimates to calculate offshore-specific storage efficiency coefficients and storage resources for the deep saline formations of interest. A hierarchical approach was used to identify select areas to locally refine storage resource estimates, conduct dynamic simulations, and classify storage resources following guidelines established by the U.S. DOE-NETL and Society of Petroleum Engineer's (SPE's) Storage Resources Management System (DOE-NETL, 2017; SPE-Storage Resources Management System (SPE-SRMS), 2017).

2.0 Methods

2.1 Task 5 Workflow Overview

The volumetric methodology developed by DOE-NETL (DOE-NETL, 2008; 2010; Goodman et al., 2011) was used to quantify and map the prospective CO_2 storage resource of deep saline formations of interest for storage and identify potential sites for further evaluation in the study area. The general workflow for storage resource calculations is shown in Figure 2.

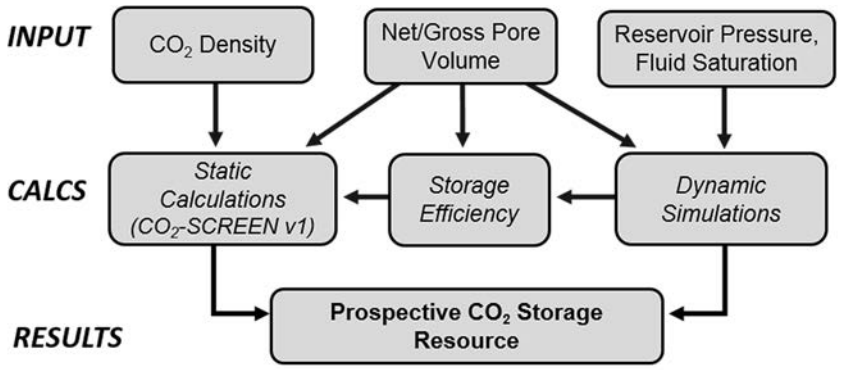

Figure 2. Schematic showing the general workflow used for storage resource calculations.

Factors such as basin age and maturity, sediment lithification, and hydrostatic pressures evaluated as part of the Risk Factors Assessment (Task 6) were incorporated into the following screening criteria to identify sub-region(s) with suitable conditions for storage resource calculations:

- Formation depth must be adequate (approximately 1,000 m [3,300 ft]) to ensure: (1) temperature and pressure conditions are sufficient to store CO_2 in a supercritical phase; (2) a consistent geothermal gradient is observed; and (3) the risk of soft-sediment deformation is minimized.
- A suitable seal/caprock must overlie the saline formation targeted for storage to inhibit the vertical migration of CO_2 to the surface.
- Hydrogeologic conditions such as structural, stratigraphic, and hydrodynamic traps must be in place to retain the injected CO_2 within the targeted storage zone(s).

The CO_2 storage resource of offshore deep saline formations was quantified via static and dynamic methods using well log, core, biostratigraphic, and seismic data. Well log correlations, biostratigraphic markers, and seismic correlations established in Tasks 2 and 3 were used to define the structural and stratigraphic framework for the storage zones of interest. This framework was integrated with petrophysical analysis of well logs, core, and hydrologic data compiled as part of Task 4 into 2D regional map grids to define reservoir pore volumes. Porosity-thickness maps were generated to evaluate the spatial distribution of pore volumes across the study area for the three storage zones. Individual depth, thickness, and porosity map grids were used as input for storage efficiency calculations and regional storage resource estimates. Results of the regional storage resource estimate for each storage zone were mapped, and the geospatial distribution of resources was evaluated along with data coverage/availability to delineate selected areas for dynamic storage simulations. All maps were

created in Petra® and/or Petrel® software using a GRS 1980 ellipsoidal map projection in zone 19N of the Universal Transverse Mercator coordinate system.

2.2 Storage Zone Structural and Stratigraphic Framework

2.2.1 Zone Definitions: Tops and Bases

Storage zone top and base depths were defined via comparison and integration of well log and seismic sequence stratigraphy, biostratigraphy, and well log and core lithostratigraphy. An initial quality assurance/quality control (QA/QC) procedure was performed for wells in the BCT and GBB to identify and correct unreliable data and misaligned interpretations to ensure seismic sequence horizons, well log sequence stratigraphic picks, and well log lithostratigraphic picks for the storage zones were consistent to within ± 100 m. The tops and bases of Cretaceous and Jurassic sequences were then correlated across wells in the study area to define three storage zones and two caprocks in the BCT (Figure 3) and three storage zones and three caprocks in the GBB (Figure 4).

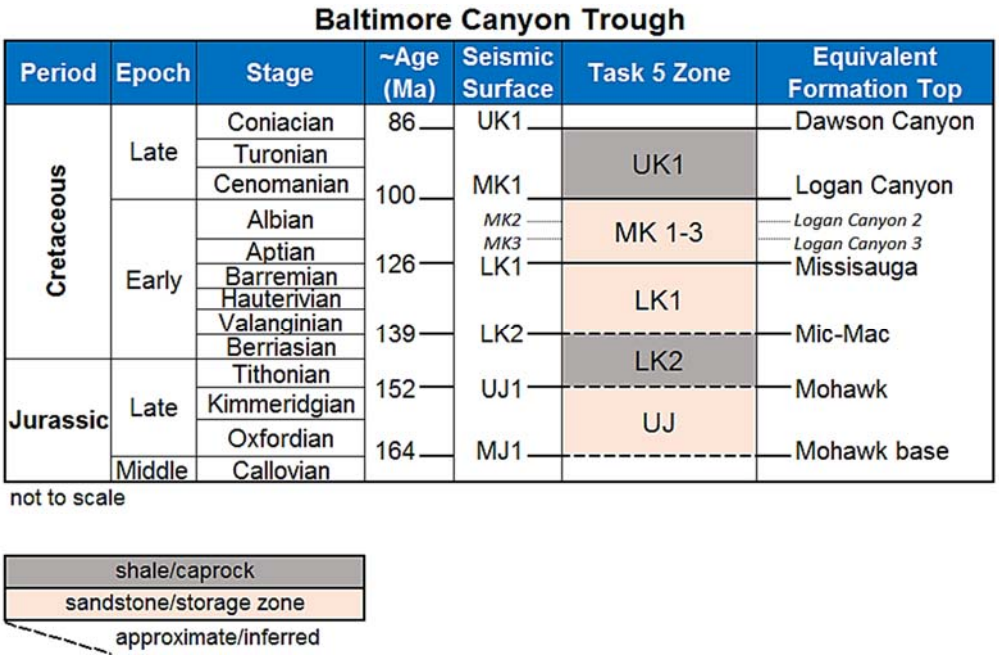

Figure 3. Correlation of chrono-, sequence-, and seismic stratigraphy and formation tops used to define Task 5 storage zone tops and bases for the BCT.

Note: These stratigraphic correlations and zone names are also assumed to apply to the western Long Island Platform with greater uncertainty due to the absence of wells.

At well locations in the BCT, sequence stratigraphic and biostratigraphic picks interpreted from well data were used to define the top depths of the regional UK1 caprock (Dawson Canyon Formation), the MK1-3 storage zone (Logan Canyon Formation), and the LK1 (Missisauga Formation) storage zone. Depths for the locally occurring LK2 caprock (Mic-Mac Formation), the UJ1 storage zone top (Mohawk sandstone), and the MJ1 top (Mohawk base) were defined in the BCT by lithostratigraphic interpretations and well log correlations, with picks chronostratigraphically constrained by biostratigraphy data when possible.

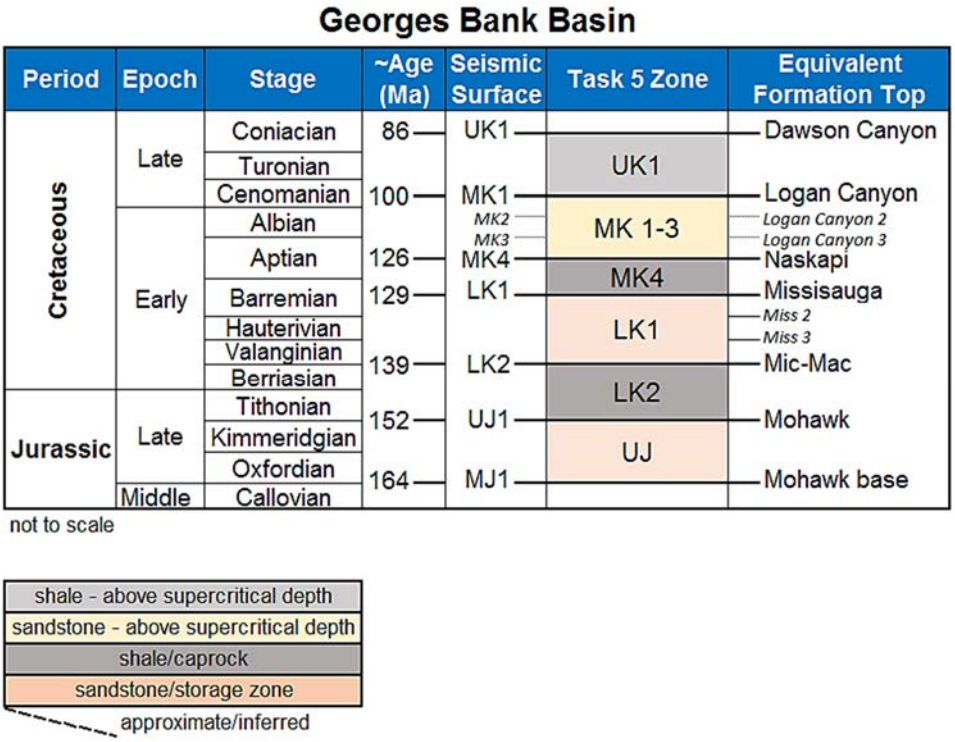

Figure 4. Correlation of chrono-, sequence-, and seismic stratigraphy and formation tops used to define Task 5 storage zone tops and bases for the GBB.

Note: These stratigraphic correlations and zone names are also assumed to apply to the eastern Long Island Platform with greater uncertainty due to the absence of wells.

In the GBB, the zones of interest include, in stratigraphic order from top to bottom: the regional UK1 caprock (Dawson Canyon Formation), the MK1-3 storage zone (Logan Canyon Formation), the locally occurring MK4 caprock (Naskapi Shale), the LK1 storage zone (Missisauga Formation), the locally occurring LK2 caprock (Mic-Mac Formation), and the UJ1 storage zone (Mohawk sandstone). At well locations, sequence stratigraphic and lithostratigraphic picks derived from well log interpretation/correlation were used to define top and base depths of all caprock and storage zones, with less biostratigraphic data available to constrain picks compared to wells in the BCT.

2.2.2 Seismic-Derived Map Grids and Calculation Boundaries

The structural and stratigraphic framework established at well locations was extended across the study region via integration with seismic data. A network of 2D seismic reflection data was tied to the available well log data and used to interpret caprock and storage zone depths, thicknesses, and continuity. Interpreted seismic horizons from Task 2 and 3 were depth-converted and integrated into one continuous, interpolated grid surface for each zone of interest to derive structural maps.

All geologic horizons were interpreted in the time domain from a combination of seismic data reprocessed as part of this project, and publicly available legacy seismic from the USGS and industry data. Localized and sub-basinal features in the BCT and GBB were integrated with basin-scale interpretations to establish a regionally consistent framework of geologic surfaces. All 2D time picks were converted to depth using the velocity functions established for the BCT,

GBB, and Long Island Platform in Klitgord et al. (1994). These depth-converted 2D interpretations were combined into one continuous, interpolated 2D surface with a grid spacing of 2,500 m for each zone of interest.

In order to verify the accuracy of the interpretation methodology and the time-to-depth conversions, the interpolated 3D depth surfaces were compared with correlative formation depths from well logs that penetrated the surfaces. Residual maps displaying graphically the difference between the depth of the interpolated, interpreted surface from seismic data and the depth of that same surface interpreted from well logs are shown in Table 1. Seismic surfaces were depth-shifted to match the well formation tops for surfaces UK1, MK1, LK1, and UJ1. As the uncertainty of the velocity model used to convert the seismic interpretation increases with depth, the depth residuals also increase. The residuals for surface MJ1 were skewed overwhelmingly in one direction and encouraged a collaborative re-interpretation of the geology, seismic surface, and petrophysical log character. After the re-interpretation, flexing of the MJ1 was not required. Maps showing the depth differences (residuals) between interpolated seismic surfaces and correlative formation tops from wells are included in Figure A-1 of Appendix A.

Table 1. Difference (residual values) between seismic surface and well tops for horizons UK1, MK1, LK1, UJ1, and MJ1 before re-interpretation.

Zone	UK1	MK1	LK1	UJ1	MJ1
Mean (m)	24	88	97	-176	573
Standard Deviation (m)	134	103	192	344	671

An initial storage resource calculation boundary was created for the Mid-Atlantic offshore region using the screening criteria discussed in Section 2.1, and the Submerged Lands Act (SLA) boundary located 3 nautical miles off the shoreline along U.S. states. The SLA defined the westernmost boundary of the polygon, with the northern, southern, and eastern extent defined by the limits of the reprocessed seismic data created during Task 3 of this project (e.g., Figure 1). Maps showing the boundary polygons created for each storage zone horizon are included in Figure A-2 of Appendix A.

The interpreted depth surfaces for each of the caprocks and storage zones were then cropped by using the initial calculation boundary polygon and applying a minimum depth cut-off of 1,000 m (3,300 ft.). Grid-to-grid calculations were applied to depth maps representing storage zone tops and bases to derive gross thickness maps (Figure 5). The depth and gross thickness maps for the three storage zones were then re-gridded to 300 grid cells to facilitate static storage resource calculations (Figure 5 and discussed in Section 2.4).

In addition to characterizing the storage reservoir units, this study delimited the geographic extent, depth, and thickness of the UK1 to evaluate the presence of a suitable caprock to inhibit the vertical migration of CO_2 to the surface. The shale-prone UK1 sequence (Dawson Canyon Formation) provides a laterally continuous seal having an average thickness of approximately 450 m across the study area with an average depth of 820 m (Figure 6). Mean depths and gross thicknesses, as well as standard deviations (σ), from the final map grids are listed in Table 2 for the UK1 caprock and the MK1-3, LK1, and UJ1 storage zones.

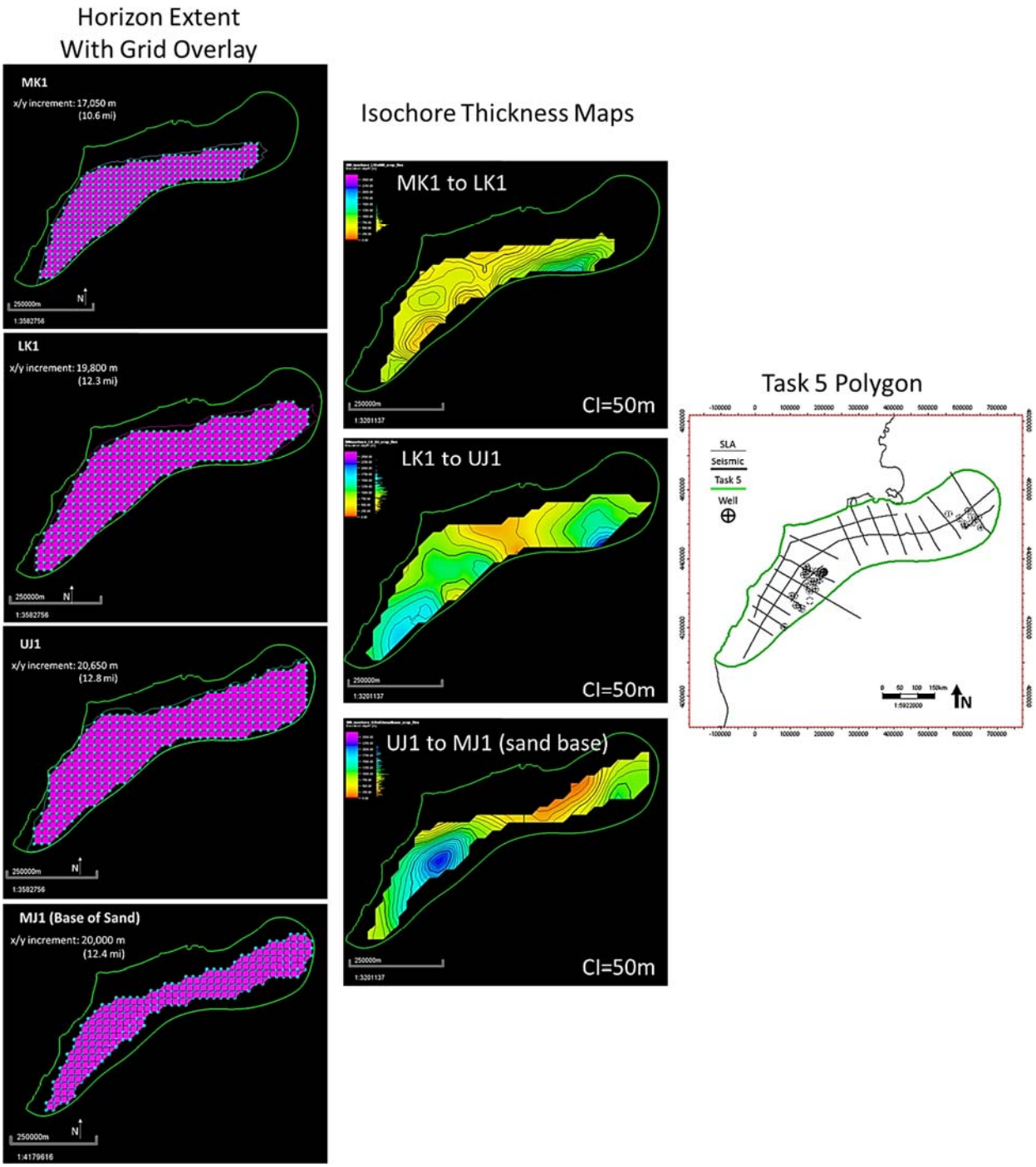

Figure 5. Geologic horizon extent with grid overlay for key storage horizons and resultant isochore thickness maps.

Table 2. Summary of depth and gross thickness data from map grids derived from seismic data.

Note that the UK1 is considered to be the primary caprock and storage volumetrics were not calculated.

Zone	Storage System Element	Interpreted Surfaces		Map Grid Cells		Depth (m)		Gross Thickness (m)	
		Top	Base	X-Y increment (km)	No. of cells	Mean	σ	Mean	σ
UK1	Caprock	UK1 top	MK1 top	NA	NA	820	643	448	247
MK1-3	Storage Reservoir	MK1 top	LK1 top	17.6	300	1,805	701	628	270
LK1	Storage Reservoir	LK1 top	LK1 base*	19.8	300	2,114	704	653	364
UJ1	Storage Reservoir	UJ1 top	UJ1 base	21.2	300	2,958	956	836	556

*Defined as LK2 top in GBB and BCT and UJ1 top in the Long Island Platform

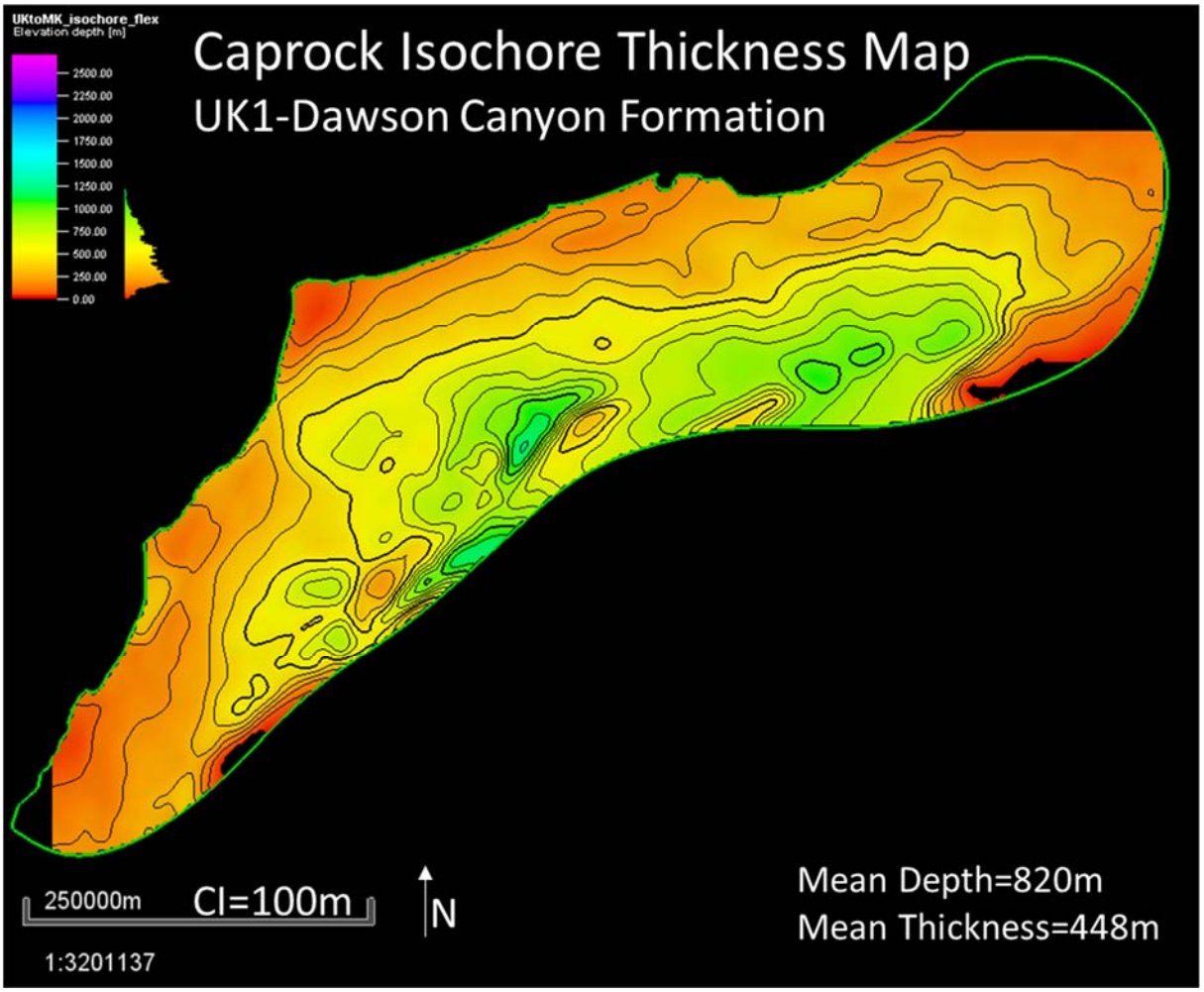

Figure 6. Isochore thickness map showing the Dawson Canyon Formation caprock interval.

2.3 Petrophysics

Petrophysical analysis was conducted for QA/QC purposes and to integrate all available core and log data in the study region to generate effective porosity and permeability logs needed for calculation of offshore-specific storage efficiencies and storage resource estimates. The workflow for core and log data integration and development of the effective porosity and permeability curves is shown in Figure 7. This general workflow was employed across all 43 wells in the three sub-regions (e.g., Figure 1). Detailed definitions of all petrophysical parameters evaluated in this study are provided in Table A-1 of Appendix A. All petrophysical calculations were conducted in Petra® for the three deep saline storage zones of interest.

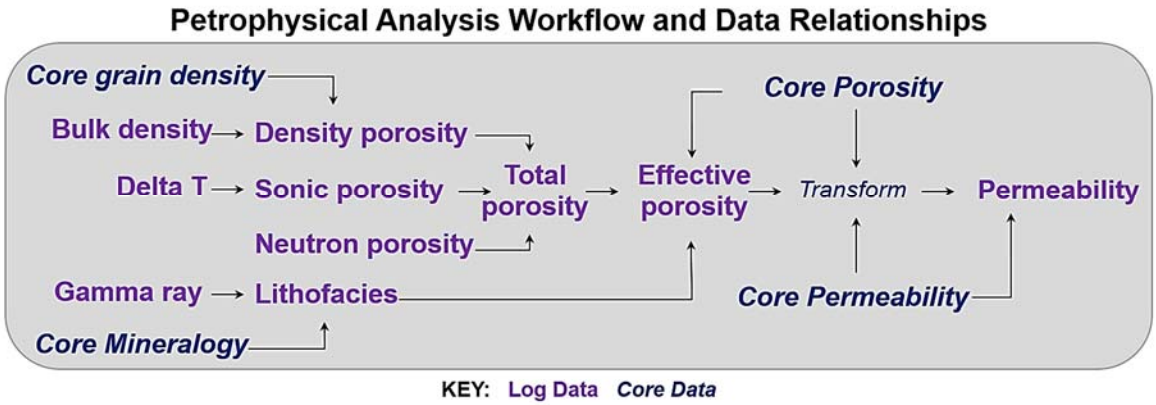

Figure 7. Schematic showing data relationships and integration for calculating petrophysical properties to be used in storage resource calculations.

Core Data

Core porosity, permeability, and grain density data from the Hydrologic Properties Database were used to correct/calibrate log data and quantify lithologic and petrophysical properties of the three storage zones. A summary of core grain density values from each storage zone is provided in Table 3. A total of 712 core measurements were used to characterize the grain density of the three storage zones, with approximately 76% of the data points from 10 wells belonging to the UJ1 zone.

Table 3. Core grain density statistics (g/cm^3) for the three storage intervals of interest.

Zone	MK1-3	LK1	UJ1
Minimum	2.66	2.66	2.61
Maximum	2.82	2.80	3.07
Mean	2.72	2.71	2.69
Number (n)	85	86	541
Well Count	4	5	10

Table 4 shows the minimum, maximum, and mean of core porosity measurements along with sample numbers and well counts for each of the three storage zones. Out of the 43 wells in the study area, core porosity data were available in 29, 31, and 32 wells for the MK1-3, LK1, and UJ1 zones, respectively. Sample counts range from 583 in the MK1-3 zone to 2,121 in the UJ1.

Table 4. Core porosity statistics (fraction) for the three storage intervals of interest.

Zone	MK1-3	LK1	UJ1
Minimum	0.01	0.01	0.01
Maximum	0.43	0.50	0.34
Mean	0.20	0.19	0.15
Number (n)	583	792	2121
Well Count	29	31	32

A summary of the core data used to evaluate the permeability of the three storage zones is shown in Table 5. Less than 200 permeability measurements were available from six wells for the MK1-3 and LK1 zones. The UJ1 zone accounted for approximately 69% of the total 914 core data points compiled for the three storage zones.

Table 5. Core permeability statistics (mD) for the three storage intervals of interest.

Zone	MK1-3	LK1	UJ1
Minimum	0.040	0.008	0.000
Maximum	2,700	3,970	949
Mean (arithmetic)	84	263	15
Mean (geometric)	3	3	1
Number (n)	126	161	627
Well Count	6	6	16

Log Data

A maximum gamma ray cut-off of 75 American Petroleum Institute gamma ray units (gAPI) is an industry standard for distinguishing between clean sandstone and carbonate reservoirs with low amounts of radioactive components (GR <75 gAPI), and non-reservoir shale and clay-bearing rocks with higher proportions of radioactive constituents (e.g., Slatt, 2006). Gamma ray logs were normalized by zone as part of a quality control procedure to eliminate varying signal intensities and establish consistent readings for sandstone, carbonate, and shale lithologies.

Gamma ray logs were normalized based on caprock and storage zone statistics from six type wells selected in the study area (Table 6): COST G-1 (GBB); Exxon 975-1 (GBB); COST B-2 (BCT); Homco 855-1(BCT); Shell 272-1 (BCT); and Shell 632-1 (BCT). These type wells are characterized by gamma ray data that generally fall within the normal range observed in sedimentary rocks (~10 to 200 gAPI), with values greater than 75 gAPI consistently calculated in formations characterized as predominately mudstone/shale and silty shale (e.g., UK1, MK4, LK2). Similarly, gamma ray logs in the type wells exhibited average values less than 75 gAPI in formations containing reservoir-quality sandstone intervals (e.g., MK1-3, LK1, UJ1) confirmed via core analysis (Smith et al., 1976; Amato and Bebout, 1980). This normalization procedure ensured mineralogically homogenous (i.e., clean) sandstones and carbonates had gamma ray values less than 75 gAPI and shale/clay-rich intervals had values above 75 gAPI.

Table 6. Gamma ray log statistics from the six type wells used to normalize gamma ray curves by zone in all wells in the study region.

Zone Name:		UK1	MK1-3	MK4	LK1	LK2	UJ1
Formation:		Dawson Canyon	Logan Canyon	Naskapi	Missisauga	Mic-Mac	Mohawk
Type Well Gamma Ray Log Statistics (gAPI)	Min. (avg.)	14	17	48	13	28	14
	Max. (avg.)	147	144	125	154	164	143
	Mean	82	73	89	71	85	72

Other logs used for characterization of reservoir lithology and petrophysical properties include bulk density (RHOB), sonic (DT), photo-electric (PE), neutron porosity (NPHI), density porosity (DPHI), and sonic porosity (SPHI) logs. Log data statistics for the Cretaceous-Jurassic interval of interest (MK1-3 - UJ1) are provided in Table A-2 of Appendix A.

Shale, Sandstone, and Carbonate Fractions

Lithologic logs representing fractions of shale (v_{shale}) and reservoir (v_{res}) components were generated from core and gamma ray log data. The lithology logs were then used to correct the total porosity log for shale and clay effects and derive a more reliable estimate of effective porosity. Both sandstone and carbonate percentages were included in the estimated reservoir fraction, with petrographic and X-ray diffraction analysis indicating an average sandstone and carbonate content of 70% and 20%, respectively, for the three storage zones of interest (Battelle, 2018a).

The normalized gamma ray curve was used as a basic index for shale volume to estimate the reservoir and non-reservoir fraction of each potential storage zone via Equation 1:

$$v_{shale} = (GR_{log} - GR_{res}) / (GR_{shale} - GR_{res}) \qquad \textbf{Equation 1}$$

Where:

- v_{shale} = shale fraction (i.e., non-reservoir)
- GR_{log} = normalized gamma ray log value
- GR_{res} = gamma ray value of clean sandstone and/or carbonate in each zone
- GR_{shale} = gamma ray value from a nearby shale interval

Average minimum gamma ray values calculated in each zone were used as input for GR_{res} (Table 6). The average maximum gamma ray value calculated in each well for the UK1, MK4, and LK2 caprocks was used as input for the GR_{shale} parameter. The estimated shale fraction (v_{shale}) was then used to derive the reservoir fraction (1-v_{shale} or v_{res}) and calculate effective log porosities for the deep saline formations of interest.

Mineral weight percentages derived from X-ray diffraction (XRD) analysis were used to calibrate and supplement the v_{shale} and v_{res} curves. XRD data were used to estimate lithology by grouping minerals characteristic of sandstone, shale, and carbonate rocks. Percentages of minerals grouped into sand consisted of quartz, rutile, anatase, plagioclase, and potassium feldspar. Percentages of minerals grouped into shale consisted of the kaolinite, micas, chlorite, and pyrite. Minerals grouped into the carbonate category consisted of calcite, dolomite, aragonite, ankerite, and siderite. The sum of the percentages of each lithology were divided by 100 to

create a normalization factor, and each lithology percent was divided by this factor to generate a normalized lithology fraction.

Whole-rock geochemical data from X-ray fluorescence (XRF) analysis was also used to supplement lithology estimates from XRD data by grouping chemical elements characteristic of sandstone, shale, and carbonate. Silicon and zirconium were assigned to sandstone, aluminum and titanium were assigned to shale, and calcium was assigned to carbonate (Turekian and Wedepohl, 1961). Concentrations from each sample were summed and normalized to 100% to derive lithologic fractions of sandstone, shale, and carbonate for each sample.

The XRD- and XRF-derived sandstone, carbonate, and shale fractions were imported into Petra, and values were compared with the v_{shale} and v_{res} logs in individual wells to evaluate consistency between the two data sets. The v_{shale} and v_{res} logs were normalized to the mean of the core data if the percent difference between the core and log values was greater than 20% in one of the storage zones. The core lithology data was then spliced directly into the v_{shale} and v_{res} curves to replace the estimated log value and generate the final integrated lithology logs.

Porosity

Total porosity, effective porosity, and reservoir facies were evaluated by assuming clean carbonate and sandstone represents the potential storage reservoir, and shale represents the non-reservoir fraction of the deep saline formation. Total porosity is defined as the combined percentage of interconnected, isolated, and clay-bound porosity of the total formation. Effective porosity is defined as the combined percentage of interconnected and isolated porosity in sandstone and/or carbonate reservoirs and does not include the clay-bound porosity associated with the non-reservoir, shale fraction. Total and effective porosity were calculated using bulk density logs, neutron porosity logs, sonic logs, and core porosity data. Density porosity was calculated from bulk density logs via Equation 2:

$$DPHI = (\rho_{matrix} - RHOB_{log}) / (\rho_{matrix} - \rho_{fluid}) \quad \textbf{Equation 2}$$

Where:

- $DPHI$ = density porosity
- ρ_{matrix} = density of rock matrix (i.e., grain density)
- $RHOB_{log}$ = bulk density log value
- ρ_{fluid} = density of pore fluids

An average grain density value of 2.72 g/cm^3 derived from core data (Table 3) was used as ρ_{matrix} input for the MK1-3. The average grain density of 2.71 g/cm^3 was used to calculate density porosity for the LK1, and an average value of 2.69 g/cm^3 was used for the UJ1. The density of pore fluids in deep saline formations was assumed to be 1 g/cm^3 for saltwater. The resulting DPHI logs were used along with NPHI logs to estimate total porosity (PHI_t) via averaging of the two curves. Sonic porosity was calculated using Equation 3:

$$SPHI = (\Delta T_{log} - \Delta T_{matrix}) / (\Delta T_{fluid} - \Delta T_{matrix}) \quad \textbf{Equation 3}$$

Where:

- *SPHI* = acoustic (sonic) porosity
- ΔT_{log} = acoustic travel time log value
- ΔT_{matrix} = acoustic travel time of rock matrix
- ΔT_{fluid} = acoustic travel time of pore fluids

A standard acoustic travel time of 52.6 microsecond per foot (µs/ft) (ΔT_{matrix}) for consolidated sandstone was assumed for all three storage zones (Carmichael, 1982). The ΔT_{fluid} value was assumed to be that of salt water, with an acoustic travel time of 189 µs/ft (Carmichael, 1982). The resulting SPHI logs were used to derive total porosity (PHI_t) curves for wells without DPHI and NPHI logs.

The estimated v_{res} curve was used to correct the total porosity curve for shale/clay effects and generate effective porosity logs. Effective porosity was estimated by calculating the porosity associated with the reservoir fraction via Equation 4:

$$PHIe = PHI_t \times (v_{res}) \qquad \textbf{Equation 4}$$

Where:

- PHI_e = effective porosity
- PHI_t= total porosity (uncorrected)
- v_{res} = reservoir fraction (i.e., sandstone and carbonate fraction)

Total and effective porosity logs were compared and evaluated for consistency with discrete core porosity measurements for individual wells (Table 7). Percent difference was calculated for the average total log porosity and core porosity for each storage zone. Results were compared to percent differences calculated for effective log porosity and core porosity to determine the reliability of the two calculated porosity logs. The percent difference between the total porosity log and core data was more than twice as high as that for the effective porosity log in the three storage zones. The effective porosity log was determined to be more reliable for storage resource calculations and was used to evaluate statistical distributions of reservoir porosity, generate porosity map grids, and derive permeability transforms.

The PHI_e logs for the 43 wells were then normalized to ensure the statistical distributions of log porosities were the same as that observed for the core data to be used in porosity-permeability transforms. All core porosity data available for an individual well were then spliced directly into the normalized PHI_e log, replacing the original PHI_e log value. The resulting final PHI_e log was used to generate porosity map grids for storage resource calculations and derive permeability curves from porosity-permeability transform equations.

Table 7. Percent difference calculated for average total log porosity versus and average effective log porosity relative to core porosity in the three storage zones.

Storage Zone:	MK1-3	LK1	UJ1
Avg. Total Log Porosity (fraction)	0.29	0.25	0.19
Avg. Core Porosity (fraction)	0.20	0.19	0.15
Percent Difference (%)	37	26	19
Avg. Effective Log Porosity (fraction)	0.17	0.18	0.14
Avg. Core Porosity (fraction)	0.20	0.19	0.15
Percent Difference (%)	16	5	7

Pseudo-wells and Seismic Inversion Porosity

Twenty pseudo-wells were placed in areas with well data gaps within the regional calculation boundary to better constrain porosity map grids for the three storage zones (Figure 8). Zone top and base depths were assigned to pseudo-wells by sampling the depth grids derived from seismic surfaces to each pseudo-well. Average effective porosities from the three nearest wells were assigned to storage zones in 15 pseudo-wells. Porosities derived from seismic inversion methods were used to characterize storage zone porosity in five pseudo-wells.

The seismic inversion process used pre-stack waveform inversion to recover detailed information about the subsurface from the entire record of seismic amplitudes and phase spectra. The inversion methodology employs a genetic algorithm using the principles of natural evolution to converge on a globally optimum result (Mallick, 1995). Forward modeling was done in the pre-stack common mid-point (CMP) domain using the reflectivity method based on the invariant imbedding algorithm by Kennett (1983). Each inversion started with a random population of primary-wave velocity (Vp), secondary-wave velocity (Vs), and density models chosen over a defined window around the velocity models built during pre-stack time migration. An objective fitness was then assigned by linear scaling of all model's cross-correlation to the real data. The models then undergo the genetic algorithm process of tournament selection, crossover, mutation, and update to advance to the next generation. This process was repeated until close correlation (~85%) between real and modeled data was achieved.

Using the inverted seismic velocities, a porosity model was derived from the empirical relationship with the P-wave velocity based on the empirical global relationship from Erickson and Jarrard (1998) that is fitted to sediments with normal consolidation histories. Assumptions included a velocity of 1.51 kilometers per second (km/s) for water, a pure sandstone matrix velocity of 5.49 km/s, and a pure shale matrix velocity of 4.3 km/s. The relationship ignores the effects of temperature, microcracks, exhumation, rebound, overpressure, anisotropy, and biogeneous sediment components. The porosity values derived from seismic inversion exhibit mean values similar to that of the well data for each storage zone of interest, though with a smaller overall range and less variability due to the limited vertical resolution of the seismic wavelet (Figure 9).

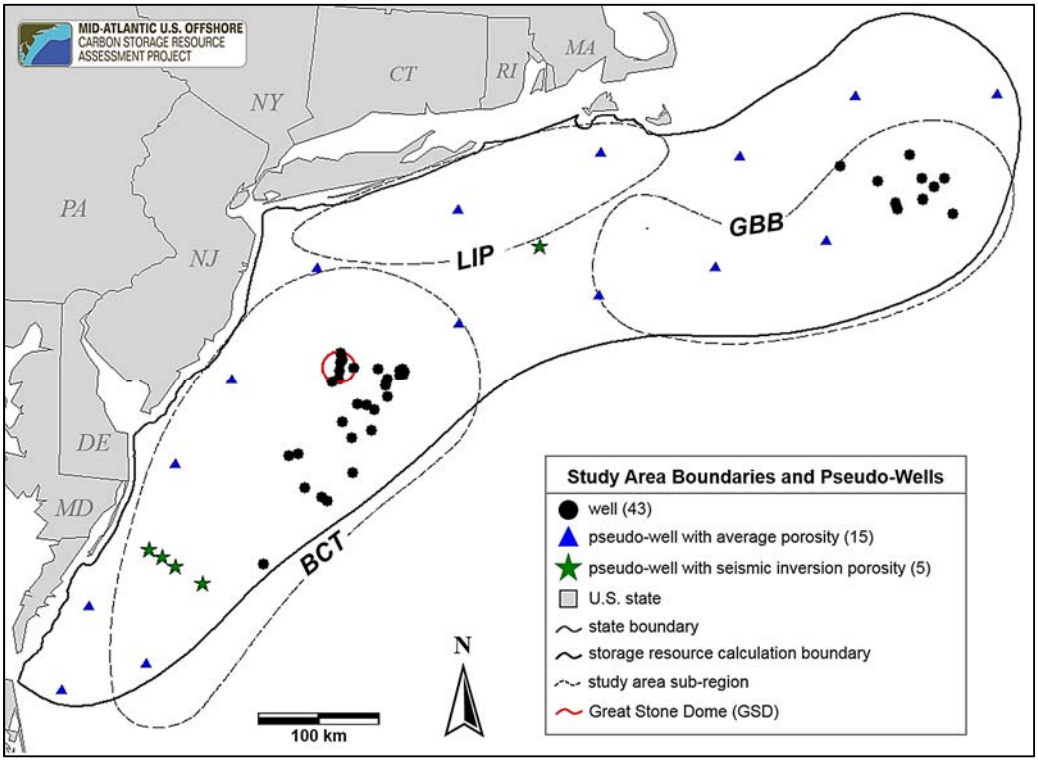

Figure 8. Map showing the locations of pseudo-wells used to constrain porosity map grids for storage resource calculations.

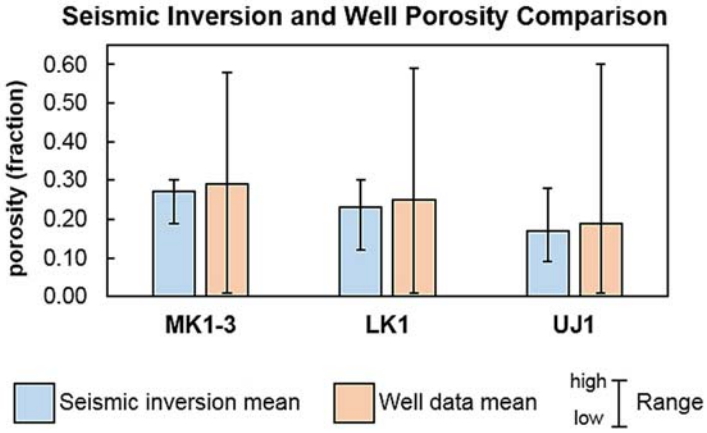

Figure 9. Comparison of porosity means and ranges from seismic inversion and PHI_e log data from wells for the three storage zones of interest.

Permeability Transforms

Cross-plots of porosity and permeability core data were generated to derive permeability transforms and permeability logs for each storage zone of interest. Transforms were based on core data from the Hydrologic Properties Database. There were 914 unique porosity and permeability core data points in the combined dataset for the three storage zones.
Figure 10 shows the resulting plots of permeability and porosity for the three storage zones with the calculated transform relationship used to derive permeability log curves for each zone.

Relative to the transforms for the LK1 and UJ1, the particularly low R-squared value observed in the regression for the MK1-3 represents a potential source of inaccuracy and uncertainty in the permeability curve derived for this zone.

The transform equation for each storage zone was applied to the PHI_e log in all 43 wells to generate an estimated permeability curve. The resulting permeability log curves were evaluated for consistency with core permeability measurements for individual wells. Unlike core porosity measurements that generally cover a range of representative depths for each storage interval, permeability measurements from core were often localized at one or two narrow depth intervals (see Figure A-3 in Appendix A). As a result, comparison of statistical distributions for the log and core data did not provide useful information for correction/normalization of the permeability log. All core permeability data available for an individual well were then spliced directly into the permeability log, and cut-offs of ≥ 10 millidarcy (mD) and ≥ 100 mD were applied to the resulting permeability curve to estimate net connected pore volumes, formation-specific storage efficiency values, and potential injectivity for static and dynamic resource calculations.

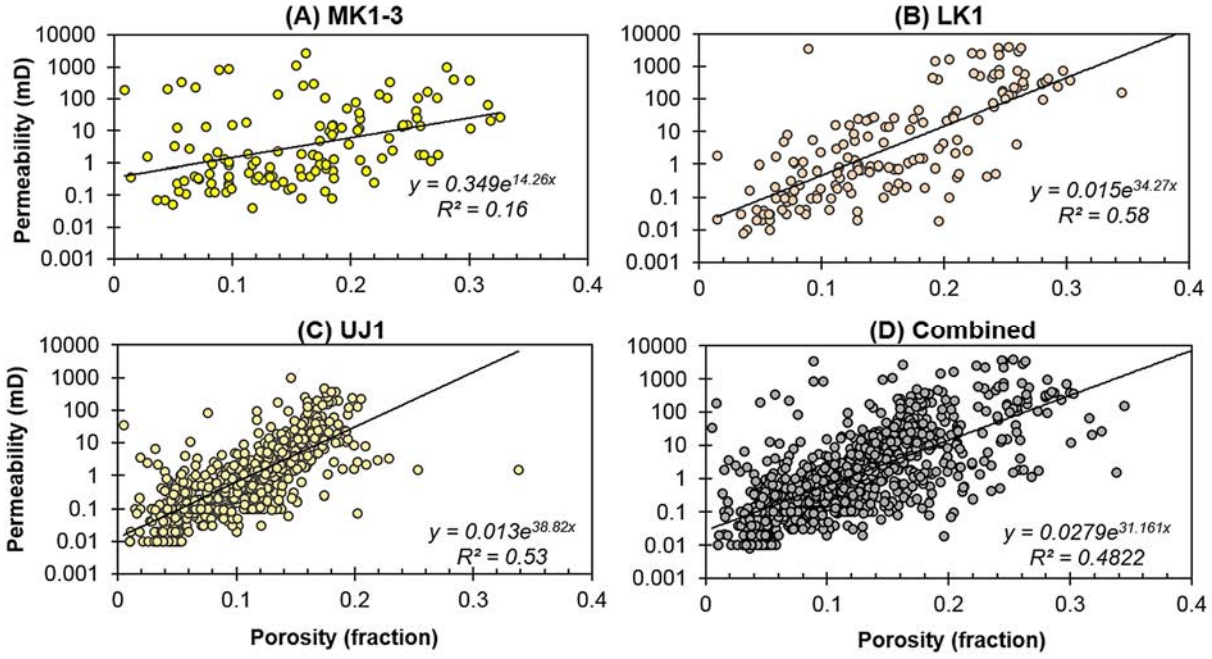

Figure 10. Porosity-permeability transforms derived from core data for (A) the MK1-3; (B) the LK1; (C) the UJ1; and (D) all three storage zones combined.

2.4 Static Prospective Storage Resource Calculations

Static CO_2 storage calculations employ estimates of subsurface pore volumes and in-situ fluid quantities to derive an equivalent volume of CO_2 that could occupy the pore space in a given storage reservoir. This method is similar to the standard equation used in the oil and gas industry to estimate original oil-in-place (Calhoun, 1982; Lake, 1989). Unlike dynamic models, static volumetric methods do not incorporate operational and temporal components such as injection rates/duration, pressure response, or well count into the storage estimate. As such, static CO_2 storage calculations are less time- and data-intensive and can be applied broadly to derive an upper bound on CO_2 storage potential during initial project phases dealing with limited subsurface data availability.

Several organizations and authors have developed static/volumetric-based methodologies to estimate static CO_2 storage potential in deep saline formations, including the Carbon Sequestration Leadership Forum (CSLF) (CSLF, 2007, 2008; Bachu et al., 2007; Bradshaw et al., 2007; Bradshaw et al., 2011; DOE-NETL, 2008, 2010, 2012; Goodman et al., 2011), the USGS (Brennan et al., 2010; Blondes et al., 2013; Zhou et al., 2008; Szulczewski et al., 2012), and international organizations such as CO_2 GeoCapacity (Vangkilde-Pedersen et al., 2009). The applicability of different methods depends on factors such as boundary conditions, reservoir type(s), CO_2 trapping mechanism(s), analysis time frame, and data availability in the basin(s) or formation(s) of interest.

DOE-NETL Methodology and CO_2-SCREEN Tool

The static methodology developed by DOE-NETL was used to quantify and map the prospective CO_2 storage resource of the offshore deep saline formations of interest (e.g., DOE-NETL 2010; Goodman et al., 2011; 2016). This methodology is represented by Equation 5:

$$G_{CO2} = A\, h\, \phi\, \rho_{CO2res}\, E_{saline} \qquad \textbf{Equation 5}$$

The storage resource equation used to estimate offshore resources includes area (A), thickness (h), and porosity (ϕ) to represent the total pore volume. This total pore volume is then reduced via the storage efficiency factor (E_{saline}) to represent the fraction of the pore volume that will be occupied by CO_2 (Goodman et al., 2011, 2016). The density of CO_2 at reservoir conditions (ρ_{CO2res}) is used to equate the CO_2-occupied pore volume to a mass of stored CO_2 (GCO_2). Storage efficiency factors account for physical limitations encountered in practice that will reduce access to the entire pore volume during CO_2 injection. The E_{saline} parameter as defined by DOE-NETL is the product of five individual efficiency factors (DOE-NETL 2008, 2010, 2012; Goodman et al., 2011). These individual efficiency parameters are shown in Equation 6 with designations used in this study to represent the fraction of the net effective pore volume that will be occupied by CO_2:

$$E_{saline} = E_{An}\, E_{hn}\, E\phi_e\, E_V\, E_d \qquad \textbf{Equation 6}$$

Definitions of parameters in Equations 5 and 6 are shown in Table 8 along with petrophysical criteria and data input used in this study to define each parameter. The net-to-total area (E_{An}), net-to-gross thickness (E_{hn}), and effective-to-total porosity ($E_{\phi e}$) parameters are geologic terms that represent the net effective pore volume of the saline formation. The two remaining efficiency factors are fluid displacement terms: volumetric displacement efficiency (E_V), which represents volume of rock surrounding an injection well that can be contacted by CO_2 due to near-wellbore fluid conditions/mobility (sweep efficiency), and microscopic displacement efficiency (E_d) to account for irreducible water saturation.

Table 8. Definitions of parameters in Equations 5 and 6.

Storage Resource Calculation Parameter	Symbol	Definition
Area	A	Total area of the storage reservoir with GR < 75 gAPI and k ≥ 10 mD
Thickness	h	Net thickness of the storage reservoir with GR < 75 gAPI and k ≥ 10 mD
Porosity	ϕ	Average effective porosity (isolated and connected) of the storage reservoir with GR < 75 gAPI and k ≥ 10 mD
CO_2 Density	ρ_{CO2res}	Density of CO_2 at reservoir temperature and pressure
Storage Efficiency	E_{saline}	Fraction of the reservoir pore volume that can be occupied by CO_2
Net-to-Total Area Efficiency	E_{An}	Net area ratio for the net ≥ 100 mD to net ≥ 10 mD reservoir intervals
Net-to-Gross Thickness Efficiency	E_{hn}	Net thickness ratio for the net ≥ 100 mD to net ≥ 10 mD reservoir intervals
Effective-to-Total Porosity Efficiency	$E_{\phi e}$	Effective porosity ratio for the net ≥ 100 mD to net ≥ 10 mD reservoir intervals
Volumetric Displacement Efficiency	E_V	Volume of the CO_2 plume surrounding an injection well; determined by numerical simulations
Microscopic Displacement Efficiency	E_d	The fraction of pore volume containing mobile water that can be displaced by the contacted CO_2 ($1-S_{Wirr}$); determined by numerical simulations

Storage calculations were conducted using the CO_2-SCREEN tool (V.1) developed by DOE-NETL (Sanguinito et al., 2016) and publicly available through the NETL Energy Data eXchange (EDX) website (https://edx.netl.doe.gov/organization/co2-screen). The tool employs Equations 5 and 6 to stochastically estimate the storage resource of open-system, saline formations, and consists of an integrated Microsoft Excel and GoldSim® calculation. The tool is intended to provide the Regional Carbon Sequestration Partnerships with a consistent method for calculating the prospective CO_2 storage resource of open-system saline formations to facilitate comparison across different partnerships and research efforts (Sanguinito et al., 2016).

To incorporate geologic heterogeneity into storage resource estimates, CO_2-SCREEN allows for up to 300 entries of grid-cell data and standard deviations to be entered for the area (A), thickness (h), porosity (ϕ), reservoir pressure, and reservoir temperature. Grid data from the depth, net thickness, and effective porosity maps generated for the reservoir interval with permeability ≥ 10 mD were used as input for each storage zone in CO_2-SCREEN. Storage zone top depth was used to derive CO_2 density at reservoir pressure and temperature based on a regional pressure gradient of 10,000 pascals per meter (Pa/m) (0.45 pounds per square inch [psi]/ft) and a geothermal gradient of 23°C/km (~1.35°F/100 ft) reported as part of the Task 6 Risk Factor Analysis (Battelle, 2018b). The CO_2 solubility model developed by Duan and Sun (2003) was used for CO_2 density calculations. The GoldSim Player module of CO_2-SCREEN accesses the input in Excel and calculates results using Monte Carlo sampling techniques and 10,000 realizations to achieve reasonable convergence for probabilistic resource estimates (Goodman et al., 2016; Sanguinito et al., 2016).

Offshore-Specific Storage Efficiency Estimates

A majority of studies define storage efficiency generally as the ratio of CO_2-occupied pore volume relative to a total pore volume (e.g., Bachu, 2015), however different studies employ slightly different procedures for arriving at that fraction of CO_2-occupied pore volume. For the purposes of this project, sandstone with gamma ray values less than 75 gAPI was used to delineate “reservoir” intervals within storage zones, and permeability was used as a proxy to represent connected pore volumes. A permeability of ≥ 10 mD was initially applied along with the gamma ray cut-off to quantify and map the total pore volume potentially available for CO_2 storage. A second permeability cut-off of ≥100 mD was applied to the ≥ 10 mD reservoir interval to quantify the net effective pore volume that will be occupied by CO_2 and derive formation-

specific storage efficiency values. The second ≥100 mD cut-off is intended to account for uncertainty in the estimated net pore volume available for CO_2 storage, and represents an order of magnitude of potential error in the permeability curves calculated from porosity-permeability transforms.

To better facilitate the use of available data to define storage efficiency inputs, the three geologic efficiency terms, E_{An}, E_{hn}, and $E_{\phi e}$, were combined into one parameter to represent the net-to-total reservoir pore volume efficiency such that:

$$E_{PVn}^{s} = E_{An}\, E_{hn}\, E_{\phi e} \qquad \textbf{Equation 7}$$

and Equation 6 can be rewritten as:

$$E_{saline} = E_{PVn}^{s}\, E_{V}^{s}\, E_{d}^{s} \qquad \textbf{Equation 8}$$

Where the "s" superscript is added to the E_{PVn} parameter to denote it as a stochastic calculation parameter defined by formation-specific data (Goodman et al., 2016). High (P90) and low (P10) probability (p) values were assigned to the geologic efficiency term based on statistical distributions of the net 100 mD to net 10 mD pore volume ratios calculated from the 300 individual grid cells in each storage zone. High and low p-values derived from results of regional dynamic injection simulations for the MK1-3 zone were used as input for the two displacement efficiency terms for all three storage zones. To be consistent with the DOE methodology, this study uses cumulative probability values such that P10 is the lower value that represents a 10% probability that the CO_2 storage resource value is less than the reported P10 value (Goodman et al., 2011). Similarly, P90 is the higher probability value that represents a 90% probability that the true CO_2 storage resource is at or below the P90 value. The P50 value is the median of the data derived from results of the 10,000 realizations. The final E_{saline} value was calculated stochastically in CO_2-SCREEN to derive G_{CO2} estimates at the P10, P50, and P90 probability ranges.

Due to the site-specific nature of the displacement efficiency factors (Sanguinito et al., 2016; Goodman et al., 2016), E_v and E_d, were determined numerically using simple equivalent homogeneous models based on regional distributions of reservoir properties supported by well data. The definition of these efficiency terms used for the calculations is reiterated below:

- E_v = volumetric sweep efficiency is given by the ratio of the pore volume contacted by CO_2 to the total pore volume within the footprint of the CO_2 plume.
- E_d = microscopic displacement efficiency is given by the fraction of pore volume containing mobile water that can be displaced by the contacted CO_2 ($1\text{-}S_{Wirr}$). As the initial gas saturation in the reservoir is 0, the average CO_2 saturation behind the front gives this displacement efficiency.
- E_v, E_d = total displacement efficiency is the product term that is input to E_{saline} storage efficiency equation (Equation 6 and Equation 8) in storage resource calculations for the formation(s) of interest.

The MK1-3 storage zone was evaluated in detail for the formation-specific displacement efficiency calculation exercise using numerical modeling. The numerical modeling used to determine E_v and E_d terms consisted of simplified models with porosity and permeability values representative of the range of conditions expected at the regional-scale in the MK1-3 zone. The reservoir volume was treated as a homogeneous radial model with an area of approximately 310 km^2 (120 mi^2) to be consistent with the area of each grid cell entered into CO_2-SCREEN for the MK1-3 static storage resource calculations.

A single CO_2 injection well was placed in the center of the model, with injection simulated across the entire formation. Figure 11 depicts the grid geometry and a sample grid property assigned to the model layers using the CMG-GEM® software.

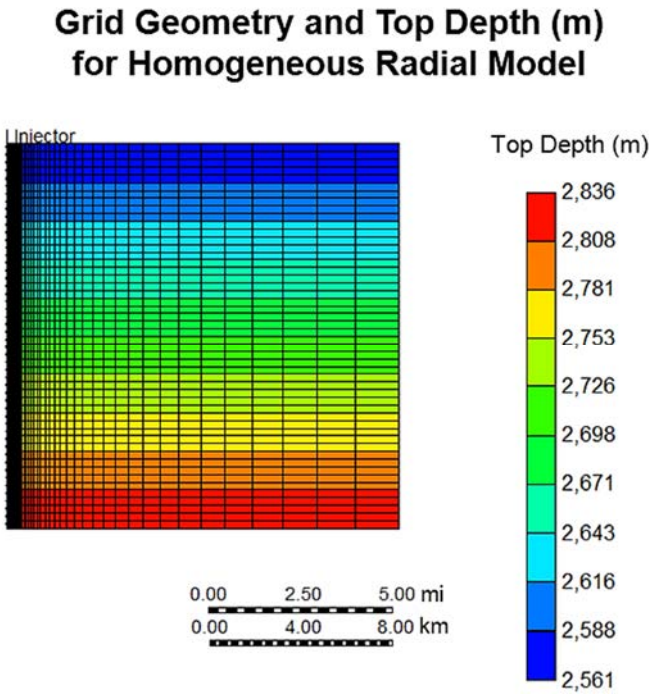

Figure 11. Model cross-section showing grid geometry and grip top (in meters) property defined at different layers in the reference depth scenario model in the MK1-3 formation.

Assuming lateral homogeneity in the compositional numerical model layers, the models were built and evaluated for their sensitivity to relative permeability curves, absolute permeability, permeability anisotropy, residual water saturation/ irreducible water saturation, amount of CO_2 injected. The list of key dynamic modeling input parameters, data sources, and storage zone assumptions and input is provided in Table A-3 of Appendix A.

Sensitivity analysis was performed using the two CO_2-brine relative permeability model variants shown in Figure 12 and one-off variation of the following model parameters to determine E_V and E_d for the formation of interest:

- Shallow through deep locations sampled in the formation with the reference depth being the formation top of 2,560 m (measured depth)
- Effective porosity and permeability values corresponding to the P10, P50, and P90 of distributions derived from regional map grids
- Net thickness values corresponding to the P10, P50, and P90 of distributions derived from regional map grids
- Fracture pressure gradients of 13,573 Pa/m (0.60 psi/ft), 14,705 Pa/m (0.65 psi/ft), and 15,833 Pa/m (0.7 psi/ft)

A total of 90 runs were evaluated to calculate the E_V and E_d for a range of conditions representative of regional variation in the MK1-3 storage zone. Key output performance metrics,

such as CO_2 saturation plume extent and amount of CO_2 injected, were extracted from the model at the end of injection to calculate the displacement storage efficiency (E_v, E_d) factors.

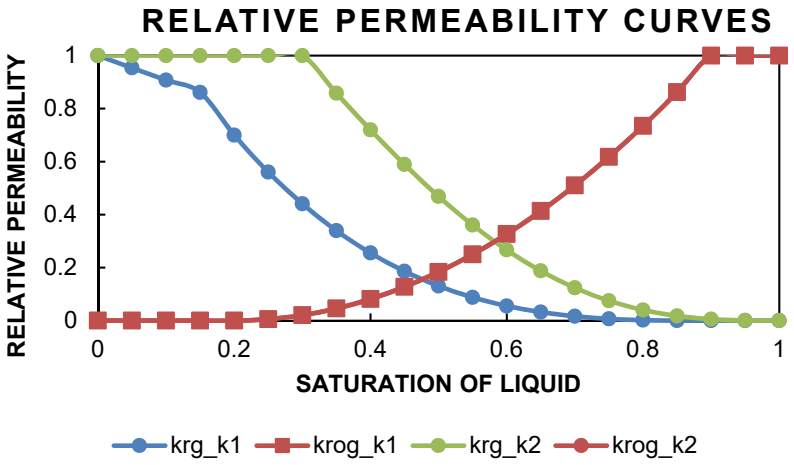

Figure 12. Relative permeability curves used in regional-scale dynamic reservoir simulations for E_V and E_d estimation.

2.5 Dynamic Injection and Storage Simulations

Simplified dynamic simulations have been used in this study for two purposes: 1) to derive offshore-specific P10 and P90 values for the E_V and E_d displacement efficiency parameters (Equations 6 and 8; Table 8); and 2) to investigate the effects of pressure and operational conditions on CO_2 injection and estimated CO_2 storage resources for a selected area in the offshore study region. Grid data averages and/or statistical distributions will be used as input in dynamic simulations to define reservoir properties for each storage zone of interest (e.g., porosity and permeability).

Using a simple CMG-GEM® model, the local storage resource of a potential commercial-scale injection interval was evaluated using dynamic reservoir simulation for a selected area in the offshore study region. The selected area for local dynamic simulations was identified via geospatial analysis of results from regional static storage resource maps along with availability of well data, such that the location with the highest storage resource and lowest well spacing per unit area was chosen. Within the selected area, the injection zone chosen for dynamic simulation was identified via analysis of net pay flag continuity (vertical and lateral) on structural cross-sections for the three storage zones of interest.

A 3D site model in the selected area was then used to predict pressure response, CO_2 injection and storage quantities, and CO_2 plume saturation front for a simulated injection operation in a vertical well located in the center of the injection interval. A sensitivity analysis for injection rates was also performed to investigate the extent of pressure buildup for a given amount of CO_2 injected. Two primary injection scenarios were evaluated for the 30-year simulation timeframe, one using an injection rate of 1.5 Mt CO_2/year (reference injection scenario) and the second using a rate of 1.0 Mt CO_2/year (variant injection scenario). A maximum CO_2 injection scenario was also examined, where CO_2 injection rates were adjusted to maintain the maximum allowable injection pressure measured at bottom-hole conditions. The pressure buildup, CO_2 storage quantity, and plume extent were analyzed at the end of injection.

Local grid refinement was implemented in the fully compositional dynamic model. An X and Y grid increment of 50 m was defined around the injection well to cover the extent of the final CO_2 plume, and an X and Y grid increment of 300 m was used toward the flanks of the model. Effective porosity and permeability logs from existing wells located within the model domain were re-scaled to 1.5 m (5 ft) sample increments to divide the injection zone into vertical layers with unique porosity and permeability values for the dynamic simulation.

All model boundaries were assumed to be closed to be consistent with structural trapping mechanisms identified in the selected area. It should be noted that both open and closed systems could potentially represent the geologic trapping mechanisms in the selected area, but a closed boundary system was determined to be the more likely scenario to encounter in practice and provides a more conservative evaluation of the CO_2 injection and storage resource relative to an open-system model.

Fluid-rock properties have the biggest impact on the dynamic simulation. For the fluid model specification, the Peng-Robinson equation of state was used, with CO_2, H_2O, and a trace constituent (to make the simulation stable) used as components in the fully compositional model. The salinity of the formation brine was assumed to be 50,000 parts per million and Henry's Law was used to model CO_2 solubility into the aqueous phase. The injection interval was assumed to be initially fully saturated with brine (i.e., no initial oil or gas saturation). The relative permeability curves used to develop the pressure and saturation profiles are represented by the relative permeability curve used for the E_v, E_d determination exercise described in Section 2.5 (Figure 12). The brine-saturated model was initialized at hydrostatic equilibrium with an assumed pressure gradient of approximately 10,000 Pa/m and geothermal gradient of 0.23°C/km.

A single vertical injection well was set to inject CO_2 at a constant rate for the 30 years while ensuring the fracture pressure constraint (translated to a maximum bottom-hole pressure constraint) was honored and then shut in at the end of the simulation period. The injection well was perforated through the entire storage zone. A conservative maximum fracture pressure gradient of 14,703 Pa/m (0.65 psi/ft) was assumed for local-scale dynamic storage resource calculations (Brown et al., 2011). If the bottom-hole pressure of the injector exceeded the fracture pressure, the formation integrity could be compromised and fractured. Hence the operating conditions simulated in the dynamic model stayed at or below this critical constraint.

3.0 Results

3.1 Reservoir Petrophysics

The petrophysical properties from the 300-grid-cell map data are summarized in Table 9 for reservoir intervals with permeability ≥ 10 mD in each storage zone of interest. The MK1-3 exhibits an average thickness of 181 m and an average effective porosity of 23%, with map grid data for resource calculations covering an area of 92,928 km^2. The resulting total pore volume of the 300 grid cells representing the MK1-3 reservoir interval with ≥ 10 mD permeability is 3,668 km^3. The total area of volumetric grid data used in storage resource calculations for the LK1 zone is 117,493 km^2. The ≥ 10 mD reservoir interval in LK1 exhibits an average thickness of 154 m and an average effective porosity of 26%, for a total pore volume of 4,635 km^3. In the UJ1 zone, the ≥ 10 mD reservoir interval has an average thickness of 211 m and an average effective porosity of 21%. The resulting total pore volume calculated for the reservoir interval with ≥ 10 mD permeability in the UJ1 is 6,511 km^3. Thickness data from the UJ1 grid exhibits the highest standard deviation (292 m) of the three storage zones, followed by the MK1-3 (112 m) and LK1 (82 m). Mean permeabilities of the ≥ 10 mD reservoir intervals range from 45 mD in the UJ1 to 71 mD in the MK1-3 zone.

Table 9. Petrophysical properties for reservoir intervals with permeability ≥ 10 mD.

Storage Zone	Area (km^2)	Thickness (m)		Effective Porosity (%)		Permeability (mD)		Total Pore Volume (km^3)
		Mean	σ	Mean	σ	Mean*	σ	
MK1-3	92,928	181	112	23	2	71	64	3,668
LK1	117,493	154	82	26	3	65	51	4,635
UJ1	134,578	211	292	21	2	45	29	6,511

*geometric mean

Table 10 shows the mean and standard deviation (σ) of pressure and temperature data derived from depth grids along with average CO_2 density estimates for the three storage zones. Mean pressures range from 18 megapascals (Mpa) in the MK1-3 to 30 Mpa in the deepest UJ1 zone. Mean reservoir temperatures are 42°C in the MK-13 zone and 49°C in the LK1 zone. Reservoir temperatures are highest in the UJ1 zone, with a mean of 68°C. Average CO_2 density is estimated at 815 kg/m^3, 809 kg/m^3, and 796 kg/m^3 for the MK1-3, LK1, and UJ1, respectively.

Table 10. Mean pressure, temperature, and CO_2 density results for the three storage zones.

Storage Zone	Pressure (MPa)		Temperature (°C)		Average CO_2 Density (kg/m^3)
	Mean	σ	Mean	σ	
MK1-3	18	7	42	16	815
LK1	22	7	49	16	809
UJ1	30	10	68	22	796

Figure 13 shows the porosity-thickness map for the MK1-3 reservoir interval with permeabilities ≥ 10 mD. MK1-3 porosity-thicknesses of 60 m and greater are observed in the northern BCT near the GSD structure (Figure 8). The lowest porosity-thicknesses are observed toward the south and east of the MK1-3 map boundary, near the shelf-slope break and in the southern BCT. High spots on porosity-thickness maps for the ≥ 10 mD reservoir interval in the LK1 and UJ1 exhibit trends similar to the MK1-3, with thicknesses of 60 m and greater occurring in the LK1 on the offshore shelf directly adjacent to New Jersey in the northern BCT (Figure 14). Porosity-thicknesses of 160 m and greater are observed in this area on the UJ1 map (Figure 15).

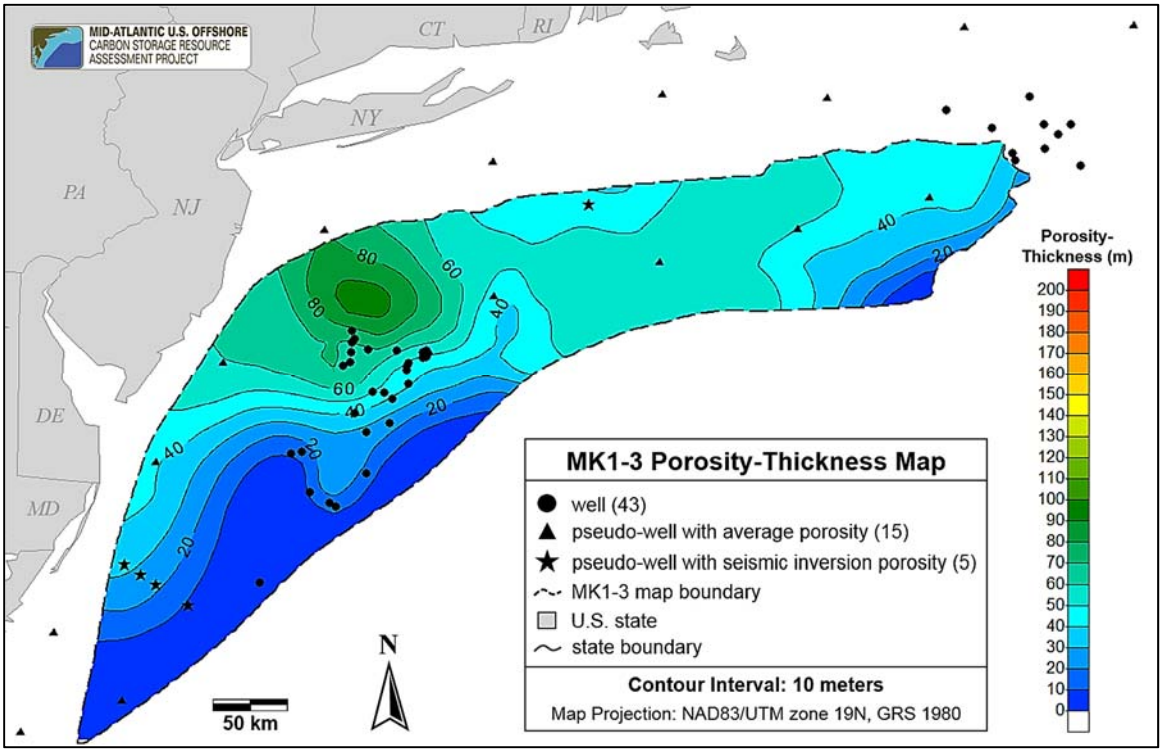

Figure 13. Porosity-thickness map for the ≥ 10 mD reservoir interval in the MK1-3 storage zone.

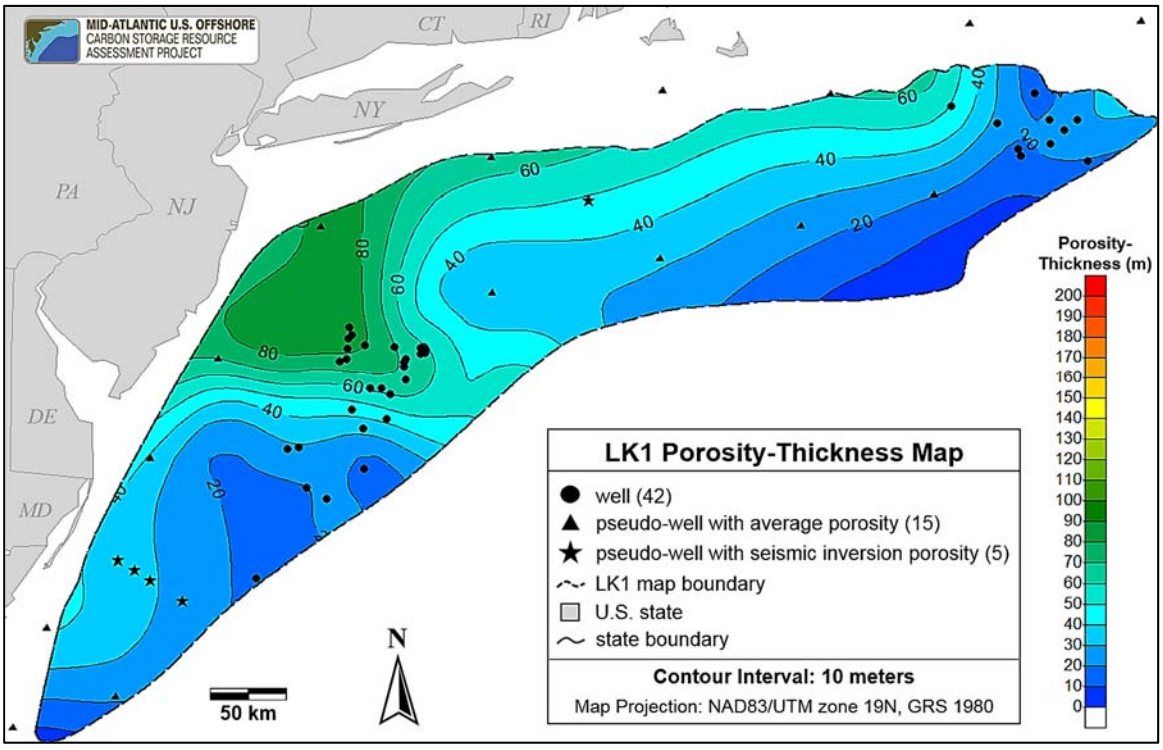

Figure 14. Porosity-thickness map for the ≥ 10 mD reservoir interval in the LK1 storage zone.

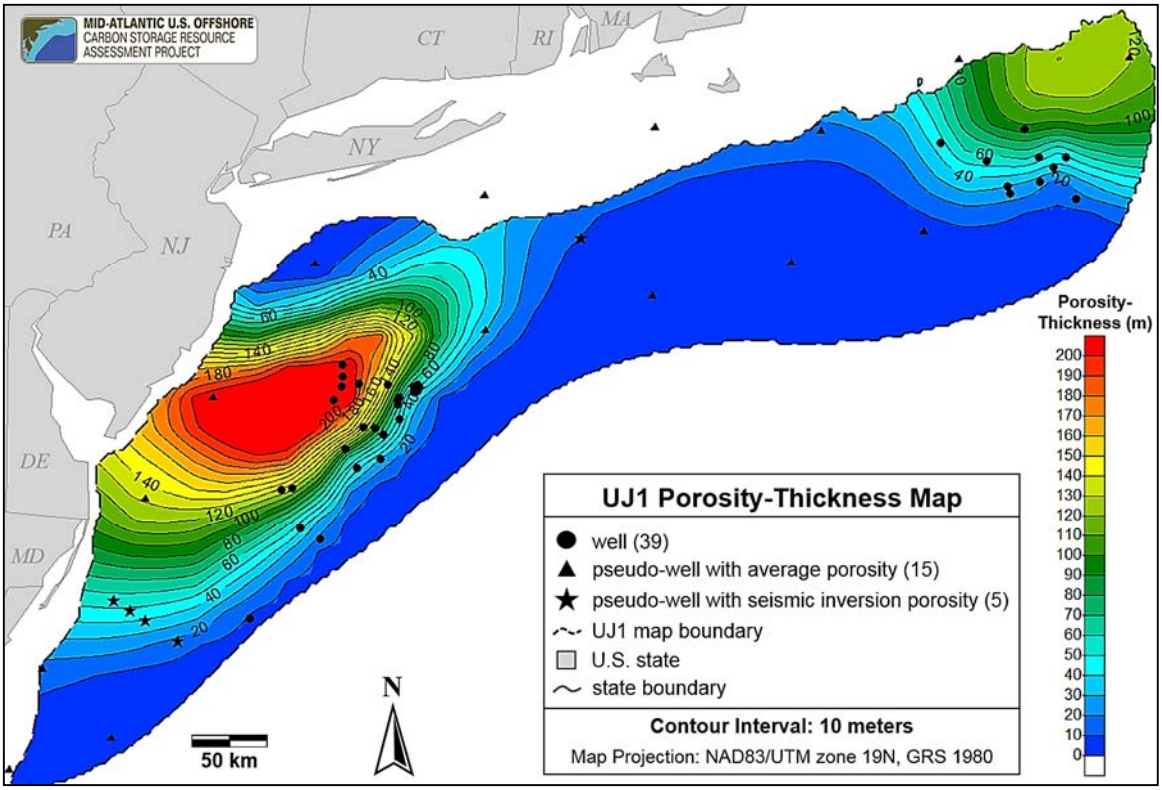

Figure 15. Porosity-thickness map for the ≥ 10 mD reservoir interval in the UJ1 storage zone.

The petrophysical properties of the net reservoir interval with permeability ≥ 100 mD are summarized for each storage zone in Table 11. The MK1-3 net reservoir interval exhibits an average net thickness of 55 m, an average effective porosity of 27%, and extends over an area of 79,918 km^2. The 300 data points representing the MK1-3 net reservoir interval with ≥ 100 mD permeability result in a combined net pore volume of 1,371 km^3. The net area of the ≥ 100 mD reservoir in the LK1 zone is 117,102 km^2. The LK1 reservoir interval exhibits an average net thickness of 40 m and an average effective porosity of 29%, for a regional net pore volume of 1,430 km^3. In the UJ1 zone, the ≥ 100 mD reservoir interval has an average net thickness of 32 m and an average effective porosity of 25%. The resulting net pore volume of the 300 grid cells representing the ≥ 100 mD reservoir interval in the UJ1 is 1,049 km^3. The mean permeability of the net reservoir interval ranges from 264 mD in the UJ1 zone to 339 mD in the LK1 zone.

Table 11. Petrophysical properties of net reservoir intervals with permeability ≥ 100 mD.

Storage Zone	Net Area (km^2)	Net Thickness (m)		Net Effective Porosity (%)		Net Permeability (mD)		Net Pore Volume (km^3)
		Mean	σ	Mean	σ	Mean*	σ	
MK1-3	79,918	55	64	27	3	314	148	1,371
LK1	117,102	40	45	29	5	339	291	1,430
UJ1	88,372	32	41	25	8	264	119	1,049

*geometric mean

3.2 Offshore-Specific Storage Efficiency

The P10, P50, and P90 values calculated for the geologic (E_{PVn}) and displacement (E_V, E_d) efficiency terms are shown in Table 12. The net-to-total pore volume ratios calculated for the 300 grid cells in the MK1-3 zone range from 0.09 (P10) to 0.70 (P90). The distribution of net-to-total pore volume ratios for LK1 has a P10 of 0.12 and a P90 of 0.59. Volumetric data from the UJ1 exhibits net-to-total values ranging from 0.08 (P10) to 0.19 (P90). Figure 16 shows the combined distribution of E_{PVn} values calculated for all three offshore deep saline storage zones. In the combined dataset, 10% of the ratios calculated were less than or equal to 0.10 (P10) and 90% of the values were less than or equal to 0.58 (P90).

Table 12. High (P90), median (P50), and low (P10) probability values of storage efficiency parameters calculated for the three storage zones of interest.

Storage Zone	E_{PVn}			E_V			E_d		
	P10	P50*	P90	P10	P50*	P90	P10	P50*	P90
MK1-3	0.09	0.36	0.70	0.34	0.72	0.89	0.22	0.28	0.30
LK1	0.12	0.36	0.59	NA	NA	NA	NA	NA	NA
UJ1	0.08	0.19	0.38	NA	NA	NA	NA	NA	NA
Combined	0.10	0.31	0.58	NA	NA	NA	NA	NA	NA

*P50 values are shown for reporting purposes only and are not used in CO_2-SCREEN (V.1) for resource calculations.
NA = Not Analyzed

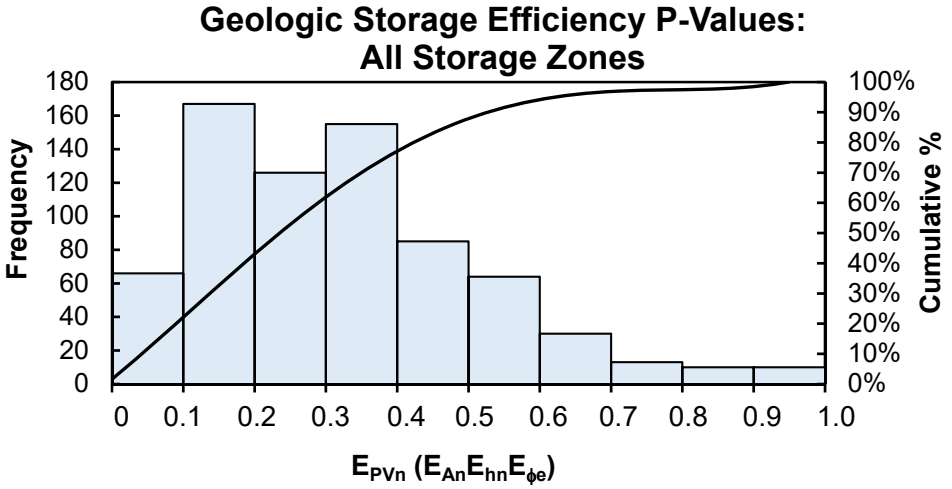

Figure 16. Histogram showing combined distribution of values calculated for the geologic storage efficiency parameter E_{PVn} ($E_{An}E_{hn}E_{\phi e}$) in the storage zones of interest.

Table 13 provides more detailed summary statistics of the offshore formation-specific displacement efficiency factors (E_V and E_d) calculated using dynamic model simulations. The displacement efficiency factors obtained in this study fall within the published range for onshore saline formations, with values between 7.4% and 26% percent reported over the P10 and P90 range by Goodman et al. (2011). The International Energy Agency Greenhouse Gas R&D Programme (IEAGHG, 2015) reported comparable storage efficiency values (4% to 17%) from 195 site-specific cartesian grid models for simulated, statistically generated site lithologies and depositional environments.

Table 13. Detailed summary statistics of the E_V and E_d displacement efficiencies obtained from the regional-scale dynamic numerical simulations in the MK1-3 zone.

Displacement Efficiency	E_V	E_d	E_V*E_d
Minimum Value	0.23	0.21	0.06
Median Value	0.72	0.28	0.18
Maximum Value	0.99	0.31	0.29
P10 Value	0.34	0.22	0.09
P50 Value	0.72	0.29	0.19
P90 Value	0.89	0.30	0.26
Number of Realizations/Runs	90		

3.3 Regional Static Storage Resource Estimates

Using the map grid data and storage efficiency p-values presented in Sections 3.1 and 3.2, respectively, the E_{saline} results and range of CO_2 storage resources estimated for each storage zone are shown in Table 14. E_{saline} results are similar for MK1-3 and LK1, with P50 values of 0.05 in both zones. The P90 value of 0.13 for the MK1-3 E_{saline} distribution is slightly higher than the P90 value of 0.11 for the LK1 zone. The distribution of E_{saline} results for UJ1 has a P10 of 0.01, a P50 of 0.03, and a P90 of 0.07.

Table 14. High (P90), median (P50), and low (P10) values for total deep saline storage efficiency (E_{saline}) results and prospective CO_2 storage resource estimates for the three storage zones.

Storage Zone	Storage Efficiency (E_{saline}) Results (fraction)			Total Prospective Storage Resources (Gt)		
	P10	P50	P90	P10	P50	P90
MK1-3	0.01	0.05	0.13	37	148	378
LK1	0.02	0.05	0.11	59	178	403
UJ1	0.01	0.03	0.07	54	153	355

Storage resource estimates for the LK1 zone exhibit the highest P10 (59 Gt) and P50 values (178 Gt) out of the three storage zones of interest, followed by the UJ1 and the MK1-3. The regional-scale storage resources estimated for MK1-3 range from 37 Gt (P10) to 378 Gt (P90), with a median P50 value of 148 Gt. The UJ1 storage resource estimates range from 54 Gt (P10) to 355 Gt (P90). The estimated storage resources for LK1 have the highest P90 value (403 Gt) of the three storage zones, followed by the MK1-3 (378 Gt) and the UJ1 (355 Gt). The P10 and P90 values for the UJ1 exhibit the smallest range of the storage resource distributions calculated for the three offshore storage zones.

The average storage resource per unit area for the MK1-3 zone is approximately 1.60 Mt CO_2/km^2 (P50). The areal distribution of P50 storage resources estimated for the MK1-3 zone is shown in Figure 17. Similar to trends observed on the MK1-3 porosity-thickness map (Figure 13), the highest storage resource values (greater than 2.4 Mt CO_2/km^2) occur in the northern BCT near the GSD (Figure 8). P50 values less than or equal to 0.2 Mt CO_2/km^2 occur along the southeastern extent of the MK1-3 map boundary.

The average storage resource per unit area for the LK1 zone is approximately 1.52 Mt CO_2/km^2 (P50). LK1 storage resource values greater than 2.4 Mt CO_2/km^2 (P50) are also observed in the northern BCT near the GSD (Figure 18). P50 storage resource estimates for the LK1 in the eastern GBB range from approximately 0.8 Mt CO_2/km^2 in the southeast to 1.6 Mt CO_2/km^2 in the northwest.

The P50 storage resource map for the UJ1 zone exhibits an average of 1.13 Mt CO_2/km^2 (Figure 19). Estimates of 3.2 Mt CO_2/km^2 and higher are observed in the northern BCT. UJ1 estimates range from approximately 0.4 Mt CO_2/km^2 to 3.4 Mt CO_2/km^2 in the eastern GBB, with values increasing to the northeast. Storage resource decreases to 0.2 Mt CO_2/km^2 along the southeastern margin of the UJ1 map boundary.

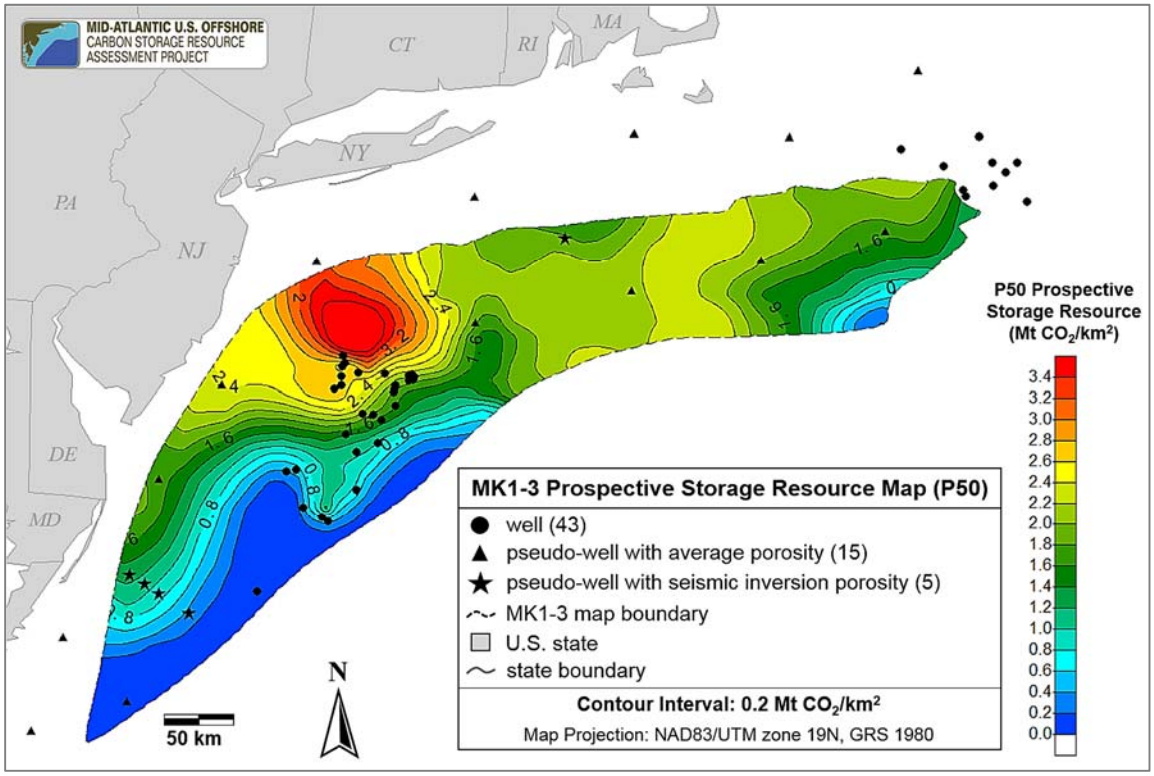

Figure 17. Map showing prospective storage resource estimates in Mt CO_2 per km^2 for MK1-3.

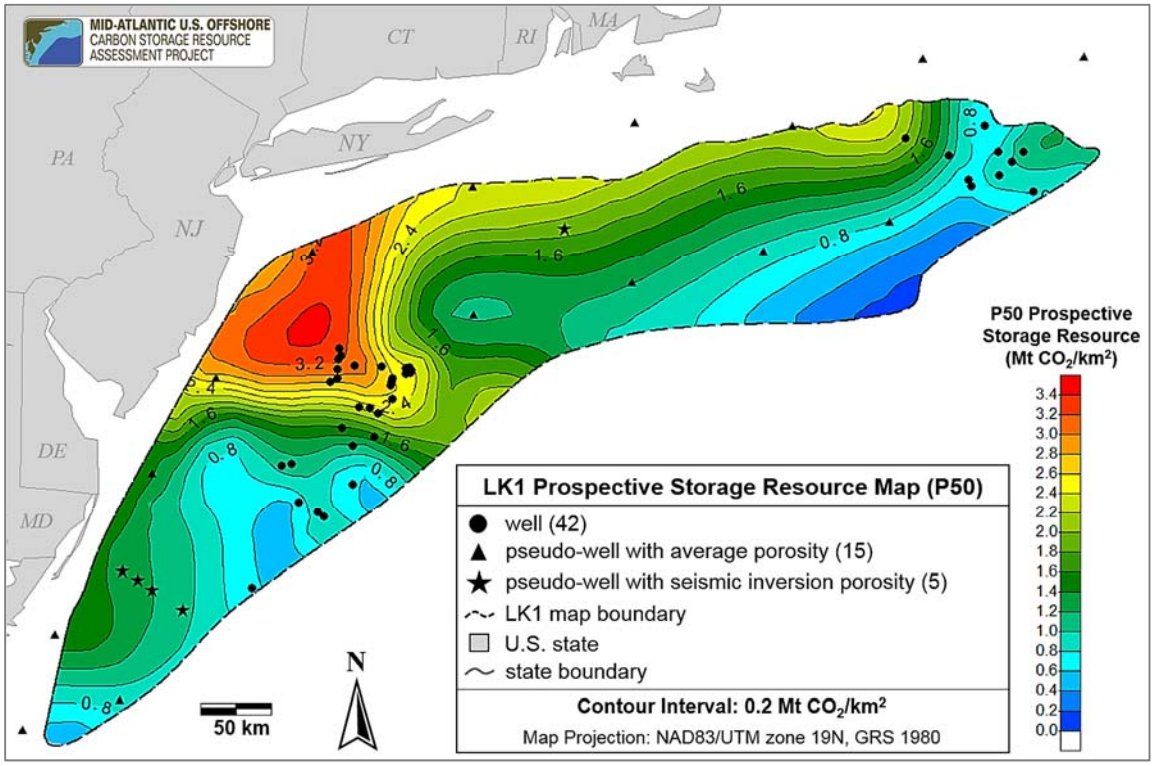

Figure 18. Map showing prospective storage resource estimates in Mt CO_2 per km^2 for LK1.

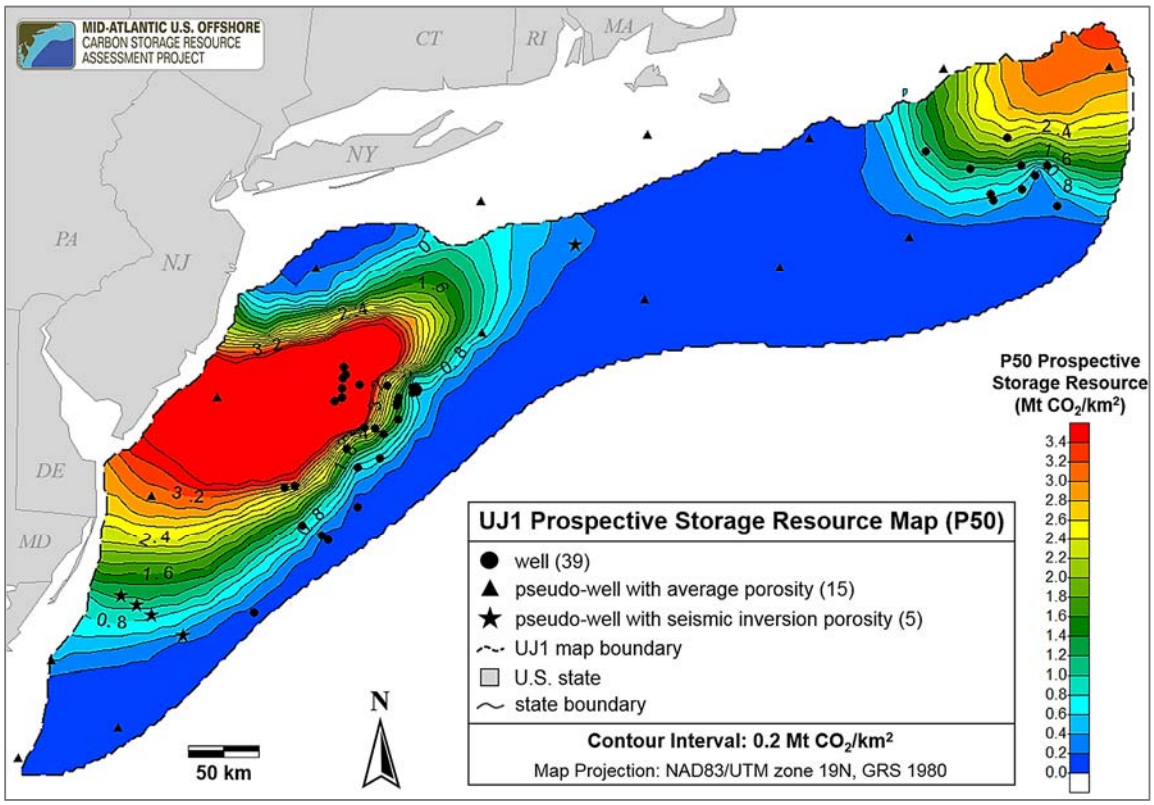

Figure 19. Map showing prospective storage resource estimates in Mt CO_2 per km^2 for UJ1.

3.4 Local Dynamic Storage Resource Estimates

The area near the GSD in the northern BCT was selected for local refinement of storage resource estimates via dynamic injection and storage simulation. P50 values greater than 2.4 Mt CO_2/km^2 were observed in the selected area on storage resource maps for all three storage zones (e.g., Figure 17, Figure 18, Figure 19). This area also exhibits relatively good well data coverage, with reservoir properties constrained by a well spacing of 5 km or less. The net thickness (GR < 75 gAPI and k ≥ 100 mD) of the interval of interest extending from the MK1 top to the UJ1 base was mapped to determine the dynamic model simulation area and injection well location (Figure 20). Structural cross-sections were examined to ensure the presence of a suitable caprock and structural trapping mechanisms in the selected area (Figure 21). A minimum continuous pay thickness of 6.1 m (20 ft.) was then applied along with the < 75 gAPI gamma ray cut-off and the ≥ 100 mD permeability cut-off to generate net pay flags over the Cretaceous-Jurassic storage interval of interest and identify the most vertically and laterally continuous pay zone to serve as the injection zone for dynamic simulation.

The potential injection well was positioned between three existing wells on the eastern margin of the GSD, with a dynamic model area of 596 km^2 (230 mi^2) delineated by net thicknesses ≥ 100 m and effective porosities ≥ 20% for the combined storage zones (e.g., Figure 20). An interval at the top of the MK3 zone having an average net thickness of 51 m (166 ft.) was delineated by net pay flags in 4 out of 7 of the wells near the GSD and was selected as the model injection zone (Figure 21). The effective porosity and permeability logs from the three surrounding wells were rescaled to 1.5 m intervals to divide the injection zone into approximately 35 vertical layers with unique porosity and permeability values for the dynamic model (Figure 22).

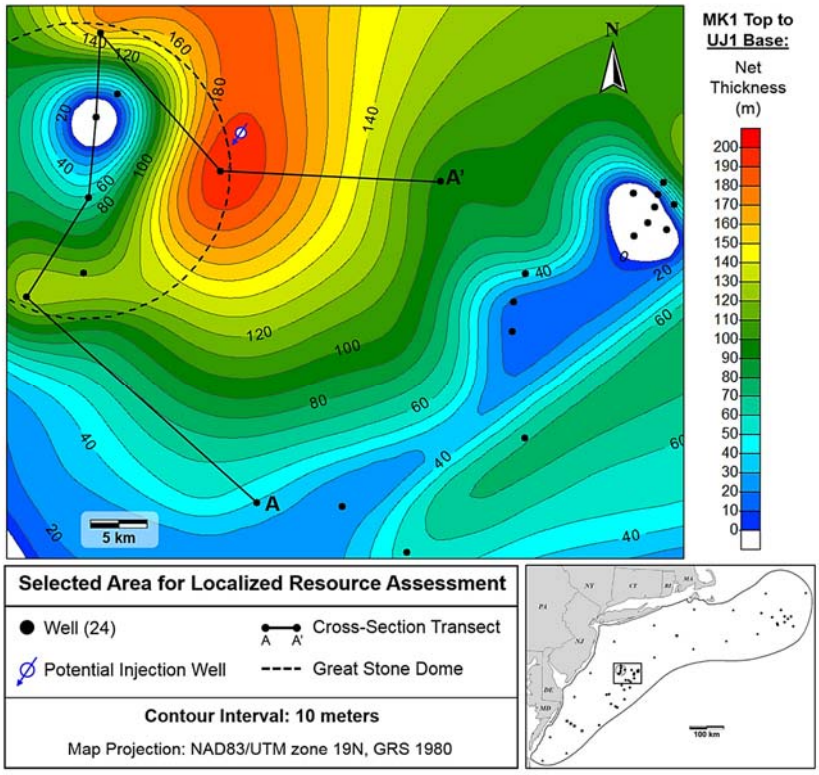

Figure 20. Net thickness map (GR< 75 gAPI, k ≥ 100 mD) for the interval extending from the MK1 top to the UJ1 base showing the selected area for localized storage resource calculations and dynamic injection simulations near the GSD.

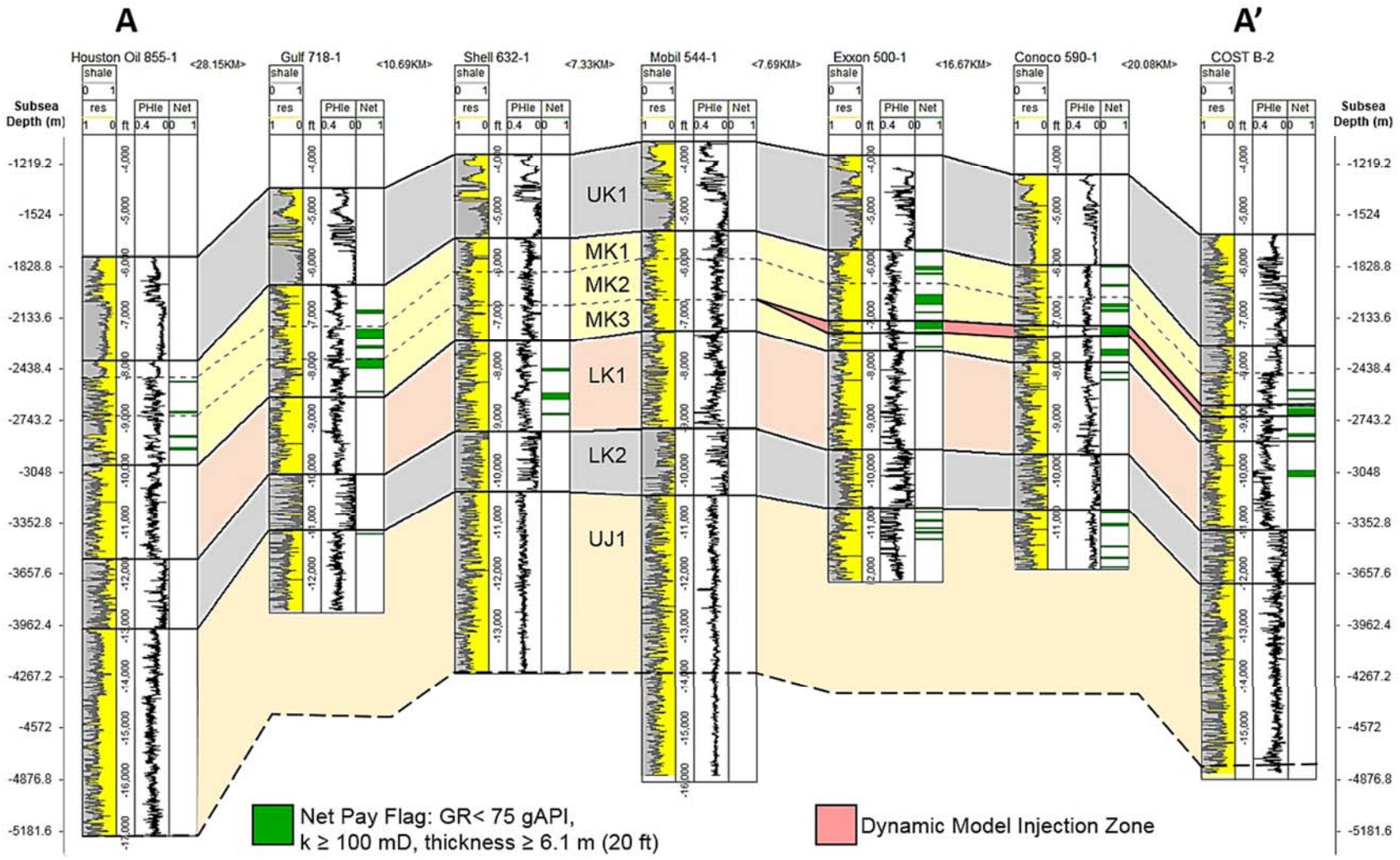

Figure 21. Structural cross-section across the GSD showing net pay flags calculated over the three storage zones and the selected injection zone for the dynamic reservoir simulation at the top of the MK3.

Figure 23 provides an oblique view of the simplified site model with a dip of approximately 1 degree assigned to the MK3 injection zone based on the calculated subsurface gradient from the model injection well to the approximate top of the GSD structure (19.2 m/km gradient over a distance of 14 km). The cumulative CO_2 injection, corresponding maximum pressure buildup, and plume extent in the MK3 injection zone were investigated for both the 1.5 Mt CO_2/year injection scenario (reference scenario) and the 1.0 Mt CO_2/year injection scenario (variant scenario). The cumulative quantity of CO_2 stored at the end of 30 years was also calculated for a maximum CO_2 injection scenario with injection rates defined by the maximum allowable injection pressure. The dynamic model results presented here are specific to the fluid-rock properties discussed in Section 3.4.

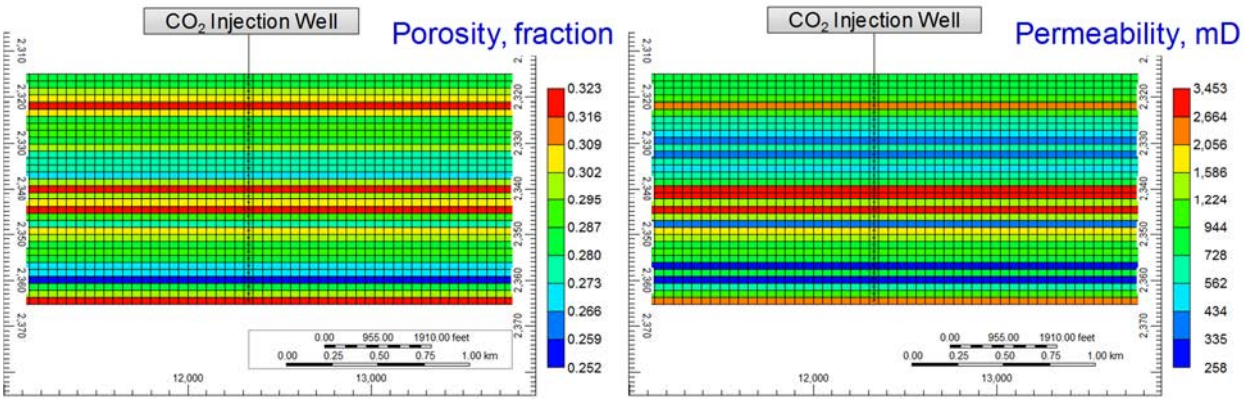

Figure 22. Snapshot of the dynamic model in the selected area near the GSD showing the vertical distribution of porosity and permeability in the MK3 injection zone.

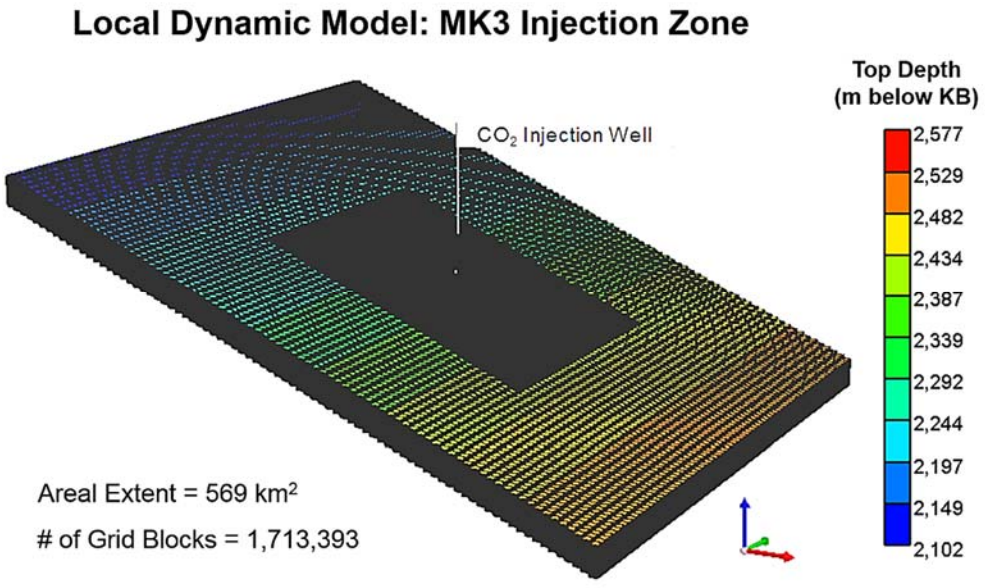

Figure 23. Dynamic model snapshot showing the injection well location in the injection zone at the top of the MK3.

The maximum amount of CO_2 that could be injected over a 30-year period was found to be 51 Mt for injection rates corresponding to the maximum allowable injection pressure of 31 MPa measured at bottom-hole conditions. Figure 24 shows the total CO_2 injected for the reference and variant injection cases modeled in the selected area. In both cases, the injection well is required to operate at the constant specified injection rate while maintaining injection pressures below the maximum bottom-hole pressure constraint specified.

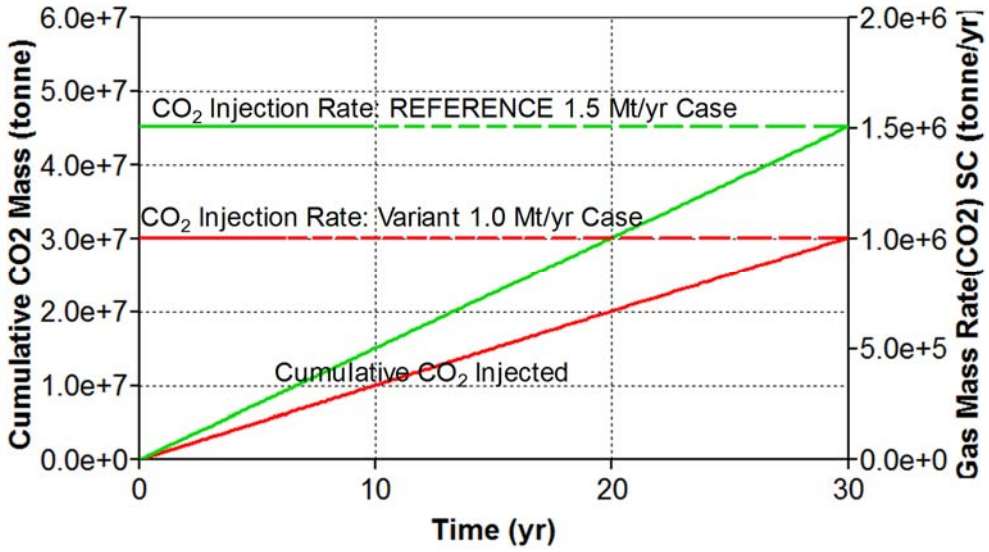

Note: Green curves correspond to the reference 1.5 Mt/year case results while the red curves correspond to results of the more conservative 1.0 Mt/year variant injection case.

Figure 24. CO_2 injection rate and cumulative injection achieved using the single vertical well in the two injection scenarios investigated.

Pressure buildup is directly related to the rate at which the fluids are added or removed from the closed system of interest. Pressure buildup in the injection zone and bottom-hole well pressure is shown through the injection period in Figure 25. For a target of 30 Mt of total CO_2 injection, a 5-MPa pressure increase was observed at 20 years in the 1.5 Mt CO_2/year reference injection scenario while a 4-MPa increase was observed after 30 years for the more conservative/variant injection scenario of 1.0 Mt of CO_2/year.

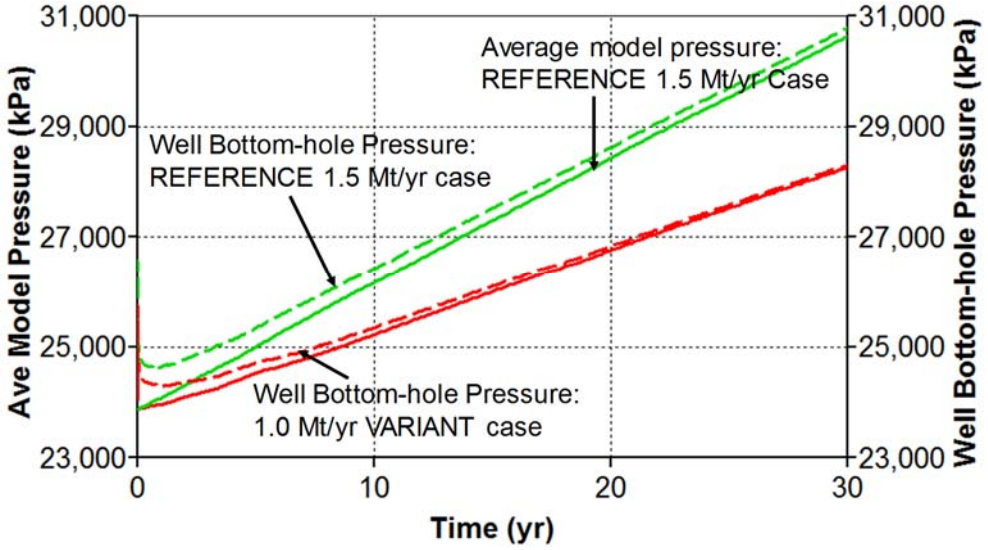

Note: Green curves correspond to the reference 1.5 Mt/year case results while the red curves correspond to results of the more conservative 1.0 Mt/year variant injection case.

Figure 25. Average reservoir pressure and injection well bottom-hole pressures tracked in the two injection scenarios investigated.

Figure 26 shows the CO_2 plume extent in the reference injection scenario (1.5 Mt CO_2 /year) at the end of 30 years of injection. The resulting CO_2 plume had an area of 32 km^2 (6.4 km diameter) and was observed to move preferentially up-dip toward the GSD, with more CO_2 accumulating in the high permeability layers of the injection zone (e.g., Figure 22). As much as 45 Mt of CO_2 was able to be injected over 30 years while maintaining bottom-hole pressures below the fracture pressure gradient.

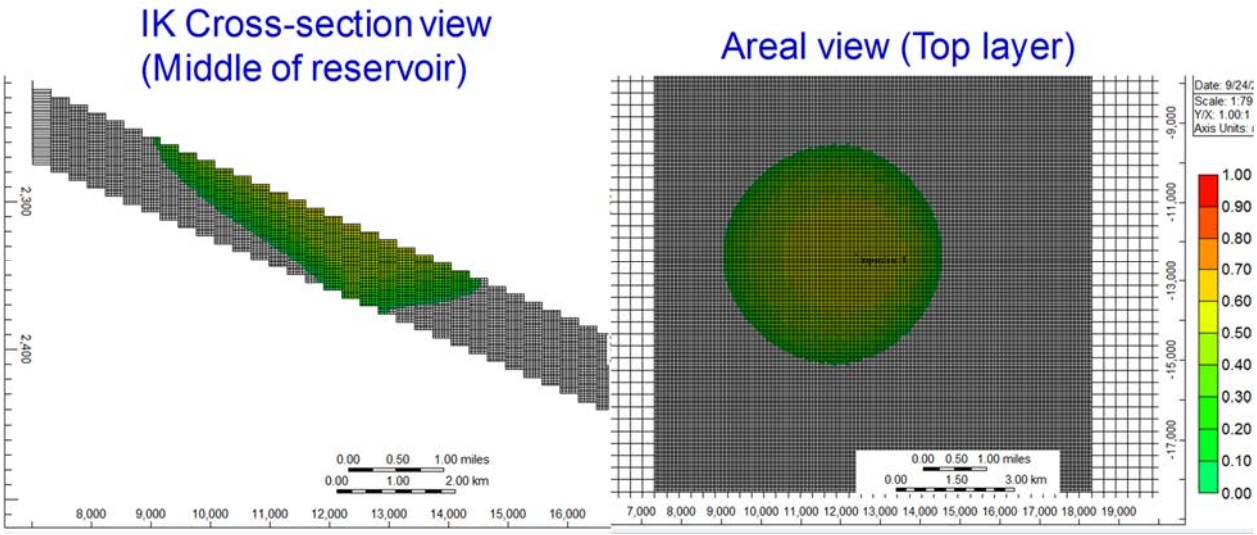

Figure 26. 45 Mt CO_2 plume extent (gas saturation) in two view planes at the end of the 30-year injection simulation.

4.0 Discussion

4.1 Key Outcomes and Offshore Storage Resource Classification

As part of the Storage Resource Calculation task, a systematic workflow has been employed to quantify and categorize CO_2 storage resources for the Mid-Atlantic U.S. offshore region extending from Maryland to Massachusetts. Based on factors unique to offshore environments, such as immature basin conditions, variation in geothermal gradient, and soft-sediment deformation, offshore-specific screening criteria were defined to identify three Cretaceous- and Jurassic-age deep saline formations suitable for CO_2 storage resource assessment. Detailed characterization of key petrophysical properties (e.g., pore volume, permeability) for the three potential storage zones suggests targeted reservoir intervals contain average porosities ranging from 21% to 29%, and mean permeabilities ranging from 45 mD to 339 mD (e.g., Table 9 and Table 11). These values are within the range of porosities and permeabilities reported for other offshore reservoirs currently being used or evaluated for commercial-scale CO_2 storage (Norwegian Petroleum Directorate, 2011; 2013; Trevino and Meckel, 2017).

Regional-scale estimates of storage resources and storage resource maps have been developed to represent portions of the Mid-Atlantic offshore region not previously characterized for carbon storage. As part of this effort, offshore-specific storage efficiency values were determined and used as input in regional-scale calculations. Resource estimates were refined at the local scale using dynamic reservoir simulation at a selected area in the northern BCT (Figure 20) with high estimated storage resource (≥ 2.4 Mt CO_2/km^2) and relatively dense well data coverage (well spacing ≤ 5 km).

The results derived from static and dynamic assessment methods employed in this study are categorized as prospective storage resources (DOE-NETL, 2017; SPE-SRMS, 2017) (Figure 27). Prospective storage resource estimates do not account for regulatory issues or system-wide techno-economics of a CCS project. Regional estimates have been calculated stochastically and reported at the P10, P50, and P90 probability ranges to represent uncertainty in the estimated net connected pore volumes and account for an order of magnitude of potential error in the permeability values assigned to the storage zones of interest. Regional storage resources reported in this work can be classified at the “Play” level in terms of project maturity (Figure 27). Local-scale storage resources estimated for the MK3 injection zone using dynamic reservoir simulation requires additional refinement to advance to the “Lead” level, which could be accomplished via development of a 3D static earth model to better characterize the geospatial variability of accessible pore volumes, reservoir injectivity, and trapping mechanisms in the selected area.

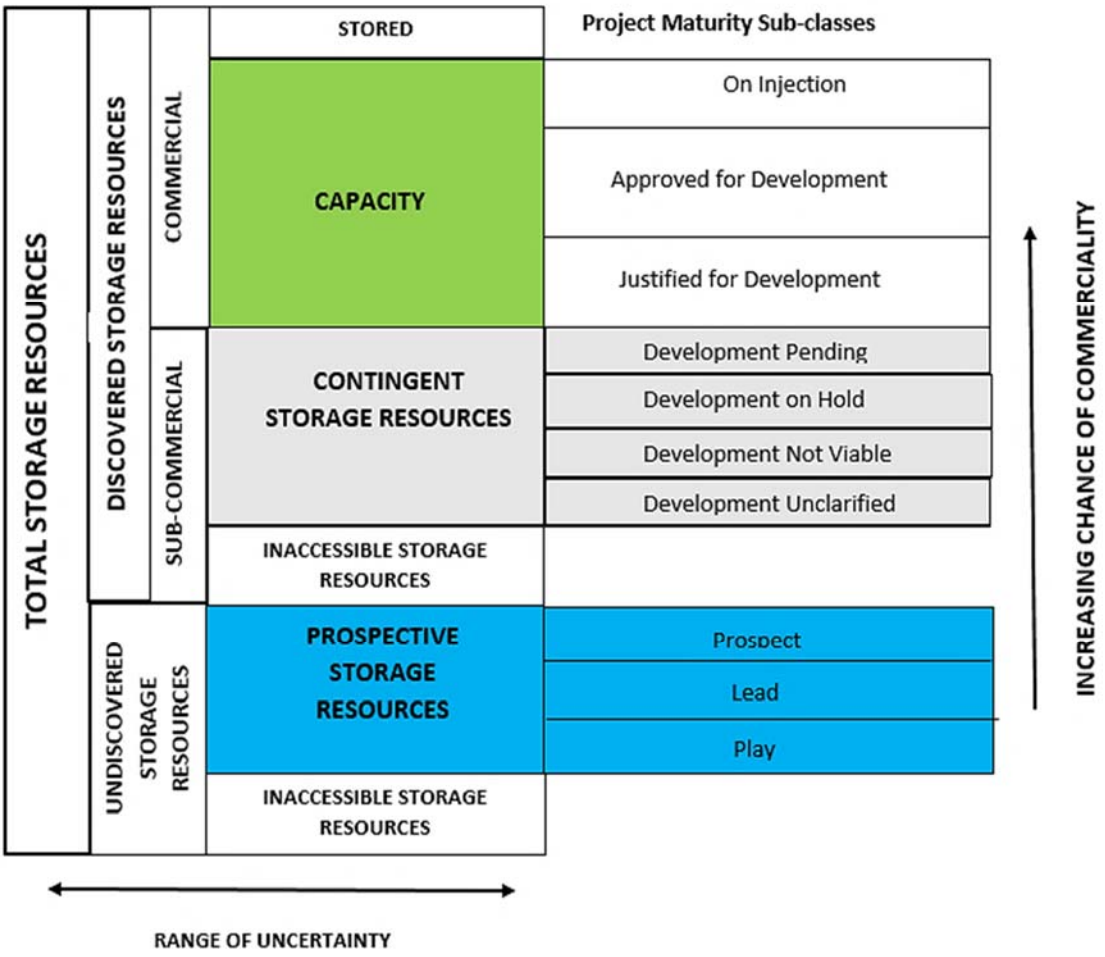

Figure 27. The SPE-SRMS storage resource classification framework and associated subclasses based on project maturity (SPE-SRMS, 2017).

4.2 Offshore-Specific Storage Efficiency

Low (P10), median (P50), and high (P90) probability values were calculated for each storage efficiency parameter (Equation 6 and 8) in order to derive offshore-specific estimates of deep saline storage efficiency (E_{saline}) and facilitate comparison with regional-scale storage efficiency ranges reported for onshore deep saline formations. Using formation-specific well log, core, and seismic data from the three offshore storage zones of interest, sandstone with gamma ray values less than 75 gAPI was used to delineate “reservoir” intervals (i.e., sandstone) from non-reservoir intervals (i.e., shale), and permeability was used as a proxy to represent connected pore volumes. Minimum permeability cut-offs of ≥ 10 mD and ≥ 100 mD were applied, respectively, along with the gamma ray cut-off to quantify the total and net effective pore volume available for CO_2 storage. Table 15 shows storage efficiency probability values calculated for offshore deep saline formations in this study compared with those reported by DOE-NETL (e.g., Goodman et al., 2011) and IEAGHG (2009).

Table 15. Storage efficiency probability values calculated in this study for offshore deep saline formations compared to values reported by DOE-NETL (Goodman et al., 2011) and IEAGHG (2009).

Study	Deep Saline Formation	Geologic Efficiency						Displacement Efficiency			
		P10			P90			P10		P90	
		E_{An}	E_{hn}	$E_{\phi\varepsilon}$	E_{An}	E_{hn}	$E_{\phi\varepsilon}$	E_V	E_d	E_V	E_d
This study	MK1-3	0.09			0.7			0.34	0.22	0.89	0.30
	LK1	0.12			0.59			NA	NA	NA	NA
	UJ1	0.08			0.38			NA	NA	NA	NA
	Combined	0.10			0.58			0.09		0.26	
IEAGHG (2009); Goodman et al. (2011)	Clastics	0.20	0.21	0.64	0.80	0.76	0.77	0.16	0.35	0.39	0.76
	Dolomite	0.20	0.17	0.53	0.80	0.68	0.71	0.26	0.57	0.43	0.64
	Limestone	0.20	0.13	0.64	0.80	0.62	0.75	0.33	0.27	0.57	0.42

NA = Not Analyzed

Figure 28 shows the resulting E_{saline} values calculated in this study for the three offshore storage zones of interest (see Table 14. High (P90), median (P50), and low (P10) values for total deep saline storage efficiency (E_{saline}) results and prospective CO_2 storage resource estimates for the three storage zones. Table 14) compared with values reported for onshore deep saline formations in the fifth edition of the U.S. DOE-NETL Carbon Storage Atlas (DOE-NETL, 2015). The MK1-3 and LK1 zones exhibit higher P50 (4.9% and 4.7%, respectively) and P90 (12.5% and 10.7%, respectively) values compared to the DOE-NETL E_{saline} values (P50 of 2.0% and P90 of 5.5%), resulting in a larger overall E_{saline} range calculated in this study for offshore deep saline formations.

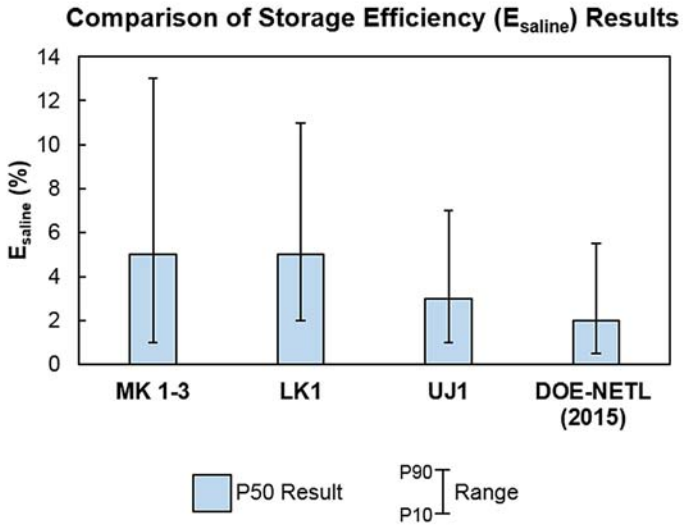

Figure 28. Storage efficiency (E_{saline}) results for the three offshore formations evaluated in this study compared to values reported for onshore deep saline formations by DOE-NETL (2015).

4.3 Regional Prospective Storage Resources

Regional prospective storage resources calculated for the three storage zones range from 37 Gt to 403 Gt of CO_2, with median P50 values of 148 Gt, 178 Gt, and 153 Gt calculated for the MK1-3, LK1, and UJ1, respectively. In 2016, total CO_2 emissions from power generation and industrial point sources in the eastern United States was approximately 0.15 Gt per year (Battelle, 2018b). Assuming CO_2 emissions increase annually by an average of 6% (EIA, 2018), P10 values of 37 Gt (MK1-3), 59 Gt (LK1), and 54 Gt (UJ1) suggest there's a high probability

that each of the potential offshore storage zones has a CO_2 storage resource greater than the cumulative 30-year quantity of CO_2 emitted (12.6 Gt) from the nearby point sources evaluated.

As previously mentioned, the regional-scale storage resource estimates reported in this study are classified at the Play level for prospective storage resources, denoting initial preliminary results should be further refined to determine project feasibility and chances of commercialization. Additional data and analysis are needed to reduce uncertainty and data gaps in each of the offshore Mid-Atlantic sub-regions, and better constrain the continuity/connectivity of reservoir pore volumes in selected area(s).

4.4 Local Prospective Storage Resources

Simplified dynamic injection and storage simulation was conducted to determine injection pressure constraints, provide local-scale CO_2 storage resource estimates, and evaluate the feasibility of commercial-scale storage operations for a selected area of the Mid-Atlantic offshore study region. Preliminary results from dynamic modeling suggest a single 51-m-thick injection zone in the MK3 sandstone sequence alone could potentially store CO_2 quantities greater than the annual and 30-year cumulative CO_2 emissions from one nearby power plant or industrial source along the eastern United States. As much as 51 Mt of CO_2 was able to be injected and stored over 30 years at the maximum allowable injection pressure determined by the fracture pressure gradient. For the reference injection scenario (1.5 Mt CO_2/year), 45 Mt of CO_2 was stored over 30 years the while maintaining injection pressures below the maximum allowable injection pressure. For comparison, 96% (468 out of 489) of the CO_2 sources identified in the eastern United States as part of the Risk Factor Analysis (Task 6) had annual CO_2 emissions of 2 Mt or less in 2016, and 90% (445 out of 489) of the sources were reported to emit 1 Mt CO_2/year or less (Battelle, 2018b).

Net pay flags (GR < 75 gAPI, k ≥ 100 mD, thickness ≥ 6.1 m) were also observed in the MK1, MK2, LK1, and UJ1 zones within the selected area near the GSD, with the MK2 net pay flag exhibiting lateral and vertical continuity comparable to that observed at the top of the MK3 reservoir selected for local-scale dynamic storage resource calculations (Figure 20). This suggests the stacked storage resources in the selected area could potentially accommodate commercial-scale CO_2 quantities from more than one industrial CO_2 source in the eastern United States. Results from the local-scale dynamic injection and storage simulation in this study are consistent with results of previous work that suggest large-scale CO_2 storage is feasible in the offshore Mid-Atlantic region (e.g., Slater et al., 2010; Brown et al., 2011; New Jersey Geological Survey, 2011).

While an injection rate of 1.5 Mt CO_2/year (reference scenario) was achieved without compromising formation integrity, dynamic simulation results for the more conservative 1.0 Mt CO_2/year injection scenario suggest injection at a lower rate for a longer period would enable the same ultimate amount of CO_2 to be stored without the additional pressure buildup observed in the closed system for the reference injection scenario. It should also be noted that aside from the uplift and structural closure formed in Cretaceous-age strata above the GSD, there were no geologic features identified in the selected area that are expected to act as lateral no-flow boundaries. Consequently, the potential pressure response during actual CO_2 injection activities may be lower than those observed in the two injection scenarios modeled in the selected area.

5.0 Conclusions

Offshore CO_2 storage resource estimates have been calculated to: 1) establish preliminary, screening-level constraints on the CO_2 storage potential of Mid-Atlantic offshore deep saline formations; and 2) help delineate prospective storage targets at the basin and sub-basin scale.

Results of this work suggest offshore storage resource estimates should be based on comprehensive data integration methods that incorporate analysis of risk factors, data availability, and formation-specific storage efficiency calculations. Factors such as basin age/maturity and sediment lithification evaluated in previous tasks (e.g., Task 2, 4, and 6) were used to establish screening criteria to identify offshore sub-region(s) with suitable conditions for storage resource calculations. A thorough data integration process involving iterative comparison and correlation of core, log, and seismic data was conducted to quantify and map petrophysical properties, pore volumes, and storage efficiency values for three potential storage zones in Middle-Lower Cretaceous and Upper Jurassic sandstone sequences.

Probability values ranging from 0.10 (low) to 0.58 (high) were derived for geologic storage efficiency terms using the combined net-to-total pore volume dataset from the three offshore storage zones. The distribution of dynamic simulation results produced displacement efficiencies with a P10 of 0.09 and a P90 of 0.26. Regional prospective storage resources calculated for the three storage zones range from 37 Gt to 403 Gt of CO_2. Storage resource maps for all three storage zones show high estimated storage resource (P50 greater than 2.4 Mt CO_2/km^2) occurring in the northern BCT near the GSD structure. Simplified dynamic reservoir simulation performed for one 51-m-thick net reservoir interval within the MK3 sequence near the GSD suggests that approximately 45 Mt to 51 Mt of CO_2 could be stored over 30 years via the specific single-well injection scenarios and pressure constraints evaluated.

Additional subsurface data analysis and acquisition is needed to reduce uncertainty and data gaps within each of the offshore sub-regions (e.g., Figure 1). Development of a 3D static earth model would help to better characterize the geospatial variability of accessible pore volumes, reservoir injectivity, caprock/confining mechanisms, and estimated storage resources in the selected area(s). Additional analysis should also consider potential regulatory issues, storage site requirements, and affected communities in the Mid-Atlantic region.

6.0 References

Amato, R. and Bebout, J. (eds.), 1980, Geologic and Operational Summary, COST No. G-1 Well, Georges Bank Area, North Atlantic OCS. USGS Open-File Report 80-268.

Bachu, S., D. Bonijoy, J. Bradshaw, R. Burruss, S. Holloway, N.P. Christensen, and O.M. Mathiassen. 2007. CO_2 storage capacity estimation: Methodology and gaps. Int. J. Greenh. Gas Con., vol. 1, no. 4, pp. 430-443.

Bachu, S. 2015. Review of CO_2 storage efficiency in deep saline aquifers. International Journal of Greenhouse Gas Control 40, 188-202.

Battelle. 2018a. Mid-Atlantic U.S. Offshore Carbon Storage Resource Assessment Project: Task 4 Hydrologic Properties Data Package Report. Submitted April 30, 2018. DOE Award Number DE-FE0026087.

Battelle. 2018b. Mid-Atlantic U.S. Offshore Carbon Storage Resource Assessment Project: Task 6 Risk Factor Analysis Report. Submitted June 30, 2018. DOE Award Number DE-FE0026087.

Blondes, M.S., S.T. Brennan, M.D. Merrill, M.L. Buursink, P.D. Warwick, S.M. Cahan, T.A. Cook, M.D. Corum, and others. 2013. National assessment of geologic carbon dioxide storage resources—Methodology implementation: U.S. Geological Survey Open-File Report 26, 2013–1055. Accessed February 19, 2017, at http://pubs.usgs.gov/of/2013/1055/.

Bradshaw, J., S. Bachu, D. Bonijoly, R. Burruss, S. Holloway, N.P. Christensen , and O.M. Mathiassen. 2007. CO_2 storage capacity estimation: Issues and development of standards. Int. J. Greenh. Gas Con., vol. 1, no. 1, pp. 62-68.

Bradshaw, B., L. Spencer, A. Lahtinen, K. Khider, D. Ryan, J. Colwell, A. Chirinos, J. Bradshaw, J. Draper, J. Hodgkinson, and M. McKillop. 2011. An Assessment of Queensland's CO_2 Geological Storage Prospectivity-The Queensland CO_2 Geological Storage Atlas.

Brennan, S.T., R.C. Burruss, M.D. Merrill, P.A. Freeman, and L.F. Ruppert. 2010. A probabilistic assessment methodology for the evaluation of geologic carbon dioxide storage: U.S. Geological Survey Open-File Report 31, 2010–1127. Accessed February 19, 2017 at http://pubs.usgs.gov/of/2010/1127.

Brown, A., Berlin, E., Butsch, R., Senel, O., Mills, J., Harichandran, A., Wang, J. 2011. Carbon Capture and Sequestration: Ascertaining CO_2 Storage Potential, Offshore New Jersey, USA. Offshore Technology Conference, Houston Texas, May 2-5, 2011.OTC 21995.

Calhoun Jr., J.C. 1982. Fundamentals of Reservoir Engineering. University of Oklahoma Press, Norman Oklahoma.

Carmichael, R.S. ed. 1982. Handbook of Physical Properties of Rocks, Vol. 2, 1-228. Boca Raton, Florida: CRC Press Inc.

CSLF. 2007. Estimation of CO_2 Storage Capacity in Geological Media: Phase II Final Report from the Task Force for Review and Identification of Standards for CO_2 Storage Capacity Estimation. CSLF-T-2007-04.

CSLF. 2008. Comparison between Methodologies Recommended for Estimation of CO_2 Storage Capacity in Geological Media: Phase III Report from the CSLF Task Force on CO_2

Storage Capacity Estimation and the US DOE Capacity and Fairways Subgroup of the Regional Carbon Sequestration Partnerships Program. CSLF-T-2008-04.

Cumming L, Gupta N, Miller K, Lombardi C, Goldberg D, ten Brink U, Schrag D, Andreasen D, Carter K. 2017. Mid-Atlantic U.S. Offshore Carbon Storage Resource Assessment. Energy Procedia v. 114 p. 4629–4636. < http://dx.doi.org/10.1016/j.egypro.2017.03.1590>

DOE-NETL (U.S. Department of Energy-National Environmental Technology Laboratory). 2008. The United States 2008 Carbon Utilization and Storage Atlas, Second Edition. Accessed February 19, 2017, at https://edx.netl.doe.gov/no/dataset/2008-carbon-storage-atlas-of-the-united-states-and-canada.

DOE-NETL (U.S. Department of Energy-National Environmental Technology Laboratory). 2010. The United States 2010 Carbon Utilization and Storage Atlas, Third Edition. Accessed February 19, 2017, at https://www.netl.doe.gov/KMD/CDs/atlasIII/2010atlasIII.pdf.

DOE-NETL (U.S. Department of Energy-National Environmental Technology Laboratory). 2012. The United States 2012 Carbon Utilization and Storage Atlas, Fourth Edition. Accessed February 19, 2017, at https://www.netl.doe.gov/File%20Library/Research/Coal/carbon-storage/atlasiv/Atlas-IV-2012.pdf.

DOE-NETL (U.S. Department of Energy-National Environmental Technology Laboratory). 2013. Best Practices for Site Screening, Selection, and Initial Characterization for Storage of CO_2 in Deep Geologic Formations. DOE/NETL-2013/1605.

DOE-NETL (U.S. Department of Energy-National Environmental Technology Laboratory). 2015. Carbon Storage Atlas, Fifth Edition. U.S. Department of Energy - National Energy Technology Laboratory - Office of Fossil Energy. Accessed February 19, 2017, at https://www.netl.doe.gov/research/coal/carbon-storage/natcarb-atlas.

DOE-NETL (U.S. Department of Energy-National Energy Technology Laboratory). 2017. Best Practices for Site Screening, Selection, and Initial Characterization for Storage of CO_2 in Deep Geologic Formations. DOE/NETL-2017/1844.

Duan, Z. and Sun, R. 2003. An improved model calculating CO_2 solubility in pure water and aqueous NaCl solutions from 273 to 533 K and from 0 to 2000 bar. Chemical Geology193, 257–271.

EIA (United States Energy Information Administration). 2018. Annual Energy Outlook 2018 with projections to 2050. U.S. Energy Information Administration Office of Energy Analysis, February 2018. < https://www.eia.gov/outlooks/aeo/pdf/AEO2018.pdf>

Erickson, S.N. and R.D. Jarrard. 1998. Velocity-porosity relationships for water-saturated siliciclastic sediments, J. Geophy. Res., 103(B12), 30385–30406, doi:10.1029/98jb02128.

Frailey, S. 2013. Estimating CO_2 plume size: A correlation for site screening. Int. J. Greenh. Gas Con., vol. 13, pp. 230-234.

Goodman, A., A. Hakala, G. Bromhal, D. Deel, T. Rodosta, S. Frailey, M. Small, D. Allen, V. Romanov, J. Fazio, N. Huerta, D. McIntyre, B. Kutchko, and G. Guthrie. 2011. U.S. DOE methodology for the development of geologic storage potential for carbon dioxide at the national and regional-scale. Int. J. Greenh. Gas Con., vol. 5, pp. 952–965.

Goodman, A., S. Sanguinito, and J. Levine. 2016. Prospective CO_2 resource estimation methodology: Refinement of existing US DOE-NETL methods based on data availability. Int. J. Greenh. Gas Con., vol. 54, pp. 242-249.

Gorecki, C., Ayash, S., Guoxiang, L.l Braunberger, J., Dotzenrod, N. 2015. A comparison of volumetric and dynamic CO_2 storage resource and efficiency in deep saline formations. International Journal of Greenhouse Gas Control, 42, 213–225.

Grow, J.A. and Sheridan, R.E. 1988. U.S. Atlantic continental margin: A typical Atlantic-type or passive continental margin, *in* Sheridan, R.E., Grow, J.A., eds., The Atlantic Continental Margin: Boulder, Colorado, Geological Society of America, Geology of North America, v. 1-2, p. 1-7.

Hutchinson DR, Klitgord KD, Detrick RS. 1986. Rift basins of the Long Island platform. Geologic Society of America Bulletin, 97, 688-702.

IEAGHG (International Energy Agency Greenhouse Gas R&D Programme). 2009. Development of Storage Coefficients for CO_2 Storage in Deep Saline Formations. Technical Study Report No. 2009/13.

Jansa, L., Pe-Piper, G. 1988. Middle Jurassic to early Cretaceous igneous rocks along eastern North American continental margin. AAPG Bulletin v. 72, p. 347-366.

Kennett, B.L.N. (1983), Seismic wave propagation in stratified media, Cambridge University Press, Cambridge [Cambridgeshire]; New York.

Klitgord, K.D., Poag, C., Schneider, C., and North, L. (1994). Geophysical database of the East Coast of the United States northern Atlantic margin—cross-sections and gridded database (Georges Bank Basin, Long Island Platform, and Baltimore Canyon Trough), 2331-1258.

Lake, L.W. 1989. Enhanced Oil Recovery. Prentice Hall, Englewood Cliffs, New Jersey.

Libby-French, J. (1984). Stratigraphic framework and petroleum potential of northeastern Baltimore Canyon Trough, Mid-Atlantic outer continental shelf: AAPG Bulletin, v. 68, no. 1, p. 50-73.

Mallick, S. (1995), Model-based inversion of amplitude-variations-with-offset data using a genetic algorithm, Geophysics, 60(4), 939-954, doi:10.1190/1.1443860.

Miller, K.G., Kominz, M.A., Browning, J.V., Wright, J.D., Mountain, G.S., Katz, M.E., Sugarman, P.J., Cramer, B.S., Christie-Blick, N., and Pekar, S.F., 2005, The Phanerozoic record of global sea-level change: Science, v. 310, p. 1293-1298.

New Jersey Geological Survey (2011). Preliminary Characterization of CO_2 Sequestration Potential in New Jersey and the Offshore Coastal Region: Midwest Regional Carbon Sequestration Partnership. Final report, 98 pp;. http://www.mrcsp.org/phase-ii-geologic-reports

Norwegian Petroleum Directorate. 2011. CO_2 Storage Atlas: Norwegian North Sea. Norwegian Petroleum Directorate, Stavanger. www.npd.no/Global/Norsk/3-Publikasjoner/Rapporter/PDF/CO2-ATLAS-lav.pdf.

Norwegian Petroleum Directorate. 2013. CO_2 Storage Atlas: Barents Sea. Norwegian Petroleum Directorate, Stavanger. www.npd.no/Global/Norsk/3-Publikasjoner/Rapporter/PDF/CO2-ATLAS-lav.pdf.

Olsen P.E. (1997). Stratigraphic record of the early Mesozoic breakup of Pangea in the Laurasia-Gondwana rift system. Annu. Rev. Earth Planet Sci., 25, 337-401.

Olsson, R.K., Gibson, T.G., Hansen, H.J., and Owens, J.P. (1988). Geology of the northern Atlantic coastal plain: Long Island to Virginia, *in* Sheridan, R.E., Grow, J.A., eds., The Atlantic

Continental Margin: Boulder, Colorado, Geological Society of America, Geology of North America, v. 1-2, p. 87-105.

Poag, W. 1978. Stratigraphy of the Atlantic continental shelf and slope of the United States. Annual Reviews of Earth and Planetary Science v. 6, p. 251-280.

Post, P. J., and Coleman, J. L., Jr. (2015). Mesozoic rift basins of the U.S. central Atlantic offshore: comparisons with onshore basins, analysis, and potential petroleum prospectivity, in GCSSEPM Foundation 34th Annual Perkins-Rosen Research Conference, Houston, Texas, p. 1-93.

Sanguinito, S., A. Goodman, and J.S. Levine. 2016. NETL CO_2 Storage prospeCtive Resource Estimation Excel aNalysis (CO_2-SCREEN) User's Manual; NETL-TRS-X-2016; Technical Report Series; U.S. Department of Energy, National Energy Technology Laboratory: Pittsburgh, Pennsylvania, 2016; p. 31. https://edx.netl.doe.gov/carbonstorage/?page_id=914.

Savva, D., Chrest, T., Saint-Ange, F., MacDonald, A., Luheshi, M., Cuilhe, L. 2016. Structural Impact of the Yarmouth Arch in the Central Atlantic Opening and on the Southwest Nova Scotian Margin Architecture. AAPG 2016 Annual Convention and Exhibition, Calgary, Alberta, Search and Discovery Article #30481.

Schlee, J., Behrendt, J. C., Grow, J. A., Robb, J. M., Mattick, R. E., Taylor, P. T., Lawson, B. J. 1976. Regional geologic framework off northeastern United States. AAPG Bulletin v. 69, p. 926-951.

Schlee, J. 1980. Seismic Stratigraphy of the Baltimore Canyon trough. United States Geological Survey Open File Report 80-1079.

Scholle, P.A., ed. (1977). Geological studies on the COST No. B-2 well, U.S. Mid-Atlantic outer continental shelf area: U.S. Geological Circular 750, 71 p.

Slater, B., Stolorow, A., and Smith, L. (2010). Potential for Supercritical Carbon Sequestration in the Offshore Bedrock Formations of the Baltimore Canyon Trough, *in* AAPG Eastern Section Meeting, Kalamazoo, Michigan, AAPG.

Slatt, R.M. 2006. Stratigraphic Reservoir Characterization for Petroleum Geologists, Geophysicists and Engineers. Handbook of Petroleum Exploration and Production v. 6.

Smith, M., Amato, R., Furbush, M., Pert, D., Nelson, M., Hendrix, J., Tamm, L., Wood, G. Jr., Shaw, D. 1976. Geological and operational summary, COST NO. B-2 well, Baltimore Canyon Trough Area, Mid-Atlantic OCS. United States Geological Survey Open File Report 76-774.

Society of Petroleum Engineers. 2017. Storage Resources Management System.

Szulczewski, M., C.W. MacMinn, H.J. Herzog, and R. Juanes. 2012. Lifetime of carbon capture and storage as a climate-change mitigation technology. Proc. Natl. Acad. Sci. vol. 109, pp. 5185–5189.

Trevino, R. and Meckel, T., (Eds). 2017. Geologic CO_2 Sequestration Atlas of Miocene Strata, Offshore Texas State Waters. Bureau of Economic Geology. The University of Texas at Austin. Report of Investigations No. 283.

Turekian, K., Wedepohl, K.H. 1961. Distribution of the Elements in Some Major Units of the Earth's Crust. Geological Society of America Bulletin v. 72, p. 175-192.

Vangkilde-Pedersen, T., H. Vosgerau, B. Willscher, F. Neele, B. van der Meer, D. Bossie-Codreanu, A. Wojcicki, Y-M Le Nindre, K. Kirk, I. von Dalwigk, and K.L. Anthonsen. 2009. EU GeoCapacity—Assessing European Capacity for Geological Storage of Carbon Dioxide. Geological Survey of Denmark and Greenland Project No. SES6-518318, pp. 45.

Watts, A.B. (1981). The U.S. Atlantic continental margin; Subsidence history, crustal structure, and thermal evolution, *in* Bally, A.W., ed., Geology of passive continental margins: History, structure, and sedimentologic record. American Association of Petroleum Geologists Education Course Note Series 19:1–75.

Zhou, Q., J.T. Birkholzer, C-F Tsang, and J. Rutqvist. 2008. A method for quick assessment of CO_2 storage capacity in closed and semi-closed saline formations. Int. J. Greenh. Gas Con. vol. 2, pp. 626-639.

Appendix A: Task 5 Storage Resource Calculation Support Tables and Graphics

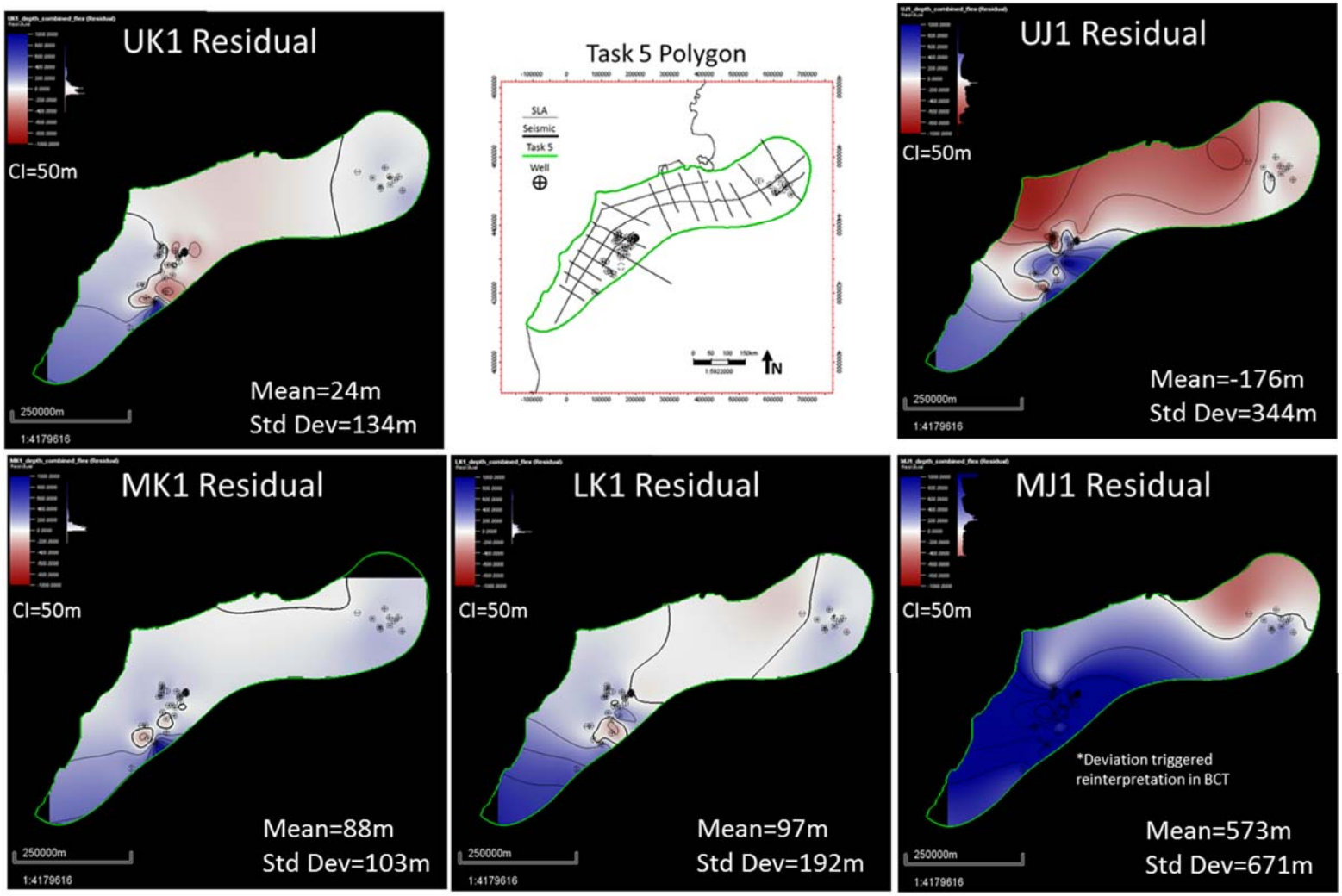

Figure A-1. Depth differences (residuals) between 3D interpolated surfaces and correlative formation tops from wells for key intervals. Note that residuals and general uncertainty increases with depth.

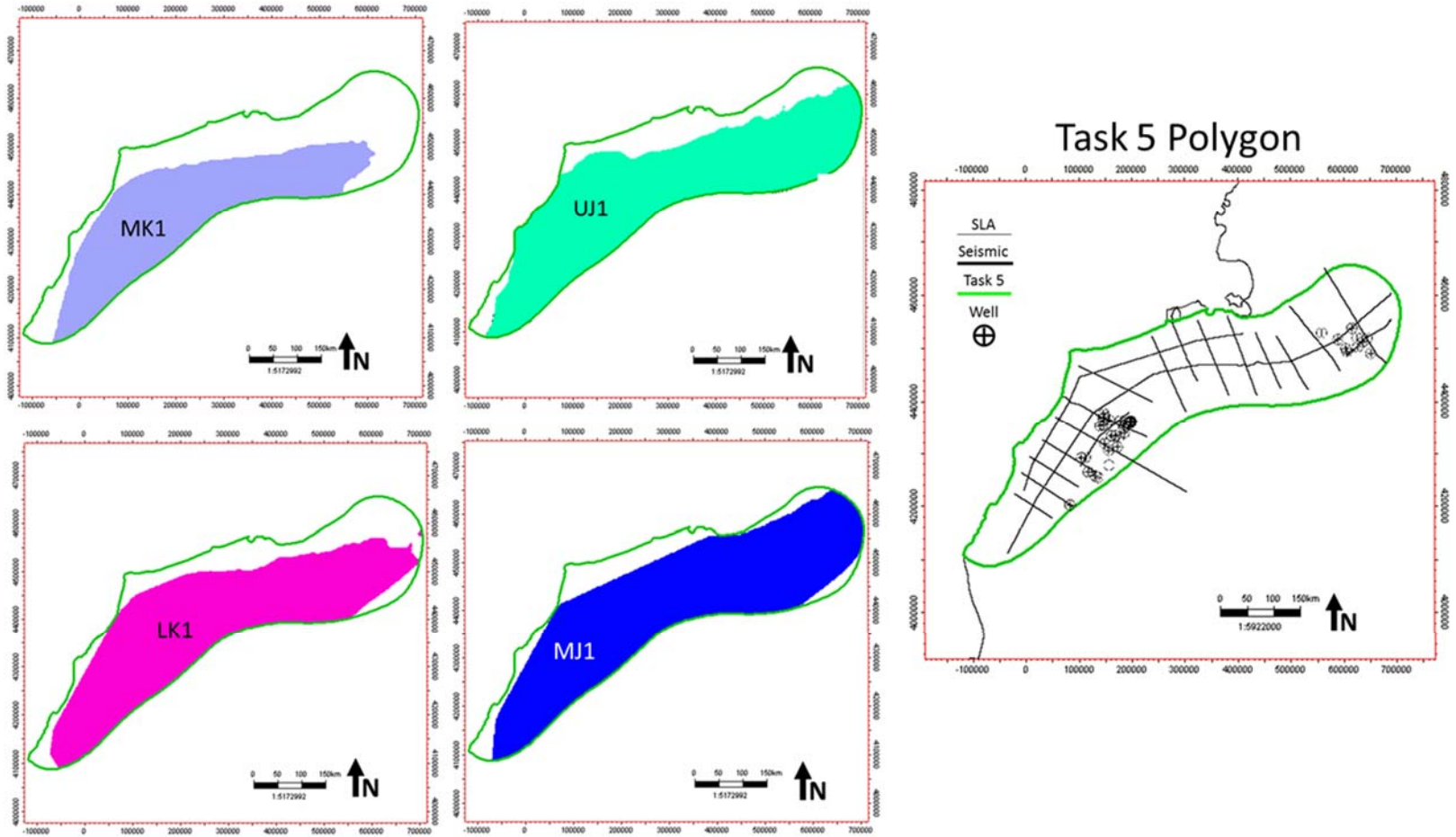

Figure A-2. Boundary polygons for key storage intervals considered in this study. Polygon limits are defined by extent of study area, presence of geologic unit, and depth below 1,000 m for supercritical CO_2 storage.

Table A-1. Petrophysical parameters evaluated for storage resource calculations.

Petrophysical Parameter/Property	Definition	Input/Calculation	Output
Depth	Depth below mean sea level to the top of the storage zone	Seismic sequence stratigraphic top in measured depth minus Kelly Bushing (KB)	Reservoir temperature, pressure, and CO_2 density
Gross Thickness	Thickness of the entire sequence/lithostratigraphic unit	Seismic sequence stratigraphic base minus top depth	Isopach / isochore map
Total Porosity	Porosity of the gross interval (isolated, connected, and clay-bound)	Average of NPHI and DPHI logs calibrated to core data	Total porosity log
Net ≥ 10 mD Reservoir Thickness	Thickness of storage zone with reservoir lithology and interconnected porosity	Maximum gamma ray log cut-off of 75 gAPI and minimum permeability log cut -off of 10 mD	Net ≥10 mD thickness map; Net pore volume efficiency (EPVn)
Net ≥ 100 mD Reservoir Thickness	Thickness of storage zone with reservoir lithology and interconnected porosity	Maximum gamma ray log cut-off of 75 gAPI and minimum permeability log cut -off of 100 mD	Net ≥100 mD thickness map; Net pore volume efficiency (EPVn)
Effective ≥ 10 mD Reservoir Porosity	Shale-corrected porosity of the net reservoir interval	Total porosity curve minus shale (vshale log) porosity over the net ≥10 mD reservoir interval	Net ≥10 mD reservoir porosity map; Net pore volume efficiency (EPVn)
Effective ≥ 100 mD Reservoir Porosity	Shale-corrected porosity of the net reservoir interval	Total porosity curve minus shale (v_{shale} log) porosity over the net ≥100 mD reservoir interval	Net ≥100 mD reservoir porosity map; Net pore volume efficiency (EPVn)
Net ≥ 10 mD Reservoir Permeability	Permeability of fluid through pore space in the net reservoir interval	Porosity-permeability transform applied to effective porosity log over the net ≥10 mD reservoir interval and calibrated to core permeability	Permeability log curve; Net pore volume efficiency (EPVn)
Net ≥ 100 mD Reservoir Permeability	Permeability of fluid through pore space in the net reservoir interval	Porosity-permeability transform applied to effective porosity log over the net ≥100 mD reservoir interval and calibrated to core permeability	Permeability log curve; Net pore volume efficiency (EPVn)

Table A-2. Wireline log statistics for the Cretaceous-Jurassic interval of interest (UK1 – UJ1)

Log Parameter	Gamma Ray (GR)	Bulk Density (RHOB)	Sonic (DT)	Photo-Electric (PE)	Neutron Porosity (NPHI)	Density Porosity (DPHI)	Sonic Porosity (SPHI)
Units	gAPI	g/cm^3	µs/ft	barns/electron	fraction	fraction	fraction
Min	1	1.17	2.9	0	-0.09	-0.07	-0.02
Max	176	3.38	271	7.5	0.60	0.70	0.44
Mean	75	2.42	81	2.7	0.26	0.20	0.19
Well Count	43	42	42	3	42	42	43

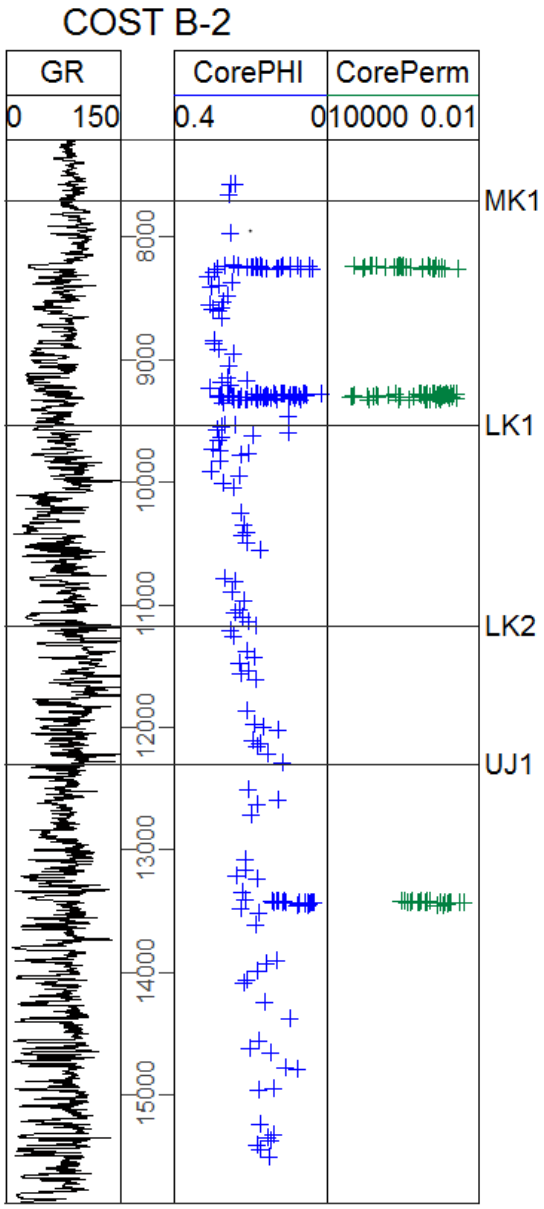

Figure A-3. Vertical section of the COST-B2 well showing representative core porosity and permeability data, with a larger depth range and number of samples observed in porosity measurements compared to fewer, more localized permeability measurements.

Table A-3. List of key dynamic modeling input parameters with input sources considered.

Input Type	Parameter (Units)	Values	Source/Comments
Rock Properties	Formation/zone tops (m)	Reference scenario: 2,560 Shallow scenario: 2,402 Deep scenario: 2,694	Assumption based on formation top depths from the regional MK1-3 structural map
	Net Thickness (m)	MK1-3 (P10, P50, P90): 36, 145, 280	P10, P50, and P90 values from regional net thickness distributions for MK1-3 intervals with ≥ 10mD permeability
	Porosity (fraction)	MK1-3 (P10, P50, P90): 0.21, 0.23, 0.28	P10, P50, and P90 values from regional effective porosity distributions for MK1-3 intervals with ≥ 10mD permeability
	Permeability (mD)	MK1-3 (P10, P50, P90): 26, 46, 120	P10, P50, and P90 values from regional permeability distributions for MK1-3 intervals with ≥ 10mD permeability, with permeability estimated from core-derived porosity-permeability transforms
	Permeability anisotropy	0.1	Assumption
	Rock compressibility (kPa)	5.8×10^{-7}	Assumption
Initial Conditions	Hydrostatic pressure gradient (Pa/m)	9,840	Based on formation tests, Task 6 report
	Geothermal temperature gradient (°C/m)	0.023	Based on formation tests, Task 6 report
	Salinity (ppm)	50,000	Based on formation tests, Task 6 report
	Initial fluid saturation (%)	100% brine	Saline aquifer assumed to be fully water saturated
Rock-Fluid Properties	CO_2-water relative permeability curve	See Figure 12 in main report	Assumption
Fluid Properties	CO_2 brine PVT properties	Literature values	Based on Peng-Robinson equation of state
Operational Constraints	Injection well perforation length (m)	MK1-3 (P10, P50, P90): 36, 145, 280	Assumes perforation length is equal to the net thickness of the MK1-3 reservoir interval with ≥ 10mD permeability
	Injection Rate (Mt CO_2/day)	Reference Scenario: 1.5 Variant Scenario: 1.0	Injection rates required to store annual CO_2 emissions from nearby CO_2 sources (e.g. Battelle, 2018b)
	Fracture Pressure Gradient (Pa/m)	14,703	Brown et al. (2011)
	Duration of CO_2 injection (years)	30	Assumption

Attachment H: Task 6 Topical Report – Task 6 Risk Factor Analysis Report

Mid-Atlantic U.S. Offshore Carbon Storage Resource Assessment Project

Task 6 Risk Factor Analysis Report

MID-ATLANTIC U.S. OFFSHORE
CARBON STORAGE RESOURCE
ASSESSMENT PROJECT

DOE Award Number DE-FE0026087

Prepared by:
Battelle
505 King Avenue
Columbus, OH 43201-2696
Principal Investigator: Dr. Neeraj Gupta
Project Manager: Ms. Lydia Cumming

Prepared for:
The U.S. Department of Energy
National Energy Technology Laboratory
Project Manager: Mr. William O'Dowd

June 30, 2018

Disclaimer

This report was prepared as an account of work sponsored by an agency of the United States Government. Neither the United States Government, nor any agency thereof, nor any of their employees, makes any warranty, express or implied, or assumes any liability or responsibility for the accuracy, completeness, or usefulness of any information, apparatus, product, or process disclosed, or represents that its use would not infringe privately owned rights. Reference herein to any specific commercial product, process, or service by trade name, trademark, manufacturer, or otherwise does not necessarily constitute or imply its endorsement, recommendations, or favoring by the United States Government or any agency thereof. The views and the opinions of authors expressed herein do not necessarily state or reflect those of the United States Government or any agency thereof.

Acknowledgments

This material is based upon work supported by the Department of Energy under Award Number DE-FE0026087. The Project Team is led by Battelle and includes the state geological surveys of Delaware, Maryland, and Pennsylvania; United States Geological Survey (USGS); Lamont-Doherty Earth Observatory at Columbia University (LDEO); and Rutgers University. Harvard University, Texas Bureau of Economic Geology, and Virginia Department of Mines, Minerals, & Energy serve as technical advisors.

Dr. Neeraj Gupta was the Battelle Principal Investigator for the Mid-Atlantic U.S. Offshore Carbon Storage Resource Assessment Project, and Ms. Lydia Cumming provided project management and technical coordination between team members. Battelle project team members J.R. Sminchak, Andrew Burchwell, Martin Jimenez, Isis Fukai, Laura Keister, Heather McCarren, and Valerie Smith were primary authors. ArcGIS work was led by David Andreasen and Andrew Staley at the Maryland Geological Survey. Task 6 analysis was based on data prepared for previous project tasks by project team members Guy Lang (USGS/Haifa University), William (John) Schmelz (Rutgers), Kenneth Miller (Rutgers), Gregory Mountain (Rutgers), Mojisola KunleDare (Delaware Geological Survey), Peter McLaughlin (Delaware Geological Survey), Kristin Carter (Pennsylvania Geological Survey), Brian Dunst (Pennsylvania Geological Survey), and many others. The analysis benefited from research performed by the Bureau of Ocean Energy Management, Bureau of Safety and Environmental Enforcement, and offshore drilling programs along the mid-Atlantic from the 1970s-1980s.

Table of Contents

List of Tables

Page

List of Figures

Acronyms and Abbreviations

AMCOR	Atlantic Margin Coring
BCT	Baltimore Canyon Trough
BOEM	Bureau of Ocean Energy Management
BSEE	Bureau of Safety and Environmental Enforcement
CCS	Carbon Capture and Storage
CO_2	Carbon Dioxide
COST	Continental Offshore Stratigraphic Test
CSB	Continental Shelf Boundary
DGS	Delaware Geological Survey
DOE	United States Department of Energy
EDS	Energy Dispersive X-ray Spectroscopy
EFH	Essential Fish Habitat
EDX	Energy Data eXchange
EFH	Essential Fish Habitat
EPA	United States Environmental Protection Agency
ESA	Endangered Species Act
ESL	Evidence Support Logic
FEPs	Features, Events, and Processes
GBB	Georges Bank Basin
HAPC	Habitat Area of Particular Concern
Hz	Hertz
IODP	Integrated Ocean Drilling Program
km	Kilometer
lb/gal	Pounds per Gallon
LDEO	Lamont-Doherty Earth Observatory
µm	Micrometer
m/s	Meters per Second
m	Meter
Ma	Million Years Ago

mD	Millidarcy
mg/L	Milligrams per Liter
MMS	Minerals Management Service
MPa	Megapascal
MPA	Marine Protected Area
msl	Mean Sea Level
NETL	National Energy Technology Laboratory
NGO	Non-Governmental Organization
NOAA	National Oceanic and Atmospheric Administration
NRAP	National Risk Assessment Partnership
OCS	Outer Continental Shelf
ODP	Ocean Drilling Program
PaGS	Pennsylvania Geological Survey
ppt	Parts per Thousand
psi/ft	Pounds per Square Inch per Foot
RFT	Repeat Formation Tester
SLA	Submerged Lands Act
USGS	United States Geological Society

Executive Summary

The Mid-Atlantic U.S. Offshore Carbon Storage Resource Assessment Project (FE0026087) is part of the U.S. Department of Energy (DOE) National Energy Technology Laboratory's (NETL) Carbon Storage Program to improve the effectiveness and reduce the costs of carbon dioxide (CO_2) storage implementation. The objectives of the Mid-Atlantic U.S. Offshore Carbon Storage Resource Assessment Project are to (1) complete a systematic carbon storage resource assessment of the offshore mid-Atlantic coastal region from the Georges Bank Basin (GBB) through the Long Island Platform to the southern Baltimore Canyon Trough (BCT), (2) define key input parameters to reduce uncertainty for offshore resource assessment and efficiency estimates, (3) examine risk factors, and (4) engage industry and regulatory stakeholders through development of a roadmap to assist future project planning and implementation.

This report presents the risk factor analysis for the Mid-Atlantic U.S. Offshore Carbon Storage Resource Assessment Project. The analysis included an initial assessment of technical risk factors in mid-Atlantic offshore areas that may affect CO_2 storage resource estimates for the following categories:

1. geologic storage processes,
2. long-term potential for CO_2 migration, and
3. environmental setting factors that could influence the development of a carbon storage facility.

The risk factor analysis provides guidance for geologic storage implementation on the long-term fate and associated risks of CO_2 injection into the subsurface, focusing on long-term CO_2 storage capacity, potential risks associated with CO_2 leakage, and other factors that may cause potential adverse impacts to logistics, economics, and infrastructure. The study covers a very large area, and conclusions presented here are meant to guide the direction of potential future feasibility assessments, with more definitive results based on field work.

The mid-Atlantic offshore area benefits from its large spatial extent, thick sequences of Cretaceous- and Jurassic-age sands, lack of previous oil and gas wellbores, and distance from populated development. No critical risk factors were identified that would impede CO_2 storage along the study areas. Faults and geomechanical stability along the mid-Atlantic slope were identified as a moderate risk factor. Reservoir variability was also noted as a moderate risk factor, especially in Cretaceous sands that have interbedded silt and clay layers. Soft sediment deformation was identified as a risk factor for semi- or unconsolidated sediments less than 1,000 meters (3,000 feet) deep, which are more prevalent in the GBB and Long Island Platform. CO_2 migration pathways and trapping mechanisms were not considered a significant risk factor for the deeper rock formations along the mid-Atlantic offshore.

There are many environmental factors, sensitive habitats, man-made features on the seabed, and marine protected areas (MPAs) along the mid-Atlantic seaboard. Most of these features are located closer to the shoreline. CO_2 sources are mainly clustered adjacent to the BCT. Stakeholder acceptance and technology adaptation is uncertain; while carbon capture and storage (CCS) has taken place for more than 20 years offshore of Norway, CCS is a relatively new concept and the number of CCS projects worldwide is limited. In addition, there is little history of oil and gas development in the region which would otherwise provide a level of familiarity with typical exploration activities.

1.0 Introduction

1.1 Project Overview

The Mid-Atlantic U.S. Offshore Carbon Storage Resource Assessment Project is a three-year project designed to (1) complete a systematic carbon storage resource assessment of the offshore mid-Atlantic coastal region from the Georges Bank Basin (GBB) through the Long Island Platform to the southern Baltimore Canyon Trough (BCT), (2) define key input parameters to reduce uncertainty for offshore resource assessment and efficiency estimates, (3) examine risk factors, and (4) engage industry and regulatory stakeholders through development of a roadmap to assist future project planning and implementation. The Project Team is led by Battelle and includes the state geological surveys of Delaware, Maryland, and Pennsylvania; United States Geological Survey (USGS); Lamont-Doherty Earth Observatory (LDEO) at Columbia University; and Rutgers University. The Project Team research is intended to develop a regional framework for offshore geologic carbon dioxide (CO_2) storage by accomplishing the following tasks:

- Define the geologic characteristics of candidate storage zones and caprocks (Task 2)
- Use seismic data to better define the continuity of storage zones and caprocks (Task 3)
- Catalog the hydrologic properties of mid-Atlantic offshore formations (Task 4)
- Determine appropriate efficiency parameters that will represent the net effective pore volume and Prospective Storage Resource specific to offshore lithologies (Task 5)
- Examine risk factors related to offshore storage (Task 6)
- Communicate with industry and other stakeholders about the future prospects for offshore storage in the mid-Atlantic (Task 7)
- Ensure that results and lessons learned are transferred to industry and other stakeholders (Task 8)

The offshore mid-Atlantic study area encompasses 170,000 square kilometers (km^2), or 66,000 square miles (mi^2), along the mid-Atlantic states of Virginia, Maryland, Delaware, New York, New Jersey, and Pennsylvania (Figure 1-1). The project study area consists of three major subregions: GBB, Long Island Platform, and BCT. The project study area extends from within 10 km to 300 km [6 to 200 miles (mi)] offshore, encompassing the outer continental shelf (OCS) and portions of the continental slope. Water depths in the mid-Atlantic continental shelf grade gently from zero depth along the shoreline to depths of 100 to 200 meters (m) [300 to 700 feet (ft)] at the continental slope. Along the continental slope, water depths plunge more than 2,000 m (7,000 ft) into the North American Basin.

The study involves integrating existing data from a wide variety of sources. A number of oil and gas companies as well as the Continental Offshore Stratigraphic Test (COST), the USGS Atlantic Margin Coring (AMCOR) project, the Ocean Drilling Program (ODP), and the Integrated Ocean Drilling Program (IODP) have drilled this area. A large amount of data, consisting mainly of wireline logs, cores, cuttings, and seismic surveys, was collected, and much of it is available for additional study.

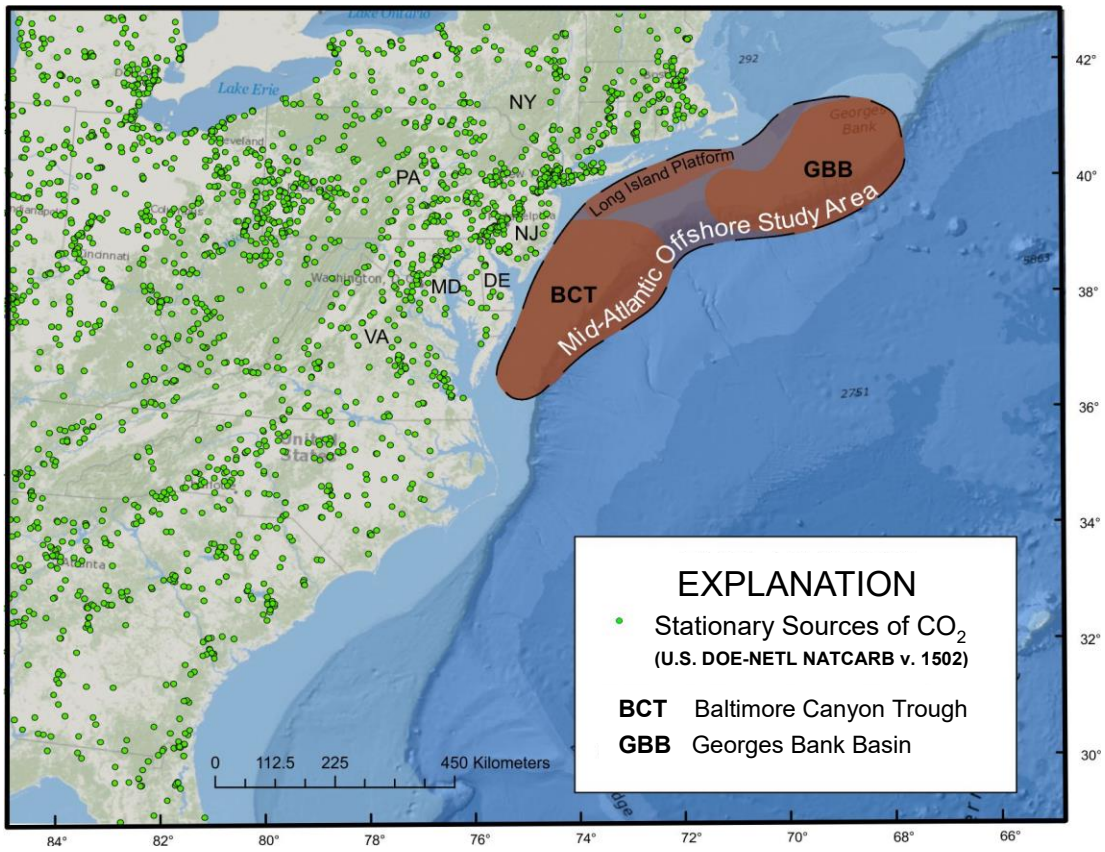

Figure 1-1. Map of the study area and large point sources of CO_2.

Previous work indicates that several sandstone formations in this region have porosities greater than 25% and permeabilities greater than 100 millidarcys (mD). These characteristics suggest an extremely large capacity for potential storage of CO_2. In addition, there are advantages to offshore storage along the mid-Atlantic offshore, including distance from population centers, absence of underground drinking water resources, limited interference with pre-existing oil and gas development, uncomplicated pore space access/mineral rights, a unified regulatory framework, and vast spatial extent.

This report presents the results of the Task 6 risk factor analysis, which was focused on identifying qualitative risk factors for consideration in resource assessment. The risks of primary concern to many stakeholder groups are those associated with unintended CO_2 migration out of the storage reservoir. In addition, the Regional Carbon Sequestration Partnerships have identified other project-related operational and financial events, such as events that take place on the surface or in the policy arena that could also have adverse impacts on a geologic storage project (DOE-NETL, 2017). Future carbon capture and storage (CCS) projects will likely assess feasibility based on storage capacity; health and environmental safety; economics; regulatory constraints; ability to deploy monitoring technologies; and other site selection criteria.

Risk communication is an important element for future CCS applications. This report is intended to help guide geologic storage implementation by providing stakeholders (e.g., operators, project developers, general public, and regulators) with preliminary information relevant to the long-term fate and associated risks of CO_2 injection into the subsurface, focusing on long-term CO_2 storage capacity, potential risks associated with CO_2 leakage, and other factors that may cause potential adverse impacts to logistics, economics, and infrastructure.

1.2 Risk Factor Analysis: Objectives and Approach

The objective of Task 6 was to perform an initial assessment of technical risk factors present in mid-Atlantic offshore areas that may affect CO_2 storage resource estimates in terms of geologic storage processes, long-term potential for CO_2 migration, and feasibility of development of a carbon storage facility (e.g., environmental setting factors). The results of the risk factor analysis were used to develop a comprehensive list of potential sources of risk and to identify site screening criteria specific to the marine environment. The results of the risk factor analysis also were used for stakeholder input and discussion about the future prospects for offshore storage in the mid-Atlantic.

Offshore Geological Storage Processes. Geological risk factors were analyzed for the study areas based on analysis of geotechnical data and geologic features such as faults, fracture zones, unstable offshore slopes, reservoir variability, and other features were portrayed with maps and geologic cross sections. The information was used to estimate the potential effect on resource estimates in relation to areas with higher storage security versus areas with more geological risk factors.

Long-Term Potential for CO_2 Migration. Long-term storage risk factors were summarized for the mid-Atlantic offshore areas to determine how they may affect CO_2 storage resource estimates. Confining layers were described in terms of their mineralogy, lithology, arrangement, thickness, and hydrologic properties. Potential for long-term CO_2 migration was evaluated based on migration pathway analysis and wellbore integrity review. Long-term processes such as CO_2 dissolution, residual saturation, and mineralization were evaluated given the offshore geologic environments.

Environmental Factors for Deployment. Features along the offshore mid-Atlantic seafloor were described as indicators of potential risk factors for exploration activities, subsurface storage, and project construction. Natural marine areas, man-made features, and CO_2 sources along the mid-Atlantic seaboard were evaluated in relation to CO_2 storage resources. In addition, stakeholder outreach and communication issues were reviewed as they may affect exploration and development of CO_2 storage resources.

Information from the risk assessment was based on results from previous tasks on hydrologic characterization, seismic interpretation, geologic mapping, and previous research studies on the offshore mid-Atlantic. Results were used to establish appropriate boundaries for the CO_2 storage resource calculations. In addition, the risk factors were identified to provide guidance for future exploration and development activities to support CO_2 storage site selection along the offshore mid-Atlantic. At this early stage of CO_2 storage resource assessment, the analysis was centered on a qualitative review of risk factors rather than a more formal risk assessment or probability-consequence evaluation.

1.3 Risk Analysis Methodologies for Carbon Storage Applications

Several different methodologies have been applied to examine risk for CO_2 storage applications (Table 1-1). Risk assessment activities may include site screening, environmental assessments, reservoir simulation of CO_2 behavior, caprock characterization, wellbore leakage analysis, surface leakage analysis, groundwater protection studies, geomechanical analysis of stress changes in the subsurface, and other studies. Results of risk analysis may be used for site selection and to provide guidance in CO_2 storage system design, operation, and closure. The mid-Atlantic offshore resource project is in the early stages of the DOE-NETL (2011) risk management process focused on identifying and characterizing CO_2 storage resource as illustrated in Figure 1-2.

Table 1-1. Summary of carbon storage risk assessment tools (after DOE-NETL, 2011).

Tool	Methodology Family
Quintessa FEP database	Qualitative, FEPs screened by experts
TNO Risk Assessment Methodology	Expert-elicited probability and consequence matrices
CO2QUALSTORE guideline, DNV	Qualitative/semi-quantitative with "panel" inputs
Carbon Storage Scenario Identification Framework (CASSIF), TNO	Qualitative, scenario-based
Risk Identification and Strategy using Quantitative Evaluation (RISQUE), URS	Semi-quantitative, expert-elicited probability and consequence matrices
Screening and Ranking Framework (SRF), LBNL	Qualitative, expert-elicited probabilities
Certification Framework (CF), LBNL	Quantitative, system-level model, probabilities partly calculated using fuzzy logic
Vulnerability Evaluation Framework (VEF), U.S. EPA	Qualitative
Performance Assessment (PA), Quintessa	Evidence support (three-valued) logic (ESL) distinguishes cases of poor-quality data from uncertain data
CarbonWorkFlow* Process for Long-term CO2 Storage	Semi-quantitative; FEPs ranked through expert elicitation using a risk matrix approach
CarbonSCORE* software to preassess potential CO2 storage sites	All evaluated criteria are quantitatively weighted, jointly evaluated, and summarized
Oxand Performance & Risk Methodology (P&RTM)	Quantitative risk matrix evaluation: semi-quantitative
CO2-PENS, LANL	Quantitative, hybrid system-process model
NRAP Risk Tools	Quantitative tools for wellbore leakage, risk-based area-of-review, groundwater, induced seismicity

Several risk analysis tools, ranging from qualitative to quantitative methods, have been developed to evaluate CO_2 storage sites (see Table 1-1). Many site assessments start with initial risk screenings like the Features, Events, and Processes (FEPs) (Savage et al., 2004). Risk assessment methods can also be used to characterize and catalog the safety attributes of storage sites (WRI, 2008; IPCC, 2005). The DOE-NETL National Risk Assessment Partnership (NRAP) program has developed a suite of tools to help delineate risk related to groundwater, wellbore leakage, induced seismicity, and subsurface pressure (Pawar et al., 2014).

Risk factors may be organized as programmatic (related to project progress and costs) and technical (related to the scientific and engineering integrity of the storage system). CO_2 is a naturally-occurring gas present throughout the environment. Consequently, CO_2 storage risk analysis methods are often focused on leakage pathways rather than the quantitative expression of risk as exposure probability times consequence.

This report presents a review of general risk factors for the broad study area in the mid-Atlantic offshore. Risk factors are described in terms of their potential impact on carbon storage resource calculations and siting carbon storage projects. More detailed risk assessment studies would be necessary for site specific projects. Furthermore, a detailed risk assessment for a site-specific project must involve stakeholder input as early in the project as possible to understand what risks (including perceived risks) must be addressed to secure project financing, obtain permits, and comply with other necessary requirements.

Figure 1-2. DOE-NETL risk management process (DOE-NETL, 2011).

1.4 Previous Research on Offshore Risk Factors

Offshore risk assessments for CO_2 storage applications involve many of the same elements that are considered for onshore sites, because deep geologic rock layers are basically the same onshore and offshore. However, the marine environment presents different risks. Some geologic features, like gas chimneys, escarpments, mass flows along slopes, and incised canyons, are distinctive to offshore settings. Temperature and pressure conditions may be much different in offshore environments, especially in deeper water. Monitoring options for offshore CO_2 storage may also be different, especially in terms of CO_2 leakage at the seafloor. Many researchers have investigated methods for detecting gas leakage along the seabed (Brown, 2017). In areas like the North Sea where there are thousands of legacy offshore wells, risk assessment studies for CO_2 storage have often concentrated on wellbore integrity as a key mechanism for CO_2 migration (Brown, 2017; Hannis et al., 2017; IEAGHG, 2016; Blackford et al., 2014; Leighton & White, 2012). A literature review was completed to help define the risk analysis for offshore CO_2 storage (Appendix A).

2.0 Risk Factors for Offshore Geological Storage Processes

Geological risk factors were analyzed for the study areas based on analysis of geotechnical data and geologic features such as faults, fracture zones, unstable offshore slopes, reservoir variability, and other features were portrayed with maps and geologic cross sections. The information was used to estimate the potential effect on resource estimates in relation to areas with higher storage security versus areas versus areas with more geological risk factors.

2.1 Geological Setting Risk Factors

2.1.1 Geological Setting

The project was divided into three major subregions based on broad geological structures present along the mid-Atlantic OCS: GBB, Long Island Platform, and BCT. These geologic structures contain sequences of sedimentary rocks deposited over four geologic time periods: the Paleogene (23 to 66 million years ago [Ma]), the Cretaceous (66 to 145 Ma), the Jurassic (145 to 201 Ma), and the Triassic (252 to 201 Ma). More recent unconsolidated marine sediments and Neogene deposits are present at the shallow seabed. Total thickness of the sediments varies from less than 200 m (700 ft) near the coastline to more than 7,600 m (25,000 ft) in the trough areas. The Cretaceous and Jurassic rock layers were emphasized in the project because they have suitable depth, pressure, and temperature conditions for supercritical CO_2 phase storage.

The mid-Atlantic U.S. passive continental margin contains thick (2- to 16-km or 1- to 9.9-mi) post-rift (upper Lower Jurassic and younger) sediments in the offshore basins and thinner (0- to 2.4-km or 0- to 1.5-mi) uppermost Jurassic-to-Holocene sediment in the onshore coastal plain in the Salisbury Embayment (e.g., Grow & Sheridan, 1988). Rifting occurred during the late Triassic to earliest Jurassic (230 to 198 Ma) followed by extrusion of early Jurassic seaward-dipping basalts. Seafloor spreading began prior to the Callovian (~165 Ma; middle Jurassic) (e.g., Grow & Sheridan, 1988), with the likely opening beginning off Georgia ca. 200 Ma and progressing northward off the mid-Atlantic margin by ca. 180 Ma (Withjack et al., 1998). This south-to-north “zipper” onset of seafloor spreading is associated with a diachronous post-rift unconformity that separates active “rift-stage” deposits from more passive margin “drift-stage” deposits that accumulated in an ever-widening and deepening basin open to the ocean. Post-rift history was generally dominated by passive simple thermoflexural subsidence and loading (Steckler & Watts, 1982; Grow & Sheridan, 1988; Kominz et al., 1998). Subsidence began offshore in the early Jurassic and progressively moved onshore from the late Jurassic to early Cretaceous (ca. 150 to 125 Ma) as a thermoflexural response to increasing crustal rigidity (Watts, 1981; Grow & Sheridan, 1988; Olsson et al., 1988). The region has provided an excellent record of relative sea-level changes (e.g., Olsson et al., 1988; Miller et al., 2005), though glacial isostatic adjustments complicate the Pliocene and younger record (e.g., Peltier, 1998; Raymo et al., 2011) and deposition has been impacted by mantle-based dynamic topography changes (Moucha et al., 2008; Rowley et al., 2011).

The U.S. mid-Atlantic offshore is a classic passive continental margin, meaning that there is sedimentation occurring above an inactive plate boundary. This tectonic setting poses inherently fewer operational and long-term storage risks than an active margin with crustal subduction or extrusion and the associated hazards such as earthquakes, faults, and volcanic activity. In the current study area, active plate movement drove rifts between blocks of continental crust

through the late Triassic and early Jurassic (230-185 Ma) (Libby-French, 1984; Klitgord et al., 1988; Olsen, 1997). The post-rift "drift" period has traditionally been subdivided into three functional periods. The first was dominated by the precipitation of carbonate reefs and platforms in the Mesozoic; the second was marked by the widespread deposition of terrigenous clastic sediments trapped on the landward side of the carbonate reefs; and finally, during the third period, the balance of processes shifted toward erosion and the shelf marched toward land throughout the Cenozoic (Brothers et al., 2013; Schlee et al., 1979).

This study focuses on the Long Island Platform, GBB, and BCT, located directly offshore several states in the northeastern United States (Figure 2-1). Potential storage zones have been identified in Jurassic sands and in lower, mid, and upper Cretaceous sands in BCT and GBB through well log analysis and seismic data interpretation. While there are no well penetrations in the Long Island Platform, mapping with seismic data suggests stratigraphic continuity into this region.

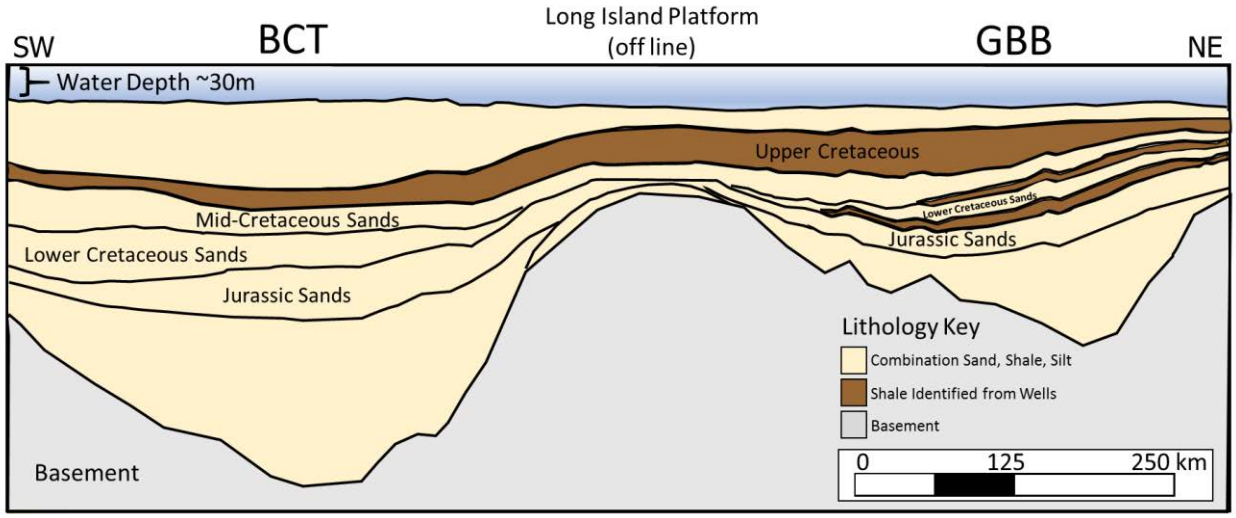

Figure 2-1. Schematic cross section of key basins in study area along strike.

2.1.2 Lithology

The offshore basins contain a thick succession of Paleogene-to-Jurassic sedimentary rocks above crystalline basement that lies at depths of 5 to 15 km (3 to 9 mi). The sedimentary rocks consist of layers of mudstone, shales, sandstone, carbonates, and evaporites that dip to the east-southeast toward the continental slope (Libby-French, 1984). The sedimentary rocks overlie deeper rift basin strata, early Jurassic flows and sills associated with the Central Atlantic Magmatic Province, continental crust, and oceanic crust. Younger quaternary clay, siltstone, and sand overlie the Paleogene-Triassic sedimentary rocks, with ocean sediments present at the ocean floor. Local structures such as igneous intrusions, salt diapirs, growth faults, and escarpments are present in portions of the mid-Atlantic offshore study area.

Previous work indicates that sandstone formations in this region have porosities of 25% and permeabilities greater than 100 mD (e.g., Amato & Bebout, 1980; Slater, 2010). Case studies from the northern Newark basin (onshore New York Metropolitan area) suggest that storage mechanisms at this candidate CO_2 storage site may translate to analog Mesozoic rift basins offshore in the Long Island Platform (e.g., Post & Coleman, 2015). This suggests an extremely large capacity for potential storage of CO_2 in the mid-Atlantic offshore study area.

2.1.3 Structural Features

Reconnaissance of 2D seismic lines and review of existing literature were conducted to determine general trends in structural features and faulting within the study area. The intent of this high-level review was not to identify every risk or fault that may be present, but instead to highlight general trends.

The present-day seafloor structure contains a broad and relatively flat shelf, an area with steeper gradient commonly referred to as the slope, and a rise which grades more gently seaward to the abyssal plain (Brothers et al., 2013). There is a subtle inner shelf edge close to shore and a high-relief, structural shelf edge located approximately 100 km (60 mi) offshore (Miller et al., 2018). The outer shelf edge is a relic of the Eocene-Miocene carbonate ramp and is not related to the paleo shoreline (Steckler et al., 1999). On the other hand, the low-relief inner shelf edge (~20 to 100 m or 70 to 300 ft deep) is the product of sea level rise and fall and has migrated landward and seaward in lock step with global eustatic cycles over the last ~120,000 years (Goff et al., 2013). The slope adjustment model of Brothers et al. (2013) demonstrates the process by which the shelf edge prograded basinward during a period of high sea level (highstand) (Figure 2-2). The slope of the shelf edge became steeper than the critical angle of repose for sediment, followed by sediment bypass of the slope and sediment-supported gravity flows. This sediment was deposited at the base of the slope and began to aggrade upward until the slope was fully buried by sediment. Once the gradient of the shelf edge slope reached equilibrium (less than the critical angle of repose), sediment clinoforms began to prograde basinward, causing the shelf edge to migrate.

The other main structural feature present in the study area is an anticline commonly referred to as the Great Stone Dome or, more rarely, the Schlee Dome. Situated in the BCT, this four-way structural closure covers an area of 400 km^2 (200 mi^2) and has 270 m (890 ft) of relief, which made it an attractive target for oil and gas exploration in the 1970s (Figure 2-3) (Amato & Giordano, 1985; Prather, 1991). The wealth of geologic samples and data provided by these failed exploration wells allowed for characterization of the late Middle Jurassic intrusive igneous activity that drove the formation of the structure (Jansa & Pe-Piper, 1988).

Faults have been identified on seismic data by the vertical offset of horizontal parallel reflections (fault plane) or by the presence of a relatively isolated vertical trending zone with chaotic reflections adjacent to horizontal parallel reflections that may or may not exhibit offset (faulted zone with gouge). Figure 2-4 provides a guide to the seismic facies analytical nomenclature used in this study.

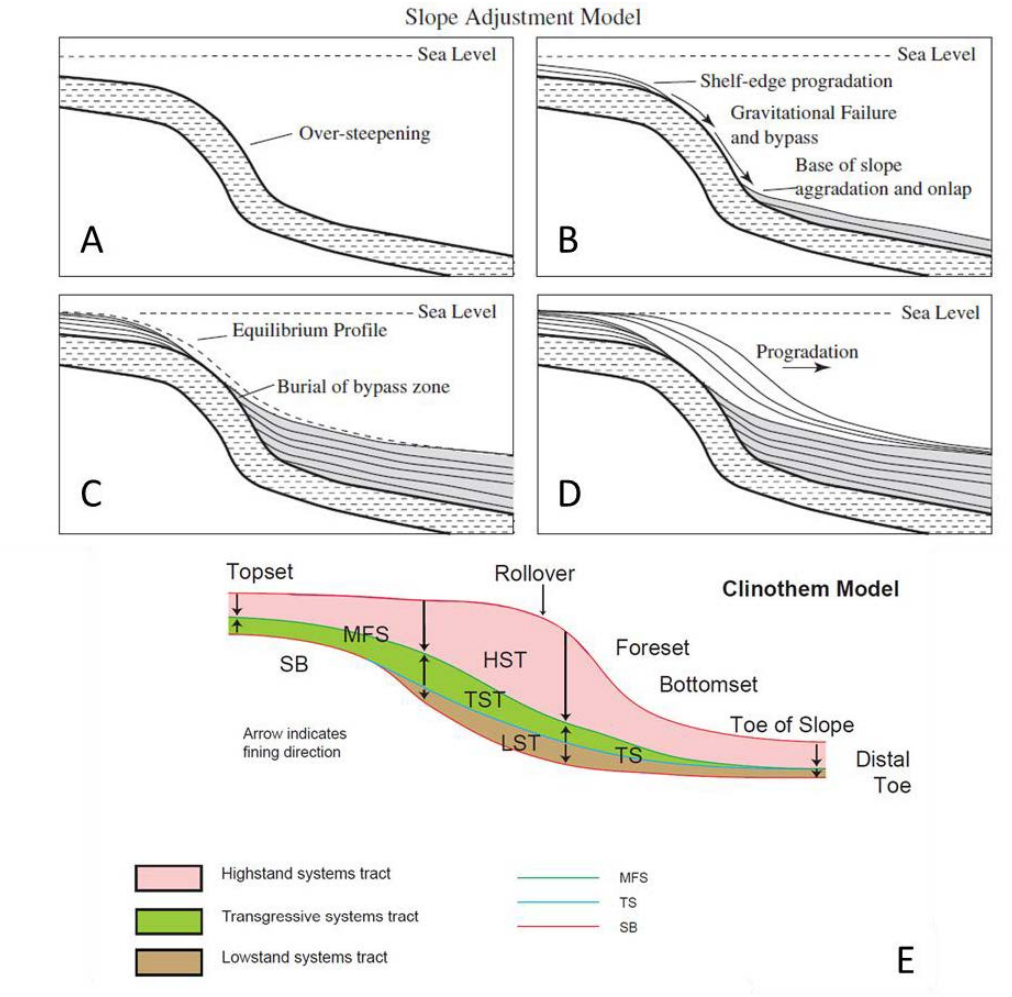

Figure 2-2. Slope adjustment model (panels A through D) (from Brothers et al., 2013) and clinothem model (panel E) (from Miller et al., 2018).

Notes: (A) Development of steep slope. (B) Sediment bypass. (C) Infill and burial of base-of-slope relief. (D) Progradation of shelf break basin-ward. (E) Arrows point in sediment-fining (water-deepening) direction. SB, sequence boundary (red lines); TS, transgressive surface (blue line); MFS, maximum flooding surface (green line). LST, lowstand systems tracts (brown fill); TST, transgressive systems tracts (green fill); HST, highstand systems tracts (pink fill). Rollover is equivalent to shelf break.

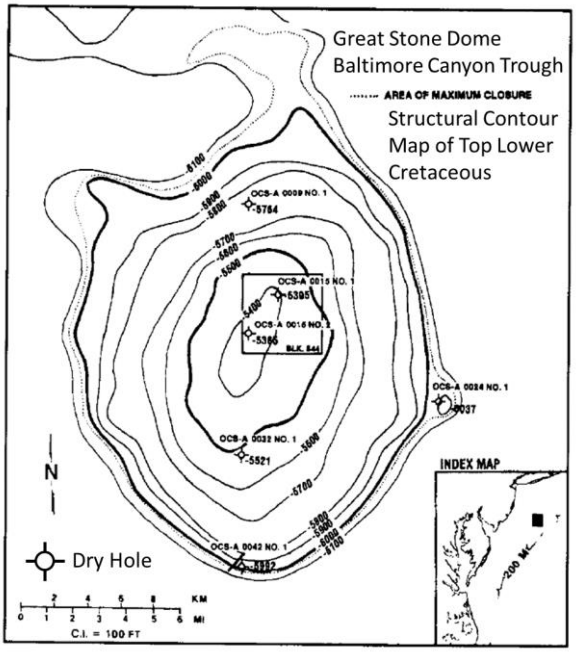

Figure 2-3. Structural contour map of the Great Stone Dome anticline in the northern BCT (from Prather, 1991).

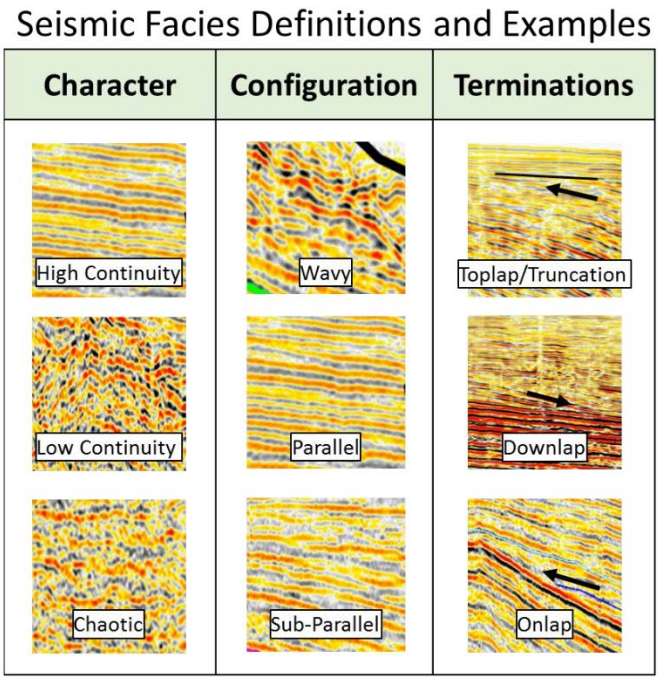

Figure 2-4. Visual description of seismic data signal elements used to define seismic facies in this study (after Hinestrosa et al., 2014).

In general, extensional mode normal faulting is observed in the subsurface near the structural shelf break, at the terminus of the buried carbonate reefs, and along the continental rise. Figures 2-5 and 2-6 display a series of 2D seismic cross sections along structural dip with faults marked in black, carbonate reef facies pointed out with white arrows, and Upper Cretaceous (UK1), Middle Cretaceous (MK1), Lower Cretaceous (LK1), Upper Jurassic (UJ), and Middle Jurassic (MJ) surfaces highlighted where applicable.

Figure 2-5 shows a seismic cross section from northern GBB, trending west to east. It exhibits normal faults with offset likely less than 300 m (1,000 ft), consistent with trends across the study area. The faults offset parallel and sub-parallel reflections below the Upper Cretaceous horizon through high-amplitude, chaotic seismic facies at depth interpreted as carbonate reef material.

A seismic cross section from the Long Island Platform, traversing the study area from northwest to southeast, is shown in Figure 2-6. No large-scale faults or structural complexities are detectable in this area. This area, located on the broad structural shelf, has been experiencing changes primarily due to sea level change and thermal subsidence on the passive continental margin. (Note that any apparent structures on this figure aside from a gentle basinward dip are artifacts of the high level of vertical exaggeration.)

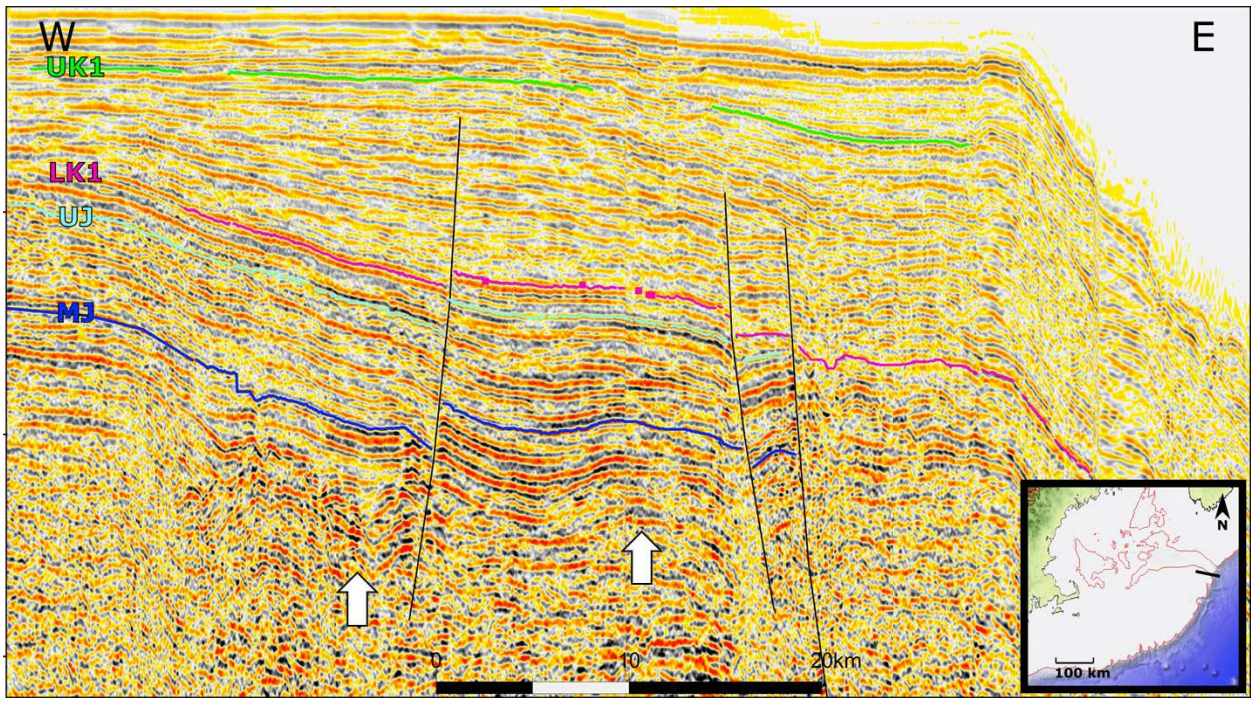

Figure 2-5. West- to east-trending seismic cross section along structural dip within GBB.

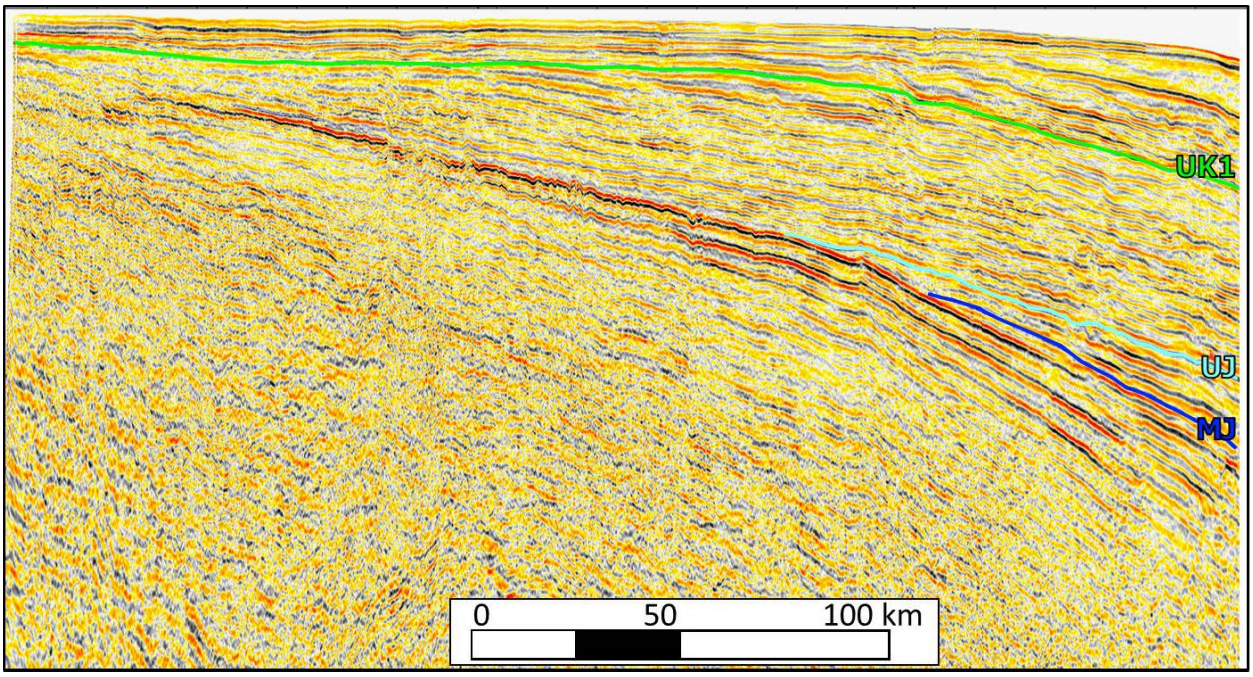

Figure 2-6. Northwest- to southeast-trending seismic cross section along structural dip across Long Island Platform. Note high ratio of vertical exaggeration (20x).

BCT faulting along the structural shelf break continued into the Miocene, evidenced by the offset of the expanded Miocene section in Figure 2-7. In both Figures 2-7 and 2-8, normal faults sole out into high-amplitude reflections, likely representing carbonate reefs as seen in GBB. Faults in BCT appear to have more listric characteristics compared to those in GBB and exhibit sediment growth on the downthrown side.

While no seafloor-broaching faults were identified on the currently available reprocessed 2D seismic lines, the presence of seafloor-broaching faults and near-surface buried faults would need to be evaluated on a site-by-site basis using higher-resolution seismic or geotechnical datasets. The limit of vertical resolution of a seismic dataset is defined by ¼ of the dominant wavelength (Kallweit & Wood, 1982). The wavelength (λ) is equal to the interval velocity (v) divided by the dominant frequency (f). An extraction of frequency spectra from the 2D seismic lines displayed in this report is given in Figure 2-9. The highest frequency at which there is a full complement of signal is at ~50 hertz (Hz). Assuming a velocity of 2,000 meters per second (m/s), or 7,000 feet per second (ft/s), for near-surface sediments, the vertical resolution of the 2D seismic lines near the water bottom is approximately 10 m (30 ft). This means that no features smaller than 10 m (30 ft) are confidently resolvable on the current dataset.

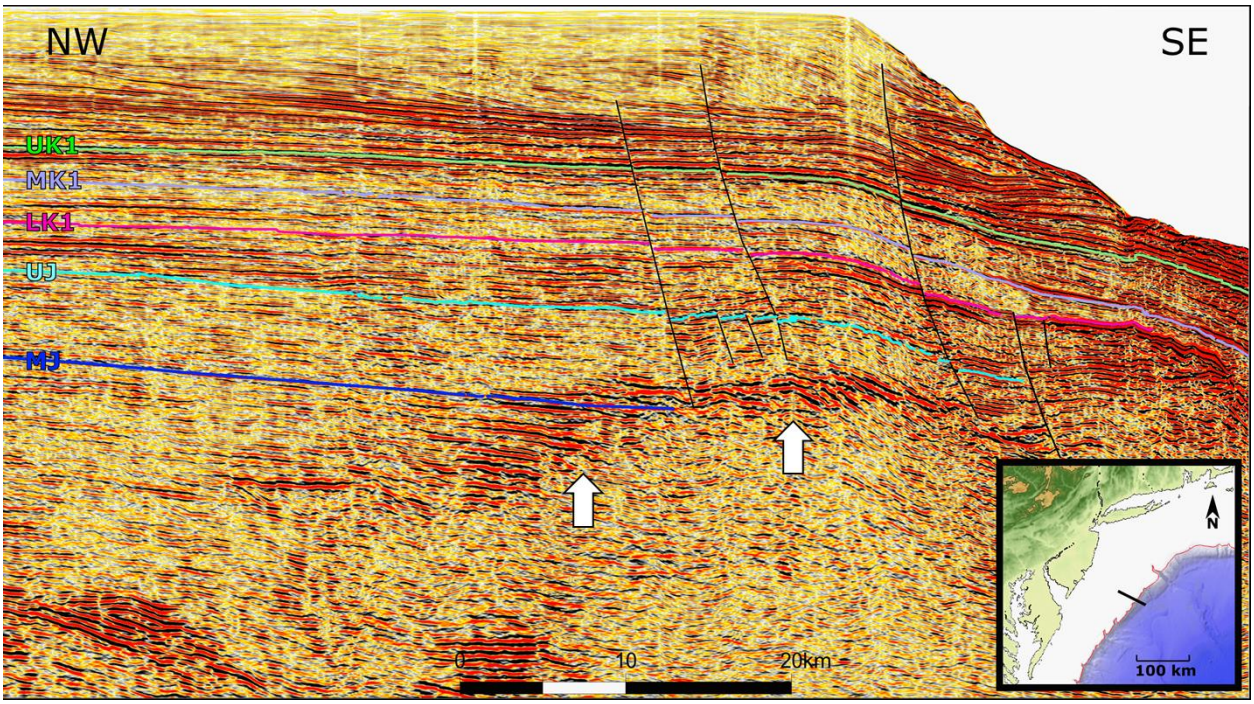

Figure 2-7. Northwest- to southeast-trending seismic cross section along structural dip within BCT. White arrows point to high-amplitude zones with geometries that suggest the presence of carbonate reef buildups.

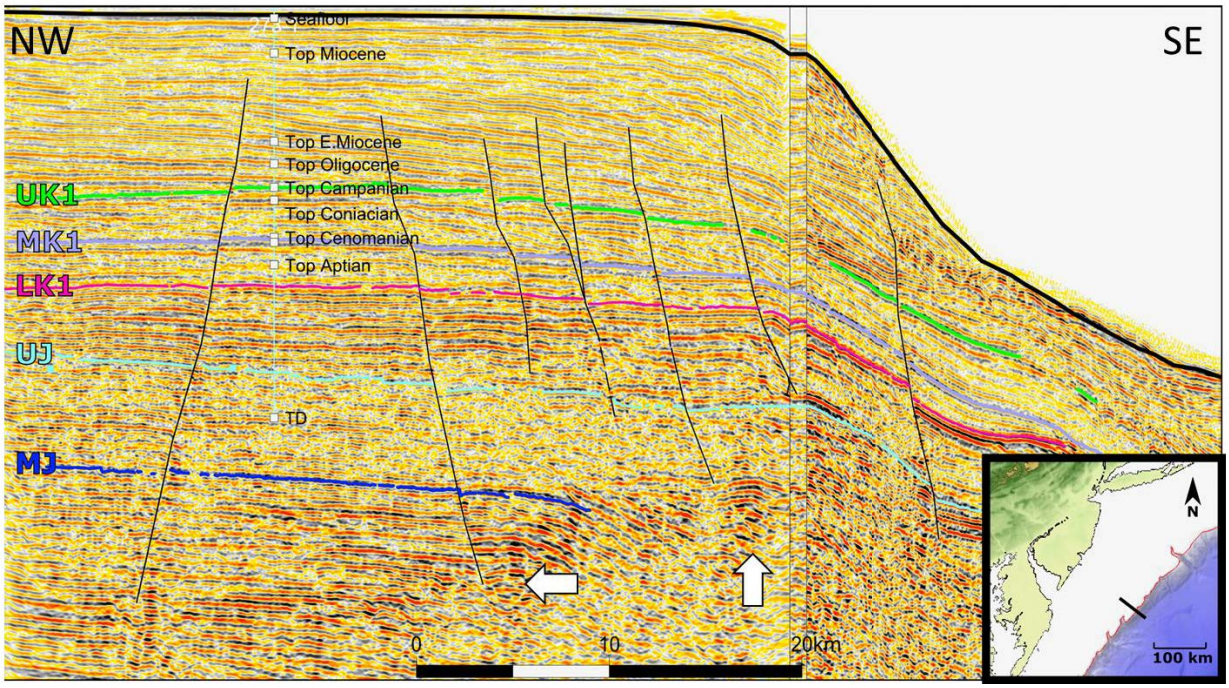

Figure 2-8. Northwest- to southeast-trending seismic cross section along structural dip within BCT. White arrows point to high-amplitude zones with geometries that suggest the presence of carbonate reef buildups.

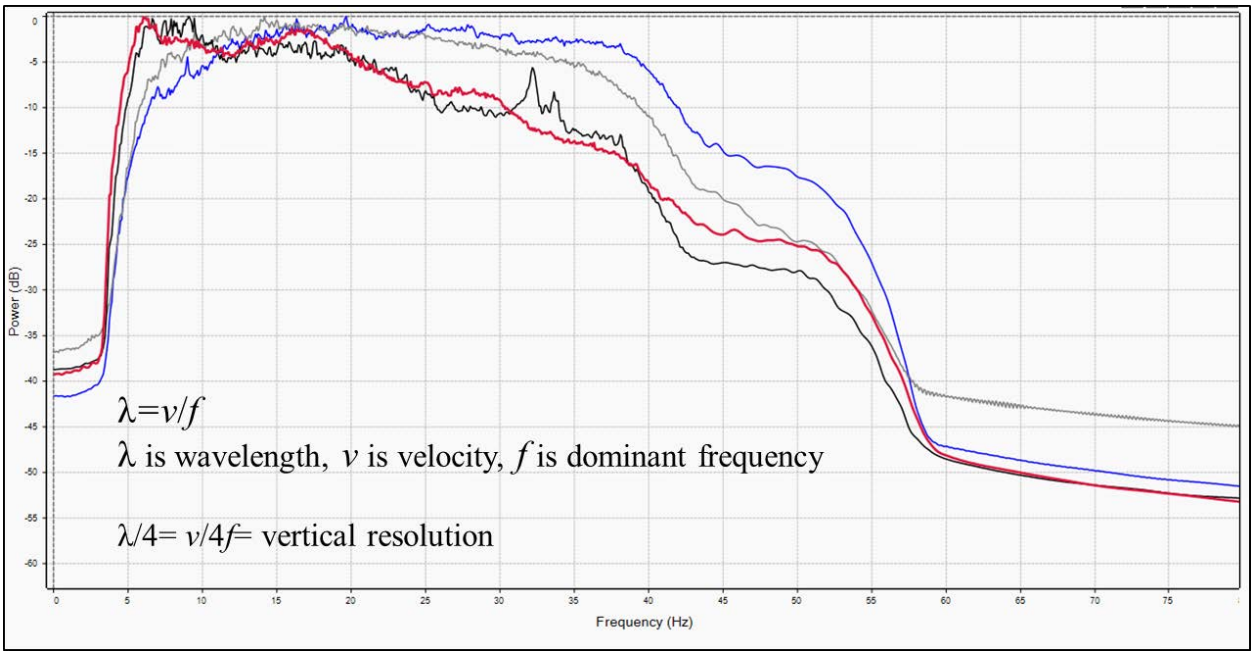

Figure 2-9. Spectra of frequency content for displayed seismic data lines and equations for calculating the threshold for vertical resolution.

2.2 Outer Continental Shelf Factors

A variety of features may be present along the OCS seafloor that are indicators of potential risk factors for exploration activities, subsurface storage, and project construction. Seawater along the shelf is mostly 25 to 200 m (80 to 700 ft) deep, a relatively shallow depth which reduces challenges associated with deepwater drilling and equipment. However, wave action and currents may disturb ocean bed sediments, making seabed characterization and monitoring methods difficult. As described in Brothers et al. (2013), the seafloor features reflect a combination of many Quaternary glacial erosion, deposition, and subsidence events related to eustatic sea level changes. Portions of the shelf are dissected by channels and canyons. More substantial relief and mass flow features are present along the slope and continental rise.

As described by Kramer & Shedd (2017), high-resolution seabed image analysis may show the presence of features related to subsurface geologic features such as gas pockmarks, salt domes, faulting, folding, escarpments, slump blocks, slides, canyons, channels, and gas chimneys. These items may be indicators of deeper geologic structures, gas migration, and other geological risk factors for CO_2 storage applications.

To examine continental shelf features on the seabed, high-resolution bathymetry data from the National Oceanic and Atmospheric Administration (NOAA), National Centers for Environmental Information, 3 arc-seconds Northeast and Southeast Atlantic Coastal Relief Model (National Geophysical Data Center, 1999a; 1999b) were imported into a mapping and visualization program. The maps were inspected for geomorphic features that may be indicators of subsurface geological processes or structures. Figure 2-10 shows a regional image of the seabed illustrating several major channels. Paleochannels are also evident parallel to current coastline in many portions of the shelf. The Georges Bank and Nantucket Shoals are evident in the northeastern portion of the study area along with the South Channel between the banks.

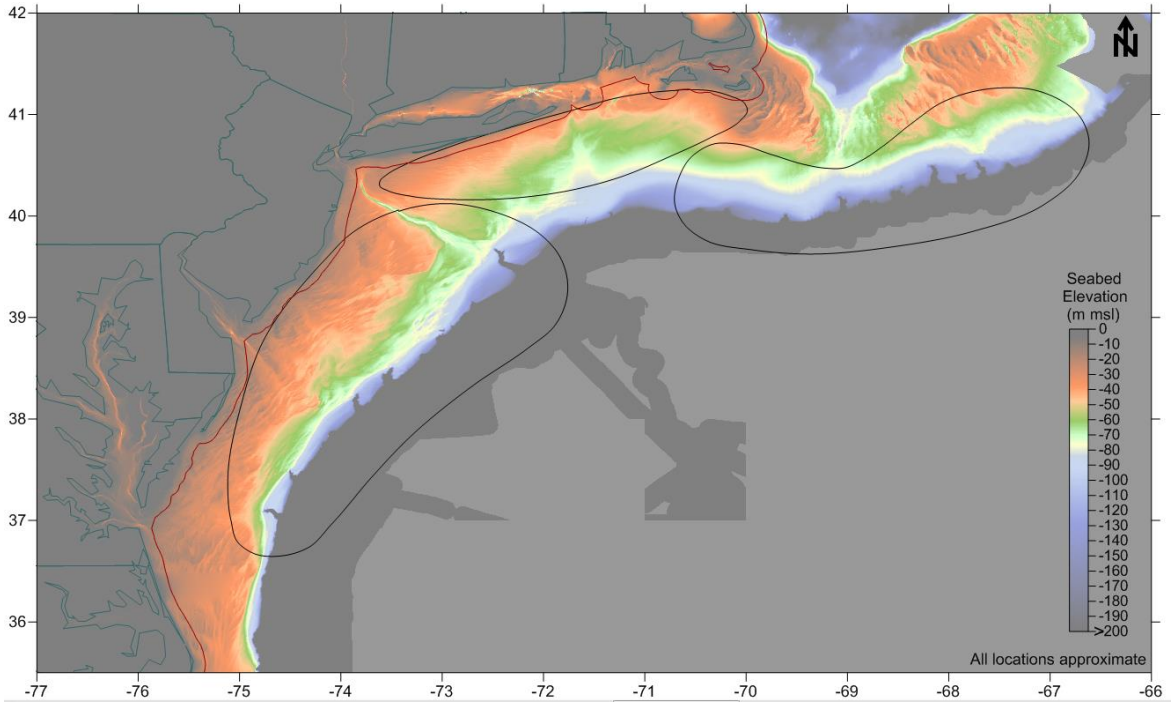

Figure 2-10. High-resolution coastal relief image for the mid-Atlantic OCS.

The relief model was examined in more detail for indicators of more localized features like faults, gas expulsions, and escarpments. Along the OCS, there are few indications of extensive features like pockmarks, gas chimneys, faulting along the seabed, salt domes, or sediment deformation. Escarpments were present near the continental slope. Along the slope, many more steeply incised canyons, mass flows, escarpments, and other were evident (Figure 2-11). More detailed seabed surveys would be necessary to determine site-specific features.

Active methane venting has been investigated along the mid-Atlantic continental shelf edge (Newman et al., 2008), indicating methane concentrations well above expected and measured background levels. These active venting sites have been categorized as elongate pockmarks on kilometers in scale, and methane venting is measured to be highest along the pockmark edges. These features are located near the shelf/slope margin and are elongated parallel to the shelf edge with steep landward walls (Hill et al., 2004). Recent post-glacial maximum shelf edge deltaic deposits show evidence of soft deformation and downslope creep, indicating a spatial correlation between the gas expulsions and the subsequent structural changes of the shelf/slope deposits.

Smaller-scale methane emission features have been detailed using multi-beam water column backscatter data; their presence is extensive along the Atlantic shelf margin, particularly between Cape Hatteras and Georges Bank (Skarke et al., 2014). In this particular study, 570 gas plumes were identified. Of these, more than 75% were identified at water depths considered to be within the uppermost limit of water column depth associated with hydrate stability in the subsurface, indicating that methane hydrate dissociation may be a driving force behind these gas seeps. Further observations indicate an absence of gas seeps along the margin between the Wilmington and Atlantis canyons. Skarke et al. (2014) hypothesize that this absence is related to thinner post-Cretaceous sedimentary deposits in this area, promoting more diffusive gas release over time, as well as less eroded and more intact shelf edge deposits (in comparison to the deposits noted above to be more deformed and eroded.)

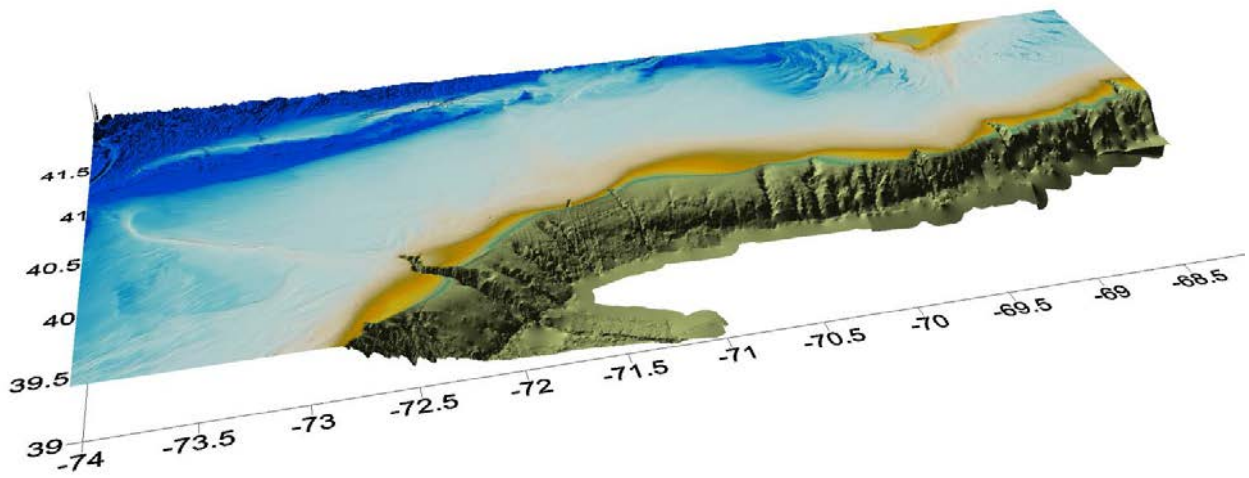

Figure 2-11. Seafloor relief image showing Hudson Canyon, escarpments, and other incised channels along the transition from the mid-Atlantic shelf to slope.

2.3 Storage Zone/Caprock Factors

CO_2 storage projects may affect large areas (thousands of square kilometers) in the subsurface, and CO_2 will migrate upward via density effects. In addition, pressure changes introduced by CO_2 injection may be transmitted to zones above and below a storage reservoir. Therefore, it is necessary to characterize the nature of the rock formations within, above, and below a storage zone.

Hannis et al. (2017) describe 'containment assurance' for offshore carbon storage in terms of deep- and shallow-focused elements. Deep containment is focused on CO_2 storage security in the reservoir zone, where containment often relies on structural traps, low-permeability caprocks, and capillary trapping. Shallow containment examines potential CO_2 leakage at the seabed into the ocean water, where gas migration along fractures, soft sediment deformation zones, and gas seeps may occur, leading to a noise or gas bubble signature at the seabed. Monitoring and risk assessments for offshore carbon storage projects will likely be concentrated on these two areas. Therefore, it is useful to examine the nature of both primary containment intervals directly above and below the storage zone, secondary containment intervals, and seabed sediments along the mid-Atlantic OCS.

Figure 2-12 shows stratigraphic columns for wells in BCT and GBB, illustrating the relationship of deep storage zones, caprocks, shallow sediments, and seawater along the mid-Atlantic OCS. Recent to Pleistocene-age marine sand with silt and clay is present at the seabed to depths of several feet in much of the OCS, but some areas may have scoured seafloor sediments. The offshore wells generally note soft to semi-consolidated Miocene- to Paleocene-age clay, mud, siltstone, limestone, shell, and sand sediments. These layers reflect various depositional and erosional periods during sea level change and vary across the shelf. Wells along the inner shelf appear to contain more clay and mud in the shallow intervals, while wells along the slope appear to contain more sand layers in the shallow intervals. Cretaceous- to Jurassic-age rock formations that are the main subject of this research are present below the Tertiary layers.

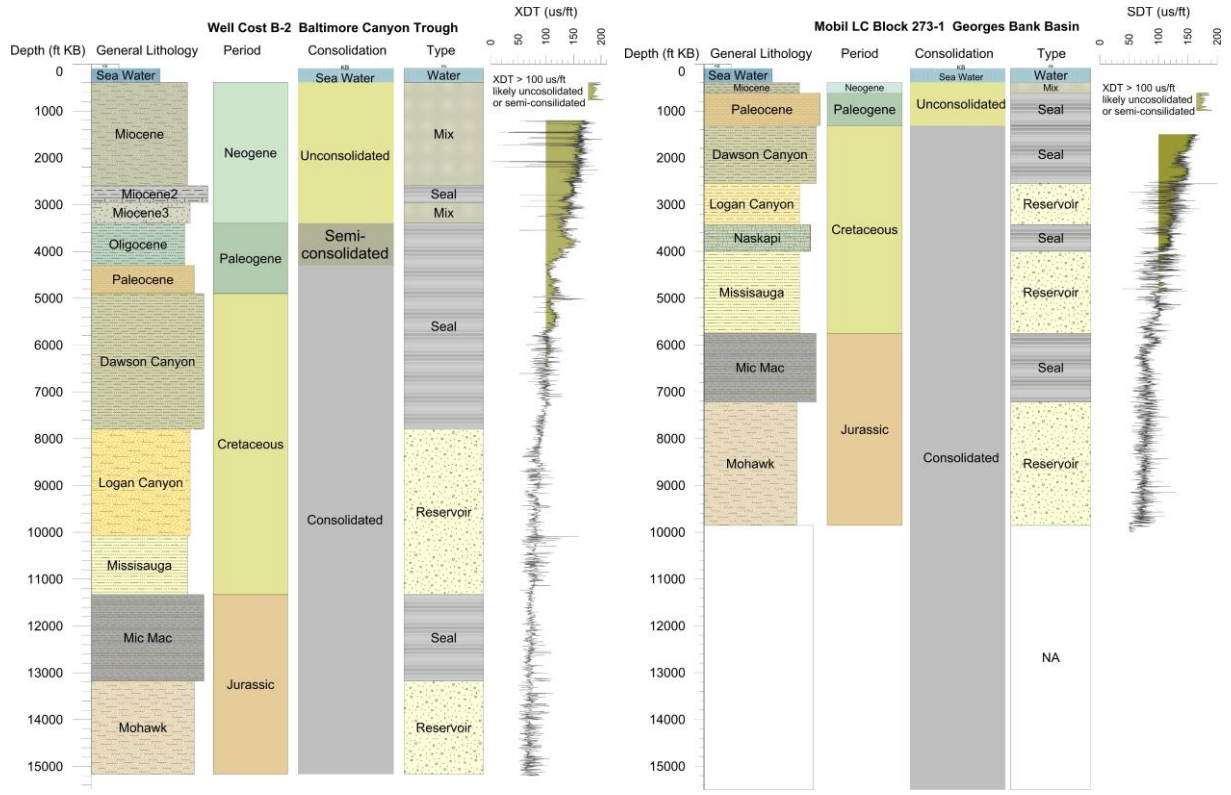

Figure 2-12. Geologic diagram illustrating sonic log (XDT) behavior in unconsolidated/semi-consolidated rocks in BCT COST B-2 and GBB Mobil 273-1 wells.

Logs and notes from exploration wells along the mid-Atlantic OCS describe unconsolidated to semi-consolidated sediments with gradual transition to more consolidated rock fabric with depth. Unconsolidated sediments are noted to depths of 500 to 1,500 m (2,000 to 4,900 ft) in wells, depending upon their location along the shelf. Sonic logs also seem to show a notable increase in velocities at depths greater than approximately 1,200 m (3,900 ft), which may be an indicator of a transition from semi-consolidated sediments to more lithified rock layer (see Figure 2-12). Combined with the phase behavior of CO_2, processes like soft sediment deformation may present risk factors in intervals above a depth of 1,000 m (3,000 ft) below mean sea level.

Variability of reservoir zones and caprocks has the potential to affect storage security and injection well performance. As discussed in the Task 4 Hydrologic Properties Data Package Report, there is a fair amount of variability in the storage zones and caprock. This reflects the series of depositional and erosional events that affected sediments over geologic time. Consequently, many of the reservoir zones have interbedded layers of sandstone, siltstone, and clay (Figure 2-13). In general, the confining layers appear more consistent and continuous in both spatial and vertical extents. The reservoir zones appear to show more variability. Consequently, these variations are important considerations for resource calculations. Site-specific storage projects would require careful examination of geologic characteristics to ensure adequate long-term storage capacity, local reservoir boundaries, and other small-scale features.

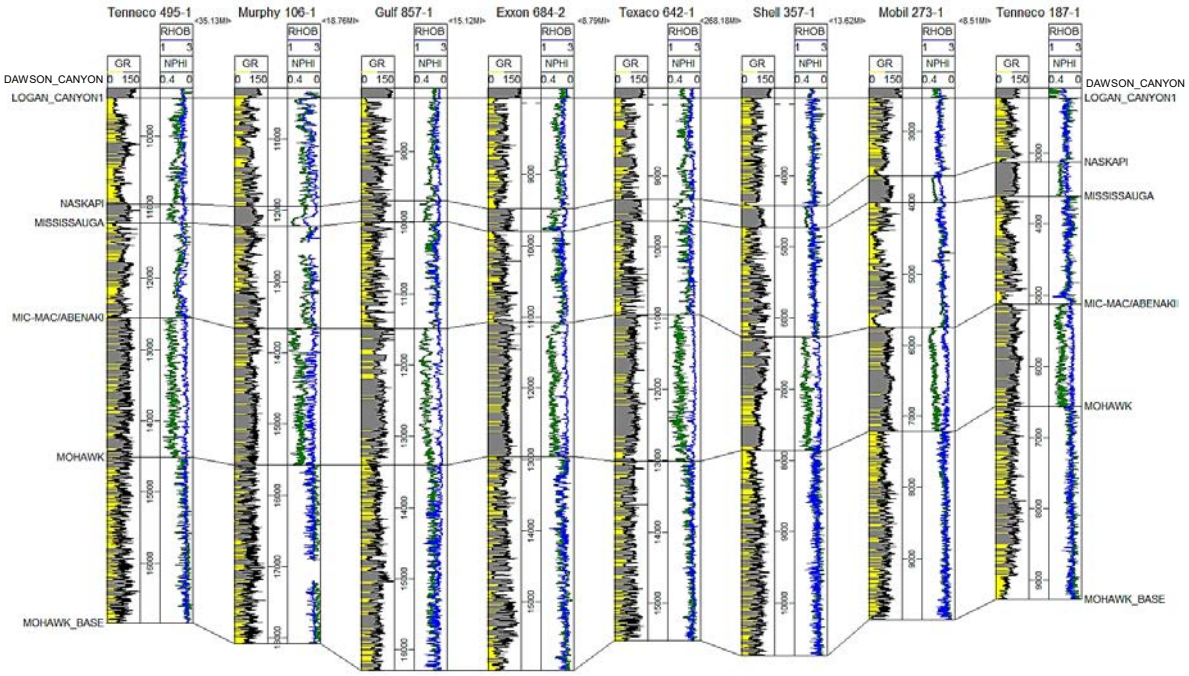

Figure 2-13. Geologic cross section through BCT and GBB illustrating reservoir variability.

2.4 Hydrologic Conditions

Hydrologic conditions along the mid-Atlantic OCS were evaluated to examine conditions in the subsurface for CO_2 storage resources. Pressure conditions, pore water salinity, geothermal gradients, and gas hydrate occurrence were analyzed based on tests, logs, and sample analysis from exploratory wells in the study areas. These conditions are important to ensure storage of CO_2 in supercritical fluid phase and also to determine potential for upward/updip migration of CO_2.

2.4.1 Subsurface Pressure Conditions

Abnormal subsurface pressure conditions may present risk factors for drilling, well completion, and injection performance along the offshore mid-Atlantic. Pore pressures may be elevated due to depositional trapping of formation fluids, tectonic compression, hydrocarbon accumulations, and other geological features. Low pore pressures may be an indicator of gas saturation, fluid migration pathways/thief zones, fracture zones, preferential flow zones, rapid erosion, isostatic rebound, and undercompaction. Pore pressures may be estimated from drilling mud weights, trends in geophysical logs, and gas kicks. Direct pore pressure may be measured with drill stem tests, leak-off tests, well tests, downhole pressure surveys, and wireline formation tests. Pore pressures are most often compared to fresh water pressure gradient of 0.433 pounds per square inch per foot (psi/ft) (8.4 pounds per gallon [lb/gal] drilling mud weight, or 9790 pascals per meter [Pa/m]). Higher salinity fluid will commonly have higher pressure gradient that reflects the column of fluid density.

Normal subsurface pressure conditions were observed. To assess subsurface pore pressure conditions in the offshore mid-Atlantic, repeat formation tests and mud weights were analyzed for exploratory wells. Repeat formation tests are wireline tools designed to isolate a 0.3- to .9 m (1- to 3 ft) vertical portion of the open borehole and measure pressure buildup over time until

pressure equalizes or seal failure occurs. The tool can be applied across multiple intervals with the open borehole. In addition, a fluid sample may be collected to verify the presence of hydrocarbons. Data from 181 repeat formation tests were compiled from 12 wells in the mid-Atlantic offshore region. The data were reviewed for quality and seal failures or inconclusive test results, resulting in 44 acceptable test results (Table 2-1). Figure 2-14 shows a plot of measured pressures versus depth for the repeat formation tests. Data indicate very good correlation to a 0.45-psi/ft (10,000 Pa/m) pressure gradient. The pressure gradient suggests consistent pressure conditions in the deeper offshore shelf geologic layers from a depth of 5,600 to 16,000 ft (1,700 to 4,900 m). Average pressure gradient was 0.45 psi/ft (10,000 Pa/m), which likely reflects salinity of more than 35,000 milligrams per liter (mg/L).

Table 2-1. Summary of repeat formation tests in mid-Atlantic offshore wells.

Well Identifier	Test No.	Depth (ft msl)	Test Pressure (psi)	Pressure Gradient (psi/ft)	Well Identifier	Test No.	Depth (ft msl)	Test Pressure (psi)	Pressure Gradient (psi/ft)
COST B-2	2	11696	5183	0.443	COST G-1	1	9770	4405	0.451
COST B-2	4	10170	4497	0.438	COST G-1	2	9265	4098	0.442
COST B-2	5	10290	4558	0.439	COST G-1	3	9265	4098	0.442
COST B-2	6	11695	5160	0.438	COST G-1	4	9264	4098	0.442
Exxon 599-1	1	12334	5539	0.446	COST G-1	5	8769	3881	0.443
Exxon 599-1	2	12384	5536	0.444	COST G-1	6	8762	3878	0.443
Exxon 684-1	3	12758	5720	0.448	COST G-1	7	8763	3880	0.443
Exxon 684-1	4	12677	5590	0.441	COST G-1	8	8502	3763	0.443
Mobil 17-2	17	12467	6145	0.493	COST G-1	9	8492	3760	0.443
Shell 273-1	1	15859	7094	0.447	COST G-1	10	7830	3458	0.442
Shell 273-1	36	11717	5176	0.442	COST G-1	11	7830	3456	0.441
Shell 273-1	37	10194	4505	0.442	COST G-1	12	7830	3457	0.442
Shell 273-1	38	12874	5719	0.444	COST G-1	13	7809	3448	0.442
Shell 586-1	1	15289	7120	0.466	COST G-1	14	6816	3009	0.441
Shell 586-1	2	15286	7119	0.466	COST G-1	15	6816	3009	0.441
Shell 586-1	3	14385	6624	0.460	COST G-1	16	5503	2404	0.437
Shell 93-1	1	8269	3718	0.450	COST G-1	17	5504	2404	0.437
Tenneco 642-3	2	13238	5960	0.450	COST G-1	18	5506	2406	0.437
Tenneco 642-3	6	8910	3995	0.448	COST G-1	19	5810	2544	0.438
Tenneco 642-3	9	8230	3685	0.448	COST G-1	7	11400	5320	0.467
Tenneco 495-1	18	13280	5536	0.417	COST G-1	9	11536	5069	0.439
Tenneco 495-1	47	9427	4333	0.460					
Tenneco 495-1	49	9527	4334	0.455					

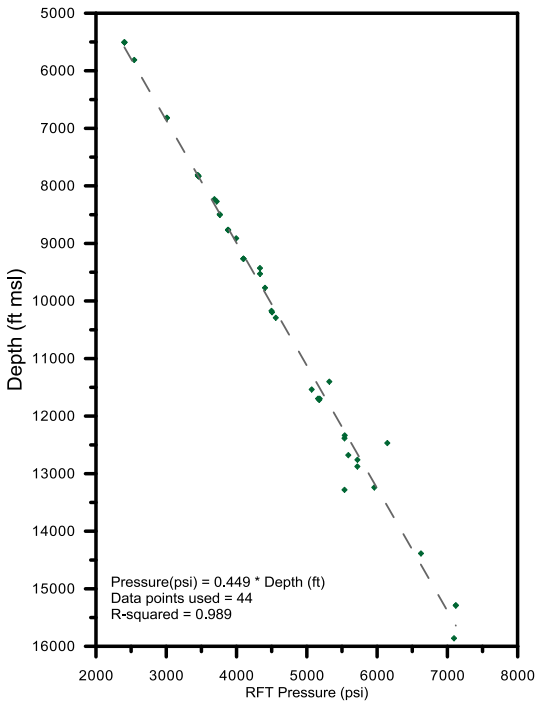

Figure 2-14. Pressure gradients from wireline repeat formation tests.

2.4.2 Subsurface Salinity Conditions

Subsurface salinity is important to determine the amount of CO_2 that may dissolve in formation fluids. Dissolved CO_2 will increase fluid density and is considered a more secure CO_2 storage mechanism than supercritical CO_2. Therefore, long-term dissolution of CO_2 in formation waters is an important process for CO_2 storage resource assessments. Several researchers have examined groundwater salinity trends along the mid-Atlantic OCS (van Geldern et al., 2013; Mountain et al., 2010; Cohen et al., 2010; Pope & Gordon, 1999; Kohout et al., 1977). The studies found salinity inversions with depth that reflect relatively fresh water trapped in sediments during lowstand sea levels and/or recharge from inland areas alternating with higher sea levels and salinity. Most of the analysis was based on water samples from a series of offshore wells drilled to depths of approximately 200 to 700 m (700 to 2,000 ft) depth mean sea level (msl). The research suggests that paleo-waters trapped in the deeper rock formations have fairly low salinity (0 to 25 parts per thousand [ppt]) near shore, with salinity increasing to 25 to 50 ppt further offshore. Cohen et al. (2010) suggest that fresh water is sequestered in sediments out to 50 km (30 mi) offshore of the present coastline and at depths up to 2,000 m (7,000 ft) near the coastline.

Salinity in the deeper rock units being considered for CO_2 storage have few well penetrations and even fewer fluid samples. Fluid samples from the repeat formation tests were mainly collected in potential oil and gas zones, so they often had gas cut in the water. Test notes also state that the samples reflected drilling mud contamination and were not formation samples. Mud weights for the offshore wells ranged from 9 lb/gal (1 gram per milliliter [g/ml]) seawater-based gel-type muds in the shallow zones to 11.3 lb/gal (1.35 g/ml) gel-type muds in deeper zones over 10,000 ft (3,000 m). Resistivity logs from the offshore wells suggest a trend of increasing salinity with depth, but the logs are difficult to interpret in terms of specific salinity values.

Overall, the precise salinity of the formation fluids in the deeper (more than 1,000-m-deep [3,000 ft]) rock formations along the mid-Atlantic OCS is challenging to define based on available information. CO_2 storage project development would require additional characterization to verify formation fluid salinity. Research and fluid sampling from Integrated Offshore Drilling Program (IODP) offshore wells suggest that salinity in the deeper formations would likely be greater than 40,000 mg/L (.3 lb/gal), especially in areas farther offshore. In areas near the coastline, protection of groundwater resources from saltwater intrusion would be a risk factor, even in the deeper formations.

2.4.3 Subsurface Geothermal Conditions

Subsurface temperature conditions are a factor for CO_2 storage in terms of phase behavior. Abnormal temperatures may result in CO_2 transition to gas phase, liquid phase, or hydrate formation in cases of low temperature and high pressures, which could affect injection operations and storage processes in the subsurface. Review of temperature logs and other research for mid-Atlantic OCS wells suggests a geothermal gradient of approximately 16 to 24 °C/km (0.9 to 1.5 °F/100 ft). Arthur (1982) describes a similar geothermal gradient along the offshore mid-Atlantic related to thermal history, depositional history, and subsidence. In general, the geothermal gradients in the offshore mid-Atlantic do not appear to present risk factors for CO_2 storage. Somewhat higher geothermal gradient may result in uncertainty in depths of approximately 700 to 1,000 m (2,000 to 3,000 ft) below msl, where CO_2 phase behavior may be sensitive to temperature/pressure conditions.

Figure 2-15 shows temperature log data for offshore mid-Atlantic wells. The logging data would suggest an average gradient of approximately 23 °C/km (1.35 °F/100 ft). Some wells (Shell 93-1, Exxon 684-1) in the thicker basin portions of the OCS appear to have lower geothermal gradients, which may be related to seawater depth and proximity to oceanic crust (Robbins, 1979; Fry, 1987).

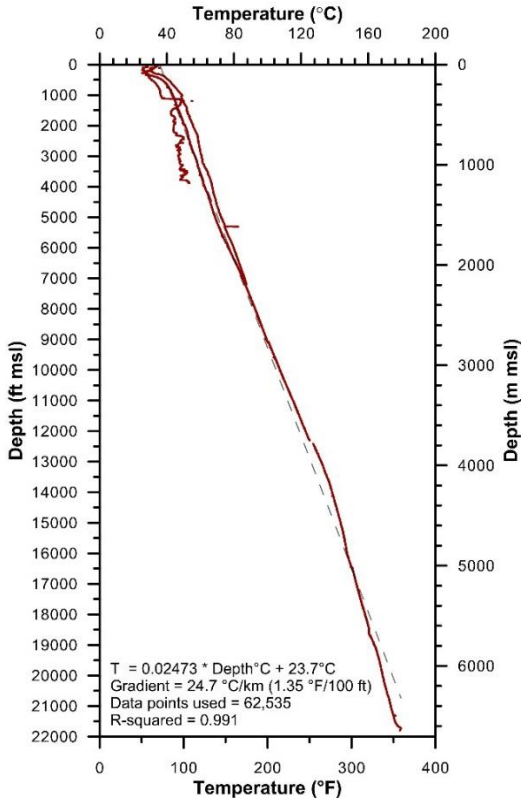

Figure 2-15. Subsurface temperatures logged in offshore mid-Atlantic wells.

2.4.4 Subsurface Hydrates

Methane gas hydrates have been observed along some areas of the Atlantic offshore continental slope. Gas hydrates may cause problems with drilling activities, CO_2 injection, and pipeline transport. Most gas hydrate formations have been observed south of BCT, generally outside of the project study area. The hydrates are also more common along the continental slope.

CO_2-water hydrates (or clathrates) may also form at high pressure (greater than 4 megapascals [MPa] or 600 psi) and low temperature (less than 10 °C or 50 °F) conditions (Kyung et al., 2013). CO_2 hydrate formation can impede injection operations since hydrates have a much higher viscosity and gel form. CO_2 hydrates would potentially clog the reservoir pore space and prevent injection (Sminchak et al., 2014). CO_2 hydrates can also form during routine CO_2 injection operations when injection cycles cause rapid depressurization in the well, resulting in low temperature conditions favorable for hydrate formation.

Subsurface temperature and pressure conditions along the offshore mid-Atlantic would generally not result in hydrate formation, mostly because the geothermal gradient is high enough in the deep rock formations to prevent hydrate formation. There may be some areas near the seabed floor where CO_2 hydrate could form, but these areas are mostly along the continental slope where seawater depth is much greater.

Laboratory experiments suggest that upward diffusion of CO_2 in subsea sediments can form hydrates within the hydrate stability zone (Tohidi et al., 2010; Babu et al., 2014). Experimentally, permeability decreases within the hydrate stability zone as hydrates are formed. This effect could act as a secondary seal, preventing further upward diffusion of CO_2 under current

conditions. Additionally, there are efforts to explore CO_2 hydrate formation as a primary mechanism for carbon sequestration by exchanging CO_2 with trapped methane gas (Schoderbak et al., 2013). Field trials in the Ignik Sikumi Gas Hydrate Field in Alaska have successfully recovered CH_4 gas using CO_2. Laboratory experiments have suggested that injection of flue gas into hydrate-bearing formations creates a fast dissociation of methane gasses and a significant formation and trapping of the CO_2 as a hydrate (Yang et al., 2017). The abundance of methane hydrates within the hydrate stability zone provides an economic incentive to recover these trapped gasses. The added potential of CO_2 sequestration further increases the argument for adoption moving forward and provides the foundation for continued exploration due to an increasing energy demand and the increasing necessity of CO_2 sequestration.

2.5 Seismic Activity along the Mid-Atlantic OCS

Earthquake activity along the offshore mid-Atlantic is low. The Atlantic OCS is a passive continental margin with very little seismic activity, tectonic movement, and/or volcanoes. Figure 2-16 shows historical earthquake activity for the study area. No earthquakes have been observed in GBB and BCT. Three earthquakes have been observed along the south-central portion of the Long Island Platform with low magnitudes of 2.5 to 3.7. Hypocenters were 10 to 30 km (20 mi) deep.

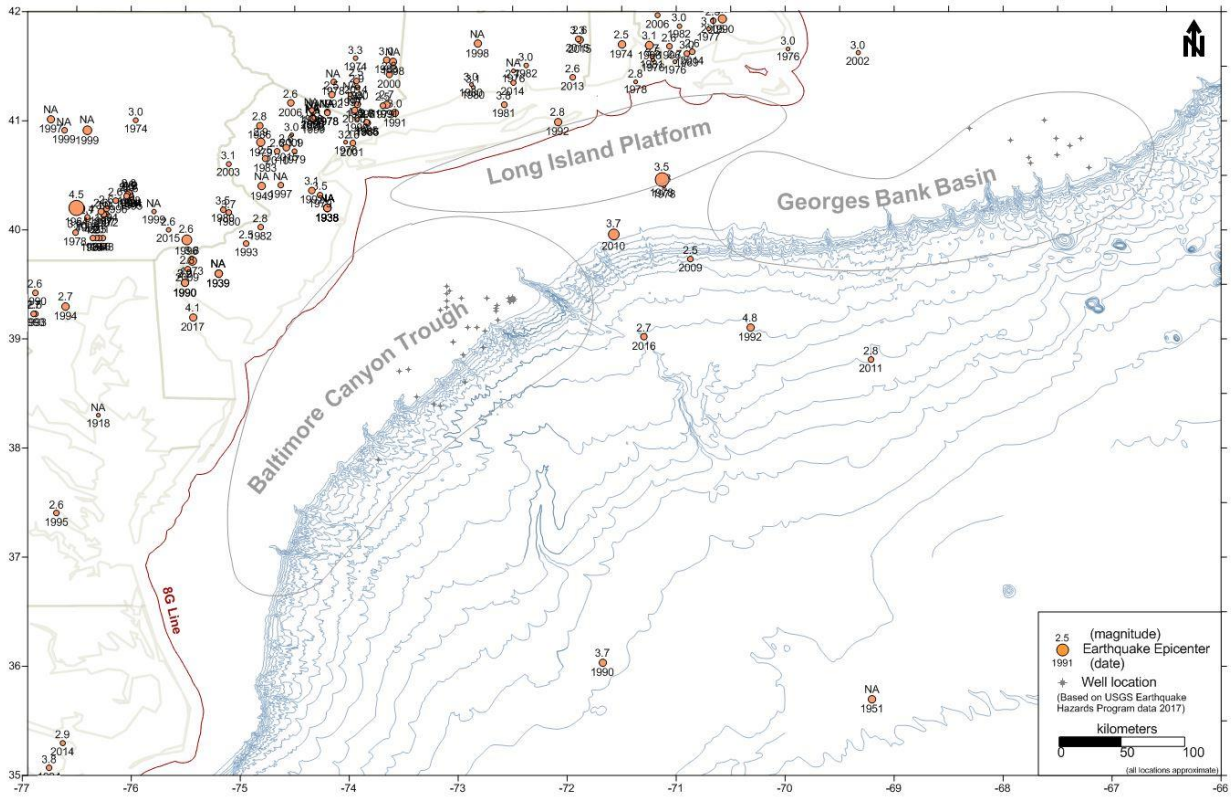

Figure 2-16. Map illustrating historical earthquakes in the mid-Atlantic region.

The USGS 2017 one-year seismic hazard forecast from induced and natural earthquakes (Figure 2-17) lists the eastern seaboard as having less than 1% chance of damage from an earthquake in 2017 (Petersen et al., 2017). The 2014 U.S. Geological Survey National Seismic

Hazard Map (Petersen et al., 2014) shows mostly low hazard, with a medium rating in the Pennsylvania-New Jersey-New York tristate area associated with Mesozoic Newark rift basin structures. While offshore areas are not specifically assessed in the seismic hazard analysis, there is a decreasing trend out toward the shelf. Escarpments and fault blocks are present along the continental slope, but these areas are not well characterized in terms of seismic hazard.

An understanding of subsurface stress conditions helps to evaluate the potential for induced seismicity, hydraulic fracturing, and critically stressed areas in relation to CO_2 injection. Stress orientations along the offshore mid-Atlantic are related to tectonic forces and mid-Atlantic spreading of oceanic crust, which results in a principal stress direction in the northeast-southwest orientation. Figure 2-18 shows data from the world stress map (Heidbach et al., 2016) illustrating stress orientation along the offshore mid-Atlantic, mostly determined from borehole breakouts observed in the offshore wells drilled in the area. Strike-slip and thrust stress regimes are most likely in the region. Stress magnitudes are not available, but they may be similar to the eastern United States where there is approximately 2:1 contrast between maximum and minimum horizontal stress magnitudes.

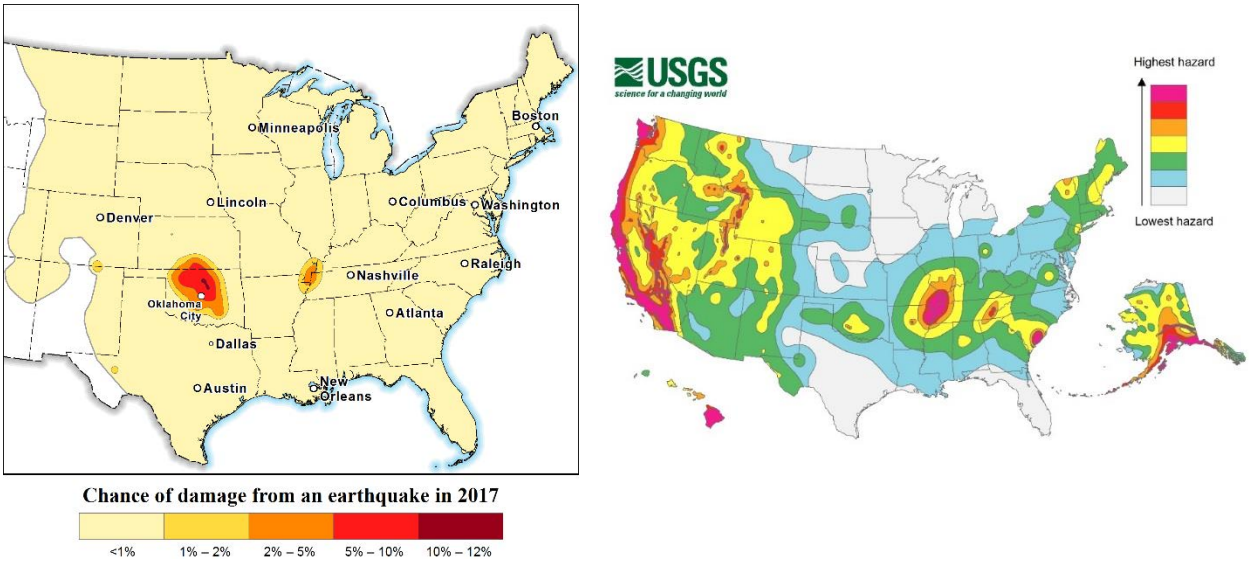

Figure 2-17. Maps of chance of damaging earthquake in 2017 (left) and seismic hazards (right) (Petersen et al., 2017; Petersen et al., 2014).

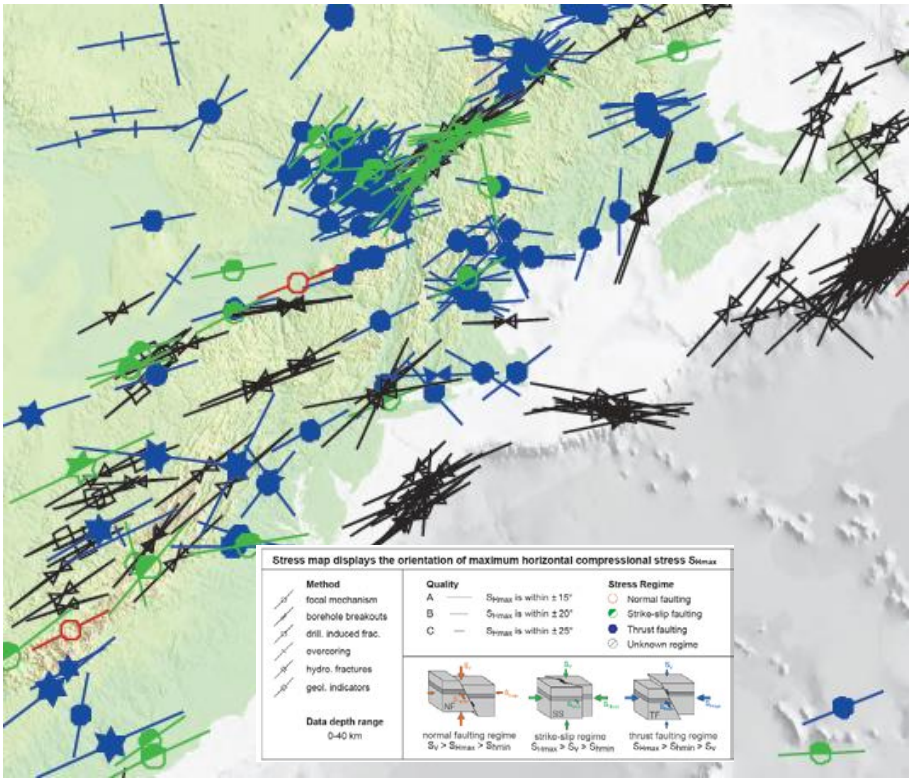

Figure 2-18. Maximum horizontal stress orientation along mid-Atlantic OCS (from Heidbach et al., 2016).

Overall, it is difficult to determine if there are critical stressed subsurface conditions in the offshore mid-Atlantic that may lead to induced seismicity due to stress changes resulting from CO_2 injection. A more detailed geomechanical characterization, testing, and analysis program would be necessary for any site-specific CO_2 storage project. Escarpments and troughs near the continental slope would require careful consideration.

3.0 Long-Term CO_2 Risk Factors

Long-term CO_2 storage risk factors were examined in terms of confining/trapping mechanisms, long-term migration patterns, and wellbore integrity. The objective of the analysis was to ensure that CO_2 would remain in the deep rock formations for geologic time periods. The offshore mid-Atlantic does not contain significant hydrocarbon plays that would attest to the ability of the rock formations to trap fluids for millions of years. Therefore, an understanding of the long-term migration potential and trapping processes is an important risk factor for carbon resource characterization in the offshore mid-Atlantic study areas.

3.1 Confining/Trapping Mechanisms

3.1.1 Confining Layers Description

The properties of the confining layers are an important factor to ensure CO_2 storage security and permanence. At depth, CO_2 will be concentrated as a supercritical phase around the injection well(s), and the CO_2 will tend to migrate upward due to buoyancy effects. Hydrocarbon plays and natural CO_2 fields provide examples of the ability of confining layers to trap natural gases for millions of years. Supercritical CO_2 has a low viscosity similar to gas, and it may penetrate further into caprock intervals than water or oil. Thus, the primary confining layer overlying the storage zone is most important for impeding upward migration of CO_2. Additional buffer layers above the primary caprock may provide added confidence in the CO_2 storage system.

Figure 3-1 illustrates the nature of the confining layers along the BCT and the GBB. In the mid-Atlantic OCS, the primary caprock for the Logan Canyon/mid-Cretaceous sands interval is the upper Cretaceous shales/Dawson Canyon Formation. In some areas of the BCT, a shale unit termed the Sable shale has been noted in the mid-Cretaceous sands. Secondary containment may be provided by shallower Miocene-Paleocene layers. However, these layers may be unconsolidated to semi-consolidated, and there may be potential for soft sediment deformation in intervals less than 3,500 ft (1,100 m) where CO_2 may transition from supercritical fluid to liquid or gas phase. The primary caprock for the lower Cretaceous sands/Missisauga Formation is the mid-Cretaceous Naskapi Formation, and the upper Jurassic Mic-Mac formation is the caprock for the Jurassic Mohawk sandstone.

As shown in Figure 3-1, the individual confining layers are generally 200 to 2,500 ft (60 to 760 m) thick. In addition, the units are fairly continuous across the mid-Atlantic OCS, although the rock properties vary with location. The depth of the upper Cretaceous shales/Dawson Canyon formation is much shallower in the GBB and Long Island Platform than in the BCT. Therefore, risk factors for containment would be present for CO_2 storage in the mid-Cretaceous sands/Logan Canyon in these areas. The distribution of the caprocks in the Long Island Platform was inferred from regional trends and seismic survey interpretation; the caprock properties would need to be confirmed with test wells.

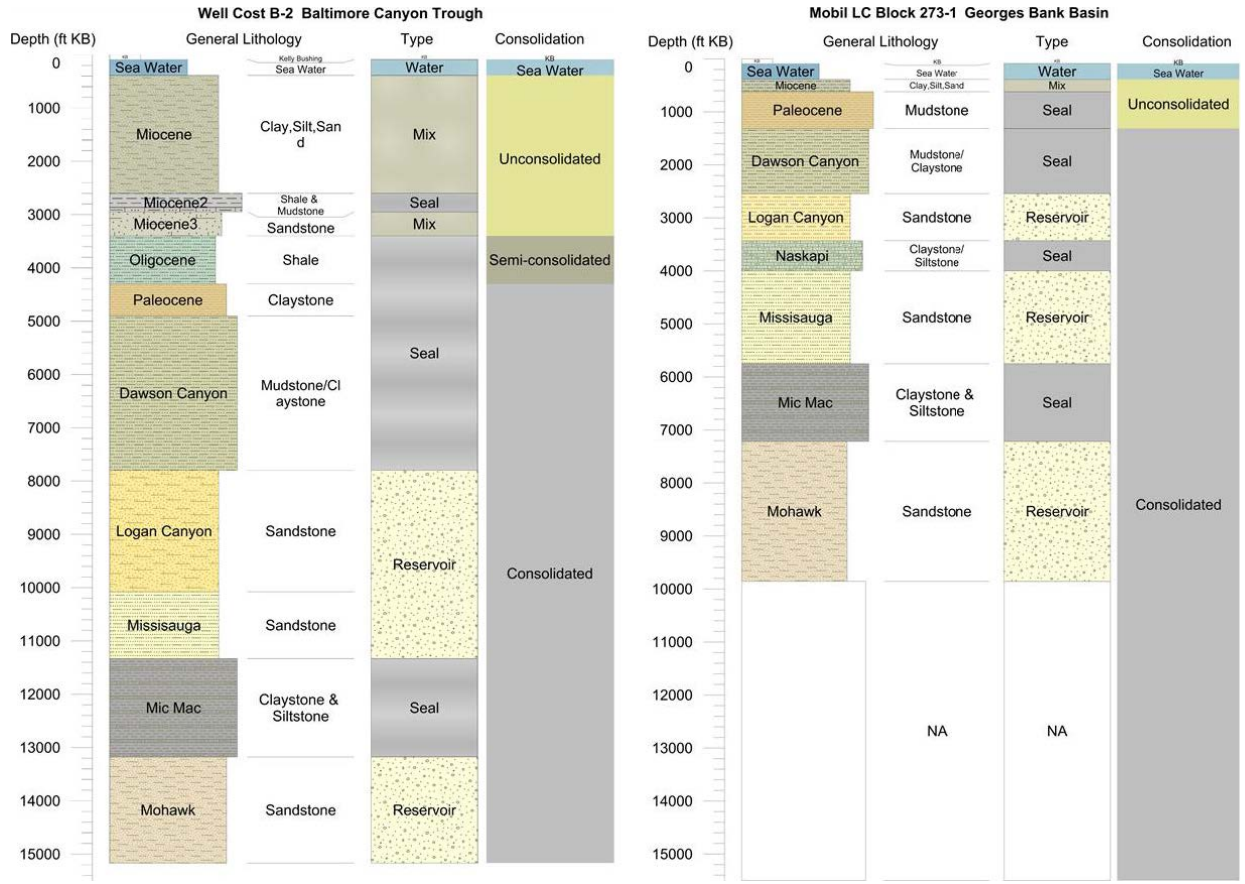

Figure 3-1. Diagram illustrating relationship of general lithology, sediment consolidation, reservoir intervals, and confining layers for BCT (left) and GBB (right).

Table 3-1 summarizes the general properties of the confining layers. In general, most of the exploration wells along the mid-Atlantic offshore did not focus on the confining layers since they were not hydrocarbon plays. Therefore, there are limited data available from these units. Threshold entry pressure tests were completed on 17 samples from the BCT Texaco 642-1 well at depths of 12,436 to 14,080 ft (3,790.5 to 4,292 m) within the upper Jurassic Mic-Mac Formation (Table 3-2). The samples had porosity of 0.6 to 5.7% and vertical permeability of 0.000001 to 0.00168 mD. Threshold pressures were mostly listed as 1,000+ psi (7 MPa), with two samples listed as 800 and 850 psi (6 MPa). These threshold entry pressures are very high, considering that threshold entry pressures of 300 to 700 psi (2 to 5 MPa) have been observed for other shale CO_2 storage caprocks (Espinoza and Santamaria, 2017; Zhou et al., 2017). The test results appear a bit general, but they suggest that a high pressure gradient may be maintained against the caprock without CO_2 breakthrough.

Table 3-1. General properties of confining layers in the mid-Atlantic OCS.

Property	Confining Layer			
	Miocene-Paleocene	UK Caprock/ Dawson Canyon	MK4/Naskapi	LK2/Mic-Mac Abenaki
Geologic Period	Tertiary	Upper Cretaceous	Middle Cretaceous	Lower Cretaceous - Upper Jurassic
Age (~MYA)	23-66	85	125	135 - 145
Lithology	Mixed clay, silt, sand	Mixed siliciclastic	shale	Mixed siliciclastic
Thickness (ft)	>1,000	1,813	593	1,757
Porosity (fraction)	NA	0.23	0.24	0.20
Permeability (mD)	NA	407	NA	122
Mineralogy	NA	quartz + illite-smectite/mica + chlorite + kaolinite + calcite + plagioclase + K-feldspar	NA	quartz + calcite + kaolinite + illite-smectite/mica + plagioclase + K-feldspar

Table 3-2. Threshold pressure test results from Texaco 642-1 well Mic-Mac Formation.

Sample Number	Sample Depth (ft KB)	Porosity	Vertical Permeability (mD)	Threshold Pressure (psi)
1	12,436.8	1.4	0.000049	1000+
2	12438.9	3.6	0.000001	1000+
3	12,442.1	2.2	0.000001	1000+
4	12,443.9	4.6	0.000023	1000+
5	12,445.9	1.4	0.000036	1000+
6	12,448.3	6.2	0.000001	850
7	12,451.1	3.6	0.000026	1000+
8	12,453.2	3.4	0.000001	1000+
9	12,455.0	4.6	0.000032	800
10	12,488.1	5.7	0.000001	1000+
11	12,490.0	0.5	0.000020	1000+
12	12,492.9	1.3	0.000001	1000+
13	12,494.2	2.2	0.000027	1000+
14	14,061.7	2.5	0.000018	1000+
15	14,068.2	0.6	0.000001	1000+
16	14,071.4	1.1	0.000001	1000+
17	14,078.5	1.6	0.000168	1000+

3.2 Long Term CO_2 Migration Analysis

The potential for long-term CO_2 migration for the mid-Atlantic outer continental shelf study areas was evaluated based on migration pathway analysis and trapping mechanisms. Long-term CO_2 migration was depicted with a CO_2 phase behavior analysis, updip flow vector pathways, and an analog study on onshore-offshore depositional systems was completed for the study areas.

3.2.1 CO_2 Phase Behavior Analysis

To examine the potential for vertical migration of CO_2, the phase behavior of CO_2 with depth was completed for the mid-Atlantic OCS study areas. Supercritical CO_2 has a density of 0.6 to 0.9 g/ml (5 to 8 lb/gal) and will migrate upward along structural trends, caprock layers, and geologic flow pathways. For example, several studies have examined the upward migration of CO_2 at the Sleipner storage site in the North Sea, where more than 15 million metric tons of CO_2 have been injected since 1996. Seismic monitoring and models have demonstrated that the injected CO_2 has migrated upward into nine vertical plume layers beneath intra-formational shale layers in the Utsira Sand storage formation (Bickle et al., 2007; Chadwick et al., 2006; Cavanagh & Haszeldine, 2014). Consequently, migration patterns are important factors for understanding risk factors related to CO_2 storage security.

Along the mid-Atlantic OCS, the rock formations being considered for CO_2 storage have a depth range of 2,000 to 15,000+ ft (600 to 5,000 m) below mean sea level with a wide range of temperature and pressure conditions. Figure 3-2 illustrates the general temperature and pressure profile along the mid-Atlantic OCS in relation to CO_2 phase behavior. In the targeted storage zones, the conditions are firmly in the supercritical phase region. Based on pressures measured with downhole repeat formation tests and geothermal gradients in the study areas, the density of supercritical CO_2 fluid is likely to range from 0.7 to 0.75 g/ml (6 lb/gal) at depths of 4,000 to 16,000 ft (1,000 to 5,000 m) msl (Figure 3-3). In general, the density would result in considerable buoyancy effects, because the CO_2 will be 25 to 30% lighter than existing fluid in the reservoir.

The pressure-temperature trends at depth suggest that a minimum depth of approximately 1,000 m (3,000 ft) below msl may be required for supercritical fluid phase storage. At depths less than 1,000 m (3,000 ft), CO_2 could potentially transition to gas phase with density less than 0.3 g/ml (3 lb/gal). The relatively high temperatures and moderate pressures generate some uncertainty as to phase behavior in these shallower zones. Gas phase CO_2 at these depths would be much more mobile, and sediments at the shallow depths are poorly consolidated. Soft sediment deformation may be possible in these zones. Gas chimneys, pockmarks, and gas expulsions may occur at the seabed when gas migrates from deeper zones. CO_2 storage at depths less than 1,000 m (3,000 ft) may involve risk factors related to CO_2 phase changes, upward migration, and soft-sediment deformation. In the shallower storage zones, caprock and reservoir structures should be carefully characterized to ensure storage permanence. These risk factors would affect the GBB and Long Island Platform, where rock formations are shallower. For example, the top of the Logan Canyon in the entire GBB and Long Island Platform is less than 1,000 m (3,000 ft) msl deep (Figure 3-4).

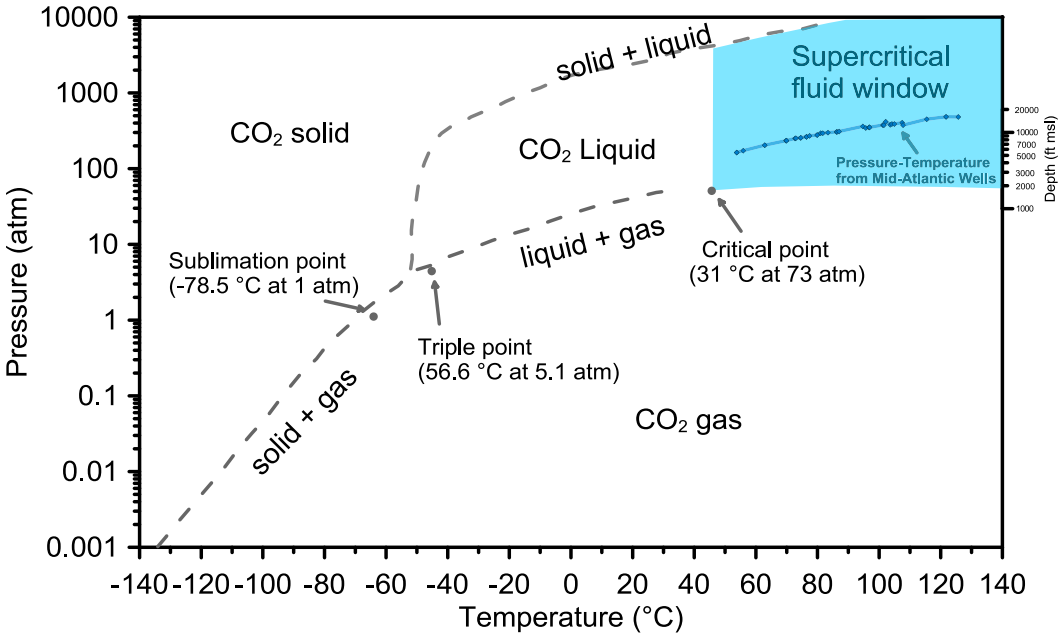

Figure 3-2. CO_2 phase diagram with pressure-temperature profile data from mid-Atlantic wells.

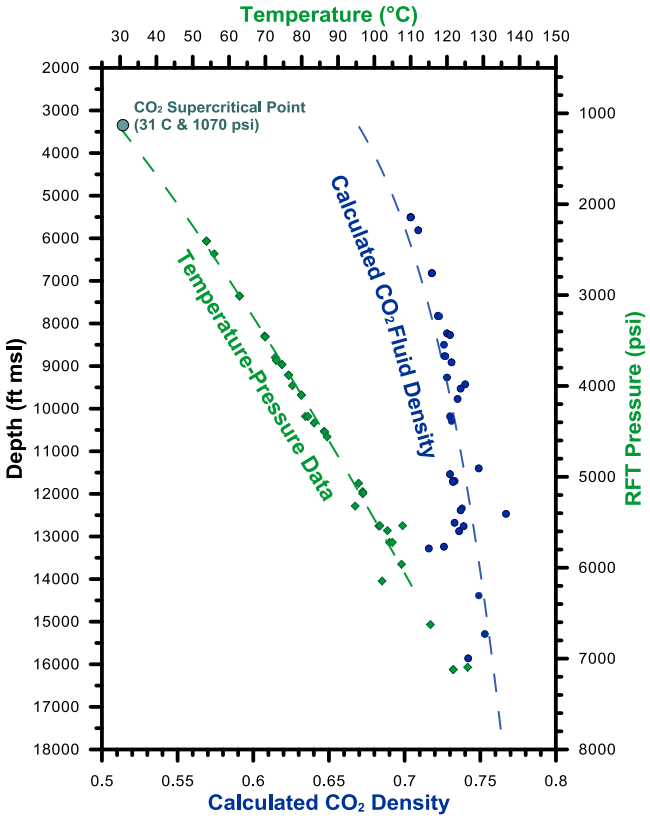

Figure 3-3. CO_2 density, pressure, and temperature trends for the offshore mid-Atlantic.

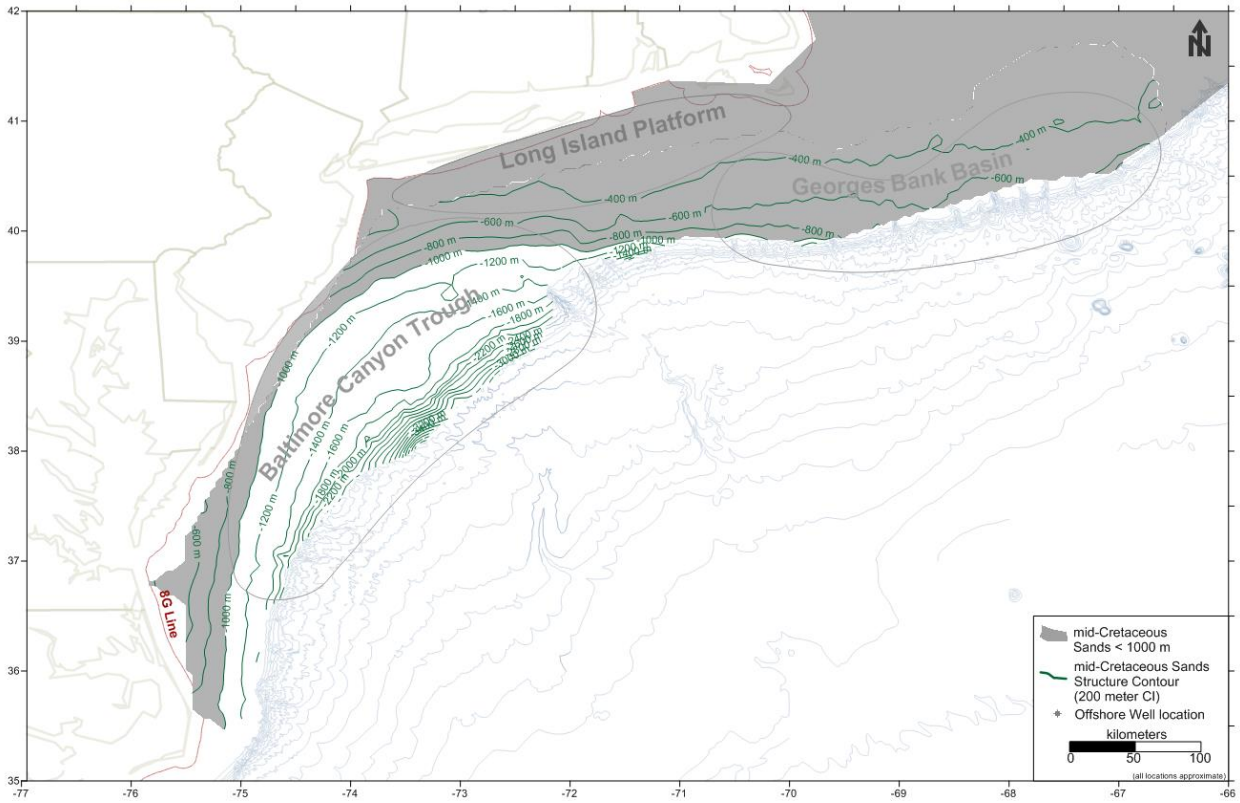

Figure 3-4. Logan Canyon structure map illustrating areas (shaded gray) where the top of the mid-Cretaceous sands is less than 1,000 m deep.

3.2.2 Updip flow vector pathway analysis

To examine the potential for long-term migration of CO_2, an updip flow vector analysis was completed for the mid-Atlantic OCS study areas. Since supercritical CO_2 has a density of 0.7 to 0.9 g/ml (6 to 8 lb/gal), the fluid will tend to migrate updip due to buoyancy processes unless there is a geologic structure, sealing fault/feature, or stratigraphic trap/pinchout.

In the mid-Atlantic OCS, the Cretaceous and deeper rock layers dip downward to the east-southeast, following the general outline of the coastline based on the surface of Logan Canyon from seismic interpretation and well logs. The rock layers' dip along the shelf is fairly low, at 0.001 to 0.02 m/m (10 to 100 ft/mi). There appear to be local undulations in some areas that may provide localized trapping structures.

Figure 3-5 shows a slope map for the top of the mid-Cretaceous sands, illustrating variations in slope across the study areas. As shown, the structural slope is low throughout most of the shelf and increases substantially along the Continental Slope. There are some areas with higher slope near the Great Stone Dome and other small areas. A channel feature may be present along the northern border of the BCT, which may present a preferable updip flow pathway for CO_2 migration.

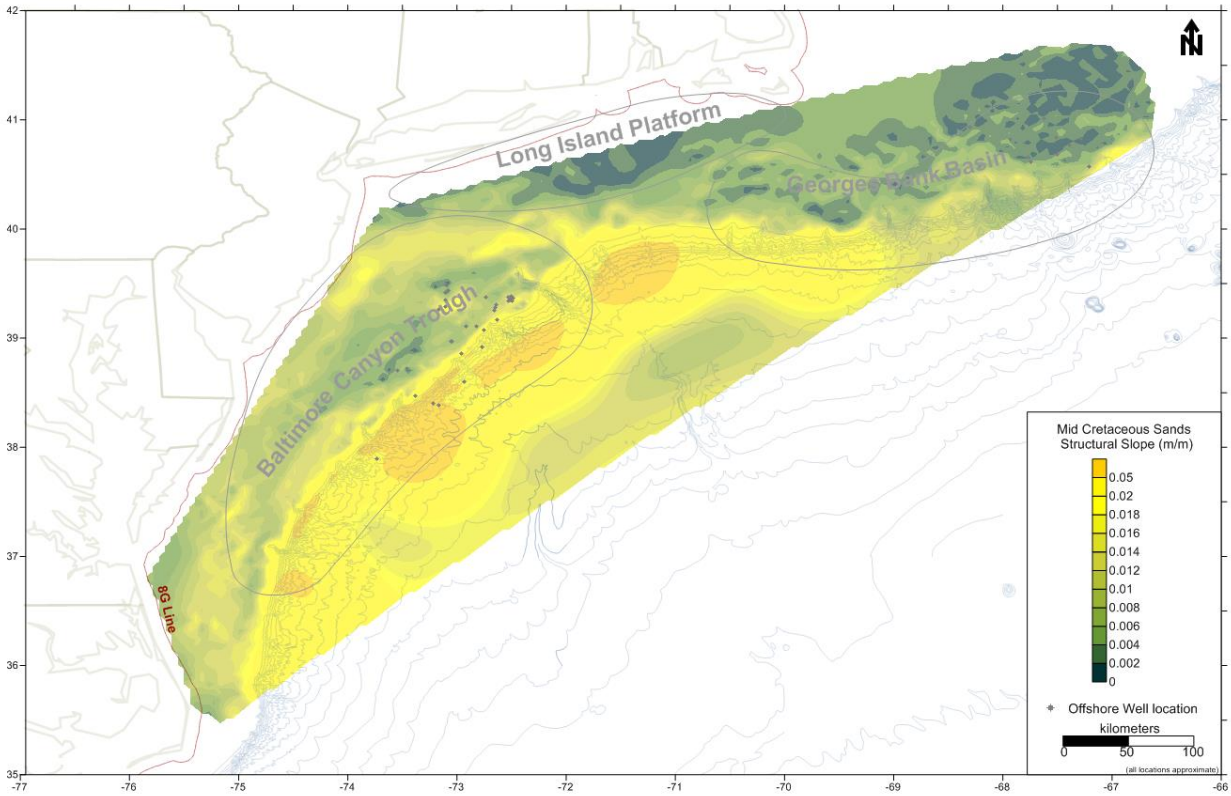

Figure 3-5. Structural slope map for the top of the mid-Cretaceous sands.

To evaluate potential CO_2 updip flow pathways, a simple fluid flow model was run for the mid-Cretaceous sands. A 3D finite difference variable density flow model was set up with the top and bottom of the mid-Cretaceous sands for the study area domain. The model grid was relatively coarse, with 50 rows, 54 columns, and 3 layers, for a total of 8,100 grid cells. Formation picks were based on a combination of well picks and seismic survey interpretation. Regional constant head nodes were prescribed to affect a small hydraulic gradient from the southeast to the northwest in a general structural updip direction. The model was run in steady-state mode to simulate hydraulic heads and correlating flow vectors. The updip flow vectors indicate the general flow direction that CO_2 would follow due to buoyancy effects. Figure 3-6 shows the simulation results. As may be expected, updip fluid flow directions are toward inland areas along the general structural updip trends. There are some minor variations, but the coarse model grid does not account for localized structures like the Great Stone Dome. More detailed reservoir simulations incorporating lithologic variations, permeability distributions, and multi-phase flow effects would be necessary to determine site-specific CO_2 injectivity and flow behavior.

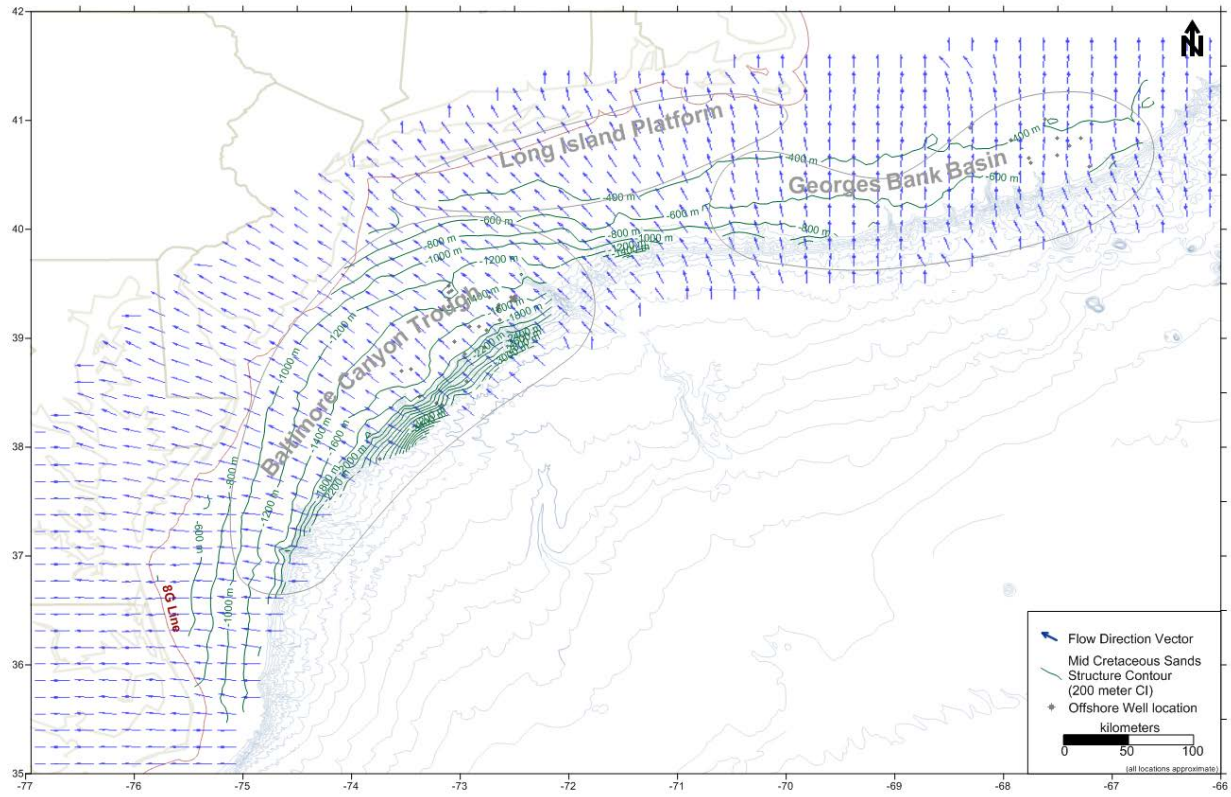

Figure 3-6. Updip fluid flow vectors based on variable density fluid flow simulation for Logan Canyon Formation.

3.2.3 Analog Study for Onshore-Offshore Depositional Systems and Stratigraphic Trapping

In order to evaluate the distribution and characteristics of confining and trapping mechanisms present in our study area, a comparable stratigraphic depositional analog was described. The analog provides an understanding of the stratigraphic architecture that makes up the mid-Atlantic offshore passive margin confining and trapping mechanisms. A detailed description of geologic settings and descriptions of the mid-Atlantic offshore passive margin can be found in the Final Regional Stratigraphic Framework Topical Report. The analog study provides insight into several processes related to CO_2 storage along the offshore mid-Atlantic:

- Long-term updip migration of CO_2 to inshore areas
- Offshore-onshore trends in reservoir quality
- Interconnectedness of porosity/permeability
- Potential for vertical migration of CO_2 within reservoir zones and/or caprocks
- Local trapping mechanisms and structures
- Continuity of caprock intervals
- Potential distribution of CO_2 within the storage reservoir
- Impact of variability on injectivity, long term injection potential

The mid-Atlantic offshore passive margin basins extend along the eastern Atlantic margin from the southern Virginia border, across to the southern extent of Massachusetts. The mid-Atlantic offshore passive margin is composed of three major depocenters: BCT, GBB, and Long Island Platform. The basins underlie the continental shelf and slope in water depths ranging from 100 to 200 m (300 to 700 ft).

This section uses data and interpretation from our project team. A key component of this study was the sequence stratigraphic and structural interpretations of 4,000+ km (2,000+ mi) of seismic survey lines, 2,500 well logs, and 5,500 core test data points (Figure 3-7). These investigations revealed that the primary formations of interest were deposited primarily under a fluvial-deltaic environment in a shallow-marine environment where progradational delta systems (Logan Canyon) developed in a fluvial dominated shoreline. These basins contain a thick and laterally continuous, prospective Logan Canyon sandstone, interpreted as three prograding stratigraphic sequences. The Logan Canyon sandstone is an attractive prospect because it is thick and continuous and is confined by the Naskapi and Dawson Canyon marine mudstones.

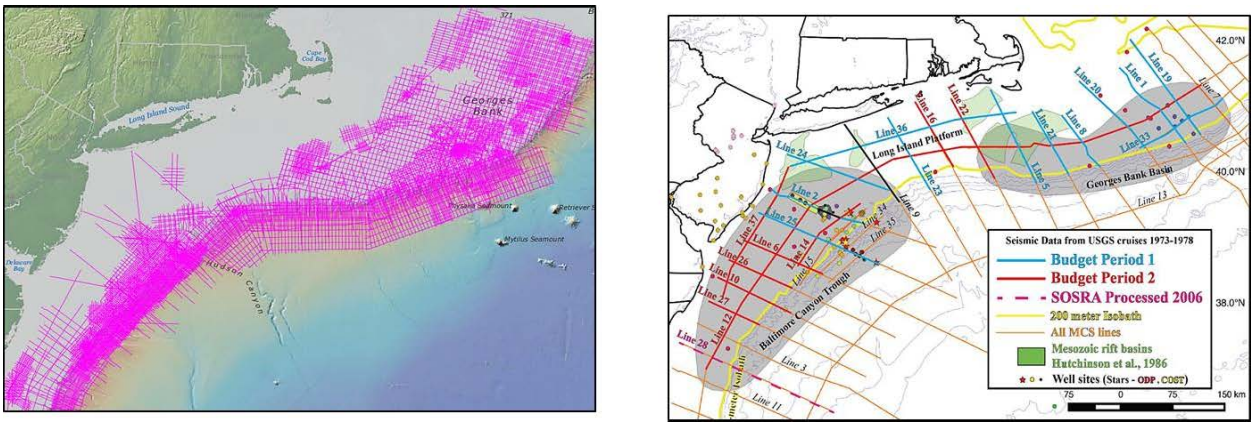

Figure 3-7. Maps showing seismic survey transects, well locations, and study areas for the offshore mid-Atlantic.

The three major depocenters of the mid-Atlantic offshore passive margin contain a Cretaceous sedimentary succession that includes the Logan Canyon sequences (reservoir) of interest and Dawson Canyon and Naskapi shale (top and bottom regional seals). These formations plunge gently to the southwest where the Naskapi-Logan Canyon-Dawson Canyon formations are generally identified in wells deeper in the BCT than those observed in the GBB. The Cretaceous sedimentary succession is overlain unconformably by a Tertiary carbonate unit followed by a thick succession of mudstone and shale.

Onshore to offshore depositional systems are characterized by a gradient of environments from the proximal to distal (Figure 3-8). On a basin scale, shallow marine shelves often occur on continental margins and interior basins, which are subsidence-prone areas. At this scale, the dynamic balance between basin subsidence, sediment input, and eustatic sea level plays a primary role in controlling and defining stratigraphic architecture (Figure 3-9). To evaluate the mid-Atlantic offshore Cretaceous formations in a qualitative approach to understand the confining and trapping risk associated with progradational fluvial-deltaic sandstones, the formations of interest were compared to the well-exposed and well-understood Lewis Shale/ Fox Hills Sandstone/Lance Formation system. This rock system represents a Late Cretaceous shallow-marine sedimentary succession deposited in the Western Interior Seaway located in the

Great Divide/Washakie basins, Wyoming. Broadly, the Lewis-Fox Hills-Lance system compares to progradational fluvial deltaic system deposited in an equivalent environment as the Naskapi-Logan Canyon-Dawson Canyon system.

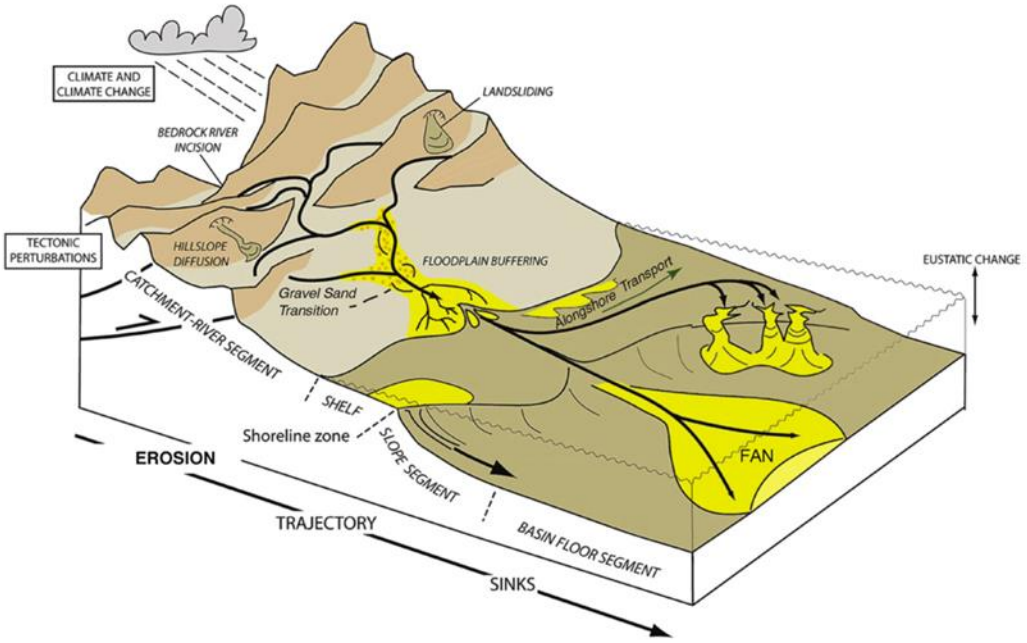

Figure 3-8. Schematic of proximal to distal environments (from Bhattacharya et al., 2016)

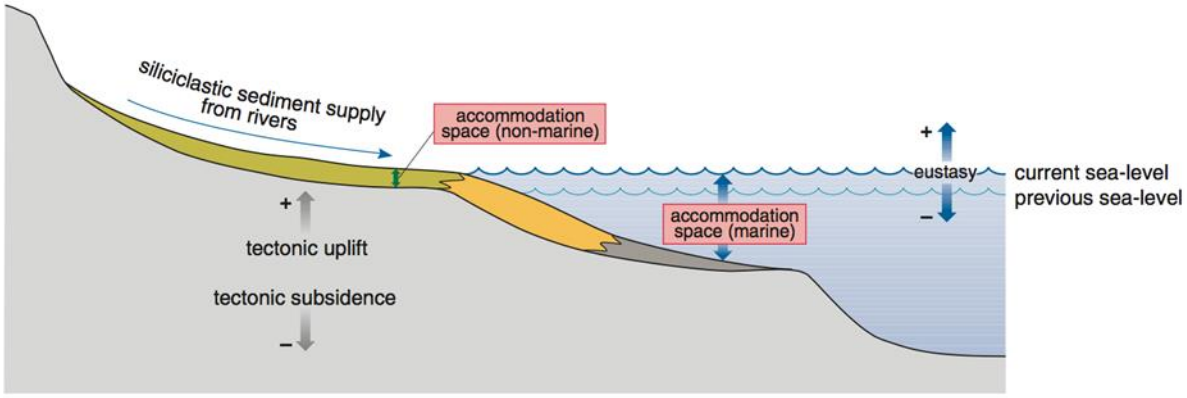

Figure 3-9. Schematic of a typical shelf environment and the controls makeup sequence stratigraphy (from Coe et al., 2003.)

Potential storage reservoir and seals in the mid-Atlantic offshore passive margin are identified and interpreted as being deposited in Cenomanian to Maastrichtian time. Three sequences containing parasequences sets and stacking patterns were also identified and interpreted using well log, seismic, and core data in the Naskapi-Logan Canyon-Dawson Canyon system. Sets of successive parasequence sets that were identified display consistent trends in thickness and lithology. For example, a parasequence set identified at the basin scale is typically composed of a topset, foreset, and bottomset (Figure 3-10).

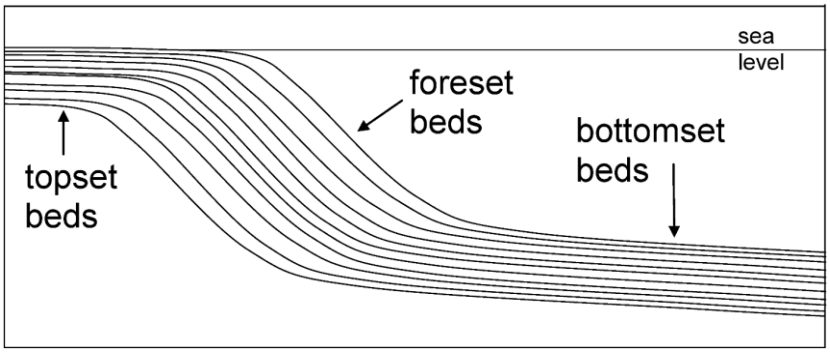

Figure 3-10. Common geometry found in offshore deltaic environments.

Topsets are the most proximal portion of the basin-margin profile characterized by low profiles. Topsets generally contain alluvial, deltaic, and shallow-marine depositional systems. The foreset portion of a parasequence is the steeply dipping portion of the basin-margin profile developed basinward of the topset. Foresets generally contain deeper-water depositional characteristics. Bottomsets describe the most distal portion of the basin-margin profile at the base of the foreset. Bottomsets are characterized by low gradients and containing deep-water depositional systems.

Sequence stratigraphic analysis of the mid-Atlantic offshore passive margin allows for powerful insights into first recognizing parasequences, then understanding and applying the predictable vertical and lateral lithologic relationship within a parasequence and determining how those relationships change by location. The Lewis-Fox Hills-Lance system shows that sandy reservoir portions of a parasequence are often associated with mudstone and shales located at the topset and bottomset of the parasequence (Figure 3-11). The sandy reservoir portions of the parasequence often shale out in both topsets and bottomsets, emplacing the reservoir often in impermeable mudstone and shales derived from different environments. In a similar way, the offshore mid-Atlantic system displays similar geometries and lithologic shifts of environments (Figure 3-12).

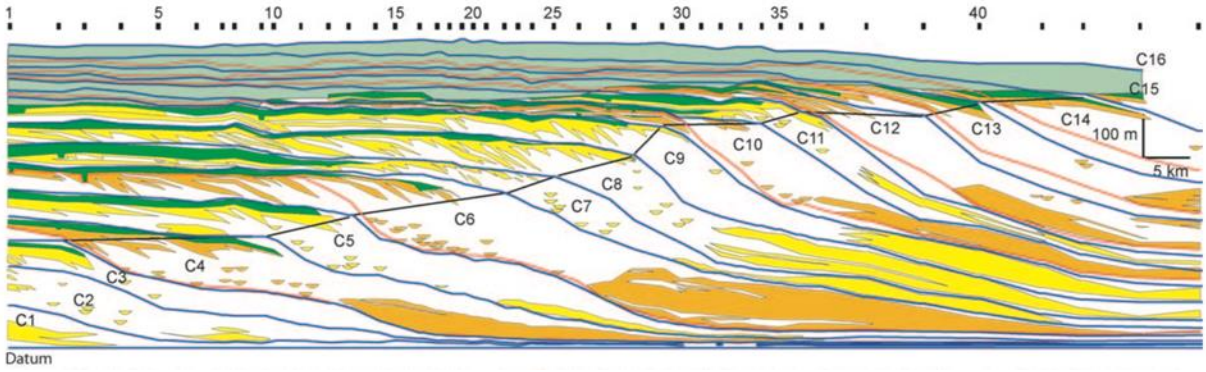

Figure 3-11. Cross section of the Great Divide and Washakie basins showing a dip-line of a coastal-plain through deep-marine transect (Carvajal & Steel, 2007).

Notes: Green represents fluvial and coastal plain deposits; yellow and orange show marine sand bodies, where yellow signifies linked deltas/strandplains to slope channels the basin floor in rising shelf-edge trajectory clinothems, and orange signifies linked deltas/strandplains to slope channels and the basin floor in flat shelf-edge trajectory clinothems. This correlation, which is based on well logs, shows how large-scale packages of marine sand bodies can be correlated and potential reservoir targets identified.

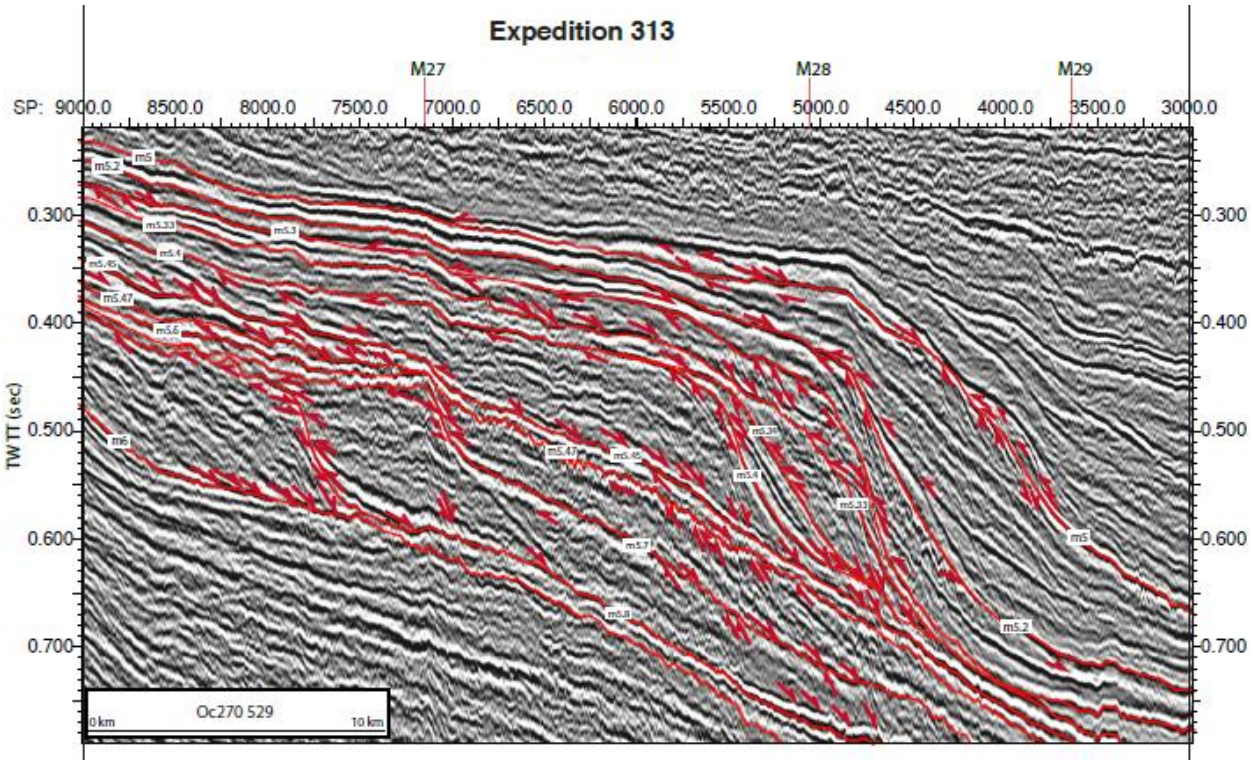

Figure 3-12. Seismic survey transect through offshore New Jersey in BCT showing topsets, foresets, and bottomsets (Source: Miller et al., 2018).

At least two types of potential trapping regimes are likely within the Logan Canyon reservoirs: depositional regime and erosional regime. Lateral depositional pinch-out traps are reservoir pinch-outs due to depositional termination of porous lithology. Lateral facies change occurs when reservoir lithology pinches out due to lateral gradation of depositional facies into a non-porous lithology (Figure 3-13). Sub-unconformity truncations are reservoir truncations beneath a regional unconformity onlap, while onto erosional surface is when strata onlap pinch-out of reservoir onto relative structural high.

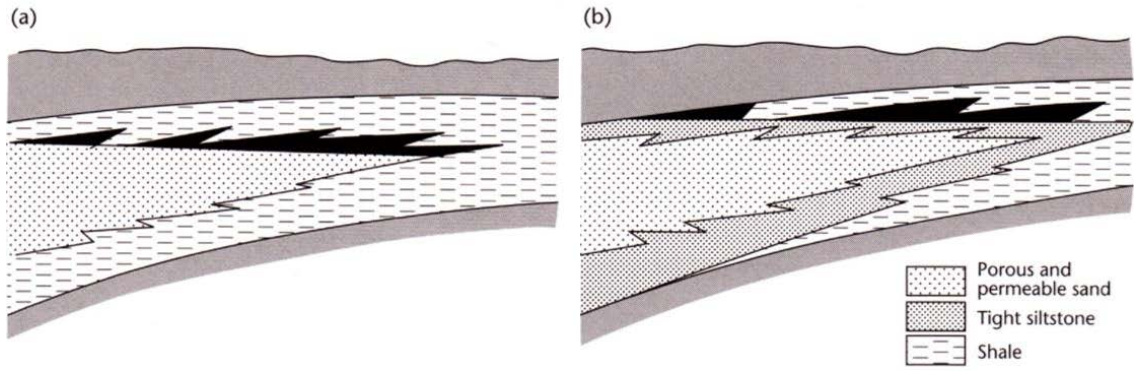

Figure 3-13. Pinch-out traps (from Allen & Allen, 2005).

Several degrees of risk are always present within any geologic storage system. However, progradational shallow-marine fluvial deltaic sandstones are an excellent potential target for CO_2 injection because their inherent stratigraphic architecture consists of clean sand bodies that grade updip and downdip into carbonaceous mudstone and shale. Furthermore, parasequences and parasequence sets often contain intraformational non-porous lithology that act as baffles to fluid flow. Commonly, fine-grained siliciclastics (clay, shale), evaporites (anhydrite, gypsum, halite), and organic-rich rocks make excellent seals, and the most effective seals should be laterally continuous. One may conclude that in the Naskapi-Logan Canyon-Dawson Canyon system, mature seal and pinch-out traps were developed, suggesting that this system presents an insignificant risk of injected fluids to migrate outside of the reservoir due to its inherent lithologic makeup.

3.3 Long-Term CO_2 Storage Process

Long-term processes such as CO_2 dissolution, residual saturation, and mineralization were analyzed for the offshore geologic environments along the mid-Atlantic OCS. These processes have been identified by Benson et al. (2009) as long-term, permanent mechanisms for CO_2 storage. The storage processes are important to understand the mobility of CO_2 in the subsurface in addition to stratigraphic and structural trapping.

3.3.1 CO_2 Solubility Trapping

After it is injected, a fraction of CO_2 will dissolve in formation water in the subsurface. Once the CO_2 is in solution, it will increase the density of the fluid and tend to sink to the bottom of the storage zone, which is considered a more permanent trapping mechanism. Consequently, the solubility of CO_2 in pore water is an important consideration for CO_2 storage resource assessments. In general, the solubility of CO_2 is higher in fresher water and lower in highly saline water. Temperature and pressure conditions will also affect CO_2 solubility. The salinity of the formation water in the deep rock formations along the mid-Atlantic OCS is uncertain, because there are few wells with fluid sample analysis and there are layers of trapped meteoric waters in some areas. Some researchers have observed hypersaline brines with salinity of 50,000 to 200,000 mg/L (.4 to 2 lb/gal) in lower Cretaceous rocks associated with salt or evaporite deposits (Sanford et al., 2013; Manheim & Paull, 1981; Meisler, 1989). Other researchers have observed “fresh paleowaters” and salinity inversions along the Atlantic Continental Shelf with relatively low salinity (<15,000 mg/L or .1 lb/gal) extending out to distances of 100 km (60 mi) off the shoreline to depths of 800 m or 3,000 ft (Cohen et al., 2010; Kohout et al., 1977). Saltwater intrusion and protection of groundwater resources are concerns along coastal plain aquifers near the shoreline.

Consequently, the solubility of CO_2 may vary with depth, location, and proximity to anhydrite layers. For example, at a depth of 10,000 ft (3,000 m), CO_2 may have solubility of 1.17 mole/kg in water with 40,000 mg/L (.3 lb/gal) salinity, but only 0.685 mole/kg (.311 mole/lb) in water with 200,000 mg/L salinity (2 lb/gal). CO_2 will also need to contact water to dissolve, and CO_2 solubility trapping may occur over long time periods as the CO_2 migrates in the storage zone.

Figure 3-14 shows calculated CO_2 solubility at depth based on observed RFT pressure, subsurface temperature, and salinity of 40,000 mg/L (.3 lb/gal). Solubility was calculated with the methods described by Zhao et al. (2015). The analysis suggests that CO_2 solubility will be 1.0 to 1.4 mole/kg (.5 to .6 mole/lb) in the subsurface along the OCS. This equates to approximately 44,000 to 60,000 mg/kg, or approximately 5% dissolved CO_2 per kilogram water by weight. In general, it appears that solubility trapping would be a moderate aspect for CO_2 storage along the offshore mid-Atlantic.

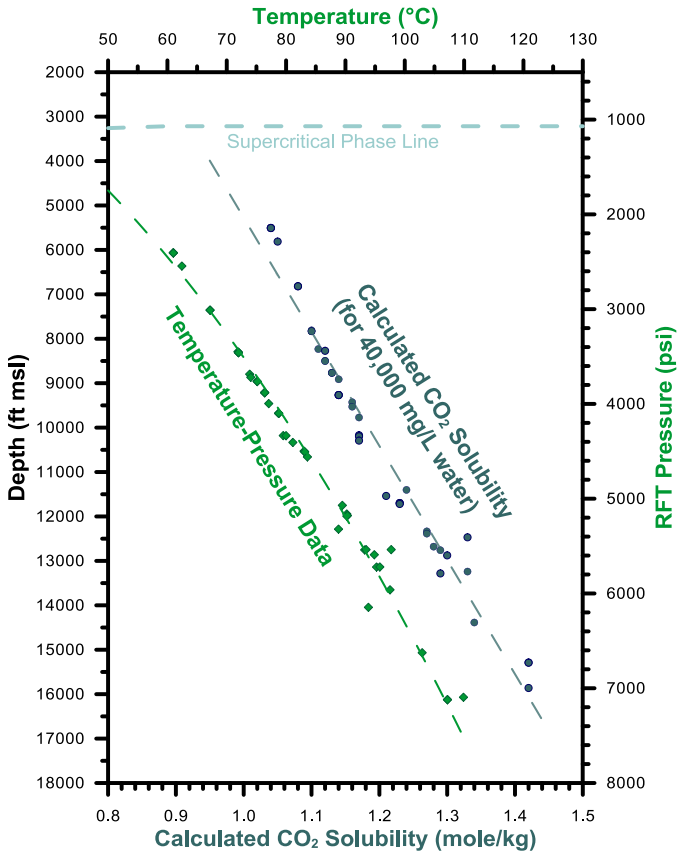

Figure 3-14. Calculated CO_2 solubility with depth based on subsurface pressure, temperature, and salinity of 40,000 mg/L.

3.3.2 CO_2 Residual Saturation Trapping

As described by research and rock core tests for CO_2 storage (Bennion & Bachu, 2008; Benson et al., 2009; Juanes et al., 2006; Krevor et al., 2015; Zuo & Benson, 2010), a fraction of injected CO_2 may be trapped within the intergranular pore space in a rock formation, a process called residual trapping. Residual trapping is related to pore network geometry, water saturation, and CO_2 saturation (Land, 1968; Larson et al., 1981; Lenhard & Parker, 1987). Relative permeability testing of rock cores with brine-CO_2 mixtures is the most accurate method to determine residual trapping potential. However, these are specialized tests that are difficult to complete because they require high-pressure conditions to keep the CO_2 in supercritical state. Consequently, residual trapping was evaluated by comparing porosity and pore size with other research on similar rocks. Figure 3-15 shows a thin-section sample from the COST B-2 well Cretaceous sands sample at a depth of 8,239 ft (2,511 m), illustrating the nature of intergranular porosity, moldic porosity, and grain/cement porosity. Total porosity was measured at 15.4%. Pore space diameters appear to be mostly in the 20- to 100-micrometer (μm) range.

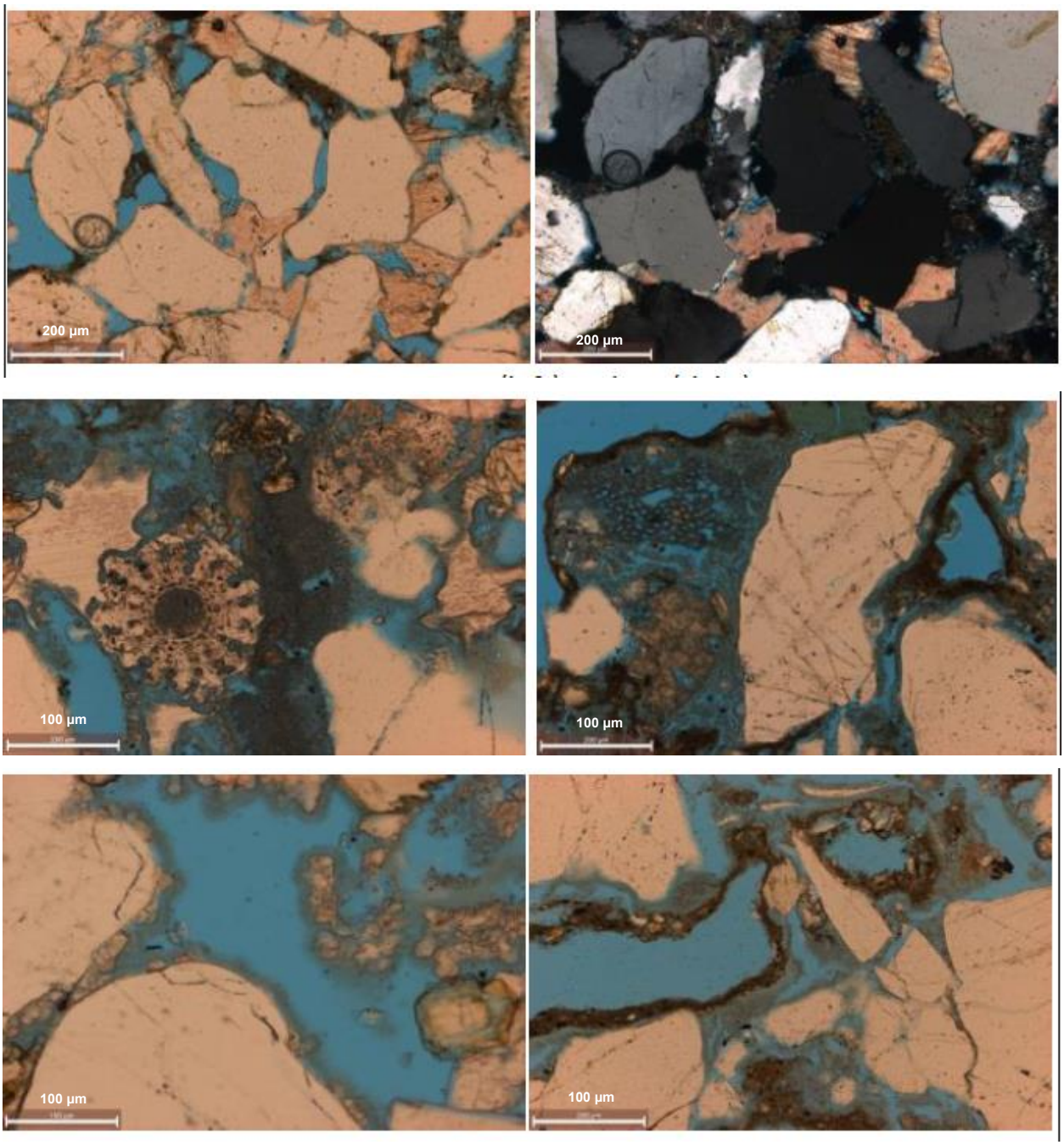

Figure 3-15. Thin section from COST B-2 at 8,239 ft from the Cretaceous sands illustrating pore space network geometry.

To estimate CO_2 residual trapping potential, the porosity distributions of mid-Atlantic offshore thin-section samples with 15 to 25% porosity were compared to brine-CO_2 relative permeability tests performed by Bachu (2013) for western Canada sandstone samples with similar 15 to 25% porosity. The pore space distribution measured by Bachu for the western Canada sandstone samples was based on threshold capillary pressure tests. This provides a quantitative measure of macroporosity (>50 nm), mesoporosity (2 to 50 nm), and microporosity (<2 nm); median pore size; and threshold capillary pressure. Threshold capillary pressure tests were not completed on

rock samples for the mid-Atlantic offshore. Consequently, the distribution of intergranular or greater, moldic/intercrystalline, and grain/cement porosity were used as a proxy for pore space distribution.

Table 3-3 compares the pore space distribution for Bachu's western Canada sandstones and the mid-Atlantic OCS samples. As shown, both sets of samples have total porosity of 15 to 25% with 70 to 90% macro (or intergranular) porosity, 8 to 11% mesoporosity, and 15 to 17% microporosity. Bachu's measurements suggest approximately 0.3 irreducible CO_2 saturation for these types of sandstones, which is on the lower end for CO_2 storage applications. Therefore, it may be concluded that a low to moderate amount of residual trapping may occur for reservoir zones in the mid-Atlantic offshore. It should be noted that many of the mid-Atlantic offshore samples had lower porosity that would likely have higher levels of residual trapping. More site-specific testing of rock samples for threshold entry pressures and residual saturation response would provide more accurate understanding of residual trapping.

3.3.3 CO_2 Mineralization Trapping

CO_2 may react upon contact with some minerals in the subsurface. CO_2 mineralization is considered a very secure mechanism for carbon storage. However, precipitation of minerals or hydrate formation can also clog pore space around an injection well, reducing injectivity of the well. CO_2 and water mixtures may also dissolve certain minerals, increasing pore space. An analog for geochemical processes in the subsurface is hydrothermal dolomite, where hot geothermal fluids upwell from faults, dissolve carbonate minerals near the fault, and precipitate dolomite away from the fault zone. Mineral trapping may be more significant in mafic igneous rocks like basalt flows, which contain abundant calcium, magnesium, and iron-bearing minerals that are much more reactive with dissolved CO_2 (Matter et al., 2016; McGrail et al., 2017). To examine the potential for geochemical CO_2 reactions along the mid-Atlantic offshore, a qualitative review of the deep rock layers' mineral composition and reactivity with CO_2-water mixtures was performed. The analysis provides a general review of the impact of CO_2 mineral interactions for the deep rock formations being considered for carbon storage along the mid-Atlantic offshore.

CO_2-rock interactions are governed by reaction thermodynamics and kinetics, which are in turn dictated by subsurface pressures, temperatures, and the composition/chemistry of in-situ minerals, pore fluids, and the injected CO_2. Mineralization of CO_2 is considered to be a secondary trapping mechanism for CO_2 storage due to the presence of relatively non-reactive or slowly reactive minerals, such as quartz and calcite, encountered in sedimentary rocks often targeted for storage (e.g., DOE-NETL, 2017). However, microscopic fluid-rock interactions induced by exposure to drilling/injection/production activities during oil and gas operations are known to result in precipitation and dissolution reactions in the near wellbore environment that can greatly impact subsequent well performance and the flow of fluids into or away from the wellbore. Similar to oil and gas activities, well drilling and injection operations during a CO_2 storage project will alter the subsurface fluids, pressure, and temperatures in the near-wellbore environment from that of the original in-situ reservoir conditions.

Table 3-3. Comparison of porosity distribution and irreducible CO_2 saturation for western Canada sandstones (from Bachu, 2013) and mid-Atlantic offshore samples with porosity of 15 to 25%.

Bachu (2013) Western Canada Sandstone Relative Permeability Tests							
Sample	Depth (ft)	Micro	Meso	Macro	Median Pore Size	Porosity	Irreducible CO_2 gas saturation
Viking Fm. #3	3090	8.7	3.0	88.4	29.8	17.2	0.223
Halfway Fm.	6725	15.8	11.8	72.4	8.8	17.7	0.459
Bellboy Fm.	5982	27.4	9.8	62.8	11.3	23.6	0.283
Deadwood Fm. #1	5407	7.8	12.9	79.3	11.3	17.6	0.382
Deadwood Fm. #2	7413	27.3	5.9	66.8	13.2	16.2	0.288
Deadwood Fm. #3	6898	7.2	6.5	86.3	16.0	19.3	0.238
Average		*15.7*	*8.3*	*76.0*	*15.1*	*18.6*	*0.3*
Mid-Atlantic OCS Thin-Section Porosity Analysis							
Sample	Depth (ft)	Grain/ Cement	Moldic/ Intercrystalline	Intergranular or greater	Median Pore Size	Porosity	
Cost B-2	5030	26.3	18.6	55.1	NA	15.6	
Cost B-2	9302	27.0	14.5	58.6	NA	15.4	
Cost B-2	9304	22.0	14.5	63.5	NA	16.0	
Cost B-3	11051	40.7	0.0	59.3	NA	22.9	
Cost B-3	11054	37.9	2.8	59.3	NA	17.9	
Mobil 544-1	7096	0.0	34.6	65.4	NA	16.2	
Mobil 544-1	7258	0.0	1.7	98.3	NA	17.8	
Mobil 544-1	9039	31.2	32.8	36.0	NA	17.2	
Exxon 684-1	9438	11.7	10.4	77.9	NA	15.4	
Exxon 684-1	9438	3.2	3.2	93.5	NA	21.6	
Exxon 684-1	9440	5.2	3.6	91.2	NA	19.3	
Cost G-1	5471	31.9	3.5	64.6	NA	22.8	
Cost G-1	5473	33.2	5.3	61.6	NA	19.0	
Cost B-2	8239	26.1	18.5	55.4	NA	15.6	
Cost B-2	9302	27.0	14.5	58.6	NA	15.4	
Cost B-2	9304	22.0	14.5	63.5	NA	16.0	
Cost B-3	11051	40.4	0.0	59.6	NA	22.9	
Cost B-3	11054	37.4	2.8	59.8	NA	17.9	
Mobil 544-1	7096	0.0	34.6	65.4	NA	16.2	
Mobil 544-1	7258	0.0	1.7	98.3	NA	17.8	
Mobil 544-1	9039	0.0	47.7	52.3	NA	17.2	
Exxon 684-1	9438	11.7	10.4	77.9	NA	15.4	
Exxon 684-1	9439	3.2	3.2	93.5	NA	21.6	
Exxon 684-1	94440	5.2	3.6	91.2	NA	19.3	
Exxon 684-1	9441	5.4	2.0	92.6	NA	20.4	
Texaco 642-1	15608	0.0	11.7	88.3	NA	21.3	
Average		*17.3*	*11.9*	*70.8*	*NA*	*18.2*	

Several studies that have investigated the influence of mineralization/dissolution on CO_2 storage operations have focused on reaction kinetics and solute transport modeling (e.g., Xu et al., 2006; Kang et al., 2010). These models depend on complex step rates, reaction paths, and intermediate reaction products that can be especially difficult to constrain/model for heterolithic sedimentary rocks that contain multi-component chemical systems (e.g., Gaus, 2010), such as the Cretaceous-Jurassic sequences in the mid-Atlantic offshore study area (e.g., Si-Al-Ca-Fe-Mg-K + H_2O) (Table 3-4). The major-element bulk-rock geochemical compositions and mineral assemblages observed in the caprocks and storage zones of interest are shown in Table 3-4 and Table 3-5, respectively.

Table 3-4. Major-element bulk-rock geochemical data for the storage zones and caprocks of interest, reported in average oxide weight-percentage and normalized to 100%.

Major-Element Bulk-Rock Geochemistry (normalized to 100%)										
Storage Zone/Caprock	SiO_2	TiO_2	Al_2O_3	FeO	MnO	MgO	CaO	K_2O	P_2O_5	TOTAL
UK Caprock/Dawson Canyon	65.14	0.99	18.12	6.23	0.07	2.09	4.41	2.46	0.48	100
LC1/MK1	66.58	0.52	8.56	4.80	0.05	1.59	16.15	1.47	0.28	100
LK1/Missisauga	67.31	0.49	8.54	2.39	0.05	1.48	17.71	1.56	0.47	100
LK2/Mic-Mac/Abenaki	72.63	0.55	12.74	2.09	0.04	1.56	8.21	1.90	0.29	100
UJ/Mohawk	74.69	0.33	8.65	1.76	0.05	1.85	11.19	1.26	0.23	100
Average	69.27	0.58	11.32	3.45	0.05	1.71	11.53	1.73	0.35	100

Table 3-5. Major mineral assemblages observed in the storage and confining zones of interest based on X-ray diffraction and thin-section petrography.

Zone	Mineral Assemblage*
UK Caprock/Dawson Canyon	quartz + illite-smectite/mica + chlorite + kaolinite + calcite + plagioclase + K-feldspar
LC1/MK1	quartz + calcite + kaolinite + chlorite + K-feldspar + illite-smectite/mica + plagioclase
LK1/Missisauga	quartz + kaolinite + dolomite + chlorite + illite-smectite/mica + calcite + K-feldspar + plagioclase
LK2/ Mic-Mac/Abenaki	quartz + calcite + kaolinite + illite-smectite/mica + plagioclase + K-feldspar
UJ/ Mohawk	quartz + plagioclase + calcite + kaolinite + illite-smectite/mica + K-feldspar

*Listed in order of relative abundance

The mineral assemblages and average bulk compositional data compiled/measured as part of Task 2 were used to qualitatively investigate potential CO_2-rock interactions and trapping mechanisms at reservoir pressures ranging from ~1,320 psi to ~6,550 psi (9.10 to 45.2 MPa) and an average reservoir temperature of ~ 57 °C (130 °F) derived from the pressure and geothermal gradients calculated for the study area. The assessment assumed that thermodynamic equilibrium has been achieved in an H_2O-CO_2 fluid-saturated, closed chemical system (no allochthonous material introduced) within the storage zones. Reactions were derived from phase equilibria based on an internally consistent thermodynamic database developed by Holland & Powell (1998; updated in 2002) and a compensated-Redlich-Kwong equation of state for H_2O-CO_2 fluid mixtures (Holland & Powell, 1991). The CO_2-rock reactions identified in the mid-Atlantic offshore storage zones as being thermodynamically possible during CO_2 injection/storage scenarios are shown in Equations 1 through 3 below. These reactions largely include dissolution and precipitation reactions among feldspars, phyllosilicates (sheet silicates), and carbonates. Based on the observed reservoir compositions, mineralogy, and temperature and pressure conditions, the introduction of CO_2 in the storage zones could result in dissolution

of K-feldspar and plagioclase followed by precipitation of muscovite, calcite, and quartz (Equation 1), and dissolution of chlorite and calcite followed by precipitation of siderite, dolomite, kaolinite and quartz (Equation 2). Chlorite and K-feldspar could dissolve completely as CO_2 concentration/ saturation in the pore fluid increases relative to H_2O, and would result in additional precipitation of muscovite, kaolinite, carbonate, and quartz (Equation 3).

$$KAlSi_3O_8 + CaAl_2Si_2O_8 + H_2O + CO_2 \leftrightarrow KAlSi_3O_{10}(OH)_2 + CaCO_3 + 2SiO_2 \quad \textbf{(1)}$$
K-feldspar plagioclase muscovite calcite quartz

$$Fe_{2.5}Mg_{2.5}Al_2Si_3O_{10}(OH)_8 + 2.5CaCO_3 + 5CO_2 \leftrightarrow 2.5FeCO_3 + 2.5CaMg(CO_3)_2 + Al_2Si_2O_5(OH)_4 + SiO_2 + 2H_2O \quad \textbf{(2)}$$
Chlorite calcite siderite dolomite kaolinite quartz

$$2.5(Fe_5Al)(AlSi_3)O_{10}(OH)_8 + KAlSi_3O_8 + 12.5CO_2 \leftrightarrow 12.5FeCO_3 + KAlSi_3O_{10}(OH)_2 + 1.5Al_2Si_2O_5(OH)_4 + 4.5SiO_2 + 6H_2O \quad \textbf{(3)}$$
Chlorite K-feldspar siderite muscovite kaolinite quartz

CO_2 mineralization in basal floods may be a potential CO_2 storage trapping mechanism in rift basins in portions of the mid-Atlantic offshore. Rift basins are present in the Long Island Platform and GBB (Hutchinson and Klitgord, 1988), where basalt flow zones may be present in the subsurface crystalline basement at reasonable depths (<10,000 ft or 3,000 m). Rift zones are also present in the BCT at deeper depths (>15,000 ft or 4,600 m). Research on the onshore Newark Rift Basin has shown the presence of high permeability/porosity zones in basalt flows (Goldberg et al., 2010), and similar rocks may be present in the offshore rift basins. The rift structures are clearly visible on seismic survey interpretations. However, the properties of these basalts need to be confirmed with drilling, because no deep wells penetrate the units in the study areas.

CO_2 Storage Process - Hydrologic conditions, geotechnical rock properties, and mineralogy of the deep rock formations in the mid-Atlantic offshore suggest that structural and stratigraphic trapping of free-phase CO_2 and residual trapping would be the primary mechanisms for storage (Figure 3-16). CO_2 dissolution may account for 3 to 5%. Mineral trapping is expected to be low at less than 1%, but there are a moderate amount of reactive clays and feldspars that may be expected to react with CO_2. CO_2 contact with formation water, plume migration, mixing with water, and reservoir variability will affect these trapping processes over time. Numerical multi-phase reservoir simulations can provide a more accurate estimate of these processes. In terms of long-term potential for CO_2 trapping, the analysis suggests that structural and lithologic traps would be important factors for the CO_2 storage system in the subsurface.

3.4 Wellbore Integrity

Wellbore integrity may be a risk factor in areas with many legacy oil and gas wells, because the wells are a potential pathway for CO_2 migration. The mid-Atlantic offshore has only 44 deep exploration wells, all of which have been plugged and abandoned. In comparison, areas like the North Sea and Gulf of Mexico have thousands of legacy oil and gas wells with variable age, construction, and status. In these areas, risk assessment studies for CO_2 storage have often concentrated on wellbore integrity as a key mechanism for CO_2 migration (Brown, 2017; Hannis et al., 2017; IEAGHG, 2016; Blackford et al., 2014; Leighton & White, 2012). In contrast, CO_2 leakage through existing wellbores in the mid-Atlantic region is not a major risk factor. However, future CO_2 storage projects may build off existing wells that provide an initial basis for reservoir characterization, and the existing wells plugging and abandonment methods should be considered.

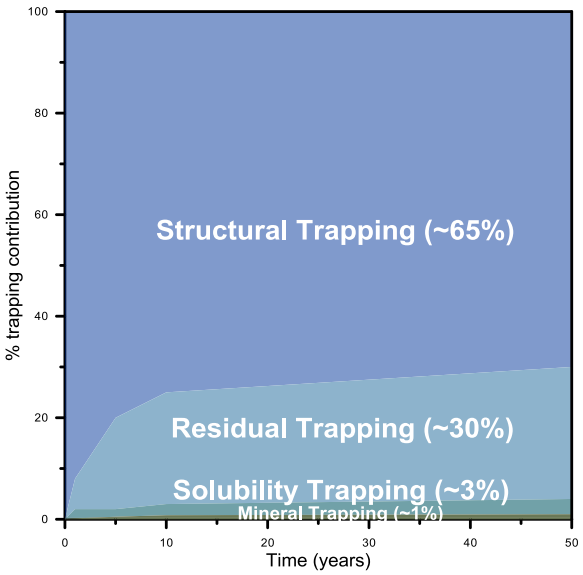

Figure 3-16. Diagram illustrating trapping processes for offshore mid-Atlantic.

Table 3-6 summarizes well plugging and abandonment specifications for wells in the mid-Atlantic OCS study areas. In general, the offshore wells were completed with three to five casing strings cemented in place with industry best practices and regulatory requirements for the late 1970s to early 1980s promulgated by the Minerals Management Service (MMS), Bureau of Ocean Energy Management (BOEM), and Bureau of Safety and Environmental Enforcement (BSEE). Because the wells were considered exploratory, a “drill and plug” procedure was followed, and the wells were plugged after drilling was completed. Records suggest that typical offshore materials (Class H cement and carbon steel casing) were used for well construction.

Many wells list squeeze jobs across perforated zones, while other wells were open-hole completions. Records indicate that well plugs were pressure-tested with drill stem tests per offshore regulations after they were set. Casing was pulled above the plugs in most wells. A few wells (Conoco 590-1, Texaco 642-1, Mobil 273-1, Shell 273-1, Mobil 273-1, Shell 410-1) appear to have few and/or thin plugs across the potential reservoir zones or casing transitions. Most wells indicate that conductor casings were cut several hundred feet below the seafloor and the drilling area was surveyed before final site demobilization. No additional monitoring or surveying of the well sites has occurred since they were drilled, and no well leakage incidents have been noted to the best of our knowledge.

Table 3-6. Summary of well plugging and abandonment specifications.

Well Name	Completion Date	Total Measured Depth (ft)	Total True Vertical Depth (ft)	Casing Strings*	#Plugs	Plug Thickness (ft)						Notes
						Deep	Intermediate				Shallow	
Conoco 590-1	6/7/1978	12000	11908	3	2	100	50				150	Class H neat + 2%CaCl
COST B-2	2/28/1976	16043	16039	4	2	305					425	
COST B-3	1/24/1979	15820	15820	4	4	100	250	300			200	Plug thicknesses are estimated
Exxon 500-1	9/28/1979	12253	12253	3	6	329	264	264	325	290	298	Class H neat
Exxon 599-1	11/2/1980	17121	17121	5	6	894	414	414	277	303	278	Class H, 2% CaCl
Exxon 684-1	12/23/1978	17620	17615	5	5	480	330	260	309		523	
Exxon 684-2	7/15/1979	16800	16759	5	5	545	316	302	347		304	
Exxon 728-1	7/5/1981	15205	15205	3	5	265	260	265	265		397	Plug thicknesses are estimated
Exxon 816-1	5/7/1981	17753	17753	5	6	377	438	370	143	125	110	Plug thicknesses are estimated
Exxon 902-1	4/15/1979	15968	15889	4	6	409	420	525	204	113	250	
Gulf 718-1	3/31/1979	12813	12800	3	4	250	250	300			200	
Gulf 857-1	1/29/1979	18554	18552	4	4	300	445	80			200	
Homco 676-1	9/22/1978	12500	12500	4	3	300	50				150	
Homco 855-1	2/8/1979	17505	17505	5	4	550	266	110			150	Plug thicknesses are estimated
Mobil 17-1	1/24/1979	1200	1200	2	2	87					165	Plug thicknesses are estimated
Mobil 17-2	5/14/1979	13992	13975	4	3	154	100				156	
Mobil 544-1	12/29/1978	17449	17449	4	4	150	354	200			390	
Mobil 544-2	10/1/1981	8312	8312	4	3	250	50				250	Plug thicknesses are estimated
Murphy 106-1	5/29/1980	18405	18401	4	3	150	403				190	Retainers, BPs set in deep interval
Shell 272-1	2/19/1979	13500	13500	3	5	150	150	150	224		88	
Shell 273-1	12/16/1978	17500	17500	6	2	225					252	
Shell 372-1	7/9/1984	11631	11631	4	4	500	695	200			200	
Shell 586-1	5/22/1984	16000	16000	5	4	2000	382	200			200	
Shell 587-1	12/21/1983	14500	14470	4	4	300	250	100			200	
Shell 632-1	7/14/1978	14000	14000	3	5	150	150	146	225		170	
Shell 93-1	11/4/1984	17740	17740	5	3	300	445				186	
Tenneco 495-1	10/11/1979	18300	18300	5	4	150	730	300			300	
Tenneco 642-2	6/10/1979	18400	18400	4	4	150	160	100			250	Plug thicknesses are estimated
Tenneco 642-3	10/14/1980	16475	16475	5	3	472	150				310	Plug thicknesses are estimated
Texaco 598-1	8/26/1978	15025	15025	5	4	845	200	200			200	Deep plug cemented wireline tool
Texaco 598-2	3/20/1979	17708	17642	NA	NA	NA	NA	NA	NA	NA	NA	No records available
Texaco 598-3	5/25/1980	16103	16103	4		90	500	50			50	Shallow plug thickness is estimated
Texaco 598-4	3/24/1981	16050	16050	NA	NA	NA	NA	NA	NA	NA	NA	No records available
Texaco 642-1	12/1/1979	17807	17797	5	2	20					30	Plug thicknesses are estimated
Conoco 145-1	8/25/1982	14500	14398	3	4	300	300	250			190	Plug thicknesses are estimated
COST G-1	7/27/1976	16071	16071	4	2	436					434	
COST G-2	8/6/1977	21874	21874	5	4	300	275	110			70	
Exxon 133-1	11/24/1981	14118	14100	5	5	363	275	554	481		290	
Exxon 975-1	3/10/1982	14605	14605	4	6	415	416	312	465	275	422	
Mobil 273-1	9/13/1982	15580	15578	3	3	100	85				186	Plug thicknesses are estimated
Mobil 312-1	6/27/1982	20000	19977	4	2	343					523	
Shell 357-1	9/27/1982	19427	19398	4	3	400	500				298	Plug thicknesses are estimated
Shell 410-1	3/31/1982	15568	15556	4	2	250					300	
Tenneco 187-1	8/21/1982	18127	18127	4	4	1653	266	350			200	

*including liners

4.0 Environmental Setting Risk Factors

Environmental resources and natural and man-made marine features present along the offshore mid-Atlantic seafloor may be indicators of potential risk factors for exploration activities, subsurface storage, and project construction. This section provides a brief description of environmental risk factors, marine features, sources of CO_2, and stakeholder risk factors that could influence efforts to implement carbon storage projects in the mid-Atlantic region.

4.1 Environmental Risk Factors

Several types of activities that may be associated with CO_2 storage projects—for example, conducting seismic surveys, drilling deep wells, installing pipelines, and placing bottom-founded equipment or structures—could cause physical disturbances on the seafloor. The *BOEM Atlantic OCS Proposed Geological and Geophysical Activities, Mid-Atlantic and South Atlantic Planning Areas* (BOEM, 2014) identified the following issues in its programmatic environmental impact statement analysis:

- impacts of underwater noise on marine mammals, sea turtles, fishes, birds, other marine life;
- impacts of underwater noise on commercial and recreational fishing (fish catch);
- impacts of vessel traffic (risk of ship strikes) on marine mammals and sea turtles, birds, and threatened and endangered fish species;
- impacts of vessel traffic on fishing, shipping, and other marine uses;
- impacts of aircraft traffic and noise on marine mammals, sea turtles, birds, and other marine life;
- impacts of seafloor-disturbing activities on sensitive benthic communities, including coral and hard/live bottom communities, chemosynthetic communities, and deepwater canyon benthos;
- impacts of seafloor-disturbing activities on Essential Fish Habitat (EFH), Habitat Areas of Particular Concern (HAPCs), and Marine Protected Areas (MPAs);
- impacts of seafloor-disturbing activities on archaeological resources, including historic shipwrecks and prehistoric archaeological sites;
- impacts of vessel exclusion zones on commercial and recreational fishing, shipping, recreational resources, and other marine uses;
- impacts of marine trash and debris on benthic communities, marine mammals, sea turtles, birds, endangered or threatened fish species, and recreational resources; and
- impacts of accidental spills on benthic communities, marine mammals, sea turtles, birds, fishes and EFH, archaeological resources, recreational resources, MPAs, other marine uses, and human resources and land use.

Development of an offshore carbon storage project would likely require a variety of exploration activities very similar to oil and gas operations. Activities related to offshore drilling and exploration that may have an environmental impact were listed as “active acoustic sound sources (airguns and electromechanical sources); vessel and equipment noise; vessel traffic; aircraft traffic and noise; vessel exclusion zones; trash and debris; seafloor disturbance; drilling discharges; onshore support activities; and accidental fuel spills.” Most of these items are not typical for the mid-Atlantic OCS.

4.2 Marine Features

Natural and man-made features were analyzed to determine their impact on exploration, drilling, and facility construction for a potential carbon storage on the mid-Atlantic OCS. In 1979, the USGS completed a survey of the mid-Atlantic shelf and slope for geologic hazards on the seafloor that may affect exploration activities (Hall & Ensminger, 1979). The analysis identified extensive sediment slumping in lease blocks along the continental slope. Seismic indicators of shallow gas deposits were present in three lease blocks, and recent shallow faulting was noted in one lease block. The shelf slopes gently seaward and is mostly covered with unconsolidated marine or detrital clay, silt, and sand with few subsea bedrock exposures. Together, these unconsolidated sediments may be up to 1,000 m (3,000 ft) thick along the shelf. Seafloor features like basins, sand waves, and terraces are present along the shelf but can change during wave or storm action. Hannis et al. (2017) note that water depths, water movement, seabed type, seabed renewal rate, and anthropogenic effects may present additional technical challenges for offshore monitoring of CO_2 storage applications. Near the continental slope, steeply incised troughs, channels, and escarpments are more prevalent.

Other marine features have been identified that are important to consider for development of an offshore carbon storage project in the mid-Atlantic United States (Table 4-1). Current or future legislation and geopolitical boundaries like the Submerged Lands Act (SLA) boundary, the 8G line, and the continental shelf boundary (CSB) could affect carbon storage implementation. Many environmentally sensitive areas for marine species and habitats are present.

In terms of CO_2 storage applications, marine features and boundaries would mainly impact exploration and infrastructure development. Figure 4-1 illustrates the locations of these features in relation to the offshore continental shelf study areas. CO_2 pipelines, injection wells, and seismic surveys may be limited in sensitive areas due to their potential to disturb the seabed or ocean surface activities. Most of the features are in near-shore areas, which may be more accessible by pipeline but less likely to be selected for a CO_2 storage site. The majority of the mid-Atlantic OCS would be accessible for CO_2 storage projects. The marine features have no direct impact on resource calculations, since the storage zones are isolated rock layers deep beneath the seabed. None of the features would appear to present a formal limitation for subsurface geologic storage. However, perception and outreach issues related to marine features may present significant challenge to siting a project, so these areas are best avoided. Since there is a very limited history of exploration activities along the mid-Atlantic OCS, there is a high degree of uncertainty on the process of developing a CO_2 storage facility in these areas.

Offshore wind energy is another consideration for carbon storage along the mid-Atlantic OCS. Figure 4-2 shows wind planning areas or areas of consideration from BOEM. These areas are in progress, under consideration, or potential planning areas. Wind energy would involve construction of many wind turbine platforms, substation platforms, and seafloor electricity transmission cables. In comparison, CO_2 storage facilities would consist of a central pipeline to a few injection well platforms. The wind energy areas may provide an opportunity to combine with CO_2 storage and minimize impact to the environment and seafloor.

Table 4-1. Marine features and boundaries that may affect carbon storage projects.

Feature	Description	Source	Impact
SLA Boundary	Limit of states' land offshore and federally managed OCS	BOEM	State coastal water limits
8G Line	Line projected 3 nautical miles seaward from SLA boundary	BOEM	Nearshore limit for federal resource management
Continental Shelf Boundary (CSB)	200 nm exclusive economic zone boundary/limit of U.S. territory from coastline	BOEM	Offshore limit of federal resource management, boundary of OCS and slope
Endangered Species Act (ESA)	Areas protected for threatened or endangered marine species and ecosystems	USFWS-NOAA NMFS	ESA covers all areas out to CSB
Critical Habitat Areas/HAPCs	Especially vulnerable habitat areas for marine species	BOEM/ NOAA	No areas designated for mid-Atlantic study area, some areas present inward of the 8G line
Marine Protected Areas (MPAs)	Areas with limited human activity to protect natural or cultural resources	NOAA	Most MPAs nearshore or in southern extent of region
Marine Sanctuary/Marine National Monuments	Federally protected underwater park areas with special marine features	NOAA	No marine sanctuaries designated in OCS study areas, Northeast Canyons and Seamounts near slope of GBB
Artificial Reefs	Man-made structures to support marine life	Mid Atl. Fishery Mgmt Council	Over 100 reef sites along mid-Atlantic, but mostly nearshore; limited extent
Fishing Vessel Density	Density of fishing vessel traffic in 2011 for the US Atlantic from vessels with AIS transponders in 100 meter grid cells	NOAA Coastal Services Center	Some areas of high vessel density in offshore fishing grounds
Shipping Lanes	Delineated shipping routes marked for commercial traffic	NOAA Office of Coast Survey	Shipping routes concentrated along major ports, bays,
Submarine Cables	Submarine communication cables in and around U.S. navigable waters	NOAA Office for Coastal Management	Submarine cables present in certain areas but have relatively minor footprint
Sand and Gravel Lease Borrow Areas	Areas with agreements in place for sand and gravel dredging	BOEM	Limited S&G borrow areas present nearshore
Shipwrecks/Obstructions	Designated shipwrecks and obstructions on seafloor within U.S. waters	NOAA, U.S. National Park Service	Several hundred wrecks present in study areas, but have limited extent
Ocean Disposal Sites	Current, historical, or discontinued sites for dumping dredging material, waste, or other materials	U.S. EPA/ Marine Protection, Research and Sanctuaries Act	There are about 15 disposal sites in mid-Atlantic OCS, which may be impediments to drill sites and pipelines

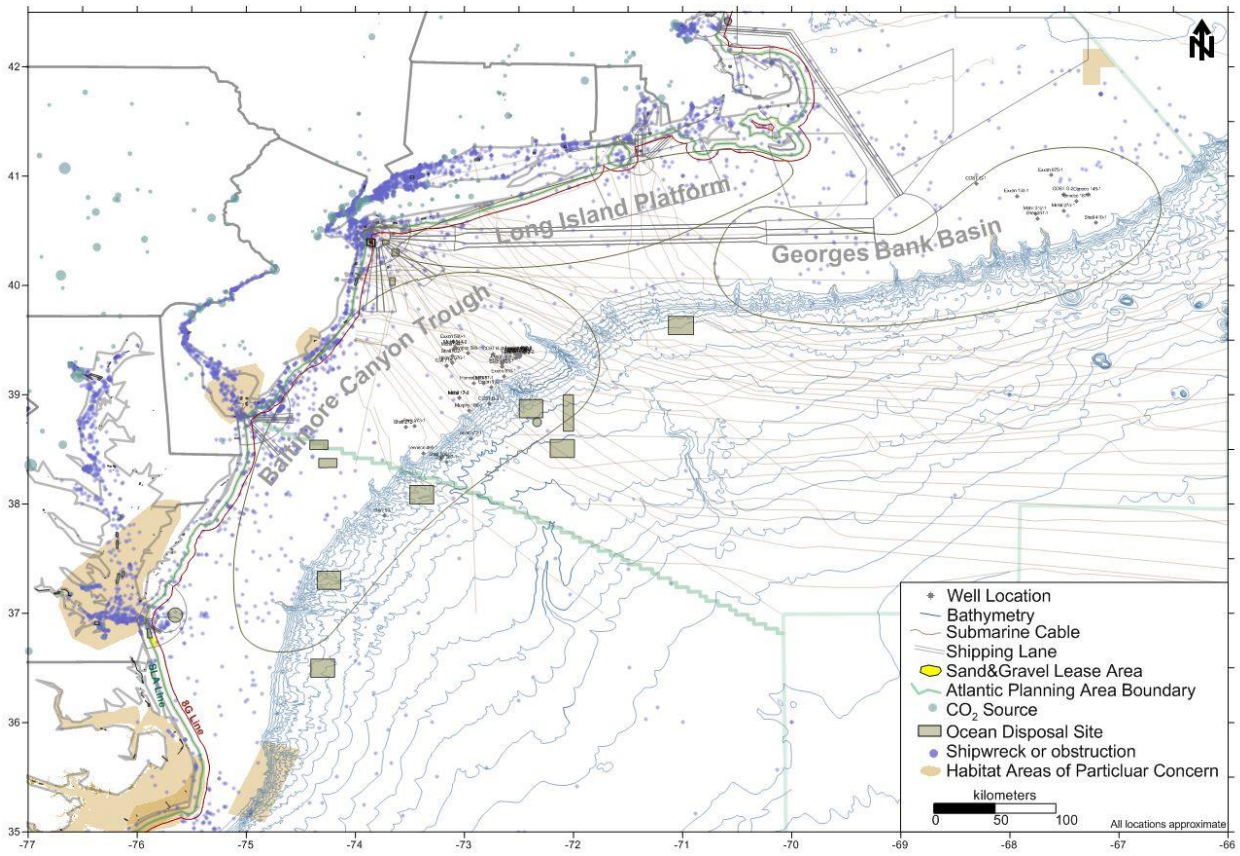

Figure 4-1. Map showing environmental and marine features in the mid-Atlantic OCS.

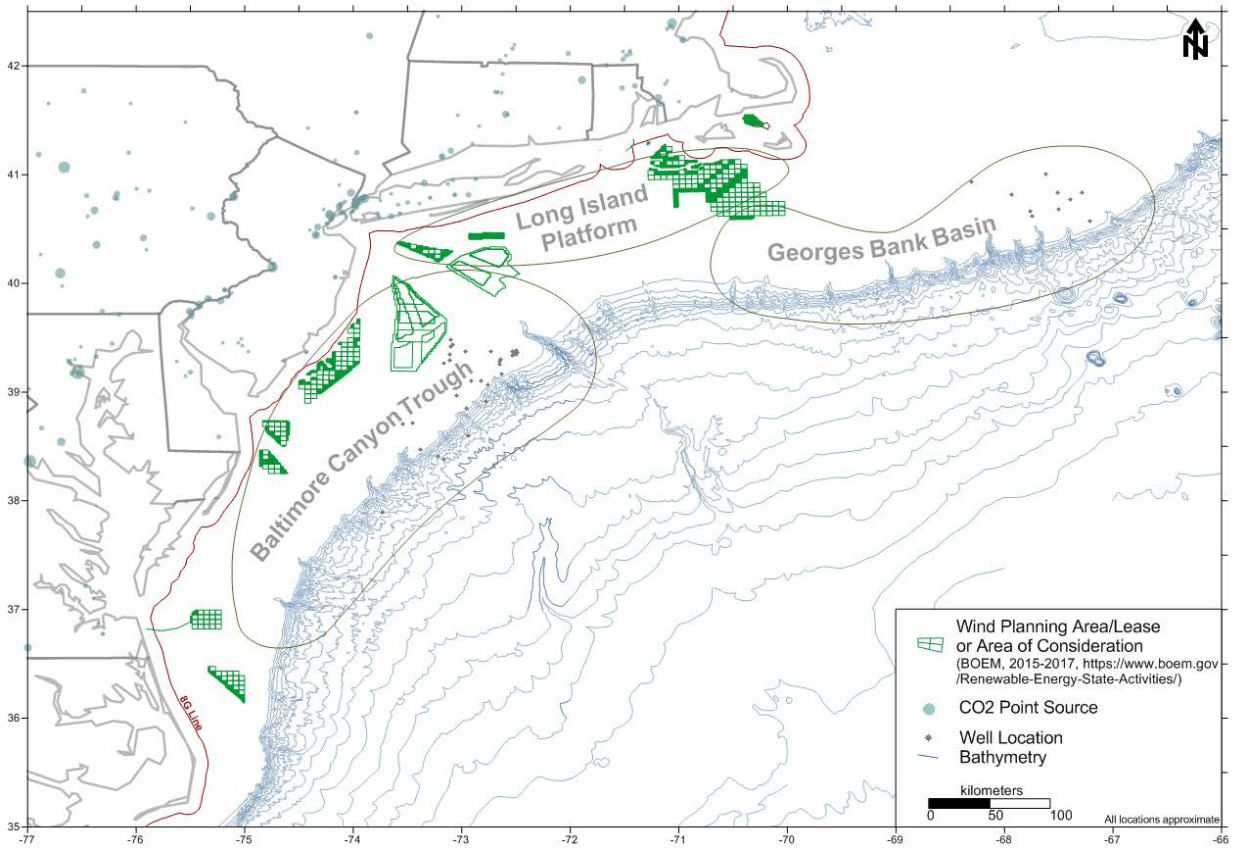

Figure 4-2. Areas of offshore wind energy development along the mid-Atlantic OCS.

4.3 CO_2 Sources in the Mid-Atlantic Region

CO_2 sources in the mid-Atlantic region were examined to determine the feasibility of linking the sources to the offshore resource locations. Figure 4-3 shows a map of CO_2 industrial point sources in the region based on the 2016 EPA Greenhouse Gas Reporting Program. There are approximately 489 sources in the region as defined by -77° W, 35° N to -66° W, 42.5° N domain. Total emissions were approximately 147 million metric tons in 2016 based on EPA Greenhouse Gas Reporting Program data. Many of the sources are clustered along industrial corridors, which have a higher CO_2 emissions intensity. There were 39 power plants and five petroleum processing facilities with emissions greater than 1 million metric tons per year. No other source types had more than 1 million metric tons per year of CO_2 emissions.

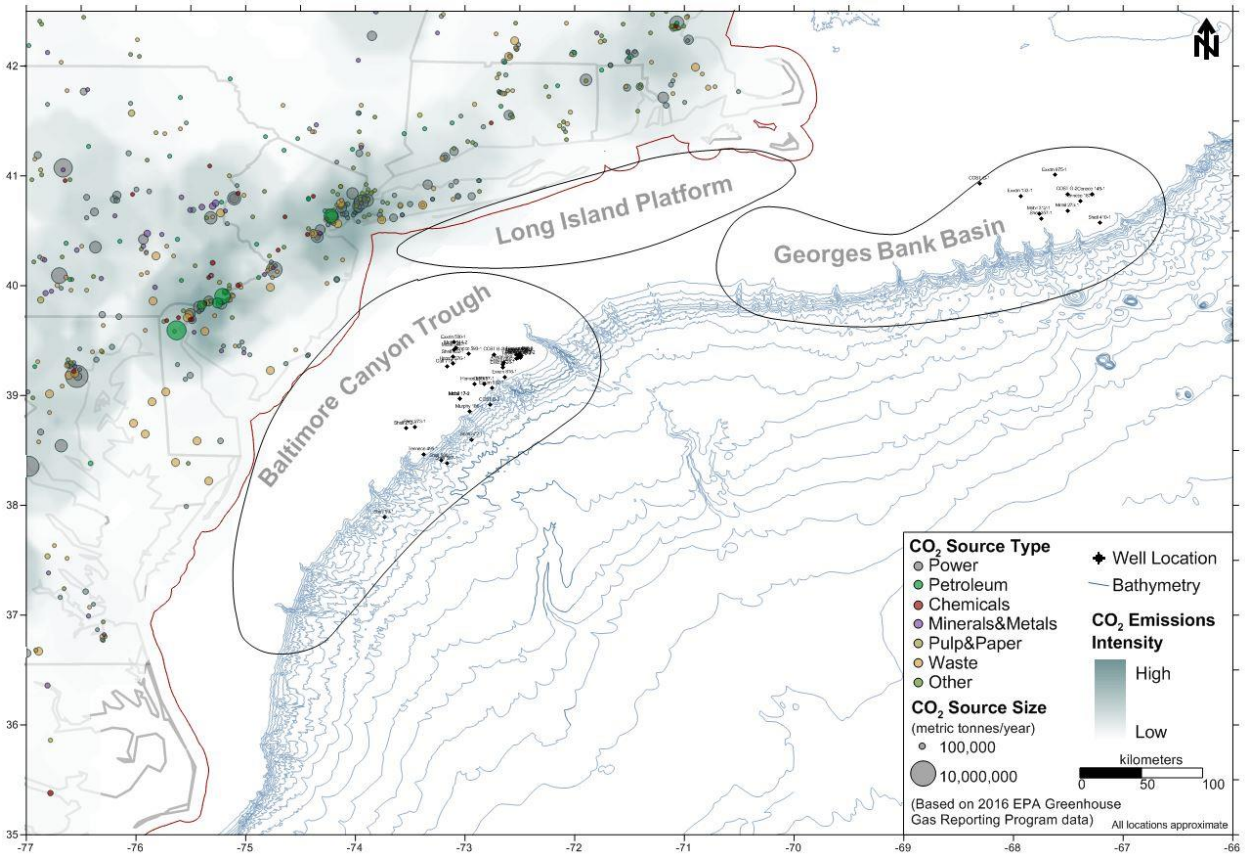

Figure 4-3. Locations of CO_2 sources in the mid-Atlantic region.

Figure 4-4 shows a graphic illustrating the distribution of 2016 CO_2 emission totals from point sources in the mid-Atlantic region. The CO_2 sources in the region reflect a mix of power generation, chemical facilities, petroleum processing, mineral and metal plants, pulp and paper, waste facilities, and other industry; power plants have the highest combined CO_2 emissions in the region (Figure 4-5). Many of the larger power plant sources are located inland from the coast. There are numerous small to moderate-sized sources in areas that may be connected with central pipelines. Combined, these sources have significant CO_2 emissions. However, carbon capture may be challenging for smaller sources that do not have well-established capture technologies.

Connecting CO_2 sources to the mid-Atlantic OCS CO_2 storage resources would likely require a pipeline network connecting multiple sources. The BCT and Long Island Platform are most accessible to existing industrial corridors. The GBB is more distant from CO_2 sources. Larger CO_2 pipelines may be considered to connect groups of power plants in the Midwestern United States with the mid-Atlantic offshore region.

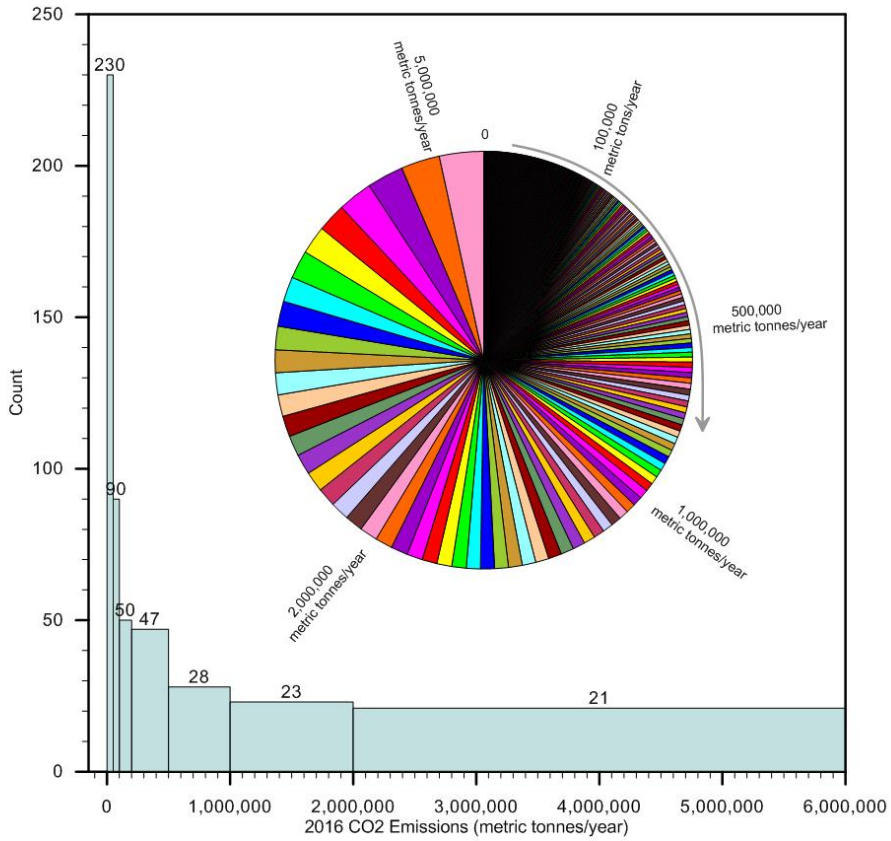

Figure 4-4. Histogram illustrating CO_2 sources in the mid-Atlantic region.

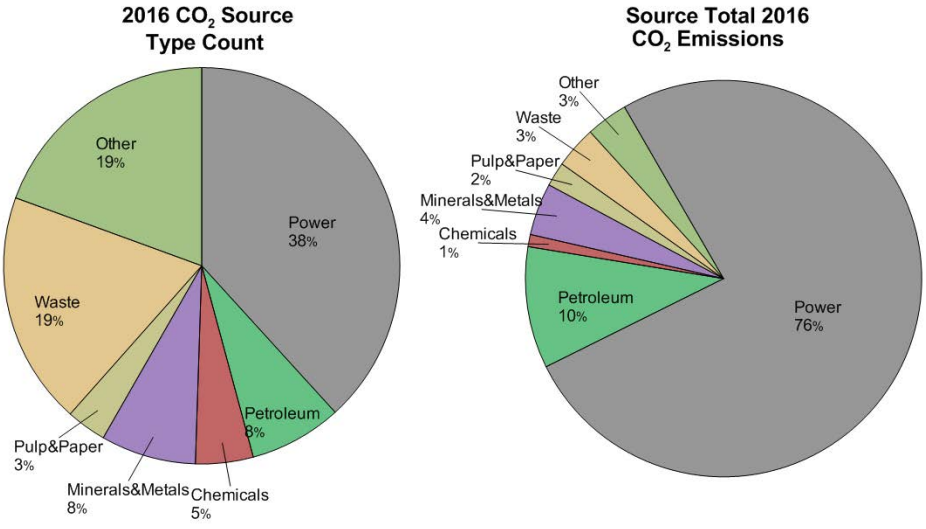

Figure 4-5. CO_2 source types and emissions in the mid-Atlantic region.

4.4 CO_2 Storage Stakeholder Risk Factors in the Mid-Atlantic Region

The objective of DOE's Carbon Storage Program is to develop and advance technologies that will significantly improve the effectiveness and reduce the cost of implementing carbon storage and be ready for widespread commercial deployment in the 2025–2035 timeframe. To accomplish deployment, technical and economic barriers need to be addressed and data collected and communicated to inform regulators and industry on the safety and permanence of carbon storage. Previous DOE investigations of the potential for geologic carbon storage in offshore resources (Litynski et al., 2011) identified several potential advantages of offshore geologic carbon storage compared to onshore storage, such as:

- Offshore storage provides additional CO_2 storage potential in the United States to supplement existing onshore capacity estimates, especially along heavily populated areas along U.S. coastlines in the Northeast.
- The use of offshore sites reduces the difficulty of establishing surface and mineral rights at candidate storage sites because, with the exception of Texas, lands more than three miles (five kilometers) offshore are owned solely by the federal government.
- Offshore storage reduces the risk to underground sources of drinking water.

The overall economics of offshore CCS may be more favorable compared to onshore CCS, despite higher capital costs (for drilling rigs, well manifolds, etc.). To promote public acceptance, it is important to provide accurate information and communicate with the public. Extensive work in stakeholder outreach and technology transfer has been undertaken under the DOE's Carbon Storage Program. The DOE has organized annual review meetings, produced the National Carbon Storage Atlas and other publications[1], and established The Energy Data eXchange (EDX), an online collection of capabilities and resources that support collaboration and technology transfer of DOE NETL research products[2].

This project is contributing to the stakeholder outreach effort by providing scientific-based data for future detailed risk assessments, which is important for building the public acceptance of offshore carbon storage. While extensive stakeholder outreach is beyond the scope of this project, the final technical report and data generated by this project will be uploaded to EDX to enable technology transfer. As part of the activities in this project, Battelle also co-hosted a stakeholder workshop on the Mid-Atlantic Offshore Carbon Storage Resource Assessment Project effort with Harvard at the Harvard University Center for the Environment in April 2018. The objective was to discuss the challenges and hurdles for offshore CCS and learn how to overcome them. Stakeholders included industry (e.g., Statoil, BP), non-governmental organizations (NGOs) (e.g., Natural Resources Defense Council, Clean Air Task Force), universities (Massachusetts Institute of Technology, University of Massachusetts Boston), and international regulators (Norwegian Petroleum Directorate). Workshop participants emphasized the need for early stakeholder outreach to identify and address *perceived* risks that are of most importance to offshore CCS stakeholders. Recommendations discussed included (1) establishing regulation and protocols specific to the offshore environment that leverage the experience of Norway, which has had an active offshore CCS industry for more than 20 years; (2) articulating risks using a quantitative analysis; (3) building a consensus that offshore CCS is for the greater good; and (4) conducting early briefings with regulators, NGOs, and the financial communities.

[1] http://www.netl.doe.gov/research/coal/carbon-storage/publications
[2] https://edx.netl.doe.gov/

5.0 Conclusions

An initial assessment was completed on technical risk factors in mid-Atlantic offshore areas that may affect CO_2 storage resource estimates by constraining the prospective resource assessment boundaries. The risk factor analysis considered the following categories:

1. geologic storage processes,
2. long-term potential for CO_2 migration, and
3. environmental setting factors that could determine the feasibility of developing a carbon storage facility.

The results of the risk factor analysis provide guidance for geologic storage implementation by providing stakeholders (e.g., operators, project developers, regulators, and the public) with preliminary information relevant to the long-term fate and associated risks of CO_2 injection into the subsurface, focusing on long-term CO_2 storage capacity, potential risks associated with CO_2 leakage, and other factors that have potential adverse impacts to logistics, economics, and infrastructure.

The risk factor analysis was based on readily available reports, maps, and data for the area. Any site-specific project would require more detailed site selection, test well drilling, geophysical logging, injection testing, seismic surveys, and storage system design. There is a great deal of uncertainty with regard to the subsurface geologic conditions. Conclusions presented here are meant to guide the direction of potential future feasibility assessments with more definitive results based on field work.

Table 5-1 summarizes the findings of the risk factor assessment. Overall, the mid-Atlantic offshore area benefits from the large spatial extent, thick sequences of Cretaceous- and Jurassic-age sands, lack of previous oil and gas wellbores, and distance from populated development. No highly critical risk factors were identified that would impede CO_2 storage along the study areas. Faults and geomechanical stability along the mid-Atlantic slope were identified as a moderate risk factor. Reservoir variability was also noted as a moderate risk factor, especially in Cretaceous sands that have interbedded silt and clay layers. Soft sediment deformation was identified as a risk factor for semi- or unconsolidated sediments less than 1,000 m deep, which are more prevalent in the GBB and Long Island Platform. CO_2 migration pathways and trapping mechanisms were not considered a significant risk factor for the deeper rock formations along the mid-Atlantic offshore.

Many environmental factors (e.g., HAPCs, man-made features on the seabed, and MPAs) are found along the mid-Atlantic seaboard. Most of these features are located closer to the shoreline. CO_2 sources are mainly clustered adjacent to the BCT. Dense population centers along the coastline may present challenges for stakeholder outreach and communication. In addition, there is little history of oil and gas development in the region which would provide a level of familiarity with typical exploration activities.

Table 5-1. Summary of risk factor analysis.

	Risk Factor	Method of Evaluation	Preliminary Findings
Geologic Storage Processes	Geologic Setting	Summarize regional structures, formation maps, geologic cross sections	Fairly continuous storage formations, regional structures affected by historical deposition/erosion events, generally passive continental margin with deep rifts
	Faults/Fractures	Seismic interpretation, examine bathymetry for indicators of structures	Seismic survey interpretation shows faults along slope areas, escarpments, uncertainty in subsurface stress/stability along slope, faults appear more prevalent along BCT slope, shelf areas appear more stable
	Seafloor/Slope Stability	Bathymetry interpretation, 3D modeling of slope	OCS shows few signs of gas migration like pockmarks, gas chimneys, fault traces; slope has features like canyons, escarpments, mass flows
	Reservoir Variability	Geophysical log analysis, geologic cross sections, analog study, hydrologic property review, core evaluation	There is a fair amount of reservoir heterogeneity in Cretaceous-age sands, caprocks appear more consistent, Jurassic sands also appear more consistent
	Seismic Activity/ Geomechanical Stability	Review earthquake historical data, subsurface stress analysis, well indicators of stress conditions	Passive continental margin with almost no earthquakes, subsurface geomechanical conditions are not well characterized, especially along slope
	Temperature/ Pressure Conditions	Compile data from well testing, temperature logs, repeat formation tests, CO_2 phase analysis	Temperature-pressure conditions suitable for CO_2 storage, soft-sediment deformation is risk factor in zones less than 1000 m deep
	Porewater Salinity	Literature search, resistivity log analysis, CO_2 solubility analysis	Salinity of deeper rock formation pore water is not well understood; some areas of low-salinity paleo waters have been observed nearshore toward GBB
	Hydrates/Mineral Precipitation & Dissolution	Literature search, pressure/temp. profile analysis, structural interpretation of the shelf/slope	Hydrates possible near slope, mainly in southern portion of BCT
Long Term CO_2 Migration	Confining Layer Rock Properties	Literature/report search, hydrologic properties aggregation, core evaluation, property mapping, statistical analysis	Thick, extensive confining layers, low permeability/porosity in shale/silt layers, interbedded sand layers may be present
	Trapping Mechanisms	Analyze solubility, structural, residual saturation, mineralogic trapping; migration pathway analysis, analog study	Significant structural trapping, moderate residual and solubility trapping likely along study area, long-term migration potential appears limited due to lithologic traps
	CO_2 Migration Pathways	Structural analysis, migration pathway analysis, trapping mechanism analysis, reservoir simulations	General structural trends suggest updip migration toward inshore areas, low dip, many structural/lithologic traps
	Gas Presence	Bathymetry analysis, seabed pockmark survey, gas analysis (formational), research review	Sediment properties & CO_2 phase behavior suggest soft sediment deformation potential at depths <1000 m, no significant indicators of gas migration along seabed
	Wellbore Integrity	Catalog well construction and plugging specifications	Few wells along study area, wells were plugged and constructed with suitable materials/methods
Environmental Factors	Environmental Setting	Catalog marine features, HAPCs, geo-political features, man-made features, CO_2 sources, exploration factors	There are numerous environmental features present in the study areas, many man-made features near shore, CO_2 sources are mainly clustered adjacent to BCT
	Regulatory Framework	Review geo-political boundaries, BOEM policy, offshore CCS risk analysis methods	Little history of oil & gas exploration, offshore development limited
	Near-Surface Features	Regulatory evaluation, locate and post GIS layers onto maps, delineation of areas where drilling will not be feasible	Many man-made features near shore for consideration
	Stakeholder/ Communication	Summarize stakeholder risk issues related to exploration & development activities along mid-ATL offshore	Many stakeholders along densely populated mid-Atlantic seaboard. Stakeholder-perceived risks need to be identified as early in the project as possible.

6.0 References

Allen, P.A., and J. R. Allen. (2005). Basin Analysis: Principles and Applications. Blackwell Publishing, Malden, Massachusetts, 549 p.

Amato, R. and Babout, J. (eds.). (1980). Geologic and Operational Summary, COST No. G-1 Well, Georges Bank Area, North Atlantic OCS. USGS Open-File Report 80-268.

Amato, R. V., & Giordano, A. C. (1985). Great Stone Dome-Great Disappointment? AAPG Eastern Section Meeting. Williamsburg, Virginia: AAPG, *69*, 1433.

Arthur, M. A. (1982). Thermal history of the Georges Bank Basin. *Geological Studies of the COST Nos. G-1 and G-2 Wells, United States North Atlantic Outer Continental Shelf.* Scholle, P. A., & Wenkam, C. R. (eds). USGS Geological Survey Circular 861.

Babu, P., Yang, S., Dasgupta, S., and Linga, P. (2014). Methane Production from Natural Gas Hydrates via Carbon Dioxide Fixation. Energy Procedia 61 (2014) 1776-1779.

Bachu, S. (2013). Drainage and imbibition CO_2/brine relative permeability curves at in-situ conditions for sandstone formations in western Canada. *Energy Procedia, 37*, 4428-4436.

Bennion, D. B., & Bachu, S. (2008). Drainage and imbibition relative permeability relationships for supercritical CO_2/brine and H_2S/brine systems in intergranular sandstone, carbonate, shale, and anhydrite rocks. *SPE Reserv. Eval. Eng. 11*, 487–496.

Benson, S., Esposito, A., Li, B., Krause, M., Krevor, S., Kuo, W., & Zou, L. (2009). Residual Trapping of Carbon Dioxide. Annual Report: Stanford Dept. of Energy Resources. 41 p.

Bhattacharya, Janok P., et al. (2016). "Estimation of source area, river paleo-discharge, paleoslope, and sediment budgets of linked deep-time depositional systems and implications for hydrocarbon potential." Earth-Science Reviews 153 (2016): 77-110.

Bickle, M., Chadwick, R., Huppert, H., Hallworth, M., & Lyle, S. (2007). Modelling CO_2 accumulation at Sleipner: implications for underground carbon storage. *Earth and Planetary Science Letters*, *255*, 164-176.

Blackford, J. C., Stahl, H., Bull, J. M., Bergès, B. J. P., Cevatoglu, M., Lichtschlag, A., … Widdicombe, S. (2014). Detection and impacts of leakage from sub-seafloor deep geological carbon dioxide storage. *Nature Climate Change, 4*, 1011-1016.

BOEM. (2014). *Atlantic OCS Proposed Geological and Geophysical Activities Mid-Atlantic and South Atlantic Planning Areas Final Programmatic Environmental Impact Statement*, Bureau of Ocean Energy Management. Prepared under Task Order No. M11PD00013. 788 p.

Brothers, D. S., ten Brink, U. S., Andrews, B. D., & Chaytor, J. D. (2013). Geomorphic characterization of the U.S. Atlantic continental margin. *Marine Geology*, *338*, 46-63.

Brown, G. (2017). Marine Monitoring for CCS…or Boaty McBoatFace's next adventure. IEAGHG Monitoring Meeting, Traverse City, Michigan, USA. June 2017.

Carvajal, Cristian, and Steel, M. (2007). Sediment Volume Partitioning, Topset Processes and Clinoform Architecture. Understanding the Role of Sediment Supply, Sea Level and Delta Types in Shelf Margin Building and Deepwater Sand Bypass: The Lance-Fox Hills-Lewis System in S. Wyoming.

Cavanagh, A., & Haszeldine, R. (2014). The Sleipner storage site: Capillary flow modeling of a layered CO_2 plume requires fractured shale barriers with the Utsira Formation. *International Journal of Greenhouse Gas Control*, *21*, 101-112.

Chadwick, A., Noy, D., Lindeberg, E., Arts, R., Eiken, O., & Williams, G. (2006). Calibrating reservoir performance with time-lapse seismic monitoring and flow simulations of the Sleipner CO_2 plume. 8th International Conference on Greenhouse Gas Control Technologies, Tronheim, Norway, June 19-22, 2006.

Coe, Angela L. (2003). The sedimentary record of sea-level change. Cambridge University Press, 2003.

Cohen, D., Person, M., Wang, P., Gable, C., Hutchinson, D., Marksamer, A., … Lane, J. W. Jr. (2010). Origin and Extent of Fresh Paleowaters on the Atlantic Continental Shelf, USA. *Ground Water*, *48*(1), 143-158.

DOE-NETL. (2011). Best Practices for Risk Analysis and Simulation for Geologic Storage of CO_2, version 1.0. U.S. Department of Energy, National Energy Technology Laboratory, DOE/NETL-2011/1459.

DOE-NETL (2017). Best Practices: Risk Management and Simulation for Geologic Storage Projects. U.S. Department of Energy, National Energy Technology Laboratory, DOE/NETL-2017/1846.

DOE-NETL. (2017). Best Practices for Site Screening, Selection, and Initial Characterization for Storage of CO_2 in Deep Geologic Formations. U.S. Department of Energy, National Energy Technology Laboratory, DOE/NETL-2017/1844.

Espinoza, D.N., and Santamaria, J.C. 2017. CO_2 breakthrough- Caprock sealing efficiency and integrity for carbon geological storage. International Journal of Greenhouse Gas Control, 66 (2017) 218-229.

Fry, C. (1987). Geothermal Gradient in Geologic and Operational Summary, COST No. B-3 Well, Baltimore Canyon Trough Area, Mid-Atlantic OCS, Open File Report 79-1159.

Gaus, I. (2010). Role and impact of CO_2–rock interactions during CO_2 storage in sedimentary rocks. *International Journal of Greenhouse Gas Control*, *4*, 73-89.

Goff, J. A., Austin, J. A., & Fulthorpe, C. S. (2013). Reinterpretation of the Franklin “Shore” in the mid-Atlantic bight as a paleo-shelf edge. *Continental Shelf Research*, *60*, 64-69.

Goldberg, D., Kent, D., & Olsen, P. (2010). Potential on-shore and off-shore reservoirs for CO_2 sequestration in Central Atlantic magmatic province basalts. *PNAS*, *107*(4), 1327-1332.

Grow, J. A., & Sheridan, R. E. (Eds.) (1988). U.S. Atlantic continental margin: A typical Atlantic-type or passive continental margin. *The Atlantic Continental Margin* (Vol. 1-2, pp. 1-7). Geological Society of America.

Hall, R., & Ensminger, H. (1979). Potential geologic hazards and constraints for blocks in proposed mid-Atlantic OCS oil and gas lease sale 49, USGS Open-File Report 79-264. 176 p.

Hannis, S., Chadwick, A., Connelly, D., Blackford, J., Leighton, T., Jones, D., … Dixon, T. (2017). Review of Offshore CO_2 Storage Monitoring: Operational and Research Experiences of Meeting Regulatory and Technical Requirements. *Energy Procedia*, *114*, 5967-5980.

Heidbach, O., Rajabi, M., Reiter, K., & Ziegler, M. (2016). World Stress Map 2016. GFZ Data Services. http://doi.org/10.5880/WSM.2016.002

Hill, J.C., Driscoll, N.W., Weissel, J.K., Goff, J.A. (2004). Large-scale elongate gas blowouts along the U.S. Atlantic margin. J. Geophys. Res. 109, B09101.

Hinestrosa, G., Webster, J. M., Beaman, R. J., & Anderson, L. M. (2014). Seismic stratigraphy and development of the shelf-edge reefs of the Great Barrier Reef, Australia. *Marine Geology*, *353*, 1-20.

Holland, T., & Powell, R. (1991). A Compensated-Redlich-Kwong (CORK) equation for volumes and fugacities of CO_2 and H_2O in the range 1 bar to 50 kbar and 100–1600°C. *Contributions to Mineralogy and Petrology, 109*, 265-273.

Holland, T., & Powell, R. (1998). An internally consistent thermodynamic data set for phases of petrological interest. *Journal of Metamorphic Geology*, *16*, 309-343.

Hutchinson, D.R., and K.D. Klitgord. (1988). Evolution of rift basins on the continental margin off southern New England, in W. Manspeizer, ed., Triassic-Jurassic Rifting, Continental Breakup and the Origin of the Atlantic Ocean Passive Margins, Part A: New York, Elsevier, p. 81-98.

IEAGHG. (2016). International Workshop on Offshore Geologic CO_2 Storage. Report: 2016/TR2, May 2016.

IPCC (2005). IPCC Special Report on Carbon Dioxide Capture and Storage. Metz, B., Davidson, O., de Coninck, H., Loos, M., and Myer, L. (eds). Prepared by Working Group III of the Intergovernmental Panel on Climate Change. Cambridge University Press, 443 p.

Jansa, L. F., & Pe-Piper, G. (1988). Middle Jurassic to Early Cretaceous Igneous Rocks Along Eastern North American Continental Margin. *AAPG Bulletin*, *72*(3), 347-366.

Juanes, R., Spiteri, E., Orr Jr., F. M., & Blunt, M. (2006). Impact of relative permeability hysteresis on geological CO_2 storage. *Water Resour. Res*., *42*, W12418.

Kallweit, R. S., & Wood, L. C. (1982). The Limits of Resolution of Zero-Phase Wavelets. *Geophysics*, *47*(7), 1035-1046.

Kang, Q., Lichtner, P. C., Viswanathan, H. S., & Abdel-Fattah, A. I. (2010). Transport in Porous Media 82, 197-213.

Klitgord, K., Hutchinson, D. R., & Schouten, H. (1988). U.S. Atlantic Continental Margin: Structural and Tectonic Framework. *The Geology of North America,* vol. I-2, The Atlantic Continental Margin: U.S., Chapter 3, Geological Society of America, pp. 19-56.

Kramer, K. V, & Shedd, W. W. (2017). A 1.4 Billion-Pixel Map of the Gulf of Mexico Seafloor. *EOS Earth & Space Science News*, *98*(8), 16-21.

Kohout, F. A., Hathaway, J., Folger, D., Bothner, M., Walker, E., Delaney, D., … Rhodehamel, E. (1977). Fresh groundwater stored in aquifers under the continental shelf, implications from a deep test, Nantucket Island, Massachusetts. J*ournal of the American Water Resources Association, 13*(2), 373-386.

Kominz, M. A., Miller, K. G., & Browning, J. V. (1998). Long-term and short-term global Cenozoic sea-level estimates. *Geology, 26*, 311-314.

Krevor, S., Blunt, M., Benson, S., Pentland, C., Reynolds, C., Al-Menhali, A., & Niu, B. (2015). Capillary trapping for geologic carbon dioxide storage – From pore scale physics to field scale implications. *International Journal of Greenhouse Gas Control*, *40*, 221-237.

Kyung, D., Lee, K., Kim, H., & Lee, W. (2013). Effect of marine environmental factors on the phase equilibrium of CO_2 hydrate. *International Journal of Greenhouse Gas Control, 20*, 285-292.

Land, C. S. (1968). Calculation of imbibition relative permeability for two- and three-phase flow from rock properties. *Society of Petroleum Engineers Journal, 8*, 149–156.

Larson, R., Davis, H., & Scriven, L. (1981). Displacement of residual nonwetting fluid from porous media. *Chem. Eng. Sci. 36*, 75–85.

Leighton, T. G., & White, P. R. (2012). Quantification of undersea gas leaks from carbon capture and storage facilities, from pipelines and from methane seeps, by their acoustic emissions. *Proceedings of the Royal Society 2012*, *468*, 485-510.

Lenhard, R., & Parker, J. (1987). A model for hysteretic constitutive relations governing multiphase flow. *Water Resour. Res., 23*, 2197–2206.

Libby-French, J. (1984). Stratigraphic Framework and Petroleum Potential of Northeastern Baltimore Canyon Trough, Mid-Atlantic Outer Continental Shelf. *AAPG Bulletin, 68*(1), 50-73.

Litynski, J. T., Brown, B. M., Vikara, D. M., & Srivastava, R. D. (2011). Carbon capture and sequestration: The U.S. Department of Energy's R&D efforts to characterize opportunities for deep geologic storage of carbon dioxide in offshore resources. OTC-21987-PP, presented at the Offshore Technology Conference Proceedings, Houston, Texas, USA, 2-5 May, 2011.

Manheim, F. T., & Paull, C. K. (1981). Patterns of groundwater salinity changes in a deep continental-oceanic transect off the southeastern Atlantic coast of the U.S.A. *Journal of Hydrology, 54*(1–3), 95-105.

Matter, J., et al. (2016). Rapid carbon mineralization for permanent disposal of anthropogenic carbon dioxide emissions. Science, v. 352, issue 6291, pp. 1312-1314.

McGrail P, Schaef, H., Spane, F., Cliff, J., et al. (2017). Field Validation of Supercritical CO_2 Reactivity with Basalts. Environ. Sci. Technol. Lett., 2017, 4, 1, pp 6-10.

Meisler, H. (1989). The occurrence and geochemistry of salty ground water in the northern Atlantic Coastal Plain. *U.S. Geol. Surv., Prof. Pap.*, Report 1404-D.

Miller, K. G., Kominz, M. A., Browning, J. V., Wright, J. D., Mountain, G. S., Katz, M. E., ... Pekar, S.F. (2005). The Phanerozoic record of global sea-level change. *Science, 310*, 1293-1298.

Miller, K.G., Browning, J.V., Sugarman, P.J., Monteverde, Andreasen, D.C., Lombardi, C., Thornburg, J, Reinfelder, Y., and Kopp, RE. (2017). Lower to mid-Cretaceous sequence stratigraphy and characterization of CO2 storage potential in the Mid-Atlantic U.S. Coastal Plain. Journal of Sedimentary Research, 87, pp. 609-629.

Miller, K. G., Lombardi, C., Browning, J. V., Schmelz, W. J., Gallegos, G., Mountain, G., & Baldwin, K. (2018). Back to Basics of Sequence Stratigraphy: Early Miocene and Mid-cretaceous Examples from the New Jersey Paleoshelf. *Journal of Sedimentary Research, 88*(1), 148-176.

Moucha, R., Forte, A. M., Mitrovica, J. X., Rowley, D. B., Quere, S., Simmons, N. A., & Grand, S. P. (2008). Dynamic topography and long–term sea level variations: there is no such thing as a stable continental platform. *Earth and Planetary Science Letters, 271*, 101–108.

Mountain, G., Proust, J.-N., McInroy, D., Cotterill, C., & the Expedition 313 Scientists. (2010). *Proceedings of the Integrated Ocean Drilling Program, 313*: Tokyo, Integrated Ocean Drilling Program Management International, Inc.

National Geophysical Data Center (1999a). U.S. Coastal Relief Model - Northeast Atlantic. National Geophysical Data Center, NOAA. doi:10.7289/V5MS3QNZ [June 17, 2018].

National Geophysical Data Center (1999b). U.S. Coastal Relief Model - Southeast Atlantic. National Geophysical Data Center, NOAA. doi:10.7289/V53R0QR5 [June 17, 2018].

Newman, KR, Cormier MH, Weissel JK, Driscoll NW, Kastner M, Solomon EA, Robertson G, Hill JC, Singh H, Camilli R, Eustice R. (2008). Active methane venting observed at giant pockmarks along the U.S. mid-Atlantic shelf break. Earth and Planetary Science Letters. 267:341-352.Olsen, P. E. (1997). Stratigraphic record of the early Mesozoic breakup of Pangea in the Laurasia–Gondwana rift system. *Annual Review of Earth and Planetary Sciences, 25*, 337-401.

Olsson, R. K., Gibson, T. G., Hansen, H. J., & Owens, J. P. (1988). Geology of the northern Atlantic Coastal Plain: Long Island to Virginia, in Sheridan, R. E., Grow, J. A., eds., *The Atlantic Continental Margin*. Boulder, Colorado, Geological Society of America, Geology of North America, v. 1-2, p. 87-105.

Pawar, R., Chu, S., Stauffer, P., Bromhal, G., Dilmore, R., Guthrie, G., … Gastelum, J. (2014). Quantification of key long-term risks at CO_2 sequestration sites: Latest results from US DOE's National Risk Assessment Partnership (NRAP) Project. *Energy Procedia. 4*, 2014, Proceedings of the 12th International Conference on Greenhouse Gas Control Technologies, Austin, Texas, USA.

Peltier, W. R. (1998). Postglacial variations in the level of the sea: Implications for climate dynamics and solid-Earth geophysics. *Reviews of Geophysics, 36*, 603-689.

Petersen, M. D., Moschetti, M. P., Powers, P. M., Mueller, C. S., Haller, K. M., Frankel, A. D., … Olsen, A. H. (2014). Documentation for the 2014 update of the United States national seismic hazard maps: U.S. Geological Survey Open-File Report 2014–1091, 243 p., https://dx.doi.org/10.3133/ofr20141091.

Petersen, M. D., Mueller, C. S., Moschetti, M. P., Hoover, S. M., Shumway, A. M., McNamara, D. E. … Rukstales, K. S. (2017). 2017 One-Year Seismic Hazard Forecast for the Central and Eastern United States from Induced and Natural Earthquakes. *Seismological Research Letters, 88*(3), 772-783.

Pope, D. A., & Gordon, A. D. (1999). Simulation of groundwater flow and movement of the freshwater-saltwater interface in the New Jersey Coastal Plain. U.S. Geological Survey Water-Resources Investigations Report, 98–4216, 169 p.

Post, P. J., & Coleman, J. L. (2015). Mesozoic Rift Basins of the U.S. Central Atlantic Offshore: Comparisons with Onshore Basins, Analysis, and Potential Petroleum Prospectivity, in GCSSEPM Foundation 34th Annual Perkins-Rosen Research Conference, Houston, Texas, p. 1-93.

Prather, B. E. (1991). Petroleum Geology of the Upper Jurassic and Lower Cretaceous, Baltimore Canyon Trough, Western North Atlantic Ocean (1). *AAPG Bulletin, 75*.

Raymo, M. E., Mitrovica, J. X., O'Leary, M. J., DeConto, R. M., & Hearty, P. J. (2011). Departures from eustasy in Pliocene sea-level records. *Nature Geoscience, 4*, 328-332.

Robbins, E. (1979). Geological Studies of the COST GE-1 Well, U.S. South Atlantic Outer Continental Shelf Area: Geothermal Gradients. U.S. Geological Survey Circular 800, 119 p.

Rowley, D. B., Forte, A. M., Moucha, R. R., Mitrovica, J. X., Simmons, N. A., & Grand, S. P. (2011). Dynamic Topography Change of the Eastern U.S. since 4 Ma: Implications for Sea Level and Stratigraphic Architecture of Passive Margins. *Science, 340*, 1563-1563.

Sanford, W., Goughten, M., Coplen, T., Hunt, A., & Bullen, T. (2013). Evidence for high salinity of Early Cretaceous sea water from the Chesapeake Bay crater. *Nature, 503*, 252-258.

Savage, D., Maul, P. R., Benbow, S., & Walke, R. C. (2004). A Generic FEP Database for the Assessment of Long-Term Performance and Safety of the Geological Storage of CO_2, Version 1.0. Quintessa Document # QRS-1060A-1.

Schlee, J., Dillon, W. P., & Grow, J. A. (1979). Structure of the Continental Slope off the Eastern United States, Special Publications. *Society of Economic Paleontologists and Mineralogists, 27*, 95-117.

Schoderbak et al. (2013). ConocoPhillips Gas Hydrate Production Test Final Technical Report. Prepared for US DOE NETL under Award DE-NT0006553, 204 p.

Skarke, A., Ruppel, C., Kodis, M, Brothers, D., and Lobecker, E. (2014). Widespread methane leakage from the sea floor on the northern US Atlantic margin. Nature Geoscience, 7, 657-661.

Slater, B., Stolorow, A., & Smith, L. (2010). Potential for Supercritical Carbon Sequestration in the Offshore Bedrock Formations of the Baltimore Canyon Trough, in AAPG Eastern Section Meeting, Kalamazoo, Michigan, AAPG, September 28, 2010.

Sminchak, J. R., Zeller, E., & Bhattacharya, I. (2014). Analysis of Unusual Scale Buildup in a CO_2 Injection Well for a Pilot-Scale CO_2 Storage Demonstration Project. *Greenhouse Gases: Science and Technology, 4*(3), 357-366.

Steckler, M. S., & Watts, A. B. (1982). Subsidence history and tectonic evolution of Atlantic-type continental margins. *Dynamics of Passive Margins*, Scrutton, R. A., ed., AGU Geodynamic Ser: 6: 184-196.

Steckler, M. S., Mountain, G., Miller, K., & Christie-Blick, N. (1999). Reconstruction of Tertiary progradation and clinoform development on the New Jersey passive margin by 2-D backstripping. *Marine Geology, 154*, 399-420.

Tohidi et al. (2010). CO_2 Hydrates Could Provide Secondary Safety Factor in Subsurface Sequestration of CO_2. Envrion. Sci. Technol., 2014, 44, 1509-1514.

van Geldern, R., Hayashi, T., Bottcher, M., Mottl, M., Barth, J., & Stadler, S. (2013). Stable isotope geochemistry of pore waters and marine sediments from the New Jersey shelf: Methane formation and fluid origin. *Geosphere, 9*(1), 96–112.

Watts, A. B. (1981). The U.S. Atlantic continental margin: Subsidence history, crustal structure, and thermal evolution. *Geology of passive continental margins: History, structure, and sedimentologic record*, Bally, A. W., ed., American Association of Petroleum Geologists Education Course Note Series 19:1–75.

Withjack, M. O., Schlische, R. W., & Olsen, P. E. (1998). Diachronous rifting, drifting, and inversion on the passive margin of central eastern North America: An analog for other passive margins. *American Association of Petroleum Geologists Bulletin, 82*, 817-835.

World Resources Institute (WRI) (2008). Guidelines for the capture, transportation and storage of carbon dioxide. Washington DC.

Xu, T., Sonnenthal, E., Spycher, N., & Pruess, K. (2006). TOUGHREACT—A simulation program for non-isothermal multiphase reactive geochemical transport in variably saturated

geologic media: Applications to geothermal injectivity and CO_2 geological sequestration. *Computers and Geosciences, 32*, 145-165.

Yang et al. (2017). Flue gas injection into gas hydrate reservoirs for methane recovery and carbon dioxide sequestration. Energy Conversion and Management 136 (2017) 431-438.

Zhao, H., Fedkin M. V., Dilmore, R. M., & Lvov, S. N. (2015). Carbon dioxide solubility in aqueous solutions of sodium chloride at geological conditions: Experimental results at 323.15, 373.15, and 423.15 K and 150 bar and modeling up to 573.15 K and 2000 bar. *Geochimica et Cosmochimica Acta, 149*, 165-189.

Zhou, Y., Dimitrios G., Hatzignatiou, Y. G., & Helland, J. O. (2017). On the estimation of CO_2 capillary entry pressure: Implications on geological CO_2 storage. *International Journal of Greenhouse Gas Control, 63*, 26-36.

Zuo, L., & Benson, S. M. (2014). Process-dependent residual trapping of CO_2 in sandstone. *Geophys. Res. Lett. 41*, 2820–2826.

Appendix A Literature Review Summary

Literature Review of Offshore CO_2 Storage Risk Assessment Approaches

CO_2 Storage Atlas – Norwegian Sea (Norwegian Petroleum Directorate, 2014)

The Storage Atlas for CO_2 in the Norwegian Sea was compiled from the experience in two offshore CO_2 storage projects (Sleipner and Snøhvit), as well as various industry exploration in the Norwegian Continental Shelf. The work spans over 40 years of experience and has culminated in best practice determinations, lessons learned, and valuable context for other offshore CO_2 storage projects. As a project in operation since 1996, Sleipner represents the longest timescale in any existing CO_2 storage project and thus provides essential detail for the successful long-term operation of a CO_2 storage project in an offshore continental shelf environment. The risk assessment and mitigation aspects of the project remain critical for any new project that comes online, and the Snøhvit project compounds the value of a long-term project like Sleipner through being able to compare and adapt strategies prior to the onset of injection based on previous lessons learned, as well as provide additional context about the important factors that can impact the success of a long term offshore storage project. Key understandings gained through the experience of these projects, as described in the CO_2 Storage Atlas include:

- In development of the Snøhvit storage project, lack of suitable injectivity was a very serious risk factor in terms of the consequence of operational inefficiencies that could lead to project stoppage, or significant reputational damage from an unsuccessful storage attempt
- Lack of well integrity remains a primary concern for storage projects, with the risk of migration into the overburden or above the seafloor being the most serious operational consequence of any storage project.
- Risks identified related to sealing capacity of the storage formation, including insufficient formation thickness, faulting near or within storage reservoirs, and geomechanical deformation response to injection all require significant forethought in assessing the likelihood and consequence of any CO_2 migration. Insufficient caprock thickness in younger sediments might present a significant risk to the project, and thus developing proper screening criteria related to candidate sites is essential.
- Monitoring techniques applied to prevent, respond, and mitigate potential impacts remain crucial for the successful operation of a storage project, for ensuring public trust and acceptance of any current of future storage effort, and for complying with regulations such as those which exist within the EU Governmental structure.
- It remains critical in an offshore environment to assess the impact on organisms and communities on the seafloor in response to a possible migration of CO_2, and to identify biological indicators and monitoring techniques to improve the accuracy and resolution of CO_2 migration prevention and early warning systems.
- Out of three potential site selections within the feasibility study for the Snøhvit project, one area was recommended to move forward (with a caveat that the terminal location will remain offshore) with a risk profile that was acceptable.

Lessons Learned from 14 years of CCS Operations: Sleipner, In Salah and Snøhvit (Eiken et al., 2014)

This summary of lessons learned through three storage projects provides key insight into the specific operational uncertainties any project will face as it moves from feasibility to demonstration. This includes the injection potential and plume development modeling work that is a key indication of storage potential, as well as the story a project tells all stakeholders regarding the safety and assuredness of long term injection. A look back at how the pre-injection models compare to the ground truth obtained during injection provides an iterative approach to developing best practice techniques for understanding risk pre-injection, and monitoring/mitigating any adverse reactions once injection has begun. Key understandings gained through this look back include:

- Sweep efficiencies during the injection period have a large degree of impact on the behavior of the supercritical CO_2 in the subsurface during injection migration. The injection period thus becomes critical for understanding and altering the course of any injection activity through the aid of detailed monitoring and iterative modeling to properly manage a reservoir (Figure 1).
- Downhole pressure and temperature measurements remove uncertainties based on wellhead conditions, and are critical for any extensive monitoring and risk mitigation approach
- High quality monitoring programs increase the resolution of data in any field, and thus decreases the threshold for detection of any CO_2 migration pathway formation. Unpredicted geologic features were further identified during injection through the use of geophysical monitoring methods like seismic and gravity surveys, thus increasing the resolution of understanding of the reservoir in real time and allows for better reservoir management.

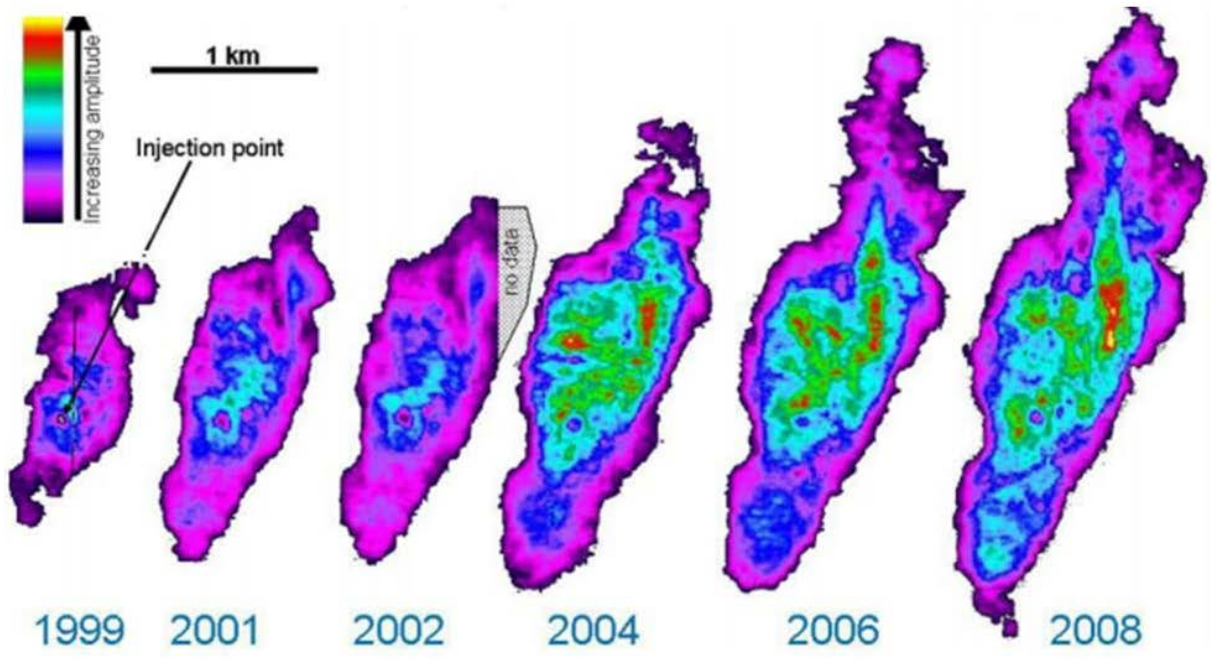

Figure 1. Time Lapsed Seismic difference reflection amplitude maps in the Sleipner Field.

Challenges for social impact assessment in coastal regions: A case study of the Tomakomai CCS Demonstration Project (Mabon et al., 2017)

This paper details the societal impact assessment of an offshore CO_2 storage project, specifically in the case of the Tomakomai Carbon Capture and Storage Demonstration Project. The additional challenge of operating in an offshore marine environment increases the complexity of a project which requires the support of the public and all relevant stakeholders. Societal impact assessment focuses on the implicit understanding of a broad informal agreement between operators and the local community acceptance of CO_2 storage projects. The argument is that both environmental assessments and societal impact assessments are necessary to fully encompass the risks and potential hinderances of a given project. The paper outlines crucial factors for consideration that developers need to consider as they approach community acceptance on the path towards viability. Key takeaways from the paper include:

- The broader public acceptance of the Tomakomai Project suggests a neutral stance towards the storage project, however for example fisheries holds large political sway due to the cultural and economic importance of the activity. This can be seen as a positive, as mitigating ocean acidification can improve the health of the fish stock. Large scale industry effects are still historically viewed through a negative lens by fishers, and thus viewed cautiously.
- Tomakomai City has largely been receptive to large scale industry, and this has general effect of allowing for a historical record of safe and trusted operation within the area, which can lead to broader acceptance of new projects
- Upscaling of CO_2 storage may present additional challenges, as pursuing a national initiative also draws in national political interest, which can generally be more risk adverse - especially if those political concerns are viewed through the lens of aiding the fossil fuel industry.
- The level of effort and engagement of the community stakeholders has a large relevance to the acceptance of large scale CO_2 storage efforts. Effective communication and engagement is necessary to move towards an operational phase. A lot of the effort would be front-loaded, however continued engagement to discuss monitoring results and requirements remains key for continued acceptance by the stakeholder community.

ECO_2 Final Publishable Summary Report - Sub-seabed CO_2 Storage: Impact on Marine Ecosystems (GEOMAR, 2015)

This final report summary highlights a 4-year study commissioned by the EU to understand sub seabed CO_2 storage impact on marine ecosystems. The document provides a high-level assessment of the potential impacts of any offshore CO_2 project, as well as specific case examples, and serves to guide future risk assessment and environmental monitoring efforts in offshore environments. This report draws upon the experience of ongoing and completed projects within the European Union, including Sleipner and Snøhvit. In addition to the identification of risks and their potential consequences, a monitoring best practice strategy is recommended. ECO_2 focused on 5 project objectives, namely:

- To investigate the likelihood of CO_2 migration from sub-seabed storage sites
- To study the potential effects of CO_2 migration on benthic organisms and marine ecosystems

- To assess the risks of sub-seabed carbon dioxide storage
- To develop a comprehensive monitoring strategy using cutting-edge monitoring techniques
- To define guidelines for the best environmental practices in implementation and management of sub-seabed storage sites

Key outcomes of this four-year study and final reporting include:

- Chimney CO_2 migration pathways in the vicinity of the Sleipner and Snøhvit fields create an increased likelihood of CO_2 migration pathways on longer timescales, and the selection of storage targets should take this into consideration to minimize CO_2 migration likelihood.
- Pockmarks above the Snøhvit storage site, some reaching several hundred meters in diameter. Pressure buildup as a result of the storage operation may reactivate gas and fluid conduits through these structures. The recommendation is to closely monitor or avoid altogether storage areas with surficial evidence of gas expulsion, especially in offshore environments with water depths less than 250 meters (850 feet).
- As opposed to looking at risk factors from the perspective of risk probability, risk is suggested to be framed from the perspective of a propensity to leak (PTL). This is in order to fully convey the nature of risk assessment behind CO_2 migration likelihood is largely heuristic in nature, and unlike other statistical analysis more driven by large databases as in the case of oil and gas drilling.
- A high-resolution sensor network is recommended to assess ongoing monitoring of potential migration of CO_2 upward through small scale features such as abandoned wells, fractures, seismic pipes. Extra attention should be paid to monitor naturally occurring CO_2 migration pathways already known to seep upwardly mobile gas or fluid.
- Due to the extensive monitoring best practice recommended in naturally occurring CO_2 migration pathways, an economic argument can be made for any prospective storage site to avoid seepage features that would require advanced baseline and monitoring surveys. This will also necessarily reduce the likelihood of CO_2 migration from storage sites.

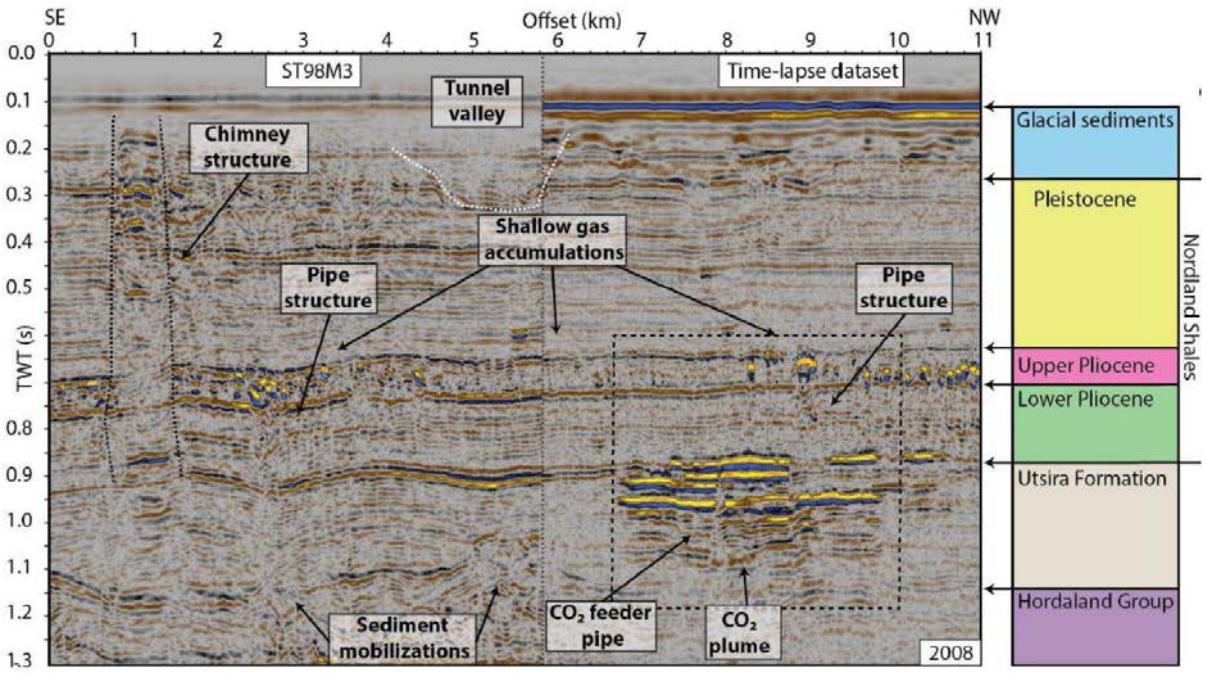

Figure 2. Seismic Profile of the Sleipner Area detailing interpreted subsurface gas and fluid CO_2 migration pathway features. Image taken from ECO_2 Final Summary Report, 2015

Integrity of Wells in the Near-shore Area Gippsland Basin Victoria (Goebe et al., 2016)

A well integrity study was undertaken to understand the state of existing wellbores in the near vicinity to the CO_2 storage site in nearshore Gippsland Basin. Storage site selection encompasses the broadest range of risk sensitivity, as the risks are necessarily increased or decreased depending on the specific site factors, and this is especially true in existing oil and gas field as in the case in the Gippsland Basin. Several site-specific storage targets were identified, and as part of the risk assessment the existing wellbores were examined to profile the potential risk of CO_2 migration pathways. As a significant identified risk, potential wellbore CO_2 migration pathways were studied in 14 wells and an assessment of likelihood of migration as well as mitigation strategies were proposed. Risker wells were identified in the process and a full understanding of the existing data was completed in order to properly inform the site selection and monitoring program as the CO_2 injection project progresses. Under an Australian regulatory framework, CO_2 storage projects must demonstrate that there are no active CO_2 migration pathways currently, as well as outline remediation and mitigation strategies if there is detection of CO_2 migration post injection. Key findings from this well integrity report include:

- Using a likelihood and consequence analysis for each well specifically towards CO_2 plume interaction with wellbores led to the judgement that the likelihood of CO_2 migration through the 14 wellbores into the overlying aquifer was generally low due to the high standards of protection applied to the wells in their original industry context.
- Risk was often higher in certain wells due to the uncertainty inherent in the access to well records and other sources of information that are no longer available the assess. As such, due to the uncertainty of an unqualified target, certain wellbores were selected to avoid certain intraformational stratigraphic targets while a few wells were to be avoided by any probable CO_2 plume.

Recent Advances in risk assessment and risk management of geologic CO_2 storage (Pawar et al., 2014)

This paper summarizes risk assessment and risk management as it has evolved over the last decade of geologic carbon storage, with a focus on offshore CO_2 storage. An important development has been the general improvement of risk definition, including the areas of performance, long term containment, public perception, and market risks. Looking at a broad range of demonstration projects globally allows for a meta-analysis of the work to date, how certain risk analyses define and communicate uncertainties, and finally allows for a proper understanding of the technical gaps that still exist in targeting and limiting risk during a storage project. The risks identified in this study helped guide the risk factor assessment efforts within the mid-Atlantic offshore study area. The paper also outlines how effective communication strategies play an integral role in increasing stakeholder confidence in a risk management setting. Highlights of the paper include:

- While the risk of CO_2 moving out of zone remains a primary concern. Existing data coverage and the quality of the containment system are key screening criteria for risk management. Also, locating sites where monitoring can be done effectively to prove conformance is an important consideration.
- Increased importance is being placed on understanding the likelihood and impact of brine displacement during injection operations, and its role as an important risk factor. Brine contamination of groundwater aquifers could be potentially much greater. (This finding highlights an advantage of off-shore CO_2 storage)
- The wellbore, near wellbore, and reservoir interaction system is crucial for controlling and efficiently operating a successful injection operative, and often initial completion plans will need to be revisited based on factual data obtained during initial injection operations.
- The collection, management, and analysis if downhole pressure gauge data should be prioritized as much as possible, as these data are essential for properly modeling the injection system through time
- Active engineering safeguards provide a first line of defense against adverse conditions, and this can be achieved by incorporating a sensor network with sufficient sensitivity, introducing logic-based decision making based on sensor data, and control responses effective enough to mitigate and control any potential adverse conditions during injection. These sensor networks can also be used to determine whether injection wells have suitable injectivity, need well intervention, or need to be abandoned in favor of a replacement well elsewhere.
- Wellbore CO_2 migration risks are primary over geologic pathway CO_2 migration in terms of likelihood of occurrence, and therefore projects must concentrate first on the additional monitoring safeguards necessary to ensure stability of the reservoir system.
- Multiple quantitative risk assessment methods have been developed in application towards storage projects; however, the variation of time scales necessary to prove permanent storage creates a gap in standardization that will require more refinement as these projects develop.

Developments since 2005 in understanding potential environmental impacts of CO_2 leakage from geological storage (Jones et al., 2015)

This summary report details 10 years of development in environmental impact assessment and risk understanding for onshore and offshore CO_2 storage projects, specifically in relation to the effects of CO_2 migration. This report highlights the various analytical techniques to understand subsea systemic effects, such as the use of laboratory experiments, natural analogue studies, and direct injection into shallow sediments as an analogue to deep injection CO_2 migration effects. Due to the limited ability to study direct CO_2 migration effects within the subsea system, modeling becomes a crucial component in understanding the spatial and temporal effects of injection and the risks inherent in any new injection project. A few key findings from study include:

- Any CO_2 migration from the geologic storage zone will impact two zones, both the near reservoir sediments and the CO_2 migration plume permeating the water column. Both leak events carry a necessary pH gradient change and is further impacted by the CO_2 migration rate.
- Baseline condition measurement can be difficult to determine due to the large spatial and temporal variance that occurs within a storage reservoir system. Local adaptation to environmental change complicates the dynamic characterization, and therefore gaps still exist in the ability to effectively capture the parameters necessary to model environmental impact within a system.
- CO_2 migration associated with existing boreholes and faults remain the likeliest possibility of occurrence. Higher CO_2 migration rates may be easily detected and thus remediated more quickly than a lower release rate from a smaller seep, giving a range of possibility that has to be considered and incorporated into any monitoring strategy.
- Natural seeps might provide a useful analogue generally, but more specifically may differ from CO_2 migration associated with storage reservoirs, as the geologic setting might vary between the two enough that they cannot be used as direct analogues.
- Little consideration has been given to brine CO_2 migration and CO_2 impurities that might cause additional impacts that need to be understood and monitored during the injection process.

References

1. Riis, F., & Halland, E. (January 01, 2014). CO_2 Storage Atlas of the Norwegian Continental Shelf: Methods Used to Evaluate Capacity and Maturity of the CO_2 Storage Potential. *Energy Procedia, 63,* 5258-5265.
2. Eiken, O., Ringrose, P., Hermanrud, C., Nazarian, B., Torp, T. A., & Høier, L. (January 01, 2011). Lessons learned from 14 years of CCS operations: Sleipner, In Salah and Snøhvit. *Energy Procedia, 4,* 5541-5548.
3. Mabon, L., Kita, J., & Xue, Z. (January 01, 2017). Challenges for social impact assessment in coastal regions: A case study of the Tomakomai CCS Demonstration Project. *Marine Policy, 83.*

4. Goebe, T., Nicolson, B.l, Hoffman, N., (February 1, 2016). Integrity of Wells in the Nearshore Area Gippsland Basin. Adapted from AAPG/SEG International Conference. Global CCS Institute.

5. GEOMAR Helmholtz Centre for Ocean Research Kiel (2015), ECO_2 Final Publishable Summary Report.

6. Pawar, R. J., Bromhal, G. S., Carey, J. W., Foxall, W., Korre, A., Ringrose, P. S., Tucker, O., ... White, J. A. (September 01, 2015). Recent advances in risk assessment and risk management of geologic CO_2 storage. *International Journal of Greenhouse Gas Control, 40,* 292-311.

7. Jones, D. G., Beaubien, S. E., Blackford, J. C., Foekema, E. M., Lions, J., Vittor, C., West, J. M., ... Queiros, A. M. (January 01, 2015). Developments since 2005 in understanding potential environmental impacts of CO_2 leakage from geological storage. *International Journal of Greenhouse Gas Control, 40,* 350-377.

Attachment I: Task 7 Stakeholder Education and Engagement Workplan

MID-ATLANTIC U.S. OFFSHORE CARBON STORAGE RESOURCE ASSESSMENT PROJECT

NATIONAL ENERGY TECHNOLOGY LABORATORY

Stakeholder Education and Engagement

1.0 Project Overview

The greatest potential for carbon storage in the northeastern United States lies in the offshore geologic formations comprising the continental shelf (Vidas and others, 2012). Offshore storage can be implemented close to large point-sources of carbon dioxide (CO_2) while avoiding many of the logistical difficulties and potential risks encountered when siting onshore projects, especially in densely populated areas of the East Coast. The technical, social and economic factors associated with offshore carbon storage have been discussed in literature (Schrag, 2009). Recent assessments of domestic offshore CO_2 storage suggest most storage potential is in sandstone and carbonate saline reservoirs, with less potential in depleted oil fields and enhanced oil recovery projects (e.g., Gulf of Mexico), as oil and gas development is currently prohibited in ~87% of U.S. offshore federal waters (Vidas and others, 2012; U.S. DOE NETL, 2012). Other potential storage formations, such as basalts, have not been comprehensively assessed, although they may become significant reservoir candidates in the Atlantic and Pacific (Vidas and others, 2012; Goldberg and others, 2010). Internationally, offshore CO_2 storage has been underway in Norway for the past 20 years and considerable research has been completed in countries including Japan, Australia, Brazil and South Africa. Offshore CO_2 storage assessment and research in the United States is still in its infancy, with significant uncertainty in potential storage resources resulting from a lack of geologic/petrophysical data and other unconstrained variables, particularly in the Mid- and North-Atlantic offshore areas (Vidas and others, 2012).

To address these data gaps and uncertainties, Battelle is leading a team of public and private entities with expertise in offshore geology to complete the Mid-Atlantic U.S. Offshore Carbon Storage Resource Assessment Project (the Project). The Project team includes state geological surveys of Delaware, Maryland and Pennsylvania; the United States Geological Survey-Woods Hole Coastal and Marine Science Center; Rutgers University; Harvard University; and Lamont-Doherty Earth Observatory at Columbia University. This team provides the U.S. Department of Energy (DOE) with multi-disciplinary

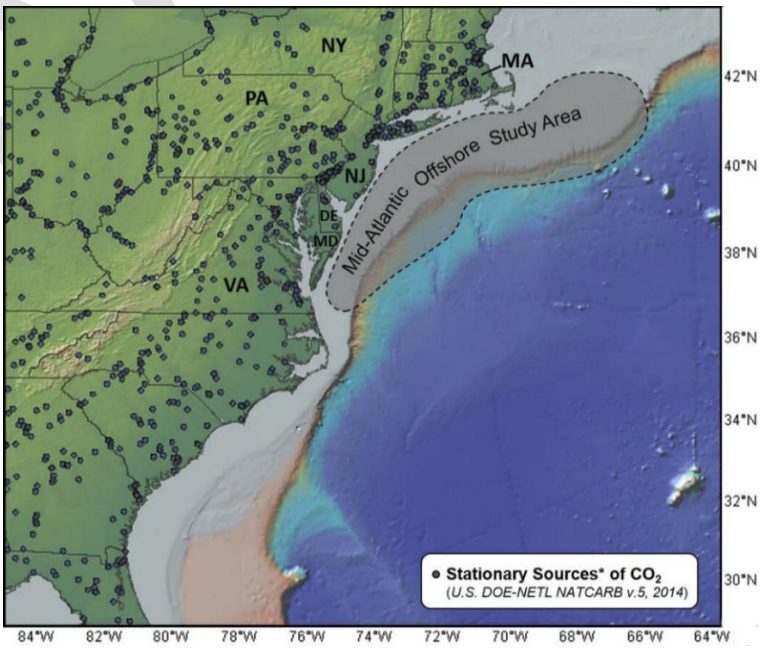

Figure 1. Map of the eastern United States coastal region showing location of the mid-Atlantic U.S. offshore study area, as well as locations of stationary CO_2 sources (U.S. DOE NETL, 2012; Ryan and others, 2009).

expertise to complete storage resource assessments for a broad region offshore of the U.S. East Coast, from Massachusetts to Virginia (Figure 1). Anticipated outcomes are high-level storage resource assessments of areas not previously characterized and improved storage resource estimates for geographically expansive portions of offshore geologic units, based on an integrated analysis of pre-existing geologic, seismic and core sample data for the Mid-Atlantic offshore area.

2.0 Education and Engagement Approach

The primary objective of the Project's Stakeholder Education and Engagement Plan (the Plan) is to build support for future carbon capture and storage (CCS) projects by developing and/or maintaining relationships with government agencies, utilities, industry and other interested parties throughout the Mid-Atlantic region. To this end, the Project team will reach out to these various stakeholders to provide educational and technical information on CO_2 storage resources for the region, as well as to gather feedback and input regarding short-term and long-term issues regarding the potential deployment of CCS technologies in the Mid-Atlantic U.S. offshore area. This two-way communication effort is intended to facilitate a greater understanding of the benefits of CCS in an offshore setting while garnering a high-level sense of how such activities may be planned, implemented and regulated from those agencies and entities who would be involved.

Given this approach, the Plan is comprised of four components, including two workshops, technology communication activities and technology transfer. The workshops will be particularly important to stakeholder education and engagement in that they provide a streamlined way to gather stakeholder perceptions, initiate information exchanges, identify potential project benefits and identify potential hurdles and how to address them. Technology communication activities will culminate in the development of a CCS planning document, and technology transfer will be accomplished through the development of a series of technical presentations and educational materials that describe important activities or findings of the Project team. Each of these components is described in more detail below.

1. Spring 2018 Stakeholder Outreach Meeting: A one-day meeting will be held in Cambridge, Massachusetts, at the Harvard University Center for the Environment (HUCE) to engage invited organizations to provide feedback regarding the Project team's preliminary findings and offer their insight on the planning and potential application of CCS technologies in the Mid-Atlantic U.S. offshore region in the years to come. Harvard University is committed to hosting a workshop with select team members and stakeholders and covering the travel and accommodation costs of the participants. HUCE has hosted numerous high-level workshops and discussions on energy and environment topics. HUCE will take the lead in developing the agenda and inviting participants in consultation with Battelle and the Pennsylvania Geological Survey (PaGS). A list of potential attendees to be invited to this meeting will be selected from the master list of government agencies, industries, technical groups and non-governmental organizations (NGOs) provided in Section 3.0 of this Plan. The workshop will likely be held during early 2018 and limited to about 25 participants.

2. Fall 2018 Industrial Outreach Meeting: The Project Team will host a one-day technical workshop to communicate the near-to-final Project results to invited industry and other interested parties in the governmental, environmental and NGO sectors (represented by the master list given in Section 3.0) and to be held at a yet-to-be-determined venue. Pennsylvania will take the lead in developing the agenda and inviting participants in consultation with Battelle and the Project team members.

3. Technology Communication Activities: A road map for future CCS project planning will be developed, which will incorporate input and feedback from attendees of the two outreach meetings. The road map will provide a synthesis of the Project findings; delineate risk factors for Mid-Atlantic U.S. Offshore Carbon Storage

Resource Assessment project areas; proffer an approach for closing data gaps regarding items such as transportation and infrastructure requirements; and summarize the accomplishments of the stakeholder education and engagement task.

4. Technology Transfer: Battelle and Project team members will develop and present technical papers at various professional meetings throughout the Project period. These include, but are not necessarily limited to, the Annual Carbon Capture Utilization and Storage (CCUS) Conference, Greenhouse Gas Control Technologies (GHGT) Conference and regional and/or national oil and gas industry meetings. In addition, a significant component of technology transfer will be through presentations, papers, and thesis prepared by graduate students working in team member institutions. A comprehensive listing of the technology transfer documents will be included in the Project's final report. In addition, a short list of fact sheets will be prepared to disseminate Project findings.

3.0 Potential Offshore CCS Stakeholders

The Project team will garner input from various organizations as we seek to engage open discussion and fact-based communications regarding offshore CCS opportunities. These organizations span both the private and public sectors, and include stakeholders in state and federal government agencies, electric utilities, technical and trade organizations and non-governmental organizations (NGOs). A current listing of entities with a history of involvement or interest in offshore related activities or CCS technology development, especially in the Atlantic Offshore is provided in Table 1. The Project team may revise and/or augment this list as necessary. The MRCSP stakeholder database will be used to help identify specific individuals, as well as Project team member networks. When needed, publicly available information will be used to identify individuals from the list of entities of interest but our new to our contact lists.

Table 1. Potential entities relevant for stakeholder education and engagement.

Federal Agencies	
U.S. Department of Energy Office of Fossil Energy	
U.S. Department of the Interior (DOI) Bureau of Ocean Energy Management (BOEM)	
U.S. Environmental Protection Agency (EPA) Regions 1, 2, 3 and 4	
U.S. National Oceanic and Atmospheric Administration (NOAA)	
National Marine Fisheries Service (NMFS)	
U.S. DOI Bureau of Safety and Environmental Enforcement (BSEE)	
State	**Public Utility Commissions**
DE	Public Service Commission
MA	Department of Public Utilities
MD	Public Service Commission
NJ	Board of Public Utilities
NY	Department of Public Service
PA	Public Utilities Commission
VA	State Corporation Commission Division of Public Utility Regulation
	National Association of Rural Utility Commissioners (NARUC)
State	**Conservation and/or Regulatory Agencies**
DE	Department of Natural Resources and Environmental Control
MA	Department of Energy Resources
MA	Department of Environmental Protection

MD	Department of Natural Resources
MD	Department of Natural Resources, Power Plant Research Program
MD	Department of the Environment
NJ	Department of Environmental Protection
NY	Department of Environmental Conservation
PA	Department of Conservation and Natural Resources
PA	Department of Environmental Protection
VA	Department of Conservation and Recreation
NRCan	Natural Resources Canada
Major Electric Utilities	
Dominion Resources	
Consolidated Edison	
Public Service Enterprise Group	
Constellation Energy Group	
Transmission Organizations	
Pennsylvania, New Jersey, Maryland Interconnection, LLC (PJM)	
Mid-Atlantic Area Council (MAAC)	
Northeast Power Coordination Council (NPCC)	
Industry / Economic Development	
New York City Economic Development Authority	
ArcelorMittal	
Occidental Petroleum	
Fugro	
Members of the Oil and Gas Climate Initiative (10 parties including Shell, BP, and Statoil)	
Regional Greenhouse Gas Initiative (RGGI)	
Professional Groups / CCS community	
Scottish CCS Center	
IEAGHG	
Society of Petroleum Engineers	
American Association of Petroleum Geologists	
Geological Society of America	
US Geological Survey	
Southeast Offshore Storage Resource Assessment Members (e.g., Southern Energy Board, Virginia Tech)	
Technical and Trade Organizations	
International Association of Geophysical Contractors (IAGC)	
American Petroleum Institute (API)	
Labor Unions	
Non-Governmental Organizations	
American Littoral Society	
Atlantic States Marine Fisheries Commission	
Cape Fear River Watch	
Center for a Sustainable Coast	
Center for Biological Diversity	
Center for Water Advocacy	
Chesapeake Bay Foundation	

Chesapeake Bay Group
Chesapeake Bay Seafood Industries Association
Citizens for Sound Conservation
Clean Ocean Action
Coastal Conservation League
Consumer Energy Alliance
Defenders of Wildlife
Earthjustice
Eastern Shore Defense Alliance
Environment New Jersey
Friends of South Shore Fisheries
Hampton Roads Chamber of Commerce
Legacy Offshore
Natural Resources Defense Council
New Jersey Sierra Club
Ocean Conservation Research
Oceana
Pender Watch and Conservancy
Sierra Club
Surfrider Foundation
The Nature Conservancy
Whale and Dolphin Conservation Society

4.0 Key Messages

Offshore CCS is an important strategy for emission reductions in the industry sector for northeastern U.S. However, the Project team recognizes that carbon storage is potentially several decades into the future and will require long-term planning. Establishing a foundation of knowledge and expertise now is critical for successful planning and implementation in the future. The current Project lays the foundation for these future CCS planning efforts by:

- Identifying the number and size of potential offshore storage reservoirs;
- Using current technology and scientific methods to assess legacy core, geophysical and seismic data for the Mid-Atlantic offshore region, thereby developing a comprehensive digital geologic database for this area that can be consulted by future projects;
- Recognizing potential risk factors associated with the deployment of offshore CCS; and
- Engaging interested parties through various technology transfer and outreach methods.

5.0 Outreach Methods and Materials

A variety of tools will be utilized to reach as diverse an audience as possible. These include, but aren't necessarily limited to, the following:

- Developing appropriate talking points, graphics and/or displays regarding the need for offshore CCS and potential timeline for deployment;
- Identifying key organizations involved in addressing potential hurdles to offshore CCS deployment;

- Preparing fact sheets describing important Project findings;
- Creating a master listing of presentations, outreach events and meetings attended by the Project team during the course of the Project;
- Conducting high-level meetings and workshops on the topic of offshore CCS deployment; and
- Providing a road map to guide future CCS planning and implementation work.

6.0 Timeline

Project completion is scheduled for December 31, 2018. The first outreach meeting for selected Project members and key stakeholder organizations is tentatively scheduled for March 2018. The second outreach meeting, intended as a technical workshop for industry and the CCS community, is tentatively planned for September 2018.

7.0 Project Team Roles and Responsibilities

The PaGS is responsible for the implementation of this Plan and will work closely with Battelle to ensure that all meetings, technology communication activities and technology transfer tasks are completed in a timely manner and are consistent with the project scope and objectives. In addition, PAGS will support and coordinate with Harvard University team members as they plan to host the first outreach meeting in Cambridge, Massachusetts.

The PaGS will query the Project team for input on meeting agendas and organization, technical presentations and topics for educational engagement, as needed. Contributions and comments will be solicited from team members as fact sheets are developed for public distribution. The Project team will also be asked to log any Project-related meetings they attend, presentations they give and/or outreach opportunities in which they participate into a master listing of outreach activities (see Section 5.0).

8.0 References Cited

Goldberg, D.S., D.V. Kent, and P.E. Olsen, 2010. Potential on-shore and off-shore reservoirs for CO2 sequestration in Central Atlantic magmatic province basalts, Proc. Nat. Acad. Sci., www.pnas.org/cgi/doi/10.1073/pnas.0913721107.

Ryan, W.B.F., S.M. Carbotte, J.O. Coplan, S. O'Hara, A. Melkonian, R. Arko, R.A. Weissel, V. Ferrini, A. Goodwillie, F. Nitsche, J. Bonczkowski, and R. Zemsky, 2009. Global multi-resolution topography synthesis, Geochem. Geophys. Geosyst., 10, Q03014, doi:10.1029/2008GC002332.

Schrag D.P., 2009. Storage of carbon dioxide in offshore sediments. Science 325, 1658-1659. DOI: 10.1126/science.1175750.

U.S. DOE NETL, 2012. Carbon utilization and storage atlas. U.S. Department of Energy, Office of Fossil Energy, National Energy Technology Laboratory.

Vidas, H., B. Hugman, A. Chikkatur, and B. Venkatesh, 2012. Analysis of the costs and benefits of CO_2 sequestration on the U.S. Outer Continental Shelf. U.S. Department of the Interior, Bureau of Ocean Energy Management. Herndon, VA. OCS Study BOEM 2012-100.

Attachment J: Road Map for Future CCS Project Planning and Implementation offshore of the Mid-Atlantic United States: Compilation of Research and Industry Views from Stakeholder Workshops

Memorandum

To: William O'Dowd, DOE-NETL

From: Neeraj Gupta and Lydia Cumming, Battelle; Kristin Carter and Brian Dunst, Pennsylvania Geological Survey

Date: December 7, 2018

RE: Road Map for Future CCS Project Planning and Implementation offshore of the Mid-Atlantic United States: Compilation of Research and Industry Views from Stakeholder Workshops

1. Introduction

Offshore carbon capture and storage (CCS) is an important strategy for reducing industrial emissions in the northeastern U.S. Furthermore, climate change experts consider CCS to be a keystone technology in the global mitigation of climate change[1]. However, widespread deployment of carbon storage will require sustained research and development (R&D) and policy framework development. Establishing a foundation of CCS knowledge and expertise now is critical for future successes in planning and implementation. The Mid-Atlantic U.S. Offshore Carbon Storage Resource Assessment Project (DE-FE0026087) lays the foundation for these future CCS planning efforts by:

- identifying the number and potential carbon dioxide storage capacity of offshore reservoirs in the study area;
- developing a comprehensive digital geologic database for this area that can be consulted by future projects;
- recognizing potential risk factors associated with the deployment of offshore CCS; and
- engaging stakeholders through various technology transfer and outreach methods.

While most of the Project research has been designed to answer technical questions, stakeholder engagement is an important strategic element for technology advancement. One outcome of this Project is a road map for future CCS project planning and implementation. A road map is a useful communication tool to assist R&D programs by facilitating stakeholder input and revealing a path for achieving desired outcomes.

2. Approach for Obtaining Stakeholder Input

The primary objective for stakeholder education and engagement is to build support for future CCS projects by developing and/or maintaining relationships with government agencies, utilities, industry and other interested parties throughout the Mid-Atlantic region. The Project team reached out to stakeholders to provide educational and technical information on CO_2 storage resources in the region, as well as to gather feedback and input on short- and long-term issues regarding the potential deployment of CCS technologies in the Mid-Atlantic U.S. offshore area. This two-way communication effort was intended to facilitate a greater understanding of the benefits of CCS in an offshore setting while garnering a high-level sense of how such activities may be planned, implemented and regulated from those agencies and entities that would be involved.

[1] International Energy Agency. Energy Technology Perspectives (2015). https://www.iea.org/etp/etp2015/

Two stakeholder workshops were held to provide a streamlined approach to gather stakeholder perceptions, initiate information exchanges, identify potential project benefits, and identify potential hurdles and how to address them. Technical presentations were provided at the meetings, followed by moderated discussion. The agenda, speakers, and attendees for both workshops are in Attachment A.

3. Key Takeaways from the Workshops

3.1 Spring 2018 Stakeholder Workshop

A one-day meeting was held in Cambridge, Massachusetts, at the Harvard University Center for the Environment to ask invited organizations to provide feedback regarding the Project team's preliminary findings and offer their insight on the planning and potential application of CCS technologies in the Mid-Atlantic U.S. offshore region in the years to come. Stakeholders included industry (e.g., Statoil, BP), non-governmental organizations (NGOs) (e.g., Natural Resources Defense Council, Clean Air Task Force), universities (MIT, UMASS Boston), and regulators (Norwegian Petroleum Directorate).

The roundtable discussion centered on three major themes, including: 1) developing appropriate regulations, 2) the role of this project and science-based data in fostering communication and public acceptance, and 3) addressing risk factors associated with CCS deployment. The key inputs from the with workshop are listed below:

- **Regulatory Framework:**
    - Norway has been performing offshore storage for 20+ years and has regulations and protocols in-place that could be referenced to help develop the regulatory framework in the USA.
    - The process of ranking sites has been important to Norway. The possibility of jobs in an onshore CO_2 plant provided a positive response.
    - In the U.S., the regulatory framework for offshore CCS is not well defined. Working with regulators and industry to build protocols and regulations that enable a project to move forward in a safe and timely manner is critical for success.
- **Science/Public Acceptance:**
    - The opportunity afforded by CCS technologies to mitigate climate change is timely and significant – the 'do nothing' option is not really an option at all. Even so, the entities that will most greatly benefit from CCS implementation should be determined so that they can be engaged early and often.
    - Public outreach needs to be incorporated early and continue throughout a project development phase to develop appropriate public outreach opportunities, technical and marketing content, and plans for focused engagement.
    - Stakeholders including regulators, NGOs, coastal communities and others must be a part of the outreach plan. Both known, current stakeholders and possible future stakeholders should be engaged to ensure effective outreach during all stages of project development and maturity.
    - NGOs can assist with early stakeholder outreach and will lend credence to any proposed technical work.
    - Any project will need to demonstrate its scientific merit and potential environmental benefits versus anticipated risks, as early as possible during project development.

- A neutral party is important for soliciting stakeholder input and providing information in situations where conflicts of interest are of concern.
- Continued focus on the scientific merit, advanced technologies being used and collaborative oversight of a CCS project will allow regulators to foster support.
- Risk mitigation (by way of providing critical scientific data and documentation of project successes) will be needed for financial institutions to back CCS projects.

- **Risk:**
  - A quantitative risk analysis is needed. Stakeholder concerns require thoughtful responses and should be addressed in the risk analysis and mitigation plan.
  - Perceived risk must be reduced. The scientific community has good reason to believe CCS works, but we must bolster understanding of CCS technologies, address risks, and maintain two-way communication to prevent the spread of misinformation.
  - Effective communication of project risk to bankers and investors may be another challenge. To address this issue, the Society of Petroleum Engineer's CO_2 Storage Resources Management System[2] can be adopted to communicate project risk and commercial potential to investors using an industry-standard classification framework.

3.2 Fall 2018 Stakeholder Workshop

The Project Team hosted a one-day technical workshop to communicate the near-to-final Project results to invited industry and other interested parties in the governmental, environmental and NGO sectors. This meeting was held in conjunction with the Midwest Regional Carbon Sequestration Partnership (MRCSP) 2018 Partners Meeting to maximize research and regional industry participation at the event. A series of technical factsheets that describe important activities and findings of the Project team, as well as a draft road map, were distributed at the workshop (see Attachment B).

A facilitated discussion was held to obtain specific input on the draft CCS road map presented at the workshop, including the following components: goals, strategies, milestones and timeline.

- **Goal:**
  - There was not enough information to reach a consensus on the desired project/program scale and timeline. For discussion purposes, an "early mover project" was envisioned as the end goal – this could be a pilot scale or a commercial scale project. However, the ultimate timing of the deployment will depend on the development of regulatory framework for carbon mitigation.
  - A suggestion was made to remove the offshore surface rig from the road map graphic and instead show images of the advanced subsea technologies used in the Snøhvit project that could be used to reduce the impact of project infrastructure/operations on coastal communities and ensure the offshore aesthetic is maintained.
- **Strategies:**
  - Early stakeholder outreach is critical. Key groups (e.g., NGOs) can be partners or roadblocks. CCS projects focus on U.S. coastal waters. Coastal communities could be great allies if we listen to their issues and can offer a direct positive economic impact to their communities.

[2] https://www.spe.org/industry/docs/SRMS.pdf

  - Regulatory and policy unknowns can make or break projects. Early mover CCS projects can help work towards development of appropriate regulations and establish regulatory certainty to promote investment, as well as to identify and implement policy mechanisms to facilitate targeted investment.

- **Milestones:**
  - A stakeholder outreach plan must be in place to garner offshore CCS champions by conveying key, targeted messages to coastal communities, international collaborators, NGOs and industry.
  - Establishing a practicable permitting/regulatory pathway is a necessary checkpoint to ensure success for CCS projects, and ultimately, CCS commercialization.
- **Timeline:**
  - The least cost portfolio for global climate change mitigation should be considered when developing the timeline. According to IEA (2018) scenario[3] for sustainable development, significant large-scale CCS deployment is needed by 2040.

4. Recommended Actions

Based on the stakeholder input received, the draft road map was revised and is shown in Figure 1. As shown in the road map, offshore CO_2 storage assessment and research of the mid-Atlantic U.S. is still in its early stages. This project represents an important first step by completing a high-level CO_2 storage resource assessment and building the knowledge infrastructure necessary to improve quantitative storage resource estimates. The data sets that have been curated under this project provide an opportunity to conduct R&D needed to address data gaps and reduce risk and uncertainty. Offshore characterization and validation strategies that are systematically designed to provide data and infrastructure that can be upscaled to meet commercial requirements should be developed. Recommended actions for future CCS project planning and implementation offshore of the Mid-Atlantic U.S. are listed below.

Near-Term Actions (Characterization Stage):

- As a practical next step, the Project team could use existing data sets to develop advanced static and dynamic geologic models to determine the geospatial variability of key storage parameters, complete the site screening process, and provide a better understanding of offshore subsurface storage opportunities and risks.
- Advanced reprocessing using existing seismic data and interpretation of modern seismic data from recent cruises should be performed to evaluate rift basin properties and reservoir capacity.
- A stakeholder outreach strategy to create champions for CCS R&D in the offshore region and streamline public acceptance of data collection in the marine environment should be implemented as early as possible.
- Identifying common industry and research goals for collaboration with international projects can build partnerships that lower research costs. Pursuit of onshore or analog data collection opportunities (e.g., drilling, core collection) could also help lower the cost of data collection.
- Development of regulatory certainty could be facilitated through U.S. regulator meetings with countries (e.g. Norway) where CCS is currently implemented and experiences from offshore oil and gas activities.

[3] International Energy Agency. 2018. World Energy Outlook. OECD/IEA WEO-2018. <https://www.iea.org/weo/>

Mid-Term Actions (Validation Stage):

- New data collection efforts should initially focus on addressing subsurface data gaps and requirements for qualifying potential sites, mitigating risk, and addressing potential regulatory/permit requirements.
- New data will be needed to validate caprock petrophysical properties, fracture pressure gradients, leakage risks, reservoir injectivity, and baseline geomechanical, geochemical, and hydrologic properties of storage zones and caprocks.
- Due to the higher costs and challenges associated with offshore characterization wells, a cost-benefit analysis will be needed to ensure the value of new data acquired meets the specific technical and economic requirements defined for the project.
- Appropriate monitoring methods will need to be investigated and validated prior to full-scale deployment and incorporated into the development phase plan.

Long-Term Actions (Development Stage):

- The development stage will establish and implement a detailed plan for large-scale CCS operations based on the findings of the preceding phases and the development of sufficient regulatory and pricing mechanisms to enable financially viable deployment. The progression to development also will depend on the strength of the stakeholder buy-in into the offshore CCS deployment in the mid-Atlantic area.
- The development stage activities typically include the assessment of CO_2 sources and transport, final site selection, detailed design, permitting, construction, operations, and monitoring. Advances in offshore technologies, such as advanced characterization, robotics, sub-sea structures, safety mechanisms, and remote operations over the next decade may facilitate cost-effective deployment with enhanced stakeholder confidence.
- Early mover projects in the U.S. and globally may help accelerate deployment of CCS through upscaling of technologies that reduce economic and policy barriers to commercial scale CCS.

5. Closing

This memorandum was prepared to document the results of two stakeholder workshops held to solicit input on what stakeholders, including Project team members, think should be done to advance offshore CCS research. We plan to draft a white paper to present a research path to address technical challenges in more detail. We will be glad to discuss these recommendations with you later on and follow through on any questions or suggestions you have.

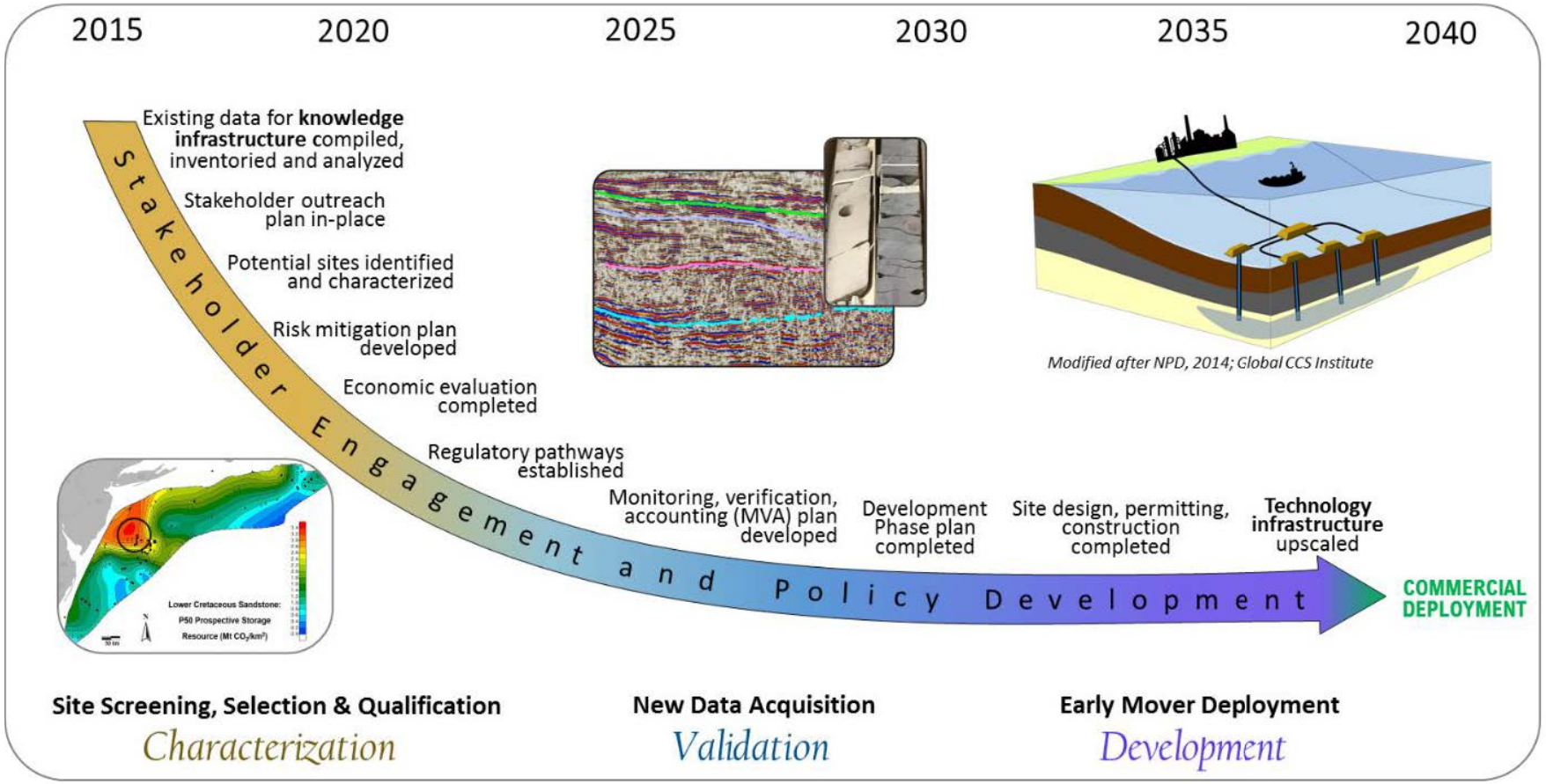

Figure 1. Draft Final Mid-Atlantic Offshore CCS Deployment Road Map

ATTACHMENT

STAKEHOLDER WORKSHOP HANDOUTS

SPRING 2018 STAKEHOLDER WORKSHOP

Stakeholder Workshop Agenda

MID-ATLANTIC U.S. OFFSHORE CARBON STORAGE RESOURCE ASSESSMENT PROJECT

Tuesday, April 3, 2018, 9:30 am to 3:30 pm
Harvard University Center for the Environment (HUCE), Cambridge Massachusetts

Meeting Host: Dan Schrag, Harvard University and Neeraj Gupta, Battelle

Meeting Purpose: The purpose of this meeting is to reach out to stakeholders to provide information on CO_2 storage resources for the region and to gather feedback and input regarding short-term and long-term issues for the potential deployment of CCS technologies in the Mid-Atlantic U.S. offshore area. This two-way communication effort is intended to facilitate a greater understanding of the benefits and challenges of CCS in an offshore setting while garnering a high-level sense of how such activities may be planned, implemented and regulated from those agencies and entities who would be involved.

Registration and Networking 9:30 AM

Welcomes and Opening Presentations 10:00 AM

Background and Lessons from Other Locations:

- *Setting the Stage: Offshore CCS Deployment in the Mid-Atlantic US (Dan Schrag, Harvard)*
- *Statoil's Offshore CO_2 Geologic Storage Experience (Philip Ringrose, Statoil)*
- *CO_2 Geologic Storage Assessments – Gulf of Mexico (*Tip Meckel, Texas Bureau of Economic Geology)
- *Environmental Regulations of Subsea Storage - Norway* (Eva Halland, Norwegian Petroleum Directorate)

Mid-Atlantic Carbon Storage:

- *Mid-Atlantic Carbon Storage Resource Assessment Project Overview (Neeraj Gupta, Battelle)*
- *Identifying and Quantifying Potential Mid-Atlantic Offshore Storage (Ken Miller, Rutgers)*
- *Discussion*

Lunch - 12:30 PM

The Path Forward - Moderated Discussion 1:30 PM

Facilitator: Dan Schrag, Harvard

- *How offshore storage could develop in areas like the Atlantic offshore*
- *Technical Evaluation and Data Availability*
- *Regulatory Issues*
- *Stakeholder Acceptance*

Workshop Ends 3:00 PM (reception to follow)

Harvard University
Center for the Environment

Stakeholders Workshop for the Mid-Atlantic U.S. Offshore Carbon Storage Resource Assessment Project
April 3, 2018

KRISTIN CARTER
Pennsylvania Geological Survey
krcarter@pa.gov

Kristin Carter serves as Assistant State Geologist for the Pennsylvania Geological Survey (the Survey) and manages its Economic Geology Division. She has worked as a petroleum geologist for the Survey since 2001, and her current research efforts involve carbon capture utilization and storage, unconventional petroleum hydrocarbon reservoir characterization, storage reservoir characterization and subsurface stratigraphy. Kristin serves as the Survey's Primary Investigator in its work with the Mid-Atlantic U.S. Offshore Carbon Storage Resource Assessment Project and the Midwest Regional Carbon Sequestration Partnership (MRCSP). She managed Pennsylvania's Carbon Sequestration Technical Assessment in 2009, an assessment of the state's subsurface geologic formations for CO_2 storage potential (prepared in accordance with Act 129 of 2008). Prior to joining the Survey, Kristin worked as a consulting hydrogeologist in the private sector, managing projects throughout the Mid-Atlantic region. In addition to her work at the Survey, she serves as an Adjunct Instructor in the Geology Department at Allegheny College (Meadville, PA) and as Eastern Region Vice President of the Potential Gas Committee (Colorado School of Mines, Golden, CO).

DAVID CASH
University of Massachusetts Boston
david.cash@umb.edu

David W. Cash is Dean of the John W. McCormack Graduate School of Policy and Global Studies at University of Massachusetts Boston. Dean Cash joined the McCormack Graduate School in July 2015. He has spent his career trying to understand and better harness knowledge to solve pressing policy challenges. Spending the past decade in Massachusetts state government in catalytic roles, Dean Cash helped to transform the commonwealth's energy and environmental policy and regulatory landscape. His job history includes positions in Massachusetts state government as Commissioner at the Department of Environmental Protection and

Harvard University
Center for the Environment

the Department of Public Utilities, and as Assistant Secretary of Policy at the Executive Office of Energy and Environmental Affairs. In these roles, he helped develop and implement nation-leading science-based environmental, climate, clean energy, water and waste management regulatory programs; innovative renewable energy and grid modernization efforts; and the development and implementation of the Regional Greenhouse Gas Initiative–the nation's first CO_2 cap-and-trade program. While working in state government positions, Dean Cash extended his efforts internationally, participating in a U.S. State Department mission to India on clean energy and climate and via USAID collaborations with regulators and policymakers in Tanzania and Ghana. Dean Cash was also a research fellow and lecturer in environmental science and public policy at Harvard University and, as a PhD student, was a White House global environmental policy intern at the Council on Environmental Quality. He has published numerous professional, peer-reviewed academic and lay articles and book chapters. He earned a PhD in public policy from the Kennedy School at Harvard University, concentrating in environment and natural resources. He also completed an MAT in science education from Lewis & Clark College and a BS in biology from Yale.

JAMES CROYLE
SCS Energy
jcroyle@scsenergyllc.com

James Croyle is CEO of SCS Energy and Hydrogen Energy California, the latter a project company requiring CCS to get built. Prior to HECA he was CEO of Purgen and in that capacity analyzed storing CO_2 off the coast of New Jersey. In 2011 Purgen was moved to the Central Valley in California after acquiring development rights in Kern County from British Petroleum. He has considerable experience with the regulatory and political environments related to energy project development both as a banker to the industry and an energy project developer. Mr. Croyle served as the President of the 1,200 MW Astoria Energy Project from 1999 to 2007 and previously had executive management responsibility for several large power projects. Mr. Croyle holds a PhD from Harvard University's Government Department.

LYDIA CUMMING
Battelle
cummingl@battelle.org

Lydia Cumming is a Project Manager at Battelle, an independent research and development organization. She has managed national and international collaborative research projects to advance carbon capture and storage (CCS) technologies through assessment of technical, risk, and other factors. She has performed outreach and project development activities for five CCS field projects in the Midwestern U.S. Her experience gained from flagship initiatives such as the Regional

Harvard University
Center for the Environment

Carbon Sequestration Partnerships and the Carbon Storage Assurance Facility Enterprise, as well as CCS Capacity Building Trust Fund projects in China and Mexico, has given her a deep appreciation for science driven innovation and collaboration. She is currently the project manager for the Mid-Atlantic U.S. Offshore Carbon Storage Resource Assessment Project, which is part of the U.S. Department of Energy's Carbon Storage Program to improve the effectiveness and reduce the costs of carbon storage. Ms. Cumming earned her Bachelor's degree in Geology from The Ohio State University, Columbus, Ohio.

BRIAN DUNST
Pennsylvania Geological Survey
bdunst@pa.gov

Brian J. Dunst, P.G. is currently a geologist supervisor with the PA Geological Survey in Pittsburgh. He supports the Survey's oil and gas well drilling tracking system (EDWIN), the Mid-Atlantic U.S. Offshore Carbon Storage Resource Assessment Project, MRCSP (Midwest Region Carbon Sequestration Partnership), and the recently completed Utica Shale play (2015) and ASH (Appalachian Storage Hub, 2017) studies. He is the Survey's seismicity and brine disposal (non-regulatory) contact. Prior to his current position, he worked in several regulatory programs, and has also been employed as a consultant in mining and oil and gas.

EMRE GENÇER
MIT Energy Initiative
egencer@mit.edu

Emre Gençer is a postdoctoral researcher in the MIT Energy Initiative since September 2016. His research interests focus on efficient and integrated process design, renewable energy conversion, multi-scale modeling and optimization. Currently, he is working on a multi-level systems analysis of carbon capture, utilization, and storage technologies and developing a novel modular life cycle analysis tool. Emre holds a PhD in Chemical Engineering from Purdue University. He received both a BSc in Chemical Engineering and BSc in Mathematics from Bogazici University in Istanbul, Turkey.

Harvard University
Center for the Environment

DAVID GOLDBERG
Columbia University
goldberg@ldeo.columbia.edu

David S. Goldberg is a Lamont Research Professor and serves as Associate Director of the Marine/Large Programs Division at the Lamont-Doherty Earth Observatory of Columbia University. His research has focused on geological carbon sequestration, marine methane hydrates, and related scientific technologies. He has published over 140 peer-reviewed articles and holds 5 patents. Goldberg has supervised field operations, engineering developments and other activities related to marine and continental drilling and mentored 11 Columbia University graduate students and 19 post-doctoral research scientists. He received B.S. and M.S. degrees in geophysics from Massachusetts Institute of Technology and a PhD degree in geophysics from Columbia University.

NEERAJ GUPTA
Battelle
gupta@battelle.org

Neeraj Gupta, a Senior Research Leader/Battelle Fellow at Battelle, provides technical and program development leadership for Battelle's subsurface resources work. He has over 25 years of domestic and international experience in CO_2 storage, CO_2-EOR, and other subsurface projects as a Principle Investigator, Project Manager, or technical advisor. He has led several field programs and research projects on CO_2 storage technology including leadership of the Midwestern Regional Carbon Sequestration Partnership (www.MRCSP.org), CO_2 storage pilot at the Mountaineer power plant in West Virginia, and regional assessments of CO_2 storage, Mid-Atlantic U.S. offshore carbon storage resource assessment, Enhanced Oil Recovery (EOR), and brine disposal in US. Dr. Gupta has also conducted international projects for CO_2 storage assessments in China, Mexico, Japan, Germany, and South Africa. Neeraj holds a PhD in Geological Sciences from The Ohio State Universities, an MS in Geochemistry from George Washington University, an MS and BSc in Geology from Panjab University, India.

Harvard University
Center for the Environment

EVA HALLAND
Norwegian Petroleum Directorate
eva.halland@npd.no

Eva Halland has held various positions within the Norwegian Petroleum Directorate (NPD), and has been a member of the management team for 17 years. Her responsibilities have included petroleum exploration, field development, field production, regulations and HSE. Her present position is as Project Director for the Norwegian CO_2 Storage Atlas and CO_2 storage projects in Norway. She is also Project Manager for FORCE, a co-operating forum for improved oil and gas recovery and improved exploration between 43 oil companies and authorities in Norway. She is Director of the Programme Board of CLIMIT, NORSAR and Natural History Museum in Oslo, member of the North Sea Basin Task Force and member of the bilateral CCS co-operation between Norway and USA. She is the leader of the Norwegian "CO_2 Storage Forum". She was the Norwegian project leader for the UK-Norway ministerial CCS project "One North Sea" and appointed member of the selection panel and project advisor for the appraisal of UK CO_2 storage sites. Eva is a member of the South African Pilot CO_2 Storage Project International Advisory Committee. She is an educated geologist from the University of Bergen, Norway.

HOWARD HERZOG
MIT Energy Initiative
hjherzog@mit.edu

Howard J. Herzog is a senior research engineer in the MIT Energy Initiative. He received his undergraduate and graduate education in chemical engineering at MIT. He has industrial experience with Eastman Kodak (1972-1974), Stone & Webster (1975-1978), Aspen Technology (1981-1986), and Spectra Physics (1986-1988). Since 1989, he has been on the MIT research staff, where he works on sponsored research involving energy and the environment, with an emphasis on greenhouse gas mitigation technologies. He was a Coordinating Lead Author for the IPCC Special Report on Carbon Dioxide Capture and Storage (released September 2005), a co-author on the MIT Future of Coal Study (released March 2007), and a US delegate to the Carbon Sequestration Leadership Forum's Technical Group (June 2003-September 2007). He was awarded the 2010 Greenman Award by the IEAGHG "in recognition of contributions made to the development of greenhouse gas control technologies".

Harvard University
Center for the Environment

JONATHAN HODGKINSON
BP
Jonathan.Hodgkinson@bp.com

Having spent twenty years in the merchant banking and commodities trading industry Jonathan moved into the geological sciences after reading for a BSc at the Birkbeck University of London and receiving a PhD from the Queensland University of Technology in Brisbane. After initial tenure as a coal geologist for the Geological Survey of Queensland he became the program manager and subsequently the director of the Queensland Carbon Geostorage Initiative jointly funded by the State and Federal governments and the Australian Coal Association. He moved to the private sector and worked for BG and Shell as a principal hydrogeologist and senior reservoir engineer before joining BP America in 2017 as a consultant CCUS Subsurface Technologist. His interests are focused across a broad spectrum of geological and reservoir engineering topics including basin analysis, petroleum hydrodynamics, geochemistry, mineral stability and reservoir management and optimization strategies.

FRANCINE KERSHAW
Natural Resources Defense Council
FKERSHAW@NRDC.ORG

As part of NRDC's Marine Mammal Protection Project and Oceans Program, Francine Kershaw identifies areas of the ocean that are crucial for marine mammals and then assesses how vulnerable those areas are to human impacts. She combines information on marine mammal behavior, genetics, and oceanography using geospatial tools to advocate for and improve marine mammal protections. Prior to joining NRDC, Kershaw worked at the United Nations Environment Programme World Conservation Monitoring Centre in Cambridge, U.K. She holds a bachelor's degree in zoology from the University of Leeds and a master's degree in biodiversity, conservation, and management from the University of Oxford. She earned her PhD in ecology and evolutionary biology from Columbia University. Kershaw is a member of the IUCN Joint WCPA/SSC Marine Mammal Protected Area Task Force (MMPATF). She works out of NRDC's New York office.

Harvard University
Center for the Environment

PETER McLAUGHLIN
Delaware Geological Survey
ppmclau@udel.edu

Peter P. McLaughlin, Jr. is Senior Scientist at University of Delaware's Delaware Geological Survey and has a secondary faculty appointment as Professor in the Department of Geological Sciences. McLaughlin has been with the University of Delaware since 1999, before which he worked for 10 years in research, exploration, and management positions at a major oil company. McLaughlin was raised in Dover, Delaware and holds a BS in Geology from the University of Delaware and a PhD in Geology from Louisiana State University. McLaughlin's primary research interests are sequence stratigraphy, micropaleontology, groundwater, and clastic depositional systems. His projects utilize many of the tools and techniques used in the oil industry to address ground-water issues of importance to Delaware. He has recently developed a research interest in geologic sequestration of carbon dioxide and the carbon storage potential of subsurface geologic formations both offshore and onshore in the U.S. Middle Atlantic region.

TIP MECKEL
Bureau of Economic Geology, University of Texas, Austin
tip.meckel@beg.utexas.edu

Dr. Tip Meckel is a research scientist investigating geologic carbon storage for the Bureau of Economic Geology at The University of Texas at Austin. During his 12 years with the Gulf Coast Carbon Center at the Bureau he has led research focusing on geologic characterization, structural geology, monitoring design, and pressure evolution for CO_2 injections. He has been directly involved with many large-scale field demonstration projects funded through the DOE-NETL Regional Carbon Sequestration Partnerships. During the past 8 years he has led the research initiative to identify offshore sequestration potential in the Gulf of Mexico with focus on capacity assessment and high-resolution 3D marine seismic monitoring technologies.

Harvard University
Center for the Environment

KEN MILLER
Rutgers University
kgm@eps.rutgers.edu

Kenneth G. Miller is a Distinguished Professor in the Department of Earth and Planetary Sciences at Rutgers University, Co-Chair of the International Ocean Discovery Program Science Evaluation Panel, and Vice Chair, of Subcommission on Neogene Stratigraphy of the International Commission on Stratigraphy. He received an A.B. from Rutgers College (1978) and a Ph.D. from the Massachusetts Institute of Technology/Woods Hole Oceanographic Institution Joint Program in Oceanography (1982). He was an Associate Research Scientist at Lamont-Doherty Geological Observatory from 1983-1988. A veteran of 8 scientific cruises, he has integrated offshore seismic and drilling activities with onshore drilling: since 1993, he has been Chief Scientist of the New Jersey Coastal Plain Drilling Project (Ocean Drilling Program Legs 150X and 174AX) that continuously cored sixteen sites. Author of over 100 peer-reviewed scientific papers, his most significant publications include widely cited synthesis of Cenozoic oxygen isotopes (Miller et al., 1987) and syntheses of global sea-level change (Miller et al., 1998, 2005, 2011, 2013). He was awarded the 2003 Rosenstiel Award from the University of Miami, is a two-time JOI/USSAC Distinguished Lecturer (1995, 2006) and an AAPG Distinguished Lecturer (2014-2015) and a Fellow of the American Geophysical Union and the Geological Society of America. A resident of Pennington, NJ, Ken grew up in Medford, NJ in the heart of the pine barrens and just sold his house in Waretown, NJ, the home of the sounds of the NJ pines, where he used to watch the inexorable rise in sea level from his deck 15 ft above Barnegat Bay.

STEVE MURPHY
Pale Blue Dot
steve.murphy@pale-blu.com

Steve Murphy has been working in the emerging CO_2 transportation and storage space since co-founding CO_2DeepStore in 2007. Project Acorn was one of the first project concepts that the company developed. The company was acquired by Petrofac and became a 50% partner in the 1st Goldeneye storage joint venture. The team did an MBO & formed Pale Blue Dot Energy in 2013 to provide strategy advice to clients involved in the energy transition. Steve has led many significant studies in CCS, including the Teesside ICCS project and the ETI CO_2 storage appraisal project. He is currently the Project Director for the Acorn project, which was recently awarded ~ €2.4m funding through the ACT co-fund program. Steve has degrees in Geophysics, Petroleum Engineering, and Business coupled with

Harvard University
Center for the Environment

around 33 years of broad experience. He describes one of his specialties as helping people make sense of complex situations and minimizing bias in strategic decision-making.

WILLIAM O'DOWD
National Energy Technology Laboratory, DOE
William.ODowd@NETL.DOE.GOV

FRANCIS O'SULLIVAN
MIT Energy Initiative
frankie@mit.edu

Dr. Francis O'Sullivan is Director of Research for the MIT Energy Initiative, and a Senior lecturer at the MIT Sloan School of Management. He works on topics related to energy technologies, policy and economics. His current research is focused on unconventional oil and gas resources, particularly the productivity and economics of North America's shale resources. He also studies global gas market dynamics, and how power systems are evolving to accommodate large-scale generation from renewable resources, particular solar power. He has written and spoken widely on these topics, and has made presentations to the President's Office of Science and Technology Policy, the EIA, the EPA, the Brookings Institute, the Bipartisan Policy Center, the Center for Strategic and International Studies, the National Governors' Association, the National Association of Regulated Utility Commissioners, at CERAWeek, the American Physical Society, the American Geophysical Union and to a range of other academic, policy and industry forums. He is a lead author of both the 2011 MIT Future of Natural Gas study, and the 2015 MIT Future of Solar Energy study.

Dr. O'Sullivan is a member of the U.S. National Academies' Roundtable on Science and Technology for Sustainability, and is a Senior Associate with the Energy and National Security Program at the Center for Strategic and International Studies. He has also served as a member of the U.S. Secretary of Energy's working group on methane emissions and as a member of the scientific advisory board for the Environmental Defense Fund's methane emissions campaign.

Harvard University
Center for the Environment

PHILIP RINGROSE
Statoil
phiri@statoil.com

Philip Ringrose is a specialist in CO_2 storage and petroleum geoscience at the Statoil Research Centre in Trondheim, Norway. He is also Adjunct Professor in CO_2 Storage at the Norwegian University of Science and Technology (NTNU) in Trondheim. He was elected as 2014-2015 President of the European Association of Geoscientists and Engineers (EAGE). He has BSc and PhD degrees in geology from Universities of Edinburgh and Strathclyde, Scotland, UK. He has published widely on reservoir geoscience and flow in rock media, and has recently published a textbook on Reservoir Model Design. He is Co-Editor for the journal Petroleum Geoscience.

TRACI RODOSTA
National Energy Technology Laboratory, Department of Energy
Traci.Rodosta@NETL.DOE.GOV

DAN SCHRAG
Harvard University
schrag@eps.harvard.edu

Daniel Schrag is the Sturgis Hooper Professor of Geology, Professor of Environmental Science and Engineering at Harvard University, and Director of the Harvard University Center for the Environment. His primary appointment is in the Department of Earth and Planetary Sciences in the Faculty of Arts and Sciences. He serves as Area Dean for Environmental Science and Engineering in the John A. Paulson School of Engineering and Applied Sciences and also co-directs the Program on Science, Technology and Public Policy at the Harvard Kennedy School with John Holdren. Dan's interests include climate change, energy technology, and energy policy. He has studied climate change over the broadest range of Earth's history, including how climate change and the chemical evolution of the atmosphere influenced the evolution of life in the past, and what steps might be taken to prepare for impacts of climate change in the future. He helped to develop the hypothesis that the Earth experienced a series of extreme glaciations, called "Snowball Earths" that may have stimulated a rise in atmospheric oxygen and the proliferation of multicellular animals. He is also interested in how we can use climate events in the geologic past to understand our current climate challenges. Dan has worked on a range of issues in energy technology and policy including advanced technologies for low-carbon transportation fuel, carbon capture and

Harvard University
Center for the Environment

storage, and risks and opportunities of shale gas. He was named a MacArthur Fellow in 2000 and served from 2009 to 2017 on President Obama's Council of Advisors for Science and Technology (PCAST), contributing to many reports to the President including energy technology and national energy policy, agricultural preparedness, climate change, and STEM education.

DAVID SPEARS
Virginia Department of Mines, Minerals and Energy
David.Spears@dmme.virginia.gov

David B. Spears is the State Geologist of Virginia. Based in Charlottesville, he manages the Division of Geology and Mineral Resources, which serves as the state geological survey. After earning a B.S. in Geology from Lafayette College and an M.S. in Geology from Virginia Tech, David began his professional career as a petroleum geologist for Chevron USA in 1983. With assignments in New Orleans and Lafayette, Louisiana, he developed oil and gas prospects using classical concepts of stratigraphy and structural geology, guided by geophysical well logs and seismic data. In 1993, David joined Virginia's geological survey as an economic geologist. His work there covered a wide range of topics including the mapping of abandoned mines, database management, field mapping in complexly deformed terranes, and assessment of natural gas resources in the Appalachian basin. From 2005 to 2009, David served as the Policy Manager for the state's Department of Mines, Minerals and Energy, where he led a major study that resulted in the development of Virginia's first offshore energy policy. During this time, he was selected by the Secretary of the Interior to serve on the Outer Continental Shelf Policy Committee. David was appointed State Geologist in 2009. He is a member of the Geological Society of America, the Society of Economic Geologists, the American Association of Petroleum Geologists, and is currently Past President of the Association of American State Geologists. He serves on the Committee on Earth Resources at the National Academies of Sciences, Engineering, and Medicine and recently completed a term as a member of the Geology and Public Policy Committee of the Geological Society of America. He has been a Professional Geologist (ASBOG) since 2002.

ANN WEEKS
Clean Air Task Force
aweeks@catf.us

Ann Weeks is the Legal Director at the Clean Air Task Force, and in that capacity she advocates for CCS as a climate mitigation technology, and has written on subseabed CCS regulatory issues. Ann holds a JD from UNC-Chapel Hill, an SM from MIT, and a BS from Boston University.

FALL 2018 STAKEHOLDER WORKSHOP

Mid-Atlantic U.S. Carbon Storage Resource Assessment Offshore Workshop Agenda

Wednesday, November 14, 2018
Historic Inns of Annapolis
58 State Circle
Annapolis, MD 21401

MID-ATLANTIC U.S. OFFSHORE CARBON STORAGE RESOURCE ASSESSMENT PROJECT

8:00 – 9:00 am ***Check-in / Continental Breakfast***

9:00 – 10:45 am ***Welcomes, Project Overview, Regional Framework***

Welcomes / Introductions	Kristin Carter, PAGS
Mid-Atlantic Offshore Program Introduction	Neeraj Gupta, Battelle
Developing Structural Framework from Legacy Seismic	David Goldberg, LDEO
Hydrogeological Assessment from Log and Core Archives	Peter McLaughlin, DGS
An Integrated Geologic Storage Framework for Atlantic Offshore	Ken Miller, Rutgers

10:45 – 11:00 am *Break*

11:00 am – 12:45 pm ***Risk Factors, Storage Resources, Road Mapping***

Storage Resources in the Mid-Atlantic Continental Shelf	Isis Fukai, Battelle
Evaluating Deployment Risk Factors	Joel Sminchak, Battelle
Considering Regulatory Issues	Melissa Batum, BOEM
Global Significance of Offshore Storage – Well Known and Frontier Areas	Sue Hovorka, BEG
Developing a “Sleipner” off the East Coast	Facilitated Discussion

1:00 pm – 1:45 pm ***Combined MRCSP Annual Meeting/Workshop Networking Lunch***

Speakers and Facilitators

Melissa Batum – *Bureau of Ocean Management*

Melissa Batum, P.G. is a Senior Program Analyst for the Bureau of Ocean Energy Management, U.S. Department of the Interior.

Kristin Carter – *Pennsylvania Geological Survey*

Kristin Carter serves as Assistant State Geologist and manages the Economic Geology Division of the Pennsylvania Department of Conservation and Natural Resources (DCNR) Bureau of Topographic and Geologic Survey. She has worked as a petroleum geologist for the Survey since 2001, and her research efforts include evaluating depleted/depleting oil and gas fields as potential storage reservoirs; characterizing unconventional petroleum hydrocarbon reservoirs; tracking oil and gas exploration, production and well abandonment activity for the state; interpreting Appalachian basin subsurface stratigraphy; and mapping subsurface geologic formations. Kristin served as Project Manager for DCNR's Carbon Sequestration Technical Assessment project, which was mandated by PA Act 129 of 2008 and completed in August 2009. She serves as Primary Investigator for the Survey's participation in both the Midwest Regional Carbon Sequestration Partnership's and the Mid-Atlantic U.S. Offshore Carbon Storage Resource Assessment Project's research. Kristin is licensed as a Professional Geologist by the Commonwealth of Pennsylvania and as a Certified Petroleum Geologist by the American Association of Petroleum Geologists.

Lydia Cumming – *Battelle*

Ms. Cumming is a Project Manager at Battelle, an independent research and development organization. She has managed national and international collaborative research projects to advance carbon capture and storage (CCS) technologies through assessment of technical, risk, and other factors. She has performed outreach and project development activities for five CCS field projects in the Midwestern U.S. Her experience gained from flagship initiatives such as the Regional Carbon Sequestration Partnerships and the Carbon Storage Assurance Facility Enterprise, as well as CCS Capacity Building Trust Fund projects in China and Mexico, has given her a deep appreciation for science driven innovation and collaboration. She is currently the project manager for the Mid-Atlantic U.S. Offshore Carbon Storage Resource Assessment Project, which is part of the U.S. Department of Energy's Carbon Storage Program to improve the effectiveness and reduce the costs of carbon storage. Ms. Cumming earned her B.S. in Geology from The Ohio State University, Columbus, Ohio.

Brian Dunst – *Pennsylvania Geological Survey*

Brian J. Dunst, P.G. is currently a geologist supervisor with the PA Geological Survey in Pittsburgh. His supports the Survey's oil and gas well drilling tracking system (EDWIN), the Mid-Atlantic U.S. Offshore Carbon Storage Resource Assessment Project, MRCSP (Midwest Region Carbon Sequestration Partnership), and the recently completed Utica Shale play (2015) and ASH (Appalachian Storage Hub, 2017) studies. He is the Survey's seismicity and brine disposal (non-regulatory) contact. Prior to his current position, he worked in several regulatory bureaus, and has also been employed as a consultant in mining and oil and gas.

Isis Fukai – *Battelle*

Isis Fukai is a geologist for Battelle's Energy Division where she currently leads various geologic characterization and CO_2 storage resource assessment efforts. Her responsibilities include assisting with field operations for characterization wells, petrophysical analysis, CO_2-EOR techno-economic analysis, and storage resource estimation. Prior to joining Battelle, Isis participated in carbon storage research as a Mickey Leland Energy Fellow and ORISE Research Associate at the U.S. Department of Energy National Energy Technology Laboratory. She is also an active committee member of the Society of Petroleum Engineer's CCUS Technical Section and contributor to the Storage Resource Management System. Isis received her Bachelor's degree from Oberlin College and her Master's degree from Louisiana State.

Speakers and Facilitators

Dave Goldberg – *Lamont-Doherty Earth Observatory of Columbia University*

David S. Goldberg is a Lamont Research Professor and serves as Associate Director of the Marine/Large Programs Division at the Lamont-Doherty Earth Observatory of Columbia University. His research has focused on geological carbon sequestration, marine methane hydrates, and related scientific technologies. He has published over 140 peer-reviewed articles and holds 5 patents. Goldberg has supervised field operations, engineering developments and other activities related to marine and continental drilling and mentored 10 Columbia University graduate students and 19 post-doctoral research scientists. He received B.S. and M.S. degrees in geophysics from Massachusetts Institute of Technology and a PhD degree in geophysics from Columbia University.

Neeraj Gupta- *Battelle*

Neeraj Gupta provides technical integration and program development leadership for the Battelle's carbon management and subsurface resources work. Dr. Gupta joined Battelle in 1993 and is currently a Senior Research Leader in the Energy Group at Battelle. Dr. Gupta has been involved in CO_2 storage technology development since mid-1990s has conducted numerous US and international projects for the US DOE and industry. As the Principal Investigator and Project Manager for Midwestern Regional Carbon Sequestration Partnership, Dr. Gupta oversees a consortium for regional assessment of field projects for CO_2 storage and Enhanced Oil Recovery (EOR), including MRCSP Michigan Basin Project. His subsurface resources work includes EOR, brine disposal, geologic characterization; regional hydrogeology; reservoir simulations; geochemical modeling and experiments; seismic assessments; and costing and regulatory aspects.

Susan D. Hovorka – *Gulf Coast Carbon Center, Bureau of Economic Geology*

Susan Hovorka is a sedimentologist who works on fluid flow in diverse applications, inlcuding water resource protection, oil production, and waste storage. She has led a team working geologic storage of CO_2 since 1998, with a focus on field studies, monitoring, and capacity estimation. Projects include saline injection at the Frio Test site and Cranfield Field and EOR studies at SACROC oil field, Cranfield, Hastings and West Ranch industrial CO_2 utilization projects. She specializes in monitoring to document retention. The Gulf Coast Carbon Center is leading efforts to develop offshore storage capacity in the the US and globaly.She has a long-term commitment to public and educational outreach. She has a BA from Earlham College and a PhD in Geology from The University of Texas at Austin.

Peter P. McLaughlin, Jr – *Delaware Geological Survey*

Peter P. McLaughlin, Jr. is Senior Scientist at University of Delaware's Delaware Geological Survey and has a secondary faculty appointment as Professor in the Department of Geological Sciences. McLaughlin has been with the University of Delaware since June 1999, before which he worked for ten years in research, exploration, and management positions in the petroleum industry. McLaughlin was raised in Dover, Delaware and holds a B.S. in Geology from the University of Delaware and a Ph.D. in Geology from Louisiana State University. McLaughlin's primary research interests are sequence stratigraphy, microfossils, groundwater, and clastic depositional systems. His projects utilize many of the tools and techniques used in the oil industry to address ground-water issues of importance to Delaware. He has recently developed an interest in geologic sequestration of carbon dioxide and the carbon storage potential of subsurface geologic formations both offshore and onshore in the U.S. Middle Atlantic region.

Speakers and Facilitators

Kenneth G. Miller – *Rutgers University*

Kenneth G. Miller is a Distinguished Professor in the Department of Earth and Planetary Sciences at Rutgers University, Co-Chair of the International Ocean Discovery Program Science Evaluation Panel, and Vice Chair of Subcommission on Neogene Stratigraphy of the International Commission on Stratigraphy. He received an A.B. from Rutgers College (1978) and a Ph.D. from the Massachusetts Institute of Technology/Woods Hole Oceanographic Institution Joint Program in Oceanography (1982). He was an Associate Research Scientist at Lamont-Doherty Geological Observatory from 1983-1988. A veteran of 8 scientific cruises, he has integrated offshore seismic and drilling activities with onshore drilling: since 1993, he has been Chief Scientist of the New Jersey Coastal Plain Drilling Project (Ocean Drilling Program Legs 150X and 174AX) that continuously cored sixteen sites. Author of over 100 peer-reviewed scientific papers, his most significant publications include widely cited synthesis of Cenozoic oxygen isotopes (Miller et al., 1987) and syntheses of global sea-level change (Miller et al., 1998, 2005, 2011, 2013). He was awarded the 2018 Laurence L. Sloss Award for Sedimentary Geology, 2003 Rosenstiel Award from the University of Miami, is a two-time JOI/USSAC Distinguished Lecturer (1995, 2006) and an AAPG Distinguished Lecturer (2014-2015) and a Fellow of the American Geophysical Union and the Geological Society of America. A resident of Pennington, NJ, Ken grew up in Medford, NJ in the heart of the pine barrens and just sold his house in Waretown, NJ, the home of the sounds of the NJ pines, where he used to watch the inexorable rise in sea level from his deck 15 ft above Barnegat Bay.

Joel Sminchak – *Battelle*

Joel Sminchak is a hydrogeologist in the Energy Division at Battelle Memorial Research Institute. He received his BSc from the University of Dayton, MSc from Ohio State University, and recently completed the Dog Training Course at Columbus Humane Society. He has been active in research on reservoir characterization, geotechnical testing, wellbore integrity, risk analysis, and performance monitoring for geologic CO_2 storage and other subsurface investigations.

MID-ATLANTIC U.S. OFFSHORE CARBON STORAGE RESOURCE ASSESSMENT PROJECT

Project Overview

The greatest potential for carbon storage in the northeastern United States lies in the offshore geologic formations comprising the continental shelf[1]. Offshore storage can be linked to large point-sources of carbon dioxide (CO_2) while avoiding many of the logistical difficulties and potential risks encountered when siting onshore projects, especially in densely populated areas of the East Coast. The technical, social and economic factors associated with offshore carbon storage have been discussed in literature[2]. Recent assessments of domestic offshore CO_2 storage suggests a majority of the storage potential is in sandstone and carbonate saline reservoirs, with less potential in depleted oil fields and enhanced oil recovery projects (e.g., Gulf of Mexico), as oil and gas development is currently prohibited in ~87% of U.S. offshore federal water[1,3]. Other potential storage formations, such as basalts, have not been comprehensively assessed, although they may become significant reservoir candidates in the Atlantic and Pacific[1,4]. Internationally, offshore CO_2 storage has been underway in Norway for the past 20 years and considerable research has been completed in countries including Japan, Australia, Brazil, and South Africa. Offshore CO_2 storage assessment and research in the United States is still in its infancy, with significant uncertainty in potential storage resources resulting from a lack of geologic/petrophysical data and other unconstrained variables, particularly in the mid- and north- Atlantic offshore area[1].

Global estimates suggest that 40% of the potential CO_2 storage resource in deep saline aquifers is located offshore in widespread porous and permeable sandstones and shelf carbonates (IEAGHG, 2009).

Given the current knowledge base and access to publicly available data, the objectives of the Mid-Atlantic U.S. Offshore Carbon Storage Resource Assessment Project are fourfold: 1) complete a systematic carbon storage resource assessment of the mid-Atlantic Offshore coastal region from the Georges Bank Basin through the Long Island Platform to the southern Baltimore Canyon Trough; 2) define key input parameters to reduce uncertainty for offshore storage resource and efficiency estimates; 3) perform a preliminary assessment of risk factors, uncertainties and data gaps; and 4) engage industry and regulatory stakeholders through development of a road map to assist future project planning and implementation.

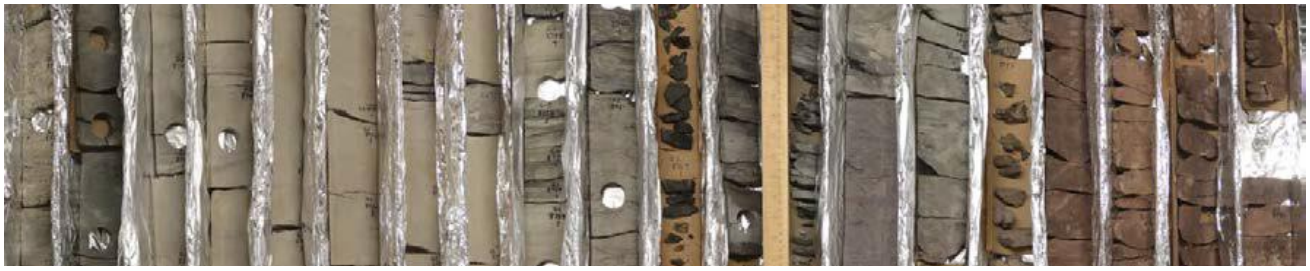

Image showing existing core material from the Continental Offshore Stratigraphic Test (COST) wells, which will be correlated with geophysical logs used to characterize rock properties relevant to carbon storage resource assessments

This project will prepare a realistic portrayal related to offshore CO_2 storage resource assessment by:

- Defining the ***geologic characteristics*** of candidate storage sites
- Using existing ***seismic data*** to better define the continuity of the storage zones and seals
- Cataloguing the ***hydrogeologic properties*** of mid-Atlantic offshore storage sites
- Calculating ***prospective CO_2 storage resources*** using net effective pore volumes and fluid displacement properties specific to offshore lithologies
- Examining ***risk factors*** related to offshore storage
- ***Communicating*** with industry and other stakeholders about the future prospects for offshore storage
- Ensuring ***technology transfer*** to industry and other stakeholders

Led by Battelle, this project is being conducted by public and private entities with expertise in offshore geology and resources for the study region, including state geological surveys of Delaware, Maryland and Pennsylvania; United States Geological Survey-Woods Hole Coastal and Marine Science Center; Rutgers University; Harvard University; and Lamont-Doherty Earth Observatory at Columbia University. This project team provides the U.S. Department of Energy with multi-disciplinary expertise to complete storage resource assessment for a broad region offshore of the U.S. East Coast, from Massachusetts to Virginia. The team will build on the success of the Midwest Regional Carbon Sequestration Partnership program (www.mrcsp.org), using a regional approach for screening and identifying candidate storage sites with the potential to deliver the most value for the East Coast. Anticipated outcomes are high-level storage resource estimates for areas not previously characterized and improved storage resource estimates for geographically expansive portions of offshore geologic units.

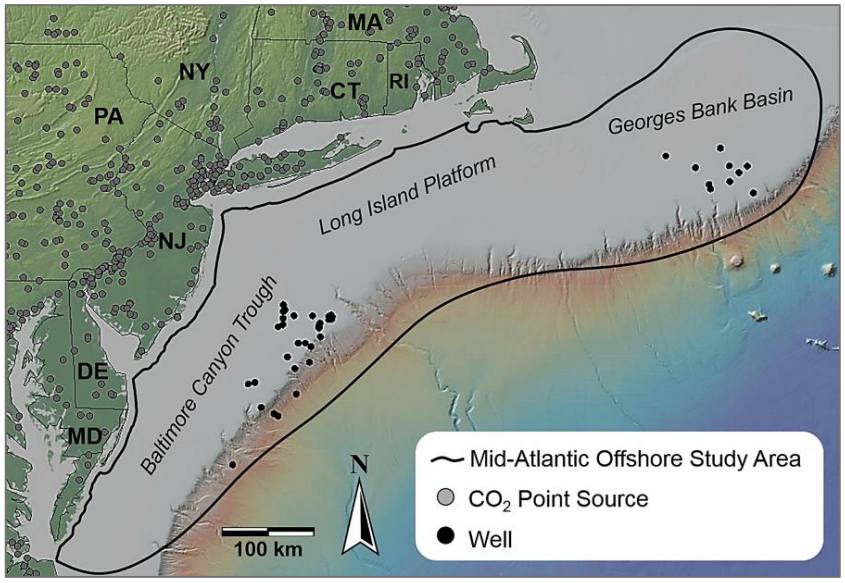

Map of the eastern United States coastal region showing location of the mid-Atlantic U.S. offshore study area, as well as locations of stationary CO_2 sources[3, 5]

Point of Contact

Neeraj Gupta, Battelle Principal Investigator, gupta@battelle.org.

References Cited

1 Vidas, H., B. Hugman, A. Chikkatur, and B. Venkatesh, 2012. Analysis of the costs and benefits of CO_2 sequestration on the U.S. Outer Continental Shelf. U.S. Department of the Interior, Bureau of Ocean Energy Management. Herndon, VA. OCS Study BOEM 2012-100.

2 Schrag D.P., 2009. Storage of carbon dioxide in offshore sediments. Science 325, 1658-1659. DOI: 10.1126/science.1175750.

3 US-DOE-NETL, 2012. Carbon Utilization and Storage Atlas. U.S. Department of Energy, Office of Fossil Energy, National Energy Technology Laboratory.

4 Goldberg, D.S., D.V. Kent, and P.E. Olsen, 2010. Potential on-shore and off-shore reservoirs for CO_2 sequestration in Central Atlantic magmatic province basalts, Proc. Nat. Acad. Sci., www.pnas.org/cgi/doi/10.1073/pnas.0913721107.

5 Ryan, W.B.F., S.M. Carbotte, J.O. Coplan, S. O'Hara, A. Melkonian, R. Arko, R.A. Weissel, V. Ferrini, A. Goodwillie, F. Nitsche, J. Bonczkowski, and R. Zemsky, 2009. Global multi-resolution topography synthesis, Geochem. Geophys. Geosyst., 10, Q03014, doi:10.1029/2008GC002332.

CO_2 Storage Resource Estimation

Estimates of CO_2 storage were calculated for Cretaceous- and Jurassic-age sandstones to establish preliminary, screening-level constraints on the geologic CO_2 storage resources in the Mid-Atlantic U.S. offshore study region. The assessment was carried out using a step-wise approach that included: **(1)** data integration and mapping, **(2)** regional-scale storage resource estimates, and **(3)** local-scale dynamic injection and storage simulation.

Data Integration

The CO_2 storage resource of offshore deep saline formations were quantified following static volumetric and dynamic methods. Static methods employ estimates of subsurface pore volumes and in-situ fluid saturations to derive an equivalent quantity of CO_2 that could occupy the pore space in a given storage reservoir. Dynamic methods use numerical models to simulate the CO_2 injection and storage performance of a reservoir under specific pressure, time, and operational constraints.

POTENTIAL OFFSHORE STORAGE ZONES

The Middle Cretaceous Logan Canyon sandstone (MK1-3), Lower Cretaceous Missisauga sandstone (LK1) and Upper Jurassic Mohawk (UJ1) units were identified as potential storage zones based on ***screening criteria derived from the risk factor analysis*** in this project and recommended best practices for onshore CO_2 storage[1].

DATASETS AND WORKFLOW

Geophysical logs from 44 existing offshore test well locations were scanned and digitized to inform interpretations of storage zone lithofacies and petrophysical properties. Seismic and well log sequence stratigraphy was used to define storage zone depth, thickness, and lateral continuity. Biostratigraphic data provided age control to help align and correlate storage zone lithofacies with sequence boundaries. ***Log data was integrated with laboratory-derived core analyses*** to better characterize effective reservoir porosity and permeability. The newly ***reprocessed seismic data provided by this project were also used to derive estimates of porosity*** in areas without well data.

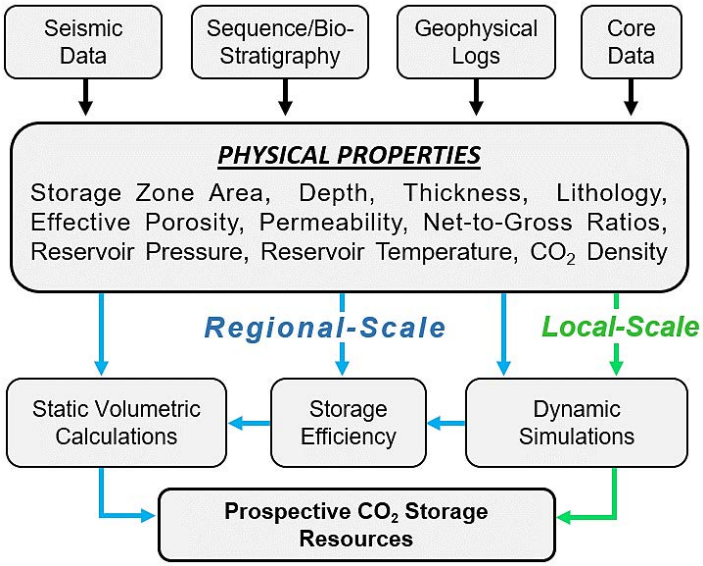

Schematic showing data input and workflow used for estimating offshore CO_2 storage resources.

STORAGE EFFICIENCY AND CALCULATION METHODS

The integrated dataset was used to develop regional maps of depth, thickness, and porosity for each storage zone within an area of ~115,000 km^2. Map grids served as input for CO_2 storage resource calculations using the static volumetric methodology[2] and CO_2-SCREEN tool[3] developed by DOE-NETL for onshore deeps saline formations. CO_2 storage efficiency is generally defined as the ratio of CO_2-occupied pore volume relative to a total pore volume, and is dependent on the specific geologic and fluid properties the reservoir(s) being evaluated for storage[4]. ***Offshore-formation specific storage efficiency values were determined*** using regional statistical and geospatial distributions of net-to-gross pore volume and permeability for the three storage zones of interest. Regional results were then mapped and locations exhibiting high CO_2 storage resource per area that were also constrained by data from three or more nearby wells were selected for further evaluation using dynamic simulation.

Regional-Scale CO_2 Storage Resource

Average effective reservoir ***porosities ranging from 21- 29% and average permeabilities ranging from 45 - 339 millidarcies*** are observed in the storage zones of interest based on detailed petrophysical analysis of available well data. These values are within range of values reported for other offshore reservoirs used for commercial-scale CO_2 storage[5].

Using formation-specific probability values derived from regional data distributions in the study area, ***calculated storage efficiencies ranged from 1% to 13%,*** with median values of 5% and 3% computed for the Cretaceous sandstones and the Upper Jurassic sandstone, respectively.

Storage Zone	Avg. Net Reservoir Properties	
	Porosity (%)	Permeability (mD)
Middle Cretaceous (MK1-3)	23 -27	71 - 314
Lower Cretaceous (LK1)	26 - 29	65 - 339
Upper Jurassic (UJ1)	21 - 25	45 - 264

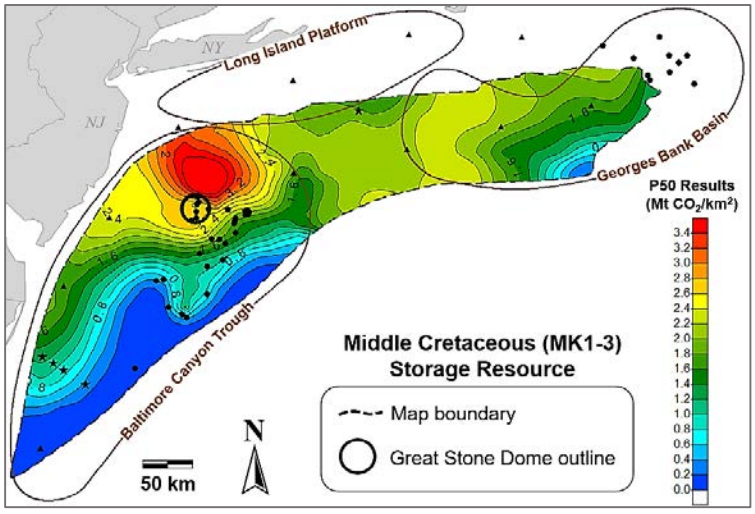

Map showing results of the regional prospective storage resource calculation (P50) for the Middle Cretaceous storage zone

Regional prospective storage resource estimates range from 37 to 403 gigatonnes (Gt) of CO_2, with median values of 148, 178 and 153 Gt computed for the Middle Cretaceous, Lower Cretaceous, and Upper Jurassic storage zones, respectively.

Local-Scale Dynamic Simulation

Dynamic CO_2 injection and storage simulation was conducted using a simplified three-dimensional site model in a selected area of the northern Baltimore Canyon Trough near the Great Stone Dome. The simulation was conducted for the lower sequence (51 m thick) of the Middle Cretaceous sandstones using an injection rate of 1.5 megatonnes (Mt) per year and a single injection well. The ***local-scale simulation results show 45 Mt of CO_2 can be stored over 30 years*** within the pressure constraints considered to be safe.

Regional estimates and dynamic simulation results both suggest ***a single offshore storage zone could potentially store commercial quantities of CO_2*** emitted from a nearby power plant or industrial source in the mid-Atlantic region. Additional data analysis and acquisition is needed to reduce uncertainty associated with data gaps throughout the offshore study area. Development of a three-dimensional static earth model to better characterize the variability of reservoir properties would provide valuable constraints on storage resource estimates and would aid in identification of candidate sites for further characterization, validation and development.

Point of Contact: Dr. Neeraj Gupta, Battelle Project Manager, gupta@battelle.org.

References Cited

1. DOE-NETL (U.S. Department of Energy-National Energy Technology Laboratory). 2017. Best Practices for Site Screening, Selection, and Initial Characterization for Storage of CO_2 in Deep Geologic Formations. DOE/NETL-2017/1844.
2. Goodman, A., S. Sanguinito, and J. Levine. 2016. Prospective CO_2 resource estimation methodology: Refinement of existing US DOE-NETL methods based on data availability. Int. J. Greenh. Gas Con., vol. 54, pp. 242-249.
3. Sanguinito, S., A. Goodman, and J.S. Levine. 2016. NETL CO_2 Storage prospeCtive Resource Estimation Excel aNalysis (CO_2-SCREEN) User's Manual; NETL-TRS-X-2016; Technical Report Series; U.S. Department of Energy, National Energy Technology Laboratory: Pittsburgh, Pennsylvania, 2016; p. 31. https://edx.netl.doe.gov/carbonstorage/?page_id=914.
4. Bachu, S. 2015. Review of CO_2 storage efficiency in deep saline aquifers. Int. J. Greenh. Gas Con 40, 188-202.
5. Norwegian Petroleum Directorate. 2011. CO_2 Storage Atlas: Norwegian North Sea. Norwegian Petroleum Directorate, Stavanger. www.npd.no/Global/Norsk/3-Publikasjoner/Rapporter/PDF/CO2-ATLAS-lav.pdf.

MID-ATLANTIC U.S. OFFSHORE CARBON STORAGE RESOURCE ASSESSMENT PROJECT

Risk Factor Analysis

A risk factor analysis was conducted as part of the Mid-Atlantic U.S. Offshore Carbon Storage Resource Assessment Project to determine whether the offshore area is suitable for geologic storage of carbon dioxide (CO_2). The analysis considered ***geologic risk factors***, ***long-term CO_2 storage risks***, and ***environmental factors*** related to the permanent storage of CO_2 in Mid-Atlantic U.S. Offshore study area.

Geologic CO_2 storage risk management process defined by the U.S. DOE-NETL[1].

Geologic Risk Factors

CO_2 CONTAINMENT: Overlying the storage zones, thick layers of Upper Cretaceous shale and mudstone occur as ***regionally continuous caprocks*** across the study region and would prevent CO_2 migration to the surface.

SEDIMENTOLOGICAL AND STRUCTURAL FEATURES: At shallower depths (<1000 m), caprocks and storage zones may occur as unconsolidated sediments subject to soft sediment deformation and CO_2 phase changes, suggesting ***lower risk at storage depths >1000 m***. Evidence of faulting was identified in localized areas near the continental slope.

SEISMICITY AND GEOMECHANICS: The eastern margin of the North American continent is a passive margin, meaning tectonic plates are not actively colliding, and very few historical earthquakes have occurred in the study region. The 2014 U.S. Geological Survey National Seismic Hazard Map[2] shows a mostly low hazard probability along this margin. Faults and geomechanical stability along the continental slope present a moderate risk factor, suggesting areas near ***the slope should be avoided*** during storage.

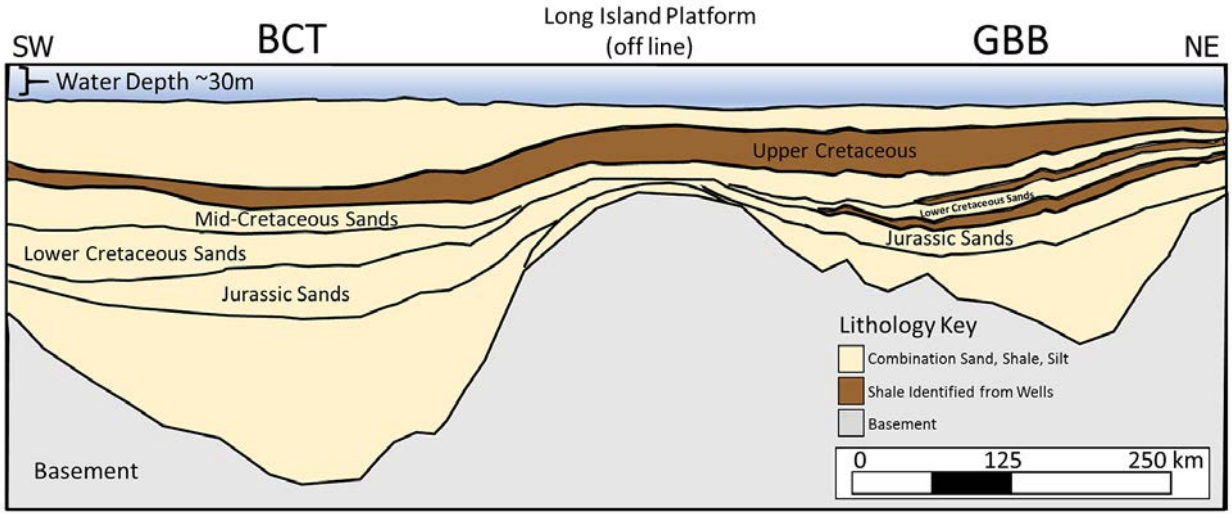

Cross-section showing regional distribution of caprocks (shale, brown) and storage zones (sandstone, tan) defined by seismic correlation across the Baltimore Canyon Trough (BCT), Long Island Platform, and Georges Bank Basin (GBB).

Long-Term CO_2 Storage Risks

Offshore CO_2 confinement and trapping mechanisms are important for ensuring long-term CO_2 storage security and permanence. CO_2 acts as a supercritical fluid below storage depths of about 1,000 m in the offshore study area, where it exhibits a higher density similar to liquid, but will flow more readily like gas. Stored CO_2 will be less dense than formation brine and will buoyantly rise to the top of the storage zone and become trapped by various mechanisms.

In the offshore study area, ***CO_2 trapping mechanisms were not identified as significant risk factors***. The majority of CO_2 stored is estimated to be trapped as a free-phase fluid in structural and stratigraphic traps. ***Approximately 34% of the CO_2 is estimated to be trapped in a less mobile state*** via residual trapping in intergranular pores, dissolution in formation brine, and mineral carbonation reactions.

General structural trends and analogous onshore-offshore depositional systems suggest up-dip migration inshore is restricted by inherent structural and lithographic traps.

A more detailed, local assessment of confining rock properties, CO_2 migration pathways, and trapping mechanisms should be conducted at candidate sites to address long-term risks.

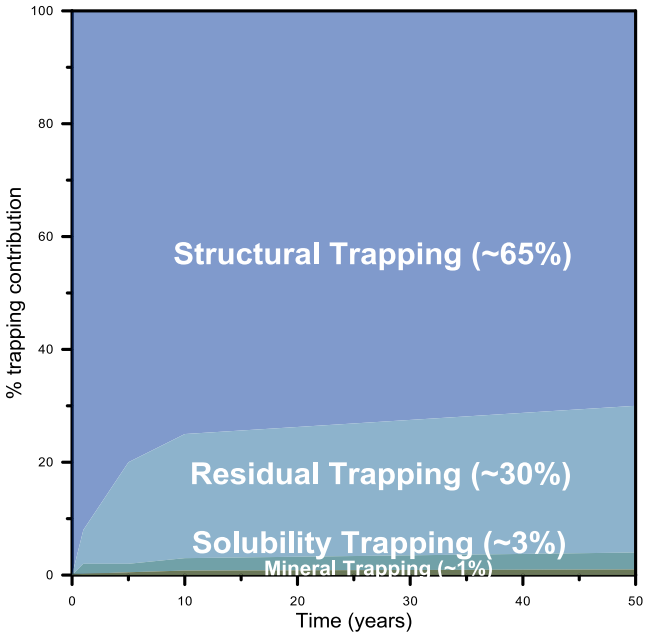

Graph showing the quantity of CO_2 estimated to be trapped by four main trapping processes in the study area

Environmental Factors

Environmental factors can have a significant impact on the deployment strategy and overall success of a potential CCS project. CO_2 storage projects involve activities such as drilling, infrastructure construction and seismic surveys that may cause environmental risks or disturbances. Some environmental factors identified as important considerations for a CO_2 storage project in the mid-Atlantic offshore study area include:

- marine life migration patterns, protected and sensitive species and marine habitats
- existing infrastructure and offshore activities such as shipping lanes, submarine cables, and ocean disposal sites
- low leakage risk from the few existing wellbores (44)
- distance from population centers and CO_2 sources

No highly critical geologic, environmental, or long-term storage risk factors were identified that would preclude deployment of CCS in the Mid-Atlantic U.S. Offshore study region.

These environmental factors should be considered when determining potential storage site locations and timing of project activities in order to reduce risks and minimize impacts to marine life, marine habitats, and other environmentally-sensitive offshore features in the study area.

Point of Contact: Dr. Neeraj Gupta, Battelle Principal Investigator, gupta@battelle.org.

References Cited

1. U.S. Department of Energy-National Energy Technology Laboratory (DOE-NETL). 2017. Risk management and Simulation for Geologic Storage Projects. DOE/NETL-2017/1846.

2. Petersen, M. D., Moschetti, M. P., Powers, P. M., Mueller, C. S., Haller, K. M., Frankel, A. D., Zeng, Y., Rezaeian, S. C., Harmsen, S., Boyd, O. S., Field, E. H., Chen, R., Rukstales, K. S., Luco, N., Wheeler, R. L., Williams, R.A., Olsen, A. H., 2014. Documentation for the 2014 update of the United States national seismic hazard maps: U.S. Geological Survey Open-File Report 2014–1091, 243 p.

3. Bureau of Ocean Energy Management (BOEM). 2014. Atlantic OCS Proposed Geological and Geophysical Activities Mid-Atlantic and South Atlantic Planning Areas Final Programmatic Environmental Impact Statement, Task Order No. M11PD00013. 788 p.

MID-ATLANTIC U.S. OFFSHORE CARBON STORAGE RESOURCE ASSESSMENT PROJECT

Road Map for U.S. Offshore CCS Deployment

Carbon capture and storage (CCS) is a critical technology for ensuring a range of clean energy options are available to meet current and future energy demand in the U.S. and abroad. The objectives of the Mid-Atlantic U.S. Offshore Carbon Storage Resource Assessment Project are to:

1) complete a systematic carbon storage resource assessment of the U.S. mid-Atlantic Offshore region
2) identify key input parameters to reduce uncertainty for offshore storage resource and efficiency estimates
3) prepare a preliminary assessment of risk factors, uncertainties and data gaps
4) engage industry and regulatory stakeholders through development of a road map to assist future project planning and implementation

The road map for full-scale development of carbon capture and storage (CCS) in the U.S. Mid-Atlantic offshore is illustrated below.

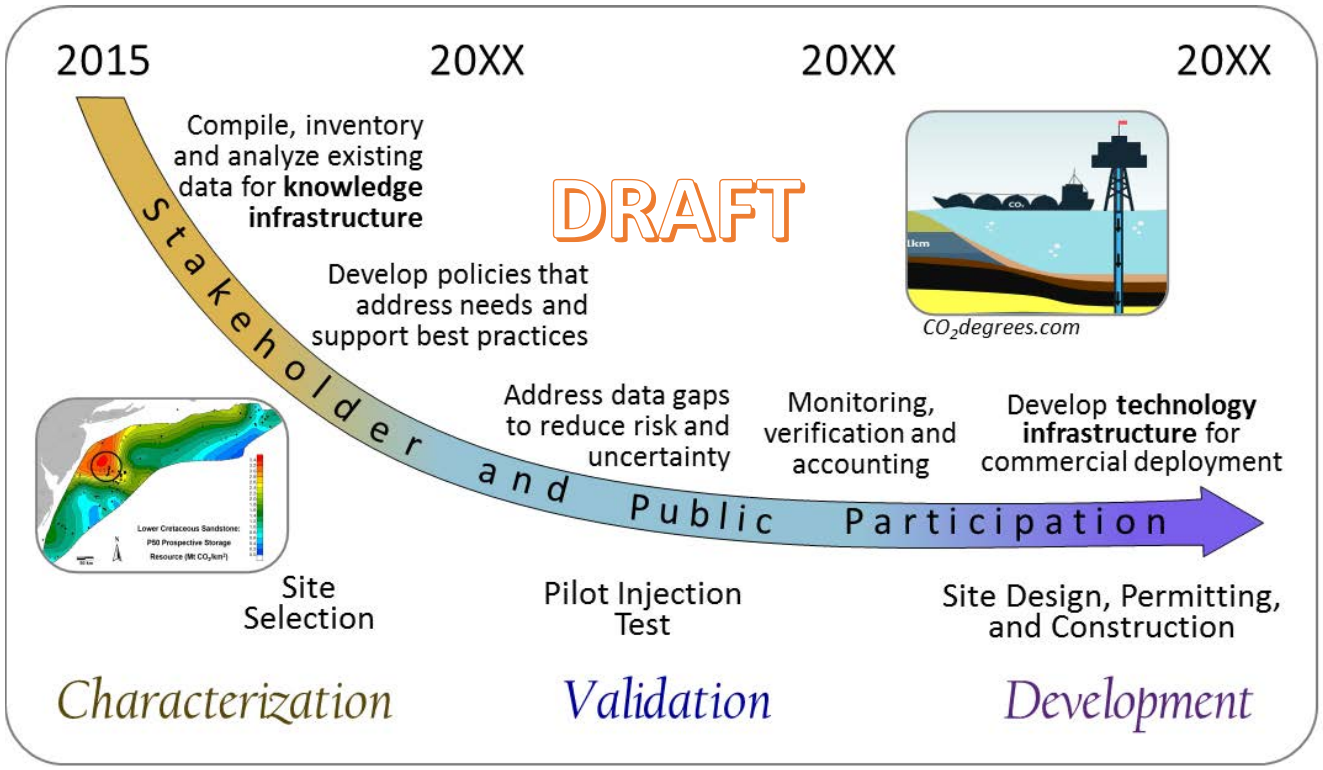

Road map for development of knowledge and technology infrastructure needed to support full-scale offshore carbon storage

Characterization: Establishing the Foundation for Knowledge Infrastructure

Over the past three years, the Project has compiled, inventoried, and assimilated various publicly available data sets to provide a strong technical basis on which future carbon storage studies and applications can be built. The knowledge infrastructure necessary to support the development of full-scale offshore carbon storage must be able to ***communicate*** our need for clean, secure energy in the context of domestic options (fuel switching, onshore storage and offshore storage); ***provide*** useful, organized data already available for the Mid-Atlantic U.S. offshore region; and ***transfer*** onshore technology knowledge in a prudent way to offshore applications.

Key Project Outcomes To-Date

SUBSURFACE DATA ANALYSIS:

- Legacy seismic, well log, core, and biostratigraphic data was digitized, reprocessed, and analyzed using modern techniques, augmenting previous characterization efforts.
- Prospective storage resource estimates suggest Mid-Atlantic U.S. Offshore formations can potentially store decades of CO_2 from industrial sources in the region.
- Advanced geologic modeling and new data acquisition are needed to address data gaps and advance CCS in key offshore areas selected for further investigation.

OFFSHORE RISK FACTORS:

- Offshore geologic risk factors include soft-sediment deformation, unit continuity, sedimentological and structural features, seismicity and hydrates.
- Carbon dioxide storage risks include inadequate seals, migration/leakage, chemical interactions leading to decreased storage
- Sensitive habitats, environmental impacts, disturbance to seafloor, and other risks need to be identified in advance of project activities and integrated into detailed mitigation plans for all project phases

STAKEHOLDER ENGAGEMENT:

- Input and participation from government, industry, and environmental groups is needed to develop the roadmap and address next steps needed for project deployment
- Early engagement and ongoing communication is key to project success

Validation: Injection Site Identification, Testing, and Verification of Storage Feasibility

The specific components of the project validation stage will be determined by stakeholder interests and concerns, injection site conditions, as well as regulatory and economic requirements. General examples of activities and milestones that could be associated with the Mid-Atlantic U.S. Offshore Storage Project include:

- ***Addressing data and technology gaps*** in areas selected for further investigation to reduce uncertainty in storage zone and caprock continuity and integrity, fault occurrence, CO_2 trapping mechanisms, pore fluid behavior and migration, geochemistry, and geomechanics.
- ***Identification of a candidate site*** for site-specific characterization to develop a well design and operational strategy in accordance with project and permit requirements
- ***Well drilling and pilot testing*** to establish injectivity, refine storage resource estimates and classification, and validate offshore CCS feasibility.
- ***Development of monitoring, verification and accounting plans*** to comply with permit/regulatory requirements, determine CO_2 fate and transport, reduce risk, and quantify storage volumes.

Development: Maturation of Knowledge and Technology Infrastructure

The project development stage will establish and implement a detailed plan for commercial offshore CCS operations, and may include activities such as: securing ***stakeholder investment and buy-in***; ongoing ***public outreach*** and communication; development of ***contingency plans*** for potential economic and technical challenges; ***upscaling*** injection and storage site infrastructure to meet project requirements and integration with CO_2 capture and transportation infrastructure; and ***implementation of monitoring, verification and accounting plans*** to provide assurance of long–term storage integrity.

Point of Contact: Dr. Neeraj Gupta, Battelle Principal Investigator, gupta@battelle.org.

MID-ATLANTIC U.S. OFFSHORE CARBON STORAGE RESOURCE ASSESSMENT PROJECT

Publications and Presentations List

Peer-Reviewed Journals

Back to Basics of Sequence Stratigraphy: Early Miocene and Mid-Cretaceous Examples from the New Jersey Paleoshelf, Miller K. G., Lombardi, C. J., Browning, J. V., Schmelz, W. J., Gallegos, G., Mountain, G. S., Baldwin, K. E., Journal of Sedimentary Research, 2018, v. 88 148-176.

Lower to Mid-Cretaceous sequence stratigraphy and characterization of CO_2 storage potential in the Mid-Atlantic U.S. Coastal Plain, Miller, K. G., Browning, J. V., Sugarman, P. J., Monteverde, D. H., Andreasen, D. C., Lombardi, C., Thornburg, J., Fan, Y., Kopp, R. E., Journal of Sedimentary Research, 2017, v. 87, 609-629.

Onshore-offshore correlations of fluvial-deltaic sequences from the mid-Cretaceous of the southern Baltimore Canyon Trough, Schmelz, W. J., Miller, K. G., Mountain, G. S, Browning, J. V., and Baldwin, K. E.; AAPG Bull., accepted

Paleopedology and Landscape Reconstruction of the mid-Cretaceous Atlantic Coastal Plain, Thornburg, J. D., Miller, K. G., Browning, J. V., McLaughlin, P. P., J. Sedimentary Research, accepted

Delineating Mid-Cretaceous seismic and well-log sequences to assess carbon storage potential in the northern Baltimore Canyon Trough, Baldwin, K. E., Miller, K. G., Mountain, G. S., and Schmelz, W. J., Geosphere, submitted

Revised age constraints for Barremian to Cenomanian sequences, offshore U.S. mid-Atlantic margin, Jordan, L., Lombardi, C.J., Miller, K. G, McLaughlin, P. P., and Browning, J. V., Geosphere, in prep.

Conferences, Workshops and Meetings

Quantitative Biostratigraphic Analysis of Middle Cretaceous Sequences in Baltimore Canyon Trough, Offshore Mid Atlantic U.S Margin, Jordan L. M., Miller, K. G., Browning, J. V., GSA, Indianapolis, IN, November 2018

Carbon Capture and Storage Potential Offshore the U. S. Coast: New Methods and Insights from Legacy Seismic Data, Fortin, W. F. J., Goldberg, G., Slagle, A. et al, 14th International Conference on Greenhouse Gas Control Technologies, GHGT-14, Melbourne, Australia, October 2018

Performing Carbon Storage Resource Assessments for Offshore Mid-Atlantic United States, Cumming, L., Fukai, I., Burchwell, A., Sminchak, J., McLaughlin, P., KunleDare, M., Gupta, N., 14th International Conference on Greenhouse Gas Control Technologies, GHGT-14, Melbourne, Australia, October 2018

CCS Potential in Basaltic Rift Basins Offshore the US East Coast: New Methods on Legacy Data, Fortin, W. F. J., Goldberg, D., Hutchinson, D., Slagle, A., 14th International Conference on Greenhouse Gas Control Technologies, GHGT-14, Melbourne, Australia October 2018

Mid-Atlantic U. S. Offshore Carbon Storage Resource Assessment DE-FE0026087, Gupta, N., Carbon Storage Technology Meeting, September 2018

Carbon Storage Resource Assessment for Offshore Mid-Atlantic United States, Cumming, L., Gupta, N. 2018 Mastering the Subsurface Through Technology Innovation, Partnerships and Collaboration: Carbon Storage and Oil and Natural Gas Technologies Review Meeting Pittsburgh, PA, August 2018

Leveraging a Legacy Sample and Data Collection for Carbon Storage Resource Assessment, KunleDare, M.A. and McLaughlin, P. P., 2018 AAPG Annual Convention & Exhibition, Salt Lake City, UT, May 2018

Mid-Atlantic U.S. Offshore Carbon Storage Resource Assessment, Cumming et al. IEAGHG, 3rd International Workshop on Offshore Geologic CO2 Storage Oslo, Norway, May 2018

Revised Stratigraphic Synthesis of the Baltimore Canyon Trough: Implications for Reservoir Identification and Analysis, Schmelz, W. J., Miller, K. G., Mountain, G. S., Browning, J. V., AAPG ACE, Salt Lake City, UT May 2018

Conferences, Workshops and Meetings (cont.)

Back to basics of sequence stratigraphy: Early Miocene and Mid-Cretaceous examples from the New Jersey Paleoshelf, Miller, K. G., Lombardi, C., Browning, J. V., Schmelz, W. J., Gallegos, G., Mountain, G. S., and Baldwin, K., Geological Society of America Abstracts with Programs. Vol. 49, No. 6, doi: 10.1130/abs/2017AM-306219, 2017

Carbon Sequestration Potential in Mesozoic Rift Basins Offshore the US East Coast: Teaching Old Seismic Data New Tricks, Fortin, W.F.J., Goldberg, D., Hutchinson, D., Slagle, A., AGU; New Orleans, LA, December 2017

Mid-Atlantic U.S. Offshore Carbon Storage Resource Assessment, Cumming, L., Gupta, N., Midwest Region Carbon Sequestration Partnership meeting, Washington, D.C., November 2017

Cross Sections from the Midwest Regional Carbon Sequestration Partnership: Visualizing Subsurface Carbon Storage Opportunities Across the Central and Eastern United States, Dinterman, P. A., Moore, J. P., Lewis, E. J., Greb, S. F., Miller, K. G., Schmelz, W. J., GSA, Seattle, WA, October 2017

Delineating Mid-Cretaceous Seismic and Well-log Sequences to Assess Carbon Storage Potential in the Northern Baltimore Canyon Trough, Baldwin, K. E., Miller, K. G, Mountain, G.S., Geological Society of America Abstracts with Programs. Vol. 49, No. 6, doi: 10.1130/abs/2017AM-308050, 2017

Mid-Atlantic U.S. Offshore Carbon Storage Resource Assessment: Project Developments and Status Update, Gupta, N., Cumming, L., IEAGHG, 2nd International Workshop on Offshore CO2 Geological Storage, Beaumont, Texas, June 2017

Geology (and policy) Matters: The Challenging Case for Carbon Storage, U.S. Mid-Atlantic Region, Miller, K.G., Browning, J. V., Kopp, R. E., Fan-Reinfelder, Y., REI Symposium; New Brunswick, NJ, May 2017

Cretaceous Sedimentation Patterns in the Southern Baltimore Canyon Trough: Correlating the Maryland Coastal Plain to the Continental Rise, Schmelz, W. J., Miller, K. G., Mountain, G. S., Browning, J. V., Geological Society of America Southeastern Section Annual Meeting, Richmond, VA, March 2017

Mid-Atlantic U.S. Offshore Carbon Storage Resource Assessment, Cumming L., Gupta, N., Miller, K., Lombardi, C., Goldberg, D., Brink, U., Schrag, D., Andreasen, D., Carter, K., Energy Procedia, 2017, v. 114:4629–4636

Mid-Atlantic U.S. Offshore Carbon Storage Resource Assessment, Cumming L., Gupta, N., Miller, K., Lombardi, C., Goldberg, D., Brink, U., Schrag, D., Andreasen, D., Carter, K., GHGT-13, Lausanne, Switzerland, November 2016

Sequence Stratigraphy in the Northern Baltimore Canyon Trough, Offshore Eastern U.S., Lombardi, C. J., Miller, K. G., Mountain, G. S., GSA, Denver, CO, September 2016

Potential for Carbon Capture and Sequestration (CCS) in the Eastern Georges Bank Basin, Offshore Massachusetts, Graham, S., Miller, K. G., Mountain, G. S. and Lombard, C. J., Geological Society of America Abstracts with Programs, v. 48, n. 7, doi: 10.1130/abs/2016AM-287229; September 2016

Mid-Atlantic U.S. Offshore Carbon Storage Resource Assessment, International Workshop on Offshore Geologic CO2 Storage; Gupta, N., Fukai, I., Cumming, L., CSLF Workshop, Austin, TX, May 2016

Overview of the Mid-Atlantic U.S. Offshore Carbon Storage Resource Assessment, Cumming et al., Carbon Capture, Utilization & Storage Conference, Tysons, VA, 2016

Palynological constraints on the stratigraphy of the Magothy Formation (Cretaceous), New Jersey and Delaware, and implications for interstate aquifer correlation, McLaughlin, P. P., Miller, K. G., Browning, J. V., Sugarman, P. J., Geological Society of America Abstracts with Programs, v. 48, n. 7, doi: 10.1130/abs/2016AM-287774, 2016

Sequence stratigraphic framework of the mid-Cretaceous nonmarine Potomac Formation in New Jersey and Delaware, Thornburg, J. D., Miller, K. G., and Browning, J. V, Geological Society of America Abstracts with Programs, v. 48, n. 7, doi: 10.1130/abs/2016AM-286710, 2016

Carbon Storage Potential at the Great Stone Dome, Northern Baltimore Canyon Trough, Lombardi, C. J., Mountain, G. S. and Miller, K. G., Geological Society of America Abstracts with Programs: v. 48, n. 7, doi: 10.1130/abs/2016AM-284924, 2016

Mid-Atlantic U.S. Offshore Carbon Storage Resource Assessment, Cumming et al., Southeast Regional Carbon Sequestration Partnership (SECARB) Annual Stakeholder Briefing, March 2016

Theses

Seismic stratigraphy of the Georges Bank Basin: Implications for seismic stratigraphy and Carbon Capture and Storage, master's thesis, Rutgers University, Adams, A., January 2019

Georges Bank Basin Stratigraphy: Cretaceous Gamma Log Sequences Correlated with Seismic Data, master's thesis, Rutgers University, Graham, S., 2019

New Insights on the Mesozoic evolution of the Mid-Atlantic Continental Margin from Integrated Sequence Stratigraphy and Numerical Modeling, master's thesis, Rutgers University, Schmelz, W., 2019

Quantitative Biostratigraphic Analysis of Middle Cretaceous Sequences in Baltimore Canyon Trough, Mid Atlantic U. S. Margin, master's thesis, Rutgers University, Jordan, L., May 2019

Sequence stratigraphic interpretation of mid-Cretaceous strata from the Great Stone Dome to the continental slope, northern Baltimore Canyon Trough: Implications to sea level and Carbon Capture and Sequestration, Ph.D. thesis, Rutgers University, Lombardi, C., May 2017

Final Participant List for Offshore Workshop

David Andreasen, Maryland Geo Survey
Robin Anthony, Pennsylvania Geo Survey
Kim Baldwin, Rutgers
Melissa Batum, BOEM
Dan Blankenau, Great Plains Energy, Inc.
Alain Bonneville, PNNL
Carol Brantley, Battelle
Joseph Camlin, Consultant
Kristin Carter, Pennsylvania Geo Survey
Thomas Coleman, Slixa
Amber Conner, Battelle
Jeff Crabaugh, ExxonMobil
Lydia Cumming, Battelle
Darin Damiani, DOE
Joe D'Amico, D'Amico Technologies
Casie Davidson, PNNL
Phillip Dinterman, West Virginia Geo Survey
Gary Draft, West Virginia Geo Survey
Brian Dunst, Pennsylvania Geo Survey
Hal Fitch, Michigan DEQ
Isis Fukai, Battelle
Jackie Gerst, Battelle
Sarah Gilliand, US EPA
Michael Godec, ARI
Dave Goldberg, LDEO
Tim Grant, NETL
Steve Greb, Kentucky Geo Survey
Janice Gregory-Sloan, Sigmacubed
Neeraj Gupta, Battelle
Bill Harrison, Western Michigan University
John Holt, NRECA
Susan Hovorka, Bureau of Economic Geology
Leslie Jordan, Rutgers
William Junkin, Maryland Geo Survey
Rebecca Kavage-Adams, Maryland Geo Survey
Bruce J. Kobelski, US EPA
George Koperna, ARI
Moji KunleDare, Delaware Geo Survey
Patricia Loria, Global CCS Institute
Kanwal Mahajan, NETL
Robert G. Mannes, Core Energy
Peter McLaughlin, Delaware Geo Survey
Andrea McNemar, NETL
Cristian Medina, Indiana Geo Survey
Ken Miller, Rutgers
Allen Modroo, Core Energy
Tomas Mora, NETL/Keylogic
Bill O'Dowd, DOE-NETL
Justin Ong, Clearpath
Richard Ortt, Maryland Geo Survey
Heather Quinn, Maryland Geo Survey
Todd Schaef, PNNL
John Schmelz, Rutgers
Katie Schmid, Pennsylvania Geo Survey
Steve Shank, Pennsylvania Geo Survey
Joel Sminchak, Battelle
Paul Spahr, Ohio Division Geo Survey
Tom Sparks, Kentucky Geo Survey
Andy Staley, Maryland Geo Survey
Jeff Summers, DOE
Andrew Theodos, NiSource
Christopher Walker, BP
Peter Warkwick, United States Geo Survey
Bob Wright, The Wright Group LLC